63RD INTERNATIONAL CONFERENCE FOR STUDENTS OF PHYSICS AND NATURAL SCIENCES

OPEN READINGS 2020

MARCH 17 -20 VILNIUS LITHUANIA

ABSTRACT BOOK

CANCELLED DUE TO COVID-19

ISBN 978-609-07-0377-9

© Vilnius University, 2020

"Open Readings" is a unique conference that has grown and developed in the past few years. Something that has begun as just a handful of students presenting their work to each other evolved into a great event where students from different countries present their research side by side with lecturers of great renown. However, the core goal of the "Open Readings" has always stayed the same – to share the joy of science. So, this year we invite you to get curious and be open minded, inspire and be inspired, learn everything you can. Whether the future looks bright or grim at the moment, "Open Readings" provides you with an opportunity to shape it yourself at least a little. Exchange ideas with your peers, get inspired by talks of famous scientists, share a cup of coffee with people who combine industry and science in their work every day.

"Open Readings" flourishes because of the passion of many young scientists. That's us and that's you. It is always exhilarating to feel a part of something bigger and to see as it becomes better for having you in it. We hope that you will experience that and make many unforgettable memories here.

Yours sincerely,

"Open Readings" organizing team

CANCELLED DUE TO COVID-19

Organizing committee would like to extend a special thank you to the Optical Society (OSA), the International Society of Optics and Photonics (SPIE) and European Physical Society (EPS Young Minds, YMCA2020A01) for their continued support of "Open Readings".

Conference Chair:
Martynas Velička, *Faculty of Physics, Vilnius University, OSA & SPIE Chapter of Vilnius University*

Organizing Committee:
Team leaders:
Rusnė Ivaškevičiūtė-Povilauskienė, *Center for Physical Sciences and Technology & SPIE Chapter of Vilnius University*
Dovilė Lengvinaitė, *Faculty of Physics, Vilnius University, OSA & SPIE Chapter of Vilnius University*
Rokas Jasiūnas, *Center for Physical Sciences and Technology*
Rasa Platakytė, *Faculty of Physics, Vilnius University, OSA & SPIE Chapter of Vilnius University*
Simona Pūkienė, *Center for Physical Sciences and Technology, OSA & SPIE Chapter of Vilnius University*
Organizers:
Nour Alsamsam, *Faculty of Physics, Vilnius University*
Bernadeta Balčiukynaitė, *Faculty of Physics, Vilnius University & SPIE Chapter of Vilnius University*
Rimantė Bandzevičiūtė, *Faculty of Physics, Vilnius University*
Živilė Čerškutė, *Faculty of Physics, Vilnius University & SPIE Chapter of Vilnius University*
Džiugas Litvinas, *Faculty of Physics, Vilnius University & SPIE Chapter of Vilnius University*
Vaida Marčiulionytė, *Faculty of Physics, Vilnius University & SPIE Chapter of Vilnius University*
Šarūnas Mickus, *Faculty of Physics, Vilnius University*
Lukas Naimovičius, *Faculty of Physics, Vilnius University*
Giedrius Pakalka, *Faculty of Physics, Vilnius University & SPIE Chapter of Vilnius University*
Dominykas Sanda, *Faculty of Physics, Vilnius University*
Kotryna Šiškauskaitė, *Faculty of Physics, Vilnius University*
Laura Tauraitė, *Faculty of Physics, Vilnius University & SPIE Chapter of Vilnius University*
Aivaras Vilutis, *Life Sciences Center, Vilnius University*

Programme Committee:
prof. Vilmantė Borutaitė, *Neurosciences Institute, Lithuanian University of Health Sciences*
dr. Kastytis Zubovas, *Department of Fundamental Research, Center for Physical Sciences and Technology*
dr. Aurimas Vyšniauskas, *Department of Molecular Compound Physics, Center for Physical Sciences and Technology*
dr. Danielis Rutkauskas, *Department of Molecular Compound Physics, Center for Physical Sciences and Technology*
dr. Ramūnas Aleksiejūnas, *Institute of Photonics and Nanotechnology, Faculty of Physics, Vilnius University*
dr. Akvilė Zabiliūtė-Karaliūnė, *Institute of Photonics and Nanotechnology, Faculty of Physics, Vilnius University*
dr. Julius Vengelis, *Laser Research Center, Faculty of Physics, Vilnius University*
dr. Rasa Pauliukaitė, *Department of Nanoengineering, Center for Physical Sciences and Technology*
dr. Linas Minkevičius, *Department of Optoelectronics, Center for Physical Sciences and Technology*
dr. Andrius Gelžinis, *Institute of Chemical Physics, Faculty of Physics, Vilnius University*
dr. Jurga Juodkazytė, *Department of Chemical Engineering and Technology, Center for Physical Sciences and Technology*
dr. Linas Vilčiauskas, *Department of Chemical Engineering and Technology, Center for Physical Sciences and Technology*
dr. Justinas Čeponkus, *Institute of Chemical Physics, Faculty of Physics, Vilnius University*
dr. Ignas Grigelionis, *Department of Optoelectronics, Center for Physical Sciences and Technology*
dr. Justina Gaidukevič, *Institute of Chemistry, Faculty of Chemistry and Geosciences, Vilnius University*
dr. Vytautas Jakštas, *Department of Optoelectronics, Center for Physical Sciences and Technology*
dr. Jevgenij Pavlov, *Institute of Photonics and Nanotechnology, Faculty of Physics, Vilnius University*
dr. Ignas Nevinskas, *Department of Optoelectronics, Center for Physical Sciences and Technology*
dr. Tomas Šalkus, *Institute of Applied Electrodynamics and Telecommunications, Faculty of Physics, Vilnius University*
dr. Saulius Daugėla, *Institute of Applied Electrodynamics and Telecommunications, Faculty of Physics, Vilnius University*
dr. Vilma Kavaliukė, *Institute of Applied Electrodynamics and Telecommunications, Faculty of Physics, Vilnius University*
dr. Ilja Ignatjev, *Department of Organic Chemistry, Center for Physical Sciences and Technology*
dr. Marius Franckevičius, *Department of Molecular Compound Physics, Center for Physical Sciences and Technology*
dr. Ieva Matulaitienė, *Department of Organic Chemistry, Center for Physical Sciences and Technology*
dr. Jurga Būdienė, *Department of Organic Chemistry, Center for Physical Sciences and Technology*
dr. Rasa Garjonytė, *Department of Organic Chemistry, Center for Physical Sciences and Technology*

CANCELLED DUE TO COVID-19

dr. Rūta Kananavičiūtė, *Institute of Biosciences, Life Sciences Center, Vilnius University*
dr. Julija Armalytė, *Institute of Biosciences, Life Sciences Center, Vilnius University*
dr. Algirdas Mikalkėnas, *Institute of Biosciences, Life Sciences Center, Vilnius University*
dr. Marijonas Tutkus, *Department of Molecular Compound Physics, Center for Physical Sciences and Technology*

Chairmen:
prof. Gintaras Valušis, *Department of Optoelectronics, Center for Physical Sciences and Technology*
prof. Mikas Vengris, *Laser Research Center, Faculty of Physics, Vilnius University*
dr. Rokas Kondrotas, *Department of Characterisation of Materials Structure, Center for Physical Sciences and Technology*
dr. Mangirdas Malinauskas, *Laser Research Center, Faculty of Physics, Vilnius University*
dr. Tomas Tamulevičius, *Institute of Materials Science, Kaunas University of Technology*
dr. Linas Vilčiauskas, *Department of Chemical Engineering and Technology, Center for Physical Sciences and Technology*
dr. Pranciškus Vitta, *Institute of Photonics and Nanotechnology, Faculty of Physics, Vilnius University*
dr. Augustinas Vizbaras, *Co-Founder at Brolis Sensor Technology*
dr. Kristijonas Vizbaras, *Co-Founder at Brolis Sensor Technology*

CANCELLED DUE TO COVID-19

TOPOLOGICAL QUANTUM COMPUTING: A MATERIALS PERSPECTIVE

Mihir Pendharkar

University of California, Santa Barbara

mihir@ece.ucsb.edu

CANCELLED DUE TO COVID-19

A quantum computer is theorized to aid in simulating nature quantum mechanically and various approaches to building a quantum computer are actively being pursued. Common to all approaches is the requirement for building a fault tolerance from errors due to external environmental perturbations (noise). Inherent fault tolerance is only native to one approach – topological quantum computation. This approach is based upon Majorana Zero Modes which are quasi-particles with no measurable charge or mass, that are bound to zero-energy. Quantum information is said to be stored non-locally in interactions of MZMs. These MZMs have been predicted to arise at the ends of 1D chain of electrons with strong spin-orbit coupling, when such a chain is transparently coupled to an s-wave superconductor and an external magnetic field is applied along the length of the chain.

This talk will focus on the materials aspects of the challenge of topological quantum computing. Namely, realizing a material system capable of hosting robust MZMs and the demonstration of MZM braiding and fusion, goals which still remain an outstanding challenge. Semiconductors like InAs and InSb when coupled to a superconductor like aluminum (Al), have been claimed to show zero energy end modes reminiscent of MZMs. Reducing disorder, i.e. increasing carrier mobility, along with increasing the g-factor and the superconducting gap of the superconductor have been proposed to be some of the ways of making more robust topological states. Apart from giving a summary of the state-of-the-art, this talk will provide insight into some new superconductor-semiconductor combinations that may enable the exploration of next generation of devices hosting the enigmatic MZMs.

DYNAMIC PLASMONICS

Laura Na Liu

Kirchhoff Institute for Physics, University of Heidelberg, Im Neuenheimer Feld 227, 69120 Heidelberg, Germany

A prerequisite to build advanced nanophotonic architectures is the ability to precisely control the organization of different optical elements, such as metal nanoparticles, fluorophores, semiconductor nanocrystals, and others in space. To this end, DNA origami represents an ideal construction platform owing to its unique sequence specificity and structural versatility. I will present sequentially a diverse set of DNA-assembled nanophotonic systems according to their characteristic optical properties. I will also discuss about the inevitable evolution from static to dynamic devices along with the fast development of this inter-disciplinary field. Finally, possible future directions and perspectives on the challenges will be elucidated.

Visit is sponsored by LIGHT CONVERSION

CANCELLED DUE TO COVID-19

ENABLING HYDROGEN AS FUTURE ENERGY CARRIER:

FROM THE LITHUANIAN CRADLE TO WHERE WE ARE TODAY

Klaus-Dieter Kreuer

Max-Planck-Institute for Solid State Research, Heisenberg Straße 1, 70569 Stuttgart, Germany
kreuer@fkf.mpg.de

CANCELLED DUE TO COVID-19

The expected end of the "oil age" (for environmental reasons) will lead to increasing focus and reliance on alternative energy conversion devices and ways for storing energy. Future scenarios may comprise "hydrogen" as an energy carrier with high energy density and potentially high conversion efficiency into electric energy and vice versa [1]. A lot will depend on further progress in PEM (polymer

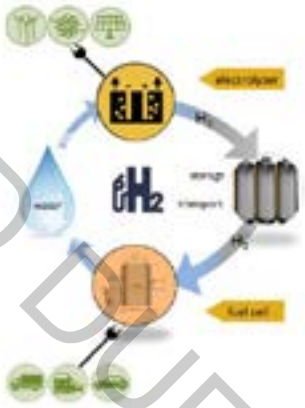

Fig 1. Hydrogen cycle.

electrolyte membrane) electrolyzer and fuel cell technology with many fundamental and engineering problems waiting to be solved.

The first who actually proposed a theory on the decomposition of water into hydrogen and oxygen by means of "électricité galvanique" [2] was the Lithuanian Freiherr Christian Johann Dietrich Theodor von Grotthuß. He introduced a concept of ionic conductivity which already captured in a qualitative way what 100 years later was described by the Nernst-Einstein relationship. In my presentation, I will tell the story starting from von Grotthuß all the way to state of the art research in an anecdotic way. I will touch upon i) the long standing issue of understanding proton conduction phenomena as an example of a process which, my no means, is unidirectional in nature, ii) the complex issue of developing materials with high performance, longevity and environmental benignity meeting critical cost targets and iii) exciting recent findings (fresh out of the lab) narrowing the gap between our visions and facts proven by good scientific practice.

---

[1] K. D. Kreuer ed.: Fuel Cells, Springer 2013, ISBN 978-1-4614-5785-5.
[2] C. J. T. de Grotthuss: Mémoire sur la décomposition de l'eau et des corps qu'elle tient en dissolution à l'acide de l'électricité galvanique, Annales Chim. (Paris) vol. 58, 1806, 54 – 74

SEMICONDUCTOR NANOWIRES FOR OPTOELECTRONICS AND ENERGY APPLICATIONS

Chennupati Jagadish
Research School of Physics, The Australian National University, Canberra, ACT 2601, Australia
c.jagadish@ieee.org

CANCELLED DUE TO COVID-19

Semiconductors have played an important role in the development of information and communications technology, solar cells, solid state lighting. Nanowires are considered as building blocks for the next generation electronics and optoelectronics. In this talk, I will introduce the importance of nanowires and their potential applications and discuss about how these nanowires can be synthesized and how the shape, size and composition of the nanowires influence their structural and optical properties. I will present results on axial and radial heterostructures and how one can engineer the optical properties to obtain high performance lasers, THz detectors, solar cells and to engineer neuronal networks. Future prospects of the semiconductor nanowires will be discussed.

Professor Jagadish is a Distinguished Professor and Head of Semiconductor Optoelectronics and Nanotechnology Group in the Research School of Physics and Engineering, Australian National University. He has served as Vice-President and Secretary Physical Sciences of the Australian Academy of Science during 2012-2016. He is currently serving as Past President of IEEE Photonics Society, Past President of Australian Materials Research Society. Prof. Jagadish is the Editor-in-Chief of Applied Physics Reviews, Editor of 3 book series and serves on editorial boards of 19 other journals. He has published more than 930 research papers (650 journal papers), holds 5 US patents, co-authored a book, co-edited 13 books and edited 12 conference proceedings and 17 special issues of Journals. He has won the 2000 IEEE Millennium Medal and received Distinguished Lecturer awards from IEEE NTC, IEEE LEOS and IEEE EDS. He is a Fellow of the Australian Academy of Science, Australian Academy of Technological Sciences and Engineering, The World Academy of Sciences, US National Academy of Inventors, Indian National Science Academy, Indian National Academy of Engineering, Indian Academy of Sciences, IEEE, APS, MRS, OSA, AVS, ECS, SPIE, AAAS, FEMA, APAM, IoP (UK), IET (UK), IoN (UK) and the AIP. He received many awards including IEEE Pioneer Award in Nanotechnology, IEEE Photonics Society Engineering Achievement Award, OSA Nick Holonyak Jr Award, Welker Award, IUMRS Somiya Award, UNESCO medal for his contributions to the development of nanoscience and nanotechnologies and Lyle medal from Australian Academy of Science for his contributions to Physics, Beattie Steel Medal from Australian Optical Society and IEEE Education Award from Electron Devices Society. He has received Australia's highest civilian honor, AC, Companion of the Order of Australia, as part of 2016 Australia day honors from the Governor General of Australia for his contributions to physics and engineering, in particular nanotechnology.

Visit is sponsored by OSA

LASER PRINTING OF NANOPARTICLES AND LIVING CELLS

Boris Chichkov

Institut für Quantenoptik, Leibniz Universität Hannover, Welfengarten 1, 20167 Hannover, Germany
chichkov@iqo.uni-hannover.de

CANCELLED DUE TO COVID-19

Laser printing can be applied for printing very small and delicate objects like nanostructures, nanoparticles, living cells, and microorganisms. We will demonstrate several laser printing techniques allowing the generation and arrangement of spherical metal and dielectric nanoparticles in a very precise manner. We will discuss prospects of this technology for printing metalenses and realization of 3d nanostructures.

In a series of publications on laser printing of living cells we demonstrated that cells are not harmed by the printing process. Different cell types, including primary cells, stem cells, iPS cells, differentiated iPS cells, and microorganisms embedded in hydrogels as extra-cellular matrix, have been printed. I will report on our recent progress and ongoing research in this field.

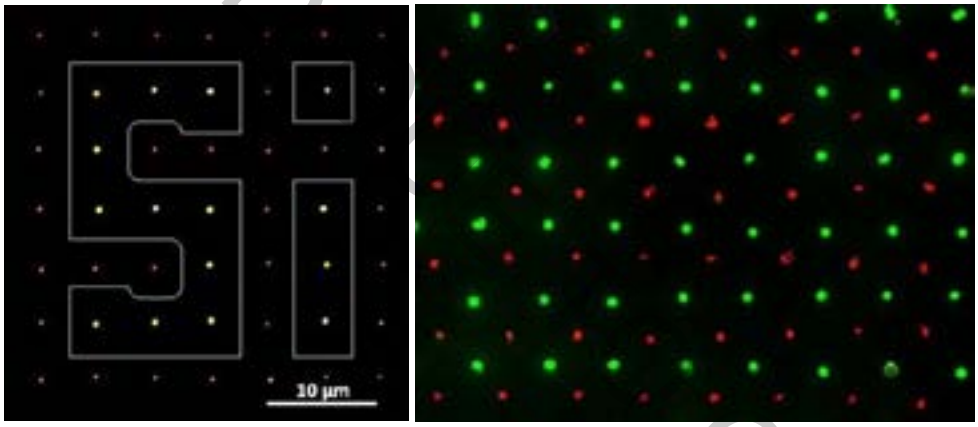

Fig. 1. Examples of laser printed arrays of Si nanoparticles, and living (endothelial and stem) cells.

Visit is sponsored by EKSPLA

ROOM-TEMPERATURE TERAHERTZ QUANTUM CASCADE LASER SOURCES BASED ON INTRA-CAVITY DIFFERENCE FREQUENCY GENERATION

Mikhail Belkin

Walter Schottky Institute and Department of Electrical and Computer Engineering
Technical University of Munich
https://www.wsi.tum.de/views/groups.php?group=belkin

CANCELLED DUE TO COVID-19

I will review the recent progress of electrically-pumped semiconductor sources of terahertz radiation based on intra-cavity difference-frequency generation (DFG) in mid-infrared quantum cascade lasers (QCLs) [1]. These devices, referred to as THz DFG-QCLs, are similar in fabrication and operation simplicity to THz QCLs, but, unlike THz QCLs, they offer room-temperature operation. With the implementation of Cherenkov phase-matching scheme [2] THz DFG-QCLs have achieved mW-level THz power output in pulsed mode and over 10 microwatts of continuous-wave THz power output at room temperature. Furthermore, these devices provide sub-1-MHz emission linewidth [3] and broadband spectral tuning in the entire 1-6 THz range [4]. I will also discuss our ongoing efforts to further improve the efficiency and power output of these devices.

Biography: Mikhail Belkin received his BS in Physics and Mathematics from Moscow Institute of Physics and Technology in 1998 and PhD degree in Physics from the University of California at Berkeley in 2004. In 2004-2008 he did his postdoctoral work in Prof. Federico Capasso group at the Harvard School of Engineering and Applied Sciences. He then joined the faculty of the Department of Electrical and Computer Engineering at The University of Texas at Austin where he rose through the academic ranks to become a Professor and a Myron L. Begeman Faculty Fellow. In 2019, Dr. Belkin joined the Walter Schottky Institute and the Department of Electrical and Computer Engineering and of the Technical University of Munich as a Chair of Semiconductor Technology. Dr. Belkin's research interests are in the field of mid-infrared and THz photonics and nonlinear optics. His recent recognitions include the 2015 Friedrich Wilhelm Bessel Research Award from Humboldt Foundation, NSF CAREER Award, the DARPA Young Faculty Award, the AFOSR Young Investigator Program Award, and the Norman Hackerman Advanced Research Program Award from the state of Texas. Dr. Belkin is the Fellow of the OSA and SPIE.

Visit is sponsored by BROLIS SEMICONDUCTORS

[1] M.A. Belkin, F. Capasso, A. Belyanin, D.L. Sivco, A.Y. Cho, D.C. Oakley, C.J. Vineis, G.W. Turner, "Terahertz quantum-cascade-laser source based on intracavity difference-frequency generation," Nat. Photon. 1, 288 (2007).
[2] K. Vijayraghavan, R.W. Adams, A. Vizbaras, M. Jang, C. Grasse, G. Boehm, M. C. Amann, and M.A. Belkin "Terahertz Sources Based on Čerenkov Difference-Frequency Generation in Quantum Cascade Lasers," Appl. Phys. Lett. 100, 251104 (2012).
[3] L. Consolino, S. Jung, A. Campa, M. De Regis, S. Pal, J. H. Kim, K. Fujita, A. Ito, M. Hitaka, S. Bartalini, P. De Natale, M. A. Belkin, and M. S. Vitiello, "Spectral purity and tunability of terahertz quantum cascade laser sources based on intracavity difference-frequency generation," Sci. Adv. 3, e160331 (2017).
[4] Y. Jiang, K. Vijayraghavan, S. Jung, F. Demmerle, G. Boehm, M. C. Amann, and M.A. Belkin, "External cavity terahertz quantum cascade laser sources based on intra-cavity frequency mixing with 1.2-5.9 THz tuning range," J. Opt., 16, 094002 (2014).

METAL-HALIDE PEROVSKITE: THE IDEAL PHOTOVOLTAIC MATERIAL?

Wolfgang Tress

Department of Chemistry and Biochemistry, University of Munich, Germany
wolfgang.tress@lmu.de

In the urgently required decarbonization of the energy sector, renewable energy technologies such as photovoltaics become increasingly relevant. Solar cells based on lead halide perovskites have recently emerged showing a high potential by combining high efficiency (up to 25%) with simple processing conditions such as deposition from solution. In this talk, the outstanding properties of this material and the device physics of perovskite solar cells are addressed. The focus is on recombination of charge carriers because understanding this process is essential to explain the high efficiency values and the ultimate limits.

The high efficiencies are accompanied by transient processes on the timescale of seconds to days. Those result in hysteresis in measured optoelectronic properties and mysterious negative capacitance effects. Furthermore, they lead to reversible performance changes during exposure to electrical bias or light. These effects are discussed based on the mixed ionic-electronic conductivity of the perovskite materials. Finally, consequences for operation of perovskite solar cells under real world conditions are addressed and opportunities for further optoelectronic applications discussed.

[1] Tress W. Perovskite Solar Cells on the Way to Their Radiative Efficiency Limit – Insights Into a Success Story of High Open-Circuit Voltage and Low Recombination. Adv. Energy Mater. 7, 1602358 (2017).

[2] Tress W. Metal Halide Perovskites as Mixed Electronic–Ionic Conductors: Challenges and Opportunities—From Hysteresis to Memristivity. J. Phys. Chem. Lett. 8, 3106–3114 (2017).

[3] Ebadi F. Taghavinia N., Mohammadpour R., Hagfeldt A. & Tress W. Origin of apparent light-enhanced and negative capacitance in perovskite solar cells. Nature Communications (2019), 10, 1574.

[4] Tress W., Domanski K., Carlsen B., Agarwalla A., Alharbi E. A., Graetzel M. & Hagfeldt A. Performance of perovskite solar cells under simulated temperature-illumination real-world operating conditions. Nat Energy 4, 568–574 (2019).

[5] Tress W., Yavari M., Domanski K., Yadav P., Niesen B., Baena J. P. C., Hagfeldt A. & Graetzel M. Interpretation and evolution of open-circuit voltage, recombination, ideality factor and subgap defect states during reversible light-soaking and irreversible degradation of perovskite solar cells. Energy Environ. Sci. 11, 151–165 (2018).

CANCELLED DUE TO COVID-19

17 March, TUESDAY

09:00	Mihir Pendharkar TOPOLOGICAL QUANTUM COMPUTING: A MATERIALS PERSPECTIVE		
	ORAL SESSION O1 (D401)		
10:00	Rusnė Ivaškevičiūtė-Povilauskienė, Linas Minkevičius, Domas Jokubauskis, Andrzej Urbanowicz, Simonas Indrišiūnas, Gintaras Valušis GRAPHITE-BASED FLEXIBLE ZONE-PLATES FOR TERAHERTZ OPTICS	O1-1	31
10:15	Julia A. Fedotova, Uladzislaw E. Gumiennik, Alexander K. Fedotov EFFECT OF MAGNETIC CO–COO PARTICLES ON THE CARRIER TRANSPORT IN SINGLE LAYER GRAPHENE	O1-2	32
10:30	Ewelina Nowak, Mirosław Szybowicz, Alicja Stachowiak, Edyta Chłopocka, Daria Piechowiak SPECTROSCOPIC STUDY ON THE INFLUENCE OF POST-PROCESSING ANNEALING ON ZNO FILMS PRODUCED WITH A SOL-GEL METHOD CENTERS IN NaF-Al2O3-P2O5 GLASSY MATRIX	O1-3	33
10:45	Rokas Jasiūnas, Huotian Zhang, Andrius Devižis, Feng Gao, Vidmantas Gulbinas FROM FS TO MS - DYNAMIC PHOTOPHYSICS OF NONFULLERENE ORGANIC SOLAR CELLS	O1-4	34
11:00	Tadas Lenkutis, Andrius Dzedziskis, Barbora Kačinskaitė, Dainius Kunkis, Vytautas Bučinskas. ENERGY GENERATION FROM VEHICLE VIBRATIONS USING SMART DAMPER	O1-5	35
	ORAL SESSION O2 (A101)		
10:00	Živilė Čerškutė, Augustas Vaitkevičius, Andrei Stancalie, Gintautas Tamulaitis. IRRADIATION INFLUENCE ON THE SPATIAL DISTRUBUTION OF PHOTOLUMINESCENCE IN OPTICAL FIBERS	O2-1	36
10:15	Edvinas Navakauskas and Simona Strazdaitė STRUCTURE DETERMINATION OF HEWL PROTEIN AGGREGATES ADSORBED AT WATER AND PHOSPHOLIPID MONOLAYER INTERFACES	O2-2	37
10:30	Juzef Kučinski, Beomseok Kim, Jin-Woo Han, Mindaugas Gicevičius, Lina Mikoliunaitė, Meyya Meyyappan POTENTIOMETRIC CO2 SENSOR FOR CREW CABIN AIR QUALITY MONITORING	O2-3	38
11:00	COFFEE BREAK		
	ORAL SESSION O3 (D401)		
11:30	Andrius Sakavicius, Gvidas Astromskas, Virginijus Bukauskas, Mindaugas Kamarauskas, Algimantas Luksa, Viktorija Nargeliene, Gediminas Niaura, Ilja Ignatjev, Marius Treideris, Arunas Setkus AIR INDUCED CHANGES IN SURFACE PROPERTIES IN GRAPHENE-METAL CONTACTS AND LONG DISTANCE DISTORTIONS IN THE GRAPHENE NEAR THE EDGE OF PLANAR METAL CONTACTS	O3-1	39
11:45	Edvinas Radiunas, Manvydas Dapkevičius, Steponas Raišys, Saulius Juršėnas, Augustina Jozeliūnaitė, Tomas Javorskis, Ugnė Šinkevičiūtė, Edvinas Orentas, Karolis Kazlauskas STRIVING FOR EFFICIENT NIR-TO-VIS UPCONVERSION: LIMITING FACTORS IN RUBRENE-BASED SYSTEMS	O3-2	40
12:00	Agnė Butkutė, Tomas, Baravykas, Titas Tičkūnas, Linas Jonušauskas, Valdas Sirutkaitis OPTIMIZATION OF SELECTIVE LASER ETCHING PROCESS FOR ARBITRARY SHAPE 3D MICRO-STRUCTURE FABRICATION	O3-3	41
12:15	Joanna Szczuka, Tomasz Buchwald, Mariusz Sandomierski SURFACE ANALYSIS OF TITANIUM ALLOY TI-6AL-4V ELI WITH OCTADECYLPHOSPHONIC ACID (ODPA) AND HYDROXYAPATITE (HA) LAYERS	O3-4	42
12:30	Džiugas Litvinas, Saulius Juršėnas, Toshinori Matsushima, Chihaya Adachi BALANCING LAYER STABILITY AND EFFECTIVE LUMINESCENCE IN PEA2FAN-1PBNBR3N+1 2D PEROVSKITES	O3-5	43
	ORAL SESSION O4 (A101)		
11:30	Matas Steponaitis, Regimantas Komskis, Egidijus Kamarauskas, Tadas Malinauskas, Saulius Jursenas and Vytautas Getautis INVESTIGATION OF PROPERTIES OF TRIARYLAMINE BASED QUATERNARY AMMONIUM SALTS	O4-1	44
11:45	Anne Loron, Christian Gardrat, Ramunė Rutkaitė, Vesta Navikaitė-Šnipaitienė, Deimantė Rosliuk, Véronique Coma TETRAHYDROCURCUMIN ENCAPSULATED IN MODIFIED STARCH BY SPRAY-DRYING FOR MICROBIOLOGICAL APPLICATIONS	O4-2	45
12:00	Deimante Vaitukaityte, Zhiping Wang, Tadas Malinauskas, Artiom Magomedov, Giedre Bubniene, Vygintas Jankauskas, Egidijus Kamarauskas, Vytautas Getautis, Henry J. Snaith EFFICIENT AND STABLE PEROVSKITE SOLAR CELLS USING LOW-COST ANILINE-BASED ENAMINE HOLE TRANSPORTING MATERIALS	O4-3	46
12:45	**PUPILS' POSTER SESSION**		
	ORAL SESSION O5 (A101)		
13:30	Gabrielė Karpickaitė, Mindaugas Mačernis MODELING CHARGE TRANSFER STATE OF CAROTENOIDS AND CHLOROPHYLL-A COMPLEXES FROM PHOTOSYNTHESIS USING DENSITY FUNCTIONAL THEORY	O5-1	47
13:45	Augustina Jozeliunaite, Domantas Valceckas, Edvinas Orentas FULLERENE-C60: FROM THE INOCCENT GUEST MOLECULE TO A PHOTOCATALYST	O5-2	48
14:00	Adrián Vicent-Claramunt, Evaldas Naujalis INFLUENCE OF WORKPLACE EXPOSURE ON VOCS PROFILE IN HUMAN BREATH	O5-3	49

CANCELLED DUE TO COVID-19

14:15	Andrei Buzykin, Oleg Smirnov SUBLIMATION ENTHALPY OF ORGANIC MOLECULES WITH DECOMPOSITION CONTROL: MASS-SPECTROMETRY APPROACH	O5-4	50
	Dzimitry Ivashenka, Elena Petrova, Vladimir Pankov SYNTHESIS AND MAGNETIC PROPERTIES OF Co0.65Zn0.35Fe2O4 MAGNETIC NANOPARTICLES WITH HIGH CRYSTALLINITY BY ULTRASONIC SPRAY PYROLYSIS METHOD	O5-5	51
14:45	BREAK		
15:00	Klaus-Dieter Kreuer ENABLING HYDROGEN AS FUTURE ENERGY CARRIER: FROM THE LITHUANIAN CRADLE TO WHERE WE ARE TODAY		
16:00-17:30	**POSTER SESSION P1**		
17:30-18:30	Opening event and discussion SUCCESS STORIES		

18 March, WEDNESDAY

09:00	Chennupati Jagadish SEMICONDUCTOR NANOWIRES FOR OPTOELECTRONICS AND ENERGY APPLICATIONS		
	ORAL SESSION O6 (A101)		
10:00	Marijus Ambrozas, Andrius Juodagalvis DRELL-YAN PROCESS BACKGROUND ESTIMATION USING THE FAKE RATE METHOD	O6-1	52
10:15	Simona Breidokaitė, Gediminas Stankūnas, Diana Adlienė CALCULATIONS OF ELECTRONS AND PHOTONS TRANSPORT IN MEDICAL LINEAR ACCELERATOR TREATMENT HEAD	O6-2	53
10:30	Simonas Draukšas, Andrius Juodagalvis ARBITRARY PRECISION IN FLEXIBLESUSY	O6-3	54
10:45	Apolodor Aristotel Raduta, Robert Poenaru, Cristian Raduta WOBBLING MOTION IN ODD-MASS LU ISOTOPES: REDEFINING THE BAND STRUCTURE FOR TRIAXIAL NUCLEI	O6-4	55
11:00	COFFEE BREAK		
	ORAL SESSION O7 (D401)		
11:30	Lena Golubewa, Mikhail Shuba, Igor Timoshchenko, Alesya Paddubskaya, Andrei Dementjev, Danielis Rutkauskas, Oleg Romanov, Renata Karpicz, Tatsiana Kulahava DESTRUCTION OF CANCER CELLS INDUCED BY INTERACTION OF NIR IRRADIATION WITH SINGLE-WALLED CARBON NANOTUBES	O7-1	56
11:45	Yatinkumar Patel, Arvydas Palevicius, Giedrius Janusas SELF ORDERED NANOPOROUS ALUMINUM OXIDE MEMBRANE FOR NANOFILTRATION USING SURFACE ACOUSTIC WAVES FOR MICROHYDRUALIC DEVICES IN BIOMEDICINE	O7-2	57
12:00	Anatoly Pushkarev, Daria Markina, Pavel Trofimov, Ivan Sinev, Sergey Makarov SIMPLE APPROACHES TOWARDS IMPROVING THE PERFORMANCE OF LEAD HALIDE PEROVSKITE NANO- AND MICROLASERS	O7-3	58
12:15	Yauhen Aniskevich, Aliaksandra Radchanka, Artsiom Antanovich, Mikhail Artemyev, Genady Ragoisha, Eugene Streltsov SPECTROELECTROCHEMISTRY OF ELECTROPHORETIC CDSE QD FILMS	O7-4	59
12:30	Audronė Šeštakauskaitė, Nadzeya Khinevich, Tomas Tamulevičius, Asta Tamulevičienė SEEDED-GROWTH OF SILVER NANOPARTICLES BY CHEMICAL REDUCTION METHOD	O7-5	60
	ORAL SESSION O8 (A101)		
11:30	Anastasiya Martynava, Anastasiya Huryna, Natallja Arekhava, Anatoli Zajogin, Maksim Shundalau THE STUDY OF THE MINERAL COMPOSITION OF THE STONY PART OF THE BRAHIN METEORITE BY LASER ATOMIC EMISSION SPECTROMETRY	O8-1	61
11:45	Karolis Daugevičius, Rokas Naujalis, Rima Stonkutė STAR CLUSTERS IN THE ANDROMEDA GALAXY. PHOTOMETRIC EFFECTS OF BACKGROUND/FOREGROUND STARS	O8-2	62
12:00	Olga Ryabukhina, Igor Zinchenko, Maria Kirsanova GAS AND DUST TEMPERATURE IN THE FILAMENTARY INFRARED DARK CLOUDS	O8-3	63
12:15	Edgaras Kolomiecas, Vidas Dobrovolskas, Arūnas Kučinskas ABUNDANCE OF ZIRCONIUM IN THE ATMOSPHERES OF RED GIANTS IN GALACTIC GLOBULAR CLUSTER 47 TUC	O8-4	64
12:45	**MAX PLANCK SCHOOL OF PHOTONICS**		
13:30	**Q&A MAX PLANCK SCHOOL OF PHOTONICS**		
	ORAL SESSION O9 (A101)		
13:30	Matas Tartėnas, Kastytis Zubovas MODELLING OF ACCRETION ON TO THE MILKY WAY'S SUPERMASSIVE BLACK HOLE	O9-1	65

CANCELLED DUE TO COVID-19

13:45	Kotryna Šiškauskaitė, Zofia Kaczmarek, Krzysztof Rybicki, Lukasz Wyrzykowski, Erika Pakštienė GRAVITATIONAL MICROLENSING SIMULATIONS THROUGH BINARY BLACK HOLES	O9-2	66
14:00	Rūta Urbonavičiūtė, Erika Pakštienė SEARCH FOR VARIABLE STARS IN THE NORTHERN SKY AND ANALYSIS OF PHOTOMETRIC TIME SERIES	O9-3	67
14:15	Algita Stankevičiūtė, Oliwia Ziółkowska, Magdalena Pawłowska, Cezary Turski, Łukasz Wyrzykowski INVESTIGATION OF BLACK HOLE LENSES WITH ADAPTIVE OPTICS	O9-4	68
14:30	Aidas Sadauskas, Kastytis Zubovas MORPHOLOGY AND KINEMATICS OF SIMULATED FERMI BUBBLES	O9-5	69
14:45	BREAK		
15:00	Laura Na Liu DYNAMIC PLASMONICS		
16:00-17:30	**POSTER SESSION P2**		

19 March, THURSDAY

09:00	Boris Chichkov LASER PRINTING OF NANOPARTICLES AND LIVING CELLS		

ORAL SESSION O10 (D401)

10:00	Vytenis Girdauskas, Paulius Mackonis, Augustinas Petrulenas, Aleksej Rodin INFLUENCE OF PICOSECOND PULSE TEMPORAL PROFILE FOR EFFECTIVE WIDE-BANDWIDTH TW-CLASS OPCPA PUMPING	O10-1	70
10:15	Akvilė Bunkeviciūtė, Balys Momgaudis, Mikas Vengris INVESTIGATION OF IMPURITIES IN LASER MEDIA: CATHODOLUMINESCENCE AND FILAMENT INDUCED LUMINESCENCE COMPARISON	O10-2	71
10:30	Augustinas Petrulėnas, Vytenis Girdauskas, Paulius Mackonis, Aleksėj Rodin BROADBAND TRANSIENT STIMULATED RAMAN AMPLIFICATION IN KGW CRYSTAL	O10-3	72
10:45	Evaldas Kažukauskas, Simas Butkus, Valdas Sirutkaitis MICROMACHINING OF TRANSPARENT BIOCOMPATIBLE POLYMERS APPLIED IN MEDICINE USING BURSTS OF FEMTOSECOND LASER PULSES	O10-4	73
11:00	Edvinas Aleksandravičius, Greta Merkininkaitė, Darius Gailevičius, Mangirdas Malinauskas, Simas Šakirzanovas ADDITIVE MANUFACTURING OF 3D GLASS-CERAMIC MICRO-STRUCTURES VIA DIRECT LASER WRITING AND ANNEALMENT	O10-5	74

ORAL SESSION O11 (A101)

10:00	Domantas Berenis, Gediminas Kreiza, Saulius Juršėnas, Tomas Javorskis, Edvinas Orentas, Dalius Gudeika, Juozas Vidas Gražulevičius, Karolis Kazlauskas SOLUTION-PROCESSED BLUE TADF-OLEDS BASED ON TWISTED ISOPHTALONITRILES	O11-1	75
10:15	Natallia S. Mahon, Olga V. Korolik, Alexander V. Mazanik, Yulia Galagan INFLUENCE OF FUNCTIONAL LAYERS ON ORGANIC-INORGANIC PEROVSKITE CHARGE CARRIERS PARAMETERS	O11-2	76
10:30	Justina Jovaišaitė, Dace Cīrule, Andris Jeminejs, Irina Novosjolova, Māris Turks, Paulius Baronas, Regimantas Komskis, Gediminas Jonušauskas and Saulius Juršėnas A NEW CONCEPT OF PURINE D-A-D' RATIOMETRIC CHEMICAL SENSOR, BASED ON INTERMOLECULAR PET	O11-3	77
11:00	COFFEE BREAK		

ORAL SESSION O12 (A101)

11:30	Danielius Samsonas, Dalius Petrulionis, Darius Grigaitis, Mikas Vengris INFLUENCE OF THE PIEZOELECTRIC RINGING ON THE POLARISATION CONTRAST OF THE KRTP POCKELS CELL IN THE MODULATION FREQUENCY RANGE UP TO 10 MHZ	O12-1	78
11:45	Robertas Grigutis, Gintaras Tamošauskas, Vaida Marčiulionytė, Danil Bulatov, Nail Garejev, Vytautas Jukna, Audrius Dubietis SUPERCONTINUUM GENERATION AND OPTICAL DAMAGE IN SOLID-STATE MEDIA AT HIGH REPETITION RATES	O12-2	79
12:00	Gabrielius Kontenis, Darius Gailevičius, Vytautas Purlys, Linas Jonušauskas, Roaldas Gadonas DYNAMIC ABERRATION CORRECTION VIA SPATIAL LIGHT MODULATOR (SLM) FOR FEMTOSECOND DIRECT LASER WRITING	O12-3	80
12:15	Mārcis Auzinsh, Laima Bušaite, Artūrs Mozers, Dace Osīte EXPERIMENTAL OBSERVATION OF ANGULAR MOMENTUM ALIGNMENT-TO-ORIENTATION CONVERSION IN RB ATOMS BY EXCITING THE D1 LINE HFS TRANSITIONS	O12-4	81
12:30	Arnas Žemaitis, Gedvinas Nemickas, Gabrielius Kontenis, Vytautas Purlys and Linas Jonušauskas EXPOSURE PARAMETER INFLUENCE ON METAL SURFACE PATTERNS FORMED USING FEMTOSECOND LASER	O12-5	82
	Dominik Czernia, Robert Pełka, Tomasz Korzeniak, Sujit Sasmal, Dawid Pinkowicz, Wojciech Nitek, Olaf Stefańczyk, Barbara Sieklucka MFA OF MAGNETIC PROPERTIES OF THE CHIRAL POLYMERIC PHOTOMAGNETS BASED ON CU2+ AND [MO2(CN)8]4- IONS	O12-6	83

CANCELLED DUE TO COVID-19

12:45 **LUNCH WITH INDUSTRY**

ORAL SESSION O13 (A101)

13:45	Lukas Jočionis, Bronislovas Čechavičius, Renata Butkutė, Saulius Tumėnas, Vytas Karpus OPTICAL ANISOTROPY OF GAASBI	O13-1	84
14:00	Justas Pagalys, Ričardas Norkus, Simona Pūkienė, Evelina Dudutienė, Vytautas Jakštas, Mindaugas Karaliūnas EMISSION MEASUREMENT OF TERAHERTZ TORCH DEVICE BASED ON GA(AS,BI)/ALGAAS NANOSTRUCTURES WITH PARABOLICALLY GRADED QUANTUM WELLS	O13-2	85
14:15	Sara Piotrowska, Mateusz Król, Katarzyna Rechcińska, Rafał Mirek, Rafał Mazur, Przemysław Morawiak, Przemysław Kula, Wiktor Piecek, Barbara Piętka, Jacek Szczytko SYNTHETIC OPTICAL SPIN-ORBIT INTERACTION IN TUNABLE LIQUID CRYSTAL MICROCAVITIES	O13-3	86
14:30	Andreea Sabadus A DETAILED PROCEDURE FOR PARAMETER EXTRACTION OF THE ONE-DIODE SOLAR CELL MODEL	O13-4	87

14:45 BREAK

15:00 Wolfgang Tress
METALE-HALIDE PEROVSKITE: THE IDEAL PHOTOVOLTAIC MATERIAL?

16:00-17:30 **POSTER SESSION P3**

20 March, FRIDAY

09:00 Mikhail Belkin
ROOM-TEMPERATURE TERAHERTZ QUANTUM CASCADE LASER SOURCES BASED ON INTRA-CAVITY DIFFERENCE FREQUENCY GENERATION

ORAL SESSION O14 (D401)

10:00	Olena Dovban, Galyna Ushakova ASTROCYTE RESPONSE UNDER MODIFIED RESTRAINT WATER IMMERSION STRESS AND ALPHA-KETOGLUTARATE SUPPLEMENTATION	O14-1	88
10:15	Greta Jarockyte, Artiom Skripka, Vitalijus Karabanovas, Riccardo Marin, Vivienne Tam, Marta Cerruti, Fiorenzo Vetrone, Ricardas Rotomskis APPLICATION OF RARE-EARTH DOPED NANOPARTICLES FOR CANCER DIAGNOSTICS AND THERAPY	O14-2	89
10:30	Ewa Borowska, Mateusz Abram, Joanna Kargul NEW APPROACH ON APPLICATION OF AN EXTREMOPHILIC RED ALGA CYANIDIOSCHYZON MEROLAE IN PHYTOREMEDIATION	O14-3	90
10:45	Andrius Sakalauskas, Mantas Ziaunys, Vytautas Smirnovas CONCENTRATION-DEPENDENT POLYMORPHISM OF INSULIN AMYLOID FIBRILS	O14-4	91
11:00	Veronika Vozniuk, Natalia Filimonova, Mykola Makarchuk, Ihor Zyma SEX DIFFERENCES OF BRAIN ACTIVITY IN VISUAL CHOICE REACTION TASK	O14-5	92

ORAL SESSION O15 (A101)

10:00	Miglė Pivoriūnaitė, Darius Stukas, Justas Žilinskas, Giedrė Šilkūnienė, Mantas Šilkūnas, Žilvinas Dambrauskas, Antanas Gulbinas, Algimantas Tamelis HAMLET CYTOTOXICITY IN COLORECTAL CANCER CELL MODELS WITH DIFFERENT MUTATION STATUS IN VITRO	O15-1	93
10:15	Margarita Kazak, Rasa Bernotienė, Tatjana Iežova AVIAN TRYPANOSOMES (TRYPANOSOMA) IN BLOODSUCKING BITING MIDGES (CERATOPOGONIDAE)	O15-2	94
10:30	Viktoriia Vasylchenko, Dunaievska Oksana, Olena Kuchmenko, Lesya Korol, Natalya Stepanova QUALITATIVE STATE OF LIPOPROTEINS UNDER ARTERIAL HYPERTENSION AND CHRONIC KIDNEY DISEASE	O15-3	95
10:45	Kumar Anubhav Tiwari, Martynas Maciulevicius, Renaldas Raisutis, Sonam Chopra, Diana Navickaite, Saulius Satkauskas ESTIMATION OF MICROBUBBLE SURVIVAL TIME FOR SONOPORATION TEMPORAL DOSIMETRY BY SIGNAL PROCESSING	O15-4	96
11:00	Victoriya Zhogla, Viktar Abashkin, Volha Dzmitruk, Jean Pierre Majoral, Dzmitry Shcharbin THE EFFECT OF COMBINED ACTION OF DOXORUBICIN AND COMPLEXES BASED ON PHOSPHORUS DENDRIMERS AND PROAPOPTOTIC SIRNA	O15-5	97

11:15 COFFEE BREAK

ORAL SESSION O16 (A101)

11:45	Jan Černuševič, Nadežda Dreižė, Algirdas Kaupinis, Silvija Urnikytė, Mindaugas Valius. DPP4/CD26 AS A MEDIATOR OF CHEMORESISTANCE AND EPITHELIAL-MESENCHYMAL TRANSITION IN HUMAN COLON CANCER CELLS	O16-1	98
12:00	Austėja Dapkutė, Egle Preikšaitienė FAMILIAL X-LINKED INTELLECTUAL DISABILITY CAUSAL MUTATION IDENTIFICATION USING WHOLE EXOME SEQUENCING	O16-2	99
12:15	Giedrė Skliutė, Raminta Baušytė, Aida Vitkevičienė, Rūta Navakauskienė GENE EXPRESSION STUDIES IN ENDOMETRIAL-DERIVED STROMAL CELLS	O16-3	100

CANCELLED DUE TO COVID-19

12:30	Yelyzaveta Makedon, Viktoriia Stetska, Taisa Dovbynchuk, Nataliia Dziubenko, Yuriy Prylutskyy, Ganna Tolstanova THE EFFECT OF PRISTINE C60 FULLERENE ON COLONIC MOTILITY IN RATS WITH 6-OHDA–INDUCED PARKINSON'S DISEASE	O16-4	101
12:45	Alona Yurchenko, Erika Patskun, Nataliya Hryshchenko CASE REPORT OF UKRAINIAN SMA FAMILY WITH RARE 5Q13 LOCUS REARRANGEMENTS	O16-5	102
13:00	Nataliya Kozak, Lubov Atramentova DYNAMICS OF NATURAL SELECTION IN THE URBANIZED UKRAINIAN POPULATION	O16-6	103
	Daria Shymon, Mariia Inomistova, Oksana Skachkova, Oleksandr Gorbach, Natalia Khranovska ASSOCIATION OF MYCN GENE AMPLIFICATION AND REARRANGEMENTS OF CHROMOSOMAL REGION 1p36 AND 11q WITH EFFICACY OF NEUROBLASTOMA TREATMENT	O16-7	104
13:15-14:45	**POSTER SESSION P4**		
19:00	**CLOSING PARTY and AWARDS CEREMONY**		

CANCELLED DUE TO COVID-19

List of poster presentations

17 March, TUESDAY

16:00-17:30 POSTER SESSION P1

Marius Bytautas, Audrius Sigitas Maruška, Kristina Bimbiraitė-Survilienė ANALYSIS OF THUJA (THUJA SPP.) BIOLOGICAL ACTIVITY	P1-1	105
Inga Gabriunaite, Aušra Valiūnienė ELECTROCHEMICAL CHARACTERISATION OF MIXED SILANE BASED SELF-ASSEMBLED MONOLAYERS FOR PHOSPHOLIPID MEMBRANE BILAYER FORMATION	P1-2	106
Aistė Ilčiukaitė, Marytė Daškevičienė, Egidijus Kamarauskas, Vygintas Jankauskas, Vytautas Getautis NEW FLUORENE DERIVATIVES AS POSITIVE CHARGE CARRIERS FOR EFFICIENT PEROVSKITE SOLAR CELLS	P1-3	107
Ieva Agnė Cechanavičiūtė, Mindaugas Gicevičius, Arūnas Ramanavičius FORMATION AND CHARACTERIZATION OF ELECTROCHROMIC METAL PLATED TEXTILE/POLYANILINE COMPOSITE	P1-4	108
Nerijus Karlonas LIQUID CHROMATOGRAPHY – TANDEM MASS SPECTROMETRY FOR THE DETERMINATION OF NEW SYNTHETIC OPIOIDS	P1-5	109
Aleksandra Buchcic, Anna Zawisza, Stanisław Leśniak, Justyna Adamczyk, Adam Marek Pieczonka, Michał Rachwalski HIGHLY ENANTIOSELECTIVE MANNICH REACTION CATALYZED BY CHIRAL PHOSPHINOYL-AZIRIDINES	P1-6	110
Aistė Kunciūtė, Remigijus Ivanauskas, Algimantas Ivanauskas INFLUENCE OF SILVER CONCENTRATION ON THE OPTICAL PROPERTIES OF TIN SELENIDE LAYERS	P1-7	111
Greta Inkrataite, Ramunas Skaudzius LUMINESCENCE PROPERTIES OF CERIUM, BORON AND/OR MAGNESIUM DOPED YTTRIUM AND LUTETIUM GARNETS COATINGS ON QUARTZ SUBSTRATE	P1-8	112
Greta Inkrataite, Ramunas Skaudzius MODIFIED STRUCTURE LUTETIUM OXYORTHOSILICATE: SYNTHESIS AND INVESTIGATION OF LUMINESCENCE PROPERTIES	P1-9	113
Rūta Aukštakojytė, Justina Gaidukevič, Jurgis Barkauskas SYNTHESIS AND STRUCTURAL CHARACTERIZATION OF THERMAL REDUCED GRAPHENE OXIDE PRODUCTS	P1-10	114
Ella Duvanova, Oleksandr Polishchuk, Serhii Radio, Georgiy Rozantsev FORMATION OF POLYOXOTUNGSTATE ANIONS IN THE SYSTEM CD2+ – WO42– (Z = 1.00) – H+/ OH-– H2O	P1-11	115
Justyna Anna Adamczyk, Adam Marek Pieczonka, Michał Rachwalski A NOVEL NONSYMMETRICAL AZINES WITH AGGREGATION INDUCED EMISSION ENHANCEMENT	P1-12	116
Karolina Koselak, Stanisław Porwański, Anna Zawisza SUGAR DERIVATIVES WITH UREA FRAGMENT	P1-13	117
Martyna Malinowska, Anna Zawisza, Stanisław Leśniak STEREOCONTROLLED SYNTHESIS OF BETTI BASES	P1-14	118
Martyna Malinowska, Aleksandra Tracz, Anna Zawisza, Stanisław Leśniak AZIRIDINES AS KEY COMPOUNDS FOR THE SYNTHESIS OF C-GLYCOSIDES	P1-15	119
Andrius Pakalniškis, Ramūnas Skaudžius, Živilė Stankevičiūtė SYNTHESIS AND INVESTIGATION OF GDPO4 BASED DIFFERENT CORE–SHELL STRUCTURES	P1-16	120
Gintarė Rimkutė, Justina Gaidukevič, Vidutė Gurevičienė, Ieva Šakinytė, Julija Razumienė INVESTIGATION AND USE OF THERMALLY REDUCED GRAPHENE OXIDE FRACTIONS IN THE DEVELOPMENT OF THIRD GENERATION BIOSENSORS	P1-17	121
Agne Kizalaite, Lauryna Sinusaite, Diana Griesiute, Anton Popov, Andris Antuzevics, Kestutis Mazeika, Dalis Baltrunas, Jen-Chang Yang, Aivaras Kareiva, Aleksej Zarkov FE AND ZN CO-SUBSTITUTED BETA-TRICALCIUM PHOSPHATE: SYNTHESIS, STRUCTURAL, MAGNETIC, MECHANICAL AND BIOLOGICAL PROPERTIES	P1-18	122
Jakub Wręczycki, Dariusz M. Bieliński, Grzegorz Mlostoń THE FLUORIDE ANION CATALYZED SULFUR TRANSFER REACTIONS OF ELEMENTAL SULFUR (S8) WITH THIOKETONES	P1-19	123
Žyginta Einorytė, Kęstutis Aidas MODELLING 17O NMR SPECTRA OF TAUTOMERIC FORMS OF CITRININ	P1-20	124
Irina Fiodorova, Rokas Skaisgiris, Tomas Serevičius, Saulius Juršėnas, Sigitas Tumkevičius SYNTHESIS AND TADF PROPERTIES OF 2-SUBSTITUTED 4,6-BIS(3,6-DIT-BUTYL-9-CARBAZOLYL)-5-METHYLPYRIMIDINES	P1-21	125
Barbara Chatinovska, Skirmantė Tutlienė, Milda Petrulevičienė, Jurgis Pilipavičius, Jurga Juodkazytė, Linas Vilčiauskas SPECIFIC PATHWAYS FOR SYNTHESIS OF CARBONACEOUS – NATI2(PO4)3 COMPOSITES AND APPLICATION AS NEGATIVE ELECTRODE MATERIALS IN AQUEOUS NA-ION BATTERIES	P1-22	126

Aivaras Labžentis, Dr. Linas Vilčiauskas, Laurynas Staišiūnas ELECTROCHEMICAL IMPEDANCE SPECTROSCOPY STUDY OF AQUEOUS NA-ION BATTERY DEGRADATION	P1-23	127
Gediminas Jakubauskas, Neringa Petrašauskienė INVESTIGATION OF COPPER SELENIDE THIN FILMS DEPOSITED USING THE SILAR METHOD AT DIFFERENT TEMPERATURES	P1-24	128
Grzegorz Mlostoń, Małgorzata Celeda, Katarzyna Urbaniak MECHANOCHEMICAL APPROACH TO THE SYNTHESIS OF 2-UNSUBSTITUTED IMIDAZOLE N-OXIDES, CONVENIENT PRECURSORS OF NEW ALKOXYIMIDAZOL-2-YLIDENES (NHCS)	P1-25	129
Miglė Liudžiūtė, Klaudija Vaičiukynaitė, Skirma Žalenkienė, Rūta Stokienė UV-VIS IVVESTIGATION OF MIXED CADMIUM SULFIDE– CADMIUM TELLURIDE LAYERS ON POLYAMIDE 6 FORMED USING DIFFERENT WAYS OF PREPARING POLYAMIDE	P1-26	130
Mantas Marcinskas, Tadas Malinauskas SYNTHESIS AND INVESTIGATION OF ORGANOMETALLIC PRECURSORS USED FOR COPPER THIOCYANATE LAYER FORMATION	P1-27	131
Karina Babiča, Zenta Balcerbule, Vitālijs Lazarenko, Māris Bērtiņš OCCURRENCE AND VARIATION OF SOME METALLIC ELEMENTS IN LINGONBERRY (VACCINIUM VITIS-IDAEA L.) AND SOIL	P1-28	132
Viktorija Krjukoviča, Zenta Balcerbule, Vitālijs Lazarenko, Māris Bērtiņš VARIATIONS OF SULPHUR AND METALLIC ELEMENTS IN LICHENS (XANTHORIA PARIETINA) IN THE DIFFERENT PARTS OF RIGA	P1-29	133
Edita Daublytė, Agnė Zdaniauskienė, Tatjana Charkova SYNTHESIS OF SILVER CORE-SILICA SHELL NANOPARTICLES UNDER MICROWAVE IRRADIATION	P1-30	134
Povilas Luizys, Maryte Daskeviciene, Vygintas Jankauskas, Egidijus Kamarauskas SYNTHESIS AND CHARACTERISTICS OF NEW ORGANIC SEMICONDUCTORS WITH N-CARBAZOLYL-BASED CHROMOPHORES	P1-31	135
Delianas Palinauskas, Gintautas Bagdžiūnas SELF-ASSEMBLED MONOLAYERS BASED ON FLAVIN COFACTOR FOR SENSING OF GLUCOSE	P1-32	136
Kamilė Tulaitė, Justina Jovaišaitė, Jelena Tamulienė, Jonas Šarlauskas, Narimantas Čėnas and Saulius Juršėnas. PHOTOPHYSICAL STUDY OF ANTICANCER DRUG TIRAPAZAMINE BASED COMPOUNDS	P1-33	137
Laurynas Butkus, Rūta Barisevičiūtė, Žilvinas Ežerinskis, Justina Šapolaitė, Evaldas Maceika, Algirdas Pabedinskas, Andrius Garbaras, Jonas Mažeika, Vytautas Rakauskas, Rūta Druteikienė, Vidmantas Remeikis TRACING STABLE CARBON ISOTOPE VARIATIONS IN LAKE DRUKSIAI	P1-34	138
Asta Bronusiene, Ingrida Ancutiene XRD AND EDX STUDIES OF TIN (II) SULFIDE FILMS FORMED AT DIFFERENT PH CONDITIONS	P1-35	139
Sarune Daskeviciute, Vytautas Getautis SYNTHESIS OF NEW DYES FOR THE DETECTION OF MERCAPTO AMINO ACIDS	P1-36	140
Adam Marek Pieczonka, Justyna Adamczyk, Lena Marciniak NEW FLUORESCENT EMITTERS EXHIBITING AGGREGATION INDUCED EMISSION FOR OLEDS	P1-37	141
Audrius Sadaunykas, Audrius Zolumskis, Evaldas Naujalis ANALYTE FOCUSING AND ENRICHMENT ON GAS CHROMATOGRAPHY COLUMN.	P1-38	142
Ruta Juodvalkyte, Simas Sakirzanovas SYNTHESIS OF SODIUM YTTRIUM FLUORIDE VIA HYDROTHERMAL METHOD AND ITS MORPHOLOGY ANALYSIS	P1-39	143
Giedrė Gaidamavičienė, Artūras Žalga SYNTHESIS AND CHARACTERIZATION OF GADOLINIUM DOPED CERIA OXIDE CERAMIC	P1-40	144
Modestas Vainoris, Natalia Tsyntsaru, Henrikas Cesiulis ELECTROCHEMICALLY DEPOSTED IRON ONTO COPPER FOAM CATALYST FOR HETEROGENOUS FENTON REACTION	P1-41	145
Benas Balandis, Guostė Ivanauskaitė, Joana Smirnovienė, Daumantas Matulis, Asta Zubrienė, Vytautas Mickevičius SYNTHESIS AND EVALUATION OF PYRROLIDINONE-BEARING BENZENESULFONAMIDES AS HUMAN CARBONIC ANHYDRASE INHIBITORS	P1-42	146
Lena Marciniak, Adam Marek Pieczonka, Michał Rachwalski SYNTHESIS OF HYDRAZIDE HYDRAZONES WITH LUMINESCENT PROPERTIES	P1-43	147
Vincenta Mikulėnaitė, Ieva Karpavičienė ELECTROPHILE-INITIATED CYCLIZATION REACTIONS OF 2-(3-SUBSTITUTED 2-PROPINILTHIO)-1H-IMIDAZOLES	P1-44	148
Aliaksei Bakavets, Yauhen Aniskevich, Genady Ragoisha, Henrikas Cesiulis, Natalia Tsyntsaru, Eugene Streltsov ELECTROCHEMICAL FABRICATION OF (BI2)M(BI2TE3)N THIN FILMS WITH CONTROLLABLE BISMUTH CONTENT	P1-45	149
Lauryna Monika Svirskaite, Ernestas Kasparavicius, Tadas Malinauskas SYNTHESIS AND INVESTIGATION OF ELECTRON TRANSPORTING ORGANIC SEMICONDUCTORS CONTAINING ANCHORING FRAGMENTS	P1-46	150
Indrė Misiūnaitė, Justas Pošiūnas, Rita Bukšnaitienė, Ieva Karpavičienė INVESTIGATION OF ELECTROPHYLIC CYCLIZATION REACTIONS OF BENZIMIDAZOL-2-YL ALKYNES	P1-47	151
Viktorija Padolskytė, Vadimas Dudoitis, Vidmantas Ulevičius CHARACTERIZATION OF AEROSOL PARTICLES IN FOREST ENVIRONMENT USING AN AEROSOL CHEMICAL SPECIATION MONITOR	P1-48	152
Aivaras Vaškevičius, Denis Baronas, Asta Zubrienė, Daumantas Matulis, Virginija Dudutienė THE SYNTHESIS OF FLUORINATED BENZENESULFONAMIDES BEARING SPECIFIC FUNCTIONAL GROUP AS INHIBITORS OF HUMAN CARBONIC ANHYDRASES	P1-49	153
Naveen Masimukku, Dalius Gudeika, Dmytro Volyniuk, Juozas Vidas Grazulevicius DESIGN, PREPARATION AND STUDIES OF NAPHTHALIMIDE MATERIALS	P1-50	154
Dovilė Ragauskaitė, Rasa Šlinkšienė DETERMINATION OF THE CHEMICAL COMPOSITION OF USED COFFEE GROUNDS	P1-51	155
Raimonda Boguzaite, Vilma Ratautaite, Arunas Ramanavicius EVALUATION OF ELECTROCHROMIC PROPERTIES OF POLYPYRROLE FILMS MODIFIED BY PHENOTHIAZINE DERIVATIVES	P1-52	156
Agnė Minderytė, Julija Pauraitė, Steigvilė Byčenkienė SOURCE APPORTIONMENT AND OPTICAL PROPERTIES OF CARBONACEOUS AEROSOL PARTICLES	P1-53	157
Evgeniia Bakhalova, Yulia Bespalko, Elena Shved THE REGIOSELECTIVITY OF ASYMMETRIC OXIRANE RING-OPENING BY BENZOATE ANION	P1-54	158
Vitālijs Lazarenko, Vita Rudoviča, Arturs Vīksna, Māris Bērtiņš, Zaiga Anna Zvaigzne, Modris Okmanis USE OF WOOD ASH IN THE FOREST AND ITS EFFECT ON THE CHEMICAL ELEMENT FLOW IN BLUEBERRIES (VACCINIUM MYRTILLUS L.)	P1-55	159

CANCELLED DUE TO COVID-19

Daria Łuczak, Adam Marek Pieczonka LEMON JUICE AS PYRAZOLE REACTION MEDIUM	P1-56	160
Julija Pauraitė, Steigvilė Byčenkienė, Kristina Plauškaitė, Vidmantas Ulevicius SINGLE SCATTERING ALBEDO DEPENDENCE ON AEROSOL SIZE AND CHEMICAL COMPOSITION	P1-57	161
Kestutis Dabrovolskas, Dalius Gudeika SYNTHESIS AND INVESTIGATION OF ORGANIC SEMICONDUCTORS FOR TADF OLEDS	P1-58	162
Gintarė Plečkaitytė, Jurgis Pilipavičius, Milda Petrulevičienė, Jurga Juodkazytė, Linas Vilčiauskas HYDRO(SOLVO)THERMAL SYNTHESIS OF NATI2(PO4)3 AS ANODE MATERIAL FOR NA-ION BATTERIES	P1-59	163
Eivydas Andriukonis, Marius Butkevicius HYDROGEL BASED MICRO AG/AGCL REFERENCE ELECTRODES. QUICK PROTOTYPING OF REFERENCE ELECTRODES	P1-60	164
Arminas Jurys, Tomas Javorskis, Ieva Karpavičienė, Gustautas Snarskis, Rita Bukšnaitienė, Edvinas Orentas HIGHLY DIASTEREOSELECTIVE SYNTHESIS OF POLYCYCLIC ALCOHOLS VIA ANIONIC CASCADE CYCLIZATION	P1-61	165
Gabija Kavaliauskaitė, Povilas Virbickas, Giedrė Medvikytė, Aušra Valiūnienė OPTICAL AND ELECTROCHEMICAL DETECTION OF UREA BY USING PRUSSIAN BLUE MODIFIED ELECTRODES	P1-62	166
Margarita Poderyte, Inga Gabriunaite, Ausra Valiuniene SCANNING ELECTROCHEMICAL MICROSCOPY APPLICATION FOR HYBRID PHOSPHOLIPID BILAYER INVESTIGATION AND MODIFICATION	P1-63	167
Milita Vagner, Karolis Motiejuitis, Valentina Plaušinaitienė. THE INFLUENCE OF GROWTH RATE AND SUBSTRATES' THERMAL EXPANSION COEFFICIENT ON PROPERTIES OF NANOCRYSTALLINE LA SR MN CO O FILMS	P1-64	168
Mantas Jakučionis, Darius Abramavičius MODELING BETA-CAROTENE INTERNAL CONVERSION IN THERMAL ENVIRONMENT USING DIRAC-FRENKEL VARIATIONAL METHOD	P1-65	169
Dominika Lubikowska, Stanisław Leśniak, Adam Marek Pieczonka AZIRIDINE/PALLADIUM COMPLEXES IN THE SYNTHESIS OF LUMINOPHORES	P1-66	170
Paulina Kaziukonytė, Inga Valionytė, Algirdas Brukštus INVESTIGATION OF 2-((SUBSTITUTED IMINO)METHYL)PHENOLS 1,3-CYCLOADDITION REACTIONS	P1-67	171
Kristaps Saršūns, Agris Bērziņš PREDICTION OF SOLID SOLUTION FORMATION AMONG CHEMICALLY SIMILAR MOLECULES USING CALCULATION OF LATTICE AND INTERMOLECULAR INTERACTION ENERGY	P1-68	172
Pavel Malakhovsky, Dmitry Murauski, Egor Minakov, Mikhail Artemyev KINETICS OF ELECTROSTATIC SELF-ASSEMBLY OF SILVER NANOPLATES ON THIN POLYELECTROLYTE FILMS	P1-69	173
Davit Tediashvili, Linas Vilčiauskas INHIBITION OF ALUMINUM CURRENT COLLECTOR CORROSION IN AQUEOUS NA-ION BATTERY	P1-70	174
Dovydas Vdovinskis, Aldona Balčiūnaitė, Loreta Tamašauskaitė-Tamašiūnaitė, Eugenijus Norkus HYDROGEN PRODUCTION FROM WATER SPLITTING USING PEROVSKITE NANOPARTICLES	P1-71	175
Algirdas Pabedinskas, Dominykas Ziemys, Evaldas Maceika, Zilvinas Ezerinskis, Justina Sapolaite, Laurynas Butkus, Laurynas Bucinskas, Vidmantas Remeikis LONG-TERM 14C ACTIVITY MEASUREMENTS IN TREE RINGS NEAR IGNALINA NUCLEAR POWER PLANT: HOW IT HELPS TO INCREASE SAFETY OF OUR ENVIRONMENT	P1-72	176
Eivilė Budrytė, Aldona Balčiūnaitė, Jūratė Vaičiūnienė, Gediminas Niaura, Sandra Stanionytė, Loreta Tamašauskaitė-Tamašiūnaitė, Eugenijus Norkus SYNTHESIS, CHARACTERISATION AND INVESTIGATION OF NITROGEN-DOPED CARBON SUPPORTED MN-CO NANOPARTICLES	P1-73	177
Aida Drevilkauskaite, Artiom Magomedov, Ernestas Kasparavicius, Tadas Malinauskas, Vytautas Getautis SYNTHESIS AND INVESTIGATION OF THE CARBAZOLE BASED PHOSPHONIC ACIDS WITH DIFFERENT ALIPHATIC LINKERS	P1-74	178
Tomas Murauskas, Mantvydas Levulis, Virgaudas Kubilius, Valentina Plaušinaitienė INVESTIGATION OF THIN PEROVSKITE LA:BASNO3 FILMS' PROPERTIES USING DIFFERENT SUBSTRATES	P1-75	179
Yauheni Malich, Anastasiya Kanunnikava, Ilya Novikov MODIFICATION OF THE METHOD FOR PREPARING OLIGOMERS FROM HIGH MOLECULAR CHITOSAN	P1-76	180
Edvinas Petraitis, Paulius Janaščius, Arūnas Maršalka, Saulius Bagdonas THE RESEARCH OF PHOTOOXIDATIVE REACTIONS OF TETRAPYRROLE COMPOUNDS USING ELECTRON PARAMAGNETIC RESONANCE SPECTROSCOPY	P1-77	181
Ramunas Levinas, Natalia Tsyntsaru, Henrikas Cesiulis APPLICATION OF INTENSITY MODULATED PHOTOCURRENT SPECTROSCOPY FOR PHOTOACTIVE MATERIAL CHARACTERIZATION	P1-78	182
Laura Baliulytė, Jelena Tamulienė IN SILICO STUDY OF L-GLUTAMIC ACID AND L-GLUTAMINE FRAGMENTATION BY LOW ENERGY ELECTRONS	P1-79	183
Tadas Žutautas, Audrius Bučinskas THE SEARCH FOR NEW ORGANIC SEMI-CONDUCTORS WITH EFFICIENT HOLE TRANSFERING PROPERTIES	P1-80	184
Lukas Šerpytis, Simas Šakirzanovas SYNTHESIS AND OPTICAL PROPERTIES OF ER3+, YB3+ AND ND3+ DOPED Y2BAZNO5	P1-81	185
Joanna Stocka, Rasa Platakytė, Justinas Čeponkus, Valdas Šablinskas, Gamil A. Guirgis, Paweł Rodziewicz COMPUTATIONAL AND EXPERIMENTAL VIBRATIONAL STUDY OF 1-CHLOROMETHYL-1-FLUOROSILACYCLOHEXANE CONFORMATIONS AND ITS REARRANGEMENTS	P1-82	186
Patrycja Szamweber, Adam Marek Pieczonka SYNTHESIS OF NONSYMMETRICAL 1,3,4-OXADIAZOLES NEW SMALL-MOLECULE METRIALS FOR OLED DIODES	P1-83	187
Kseniia Yutilova, Elena Shved, Yuliia Bespalko THEORETICAL AND EXPERIMENTAL STUDY OF THE BEHAVIOR OF E+–NU– SALTS IN THE NUCLEOPHILIC RING OPENING REACTION OF 2-(CHLOROMETHYL)OXIRANE	P1-84	188
Yaraslau Dzichenka, Eugene Hudny CYTOCHROME P450 7B1 F470I MUTATION AFFECTS ON LIGAND BINDING PROPERTIES	P1-85	189
Lina Jatautė, Valentina Krylova, Nijolė Dukštienė, Martynas Lelis COMPOSITION OF AG-IN-SE LAYERS DEPOSITED ON PES/PVC SURFACE	P1-86	190
Dmytro Smychko, Olena Shvets, Olga Bui, Volodymyr Vakula SYNTHESIS OF NEW 1- (4-OXOTHIAZOLIN-2-IL) PYRAZOLINES BASED ON CHALCONS	P1-87	191

CANCELLED DUE TO COVID-19

Karolis Treinys, Vilma Ratautaitė, Simonas Ramanavičius, Andrius Maneikis, Urtė Samukaitė-Bubnienė, Povilas Genys, Arūnas Ramanavičius SYNTHESIS AND ANALYSIS OF TUNGSTEN OXIDE THIN FILMS FORMED BY MAGNETRON SPUTTERING.	P1-88	192
Sergey Barsuk, Leonid Burmistrov, Veronique Puill, Patrick Robbe, Oleg Bezshyyko, Larisa Golinka-Bezshyyko, Vladyslav Orlov, Vsevolod Yeroshenko DETECTOR FOR LUMINOSITY MEASUREMENT AT HIGH ENERGY PHYSICS EXPERIMENTS	P1-89	193
Victoria Bundyukova, Dzmitry Yakimchuk, Vladislav Prigodich GOLD PATTERNS ON N-SILICON SURFACE FOR SENSORIC APPLICATION	P1-90	194
Alexandr Vasilevsky, Anna Kozhevnikova, Viktoryia Zhautok, Alex Malevich, George Pitsevich, Valdas Sablinskas MODELING OF LOW-TEMPERATURE TORSIONAL SPECTRA OF THE DOOOH AND DOOOD MOLECULES	P1-91	195
Artem Shlyk, Sergei Yanushkevich, Darya Kisuryna, Alex Malevich, George Pitsevich, Vitas Balevicius NUMERICAL SIMULATION OF QUANTUM EFFECTS DUE TO INTERNAL ROTATION IN A HYDROGEN PEROXIDE MOLECULE	P1-92	196
Alexandr Vasilevich, Andrei Ostyakov, Aryna Khrapunova, Alex Malevich, George Pitsevich, Valdas Sablinskas GROUP-THEORETICAL ANALYSIS OF THE TORSIONAL VIBRATIONS IN NON-RIGID MOLECULES HXYXH TYPE	P1-93	197
Darya Meniailava, Ulada Vysotskaya, Aliaksandr Ruskikh, Anna Matsukovich, Maksim Shundalau STRUCTURAL AND SPECTRAL PROPERTIES OF THE (Z)-3-(ADAMANTAN-1-YL)-1-(3-CHLOROPHENYL)-S-BENZYLISOTHIOUREA	P1-94	198
Karolina Maleckaitė, Jelena Dodonova, Sigitas Tumkevičius, Aurimas Vyšniauskas PHOTOPHYSICAL PROPERTIES OF THIOPHENE-SUBSTITUTED BODIPY MOLECULAR ROTORS	P1-95	199
Edvinas Zacharovas, Martynas Velička, Gediminas Platkevičius, Arūnas Želvys, Valdas Šablinskas STUDY OF URINARY BLADDER CANCER BY MEANS OF SURFACE ENHANCED RAMAN SCATTERING SPECTROSCOPY	P1-96	200
Gerda Mickūnaitė, Rimantė Bandzevičiūtė, Justinas Čeponkus, Eglė Lastauskienė, Renata Gudiukaitė, Valdas Šablinskas IDENTIFICATION OF THE PATHOGENIC FUNGI AND BACTERIA. THEIR LIFE-CYCLE STUDY USING INFRARED SPECTROSCOPY	P1-97	201
Rimantė Bandzevičiūtė, Justinas Čeponkus, Valdas Šablinskas, Christian Teske, Gerald Steiner IDENTIFICATION OF PANCREATIC CANCER BY FIBER BASED ATR IR SPECTROSCOPY	P1-98	202
Sonata Gailiūnaitė, Saulutė Budrienė UNSATURATED POLYESTERS FOR BIO-TISSUE: EFFECT OF PDMS AND MULTIFUNCTIONAL HYDROXY COMPOUNDS ON STRUCTURE AND PROPERTIES	P1-99	203
Rugilė Lukaševičiūtė, Renata Karpič SPECTROSCOPIC PROPERTIES AND ACTIVITY OF GLUCOSE OXIDASE	P1-100	204
Domantas Česnys, Rasa Platakytė, Justinas Čeponkus, Claudine Crepin STUDY OF ACETYLSALICYLIC ACID MOLECULES BY THE MEANS OF MATRIX ISOLATION	P1-101	205
Romanenko Vitaliy, Lujanienė Galina, Šemčuk Sergej, Jonas Mažeika, Olga Jevanova, Ezhova Elena, Garnaga-Budrė Galina, Povinec Pavel APPLICATION OF AM AND PU ISOTOPES TO TRACE SEDIMENT REDISTRIBUTION IN THE BALTIC SEA	P1-102	206
Vaida Grasyte, Ernesta Buzavaite-Verteliene, Zigmas Balevicius DISPERSION RELATION ANALYSIS OF BLOCH SURFACE WAVES AND SURFACE PLASMON POLARITONS USING TOTAL INTERNAL REFLECTION ELLIPSOMETRY	P1-103	207
P1-104 Sridhar Hariharaputran, Arul Murugan Natarajan, Zilvinas Rinkevicius COMPUTATIONAL MULTISCALE MODELING AND ANALYSIS OF LIPID MEMBRANES: A CASE STUDY ON GRAM-NEGATIVE BACTERIA	P1-104	208
Izolda Marcinoniene ANALYSIS OF VERY LARGE HAIL AND TORNADOS IN LITHUANIA IN THE PERIOD 1962-2019	P1-105	209
Malek Mahmoudi, Dalius Gudeika, Dmytro Volniuk, Jouzas V.Grazulevicius EFFICIENT NON-DOPED OLEDS BASED ON MULTI-CARBAZOLE DERIVATIVES SUBSTITUTED BY DIFFERENT ACCEPTORS	P1-106	210
Alena Vabishchevich, Aliaksandra Kazak, Olga Emeliyanova, Goran Sretenovich SPECTRAL ANALYSIS OF AIR PLASMA JETS AT ATMOSPHERIC PRESSURE	P1-107	211
Krzysztof Gadomski, Tomasz K. Pietrzak SYNTHESIS AND CHARACTERISATION OF GLASSY AND NANOCRYSTALLINE ANALOGUES OF LiFePO4 OLIVINES	P1-108	212
Dzmitry Kacharhin EVALUATION OF THE DOSE ACCUMULATION COEFFICIENT BY IN SILICO MODELLING OF THE X-RAY DIAGNOSTICS	P1-109	213

18 March, WEDNESDAY

16:00-17:30 POSTER SESSION P2

Eimantas Kriščiūnas, Rima Stonkutė PHOTOMETRIC PROPERTIES OF STAR CLUSTERS IN THE ANDROMEDA GALAXY	P2-1	214
Sebastian Szybka, Adam Cieślik STANDING WAVES IN GENERAL RELATIVITY	P2-2	215
Maksim Kravchenko, Tamara Korbut, Eduard Rudak, Andrey Petrovski, Maria Bobkova ON A GENERALIZED BIRTH AND DEATH MODEL APPLIED TO A POINT NUCLEAR REACTOR THEORY	P2-3	216
M. Sizova, E. Postnikova, N. Chupina, S. Vereshchagin HYADES STAR CLUSTER AND THE NEW COMETS	P2-4	217
Kristians Draguns, Karlis Grundsteins, Inga Brice, Janis Alnis, Aigars Atvars COMPUTER MODELLING OF WGM MICRORESONATORS WITH A ZINC OXIDE NANOLAYER USING COMSOL MULTIPHYSICS SOFTWARE	P2-5	218
Raminta Bartuliene, Ruta Narvilaite, Gustavas Davidavicius, Ausra Saudargiene, Sarunas Asmantas, Saulius Satkauskas A CASE STUDY OF A SYNESTHETIC APPLYING NEURAL NETWORK	P2-6	219
Yauheniya Lisitsa, Victor Skakun CLASSIFICATION OF SUPERPIXELS FOR TUMOR SEGMENTATION ON IMMUNOHISTOCHEMISTRY IMAGES	P2-7	220
Austėja Mikalčiūtė, Linas Vilčiauskas THE HYDROGEN BOND NETWORK TOPOLOGY OF PHOSPHORIC ACID AND WATER SYSTEMS	P2-8	221

CANCELLED DUE TO COVID-19

Saulius Lozovskis, Saulius Šliaupa, Jurga Lazauskienė, Rasa Šliaupienė NEW STUDIES ON PETROPHYSICAL PROPERTIES OF SHALES FOR POTENTIAL GAS EXPLORATION	P2-9	222
Tautvydas Brazaitis, Sigita Kasetaite, Jolita Ostrauskaite ACRYLATED GLYCEROL-BASED PHOTOCROSS-LINKED POLYMERS	P2-10	223
Vidmantas Klimaitis, Migle Lebedevaite, Jolita Ostrauskaite SYNTHESIS AND INVESTIGATION OF POLYMERS COMPOSED OF BIOBASED METHACRYLATES	P2-11	224
Lauryna Sinušaitė, Diana Griesiūtė, Andris Antuzevičs, Artūras Katelnikovas, Aleksej Žarkov HIGH-TEMPERATURE SYNTHESIS, STRUCTURAL AND LUMINESCENT PROPERTIES OF MN-DOPED α-TRICALCIUM PHOSPHATE	P2-12	225
Asta Kabelkaite-Lukosevice, Ilona Kapociute, Ingrida Venyte, Laura Gegeckiene, Georgij Petriaszwili RESEARCH ON ADHESION OF PASTEURIZED ADHESIVE LABELS	P2-13	226
Paulius Andriūnas, Arvaidas Galdikas MODELING OF THE INFLUENCE OF CH4 FRACTION GAS ON OXYGEN ION DIFFUSION IN ELECTROLYTE IN SINGLE-CHAMBER SOLID OXIDE FUEL CELLS	P2-14	227
Tomas Vaitkūnas, Audrius Jutas LATTICE DISTORTION MODEL ANALYSIS SIMULATING POISSON'S RATIO ON CRYSTALLINE MATERIALS OF BCC-LATTICES	P2-15	228
Gusautas Snarskis, Linas Vilčiauskas ANALYSIS OF THE NA-MN-TI-PO4 PHASE DIAGRAM USING FIRST-PRINCIPLES CALCULATIONS	P2-16	229
Martynas Bertašius, Rokas Kondrotas THEORETICAL PREDICTION OF SB2SE3 GROWTH MORPHOLOGY AND ORIENTATION ON MUSCOVITE MICA SUBSTRATES	P2-17	230
Ada Steponavičiūtė, Genrik Mordas, Karolis Stravinskas, Aušra Selskienė MICROSTRUCTURAL ANALYSIS OF ADDITIVELY MANUFACTURED STAINLESS STEEL PARTS	P2-18	231
Sohrab Nasiri, Simas Macionis, Dalius Gudeika , Dmytro Volyniuk , Juozas V. Grazulevicius SYNTHESIS AND INVESTIGATION OF XANTHENONE BASED OLED EMITTERS EXHIBITING BOTH AIEE AND TADF	P2-19	232
Khaja Naib Rasool Shaik, Gopi Kompelli, Hari Prasanna Manimaran, Dr. Elena Jasiūnienė SCANNING BEHAVIOR IN ULTRASONIC NDE OF T-SHAPED CFRP COMPONENT	P2-20	233
Sandra Navickytė, Skirmantas Norkus, Brigita Abakevičienė SURFACE MODIFICATION OF 3D PRINTED TRABECULAR TITANIUM ALLOY STRUCTURE	P2-21	234
Greta Motiekaitytė, Auksė Navaruckienė, Jolita Ostrauskaitė PHOTORHEOMETRICAL STUDY OF ACRYLATED VANILLIN-BASED RESINS	P2-22	235
Karolis Stravinskas, Sergejus Borodinas, Ada Steponavičiūtė, Genrik Mordas NEW TYPE OF METAL PARTICLE DOSING, TRANSPORTATION AND POSITIONING SYSTEM	P2-23	236
Rytis Šalaševičius, Sergejus Balčiūnas, Jūras Banys, Satoshi Wada NANOCOMPOSITE BROADBAND DIELECTRIC SPECTROSCOPY	P2-24	237
Viktor Kovalevskyi, Darius Viržonis, Vytautas Bučinskas, Rimgaudas Urbonas, Sigitas Petkevičius, Inga Morkvėnaitė –Vilkončienė, Andrius Dzedzickis RESEARCH OF THE HORIZONTAL PENDULUM BASE HARVESTER FOR LOW ENERGY DENSITY SYSTEMS	P2-25	238
Viktor Kovalevskyi, Darius Viržonis, Vytautas Bučinskas, Rimgaudas Urbonas, Sigitas Petkevičius, Inga Morkvėnaitė –Vilkončienė, Andrius Dzedzickis INVESTIGATION OF CHAOTIC LOW FREQUENCY VIBRATIONS TRANSFORMATION EFFICIENCY OF HORIZONTAL PENDULUM BASE HARVESTER	P2-26	239
Paulius Dolmantas, Andrius Vasiliauskas, Šarūnas Meškinis GRAPHENE FORMATION THROUGH CARBON SEGREGATION ON AMORPHOUS CARBON AND TRANSITION METAL COMPOSITES	P2-27	240
Augusto Hernandez, Nadzeya Khinevich, Nikita Grevtsov, Alex Burko, Hanna Banadrenka, Tomas Tamulevičius, Sigitas Tamulevičius POROUS PERIODICAL SILICON STRUCTURE AS SUBSTRATE FOR SERS APPLICATION	P2-28	241
Alexander K. Fedotov, Uladzislaw E. Gumiennik, Dmitry V. Yurasov, Alexey V. Novikov, Pavel Yu. Apel CHANGES OF ELECTRIC AND MAGNETOTRANSPORT PROPERTIES OF DELTA-LAYERS DUE TO SWIFT HEAVY IONS IRRADIATION	P2-29	242
Naglis Kyžas, Alexandr Belosludtsev, Algirdas Selskis REACTIVE MAGNETRON SPUTTERING OF ALUMINIUM OXYNITRIDE FILMS FOR OPTICAL COATINGS APPLICATIONS	P2-30	243
Ugne Naruseviciute, Laura Peciulyte INFLUENCE OF CATALYST ON SYNTHESIS AND PROPERTIES OF STARCH ACETATE	P2-31	244
Serhii Mazura, Volodymyr Bessarabov, Liubov Vakhitova POLYMER SYSTEM FOR DECONTAMINATION OF PHOSPHORORGANIC TOXIC SUBSTANCES	P2-32	245
Manvydas Dapkevičius, Edvinas Radiunas, Steponas Raišys, Augustina Jozeliūnaitė, Tomas Javorskis, Ugnė Šinkevičiūtė, Edvinas Orentas, Saulius Juršėnas, Karolis Kazlauskas SUPRESSED CONCENTRATION QUENCHING BY 3,5-DI-TERT-BUTYL-PHENYL SUBSTITUTION IN RUBRENE FOR SOLID-STATE PHOTON UPCONVERSION	P2-33	246
Lukas Naimovičius, Edvinas Radiunas, Karolis Kazlauskas, Steponas Raišys, Augustina Jozeliūnaitė, Tomas Jarovskis, Ugnė Šinkevičiūtė, Edvinas Orentas TERT-BUTYL-PHENYL RUBRENE EMITTER FOR TRIPLET-TRIPLET ANNIHILATION MEDIATED NIR-TO-VISIBLE PHOTON UPCONVERSION	P2-34	247
Uliana Tsiko, Galyna Sych, Yan Danyliv, Iryna Hladka, Juozas Vidas Grazulevicius TRIPHENYLAMINE- AND CARBAZOLE-BASED COMPOUNDS EXHIBITING DELAYED FLUORESCENCE	P2-35	248
Olga Bulderberga, Edvins Druska, Andrey Aniskevich UV STABILITY OF THERMOCHROMIC MICROCAPSULES FOR SMART POLYMER COMPOSITE STRUCTURES	P2-36	249
Dominik Suwala, Grzegorz Wryk, Aleksandra Szymanska, Krzysztof Domanski, Alicja Kalucka, Ola Bednarczyk, Dana Binczuk, Wojciech Mech, Adam Wincukiewicz, Maciej Krajewski, Joanna Sitnicka, Krzysztof P. Korona, Maria Kaminska PRODUCTION OF VARIOUS SIZE ORGANIC PHOTOVOLTAIC CELLS WITH P3HT:PC61BM AS AN ACTIVE LAYER	P2-37	250
Laurynas Endriukaitis, Andrius Devižis EFFECT OF ANNEALING ON EXCITED STATES RELAXATION IN FPMAI/MAPBI3 PEROVSKITE NANOPARTICLES	P2-38	251
Ranush Durgaryan, Yan Danyliv, Dmitriy Volyniuk, Juozas Vidas Gražulevičius SIMPLY DESIGNED HOLE TRANSPORTING MATERIALS FOR EFFICIENT PEROVSKITE SOLAR CELLS	P2-39	252

CANCELLED DUE TO COVID-19

Andrius Aukštuolis, Nerijus Nekrašas, Kristijonas Genevičius, Jūratė Jonikaitė-Švėgždienė, Giedrius Juška HOLES' MOBILITY PROPERTIES OF PCPDTBT THIN FILM HYBRID TRANSISTORS	P2-40	253
Gytis Vėjelis, Vilius Dovydaitis. SUBSTRATE BIAS VOLTAGE EFFECT ON AMORPHOUS CARBON FILM GROWTH RATE AND OPTICAL PROPERTIES	P2-41	254
Vytautas Vosylius, Karolis Ratautas, Inga Andriulionytė, Aldona Jagminienė, Ina Stankevičienė, Eugenijus Norkus, Gediminas Račiukaitis GALVO-SCANNER LASER PULSE DELIVERY TECHNIQUES FOR ELECROLESS COPPER DEPOSITION ON PC-ABS.	P2-42	255
Dmitrij Smirnov, Andrius Bartašiūnas, Rimantas Miškinis, Emilis Urba, Victor Plessky NETWORK OF SURFACE ACOUSTIC WAVE SENSORS WITH WIDE-BAND HYPERBOLICALLY FREQUENCY-MODULATED TECHNOLOGY	P2-43	256
Kristina Radinović, Jadranka Milikić, Aldona Balčiūnaitė, Zita Sukackienė, Loreta Tamašauskaitė-Tamašiūnaitė, Biljana Šljukić	P2-44	257
Laura Tauraitė, Erminas Kozlovskis, Antanas Urbas, Sergejus Orlovas, Ilja Ignatjev RAMAN SPECTROSCOPY ANALYSIS OF FS LASER INDUCED STRUCTURAL DAMAGE ON SODA-LIME GLASS	P2-45	258
Lukas Ramalis, Lina Grinevičiūtė, Rytis Buzelis and Tomas Tolenis ANISOTROPIC THIN FILMS BASED POLARIZING COATINGS FOR HIGH POWER LASERS	P2-46	259
Anton Sikorski, Evgeny Bondarenko, Natallia Mahon, Olga V. Korolik, Tomas Ingr, Denis Esipenko INFLUENCE OF ELECTROLYTE COMPOSITION ON PHYSICAL PROPERTIES OF COPPER (I) OXIDE THIN FILMS	P2-47	260
Diana Pavlovaitė, Sergejus Balčiūnas, Šarūnas Svirskas, Mirosław Mączka, Jūras Banys DIELECTRIC ANISOTROPY OF METHYLAMMONIUM LEAD IODIDE	P2-48	261
Tomas Grigaitis, Andrius Aukštuolis INFLUENCE OF DEPOSITION PARAMETERS ON PROPERTIES OF POLY CRYSTALLINE DIAMOND FILMS	P2-49	262
Paulius Dapkus, Liudas Mažeika A STUDY OF SUPERVISED COMBINED NEURAL-NETWORK-BASED ULTRASONIC METHOD FOR RECONSTRUCTION OF SPATIAL DISTRIBUTION OF MATERIAL PROPERTIES	P2-50	263
Agnieszka Anna Wiciak, Veit Hoffmann, Sven Einfeld ANALYSIS OF LASERS DIODES BASED ON INGAN / GAN	P2-51	264
Maliha Parvin, Milda Petrulevičienė, Irena Savickaja, Benjaminas Šebeka, Arnas Naujokaitis, Vidas Pakštas, Jurga Juodkazytė TUNING OF PHOTOELECTROCHEMICAL ACTIVITY OF NANOSTRUCTURED WO3 FILMS THROUGH MODIFICATION OF SOL-GEL SYNTHESIS PROCEDURE	P2-52	265
Gleb Gribovskii STRESS-STRAIN STATE AND DAMAGED VOLUME IN CONTACT AREA OF CAR TIRE–ASPHALT CONCRETE SYSTEM UNDER VARIOUS LOADS	P2-53	266
Nadzeya Brezhneva, Sviatlana A. Ulasevich, Nikolai V. Dezhkunov, Ekaterina V. Skorb PHYSICO-CHEMICAL ASPECTS OF ULTRASONIC METAL NANOSTRUCTURING	P2-54	267
Aliaksei Pashkevich, Alexander K. Fedotov, Krystsina Kirylchyk, Viktoryia Halauchuk PHASE COMPOSITION AND PROPERTIES OF ZNO-METAL OXIDES CERAMICS	P2-55	268
Augustas Morkvėnas, Živilė Jurgelėnė, Sergej Šemčiuk, Mindaugas Kazlauskas, Vitalijus Karabanovas BIODISTRIBUTION OF GRAPHENE OXIDE IN CHORION OF SALMO TRUTTA EMBRYOS	P2-56	269
Kanak Kalita, Ranjan Kumar Ghadai AN EXPERIEMENTAL STUDY OF ALUMINIUM (AL) INCORPORATED DIAMOND LIKE CARBON (DLC) THIN FILMS	P2-57	270
Edith Flora Joel, Galina Lujanienė, Ieva Uogintė, Sandra Stanionytė, Martynas Skapas, Loreta Leviskaitė GRAPHENE OXIDE CHITOSAN COPPER PLATINUM NANO COMPOSITE THIN FILM METHOD FOR ANTI-BACTERIAL APPLICATION	P2-58	271
Paulius Gaigalas, Arūnas Jagminas, Arnas Naujokaitis, Simonas Ramanavičius, Marija Kurtinaitienė, Rolandas Trusovas SUBSTRATE IMPACT ON THE STRUCTURE AND ELECTROCATALYST PROPERTIES OF MOLYBDENUM DISULFIDE FOR HER FROM WATER	P2-59	272
Virginija Kleivaitė, Rimvydas Milašius MATHEMATICAL ANALYSIS OF POROSITY IN NANOFIBERS	P2-60	273
Hanna Maltanava, Semyon Mazheika, Evgeni Ovodok, Sergei Voitekhovich, Tatyana Gaevskaya, Sergey Poznyak ELECTROCATALYTIC ACTIVITY OF TITANIA NANOTUBULAR LAYERS DECORATED BY GOLD NANOPARTICLES IN OXYGEN ELECTROREDUCTION	P2-61	274
Aliaksandra Radchanka, Varvara Hrybouskaya WATER-SOLUBLE SEMICONDUCTOR CORE-SHELL NANOCRYSTALS WITH CONTROLLED SURFACE CHARGE	P2-62	275
Gerda Klimaitė, Domantas Peckus, Mantas Mikalkevičius, Asta Tamulevičienė, Tomas Tamulevičius, Sigitas Tamulevičius. ULTRAFAST PLASMON RELAXATION DYNAMICS OF LASER AFFECTED SILVER NANOPARTICLES	P2-63	276
Greta Urbonaitė, Tibor Szabo, Radmila Panajotović, Jasna Vujin, Tijana Tomašević-Ilić, Ieva Bagdanavičiūtė, Richard Cseko, Klara Hernadi, Gyorgy Varof and Laszlo Nagy PHOTOELECTRIC ACTIVITY OF GRAPHENE/BACTERIAL REACTION CENTER NANOCOMPOSITE	P2-64	277
Raman Novikau, Galina Lujanienė, Kęstutis Mažeika, Sergej Šemčuk DEVELOPMENT OF CLAY-BASED NANOCOMPOSITE MATERIALS	P2-65	278
Julianija Nikitina, Tomas Tolenis, Lina Grinevičiūtė DEPOSITION OF MULTILAYER OPTICAL COATINGS ON CORRUGATED SURFACES	P2-66	279
Simona Vyčaitė, Asta Tamulevičienė STUDY OF THE TEMPERATURE INFLUENCE ON THE GEOMETRY OF THE SILVER NANOPARTICLES DURING POLYOL SYNTHESIS	P2-67	280
Mantas Mikalkevičius, Mindaugas Juodėnas, Tomas Tamulevičius, Saulius Burinskas, Asta Tamulevičienė CONTROL OF THE STAINLESS STEEL WETTABILITY VIA FEMTOSECOND LASER-INDUCED PERIODIC STRUCTURES AND DEPOSITION OF AMORPHOUS DIAMOND LIKE CARBON THIN FILMS	P2-68	281
Šarūnas Jankauskas, Rimantas Gudaitis, Andrius Vasiliauskas, Šarūnas Meškinis EFFECTS OF THERMAL ANNEALING ON GRAPHENE STRUCTURE DIRECTLY SYNTHESISED ON SI(100) SUBSTRATE	P2-69	282
Alena Mikitchuk, Konstantin Kozadaev, Elizaveta Girshova, Liubou Hauryk, Uladzislau Dolnikau, Anton Talkachov OUTPUT CHARACTERISTICS OF THE EXPERIMENTAL PHOTOACOUSTIC TRANSDUCER WITH SILVER NANOPARTICLES AT OPTICAL FIBER EDGE	P2-70	283

POSTPONED DUE TO COVID-19

Liubou Hauryk, Anton Talkachov, Alena Mikitchuk, Uladzislau Dolnikau, Elizaveta Girshova MODELING THE OPTICAL PROPERTIES OF AG AND AU NANOPARTICLES ON THE BUTT OF AN OPTICAL FIBER FOR A COMPACT ULTRASONIC EMITTER	P2-71	284
Magdalena Bartolewska, Maciej Mazur PREPARATION OF NANOSIZED SULFUR PARTICLES	P2-72	285
Eimantas Bucmys, Anton Popov, Auguste Adamonyte, Ieva Plikusiene PROTEIN IMMOBILIZATION ON SURFACE OF ZNO NANOSTRUCTURES FOR OPTICAL BIOSENSOR DESIGN	P2-73	286
Aleksandra Shulga, Leonid Butusov, Galina Chudinova, Tatiana Sheshko, Vladimir Kopylov CERIUM DOPED ZINC OXIDE NANOSTRUCTURES OBTAINED BY MICROWAVE ASSISTED METHOD WITH THE USE OF AMINO-GROUP CONTAINING PRECURSORS	P2-74	287
Ema Baliūnaitė, Ernesta Lubinaitė, Almira Ramanavičienė SYNTHESIS OF GOLD COATED MAGNETIC NANOPARTICLES AND MODIFICATION WITH ANTIBODIES AT OPTIMAL CONDITIONS	P2-75	288
Gabija Grudzinskaite, Vaidas Klimkevicius, Simas Sakirzanovas SURFACE MODIFICATION AND STABILIZATION OF UPCONVERTING NAGDF4:YB3+/ER3+ NANOPARTICLES IN AQUEOUS MEDIA USING ANIONIC BRUSH-TYPE PLYELECTROLYTES	P2-76	289
Andrey Iodchik, Aliaksandra Radchanka, Tatsiana Terpinskaya, Tatjana Balashevich, Tatsiana Yanchanka, Palukoshka Alena, Svetlana Sizova, Vladimir Oleinikov, Alexei Feofanov, Mikhail Artemyev CADMIUM CHALCOGENIDE NANOPLATELETS FOR CELL LABELING AND VISUALIZATION WITH TWO-PHOTON EXCITATION	P2-77	290
Justinas Januškevičius, Živilė Stankevičiūtė, Aldona Beganskienė, Aivaras Kareiva SYNTHESIS AND INVESTIGATION OF YTTRIUM IRON GARNET, YTTRIUM AND TERBIUM IRON PEROVSKITE NANOTUBES	P2-78	291
Aliaksandra Radchanka, Alexander W. Achtstein, Mikhail V. Artemyev TUNABILITY OF OPTICAL PROPERTIES OF WATER-SOLUBLE SEMICONDUCTOR NANOCRYSTALS VIA ZETA-POTENTIAL	P2-79	292
Vytautas Žalandauskas, Mažena Mackoit-Sinkevičienė, Audrius Alkauskas DISCLOCATION-INDUCED STRAIN EFFECTS ON OPTICAL PROPERTIES OF CARBON DIMER DEFECTS IN HEXAGONAL BORON NITRIDE	P2-80	293
Laima Busaite, Reinis Lazda, Florian Gahbauer, Andris Berzins, Ruvin Ferber, Marcis Auzinsh NUCLEAR SPIN POLARIZATION OF NV CENTERS IN DIAMOND	P2-81	294
Nastassia Savina, Irina Shapochkina SYMMETRY BASED MODELING THE FUNCTIONING OF POLAR BROWNIAN ROTOR	P2-82	295
Lizaveta Hvazdouskaya, Sergei Lazarouk THE FORMATION OF FILMS OF ANODIC TITANIUM OXIDE AND THEIR USE IN MAXILLOFACIAL SURGERY	P2-83	296
Dzmitry Hvazdouski, Maryia Baranava ELECTRONIC AND MAGNETIC PROPERTIES OF THE GRAPHENE-FERROMAGNET INTERFACES: AB INITIO SIMULATION	P2-84	297
Aliaksandr V. Zaparozhtsau, Aliaksandr S. Fedotov BEHAVIOR OF NANOCOMPOSITES PERCOLATION THRESHOLD IN THE INSULATION SHELLS MODEL.	P2-85	298
Ranjan Kumar Ghadai, Soham Das, Ashis Sharma INVESTIGATION OF BIOMEDICAL AND TRIBOLOGICAL PROPERTIES OF SILICON (SI) DOPED DLC COATING	P2-86	299
Uladzimir Lazicki, Zlata Lepenkova, Darya Kisuryna, Alex Malevich, George Pitsevich, Vitas Balevicius TORSIONAL SPECTRUM OF THE METHYL HYDROPEROXIDE MOLECULE CALCULATED AT MP2/CC-PVQZ	P2-87	300
Siarhei Sadau, Igor Kheidorov A COMPREHENSIVE BIOINFORMATION SYSTEM OF HUMAN EMOTION RECOGNITION	P2-88	301
Saulius Pakalka, Aušra Kynienė, Sigitas Kučas, Šarūnas Masys, Valdas Jonauskas ELECTRON IMPACT IONIZATION OF W5+	P2-89	302
Aliaksandr Dubrouski, Hanna Kiyavitskaya SIMULATION OF AN ACCELERATOR DRIVEN SYSTEM WITH DIFFERENT SPALLATION TARGETS	P2-90	303
Eduard Gohman, Viktor Zhaba CLARIFICATION OF ENERGY VALUE FOR THE ACTIVATION LEVEL IN THE REACTION 103RH(γ,γ')103MRH	P2-91	304
Povilas Račkauskas, Viktor Novičenko, Han Pu, Gediminas Juzeliūnas NON-ABELIAN GEOMETRIC POTENTIALS AND SPIN-ORBIT COUPLING FOR PERIODICALLY DRIVEN SYSTEMS	P2-92	305
Giedrius Žlabys, Mantas Račiūnas, Egidijus Anisimovas LEARNING QUANTUM STRUCTURES IN COMPACT LOCALIZED EIGENSTATES	P2-93	306
Vytautas Bubilaitis, Darius Abramavičius MODELING OF PUMP-PROBE SPECTRA AT HIGH EXCITATION INTENSITY IN MOLECULAR AGGREGATES	P2-94	307
Jurgita Koncevičiūtė, Valdas Jonauskas ELECTRON-IMPACT DOUBLE IONIZATION OF B+	P2-95	308
Ignas Kazakevičius, Vygintas Gontis APPROXIMATION OF BURST DURATION'S PDFS OF BIRTH-DEATH PROCESSES	P2-96	309
Rokas Garbačauskas Thomas Gajdosik RENORMALIZATION FLOW OF THE GRIMUS-NEUFELD MODEL AT ONE LOOP LEVEL	P2-97	310
Simonas Draukšas, Thomas Gajdosik ON-SHELL CALCULATION OF FIELD STRENGTH AND CHARGE COUNTERTERMS IN ARBITRARY COVARIANT GAUGE IN SCALAR QED	P2-98	311
Sebastian Wilman, Magdalena Elantkowska, Jaroslaw Ruczkowski SEMIEMPIRICAL INVESTIGATIONS OF THE IONIC BISMUTH (BI II) ENERGY STRUCTURE FOR ELECTRIC QUADRUPLE MOMENT CALCULATION	P2-99	312
Viktoriia Len, Andrii Semenov BOSON SAMPLING WITH CONTINUOUS-WAVE DETECTION	P2-100	313
Mariia Byelova, Andrii Semenov NON-UNIVERSAL OPTICAL QUANTUM COMPUTING WITH ARRAY DETECTORS	P2-101	314
Apoorva Devaraj, Mastan Raja Papanaboina, Dr. Elena Jasiūnienė ACCURACY ASSEMENT OF REVERSE ENGINEERING PROCESS OF PLEXIGLASS STEP CYLINDER SAMPLE	P2-102	315
Mastan Raja Papanaboina, Apoorva Devraj, Dr. Elena Jasiūnienė, Dr. Egidijus Zukauskas DAMAGE CHARACTERIZATION ON ALUMINUM PLATE USING FINITE ELEMENT METHOD	P2-103	316

CANCELLED DUE TO COVID-19

Aleksandra Cuper, Przemysław P. Michalski, Jerzy E. Garbarczyk STUDY OF STRUCTURAL PROPERTIES OF LITHIUM-IRON SILICATE (LI2FESIO4) OBTAINED BY SOL-GEL METHOD	P2-104	317
Klaudia Pachulska, Przemysław P. Michalski, Jerzy E. Garbarczyk STUDY OF THERMAL PROPERTIES OF LITHIUM-IRON SILICATE (LI2FESIO4) GELS	P2-105	318
Maksymilian Odziemczyk, Przemysław P. Michalski, Jerzy E. Garbarczyk SYNTHESIS OF LITHIUM-IRON SILICATE LI2FESIO4 USING SOL-GEL METHOD	P2-106	319
Karol Olszewski, Aleksander Tecza, Paulina Kruk-Fura, Jan Jamroz STRUCTURAL PROPERTIES OF GLASS-CERAMIC COMPOSITE MATERIALS IN Bi2O3-Pr2O3 SYSTEM	P2-107	320
Michał Ołowski SYNTHESIS AND STUDIES ON THERMOLUMINESCENCE OF LITHIUM FLUORIDE DOPED WITH SELECTED ELEMENTS	P2-108	321
Jakub Mrówczyński, Przemysław Piotr Michalski SYNTHESIS OF VANADIUM-DOPED LITHIUM-MANGANESE BORATE BY SOL-GEL METHOD	P2-109	322
Aleksander Tecza, Karol Olszewski, Paulina Kruk-Fura, Jan Jamroz INVESTIGATION OF STRUCTURAL PROPERTIES OF GLASS-CERAMIC COMOPOSITE MATERIALS Bi2O3-Yb2O3 SYSTEM	P2-110	323
Paulina Kruk-Fura, Tomasz K. Pietrzak, Jerzy E. Garbarczyk STRUCTURAL AND ELECTRICAL PROPERTIES OF NANOCOMPOSITES IN BI2O3-AL2O3-SIO2 SYSTEM OBTAINED WITH FAST COOLING TECHNIQUE	P2-111	324
Przemysław P. Michalski, Agata Jarocka, Jakub S. Otrębski, Olivier Lafon, Julien Trebosc, Tomasz K. Pietrzak, Jan L. Nowiński COMPREHENSIVE STUDY OF GLASSES AND COMPOSITES IN LITHIUM-BORATE SYSTEM	P2-112	325
Maciej Nowagiel, Tomasz K. Pietrzak TOWARDS EFFICIENT SODIUM BATTERIES: NANOCRYSTALLIZATION OF GLASSY ALLUAUDITE Na2Fe2V(PO4)3	P2-113	326
Agata Jarocka, Przemysław P. Michalski, Jacek Ryl, Tomasz K. Pietrzak, Marek Wasiucionek XPS STUDIES OF VANADIUM-DOPED LITHIUM-MANGANESE-BORATE GLASSES AND NANOCOMPOSITES	P2-114	327
Mateusz Samsel, Tomasz Pietrzak HOLDER FOR IMPEDANCE SPECTROSCOPY MEASUREMENTS OF MIXED CONDUCTORS IN INERT ATMOSPHERE	P2-115	328

19 March, THURSDAY

16:00-17:30 POSTER SESSION P3

Romuald Petkevič, Ada Steponavičiūtė, Sergejus Borodinas, Genrik Mordas DEVELOPMENT OF THE LASERMETALDEPOSITIONTECHNOLOGY	P3-1	329
Nadiia Roik, Lyudmila Belyakova, Marina Dzyazko EFFECT OF ADDITIVES ON STRUCTURAL CHARACTERISTICS OF MCM-41-TYPE NANOPARTICLES	P3-2	330
Sergey Anoshkin, Arnas Naujokaitis, Anatoly Pushkarev, Sergey Makarov ELECTROLUMINESCENT PROPERTIES OF PEROVSKITE NANOPARTICLES EMBEDDED IN A POLYMER ELECTROLYTE THIN LAYER	P3-3	331
Volodymyr Sendiuk, Tomas Serevicius, Rokas Skaisgiris, Ausra Tomkeviciene, Juozas Vidas Grazulevicius, Karolis Kazlauskas, Saulius Jursenas SWITCHING BETWEEN TADF AND RTP IN THE METHYL SUBSTITUTED PHENOTHIAZINE COMPOUNDS	P3-4	332
Karolis Leitonas, Rasa Keruckiene, Dmytro Volyniuk, Juozas Vidas Grazulevicius INVESTIGATION OF ROOM-TEMPERATURE PHOSPHORESCENCE SENSITIVITY TO OXYGEN USING BENZOTRIFLUORIDE AND PHENOTHIAZINE DERIVATIVES	P3-5	333
Egle Ezerskyte, Arturas Katelnikovas CONVENTIONAL AND UPCONVERSION LUMINESCENCE OF POLYMORPHOUS BIPO4:YB3+,TB3+,EU3+ PHOSPHORS	P3-6	334
Vincentas Mindaugas Mačiulis, Ieva Plikusiene, Almira Ramanaviciene, Anton Popov, Octavio Graniel, Mikchael Bechelany, Arunas Ramanavicius INVESTIGATION OF PLANAR AND NANOSTRUCTURED ZNO AND AL2O3 APPLICATION IN BIOSENSORS DESIGN	P3-7	335
Deimante Rosliuk, Dovile Liudvinaviciute, Anne Loron, Ramune Rutkaite, Véronique Coma FORMATION OF CHITOSAN AND GREEN COFFEE BEAN OR ARTICHOKE EXTRACT COMPLEXES AND THEIR ANTIFUNGAL ACTIVITY	P3-8	336
Paulina Andriunaite, Vesta Navikaite-Snipaitiene, Deimante Rosliuk ADSORPTION OF IBUPROFEN FROM AQUEOUS MEDIUM ON CHEMICALLY MODIFIED STARCH	P3-9	337
Diana Masiulionyte, Deimante Rosliuk, Ramune Rutkaite, Véronique Coma IMMOBILIZATION OF CAFFEIC ACID ON CROSS-LINKED CATIONIC STARCHES WITH DIFFERENT DEGREE OF SUBSTITUTION	P3-10	338
Marius Navickas, Laisvydas Giriūnas, Vidmantas Kalendra, Timur Biktagirov, Uwe Gerstmann, Wolf Gero Schmidt, Mirosław Mączka, Andreas Pöppl, Jūras Banys, Mantas Šimėnas EPR SPECTROSCOPY OF MANGANESE DOPED [NH4][ZN(HCOO)3] FORMATE FRAMEWORK	P3-11	339
Karolina Aleknaite, Deimante Rosliuk, Ugne Naruseviciute STARCH ACETATE SORBENT FOR REMOVAL OF METILPARABEN FROM WATER	P3-12	340
Julija Grigorjevaite, Arturas Katelnikovas SYNTHESIS AND APPLICATION OF UPCONVERSION MATERIALS IN ANTICOUNTERFEITING	P3-13	341
Greta Cizauskaite, Karolina Almonaityte, Joana Bendoraitiene THE DETERMINATION OF VARIOUS BOTANICAL ORIGIN STARCH CROSSLINKING WITH EPICHLOROHYDRIN AND CROSLINKING DEGREE METHODOLOGY	P3-14	342
Vesta Navikaite-Snipaitiene, Ramune Rutkaite, Deimante Rosliuk, Karolina Almonaityte, Vaida Vaskeliene, Renaldas Raisutis, MODIFIED STARCH SORBENTS FOR THE REMOVAL OF DICLOFENAC AND IBUPROFEN FROM WATER	P3-15	343
Laisvydas Giriūnas, Marko Bertmer, Mirosław Mączka, Jūras Banys, Mantas Šimėnas NMR SPECTROSCOPY OF STRUCTURAL PHASE TRANSITION IN CH3NH2NH2PBCL3 HYBRID PEROVSKITE	P3-16	344
Evgeni Ovodok, Hanna Maltanava, Sergey Poznyak, Vladimir Kurilo, Gediminas Monastyreckis, Daiva Zeleniakiene, Maria Omastava, Matej Micusik EPOXY COMPOSITES LOADED WITH CARBON NANOTUBES AND GRAPHENE	P3-17	345
Tomas Kudrevičius, Artyom Plyushch, Šarūnas Svirskas, Algirdas Selskis, Marija Dunce, Eriks Birks, Jūras Banys TAPE CASTING AND DIELECTRIC CHARACTERISTICS OF NBYT THICK FILMS	P3-18	346
Edgaras Narbutaitis, Matas Gužauskas, Dmytro Volyniuk, Juozas Vidas Gražulevičius SYNTHESIS AND PHOTOPHYSICAL PROPERTIES OF PHENOTHIAZINE-5,5-DIOXIDE BASED TADF DERIVATIVES	P3-19	347

CANCELLED DUE TO COVID-19

Arnoldas Solovjovas, Šarūnas Svirskas, Džiugas Jablonskas, Shinya Tsukada, Seiji Kojima, Jūras Banys DIELECTRIC PROPERTIES OF THE RELAXOR FERROELECTRIC (1-X)PB(ZN1/3NB2/3)O3- XPBTIO3	P3-20	348
Matas Guzauskas, Edgaras Narbutaitis, Dmytro Volyniuk, Juozas Vidas Grazulevicius INVESTIGATION OF PHOTO INDUCED CONFORMATIONAL CHANGES IN ORGANIC FLUORESCENCE EMITTERS	P3-21	349
Eglė Tankelevičiūtė, Paulius Baronas, Gediminas Kreiza, Povilas Adomėnas, Karolis Kazlauskas, Chihaya Adachi, and Saulius Juršėnas THE ROLE OF EXCITONIC COUPLING IN BIFLUORENE CRYSTALS FOR LASER APPLICATIONS	P3-22	350
Gytis Baranovas, Jurgis Pilipavicius, Linas Vilciauskas ANALYSIS OF MANGANESE CONTENT INFLUENCE IN NASICON-STRUCTURED NA2XZR2-XMNX(PO4)3 PREPARED VIA SOL-GEL METHOD AND ITS USE AS A CATHODE IN AQUEOUS NA-BASED BATTERIES	P3-23	351
Dovydas Banevičius, Gediminas Kreiza, Justina Jovaišaitė, Tomas Javorskis, Vytenis Vaitkevičius, Edvinas Orentas, Saulius Antanas Juršėnas, Karolis Kazlauskas DEEP BLUE TO BLUE TADF-OLEDS WITH LOW EFFICIENCY ROLL-OFF BASED ON NEW NAPHTHYRIDINE EMITTERS	P3-24	352
Simas Mačionis, Dalius Gudeika, Dmytro Volyniuk, Juozas Vidas Gražulevičius, Jiun Haw Lee, Tien-Lung Chiu SYNTHESIS AND INVESTIGATION OF BENZIMIDAZOLE/TERT-BUTYLCARBAZOLE HYBRID BIPOLAR MATERIALS FOR HIGHLY EFFICIENT OLEDS	P3-25	353
Simona Vekteryte, Rasa Keruckiene, Eimantas Vijaikis, Matas Guzauskas, Juozas Vidas Grazulevicius SYNTHESIS AND PROPERTIES OF QUINAZOLINE-BASED ELECTROACTIVE COMPOUNDS	P3-26	354
Rugile Zilenaite, Egle Ezerskyte, David Van der Heggen, Philippe F. Smet, Arturas Katelnikovas, Simas Sakirzanovas SYNTHESIS OF SRAL2O4:EU2+,SM3+ PHOSPHORS AND THEIR SPECTROSCOPIC CHARACTERIZATION	P3-27	355
Ronit Sebastine Bernard, Galyna Sych, Sohrab Nasiri, Oleksandr Bezvikonnyi, Dmytro Volyniuk, Azhar Ariffin, Juozas V. Grazulevicius. EFFECT OF FLUORINE ON ELECTROACTIVE MATERIALS WITH AGGREGATION INDUCED ENHANCED EMISSION PROPERTIES	P3-28	356
Rokas Skaisgiris, Tomas Serevičius, Jelena Dodonova, Laimis Jagintavičius, Jonas Bucevičius, Karolis Kazlauskas, Saulius Juršėnas, Sigitas Tumkevičius TADF EMISSION WAVELENGTH INSTABILITY DUE TO CONFORMATIONAL DISORDER	P3-29	357
Edvinas Staišiūnas, Jurgis Pilipavičius, Linas Vilčiauskas NASICON-STRUCTURED NA2XTI2-XMNX(PO4)3 AS AN ELECTRODE IN SYMMETRICAL SODIUM AQUEOUS BATTERY SYNTHESIZED VIA SOL-GEL METHOD	P3-30	358
Nizy Sara Samuel, Dalius Gudeika DESIGN, SYNTHESIS AND INVESTIGATION OF COUMARINE-BASED DERIVATIVES	P3-31	359
Wojciech Sas, Marcin Perzanowski, Magdalena Fitta MAGNETIC PROPERTIES OF PRUSSIAN BLUE ANALOGUE FE3[CR(CN)6]2·NH2O NANORODS OBTAINED BY ELECTRODEPOSITION METHOD	P3-32	360
Eimantas Tarailis, Audrius Valavičius, Mantas Drazdys, Darija Astrauskytė, Ramutis Drazdys ULTRATHIN METAL FILMS OPTICAL PROPERTIES DEPENDENCIES ON DEPOSITION PARAMETERS	P3-33	361
Danas Buožius, Julius Jokubaitis, Maksym Ivanov VORTEX TERAHERTZ WAVE GENERATION IN AIR BY FEMTOSECOND OPTICAL VORTEX PULSES	P3-34	362
Gabija Petrauskaitė, Lina Grinevičiūtė, Lukas Ramalis and Tomas Tolenis INVESTIGATION OF SCULPTURED THIN FILM GROWTH BY OPTICAL MONITORING	P3-35	363
Justas Deveikis, Ausrine Jurkeviciute, Tomas Tamulevicius, Sigitas Tamulevicius. THE DETERMINATION OF DISPERSION AND MODELLING OF ABSORPTION DIAMOND-LIKE CARBON:SILVER NANOCOMPOSITE THIN FILMS	P3-36	364
Jonas Banys, Giedrius Sinkevičius, Julius Vengelis, Rimantas Grigonis INVESTIGATION OF THERMAL EFFECTS IN POCKELS CELL WITH BBO CRYSTAL IN A HIGH AVERAGE POWER LASER SYSTEM	P3-37	365
Gabrielė Stanionytė, Miglė Kuliešaitė, Vygandas Jarutis, Julius Vengelis INVESTIGATION OF SUPERCONTINUUM GENERATION IN POLIARIZATION-MAINTAINING PHOTONIC CRISTAL FIBER	P3-38	366
Tomas Klinavičius, Tomas Tamulevičius SPECTRAL CHARACTERISTICS OF TRUE-COLOR DOT-MATRIX HOLOGRAMS	P3-39	367
Gustas Liaugminas, Julijanas Želudevičius, Kęstutis Regelskis PARAMETRIC GENERATION AT 648 NM IN A LMA PHOTONIC CRYSTAL FIBER.	P3-40	368
Agnė Šuminienė, Rosvaldas Šuminas, Vytautas Jukna, Gintaras Tamošauskas, Mikas Vengris, Audrius Dubietis DEEP UV SUPERCONTINUUM GENERATION IN LISAF CRYSTAL USING FEMTOSECOND LASER PULSES	P3-41	369
Tomas Jurkšas, Mindaugas Juodėnas, Tomas Tamulevičius, Artūras Vailionis, Sigitas Tamulevičius FORMATION OF 3D MICROSTRUCTURES IN POLYDIMETHYLSILOXANE VIA FEMTOSECOND LASER IRRADIATION	P3-42	370
Evaldas Svirplys, Simonas Indrišiūnas INVESTIGATION OF LASER SCRIBING CAUSED DAMAGE TO THE METAL COATING OF THE TRANSPARENT MATERIAL	P3-43	371
Lase Milgrave, Pauls Kristaps Reinis, Janis Alnis, Aigars Atvars WHISPERING GALLERY MODE MICRORESONATOR AS A HUMIDITY SENSOR: SENSING MECHANISMS AND APPLICATIONS	P3-44	372
Vaida Marčiulionytė, Danil Bulatov, Robertas Grigutis, Nail Garejev, Gintaras Tamošauskas, Audrius Dubietis SUPERCONTINUUM GENERATION IN SAPPHIRE AND YAG: A COMPARATIVE STUDY	P3-45	373
Laimis Zubauskas, Edgaras Markauskas WATER-ASSISTED GLASS ABLATION WITH PICOSECOND LASER	P3-46	374
Ivona Juchnevičiūtė, Lina Grinevičiūtė, Tomas Tolenis MATHEMATICAL MODELING OF COATING BASED ACHROMATIC WAVEPLATE	P3-47	375
Raimundas Burokas, Pierre-Marc Dansette, Tadas Bartulevičius, Andrejus Michailovas GROUP DELAY DISPERSION IMPACT ON SECOND HARMONIC GENARATION WITH ULTRASHORT LASER PULSES	P3-48	376
Danielius Samsonas, Lukas Kontenis, Mikas Vengris LABEL-FREE IMAGING OF BIOLOGICAL TISSUE USING WIDEFIELD SECOND-HARMONIC GENERATION MICROSCOPY	P3-49	377
Kamilė Kasačiūnaitė, Antanas Urbas, Sergej Orlov, Ina Stankevičienė, Aldona Jagminienė. COHERENT RESEARCH OF METAL DEPOSITION ON D263 GLASS USING LASER PULSES AND CHEMICAL ETCHING	P3-50	378
Dominyka Stonytė, Domas Paipulas MICRO-MECHANICAL VOLTAGE ACTUATED CANTILEVER BEAM FEM ANALYSIS AND MANUFACTURE IN A FUSED QUARTZ GLASS	P3-51	379

CANCELLED DUE TO COVID-19

Roberts Berķis, Aigars Atvars, Inga Brice, Kārlis Grundšteins, Jānis Alnis PMMA WGM MICROSPHERE RESONATOR QUALITY FACTOR MEASUREMENTS USING VIDEO RECOGNITION, TEMPERATURE CHANGES AND FIXED WAVELENGHT LASER	P3-52	380
Ramūnas Logminas, Arūnas Varanavičius SUPERCONTINUUM GENERATION IN A MULTI-PLATE SYSTEM	P3-53	381
Nikolai Mitetelo, Mikhail Popov, Evgeniy Mamonov, Rajadurai Chandrasekar, Tatiana Murzina CHIRALITY DRIVEN EFFECTS IN MULTIPHOTON EXCITED ORGANIC WHISPERING GALLERY MODE MICRORESONATORS	P3-54	382
Ignas Stasevicius, Giedrius Martynaitis, Mikas Vengris CASCADED NONLINEARITY INFLUENCE TO HIGH POWER FEMTOSECOND OPTICAL PARAMETRIC OSCILLATOR	P3-55	383
Artūrs Mozers, Mārcis Auzinsh, Laima Bušaite, Dace Osīte THE INFLUENCE OF COHERENT EFFECTS ON ANGULAR MOMENTUM DISTRIBUTION DEPENDENCE ON MAGNETIC FIELD IN 85RB: MAGNETOOPTICAL SIGNALS WITHOUT THE DOPPLER EFFECT	P3-56	384
Mikhail Popov, Nikolai Mitetelo, Evgeniy Mamonov, Tatiana Murzina INTENSITY DEPENDENT PROCESSES IN NONLINEAR-OPTICAL RESPONSE OF ORGANIC WGM CAVITY MICROSTRUCTURES	P3-57	385
Domantas Barisevičius, Pranciškus Vitta INVESTIGATION AND DEVELOPMENT OF THE SMART ILLUMINATION SYSTEM FOR ENHANCED COLOR DISCRIMINATION	P3-58	386
Simonas Driukas, Rokas Gegevičius, Rokas Jasiūnas, Vidmantas Gulbinas LIGHT-INDUCED CURING OF MAPBI3 PEROVSKITE AND ITS EFFECTS ON OPTICAL PROPERTIES	P3-60	387
Kornelijus Raugas, Pranciškus Vitta DEVELOPMENT OF A PROTOTYPE ILLUMINATION SYSTEM FOR PHOTODYNAMICAL TREATMENT OF BIOLOGICAL SAMPLES	P3-61	388
Pauls Kristaps Reinis, Lase Milgrave, Aigars Atvars, Janis Alnis WHISPERING GALLERY MODE HUMIDITY SENSOR: PHYSICAL PROPERTIES	P3-62	389
Vytautas Lukas Paukštė, Linas Minkevičius SIMULATION OF SILICON-BASED BESSEL ZONE PLATES FOCUSING PERFORMANCE AT SUB-TERAHERTZ RANGE	P3-63	390
Gaudenis Jansonas, Rimantas Budriūnas NUMERICAL SIMULATION TECHNIQUES FOR THE PROCESSING OF NONLINEAR REFRACTIVE INDEX MEASUREMENTS	P3-64	391
Simonas Stasiūnas, Greta Inkrataitė, Akvilė Zabiliūtė-Karaliūnė, Ramūnas Skaudžius, Pranciškus Vitta INVESTIGATION OF PHOSPHOR PHOTOLUMINESCENCE QUANTUM EFFICIENCY	P3-65	392
Simas Melnikas, Lukas Ramalis, Simonas Kičas, Tomas Tolenis BROADBAND CHIRPED MIRRORS FEATURING LOW GROUP DELAY DISPERSION OSCILLATIONS	P3-66	393
Sandesh Mysore Sathyaraj, Divyesh Mune Gowda, Ajith Kumar Rajendra HEAT SOURCE DETECTION USING THE THERMOGRAPHIC METHOD FLIR ONE THERMAL CAMERA SYSTEM	P3-67	394
Sandesh Mysore Sathyaraj, Divyesh Mune Gowda, Ajith Kumar Rajendra REMOTE DETECTION IN HIGH-VOLTAGE DEVICES USING THE ULTRASONIC METHOD	P3-68	395
Aivaras Pečiulis, Mikas Vengris, Linas Smalakys, Andrius Melninkaitis INVESTIGATION OF LASER INDUCED DAMAGE DYNAMICS IN TRANSPARENT MEDIA AND DIELECTRIC COATING BY ULTRAFAST SPECTROSCOPY	P3-69	396
Maciej Chomski, Gustaw Szawioła, Bogusław Furmann THE ORBITAL ANGULAR MOMENTUM OF LIGHT IN LASER SPECTROSCOPY	P3-70	397
Sergei Anishchenko, Illia Maroz, Anatoli Rouba RADIATION INSTABILITY IN RELATIVISTIC SPLIT-CAVITY OSCILLATOR	P3-71	398
Yuliya Osika, Maksim Shundalau AB INITIO MULTI-REFERENCE PERTURBATION THEORY STUDY ON THE RACL MOLECULE PROMISING FOR LASER COOLING	P3-72	399
Monika Baronaitė, Simonas Ramanavičius, Milda Petrulevičienė, Jurga Juodkazytė, Asta Griguceviciene, Maliha Parvin, Vilma Ratautaitė, Urte Samukaitė-Bubnienė, Renata Karpicz, Arūnas Ramanavičius WO3/WOX COMPOSITES FORMATION BY SOL-GEL METHOD	P3-73	400
Eugene Petrenko, Andrei Solovjov, Lyudmila Omelchenko, Elena Nazarova, Krastyo Buchkov, Krzysztof Rogacki EXCESS CONDUCTIVITY AND POSSIBLE PSEUDOGAP STATE IN FESE SUPERCONDUCTORS	P3-74	401
Romualdas Jonas Čepas, Lukas Kukulas, Gytis Juška, Kristijonas Genevičius THE INVESTIGATION OF RECOMBINATION PROCESSES BY EXTRACTION OF THE INJECTED CHARGE CARRIERS	P3-75	402
Vaiva Soriūtė, Džiugas Litvinas, Patrik Ščajev, Saulius Juršėnas, Chuanjiang Qin, Takashi Fujihara, Toshinori Matsushima, Chihaya Adachi IMPACT OF DIMENSIONALITY TO DIFFUSION AND RECOMBINATION PROCESSES IN LAYERED PEROVSKITES	P3-76	403
Lyudmila Omelchenko, Andrei Solovjov, Eugene Petrenko, Andrei Terekhov EXCESS CONDUCTIVITY IN MAGNETIC SUPERCONDUCTOR DY0.6Y0.4RH3.85RU0.15B4	P3-77	404
Laimonas Deveikis, Tomas Čeponis, Eugenijus Gaubas RECOMBINATION CHARACTERISTICS AND DEEP LEVEL SPECTRA OF GAN/SI INTERFACES	P3-78	405
Vaiva Soriūtė, Patrik Ščajev, Pavels Onufrijevs, Arturs Medvids, Hung-Hsiang Cheng TEMPERATURE DEPENDENT DIFFUSION COEFFICIENT, DIFFUSION LENGTH AND LIFETIME IN GESN EPILAYER	P3-79	406
Jonas Gradauskas, Steponas Ašmontas, Algirdas Sužiedėlis, Aldis Šilėnas, Viktoras Vaičikauskas, Ovidijus Žalys, Oleksandr Masalskyi HOT CARRIER EVIDENCE IN SOLAR CELLS	P3-80	407
Gabrielė Kavaliauskaitė, Gintarė Kuksėnaitė, Rokas Gegevičius, Vidas Pakštas, Viktorija Strazdienė, Edvinas Orentas, Marius Franckevičius, Vidmantas Gulbinas S-METHYLTHIOURONIUM IODIDE IMPROVES PHOTOSTABILITY OF METHYLAMMONIUM LEAD IODIDE PEROVSKITES	P3-81	408
Mikhail Lobanok, Stanislau Prakopyeu, Olga Korolik, Peter Gaiduk RAMAN SPECTROSCOPY OF SIC LAYERS GROWN BY RAPID THERMAL CARBONIZATION OF (100) SI	P3-82	409
Alexei Bondarev, Mikhail Korjik, Andrei Fedorov, Yauheni Talochka, Vitalii Mechinski COINCIDENCE TIME RESOLUTION OF FAST INORGANIC SCINTILLATION CRYSTALS: GAGG:CE, LYSO:CE AND BGO	P3-83	410
Ilya Zur, Alexander Fedotov. THE INFLUENCE OF EXTERNAL LOW-FREQUENCY ACOUSTIC FIELDS ON COMBUSTION OF HEXAMINE	P3-84	411
Mantas Vaičiulis, Kazimieras Nomeika, Ramūnas Aleksiejūnas CARRIER LOCALIZATION IN INGAN STRUCTURES INVESTIGATED BY LIGHT-INDUCED TRANSIENT GRATING TECHNIQUE	P3-85	412

CANCELLED DUE TO COVID-19

Tomas Jurgutis INFLUENCE OF EXCITATION RELAXATION ON LSO:CE QUANTUM YIELD	P3-86	413
Maksimas Anbinderis, Algirdas Sužiedėlis SENSITIVE PLANAR MICROWAVE DIODES ON THE BASE OF TERNARY ALXGA1-XAS SEMICONDUCTOR COMPOUND	P3-87	414
Anatoly Ivashchuk, Dusheiko Mychailo, Mykola Koliada, Oleksandr Masalskyi LINEARIZATION OF ANGULAR CHARACTERISTICS OF THE SUN SENSOR FOR THE POLYITAN-3 SATELLITE	P3-88	415
Simona Pūkienė, Algirdas Jasinskas, Virginijus Bukauskas, Vladimir Agafonov, Mindaugas Kamarauskas, Andrius Bičiūnas, Bronislovas Čechavičius, Arūnas Šetkus, Renata Butkutė NEAR-IR LIGHT EMITTING SOURCES: ELECTRO-OPTICAL CHARACTERISTICS	P3-89	416
Andrea Zelioli, Algirdas Jasinskas, Simona Pūkienė, Lukas Jočionis, Bronislovas Čechavičius, Renata Butkutė GAINAS/GAAS QUANTUM STRUCTURES FOR NEAR INFRARED VERTICAL-EXTERNAL-CAVITY SURFACE-EMITTING LASERS	P3-90	417
Anastasia Chertkova, Vera Tiunova, Alexey Rubtsov QUANTUM MONTE-CARLO SIMULATION OF POLARON TUNNELING	P3-91	418
Daniil Pashnev, Vadym Korotyeyev, Andrzej Urbanowicz, Irmantas Kašalynas TERAHERTZ TRANSMISSION SPECTROSCOPY OF GRATING-COUPLED TWO-DIMENSIONAL ELECTRON GAS IN THE ALGAN/GAN HETEROSTRUCTURES	P3-92	419
Justinas Jorudas, Irmantas Kašalynas TERAHERTZ DETECTION WITH ALGAN/GAN BOW-TIE DIODES AT 300 K AND 80 K TEMPERATURES	P3-93	420
Paweł Dębowski, Joanna Kłosaj, Agata Jarocka, Tomasz Karol Pietrzak INFLUENCE OF EXCITATION WAVELENGTH ON THE EUROPIUM IONS PHOTOLUMINESCENCE IN THE GLASSY MATRIX	P3-94	421
Agata Jarocka, Dominika Wąs, Jakub Płachta, Tomasz K. Pietrzak INVESTIGATION OF OPTICAL PROPERTIES OF CaAlBO3F2 GLASSY MATRIX DOPED WITH EUROPIUM AND SAMARIUM IONS	P3-95	422
Karol Tomasz Płochocki, Agata Jarocka, Tomasz Karol Pietrzak INVESTIGATION OF OPTICAL PROPERTIES OF PHOSPHATE GLASSES DOPED WITH YTTERBIUM AND ERBIUM IONS	P3-96	423
Wojciech Sas, Marcin Perzanowski, Magdalena Fitta MAGNETIC PROPERTIES OF PRUSSIAN BLUE ANALOGUE Fe3[Cr(CN)6]2·nH2O NANORODS OBTAINED BY ELECTRODEPOSITION METHOD	P3-97	424
Agata Jarocka, Tomasz K. Pietrzak, Jakub Płachta, Joanna Kłosaj, Michał Jarczewski, Jacek Ryl, Marek Wasiucionek ROBUST TECHNIQUE FOR TUNABLE PHOSPHORS PHOTOLUMNESCENCE – OPTIMIZATION OF EUROPIUM IONS REDUCTION PROCESS	P3-98	425
Filip Łabaj, Witold Stępień, Wiktor Kulesza, Klaudia Gębala, Michał Wincel HOLOGRAPHIC, LOW-COST DIGITAL MICROSCOPE	P3-99	426
Julia Chepurnaya, Liliya Odanets, Elena Levchuk ELECTRIC FIELD CONTROL OF TWO-ELECTRON STATES IN CYLINDRICALLY SYMMETRIC QUANTUM DOT	P3-100	427

20 March, FRIDAY

13:15-14:45 POSTER SESSION P4

Vaida Vaičiulytė, Kristina Ložienė YIELD AND CHEMICAL COMPOSITION OF ESSENTIAL OIL IN GERANIOL BEARING LARGE THYME (THYMUS PULEGIOIDES)	P4-1	428
Jolita Jagelaviciute, Dalia Cizeikiene IN VITRO EVALUATION OF ANTIMICROBIAL ACTIVITY OF PROBIOTIC PRODUCED METABOLITES AGAINST PATHOGENS	P4-2	429
Džiugas Jurgutis, Greta Jarockytė, Aurimas Vyšniauskas, Vitalijus Karabanovas, Ričardas Rotomskis. EXPLORING PROPERTIES OF VISCOSITY-SENSITIVE BODIPY BASED MOLECULAR ROTOR IN HUMAN MESENCHYMAL STEM CELLS	P4-3	430
Justas Martūnas, Lilija Kalėdienė, Arnoldas Kaunietis NEW LINEAR AZOL IN)E CONTAINIG ANTIMICROBIAL PEPTIDE IDENTIFICATION IN THERMOPHILIC BACTERIUM	P4-4	431
Rokas Jonaitis, Rugilė Chmieliauskaitė, Natalija German THE DEVELOPMENT OF GLUCOSE BIOLOGICAL SENSORS MODIFIED BY VARIOUS GOLD DERIVATIVES	P4-5	432
Aistė Lisavičiūtė, Ernesta Bužavaitė-Vertelienė, Ieva Plikusienė, Zigmas Balevičius, Gitana Mickienė, Milda Plečkaitytė, Gintautas Žvirblis EVALUATION OF INTERACTION KINETICS BETWEEN FUSED CYTOKINES AND RECEPTORS USING TOTAL INTERNAL REFLECTION ELLIPSOMETRY	P4-6	433
Mantas Žiaunys, Vytautas Smirnovas ADDITIONAL THIOFLAVIN-T BINDING MODE IN INSULIN FIBRIL INNER CORE REGION	P4-7	434
Jurga Andrėja Kazlauskaitė, Gražina Juodeikienė, Daiva Žadeikė, Valdas Jakštas, Jurga Bernatonienė, Mindaugas Marksa, Liudas Ivanauskas, Elena Bartkiene, Vita Lėlė, Pranas Viškelis ANTIMICROBIAL NUTRACEUTICALS: RASPBERRY PRESS CAKES COMBINATIONS WITH ESSENTIAL OILS AND LAB FERMENTED BOVINE COLOSTRUM	P4-8	435
Evelina Jankaitytė, Rima Budvytytė, Gintaras Valinčius, Vytautas Smirnovas, Nguyen Ngoc Mai STUDY OF THE INTERACTION OF S100A9 PROTEIN WITH TETHERED LIPID BILAYER MEMBRANES	P4-9	436
Ruta Snieckute, Andrius Sakalauskas, Mantas Ziaunys, Vytautas Smirnovas POLYMORPHISM OF PRION PROTEIN AMYLOID FIBRILS	P4-10	437
Milda Bulotaitė, Vilma Kaškonienė, Audrius Maruška VARIATION OF BIOLOGICALLY ACTIVE COMPOUNDS OF KOMBUCHA PREPARED FROM LITHUANIAN MEDICAL HERBS	P4-11	438
Aleksandra A. Dobysh, Michail A. Shapira, Aleksei V. Yantsevich MICROBIAL CHOLESTEROL OXIDASE: PRODUCTION CHARACTERISTICS AND FEATURES OF ENZYMATIC CATALYSIS.	P4-12	439
Jolita Pachaleva, Ruta Gruskiene, Alma Bockuviene, Jolanta Sereikaite. PREPARATION OF NISIN-LOADED PECTIN-CHITOOLIGOSACCHARIDES PARTICLES	P4-13	440
Edita Kodyte, Ruta Gruskiene, Jolanta Sereikaite NEW NISIN-ULVAN PARTICLES: LOADING EFFICIENCY	P4-14	441
Vita Tumosaitė, Mantas Stankevičius, Tomas Drevinskas, Audrius Maruška GEL COMPOSITES FOR CAPILLARY ELECTROCHROMATOGRAPHY	P4-15	442

CANCELLED DUE TO COVID-19

Domantas Armonavičius, Audrius Maruška, Tomas Drevinskas GENETICAL IDENTIFICATION OF ANTIBACTERIAL AGENTS PRODUCING MICROORGANISMS, ANALYSIS OF THEIR BACTERIOCINS AND KILLER TOXINS AND FOOD FERMENTATION ASSAY	P4-16	443
Tomas Nenartavičius, Neringa Kuliešienė, Sandra Sakalauskaitė, Samy Yousef, Rimantas Daugelavičius RECYCLING OF WASTE MONEY BILLS BY USING MICROBIAL HYDROLYSIS AND ETHANOL FERMENTATION	P4-17	444
Ona Bartininkaitė, Aleksandras Konovalovas, Justas Lazutka, Saulius Serva, Elena Servienė BIOSYNTHESIS AND CHARACTERIZATION OF RECOMBINANT VIRUS LIKE PARTICLES OF TORULASPORA DELBRUECKII VIRUS TDV-1	P4-18	445
Augustė Rastenienė, Kamilė Šimelytė, Monika Kisieliūtė, Rūta Gruškienė, Ramunė Stanevičienė, Elena Servienė, Jolanta Sereikaitė THE CHARACTERISTICS OF AN ANTIMICROBIAL PEPTIDE FROM PEDIOCOCCUS ACIDILACTICI JEM-1	P4-19	446
Justinas Babinskas, Inga Matijošytė SYNTHESIS AND INVESTIGATION OF OLIGOMERIZED AROMATIC AMINE FOR LACCASE ACTIVITY ASSAY	P4-20	447
Julius Andriuškevičius, Eglė Žalytė, Marija Ger, Marius Petrulionis, Benediktas Kurlinkus, Audrius Šileikis, Mindaugas Valius FLT3 RECEPTOR AS A POTENTIAL PROGNOSTIC BIOMARKER AND THERAPEUTIC TARGET IN PANCREATIC CANCER	P4-21	448
Viktoras Mažeika, Dominyka Dapkutė, Artiom Skripka, Riccardo Marin, Patrizia Canton, Fiorenzo Vetrone, Vitalijus Karabanovas BIOCOMPATIBLE CARBOXYLATED CUINS2/ZNS QUANTUM DOTS FOR BRAIN TUMOR DIAGNOSTICS	P4-22	449
Veronika Reut, Daria Grigorieva ACETAMINOPHEN AS A REGULATOR OF NEUTROPHILS' ROS AND RHS PRODUCTION	P4-23	450
Oleksandr Ladan, Volodymyr Bessarabov, Galyna Kuzmina, Ganna Kharitonenko, Iryna Pashchenko, Nadiya Matvieieva ANTI-INFLAMMATORY PROPERTIES OF ARTEMISIA TILESII BIOTECHNOLOGICAL RAW MATERIAL	P4-24	451
Dovilė Jurevičiūtė, Audrius Sigitas Maruška, Vita Tilvikienė, Aušra Bakšinskaitė SPECTROPHOTOMETRIC ANALYSIS OF PURE EXTRACTS AND THEIR FRACTIONS FROM DIFFERENT PARTS OF ARTEMISIA DUBIA WALL.	P4-25	452
Gerda Skinderytė, Saulius Serva, Aleksandras Konovalovas ROLE OF SCV-LA VIRUS IN TRANSPOSITION FREQUENCY OF YEAST SACCHAROMYCES CEREVISIAE	P4-26	453
Agnė Savickaitė, Eglė Lastauskienė, Renata Gudiukaitė PHYSICOCHEMICAL CHARACTERIZATION OF IMMOBILIZED LIPOLYTIC GDEST-LIP ENZYME AND ITS APPLICATION FOR TRANSESTERIFICATION REACTION	P4-27	454
Deimantė Purytė, Irina Buchovec, Pranciškus Vitta OPTICAL PROPERTIES ANALYSIS OF THE NATURAL PHOTOSENSITIZERS	P4-28	455
Lukas Budginas, Rytis Rugienius, Jurgita Vinskienė, Danas Baniulis, Vidmantas Stanys PRODUCTION OF RECOMBINANT EXTRACLLULAR MATRIX MIMICKING PEPTIDES IN TOBACCO PLANT	P4-29	456
Karina Vitchuk, Anastasia Lapina, Andrey Demidov, Viktor Zhilkin, Gennady Fedorov, Vladimir Glotov GENERATION OF EFFECTIVE ENDOTHELIAL CELL POPULATIONS FOR MICROFLUIDIC TECHNIQUES	P4-30	457
Valentinas Černiauskas, Alytis Gruodis, Raminta Rodaitė-Riševičienė, Gintautas Saulis MECHANISM OF EFFECTIVE QUENCHING OF CALCEIN FLUORESCENCE BY IRON. AB INITIO STUDY	P4-31	458
Gintarė Surplytė, Vilius Poderys, Vitalijus Karabanovas, Ričardas Rotomskis GENERATION OF REACTIVE OXYGEN SPECIES INDUCED BY GOLD NANOCLUSTERS STABILIZED BY HUMAN BLOOD PLASMA PROTEINS	P4-32	459
Vilius Aukscionis, Antanas Zinovicius, Aura Kisieliute, Almira Ramanaviciene, Arunas Ramanavicius INVESTIGATION OF MODIFIED SACCHAROMYCES CEREVISIAE USING AMPEROMETRIC AND IMPEDANCE SPECTROSCOPY METHODS	P4-33	460
Ieva Nekrošiūtė, Vilma Kaškonienė, Rūta Mickienė, Audrius Maruška EVALUATION OF BIOLOGICAL ACTIVITY OF PICEA ABIES (L.) KARST SEEDS COLECTED IN LITHUANIA	P4-34	461
Vilmantas Pupkis, Indre Lapeikaite, Vilma Kisnieriene ELECTROPHYSIOLOGICAL TECHNIQUES REVEAL CS+ EFFECT ON ELECTRICAL SIGNALING IN MACROALGAE NITELLOPSIS OBTUSA	P4-35	462
Gabriele Agne Stasiukynaite, Greta Jarockyte, Marijus Pleckaitis, Saulius Bagdonas, Virginijus Barzda, Vitalijus Karabanovas, Ricardas Rotomskis UPTAKE AND INTRACELLULAR LOCALIZATION OF TPPS4 IN LIVING CELLS	P4-36	463
Marijus Pleckaitis, Vitalijus Karabanovas, Saulius Bagdonas, Ricardas Rotomskis, Virginijus Barzda EVOLUTION OF SELF-ASSEMBLING TPPS4 STRUCTURES. FROM NANO TO MACROAGGREGATES	P4-37	464
Lukas Krasauskas, Vytautas Smirnovas AGGREGATION OF RECOMBINANT TAU PROTEIN ISOFORM 2N4R DEPENDENCE ON DIFFERENT ENVIRONMENTAL CONDITIONS	P4-38	465
Alena Kavalenka, Alexei Svechko, Ekaterina Sobolevskaya MODIFICATION OF ERYTHROCYTES UNDER THE ACTION OF CARBON NANOTUBES FUNCTIONALIZED BY POLYMERS	P4-39	466
Alena Kavalenka, Ekaterina Sobolevskaya, Alexei Svechko, Tatsiana Kulahava EFFECTS OF MULTI-WALLED CARBON NANOTUBES ON NEUTROPHIL ACTIVITY IN VITRO	P4-40	467
Ksenija Godlevskaja, Evelina Voronovic, Artiom Skripka, Vitalijus Karabanovas, Fiorenzo Vetrone, Ricardas Rotomskis NANOPARTICLES IN THE BIOLOGICAL ENVIRONMENT: COLLOIDAL STABILITY AND THEIR CELLULAR UPTAKE	P4-41	468
Greta Bigelyte, Tautvydas Karvelis, Joshua K. Young, Zhenglin Hou, Rimante Zedaveinyte, Karolina Pociute, Arunas Silanskas, Česlovas Venclovas, Virginijus Siksnys MINIATURE CRISPR-CAS SYSTEM CHARACTERIZATION	P4-42	469
Danguolė Norkūnaitė, Tomas Šinkūnas THE ROLE OF TARGET SEQUENCE LENGTH FOR DNA INTERFERENCE IN THE TYPE I-F CRISPR-CAS SYSTEM	P4-43	470
Konstanty Keda, Irmantas Mogila, Gintautas Tamulaitis, Virginijus Šikšnys CRISPR-CAS EFFECTOR COMPLEX OPTIMIZATION FOR SINGLE MOLECULE STUDIES	P4-44	471
Kamilė Mikalauskaitė, Mantas Žiaunys, Vytautas Smirnovas AMYLOIDOPHILIC MOLECULE INTERACTIONS ON THE SURFACE OF AMYLOID FIBRILS: COOPERATIVE BINDING AND FLUORESCENCE QUENCHING	P4-45	472
Mindaugas Zaremba, Elena Manakova, Edvardas Golovinas, Saulius Gražulis and Virginijus Šikšnys SPECIFICITY OF THE ARGONAUTE PROTEIN FROM ARCHAEOGLOBUS FULGIDUS TO THE 5'-END OF THE GUIDE	P4-46	473
Deimantė Galalytė, Neringa Kuliešienė, Simona Vaitkienė, Rimantas Daugelavičius ANTIFUNGAL ACTIVITY OF PYRIDINIUM COMPOUNDS IN COMBINATION WITH FLUCONAZOLE AGAINST CANDIDA ALBICANS PLANKTONIC CELLS AND BIOFILMS	P4-47	474

CANCELLED DUE TO COVID-19

Matas Tiškus, Nina Urbelienė, Audrius Laurynėnas, Rolandas Meškys IDENTIFICATION OF AMINO ACIDS RESPONSIBLE FOR ACTIVITY OF THE HYDROLASE MO13 SELECTED FROM METAGENOME	P4-48	475
Greta Koženevska, Augustina Naciūtė, Karolina Kavaliauskaitė, Kamilė Butkutė, Daiva Tauraitė ENZYME/PRODRUG SYSTEMS FOR CANCER TREATMENT	P4-49	476
Reda Nalivaikienė, Virginija Kalcienė, Laura Butrimavičienė RESPONSE OF OXIDATIVE STRESS AND NEUROTOXICITY BIOMARKER IN RAINBOW TROUT (ONCORHYNCHUS MYKISS) AFTER EXPOSURE TO SIX-METALS MIXTURES	P4-50	477
Wojciech Marciniak, Joanna Marciniak, Karolina Olszewska AB INITIO CONFORMATIONAL AND ELECTRONIC STRUCTURE ANALYSIS OF INOSITOL PHOSPHATES	P4-51	478
Tomas Urbaitis, Giedrius Gasiunas, Joshua K. Young, Monika Jasnauskaite, Mantvyda Grusyte, Sushmitha Paulraj, Jennifer L. Curcuru, Megumu Mabuchi, Ryan T. Fuchs, Ezra Schildkraut, G. Brett Robb, and Virginijus Siksnys	P4-52	479
Oleksii Fedorenko, Valentina Tararina, Olesya Moroz PROTEIN KINASE C SIGNALING IN STIMULATED MYOMETRIUM CONTRACTILITY	P4-53	480
Marius Žagunis, Nicola Tiso, Jurgita Mikašauskaitė, Audrius Maruška CAPACITY OF IRPEX LACTEUS TO DECOLORIZE VARIOUS TEXTILE DYES	P4-54	481
Aušrinė Venckaitytė, Vilma Kaškonienė, Rūta Mickienė, Audrius Maruška EVALUATION OF MICROORGANISMS, ISOLATED FROM BEES PRODUCTS	P4-55	482
Vaida Adaškevičiūtė, Vilma Kaškonienė, Audrius Maruška COMPARISON OF BEE POLLEN ANTIOXIDANT PROFILE AFTER ENZYMATIC HYDROLYSIS AND LACTIC ACID FERMENTATION	P4-56	483
Aistė Rimgailaitė, Paulius Ruzgys, Sonam Chopra, Saulius Šatkauskas ENHANCEMENT OF BLEOMYCIN CYTOTOXIC EFFECT AND REGULATION OF GENE EXPRESSION USING SIMULTANEOUS PLASMID DNA AND BLEOMYCIN ELECTOTRANSFER	P4-57	484
Eglė Žalytė, Kęstutis Strupas, Mindaugas Valius ESTABLISHMENT AND CHARACTERIZATION OF A NEW HUMAN PANCREATIC CANCER CELL LINE CAPAN-26	P4-58	485
Dovilė Daunoraitė, Marius Gedgaudas, Aurelija Mickevičiūtė, Egidijus Kazlauskas, Daumantas Matulis TRYPANOSOMA CRUZI CHAPERONE HSP90 AS A TARGET FOR CHAGAS DISEASE TREATMENT	P4-59	486
Inga Songailienė, Jonas Juozapaitis, Giedrė Tamulaitienė, Giedrius Sasnauskas, Audronė Rukšėnaitė, Virginijus Šikšnys CHARACTERIZATION OF TOXIN-ANTITOXIN SYSTEM IN THE VICINITY OF CRISPR-CAS OPERON	P4-60	487
Maryia Kisel, Irina Haidukevich, Tatsiana Sushko, Andrei Gilep OPTIMIZATION OF CULTURE CONDITIONS FOR THE EXPRESSION OF MEMBRANE SCAFFOLD PROTEIN 1 FOR THE DESIGN OF DISCOIDAL PHOSPHOLIPID BILAYER NANOPARTICLES	P4-61	488
Akvilė Milašiutė, Rima Budvytytė, Tadas Ragaliauskas, Gintaras Valinčius CHARACTERIZATION OF MULTILAMELLAR LIPID VESICLES	P4-62	489
Kornelija Beresnevičiutė, Rūta Mickienė, Vilma Kaškonienė, Audrius Maruška INVESTIGATION OF THE INFLUENCE OF DIFFERENT MICROORGANISMS ON PLANT BIOMASS	P4-63	490
Kristina Gluščiukaitė, Vaida Paketurytė, Alexey Smirnov, Vaida Juozapaitienė, Daumantas Matulis NON-CLASSICAL BINDING MODE BETWEEN ORTHO-, PARA- DISUBSTITUTED FLUORINATED PRIMARY BENZENESULFONAMIDES AND NATIVE OR MUTATED HUMAN CARBONIC ANHYDRASES	P4-64	491
Valeryia Klopava, Jan Panada, Tatsiana Kulahava, Yaroslav Faletrov, Vladimir Shkumatov THE EFFECT OF NEWLY SYNTHESIZED DERIVATIVE OF DEHYDROEPIANDROSTERONE ON GLIOMA CELL PROLIFERATION AND REACTIVE OXYGEN SPECIES GENERATION.	P4-65	492
Shamish Ganpule, Giulio Preta PLEIOTROPIC EFFECTS OF STATINS	P4-66	493
Lavryk Roman, Sukha Iryna, Moroz Olesya TRPV4 IN RAT MYOMETRIUM CONTRACTILITY	P4-67	494
Maria Terekhova, Anatoli Kokhan, Daria Grigorieva STRUCTURAL PROPERTIES AND IRON-BINDING CAPACITY OF LACTOFERRIN DURING OXIDATIVE/HALOGENATIVE STRESS	P4-68	495
Arthur F. Chaikovskii **SPECTRAL-KINETIC PROPERTIES OF LOWER EXCITED ELECTRONIC STATES IN OXYHEMOGLOBIN**	P4-69	496
Ivan Kablov, Yulia Kuziv ANALYSIS OF RELEASE PROCESSES OF TEMOPORFIN (MTHPC) FROM DEXTRAN70-POLY (N-ISOPROPYLACRYLAMIDE) COPOLYMER IN BLOOD SERUM	P4-70	497
Mantė Rakauskaitė, Marija Jankunec, Arnoldas Kaunietis THE ANTIMICROBIAL ACTIVITY OF GEOBACILLIN 26: ARTIFICIAL VS BACTERIAL CELL MEMBRANE	P4-71	498
Antanas Zinovicius, Juste Rozene, Inga Morkvenaite-Vilkonciene, Almira Ramanaviciene, Arunas Ramanavicius MINIATURIZED GLUCOSE BIOSENSOR BASED ON LOCALIZED ELECTROCHEMICAL IMPEDANCE SPECTROSCOPY	P4-72	499
Povilas Šimonis, Rasa Garjonytė, Arūnas Stirkė INVESTIGATION OF ELECTROPORATION EFFECTS BY MEDIATED AMPEROMETRY AT YEAST MODIFIED ELECTRODES	P4-73	500
Kestutis Dabravolskas, Ilona Jonuskiene, Simona Sutkuviene, Dalius Gudeika SYNTHESIS AND ANTIBACTERIAL ACTIVITY EVALUATION OF CARBAZOLE-BASED COMPOUNDS	P4-74	501
Jolanta Bukauskaite, Edvardas Bagdonas, Ausra Unguryte, Paulius Lukas Tamosiunas, Vaidas Dirse, Dainius Daunoravicius, Ali Mobasheri, Eiva Bernotiene. EARLY AND PROLONGED MESENCHYMAL INDUCTION FOR CHONDROGENIC DIFFERENTIATION OF HUMAN DERMAL FIBROBLAST-DERIVED INDUCED PLURIPOTENT STEM CELLS (HDF-HIPSCS)	P4-75	502
Veronika Malyško, Vitalij Novickij, Augustinas Želvys, Austėja Balevičiūtė, Auksė Zinkevičienė, Jurij Novickij, Gediminas Staigvila and Irutė Girkontaitė PULSED CURRENT AS AN INDICATOR OF SUCCESSFUL TUMOR ELECTROCHEMOTHERAPY	P4-76	503
Arūnas Murauskas, Gediminas Staigvila, Vitalij Novickij APPLICATOR PROTOTYPE FOR DIELECTROPHORESIS-ENHANCED ELECTROTRANSFER OF MOLECULES INTO BIOLOGICAL CELLS	P4-77	504
Gabrielė Bumbulytė, prof. habil. dr. Vincas Būda EFFECTS OF ESSENTIAL OILS AND THEIR COMPOUNDS ON MEALWORMS (TENEBRIO MOLITOR L.) LARVAE	P4-78	505
Aušra Kondrataitė, Arnoldas Kaunietis OPTIMIZATION OF CONDITIONS FOR GENETIC TRANSFORMATION OF THERMOPHILIC BACTERIA	P4-79	506

CANCELLED DUE TO COVID-19

Sandra Saunoriūtė, Ona Ragažinskienė, Liudas Ivanauskas, Mindaugas Marksa EVALUATION OF ESSENTIAL OILS COMPOSITION OF ARTEMISIA ABSINTHIUM L. USING GC-MS	P4-80	507
Zhanna Hladkova EFFECT OF ESCHERICHIA COLI ENDOTOXIN ON VITAL FUNCTIONS OF RATS AFTER INTRANASAL INJECTION	P4-81	508
Gintarė Sauliutė, Arvydas Markuckas, Brigita Čapukoitienė, Milda Stankevičiūtė RESPONSE PATTERNS OF BIOMARKERS IN DIFFERENT FISH SPECIES EXPOSED TO MULTICOMPONENT METAL (CD, CR, CU, NI, PB AND ZN) MIXTURE	P4-82	509
Brigita Čapukoitienė, Gintarė Sauliutė, Tomas Makaras, Svetlana Markovskaja, Milda Stankevičiūtė HAEMATOLOGICAL RESPONSES UNDER MULTIPLE STRESS EXPOSURE IN PERCH (PERCA FLUVIATILIS)	P4-83	510
Vitalijus Stirkė, Linas Balčiauskas, Laima Balčiauskienė, Raminta Skipitytė, Andrius Garbaras TROPHIC ECOLOGY OF SMALL MAMMALS IN COMMERCIAL ORCHARDS: INSIGHTS FROM STABLE ISOTOPE STUDIES	P4-84	511
Vaidas Maciulskis, Jurate Skerniskyte, Edita Suziedeliene ISOLATION OF A HIGH MOLECULAR MASS PLASMID FROM OPPORTUNISTIC PATHOGEN ACINETOBACTER BAUMANNII	P4-85	512
Giedrė Miniotaitė, Indrė Valiulytė, Arūnas Kazlauskas THE EFFECTS OF CLASS-3 SEMAPHORIN PROTEINS ON ANGIOGENESIS IN VITRO SYSTEM	P4-86	513
Ana Koniuchovaitė, Lilija Kalėdienė Arnoldas Kaunietis IDENTIFICATION OF NEW ANTIMICROBIAL PEPTIDES FROM THERMOPHILIC BACTERIA	P4-87	514
Miriama Peklanska, Federica Serati & Alexander W. Bruce UTILISING CRISPR-CAS9 TO TAG ENDOGENOUS GENE LOCI WITH C-TERMINAL FLUORESCENT PROTEIN FUSIONS IN PREIMPLANTATION MOUSE EMBRYOS.	P4-88	515
Saulė Ulinauskaitė, Algirdas Kaupinis, Mindaugas Valius, Lilija Kalėdienė, Arnoldas Kaunietis GEOBACILLIN 19, NOVEL BACTERIOCIN FROM A THERMOPHILIC BACTERIUM	P4-89	516
Julius Martinkus, Renatas Krasauskas, Jūratė Skerniškytė, Julija Armalytė, Edita Sužiedėlienė TAGGING A. BAUMANNII TYPE VI SECRETION SYSTEM COMPONENTS WITH A GREEN FLUORESCENT PROTEIN	P4-90	517
Volodymyr Vasylenko, Volodymyr Bessarabov, Galyna Kuzmina, Victoria Chumak, Marina Sidorenko, Saulius Mickevičius USING OF HESPERIDINE FOR PREVENTION POISONING OF PHOSPHORORGANIC SUBSTANCES	P4-91	518
Elizabet Beržanskytė, Aistė Zentelytė, Giedrė Valiulienė, Rūta Navakauskienė NEURAL GENE EXPRESSION PATTERNS OF DIFFERENTIATED HUMAN AMNIOTIC FLUID STEM CELLS	P4-92	519
Edvina Krokaitė, Tomas Rekašius, Lina Jocienė, Donatas Žvingila, Eugenija Kupčinskienė NITROGEN AS A KEY NUTRIENT AMONG POPULATIONS OF PHALARIS ARUNDINACEA	P4-93	520
Edvina Krokaitė, Dinara Shakeneva, Tomas Rekašius, Lina Jocienė, Donatas Žvingila, Eugenija Kupčinskienė SOME PECULIARITIES OF LYTHRUM SALICARIA NUTRITION	P4-94	521
Austėja Dapkutė, Egle Preikšaitienė COMPARISON OF INTELLECTUAL DISABILITY ASSOCIATED GENES IN X CHROMOSOME AND AUTOSOMES	P4-95	522
Benita Buragaite-Staponkiene, Kristina Stuopelyte, Adomas Rovas, Egle Puneviciene, Irena Butrimiene, Alina Puriene, Sonata Jarmalaite MIRNAS AS THE POTENTIAL BIOMARKERS FOR CHRONIC PERIODONTITIS	P4-96	523
Illia Kostiuk, Daria Hamova, Mariia Harkusha-Omelchenko, Yuliia Faidiuk, Pavlina Zelena, Larysa Skivka, Oleksandr Tereshchenko, Oleksandr Bului, Vasyl Nazarenko MODELING NATURAL HABITATS WITH LIQUID CRYSTALS: MOTILE BACTERIA IN ANISOTROPIC ENVIRONMENT	P4-97	524
Gabija Šakalytė , Julija Armalytė, Edita Sužiedelienė ACETYLTRANSFERASE CHEA IN ACINETOBACTER BAUMANNII STRESS RESPONSE	P4-98	525
Katažyna Samaitė, Arimantas Tamašauskas, Giedrius Steponaitis THE STUDY OF M6A EPIMODIFICATION REGULATING GENES EXPRESSION AND M6A EPIMARK LEVEL IN HUMAN ASTROCYTOMAS	P4-99	526
Mariia Popova, Olena Saliy, Aleksey Godovskiy TECHNOLOGICAL ASPECTS OF DEPROTEINIZED CALF BLOOD HEMODERIVATIVE PREPARATION	P4-100	527
Agnė Šeštokaitė, Rasa Sabaliauskaitė, Vaida Gedvilaitė, Saulius Cicėnas, Sonata Jarmalaitė MUTATION ANALYSIS IN LIQUID BIOPSY FROM NON-SMALL CELL LUNG CANCER PATIENTS	P4-101	528
Ignas Ragaišis, Laurita Klimkaitė, Renatas Krasauskas, Julija Armalytė, Edita Sužiedėlienė ANALYSIS OF METALLO-B-LACTAMASES FROM CHRYSEOBACTERIUM SPP. OF SOIL ORIGIN	P4-102	529
Sima Garberytė, Margarita Žvirblė, Karolina Žilionytė, Jan Aleksander Kraśko, Nijolė Matusevičienė, Božena Pavliukevičienė, Gintaras Zaleskis DOXORUBICIN CELLULAR RETENTION PATTERNS CORRELATES WITH THERAPEUTIC RESPONSE IN ASCITIC LYMPHOMA BEARING MICE	P4-103	530
Andre Aleksandraviciute, Rokas Miksiunas, Ieva Kulvinskiene, Ruta Aldonyte, Kestutis Rucinskas, Vilius Janusauskas, Siegfried Labeit, Daiva Bironaite INVESTIGATION OF CYTOTOXIC RESPONSE OF HEALTHY AND PATHOLOGICAL HUMAN MYOCARDIUM-DERIVED MESENCHYMAL STEM CELLS	P4-104	531
Justas Šidiškis, Gintarė Povilaitytė, Lilija Kalėdienė, Alisa Gricajeva IDENTIFICATION AND QUALITATIVE EXPRESSION ANALYSIS OF UNUSUAL ESTERASE FROM STAPHYLOCOCCUS SAPROPHYTICUS AG1	P4-105	532
Raminta Vaičiulevičiūtė, Ilona Uzielienė, Vitalij Novickij, Ali Mobasheri , Edvardas Bagdonas, Narūnas Porvaneckas, Giedrius Kvederas, Eiva Bernotienė THE EFFECTS OF ELECTROSTIMULATION ON HUMAN MESENCHYMAL STEM CELL CHONDROGENIC DIFFERENTIATION	P4-106	533
Nataliia Shtefan, Oleksiy Boldyriev, Taras Vereshak, Yaroslav Shuba THE FLOCALIN ACTION ON HEART-SPECIFIC COMBINATION OF K-ATP CHANNELS AND ITS DOSE-RESPONSE	P4-107	534
Martynas Rojus Bartkus, Bazilė Ravoitytė, Ramunė Stanevičienė, Elena Servienė THE INTERFACE BETWEEN CHRONOLOGICAL AGING AND KILLER MAINTENANCE IN SACCHAROMYCES YEASTS	P4-108	535
Greta Rakauskienė, Emilija Sadauskaitė, Eiva Bernotienė, Edvardas Bagdonas, Ali Mobasheri, Narūnas Porvaneckas, Giedrius Kvederas, Ilona Uzielienė THE INTRACELLULAR CALCIUM CONCENTRATION IN HUMAN MESENCHYMAL STEM CELLS AS A POTENTIAL TARGET FOR IMPROVEMENT OF CHONDROGENIC DIFFERENTIATION	P4-109	536

CONFERENCE DUE TO COVID-19

Emilija Sadauskaitė, Ilona Uzielienė, Greta Rakauskienė, Rokas Mikšiūnas, Edvardas Bagdonas, Daiva Bironaitė, Ali Mobasheri, Narūnas Porvaneckas, Giedrius Kvedaras, Eiva Bernotienė THE EXPRESSION OF L-TYPE VOLTAGE-OPERATED CALCIUM CHANNEL SUBUNIT CAV1.2 IN HUMAN MESENCHYMAL STEM CELL CHONDROGENIC DIFFERENTIATION	P4-110	537
Jurgita Rutkauskaitė-Sucilienė, Ingrida Šatkauskienė, Simona Tučkutė MORPHOLOGY AND ELEMENTAL ANALYSIS OF LEECHES COCOONS USING SEM-EDS	P4-111	538
Aušra Bakšinskaitė, Vita Tilvikienė, Modupe Doyeni, Urtė Stulpinaitė USE OF DIGESTATE FOR PLANT FERTILIZATION - INFLUENCE ON SOIL AND PLANT QUALITY AND GHG EMISSIONS	P4-112	539
Solveiga Braknytė, Aušra Bakšinskaitė, Vita Tilvikienė, Karolina Barčauskaitė DETERMINATION OF MINERAL COMPOSITION OF HEMP MORPHOLOGICAL PARTS (CANNABIS SATIVA L.) DURING VEGETATION BY MEANS ICP-MS	P4-113	540
Rūta Zabitaitė, Daina Skiriutė, Rūta Urbanavičiūtė IDENTIFICATION OF 6 POTENTIAL SERUM MARKERS OF ASTROCYTOMA	P4-114	541
Gintarė Šidlauskaitė, Žydrė Kadžiulienė EVALUATION OF FECUNDITY OF PERENNIAL RYEGRASS OF DIFFERENT GENETIC ORIGIN	P4-115	542
Jovita Kybartaitė, Lina Šernaitė, Neringa Rasiukevičiūtė, Alma Valiuškaitė SUPPRESSING FUNGAL SOFT FRUIT PATHOGENS GROWTH USING PLANT EXTRACT	P4-116	543
Anastasiya Kanunnikava, Vladimir Gureev, Arkadiy Nesterov, Evgenij Patrakhanov, Vladimir Pokrovsky, Vitaly Tilikin THE PREVENTION OF POSTOPERATIVE PERITONEAL ADHESIONS IN A RAT MODEL BY THE NOVEL ANTI-ADHESION POLYSACCHARIDE-BASED FILMS	P4-117	544
Marlena Szeligowska, Emilia Trudnowska, Anna Maria Dąbrowska, Rafał Boehnke, Sławomir Sagan, Józef Wiktor, Katarzyna Błachowiak-Samołyk SPATIAL PATTERNS OF PARTICLES&PLANKTON IN THE WARMING ARCTIC FJORD (ISFJORDEN,WEST SPITSBERGEN) IN 7 CONSECUTIVE MID-SUMMERS (2013-2019)	P4-118	545
Simona Lukošiūtė, Alma Valiuškaitė, Neringa Rasiukevičiūtė NATURAL BIOACTIVE PRODUCTS FOR VEGETABLE DISEASE	P4-119	546
Rodionova Elena Yurievna, Sazhnev Alexey Sergeevich THE USE OF A CONDENSER MICROPHONE FOR THE STUDY OF STRIDULATION OF AQUATIC AND SEMI-AQUATIC BEETLES	P4-120	547
Vladimir Pokrovsky, Anastasiya Kanunnikava, Arkadiy Nesterov, Yury Linnik, Alexandr Filchakov, Ivan Arkhipov, Petr Lebedev THE NOVEL EXPERIMENTAL RAT MODEL OF POSTOPERATIVE PERITONEAL ADHESIONS	P4-122	548
Sofiia Shapoval, Yevheniia Minchuk, Yuliia Faidiuk, Maksym Kharkhota, Svitlana Moroz, Tetiana Gorb, Fedir Tovkach FIRE-BLIGHT PATHOGEN ERWINIA AMYLOVORA, PERSISTING IN UKRAINE: MULTI-APPROACH ANALYSIS	P4-123	549
Anastasiia Tsymbaliuk, Viktoriia Stetska, Taisa Dovbynchuk, Yelyzaveta Makedon, Nataliia Dziubenko, Yuriy Prylutskyy, Ganna Tolstanova THE EFFECT OF PRISTINE C60 FULLERENE ON COGNITIVE DYSFUNCTIONS IN 6-OHDA–INDUCED MODEL OF PARKINSON'S DISEASE IN RATS	P4-124	550
Marharyta Skovorodka, Iryna Akulenko, Hennadii Suslov, Tetiana Serhiychuk, Ganna Tolstanova SCREENING OF PROBIOTIC STRAINS OF BACTERIA WITH HIGH OXALATE-DEGRADING ACTIVITY	P4-125	551
Ernestas Brazys, Vilma Ratautaitė, Gintautas Bagdžiūnas, Arūnas Ramanavičius. CHARACTERIZATION OF L-TRYPTOPHAN IMPRINTED POLYPYRROLE DEPOSITED ON THE GRAPHITE ELECTRODE	P4-126	552
Vadym Lisovyi, Iryna Povshedna, Dmytro Danylenko, Volodymyr Bessarabov, Galyna Kuzmina INCREASING OF THE BIOAVAILABILITY OF MODEL FLAVONOID IN SOLID DISPERSION SYSTEM WITH UREA	P4-127	553
Justinas Baleišis, Romualdas Rudys LASER INDUCED OPTICAL BREAKDOWN WITH FRACTIONAL PICOSECOND ND:YAG 1064 NM LASER IN VIVO ON PORCINE MODEL	P4-128	554

CANCELLED DUE TO COVID-19

GRAPHITE-BASED FLEXIBLE ZONE-PLATES FOR TERAHERTZ OPTICS

Rusnė Ivaškevičiūtė-Povilauskienė[1], Linas Minkevičius[1,2], Domas Jokubauskis[1], Andrzej Urbanowicz[1], Simonas Indrišiūnas[3], Gintaras Valušis[1,2]

[1] Department of Optoelectronics, Center for Physical Sciences and Technology, Lithuania
[2] Institute of Photonics and Nanotechnology, Department of Physics, Vilnius University, Lithuania
[3] Department of Laser Technologies, Center for Physical Sciences and Technology, Lithuania
rusne.ivaskeviciute@ftmc.lt

CANCELLED DUE TO COVID-19

One of the most relevant topics in terahertz (THz) photonics is a search of new ways to control THz radiation using compact planar solutions for THz imaging systems [1]. In particular, these issues become essential designing imaging systems using on-chip approach, because metal diffusion cannot be further used as suitable tool to fabricate THz diffractive optics components. We consider graphite that displays high electrical conductivity, is cheap and ecofriendly material. Moreover under standard conditions it is the most stable form of carbon.

In this communication, we extend our previous study of silicon based Terahertz zone plates (TZP) [2] by exploring graphite TZPs as possible solutions for diffractive THz optical components [3]. We have investigated and explored the optical properties of flexible TZPs with integrated cross-shaped filters fabricated from three different materials. The first TZP was made of 10 μm thick graphite foil placed on 75 μm plastic. The second one was a few micron thick graphite layer produced by shading HB graphite pencil on a 100 μm thick paper sheet. To evaluate the impact of thin graphite layer on the second TZP, 100 μm thick paper sheet TZP was made in order to serve as reference for the second TZP. Finally, the metallic reference zone plate was made from 30 μm thick steel foil.

At first, flexible materials for TZPs were investigated using THz Time-Domain Spectroscopy (THz-TDS) by measuring their transmittance spectras. Results showed that graphite foil TZP and its reference metallic TZP had similarly expressed resonances around expected 0.6 THz frequency. Also, focusing performance was evaluated by recording imaging beam cross-sections in the focus plane using THz Continuous Wave (THz-CW) system. Results showed that graphite foil TZP operation was effective and very simmilar to the metallic TZP.

The findings suggest that graphite-based THz zone plates can provide an inexpensive alternative to metal-based elements for design of passive optical elements in THz imaging systems.

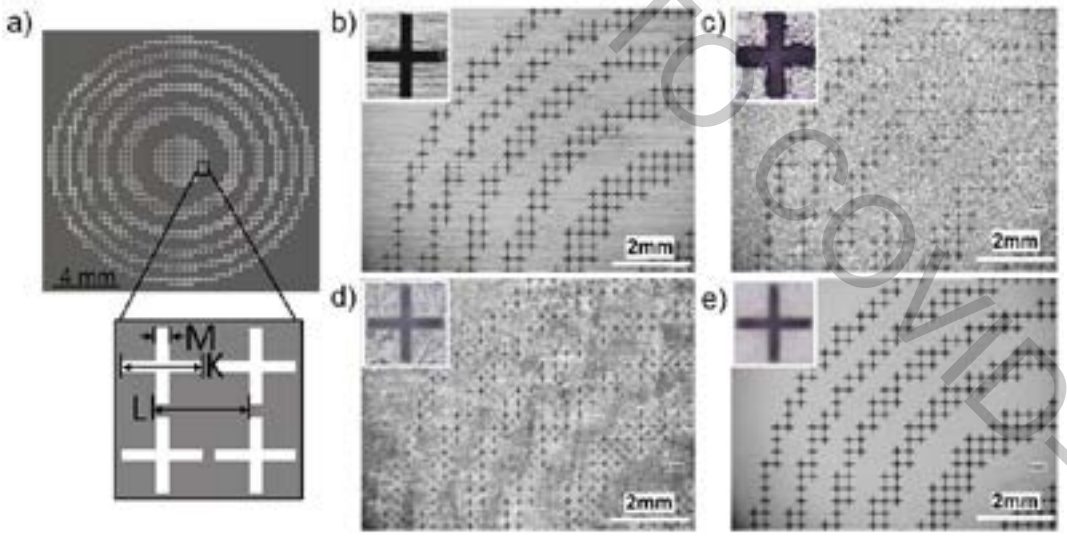

Fig. 1. a) Design of the graphite foil terahertz zone plate for 0.6 THz and geometry of cross-shaped filters (M=40 μm, K=260 μm, L=290 μm). Photos of the quarter of TZP made from different materials: b) metal; c) graphite foil on plastic; d) graphite on paper and e) paper. Insets depicts the shape of cross-shaped aperture element.

[1] L. Minkevičius et al., Focusing Performance of Terahertz Zone Plates with Integrated Cross-shape Apertures, J. Infrared, Millimeter, Terahertz Waves, **35**, 699–702 (2014).
[2] L. Minkevičius et al., Compact Diffractive Optics for THz Imaging, Lithuanian J. of Phys., **58** (1), 99-107 (2018).
[3] R. Ivaškevičiūtė-Povilauskienė et al., Flexible Materials for Terahertz Optics: Advantages of Graphite-based Structures, Optical Materials Express, **9** (11), 4438-4446 (2019).

EFFECT OF MAGNETIC Co–CoO PARTICLES ON THE CARRIER TRANSPORT IN SINGLE LAYER GRAPHENE

Julia A. Fedotova[1], Uladzislaw E. Gumiennik[1,2], Alexander K. Fedotov[1]

[1] Institute for Nuclear Problems, Belarusian State University, Babrujskaja Str. 11, 220030 Minsk, Belarus
[2] Belarusian State University, Praspiekt Niezaliežnasci 2, 220030 Minsk, Belarus
gumennik@gmail.com

CANCELLED DUE TO COVID-19

Fabrication and studying of magnetic and magnetoresistive graphene-based hybrid structures is a highly relevant problem, because it opens new perspectives for their use in magnetic tunneling transitions, spin valves and filters, magnetoresistive memory devices, and other spintronic elements [1][2][3]. These kinds of structures can be successfully fabricated by depositing particles or layers of various ferromagnetic materials (e.g., *Co* and *Ni*) onto graphene [2][4]. We note that specific features characteristic of deposition of metallic particles on graphene constitute one of the issues related to its prospective use in electronic devices, and these must be investigated in order to overcome the difficulty of making low-resistance ohmic contacts to the graphene surface.

The aim of this work is to investigate the interrelation between the electric and magnetic properties of composite structures consisting of a ferromagnetic metal and graphene that are fabricated by electrochemical deposition of cobalt nanoparticles onto monolayer CVD graphene, since this will enable us to identify the effects that covered with *CoO* shells have on carrier transport in zero and nonzero external magnetic fields.

Graphene was synthesized on copper foil by CVD-method using a PlanarTech G2 unit. Cobalt nanoparticles were deposited onto graphene from a solution containing 1.25 $g/L\ CoSO_4{\cdot}6H_2O$ and 0.064 $g/L\ NaCl$ using a PI-50-1.1 potentiostat coupled to a PR-8 programming unit. Depositions were performed in the pulse reverse mode, a controlled- current technique, at a cathodic current density of 2.5 mA/cm^2 (pulse duration, 5 *s*) and anodic current density of 1.25 mA/cm^2 (pulse duration, 2 *s*); the total deposition time was 30 *s*.

Temperature and magnetic field dependences of electrical resistivity $R(T,B)$ were measured by the four-point probe method in the temperature range of 2 to 300 *K* and in a transversal magnetic field with magnetic flux density *B* up to 8 *T* using a noncryogenic measuring system (Cryogenics Ltd) on the basis of a closed-cycle refrigerator.

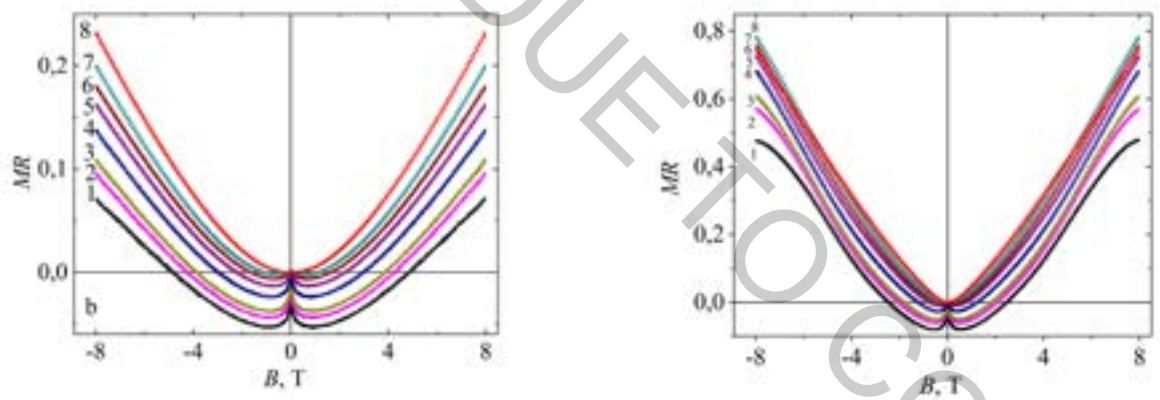

Fig. 1. Relative magnetoresistance MR(B)=$\frac{[R(B)-R(0)]}{R(0)}$ on magnetic flux density *B* for Gr/SiO_2 and $Co-Gr/SiO_2$ sample at different temperatures covering the range of 2–300*K*: (1) - 2, (2) - 7, (3) - 10, (4) - 25, (5) - 50, (6) - 75, (7) - 125, and (8) - 275 *K*.

Electrochemical deposition onto CVD graphene in the pulse-reverse mode from an electrolyte containing $CoSO_4 \cdot 6H_2O$ produced with size (up to 500 *nm*) on the graphene surface consisting of polydisperse agglomerates with prolate shapes.

The deposition of *Co–CoO* particles was shown the increase of resistance of graphene samples due to a lower electron concentration in dielectric *CoO*. For the Gr/SiO_2 and $Co-Gr/SiO_2$ samples, we revealed the existence of a competition between the NMR and PMR contributions to the observed magnetoresistance effect and at the low-temperature carrier transport in the NMR region was due to quantum localization correction to the Drude conductivity, while the enhancement in PMR after depositing *Co–CoO* particles onto graphene may be attributed to the Lorentz mechanism operating within *Co* cores.

[1] I.S. Zhidkov, N.A. Skorikov, A.V. Korolev, A.I. Kukharenko, E.Z. Kurmaev, V.E. Fedorov, S.O. Cholakh. Carbon **91**, 298 (2015).
[2] P.U. Asshoff, J.L. Sambricio, A.P. Rooney, S. Slizovskiy, A. Mishchenko, A.M. Rakowski, E.W. Hill, A.K. Geim, S.J Haigh, V.I. Fal'ko, I.J. Vera-Marun, I.V. Grigorieva. 2D Mater. **4**, 031004 (2017).
[3] M.Z. Iqbal, M.W. Iqbal, J.H. Lee, Y.S. Kim, S. Chun, J. Eom. NanoResearch **6**, 5, 373 (2013).
[4] V.C. De Franco, G.M.B. Castro, J. Corredor, D. Mendes, J.E. Schmidt. Carbon Lett. **21**, 16 (2017).

SPECTROSCOPIC STUDY ON THE INFLUENCE OF POST-PROCESSING ANNEALING ON ZNO FILMS PRODUCED WITH A SOL-GEL METHOD

Ewelina Nowak[1], Mirosław Szybowicz[1], Alicja Stachowiak[2], Edyta Chłopocka[1], Daria Piechowiak[3]

[1] Institute of Materials Research and Quantum Engineering, Faculty of Materials Engineering and Technical Physics, Poznań University of Technology, Poland
[2] Institute of Physics, Faculty of Materials Engineering and Technical Physics, Poznań University of Technology, Poland
[3] Institute of Materials Engineering, Faculty of Materials Engineering and Technical Physics, Poznań University of Technology, Poland
ewelina.k.nowak@doctorate.put.poznan.pl

CANCELLED DUE TO COVID-19

Zinc oxide (ZnO), due to its electrical and optical properties is a promising material for optoelectronic and high power devices. ZnO is a II–VI compound semiconductor with a wide direct bandgap (3.37 eV at room temperature) and large excitation binding energy (around 60 meV). Depending on the specific application, ZnO can be used in the form of powder, nanostructures or single crystals. However, the most popular way to achieve material for electronic purposes is growing of thin layer [1].

In most cases, thin layers of ZnO tend to form zinc blend or wurtzite structure crystallites from an amorphous phase in high temperature [1]. One of the techniques used for ZnO film production is a sol-gel method, which due to ease and low cost of production and deposition, is one of the most popular methods of obtaining functional films for optoelectronics. Unfortunately, besides numerous research focused on the properties of acquired layers [2], the universal method of achieving repeatable samples is still not developed. One of the main problems in production is the appearance of native defects. Undoped ZnO usually contains various intrinsic defects such as Zn vacancies, interstitial Zn, O vacancies, interstitial O, and antisite O. These intrinsic defects form either acceptor level or donor level in the bandgap and greatly affect the optical and electrical properties of ZnO [2].

Moreover, in the growth of ZnO layers, besides native defects, we should take a glance at the behavior of grain growth during the annealing process, which is the basic procedure due to getting rid of organic substances and recrystallization of layers [3]. Understanding the course of the recrystallization process – with special consideration of the influence of the crystal growth kinetics on the substrate's orientation and the presence of defects – seems to be one of the main goals in the development of methods for sol-gel synthesis of thin films on amorphous substrates [3].

The presented research is a comprehensive study on the influence of post-processing annealing on ZnO films produced with a sol-gel method. The main issue was to prepare the sol-gel spin-coated layers in exact same conditions and anneal them in different temperatures and at a different time rate. The purity and chemical composition of samples were investigated with the X-ray photoelectron spectroscopy (XPS). The quality and structure were determined by x-ray diffraction. Complementary measurements, which enabled to estimate the grain sizes and orientation, were conducted with Raman microscopy at room temperature.

Due to the process of the reorientation and growth of crystallites, the defects may be introduced into the material, which leads to fine-tuning the electrons states. That is why for complementary information UV-VIS absorption and photoluminescence measurements were conducted.

This research was funded by the Ministry of Science and Higher Education of Republic of Poland.

[1] C. F. Klingshirn, ZnO: Material, physics and applications, ChemPhysChem **8**, 6, 782–803, 2007
[2] J.C. Fan, et al., P-Type ZnO materials: Theory, growth, properties and devices, Progress in Materials Science. **58,** 2013
[3] L. Znaidi, Sol-gel-deposited ZnO thin films: A review, Mater. Sci. Eng. B Solid-State Mater. Adv. Technol. **174**, 18–30, 2010
[4] O. Schmidt et al., Effects of an electrically conducting layer at the zinc oxide surface, Jpn. J. Appl. Phys. **44**, 7271–7274, 2005

FROM FEMTO TO MICROSECONDS - DYANMIC PHOTOPHYSICS OF NONFULLERENE ORGANIC SOLAR CELLS

Rokas Jasiūnas[1], Huotian Zhang[2], Andrius Devižis[1], Feng Gao[2], Vidmantas Gulbinas[1]

[1]Department of Molecular Compound Physics, Center for Physical Sciences and Technology, Saulėtekio av. 3, LT-10257 Vilnius, Lithuania

[2]Department of Physics Chemistry and Biology (IFM), Linköping University, Linköping SE-58183, Sweden

rokas.jasiunas@ftmc.lt

Organic photovoltaics (OPV) has been steadily progressing as one of the alternative solar energy-harvesting technology, ever since their first appearance over three decades ago [1]. Favorable properties such as lightness, flexibility, transparency and low-cost encouraged the research in materials design, device engineering and photophysical processes study. Even though one of the main photovoltaic parameter, solar-to-electrical power conversion efficiency (PCE), has remarkably increased since OPV appearance, now exceeding 16% for single-junction OPV devices, yet it falls behind state-of-the-art silicon or perovskite photovoltaic technology [2]. In recent years, the inventive substitution of well-established fullerene type acceptors by small low-bandgap molecules has led to a significant PCE increase. Such gain was enabled by numerous advantages of non-fullerene (NF) molecules over fullerene-based acceptors, including a broader absorption spectrum, which leads to higher short-circuit current and tunability of energy levels, enabling the open-circuit voltage gain. The superior photovoltaic performance of NF based OSCs is also believed to originate from the favorable morphology and charge dynamic properties in blends; however, the understanding of the latter is still very obscure and requires more in-depth investigation.

In this work, we use several time-resolved electro-optical measurement techniques covering an exceptionally wide time span (from sub-ps up to μs) to study the whole life cycle of photogenerated charge carriers, starting with their generation and finishing with extraction. We intently inquire into carrier mobility kinetics and disentangle geminate and nongeminate recombination processes in various bulk heterojunction systems. We comparatively investigated OPV systems comprising the well established PBDB-T donor molecule blended with either novel NF acceptor Y1 or archetypal $PC_{71}BM$ acceptor. Additionally, were investigated, BHJ systems based on benchmark NF acceptor ITIC with PBDB-T-2Cl and PDCBT-2F donor materials specifically chosen to have small HOMO level offsets.

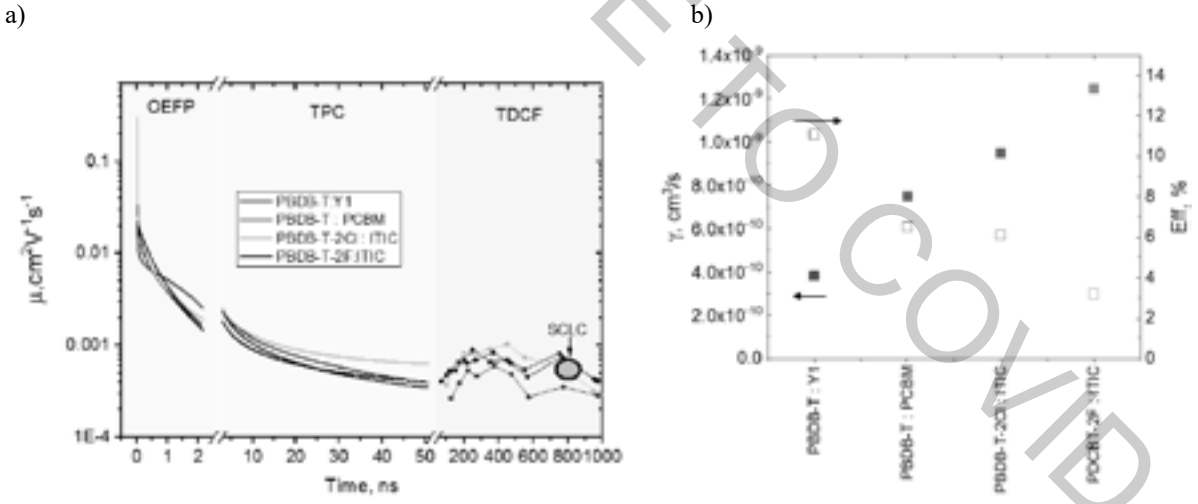

Fig. 1. a) Mobility kinetics of indicated OPV devices, obtained by optical electric-field probing (OEFP), transient photocurrent (TPC), time-delayed collection field (TDCF) measurement techniques. The black dot indicates PBDB-T:Y1 mobility value obtained by surface-charge limited current technique. b) Bimolecular recombination rate and power conversion efficiency values for indicated devices.

[1] Inganäs O. Organic Photovoltaics over Three Decades. Advanced Materials **30(35)**, 1800388, (2018).

[2] Fan B, Zhang D, Li M, et al. Achieving over 16% efficiency for single-junction organic solar cells. Sci China Chem. **62(6),** 746-752 (2019).

CANCELLED DUE TO COVID-19

ENERGY GENERATION FROM VEHICLE VIBRATIONS USING SMART DAMPER

Tadas Lenkutis[1], Andrius Dzedzickis[1], Barbora Kačinskaitė[1], Dainius Kunkis[1], Vytautas Bučinskas[1]

[1] Department of Mechatronics, robotics and digital manufacturing, Vilnius Gediminas technical university
tadas.lenkutis@vgtu.lt

CANCELLED DUE TO COVID-19

Vibrations energy is one of the biggest unused energy sources in nowadays engineering. This happens, because collecting energy from vibrations is uncommon task and requires non-standard solutions. This paper presents shock absorber construction that has implemented energy generation function and can fulfill vibrations energy generation task.

Vibrations in vehicle appears then vehicle tire contacts road [1]. More then 100 years these vibrations were named as harmful and only solution to avoid them was to absorb the energy and dissipate it as heat. Possibility to collect vibrations energy can lower travel energy costs from 2 % to 10 %, depending on vehicle type [2]. The biggest challenge is to convert energy only few shock absorbers types prevails in researches: Mechanical shock absorbers, where linear movement is changed to rotary by pinion gear [3] and Magnetic absorbers [4].

Our proposed solution is shock absorber with magneto-rheological fluid. Magneto-rheological fluid also known as smart fluid consists of two main elements: oil and magnetic parts. The main feature of smart fluid is that then magnetic field is applied the magnetic parts in fluid organizes and fluid gets thicker. In our case the smart fluid performs three tasks: holds permanent magnetic field for energy generation, lubricates the system and allows to change shock absorbers damping coefficient.

For experimental research were created prototype of shock absorber, which is shown in fig. 1 A. where: 1 – frame; 2 – solenoid coil; 3 – piston stem for force application; 4 – piston; 5 – smart fluid; 6 – fixing eye; 7 – compensating spring; 8 – air piston. This prototype was created for generated energy size determination. Experiments were performed using test rig SPA PSD 2004. Prototype was tested in various regimes applying two different excitation amplitudes: 25 mm and 50mm and frequencies: 1 Hz, 2 Hz, 3 Hz, 4 Hz, 5 Hz, 5,5 Hz, 6 Hz, 6,5 Hz, 7 Hz, 7,5 Hz. Generated voltage was measured in two coils (1st and 3rd from top) obtained results are shown in fig. 1 B.

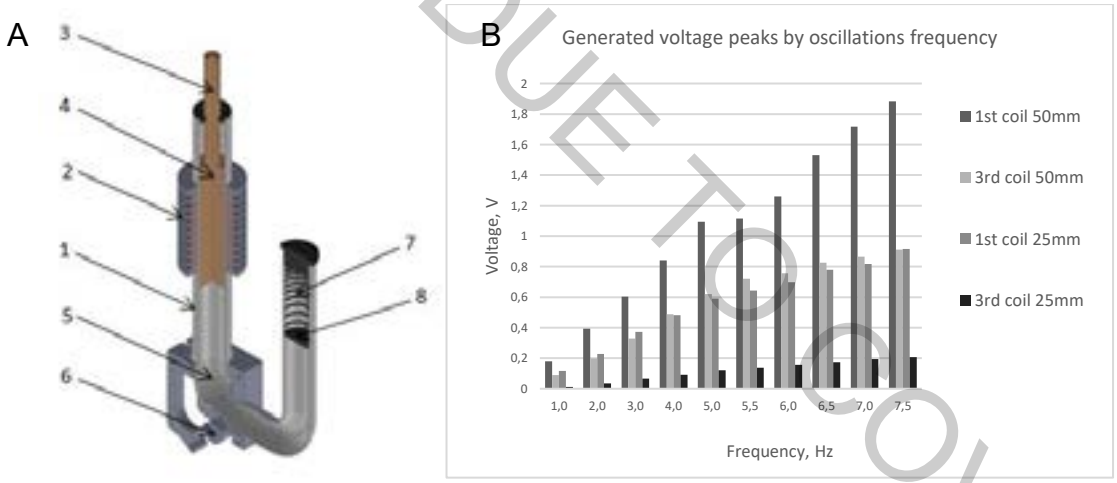

Fig. 1. A- Experiments prototype, B – Energy generation results.

Performed experimental research revealed many interesting effects of implementing such design of the shock absorber. Firstly, this type of liquid core generator can operate and it is really functional. Secondly, obtained voltages are enough high, and this proves that amount of energy harvested from vehicle vibrations is significant and can be used for a variety of purposes, for example powering sensors in autonomous vehicles. In the other hand, many features of this type of electric machines are unknown and need to be further researched.

[1] A. Kumar, A. Dwivedi, H. Jaiswal, and P. P. Patil, "Material-Based Vibration Characteristic Analysis of Heavy Vehicle Transmission Gearbox Casing Using Finite Element Analysis ", Intelligent Computing, Communication and Devices, Springer pp. 527-533, 2015.
[2] M. A. Abdelkareem, L. Xu, M. K. A. Ali, A. Elagouz, J. Mi, S. Guo and L. Zuo, "Vibration energy harvesting in automotive suspension system: A detailed review", Applied energy, vol. 229, pp. 672-699, 2018.
[3] Z. Li, L. Zuo, G. Luhrs, L. Lin and Y. X. Qin, "Electromagnetic energy-harvesting shock absorbers: design, modeling, and road tests". IEEE Transactions on vehicular technology, vol. 62, no. 3, pp. 1065-1074, 2012.
[4] B. Sapiński, "Energy-harvesting linear MR damper: prototyping and testing", Smart Materials and Structures, vol. 23 no. 3, 2014.

IRRADIATION INFLUENCE ON THE SPATIAL DISTRUBUTION OF PHOTOLUMINESCENCE IN OPTICAL FIBERS

Živilė Čerškutė[1], Augustas Vaitkevičius[1], Andrei Stancalie[2], Gintautas Tamulaitis[1]

[1]Institute of Photonics and Nanotechnology, Vilnius University, Lithuania
[2] Center for Advanced Laser Technologies, National Institute for Laser Plasma and Radiation Physics, Romania
zivile.cerskute@ff.stud.vu.lt

CANCELLED DUE TO COVID-19

Optical fibers sometimes have to be exploited in environment affected by strong ionizing radiation. Therefore, radiation tolerance is an important parameter for such fibers. On the other hand, sensitivity to irradiation might be exploited for monitoring of the radiation. In this work, we analyzed the influence of the irradiation on the properties of optical fibers of various types by studying the radiation influence on the spatial distribution of photoluminescence (PL).

The experiment was performed using confocal microscope *Witec Alpha 300s*. All of the samples were excited with *Alphalas* laser emitting at 405 nm. PL signals were analyzed by a spectrometer and registered by a thermoelectrically coolled CCD camera. The spatial PL parameters were analyzed in commercially produced fibers of 6 different types: DRAKA SMF, DRAKA MMF, Nufern, Nufern RI310 HTA, Ver-MMF-50-4-P-12, and VIP-125-3. For all 6 types, two samples have been prepared. One of them was irradiated, whereas the second one was virgin.

Typical results for fibers of two types, VIP-125-3 and DRAKA MMF, are presented in Figs. 1 and 2, respectively. Optical fiber VIP-125-3 consists of two layers: a core is surrounded by a coating layer. As evident in Fig. 1, the spectra of this fiber has significantly changed after being exposed to intense irradiation. The irradiation results in a blue shift of the main emission band of the fiber by 120nm.

The optical fiber DRAKA MMF has three layers: the core in this fiber is surrounded by inner and outer coatings. As seen in Fig. 2b, the radiation has no impact on the peak position of PL in high intensity areas of fiber cross section. The PL band is peaked at ~475nm.

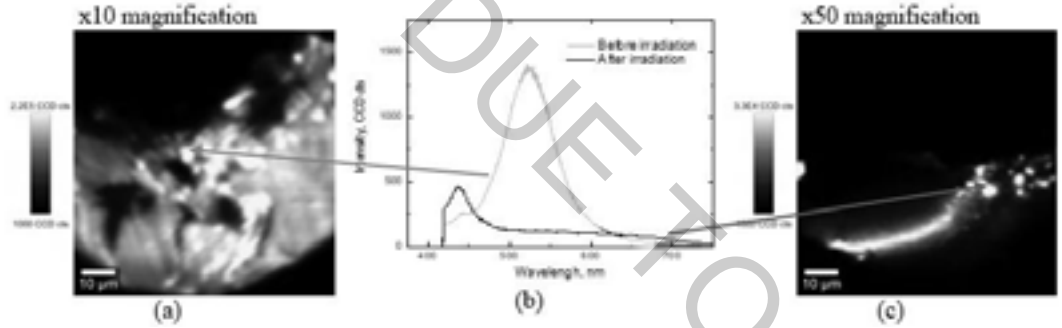

Fig. 1 Spatial distribution of PL intensity in virgin (a) and irradiated (c) optical fiber VIP-125-3 and PL spectra (b) from high brightness areas indicated by arrows.

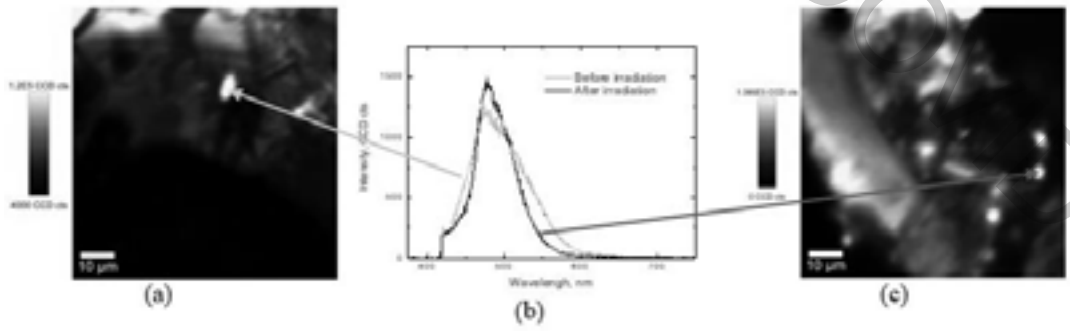

Fig. 2 Spatial distribution of PL intensity in virgin (a) and irradiated (c) optical fiber DRAKA MMF and PL spectra (b) from high brightness areas indicated by arrows.

Our results show that DRAKA MMF fibers exhibit a high radiation tolerance and might be exploited in harsh irradiation environments. Meanwhile both intensity and band position of PL band in VIP-125-3 is sensitive to irradiation. Thus, this type of fiber might be used for measuring irradiation dose. Fibers of other four types are also analyzed from this point of view.

STRUCTURE DETERMINATION OF *HEWL* PROTEIN AGGREGATES ADSORBED AT WATER AND PHOSPHOLIPID MONOLAYER INTERFACES

Edvinas Navakauskas[1] and Simona Strazdaitė[1]

Center of Physical Sciences and Technology, Department of Organic Chemistry, Saulėtekis ave. 3, LT-10257 Vilnius
Edvinas.Navakauskas@ftmc.lt

Protein aggregation is associated with more than 30 different human diseases including Alzheimer's, Parkinson's, Huntington's and others. Each of these diseases is caused by the aggregation of a particular protein, which is a normal product of a cellular metabolism, however, it starts to aggregate when production and elimination cycle is disrupted.

In order to understand protein aggregation at the molecular level, it is essential to identify the structure of protein aggregates. Many different methods are used for this purpose, for example: nuclear magnetic resonance (NMR), Fourier-transform infrared (FTIR) and Thioflavin T fluorescence (ThT) spectroscopies. These methods can only characterize the structures formed in the volume of the solution. Meanwhile, the most recent studies suggest that interaction between protein and cell membrane can accelerate protein aggregation. Thus the characterization of structures at the surface of the liquid, especially at the Lipid/Water interface, remains a major subject of the protein aggregation research. Vibrational sum frequency generation (VSFG) spectroscopy enables the detection of a single molecular layer adsorbed at any liquid surface and structure determination of the adsorbed molecules.

This paper seeks to understand and compare the adsorption behavior of hen egg white lysozyme (HEWL) and its aggregates at Air/Water and Lipid/Water interfaces. HEWL is used as a model protein to study the adsorption of aggregates and their structure. In our study Fourier transform infrared spectroscopy and atomic force microscopy (AFM) served as tools to verify the structure of lysozyme aggregates formed in the bulk solution and their morphology. Whereas measurements at Air/Water and Lipid/Water interfaces were performed using VSFG spectroscopy. In both cases, the aggregated lysozyme solution was injected below the interface. Different combinations of VSFG beam polarization were used to determine the structures of protein aggregates adsorbed at the interfaces. We found that protein in disordered form together with small aggregates, such as dimers and trimers, and larger aggregates with parallel and anti-parallel β-sheet structures, were adsorbed at both interfaces. However, adsorbtion had a very different kinetics. Adsorbtion at Air/Water interface was mainly governed by hydrophobic interaction, whereas at Lipid/Water interface, electrostatic interaction was the main driving force for adsorbtion with a possible contribution of a hydrophobic interaction as well.

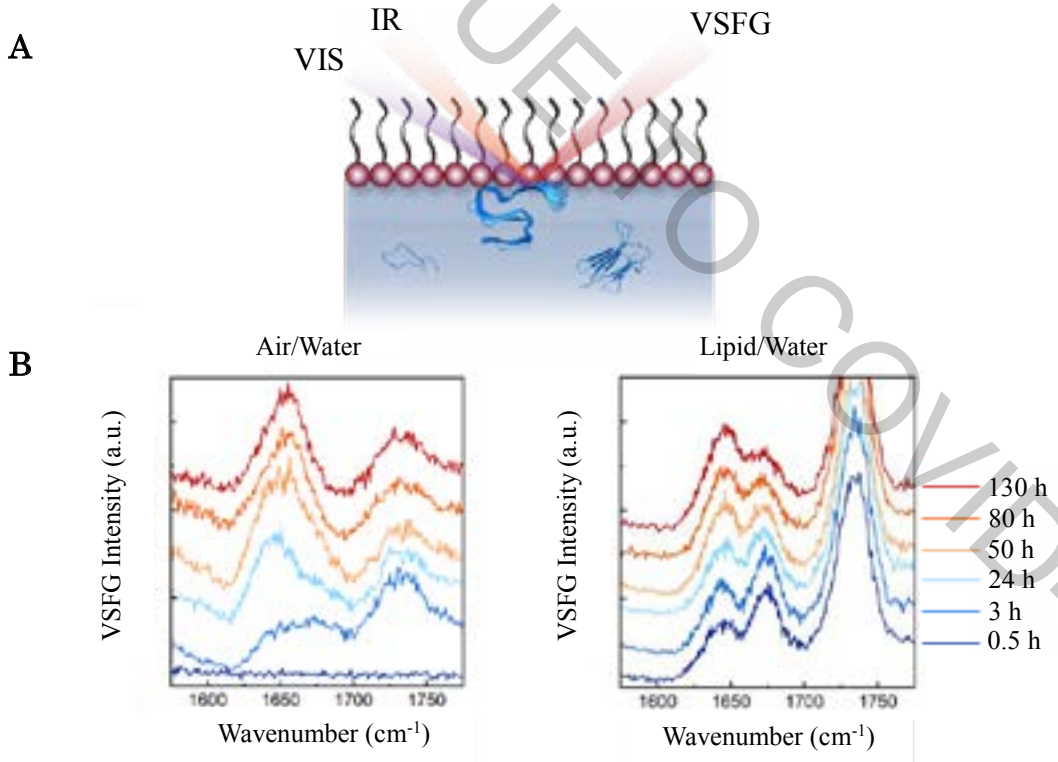

Fig. 1 (A) Schematics of the VSFG experiment **(B)** The VSFG spectra of HEWL and its aggregates adsorbed at Air/Water and Lipid/Water interfaces in Amide I vibrational region. Different spectra correspond to aliquots that were heated for various times (see the legend).

CANCELLED DUE TO COVID-19

POTENTIOMETRIC CO_2 SENSOR FOR CREW CABIN AIR QUALITY MONITORING

Juzef Kučinski[1], Beomseok Kim[2], Jin-Woo Han[2], Mindaugas Gicevičius[1], Lina Mikoliunaitė[1], Meyya Meyyappan[2]

[1] Faculty of Chemistry and Geosciences, Vilnius University, Lithuania
[2] Center for Nanotechnology, NASA Ames Research Center, USA
juzef.kucinski@gmail.com

CANCELLED DUE TO COVID-19

Monitoring pressure, temperature and the concentration of carbon dioxide on International Space Station (ISS) is an integral part of keeping astronauts safe and preventing any possible accidents. The level of CO_2 on ISS is a few times higher than normal CO_2 concentration on Earth because of the limitations of technology as well as limited space. That is why even a slight increase in the concentration of carbon dioxide can result in headaches, sleepiness and tiredness of the orbital station inhabitants. Due to these reasons, constant monitoring of CO_2 levels at various points of cabin is of crucial importance for successful operation of ISS and the well-being of its crew.

There are numerous reported gas sensors that can detect low levels of CO_2 in comparably short amount of time, however, there are few issues that must be addressed: long term stability, effects of relative humidity (R.H.) on sensor response (SR), high power consumption, bulkiness and high cost. Infrared spectroscopy based gas sensors are commonly used in CO_2 level detection, although they have several drawbacks, such as large size and high cost. This creates a demand for inexpensive, maintenance-free and easy-to-make CO_2 sensors, whose development is reported in this work.

The developed sensor is based on metal/metal oxide working electrode, solid state Ag/AgCl reference electrode and gel electrolyte [1]. Gel electrolyte used in the sensor is composed of glycerol or ethylene glycol as a humectant that absorbs water from air even at low levels of R.H. This makes sensor resistant to drying out under low humidity conditions. Alongside H_2O vapor, carbon dioxide is absorbed into the electrolyte as well. Carbon dioxide reacts with OH^- to form a stable HCO_3^-, in turn lowering the pH of the electrolyte (Eq. 1). Metal/metal oxide electrodes are known for having pH-

$$H_2O + CO_2 \leftrightarrow HCO_3^- + H^+ \quad (1)$$

dependent electrochemical potential, for this reason they are commonly used as working electrodes for pH sensors. The electrochemical potential of Ti/TiO_2 electrode changes with respect to the pH of the media (Eq. 2), whereas the reference

$$E = E^0_{Ti,TiO_2,H^+} - 2.303\frac{RT}{F}pH \quad (2)$$

Ag/AgCl electrode potential is independent of pH. As Cl^- ions are sealed with layers of Nafion, it can be assumed that the electrochemical potential of Ag/AgCl electrode remains stable throughout the measurement. From the registered potential difference between the sensing and the reference electrodes, sensor response can be derived and calculated.

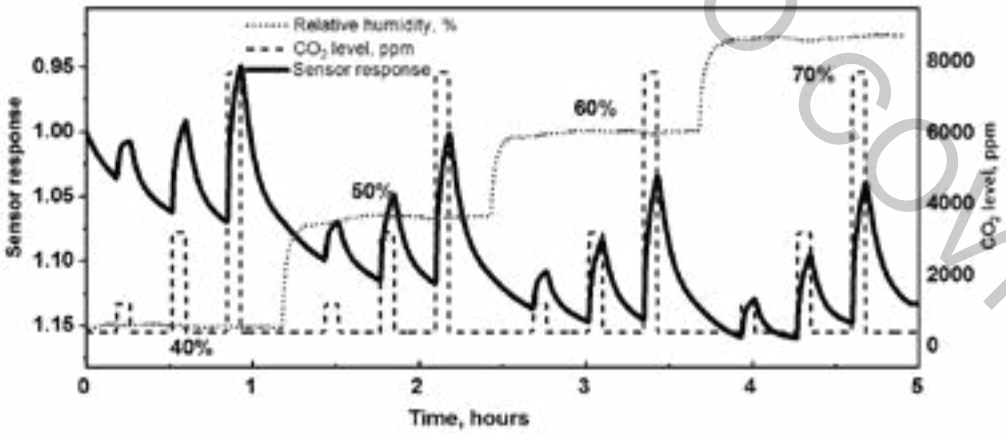

Fig. 1. Sensor response graph as a function from relative humidity and carbon dioxide level.

The main focus of this research was to determine the optimal composition of gel electrolyte. Different electrolytes (salts, acids, bases), humectants and concentrations of the aforementioned components were tested and formula with best sensor response was chosen to use for further research.

[1] Bhadra, S., Thomson, D. J., & Bridges, G. E. (2015). Sensors and Actuators B : Chemical Monitoring acidic and basic volatile concentration using a pH-electrode based wireless passive sensor. Sensors & Actuators: B. Chemical, 209, 803–810. https://doi.org/10.1016/j.snb.2014.12.021

AIR INDUCED CHANGES IN SURFACE PROPERTIES IN GRAPHENE-METAL CONTACTS AND LONG DISTANCE DISTORTIONS IN THE GRAPHENE NEAR THE EDGE OF PLANAR METAL CONTACTS

Andrius Sakavicius, Gvidas Astromskas, Virginijus Bukauskas, Mindaugas Kamarauskas, Algimantas Luksa, Viktorija Nargeliene, Gediminas Niaura, Ilja Ignatjev, Marius Treideris, Arunas Setkus

Center for Physical Sciences and Technology, Sauletekio av. 3, 10257 Vilnius, Lithuania
andrius.sakavicius@ftmc.lt

CANCELLED DUE TO COVID-19

The variation of electrical, surface charge and strain properties of CVD graphene based Au and Ni contacts were investigated after samples were exposed to air. Long thermal treatment of samples was performed to compensate the atmospheric influence in graphene structures, moreover thermal process induced changes were investigated analyzing the changes of strain and doping in graphene sheet. Raman spectroscopy and Kelvin force probe microscopy were exploit to observe charge doping, strain and work function in graphene on SiO_2 substrate and metal films. Values of these characteristics before and after sample thermal treatment were compared.

The properties of the planar junction between graphene layer and thin film metal structures are important for formation of the electronic devices integrating the structures of the two-dimensional materials. However, the properties of the graphene-metal contacts are still weakly controlled in the large area device fabrication. We demonstrated an approach acceptable to characterise the long distance distortion area produced by the metal contact edges in the graphene monolayer. The systematic analysis of the Raman maps of the graphene is performed aiming to describe the changes in the graphene monolayer produced by the technology dependent parameters in the planar structures used for the measurements by the circular transmission line method. It was proved that Au contacts produce the compressive strain in the graphene layer in the distances up to about 2-4 μm from the contact edges. The transition between the n and p-type of the doping is combined with the compression strain in the long distance graphene distortion area close to the Ni-contact edges. An equivalent electrical circuit is proposed for description of the graphene distortion area near the contact edges.

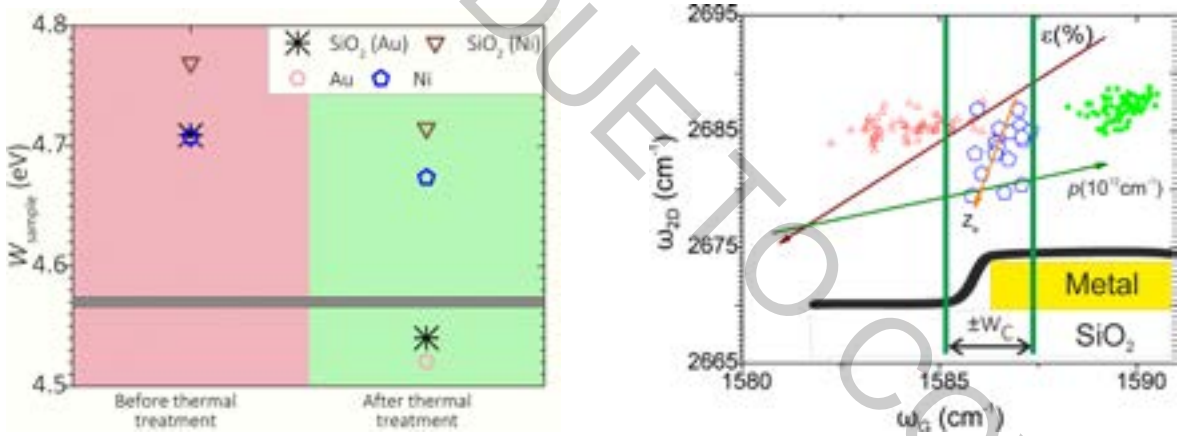

(a) (b)

Fig. 1. (a) Dependence of work function W_{Gr} on thermal process on different surfaces. Symbols depict the variation of work function of graphene on SiO_2 substrate, Au and Ni films. (b) Correlation between ω_{2D} and ω_G Raman modes of metal-graphene CTLM structures. Raman map was scanned on SiO_2 substrate, contact transition zone and metal film.

The largest decrease of W_{Gr} of CVD graphene observed in Au contacts. Raman analysis indicated the increase of p-type doping in graphene on metal films (on both Au and Ni). Graphene on SiO_2 substrate demonstrated higher values of p-type doping. The correlation between doping in graphene layer and variation of resistance implicated the idea that atmospheric induced changes occur mainly in graphene layer on SiO_2 substrate. Graphene doping and strain changes caused by exposing to air on metal films were minor.

Based on the principles of the method it was demonstrated that the metal contact edges produce the changes in the properties of the graphene monolayer at sufficiently large distances from the edges. The distortion of the graphene can be identified at the distances from 2 μm to more than 8 μm. The compressive strain was detected for all the samples in the close vicinity of the contact edges.

[1] In press: A. Sakavicius, G. Astromskas, V. Bukauskas, M. Kamarauskas, A. Luksa , V. Nargeliene, G. Niaura , I. Ignatjev, M. Treideris and A. Setkus, Thin Solid Films, 2020, https://doi.org/10.1016/j.tsf.2020.137850

STRIVING FOR EFFICIENT NIR-TO-VIS UPCONVERSION: LIMITING FACTORS IN RUBRENE-BASED SYSTEMS

Edvinas Radiunas[1], Manvydas Dapkevičius[1], Steponas Raišys[1], Saulius Juršėnas[1], Augustina Jozeliūnaitė[2], Tomas Javorskis[2], Ugnė Šinkevičiūtė[2], Edvinas Orentas[2], Karolis Kazlauskas[1]

[1]Institute of Photonics and Nanotechnology, Vilnius University, Lithuania
[2]Department of Organic Chemistry, Vilnius University, Lithuania
edvinas.radiunas@ff.vu.lt

CANCELLED DUE TO COVID-19

The growing interest in triplet-triplet annihilation (TTA) mediated light upconversion (UC) utilizing organic compounds is associated with potential applications in photocatalysis, bioimaging, stress sensing, night vision, memory devices, photovoltaics, targeted drug delivery and many others [1-2]. Although numerous efficient UC systems with a quantum yield (Φ_{UC}) of up to ~30% were demonstrated in the visible (vis) spectral region, only a handful of molecular systems was shown to produce near-infrared-(NIR)-to-vis UC with Φ_{UC} above 2%. Lack of efficient IR-to-visible UC devices is partly attributed to a limited number of efficient triplet sensitizers in the IR range, which suffer from large non-radiative losses [3]. Another less studied issue in such systems is related to low statistical factor (f) representing probability to obtain a singlet from two emitter triplets via TTA.

In this work, we investigate limiting factors of NIR-to-vis UC in the systems consisting of novel (Pd,Pt)phthalocyanine (Pc) sensitizers coupled with most popular TTA emitter rubrene (Rub). The study focuses on UC in both liquid as well as rigid environment best suited for practical application. Rubrene is additionally modified with tert-butyl side groups to preserve high emission quantum yield (Φ_{FL}) at high concentrations, which are required for efficient triplet diffusion and TTA. Since the UC systems are sensitive to oxygen, all UC samples were fabricated and encapsulated in nitrogen ambient (with O_2 and H_2O level < 0.1 ppm). Sensitizer and emitter concentrations were varied to obtain efficient triplet transfer that was estimated to be up to 82%. A key limiting factor in the optimized liquid UC systems was found to be rubrene's low statistical probability (f = 15.5±3%) to obtain a singlet from two triplets via TTA (see Fig. 1). Modified t-butyl-rubrene demonstrated 3-fold lower statistical factor (f = 5.3±1%) as well as reduced triplet energy transfer (Φ_{TET}=52%) and thus lower Φ_{UC}. Interestingly, the opposite result was obtained in rigid films. The 4-fold higher UC efficiency of t-butyl-rubrene films was determined by reduced singlet fission and thus higher Φ_{FL}. The obtained results strongly encourage to search for new alternatives to popular rubrene emitter.

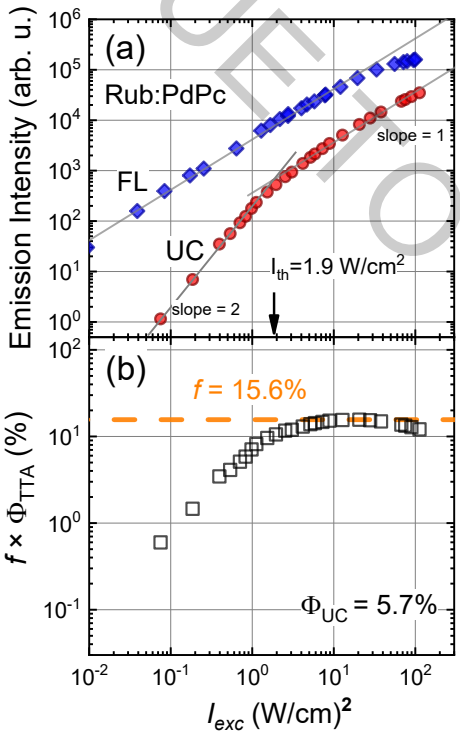

Fig. 1. a) Fluorescence and UC intensities under CW excitation at 485 nm and 730 nm, respectively, as a function of excitation power density for Rub (18mM):PdPc (15μM) in toluene. UC threshold values (I_{th}), indicated. b) Excitation dependences of the product [$f \cdot \Phi_{TTA}$] of the same system. f values, indicated.

[1] J. Zhou, Q. Liu, W. Feng et al., Upconversion luminescent materials: advances and applications, Chemical Reviews **115**, 395-465 (2015).
[2] S. Wen, J. Zhou, J. Schuck et al., Future and challenges for hybrid upconversion nanosystems , Nature Photonics **13**, 828-838 (2019).
[3] R. Englman, J. Jortner, The energy gap law for radiationless transitions in large molecules, Molecular Physics, **18**, 145-164 (1970).

OPTIMIZATION OF SELECTIVE LASER ETCHING PROCESS FOR ARBITRARY SHAPE 3D MICRO-STRUCTURE FABRICATION

Agnė Butkutė[1,2], Tomas Baravykas[2], Titas Tičkūnas[1,2], Linas Jonušauskas[1,2], Valdas Sirutkaitis[1]

[1] Laser Research Center, Vilnius University, Lithuania
[2] Femtika, Lithuania
agne@femtika.lt

Glass was proven to be material of choice in multitude of rapidly developed science and engineering fileds. Popularity of this material arises from its superb mechanical properties, being completely transparent for the visible and near infrared (IR) radiation and being chemically inert in organic solvents. While various glass processing techniques exist, most of them are unable to produce required 3D high-fidelity structures out of glass or it is highly complicated. It is limiting the adoption of 3D glass structures in a lot of areas.

One the most promising technology to produce 3D glass structures is selective laser etching (SLE) [1]. Potentially, many types of glasses and crystals can be processed this way. Nevertheless, this process is not exploited widely. The problem lies in the complex nature of light-matter interaction and challenges in optimising the technique for true 3D fabrication. Laser parameters, translation velocity, etchant concentration and etching time are all important factors that cannot be disregarded [2,3]. Thus, overall, while the premise of SLE is simple, so far realisation was proven to be rather complicated.

The aim of this work is to uncover the ways to simplify the production methodology of SLE while still maintaining good quality. The improvements of the technique include adoption of circular polarization, high scanning speed (a few cm/s) , KOH etching and high-spacing between scaning lines in all space directions which in turn both simplify and accelerate the processing. The methods are employed to manufacture complex microfluidic systems and assembly-free micromechanical structures. These include various channels, deformable 3D objects, chainmail-like structures, flexible structures with ball joints, and freely rotatable gears (e.g. *Geneva mechanism*) (fig. 1). All of these structures are evaluated qualitatively and quantitatively showing that simplified fabrication techniques do not compromise quality or functionality of the structures. The smooth rotation of the mechanism is enabled by capability to produce such glass structures with a few micrometers tolerances. The acquired results are shown in the broader picture, relating it to previous SLE works, additive manufacturing and potential application areas.

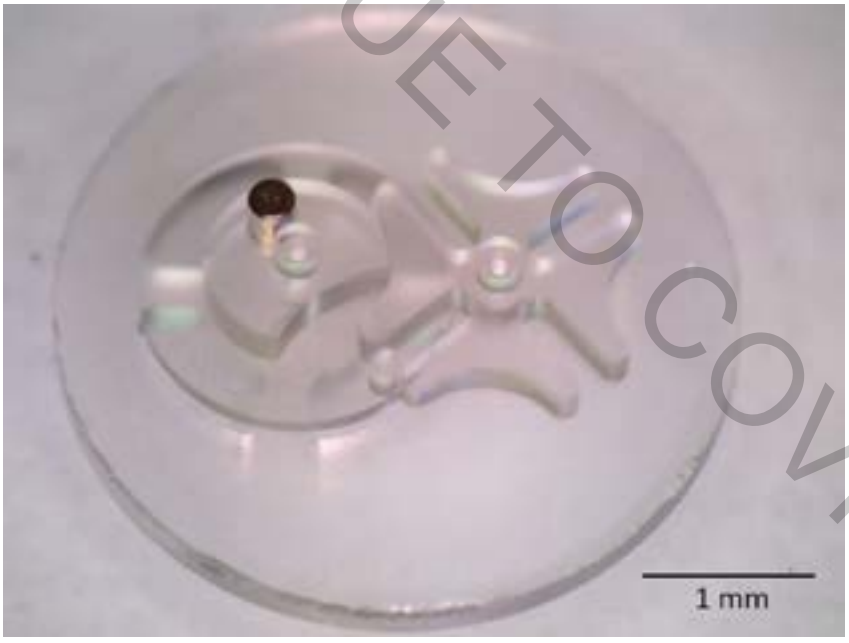

Fig. 1. Photo of free rotateable asemble-free Geneva machanism made out of single piece of fused silica by using SLE method.

[1] J. Gottmann, M. Hermans, N. Repiev, J. Ortmann, Selective laser-induced etching of 3D precision quartz glass components for microfluidic applications - up-scaling of complexity and speed, Micromachines **8**(4), 110 (2017).
[2] C. A. Ross, D. G. Maclachan, D. Choudrury, R. R. Thomson, Optimisation of ultrafast laser assisted etching in fused silica, Opt. Express **26**(19), 24343 - 24356 (2018).
[3] S. Butkus, M. Rickus, R. Sirutkaitis, D. Paipulas, V. Sirutkaitis, Fabrication of high aspect ratio channels in fused silica using femtosecond pulses and chemical etching at different conditions, J. Laser Micro. Nanoen. **14**(1), 19 - 24 (2019).

CANCELLED DUE TO COVID-19

SURFACE ANALYSIS OF TITANIUM ALLOY Ti-6Al-4V ELI WITH OCTADECYLPHOSPHONIC ACID (ODPA) AND HYDROXYAPATITE (HA) LAYERS

Joanna Szczuka[1], Tomasz Buchwald[1], Mariusz Sandomierski[2]

[1] Institute of Materials Research and Quantum Engineering, Poznan University of Technology, Poland
[2] Institute of Chemical Technology and Engineering, Poznan University of Technology, Poland
joanna.p.szczuka@doctorate.put.poznan.pl

CANCELLED DUE TO COVID-19

Titanium alloy Ti6Al4V ELI, made in accordance with ASTM F 136/1472 standards [1] is recommended for surgical applications [2], including for the construction of endoprostheses. It has very good mechanical properties such as low density and corrosion resistance. Unfortunately, due to doping with toxic elements - Al, V [3], modification of its surface is very important [4]. The aim of the project is to optimize the surface modification process of Ti6Al4V ELI with phosphonic compounds. It has already been proven that octadecylphosphonic acid (ODPA) (fig. 1.) shows sorption with hydroxyapatite (HA) (fig. 2.) – bone building material [5]. Titanium alloy and phosphonium compounds are very common in medicine [6]. There are many publications on their properties or specific applications [7]. However, no research could be found that would accurately describe the manner in which the monolayers would arrange on the surface of the titanium alloy as well as the subsequent interaction with hydroxyapatite.

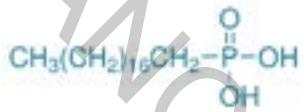

Fig. 1. the ODPA

Fig. 2. the hydroxyapatite

Ti-6Al-4V ELI titanium alloy plates measuring 30 mm x 15 mm x 11 mm (from Wolften) were used for the tests, (percentage alloy composition: Fe – 0.12; V – 3.85; Al - 6.15; C - 0.008; O – 0.13; N – 0.004; Y - <0.0004; Ti - 89.74). Current research has focused on creating an ODPA layer on the surface of the titanium alloy plate and then creating the HA layer through the crystallization process. The application of the ODPA layer consisted of complete evaporation of the solvent – THF. Figures 3 and 4 show the difference before and after ODPA application on the plate surface.

For analysis of Ti-6Al-4V ELI surface modified with ODPA and HA, inVia confocal Raman microscope (Renishaw) was used, with a 785 nm beam laser and 50x and 100x magnification lenses. To confirm the correctness of the results, measurements using Fourier-transform infrared spectroscopy (FTIR) were carried out for the same samples. In addition, to check the wettability of the surface, contact angle measurements were realized. The obtained results confirm the presence of ODPA together with HA on the surface of the titanium alloy plate.

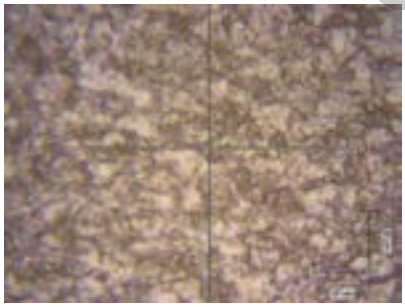

Fig. 3. Ti-6Al-4V ELI surface at 50x magnification, before applying the ODPA layer

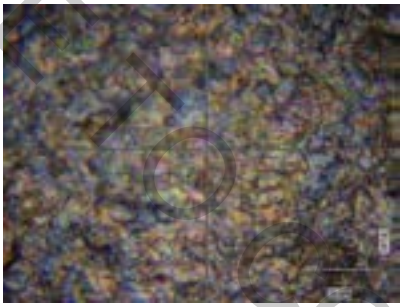

Fig. 4. Ti-6Al-4V ELI surface at 50x magnification, after applying the ODPA layer

Acknowledgments: This research was funded by the Ministry of Science and Higher Education of the Republic of Poland

[1] ASTM, Standard Specification for Wrought Titanium-6Aluminum-4Vanadium ELI (Extra Low Interstitial) Alloy for Surgical Implant Applications (UNSR56401).
[2] L.Under. Osseointegration of metallic implants: I. Light microscopy in the rabbit. Acta Orthopaedica Scandinavica, 1989, 60.2: 129-134.
[3] Niinomi, Mitsuo. Recent titanium R&D for biomedical applications in Japan. Jom 51.6 (1999): 32-34
[4] W.Liu, et all. Surface Modification of Biomedical Titanium Alloy: Micromorphology, Microstructure Evolution and Biomedical Applications. Coatings, 2019, 9.4: 249
[5] M. Pietrzyńska. Experimental and in silico investigations of organic phosphates and phosphonates sorption on polymer-ceramic monolithic materials and hydroxyapatite., European Journal of Pharmaceutical Sciences 93, 2016, pp. 295-303
[6] M.Yoshinari, et all. Bone response to calcium phosphate-coated and bisphosphonate-immobilized titanium implants. Biomaterials, 2002, 23.14: 2879-2885
[7] N. Adden, et all. Phosphonic acid monolayers for binding of bioactive molecules to titanium surfaces. Langmuir, 2006, 22.19: 8197-8204.

BALANCING LAYER STABILITY AND EFFECTIVE LUMINESCENCE IN $PEA_2FA_{n-1}Pb_nBr_{3n+1}$ 2D PEROVSKITES.

Džiugas Litvinas[1], Saulius Juršėnas[1], Toshinori Matsushima[2], Chihaya Adachi[2].

[1]Institute of Photonics and Nanotechnology, Vilnius University, Saulėtekio al. 3, LT-10257 Vilnius, Lithuania
[2]Center for Organic Photonics and Electronics Research (OPERA), Kyushu University, 744 Motooka, Nishi, Fukuoka 819-0395, Japan
dziugas.litvinas@ff.stud.vu.lt

CANCELLED DUE TO COVID-19

Hybrid perovskites are attractive due to their high carrier mobility [1], diffusion length [2], large crystal grains, tunable bandgap and inexpensive production via spin-coating. Impressive results have been demonstrated in conditions similar to those in optically-pumped lasers [3], [4]. In spite of this, the perovskite phase can degrade rapidly due to humidity and high excitation density induced ion migration. To increase stability for applications the 2D perovskite (2DP) phase has been developed. Organic ligand layers in 2DP separate crystalline perovskite nanosheets of average thickness n (in units of lattice period), thus inducing quantum confinement for the generated carriers. This leads to higher bimolecular recombination, however, a reduction in perovskite absorption is present, raising the amplified spontaneous emission (ASE) threshold Δn_{ASE}. In this work, we optimised the 2DP layer dimensionality n for characteristics appropriate to a laser medium in $PEA_2FA_{n-1}Pb_nBr_{3n+1}$ perovskites.

Sample preparation was done in collaboration with Kyushu University. Prior to use, ultrasonication followed by ultraviolet-ozone treatment were used to clean quartz substrates. The precursor solutions consisted of dissolved phenetylammonium bromide (PEABr), formamidinium bromide (FABr) and lead bromide (PbBr) in various ratios. Thus, 2DP dimensionalities of n = 1, 2, 3, 4 and ∞ (3D) were achieved. The spin-coated layers were encapsulated between 2 quartz substrates using epoxy glue.

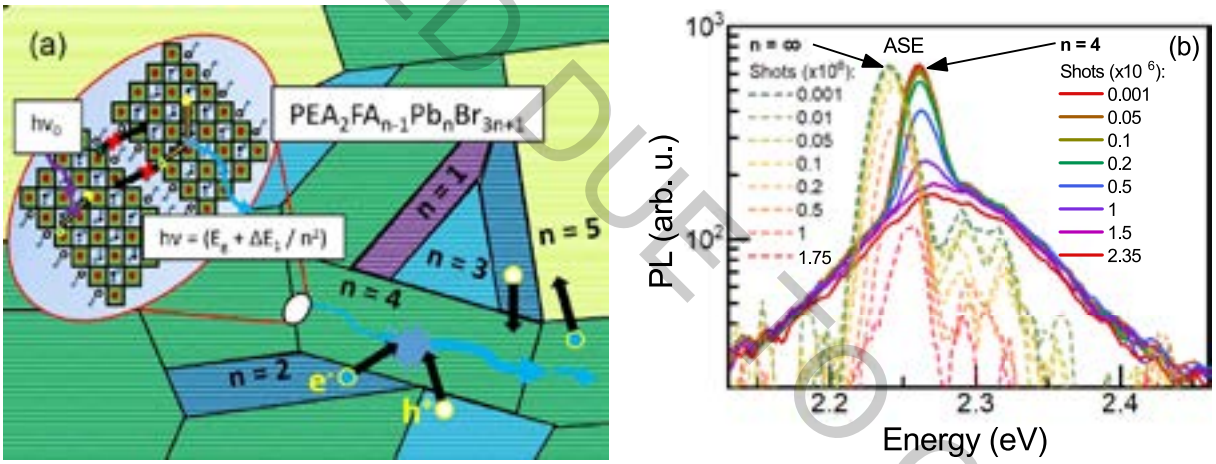

Fig. 1. (a) Illustration of the microscopic crystal domains in the 2D perovskite with various dimensionalities n and the appropriate photo-generated carrier funneling; domain colors roughly correllate with their emission spectra. (b) Degradation of appearing ASE lines in the PL spectra under 350nm excitation ($\Delta n = 2\Delta n_{ASE}$).

As seen in Fig. 1 (a), the 2DP bandgap gets a larger blueshift in lower dimensionalitites n, that is $\Delta E_g \propto 1/n^2$. Also, perovskite domains composed of crystallites with various thicknesses n_{cryst} form in the layers [5], not necessarily $n = n_{cryst}$. This, together with random domain orientations prevents population inversion within a single desired band to appear in the 2DP layers, as excited carriers tend to funnel through crystallite surface boundaries into states of lower energy. Thus, ASE lines with thresholds Δn_{ASE} = 1.72 and 1.53 ($x10^{18}cm^{-3}$) appear in n = 4 and ∞ respectively, i.e. in samples of smaller quantum confinement, more beneficial for a homogenous phase to form. Even though at low excitation intensity samples n = 1, 3 have higher external quantum yields (EQE = 1.1%, 1.7%), at higher excitations (for example, $\Delta n = 2\Delta n_{ASE}$) n = 4 catches up with an EQE ≈ 20%. In addition, the 2DP phase endures longer in an active ASE regime compared to the 3D perovskite (Fig. 1 (b)). So, the 2D perovskite with dimensionality n = 4 seems best fit for the role of a laser active medium, given future domain orientation unification during the production process.

[1] C. Wehrenfennig, G. E. Eperon, M. B. Johnston, H. J. Snaith, and L. M. Herz, "High Charge Carrier Mobilities and Lifetimes in Organolead Trihalide Perovskites," Adv. Mater., **26**, 10, 1584–1589 (2014).
[2] S. D. Stranks et al., "Electron-hole diffusion lengths exceeding 1 micrometer in an organometal trihalide perovskite absorber," Science, **342**, 6156, 341–344 (2013).
[3] S. Yakunin et al., "Low-threshold amplified spontaneous emission and lasing from colloidal nanocrystals of caesium lead halide perovskites," Nat. Commun., **6**, 1, 1–9, (2015).
[4] H. Zhu et al., "Lead halide perovskite nanowire lasers with low lasing thresholds and high quality factors," Nat. Mater., (14), 6, 636–642, (2015).
[5] M. Yuan et al., "Perovskite energy funnels for efficient light-emitting diodes," Nat. Nanotechnol., **11**, 10, 872–877, (2016).

INVESTIGATION OF PROPERTIES OF TRIARYLAMINE BASED QUATERNARY AMMONIUM SALTS

Matas Steponaitis[1], Regimantas Komskis[2], Egidijus Kamarauskas[3], Tadas Malinauskas[1], Saulius Jursenas[2] and Vytautas Getautis[1]

[1] Department of Organic Chemistry, Kaunas University of Technology, Kaunas, Lithuania
[2] Institute of Photonics and Nanotechnology, Vilnius, Lithuania.
[3] Department of Solid State Electronics, Vilnius University, Vilnius, Lithuania.
matas.steponaitis@ktu.lt

Triphenylamine (TPA) compounds are versatile charge transport materials, demonstrating high emission efficiency and interesting interactions in solid state. Their spectroscopic emission parameters highly depend on surrounding medium owning to strong CT character in solution. Although TPA compounds demonstrate good charge transport capabilities, further optimization via molecular design is required.

In this work, various TPA molecular systems with varying number of additional dimethylamine and phenylethenyl substituents were thoroughly investigated. Additionally, influence of quaternarization of tertiary amine groups in the triphenylamine backbone on emission and electronic properties was analyzed.

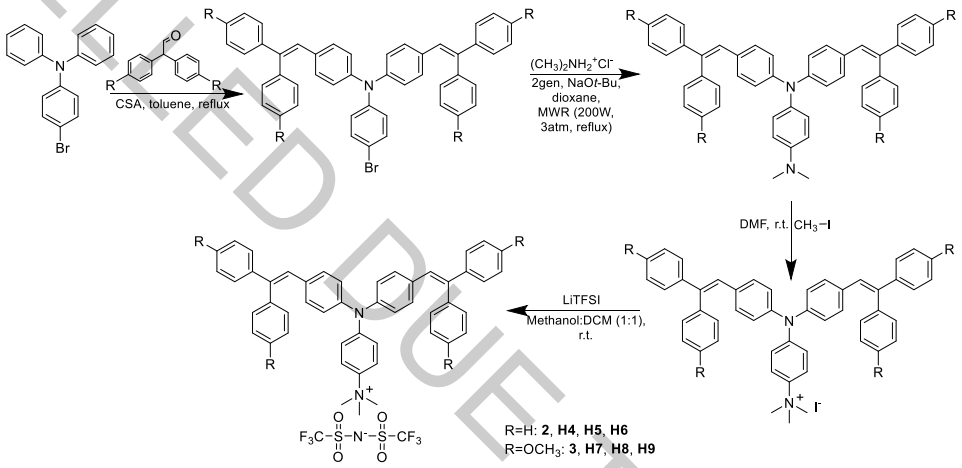

Fig. 1. Synthesis of quaternary ammonium compounds.

CANCELLED DUE TO COVID-19

TETRAHYDROCURCUMIN ENCAPSULATED IN MODIFIED STARCH BY SPRAY-DRYING FOR MICROBIOLOGICAL APPLICATIONS

Anne Loron[1], Christian Gardrat[1], Ramunė Rutkaitė[2], Vesta Navikaitė-Šnipaitienė[2], Deimantė Rosliuk[2], Véronique Coma[1]

[1] Université de Bordeaux, CNRS, Bordeaux INP, LCPO, UMR 5629, 16 avenue Pey Berland, Pessac F-33600, France
[2] Department of Polymer Chemistry and Technology, Faculty of Chemical Technology, Kaunas University of Technology, Radvilenu plentas 19, Kaunas LT-50254, Lithuania
anne.loron@enscbp.fr

CANCELLED PROCEED-19

The pathogenic fungus *Fusarium graminearum* is responsible for the disease Gibberella Ear Rot in maize and Fusarium Head Blight in wheat. The diseases caused by *Fusarium* not only severely decrease grain yield, but also result in contaminated grains with an unacceptable levels of mycotoxins, which are toxic secondary metabolites. Hence, such fungal strains can drive the outbreaks of mycotoxicosis in humans and animals.

In constant search for bio-sourced and non-toxic efficient compounds to deal with pathogenic fungi, our lab is currently working with tetrahydrocurcumin (THC, Fig. 1). This colorless curcumin derivative possess anti-oxidant, anti-fungal [1-2] and anti-carcinogenic properties [3]. THC is unfortunately a scarcely water-soluble molecule. However we need an acceptable solubility in water to add this phenolic compound in an aqueous formulation of bio-fungicide. That is the reason why we chose to encapsulate the molecule to enhance its apparent solubility.

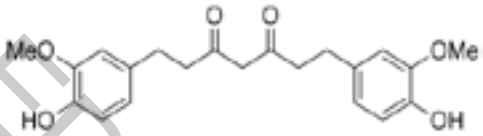

Fig. 1 Structure of tetrahydrocurcumin (THC)

Spray-drying was chosen as encapsulation technique, as is it widely used in industry due to high flexibility and the possibility to work in continuous process [3-4]. Before spraying, THC is trapped in vegetable oil in water emulsion stabilized with octenyl succinic acid modified-starch. The size of the droplets was optimized and visual control of emulsion stability was performed. After spray-drying, particles were characterized with scanning electron microscopy (SEM), nuclear magnetic resonance, UV-spectrophotometry and differential scanning calorimetry. One can observe emulsion used for spraying in Fig. 2 (a). SEM views confirmed that no free THC was visible in synthetized THC-loaded particles (Fig. 2 (b) and (c)). Microbiological assays were then performed on *F. graminearum.*

(a) (b) 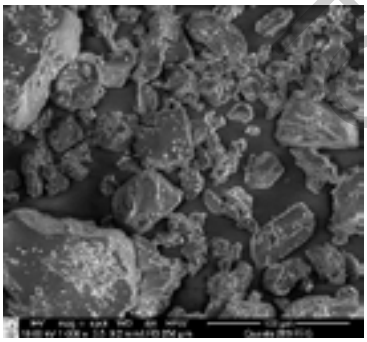 (c) 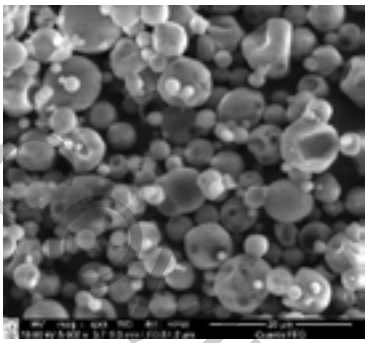

Fig. 2 (a) Emulsion before spraying (b) SEM view of THC (c) SEM view of THC-loaded particles obtained from spray-drying

Acknowledgement. The financial support of the Research Council of Lithuania and Campus France for the Lithuanian-French programme “Gilibert” project No. S-LZ-19-6 is highly acknowledged.

[1] V. Coma, E. Portes, C. Gardrat, F. Richard-Forget, A. Castellan, In vitro inhibitory effect of tetrahydrocurcuminoids on *Fusarium proliferatum* growth and fumonisin B $_1$ biosynthesis. Food Additives & Contaminants: Part A **28(2)**, 218-225 (2011).
[2] E. Portes, C. Gardrat, A. Castellan, A comparative study on the antioxidant properties of tetrahydrocurcuminoids and curcuminoids. Tetrahedron **63(37)**, 9092-9099 (2007).
[3] J.-C. Wu, M.-L. Tsai, C.-S. Lai, Y.-J. Wang, C.-T. Ho, M.-H., Pan Chemopreventative effects of tetrahydrocurcumin on human diseases. Food Funct. **5(1)**, 12-17 (2014).
[4] B. N. Estevinho, F. Rocha, L. Santos, A. Alves, Microencapsulation with chitosan by spray drying for industry applications – A review. Trends in Food Science & Technology **31(2)**, 138-155 (2013).
[5] V. Nedovic, A. Kalusevic, V. Manojlovic, S. Levic, B. Bugarski, An overview of encapsulation technologies for food applications. Procedia Food Science **1**, 1806-1815 (2011).

EFFICIENT AND STABLE PEROVSKITE SOLAR CELLS USING LOW-COST ANILINE-BASED ENAMINE HOLE TRANSPORTING MATERIALS

Deimante Vaitukaityte[1], Zhiping Wang[2], Tadas Malinauskas[1], Artiom Magomedov[1], Giedre Bubniene[1], Vygintas Jankauskas[3], Egidijus Kamarauskas[3], Vytautas Getautis[1], Henry J. Snaith[2]

[1] Department of Organic Chemistry, Kaunas University of Technology, Lithuania
[2] Clarendon Laboratory, Department of Physics, University of Oxford, United Kingdom
[3] Department of Solid State Electronics, Vilnius University, Lithuania
deimante.vaitukaityte@ktu.edu

CANCELLED DUE TO COVID-19

Over the last few years perovskite solar cell (PSC) technology has evolved from a scientific curiosity to a major research subject in the field of photovoltaics. In that short period of time they have gained recognition as one of the most promising photovoltaic technologies and managed to demonstrate remarkable achievements in the power conversion efficiency (PCE) exceeding 25% certified by the NREL [1]. Most of the high efficiency n-i-p structured perovskite solar cells are based on 2,2′,7,7′-tetrakis(*N*,*N*-di-*p*-methoxy-phenylamine)-9-9′-spirobifluorene (Spiro-OMeTAD) hole transporting material (HTM), which is very expensive [2]. The generated high cost is mainly due to the multi-step synthesis, complicated purification procedures and use of transition metal catalysts [3].

In this work, four low-cost enamines were functionalized *via* single-step synthetic procedure from commercially available aniline precursors without the use of expensive and problematic oraganometallic catalysts. Depending on the ration of the reagents enamines with two (**V1092**) or three (**V1091**) diphenylethenyl groups have been isolated. Additionally, aniline derivative with methoxy group in *para*-position (**V1056**) and 3,5-dimethyl substituted analogue (**V1102**) were also used for the synthesis.

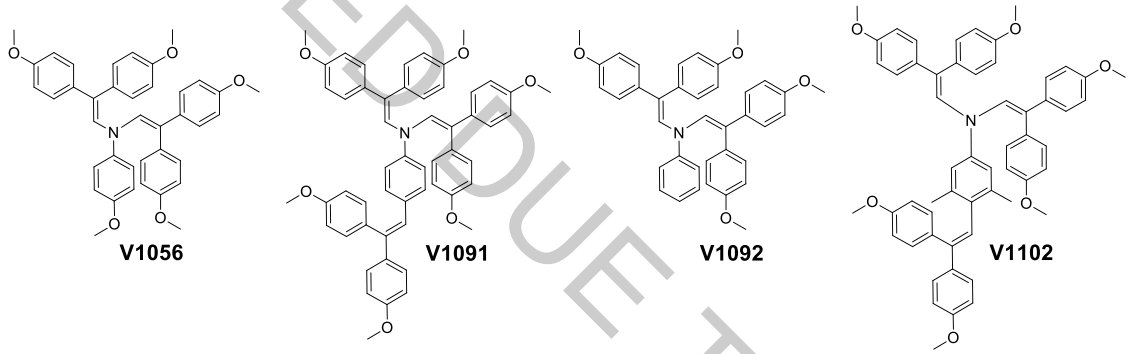

Fig. 1. Structures of aniline-based hole transporting materials **V1056**, **V1091**, **V1092** and **V1102**.

To investigate photoelectrical properties of synthesized HTMs hole drift mobility and ionization potential were measured. Photoelectron spectroscopy in air method was used to measure ionization potentials (I_p). Aniline derivative containing two diphenylethenyl groups (**V1092**) exhibits the highest ionization energy (5.3 eV). Additional electron donating diphenylethenyl (**V1091**) or methoxy (**V1056**) group lowers I_p of the HTM by ~0.1 eV. With the addition of methyl groups at 3,5-positions of the phenyl ring in **V1102**, negligible changes were observed in ionization energy. On the whole, the investigated HTMs show slightly higher ionization energy than Spiro-OMeTAD (5.0 eV), but still suitable for the hole extraction in PSCs. Charge transport properties of the investigated HTMs were measured using xerographic time-of-flight technique. **V1056** shows a similar hole mobility (7.8×10^{-4} cm^2/Vs) as compared to Spiro-OMeTAD (5.0×10^{-4} cm^2/Vs). In contrast, **V1091**, containing three diphenylethenyl moieties, displays significantly better hole drift mobilities (1.7×10^{-2} cm^2/Vs) at high electric fields. Addition of the methyl groups at 3,5-positions of the phenyl ring in **V1102** results in reduced charge mobility (1.5×10^{-4} cm^2/Vs).

The materials were tested as a HTM in planar heterojunction perovskite solar cells (with a device structure: fluorine doped tin oxide (FTO)/SnO_2/perovskite/HTM/Au). The device using **V1102** and **V1056** shows a champion efficiency of 17.6% and 18.7%, respectively, which is slightly lower than the PCE of 20.2% for the control device using Spiro-OMeTAD. In contrast, the PSC using **V1091** exhibits a high efficiency of 20.2%. To access device stability using the HTMs, non-encapsulated high efficiency devices were aged with **V1091** and Spiro-OMeTAD hole transporting layers in ambient air with a relative humidity of ~ 45% under dark conditions. **V1091** device showed superior stability sustaining 96% of its original efficiency after 820 h. In contrast, stabilized power output of the control device dropped to 42% after aging.

[1] https://www.nrel.gov/pv/assets/pdfs/best-research-cell-efficiencies.20191106.pdf.
[2] K. Rakstys, C. Igci and M. K. Nazeeruddin, Efficiency *vs*. stability: dopant-free hole transporting materials towards stabilized perovskite solar cells, Chemical Science, **10**, 6748-6769 (2019). https://doi.org/10.1039/C9SC01184F.
[3] D. Vaitukaityte, Z. Wang, T. Malinauskas, et al., Efficient and Stable Perovskite Solar Cells Using Low-Cost Aniline-Based Enamine Hole-Transporting Materials, Advanced Materials, **30**, 45, 1803735 (2018). https://doi.org/10.1002/adma.201803735.

MODELING CHARGE TRANSFER STATE OF CAROTENOIDS AND CHLOROPHYLL-A COMPLEXES FROM PHOTOSYNTHESIS USING DENSITY FUNCTIONAL THEORY

Gabrielė Karpickaitė[1], Mindaugas Mačernis[1]

[1]Institute of Chemical Physics, Vilnius University, Lithuania
gabriele.karpickaite@ff.stud.vu.lt

CANCELLED DUE TO COVID-19

Photosynthesis is an important process used by plants and other organisms to convert light energy into chemical energy. Therefore, it is essential to have a good understanding of the processes that occur in these systems. Carotenoids in marine environment, including fucoxanthin in diatoms and peridinin in dinoflagellates, play an important role not only because of their high content relative to chlorophylls, but also because of a structural modification involving a carbonyl group that binds to the backbone of polyene. As a result, their light absorption range is extended to the blue-green range required for successful photosynthesis in the oceans. This property also makes carotenoids efficient channels for transferring the absorbed energy to chlorophyll-a. This functionality of carotenoids may be better understood by reference to the C_{2h} point group of linear polyenes, where the strongly allowed π-π* transition is not to the lowest-energy singlet S_1 state, but to a higher state, that is, $S_0 \rightarrow S_n$ (often n = 2). The large change in dipole moment indicates that carotenoid undergoes photoinduced charge transfer. [1]

In this work Gaussian09 software [2] was used to analyze excited singlet states and to examine possible interactions of carotenoids fucoxanthin and peridinin with chlorophyll-*a* (Figure 1 A). The arrangements of complexes were taken as in PDB crystallographic structure 1PPR [3]. Computations were performed on resources at the High Performance Computing Center "HPC Sauletekis" in Vilnius University Faculty of Physics.

According to calculations the charge transfer state below carotenoid S_2 state was observed in complexes 624. Results obtained were implying that for the existence of a charge transfer state below carotenoid S_2 state the position between carotenoid and chlorophyll-a in complexes was crucial (Figure 1 B) as well as the structure of chlorophyll-*a,* especially a carbonyl group attached to a chlorin ring.

The results obtained may exist in the protein because the investigated structures are based on naturally existing protein *amphidinium carterae*. The possible excited states of the carotenoids and chlorophyll-a complexes discussed above and the conditions of the charge transfer state existence below the carotenoid S_2 state were investigated.

The charge transfer state has not been fully analyzed. The results show that the charge transfer state depends on the positions between carotenoid and chlorophyll-*a*.

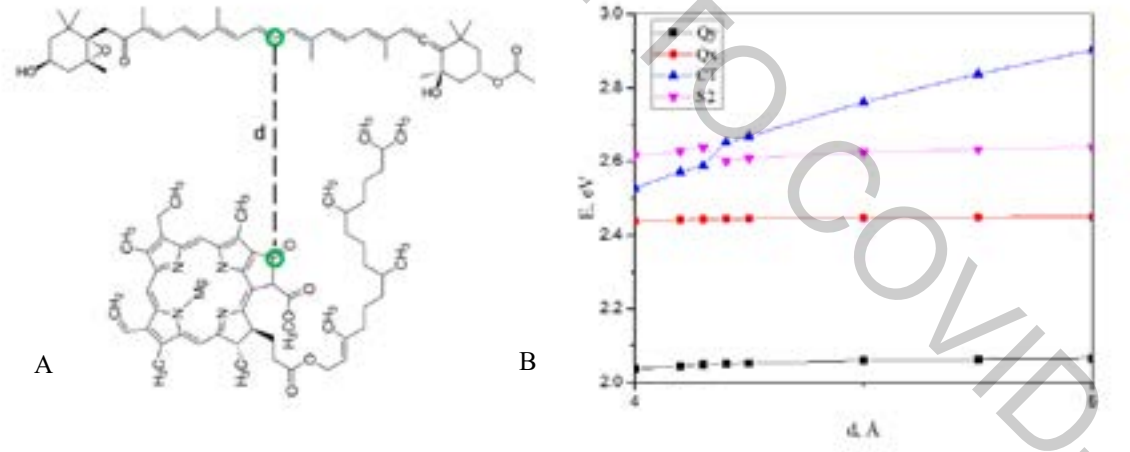

Fig. 1. A: Complex of fucoxanthin with chlorophyll-*a* and the shortest distance d between chosen atoms. B: Dependence of the first four excited states energies on the distance between chosen atoms in fucoxanthin and chlorophyll-a complex.

[1] Premvardhan, L., Sandberg, D. J., Fey, H. & Birge, R. The Charge-Transfer Properties of the S2 State of Fucoxanthin in Solution and in Fucoxanthin Chlorophyll-a/c2 Protein (FCP) Based on Stark Spectroscopy and Molecular-Orbital Theory. **112**, 11838–11853 (2010).
[2] M. J. Frisch, G. W. Trucks, H. B. Schlegel, G. E. S. *et al.* Gaussian 09. (2013)
[3] Valentin, M. Di & Carbonera, D. The fine tuning of carotenoid – chlorophyll interactions in light-harvesting complexes : an important requisite to guarantee ef fi cient photoprotection via triplet – triplet energy transfer in the complex balance of the energy transfer processes. *J. Phys. B At. Mol. Opt. Phys.* **50**, 162001 (2017).

FULLERENE-C60: FROM THE INOCCENT GUEST MOLECULE TO A PHOTOCATALYST

Augustina Jozeliunaite[1], Domantas Valceckas[1], Edvinas Orentas[1*]

[1] Department of Organic Chemistry, Vilnius University, Lithuania
augustina.jozeliunaite@chgf.vu.lt

The tubular nanoscale self-assembled systems are highly desired due to their possible application in the drug delivery, molecular encapsulation or flow-through catalysis. Such tubular assemblies can be obtained either by utilization of various growth templates, ring stacking or by bio-inspired supramolecular chemistry employing weak intermolecular forces. On the contrary, the synthesis of such systems comprising large cavities still remains challenging[1]. Herein we present the strategy of using chiral C_2-symmetric bicyclo[3.3.1.]nonane framework encompassing self-complementary ureidopyrimidinone (Upy) moiety as our synthon for supramolecular cyclic tetrameric structures[2]. We noticed that introduction of fullerene guest molecule into the cavity of our supramolecular aggregate enhances fullerene's ability to generate singlet oxygen without external stimuli which oxidizes sulfide groups in the side chains of the cyclic tetramer.

Based on our observations we developed a green and mild method which facilitates chemoselective oxidation of sulfides using oxygen as the terminal oxidant under heterogeneous catalysis. Thus, we propose light-driven sulfide oxidation catalyzed by non-soluble fullerene (C60) in ethanol without further overoxidation to sulfones. We took this even further by employing much cheaper fullerene soot as a heterogenous catalyst which would allow us to recover the catalyst by simple filtration and reuse it many times without losing its intrinsic properties. The fullerene soot could possess the huge advantage amongst other reusable catalyst because it does not require the catalyst immobilization to any heterogenous supports such as resins or insoluble polymers, it is available from multiple suppliers and is very cheap.

Fig. 1. Photoxidation of sulfides to sulfoxides using a heterogeneous catalyst

CANCELLED DUE TO COVID-19

[1] M. A. B. Block, C. Kaiser, A. Khan, S. Hecht, Top. Curr. Chem., **245**, 89-150 (2005).
[2] D. Rackauskaite, R. Gegevicius, Y. Matsuo, K. Wärnmark, E. Orentas, Angew. Chem. Int. Ed., **55**, 208-212 (2016).

INFLUENCE OF WORKPLACE EXPOSURE ON VOCs PROFILE IN HUMAN BREATH

Adrián Vicent-Claramunt[1], Evaldas Naujalis[1]

[1]State Research Institute Center for Physical Sciences and Technology,
Savanorių Ave. 231, LT-02300 Vilnius, Lithuania.
adrian.vicent@ftmc.lt

Nowadays people spend most of their time indoors: sleeping at home, working in offices, eating in canteens or restaurants, or spending free time in cinemas, shopping malls and other stores. It is in those places where we are exposed to a high content of volatile organic compounds (VOCs). In this work, we focused on places where we spend a great part of our time every day.

Human breath contains more than 1000 different VOCs [1], and some of them can be used as biomarkers for several diseases like diabetes [2], several types of cancer [3], and fungal infections [4] among others. In this work we will focus on the understanding of the background VOC profile in breath of healthy volunteers; and how their exposure to environmental compounds could modify this profile.

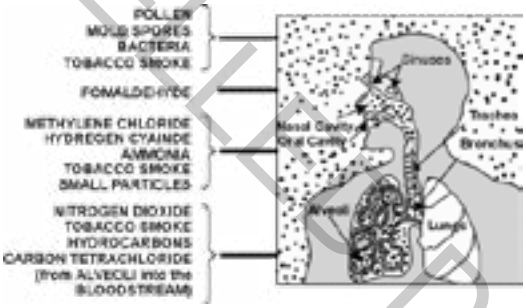

Fig.1: Sources of VOCs indoors.

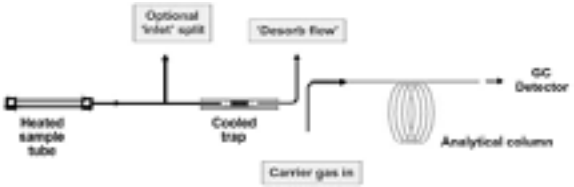

Fig.2: TD/GC-MS configuration

Air samples were taken from the selected places, to benchmark the background compounds. Samples were collected using thermal desorption (TD) tubes and purged into a gas chromatography with mass spectrometer (GC-MS). Then, breath samples from participants were collected before starting their daily work, and at the end of the workday. Breath sampling was obtained using a self-made plastic bag collection system. Optimization of system parameters was performed to get good compound separation and identification.

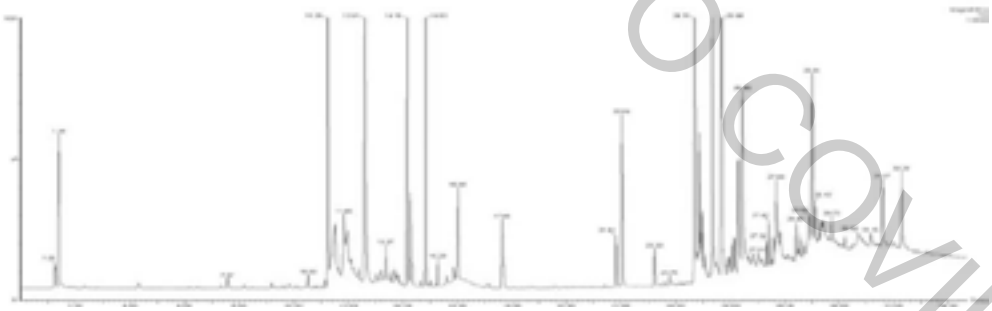

Fig.3: Chromatogram from air sample after air freshener used.
Column DB-5MS (60x0.25x0.1). Magnet Scan 50-200m/z. Temp. range: 40 to 280 ºC

Figure 3 shows the high concentration of several VOCs in a study place after using some air freshener, like Pinene, Limonene among plenty of other terpenes; and some more toxic compounds like Benzaldehyde or Benzyl acetate. If people are exposed to VOCs, some of them are incorporated into respiratory system and their variation in breath could tell us how those compounds behave inside our body, some will be exhaled, others might be retained and different metabolites can be formed. In conclusion, when using breath samples for disease diagnosis we should take into consideration the exposure to external contaminants which could influence the VOCs profile.

[1] de Lacy Costello B et al., *A review of the volatiles from the healthy human body,* J Breath Res. 2014 Mar; 8(1) 014001.
[2] Neupane S et al., *Exhaled breath isoprene rises during hypoglycemia in type 1 diabetes,* Diabetes Care. 2016 Jul; 39(7) e97-e98
[3] Zhou J et al., *Review of recent developments in determining volatile organic compounds in exhaled breath as biomarkers for lung cancer diagnosis*, Anal Chim Acta. 2017 Dec 15; 996 1-9
[4] Thalavitiya Acharige MJ, *Breath based diagnosis of fungal infections,* J Breath Res. 2017 Nov 07

CANCELLED DUE TO COVID-19

SUBLIMATION ENTHALPY OF ORGANIC MOLECULES WITH DECOMPOSITION CONTROL: MASS-SPECTROMETRY APPROACH

Andrei Buzykin[1,2], Oleg Smirnov[2]

[1]Institute of Physics, Nanotechnology and Telecommunications, Peter the Great St. Petersburg Polytechnic University, St. Petersburg, Russia
[2] Ioffe Institute, St. Petersburg, Russia
Buzykin7@gmail.com

CANCELLED DUE TO COVID-19

Interest to single molecule spectroscopy and mechanisms of interaction of the light and other energy carriers with isolated molecules has enhanced through last years. However, isolated organic molecules may decompose due to interaction with atmospheric oxidizers, temperature growth and chemical interaction. That's why it is important to distinguish thermal-induced decomposition, radiation-induced and chemical one for accurate experimental measurements, as well as for application of some organic compounds in industry[1].

In modern quantum chemistry a big attention is devoted to studies of organic molecules and compounds and various homologues of wide-known molecules. In this study, authors present an experimental approach in application to fragmentation of organic molecules, evaporated from a Knudsen cell and fragmented with single or multiple charged ions with energies from 2 to 100 kEv. Mass-spectra obtained with a time-of-flight fragment detection method allows to judge about probabilities for possible decomposition reaction channels, while sublimation enthalpy is received due to theoretical treatment.The experiment is held under conditions of vacuum 10^-6 Torr, and mass-spectra, showing native and/or fragment peak allows to consider if the process is a kind of thermal decomposition, or ion-induced.

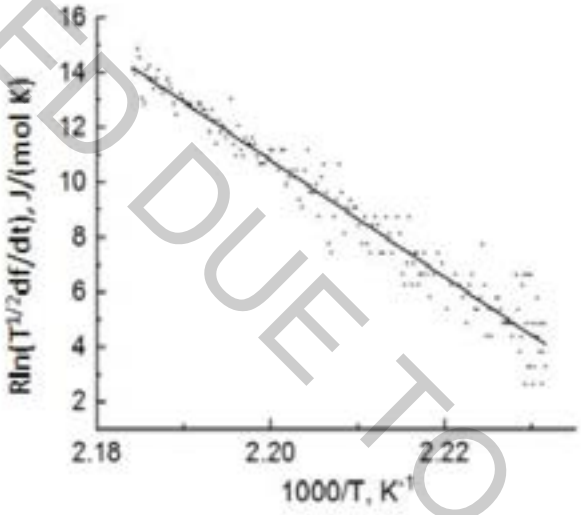

Fig. 1. Enthalpy of sublimation is represented in accordance with Eq (1). Figure 1 represents sublimation enthalpy for N-Glycylglycine ($C_4H_8N_2O_3$) in accordance with results of article [2]

Our treatment is based on pressure, enthalpy and temperature dependence, considered in the Eq (1). Value, obtained from peak information, allow us to receive pressure. Basically, we measure vapor temperature and signal current, associated with concentration of molecules. Enthalpy value is obtained from least squares method for linear dependence of logarithmic pressure from inversed temperature according to Fig. (1).

$$\ln p = -{}^{\Delta H}/_{RT} + Const \quad (1)$$

Our approach is supposed to be effective for high-energy compounds due to strong vacuum conditions and decomposition control, distinguishing it from other techniques[3] ,which allows to measure sublimation enthalpy of isolated molecules, relevant both for theoretical consideration, and practical application.

[1] A.G. Buzykin, A.A. Basalaev,Proceedings of the Polytechnic Science week, 2018, 299-301.{In Russian}
[2] A ABasalaev et al 2019 J. Phys.: Conf. Ser. 1400 033017.
[3] Badelin, V.G., Tyunina, E.Y., Girichev, G.V. et al. Relationship between the molecular structure of amino acids and dipeptides and thermal sublimation effects. J Struct Chem 48, 647–653 (2007).

SYNTHESIS AND MAGNETIC PROPERTIES OF $Co_{0.65}Zn_{0.35}Fe_2O_4$ MAGNETIC NANOPARTICLES WITH HIGH CRYSTALLINITY BY ULTRASONIC SPRAY PYROLYSIS METHOD

Dzimitry Ivashenka[1], Elena Petrova[1], Vladimir Pankov[1]

[1]Department of Physical Chemistry, Belarusian State University, Belarus
che.ivashenkDV@bsu.by

Over the past decades, the production of spinel ferrite nanoparticles has been intensively studied due to their promising magnetic properties. Cobalt ferrite ($CoFe_2O_4$) is especially attractive because of its high coercivity and moderate saturation magnetization. It was shown that substitution of Co^{2+} with Zn^{2+} leads to enhanced magnetic properties of nanocrystalline ferrites [1]. Zinc substituted cobalt ferrites are considered to be suitable magnetic materials for such applications as magnetic drug delivery [2], magnetic resonance imaging, information storage system, ferrofluids [3], etc.

Our study is devoted to improvement of ultrasonic spray pyrolysis (USP) technique in order to enhance magnetic properties of ferrite nanoparticles. It's generally known that increasing crystallinity of magnetic nanoparticles leads to the increase of saturation magnetization. Therefore, the main aim of this research is to increase nanoparticle's crystallinity by calcination at high temperatures. At first, cobalt-zinc ferrite suspension was prepared by co-precipitation from a solution of metal nitrates taken in stoichiometric amount. Sodium chloride (wt. concentration 5: 1 with respect to ferrite) was added to the suspension to prevent aggregation and sintering during calcination. Magnetic nanoparticles were obtained from as-prepared suspension by USP method at 600°C. Thus, cobalt-zinc ferrite nanoparticles in inert matrix were synthesized. Finally, calcination was carried out within temperature range from 300 to 900 °C in order to improve crystallinity.

The phase composition and structure of ferrites were studied by XRD and FT-IR spectroscopy. The size and morphology of the particles were examined by SEM, saturation magnetization of samples was measured by SQUID magnetometry. The average size of nanoparticles annealed at 300°C is about 7 nm (Fig.1). It was found that significant growth of those occurs during annealing process at 900°C. Nevertheless, major fraction of the particles remained within nanoscale range (about 80 nm) although recrystallization process caused formation of the larger particles fraction (200 nm and higher). The calculations of the crystallite size based on the diffraction reflection broadening correlate to average size data obtained from SEM. The average crystallite size was found to be 53 nm for annealing at 900°C, 7 nm –at 300°C. With increasing annealing temperature from 300°C to 900°C saturation magnetization increased from 45.0 emu/g to 78.6 emu/g. (Table.1)

Table 1. Magnetic properties of the ferrite nanoparticles annealed at different temperatures

T, °C	900	700	500	300
M_s, emu/g	78,6	54,7	45,6	45,0

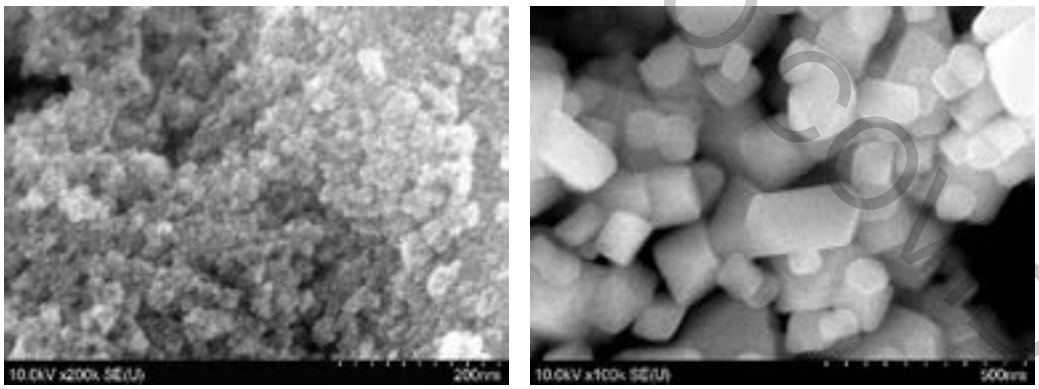

a b

Fig.1. SEM images of CoZnFe2O4 nanoparticles annealed at 300°C (a), 900°C (b)

[1] S. Dey, J. Ghose, Synthesis, characterisation and magnetic studies on nanocrystalline $Co_{0.2}Zn_{0.8}Fe_2O_4$, Materials Research Bulletin 38.11-12, 1653-1660 (2003):

[2] W. Pon-On, N. Charoenphandhun et al., Encapsulation of magnetic $CoFe_2O_4$ in SiO_2 nanocomposites using hydroxyapatite as templates: A drug delivery system, Materials Chemistry and Physics 131(1-2), 485-494 (2011).

[3] K. Raj, B. Moskowitz, R. Casciari, Advances in ferrofluid technology, Journal of magnetism and magnetic materials 149.1-2, 174-180 (1995):

CORRECTED PROOF COVID-19

DRELL-YAN PROCESS BACKGROUND ESTIMATION USING THE FAKE RATE METHOD

Marijus Ambrozas, Andrius Juodagalvis

Institute of Theoretical Physics and Astronomy, Faculty of Physics, Vilnius University, Lithuania
marijus.ambrozas@ff.stud.vu.lt

The Large Hadron Collider (LHC) at CERN produces high energy proton-proton collisions which allow us to peek into the smallest building blocks of the Universe. Protons in the collider can be seen as streams of quarks and gluons, according to the parton model. Many different parton-parton interactions are possible during the proton collision. Probabilities of different outcomes depend on the parton distribution functions (PDFs), which describe the inner structure of the proton. Precise knowledge of the PDFs is required for realistic estimation of the probabilities of very rare events.

The Drell-Yan process is a quark-antiquark annihilation resulting in a lepton-antilepton pair [1]. High-precision measurements of the differential Drell-Yan cross section are useful for constraining the PDFs, as well as for testing the perturbative framework of the Standard Model [2]. They are also important for many other experimental measurements where the Drell-Yan process is a significant background [3, 4, 5].

Lepton tracks that emerge from the Drell-Yan process are ususally well separated from any other particle tracks produced in the event. They are called "isolated leptons." Several other processes can also lead to production of the isolated lepton pairs (for example, the leptonic decay of a top quark-antiquark pair). These processes can be easily confused with the Drell-Yan process and are referred to as backgrounds. However, non Drell-Yan production of the isolated lepton pairs is not the only possible background.

A quark or a gluon may also be produced in the proton-proton collision. Due to the confinement, it undergoes the hadronization process which results in a cone-shaped hadron stream, called a jet. Heavy flavor jets (for example, bottom or charm jets) may contain an energetic lepton. On very rare cases, some hadrons from a jet may reach muon detectors, which are located on the outermost layers of modern particle detectors, and be confused with muons. Ideally, in both of these cases the lepton track should not be isolated (it should be surrounded by a stream of hadrons). Though, it is still possible for the event reconstruction algorithm to misidentify a jet as an isolated lepton. Therefore, jet events also contribute to the Drell-Yan backgrounds.

It is very difficult to predict the ammount of jet backgrounds from the simulation, because jet events have a very large cross section and a very low probability to be misidentified as isolated lepton events. Data-driven methods are used to estimate these kind of backgrounds. The fake rate method is one of them. This method relies on estimating the probability for a jet to be misidentified. The estimated probability is then used to predict the ammount of jet events in experimental data. The fake rate method and its use with the 2016 CERN CMS proton-proton collision data will be discussed in the presentation

The work is performed in collaboration with scientists from Seoul National University and University of Nebraska Lincoln. Collaboration with CERN CMS experiment is supported by Lithuanian academy of sciences.

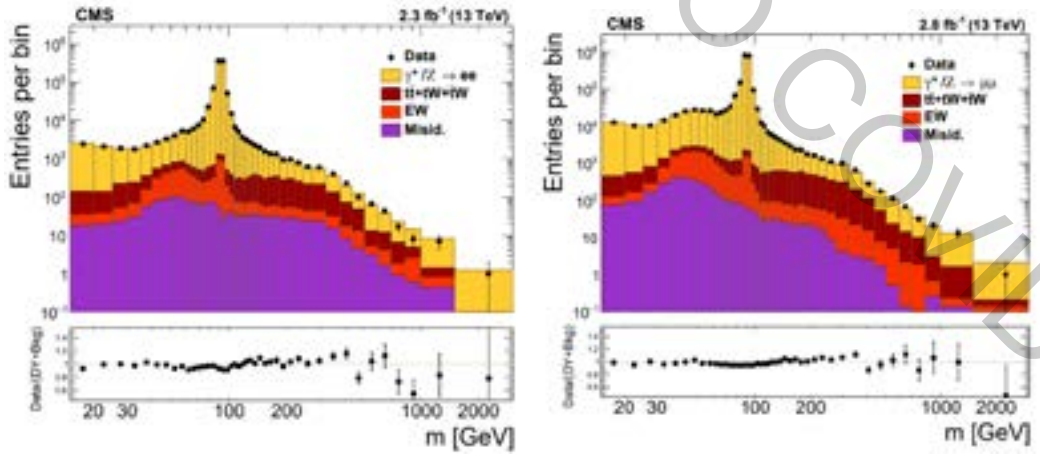

Fig. 1. Dielectron (left) and dimuon (right) invariant mass distributions in 2015 CMS data [2]. Black dots represent the number of events measured with the CMS detector. Colored bars represent contribution of different processes. Yellow color marks the signal, i.e. the Drell-Yan process. "EW" denotes electroweak backgrounds. "Misid." marks the contribution from misidentified jet events, estimated using the fake rate method.

[1] S. D. Drell, T. M. Yan, Massive Lepton Pair Production in Hadron-Hadron Collisions at High-Energies, Phys. Rev. Lett. **25**, 316 (1970).
[2] CMS Collaboration, Measurement of the differential Drell-Yan cross section in proton-proton collisions at $\sqrt{s} = 13$ TeV, JHEP **12** 059 (2019).
[3] CMS Collaboration. Observation of the Higgs boson decay to a pair of tau leptons with the CMS detector. Phys. Lett. B **779**, 283 (2018).
[4] CMS Collaboration. Search for high-mass resonances in dilepton final states in proton-proton collisions at $\sqrt{s} = 13$ TeV. JHEP **06** 120 (2018).
[5] CMS Collaboration. Search for supersymmetric partners of electrons and muons in proton-proton collisions at $\sqrt{s} = 13$ TeV. Phys. Lett. B **790** 005 (2019).

CANCELLED DUE TO COVID-19

CALCULATIONS OF ELECTRON AND PHOTON TRANSPORT IN MEDICAL LINEAR ACCELERATOR TREATMENT HEAD

Simona Breidokaitė[1], Gediminas Stankunas[1], Diana Adliene[2],

[1] Laboratory of Nuclear Installation safety, Lithuania Energy Institute, Lithuania
[2] Department of Physics, Kaunas University of Technology, Lithuania
simona.breidokaite@lei.lt

The first Linear accelerator (LINAC) for cancer treatment was firstly applied in Hammersmith Hospital (London, UK), in 1953 [1], which operated with the 8 MeV electron beam energy. Electrons in LINAC are usually generated by a Pierce-type electron gun [2]. In modern LINACs different electron beam energies can be generated depending on equipment provider. For example, Varian linear accelerators currently offer selected electron beams of 4, 6, 9, 12, 16, and 20 MeV energies [3]. For the safe performance it is important to know the distribution of electron/photon beams and their interaction with matter process.

In this work, the interaction processes induced by electrons, when energies are 9, 16 and 20 MeV were studied. Attention is also drawn to the resulting photons and their interaction processes. In general, particle transport calculations of electron are fundamentally different from photons. Neutral particle interactions are characterized by relatively uncommon collisions and long mean free path, while electrons interaction with matter is supported by the Coulomb laws. For example: When photon or electron interacts with an aluminium plate. In case, when energy is decreasing from 0.5 MeV to 0.0625 MeV, photons will have less than 10 interactions, while electrons have more than 10^5 [4].

This work presents the pilot model of medical linear accelerator treatment head, which was created using MCNP-VIS (see figure 1) and particle transport calculations were performed with 10^6 particles. Calculations have shown that increasing energy secondary electron generation is by electrons is reduced, however improved for photons. The number of reactions for both photons and electrons increased by the factor of 1.2 and the average energy of the reactions increased by 10 MeV and 26 MeV respectively. In addition, dose rate calculations were also performed and results shown that increase of electron energy from 9 to 20 MeV was able for dose rate changes from 0.54 Sv/h to 0.89 Sv/h.

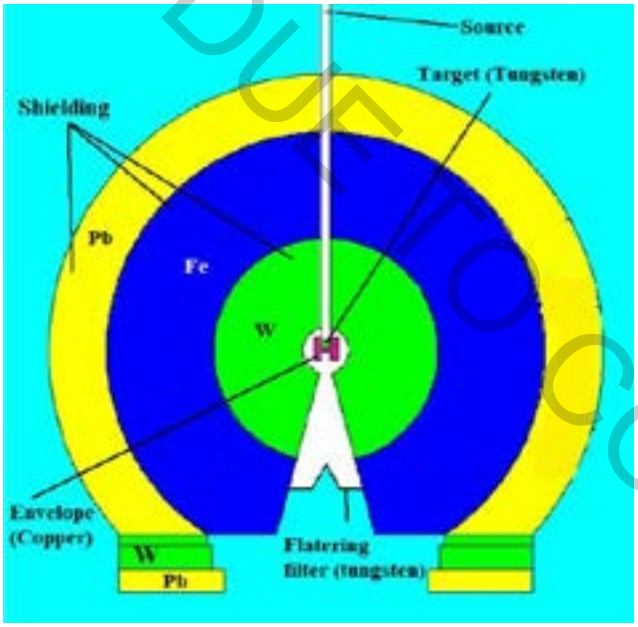

Fig. 1. MCNP model of linear accelerator treatment head in the Y-Z plane.

[1] Thwaites, DI; Tuohy J, Back to the future: the history and development of the clinical linear accelerator, Phys, Med, Biol, 51 (2006) R343–R36, prieiga per doi:10,1088/0031-9155/51/13/R20
[2] J. R. Pierce, *Theory and Design of Electron Beams*, (1954) 182-192,
[3] Zhang S, et al., Clinical implementation of electron energy changes of varian linear accelerators, Appl Clin Med Phys, (2009)
[4] X-5 MONTE CARLO TEAM, *MCNP- a General Monte Carlo N-particle transport code, version 5*, 2003m

ATŠAUKTA DĖL COVID-19

ARBITRARY PRECISION IN FLEXIBLESUSY

Simonas Draukšas[1], Andrius Juodagalvis[1]

[1]Institute of Theoretical Physics and Astrophysics, Vilnius University, Lithuania
simonas.drauksas@ff.stud.vu.lt

Properties of multi-parameter particle physics models are usually explored using either generalized or dedicated computer software that allows to perform parameter scans and evaluate quantities of interest, like, the particle mass spectra or their decay rates. Numerical evaluation often faces the difficulty of huge separation of scales of the calculated quantities. Analytical evaluation takes this into account easily. However, the limited numerical accuracy causes problems when performing parameter scans as the huge scale differences could mean losing numerical precision up to the point where the result is random and, hence, useless. We have encountered this problem while working on the Grimus-Neufeld model [1] with the FlexibleSUSY [2, 3, 4] spectrum generator. The Grimus-Neufeld model is an extension of the Standard Model and uses the seesaw mechanism to generate the light neutrino masses. Due to the seesaw mechanism and extremely small masses of the light neutrinos the model can have scale differences of 10^{20} or even more. Hence, FlexibleSUSY cannot properly handle this difference with the usual `double` precision.

We tackle this problem by implementing arbitrary precision libraries in FlexibleSUSY. While there is still work to be done before this development is available officially and for any model, we present the proof of principle with the Grimus-Neufeld model as an example.

The authors thank the Lithuanian Academy of Sciences for the support (the project DaFi2019).

[1] W. Grimus and H. Neufeld, *Radiative neutrino masses in an SU(2) × U(1) model*, Nuclear Physics B 325.1 (1989), pp. 18-32, ISSN: 0550-3213
[2] P. Athron et al., *FlexibleSUSY - A spectrum generator generator for supersymmetric models*, Comput. Phys. Commun. 190 (2015), pp. 139-172, arXiv: 1406.2319 [hep-ph]
[3] B. C. Allanach, *SOFTSUSY: A program for calculating supersymmetric spectra*, Comput. Phys. Commun. 143 (2002), pp. 305-331, arXiv: hep-ph/0104145
[4] B. C. Allanach et al., *Next-to-minimal SOFTSUSY*, Comput. Phys. Commun. 185 (2014), pp. 2322-2339, arXiv: 1311.7659 [hep-ph]

CANCELLED DUE TO COVID-19

WOBBLING MOTION IN ODD-MASS LU ISOTOPES: REDEFINING THE BAND STURCTURE FOR TRIAXIAL NUCLEI

Apolodor Aristotel Raduta[1,2], Robert Poenaru[1,3,a)], Cristian Raduta[1]

[1] Department of Theoretical Physics, Institute of Physics and Nuclear Engineering, Bucharest, PO Box MG6, Romania
[2] Academy of Romanian Scientists, 54 Splaiul Independentei, Bucharest 050094, Romania
[3] Doctoral School of Physics, Bucharest University, 405 Atomistilor Str., Magurele, Romania
[a)] robert.poenaru@drd.unibuc.ro

The wobbling motion, a unique fingerprint for highly triaxial deformation in nuclei, is described for odd-mass Lu isotopes within a Particle Rotor Model where an even-even core is coupled to a single j-shell nucleon. Compared to the previous work that aimed to describe the wobbling states in Lu isotopes (where the Triaxial Strongly Deformed (TSD) bands were defined as zero (ground), one, two and three phonon wobbling bands, namely, TSD1, TSD2 TSD3 and TSD4), this new approach redefines the deformed states as two ground bands (zero phonon) for a coupling of the core's angular momentum R with the single particle angular momentum $j=i(13/2)$ equal to $I = R + j$, with $R=0,2,4,\ldots$ for TSD1 and $I = R + j$ and $R = 1, 3, 5, \ldots$ for TSD2, a one-wobbling phonon band for TSD3 and another ground band for TSD4, where this time the core couples to a different particle with angular momentum $j=h(11/2)$. In this model, the moments of inertia (MOI) of the even-mass core are considered as free parameters, and they differ with respect to the odd-particle's angular momentum j, so the MOIs for TSD4 are different. The results for both excitation energies and transition probabilities are compared with the available experimental data for all the studied isotopes and the agreement between the two is fairly accurate. A phase diagram for the whole deformed system is also schematically developed, which represents the start of an outgoing fully consistent study that tries to locate regions where the *transversal wobbling* mode arises and also where wobbling motion is totally forbidden.

CANCELLED DUE TO COVID-19

DESTRUCTION OF CANCER CELLS INDUCED BY INTERACTION OF NIR IRRADIATION WITH SINGLE-WALLED CARBON NANOTUBES

Lena Golubewa[1,2], Mikhail Shuba[2], Igor Timoshchenko[3], Alesya Paddubskaya[2], Andrei Dementjev[1], Danielis Rutkauskas[1], Oleg Romanov[3], Renata Karpicz[1], Tatsiana Kulahava[2,3]

[1] Department of Molecular Compounds Physics, State research institute Center for Physical Sciences and Technology, Lithuania

[2] Department of Nanoelectromagnetism, Research Institute for Nuclear Problems of Belarusian State University, Belarus

[3] Department of Computer modelling, Belarusian State University, Belarus

lena.golubewa@ftmc.lt

Single-walled carbon nanotubes (SWCNTs) are among the most promising nanomaterials for theranostics. Due to their specific physico-chemical characteristics SWCNTs have the potential to be used both for cancer cell imaging [1] and destruction [2]. Carbon nanotubes are supposed to be used in bioapplications as photoacoustic imaging contrast agents or as photothermal therapy heating agents [3]. Under the influence of pulsed laser radiation on an absorbing medium, its local heating, thermal expansion, and generation of compression and rarefaction waves occur.

In present study we show the effect of continuous and pulsed laser irradiation of near-infrared (NIR) spectral range on rat C6 glioma cells in three different model systems: 1) cells, accumulated SWCNTs inside the cytoplasm as small agglomerates of micrometer size, 2) cells, exposed to nanofluid of separately dispersed single (or small bundles of several nanotubes) SWCNTs in non-covalent complexes with DNA molecules, 3) cells without SWCNTs either inside or outside the cell.

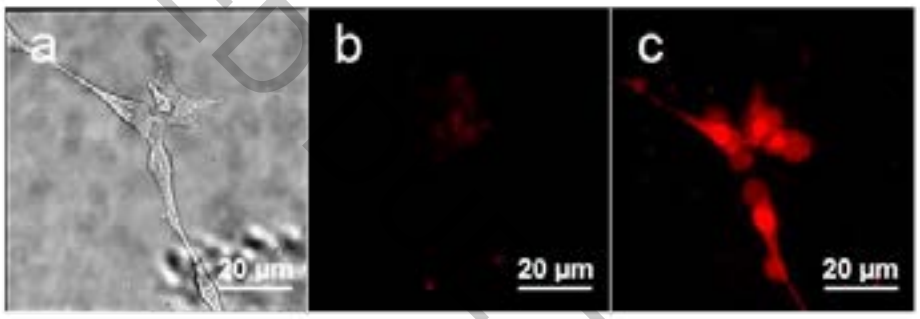

Fig. 1. Typical cell images before and after irradiation with laser pulses (t_p = 10 ps, λ_{ex} = 909 nm). a – reflected light microscopy of cells before irradiation, b – propidium iodide fluorescence in cells with SWCNTs before laser irradiation, c – propidium iodide fluorescence in cells with SWCNTs after laser irradiation.

By means of Raman spectroscopy we demonstrate the accumulation of SWCNTs inside the cell cytoplasm in the form of micrometer-sized agglomerates presumably in the endoplasmic reticulum after 24 h of cells exposure to SWCNTs. Glioma cells irradiation with lasers of λ_{ex} = 635 nm and λ_{ex} = 785 nm in continuous mode does not influence cell viability neither in the presence of SWCNTs nor in their absence, excluding the probability of cell destruction due only to the conversion of absorbed radiation by carbon nanotubes into heat. Cell viability was detected by fluorescence microscopy using. Exposure of glioma cells with SWCNTs accumulated inside the cell to pulsed irradiation with λ_{ex} = 909 nm and picosecond laser pulse duration leads to effective cancer cell destruction (Fig. 1), while similar impact on cells in a medium with dispersed individual nanotubes does not affect their viability. We propose theoretical model of vis-NIR laser irradiation interaction with SWCNTs and cancer cells. We consider the problems of energy absorption of pulsed laser radiation by cylindrical and spherical nano- and microparticles (SWCNT individually and in agglomerates, respectively), which differ in physical characteristics from the environment (biostructure). The results of simulation confirm that photo-induced destruction of cancer cells with picosecond pulsed irradiation in NIR spectral range can be achieved only when SWCNTs are accumulated inside the cell, but not when SWCNTs are dispersed in the external medium (under the same exposure conditions).

[1] P.K. Avti, B. Sitharaman, Luminescent single-walled carbon nanotube-sensitized europium nanoprobes for cellular imaging, Int. J. Nanomed. https://doi.org/10.2147/IJN.S29545 (2012).

[2] R. Singh., S.V. Torti, Carbon nanotubes in hyperthermia therapy, Adv. Drug Deliv. Rev. **65**(15), 2045–2060 (2013.).

[3] A. De La Zerda et al., Carbon nanotubes as photoacoustic molecular imaging agents in living mice, Nat. Nanotechnol. Nature Publishing Group **3**(9) 557-562 (2008).

CANCELLED DUE TO COVID-19

SELF ORDERED NANOPOROUS ALUMINUM OXIDE MEMBRANE FOR NANOFILTRATION USING SURFACE ACOUSTIC WAVES FOR MICROHYDRUALIC DEVICES IN BIOMEDICINE

Yatinkumar Patel[1*], Arvydas Palevicius[1], Giedrius Janusas[1]

[1] Department of Mechanical Engineering, Kaunas University of Technology, Lithuania
y.patel@ktu.lt

Aluminum is ubiquitous metal. There are plenty of methods developed in last few decades for the development of nanoporous aluminum oxide membrane using different electrolytes such as Oxalic acid ($C_2H_2O_4$), phosphoric acid (H_3PO_4), chromic acid (H_2CrO_4) or sulphuric acid (H_2SO_4). Moreover, there are possibilities to control their geometry of the pores such as diameter of hole and interpore distance by controlling the voltage applied during the electrochemical process and duration of the anodization process. Also, it is possible to fabricate aluminum oxide membrane by applying two step anodization methods mild anodization (MA) and hard anodization (HA) [1]. By improving the geometrical dimensions and functionality of the nano membrane could be increase in the applicability in micro hydraulic devices at nano level such as particle separation, filtration of nano powders, phase separation and so on [2]. There are huge number of researches is going on in the field of the microsystem for development and applicability of the aluminum oxide membrane in microhydraulic devices.

The major mechanical challenge in the filtration process is to pass the biocells from the nano holes fabricated in aluminum oxide membrane without mechanical damge [3]. Surface acoustic waves (SAW) is widely used and most approprite method because of such a small scale, wide range of frequency and excellent stability. The surface acoustic wave effect possible to produce using the actuating agent such as piezoelectric materials. By actuating the piezoelectric cylinder at different range of frequency it is possinle to generate SAW effect on the suraface of nanomemnrane. Using standing and travelling waves principle concentration of the particles for the seperation and filtration can be done in rapidy [2,4].

The objective of the work is to fabricate the nanoporous aluminum oxide membrane with predefined geometry of hole size and interpore distance for nanofiltration and actuating the nano membrane at different range of frequency by using the piezoelectric cylinder to produce the SAW effect which is usefull as a filtering agent for microhyraulics in the field of biomedicine.

Firstly, By applying two step anodization mehod (MA & HA) self orderd nanoporous aluminum oxide membrane was fabricated using custom made anodization experimental setup. After fabrication the confirmation of the diamer and interpore distance was identified by scanning electron microscopy (SEM) and surface morphology. Diameter of fabricated nano memnrane is 30 mm, diameter of the nano pores 70 ±20 nm and interpore distance 110± 10 at constant voltage 60 V and oxalic acid as electrolyte during anodization.

After fabrication of the nano membrane actuation was performed using the piezoelectric cylinder. Nano membrane was fixed on the piezoelectric cylinder. Piezoelectric cylinder was actuated at the frequency range of 1-100 kHz. The nondestructive testing methods was used to analyze the different mode of vibration acting on the surface of aluminum oxide nano membrane. PSV-500-3D Scanning Vibrometer (Polytech) and holographic PRISM optical system (USA by HYTECH) was used to analyses the distribution of the vibration on the nanoporous aluminum oxide membrane by mounting nano membrane on the piezoelectric ring. Those methods confirm the different mode of the vibrations and patterns of the surface acoustic waves which is useful for the particle filtration and separation in microhydraulic devices in biomedicine.

CANCELLED DUE TO COVID-19

Acknowledgement: This research was funded by a Grant S-MIP-17-102 from the Research Council of Lithuania.

[1] Zhou, Z., & Nonnenmann, S. S. (2019, August 1). Progress in nanoporous templates: Beyond anodic aluminum oxide and towards functional complex materials. Materials, Vol. 12. https://doi.org/10.3390/ma12162535

[2] Janusas, G., Guobiene, A., Palevicius, A., & Ramalis, L. (2017). Nanoporous aluminum oxide membranes for biomedical micro hydraulic devices. Vibroengineering Procedia, 15, 110–114. https://doi.org/10.21595/vp.2017.19448

[3] Sara Salehyar and Qiang Zhu. (2016) Deformation and internal stress in a red blood cell as it is driven through a slit by an incoming flow. Soft Matter, 12, 3156-3164.

[4] Zhang, A., Liu, W., Jiang, Z., & Fei, J. (2009). Rapid concentration of particle and bioparticle suspension based on surface acoustic wave. Applied Acoustics, 70(8), 1137–1142. https://doi.org/10.1016/j.apacoust.2009.02.007

SIMPLE APPROACHES TOWARDS IMPROVING THE PERFORMANCE OF LEAD HALIDE PEROVSKITE NANO- AND MICROLASERS

Anatoly Pushkarev, Daria Markina, Pavel Trofimov, Ivan Sinev, Sergey Makarov

Department of Physics and Engineering, ITMO University, Russia
anatoly.pushkarev@metalab.ifmo.ru

Over the last decade, halide perovskites have emerged as promising materials to supersede conventional $A^{III}B^{V}$ semiconducting nano- and microstructures for photonics applications. Great interest in perovskites is caused by their unique structural and photophysical properties such as defect tolerance, highly efficient absorption and emission, and long diffusion length. Moreover, these materials tend to form regular shaped nano- and microcrystals - optical resonant cavities. The electromagnetic field in such cavities is distributed in the form of resonant modes (e.g. Mie, Fabry-Pérot, or whispering gallery modes) and mediates laser action because of both optical gain and refractive index of the medium are sufficient. Generally, perovskite resonators exhibit high-quality lasing ($Q_{las} \sim 10^3 - 10^4$) at low threshold power. [1, 2, 3, 4, 5] The outcoupled light propagates in certain directions defined by the shape of the resonator. However, the improvement of laser performance as well as light management could be realized by integrating the perovskite cavities with various nanomaterials.

Herein we report on $CsPbBr_3$ nanowires deposited on nanostructured indium-tin-oxide substrates (Fig. 1a) by using a simple wet chemical approach. Surface passivation of the substrates is found out to govern the regularity of the perovskite resonators shape. The nanowires show room-temperature lasing with quality factors that are $3-4$ times higher than that of similar structures on a flat indium-tin-oxide layer (Fig. 1b). Concerning the light management, we show simple integration of $CsPbBr_3$ microlasers with GaP nanowaveguides (Fig. 1c) resulting in the direct output of coherent light from the end facet of the latter (Fig. 1d). Importantly, long-range guiding of visible light could be realized in $CsPbBr_3$-GaP structures since GaP exhibits low ohmic losses in the range of perovskite photoluminescence.

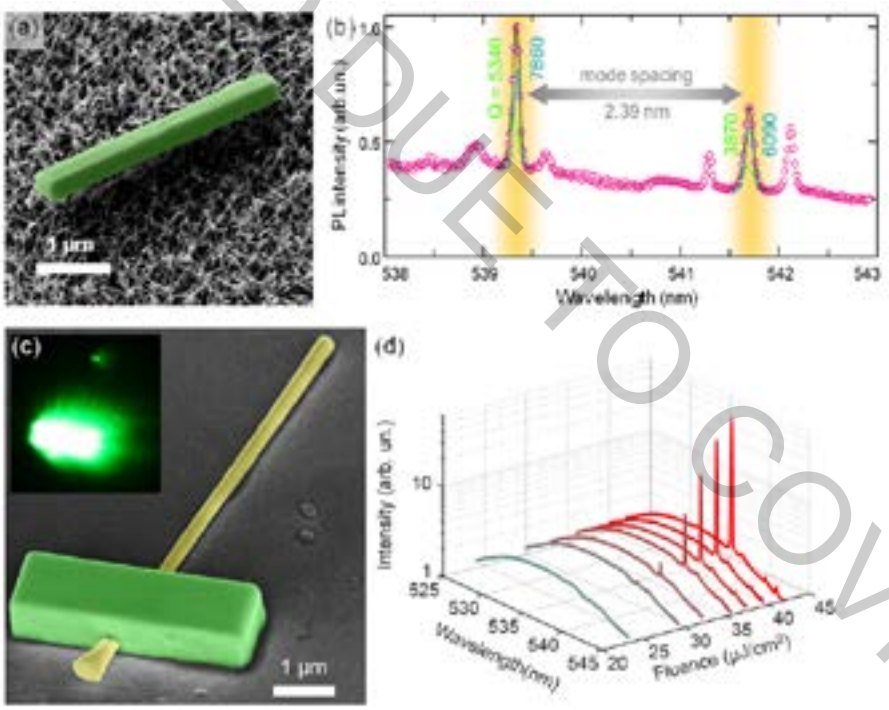

Fig. 1. (a) SEM image of $CsPbBr_3$ NW on nanostructured ITO substrate. (b) Laser emission of NW with 9 μm length. (c) SEM and fluorescent (inset picture) images of GaP nanowaveguide embedded into $CsPbBr_3$ microcavity. (d) PL intensity collected from GaP end facet versus fluence characteristics.

Acknowledgement: Russian Science Foundation (grant no. 18-73-00346)

[1] Q. Liao, K. Hu, H. Zhang et al., Perovskite microdisk microlasers self-assembled from solution, Advanced Materials **27**, 3405-3410, (2015).
[2] Q. Zhang, S. T. Ha, X. Liu et al., Room-temperature near-infrared high-Q perovskite whispering-gallery planar nanolasers, Nano letters **14**, 5995-6001 (2014).
[3] A. P. Pushkarev, V. I. Korolev, D. I. Markina et al., A few-minute synthesis of CsPbBr3 nanolasers with a high quality factor by spraying at ambient conditions, ACS applied materials & interfaces **11**, 1040-1048 (2019).
[4] A. Zhizhchenko, S. Syubaev, A. Berestennikov et al., Single-mode lasing from imprinted halide-perovskite microdisks, ACS Nano **13**, 4140-4147 (2019).
[5] E. Yu. Tiguntseva, K. L. Koshelev, A. D. Furasova et al., Single-particle Mie-resonant all-dielectric nanolasers, arXiv:1905.08646 (2019).

CANCELLED DUE TO COVID-19

SPECTROELECTROCHEMISTRY OF ELECTROPHORETIC CdSe QD FILMS

Yauhen Aniskevich[1,2], Aliaksandra Radchanka[1], Artsiom Antanovich[1], Mikhail Artemyev[1], Genady Ragoisha[1], Eugene Streltsov[2]

[1]Research Institute for Physical Chemical Problems of the Belarusian State University, Minsk, 220006, Belarus
[2]Department of Chemistry, Belarusian State University, Minsk, 220030, Belarus
aniskevich.y.m@gmail.com

CANCELLED DUE TO COVID-19

Quantum dots (QDs) are known to be attractive for use in photovoltaics, optoelectronics, and photonics due to tunability of their properties by size, shape and surface chemistry [1]. Moreover, several QD properties can be modulated by electrochemical treatment. For instance, electrochemical injection of electrons into QD conduction band (CB) results in absorbance spectra change due to exciton absorption bleaching [2, 3].

Here we investigate electrochemistry and spectroelectrochemistry of CdSe QD films obtained by electrophoretic deposition on FTO. Cyclic voltammetry of CdSe QD films in NBu_4PF_6/acetonitrile electrolyte reveals two pairs of redox peaks, observable at −1.1 and −1.3 V (Fig. 1a) for 6.3 nm particles. The cathodic and anodic peaks correspond to electron injection to CdSe CB levels and its withdrawal after scan reversal which is seen by changes in absorbance spectra of films (Fig. 1b). Figure 1b shows CdSe QD film differentitial visible spectra variation in negative and positive scans of the electrode potential. As the electrode potential is scanned negatively, absorbance of the first exciton (635 nm) drops gradually and recoveres reversibly after scan reversal. The first exciton absorption was completely bleached and this indicates the whole filling of the $1S_e$ level of each particle with electrons and that the whole film is electrochemically active. The changes in optical properties were also observable with a naked eye while the electrode potential was scanned.

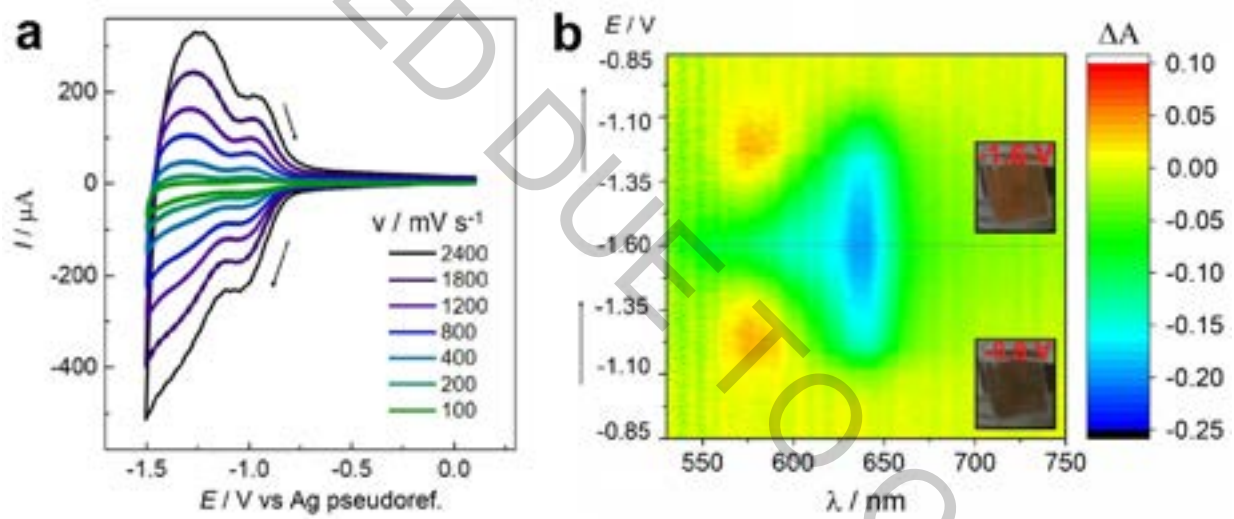

Fig. 1. (a) Cyclic voltammetry of a CdSe QD film electrode in 0.1 M NBu_4PF_6/CH_3CN electrolyte. (b) Differential spectra of the QD film upon cyclic potential scan at 0.2 V/s (transmission mode). The inserts show the film color at different states.

An analysis of electrochromism kinetics showed that the transition between charged and uncharged QD states completes within 200 ms for 500 nm thick films. We have also studied effects of the QD size, capping ligand length and film thickness on volatmmetric and spectroelectrochemical response.

Thus, our investigation has revealed fast and reversible electrochromic behavior of electrophoretically deposited CdSe QD films.

This work has been supported by Horizon 2020 research and innovation program under MSCA-RISE-2017 grant agreement No. 778357.

[1] Semiconductor Nanocrystal Quantum Dots: Synthesis, Assembly, Spectroscopy and Applications; Rogach, A. L., Ed.; Springer, 2008.
[2] C. Wang, M. Shim, P. Guyot-Sionnest, Electrochromic Nanocrystal Quantum Dots. Science, 291, 2390-2392 (2001).
[3] S.C. Boehme et al., Electrochemical Charging of CdSe Quantum Dot Films: Dependence on Void Size and Counterion Proximity. ACS Nano, 7, 2500-2508 (2013).

SEEDED-GROWTH OF SILVER NANOPARTICLES BY CHEMICAL REDUCTION METHOD

Audronė Šeštakauskaitė[1], Nadzeya Khinevich[2], Tomas Tamulevičius[1,2], Asta Tamulevičienė[1,2]

[1] Department of Physics, Kaunas University of Technology, Studentų Str. 50, Kaunas, Lithuania
[2] Institute of Materials Science of Kaunas University of Technology, K. Baršausko Str. 59, Kaunas, Lithuania
audrone.sestakauskaite@ktu.edu

The ability to create silver nanoparticles with precise control of their physical, chemical and structural properties is crucial for expanding their applicability in various applications, e.g. optoelectronics, energy storage, catalysis [1], chemical and biological sensors [2], biomedicine [3] and others. Because of its properties, silver can be used in surface-enhanced Raman scattering (SERS) sensors, which allow the detection of vanishingly small amounts of various materials and, in some cases, single molecules [4-5].

The aim of this work was to synthesize spherical silver nanoparticles employing simple and reproducible chemical reduction method. Silver nitrate ($AgNO_3$), tannic acid ($C_{76}H_{52}O_{46}$) and trisodium citrate ($Na_3C_6H_5O_7$) were used as precursor, redactor and stabilizer respectively. The results of UV-Vis absorption spectra were recorded on an AvaSpec-2048 fiber optic spectrometer (172 - 1100 nm, 1.4 nm resolution). The size and shape of silver nanoparticles were determined by microscopic analysis using scanning electron microscope QUANTA 200FEG (1.2 nm (30 kV, SE)). The SEM images were analysed with ImageJ software [6] and size distribution of particles was determined measuring at least 50 particles in each image. The absorption spectrum of silver nanoparticles was theoretically calculated using the MiePlot program [7].

Colloidal solutions with small particles (11 nm diameter) appear yellow and clear and this solution was used as seeds for further growth of nanoparticles. After the growth process solutions with larger particles lose characteristic yellow colour due to the multipole plasmon resonance, which becomes the dominant spectral component. The UV-VIS absorption spectra of different size silver nanoparticles is presented in Fig 1. From the absorption spectra, one can see that the peak position is shifting towards longer wavelengths and becoming broader, suggesting that the particle size is increasing. When the size of Ag nanoparticles reach 53 nm, the absorption peak begins to develop a "hump" at 405 nm, which represents the quadrupole resonance of silver nanoparticles. SEM analysis has shown that synthesized particles prevail spherical shape and Mie scattering theory was used to model the optical response of the particles (Fig. 2). Comparing the theoretical and experimental results one can see that theoretically generated curves are much narrower compared to the experimental ones. This can be explained by the fact that in theoretical calculations only single value of particle radius was used and the experimental spectrum is a sum of signals generated of different size particles.

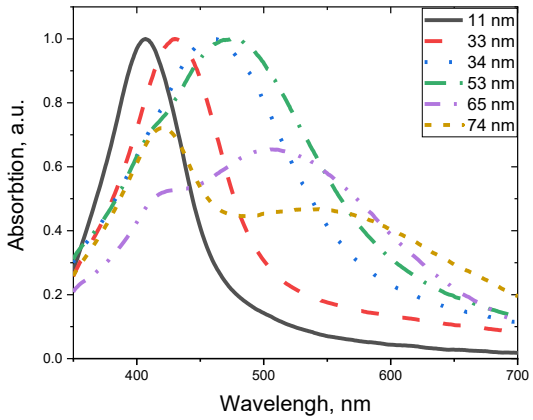

Fig. 1. UV-VIS absorption spectra of silver nanoparticles

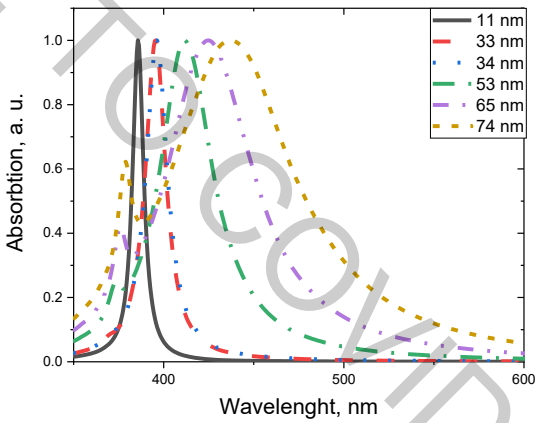

Fig. 2. Theoretical absorption spectra of Ag nanoparticles

[1] M. Rycenga *et al.*, "Controlling the synthesis and assembly of silver nanostructures for plasmonic applications," in *Chemical Reviews*, vol. 111, no. 6, 2011, pp. 3669–3712.
[2] A. Loiseau, V. Asila, G. Boitel-Aullen, M. Lam, M. Salmain, and S. Boujday, "Silver-based plasmonic nanoparticles for and their use in biosensing," in *Biosensors*, vol. 9, no. 2, MDPI AG, 2019.
[3] S. Nakamura *et al.*, "Synthesis and application of silver nanoparticles (Ag nps) for the prevention of infection in healthcare workers," *Int. J. Mol. Sci.*, vol. 20, no. 15, 2019.
[4] M. Fan and A. G. Brolo, "Silver nanoparticles self assembly as SERS substrates with near single molecule detection limit," *Phys. Chem. Chem. Phys.*, vol. 11, no. 34, pp. 7381–7389, 2009.
[5] T. Y. Chan *et al.*, "SERS Detection of Biomolecules by Highly Sensitive and Reproducible Raman-Enhancing Nanoparticle Array," *Nanoscale Res. Lett.*, vol. 12, pp. 0–7, 2017.
[6] "ImageJ." [Online]. Available: https://imagej.nih.gov/ij/. [Accessed: 23-Dec-2019].
[7] "MiePlot." [Online]. Available: http://www.philiplaven.com/mieplot.htm. [Accessed: 23-Dec-2019].

ORGELFREE TO COVID-19

THE STUDY OF THE MINERAL COMPOSITION OF THE STONY PART OF THE BRAHIN METEORITE BY LASER ATOMIC EMISSION SPECTROMETRY

Anastasiya Martynava[1], Anastasiya Huryna[1], Natallja Arekhava[1],
Anatoli Zajogin[2], Maksim Shundalau[2]

[1] Secondary School No. 64, Minsk, Belarus
[2] Faculty of Physics, Belarusian State University, Minsk, Belarus
nastzmart2002@mail.ru

CREATED DUE TO COVID-19

During the long time meteorites were the only source of information about the protoplanetary and early planetary history of the Solar System. Nowadays, despite of the intensive development of space research, meteorites remain the key source of the above-mentioned information. The studies of mineral and chemical composition of meteorites expand our knowledge of the Solar System cosmogony [1-4]. According to the mineralogical and chemical composition, all meteorites are divided into three groups: stony, stony-iron, and iron meteorites. The stony-iron meteorites consist of nearly equal parts of iron and stone (silicates). The stony-irons are divided into two classes: mesosiderites and pallasites. Their main difference is following: the mesosiderites' silicates are mainly represented by pyroxene and plagioclase, and the pallasites' silicates are olivines of various sizes and shapes.

The Brahin meteorite represents a group of fragments that were found over 200 years ago in the Brahin District (former Russian Empire, now Belarus). All fragments have the same structure and composition. Despite of long history of the Brahin meteorite, it remains poorly studied [1].

The olivines are the most common minerals in the Brahin meteorite. They visually compose approximately 50% of the plate area of the Brahin meteorite. The second most common mineral is the nickel iron, which accounts for approximately 45% of the plate area.

The main goal of this work is studying of the mineral composition of the stony part of the sample of the Brahin meteorite. The local spatial and volume distribution of the elements was determined by laser multichannel spectrometry using the laser atomic emission multichannel LSS-1 spectrometer, which has the following characteristics: the pulse duration is around 15 ns, the laser radiation is focused on the sample using an achromatic condenser with a focal length of 104 mm, the size of the focus spot is approximately 50 μm, the pulse energy is 35 mJ.

The Fig. 1*a* represents a portion of the stony part of the meteorite. The places of the double laser pulses impacts are the black dot in the light part, and the white one in the dark part. Figs. 1*b* and 1*c* show layer-by-layer (20 pulses per layer) distribution of Mg, Ca, and Fe in the indicated points.

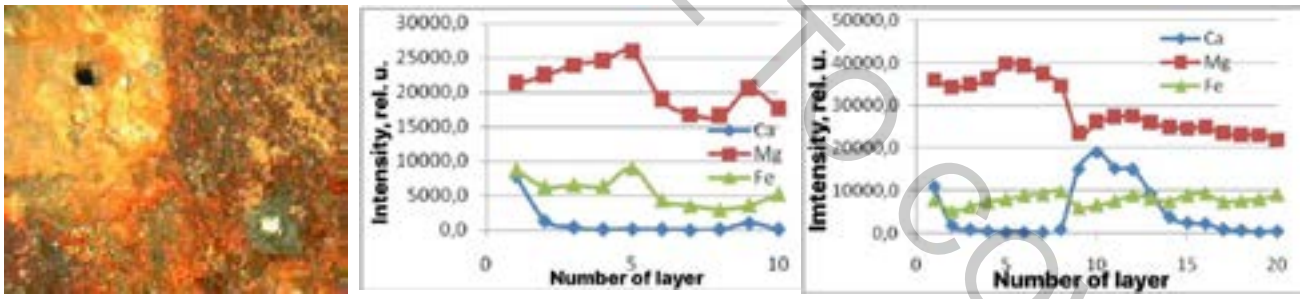

a *b* *c*

Fig. 1. The stony part of the Brahin meteorite (*a*), layer-by-layer distributions of elements in the light (*b*) and the dark (*c*) parts of the sample.

There is a significant difference between distributions of Ca in the light and the dark parts of the meteorite. It can be assumed that there is an inclusion of a new mineral in the dark part at the depth between 9th and 15th layers. Taking in the account the fact that the average ablation per pulse is of the order of 10-15 μm, the thickness of the mineral sample is approximately 50-150 μm. To assess the size of the inclusion, the analysis of the calcium content was made in two mutually perpendicular directions. The approximate size of the inclusion is 1×1.3 mm.

It should be worth mentioned that earlier (see, for example, the most detailed study of the chemical and mineral composition of the stony part of the Brahin meteorite [1]) the presence of a mineral containing together these three elements was not found. Apparently, the mineral belongs to a variety of Ca-containing olivines [4].

[1] A.I. Bakhtin, A.A. Eskin, R.Kh. Sungatullin, G.V. Sonin, R.D. Petrova, Peculiarities of the composition and genesis of the Brahin meteorite. Uchenye Zapiski Kazanskogo Universiteta. Seriya Estestvennye Nauki **160**, 324–338 (2018) (In Russian).
[2] P.R. Buseek, Pallasite meteorites—mineralogy, petrology and geochemistry, Geochim. Cosmochim. Acta **41**, 711–740 (1977).
[3] Z.A. Lavrentjeva, A.Y. Lyul, G.M. Kolesov, The Omolon pallasite: Chemical composition, mineralogy, and genetic implications, Geochem. Int. **50**, 34–43 (2012).
[4] A.V. Ivanov, A.A. Yaroshevskiy, M.A. Ivanova, Meteorite minerals, Geochem. Int. **57**, 931–939 (2019).

STAR CLUSTERS IN THE ANDROMEDA GALAXY. PHOTOMETRIC EFFECTS OF BACKGROUND/FOREGROUND STARS

Karolis Daugevičius[1,2], Rokas Naujalis[1], Rima Stonkutė[1]

[1] Center for Physical Sciences and Technology, Saulėtekio av. 3, 10257 Vilnius, Lithuania
[2] Vilnius University Observatory, Saulėtekio av. 3, 10257 Vilnius, Lithuania
karolis.daugevicius@ff.stud.vu.lt

ACCEPTED DUE TO COVID-19

Deriving physical parameters of star clusters using aperture photometry is an effective method to investigate evolution of galaxies. However, in majority cases bright background or foreground stars projecting within photometry apertures make measurement results unreliable, which in turn leads to inaccurately derived physical parameters of star clusters. In this study we aimed to improve the accuracy of star cluster photometry (the Panchromatic *Hubble* Andromeda Treasury survey, PHAT [1]) by correcting for background/foreground ("suspected") stars interactively.

We used the subsample of PHAT star clusters analysed in [2]. For each of these 1183 clusters we located objects within their aperture radius using PHAT star catalogue [3]. To identify "suspected" stars projecting onto the cluster, we analysed cluster colour images (Fig. 1a) in various passbands and distribution of stars in the colour-magnitude diagram (CMD, Fig. 1b). We selected bright objects that likely do not belong to a given cluster based on their colours and unusual positions in the CMD. Majority of the selected "suspected" stars are red, i.e., bright objects in the infrared passbands. However, in some cases bright in the ultraviolet passbands "suspected" stars also were selected.

Quality of the PHAT cluster photometry was improved considerably by subtracting those "suspected" stars. Positions of all reduced clusters in the colour-colour diagram are shown before (red) and after (blue) subtracting of the "suspected" stars (Fig. 1c). Also, in Fig. 1c are plotted stochastic theoretical models by applying various extinction values (small grey dots). A better match of the star cluster photometry data with theoretical models in the ultraviolet and visual passbands is noticeable. However, in the infrared passbands a spread of corrected cluster photometry data increased significantly. We found that subtraction of "suspected" stars imitates interstellar extinction effects.

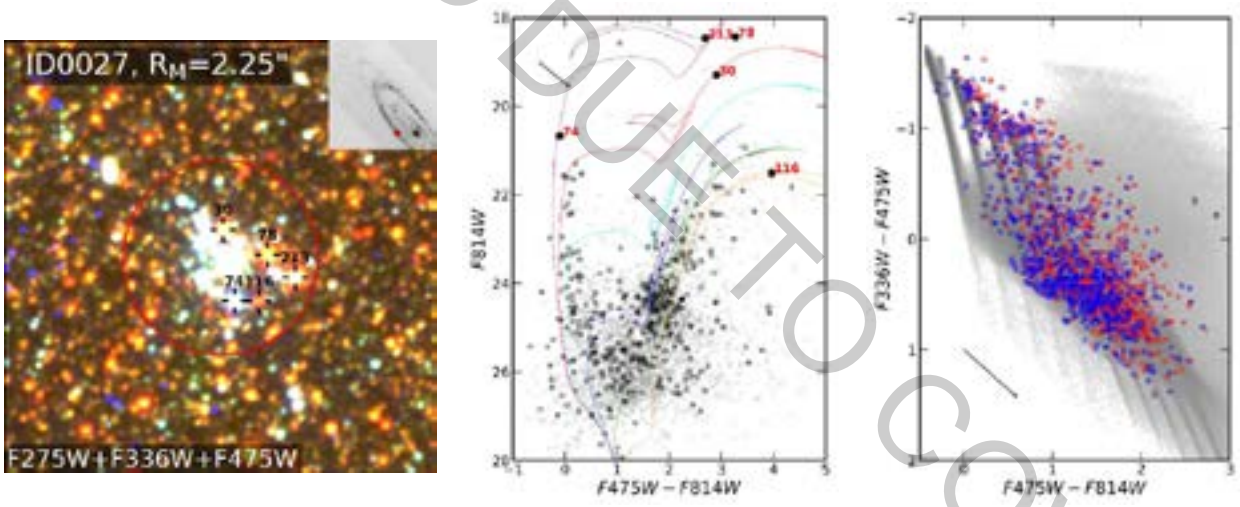

a) b) c)

Fig. 1. a) The multi-colour image of the PHAT cluster ID0027 with marked "suspected" stars. A position of the star cluster ID0027 in the Andromeda galaxy is shown in the inset (upper-right corner, red dot). b) the CMD; black numbered dots mark "suspected" stars, black open circles – stars inside the aperture radius, grey dots – stars around the cluster. c) The colour-colour diagram of the PHAT star clusters in the Andromeda galaxy. Red open circles mark star clusters before subtraction of the "suspected" stars; blue open circles – after subtraction. Stochastic theoretical models are shown in grey. Arrows indicate extinction vector, $A_V = 1$.

[1] Johnson, L. C., Seth, A. C., Dalcanton, J. J., et al. 2015, ApJ, 802, 127
[2] Naujalis, R., Daugevičius, K., Stonkutė, R., Vansevičius, V. 2019, Star clusters of the Andromeda galaxy. Conf. LNFK-43, Kaunas, Lithuania
[3] Williams, B. F., Lang, D., Dalcanton, J. J., et al. 2014, ApJS, 215, 9

GAS AND DUST TEMPERATURE IN THE INTERSTELLAR FILAMENTARY INFRARED DARK CLOUDS

Olga Ryabukhina[1,2], Igor Zinchenko[2], Maria Kirsanova[1]

[1]Institute of Astronomy of the Russian Academy of Sciences, Moscow, Russia
[2]Institute of Applied Physics of the Russian Academy of Sciences, Nizhny Novgorod, Russia
ryabukhina@ipfran.ru

CANCELLED DUE TO COVID-19

The study of the processes of star formation in interstellar clouds is one of the most relevant topics in astrophysics. Recent studies have shown that these clouds have a filamentary structure [1]. To build a deeper model of the processes of star formation, we must restore the physical parameters in dark infrared clouds. One of these parameters is the temperature, for the determination of which various methods based on radio or infrared observations are used.

The conditions of local thermodynamic equilibrium (LTE) are often realized in dense interstellar clouds, under which the excitation temperature (T_{ex}) of the second most abundant ^{12}CO molecule approaches the kinetic temperature (T_{kin}) of the gas. T_{ex} of ^{12}CO is calculated by:

$$T_{ex} = 10.6/ln\left(1 + \frac{10.6}{T_B + 0.2132}\right), \tag{1}$$

where T_B^{12} is the brightness temperature of the optically thick line J = 2–1 ^{12}CO at 230.538 GHz [2]. However, due to the high optical thickness in the line, it shows the conditions on the cloud surface.

Analysis of the thermal emission in the far infrared range can be used to obtain the dust temperature (T_d). To do this, we simulated the spectral energy distribution of dust emission according to Herschel (160-500 m). Blackbody expression with free parameters T_d and column density of hydrogen N(H_2) was built:

$$S_\nu(\nu) = \Omega(1 - e^{-\tau(\nu)})(B_\nu(\nu, T_d) - I_{bg}(\nu)) \tag{2}$$

$$\tau(\nu) = N_H m_H k_d(\nu) M_d/M_H, \tag{3}$$

where $S_\nu(\nu)$ is the observed flux density at frequency ν, Ω is the solid angle, $\tau(\nu)$ is the optical depth, $B_\nu(\nu, T_d)$ is the Planck function, $I_{bg}(\nu)$ is the background flux level, $N_H = 2 \times N(H_2) + N(H)$ is the total hydrogen column density, m_H is the hydrogen mass, M_d/M_H is the dust-to-hydrogen mass ratio, and $k_d(\nu)$ is the dust mass absorption coefficient. Thus, the temperature of the gas in the filament G192.76+00.10 which is located in the star forming complex S254–S258 was calculated using CO (2–1) emission, the temperature of the dust using Herschel data.

The kinetic temperature of the gas can be calculated from the emission of inversion transitions of ammonia. Due to the tunneling of the nitrogen through the plane created by the hydrogen nuclei, the transitions have hyperfine splitting. The populations of the metastable levels (1,1) and (2,2) are determined by collisions.

$$T_{kin} = \frac{T_{rot}}{1 - \frac{T_{rot}}{42K} ln(1 + 1.1exp(\frac{-16K}{T_{rot}}))}(K), \tag{4}$$

where T_{rot} is rotational temperature which can be derived from the intensity of the lines NH_3 (1,1) and (2,2) and the optical depth of NH_3 (1,1) [2]. The temperature of the gas in the filament WB 673 was calculated from the emission of ammonia.

The kinetic temperature of the gas was estimated from observations of the CH_3CCH line using the "population diagrams" method. The methylacetylene molecule is a type of symmetric top and is a reliable indicator of kinetic temperature, since it may separate the effect of temperature and density on the excitation of rotational transitions [3]. The dependence on E_u was built:

$$\ln\left(\int T_A dv/[g_I g_K (J^2 - K^2)]\right), \tag{5}$$

where E_u is the energy of the upper level, T_A is the brightness temperature in a line, v is the radial velocity, $\int T_A dv$ is the integrated intensity of the line, g_K is the statistical weight of the level K, g_I is the statistical weight due to nuclear spin, J is a quantum number that determines the moment of the momentum of motion; K is a quantum number that determines the projection of the moment on the axis of symmetry of the molecule. The kinetic temperature is found as the reciprocal of the slope of a straight line approximated by this dependence. Thus the temperature in the filament G351.78-0.53 was calculated.

This research was supported by the Russian Foundation for Basic Research (grant No. 18-02-00660)

[1] André, P. and Di Francesco, J. et al., From Filamentary Networks to Dense Cores in Molecular Clouds: Toward a New Paradigm for Star Formation, Protostars and Planets VI, 27 (2014).
[2] Rohlfs, Kristen and Wilson, Thomas L., Tools of radio astronomy (2004).
[3] Bergin, E. A. and Goldsmith, P. F. et al., CH3C2H as a temperature probe in dense giant molecular cloud cores, The Astrophysical Journal, **431**, 674-688 (1994).
[4] Wienen, M. and Wyrowski et al., Ammonia from cold high-mass clumps discovered in the inner Galactic disk by the ATLASGAL survey, Astronomy & Astrophysics, **544**, A146, (2012).

ABUNDANCE OF ZIRCONIUM IN THE ATMOSPHERES OF RED GIANTS IN GALACTIC GLOBULAR CLUSTER 47 TUC

Edgaras Kolomiecas[1], Vidas Dobrovolskas[1], Arūnas Kučinskas[1]

[1] Institute of Theoretical Physics and Astronomy, Faculty of Physics, Vilnius University, Lithuania
edgaras.kolomiecas@ff.vu.lt

It has been long held that Galactic globular clusters (GGCs) are homogeneous objects consisting of stars that have the same age and chemical composition. However, research done during the past decade has shown that stars in the GGCs do not share the same chemical composition and may have formed during different star formation episodes (see, e.g., [1]). This suggests that GGCs may consist of two (or more) generations of stars, with the second generation born from the material enriched by the ejecta of first-generation stars, with the most plausible candidates being fast-rotating massive stars [2] and asymptotic giant branch (AGB) stars [3], the so called polluters. Unfortunately, our current knowledge about the GGCs does not allow us to discriminate between the possible pollution scenarios.

In order to determine which polluters were most likely to enrich the intracluster medium during the early stages of GGC formation, one may look at the abundances of *s*-process elements. Since AGB stars produce *s*-process elements and fast-rotating massive stars do not, abundance correlations between the light and *s*-process chemical elements would indicate that the polluters were AGB stars. On the other hand, no such correlation would indicate that the polluters were fast-rotating massive stars. One earlier study has suggested a tentative existence of a correlation between the abundances of Na and Ba in the globular cluster 47 Tuc [4]. In order to check if such correlation may also exist in the case of Zr, which, like Ba, is also an *s*-process element, we determined Zr abundance in 327 RGB stars in 47 Tuc. Importantly, the studies of Zr abundance in the GGCs have been very scarce until now and the results were inconclusive, i.e., not only for this but also other GGCs.

Abundance analysis was based on the archival spectra of RGB stars in 47 Tuc that were obtained with GIRAFFE spectrograph mounted on the VLT UT2 telescope (ESO, Chile). Two spectral lines of neutral Zr were used, with their central wavelengths located at 613.4585 nm and 614.3252 nm. Line equivalent widths were measured using IRAF package, by fitting Gaussian profiles to the observed spectral lines. Stellar model atmospheres were computed using the ATLAS9 code and were further employed to derive 1D LTE Zr abundances with the WIDTH9 package.

The mean Zr to Fe abundance ratio that we obtained in a sample of 327 RGB stars in 47 Tuc is [Zr/Fe] = +0.38 ± 0.12 (the error is standard deviation due to star-to-star abundance variation). This is so far the largest sample of RGB stars analyzed in this cluster for Zr abundance. Analysis of Zr and Na abundances shows weak but statistically significant correlation: Pearson correlation coefficient is 0.36 and Student's *t*-test probability is $< 10^{-4}$ (Fig. 1). This suggests that AGB stars played a significant role in the enrichment of the intracluster medium in 47 Tuc.

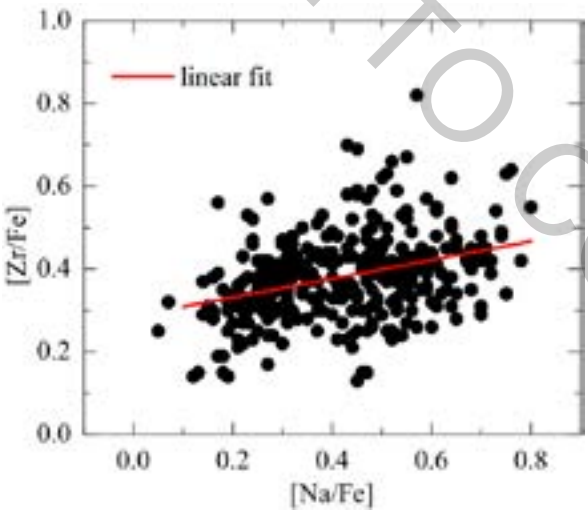

Fig. 1. Abundance of Zr in the RGB stars of 47 Tuc plotted against the sodium-to-iron abundance ratio.

[1] Bastian, N. & Lardo, C. 2018, ARA&A, 56, 83.
[2] Krause, M., Charbonnel, C., Decressin, T., Meynet, G., & Prantzos, N. 2013, A&A, 552, A121.
[3] Ventura P., D'Antona F., Mazzitelli I., Gratton, R., 2001, ApJ, 550, L65.
[4] Gratton, R. G., Lucatello, S., Sollima, A., Carretta, E., Bragaglia, A., Momany, Y., D'Orazi, V., Cassisi, S., Pietrinferni, A., & Salaris, M. 2013, A&A, 549, A41.

CANCELLED DUE TO COVID-19

MODELLING OF ACCRETION ON TO THE MILKY WAY'S SUPERMASSIVE BLACK HOLE

Matas Tartėnas[1], Kastytis Zubovas[1,2]

[1]Faculty of Physics, Vilnius University, Lithuania
[2]Department of Fundamental Research, Center for Physical Sciences and Technology, Vilnius, Lithuania
matas.tartenas@gmail.com

CANCELLED DUE TO COVID-19

Currently, the black hole at the center of the Milky Way is inactive, but a few million years ago there was a period of increased activity leaving traces in the surrounding environment [1]. It is suggested that an active galactic nucleus (AGN) phase could follow a collision of the molecular gas ring that surrounds the black hole (the circumnuclear ring or CNR) and an infalling molecular cloud. The observed ~ 6 Myr stellar population in the central parsec as well as the *Fermi* bubbles could be linked to this AGN phase [1, 2].

We aim to reproduce the activity period with a hydrodynamical Gadget-3 model of the several-parsec-wide region of the Galactic centre. The model consists of three main components: the central black hole ($M_{\rm bh} = 4 \times 10^6\,{\rm M}_\odot$), the CNR-like toroidal gas ring ($M_{\rm r} = 10^5\,{\rm M}_\odot$, $R_{\rm in} = 1.5\,{\rm pc}$, $R_2 = 4\,{\rm pc}$) and the infalling molecular cloud ($M_{\rm mc} = 10^5\,{\rm M}_\odot$, $R_{\rm mc} = 3\,{\rm pc}$). The central black hole is fed by the gas that crosses a sink boundary ($r_{\rm sink} = 0.01\,{\rm pc}$) in the hydrodynamical model. We also allow for star formation.

By varying the initial inclination angle (γ) of the orbit of the molecular cloud we change the outcome of the encounter, including the feeding rate of the central accretion disc and the morphology of resulting structures.

We find that larger angles result in more compact systems with more mass concentrated in the centre. Large angle collisions also result in significant star formation in the central parsec. We also find that in the case of the most extreme collisions ($\gamma = 175^\circ$ and 180°) about one quarter to a half of the initial gas mass is accreted by the central black hole, although the accretion rate is well above Eddington limit. We account for this by using a simple model of the accretion disc and find that the energy released during the activity period is reduced by at least a half.

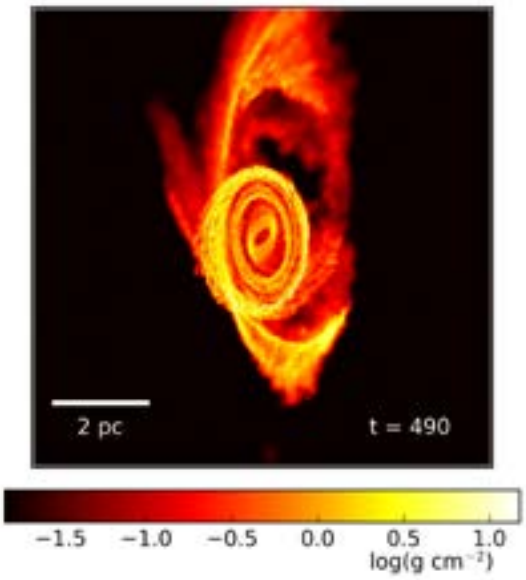

Fig. 1. Density map of the resultant system with $\gamma = 120^\circ$ at the time $t = 490$ kyr

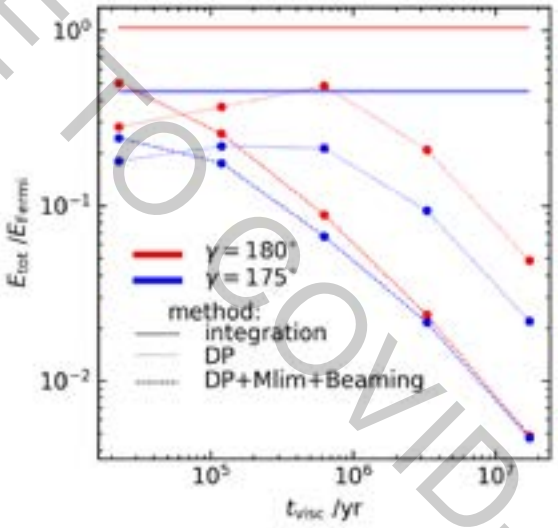

Fig. 2. The total energy released during the activity period depending on the viscous timescale $t_{\rm visc}$ of the accretion disc in the units of $E_{\rm Fermi}$

[1] Ponti G., Morris M. R., Terrier R., Goldwurm A., 2013, in Cosmic Rays in Star-forming Environments, edited by D. F. Torres, O. Reimer, vol. 34 of Astrophysics and Space Science Proceedings, 331.
[2] Zubovas K., Nayakshin S., 2012, MNRAS, 424, 666.

GRAVITATIONAL MICROLENSING SIMULATIONS THROUGH BINARY BLACK HOLES

Kotryna Šiškauskaitė[1], Zofia Kaczmarek[2], Krzysztof Rybicki[2], Lukasz Wyrzykowski[2], Erika Pakštienė[1]

[1] Institute of Theoretical Physics and Astronomy, Vilnius University, Lithuania
[2] Warsaw Astronomical Observatory, University of Warsaw, Poland
kotryna.siskauskaite@ff.vu.lt

In large and complex stellar populations such as galaxies it is difficult to predict the number of black holes and parameters of black hole (BH) population. Even more so for binary black hole systems, as the population of these systems is highly influenced by violent binary interactions during their evolution. Different initial parameters, such as metallicity or IMF also influence the binary black hole population. Natal kicks and binary mergers greatly reduce the number of black holes remaining in binaries. however according to a recent population synthesis study there should be around 3 million black holes remaining in binaries in the Milky Way. Based on OGLE-IV survey results that capture 2000 new gravitational microlensing events each year, 26 are caused by black holes. Out of those 26 events, 8 are estimated to be caused by binary black holes and in our study we found that one of these events should be resolvable as two peaks within single magnification period. We used a synthetic binary black hole population database to create gravitational microlensing events and generate theoretical light curves to check for resolvability of microlensing caused by these systems.

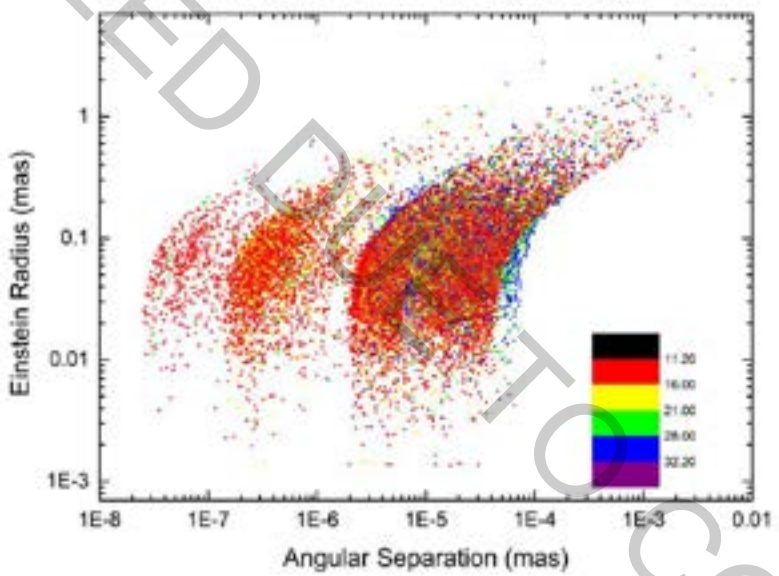

Fig. 1. Simulated binary black hole microlensing (BBH) events. Colors indicate total mass of the system. In the log x axis the angular separation is in milliarcseconds and log y is the Einstein Radii of BBH lens.

In order to simulate the microlensing events I used the database Universe@Home [1] with synthetic BBH population and used their derived parameters of these systems. I calculated Einstein radii of these events and mass lens separation ratio of these binary systems in order to create caustic maps. Our program solves general gravitational lensing equation for a binary system [2] and plots magnification maps of microlensing events with binary black holes as lens using inverse ray shooting. Based on magnification of the source, I generated theoretical light curves of the microlensing events to study the resolvability of these events. Based on my results I found that around 3% of the events are unseparable, 17% are distinct with two peaks over each component of the binary system and 80% have two different magnification periods on a single plane, resembling two different lensing events. Since OGLE-IV finds 8 microlensing events per year caused by binary black holes such event should be found once per year having single magnification period and two peaks, caused by the binarity of the system.

[1] Wiktorowicz, G., Wyrzykowsi, L., Chrulinska, M., Populations of Stellar-mass Black Holes from Binary Systems, The Astrophysical Journal 885:1 (2019).
[2] Witt, H., Shude, M. On the Minimum Magnification between Caustic Crossings for Microlensing by Binary and Multiple Stars, The Astrophysical Journal, L105 (1995).

CANCELLED DUE TO COVID-19

SEARCH FOR VARIABLE STARS IN THE NORTHERN SKY AND ANALYSIS OF PHOTOMETRIC TIME SERIES

Rūta Urbonavičiūtė[1], Erika Pakštienė[2]

[1] Faculty of Physics, Vilnius University, Lithuania
[2] Institute of Theoretical Physics and Astronomy, Vilnius University, Lithuania
ruta.urbonaviciute@ff.stud.vu.lt

As more space telescopes enter space, TESS (Transit Exoplanet Survey Satellite) launched in April 2018, and more to be launched, as JWST (James Webb Space Telescope) in 2021 and PLATO (PLAnetary Star Transit and Oscillation) in 2026. Their main purpose is to search and study exoplanets, but observing exoplanets with such cosmic telescopes, we also can observe brightness fluctuations of the stars, since the methodology for observing these objects is very similar. Variable stars have been recognized to offer crucial insights into stellar structure and evolution. With ground based observations, we search for most suitable variables - candidates stars, to study them further with space telescopes. The aim of this work was to find variable stars in five fields, which all of them are in northern sky. Observations of northern sky stars are vital, because vast majority of observatories are located in the southern hemisphere or closer to the equator, so stars near the north pole are inaccessible to them and therefore, the stars seen in this part of the sky are less studied. To attain this intent, chosen fields were near the north pole. We studied five fields, of which the central stars are NSV26138, NSV0255, NSV13673, NSV15053, NSV25919. To achieve this we used *Muniwin* [1] computer program to perform phomoteric reduction for these five fields. To determine variability of the stars we used Lomb-Scargle periodogramas and *Period04* [2] statistical analysis program to determine variability parameters of the stars. We found twenty previously unknown candidates of variable stars. For them we determined amplitudes, periods, phases of their brightness variations and possible variability types.

Among twenty previously unknown variable stars is a late type W Ursae Majoris binary which orbital period is 6 hours 27 minutes and two Algol type binary stars - candidates. We also observed one δ Scuti candidate with period - 20 hours 53 minutes. Together with them we found seven slowly variable stars and nine periodic variable stars.

Also we present recommendations for further investigations. We will use new data sets from cosmic telescope TESS (Transiting Exoplanet Survey Satellite) to study more profoundly Algol type stars. For all long period variables need more photometric observations for longer periods of time to prove their variability, to determine more precisely variability parameters and to conclude their type of variability. For three of them additional spectroscopic observations or multicolour photometric observations are needed in order to determine luminosity. We recommend spectroscopic or multicolour photometric observations for T-Tauri or BY Draconis candidates in order to determine their real type. For two unknown type short period variables we recommend also spectroscopic observations in order to determine their temperatures and luminosity.

---

[1] Hroch,F. 2014, Munipack:GeneralAstronomicalImageProcessingSoftware, *Astrophysics Source Code Library,* 140.006
[2] Lenz, P., Breger, M., 2005, *Communications in Asteroseismology,* 146, 53

CANCELLED DUE TO COVID-19

INVESTIGATION OF BLACK HOLE LENSES WITH ADAPTIVE OPTICS

Algita Stankevičiūtė[1], Oliwia Ziółkowska[1], Magdalena Pawłowska[1], Cezary Turski[1], Łukasz Wyrzykowski[1]

[1] Astronomical Observatory, Faculty of Physics, University of Warsaw, Poland
algita@astrouw.edu.pl, atigla@gmail.com

Gravitational microlensing phenomenon [1] is one of the most persuasive techniques to demonstrate the effectiveness of Einstein's general relativity [2]. The method relies on the space-time bending due to a massive object (e.g., black hole) and change in the trajectory of the light rays [3]. Resolving the images created during the lensing can lead to investigating massive astronomical objects, including black holes or planets, no matter how faint they are [4]. This gives a unique opportunity to investigate black holes lenses [5], different scenarios of their formation, in conjunction with the explanation of the nature of the dark matter and stellar evolution [6].

Gravitational microlensing phenomenon due to massive objects can be investigated with the ground-based astronomical instruments, however, one of the biggest issues with the ground-based observations is that the photon wavefront coming to the telescope is distorted due to atmospheric turbulence. It is caused by multiple atmospheric layers [7] which have different wind speeds and directions, also including absorption and scattering of the particles [8] in the atmosphere.

The easiest way to eliminate such instabilities and achieve high-resolution images is to use the Adaptive Optics (AO) system in telescope's interferometer that is able to correct distorted wavefront by collimator and deformable mirrors. It makes the wavefront planar that is detected by Shack-Hartman wavefront sensor [9].

In this research, we used ESO's VLT (Very Large Telescopes system) interferometric instrument NaCo [10] which is capable to provide multimode, corrected observations by AO system in the range of 1-5 μm. AO system performance possesses 50% Strehl ratio (SR) under good atmospheric conditions and good correction the K-band corresponds to an SR larger than 30% [10].

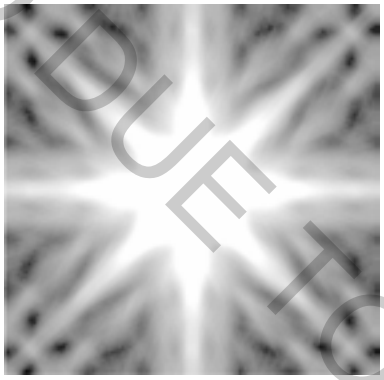

Fig. 1. Simulated PSF in log color scale

Using *soapy* [11] we simulated the point spread function (PSF) of NaCo. We created a set of artificial images of two point sources - a lens and a star, with varying separation and magnitude difference. We then convolved the artificial images with the PSF, which resulted in simulated NaCo images (in Fig. 1). Studying the shape of the simulated images and comparing it with the real NaCo image allowed us to determine whether a potential lens would be visible and to constrain its parameters.

In resume, by using NaCo and gravitational microlensing phenomenon, we hope to find Black Hole candidates.

[1] B. Paczynski. Gravitational Microlensing: Black Holes, Planets; OGLE, VLTI, HST and Space Probes. arXiv: 0306564 [astro-ph/] 26 Jun 2003.
[2] F. Delplancke, M. A. Górski and A. Richichi. Resolving gravitational microlensing events with long-baseline optical interferometry Prospects for the ESO Very Large Telescope Interferometer, Astronomy & Astrophysics **375(2),** 701-710 (2001).
[3] P. Murdin. *Encyclopedia of Astronomy and Astrophysics* (Nature Publishing Group, London, New York, Tokyo, 2001).
[4] P. Schneider, C. Kochanek and J. Wambsganss. *Gravitational Lensing: Strong, Weak and Micro* (Springer-Verlag Berlin, Heidelberg, 2006).
[5] Ł. Wyrzykowski, Z. Kostrzewa-Rutkowska and K. Rybicki. Microlensing by single black-holes in the Galaxy. arXiv:1601.02830 [astro-ph/] 12 Jan 2016.
[6] R. M. Wald. *General Relativity* (University of Chicago Press, Chicago and London, 1984).
[7] C. S. Gardner and J. D. Shelton. Density response of neutral atmospheric layers to gravity wave perturbations. Journal of Geophysical Research: Space Physics **90(A2)**, 1745-1754 (1985).
[8] A. Alkholidi and K. Altowij. Effect of clear atmospheric turbulence on quality of free space optical communications in Western Asia. Optical Communications Systems **41** (2012).
[9] R. K. Tyson. *Principles of Adaptive Optics* (CRC Press, London and New York, 2010).
[10] J. Girard, C. Dumas and A. Kaufer *Very Large Telescope NACO User Manual* (2011).
[11] A. Reeves. Soapy: an adaptive optics simulation written purely in Python for rapid concept development, Proc. SPIE **9909** (2016).

CANCELLED DUE TO COVID19

MORPHOLOGY AND KINEMATICS OF SIMULATED FERMI BUBBLES

Aidas Sadauskas, Kastytis Zubovas

Department of Fundamental Research, Center for Physical Sciences and Technology, Lithuania
a.sadauskass@gmail.com

SgrA*, the supermassive black hole in the center of the Milky Way, is probably one of the most important ingredients in the formation and evolution of our Galaxy. Young star clusters Arches & Quintuplet and young massive stars in the central parsec indicate that Sgr A* might have been active in the past <10 Myr. Recently discovered giant gamma-ray structures, known as the Fermi Bubbles [1], could be one of the activity footprints of SgrA*. The age and formation mechanisms of these structures are still unclear, therefore understanding the kinematics of Fermi Bubbles would help to determine their origin which in principle can be explained by an accretion episode of Sgr A*. In this work we perform numerical hydrodynamical simulations designed to reproduce the Fermi Bubbles and analyze the resulting gas morphology and kinematics. Studying the evolution of the simulated bubble sizes and shapes we find age estimates of these bubbles to be between 6 and 8 Myr, consistent with other indicators of past activity of Sgr A*.

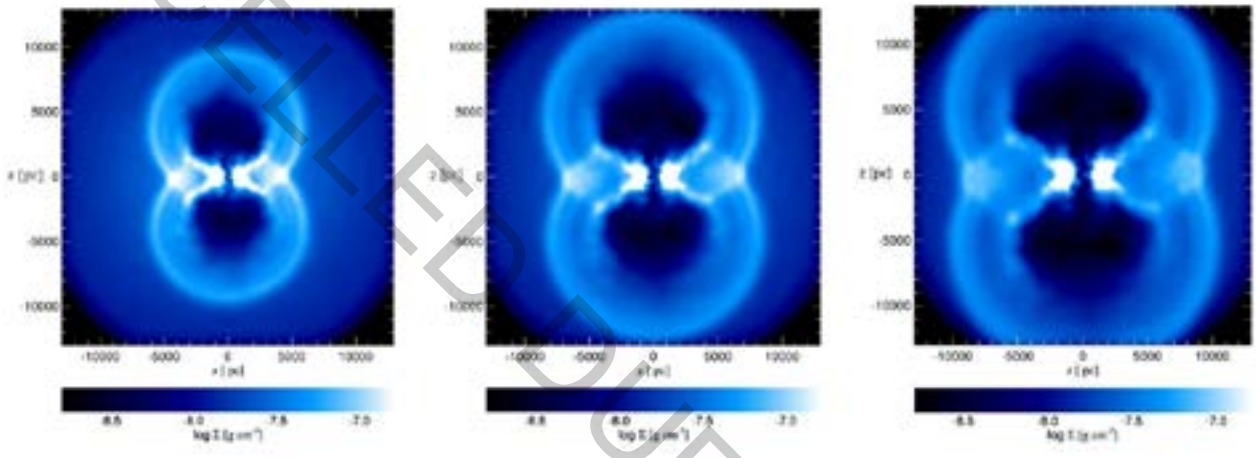

Fig. 1. The evolution of the simulated Fermi bubbles. Density maps. Left - 4 Myr, center - 6 Myr, right - 8 Myr after AGN activity episode. View from side, z axis perpendicular to galactic plane.

[1] Su M., Slatyer T. R., Finkbeiner D. P., 2010, The Astrophysical Journal, 724, 1044 [2] M. A. Green, *High Efficiency Silicon Solar Cells* (Trans. Tech. Publications, Switzerland, 1987).

CANCELLED DUE TO COVID-19

INFLUENCE OF PICOSECOND PULSE TEMPORAL PROFILE FOR EFFECTIVE WIDE-BANDWIDTH TW-CLASS OPCPA PUMPING

Vytenis Girdauskas[1], Paulius Mackonis[1], Augustinas Petrulenas[1], Aleksej Rodin[1]

[1]Solid-State Lasers Laboratory, Department of Laser Technologies, State research institute Center for Physical Sciences and Technology, Savanoriu ave. 231, LT-02300 Vilnius, Lithuania
vytenis.girdauskas@ff.stud.vu.lt

Compact and cost-effective TW-class peak power lasers are in demand for emerging applications in nonlinear optics, material science, biology and medicine. Since the first demonstration in 1992 [1] the Optical Parametric Chirped Pulse Amplification (OPCPA) has become an attractive alternative to Ti:Sapphire based amplifier systems and has opened a new path towards generation of few-cycle, high intensity pulses.

In the OPCPA process the resulting gain depends on the pump intensity and hence on the temporal shape of the pump pulses. In most cases pump with a Gaussian temporal profile is used and a fraction of energy is discarded, thereby lowering the overall efficiency of the parametric amplification process. If the seed and pump pulses are of comparable duration, the gain along the chirped seed pulse replicates pulse temporal shape and usually leads to the narrowing of the amplified pulse spectrum. The pump pulses with a rectangular temporal profile and duration comparable to seed pulse would provide a uniform gain for whole seed spectral range, thereby avoiding spectral gain narrowing and increasing pump-to-signal conversion efficiency.

Purpose of this study was to investigate picosecond pump pulse temporal profile influence on OPCPA performance and to determine optimal conditions for effective energy transfer and shortest amplified pulse width after compression.

Pulses with an energy up to 20 mJ, a pulse width of 1.2 ps and excellent beam quality $M^2 \sim 1.1$ at a wavelength of 1030 nm were obtained from a two-stage double-pass Chirped Pulse Amplifier (CPA) based on Yb:YAG rods [2]. Under optimal conditions, the stability of the generated white light continuum (WLC) pulse energy and beam pointing in the wavelength range from 500 to 2500 nm is several times higher than the source stability [3]. The second harmonic was generated in two successive cascades with an overall conversion efficiency of 85%, where M-shaped pulses were formed in the second cascade due to the strong depletion of fundamental radiation in the first cascade. When reducing the first SHG stage conversion efficiency, pulse temporal shape becomes flat-top or even Gaussian distribution (Fig. 1, left).

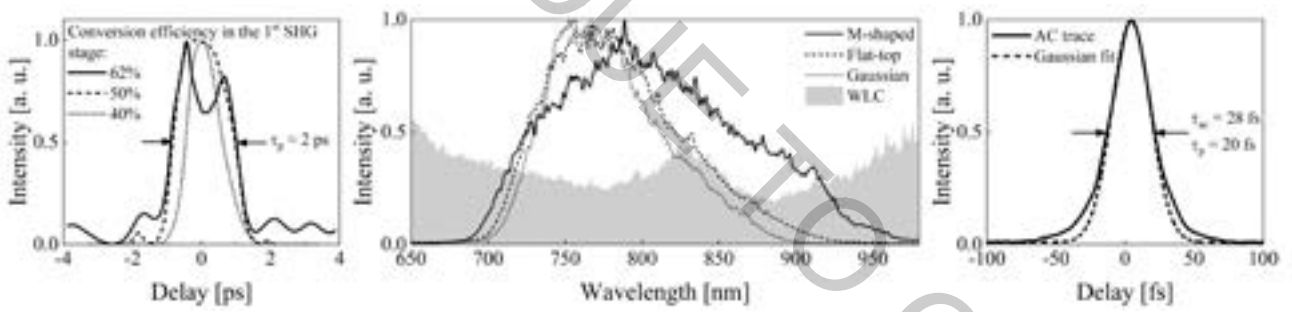

Fig. 1. The measured pulse temporal profile after second SHG stage with 62% (solid), 50% (dashed) and 40% (dotted) conversion efficiency in the first SHG cascade (left), output amplified spectrum after two OPCPA stages when pumped with M-shaped (solid), flat-top (dashed) and Gaussian (dotted) pulses (middle), the measured autocorrelation trace of amplified and compressed pulse (right).

Pulses with an energy up to 14.2 mJ at wavelength of 515 nm were used to pump three OPCPA stages. The use of M-shaped pulses helped to support a wide spectral bandwidth of amplified pulses in OPCPA cascades with a high gain (Fig. 1, middle), while Gaussian pump pulses provided efficient energy extraction of 20% at the last cascade. The output energy after three stages exceeds 2.1 mJ with the support of a spectral bandwidth sufficient for a transform-limited pulsewidth of 8.6 fs. For comparison, using flat-top or Gaussian pulse temporal profile amplified signal pulse transform limit is 9,7 fs and 11 fs respectively. The measured autocorrelation trace of the pulses after prism compressor corresponds to a pulsewidth of 20 fs (Fig. 1, right). In our opinion, a combination of chirped mirrors and prisms or adaptive dispersion control would allow obtaining much shorter pulses.

Acknowledgement: This research was partially funded by the European Social Fund under the No 09.3.3-LMT-K-712-16-0089 Development of Competences of Scientists, other Researchers and Students through Practical Research Activities measure.

[1] A. Dubietis, G. Jonuauskas, A. Piskarskas, Powerful femtosecond pulse generation by chirped and stretched pulse parametric amplification in BBO crystal, *Opt. Commun.* **88**(46), 437-440 (1992).

[2] P. Mackonis, A.M. Rodin, Laser with 1.2 ps, 20 mJ pulses at 100 Hz based on CPA with a low doping level Yb:YAG rods for seeding and pumping of OPCPA, *Opt. Express* **28**(2), 1261-1268 (2020).

[3] P. Mackonis, A. Petrulenas, V. Girdauskas, A. Rodin, Observation of a stable supercontinuum from 1100 nm to 2400 nm in YAG pumped with 1.2 ps pulses for a cost-effective 1 TW-class OPCPA, 8th EPS-QEOD Europhoton Conference, paper TuPD4, Barcelona, 27 September 2018.

CANCELLED DUE TO COVID-19

INVESTIGATION OF IMPURITIES IN LASER MEDIA: CATHODOLUMINESCENCE AND FILAMENT INDUCED LUMINESCENCE COMPARISON

Akvilė Bunkevičiūtė, Balys Momgaudis, Mikas Vengris

Laser Reasearch center, Vilnius University, Saulėtekio Ave. 10, LT-10223 Vilnius, Lithuania
akvile.bunkeviciute@ff.stud.vu.lt

CANCELLED DUE TO COVID-19

Luminescence is the light emitting process when an electron jumps from excited to a ground state. In order to observe this phenomena within undoped laser host material a very strong electromagnetic field is required. Such intensities can only be reached during such experiments as cathodoluminescence, X-ray luminescence, nonlinear photoluminescence, etc.

In this work we are using filaments of light in order to induce luminescence and observe the resulting spectrum. This method is more convenient compared to cathodoluminescence or X-ray luminescence because the specimen is excited by laser beam. Besides, it allows to study decay of excited states which is not possible during other experiments. In this way, we have system which is easily adjustable and requires no complex optical elements. Use of filaments in luminescence spectroscopy is a nondestructive way to examine transparent solid material in order to determine it's quality.

By focusing femtosecond laser pulses in transparent medium, wide spectrum coherent radiation - white light continuum can be generated. When light self-action occurs, laser beam can shrink to micro-meter size and pulse spectrum can spread over several octaves. Within the generated filament there is enough electromagnetic field to excite impurities and charge carriers. Filament induced luminescence is observed and registered from the side of the filament. The main purpose of this work is to compare two different methods:: filament induced luminescence and cathodoliuminescence. Therefore, spectra were registered in different popular laser media such as YAG, Al_2O_3 and KGW. Specimens were provided by different manufacturers.

Overall,it was shown that characterizing lines of impurities are repeated in both experiments. For instance, Fig. 1 reveals that same ions of impurities were found in YAG crystals. On the other hand, it can be seen that the characteristic peaks differ in intensity, depending on the type of the excitation. Generation of optical filament is more suitable way to investigate luminescence in samples which have intense luminescence. When intensity is low it is better to use cathodoluminescence experiment because light is collected from larger area of the sample's surface.

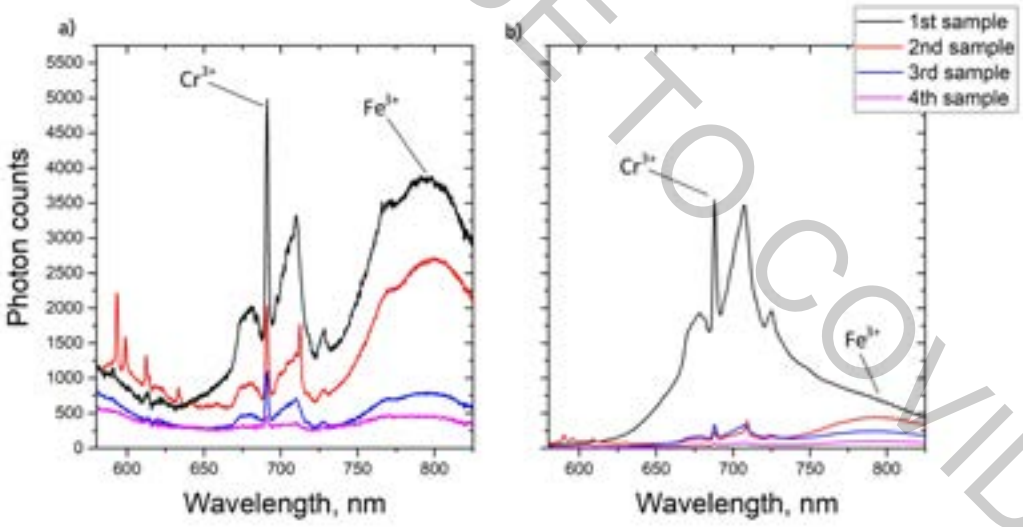

Fig. 1. Filament induced luminescence (a) and cathodolimonescence (b) spectra in YAG samples.

BROADBAND TRANSIENT STIMULATED RAMAN AMPLIFICATION IN KGW CRYSTAL

Augutinas Petrulėnas[1], Vytenis Girdauskas[1], Paulius Mackonis[1], Aleksėj Rodin[1]

[1] Solid State Laser Laboratory, Center for Physical Sciences and Technology, Vilnius, Lithuania
augustinas.petrulenas@gmail.com

In recent decades, Optical Parametric Chirped Pulse Amplification (OPCPA) has become a common method for generating few-cycle pulses of high intensity. However, maintaining a wide amplification bandwidth in the IR range well above 1 μm is more difficult due to the lack of suitable broadband gain media. Alternatively, Stimulated Raman Amplification (SRA) not critical to phase matching can be used.

In the transient SRA regime, when the pulse width of the pump pulse is comparable or even shorter than the dephasing time of molecular vibrations, a wider gain bandwidth becomes possible. Moreover, under certain excitation conditions, multiple Raman lines can be involved to significantly expand the SRA gain bandwidth. In this work, we report the efficient amplification of weak supercontinuum pulses using SRA in a KGW crystal pumped with 1.2 ps transform-limited pulses from a two-stage double-pass Chirped Pulse Amplifier (CPA) [1]. Significant broadening of the SRA spectrum was investigated for different directions of pump and seed polarization.

A picosecond laser, consisting of a two-stage double-pass CPA based on a low doping level Yb:YAG rods, operates at a repetition rate of 100 Hz. The laser provides amplified pulses with pulse width of 1.2 ps and an energy up to 20 mJ. Pulses with a higher energy after passing through a controlled optical delay line are used for pumping a Raman amplifier based on N_p-cut 5×5×30 mm^3 KGW crystal. Supercontinuum pulses in the wavelength range of 1100 – 2500 nm, obtained in a 15 mm YAG crystal [2] under focusing the weaker portion of the laser pulses are used as seed pulses for the Raman amplifier. The seed and pump pulses are combined in space and time in a Raman-active crystal. Their polarizations were oriented for beams propagation along the N_p axis (Fig. 1a – inset), so that SRA could be achieved with an electric field vector E parallel to either N_g or N_m crystal axes with Raman frequency shifts of 768 and 901 cm^{-1}, respectively. In addition, polarizations were set at different angles with respect to the N_g axis, in order to simultaneously generate multiple Raman lines.

The output spectra of SRA pulses centered at 1118 nm and 1135 nm were observed for the E II N_g, E II N_m pump polarizations (Fig. 1a and b). The bandwidth of amplified Raman pulses ~8 nm FWHM is about 5 times wider than that of incident pump pulses. At the optimum pump energy, the maximum conversion efficiencies of 14% and 8% were achieved, and the threshold SRA energies were 0.35 mJ and 0.8 mJ, respectively.

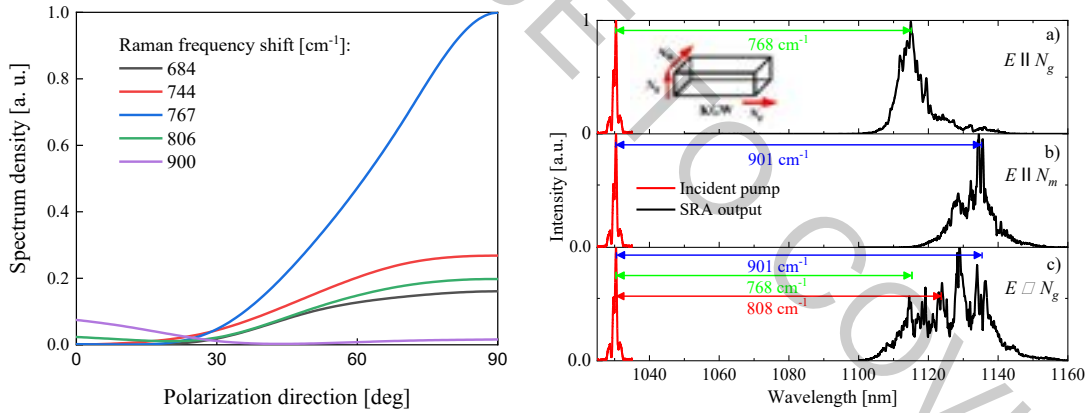

Fig. 1. The dependence of the spectrum densities of the first Stokes pulses on the pump and seed polarization direction at a pump pulse energy of 2 mJ – left. The output SRA spectrum for a) 768 cm^{-1}, b) 901 cm^{-1} and c) multiple Raman frequency shifts with pump polarizations E II Ng, E II Nm and $E \angle Ng$, respectively – right.

When the pump and seed polarizations were oriented at an angle between 24 and 27° with relative to the Ng axis (Fig.1. left), multiple Raman frequency shifts become possible. In this case, Raman lines 768, 808 and 901 cm^{-1} of the KGW crystal were involved in the formation of a common SRA gain bandwidth of ~25 nm FWHM (Fig. 1c). Thus, SRA gain bandwidth in KGW is more than 15 times the spectrum width of the incident pump pulse of ~1.6 nm. With a pump energy of 3 mJ, an SRA conversion efficiency of 8% was achieved.

[1] P. Mackonis and A.M. Rodin, "Laser with 1.2 ps, 20 mJ pulses at 100 Hz based on CPA with a low doping level Yb:YAG rods for seeding and pumping of OPCPA," Opt. Express **28**, 1261-1268 (2020).

[2] P. Mackonis, A. Petrulenas, V. Girdauskas, and A. Rodin, "Stable 1100 – 2400 nm supercontinuum in YAG with picosecond pumping for simplifiedOPCPA," in 2019 Conference on Lasers and Electro-Optics Europe and European Quantum Electronics Conference, OSA Technical Digest (Optical Society of America, 2019), paper ca_p_43).

CANCELLED DUE TO COVID-19

MICROMACHINING OF TRANSPARENT BIOCOMPATIBLE POLYMERS APPLIED IN MEDICINE USING BURSTS OF FEMTOSECOND LASER PULSES

Evaldas Kažukauskas[1], Simas Butkus[1] and Valdas Sirutkaitis[1]

[1] Laser Research center, Faculty of Physics, Vilnius University, Lithuania
evaldas.kazukauskas@ff.stud.vu.lt

Biocompatible plastics are used for many different purposes (catheters, artificial heart components, dentistry products, etc. [1]). One important field is the use of specificaly designed surfaces from these types of materials to be used as vision implants. It is estimated that half of the white Americans at the age of 75 or above have developed cataracts [2]. A cataract is the clouding of the lens in the eye which leads to a decrease in vision quality.

This condition may be curable by surgically replacing the original eye lens with an artificial lens, known as an intraocular lens (IOL). One of the most favorable materials in IOL manufacturing is hydrophilic acrylic – a soft, biocompatible polymer. Typically, curved surfaces are manufactured by applying abrasive grinding method via CNC machines. In addition, 2.5D objects/surfaces can also be manufactured by means of laser micromachining, however, due to the light-matter interaction mechanisms, the surface of the micromachined objects appears rough (> 1 µm Ra) therefore is not usable for optical applications. These surfaces may be polished via mechanical methods, however, the process may take up to a few days [3], which makes it economically challenging. To speed up this process, alternative ways to polish IOLs are on the search.

The aim of this study is the investigation of the polishing capabilities of rough (> 1 µm Ra) hydrophilic acrylic surfaces using bursts of femtosecond laser pulses (laser "Carbide"). To start off, femtosecond laser pulses were divided into burst packets of 2, 5, 10, 25 pulses. By changing the burst envelope parameter, different configurations of sub-pulse amplitudes were obtained. It was determined that it is possible to level all sub pulses within the burst to the same value with the error of 10%. The next step was the preparation of samples, where a surface area of (10x10) mm was ablated up to a depth of 0.5 mm. As was expected, the surface after ablation was rough and non-transparent. Afterwards, surface polishing experiments were conducted using a galvo-scanner based scanning/focusing system. By changing the average laser power, the scanning velocity of the beam on the surface of the sample, the line scanning pitch and the number of sub-pulses within the burst it was possible to find a regime where the surface roughness can be minimized to 88 nm Ra (the initial value of ~ 1 µm). The produced surface resembles a transparent appearance (see fig. 1b). It was determined that using bursts of femtosecond laser pulses the surface quality can be increased by ~10-fold compared to using the conventional femtosecond regime.

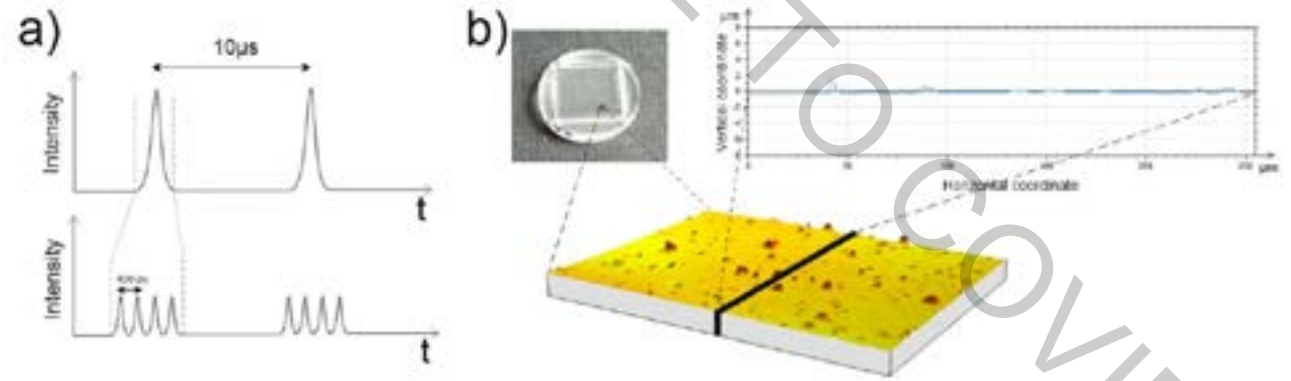

Fig. 1. Femtosecond laser pulse divided into bursts schematic (a), hydrophilic acrylic after polishing using parameters: avg. power = 29 W, scanning velocity = 1 m/s, scanning pitch = 10 µm, number of sub-pulses = 10 (b).

[1] A. Šešok, *Medžiagos medicinoje* (Mokomoji knyga, Vilnius: Technika, 2012).
[2] Cataract Data and Statistics, https://www.nei.nih.gov/eyedata/cataract [viewed 2020-01-28].
[3] M. A. Valle, A. Yamada, R. J. Kellar, *INTRAOCULAR LENS TUMBLING PROCESS USING COATED BEADS* (Chiron Vision Corporation, United States, 1999).

CANCELLED DUE TO COVID-19

ADDITIVE MANUFACTURING OF 3D GLASS-CERAMIC MICRO-STRUCTURES VIA DIRECT LASER WRITING AND ANNEALMENT

Edvinas Aleksandravičius[1], Greta Merkininkaitė[2,3], Darius Gailevičius[1,3], Mangirdas Malinauskas[1], Simas Šakirzanovas[2]

[1]Laser Research Center, Vilnius Universtity, Lithuania
[2]Faculty of Chemistry and Geosciences, Vilnius Universtity, Lithuania
[3]Femtika Ltd., Lithuania
edvinas.aleksandravicius@ff.stud.vu.lt

CANCELLED DUE TO COVID-19

Ceramic materials possess a wide range of useful properties including great mechanical and chemical resistance and thermal stability. This has lead to them being extensively used in science and industry, with intensive research being done on the methods of manufacturing of ceramic structures. One option for the fabrication of ceramic micro-structures is to use direct laser writing. Direct laser writing using multi-photon polymerization is powerful method for the additive manufacturing of fully 3D micro- and nano-structures for diverse applications in microfluidic, micromechanic and electronic, biomedical, metamaterial as well as nanophotonic research fields [1]. It has been demonstrated that using direct laser writing in conjunction with calcination of the hybrid organic-inorganic polymer SZ8020 it is possible to manufacture glass-ceramic micro-structures with sub-100 nm resolution [2].

The goal of this study was to investigate the 3D micro-structurability of a series of organic-inorganic polymer precursors and evaluate the effects that annealment has on the fabricated structures. First, a series of silicon and zirconium based hybrid prepolymers SZXY were synthesized via the sol-gel method [3] with a varying molar ratio of silicon (Si) and zirconium (Zr) (X:Y indicate the ratio Si:Zr, the following ratios were tested: 9010, 8020, 7030, 6040, 5050). Secondly, in order to determine the suitability of the prepolymers for laser lithography and the effect of the subsequent heat-treatment, various microstructures were fabricated including woodpiles, solid cubes and resolution bridges. Scanning electron microscopy was used to measure fabricated feature sizes. It was shown that highest resolution is obtained by using a polymer precursor with the least amount of zirconium. It was also found that polymers with a smaller amount of zirconium shrink more during calcination with no significant deformation. In order to determine the crystalline phases that form as a result of the heat-treatment, X-ray diffraction of the polymer powders and micro X-ray diffraction of fabricated hexagonal scaffold structures (Figure 1b) experiments were performed. It can be seen (Figure 1a), that the heat-treatment leads to the formation of four different crystalline phases: cristobalite, zirconium orthosilicate, tetragonal and monoclinic zirconia.

Overall, it can be seen that direct laser writing in conjunction with annealment of various ratios of SZXY is an effective method for the additive manufacturing of 3D glass-ceramic micro-structures. Zirconium orthosilicate and monoclinic zirconia are new material phases that were not observed previously on 3D micro-structures and will probably result in new physical properties to explore.

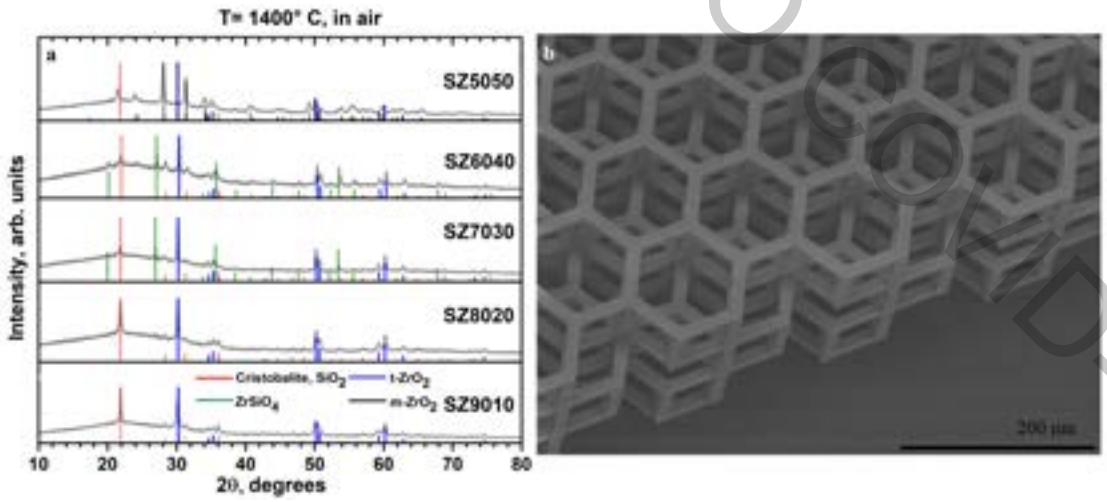

Fig. 1. (a) XRD spectra of the SZXY powder heat-treated at 1400 °C for 5 h in an atmosphere of air at ambient pressure, showing the formation of four different cristalline phases. (b) SEM micrograph of a hexagonal scaffold structure fabricated for the micro X-ray diffraction experiments.

[1] M. Malinauskas et al., Ultrafast laser processing of materials: from science to industry, Light Sci. Appl. **5**, e16133-e16133 (2016).
[2] D. Gailevičius et al., Additive-manufacturing of 3D glass-ceramics down to nanoscale resolution, Nanoscale Horizons **4**, 647-651 (2019).
[3] A. Ovsianikov et al., Ultra-Low Shrinkage Hybrid Photosensitive Material for Two-Photon Polymerization Microfabrication, ACS Nano **2**, 2257-2262 (2008).

SOLUTION-PROCESSED BLUE TADF-OLEDs BASED ON TWISTED ISOPHTALONITRILES

Domantas Berenis[1], Gediminas Kreiza[1], Saulius Juršėnas[1], Tomas Javorskis[2], Edvinas Orentas[2], Dalius Gudeika[3], Juozas Vidas Gražulevičius[3], Karolis Kazlauskas[1]

[1] Institute of Photonics and Nanotechnology, Vilnius University, Lithuania
[2] Department of Organic Chemistry, Vilnius University, Lithuania
[2] Department of Polymer Chemistry and Technology, Kaunas University of Technology, Kaunas, Lithuania
domantas.berenis@ff.stud.vu.lt

Due to the small singlet-triplet energy gap thermally activated delayed fluorescence (TADF) emitters can harvest all triplet excitons by upconversion to the singlet manifold and achieve up to 100% internal quantum efficiency [1]. Therefore they are attractive for replacing expensive phosphorescent emitters containing heavy metals and having issues with OLED stability in the blue spectral region [2]. Studied TADF emitters consist of carbazole (Cz) donor and isophtalonitrile (IPN) acceptor moieties. Such type of molecules are known to exhibit blue emission [3], however with significantly lower efficiency as compared to their green-emitting IPN counterparts [4].

In this work, photoluminescence properties of two IPN emitters, namely, unmodified DCzIPN [3] and modified DCzIPNMe were investigated. Methyl substituents were intentionally introduced at *ortho* positions of Cz moieties to alter TADF properties. The emitters were tested in solution-processed TADF OLEDs. An extra hole transport layer in OLEDs was introduced using crosslinking technique to ensure charge balance and exciton localisation in the emission layer [5].

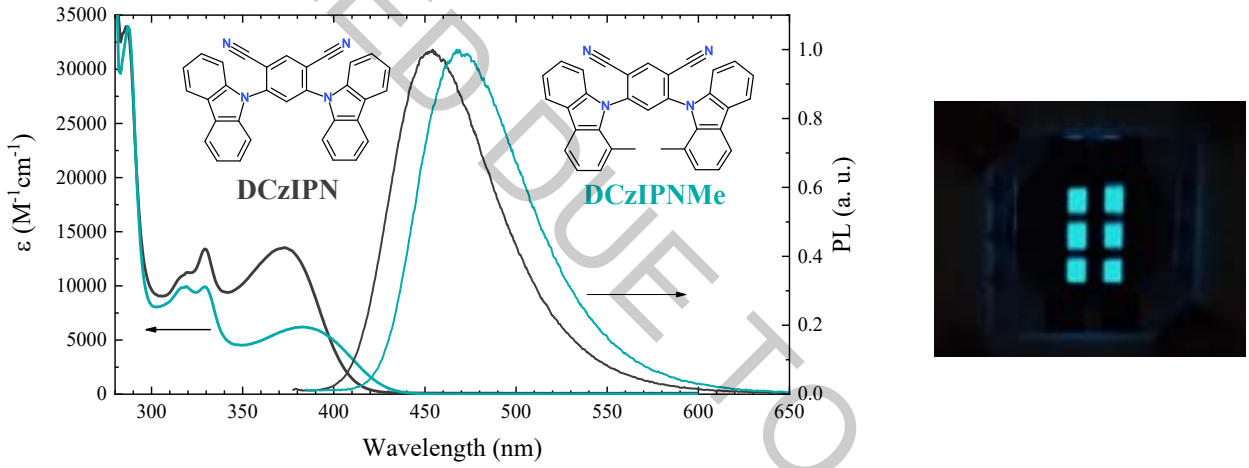

Fig. 1. Absorption and photoluminescence (PL) spectra of the studied isophtalonitrile TADF emitters (left), picture of blue emitting OLED based on DCzIPN emitter (right).

It was found that modified DCzIPNMe emitter dispersed in mCP host at 7 wt% concentration demonstrated enhanced charge transfer and TADF properties (~1.5 higher quantum efficiency and ~15 times larger delayed fluorescence rate). However, this modification of molecular structure resulted in reduced S_1 energy (by 72meV), thus making difficult to realize emission in a deep blue range. OLED containing modified DCzIPNMe emitter exhibited much higher external quantum efficiency (EQE_{max} = 17.5%) as compared to that with DCzIPN (EQE_{max} = 9.2%). Additionally, maximum EQE of DCzIPNMe-based OLED was achieved at several times higher current density and brightness levels as compared to DCzIPN. The obtained results imply great potential of the modified DCzIPNMe emitter for OLED applications.

[1] H. Uoyama, K. Goushi, K. Shizu, H. Nomura, C. Adachi, Highly efficient organic light-emitting diodes from delayed fluorescence, Nature. 492 (2012) 234–238. doi:10.1038/nature11687.
[2] S. Schmidbauer, A. Hohenleutner, B. König, Chemical degradation in organic light-emitting devices: Mechanisms and implications for the design of new materials, Adv. Mater. 25 (2013) 2114–2129. doi:10.1002/adma.201205022.
[3] Y.J. Cho, K.S. Yook, J.Y. Lee, Cool and warm hybrid white organic light-emitting diode with blue delayed fluorescent emitter both as blue emitter and triplet host, Sci. Rep. 5 (2015) 1–7. doi:10.1038/srep07859.
[4] M.Y. Wong, E. Zysman-Colman, Purely Organic Thermally Activated Delayed Fluorescence Materials for Organic Light-Emitting Diodes, Adv. Mater. 29 (2017). doi:10.1002/adma.201605444.
[5] K.W. Tsai, M.K. Hung, Y.H. Mao, S.A. Chen, Solution-Processed Thermally Activated Delayed Fluorescent OLED with High EQE as 31% Using High Triplet Energy Crosslinkable Hole Transport Materials, Adv. Funct. Mater. 29 (2019) 1–10. doi:10.1002/adfm.201901025.

CANCELLED DUE TO COVID-19

INFLUENCE OF FUNCTIONAL LAYERS ON ORGANIC-INORGANIC PEROVSKITE CHARGE CARRIERS PARAMETERS

Natallia S. Mahon[1*], Olga V. Korolik[1], Alexander V. Mazanik [1], Yulia Galagan[2]

[1] Energy Physics Department, Belarusian State University, Republic of Belarus
[2] TNO – Solliance, The Netherlands
natalimahon@gmail.com

Nowadays, organic-inorganic perovskite (OIP) is the most perspective photoabsorbing layer for photovoltaic application [1]. Power conversion efficiency of the OIP solar cells reaches over 25% [2] with the possibility of cheap and easy synthesis from solutions [3]. Actually, the main problem of them is fast degradation under environmental influence: moisture, oxygen, heat and light-soaking [4]. We are able to prevent the impact of the first 3 factors using encapsulation and chemical modification of OIP layer [4], but we can't limit illumination. So, scientists try to reveal mechanisms and reasons of photoinduced processes in OIPs.

Our recent investigation [5] showed that functional layers as electron-transport layer (ETL), hole-transport layer (HTL) and contact layers have strong influence on the OIP properties especially on the charge carriers' transport and recombination. We have been studied organic-inorganic perovskite solar cells and the simplest structures based on $(Cs/FA)Pb(I/Br)_3$ perovskite with different combinations of functional layers: (a) individual perovskite, (b) SnO_2/perovskite (SnO_2 is ETL), (c) perovskite/Spiro-MeOTAD (Spiro-MeOTAD is HTL), (d) SnO_2/perovskite/Spiro-MeOTAD, (e) ITO/SnO_2/perovskite/Spiro-MeOTAD, (f) SnO_2/perovskite/Spiro-MeOTAD/Au, and (g) full solar cell structure ITO/SnO_2/perovskite/Spiro-MeOTAD/Au.

Using confocal spectroscopy, we obtained photoluminescence kinetics (Fig.1) and established that the biggest changes in perovskite charge carrier's properties occurred at the HTL – perovskite interface. It is interesting to note that this influence is powered by gold contact. The obtained results have shown the necessity of the next investigation of photoinduced processes in the OIP solar cells and structures with different HTL and back contact layer.

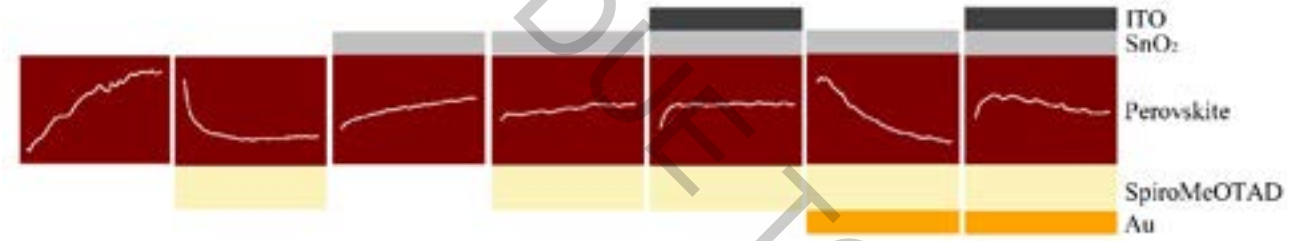

Fig. 1. Kinetics of photoluminescence intensity in dependence on functional layers set with $(Cs/FA)Pb(I/Br)_3$ perovskite. Data was obtained with 532 nm, 0.6 μW and 250 s accumulation time.

[1] Q. Tai, K.-C. Tang, F. Yan., Recent progress of inorganic perovskite solar cells, Energy Environ. Sci., **12**, 2375-2405 (2019).
[2] NREL, Best Research-Cell Efficiency Chart (2020).
[3] M. I. H. Ansari, A. Qurashi, M. K. Nazeeruddin, Frontiers, opportunities, and challenges in perovskite solar cells: A critical review, Journal of Photochemistry and Photobiology C: Photochemistry Reviews, **35**, 1-24 (2018).
[4] R. Wang, M. Mujahid, Y. Duan et.al., A review of perovskites solar cell stability, Adv. Funct. Mater., **2019**, 1808843 (2019)
[5] N. S. Mahon, O. V. Korolik, M. V. Khenkin et.al., Photoluminescence kinetics for monitoring photoinduced processes in perovskite solar cells, Solar Energy, **195**, 114-120 (2020).

CANCELLED DUE TO COVID-19

A NEW CONCEPT OF PURINE D-A-D' RATIOMETRIC CHEMICAL SENSOR, BASED ON INTERMOLECULAR PET

Justina Jovaišaitė[1], Dace Cīrule[2], Andris Jeminejs[2], Irina Novosjolova[2], Māris Turks[2], Paulius Baronas[1], Regimantas Komskis[1], Gediminas Jonušauskas[3] and Saulius Juršėnas[1]

[1] Institute of Photonics and Nanotechnology, Faculty of Physics, Vilnius University, Lithuania
[2] Institute of Technology of Organic Chemistry, Faculty of Materials Science and Applied Chemistry, Riga Technical University, Latvia
[3] Laboratoire Ondes et Matière d'Aquitaine, Bordeaux University, UMR CNRS 5798, France
justina.jovaisaite@ff.vu.lt

The control of photophysical properties of purine-based compounds is of a great importance. The wide possibilities of purine core modification by addition of electron accepting or donating substituents allow creating push-pull molecular systems with desired features. Here we present four 9-(3',5'-di-O-acetyl-2'-deoxy-β-D-ribofuranosyl)-2,6-bis-(1H-1,2,3-triazol-1-yl)-9H-purine derivatives which in case of electron donating substituents become unique Donor-Acceptor-Donor' systems with unusual character of dual emission. The steady-state absorption, fluorescence and excitation, time-resolved fluorescence experiments and DFT calculations were employed to study the nature of dual fluorescence, which was attributed to distinct transitions within electron donating branches. The NMR study of 9-(3',5'-Di-O-acetyl-2'-deoxy-β-d-ribofuranosyl)-2,6-bis-[4-(4-methoxyphenyl)-1H-1,2,3-triazol-1-yl]-9H-purine with metal ions proved the efficient assembly of three purine molecules to one metal ions. As revealed by steady-state fluorescence titration experiments, the complexation causes the quenching of blue side band of dual fluorescence, determined by an efficient interbranch intermolecular photoinduced electron transfer (PET), which was further analyzed by transient absorption experiments. The unique dual fluorescence along with an efficient PET as metal ion sensing mechanism enables to propose a new concept of a ratiometric chemical sensor.

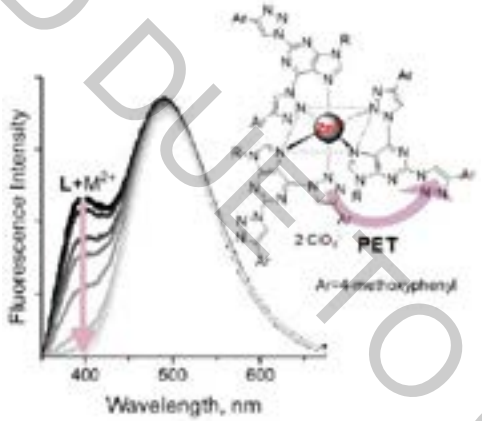

Fig. 1. The fluorescence spectrum response of purine ligand (**L**) to metal ions present in the system. The inset demonstrates the complexation mode of three purine molecules to one Zn^{2+} metal ion along with PET process between two separate molecules.

CANCELLED DUE TO COVID-19

INFLUENCE OF THE PIEZOELECTRIC RINGING ON THE POLARISATION CONTRAST OF THE KRTP POCKELS CELL IN THE MODULATION FREQUENCY RANGE UP TO 10 MHZ

Danielius Samsonas[1,2], Dalius Petrulionis[2], Darius Grigaitis[2], Mikas Vengris[1,2]

[1]Faculty of Physics, Vilnius University, Vilnius, Lithuania
[2]Light Conversion, Vilnius, Lithuania
danielius.samsonas@ff.vu.lt

CANCELLED DUE TO COVID-19

Pockels cell is one of the major components limiting the pulse repetition rate of high power laser sources. The birefringence in an the electro-optical crystal can be changed by variable electric voltage. It therefore acts as a voltage-controlled waveplate. This allows high frequency modulation of intercavity losses, unlocking the MHz frequency band for pulse repetition rate.

In this study Potassium Rubidium Titanyl Phosphate (KRTP) crystals were used due to their low quarter-wave voltage. This material property is critical for achieving high modulation frequency while maintaining steep edges (∼4 ns) of high voltage (HV) pulses required in order to use the crystals in femtosecond regenerative amplifiers. In addition to birefringence, HV pulses induce converse-piezoelectric effect — deformation of the crystal when an external electric field is applied. When modulation frequency matches the natural frequency of the crystal, piezoelectric ringing occurs.

The effect of piezoelectric ringing on the polarisation contrast (PC) of the Pockels cells based on BBO crystals have already been studied in the modulation frequency range up to 1 MHz [1]. However, there are no studies dedicated to the analysis of the piezoelectric ringing behaviour of KRTP based Pockels cells in high modulation frequencies. The purpose of this work is to investigate this phenomena in the modulation frequency range up to 10 MHz.

We have investigated the behavior of 4 mm × 4 mm × 20 mm KRTP based Pockels cell by measuring its polarization contrast and surface temperature as a function of modulation frequency.

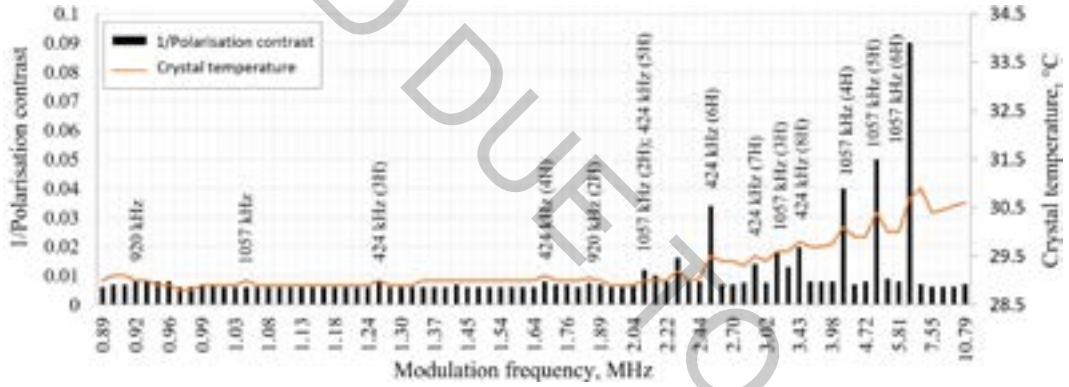

Fig. 1. Polarisation contract and crystal surface temperature dependence on the modulation frequency in the KRTP crystal based Pockels cell. Resonant frequencies are matched with the harmonics of calculated fundamental natural frequencies.

It was found that most of the resonant frequencies can be grouped as the harmonics of three theoretically calculated fundamental natural frequencies of the crystal (424 kHz, 920 kHz, 1057 kHz). The behaviour and dominant mechanism behind the effects of piezoelectric ringing were found to be distinct in the three following modulation frequency ranges:

For resonant modulation frequencies up to 2 MHz, the effect of standing acoustic wave in the crystal was seen as a harmonic wave of PC reduction in the modulated pulse-train. It was concluded that in this modulation frequency range, depolarisation mechanism is dominated by the photoelastic effect.

For modulation frequencies above 2 MHz, crystal surface temperature was found to be increasing by $\sim 0.2\,C^o$/MHz. This steady temperature gain did not affect the PC at non-resonant modulation frequencies due to thermally compensated configuration of the Pockels cell [2]. However, when piezoelectric ringing occurred, an additional temperature gain was observed, which took up to 90 *s* to stabilise. The effect on the PC in this frequency range was found to be greater and took longer to settle (up to 30 *s*). It was concluded that in this modulation frequency range, depolarisation mechanism is dominated by thermal gradient formation due to acoustic wave propagation losses in the crystal. These losses are higher for shorter acoustic waves and hence greater PC drop is observed at high resonant modulation frequencies.

Above 6.3 MHz modulation frequency, piezoelectric ringing has not been observed. It was postulated that high frequency acoustic modes are more effectively damped in the adhesive layer holding the crystal to its mount, however, further research is needed to verify this hypothesis.

[1] J. Vengelis, G. Sinkevičius, J. Banys, L. Masiulis, R. Grigonis, J. Domarkas, and V. Sirutkaitis, "Investigation of piezoelectric ringing effects in Pockels cells based on beta barium borate crystals," Applied Optics, vol. 58, no. 33, pp. 9240–9250, nov 2019.

[2] J. P. Salvestrini, M. Abarkan, and M. D. Fontana, "Comparative study of nonlinear optical crystals for electro-optic Q-switching of laser resonators," Optical Materials, vol. 26, no. 4, pp. 449–458, 2004.

SUPERCONTINUUM GENERATION AND OPTICAL DAMAGE IN SOLID-STATE MEDIA AT HIGH REPETITION RATES

Robertas Grigutis, Gintaras Tamošauskas, Vaida Marčiulionytė, Danil Bulatov, Nail Garejev, Vytautas Jukna, Audrius Dubietis

Laser Research Center, Vilnius University, Saulėtekio Avenue 10, LT-10223 Vilnius, Lithuania
robertas.grigutis@ff.vu.lt

CANCELLED DUE TO COVID-19

Supercontinuum (SC) generation is one of the most spectacular optical phenomena produced by filamentation process as the intense ultrashort laser pulses propagate in transparent bulk materials [1]. SC represents extremely broadband radiation with high spatio-temporal coherence. SC generation is mainly used in production of broadly tunable femtosecond pulses in ultrafast optical parametric amplifiers [2] as well as in high repetition rate noncollinear optical parametric amplifiers [3] and more recently, in optical parametric chirped pulse amplification (OPCPA) systems [4] which employ high repetition rate (hundreds of kHz and more) and high energy ultrashort pulse lasers based on Yb-doped lasing media.The induced accumulation effects by repetitive pulse exposure may lead to the gradual degradation and even optical damage of the nonlinear material. Optimization of SC generation conditions could solve the optical degradation problems, however there are no consistent studies on early indications and evolution of the optical damage at high repetition rate condition.

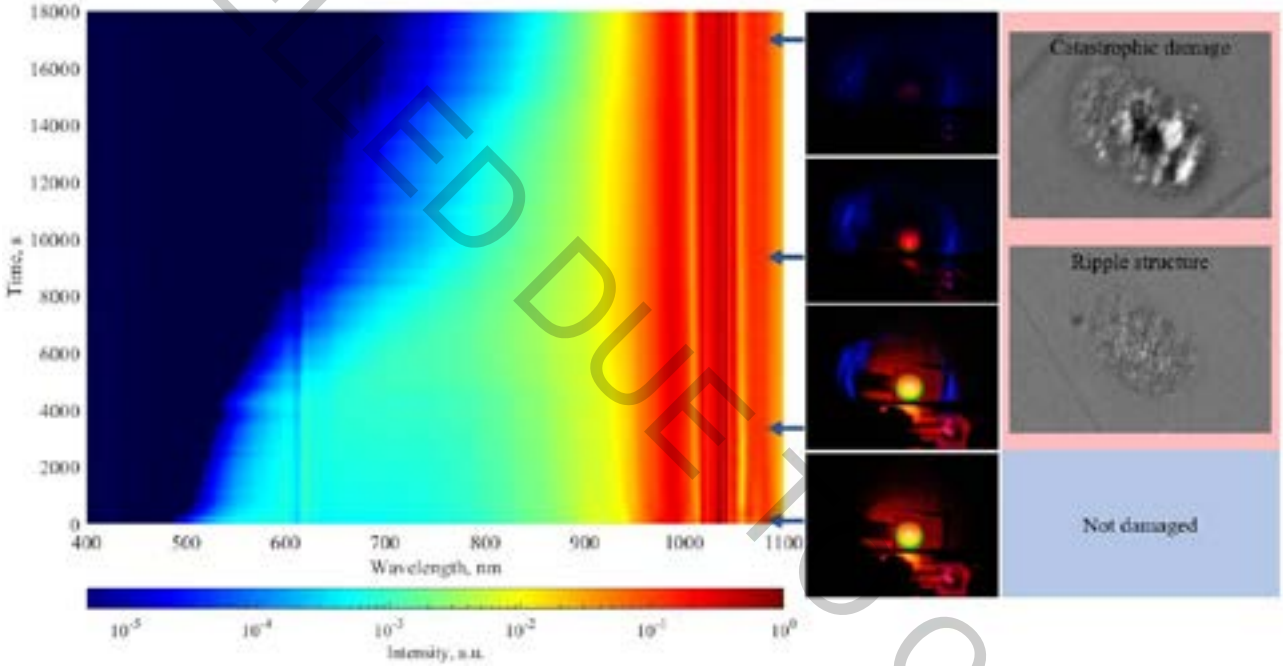

Fig. 1. The time evolution of the SC spectrum in sapphire at 20 kHz repetition rate, NA=0.051 (left image). Screenshots of the crystal output showing the decay of SC and occurrence of diffracted third harmonic (middle column). Related damage structures at the crystal output (right column).

The aim of our study was to experimentally investigate the SC generation and optical degradation effect in sapphire and YAG nonlinear crystals at high laser pulse repetition rates and provide some practical guidelines on SC application at these conditions. During the experiments the nonlinear materials were irradiated with 1030 nm, 180 fs pulses from an amplified Yb:KGW laser varying the laser repetition rates from 2 kHz to 200 kHz and beam focusing conditions from tight (NA=0.085) to loose (NA=0.025). The time evolution of the SC spectrum, changes in filament-induced luminescence and third harmonic generation due to damage formation were investigated (Fig. 1). We found that the optical damage is initiated in the bulk of the nonlinear crystal at the nonlinear focus of the pump beam in the form of the ripple structure. As the early indicator of optical degradation process is third harmonic diffraction from this ripple structure which correlates with the shrinking of the SC spectrum. We believe that these results could provide a better practical understanding on how to optimize SC generation in bulk materials at high repetition rates.

[1] A. Dubietis, G. Tamošauskas, R. Šuminas, V. Jukna, and A. Couairon, Ultrafast supercontinuum generation in bulk condensed media, Lith. J. Phys. **57**, 113–157 (2017).
[2] C. Manzoni and G. Cerullo, Design criteria for ultrafast optical parametric amplifiers, J. Opt. **18**, 103501 (2016).
[3] A. Steinmann, A. Killi, G. Palmer, T. Binhammer, and U. Morgner, Generation of few-cycle pulses directly from a MHz-NOPA, Opt. Express **14**, 10627–10630 (2006).
[4] A. Harth, M. Schultze, T. Lang, T. Binhammer, S. Rausch, and U. Morgner, Two-color pumped OPCPA system emitting spectra spanning 1.5 octaves from VIS to NIR, Opt. Express **20**, 3076–3081 (2012).

DYNAMIC ABERRATION CORRECTION *VIA* SPATIAL LIGHT MODULATOR (SLM) FOR FEMTOSECOND DIRECT LASER WRITING

Gabrielius Kontenis[1,2], Darius Gailevičius[1,2], Vytautas Purlys[1,2], Linas Jonušauskas[1,2], Roaldas Gadonas[1,2]

[1] Laser Research Center, Vilnius University, Saulėtekio Ave. 10, Vilnius LT-10223, Lithuania
[2] Femtika Ltd., Saulėtekio Ave. 15, Vilnius LT-10224, Lithuania
gabrielius.kontenis@ff.vu.lt.

Femtosecond (fs) lasers are becoming a preferred tool in transparent media processing due to the possibility to induce highly localized and well-defined modification on the surface or in the volume of the material [1]. It was proven to be suitable to produce components or whole functional devices out of crystals, ceramics, glasses, polymers or working directly with living organisms in the whole meso-scale. With such versatility and capabilities there is a huge drive to transfer current know-how from experimental laboratories to industry [2].

Aberrations and associated optical distortions are one of the key issues hindering the structuring quality in high definition direct laser writing. The most troublesome being spherical aberrations. These aberrations distort the voxel shape and aspect ratio depending on the focusing depth, making structuring deep inside transparent medium challenging. The problem lies in voxel elongation and subsequent energy density decrease. This limit direct laser fabrication in terms of how deep high-precision fabrication can be carried out in the volume of transparent mediums while still maintaining acceptable and controllable writing resolution. Because spherical aberrations increase the larger the refractive index difference between the specimen and the surrounding medium it is more pronounced in high refractive index (n=2.4) materials, such as diamonds, or crystals with optical anisotropy (like LinBO3) [3,4]. In glass or polymer samples it is possible to compensate for refractive index mismatch by using immersion oils that have similar refractive index values, whereas for diamond – no such oils exist. Some objectives have correction collars that can be tuned for certain depths, but their tuning range is very limited, and tuning speed is slow. Therefore, more dynamic and broad range solutions are required for tackling these optical aberrations.

In this work, we demonstrate how a spatial light modulator (SLM) can be used to minimize aberrations when fabricating single lines in transparent medium – soda lime glass. Phase mask calculation method based on Zernike polynomials is applied. An iterative algorithm for determining the exact phase mask is discussed in detail, showing which types of aberrations (spherical, defocusing, coma) have to be accounted for and to what extent. Aberration correction is demonstrated for 100x 0.9 NA objective in sample depths up to 1 mm. We show that a combination of SLM and Zernike polynomial calculation method allows to achieve nearly spherical few μm sized voxels written in arbitrary depths of glass with a femtosecond laser. Results are shown in a broader sense, highlighting how it can influence such research areas as integrated photonics or microfluidics. Possible future challenges of using SLM for aberration control, such as limited refresh rate of most SLMs (up to 60 kHz) or relatively large pixel sizes (up to 20 μm) are discussed, possible solutions highlighted.

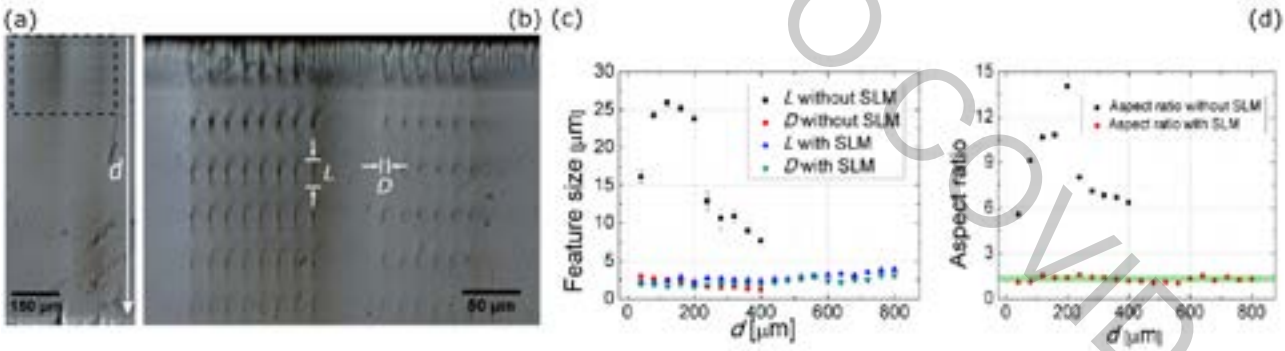

Figure 1 (a) and (b) shows optical images of the cross sections of fabricated lines and what was considered to be lateral and longitudinal resolutions D and L. (c) Shows feature sizes acquired in different d with and without aberration correction. (d) Aspect ratios in various d acquired with and without SLM. Corrected lines have an aspect ratio in the range from 1 to 1.5 proving, that the acquired voxels were near-spherical.

[1] R. R. Gattass and E. Mazur, "Femtosecond laser micromachining in transparent materials," Nat. Photonics 2, 219–225 (2008).
[2].L.Jonušauskas, D. Mackeviciute, G. Kontenis, and V. Purlys, "Femtosecond Lasers: The Ultimate Tool for High Precision 3D Manufacturing," Adv. Opt. Techn. (2019)
[3] R. D. Simmonds, P. S. Salter, A. Jesacher, and M. J. Booth, "Three dimensional laser microfabrication in diamond using a dual adaptive optics system," Opt. Express 19, 24122–24128 (2011).
[4] B. P. Cumming, A. Jesacher, M. J. Booth, T. Wilson, and M. Gu, "Adaptive aberration compensation for three- dimensional micro-fabrication of photonic crystals in lithium niobate," Opt. Express 19, 9419–9425 (2011).

СТЕКЛО ВЕРТОСОУВ-19

EXPERIMENTAL OBSERVATION OF ANGULAR MOMENTUM ALIGNMENT-TO-ORIENTATION CONVERSION IN RB ATOMS BY EXCITING THE D1 LINE HFS TRANSITIONS

Mārcis Auzinsh, Laima Bušaite, Artūrs Mozers, Dace Osīte

Laser Centre, University of Latvia, Latvia
dace.osite@gmail.com

CANCELLED DUE TO COVID-19

The experiment was conducted by exciting D_1 line hyperfine structure (HFS) transitions in rubidium vapor. The results of this experiment show that the total angular momentum of rubidium atoms can be changed from an aligned to an oriented state also known as alignment-to-orientation conversion (AOC). When the magnetic field is zero, linearly polarized laser radiation can only create an aligned state – angular momentum is symmetrically distributed along a determined axis. When an external magnetic field is applied, the angular momentum changes its distribution due to the nonlinear Zeeman effect and starts to have a preferred spatial direction – it becomes oriented.

To create AOC, exciting linearly polarized laser radiation **E** forms an angle of $\pi/4$ with respect to the magnetic field **B**. The magnetic field **B** defines the quantization axis. Two circularly polarized fluorescence components are observed in the direction perpendicular to both **E** and **B** (see Fig. 1).

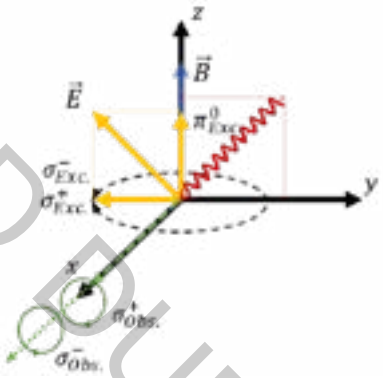

Fig. 1. Excitation and observation geometry.

In the previous work [1], where the same excitation and observation geometry was used, the AOC phenomenon was studied in the excited state of D_2 line, where magnetic sublevel crossings occurred due to the nonlinear Zeeman effect. In contrast, there are no magnetic sublevel crossings in the D_1 line of rubidium and one would not expect to observe AOC. However, the results show that the difference between these two components is a non-zero signal, which is a direct indication of partial orientation of total angular-momentum. This difference normalized to the sum of the components is known as circularity.

The observed fluorescence components and their circularities were compared with theoretical data, obtained with the theoretical model [2], developed in the Laser Centre of UL, which takes into account all neighbouring hyperfine transitions, the mixing of magnetic sublevels in an external magnetic field, the coherence properties of the exciting laser radiation, and the Doppler effect.

The maximum amplitude of the observed circularity is 4%, when the laser frequency was fixed to the F_g=2→F_e=2 transition. In contrast to the observed signals when the laser frequency was fixed to other transitions where the orientation is in one direction with varying amplitude, in the case for F_g=2→F_e=3 transition the amplitude changes direction as the magnetic field changes – at relatively smaller magnetic fields the orientation is in a positive direction, but with higher magnetic fields the orientation changes to a negative direction. Additionally, when laser intensity is increased, the orientation no longer changes its sign depending on magnetic field – similarly to other transitions.

A. Mozers acknowledges support from ERAF PostDoc Latvia project No. 1.1.1.2/16/117 "Experimental and theoretical signals of ground-state angular momentum alignment-to-orientation conversion by the influence of laser radiation and external magnetic field in atomic alkali metal vapor".

.

[1] M. Auzinsh, A. Berzins, R. Ferber, F. Gahbauer, L. Kalvans, A. Mozers, and A. Spiss, Phys. Rev. A 91, 053418 (2015).
[2] M. Auzinsh, R. Ferber, F. Gahbauer, A. Jarmola, and L. Kalvans, Phys. Rev. A 79, 053404 (2009).

EXPOSURE PARAMETER INFLUENCE ON METAL SURFACE PATTERNS FORMED USING FEMTOSECOND LASER

Arnas Žemaitis[1,2], Gedvinas Nemickas[1,2], Gabrielius Kontenis[1,2], Vytautas Purlys[1,2] and Linas Jonušauskas[1,2]

[1] Femtika Ltd., Saulėtekis Ave. 15, Vilnius LT-10224, Lithuania
[2] Laser Research Center, Vilnius University, Saulėtekis Ave. 10, Vilnius LT-10223, Lithuania
arnas@femtika.lt

CANCELLED DUE TO COVID-19

Laser technology provides new and revolutionizing solutions to many different fields ranging from agriculture [1] to military [2] and space industries [3]. Annual increase in the photon-based solutions provides us with highly precise tools that do not require contact to obtain information or perform certain tasks. Currently, mostly high-power continuous wave or long pulse (millisecond-nanosecond) laser systems are used in the industry. Nevertheless, in order to achieve nano-level precision ultrashort picosecond (ps) and femtosecond (fs) laser pulses are needed. They allow initiation of vast array of highly localized nonlinear light-matter interactions which became the basis for variety of novel laser material processing techniques [4].

One of the areas that highly benefited from these developments was ultra-precise surface patterning. It allows to produce hierarchical surface patterns with feature sizes ranging from hundreds of nm to tens of μm [Fig. 1]. Such surface topographies allow to control multitude of surface parameters allowing it to become hydrophobic, hydrophilic, repulsive or highly adhering. In addition, change between these surface properties are easily induced by changing exposure parameters during the fabrication process. For this reason, complete understanding of how laser parameters influence relevant surface properties is extremely important.

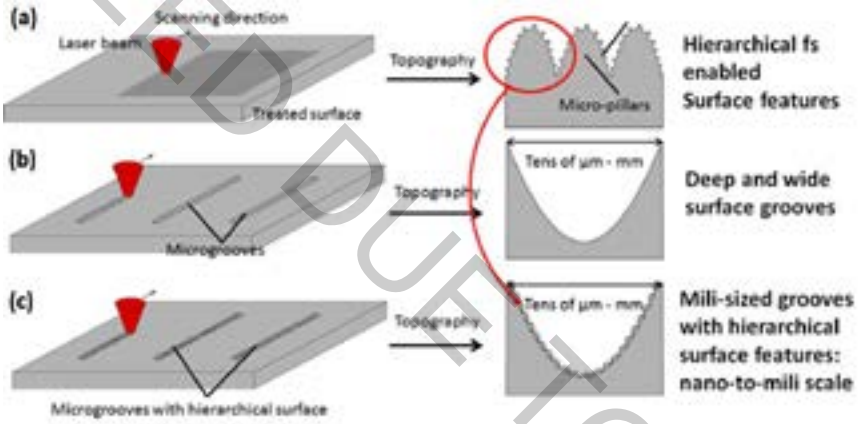

Fig. 1. Application of fs laser allows to achieve hierarchical nanogrooves (a), micro-features (b) or combine them together (c). This enables the control of surface wetting, photonic and related properties.

In this work we investigated how fabrication parameters such as wavelength, pulse duration, repetition rate, pulse energy, overlap and spot size influence the wetting properties of various metal sample. The chosen metal samples represent alloys most prominent in industries like medicine, maritime and aviation. SEM analysis as well as contact angle measurements and profilometer readings were used for qualitative surface analysis. At the same time their wetting properties were tested, showing contact angles in the range of 5 to 170 degrees [Fig. 2]. These results are presented in the context of current state-of-the-art highlighting possibilities and challenges in further developing this technology.

Fig. 2. Example of water drop on fs laser textured metal surface. Clear hydrophobicity at contact angle of 160 degrees is visible.

[1] B. Blackwell et al., Lasers as nonlethal avian repellents, J. Wildl. Manag. **66** (1), 250-258 (2002).
[2] A. Sijan, Development of military lasers for optical countermeasures in the mid-IR, Proc. SPIE **7483**, 748304 (2009).
[3] R. J. DeYoung et al., Comparison of electrically driven lasers for space power transmission, NASA-TM-4045, L-16431, NAS 1.15:4045 (1988).
[4] L. Jonušauskas et al., Femtosecond lasers: the ultimate tool for high-precision 3D manufacturing, Adv. Opt. Technol. **8** (3-4), 241-251 (2019).

MFA OF MAGNETIC PROPERTIES OF THE CHIRAL POLYMERIC PHOTOMAGNETS BASED ON Cu^{2+} AND $[MO_2(CN)_8]^{4-}$ IONS

Dominik Czernia[1], Robert Pełka[1], Tomasz Korzeniak[2], Sujit Sasmal[2], Dawid Pinkowicz[2], Wojciech Nitek[2], Olaf Stefańczyk[3], Barbara Sieklucka[2]

[1] Institute of Nuclear Physics Polish Academy of Sciences, Cracow, Poland
[2] Faculty of Chemistry, Jagiellonian University, Cracow, Poland
[2] Department of Chemistry, School of Science, The University of Tokyo, Tokyo, Japan
dominik.czernia@ifj.edu.pl

Multifunctional molecular systems offer a wide range of unique properties promising in the development of future technologies. One of them is magnetic sensing technology operated by external stimuli such as applied light. In photomagnets two distinct switchable magnetic states can be obtained upon light irradiation due to the presence of the photomagnetically-active ions.

Magnetic and photomagnetic properties of three photoactive coordination polymers based on Cu^{2+} and $[Mo_2(CN)_8]^{4-}$ ions were investigated in this work: racemic 2-D system $[Cu(chxn)_2]_2[Mo(CN)_8]\cdot 3H_2O$, chiral 1-D chain $[Cu(RR\text{-}chxn)_2]_2[Mo(CN)_8]\cdot H_2O$, and chiral 1-D chain $[Cu(SS\text{-}chxn)_2]_2[Mo(CN)_8]\cdot 1.5H_2O$.

Analysis of the properties of the samples would require non-trivial and time-consuming Monte Carlo simulations. Instead, a simplified approach based on the molecular field approximation (MFA) was taken. As the efficiency of the irradiation process was not known (the molecular fraction of the Mo^{IV} that undergo the spin-crossover transition to the metastable state Mo^{IV}_{HS}), two independent models were considered for the excited samples. The first one corresponds to the situation where a relatively small fraction of Mo^{IV} becomes excited (formation of isolated $[Cu^{II}]_3Mo^{IV}_{HS}$ units), and the second assumes a 100% efficiency of light irradiation (Fig. 1).

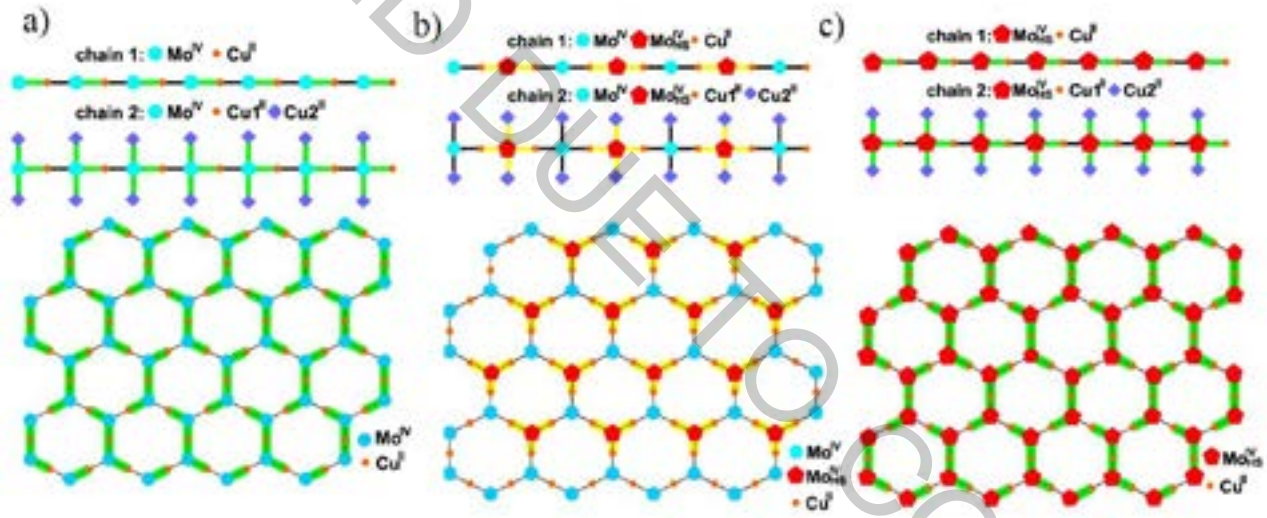

Figure 1. Schematic representation of the employed models: a) unexcited state, b) low efficiency of light irradiation, c) high efficiency of light irradiation.

CANCELLED DUE TO COVID-19

OPTICAL ANISOTROPY OF GaAsBi

Lukas Jočionis, Bronislovas Čechavičius, Renata Butkutė, Saulius Tumėnas, Vytas Karpus

Center for Physical Sciences and Technology, Saulėtekio av. 3, LT-10257, Vilnius, Lithuania
lukas.jocionis@ftmc.lt

The spontaneous atomic ordering in the conventional $A^{III}(B_{1-x}C_x)^V$ [or $(A_{1-x}B_x)^{III}C^V$] semiconductor alloys was discovered in the late 1980s [1]. Usually, the ordering is of the $CuPt_B$ type, when elements of the V (or III) group arrange themselves in alternating $(\bar{1}11)$ or $(1\bar{1}1)$ planes. The ordering induces changes in the electronic structure of alloys and, therefore, their optical properties.

Recently, the $CuPt_B$ ordering was reported for GaAsBi bismides [2]. However, no optical studies of the ordering-induced optical properties of bismides have been carried out so far.

In this work, photomodulated transmittance (PT) and Mueller matrix ellipsometry techniques were used to investigate the optical anisotropy of GaAsBi induced by the atomic ordering. GaAsBi sample with 3.86% bismuth concentration was grown by molecular beam epitaxy on a semi-insulating (001) GaAs substrate. Figure 1(a) presents PT spectra measured at different polarizations of the incident light beam. The spectra show a distinct polarization dependence of two optical features, positioned at 1.122 eV and 1.179 eV, which correspond to valence band splitting Δ_c = 57 meV. The polarization dependence is determined by the $[1\bar{1}0]$ direction, which is a projection of the atomic ordering axis $[1\bar{1}1]$ to the sample surface.

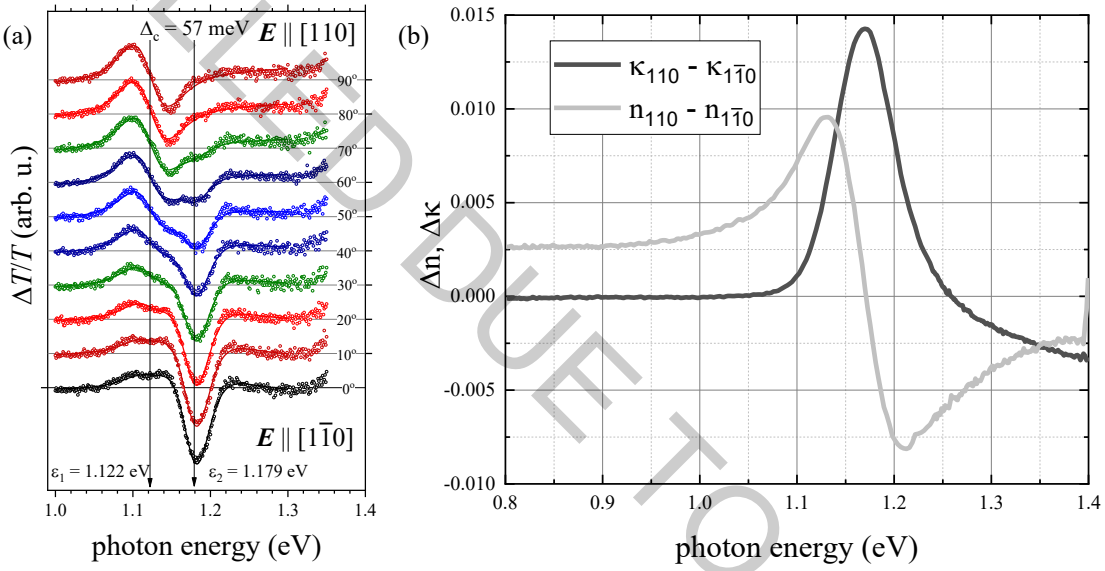

Fig. 1. (a) Photomodulated transmittance spectra at different polarizations of the incident light beam. (b) Linear dichroism and birefringence spectra determined by the Mueller matrix ellipsometry.

Figure 1(b) presents results of ellipsometric measurements in transmission geometry. Making use of the Mueller matrix analytic inversion method [3], the linear birefringence and dichroism (along [110] and $[1\bar{1}0]$ directions) spectra were determined. The sample is clearly anisotropic with its optical axis parallel to the atomic ordering $[1\bar{1}1]$ (or $[\bar{1}11]$) direction. The highest birefringence value reached 0.0097 at 1.13 eV and the dichroism peaked at 1.17 eV with a value of 0.0144. Another characteristic tail is seen above 1.25 eV, however this feature is hidden behind GaAs absorption.

The optical anisotropy of GaAsBi observed both in polarized transmittance and ellipsometric spectra is induced by spontaneous $CuPt_B$-type atomic ordering of bismuth atoms.

[1] A. Mascarenhas, *Spontaneous Ordering in Semiconductor Alloys* (Springer Science, New York, 2002).
[2] A. G. Norman, R. France and A. J. Ptak, "Atomic ordering and phase separation in MBE GaAs1−xBix," Journal of Vacuum Science & Technology B 29, 03C121 (2011).
[3] O. Arteaga and A. Canillas, "Analytic inversion of the Mueller–Jones polarization matrices for homogeneous media," Optics Letters 35(4), 559-561 (2010).

CANCELLED DUE TO COVID-19

EMISSION MEASUREMENT OF TERAHERTZ TORCH DEVICE BASED ON Ga(As,Bi)/AlGaAs NANOSTRUCTURES WITH PARABOLICALLY GRADED QUANTUM WELLS

Justas Pagalys, Ričardas Norkus, Simona Pūkienė, Evelina Dudutienė, Vytautas Jakštas, Mindaugas Karaliūnas

Center for Physical Sciences and Technology, Sauletekio Ave. 3, 10257 Vilnius, Lithuania
justas.pagalys@ftmc.lt

Terahertz (THz) frequency range radiation has various applications such as security, medical diagnosis, high speed communication, etc. Due to the fact that THz radiation is non-ionizing, the imaging and spectroscopy in THz spectral range are promising techniques for non-destructive inspection [1]. For the development of room temperature operating THz technology the compact and efficient THz emitters are crucial elements. One of the methods to meet requirements for THz generation is emission from parabolic quantum wells (PQWs) through intersubband carrier transition. In this work, the investigation of emission from Ga(As,Bi)/AlGaAs nanostrutures with PQWs is presented.

GaAsBi/GaAs rectangular quantum wells (QW) in GaAs/AlGaAs PQWs were grown using molecular beam epitaxy [2]. The active region consists of 52 nm width undoped PQW designed for equidistant energy subbands structure to meet the energy difference between subbands of 29 meV (7 THz). At the center of single GaAs/AlGaAs PQW single 7 nm wide GaAsBi rectangular QW is introduced to enable faster carrier depopulation form the PQW subbands [3]. The active region is sandwiched between undoped $Al_{0.3}Ga_{0.7}As$ layers and then between doped $Al_{0.3}Ga_{0.7}As$ layers with *n*-type from bottom side and *p*-type from top side. Doped structures were grown on the n^+-type GaAs substrate. Then metal ohmic contacts were deposited. For optical characterization undoped samples were also prepared.

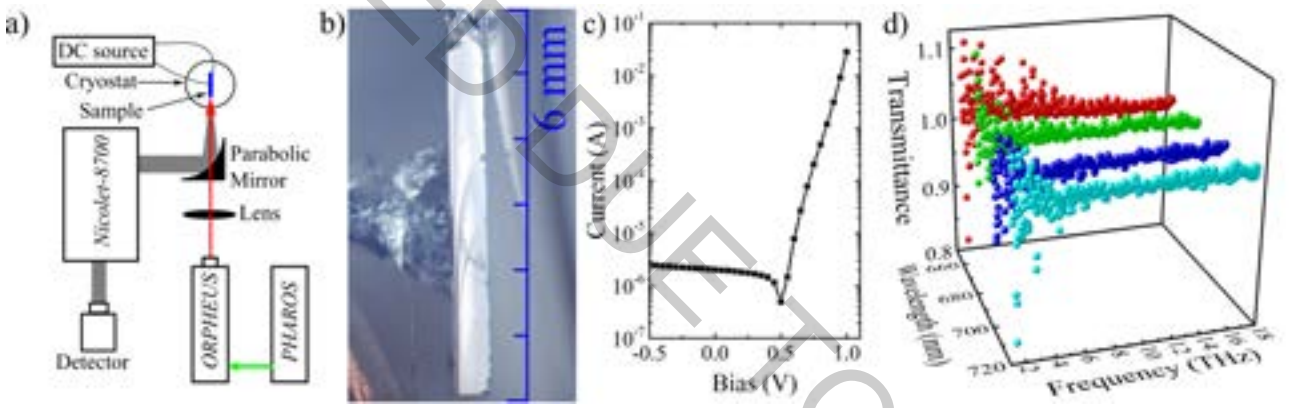

Fig. 1. a) Experimental set-up for measuring edge emission from the sample. b) Side view of the sample. c) typical I-V characteristic of the Ga(As,Bi)/AlGaAs nanostructure sample. d) Emission spectra of the sample with 300 mV applied bias and different laser excitation wavelengths, namely 655 nm (red points), 675 nm (green points), 695 nm (blue points), and 715 nm (cyan points).

Prior to THz emission experiment the low temperature photoluminescence (PL) spectroscopy was carried out for the undoped samples. The 4th harmonic of the solid state laser with 4.66 eV photon energy, 0.5 m focal length monochromator and thermo-electrically cooled photo-multiplier tube were used in PL set-up. Measurements of THz transmission spectroscopy carried out with *Nicolet-8700* (*Thermo Scientific*) far infrared Fourier transform spectrometer. For emission measurements samples were set as the external source of THz radiation for spectrometer (Fig. 1a). For excitation *PHAROS* femtosecond laser with *ORPHEUS* collinear optical parametric amplifier (*Light conversion*) was used. Excitation power density was kept at 3.5 W/cm^2. Samples have electrical wires (Fig. 1b) in order to apply external DC bias and were put in the cryostat which was cooled down to 80 K.

PL spectra revealed that the structure of energy subbands in the PQW is nearly to the designed one. From transmission spectroscopy measurements spectral features were observed at 4.69 THz and 7.1 THz [4]. Measured I-V characteristics of doped samples show asymmetrical *pn* junction behaviour (Fig.1c). Fig.1d shows the measured emission spectra for one of samples with 300 mV applied bias and at different excitation wavelengths. With current experimental set-up the THz torch device emission was below detection limit. However, the new approach of the measurement using 45° angle polished device geometry is very likely to allow to prove the working principle of the THz torch by measuring emission signal.

[1] M.Karaliūnas et al. Sci. Rep. **8**, 18025 (2018)
[2] S. Pūkienė et al. Nanotechnology **30**, 455001 (2019).
[3] M.Karaliūnas et al. Lith. J. Phys., accepted (2020).
[4] M. Karaliūnas et al. Proc. of SPIE, **11124**, 27 – 34 (2019).

CANCELLED DUE TO COVID-19

EXPOSURE PARAMETER INFLUENCE ON METAL SURFACE PATTERNS FORMED USING FEMTOSECOND LASER

Arnas Žemaitis[1,2], Gedvinas Nemickas[1,2], Gabrielius Kontenis[1,2], Vytautas Purlys[1,2] and Linas Jonušauskas[1,2]

[1] Femtika Ltd., Saulėtekis Ave. 15, Vilnius LT-10224, Lithuania
[2] Laser Research Center, Vilnius University, Saulėtekis Ave. 10, Vilnius LT-10223, Lithuania
arnas@femtika.lt

CANCELLED DUE TO COVID-19

Laser technology provides new and revolutionizing solutions to many different fields ranging from agriculture [1] to military [2] and space industries [3]. Annual increase in the photon-based solutions provides us with highly precise tools that do not require contact to obtain information or perform certain tasks. Currently, mostly high-power continuous wave or long pulse (millisecond-nanosecond) laser systems are used in the industry. Nevertheless, in order to achieve nano-level precision ultrashort picosecond (ps) and femtosecond (fs) laser pulses are needed. They allow initiation of vast array of highly localized nonlinear light-matter interactions which became the basis for variety of novel laser material processing techniques [4].

One of the areas that highly benefited from these developments was ultra-precise surface patterning. It allows to produce hierarchical surface patterns with feature sizes ranging from hundreds of nm to tens of μm [Fig. 1]. Such surface topographies allow to control multitude of surface parameters allowing it to become hydrophobic, hydrophilic, repulsive or highly adhering. In addition, change between these surface properties are easily induced by changing exposure parameters during the fabrication process. For this reason, complete understanding of how laser parameters influence relevant surface properties is extremely important.

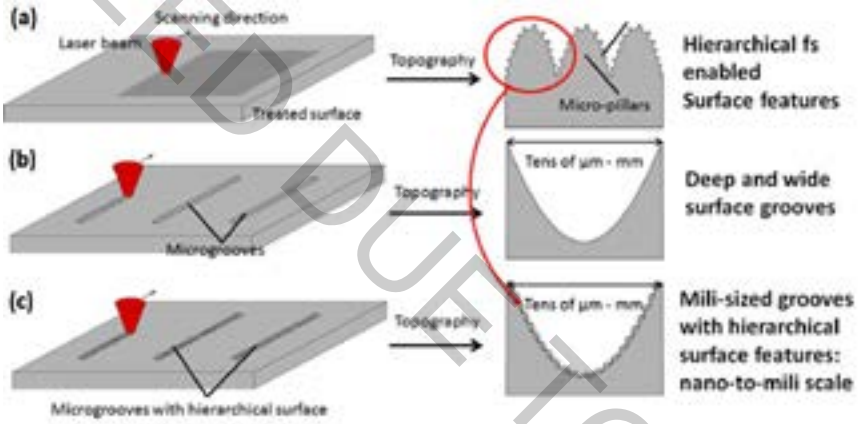

Fig. 1. Application of fs laser allows to achieve hierarchical nanogrooves (a), micro-features (b) or combine them together (c). This enables the control of surface wetting, photonic and related properties.

In this work we investigated how fabrication parameters such as wavelength, pulse duration, repetition rate, pulse energy, overlap and spot size influence the wetting properties of various metal sample. The chosen metal samples represent alloys most prominent in industries like medicine, maritime and aviation. SEM analysis as well as contact angle measurements and profilometer readings were used for qualitative surface analysis. At the same time their wetting properties were tested, showing contact angles in the range of 5 to 170 degrees [Fig. 2]. These results are presented in the context of current state-of-the-art highlighting possibilities and challenges in further developing this technology.

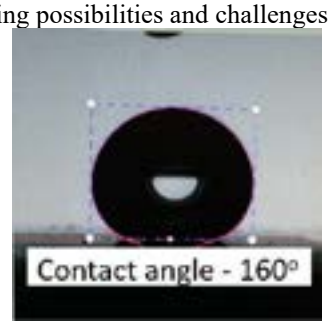

Fig. 2. Example of water drop on fs laser textured metal surface. Clear hydrophobicity at contact angle of 160 degrees is visible.

[1] B. Blackwell et al., Lasers as nonlethal avian repellents, J. Wildl. Manag. **66** (1), 250-258 (2002).
[2] A. Sijan, Development of military lasers for optical countermeasures in the mid-IR, Proc. SPIE **7483**, 748304 (2009).
[3] R. J. DeYoung et al., Comparison of electrically driven lasers for space power transmission, NASA-TM-4045, L-16431, NAS 1.15:4045 (1988).
[4] L. Jonušauskas et al., Femtosecond lasers: the ultimate tool for high-precision 3D manufacturing, Adv. Opt. Technol. **8** (3-4), 241-251 (2019).

A DETAILED PROCEDURE FOR PARAMETER EXTRACTION OF THE ONE-DIODE SOLAR CELL MODEL

Andreea Sabadus

Faculty of Physics, West University of Timisoara, V Parvan 4, 300223, Timisoara, Romania
sabadus.andreea@yahoo.com

CANCELLED DUE TO COVID-19

Many models for solar cells operation were developed on the basis of the Shockley theory of the illuminated p-n junction [1]. As a result, the equivalent circuit of the solar cell can be described at different levels of approximation. The one-diode model defines the most common approximation of the current-voltage (I-V) characteristics of a solar cell operating in standard test conditions (STC) (Fig. 1). STC specifies the global irradiance incident normal on the surface of a PV module at $G_{STC} = 1000\,\mathrm{W/m^2}$ with a spectral distribution *AM1.5G* and cell temperature $T_{STC} = 25°C$. The equivalent circuit captures the physical process that governs the operation of a solar cell. The photocurrent (I_L) is modeled by a current source mainly depending on solar irradiance. The diode models the dark current losses (D). Current loss caused by increased junction conductivity at cell edges is modeled by the shunt resistance (R_P). The series resistance (R_S) captures the resistive loses in the cell such as the contact resistances and neutral regions resistances.

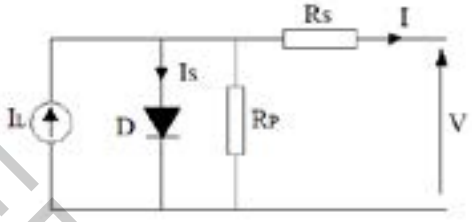

Fig. 1. One-diode model of a solar cell: the electrical circuit.

The most popular equation developed in the frame of one-diode model is the five-parameter equation:

$$I(V) = I_L - I_S\left[\exp\left(\frac{e(V+IR_S)}{mk_BT}\right) - 1\right] - \frac{V+IR_S}{R_P} \quad (1)$$

where e is the elementary charge and k_B is the Boltzmann constant.

The I-V characteristics of a PV module consist of a superposition of the I-V characteristics of its constituent solar cells. A PV module is usually delivered by manufacturer with a datasheet which emphasizes three notable points on the I-V characteristic: the short-circuit current, the open-circuit voltage and the maximum power point (MPP). These points are measured at STC.

In this paper a detailed procedure [2] for parameters extraction is presented and assessed from the perspective of performance in modeling the I-V characteristics. The procedure uses only the information provided in datasheets, i.e the three notable points of the I-V characteristic. For this, the numerical results are compared with measured data. The samples were prepared at ISC Konstanz and characterized at the PV Laboratory of the West University of Timisoara.

[1] S. Lineykin, M. Averbukh, A. Kuperman, An improved approach to extract the single-diode equivalent circuit parameters of a photovoltaic cell/panel, Renew Sustain Energy Rev **30**, 282-289 (2014).

[2] A. Sabadus, V. Mihailetchi, M. Paulescu, Parameter extraction for the one-diode model of a solar cell, American Institute of Physics Proceedings Series, article number: 040005 (2017).

ASTROCYTE RESPONSE UNDER MODIFIED RESTRAINT WATER IMMERSION STRESS AND ALPHA-KETOGLUTARATE SUPPLEMENTATION

Olena Dovban, Galyna Ushakova

Department of Biochemistry and Physiology, Oles Honchar Dnipro National University, Ukraine
dovbanelena@gmail.com

Stress research is one of the relevant issues of modern biology and medicine. Stress is a condition of the organism that responds to various types of exogenous and endogenous effects that lead to physical and psychological dysfunctions [1]. The most widely used experimental stress model is the restraint water-immersion stress (RWIS), a compound stress model that includes both psychological and physical stimulations [2, 3]. Several stressors, such as exposure to temperature, biorhythmic changes, and restriction, often work in combination. The reaction of glial cells that support neuron function under stress is actual today. Astrocytes behavior can be evaluated by the level of specific proteins - Ca^{2+}-binding protein S-100b and glial fibrillary acidic protein (GFAP).

Our study aimed to investigate the changes in the levels of glial fibrillary acidic protein (GFAP) and Ca^{2+}-binding protein S-100b in different rat's brain areas under modified RWIS condition, during physiological recovery and alpha-ketoglutarate supplementation.

The brains of 24 Wistar rats were used for investigation. Animals were kept under standard vivarium conditions, and all manipulations were performed according to the animal protection convention used in the experiments. The experimental model was created within 3 days using prolonged and modified restraint water-immersion stress [4]. Animals were divided into four groups (n = 6). 1 - rats of the control group; 2 - rats subjected to modified RWIS for 3 days using a stress protocol with immersion in water with changing of the temperature and under permanent light, 3 - rats that were kept under normal conditions for 14 days without stress factors after 3days RWIS, 4 - rats receiving 2% alpha-ketoglutarate with drinking water during 14 days after stress exposure. The animals were decapitated under mild anesthesia; four brain areas were isolated: cerebellum, visual cortex, thalamus, and hippocampus. Quantification of S-100b and GFAP was performed according to the competitive ELISA. The results were statistically processed using one-way ANOVA followed by post-hoc Tuckey test to compare different groups. Data at $P<0.05$ were considered as significant.

It was shown that under modified RWIS exposure the level of S-100b protein increased in cerebellum by 61% compared to control. In other brain areas were no significant changes after RWIS. In the thalamus, visual cortex and hippocampus increase of the level of S-100b protein was shown in the group with 14 days of the physiological recovery by 97%, 81% and 78% compare to control animals. Obtained data of the S-100b level indicate a delayed effect of modified RWIS.

The GFAP level was shown with 31% deficit in the hippocampus, an 18% increase in the thalamus, and a 23% increase in the visual cortex after 3-days stress exposure.

Supplementation for 14-days with 2% alpha-ketoglutarate dissolved in drinking water had a positive impact on astroglial cells after exposure to 3-days stress.

Previous data from our lab had shown the positive impact of alpha-ketoglutarate on the astrocyte condition with age-dependent changes in GFAP concentration [5], and under ischemic conditions [6].

The findings suggest that alpha ketoglutarate as a natural compound may serve as a protector against stress impact.

[1] McEwen, B. S. Mechanisms of Stress in the Brain. Nature neuroscience, 18(10), 1353–1363. (2015)
[2] Sun, H., Li, R., Xu, S., Liu, Z., & Ma, X. Hypothalamic Astrocytes Respond to Gastric Mucosal Damage Induced by Restraint Water-Immersion Stress in Rat. Frontiers in behavioral neuroscience, 10, 210. (2016).
[3] Fan F., Yang M., Geng X., Ma X., Sun H. Effects of Restraint Water-Immersion Stress-Induced Gastric Mucosal Damage on Astrocytes and Neurons in the Nucleus Raphe Magnus of Rats via the ERK1/2 Signaling Pathway. Neurochem Res. 44:1841–1850. (2019).
[4] Uhakova GO, Dovban OO. Method of modeling of acute combined water-immobilization stress with change of light biorhythm. UA Patent 133796, 25 Apr 2019
[5] Kovalchuk YP, Ushakova HO. The changes of glial fibrillary acid protein level in the different brain areas of gerbils under development, aging and alpha-ketoglutarate effect. Med Clin Chem. 1, 29-35 (2016).
[6] Kovalenko T.N., Ushakova G.A., Osadchenko I., Skibo G.G., Pierzynowski S.G. The neuroprotective effect of 2-oxoglutarate in the experimental ischemia of hippocampus. J Physiol Pharmacol.; 62, 239–46. (2011).

CANCELLED DUE TO COVID-19

APPLICATION OF RARE-EARTH DOPED NANOPARTICLES FOR CANCER DIAGNOSTICS AND THERAPY

Greta Jarockyte[1,2], Artiom Skripka[3], Vitalijus Karabanovas[1,4], Riccardo Marin[3], Vivienne Tam[3,5], Marta Cerruti[5], Fiorenzo Vetrone[3], Ricardas Rotomskis[1,6]

[1]Biomedical Physics Laboratory, National Cancer Institute, Vilnius, Lithuania
[2]Life Sciences Center, Vilnius University, Vilnius, Lithuania
[3]Centre Énergie, Matériaux et Télécommunications, Institut National de la Recherche Scientifique, Université du Québec, Varennes, QC, Canada
[4]Department of Chemistry and Bioengineering, Vilnius Gediminas Technical University, Vilnius, Lithuania
[5]Department of Mining and Materials engineering, McGill University, Montréal, QC, Canada
[6]Biophotonics group of Laser Research Centre, Vilnius University, Vilnius, Lithuania
greta.jarockyte@nvi.lt

Despite recent progress in medicine there still are many challenges in the fight against cancer. Nanotechnology tools have potential to improve early cancer diagnostic and therapy. One of the possible ways to improve cancer treatment is to combine diagnostic and therapeutic properties, creating multifunctional theranostics agents. The concept of theranostics emerged around 2002 and within the past decade has transformed into a rapidly expanding field that is located at the interface of diagnosis and therapy.

In our study, we present a new generation theranostic nanomedicines. The theranostic approach within these nanoparticles is functionally decoupled, meaning that the therapeutic or diagnostic faculties are prompted individually, on-demand, by the wavelength specific optical excitation. Decoupled rare-earth nanoparticles (dNPs) operate entirely in the near-infrared (NIR) spectral region, for minimized light interference with target and extended tissue depth action. Heating-free 806 nm irradiated dNPs behave solely as high-contrast NIR-to-NIR optical probes. While exclusively excited by light of 980 nm, dNPs can prompt a therapeutic effect via upconversion emission in the UV/blue spectral regions.

Specifically, we have made multilayered $LiYF_4$:Tm^{3+},Yb^{3+}@$LiYF_4$@$LiYF_4$:Nd^{3+} nanoparticles that behave as dNPs in early cancer diagnostics and photosensitized tumor therapy [1]. dNPs optical properties *in vitro* were explored upon 806 nm and 980 nm excitation to prove that dNPs have NIR downshifting emission under heating-free 806 nm excitation and UV and blue radiation when dNPs are excited by the therapeutic 980 nm light. Also, dNPs' cytotoxicity and uptake in cancer cells were evaluated. Moreover, as an example, we formed a dNPs and photosensitizer chlorine e_6 (Ce_6) (dNPs-Ce_6) complex that was able to generate reactive oxygen species solely under 980 nm of excitation, and cause cancer cell death in 2D and 3D cell cultures.

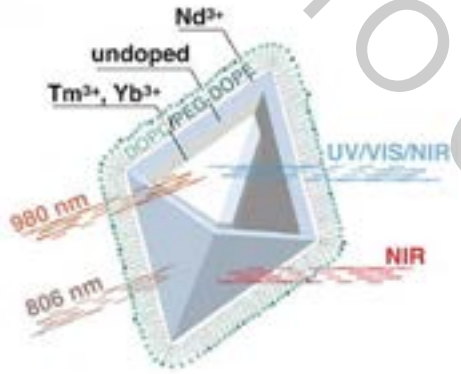

Fig. 1. Schematic representation of the dNPs. The $LiYF_4$: Tm^{3+}, Yb^{3+} core absorbs only 980 nm photons and emits UC light from UV to NIR. The core of dNPs is separated by an undoped LiYF4 shell #1 from the $LiYF_4$: Nd^{3+} shell #2 which can be excited by 806 nm irradiation and emit in the NIR spectral region. dNPs are encapsulated in phospholipid micelles, ensuring aqueous colloidal stability and biological applicability.

Overall, these dNPs represent a new class of theranostic agents in which the therapy and diagnostics are not prompted simultaneously, but rather on-demand, potentially increasing the safety and versatility of such nanostructures in the future.

[1] A. Skripka, V. Karabanovas, G, Jarockyte, R. Marin, V. Tam, M. Cerruti, R. Rotomskis, F. Vetrone, Decoupling Theranostics with Rare Earth Doped Nanoparticles, Advanced Functional Materials., 29(1), 1-12 (2019).

CANCELLED DUE TO COVID-19

NOVEL APPROACH ON APPLICATION OF AN EXTREMOPHILIC RED ALGA *CYANIDIOSCHYZON MEROLAE* IN PHYTOREMEDIATION

Ewa Borowska[1], Mateusz Abram[2], Joanna Kargul[2]

[1] The College of Inter-Faculty Individual Studies in Mathematics and Natural Sciences (MISMaP), University of Warsaw, Poland
[2] Solar Fuels Laboratory, Centre of New Technologies, University of Warsaw, Poland
e.borowska@biol.uw.edu.pl, ewa.borowska86@gmail.com

CANCELLED DUE TO COVID-19

Nowadays, water pollution and bioremediation are the most important issue. Scientists endeavouring and trying to discover novel methods for removing pollutants from water or clean sludges for reuse contaminated waters. Most of the mentioned environmental hazards are created in human environment, like acid and metalliferous drainage that also contain heavy metals. Acidic and eutrophic waters can determine further dangerous conditions for biodiversity as increase of biogenic elements or acidity of ground and sea waters. Organisms, especially those one that can thrive in naturally polluted habitats, can give us a great possibility to use their features for understanding cleaning, transforming and removing processes [1].

One of the possibilities of reducing toxicity of waste is to apply microorganisms in bioremediation. Thus, the best opportunity is to use relevant organisms with a wide spectrum of activity and adaptation to harmful conditions (e.g., extremophiles).

Cyanidioschyzon merolae is a red microalgae, which is the one of the most primitive algae, naturally exist in sulphate-rich hot springs habitat (pH 1.5, at 45 – 56 °C) associated with high heavy metal concentrations [2, 3]. In this research, we present the first steps to assess the bioremediation potential of C. merolae. We measured cell survivability in the presence of selected high salt concentrations at two growth temperatures (42 °C and 25 °C). It is worth to mention that this research firstly introduce a new cell strain of Cyanidioschyzon merolae based on the NIES-1332 strain (Microbial Culture Collection from the National Institute for Environmental Studies (Tsukuba, Japan)), which is adapted to vary pH and capable of being effective growth under pH conditions in the range of 2.5 to 6.7. Likewise, it can be cultivated in temperature range 25 – 65 °C, although the optimal range is 40 – 42 °C.

Our research implies new facet to cope with such peculiar pollution with a different pH range. (This research is based on Patent notification by Polish Patent Office: No. P.432684).

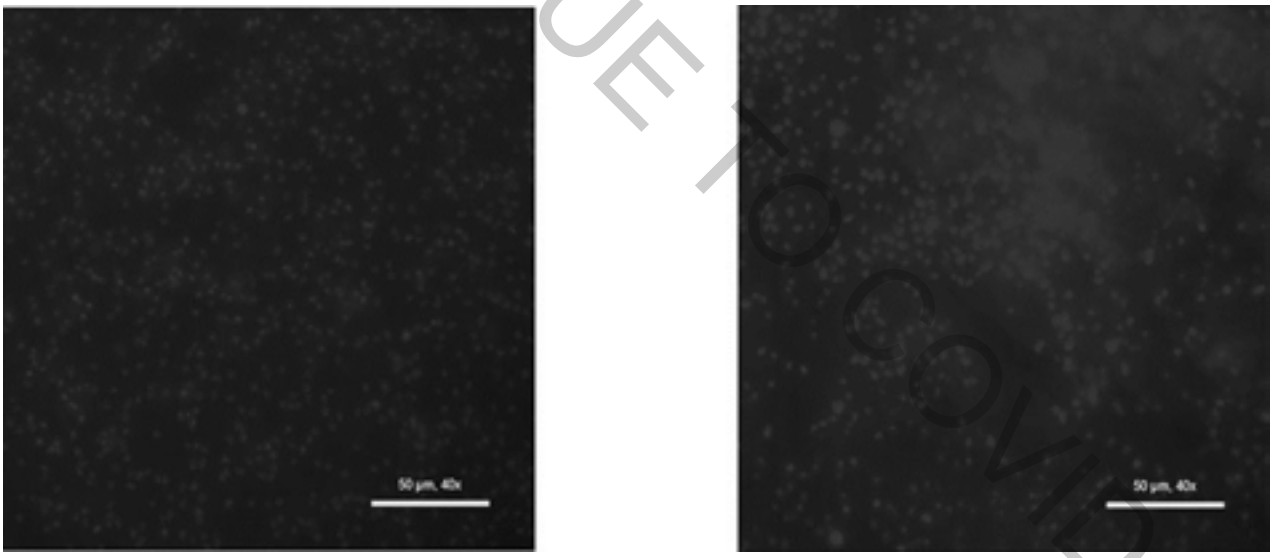

Fig. 1. Fluorescence microscopy images of chlorophyll emissions from C. merolae cells cultured at different pH: (a) 2.5 (b) >6.

We discovered differences between cells in varying pH conditions, for instance the size and shape (in Fig. 1). Microscopic analysis was performed via LS720 fluorescence microscope (Etaluma) at 40x magnification and chlorophyll excitation at 580 – 598 nm. 50 µM scale. Both micrographs show fluorescence of individual chloroplasts in C. merolae cells, thus, showing cell viability in both cultures.

In conclusions, this preliminary data and new cell strain open further possibilities of investigation of bioremediation potential of C. merolae.

[1] S. K. Gupta. *Application of Microalgae in Wastewater Treatment* (Springer, Switzerland, 2019).
[2] T. Kuroiwa, et al. *Cyanidioschyzon merolae. A New Model Eukaryote for Cell and Organelle Biology* (Springer, Singapore, 2017).
[3] P. De Luca, et al. Cyanidioschyzon merolae a new alga of thermal acidic environments. Journal of Plant Taxonomy and Geography **31** (1978).

CONCENTRATION-DEPENDENT POLYMORPHISM OF INSULIN AMYLOID FIBRILS

Andrius Sakalauskas, Mantas Ziaunys, Vytautas Smirnovas

Institute of Biotechnology, Life Sciences Center, Vilnius University, Vilnius, Lithuania
sakalauskas.and@gmail.com

Protein aggregation into insoluble amyloid aggregates is associated with several neurodegenerative diseases, such as Alzheimer's, Parkinson's and Prion diseases [1]. Polymorphism of amyloidogenic proteins is one of the factors that complicate the disease mechanisms which may be the cause of failure in research for anti-amyloid drugs. In this study we show that protein concentration is another factor which leads to formation of structurally distinct insulin fibrils [2]. Experimental data suggests that distinct insulin fibrils self-replicate via elongation, while seed-induced nucleation will lead to environment-defined conformation of fibrils.

We have characterized insulin amyloid fibrils formed at protein concentration range from 0.2 mM to 1.0 mM. Insulin aggregation kinetics were measured using amyloid-specific fluorescent dye – Thioflavin T (ThT). After insulin aggregation, data revealed two different fibrils populations – low concentration fibrils (LCF) and high concentration fibrils (HCF) which had a major difference in ThT fluorescence intensity and fibril concentration ratio values. Further assessment of secondary structures using Fourier-transform infrared spectroscopy confirmed two different fibril conformations formed at 0.2 mM and 1.0 mM insulin concentration. Fibrils morphology was imaged by AFM and fibril height distribution was estimated from the images.

[1] F. Chiti and C. M. Dobson, "Protein Misfolding, Amyloid Formation, and Human Disease: A Summary of Progress Over the Last Decade," *Annu. Rev. Biochem.*, vol. 86, no. 1, pp. 27–68, 2017.
[2] A. Sakalauskas, M. Ziaunys, and V. Smirnovas, "Concentration-dependent polymorphism of insulin amyloid fibrils," *PeerJ*, vol. 7, p. e8208, Dec. 2019.

CANCELLED DUE TO COVID-19

SEX DIFFERENCES OF BRAIN ACTIVITY IN VISUAL CHOICE REACTION TASK

Veronika Vozniuk[1], Natalia Filimonova[1], Mykola Makarchuk[1], Ihor Zyma[1]

[1] Department of physiology and anatomy, ESC Institute of biology and medicine, Taras Shevchenko National University of Kyiv, Ukraine
veronicavozniuk@gmail.com

It is well known phenomenon in psychology that men and women usually make decision/choice using different mind strategies. The existence of such phenomen is obvious due to different ratio of determinant sex steroids that cause very powerful impact on brain development and functioning as there are specific receptors to estrogen and testosterone in numerous brain structures. However, the neurobiological aspects of men's and women's decision making strategies are still ambiguous and require more data. The knowledge of sex differences of brain activity potentially could provide better rehabilitation for men and women with various brain injuries.

Decision making implies execution of basic cognitive processes which are based on choice reaction. Thereby, in this study visual choice reaction task with 2 simple stimuli was used.

The aim of the study was to investigate whether there are any differences in brain activity and choice reaction time between male and female subjects during choice reaction task performance.

The study involved 30 male volunteers, right-handed, 23,2±3,1 y.o., and 25 female volunteers, right-handed, 18,4±0,6 y.o.. All participants were students of Taras Shevchenko National University of Kyiv and have no health complaints, reported brain injuries or psychiatric disorders.

In the study choice reaction time (CRT) of motor responses made by right (rhCRT) and left hands (lhCRT) were detected. Mean CRT was evaluated as well. CRT data is presented below as Median [Lower Quartile (25%); Upper Quartile (75%)]. EEG was recorded during choice reaction task perfomence. EEG was done with 19 leads placed on the scalp according to the International 10-20 System. Localization and statistical analysis of 3D distribution of the generating electric neuronal activity were performed applying the LORETA-software package v.20181107 [1,2]. Coherence analysis was performed for all possible coupled pairs of leads in delta (0,5-3,9 Hz), theta (4-7,9 Hz), alpha (8-12 Hz), beta-1 (14-19,9 Hz) and beta-2 (19-35 Hz) bands applying the Neuron-Spectrum software. Significant level of coherence value was established equal or greater than 0,7 [3].

There was no significant difference between results of male and female subjects in mean CRT (409 [392;430] ms vs. 420 [397; 460] ms (p=0,185)), rhCRT (402 [392; 435] ms vs. 413 [390;462] ms (p=0,473)) and lhCRT (413 [390;430] ms vs. 426 [409;476] ms (p=0,112)). Nevertheless, males demonstrated greater activation mostly of right hemisphere compared to females (p=0,013, threshold=0,487): BA 11 (rectus gyrus, medial frontal gyrus); BA 17, 18, 19, 23 (cuneus, lingual gyrus, fusiform gyrus, inferior occipital gyrus, middle occipital gyrus); BA 19 (inferior temporal gyrus); BA 24, 25, 32, 33 (anterior cingulate cortex); BA 30, 31 (posterior cingulate cortex); BA 28, 34 (parahippocampal gyrus); BA 28, 34, 36, 38 (uncus); BA 31 (precuneus); BA 38 (superior temporal gyrus); BA 22, 37, 39 (middle temporal gyrus); BA 47 (inferior frontal gyrus). There are few left hemispheric brain zones that also were more active in males: BA 11, 17, 18, 19, 24, 25, 28, 32 and 33. Coherence analysis revealed both males and females had distributed fronto-parieto-occipital network in teta band within the left hemisphere. For males the same network in the right hemisphere was interconnected with lateral sites in fronto-temporal regions. Furthermore, females demonstrated no activation of right centro-parieto-occipital networks in alpha and beta-1 bands. Centro-parieto-occipital networks in beta-2 band were present bilaterally in females, while the activation of left fronto-parieto-occipital and right hemispheric centro-parieto-occipital networks was distinctive for males. Also bilateral activation of centro-parieto-occipital networks in delta band was specific solely to females.

[1] Pascual-Marqui RD, Michel CM, Lehmann D. Low resolution electromagnetic tomography: A new method for localizing electrical activity in the brain. Int J Psychophysiol. 1994;18:49-65. doi: 10.1016/0167-8760(84)90014-x

[2] Nichols TE, Holmes AP. Nonparametric permutation tests for functional neuroimaging: A primer with examples. Hum Brain Mapp. 2002;15(1):1-25. doi: 10.1002/hbm.1058

[3] Kulaichev AP. The informativeness of coherence analysis in EEG studies. Neurosci Behav Physiol. 2011;41(3):321-328. doi: 10.1007/s11055-011-9419-4

CANCELLED DUE TO COVID-19

HAMLET CYTOTOXICITY IN COLORECTAL CANCER CELL MODELS WITH DIFFERENT MUTATION STATUS IN VITRO

Miglė Pivoriūnaitė[1,3], Darius Stukas[1,3], Justas Žilinskas[2], Giedrė Šilkūnienė[1], Mantas Šilkūnas[1], Žilvinas Dambrauskas[1,2], Antanas Gulbinas[1], Algimantas Tamelis[2]

[1]Institute for Digestive Research, Medical Academy, Lithuanian University of Health Sciences, Lithuania
[2]Clinic of Surgery, Lithuanian University of Health Sciences, Lithuania
[3]Faculty of Natural Sciences, Vytautas Magnus University, Lithuania
m.pivoriunaite@gmail.com

CANCELLED DUE TO COVID-19

HAMLET (Human Alpha-lactalbumin Made LEthal to Tumor cells) is a proteolipid complex of partially unfolded α-lactalbumin and several oleate residues. Its efficacy as a selective killer of tumor cells has been documented *in vitro* and *in vivo* in several animal models [1]. HAMLET interacts with multiple tumor cell compartments, affecting cell morphology, metabolism, proteasome function, chromatin structure and cell viability [2]. Colorectal cancer is one of the most frequent malignancies worldwide, being second in males and third in females for its frequency and ranking fourth and third for cancer-related deaths among males and females, respectively [3]. KRAS and BRAF are major oncogenic drivers of colorectal cancer (CRC) [4].

The aim of this study was to evaluate antitumoral activity of the HAMLET complex on three different CRC cell lines (LoVo, WiDr, Caco-2) with different mutation status (KRAS/BRAF, wild type).

HAMLET complex was prepared using controlled temperature (partial protein unfold) combined with mixing/shaking with olein acid additive (acid incorporation in protein structure) [5]. Cytotoxicity of complex (metabolic activity and viability of the cells) was evaluated using 6 h exposition and different concentration in compliance with MTT and clonogenic assay protocols.

The results suggest that HAMLET affects cell metabolism, this effect is severe and at the same time irreparable for cells, leading to cell death. The complex exhibits cytotoxicity in dose-response manner against all cell lines. However, BRAF mutant cells seems to be more resistant to HAMLET in comparison to KRAS mutants and wild type cells. HAMLET has anticancer potency for CRC in *in vitro* model.

Acknowledgments: This project has received funding from European Social Fund (project No 09.3.3-LMT-K-712-15-0288) under grant agreement with the Research Council of Lithuania (LMTLT).

[1] Ho, J., Nadeem, A., Rydström, A. *et al.* Targeting of nucleotide-binding proteins by HAMLET—a conserved tumor cell death mechanism. *Oncogene* 35, 897–907 (2016) doi:10.1038/onc.2015.144

[2] Ho, J., Sielaff, H., Nadeem, A., Svanborg, C., & Grueber, G. (2015). The molecular motor F-ATP synthase is targeted by the tumoricidal protein HAMLET. *Journal of molecular biology, 427 10*, 1866-74

[3]Testa, U., Pelosi, E., & Castelli, G. (2018). Colorectal cancer: genetic abnormalities, tumor progression, tumor heterogeneity, clonal evolution and tumor-initiating cells. *Medical sciences (Basel, Switzerland)*, *6*(2), 31. doi:10.3390/medsci6020031

[4] Morkel, M., Riemer, P., Bläker, H., & Sers, C. (2015). Similar but different: distinct roles for KRAS and BRAF oncogenes in colorectal cancer development and therapy resistance. *Oncotarget*, *6*(25), 20785–20800. doi:10.18632/oncotarget.4750

[5] Kamijima T1, Ohmura A, Sato T, Akimoto K, Itabashi M, Mizuguchi M, Kamiya M, Kikukawa T, Aizawa T, Takahashi M, Kawano K, Demura M. Heat-treatment method for producing fatty acid-bound alpha-lactalbumin that induces tumor cell death. Biochem Biophys Res Commun. 2008 Nov 7;376(1):211-4.

AVIAN TRYPANOSOMES (*TRYPANOSOMA*) IN BLOODSUCKING BITING MIDGES (CERATOPOGONIDAE)

Margarita Kazak[1], Rasa Bernotienė[2], Tatjana Iežova[3]

[1] Life Sciences Center, Vilnius University, Lithuania
[2] Laboratory of Entomology, The Nature Research Centre, Lithuania
[3] P.B. Šivickis Laboratory of Parasitology, The Nature Research Centre, Lithuania
margusix@gmail.com

Protozoa of the genus *Trypanosoma* (Sarcomastigophora, Kinetoplastida) causes Chagas disease and African sleeping sickness in humans. Trypanosomiasis is not as well studied in birds, but the parasite does affect the growth and fitness of highly infected individuals [1]. More than 100 species of avian trypanosomes have been described and prevalence of these parasites in avian populations is close to 30 %, however most species biology and life cycles are unknown. Vectors of avian trypanosomes are bloodsucking insects, mostly from order Diptera – blackflies, biting midges and mosquitoes, but most vectors remain unknown [2-3]. Nowadays flagellates from genus *Trypanosoma* became one of the main objects in bird studies because of their ecological and evolutional importance [4].

The main purpose of this study was to investigate trypanosome infections in biting midges (Ceratopogonidae, *Culicoides*). Goals of the study were: to collect parous biting midges for research in wild; to screen biting midges for natural trypanosome infections; to determine if two *Trypanosoma* species naturally found in Lithuanian birds can develop in *Culicoides nubeculosus* and *C. impunctatus* biting midges under laboratory conditions.

Biting midges were collected using UV light trap in Verkiai regional park in 2018 - 2019. Parous females were screened for the presence of *Trypanosoma* using molecular methods (PCR, DNA sequencing and sequence analysis). Birds naturally infected with *Trypanosoma* parasites were collected in Ventės Ragas and Labanoras. *Culicoides nubeculosus* (from the colony cultivated in laboratory) and *C. impunctatus* (wild) biting midges were allowed to feed on infected bird blood, were kept in laboratory, dissected daily and screened for the presence of *Trypanosoma* parasites using microscopy and PCR-based methods. Investigations were carried out at Nature Research Centre, laboratories of Entomology and P. B. Šivickis parasitology.

During research 235 parous wild caught biting midges (*Culicoides*) were investigated. Two *Trypanosoma* species and 2 species of related to trypanosomes flagellate parasites were detected in 16 biting midges belonging to 10 species. Experimental infections of *C. impunctatus* and *C. nubeculosus* biting midges with 2 species of trypanosomes (*Trypanosoma avium* and *T. everetti*) showed, that *T. everetti* can develop in *C. nubeculosus* and *C. impunctatus*. These parasites were detected in biting midges up to 9 days after feeding with infected blood. Only one out of 8 blood fed *C. impunctatus* biting midge was found to be infected with *T. avium*. There is not enough evidence that *T. avium* can develop in *C. impunctatus* under laboratory conditions and further investigation is needed.

[1] Sehgal, R. N. M., Jones, H. I., & Smith, T. B., 2001. Host specificity and incidence of Trypanosoma in some African rainforest birds: A molecular approach. Molecular Ecology, 10(9), 2319–2327).
[2] Svobodová, M., Dolnik, O. V., Čepička, I., & Rádrová, J., 2017. Biting midges (Ceratopogonidae) as vectors of avian trypanosomes. Parasites and Vectors, 10(1), 1–9.
[3] Zídková, L., Cepicka, I., Szabová, J., & Svobodová, M., 2012. Biodiversity of avian trypanosomes. Infection, Genetics and Evolution, Vol. 12, pp. 102–112.
[4] Masello, J. F., Martínez, J., Calderón, L., Wink, M., Quillfeldt, P., Sanz, V., Hauber, M. E., 2018. Can the intake of antiparasitic secondary metabolites explain the low prevalence of hemoparasites among wild Psittaciformes? Parasites and Vectors;11(1):357.

CANCELLED DUE TO COVID-19

QUALITATIVE STATE OF LIPOPROTEINS UNDER ARTERIAL HYPERTENSION AND CHRONIC KIDNEY DISEASE

Viktoriia Vasylchenko[1, 2], Oksana Dunaievska[3], Olena Kuchmenko[1, 2], Lesya Korol[2], Natalya Stepanova[3]

[1]Department of Biology, National University of Kyiv-Mohyla Academy, Ukraine
[2]Laboratory of Biochemistry, State Institution "Institute of Nephrology NAMS of Ukraine", Ukraine
[3]Pharmaceutical and Laboratory Department, Zhytomyr College of Pharmacy, Ukraine
vasylchenkovita@gmail.com

The changing the enzyme's activity which conjugated with high-density lipoproteins under dysfunctional of the metabolic process caused disease in the cardiovascular system. Preventing their complications is paramount for patients with chronic kidney disease (CKD) [1]. For investigating the development of pathogenesis in lipoprotein, the activity of lipoprotein-associated enzymes (paraoxonase-1 and myeloperoxidase) were evaluated in patients with the II stage arterial hypertension (AH) and CKD. The study included 50 patients (mean age 54 years) with AH, 30 (mean age 48 years) with CKD and 30 conditionally healthy donors (mean age 46 years). The Kruskal-Wallis criterion was performed for processing the data ($P < 0.01$) [2].

The activity of paraoxonase-1 in blood plasma in both groups of patients was two times lower under this index in the control group. The activity of myeloperoxidase, conversely, was approximately two times increase in the patient with AH and one and a half times increase in the patient with CKD which signals about the activation of free radical oxidation processes.

Consequently, the decreased activity of paraoxonase-1 leads to the loss of antioxidant and anti-atherogenic properties of high-density lipoprotein and may be used as predictive markers for cardiovascular disease.

[1] Zhou C, Cao J, Shang L, Tong C, Hu H, Wang H, et al. Reduced Paraoxonase 1 Activity as a Marker for Severe Coronary Artery Disease. Dis Markers 2013; 35(2):97-103. doi: 10.1155/2013/816189.

[2] Ungurianu A, Margina D, Gradinaru D, Bacanu C, Ilie M, Tsitismpikoungurianu C, et al. Lipoprotein redox status evaluation as a marker of cardiovascular disease risk in patients with inflammatory disease. Mol Med Rep 2017;15:256-62. doi: 10.3892/mmr.2016.5972

CANCELLED DUE TO COVID-19

ESTIMATION OF MICROBUBBLE SURVIVAL TIME FOR SONOPORATION TEMPORAL DOSIMETRY BY SIGNAL PROCESSING

Kumar Anubhav Tiwari[1,3], Martynas Maciulevicius[2], Renaldas Raisutis[1], Sonam Chopra[2], Diana Navickaite[2], Saulius Satkauskas[2]

[1]Ultrasound Research Institute, Kaunas University of Technology, Lithuania
[2]Biophysical Research Group, Faculty of Natural Sciences, Vytautas Magnus University, Lithuania
[3]Department of Multimedia Engineering, Kaunas University of Technology, Lithuania
k.tiwari@ktu.lt

CANCELLED DUE TO COVID-19

The microbubbles (MBs) are ultrasound (US) contrast agents, which are used to improve the visibility in diagnosis by contrast imaging techniques. Moreover, in the therapeutic applications of sonoporation, it causes a significant reduction of acoustic cavitation threshold. In the cell sonoporation phenomenon, the microbubble (MB) cavitation results due to the interaction of MBs with US. At low acoustic pressure, MB stable cavity (MB-SC) exists and MB acts as a linear system exhibiting linear and periodic oscillations in response to the ultrasonic excitation. In this state, scattered US is generated comprising the harmonic, subharmonic and ultra harmonic spectral contents of the fundamental frequency [1]. However, at higher acoustic pressures, the MBs oscillate and continuously grow in size until the drastically implosion. In this transitional state, the cavitation is called as MB inertial cavitation (MB-IC). This phenomenon leads to introduce the broadband noise in the scattered spectrum, which can be used for the quantification of MB-IC extent. The explosion of MB exhibits various physical effects such as sudden temperature increase, microjets, shock waves, etc. In order to form sonoporation an effective and controllable drug delivery system in the temporal and spatial domain, one of the prime necessities is the development of an adequate and precise MB-IC dosimetry system [2, 3].

The objective of this work is to apply the signal processing approach for the estimation of optimal value of MB exposure time in order to achieve the maximum sonoporation efficiency with high cell viability. During the experiment, sonoporation cuvette of 1 cm path-length is used. It was filled either by 1 ml of MB suspension (+MB) or 1 ml of the phosphate-buffered saline-background group (MB-). The US waves were excited by an ultrasonic transducer having center frequency of 1 MHz and bandwidth up to 1.2 MHz (– 6 dB). The other parameters were: pulse repetition frequency of 1 kHz, 10 % duty cycle, 100 to 700 kPa peak-negative-pressure (PNP) and overall exposure duration of 6 s. The receiving transducer to detect the scattered US signals was positioned 90º to the transmitter.

Firstly, the denoising of received US signals was performed by applying the discrete wavelet transform (DWT) with the Daubechies mother wavelet [4]. Later on, the time-frequency analysis of amplitudes of magnitude spectrums in each case (with or without MBs) at different pressures (100-700 kPa) was performed for better visualization. In order, to estimate the optimal frequency, the differential root-mean-square (RMS) amplitudes (the difference between the RMS amplitudes obtained with MBs and without MBs) and differential inertial cavitation dose (ICD) are compared for different frequency ranges from 1.5-1.8 up to 9.5-9.8 MHz. After selecting the optimal frequency range (1.5-1.8 MHz in this case), the MB survival time and rate of MB survival time were estimated at different pressure conditions, which are the proposed metrics for the optimal MB exposure duration and cavitation control respectively.

[1] Gong, Y., Zhang, D., & Gong, X. (2005). Subharmonic and ultraharmonic emissions based on the nonlinear oscillation of encapsulated microbubbles in ultrasound contrast agents. *Chinese Science Bulletin, 50*(18), 1975-1978.
[2] Chen, X., Wu, W., Wang, S., Zhong, J., Djama, N. M., Wei, G., et al. (2019). Magnetic targeting improves the therapeutic efficacy of microbubble-mediated obstructive thrombus sonothrombolysis. *Thrombosis and haemostasis, 119*(11), 1752-1766.
[3] Maciulevicius, M., Tamosiunas, M., Jakstys, B., Jurkonis, R., Venslauskas, M. S., & Satkauskas, S. (2016). Investigation of microbubble cavitation-induced calcein release from cells in vitro. *Ultrasound in medicine & biology, 42*(12), 2990-3000.
[4] Tiwari, K. A., & Raisutis, R. (2018). Identification and characterization of defects in glass fiber reinforced plastic by refining the guided lamb waves. *Materials, 11*(7), 1173.

THE EFFECT OF COMBINED ACTION OF DOXORUBICIN AND COMPLEXES BASED ON PHOSPHORUS DENDRIMERS AND PROAPOPTOTIC siRNA

Victoriya Zhogla[1, 2], Viktar Abashkin[1], Volha Dzmitruk[1], Jean Pierre Majoral[3], Dzmitry Shcharbin[1]

[1]Institute of Biophysics and Cell Engineering of NASB, Minsk, Belarus,
[2]Department of Biophysics, Belarusian State University, Belarus
[3]Laboratoire de Chimie de Coordinations du CNRS, Toulouse, France
vika.physics@yandex.ru

Chemotherapeutic agents have the nonspecific toxicity and can affect healthy cells that leads to various side effects in the cancer treatment. Also, drug resistance in malignant tumors often complicates the treatment. Proapoptotic anticancer small interfering RNAs (siRNAs) can reduce the effective dose of drugs and can decrease the side effects. For efficient delivery siRNAs into cells the different carriers are used including nanocarriers such as nanoparticles, quantum dots, liposomes, dendrimers. Dendrimers, which are spherical hyperbranched polymers, proved themselves as effective carriers for DNA and siRNA delivery.

The aim of this work was to study the efficiency of combined use both dendriplexes (complexes of dendrimers and siRNAs) and doxorubicin – anthracycline antibiotic that used to treat many types of cancer, including acute lymphoblastic leukemia, cervical cancer, etc. Studies were performed using three cell lines: HT29, HeLa and HL-60.

To study the internalization of dendriplexes, the non-targeting FITC-labeled siRNAs were used. SiRNAs were complexed with third generation cationic phosphorus dendrimers and incubated with studied cell lines for 3 hours. Level of internalization was measured by flow cytometry (CytoFLEX, Beckman Coulter). The cellular uptake of complexes was 70% for HT29 cell line, 83% for HeLa and– 98% for HL-60.

For detection of the cytotoxicity of dendriplexes and doxorubicin the cell viability tests were used. Concentrations of doxorubicin were 0.1, 1 and 10 μM for HL-60, HeLa and HT29 respectively. Dendrimers were complexed with siRNAs siBCL-xL (HL-60, HT29) and siMCL-1 (HeLa), which silences genes of corresponding antiapoptotic proteins BCL-xL and MCL-1. The dendrimer/siRNA charge ratio was 10:1. Cells were treated with complexes and doxorubicin for 24 hours. After incubation, cell viability was measured by Alamar Blue assay for suspension cells (HL-60) or MTT-test for adherent cells (HeLa, HT29). As a result of the combined action of doxorubicin and dendriplexes cell death was 80% for HL-60 and HeLa (Fig. 1). This effect is higher with a statistically significant difference than the sum of the effects of the components *per se*, which means the presence of a synergistic effect. For HT29, no significant difference was observed and the effect of combined action is additive.

This work was partially supported by the Belarusian Republican Foundation for Fundamental Research and State Committee of Science and Technology of Belarus, grants number B18TYUB-001, B19ARMG-002.

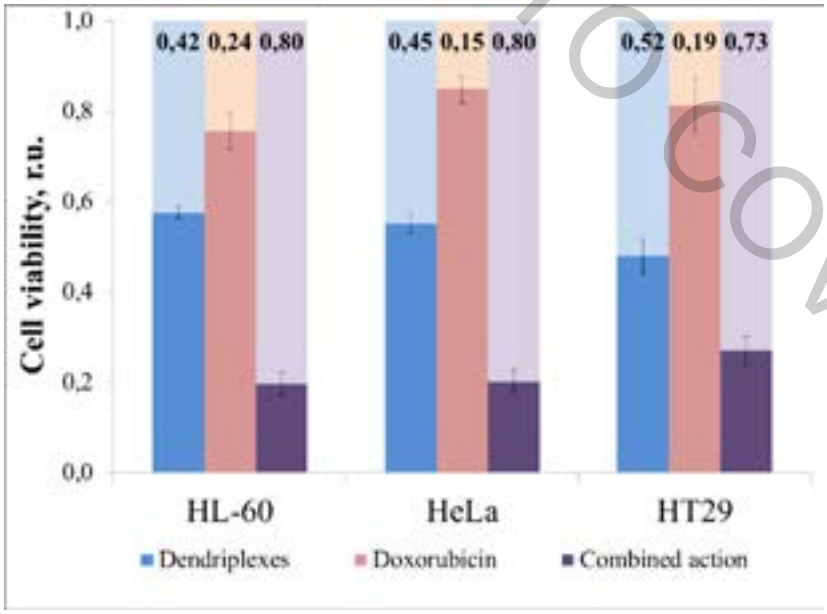

Fig. 1. Viability of HL-60, HeLa and HT29 cells after 24h exposure by doxorubicin, dendriplexes and the combination of both.

CARCINOGENESIS TO COVID-19

DPP4/CD26 AS A MEDIATOR OF CHEMORESISTANCE AND EPITHELIAL-MESENCHYMAL TRANSITION IN HUMAN COLON CANCER CELLS

Jan Černuševič[1], Nadežda Dreižė[1], Algirdas Kaupinis[1], Silvija Urnikytė[1], Mindaugas Valius[1]

[1] Proteomics Center, Institute of Biochemistry, Vilnius University Life Sciences Center, Vilnius, Lithuania
jan.cernusevic@gmail.com

Dipeptidyl peptidase 4 or Cluster of differentiation 26 (DPP4/CD26) is a multifunctional type II transmembrane glycoprotein, which regulates various biological processes *in vivo* and *in vitro* by cleaving N-terminal dipeptides with its extracellular domain [1]. Moreover, it can act as a receptor, transducing T cell costimulatory activation signal during interaction with different membrane proteins like ADA, CAV1, IGF2R, and PTPRC [2]. Also, DPP4/CD26 was shown to interact with extracellular matrix (ECM) proteins such as fibronectin and collagen, thus playing role in cellular processes as adhesion, migration and metastasis [3].

DPP4/CD26 has been intensively investigated as a potentional biomarker of various cancers and its impact on cancer malignancy and chemoresistance as well as a novel therapeutic target for different cancers during past decades. It can act as a tumor suppressor or activator depending on tumor type and some other conditions [3] [4]. It has been reported that subpopulation of $DPP4^+/CD26^+$ colon cancer cells showed elevated levels of epithelial–mesenchymal transition (EMT) protein markers in comparison with $DPP4^-/CD26^-$ subpopulation. DPP4/CD26 knock down in $DPP4^+/CD26^+$ subpopulation cells resulted in downregulation of EMT protein markers and upregulation of E-cadherin [5]. Also, DPP4/CD26 knock down was shown to downregulate some EMT markers in NLCSC cell lines *in vitro* [6]. In addition, vildagliptin, DPP4/CD26 enzymatic activity inhibitor, which is used to treat type 2 *diabetes mellitus* in clinical practice, contributed to elevated E-cadherin expression levels in MC38 cell line *in vitro* and suppressed colorectal lung metastases formation *in vivo* in mouse model [7]. However, in human breast cancer cell lines MCF 10A, MCF-7 and MDA-MB-231 DPP4/CD26 acts as an EMT negative regulator [8]. Moreover, this protein was proposed as a cancer stem cells marker, especially for colorectal cancer [5].

Colorectal cancer is the third in men and the second in women most common cancer worldwide, with nearly 1,8 million new cases diagnosed in 2018. Common therapy includes FOLFOX protocol, which consists of oxaliplatin (L-OHP) and 5-fluoruracil (5-FU) combination. However, colon tumor cells undergo fast adaptation and become resistant to anticancer agents. In addition, drug-resistant colorectal cell lines can demonstrate cancer stem cells-like properties, including DPP4/CD26 elevated expression [9]. However, it has not been investigated whether elevated DPP4/CD26 expression levels alone could cause development of chemoresistance or alter EMT status of colorectal cancer cells *in vitro*.

In this research, our proteomic analysis data showed, that colorectal cancer cell line HCT116, resistant to L-OHP (HCT-Oxa), exibited elevated DPP4/CD26 protein levels in comparison to parental HCT116 cell line (HCT-P), while HCT116 cell line, resistant to 5-FU (HCT-Fu), demonstrated comparable to HCT-P cell line DPP4/CD26 levels. Results were confirmed by western blot. Therefore, we checked if vildagliptin could alter resistance to L-OHP and 5-FU in HCT-P, HCT-Oxa and HCT-Fu cell lines. Also, vildagliptin influence on EMT status in these cell lines was investigated. After that, *DPP4* gene was amplified by polymerase chain reaction (PCR), using HCT-P cell line copy DNA (cDNA), cloned into pJET vector and sequenced. Consequently, *DPP4* sequence was transferred to pcDNA3 vector and this construct was used to investigate if transiently overexpressed DPP4/CD26 alters resistance to anticancer drugs in HCT-P and HCT-Oxa cell lines. Our next step was to clone *DPP4* sequence in all-in-one TET ON system lentiviral vector. Stable HCT-P and HCT-Oxa cell lines with an option of inducible DPP4/CD26 expression (HCT-P iDPP4, HCT-Oxa iDPP4) were created. Titration of DPP4/CD26 expression levels depending on doxycycline concentrations in these cell lines was completed. Finally, we investigated influence of maximum DPP4/CD26 expression level on chemoresistance and EMT status in HCT-P iDPP4 cell line.

[1] Pamela, A. H. The role of CD26/dipeptidyl peptidase IV in cancer. *Frontiers in Bioscience*, 13(13), 1634 (2008).
[2] Wagner, L., Klemann, C., Stephan et al. Unravelling the immunological roles of dipeptidyl peptidase 4 (DPP4) activity and/or structure homologue (DASH) proteins. *Clinical & Experimental Immunology,* 184(3), 265–283 (2016).
[3] Beckenkamp, A., Davies, S., Willig et al. DPPIV/CD26: a tumor suppressor or a marker of malignancy? *Tumor Biology*, 37(6), 7059–7073 (2016).
[4] Enz, N., Vliegen, G., Meester et al. CD26/DPP4 - a potential biomarker and target for cancer therapy. *Pharmacology & Therapeutics*, 198, 135–159 (2019).
[5] Pang, R., Law, W. L., Chu et al. A Subpopulation of CD26 Cancer Stem Cells with Metastatic Capacity in Human Colorectal Cancer. *Cell Stem Cell*, 6(6), 603–615 (2010).
[6] Chang, J.-H., Cheng, C.-W., Yang et al. Downregulating CD26/DPPIV by apigenin modulates the interplay between Akt and Snail/Slug signaling to restrain metastasis of lung cancer with multiple EGFR statuses. *Journal of Experimental & Clinical Cancer Research*, 37(1) (2018).
[7] Jang, J.-H., Baerts, L., Waumans et al. Suppression of lung metastases by the CD26/DPP4 inhibitor Vildagliptin in mice. *Clinical & Experimental Metastasis*, 32(7), 677–687 (2015).
[8] Yang, F., Takagaki, Y., Yoshitomi et al. Inhibition of Dipeptidyl Peptidase-4 Accelerates Epithelial–Mesenchymal Transition and Breast Cancer Metastasis via the CXCL12/CXCR4/mTOR Axis. *Cancer Research*, 79(4), 735–746 (2018).
[9] Khoury, F. E., Corcos, L., Durand et al. Acquisition of anticancer drug resistance is partially associated with cancer stemness in human colon cancer cells. *International Journal of Oncology*, 49(6), 2558–2568 (2016).

CANCELLED DUE TO COVID-19

FAMILIAL X-LINKED INTELLECTUAL DISABILITY CAUSAL MUTATION IDENTIFICATION USING WHOLE EXOME SEQUENCING

Austėja Dapkutė[1], Egle Preikšaitienė[2]

[1] Faculty of Medicine, Vilnius University, Lithuania
[2] Department of Human and Medical Genetics, Institute of Biomedicine sciences, Faculty of Medicine, Vilnius University, Lithuania
austeja.dapkute@mf.stud.vu.lt

The relatively high prevalence of an intellectual disability and its variability induce active research of the etiology of this disorder. Upon the observation that it occurs with 20 % higher frequency in males than females [1] extensive studies of X chromosome-linked disorders affecting intelligence are held. 145 genes in X chromosome are currently known to be linked with intellectual disability and it comprises 17,12% of all coding sequences in X chromosome, in comparison with 5,43% on average in autosomes. [2]

We were presented with two male brothers (patient A, a 12-year-old boy and patient B, an 8-year-old boy). Both patients were cognitively and motorically delayed. Patient A was unable to construct sentences and started to walk at the age of 4,5, in addition, he experienced stereotypical arm movements. Patient B at the age of 8 was evaluated to produce speech, typical for 15-16-month-old children, he started to walk at the age of 4 and presents grimacing smiling. Both patients experience seizures and intellectual disability of an unknown cause. Based on the genealogical analysis, we predicted that the inheritance pattern of the mutation is X-linked because of the mild presentation in mother (reported seizures in childhood and marginal intelligence) and unconfirmed family history of mother's brother having seizures, developmental delay and death at the age of 9. Our aim was to analyze whole exome sequencing (WES) data of two sibs and their parents using *in silico* methods in order to find potential intellectual disability causing genes and to create a further investigation plan for confirmation of the causal pathogenic variant.

Samples for WES were taken from both sibs and their parents. In total, 3974 pathogenic variants were automatically annotated and filtered according to their frequency in the population (MAF<2%). Therefore, 6 pathogenic variants in X chromosome common for both sibs, and the mother but not found in the genome of the healthy father, were used for further investigation. They were analyzed using Sift, PolyPhen, Mutation Taster (MutT) and Human Splicing Finder (HSF) software. For further description, ExAC, 1000G and HGMD databases were used. According to the analysis, it was concluded that two genes, ARHGEF6 and SLC9A6, are associated with intellectual disability. ARHGEF6 mutation appeared to be a variant of unknown significance and it is usually associated with non-syndromic intellectual disability. Another candidate gene, SLC9A6, mutation was likely to be a pathogenic splice donor variant. This gene is associated with Christianson syndrome, which frequency in the population is <1/1 000 000. Clinical presentation of this syndrome involves intellectual disability, seizures, absent speech and stereotypical movements [3] which strongly fits the clinical presentation of our patients. Furthermore, SLC9A6 pathogenic variant carriers are often presented with milder symptoms. [4]

Our investigated SLC9A6 pathogenic variant was not previously described in literature. Therefore, it was decided to model this mutation and analyze its theoretical significance. Fig. 1 depicts 3D models of a Na/H antiporter 6, an SLC9A6 gene product, with and without the mutation. Both models were created using Phyre 2 software.

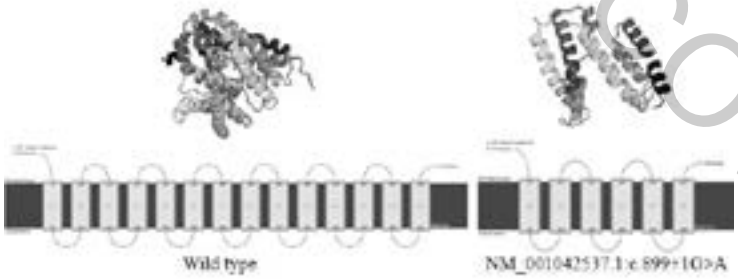

Fig. 1. 3D models of a wild type and mutated SLC9A6 products

It was concluded that the identified SLC9A6 pathogenic variant is fitting our patients' clinical presentation and is altering the gene product significantly and sufficiently to induce symptoms. For the confirmation of this mutation causing altered splicing, it is planned to perform *in vitro* analysis of the SLC9A6 mRNA/cDNA.

[1] Knight SJL. Genetics of mental retardation: an overview encompassing learning disability and intellectual disability. Karger Medical and Scientific Publishers; 2010.
[2] Dapkute A, Preiksaitiene E. Su X chromosoma susijusi intelektinė negalia: Literatūros apžvalga. Laboratorinė Medicina 2017, 19(4), 255-262.
[3] Morrow, E. M., & Pescosolido, M. F. (2018). Christianson syndrome. In GeneReviews®[Internet]. University of Washington, Seattle.
[4] Sinajon, P., Verbaan, D., & So, J. (2016). The expanding phenotypic spectrum of female SLC9A6 mutation carriers: a case series and review of the literature. Human genetics, 135(8), 841-850.

COVID-19

GENE EXPRESSION STUDIES IN ENDOMETRIAL-DERIVED STROMAL CELLS

Giedrė Skliutė, Raminta Baušytė, Aida Vitkevičienė, Rūta Navakauskienė

Department of Molecular Cell Biology, Institute of Biochemistry, Life Sciences Center, Vilnius University, Lithuania
giedre.skliute@gmc.stud.vu.lt

Infertility is a disease of the reproductive system defined by the failure to achieve a pregnancy after 12 months or more of regular unprotected sexual intercourse [1]. According to statistics, 10 - 15 % of couples in the world face this problem, of which 20 % are diagnosed with unexplained infertility. Unexplained infertility is a condition in which no reproductive system pathology is detected, but pregnancy still fails. The main treatments include intrauterine insemination with ovarian hyperstimulation and *in vitro* fertilization. The effectiveness of the procedures is 18 % and 40 % respectively [2]. Therefore, there is a demand for new diagnostic and therapeutic methods. Studies show that endometrial dysfunction can lead to failed implantation and early pregnancy loss making endometrial cellular changes an attractive target for studies of unexplained infertility [3].

In the present study, we aimed to investigate the expression of pluripotency markers (*OCT4, SOX2, NANOG, NOTCH1, LIN28*), genes related to aging and epigenetic regulation (*CCNA2, HMGA2, TOP2A, TERF1, HDAC1, DNMT1, DNMT3A, DNMT3B*) and proliferation and regeneration related genes (*PDGFB, PDGFRB, P53, VIMENTIN, VEGFR2, E-CADHERIN*) *ex vivo* in cells of patients who conceived or did not conceive after *in vitro* fertilization procedures. Gene expression changes were evaluated by using RT-qPCR. Our study revealed that expression of pluripotency markers during cell cultivation increased in cells of patients who conceived, while decreased or remained unchanged in cells of patients who did not conceive. Expression of aging-related genes changed only in cells of patients who did not conceive, whilst expression of epigenetic regulation related genes changed in both cells of patients who conceived and patients who did not. Expression of proliferation and regeneration related genes showed similar changes in cells of patients who conceived and who did not conceive (Fig. 1).

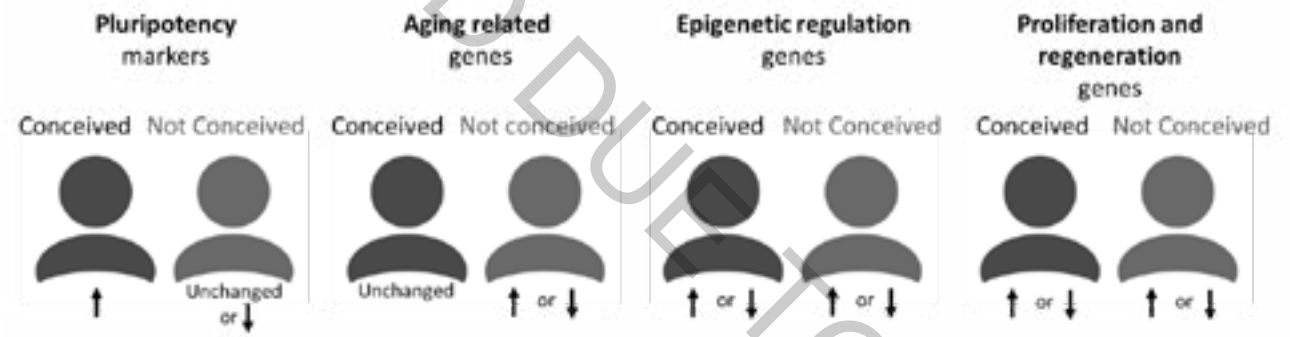

Fig. 1. Relative gene expression changes in after *in vitro* fertilization conceived and not conceived patient endometrial-derived stromal cells *ex vivo*

Consequently, we suggest that the differences in pluripotency markers' gene expression could be important for diagnostics of unexplained infertility.

CANCELLED DUE TO COVID-19

[1] World Health Organization (2019). Infertility definitions and terminology. (2016, October 21). Retrieved from https://www.who.int/reproductivehealth/topics/infertility/definitions/en/.
[2] A. Quaas and A. Dokras, Diagnosis and Treatment of Unexplained Infertility, Reviews in Obstetrics and Gynecology **1** (2), 69–76 (2008).
[3] S. Morelli, P. Yi, L.T. Goldsmith, Endometrial Stem Cells and Repoduction, Obstetrics and Gynecology International **2012**, 851367, (2012).

THE EFFECT OF PRISTINE C_{60} FULLERENE ON COLONIC MOTILITY IN RATS WITH 6-OHDA–INDUCED PARKINSON'S DISEASE

Yelyzaveta Makedon[1], Viktoriia Stetska[1], Taisa Dovbynchuk[1], Nataliia Dziubenko[1], Yuriy Prylutskyy[1], Ganna Tolstanova[1,2]

[1]ESC "Institute of Biology and Medicine" Taras Shevchenko National University of Kyiv,
[2] Institute of High Technologies Taras Shevchenko National University of Kyiv,
64/13, Volodymyrska Street, Kyiv, 01601, Ukraine
elisavetamadon@gmail.com

CANCELLED DUE TO COVID-19

Diagnosis of Parkinson's disease (PD) are preceded 20 years or more by numerous non-motor symptoms (prodromal phase), such as delayed motility of gastrointestinal tract (constipation) [1]. The pathogenic process that causes PD is presumed to be underway during the prodromal phase, involving regions of the peripheral and central nervous system in addition to the dopaminergic neurons of the SN. Oxidative stress is thought to be one of the mechanisms of PD pathogenesis [2]. In present study we tested the hypothesis that treatment with C_{60}FAS, which has antioxidant properties, can improve colon motility in rats with 6-OHDA–PD.

The unilateral dopamine deficiency was induced in male Wistar rats (220-250 g) by stereotaxic (AP = -2,2; ML = -1,5; DV = 8,8) microinjections of selective neurotoxin 6-hydroxydopamine (6-OHDA, 12 μg). The control group was injected 2 μl 0,9 % NaCl. The C_{60}FAS was given daily for 2-11 days i.p. at doze 75 mg/kg. The percentage of destroyed dopaminergic neurons was evaluated by IHC staining of tyrosine hydroxylase (TH)-positive neurons in midbrain. Levels of spontaneous and carbachol-stimulated colon motility was estimated by ballonographic method *in vivo.*

6-OHDA rats treated by C_{60}FAS showed positive tendency to increase the number of tyrosine hydroxylase (TH)-positive cells in midbrain and increased by 7% the body weight *vs.* placebo-treated animals. We found profoundly decreased carbachol-stimulated colon motility in rats with 6-OHDA-PD *vs.* the sham-lesioned animals. C_{60}FAS improved increased in 2-fold the index of stimulated colon motility, tonic and phase index *vs.* sham-lesioned rats.

These findings suggest that C_{60}FAS might be promising experimental basis for the treatment of the early non-motor symptoms of PD.

---

[1] L. V. Kalia, A. E. Lang, Parkinson's disease, The Lancet, 386(9996), 896–912 (2015).
[2] J. Guo, X. Zhao, Y.Li et al., Damage to dopaminergic neurons by oxidative stress in Parkinson's disease (Review), International Journal of Molecular Medicine 41, 1817-1825 (2018).

CASE REPORT OF UKRAINIAN SMA FAMILY WITH RARE 5Q13 LOCUS REARRANGEMENTS

Alona Yurchenko[1], Erika Patskun[2], Nataliya Hryshchenko[3]

[1]Kiev National University, Educational and Scientific Center "Institute of Biology and Medicine", Kyiv, Ukraine
[2]Municipal Non-profit Enterprise "Transkarpathian Clinical Regional Hospital named after A.Novak", Uzhgorod, Ukraine
[3] Institute of Molecular Biology and Genetics National Academy of Sciences of Ukraine, Kyiv, Ukraine
alenaurchenko001@gmail.com

CANCELLED DUE TO COVID-19

Spinal muscular atrophy (SMA) is an autosomal recessive genetic disorder which is characterized by the degeneration of alpha motor neurons and progressive peripheral muscle weakness. The great majority of SMA patients have homozygous deletion in *SMN1* gene of 5q13 locus and the SMA carriers have the heterozygous deletion with typical "1+0" *SMN1* genotype. The highly homologous *SMN2* gene is located in the same locus, and SMA patients have 1 to 6 copies of this gene. *SMN2* would partially compensate a deficiency of the SMN protein in SMA patients. An increased *SMN2* copies result in an increased amount of the protein and lead to milder SMA phenotype [1].

A routine screening for SMA carriers is performed using quantitative PCR (qPCR) or Multiplex Ligation-Dependent Probe Amplification technology. These methods cannot determine the silent SMA carriers, who have *SMN1* duplication (2 copies) in 5q13 locus and *SMN1* deletion on the homological chromosome ("2+0" *SMN1* genotype). In some populations *SMN1* duplication is associated with rare haplotype of intragenic *SMN1* polymorphisms (g.27134G and g.27706_27707delAT) due to "founder" effect [2]. Analysis of these markers in a combination with dosage-sensitive methods would be used to determine "2+0" silent carriers improving the overall SMA carrier detection rate. However, the frequency of the "founder" *SMN1* haplotype is different in the populations, leading to different informativeness of the "2+0" haplotype determination [3].

A 10-year-old SMA patient (proband) from a large Transcarpathian unrelated family has homozygous *SMN1* deletion, but his phenotype is atypically mild as compared with other SMA patients with same *SMN1* mutation: he had proximal lower limb amyotrophy but saved the ability to walk independently. One of his elder sisters had proximal lower limb weakness (has never been examined) but other relatives had no specific SMA phenotypic symptoms. The molecular testing showed that proband's mother had heterozygous deletion in *SMN1* representing a typical *SMN1* genotype ("1+0"). The father had two *SMN1* copies which required further clarification.

The aim of our study was to determine an origin of the patient's paternal 5q13 rearrangement. We performed the qPCR of *SMN1* and *SMN2* genes as well as a segregation analysis of 5q13 region polymorphic markers LAS96 and 2AE9.1 in all available family members. The results are presented in the table 1.

Family member	*SMN1* copies / genotypes	*SMN2* copies/ genotypes	2AE9.1 alleles	LAS96 alleles	SMA status
proband	**0 / 0+0**	**4 / 2+2**	**2-2**	**6-6**	**SMA**
mother	1 / 1+0	3 / 1+2	2-4	3-6	SMA carrier
father	2 / 2+0	2 / 0+2	2-4	6-6	SMA carrier
sibs 1	3 / 1+2	1 / 1+0	4-4	3-6	Non carrier
sibs 2	**0 / 0+0**	**4 / 2+2**	**2-2**	**6-6**	**SMA**
sibs 3	3 / 1+2	1 / 1+0	4-4	3-6	Non carrier
sibs 4	1 / 1+0	3 / 1+2	2-4	3-6	SMA carrier
sibs 5	1 / 1+0	3 / 1+2	2-4	3-6	SMA carrier

Table 1. 5q13 rearrangement study in the family members

It would be noted that proband`s sibs 2 (13 years old female without specific SMA sings) had the same *SMN1* homozygous deletion. According to obtained result, it was found that the father is the carrier of rare *SMN1* ("2+0"). The chromosome with *SMN1* duplication inherited within the family (father, sibs 1 and sibs 3) hadn't g.27134G allele indicating the origin of the rearrangement is not due to mentioned above "founder" effect. The proband`s parents have *SMN2* heterozygous duplication (mother: "2 + 1", father: "2 + 0"). Consequently, the proband and sibs 2 inherited *SMN2* duplication from both of parents and have 4 *SMN2* copies.

We can conclude that two children inherited the *SMN1* deletion from both the parents; but the father is a silent carrier of a rare *SMN1* genotype. The proband and sibs 2 inherited from the parents 4 *SMN2* copies, that could explain their mild SMA phenotypes. The parental *SMN1* duplication has a recurrent origin possibly due to *de novo* mutation.

[1] S.Ogino, R. B. Wilson, Spinal muscular atrophy: molecular genetics and diagnostics, Expert Review of Molecular Diagnostics **4(1)**, 15-29 (2004).
[2] L. Edelmann, R. J. Desnick, Materials and method for identifying spinal muscular atrophy carriers (International application published under the patent cooperation treaty, 2012).
[3] L. Alías, S. Bernal, M. Caluchoet et al., Utility of two *SMN1* variants to improve spinal muscular atrophy carrier diagnosis and genetic counselling, Eur J Hum Genet **26(10)**, 1554-1557 (2018).

DYNAMICS OF NATURAL SELECTION IN THE URBANIZED UKRAINIAN POPULATION

Nataliya Kozak[1,2], Lubov Atramentova[1]

[1] Department of genetic and cytology, V. N. Karazin Kharkiv National University, Ukraine
[2] Department of medical biology, Kharkiv National Medical University, Ukraine
kozaknatali93@gmail.com

Selection is the most important driving power of evolution and it occurs in all types of living organisms, and human is not an exception. In the context of genetics, selection is the differential reproduction of genotypes. It occurs at different stages of the development of the human body: at the prenatal stage it happens in the form of spontaneous abortions and ectopic pregnancies; in postnatal is in the form of infant mortality. Reproduction of genotypes is associated with the reproductive behavior of women, which depends on many factors such as age, education, cultural level, traditions, etc. The structure of indicator of total selection is changing with the development of civilization, increasing in the standards of living and the success of medicine [1]. The main tendency of these changes is moving selection to the prenatal stage of development and it is manifested in increasing of the frequency of spontaneous abortions, which are caused by genetic defects of the fetus or inability of a female body for childbearing. The practice of family size planning eliminates differences in the number of offspring in women with different reproductive potentials [2, 3].

The intensity and direction of the selection is described quantitatively by indicators called Crow's indexes. The total selection rate (I_{tot}) includes two components: the differential mortality rate (I_m) and the differential fertility rate (I_f). The structure of the total index (specific weight of each component) is not the same in different populations and depends on the level of civilizational development of the community and is changing during the historical development of society [4]. Therefore, the purpose of this study was to investigate how these processes take place in Ukraine, where 70% of the population lives in cities. It was carried out on the example of Kharkiv city. The task was to assess the intensity of selection in the dynamics of three successive generations.

The information of the obstetric-gynecological history of the female residents of Kharkiv with completed reproduction was used. Material was collected in 1990 and 2017. Information was received from 1121 women who were divided into three generations according to the year of birth: the first generation (1900 – 1924), the second (1928 – 1955), and the third (1956 – 1979). According to the obstetric and gynecological history, the total selection index (Crow's index) was calculated.

It has been established that in the studied population from the older generation to the younger one the total selection index has been decreased. In the first generation this indicator is as twice as large (I_{tot} = 0.56) than in the second (I_{tot} = 0.29) and third (I_{tot} = 0.28) generations. In countries with low infant mortality the proportion of the specific weight of the selection component associated with differential fertility (I_f) is higher than the component of differential mortality (I_m). In the population of Kharkiv the same orientation has been observed: for the first generation, I_m = 0.04, which is 7.2% of the total index, for the second generation, I_m = 0.02, which is 7.3% of I_{tot}, and for the third generation I_m = 0.01, which is 4.1 in percentage terms. The I_f component depends on the dispersion of the number of children and is equal to 0.52 in the first generation; 0.26 in the second and 0.27 in the third, which is approximately 93; 91 and 95% out of the total index in generations. The selection intensity slightly goes down mainly due to the decrease in the differential mortality component, which can be associated with an improvement of the quality of medicine and other social factors.

Comparison of the reproductive characteristics of residents of Kharkiv city among adjacent generations showed that their reproductive dynamics are, in general, on line with global trends, which is expressed in a decreasing of fertility due to its artificial regulation. The Kharkiv population is characterized by a narrowed type of reproduction. Natural selection is weakening due to development of civilization, success of medicine, and improvement of living conditions for a human. The selection rate (I_{tot}) is decreasing due to a reduction in differential mortality and changes in the index of differential fertility. Studying of the structure of the population and the intensity of selection processes, especially in the presence of the phenomenon of its natural relaxation, increases the relevance of predicting of dynamic of the gene pool of concrete population, and popularization of medical and genetic counseling and dissemination of methods for preventing the appearance of sick children in families predisposed to genetic pathologies.

The authors are grateful to all medical institutions and persons who contribute for collecting material.

[1] O.L. Kurbatova, Demographic genetics of urban population (abstract. dis. Sc.D. Moskow, 2014).
[2] L.A. Atramentova, I.P. Meshcheryakova, O.V. Filiptsova, Reproductive characteristics and the Crow's index in different populations of Evpatoria, Genetika 49 № 12, 1398–1406 (2013).
[3] L.A. Atramentova, L.I. Fedchun, S.A. Povolockij, Differential fertility in the Kharkov population. Genetika 29, № 3, 520–530 (1993).
[4] Ed. by Ju.P. Altuhov, *Dynamics of population gene pools under anthropogenic pressures.* (Moskow, Nauka, 2004).

CARELESS PROOF 2019

ASSOCIATION OF MYCN GENE AMPLIFICATION AND REARRANGEMENTS OF CHROMOSOMAL REGION 1p36 AND 11q WITH EFFICACY OF NEUROBLASTOMA TREATMENT

Daria Shymon[1,2], Mariia Inomistova[1,2], Oksana Skachkova[1], Oleksandr Gorbach[1], Natalia Khranovska[1]

[1]National Cancer Institute of Ukraine, Kyiv, Ukraine
[2]ESC "Institute of Biology and Medicine" of Taras Shevchenko National University, Kyiv, Ukraine
shimon1803@ukr.net

Neuroblastoma (NB) is an embryonal tumor of the sympathetic nervous system, which causes 15% of pediatric cancer deaths [1]. NB cells with *MYCN* amplification is one of the most aggressive NB subgroups that comprises 20–25% of all primary tumors and is associated with tumor progression with poor prognosis [2]. 1p36 deletion is a frequent chromosomal abnormality observed in NB cell lines and primary tumors; 11q deletion is one of the most frequent events that occurs during NB aggressive development [3].

The current project aim is to determine the frequency of *MYCN* gene amplification occurrence; also to describe the rearrangement of chromosomal region 1p36 and 11q in pediatric patients with NB; and then to investigate its association with the effectiveness of treatment.

Paraffin-embedded tumor tissues of 103 patients, from 2 months old to 16 years old (54.5 ± 42 months), with verified NB were used in the study. All samples were analyzed on *MYCN* amplification and rearrangements of chromosomal regions 1p36 and 11q. Tumor samples were obtained prior to chemotherapy treatment. *MYCN* amplification was analyzed by FISH microscopy and real-time PCR, and deletions of 1p36 and 11q chromosomal regions were determined by FISH microscopy.

In tumor tissues, 11q deletion was determined in 3.9% (4/103) of patients with NB. Deletion of the chromosomal region 1p36 was detected in 4.9 % (5/103) of NB patient tumor tissues. *MYCN* gene amplification was detected in 35% (36/103) out of patients with NB. Amplification of the *MYCN* gene was detected in 2 patients (1.9%) out of 4 with detected 11q deletion, which is the most commonly observed in female (3/4) patients, older than 2 years (2/4). A statistically significant difference between groups of patients with and without deletion of the 11q chromosome, such as sex ($\chi2 = 0.714$, $p = 0.399$), age ($\chi2 = 0.121$, $p = 0.94$), and *MYCN* gene status ($\chi2 = 0.42$, $g = 0.52$), was not observed. Amplification of the *MYCN* gene was detected in all patients with 1p36 deletion. The 1p36 deletion was most commonly detected in female (3/5) patients older than 2 years (3/5). The difference between the presence / absence of 1p36 deletion and *MYCN* gene status was statistically significant ($\chi2 = 9.8$, $p = 0.002$). According to the Kaplan-Meier method, the deletion of 11 chromosome`s long arm didn't affect the duration of recurrent period, $p = 0.07$. Similarly, the *MYCN* gene amplification didnt't affect the duration of progression free period, $p = 0.6$. However, the deletion of the 1p36 chromosome significantly reduced the duration of relapse-free period in children with NB ($p = 0.002$). NB patient's with 1p36 deletion 6-month disease-free survival was 60 ± 2%, but throughout the one year all patients with 1p36 deletion had local recurrences and / or distant metastases. Among the patients without 1p36 deletion the 6-month progression free survival rate was 90.6 ± 4% and the one-year progression free survival was 87 ± 5%.

We established that only 1p36 deletion was decreased significantly progression free survival rate in patients with NB and all patients with 1p36 deletion had local recurrences and/or distant metastases in one year period.

[1] J. A. Tomolonis, S. Agarwal, and J. M. Shohet, Neuroblastoma pathogenesis: deregulation of embryonic neural crest development, Cell Tissue Res., 372(2), 245–262 (2018).
[2] D. Bogen, C. Brunner, D. Walder et al., The genetic tumor background is an important determinant for heterogeneous *MYCN*-amplified neuroblastoma, Int J Cancer, 139(1), 153–163(2016).
[3] V. Mlakar, S. Jurkovic Mlakar, G. Lopez et al., 11q deletion in neuroblastoma: a review of biological and clinical implications(Mol Cancer, 16:114 (2017).

CPHCR-EUSPRI-COVID-19

ANALYSIS OF THUJA (THUJA SPP.) BIOLOGICAL ACTIVITY

Marius Bytautas, Audrius Sigitas Maruška, Kristina Bimbiraitė-Survilienė

Faculty of Natural Sciences, Vytautas Magnus University, Lithuania
marius.bytautas@stud.vdu.lt

The object of interest for this research were leaves and bark of Thuja standishii (Gord.) Carr., Thuja occidentalis L. and Thuja occidentalis 'Aurescens'. The aim was to measure the quantities of flavonoids and phenolic compounds, the radical scavenging activities, compare the results to find out which parts of the plant and which species produce the most of the compounds,evaluate the effects of storage, allelopathic properties, antifungal and antibacterial activities.

The quantities of the compounds were measured using spectrophotometric methods [1]. The quantities of flavonoids in leaves varied from 1.02 % to 2.36 %, of phenolic compounds in bark from 4.51 % to 8.97 % fraction mass and radical scavenging activity was determined to be from 0.81 % to 1.23 % rutin equivalents in leaves.

Leaves turned out to be the richest part in flavanoids and bark in phenolic compounds. T.occidentalis 'Aurescens' had the largest quantities of both of the desired compounds. Radical scavenging activity was highest in the bark of T. occidentalis.

The results of other analysis will be presented during the conference.

---

[1] V. Kaškonienė, G. Ruočkuvienė, P. Kaškonas, I. Akuneca, A. Maruška. 2015, Chemometric analysis of bee pollen based on volatile and phenolic compound compositions and antioxidant properties, Food Analytical Methods, 8(5), 1150-1163.

CANCELLED DUE TO COVID-19

ELECTROCHEMICAL CHARACTERISATION OF MIXED SILANE BASED SELF-ASSEMBLED MONOLAYERS FOR PHOSPHOLIPID MEMBRANE BILAYER FORMATION

Inga Gabriunaite[1], Aušra Valiūnienė[1]

[1] Department of Physical Chemistry, Faculty of Chemistry and Geosciences, Vilnius University
inga.gabriunaite@chf.vu.lt

Biological lipid membrane mimicking systems are convenient subject for investigating interactions between enzymes, toxins, other proteins and biological membranes. Such systems were designed as membranes on solid supports. They are physically stable enough and they could be investigated using different surface sensitive methods, such as various electrochemical methods, surface plasmon resonance or atomic force microscopy.

So far, such system was designed on gold substrate with alkanethiol self-assembled monolayers (SAM) and widely investigated [1]. Even though such system shows great properties but it has some flaws. Gold is expensive material and to fabricate thin films one needs expensive devices. Additionally, atoms on the Au surface are mobile, so Au–SH bond is mobile across the substrate. After being in a contact with aqueous solution, SAM reassembles into islands and it is no longer uniform. This leads to a system which could be used only one time [2].

In this study, inexpensive and commercially available fluorine doped tin oxide was functionalized with octadecyltrichlorosilane (OTS), methyltrichlorosilane (MTS) and vinyltrimethoxysilane (VTS) self-assembled monolayer (SAM). OTS-MTS and OTS-VTS were mixed at different molar ratios to produce anchoring SAM for phospholipid membrane formation via vesicle fusion method. Vesicle solution contained 60 mol% 1,2-dioleoyl-sn-glycero-3-phosphocholine (DOPC) and 40 mol% cholesterol (Chol) while total lipid concentration was 1.5 mM.

To investigate SAM and membrane, contact angle (CA), cyclic voltammetry (CV) and electrochemical impedance spectroscopy (EIS) methods were used. From recorded EI spectra presented in Cole – Cole and Bode plot it is possible to make assumptions about surface coverage with SAM, calculate number of defects [3]. After analyzing CA, CV and EIS results, SAM and bilayer formation was attested. Obtained results were comparable with developed system of Au/SH [4]. Three different proteins were able to penetrate formed phospholipid membrane system and confirm the biological activity.

To conclude, biologically relevant membrane was formed on OTS-VTS and OTS-MTS monolayers. In near future, such systems could be successfully applied for protein investigation, such as toxin detection or analyzing electron transfer proteins.

CANCELLED DUE TO COVID-19

[1] T. Ragaliauskas, M. Mickevicius, B. Rakovska et al. Fast formation of low-defect-density tethered bilayers by fusion of multilamellar vesicles, Biochimica et Biophysica Acta (BBA) – Biomembranes **1859,** 669-679 (2017).

[2] B. Rakovska, T. Ragaliauskas, M. Mickevicius et al. Structure and Function of the Membrane Anchoring Self-Assembled Monolayers, Langmuir **31**, 846-857 (2015).

[3] G. Valincius, T. Meškauskas, F. Ivanauskas, Electrochemical Impedance Spectroscopy of Tethered Bilayer Membranes, Langmuir **28**, 977-990 (2012).

[4] V. I. Silin, H. Wieder, J. T. Woodward, et al. The Role of Surface Free Energy on the Formation of Hybrid Bilayer Membranes, J. Am. Chem. Soc. **124**, 14676-14683 (2002).

NEW FLUORENE DERIVATIVES AS POSITIVE CHARGE CARRIERS FOR EFFICIENT PEROVSKITE SOLAR CELLS

Aistė Ilčiukaitė[1], Marytė Daškevičienė[1], Egidijus Kamarauskas[2], Vygintas Jankauskas[2], Vytautas Getautis[1]

[1] Department of Organic Chemistry, Kaunas University of Technology, Lithuania
[2] Institute of Chemical Physics, Vilnius University, Lithuania
aiste.ilciukaite@ktu.edu

CANCELLED DUE TO COVID-19

Solar energy is the most powerful source of renewable energy. Properly refined solar cell technology can fully meet society's energy needs. Currently, silicon solar elements are mainly used, but they are expensive and complicated to manufacture. However, in the last decade organic and hybrid solar cells are gaining ground. Among them are the perovskite solar cells (PSCs), which have already reached 24% efficient [1]. The benefits of these elements are cheap starting materials and a variety of different fabrication methods that could simplify industrial applications. However, there are still several drawbacks of PSCs. First is the high cost of the widely used hole transporting material spiro-OMETAD [2], and secondly the unresolved stability problem of these devices. There is a vigorous search for simpler and cheaper methods for the synthesis of organic semiconductors. The aim of this work was to synthesize new p-type organic semiconductors containing carbazolyl-and fluorenylchromophores for efficient perovskite solar cells and estimate the influence of the length of alkyl chains on the properties of new compounds.

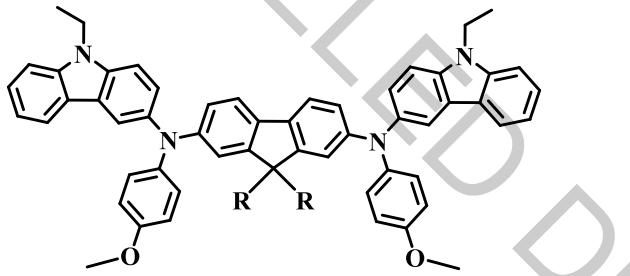

1-4

R: **1** $-CH_3$;
2 $-CH_2CH_2CH_3$;
3 $-CH_2CH2(CHCH_3)CH_2(CH_2)_2CH_3$;
4 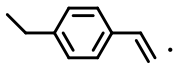 .

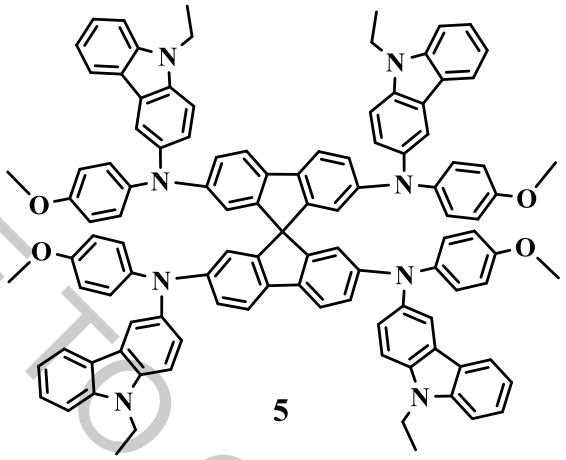

5

Fig. 1. Structures of new fluorene-based derivatives.

During this work, new fluorene class compounds (**1**-**5**) were obtained in three-step reaction. From investigated optical properties, it is evident that all compounds have two maximum absorption peaks between 303 and 377 nm. All target substances are amorphous and have thermal stability greater than 400 °C. It has been observed that longer alkyl chains reduce the thermal stability and glass transition temperature. Ionization potential (3,77-5,28 eV) and hole drift mobility ($3{,}25 \cdot 10^{-5} - 3 \cdot 10^{-3}$ $cm^2/V \cdot s$) of new compounds are favorable for the use in PSCs as hole transporting materials. However, the obtained data show that the increase in the length of alkyl chains tend to rise the numeric value of ionization potential and decrease the charge carrier mobility.

[1] Q. Jiang, Y. Zhao et al. Surface passivation of perovskite film for efficient solar cells, Nat. Photonics **13,** 460–466 (2019).
[2] T. P. I. Saragi, T.Spehr et al. Spiro Compounds for Organic Optoelectronics, Chem. Rev. 107, 1011-1065 (2007).

FORMATION AND CHARACTERIZATION OF ELECTROCHROMIC METAL PLATED TEXTILE/POLYANILINE COMPOSITE

Ieva Agne Cechanaviciute, Mindaugas Gicevicius, Arunas Ramanavicius

Faculty of Chemistry and Geosciences, Vilnius University, Naugarduko str. 24, Vilnius, Lithuania
ievaagne@gmail.com

To this day, despite all technological achievements, color changing clothes are still found to be futuristic. Controlled color change clothing could be entitled as a product of a smart textile - fabrics that have been developed with new technologies to provide additional functionality and value. Light emitting elements are often used in a formation of color adjustable wearable devices [1]. However, this method suffers from some major drawbacks: high cost, color dependency on the environment lighting and continuous electrical consumption. Chromic materials can also be employed in the development of smart fabrics [2]. Because of their low power consumption, good stability and high color contrast exploration of electrochromic materials is a promising way to create a color changing textile-based devices [3]. In this study conducting polymer polyaniline was deposited on the metal-plated textile surface and the electrochromic properties of the obtained composite investigated.

Aniline was polymerized electrochemically on polyester fabric, plated with copper-nickel, which was used as working electrode. Deposition was carried from a 0.2 M aniline solution in 0.5 M H_2SO_4 (Fig. 1). The obtained composite structures were further investigated by recording electrochemical potential-induced color change with smartphone video camera and analyzing captured material with digital image analysis software ImageJ (National institution of health (USA)). All colors can be expressed as numeric value from 0 to 255 (mean gray value - MGV), thus the difference between two electrochromic states can be expressed as a mathematical subtraction of those states numeric values (ΔMGV).

By manipulating the values and the duration of the potential applied, optimal working conditions for polyaniline/textile composites were achieved. Potential switching values for maximum optical contrast between reduced and oxidized states were obtained. However, by lowering determined anodic potential, significant increase in electrochromic stability can be obtained by losing negligible part of optical contrast. It was also observed that the stability of electrochromic composite can be further improved by applying reduction potential for longer times than anodic potential.

Fig. 1 Schematics of electrochemical deposition of PANI onto conducting textile electrode and the principle of reversible electrochromic switching

Polyaniline/textile composites demonstrated reversible electrochromic color change. By manipulating the applied electrochemical potential, optimal operating conditions for maximum stability and lifetime of composite were achieved. Combining electrochromic materials with metal plated textiles is a promising way to produce color changing textiles that can lead to a further development of a smart wearable displays.

[1] Z. Zhang, X. Shi, H. Lou, et al., A stretchable and sensitive light-emitting fabric, Journal of Materials Chemistry C **5**, 4139–4144 (2017).
[2] P. Bamfield, Chromic phenomena: the technological applications of colour chemistry, The Royal Society of Chemistry, Cambridge (2010).
[3] Kelly F.M., Cochrane C., Color-Changing Textiles and Electrochromism. In: Tao X. (eds) Handbook of Smart Textiles, Springer, Singapore (2015).

CANCELLED DUE TO COVID-19

LIQUID CHROMATOGRAPHY – TANDEM MASS SPECTROMETRY FOR THE DETERMINATION OF NEW SYNTHETIC OPIOIDS

Nerijus Karlonas

The State Forensic Medicine Service, Toxicology Laboratory, Didlaukio 86E, LT-08303 Vilnius, Lithuania
nerijuskarlonas@yahoo.com

In many clinical or toxicology laboratories gas chromatography/mass spectrometry using electron impact ionization (GC/EI-MS) or electron capture ionization, and finally, liquid chromatography with ultraviolet detection (LC-UV) or with tandem mass spectrometry (LC-MS/MS) have been used for comprehensive illicit drugs confirming [1]. Unfortunately, GC/EI-MS is not capable of directly analyzing illicit drugs that are non-volatile, polar or thermally labile. Besides, lengthy sample preparations, which include hydrolysis and derivatization, are required prior to GC/EI-MS analysis [2]. The limitations of LC-UV are well established [2], which include the limited specificity and variability of UV spectra. Also, many illicit drugs have little to no UV absorbance, restricting the menu of detectable drugs. LC-MS/MS method has higher sensitivity and specificity than LC-UV and GC/EI-MS methods [1, 2].

Recently, some clinical or toxicology laboratories have adopted liquid chromatography-mass spectrometry (LC-MS) as a complementary method to LC-MS/MS [2]. However, unlike LC-MS, LC-MS/MS using electrospray ionization (ESI+) is capable of detecting non-volatile, polar and thermally labile illicit drugs and provides a means of detecting a broad range of drugs without the need for lengthy sample preparations. Also, in this study, LC-MS/MS is the analytical method of choice because it's commonly used in forensic toxicology laboratories [1-3].

New synthetic opioids, especially fentanyl analogues are popular in recent years among drug addicts and have been related to many overdoses and deaths worldwide [4, 5]. Therefore, the main aim of my study was to develop a new sensitive and specific method based on LC-MS/MS using solid-phase extraction (SPE) on ChemElute® columns for the determination of new synthetic opioids (fentanyl, norfentanyl, carfentanyl, norcarfentanyl, sufentanyl, norsufentanyl, 3-methylfentanyl, acrylfentanyl, furanylfentanyl, AH-7921, U-47700) in whole blood and urine samples. A diatomaceous earth sorbent was used for SPE of biological samples. The use of extraction solvents for the elution of the adsorbed new synthetic opioids and finally sample pretreatment at different pH values from pH 4.5 to pH 12.0 were also optimized. For the quantitative bioanalytical methods there is a general agreement that at least the following validation parameters should be evaluated [5, 6]: the limit of detection (LOD), quantification (LOQ), selectivity, calibration model (linearity), accuracy, precision (RSD), recovery, robustness and stability. The reliability of this method was certified using an exhaustive validation study.

In this study, liquid chromatography with an efficient separation column (particles size of 2.7 microns) has become the leading separation technique in chromatography due to its flexibility, accuracy, and efficiency. Although liquid chromatography achieved physical separation of new synthetic opioids in a mixture, the MS spectrum offered more information about their structural identity. The addition of tandem MS technology has improved the specificity and accuracy of the detection method, especially for AH-7921 and U-47700 substances. The triple-quadrupole mass spectrometry capability of the selected system has facilitated the simultaneous identification and quantification of all analytes. In the experimental, especially chromatographic conditions and MS/MS parameters were also optimized.

The presented method has several advantages when compared with other previously published data [5-7]. The LOD and LOQ for new synthetic opioids in whole blood and urine samples for the developed method were in the range of 0.01 – 0.10 ng mL^{-1} and 0.03 – 0.25 ng mL^{-1}, respectively. The linear relationships with the coefficient of determination (r2) were in the range from 0.9991 to 0.9997. Furthermore, no interferences were observed from the tested substances at the retention times of new synthetic opioids. The results of intraday and interday accuracy tests for three different concentrations of analyte were in the range of 80.6 – 109.7 %, while all RSDs (precision) for replicate determinations were in the range of 3.28 - 8.64 %. Moreover, it was determined that extraction efficiency ranged from 84.6 (±5.2) % to 96.8 (±3.0) %. The absolute recoveries for most of the new synthetic opioids ranged from 81.8 to 90.4 %, except for AH-7921 (72.4 %) and U-47700 (68.9 %). Moreover, this method has several advantages: elimination of interferences, a multi-residue analysis, and very fast chromatographic separation of eleven analytes, the total run time was 9.5 min.

Obtained results showed, that the developed LC-MS/MS and solid-phase extraction method is accurate, sensitive, selective and specific enough to detect analytes after a long time of a single injection or oral administration of some illicit drugs. Finally, it was demonstrated, that this method is applicable for the determination of trace concentrations of new synthetic opioids in real blood and urine samples. The developed method can be applied in routine toxicological analysis during the investigations of both clinical and forensic cases.

[1] K. Sze-Yin, B. Mei-Wah. Analytical and Bioanalytical Chemistry **406**, 2289-2301 (2014).
[2] A. C. Moffat, M. D. Osselton. Clarke's analysis of drugs and poisons, fourth ed., Pharmaceutical Press, London, UK (2011).
[3] D. French. Bioanalysis **22**, 2803-2820 (2013).
[4] European Monitoring Centre for Drugs and Drug Addiction; European Drug Report 2019: Trends and Developments, Publications Office of the European Union, Luxembourg, ISSN 2314-9086 (2019).
[5] K. E. Strayer, H. M. Antonides, M. P. Juhascik, R. Daniulaityte, I. E. Sizemore. ACS Omega **3**, 514-523 (2018).
[6] N. Misailidi, S. Athanaselis, P. Nikolaou, M. Katselou, Y. Dotsikas, C. Spiliopoulou, I. Papoutsis. Forensic Toxicology **37**, 238-244 (2019).
[7] L. Wang, J. T. Bernert. Journal of Analytical Toxicology **30**, 335-341 (2006).

CORRECTED PROOF

HIGHLY ENANTIOSELECTIVE MANNICH REACTION CATALYZED BY CHIRAL PHOSPHINOYL-AZIRIDINES

Aleksandra Buchcic, Anna Zawisza, Stanisław Leśniak, Justyna Adamczyk, Adam Marek Pieczonka, Michał Rachwalski

Department of Organic and Applied Chemistry, University of Lodz, Faculty of Chemistry, Poland
Aleksandra.buchcic.ul@gmail.com

Asymmetric synthesis is still extensively explored field of organic chemistry due to high interest on developing new methods of producing optically pure compounds. Each enantiomer could have significantly different biological activities or organoleptic properties, which often occurs in compounds used in pharmaceutical or cosmetic industry. Organocatalysis could be the right option for the synthesis of optically active (or pure) compounds since there is no presence of metal ions. It is also noteworthy that catalyst molecules are usually quite simple in structure and easy to synthesize. Over the last decade, one or more organocatalytic approaches were applied in synthesis of biologically active species [1]. The organocatalyzed enantioselective Mannich reaction constitutes one of the ways on constructing nitrogen-containing systems. Various molecules (originated from the nature) such as proline, D-glucosamine derivatives or protease were tested in this transformations.

The chiral aziridines containing phosphinoyl moiety are only scarcely mentioned in chemical literature. Taking into account our experience in the area of asymmetric organocatalysis we decided to prepare series of chiral phosphinoyl-functionalized aziridines in order to investigate their activity in the direct asymmetric Mannich reaction of *p*-anisidine, hydroxyacetone and various aromatic aldehydes (Fig. 1). The influence of the catalyst on the absolute configuration of the desired product is discussed [2].

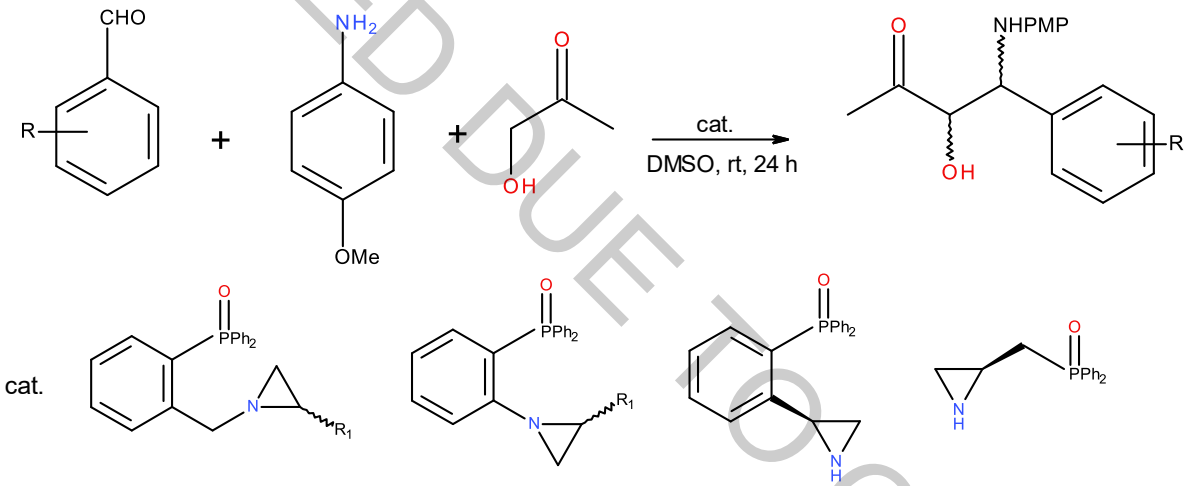

R = H, 4-NO_2, 4-OMe, 2-OMe

R_1 = *i*-Pr, *i*-Bu, Ph

rt - room temperature; Me - methyl; cat. - catalyst, PMP - p-methoxyphenyl, *i*-Pr - isopropyl, *i*-Bu - isobutyl; Ph - phenyl

Fig. 1. Organocatalytic Mannich reaction promoted by chiral phosphinoyl-aziridines.

This project is supported by National Science Centre (NCN) (Grant no. 2016/21/B/ST5/00421).

[1] V. da Gama Oliveira, M. F. do Carmo Cardoso, L. da Silva Magalhães Forezi, Organocatalysis: a brief overview on its evolution and applications, Catalysts **8**, 605-634 (2018).

[2] A. Buchcic, A. Zawisza, S. Leśniak, J. Adamczyk, A. M. Pieczonka, M. Rachwalski, Enantioselective Mannich reaction promoted by chiral phosphinoyl-aziridines, Catalysts **9**, 837-846 (2019).

CANCELLED DUE TO COVID-19

INFLUENCE OF SILVER CONCENTRATION ON THE OPTICAL PROPERTIES OF TIN SELENIDE LAYERS

Aistė Kunciūtė, Remigijus Ivanauskas, Algimantas Ivanauskas

Department of Physical and Inorganic Chemistry, Kaunas University of Technology, Kaunas, Lithuania
aiste.kunciute@ktu.edu

Tin selenide films are valued for such properties as non-toxicity, financial availability and good optical properties, which depend on tin selenide structure (Table 1). It is known that different tin selenide forms have different bandgap value, for example, direct bandgap value for tin selenide nanocrystals is 1.71eV and for monolayers – 1.66eV [1].

Table 1. Bandgap values of tin selenide

Structure	Direct bandgap, eV	Indirect bandgap, eV
Bulk	1,3	0,9
Nanosheets	1,10	0,86
Nanocolumns	-	0,93
Nanocrystals	1,71	-
Single layer	1,66	1,63
Double layer	1,62	1,47

Nowadays great attention is given to use this tin selenide films as semiconductive layers in solar cells systems. These layers have a potential to replace such materials as gallium telluride (direct bandgap value – 1.65 eV) or gallium arsenide (direct bandgap value – 1.55 eV), which are now used in second generation solar cells structures. Also, it is known, that doping of primary semiconductive layer has an ability to chance its optical parameters [2, 3].

In this work was investigated how different concentration of silver dopants change primary tin selenide layers bandgaps values. All layers were formed by using simple and cost-efficient sorption-diffusion method. During this method polyamide 6 sheets are immersed into precursors solutions as it is shown in figure 1.

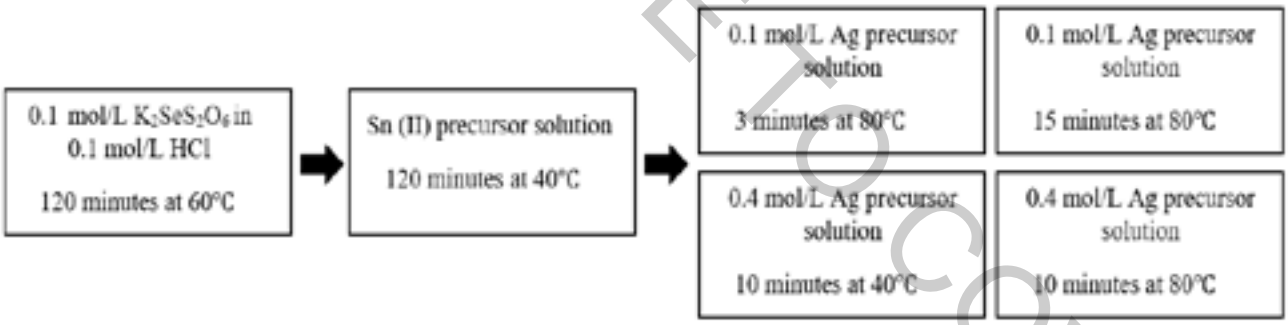

Fig. 1. Scheme of semiconductor layers formation

Optical properties and quantitative analysis of the obtained layers were investigated by UV/VIS spectroscopy and atomic absorption spectroscopy. These analyses indicate that with increasing of silver dopants concentration the bandgap value of primary tin selenide layer decrease.

[1] Shi, W., Gao, M., Wei, J. et al., Tin Selenide (SnSe): Growth, Properties, and Applications, Advanced Science, 5(4), 2018, ISSN: 2198-3844.
[2] Mrinalini M., Islavath N., Prasanthkumar S., et al. Stipulating Low Production Cost Solar Cells All Set to Retail, Chem. Rec 18, 1–15 (2018).
[3] Xi Y., Bounami L.E., Xu Z., et al., Solution-based Ag-doped ZnSe thin films with tunable electrical and optical properties, Journal of Materials Chemistry, 3(38), 9781-9788 (2015).

CANCELLED DUE TO COVID-19

LUMINESCENCE PROPERTIES OF CERIUM, BORON AND/OR MAGNESIUM DOPED YTTRIUM AND LUTETIUM GARNETS COATINGS ON QUARTZ SUBSTRATE

Greta Inkrataitė[1], Ramūnas Skaudžius[1]

[1] Institute of Chemistry, Faculty of Chemistry and Geosciences, Vilnius University, Vilnius, Lithuania
greta.inkrataite@chgf.vu.lt

In recent years materials with luminescent properties have become very popular. In addition, these materials are very popular for usage in lamps and other light emitting devices, but nowadays scintillators and their research is becoming a very interesting subject for scientists. Scintillators are the basis for devices, that are used for radioactive contamination detection and measurement, nuclear material monitoring, also they are included in the computer detector composition of the tomography devices. There are various compounds that can be used as scintillators, but one of the most popular are those which have a garnet structure [1]. Amongst others, these can be yttrium or lutetium aluminum garnet, doped with different lanthanides (YAG:Ln; LuAG:Ln). These inorganics compounds have the required optical properties and radiation resistance [2]. The development of new scintillators is important. However, not the materials which are used are important but also their form. The preparation of powder is the simplest, but they are not suitable for the construction of scintillator detectors. Best suited and used for the manufacture of various devices are single crystals. In addition to single crystals, coatings on various pallets or microfibers can be used [3]. Due to the possibility of using different substrates, different methods of coating, materials with different properties can be prepared, which makes this method widely used. Using the sol-gel method we can obtain homogeneous multicomponent coatings at low temperature, leaving the possibility of synthesizing compounds with emission intensity [4].

Improvement of luminescence is essential for getting the fastest scintillators properties. One way to do this is to additionally dope compounds with other elements. Replacing one element with another in the crystal lattice can influence the properties of the materials. The most common goal is to improve key parameters: compound emission intensity, quantum efficiency and decay times. One of the greatest scintillators drawbacks that is being addressed is that decay time is too long. When it is extremely long, then these second signal captured by the materials overlaps with the first, making the results unreliable and provides less data than it could. Scintillators such as YAG:Ce and LuAG:Ce doped with boron or magnesium can solve this problem. If a quick quench of decay time was obtained given result would be more accurate, and this method of synthesizing scintillators could be practically applicable [5, 6].

In this work cerium boron and/or magnesium doped YAG and LuAG are synthesized on quartz substrates using sol-gel coating method. Boron and magnesium are expected to improve required luminescent properties, and with the sol-gel method, homogeneous compounds will be synthesized at low temperatures. Phosphor coatings were analyzed by x-ray diffraction (XRD) and scanning electron microscopy (SEM) and atomic force microscopy (AFM). Of course, emission, excitation spectra and decay times have been investigated as well.

[1] D. S. McGregor, Materials for Gamma-Ray Spectrometers: Inorganic Scintillators, Annual Review of Materials Research, **48**, 254-277 (2018).
[2] A.D. Sontakke, J. Ueda, J. Xu, et. al., A Comparison on Ce3+ Luminescence in Borate Glass and YAG Ceramic: Understanding the Role of Host's Characteristics, The Journal of Physical Chemistry C, **120**, 31, 17683 – 17691 (2016).
[3] S. Rawat, M. Tyagi, P. K. Netrakanti, et. al., Pulse shape discrimination properties of Gd3Ga3Al2O12:Ce,B single crystal in comparison with CsI:Tl, Nuclear Instruments and Methods in Physics Research Section A: Accelerators, Spectrometers, Detectors and Associated Equipment, **840**, 186 – 191 (2016).
[4] A. Potdevin, G. Chadeyron, D. Boyer, et. al., Sol–gel based YAG: Tb3+ or Eu3+ phosphors for application in lighting sources, Journal Of Physics D: Applied Physics, 3251 – 3260 (2005).
[5] C. Foster, Y. Wu, M. Koschan, et. al., Boron Codoping of Czochralski Grown Lutetium Aluminum Garnet and the Effect on Scintillation Properties, Journal of Crystal Growth, **486**, 126 – 129 (2018).
[6] H. S. Yoo, W. B. Im, J. H. Kang, D. Y. Jeon, Preparation and photoluminescence properties of YAl3(BO3)4:Tb3+, Bi3+ phosphor under VUV/UV excitation Optical Materials, **31**, 2, 131 – 135 (2008).

CANCELLED DUE TO COVID-19

MODIFIED STRUCTURE LUTETIUM OXYORTHOSILICATE: SYNTHESIS AND INVESTIGATION OF LUMINESCENCE PROPERTIES

Greta Inkrataitė[1], Ramūnas Skaudžius[1]

[1] Institute of Chemistry, Faculty of Chemistry and Geosciences, Vilnius University, Vilnius, Lithuania
greta.inkrataite@chgf.vu.lt

Scintillators have already been used for decades. They are included in computed tomography (CT) instrument detectors, positron emission tomography (PET), and are the basis for devices that measure and detect radioactive contamination. Scientists are putting a lot of work into the development of scintillation agents, which are materials for devices that can help preserve health, detect cellular changes, cancer or alert to imminent health threats. In addition to the need for intensive emission, the decay time of the compounds is very important and should be as short as possible. Material with short decay times can capture more signals at the same time, resulting in a brighter and higher contrast image on CT or PET devices, or a higher quality result on radioactive contamination [1].

One of the materials, which can be used as a scintillator is cerium doped lutetium oxyorthosilicate (LSO:Ce). This compound as compared to a very popular and useful cerium doped yttrium aluminium garnet has better energy resolution and higher material density [2]. Because of these advantages and good luminescence properties, cerium doped LSO scintillators are widely used in PET and radioactive contamination detection equipment. All of the important characteristics can be modified by introducing other elements into the structure. Co-doping with ions such as Mg^{2+} potentially might improve the physical properties. The decay time would decrease and emission intensity would be better than without the extra dopant. Magnesium's contribution to the improvement of luminescence properties is obvious, such results have been reported in [3]. Other, not as investigated opportunity to obtain better properties of scintillators is to incorporate boron into the crystal lattice. This element effects inside lutetium aluminium garnet matrix was studied but to a lesser extent as compared to Mg^{2+}, and off course, it gives better luminescence characteristics [4]. In our study, we believe that the synthesized LSO:Ce:B, together with the extra magnesium dopant would exhibit the desired property improvement.

For this project, different cerium doped lutetium oxyorthasilicate compounds were prepared using sol-gel method. These phosphors could be used in scintillators and show faster decay times than the silicates without boron/magnesium. Samples were analyzed by x-ray diffraction (XRD) and scanning electron microscopy (SEM) in order to determine phase purity and structure as well as particle morphology. Luminescence properties such as quantum efficiency, decay times, emission and excitation spectrum were also measured.

ACKNOWLEDGEMENTS:

This project has received funding from European Social Fund (project No [09.3.3-LMT-K-712-16-0271]) under grant agreement with the Research Council of Lithuania (LMTLT).

[1] Y. Wu, M. Koschan, Q. Li, et. al., Revealing the role of calcium codoping on optical and scintillation homogeneity in Lu2SiO5:Ce single crystals, Journal of Crystal Growth, **498**, 362-371 (2018).

[2] V.V. Avdeichikov, L. Bergholt, M. Guttormsen, et. al. Light output and energy resolution of CsI, YAG, GSO, BGO and LSO scintillators for light ions, Nuclear Instruments and Methods in Physics Research A, **349**, 216-224 (1994).

[3] Y. Wu, M. Koschan, C. Foster et. al., Czochralski Growth, Optical, Scintillation, and Defect Properties of Cu2+ Codoped Lu2SiO5:Ce3+ Single Crystals, Crystal Growth Design, **19**, 7, 4081-4089 (2019).

[4] C. Foster, Y. Wu, M. Koschan, et. al., Boron Codoping of Czochralski Grown Lutetium Aluminum Garnet and the Effect on Scintillation Properties, Journal of Crystal Growth, **486**, 126 – 129 (2018).

CANCELLED DUE TO COVID-19

SYNTHESIS AND STRUCTURAL CHARACTERIZATION OF THERMAL REDUCED GRAPHENE OXIDE PRODUCTS

Rūta Aukštakojytė[1], Justina Gaidukevič[1], Jurgis Barkauskas[1]

[1] Institute of Chemistry, Faculty of Chemistry and Geosciences, Vilnius University,
Naugarduko 24, LT-03225 Vilnius, Lithuania
ruta.aukstakojyte@chgf.vu.lt

Graphene is a two dimensional (2D) material with sp^2 hybridized carbon atoms configured in a honeycomb-like structure. Unique thermal, electrical, optical, physical and mechanical properties make it highly promising energetic material for various applications in electronics or electrochemical power sources such as fuel or solar cells and supercapacitors. [1] Today thermal reduction of graphene oxide (GO) is one of the potential synthesis methods to obtain graphene in a simple, low-cost, high yield and time-saving way. However, high volume of CO_2, CO and H_2O is released due to the deoxygenation of functional groups in GO lattice. The vigorous process of deoxygenation generates topological defects and C vacancies in the final product and causes poor electrical conductivity of graphene prepared this way. Also, high temperature of exfoliation leads to the fragmentation of graphene structure. [2] To overcome these drawbacks, efficiency recovery of conjugated π-electron system could be achieved by using lower temperature of reduction and suitable source of elemental carbon. According to the literature, reaction between malonic acid (MA) and phosphorus pentoxide gives carbon suboxide (C_3O_2) that decomposes into carbon atoms at low temperatures. [3] By addition of these compounds in reduction of GO lower defects concentration and better structural properties of thermal reduced graphene can be achieved.

In this work, we present a new approach of thermal reduction of GO in the presence of additives. Three GO samples were prepared using different oxidizing agents and exfoliated by adding various amounts of MA and P_2O_5 .The thermal annealing under Ar gas atmosphere was performed for 30 min at different temperatures: 100 ºC, 150 ºC, 250 ºC and 500 ºC. Reduced GO products were analyzed by Fourier Transform infrared (FTIR) and Raman spectroscopy, scanning electrone microscopy (SEM) and X-ray diffraction (XRD) analysis. Furthermore, measurements of electrical conductivity have also been carried out.

ACKNOWLEDGEMENTS:
This project has received funding from European Social Fund (project No 09.3.3-LMT-K-712-16-0154) under grant agreement with the Research Council of Lithuania (LMTLT).

[1] Q. Ke, J. Wang, Graphene-based materials for supercapacitor electrodes – A review, Journal of Materiomics **2**, 37-54 (2016).
[2] S. Pei, H. Cheng, The reduction of graphene oxide, Carbon **50,** 3210-3228 (2012).
[3] A. Ganguly, Fundamentals of Inorganic Chemistry, ISBN 8131776220, Pearson Education India, (2011).

CANCELLED DUE TO COVID-19

FORMATION OF POLYOXOTUNGSTATE ANIONS IN THE SYSTEM $Cd^{2+} – WO_4^{2–}$ (Z = 1.00) – H^+/ OH^-– H_2O

Ella Duvanova[1], Oleksandr Polishchuk[1], Serhii Radio[1], Georgiy Rozantsev[1]

[1] Faculty of Chemistry, Biology, and Biotechnology, Vasyl' Stus Donetsk National University, Ukraine
e.ivantsova@donnu.edu.ua

Polyoxotungstates have a variety of interesting properties, which determine the main areas of their using as organic synthesis catalysts, radioactive waste disposal materials, anticorrosion coatings, antiviral and antitumor medicines, etc. Considering this, the search of new synthesis procedures, and the structure and properties characterization of this compounds is an actual research problem.

Usually, isopoly tungstates of the d-metals are synthesized by the self-assembly reactions in aqueous solutions, which are acidified to the needed acidity ($Z = C(H^+) / C(WO_4^{2–})$). This synthesis method is simple, fast, convenient, and takes minimum of energy. The existence areas of isopoly anions are quite long, so the synthesis can be done in a wide range of pH values of solution, which is set by different acidity values.

Various forms of paratungstate anion are mainly formed in solutions with a pH close to neutral, which corresponds to a range of acidity from 1.00 to 1.40: $[H_nW_{12}O_{40}(OH)_2]^{(10–n)–}$, $n \le 3$: Z = 1.17, n = 0; Z = 1.25, n = 1; Z = 1.33, n = 2; Z = 1.42, n = 3. The stoichiometry of the starting isopoly anions, which is determined by the reaction $12\ WO_4^{2–} + (14 + n)\ H^+$, and salts, which are formed, has already been sufficiently studied for $Z \ge 1.17$. While the question of the low acidity range of $1.00 \le Z \le 1.17$ is still unclear.

In this regard, the solution of orthotungstate anion, which contained cadmium cations in a molar ratio $C(Cd^{2+}):C(WO_4^{2–}) = 1:6$, was acidified to Z = 1.00. The pH-potentiometric titration of this solution was carried out with an increment $\Delta Z = 0.02$ by the acid and alkali in the acidity intervals Z = 1.00–1.68, and 1.00–0.74, respectively. Ionic strengths (I = 0.05, 0.10, 0.20, 0.30, 0.40, and 0.50 $mol \cdot L^{-1}$) in the solutions were created by adding the required quantity of a $NaNO_3$ solution before the titration. Based on the titration results, a modeling in the CLINP 2.1 software showed that the Anderson heteropoly anions, which were expected at this acidity $Cd^{2+} + 6\ WO_4^{2–} + 6\ H^+ \leftrightarrows [Cd(OH)_6W_6O_{18}]^{4–}$, didn't formed. Therefore, there was a problem of creating a model, that, on the one hand, would describe, the formation of isopoly tungstate anions, and, on the other hand, would consider the presence of Cd^{2+} cations without the formation of a heterogeneous system. For this, the interaction in the system was studied first by the conductometric method.

It was found that the conductivity change in the solution of Na_2WO_4 acidified by HNO_3 to Z=1.00 during adding a solution of $Cd(NO_3)_2$, is not linear. A parabolic dependence of conductivity changes values from the ratio $[C(Cd^{2+}):C(WO_4^{2–})]$, with a minimum at a point that corresponds to the ratio (1.10:12.00), was obtained. This can be explained by the presence of ion pairs between the possible cadmium cations and the isopoly tungstate anions of the 12th row.

As a result, among a number of tested models, there was selected a model which contains a ion pairs $[CdOH^+, W_{12}O_{40}(OH)_2]^{9-}$, $[Cd^{2+}, W_{12}O_{40}(OH)_2]^{8–}$, $[Cd^{2+}, HW_{12}O_{40}(OH)_2]^{7–}$, $[Cd^{2+}, H_2W_{12}O_{40}(OH)_2]^{6–}$, $[Cd^{2+}, W_{12}O_{38}(OH)_2]^{4–}$, $[Cd^{2+}, HW_{12}O_{38}(OH)_2]^{3–}$. This model explains the homogeneity preservation of the system with rather high content of free ions Cd^{2+} and WO_4^{2-}. The model has the low criterion function value CF = 27.39, the good global adequacy criterion $\chi^2_{exp} = 7.94 << \chi^2_{f,\ \alpha=0.05} = 58.12$ and is not redundant. The logarithms of concentration constants of the anions formation at appropriate ionic strengths, which were obtained by the modeling, were then used to calculate the logarithms of thermodynamic constants lgK^0 by the Pitzer method.

The synthesis was done at room temperature in an aqueous solution acidified to Z = 1.00, $C(Na_2WO_4) = C(CH_3COOH) = 0.10$ ($mol \cdot L^{-1}$), with adding the solution of cadmium nitrate $C(Cd(NO_3)_2) = 1.67 \cdot 10^{-2}$ ($mol \cdot L^{-1}$). As a result, after 2 days, the precipitate of colorless salt was formed. The single-phase nature and composition of the isolated salt $Na_2Cd_4[W_{12}O_{40}(OH)_2] \cdot 22H_2O$ were found by chemical analysis and scanning electron microscopy. The presence of paratungstate B anion in the salt composition was shown by FT–IR spectroscopy. The study of surface micromorphology showed that salt exists in the form of plates with 150-295 nm grain sizes (Fig. 1).

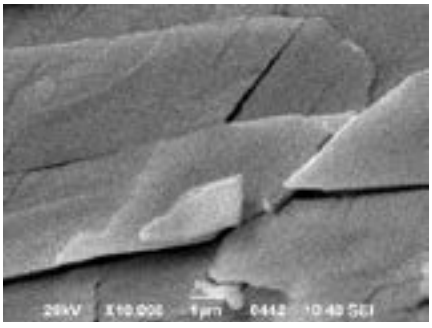

Fig. 1. SEM image of $Na_2[Cd_4W_{12}O_{40}(OH)_2] \cdot 22H_2O$ in SEI electron mode (× 10.000)

ORCID ERROR-ID-19

A NOVEL NONSYMMETRICAL AZINES WITH AGGREGATION INDUCED EMISSION ENHANCEMENT

Justyna Anna Adamczyk[1], Adam Marek Pieczonka[1], Michał Rachwalski[1]

[1] Department of Organic and Applied Chemistry, Faculty of Chemistry, University of Lodz, Poland
justyna.adamczyk@unilodz.eu

Many organic fluorophores show good emission in dilute solutions. However, their emissions will be weakened or completely quenched when they aggregate in solid state or at a high concentration because of the strong π-π interactions. This phenomenon is called the aggregation-caused quenching (ACQ) effect. In contrast to conventional fluorophores with ACQ drawbacks, salicylaldehydes derivatives exhibit Aggregation Induced Emission (AIE). AIEgens are almost non-emissive in dilute solution, but become highly emissive in the aggregate state because of restricted intramolecular motion [1-4].

Salicylaldehyde azines are highly stable condensation products with hydrazine which display several advantages such as easy synthesis and product purifications, low costs or high melting points. They exhibit strong aggregation induced emission in aggregate/solid state which were used in various applications such as optoelectronics [5], chemosensors [6, 7] or for bio-imaging [8, 9]. Azines also exhibit keto-enol tautomerism upon photoexcitation. Tautomerism in azines is characterized by translocation of a proton with a pre-established intramolecular hydrogen bond giving birth to a phototautomer phenomenon, commonly termed as excited state intramolecular proton transfer (ESIPT) [10].

New group of nonsymmetrical salicylaldehyde azine derivatives was prepared and investigated starting from differently substituted salicylaldehydes (Fig.1.).

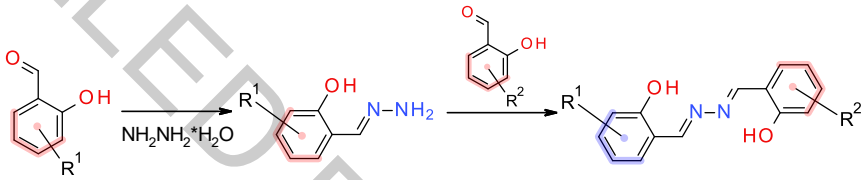

Fig.1. Synthesis pathway of nonsymetrical azines

The introduction of two different substituents into the fluorescent core has a significant effect on the physicochemical properties of the obtained compounds.

CANCELLED DUE TO COVID-19

[1] Y. Hong, J.W.Y. Lam, B.Z. Tang, Aggregation-induced emission, Chemical Society Reviews, 40 (2011) 5361 - 5388.
[2] J. Mei, N.L.C. Leung, R.T.K. Kwok, J.W.Y. Lam, B.Z. Tang, Aggregation-Induced Emission: Together We Shine, United We Soar!, Chemical Reviews, 115 (2015) 11718 - 11940.
[3] J. Mei, Y. Hong, J.W.Y. Lam, A. Qin, Y. Tang, B.Z. Tang, Aggregation-induced emission: The whole is more brilliant than the parts, Advanced Materials, 26 (2014) 5429 - 5479.
[4] S. Kagatikar, D. Sunil, Aggregation-induced emission of azines: An up-to-date review, Journal of Molecular Liquids, 292 (2019).
[5] Z. Wang, F. Zhou, J. Wang, Z. Zhao, A. Qin, Z. Yu, B.Z. Tang, Electronic effect on the optical properties and sensing ability of AIEgens with ESIPT process based on salicylaldehyde azine, Science China Chemistry, 61 (2018) 76 - 87.
[6] X. Ma, J. Cheng, J. Liu, X. Zhou, H. Xiang, Ratiometric fluorescent pH probes based on aggregation-induced emission-active salicylaldehyde azines, New Journal of Chemistry, 39 (2015) 492 - 500.
[7] P.-X. Pei, J.-H. Hu, Y. Chen, Y. Sun, J. Qi, A novel dual-channel chemosensor for CN? using asymmetric double-azine derivatives in aqueous media and its application in bitter almond, Spectrochimica Acta Part A: Molecular and Biomolecular Spectroscopy, 181 (2017) 131 - 136.
[8] M. Gao, C.K.i. Sim, C.W.a.T. Leung, Q. Hu, G. Feng, F. Xu, B.Z.h. Tang, B. Liu, A fluorescent light-up probe with AIE characteristics for specific mitochondrial imaging to identify differentiating brown adipose cells, Chemical communications (Cambridge, England), 50 (2014) 8312 - 8315.
[9] M. Gao, Q. Hu, G. Feng, B.Z. Tang, B. Liu, A fluorescent light-up probe with "aIE + ESIPT" characteristics for specific detection of lysosomal esterase, Journal of Materials Chemistry B, 2 (2014) 3438 - 3442.
[10] S.S. Chourasiya, D. Kathuria, S.S. Nikam, A. Ramakrishnan, S. Khullar, S.K. Mandal, A.K. Chakraborti, P.V. Bharatam, Azine-Hydrazone Tautomerism of Guanylhydrazones: Evidence for the Preference Toward the Azine Tautomer, Journal of Organic Chemistry, 81 (2016) 7574 - 7583.

SUGAR DERIVATIVES WITH UREA FRAGMENT

Karolina Koselak[1], Stanisław Porwański[1], Anna Zawisza[1]

[1] Faculty of Chemistry, Department of Organic and Applied Chemistry, University of Lodz, Poland
karolina.koselak@chemia.uni.lodz.pl

In researching aspects of asymmetric synthesis, a very important element is the appropriate reaction promoter that allows to receive planned products in an enantioselective approach. Following closely the literature reports of the last decade, we observe an increasing interest in organocatalysts or chiral ligands. Among them, an important group are sugar derivatives, including structures with urea fragment, which are the main research trend in our team. Our work resulted in obtaining a large library of organocatalysts containing both mono and disaccharide rings. These derivatives were tested in many asymmetric reactions such as: aza-Henry, Michael and others [1,2].

My research is a continuation of the work of the team from the Unit of Catalysis and Organic Synthesis at the Department of Organic and Applied Chemistry of the University of Lodz. The catalysts mentioned above are obtained as a result of the Staudinger-aza-Wittig reaction from the corresponding sugar azide and nitrogen nucleophile in the presence of triphenylphosphine and CO_2 [3].

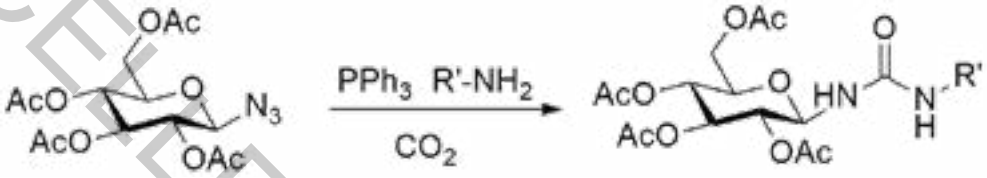

Fig. 1. Staudinger-aza-Wittig reaction.

Their effectiveness in selected asymmetric reactions varied in terms of yield and enantiomeric excess and ranged from average to very good.

[1] S. Porwański, New ureas containing glycosyl and diphenylphosphinyl scaffolds: synthesis and the first attempts to use them in asymmetric synthesis, Carbohydrate Research **394**, 7-12 (2014).
[2] J. Robak, B. Kryczka, B. Świerczyńska et all., New sugar-derived bifunctional chiral ureas as highly effective organocatalysts in asymmetric aza-Henry reaction, Carbohydrate Research **404**, 83-86 (2015).
[3] J. Kovacs, I. Pinter, A. Messmer, G. Toth, Unprotected sugar phosphinimines: A facile route to cyclic carbamates of amino sugars, Carbohydrate Research **141**, 57 (1985).

CANCELLED DUE TO COVID-19

STEREOCONTROLLED SYNTHESIS OF BETTI BASES

Martyna Malinowska, Anna Zawisza, Stanisław Leśniak

Department of Organic and Applied Chemistry, University of Lodz, Poland
martyna.malinowska@chemia.uni.lodz.pl

The Betti reaction is a special case of the aza-Friedel-Crafts reaction - one of the most useful method to create a carbon – carbon bond. The substrates used in the reaction are derivatives of imines and naphthol, which leads to 1-(α-aminoalkyl)-2-naphthols, called Betti bases [1]. Stereocontrolled variant of Betti reaction (Fig. 1) using chiral ligands and catalysts is an effective method leading to compounds with high application potential, commonly found in many biologically active compounds [2]. Due to the promising biological and catalytic properties, synthesis of variously substituted derivatives of Betti bases become an interesting research problem for scientists from around the world. Based on previous literature, it can be concluded that there are only a few examples of this reaction carried out in the stereocontrolled way [3,4,5].

My poster will present the results that I obtained using new ligands based the aziridine ring in the Betti reaction.

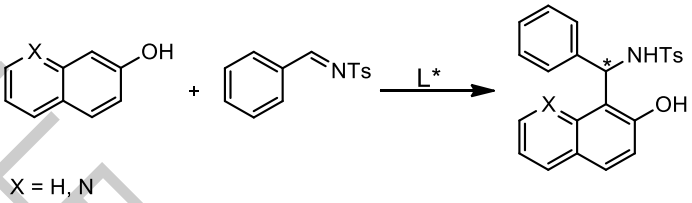

Fig. 1. Stereocontrolled Betti reaction.

[1] C. Cardellicchio, M. A. M. Capozzi, F. Naso, The Betti base: the awakening of a sleeping beauty, Tetrahedron: Asymmetry **21**, 507-517 (2010).
[2] H. Sasai et al., Enantio- and Diastereoselective Betti/aza-Michael Sequence: Single Operated Preparation of Chiral 1,3-Disubstituted Isoindolines, Organic Letters **19**, 5426-5429 (2017).
[3] G. Bian, S. Yang, H. Huang, L. Song, A New Method for the Synthesis of Enantiomerically Pure Betti Bases, Synthesis **45**, 899-902 (2013).
[4] X.-P. Hui et al., Asymmetric Aza-Friedel-Crafts Reaction of 2-Naphthol with Tosylimines Catalyzed by a Dinuclear Zinc Complex, Synlett **5**, 765-768 (2010).
[5] P. Chauhan, S. S. Chimni, Asymmetric Organocatalytic Aza-Friedel–Crafts Reaction of Naphthols with N-Sulfonyl Imines, European Journal of Organic Chemistry **9**, 1636-1640 (2011).

CANCELLED DUE TO COVID-19

AZIRIDINES AS KEY COMPOUNDS FOR THE SYNTHESIS OF *C*-GLYCOSIDES

Martyna Malinowska, Aleksandra Tracz, Anna Zawisza, Stanisław Leśniak

Department of Organic and Applied Chemistry, University of Lodz, Poland
martyna.malinowska@chemia.uni.lodz.pl

Thanks to plants, carbohydrates are an inexhaustible source of substrates for the synthesis of many chemical compounds. Understanding the role carbohydrates and glycoconjugates play in living organisms is the basis for the development of more and more effective therapeutic agents. An extremely important element in the construction of glycosides and glycoconjugates is the glycosidic bond, which is an essential part of such important substances as: antibiotics, antineoplastic drugs and cardiac glycosides. Therefore, research on glycosylation reactions is such an important research problem in carbohydrate chemistry. In nature, carbohydrate connections are based on *O*- and *N*-glycosidic bonds, but studies show that they are not stable enough under therapeutic conditions [1]. Replacement of this type of bonds with a *C*-glycosidic bond leads to derivatives with excellent chemical and enzymatic stability without negative influence on their biological properties [2,3].

The statement will present a synthesis path of new building blocks, which orginality is based on the use of aziridine as a connector with a defined configuration that combines an aminoacid with a saccharide (Fig. 1).

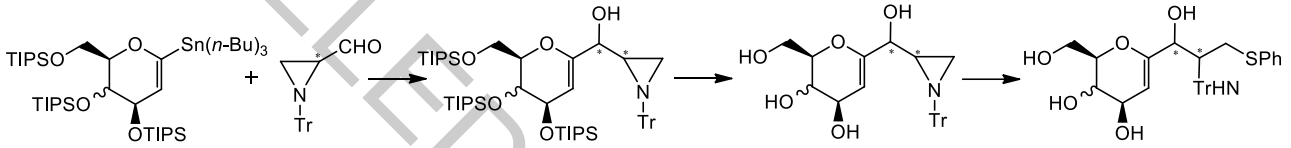

Fig. 1. Scheme of planned synthesis steps.

[1] B. Ernst, J. L. Magnani, From carbohydrate leads to glycomimetic drugs, Nature Reviews Drug Discovery **8**, 661-667 (2009).
[2] M. Sparks, W. Williams, M. Whitesides, Neuraminidase-resistant hemagglutination inhibitors: acrylamide copolymers containing a C-glycoside of N-acetylneuraminic acid, Journal of Medicinal Chemistry **36**, 778-783 (1993).
[3] D. E. Levy, *The Chemistry of C-Glycosides* (Pergamon, Oxford, 1995).

CANCELLED DUE TO COVID-19

SYNTHESIS AND INVESTIGATION OF $GdPO_4$ BASED DIFFERENT CORE–SHELL STRUCTURES

Andrius Pakalniškis[1], Ramūnas Skaudžius[1], Živilė Stankevičiūtė[1]

[1]Institute of Chemistry, Vilnius University, Naugarduko 24, LT-03225 Vilnius, Lithuania
andrius.pakalniskis@chgf.vu.lt

Conventional treatment for cancer is chemotherapy, which has many limitations such as drug stability and solubility. It also causes adverse side effects like hair loss, healthy cell death, loss of appetite and etc [1]. For these reasons the cancer research has attracted a lot of attention from scientists around the world. Many different approaches have been taking to battling the disease. These range from simple such as new and more effective cancer drug creation, improving the early stage detection of tumors to more complex such as immunotherapy and vaccines [2]. One other emerging treatment with high potential in both detection and treatment of cancer is the use of multifunctional nanoparticles. These particles could combine both luminescence bioimaging as well as act as contrast agents for MRI in order to improve the detection of cancer [3]. Also, as potential drug carriers for improved and more direct drug delivery. Due to the fact that nanoparticles tend to accumulate in the tumor itself rather than to disperse into the whole organism drugs would be delivered directly to the tumor and many side effects could be prevented. One of such potential compounds could be rare-earth element doped $GdPO_4$. Since Gd^{3+} ions already have 7 unpaired f electrons they induce strong contrast during magnetic resonance imaging. In addition, doping by optically active ions such as Eu^{3+}, Er^{3+}, Yb^{3+}, and so on could be used for conventional or upconverting luminescence imaging. Anyway, there are still many problems related to both the production and the properties related to them. Such compounds have to match many of the needed criteria such as very small particle size of around 100 nm, not soluble in the biological fluid, do not degrade over time and so on [4]. However, the small particle size reduces the luminescence intensity of the particles, making one of the functionalities hampered. In order to avoid this drawback, core-shell structures are created [5]. $GdPO_4$ can also have several different crystal structures which could also influence the luminesce properties as well as particle stability, so much research is still needed to evaluate all of the factors involved.

In this work europium doped conventional luminescence as well as upconverting ytterbium and erbium/thulium co-doped $GdPO_4$ nanoparticles were using the hydrothermal method synthesized. Different shell structures of $GdPO_4$, SiO_2, and Ag were prepared. X-ray diffraction analysis was used to determine the thermal stability and purity of obtained samples. Scanning electron microscopy and transmission electron microscopy were used to determine the shape and size of particles. Luminescence measurements of particles and their solutions in the biological medium were performed.

Acknowledgements. This project has received funding from European Social Fund (project No [09.3.3-LMT-K-712-16-0290]) under grant agreement with the Research Council of Lithuania (LMTLT).

[1] Nurgali, K., R.T. Jagoe, and R. Abalo, Adverse Effects of Cancer Chemotherapy: Anything New to Improve Tolerance and Reduce Sequelae? Frontiers in pharmacology **9,** 245-245 (2018).
[2] Ramaswami, R., V. Harding, and T. Newsom-Davis, Novel cancer therapies: treatments driven by tumour biology. Postgraduate Medical Journal, **89,** 652 (2013).
[3] Cheng, L., et al., Multifunctional nanoparticles for upconversion luminescence/MR multimodal imaging and magnetically targeted photothermal therapy. Biomaterials, **33,** 2215-2222 (2012).
[4] Yoshioka, Y., K. Higashisaka, and Y. Tsutsumi, Biocompatibility of Nanomaterials. Nanomaterials in Pharmacology, **39,** 185-199 **(**2016).
[5] Homann, C., et al., NaYF4:Yb,Er/NaYF4 Core/Shell Nanocrystals with High Upconversion Luminescence Quantum Yield. Angewandte Chemie International Edition, **57,** 8765-8769 **(**2018).

CANCELLED DUE TO COVID-19

INVESTIGATION AND USE OF THERMALLY REDUCED GRAPHENE OXIDE FRACTIONS IN THE DEVELOPMENT OF THIRD GENERATION BIOSENSORS

Gintarė Rimkutė[1,2], Justina Gaidukevič[1], Vidutė Gurevičienė[2], Ieva Šakinytė[2], Julija Razumienė[2]

[1]Institute of Chemistry, Faculty of Chemistry and Geosciences, Vilnius University, Lithuania
[2] Institute of Biochemistry, Life Sciences Center, Vilnius University, Lithuania
gintare.rimkute@chgf.stud.vu.lt

The increasing demand for inexpensive and portable analytical devices, which require low-sample consumption and real-time response, has greatly raised the novelty in the design of biosensors [1]. Researchers have especially focused on new materials, which could improve portability and miniaturization of mentioned devices [2]. This can be achieved by integrating carbon materials, which are characterized by unique properties, into analytical systems. One of the most promising carbon materials is graphene, which after special modification could help to create third-generation biosensors that use direct electron transfer (DET) between the enzyme and the electrode and therefore do not require any intermediate mediating materials [3].

This study aims to synthesize and investigate fractions of thermally reduced graphene oxide (TRGO) and to use them in construction of third-generation biosensors based on pyrroloquinoline quinone-dependent glucose dehydrogenase (PQQ-GDH) from *Acinetobacter calcoaceticus* sp. and urease from *Canavalia ensiformis.* While PQQ-GDH enzyme could be very promising for creation of new technologies for investigation of diseases related to release of carbohydrates, urea sensitive analytical devices can be significant in medicine, agriculture and chemical industries too.

TRGO fractions were synthesized from graphite oxide (GO), which was initially prepared using modified Hummers' method and pre-washed 13 days from excess of sulphate ions. Afterwards GO was reduced using thermal reduction and fractionation equipment. Properties of obtained TRGO fractions were characterised by x–ray diffraction, thermogravimetric and Brunauer–Emmett–Teller analysis. The amperometric biosensors were constructed using membranes made from PQQ-GDH/urease immobilised into layer of TRGO. Characteristics of proposed biosensors, such as sensitivity, substrate selectivity, optimal working electrode potential, pH and concentration of buffer solution were determined. On a base of these data, an influence of TRGO properties to the efficacy of biosensors were concluded. Obtained results will be presented in more detail during the poster session.

This research was partly supported by Research Council of Lithuania (Project No. 09.3.3-LMT-K-712-16-0125).

[1] Lopez G.A., Estevez M.-C., Soler M., Lechuga L.M., Recent advances in nanoplasmonic biosensors: applications and lab-on-a-chip integration, Nanophotonics **6**, 123-136 (2017).
[2] da Silva Neves M.M.P., González-García M.B., Hernández-Santos D., Fanjul-Bolado P., Future trends in the market for electrochemical biosensing, Current Opinion in Electrochemistry **10**, 107-111 (2018).
[3] Sakinyte I., Barkauskas J., Gaidukevic J., Razumiene J., Thermally reduced graphene oxide: The study and use for reagentless amperometric D-fructose biosensors, Talanta **144**, 1096-1103 (2015).

CANCELLED DUE TO COVID-19

Fe AND Zn CO-SUBSTITUTED BETA-TRICALCIUM PHOSPHATE: SYNTHESIS, STRUCTURAL, MAGNETIC, MECHANICAL AND BIOLOGICAL PROPERTIES

Agne Kizalaite[1], Lauryna Sinusaite[1], Diana Griesiute[1], Anton Popov[1], Andris Antuzevics[2], Kestutis Mazeika[3], Dalis Baltrunas[3], Jen-Chang Yang[4], Aivaras Kareiva[1], Aleksej Zarkov[1]

[1] Institute of Chemistry, Vilnius University, Naugarduko 24, LT-03225 Vilnius, Lithuania
[2] Institute of Solid State Physics, University of Latvia, Kengaraga 8, LV-1063 Riga, Latvia
[3] Center for Physical Sciences and Technology, Vilnius LT-02300, Lithuania
[4]College of Biomedical Engineering, Taipei Medical University, 250 Wu-Hsing St, Taipei 11052, Taiwan
agne.kizalaite@chgf.vu.lt

Calcium phosphates (CPs) are the main inorganic part of biological hard tissues such as bones or teeth and play an essential role in human life. This reason makes synthetic CPs widely used in medicine for repair and reconstruction of diseased or damaged parts of bone. For these purposes CPs can be used in different forms varying from thin coatings on metallic implants to sintered bioceramics [1-3]. One of the CPs most frequently used for the fabrication of bioceramics is beta-tricalcium phosphate (β-TCP, $Ca_3(PO_4)_2$), which attracts practical interest due to several reasons such as excellent biocompatibility, osteoconductivity and chemical composition similar to natural bone [4].

Partial substitution of Ca by other biologically active ions has been proposed as a promising tool to the superior biological performance of CP based materials [5]. Chemical modification can drastically affect physicochemical, mechanical and anti-bacterial properties of materials, to cause changes in morphology, density, solubility and ion release kinetics [6]. Substitution-induced properties allow to combine biocompatibility of CPs with newly obtained properties resulting in application of these materials in new areas such as various imaging modalities including fluorescence, magnetic resonance or multimodal imaging, as well as for various therapeutic approaches including chemotherapy, gene therapy, hyperthermia or combination therapy [7].

Despite the fact that different CPs have been reported to be substituted with a huge variety of ions, co-doping of CPs still remains relatively new approach. Since substitution with single ions opens so many horizons for new applications, it makes sense to use multielement substitution for the synergistic effect or multifunctioning of CP-based materials [8]. The main goal of the present work was to develop synthetic approach and comprehensively characterize β-TCP bioceramics with magnetic and biological properties. Due to these reasons β-TCP partially substituted with Fe^{3+} and Zn^{2+} ions was chosen and series of products with different substitution level was investigated in detail.

Fe^{3+} and Zn^{2+} co-substituted β-tricalcium phosphate (β-TCP) has been synthesized by wet co-precipitation method. Co-substitution level in the range from 1 to 5 mol% has been studied. The thermal decomposition of the as-prepared precipitates was analysed through thermogravimetric (TG) analysis. The phase purity and structure of the synthesized compounds were evaluated using X-ray diffraction (XRD) analysis, electron paramagnetic resonance (EPR) and Fourier-transform infrared spectroscopy (FTIR). Scanning electron microscopy (SEM) was used for the characterization of morphological features of the synthesized products. Chemical composition of the compounds was confirmed by inductively coupled plasma optical emission spectrometry (ICP-OES). Cytotoxicity of the synthesized species was estimated by in vivo assay using zebrafish (*Danio rerio*).

Acknowledgements

This research was funded by the European Social Fund under the No. 09.3.3-LMT-K-712 "Development of Competences of Scientists, other Researchers and Students through Practical Research Activities" measure (grant No. 09.3.3.-LMT-K-712-16-0157).

[1] W. Habraken, P. Habibovic, M. Epple et al., Calcium phosphates in biomedical applications: materials for the future?, Mater. Today **19**, 69-87 (2016).
[2] E.A. Chudinova, M.A. Surmeneva, A.S. Timin et al., Adhesion, proliferation, and osteogenic differentiation of human mesenchymal stem cells on additively manufactured Ti6Al4V alloy scaffolds modified with calcium phosphate nanoparticles, Colloids Surf. B **176**, 130-139 (2019).
[3] S.V. Dorozhkin, Calcium orthophosphate-based bioceramics, Materials, **6**, 3840-3942 (2013).
[4] R.G. Carrodeguas, S. De Aza, α-Tricalcium phosphate: Synthesis, properties and biomedical applications, Acta Biomater. **7**, 3536-3546 (2011).
[5] E. Boanini, M. Gazzano, A. Bigi, Ionic substitutions in calcium phosphates synthesized at low temperature, Acta Biomater. **6**, 1882-1894 (2010).
[6] B. Yilmaz, A.Z. Alshemary, Z. Evis, Co-doped hydroxyapatites as potential materials for biomedical applications, Microchem. J. **144**, 443-453 (2019).
[7] C. Qi, J. Lin, L.H. Fu, P. Huang, Calcium-based biomaterials for diagnosis, treatment, and theranostics, Chem. Soc. Rev. **47**, 357-403 (2018).
[8] S. Sprio, L. Preti, M. Montesi et al. Surface phenomena enhancing the antibacterial and osteogenic ability of nanocrystalline hydroxyapatite, activated by multiple-ion doping, ACS Biomater. Sci. Eng. **5**, 5947-5959 (2019).

CANCELLED DUE TO COVID-19

THE FLUORIDE ANION CATALYZED SULFUR TRANSFER REACTIONS OF ELEMENTAL SULFUR (S_8) WITH THIOKETONES

Jakub Wręczycki[1], Dariusz M. Bieliński[1], Grzegorz Mlostoń[2*]

[1] Faculty of Chemistry, Lodz University of Technology, Żeromskiego 116, 90-924, Lodz, Poland
[2] Faculty of Chemistry, University of Lodz, Tamka 12, 91-403, Lodz, Poland
jakub.wreczycki@edu.p.lodz.pl

CANCELLED DUE TO COVID-19

It is well known that thiocarbonyl compounds such as aryl, hetaryl or cycloaliphatic thioketones ($R_2C=S$) are important building blocks, widely applied for preparation of sulfur heterocycles with diverse ring size. Their superior ability to react with 1,3-dipoles or dienes via the C=S group brought them into prominence as 'superdipolarophiles' and 'superdienophiles' in [3+2] and [4+2] cycloadditions reactions, respectively [1,2]. Sulfurization of the C=S bond leads to so called "thiosulfines" (thiocarbonyl *S*-sulfides). They are considered as a class of elusive 1,3-dipoles that *in situ* undergo further conversions. The evidence of their supposed existence was unambiguously demonstrated in 1987 by R. Huisgen and J. Rapp [3-5]. The sulfur transfer reaction involving elemental sulfur (S_8) as a sulfur source, require its activation via homolytic or heterolytic cleavage of the S−S bond. Various chemical species are known to activate the S_8 ring, however one of the unorthodox but only little-known approaches is the usage of the fluoride anion F^- as a catalyst.

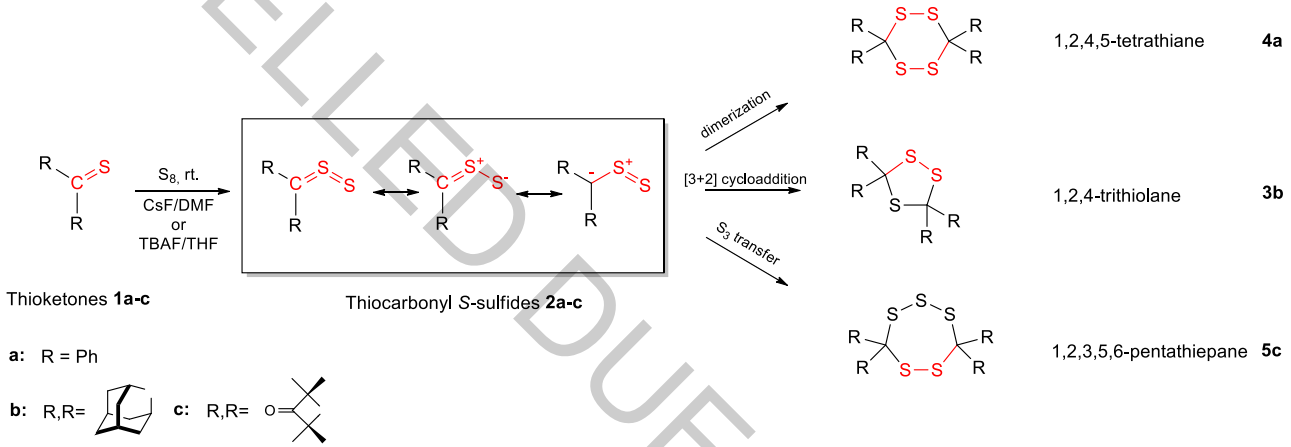

Fig. 1. *In situ* generation of thiocarbonyl *S*-sulfide with the use of fluoride anion and its further pathway conversation to heterocyclic compounds.

In our ongoing research, we found that sulfurization of aryl and cycloaliphatic thioketones **1a-c** by treatment with elemental sulfur (S_8) in the presence of cat. amounts of fluoride anion (cesium fluoride (CsF) or tetra-*n*-butyl ammonium fluoride (TBAF)), leads to formation of thiocarbonyl *S*-sulfides **2a-c** that *in situ* undergo further conversations. We also found that, depending on thioketone type, the product can be formed as 5-, 6- or 7-membered heterocyclic ring with four (1,2,4,5-tetrathiane) **4a**, three (1,2,4-trithiolanes) **3b**, or five (1,2,3,5,6-pentathiepanes) **5c** sulfur atoms. A novel, unique and efficient method for the *S*-transfer to the C=S bond *via* activation of S_8 with fluoride anion as well as mechanisms of the formation of sulfur rich heterocycles **3-5** will be discussed.

Acknowledgement: Authors acknowledge financial support by the National Centre for Research and Development (Warsaw, Poland) within the grant InterChemMed (WND-POWR.03.02.00-00-I029/16-01).

[1] G. Mlostoń et al., Aryl, hetaryl, and ferrocenyl thioketones as versatile building blocks for exploration inthe organic chemistry of sulfur, Phosphorus Sulfur and Silicon and Related Elements **192**, 204-211 (2017)
[2] P. Grzelak, G. Utecht, M. Jasiński, G. Mlostoń., First (3+2)-cycloadditions of thiochalcones as C=S dipolarophiles: efficient synthesis of 1,3,4-thiadiazoles via reactions with fluorinated nitrile imines, Synthesis **49**, 2129-2137 (2017)
[3] R. Huisgen, J. Rapp, The conversion of thioketones to 1,2,4,5-tetrathianes and its mechanism, Heterocycles **45**, 507-525 (1997)
[4] R.Huisgen, J. Rapp, The chemistry of thiocarbonyl S-sulfides, Tetrahedron **53**, 939-960 (1997)
[5] R. Huisgen, J. Rapp, Thiocarbonyl S-sulfides, a new class of 1,3-dipoles, J. Am. Chem. Soc. **109,** 902- (1987)

MODELLING ^{17}O NMR SPECTRA OF TAUTOMERIC FORMS OF CITRININ

Žyginta Einorytė[1,2], Kęstutis Aidas[2]

[1] Institute of Chemistry, Faculty of Chemistry and Geosciences, Vilnius University, Lithuania
[2] Institute of Chemical Physics, Faculty of Physics, Vilnius University, Lithuania
zyginta.einoryte@chf.stud.vu.lt

Citrinin is a mycotoxin which causes contamination of food with various toxic effects. Two tautomeric forms of citrinin exist – *para* or *ortho* quinone methide (analogous to a quinone but having one of the carboxylic oxygens replaced with a carbon) (Fig. 1). Citrinin is synthesized as a secondary metabolite by several fungal strains of *Penicillium, Aspergillus* and *Monascus* genera and is often found along with another nephrotoxic compound, ochratoxin A. As many other mycotoxins, citrinin is considered a perspective antimicrobial, antitumor and even neuroprotective agent due to its toxicity. Citrinin is known for having toxic effects on the heart, kidneys, liver, reproductive system. Oxidative stress and modified antioxidative enzymatic defences (e.g. glutathione) are thought to be two major causes of citrinin's mediated toxic effects but the precise mechanism of its action is yet to be discovered [1]. More detailed understanding of citrinin's distribution between two tautomeric forms would help in dissecting the possible mechanism of its action.

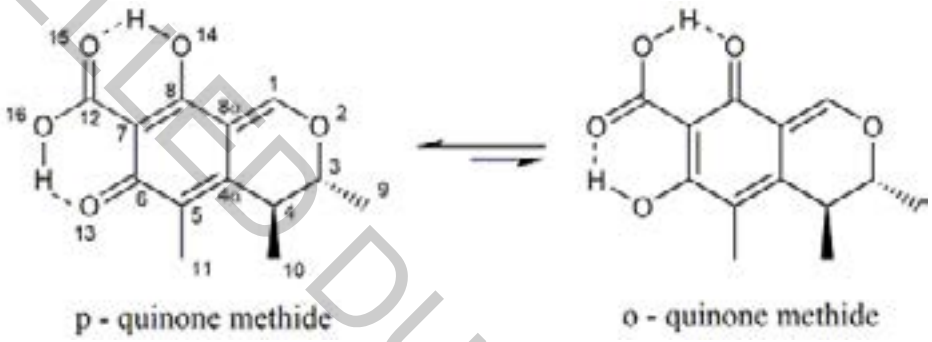

Fig. 1. Tautomeric forms of citrinin

The main goal of this study is to model the ^{17}O NMR spectrum of citrinin in the dichloromethane (DCM) solution in order to compare it to an experimental spectrum from previous studies [2]. The measured ^{17}O NMR spectrum of citrinin is interesting as its qualitative shape is not consistent with citrinin's tautomeric distribution implied by the ^{1}H and ^{13}C NMR spectra measured in the same study. In addition, the ^{17}O NMR signals from oxygen atoms 13 and 14 exhibit additional peaks, almost doublets, which is intriguing because the interconversion between two tautomers should occur at a high rate so that only single peak should be seen in the spectrum [2]. Our computational approach allows evaluating the ^{17}O NMR spectrum of both individual tautomers. Thus, the comparison between theoretical tautomer-averaged spectrum and the experimental spectrum allows us to estimate the populations of each tautomer of citrinin in DCM solution.

Molecular dynamics (MD) simulations were executed for *para*- and *ortho*-citrinin in DCM using an all-atom OPLS force field. The standard Coulomb plus 12-6-type Lennard-Jones potential was used, and atomic point charges were derived by fitting to the quantum mechanical electrostatic potential according to the CHelpG scheme. NMR shielding constants were calculated for isolated molecular species of citrinin. To account for solvation, the hybrid quantum mechanics/molecular mechanics (QM/MM) calculations were considered. These calculations were performed for a set of molecular solute-solvent snapshots extracted from the MD trajectory for each tautomer. The comparisons between experimental data and our computational results will be discussed in the presentation.

[1] J. W. G. de Oliveira Filho, et al. A comprehensive review on biological properties of citrinin. Food Chem. Toxicol. 110, 130–141 (2017).
[2] R. Poupko, Z. Luz, Carbon-13 NMR of Citrinin in the Solid State and in Solutions. Journal of Physical Chemistry A - J PHYS CHEM A 101, (1997).

CANCELLED DUE TO COVID-19

SYNTHESIS AND TADF PROPERTIES OF 2-SUBSTITUTED 4,6-BIS(3,6-DI-*t*-BUTYL-9-CARBAZOLYL)-5-METHYLPYRIMIDINES

Irina Fiodorova[1], Rokas Skaisgiris[2], Tomas Serevičius[2], Saulius Juršėnas[2], Sigitas Tumkevičius[1]

[1] Department of Organic Chemistry, Faculty of Chemistry and Geosciences, Vilnius University, Naugarduko 24, LT-03225 Vilnius, Lithuania

[2] Institute of Photonics and Nanotechnology, Faculty of Physics, Vilnius University, Sauletekio 3, LT-10257 Vilnius, Lithuania.

irina.fiodorova@chgf.vu.lt

CANCELLED DUE TO COVID-19

Thermally Activated Delayed Fluorescence (TADF) is an attractive way to achieve 100% internal fluorescence quantum yield without involving any expensive heavy atoms by converting all excitations to singlet ones by thermal activation [1]. Usually, this is achieved by constructing TADF compounds from electron-donating (D) and electron-accepting (A) units, decreasing the spatial overlap of electron density distribution in HOMO and LUMO and narrowing the singlet-triplet energy gap (ΔE_{ST}) up to values, comparable to thermal energy at room temperature [1,2]. It is rather difficult to find suitable D and A units with limited conjugation length and high triplet energy and bound them in a suitable architecture. Among numerous candidates for D and A units, carbazole as D unit and aromatic nitrogen heterocycles as A moieties are considered as being stable-enough and preferable for high stability OLEDs [3]. Recently, compounds containing pyrimidine heterocycle as an A unit have been demonstrated to be promising for TADF applications [4]. Seeing the potential of carbazole-pyrimidine pair for achieving efficient deep-blue TADF, we performed the design, synthesis, photophysical characterization as well as application in OLED devices of some novel single bonded carbazole-pyrimidine conjugates (Scheme 1).

The designed molecules were synthesized starting from an easily accessible pyrimidine derivative **1**. The chlorine groups substitution of **1** with 3,6-di-*t*-butylcarbazole to give compound **2a** was carried out by the palladium-catalyzed Buchwald-Hartwig amination reaction in the presence of Pd_2dba_3 and $P(t\text{-}Bu)_3 \cdot HBF_4$ as a catalyst system and NaO*t*-Bu as a base. Synthesis of compounds **2b-d** was accomplished by using Liebeskind-Srogl coupling of 2-methylthiopyrimidine derivative **2a** with substituted phenylboronic acids in the presence of $Pd(PPh_3)_4$ and CuMeSal as catalysts.

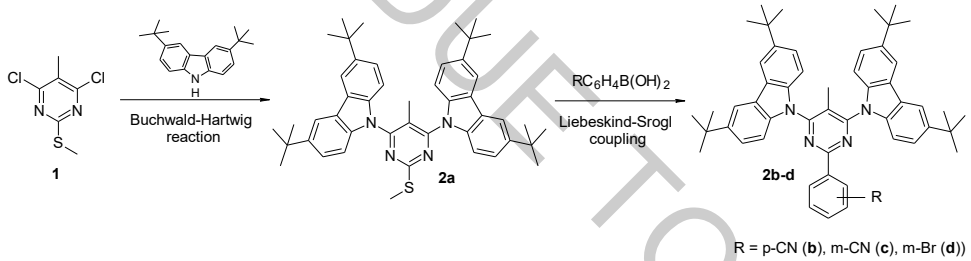

Fig. 1. Synthesis of 2-substituted 4,6-bis(3,6-di-*t*-butyl-9-carbazolyl)-5-methylpyrimidines (**2a-d**).

Optical properties of the synthesized materials **2a-d** were assessed by DFT calculations and investigated by absorption, time integrated and time-resolved fluorescence spectroscopies and fluorescence quantum yield and lifetime measurements. The enhancement of electron-donating properties of carbazole, the increase of twisting angle between D and A units as well as the increase of conjugation length by introduction substituents into the 2nd position of pyrimidine ring was shown to shift the emission towards deep-blue together with lowering the singlet-triplet gap and emergence of TADF. Compound **2a** was shown to be an efficient TADF emitter with peak wavelength of 428 nm, 0.5 solid-state emission yield and average delayed fluorescence lifetime of 143 μs. When used in OLED device, compound **2a** based OLED showed electroluminescence with 8.7% EQE and CIE coordinates of (0.16; 0.12). Thus, simple molecular design steps were shown to be the successful strategy for achieving deep-blue TADF in highly promising carbazole-pyrimidine compounds.

Acknowledgements

This research was funded by a grant (no. S-MIP-17-73) from the Research Council of Lithuania.

[1] H. Uoyama, K. Goushi, K. Shizu et al. Highly Efficient Organic Light-emitting Diodes from Delayed Fluorescence, Nature, **492**, 234-238 (2012).

[2] M. K. Etherington, J. Gibson, H. F. Higginbotham et al., Revealing the spin-vibronic coupling mechanism of thermally activated delayed fluorescence. Nature Communications, **7**, 13680 (2016).

[3] Y. Im, M. Kim, Y. J. Cho et al. Molecular Design Strategy of Organic Thermally Activated Delayed Fluorescence Emitters. Chemistry of Materials, **29**, 1946–1963 (2017).

[4] (a) R. Komatsu, H. Sasabe, J. Kido, Recent progress of pyrimidine derivatives for high-performance organic light-emitting devices, J. Photon. Energy, **8**, 032108 (2018); (b) T. Serevicius, T. Buciunas, J. Bucevicius et al. Room temperature phosphorescence vs. thermally activated delayed fluorescence in carbazole–pyrimidine cored compounds, J. Mater. Chem. C, **6**, 11128-11136 (2018); (c) T. Serevičius, R. Skaisgiris, J. Dodonova et al. Emission wavelength dependence on the rISC rate in TADF compounds with large conformational disorder. Chemical Communications, **55**, 1975-1978 (2019).

SPECIFIC PATHWAYS FOR SYNTHESIS OF CARBONACEOUS – $NaTi_2(PO_4)_3$ COMPOSITES AND APPLICATION AS NEGATIVE ELECTRODE MATERIALS IN AQUEOUS Na-ION BATTERIES

Barbara Chatinovska[1,2], Skirmantė Tutlienė[2], Milda Petrulevičienė[2], Jurgis Pilipavičius[2], Jurga Juodkazytė[2], Linas Vilčiauskas[2]

[1] Institute of Chemistry, Faculty of Chemistry and Geosciences, Vilnius University, Lithuania
[2] Center for Physical Sciences and Technology, Saulėtekio al. 3, LT-10257 Vilnius, Lithuania
barbara.chatinovska@chgf.stud.vu.lt

CANCELLED DUE TO COVID-19

The most recent Nobel Prize in Chemistry was awarded to John Goodenough, M. Stanley Whittingham and Akira Yoshino "for the development of lithium-ion batteries". Although Li-ion batteries (LIBs) are revolutionary and surely are the main electrochemical energy storage technology today, there are ongoing issues with these batteries, caused by the natural scarcity of lithium and cobalt; furthermore, some issues remain concerning the safety due to the use of organic electrolytes. Therefore, alternative technologies are being intensively explored, one of them being the sodium ion battery (SIB) [1].

The aim of our research is to develop suitable electrode materials for aqueous SIBs that would ensure high capacity, long lifespan and superior cycling performance. One material that stands out in its suitable electrode potential, high theoretical capacity and ionic conductivity, structural and electrochemical stability is the Sodium SuperIonic Conductor (NASICON)-structured $NaTi_2(PO_4)_3$ (NTP) [2]. We present the detailed aqueous sol-gel synthesis pathway of carbonaceous-NTP composites and a thorough analysis of prepared samples.

The main issue with aqueous sol-gel synthesis of NTP is the stabilization of titanium precursor (in this case-titanium tetraisopropoxide ($Ti(^iOPr)_4$)), as titanium alkoxides are irreversibly hydrolyzed in water. A procedure to make a stable organometallic titanium complex is the reaction of $Ti(^iOPr)_4$ with lactic acid [3]. After preparing the stable titanium precursor, different synthesis pathways were employed to prepare the NTP powder. The obtained NTP powder (the active material for electrode preparation) were analyzed by powder X-ray diffraction (XRD) (Fig. 1a), Scanning electron microscopy (SEM) and Fourier Transform infrared spectroscopy (FTIR). The electrodes were prepared by mixing the synthesized active materials (carbonaceous-NTP composites) with conducting carbon filler and polyvinylidene fluoride binder in the ratio 7:2:1 (using N-methyl-2-pyrrolidone as the solvent) and casting the slurry in a uniform layer on aluminum foil. The electrochemical properties of prepared electrodes were characterized in the in-house built three-electrode bottom mount flat sample cells using cyclic voltammetry and galvanostatic charge/discharge cycling (Fig. 1b).

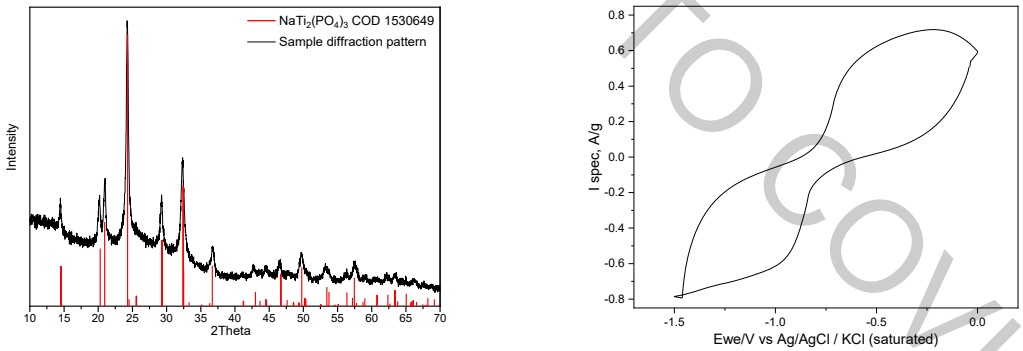

Fig.1 a) XRD pattern; **b)** Cyclic voltammetry of carbonaceous-NTP composite

In our presentation, we will analyze in detail the pathways of carbonaceous-NTP synthesis, present the obtained material phase-purity and morphology analysis results and further investigate the differences in electrochemical properties and their co-dependence with employed synthesis pathways.

[1] Palomares, V., Serras, P., Villaluenga, I., Hueso, K. B., Carretero-González, J., & Rojo, T. Na-ion batteries, recent advances and present challenges to become low cost energy storage systems. Energy Environ. Sci. (2012) 5, 5884.
[2] Wu M., Ni W., Hu J. Ma & J. Wei. NASICON-Structured NaTi2(PO4)3 for Sustainable Energy Storage. Nano-Micro Lett. (2019) 11:44.
[3] Ohya T., Ito M., Yamada K., Ban T., Ohya Y. & Takahashi Y. Aqueous Titanate Sols from Ti Alkoxide-α-Hydroxycarboxylic Acid System and Preparation of Titania Films from the Sols. Journal od Sol-Gel Science and Technology 30, 71-81, 2004.

Acknowledgements: This project has received funding from the European Regional Development Fund (Project No. 01.2.2-LMT-K-718-02-0005) under grant agreement with the Research Council of Lithuania (LMTLT).

ELECTROCHEMICAL IMPEDANCE SPECTROSCOPY STUDY OF AQUEOUS NA-ION BATTERY DEGRADATION

Aivaras Labžentis[1], Laurynas Staišiūnas[2], Linas Vilčiauskas[2]

[1]Faculty of Physics, Vilnius University, Lithuania
[2]Center for Physical Sciences and Technology, Saulėtekio al. 3, LT-10257 Vilnius, Lithuania
aivaras.labzentis@ff.stud.vu.lt

CANCELLED DUE TO COVID-19

Increasing energy consumption and changing people attitude towards more sustainable energy calls for new ways how to produce and store electricity [1]. One of the alternatives is the use of aqueous Na-ion batteries due to their low cost, environmental friendliness and durability. However, water based electrolytes suffer due to the limited electrochemical window of water and limited electrode material stability [1, 2].

The main goals of this study are to choose and investigate the effects of cell type and geometry to the Electrochemical Impedance Spectroscopy (EIS) measurements, record the EIS spectra of a negative Na-ion battery electrode during the galvanostatic charge/discharge cycling, fit the data using the equivalent circuit model and analyze the results in terms of electrode degradation mechanisms [3]. All the studied electrodes were developed in house using the NASICON–structured $Na_3Ti_2(PO_4)_3$ as active material and 1M Na_2SO_4(aq.) as electrolyte. All measurements were conducted at room temperature.

In the simulation an equivalent electrical circuit is used in order to fit the EIS results (Fig. 1). The data presented in Table 1 show the increase in one of the resistances (R_1) upon cycling, which correlates directly with the shrinking electrode charge capacity. This indicates the electrode degradation process caused by such processes as electrode material dissolution and subsequent deposition of certain blocking layer or corrosion of electrode component due to water decomposition reactions taking place. Nevertheless, the Coulombic efficiency does not deteriorate but actually increases with cycle number indicating a certain stabilization and corrosion inhibition processes.

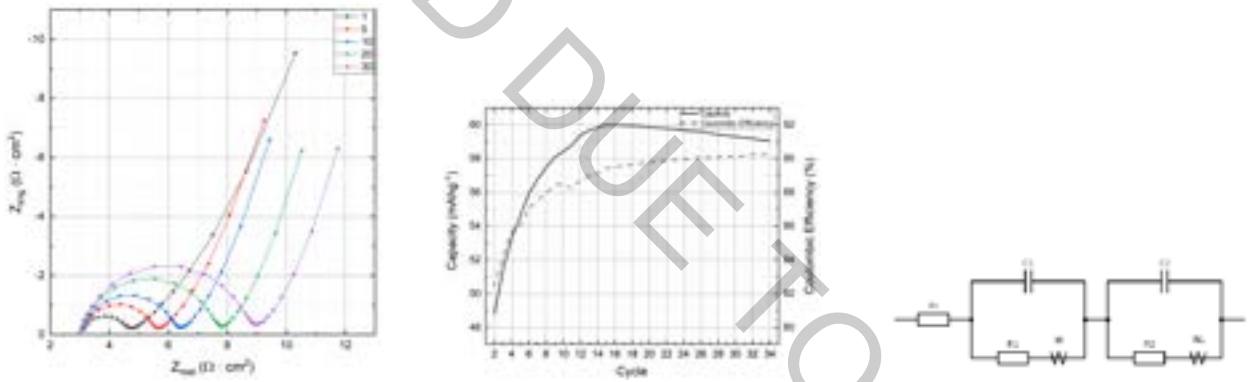

(a) (b) (c)

Fig. 1. Electrode degradation. (a) EIS change with cycle number, (b) charge capacity and Coulombic efficiency change with cycle number, (c) fitted electrical circuit.

Table 1. Fitted measurement data

Cycle No.	R_t	C_1	R_1	W	C_2	R_2	W_{or}	W_{oc}
	$\Omega\cdot cm^2$	F/cm^2	$\Omega\cdot cm^2$	$\Omega\cdot cm^2/s^{\frac{1}{2}}$	F/cm^2	$\Omega\cdot cm^2$	$\Omega\cdot cm^2/s^{\frac{1}{2}}$	$s^{\frac{1}{2}}$
1	3,15	$1{,}29\cdot10^{-4}$	0,43	3,69	$6{,}83\cdot10^{-6}$	1,32	0,90	0,52
5	3,12	$7{,}64\cdot10^{-5}$	0,77	2,74	$8{,}53\cdot10^{-6}$	1,65	0,79	0,48
10	3,11	$4{,}56\cdot10^{-5}$	1,37	2,34	$9{,}34\cdot10^{-6}$	1,77	0,78	0,49
20	3,08	$2{,}81\cdot10^{-5}$	2,74	2,13	$1{,}16\cdot10^{-5}$	1,74	0,89	0,57
30	3,07	$2{,}57\cdot10^{-5}$	3,74	2,20	$1{,}26\cdot10^{-5}$	1,82	1,04	0,68

Acknowledgements:
This project has received funding from the European Regional Development Fund (Project No. 01.2.2-LMT-K-718-02-0005) under grant agreement with the Research Council of Lithuania (LMTLT).

[1] J. Liu, C. Xu, Z. Chen, S. Ni, Z. X. Shen. Progress in aqueous rechargeable batteries, Green Energy & Environment 3 (1), 20-41 (2018).
[2] R. Demir-Cakan, M. R. Palacin, L. Croguennec, Rechargeable aqueous electrolyte batteries: from univalent to multivalent cation chemistry, Journal of Materials Chemistry A 7, 20519–20539 (2019).
[3] M. E. Orazem, B. Tribollet, Electrochemical Impedance Spectroscopy (Wiley, 2008).

INVESTIGATION OF COPPER SELENIDE THIN FILMS DEPOSITED USING THE SILAR METHOD AT DIFFERENT TEMPERATURES

Gediminas Jakubauskas, Neringa Petrašauskienė

Department of Physical and Inorganic Chemistry, Kaunas University of Technology, Lithuania
gediminas.jakubauskas@ktu.edu

Copper selenide belongs to I–VI compound semiconductor materials. Cu_xSe (x = 1-2) thin films have been one of the most studied in recent years, with stoichiometric (Cu_2Se, Cu_3Se_2, CuSe, and Cu_2Se) and non-stoichiometric ($Cu_{2-x}Se$) compositions exhibiting a continuous change of physical properties. Cu_xSe can been used in the fabrication of photovoltaic devices such as window materials, super ionic conductors, electro-optical devices, optical filters, thermo electric converters and photo electrochemical cells. Copper selenides can be formed on various substrates, such as glass, silicon, silicon oxide, titanium, various polymers, etc., using techniques, like chemical vapor deposition, chemical spray pyrolysis, atomic layer deposition or electrochemical deposition. All mentioned deposition methods usually require specialized equipment, vacuum, high temperature, use of electrolytes, it is hard to form layers across large surfaces, thus making them expensive and not suitable for all substrates.

Here is reported the preparation of electrically conductive Cu_xSe-PA films (PA – polyamide 6) by deposition of copper selenides from aqueous solutions on the PA film surface using Successive Ionic Layer Adsorption and Reaction (SILAR) method. This method used with the polymer differs from other methods, as it does not require specialized equipment or conditions, is cheap and simple, can be used at room temperatures. It has two stages: first – copper ions are adsorbed on polyamide surface from a precursor solution, containing copper ions, second – copper selenide layers are formed by treating the layer formed in the first stage with a solution containing selenium ions. The substrate is rinsed in distilled water after treatment in either solution.

Copper selenide thin films on the PA substrate were formed using the SILAR method at room temperature (20°C) and at 50°C. Their characterization was carried out through X-ray diffraction (XRD), scanning electron microscopy (SEM) and energy-dispersive X-ray spectroscopy (EDX).

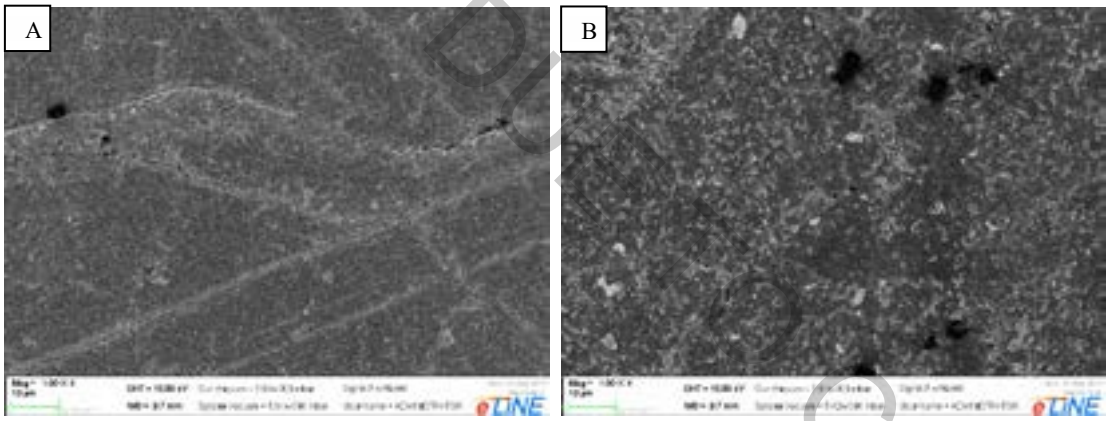

Fig. 1. SEM images of Cu_xSe layers deposited at A - 20°C and B - 50°C, magnified 1000 times

Observations about crystal size and homogeneity of Cu_xSe films can be made from the SEM images shown in Fig. 1. The size of the crystals deposited at 50°C is larger than the size of those deposited at 20°C. The film in image A appears to be more homogenous than that of image B, due to a smaller variation of crystal sizes. From these observations, it can be concluded that at higher temperatures the rate of Cu_xSe crystal growth increases more than the rate of formation of crystal nucleation sites.

EDX results show an overall higher amount of copper selenide deposited at 50°C than 20°C, with copper to selenium ratio being 1.6 and 1.5 respectively. XRD analysis is not sensitive enough to show what phases of copper selenides formed on the sample treated at 20°C, however $Cu_{2-x}Se$ phase is observed on the 50°C sample.

CANCELLED DUE TO COVID-19

MECHANOCHEMICAL APPROACH TO THE SYNTHESIS OF 2-UNSUBSTITUTED IMIDAZOLE *N*-OXIDES, CONVENIENT PRECURSORS OF NEW ALKOXYIMIDAZOL-2-YLIDENES (NHCS)

Grzegorz Mlostoń,* Małgorzata Celeda, Katarzyna Urbaniak

Department of Organic & Applied Chemistry, University of Łódź, Tamka 12, 91-403 Łódź, Poland
grzegorz.mloston@chemia.uni.lodz.pl

CANCELLED DUE TO COVID-19

2-Unsubstituted imidazole *N*-oxides of type **1** are known as useful precursors for the preparation of a wide range of imidazole derivatives [1]. Their *O*-alkylation, leading to imidazolium salts **2**, opens a convenient route to alkoxyimidazol-2-ylidenes **3**, which constitute a new group of nucleophilic carbenes NHCs [2,3] (Fig. 1).

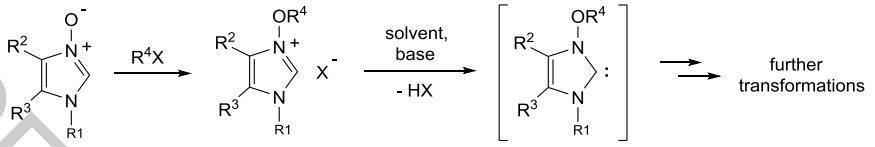

Fig. 1. In situ generation of alkoxy imidazol-2-ylidenes **3** starting with 2-unsubstituted imidazole *N*-oxides **1**.

The best known protocol for synthesis of **1** is heterocyclization of α-hydroxyiminoketones **4** by treatment with formaldimines **5** in boiling EtOH or in AcOH at room temperature [1,2]. In the first case, however, isomerization of the starting *N*-oxide to corresponding imidazol-2-one is a serious disadvantage. Moreover, this method can't be applied for formaldimines derived from aromatic primary amines. On the other hand, reactions performed in acetic acid require longer reaction times (an overnight protocol) and a multi-step workup.

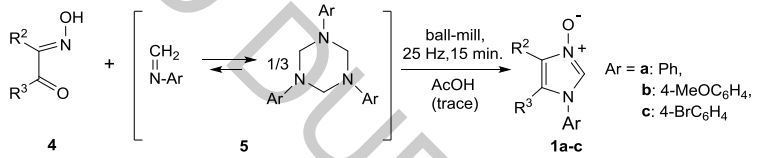

Fig. 2. Mechanochemical synthesis of N(1)-aryl functionalzed imidazole *N*-oxides **1**.

Now, we report mechanochemical approach to the synthesis of imidazole *N*-oxides **1** bearing aryl (Ar) substituent at the N(1). Ball milling of α-hydroxyiminoketone **4** with corresponding formaldimine **5** ($Ar\text{-}NH_2$) led to desired products **1a-c** in 69-80% yield (Scheme 2). The same protocol was applied for N(1)-alkyl substituted imidazole *N*-oxides **1** including optically active derivatives of *trans*-1,2-diaminocyclohexane [3].

Acknowledgement: Authors thank the National Science Center (Cracow, Poland) for generous support within the Beethoven-2 project (grant #2016/23/G/ST5/04115/l).

[1] G. Mlostoń, M. Jasiński, A. Wróblewska, and H. Heimgartner, Recent progress in the chemistry of 2-unsubstituted imidazole N-oxides, Curr. Org. Chem., **20**, 1359–1369 (2016).
[2] G. Mlostoń, M. Celeda, K. Urbaniak, M. Jasiński, V. Bakhonsky, P. R. Schreiner, H. Heimgartner, Synthesis and selected transformations of 2-unsubstituted 1-(adamantyloxy)imidazole 3-oxides: strightforward access to non-symmetric 1,3-dialkoxy imidazolium salts, Beilstein J. Org. Chem., **15**, 497–505 (2019).
[3] G. Mlostoń, M. Celeda, M. Jasiński, K. Urbaniak, P. J. Boratyński, P. R. Schreiner, H. Heimgartner, Synthesis 2-Unsubstituted imidazole *N*-oxides as novel precursors of chiral 3-alkoxyimidazol-2-ylidenes derived from *trans*-1,2-diaminocyclohexane and other chiral amino compounds Molecules, **24**, 4398 (2019).

UV-VIS IVVESTIGATION OF MIXED CADMIUM SULFIDE– CADMIUM TELLURIDE LAYERS ON POLYAMIDE 6 FORMED USING DIFFERENT WAYS OF PREPARING POLYAMIDE

Miglė Liudžiūtė[1], Klaudija Vaičiukynaitė[1], Skirma Žalenkienė[1], Rūta Stokienė[1]

[1]Department of Physical and Inorganic Chemistry of Kaunas University of Technology, Lithuania
migle.liudziute@ktu.edu

CANCELLED DUE TO COVID-19

Cadmium sulfide (CdS), cadmium telluride (CdTe) and cadmium selenide (CdSe) are three of the II–VI compounds that have played a diverse role in investigating and seeking to use phenomena involving the interaction of light with semiconductors. In their pristine form, the electrodes normally exhibit low light-to-electricity conversion efficiency [1].These compounds have been studied both as single crystal materials, and as thin-film materials [2].CdTe is a material with a high absorption coefficient [3] and is mainly used in solar cells, finds application in IR detectors, radiation detectors, electrooptic modulators [4]. Cadmium sulfide has wide direct bandgap and high stability [5]. CdS is a semiconductor, which has a worldwide interest in photocatalytic applications [6].

Polyamide 6 films used in this study were obtained from Ensinger (Germany). PA 6 film was 500 μm thick with the density of 1.13 g/cm^3. Prior to the experiments, PA film 15×70 mm in sizes were boiled in distilled water for 2 h (Sample 1). Other samples were stored in concentrated acetic acid at 20 ° C for 0.5 h (Sample 2). Then they were dried using a filter paper and kept in a desiccator over anhydrous $CaCl_2$. The salts of potassium telluropentathionate ($K_2TeS_4O_6 \cdot 1.5H_2O$), were prepared and chemically analyzed according to published procedure [7]. In the first stage, the PA 6 films were chalcogenized from 1.0 to 5 h at 20 ºC, using a continually stirred acidified (0.2 mol·dm^{-3} HCl) 0.1 mol·dm^{-3} solution of $K_2TeS_4O_6$. In the second stage, the samples of chalcogenized PA were treated with the 0.1 mol·dm^{-3} solution of cadmium acetate, ($Cd(CH_3COO)_2 \cdot 2H_2O$), for 10 min at the temperature 80 ºC.

UV-VIS spectra were recorded on a Spectronic^R Genesys^{TM} 8 UV/VIS spectrophotometer with compensation of the absorption of PA 6, the range of 200–800 nm.

UV-VIS absorption spectral analysis of the chalcogenated PA 6 films showed that the absorbance of polyamide 6, sample 1 was significantly lower than PA 6 sample 2, which absorbs and diffuses more telluropentathionate, $TeS_4O_6^{2-}$, ions into the films thus treated [8].

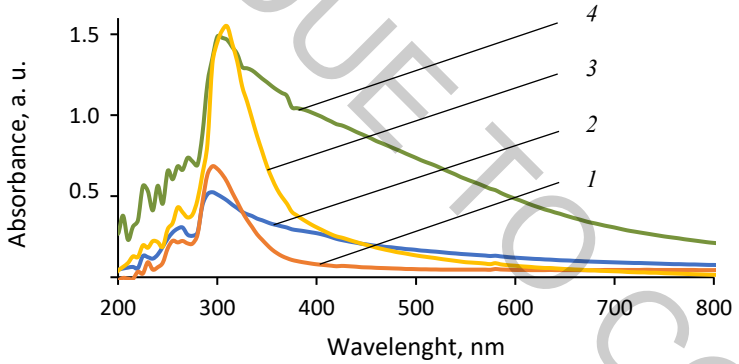

Fig.1. UV-VIS spektra of PA 6 film chalcogenized in $K_2TeS_4O_6$ solution for 5 h at 20 ºC, and then treated in $Cd(CH_3COO)_2 \cdot 2H_2O$ solution: 1, 2 – sample 1; 3, 4 – sample 2

After interaction of the chalcogenated PA 6 with cadmium ions, peaks at 220, 245 and 260 nm are observed in the UV–VIS spectra. The absorption maximum at 295-310 nm is slightly lower in intensity and significantly wider (Fig. 1). Sample 1 after interaction with $Cd(CH_3COO)_2 \cdot 2H_2O$, reached peak intensities at 0.275–0.593 nm. Otherwise sample 2 – has more intense peaks – from 0.767 to 1.668 nm. These changes in absorption are thought to indicate the formation of cadmium sulfide-cadmium telluride following the interaction of chalcogenated PA with cadmium ions.

[1] Ahed Zyoud, et. al, Electrochemically and chemically deposited polycrystalline CdSe electrodes with high photoelectrochemical performance by recycling from waste films, Materials Science in Semiconductor Processing Vol. 107. (2019)
[2] R. H. Bube, Cadmium Sulfide and Telluride, Encyclopedia of Materials: Science and Technology (second edition), p.873-879.(2001)
[3] J. A. Ríos-González, et. al, Inducing a level inside of CdTe bandgap doping with Sn using a co-sublimation technique by CSS, Materials Science in Semiconductor Processing Vol. 107. (2019)
[4] Bruce A. Fowler, Chapter 3 Toxicology of E-Waste Chemicals-Mechanisms of Action, Electronic Waste, p. 33-54 (2017)
[5] M. Aslam Manthrammel, et. al, Facile spray pyrolysis fabrication of Al:CdS thin films and their key linear and third order nonlinear optical analysis for optoelectronic applications, Optical Materials Vol. 100. (2019)
[6] J. Gobinath,P. Gowthaman et al, Effect of annealing temperature on the structural, optical and dye degradation properties of cadmium sulfide thin films, Materials Today: Proceedings. (2020)
[7] Foss O. Salts of Monotelluropentathionic Acid // Acta Chemica Scandinavica. Vol. 3, p. 708–716. (1949)
[8] L. Kapočius, G. Garlaitė, S. Žalenkienė. Poliamido 6 paviršiaus paruošimas kadmio telūrido sluoksnių sudarymui, Proceedings of the national scientific students' conference "Chemistry and chemical technology 2019". Vilnius University, 116-119 (2019).

SYNTHESIS AND INVESTIGATION OF ORGANOMETALLIC PRECURSORS USED FOR COPPER THIOCYANATE LAYER FORMATION

Mantas Marčinskas, Tadas Malinauskas

Faculty of Chemical Technology, Kaunas University of Technology, Lithuania
mantas.marcinskas@ktu.edu

Growing population is always linked to the increases in energy demands. Fossil fuels – the main source of energy is rather limited, therefore more and more attention is paid to the renewable energy sources. Among them, photovoltaics can be considered as one of the most promising renewable energy technologies to be developed [1]. Up to now, silicon-based solar cells (Si-SC) are dominating the photovoltaic devices industry, well-known manufacturing processes, reliable efficiencies, long-term stability can be named as the main reasons [2]. However, Si-SC production costs are still relatively high, therefore these devices cannot fully compete and replace fossil fuels [3].

Perovskite solar cells (PSCs) can be considered as a possible future competitor for Si-SC. The crucial component of PSC – perovskite offers a lot of benefits, such as: variety of perovskite coating methods, light absorption in a wide spectrum, good conductivity and tolerance to defects [1]. Efficient PSCs usually contain additional charge transporting semiconductors of which hole transporting materials (HTMs) play important role both to the power conversion efficiency (PCE) and the stability of perovskite. Yet, the most popular HTMs are organic small molecules and polymers, which are often relatively expensive and require to be doped to increase their conductivity. As a consequence, presence of dopants decreases the stability of PSCs, which is one of the largest barriers towards PSC commercialization [4].

Inorganic HTMs can be promising candidates to replace organic analogues, since their conductivity is usually significantly higher, therefore they don't need to be doped. Most of them do not absorb light in the visible and infrared regions, therefore the absorption of inorganic HTMs do not interfere or overlap with the perovskite absorption. Additionally, inorganic semiconductors are considerably less expensive, which is important for the solar cells manufacturers. So far, NiO_x, CuSCN, CuO_x, V_2O_5, CuS and MoO_2 were investigated as *p*-type inorganic semiconductors for application in PSCs. Among them, one of the best efficiency results have been achieved using CuSCN, reaching 20.4%. However, CuSCN can be only dissolved in ammonia solution and diethyl sulfide (DES); both solvents affect perovskite negatively and induce degradation by damaging or dissolving its structure components [5].

In this work a series of organometallic complexes were synthesized as precursors of CuSCN. All synthesized precursors were obtained in one-step synthesis, purified by quick and inexpensive methods and shown relatively low thermal decomposition temperatures. The best solubility in different organic solvents was demonstrated by CuSCN complexes containing aliphatic amines and 4-(5-nonyl)-pyridine ligands.

The solutions of different precursors were deposited on the glass surface via spin-coating. Subsequently, the formed layers were heated above the relevant organometallic compound decomposition temperature, initiating organic part evaporation and the layer of CuSCN was obtained.

This research was funded by the European Social Fund under the No 09.3.3-LMT-K-712-16-0098 „Development of Competences of Scientists, other Researchers and Students through Practical Research Activities" measure.

[1] R. Wang, M. Mujahid, Y. Duan, Z. K. Wang, J. Xue, Y. Yang. A Review of Perovskites Solar Cell stability. *Adv. Funct. Mater.* 2019, 29, 47, 1808843.
[2] A. Bozzola, P. Kowalczewski, M. Liscidini, L. Redorici. Silicon Solar Cells: Towards the Efficiency Limits. *Advances in Physics: X*. 2019, 4, 1, 1548305.
[3] A. Louwen, W. Sark, R. Schropp, A. Faaij. A Cost Roadmap for Silicon Heterojunction Solar Cells. *Sol. Energy Mater. Sol. Cells*. 2016, 147, 295-314.
[4] L. Calió, S. Kazim, M. Grätzel, S. Ahmad. Hole-Transport Materials for Perovskite Solar Cells. *Angew. Chem. Int. Ed*. 2016, 55, 47, 14522-14545
[5] Y. Yang, N. D. Pham, D. Yao, H. Zhu, P. Yarlagadda, X. Wang. Inorganic p-type Semiconductors and Carbon Materials Based Hole Transport Materials for Perovskite Solar Cells. *Chin. Chem. Lett.* 29, 8, 1242-1250.

CANCELLED DUE TO COVID-19

OCCURRENCE AND VARIATION OF SOME METALLIC ELEMENTS IN LINGONBERRY *(VACCINIUM VITIS-IDAEA L.)* AND SOIL

Karina Babiča, Zenta Balcerbule, Vitālijs Lazarenko, Māris Bērtiņš

University of Latvia, Faculty of Chemistry, Jelgavas iela 1, Riga, Latvia
babichkarinaa@gmail.com

The geographic distribution of lingonberries *(Vaccinium vitis-idaea L.)* in the world extends from Scandinavia to North America. In 1962, the first lingonberry plantations were created in Sweden for research studies. The climatic conditions in Latvia are favourable for the growth of these plants. The chemical composition of lingonberries is characterized by a diverse content of macro and micro elements.

The use of various berries, both wild and cultivated, in medicine, food production, pharmacology, and cosmetology are becoming increasingly popular. In recent years, the use of lingonberries in the production of medicinal products and nutritional supplements has been actively researched, not only lingonberry berries but also their components (leaves and roots) are being analysed.

The aim of our research was to evaluate the variation of some metallic elements in lingonberries *(Vaccinium vitis-idaea L.)* depending on their growing place and soil. The roots of lingonberry have also been collected to study the transfer of metallic elements from soil to plants. Lingonberry (berries and roots) and soil samples were collected in September 2019 in two different areas:

1) Garkane pines forest. In this area are located Riga-Lugazi railway line, where passenger trains pass through);
2) Vecumu forest in Ziguri parish. The territory is located ~8 km from the Latvia-Russia border.

The lingonberry samples were air-dried and digested using dry and microwave assisted digestion method.

The forest soil is very acidic (pH_{KCl} 3.4 – 4.0) at the places of lingonberry growth sites. The low content of Zn and Cu in the soil indicates the mobility of these elements and the leaching into the deeper layers of the soil.

Iron content of digested lingonberry samples and soil was determined both photometrically and by flame atomic absorption spectrometry (FAAS). Iron content in soil varies in wide range in the Garkalne and Vecumu forest (8 $mg \cdot kg^{-1}$ to 1250 $mg \cdot kg^{-1}$), but in lingonberries iron content is similar 10 $mg \cdot kg^{-1}$.

Zinc and copper content were determined by flame atomic absorption spectrometry. The content of copper and zinc in lingonberries are similar and does not depend from sampling site and soil chemical composition. Copper and zinc content in lingonberries are as follows: copper ~4 $mg \cdot kg^{-1}$ and zinc ~10 $mg \cdot kg^{-1}$. For determination of other microelements, the ICP-MS analysis method was used.

CANCELLED DUE TO COVID-19

VARIATIONS OF SULPHUR AND METALLIC ELEMENTS IN LICHENS *(XANTHORIA PARIETINA)* IN THE DIFFERENT PARTS OF RIGA

Viktorija Krjukoviča, Zenta Balcerbule, Vitālijs Lazarenko, Māris Bērtiņš

University of Latvia, Faculty of Chemistry, Jelgavas iela 1, Riga, Latvia
viktorija.krjukovica95@gmail.com

Lichens *(lichenes)* are symbiotic organisms which consist of two organic parts: fungi and algae or cyanobacteria. They are considered as one of the slowest growing plants with growth rate 1-30 mm·year^{-1}. Lichens absorb water and nutrients directly from air and therefore, they are sensitive to air pollution. Sulphur dioxide (SO_2), heavy and radioactive metallic elements are considered toxic which may negatively affect further development of lichens.

Lichens are widely used as bioindicators for monitoring the status of the environment, especially quality of the air. Air quality can be estimated not only by diversity of lichen species but also by their chemical composition. The more polluted the air is, the higher concentration of chemical elements will be found in the lichens.

(Xanthoria parietina) is foliose (leafy) lichen which can be found in wide geographical area. They often are spotted on tree branches and barks and belong to the one of durable lichen species whose growth is affected only by high air pollution level.

The aim of our research was to evaluate sulphur and metallic element content in foliose lichens *(Xanthoria parietina)* in the different parts of Riga. Lichens samples were collected on different tree species with similar bark structure ~1-2 m above the ground. For the analyses had chosen three different locations:

1. Freeport of Riga, Kundzinsala;
2. Residential area, Sarkandaugava;
3. Mezaparks (green area of the city).

During the research it was important to evaluate the level of pollution in the Freeport of Riga. This area is characterized by intensive coal cargo transportation, both by ships and trucks. Therefore, high air pollution level in this area could significantly affect other neighbourhoods depending on wind direction. When analysing lichens, it was important to evaluate how far dust from the coal storage area could spread to adjacent areas.

Unwashed lichens were air-dried at 50 ºC for 24 h, homogenized and digested in the mixture of HNO_3:H_2O_2 using microwave assisted digestion method. Metallic element content in lichens was determined by ICP-MS analysis method but sulphur was determined as sulphate ions by turbidimetry.

The determined sulphur content in lichens in the territory of the Freeport of Riga is ~5-7 times higher than in other areas. The determined Ca, Mn, Fe and Cu content in lichens from the Freeport of Riga is ~2 times higher than Sarkandaugava and Mezaparks.

The content of sulphur and iron content in lichens that were sampled from the Freeport of Riga varies in a wide range, whereas in the territory of Mezaparks determined concentrations are quite similar.

There is observed tendency that As and Pb content in the analysed lichens decreases in the following order: Freeport of Riga → residential area, Sarkandaugava → Mezaparks.

CANCELLED DUE TO COVID-19

SYNTHESIS OF SILVER CORE-SILICA SHELL NANOPARTICLES UNDER MICROWAVE IRRADIATION

Edita Daublytė[1], Agnė Zdaniauskienė[2], Tatjana Charkova[2]

[1] Faculty of Chemistry and Geosciences, Vilnius University, Lithuania
[2] Department of Organic Chemistry, Center for Physical Sciences and Technology, Lithuania
editadaublyte@gmail.com

CANCELLED DUE TO COVID-19

The silica shell-isolated nanoparticles spread over the surface of sample material are widely used in various fields such as nanoelectronics, biomedicine or environment science. Shell-isolated nanoparticle-enhanced Raman spectroscopy (SHINERS) is one of the most powerful tool to investigate various materials with diverse morphologies [1]. Typically, such nanoparticles are prepared by reduction with sodium citrate in boiling aqueous medium [2]. We have successfully modified the most used synthesis protocol [2, 3] and applied it for microwave synthesis (Fig. 1). This more convenient, efficient, fast method of synthesis allows to obtain 90 ± 5 nm size silver nanoparticles with 3 nm of silica shell ($Ag@SiO_2$).

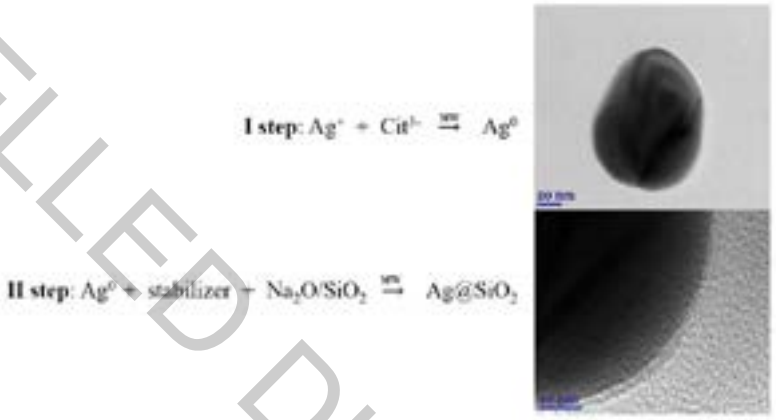

Fig. 1. Synthesis steps and HR-TEM images of Ag and $Ag@SiO_2$ nanoparticles.

In order to show that synthesized $Ag@SiO_2$ nanoparticles enhance Raman signal, a self-assembled monolayer of 4-mercaptobenzoic acid (MBA) was formed onto smooth gold surface. $Ag@SiO_2$ nanoparticles allowed to collect significantly enhanced SHINERS spectra of MBA compared to the Raman spectra (Fig. 2). Also, it was observed that there were no additional bands from impurities of the synthesis in SHINERS spectra of MBA.

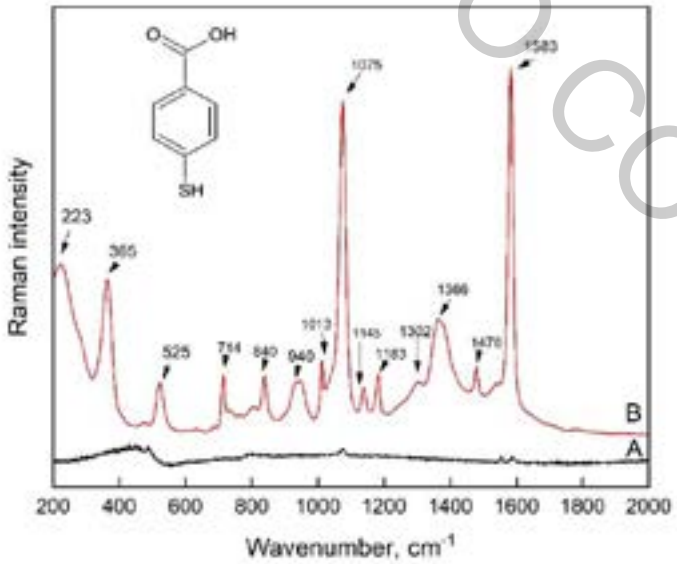

Fig. 2. Raman spectrum of MBA adsorbed on smooth Au surface without nanoparticles (A – black), and SHINERS spectra of MBA with $Ag@SiO_2$ nanoparticles (B – red).

[1] J.-F. Li, Y.-J. Zhang et al., Core–Shell Nanoparticle-Enhanced Raman Spectroscopy, Chem. Rev. **117**, 5002-5069 (2017).
[2] P. C. Lee, D. Meisel, Adsorption and surface-enhanced Raman of dyes on silver and gold sols, J. Phys. Chem. **86**, 3391-3395 (1982).
[3] H. B. Abdulrahman, J. Krajczewski, A. Kudelski, Modification of surfaces of silver nanoparticles for controlled deposition of silicon, manganese, and titanium dioxides, Appl. Surf. Sci. B **427**, 334-339 (2018).

SYNTHESIS AND CHARACTERISTICS OF NEW ORGANIC SEMICONDUCTORS WITH *N*-CARBAZOLYL-BASED CHROMOPHORES

Povilas Luizys[1], Maryte Daskeviciene[1], Vygintas Jankauskas[2], Egidijus Kamarauskas[2]

[1]Department of Organic Chemistry, Kaunas University of Technology, Lithuania
[2] Institute of Chemical Physics, Vilnius University, Lithuania
povilas.luizys@ktu.lt

CANCELLED DUE TO COVID-19

Global warming and environmental damage caused by burning of fossil fuels are increasing world attention to renewable energy sources and one of the most promising is solar energy. Solar energy, which is converted into electricity via different types of solar cells, could theoretically satisfy the energy needs of mankind. Therefore, in many countries, development of technologies utilizing solar energy is stimulated in various ways. Silicon solar cells are currently the most widely used on the market. Because of their high production costs, intensive search of alternatives is underway. One of them is perovskite solar cells, which just in a last decade have become a subject of great interest in the development of next generation solar cells that have already exceeded 25,2% power conversion efficiency [1]. Perovskite solar cells are characterized by simplicity of construction and inexpensive raw materials. Commercialization of the perovskite solar cell technology is hindered by drawbacks which need to be resolved. One of them is that hole transporting organic semiconductor spiro-OMeTAD crystallizes in the device over the time, thus reducing its efficiency [2], furthermore additives are needed to increase the conductivity, which may cause the device degradation. Therefore, the search for new efficient organic semiconductors remains highly relevant.

In this work, new organic semiconductors utilizing one, two, three and four *N*-carbazolyl chromophores (Fig.1) were synthesized to function as hole transporting materials in perovskite solar cells.

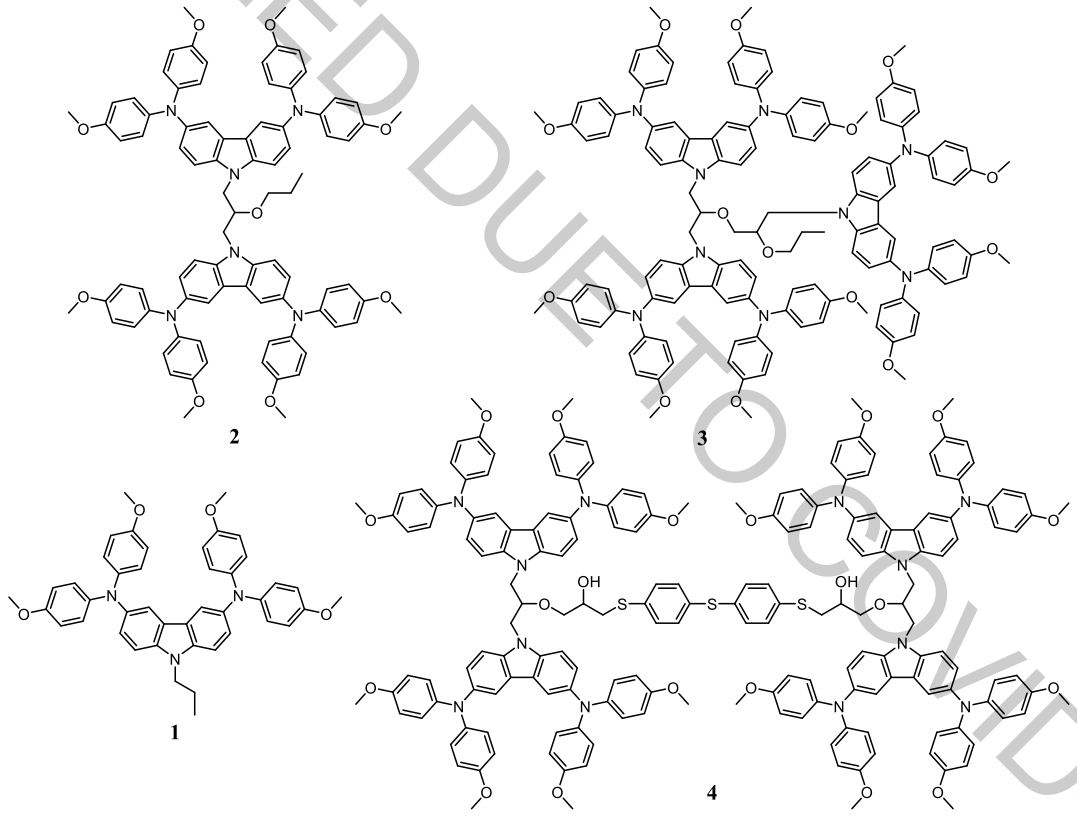

Fig. 1. Structures of synthesized organic semiconductors with carbazolyl chromophores.

New organic compounds were obtained via step-by-step synthesis. The structure of the newly synthesized semiconductors was confirmed by ^{1}H NMR, ^{13}C NMR and IR spectroscopy. Thermal properties of target compounds proved that they are molecular glasses, demonstrate stable amorphous state and are thermally stable at relatively high temperatures. Ionization potential measurement results (4,92 - 5,16 eV) indicate that the HOMO energy level of the synthesized products is compatible with the valence band of the photoactive perovskite layer. Compounds **2**, **3**, and **4** exhibit sufficient hole mobility for their use in construction of solar cells.

[1] Best Research-Cell Efficiencies, https://www.nrel.gov/pv/assets/pdfs/best-research-cell-efficiencies.20190802.pdf (accessed 2020-01-26), (2019).
[2] Tobat P. I. Saragi, T. Spehr, A. Siebert et al., Spiro compounds for organic optoelectronics, Chem. Rev. 107, 1011-1065 (2007).

SELF-ASSEMBLED MONOLAYERS BASED ON FLAVIN COFACTOR FOR SENSING OF GLUCOSE

Delianas Palinauskas[1], Gintautas Bagdžiūnas[1,2]

[1] Department of Material Science and Electrical Engineering, Center for Physical Sciences and Technology, Sauletekio av. 3, Lithuania

[2] Institute of Biochemistry, Department of Bioanalysis, Life Sciences Centre, Vilnius University, Sauletekio av. 7, LT-10223, Vilnius, Lithuania

delianas.palinauskas@chgf.vu.lt

CANCELLED DUE TO COVID-19

The recognition of bioanalyte toward self-assembled monolayers (SAMs) mostly on conducting surfaces can be employed as the sensing element of an electrochemical sensor. These SAMs as 2D layers seem to be the ideal approach of tailoring a surface and controlling electron transfer, which is the basis of an electrochemical sensor [1]. On the other hand, a number of experimental techniques [2,3] and theoretical methodologies [4] have been used for sensing of glucose in our group. In turn, flavin function group in flavin adenine dinucleotide (FAD) is a redox-active coenzyme associated with various proteins such as glucose oxidase, which is oxidized glucose to gluconic acid [2, 3].

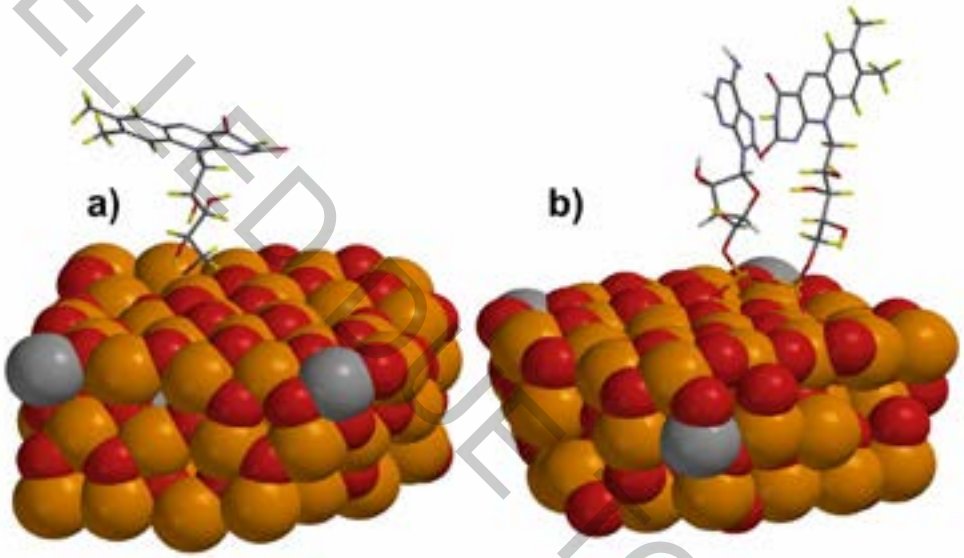

Fig. 1. Optimized molecules of RFL (a) and FAD (b) on surface of ITO.

Herein, for the first time, an electrochemical investigation of SAMs based on riboflavin (RFL), also known as vitamin B_2, and flavin adenine dinucleotide (FAD) on indium tin oxide (ITO) coated glass as the working electrodes will be presented. These monolayers were studied by using the cyclo voltamperometry (CV), chronoamperometry, Raman spectroscopy, as well as theoretical methods. Prepared SAMs based on these molecules were employed for sensing of glucose. We hope that this work will be useful for further research of electrochemistry of SAMs. These promising studies are ongoing in our scientific group.

Acknowledgments: Financial support from the Research Council of Lithuania a grant No. 09.3.3.-LMT-K-712-16-0260 is gratefully acknowledged.

[1] Mandler, D.; Kraus-Ophir, S. Self-Assembled Monolayers (SAMs) for Electrochemical Sensing. J Solid State Electrochem 2011, 15 (7–8), 1535–1558.

[2] Žukauskas, Š.; Ramanavičius, A.; Bagdžiūnas, G. Organic Semiconductors with Carbazole and Triphenylamine Moieties for Glucose Oxidase-Based Biosensors. J. Electrochem. Soc. 2019, 166 (6), B316–B321.

[3] Bagdžiūnas, G.; Žukauskas, Š.; Ramanavičius, A. Insights into a Hole Transfer Mechanism between Glucose Oxidase and a p-Type Organic Semiconductor. Biosensors and Bioelectronics 2018, 102, 449–455.

[4] Bagdžiūnas, G.; Ramanavičius, A. Towards Direct Enzyme Wiring: A Theoretical Investigation of Charge Carrier Transfer Mechanisms between Glucose Oxidase and Organic Semiconductors. Phys. Chem. Chem. Phys. 2019, 21 (6), 2968–2976.

PHOTOPHYSICAL STUDY OF ANTICANCER DRUG TIRAPAZAMINE BASED COMPOUNDS

Kamilė Tulaitė[1], Justina Jovaišaitė[1], Jelena Tamulienė[2], Jonas Šarlauskas[3], Narimantas Čėnas[3] and Saulius Juršėnas[1]

[1]Institute of Photonics and Nanotechnology, Faculty of Physics, Vilnius University, Lithuania
[2]Institute of Theoretical Physics and Astronomy, Vilnius University, Lithuania
[3]Institute of Biochemistry, Life Sciences Center, Vilnius University, Lithuania
kamile.tulaite@ff.stud.vu.lt

Tirapazamine (TPZ) is a compound in the benzotriazine-di-N-oxide class of cytotoxins [1]. It is an anticancer drug, that selectively acts in hypoxic (low oxygen levels) conditions that are found in solid tumors. Tumor hypoxia is still a big challenge in the treatment of cancer as the hypoxic regions are resistant to the effect of radiation therapy and other anticancer drugs [2]. During the treatment stage, TPZ compound can attach oxygen to its molecule and so reduce to a radical that causes DNA double-strand, single-strand breaks and base damage [3]. The use of TPZ derivatives in medicine has been widely investigated for several decades. However, the photophysical examination of these compounds remains scarce. In order to successfully understand their usability, more studies of TPZ optical properties need to be performed.

Here we present a photophysical study of tirapazamine based derivatives, that have no oxygen atoms, one double bonded oxygen atoms at N1 position of tirapazamine core or two double bonded oxygen atoms at N1 and N4 positions. In addition, the substituents at C8 were also altered. The optical properties of TPZ compounds were tested in polar environment: ethylacetate, acetonitrile and 1 v/v% dimethylsulfoxide (DMSO)/water mixture. Various characterization techniques, such as steady-state absorption and fluorescence and time-resolved fluorescence spectroscopy, were employed. Photophysical properties of TPZ compounds are changing dramatically in the presence of one double bonded oxygen atom and can be controlled by the different substituents at C8. Furthermore, another interesting feature is observed as the fluorescence quantum yields tend to increase in solvent of higher polarity. The experiments in DMSO/water mixture also gave promising results as sufficient fluorescence quantum yields were recorded. This may allow using new TPZ derivatives for the applications in biological systems.

[1] M. J. Done and J. M. Brown, Tumor-specific, Schedule-dependent Interaction between Tirapazamine (SR 4233) and Cisplatin, Cancer Res., **53**, 4633–4636 (1993).
[2] S. B. Reddy and S. K. Williamson, Tirapazamine: A novel agent targeting hypoxic tumor cells, Expert Opinion on Investigational Drugs, **18**, 77–87 (2009) .
[3] G. D. Jones and M. Weinfeld, Dual action of tirapazamine in the induction of DNA strand breaks., Cancer Res., **56**, 1584–90 (1996).

CANCELLED DUE TO COVID-19

TRACING STABLE CARBON ISOTOPE VARIATIONS IN LAKE DRUKSIAI

Laurynas Butkus[1], Rūta Barisevičiūtė[1], Žilvinas Ežerinskis[1], Justina Šapolaitė[1], Evaldas Maceika[1], Algirdas Pabedinskas[1], Andrius Garbaras[1], Jonas Mažeika[2], Vytautas Rakauskas[2], Rūta Druteikienė[1], Vidmantas Remeikis[1]

[1] Center for Physical Sciences and Technology, Vilnius, Lithuania
[2] Nature Research Centre, Vilnius, Lithuania
laurynas.butkus@ftmc.lt

CANCELLED DUE TO COVID-19

According to the Intergovernmental Panel on Climate Change (IPCC), the global mean temperature is likely to increase by 1.8-4.8 degrees C by 2100 [1]. Rising global temperature will have an impact on water bodies, such as oceans, lakes, etc. As a result, higher temperatures could cause an increase of eutrophication in lakes and induce major changes in the ecosystem of a water body.

During the period 1983-2004, Lake Druksiai was used as the source of cooling water for the Ignalina Nuclear Power Plant (INPP). This raised the average monthly surface temperature of the lake by 3-4 °C [2].

The aim of this research was to analyze the variations of stable carbon isotope concentrations in the Lake Druksiai due to anthropogenic influence. The lake sediment and vendace (*C. albula*) scale samples were collected from the Druksiai lake. This species of pelagic fish was chosen because it was proved by earlier investigations that the planktivorous vendace feeds exclusively on zooplankton and a relatively short food chain (dissolved inorganic carbon (DIC) → phytoplankton → zooplankton → vendace) is expected. Thus, fish scales reflect averaged $\delta^{13}C$ values of 2 years in DIC of the lake water. ABA (acid-base-acid) chemical pretreatment procedure was used to extract humin (HM) and humic acid (HA) fractions from the sediments. $\delta^{13}C$ measurements in the lake sediment organic fractions and vendace scale samples were performed using the Thermo Flash EA 1112 elemental analyzer connected to the Thermo Scientific Delta V Advantage isotope ratio mass spectrometer.

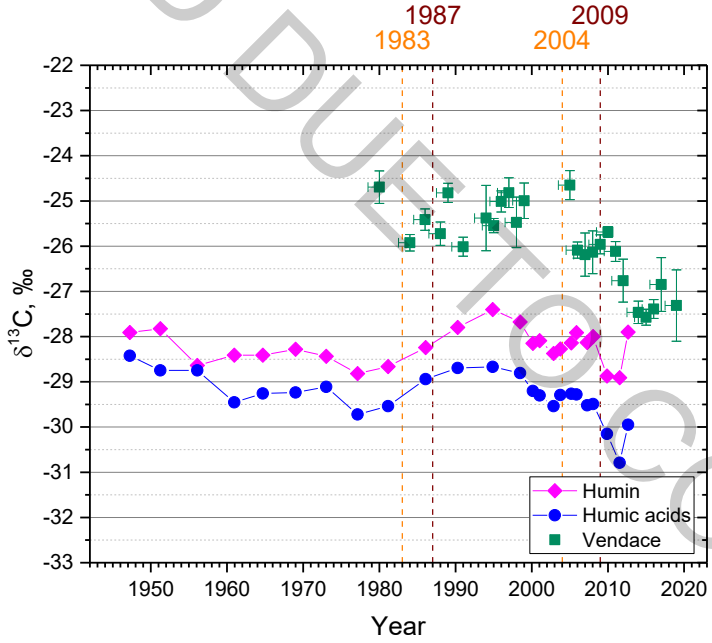

Fig. 1. Temporal $\delta^{13}C$ variations in the Lake Druksiai

$\delta^{13}C$ measurements in humin and humic acid fractions (Fig. 1) have shown that eutrophication of the lake caused an increase in $\delta^{13}C$ values of the lake sediments (1983-1995). In 1995, there was a change in predominant aquatic plants (shift from phytoplankton to submerged macrophytes) of the Lake Druksiai which caused $\delta^{13}C$ in sediments to decrease. Since 2005, stable carbon isotope concentration in both sediments and fish samples follow the same trend: during 2005-2009, $\delta^{13}C$ values are constant and after the shutdown of the INPP in 2009 the $\delta^{13}C$ values are decreasing. The reduction of thermal and chemical pollution significantly reduced the impact of these local effects on the ecosystem of Lake Druksiai.

[1] Intergovernmental Panel on Climate Change, „Climate Change 2014: Synthesis Report. Contribution of Working Groups I, II and III to the Fifth Assessment Report of the Intergovernmental Panel on Climate Change“, 2014.

[2] P. Meire, M. Coenen, C. Lombardo, M. Robba, ir R. Sacile, Sud., „Integrated Water Management“, t. 80, Dordrecht: Springer Netherlands, 2008.

XRD AND EDX STUDIES OF TIN (II) SULFIDE FILMS FORMED AT DIFFERENT pH CONDITIONS

Asta Bronušienė, Ingrida Ancutienė

Department of Physical and Inorganic Chemistry, Kaunas University of Technology, Lithuania
assta09@gmail.com

Metal chalcogenides are important because of their physical, chemical, optical properties and extensive potential applications in a lot of research areas [1]. Because of their different types of morphology, metal chalcogenides are applied for solar cells, Li-ion battery, Na-ion battery, photodetector, gas sensor and one of the newest application – ethanol gas sensor [1], [2], [3]. Tin compounds are abundant in nature and relatively cheap. For the fabrication is not needful expensive materials and toxic conditions.

The preparation of tin(II) sulfide was made using SILAR method. This method have some advantages, such as simplicity, easy to control the thickness and the composition of the films. For the synthesis of SnS films as a substrate FTO glass slide was used. Glass slides were ultrasonically cleaned in acetone at 40 °C, then washed with water and dried in air. For the SILAR cycles as a cationic precursor 0.1M tin(II) chloride acidic with a pH=1.5 (marked ac.) or alkaline solution with a pH=8 (marked al.) at 40 °C was used. As an anionic precursor 0.1M sodium sulfide solution at 40 °C was used. Firstly pre-cleaned substrate was immersed in the cationic precursor for 30s and tin ions adsorbed on the top of the substrate. Then sample was immersed in the anionic precursor for 30s, where sulfide ions react with adsorbed tin ions, and lastly in room temperature distilled water for 20s. 20 such deposition cycles were repeated in order to get adherent films. The last step was dip in the cationic precursor for 30s, then washed with distilled water and dried in air. The XRD technique was carried out by using a Bruker AXS D8 Advance diffractometer. EDX analysis was carried out using QUANTAX with X-Flash Detector 3001 and ESPRIT software.

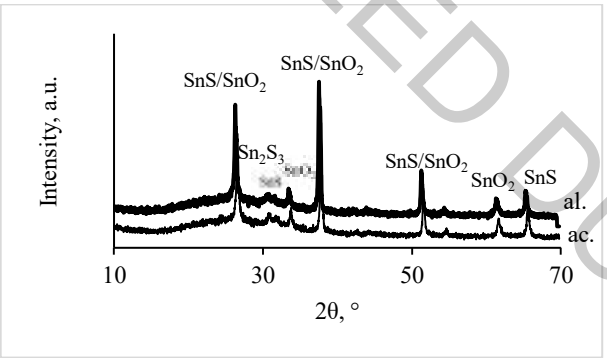

Fig. 1. X-Ray diffractograms of formed layers.

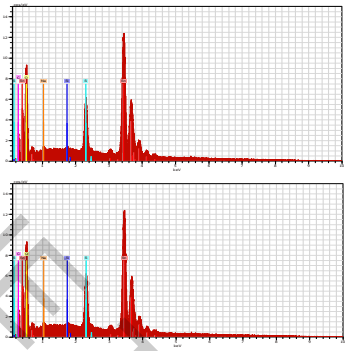

Fig. 2. EDX spectra: on the top sample ac, on the bottom sample al.

Figure 1 shows the results of X-Ray diffractions analysis and here it could be seen that the phase composition of both samples is very similar. The most intensive peak is at 2θ=37.8° and assigned to SnS (JCPDS card number 83-47). This peak also could be attributed to SnO_2 (JCPDS card number 46-1088), which is on the glass slide. Other peaks with a similar situation are at 2θ=26.59 and 51.5°. There are two small peaks at 2θ=31.8 and 65.5°, assigned to SnS. Both samples have one peak at 2θ=30.8°, assigned to Sn_2S_3 (JCPDS card number 72-31). Based on the article [4], it is possible to get tin(III) sulfide at almost room temperature. From diffractograms it is clearly seen that using the cationic precursor alkaline solution the peaks of SnS are a little bit more intensive than by the use of acidic cationic solution.

Figure 2 shows the EDX results of both samples. There are two high peaks of tin and sulfur, which clearly show the formation of tin sulfides. Also, there is the peak of oxygen, showing the existence of tin oxide, which is on the top of the substrate. There also is a very small amount of sodium, left from the anionic precursor.

Based on XRD analysis it can be concluded that there is no strong difference between tin(II) chloride solution pH in order to get tin(II) sulfide films. The main products are the same, but the peaks of target products are a little bit higher using the alkaline solution of cationic precursor.

[1] C. Rana, S. R. Bera, and S. Saha, "Growth of SnS nanoparticles and its ability as ethanol gas sensor," *J. Mater. Sci. Mater. Electron.*, vol. 30, no. 3, pp. 2016–2029, Feb. 2019.

[2] W. Wang, L. Shi, D. Lan, and Q. Li, "Improving cycle stability of SnS anode for sodium-ion batteries by limiting Sn agglomeration," *J. Power Sources*, vol. 377, no. August 2017, pp. 1–6, 2018.

[3] M. F. Afsar, M. A. Rafiq, and A. I. Y. Tok, "Two-dimensional SnS nanoflakes: synthesis and application to acetone and alcohol sensors," *RSC Adv.*, vol. 7, no. 35, pp. 21556–21566, Apr. 2017.

[4] E. Güneri, F. Göde, B. Boyarbay, and C. Gümüş, "Structural and optical studies of chemically deposited Sn2S3 thin films," *Mater. Res. Bull.*, vol. 47, no. 11, pp. 3738–3742, Nov. 2012.

CORRECTED PUBLISHED 19

SYNTHESIS OF NEW DYES FOR THE DETECTION OF MERCAPTO AMINO ACIDS

Sarune Daskeviciute, Vytautas Getautis

Department of Organic Chemistry, Kaunas University of Technology, Lithuania
sarune.daskeviciute@ktu.lt

Amino acids are important body building materials. Mercapto amino acids attract considerable attention and are especially widely investigated. There are three mercapto biomolecules of the similar structure – cysteine, homocysteine and glutathione – that play crucial role in maintaining biological systems. Generally, alternations in concentration levels of biothiols in cells have been linked to a number of diseases. Therefore, detection of these mercapto biomolecules in biological samples is of crucial importance. For that purpose, a fluorescent Michael addition method for the detection of mercapto amino acids by employing a fragment of the maleimide as biothiols receptor is widely used [1]. The main goal of this project was synthesis of new dyes with a maleimide fragment, which could react selectively with mercapto amino acids and identify them.

New cyanine dyes (probes) with different number of double bonds in the conjugated chain connecting the electron donor and electron acceptor parts of dyes were synthesized [2]. Fluorescent cysteine, homocysteine and glutathione probes were prepared on their basis (Fig. 1).

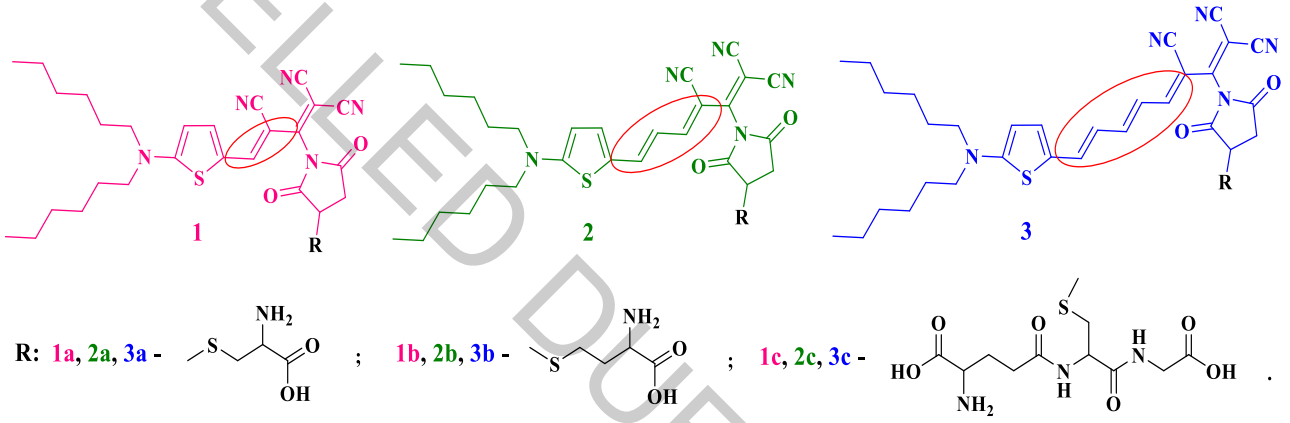

Fig. 1. Fluorescent cysteine, homocysteine and glutathione probes with a different number of double bonds

In the fluorescence spectra of the novel probes, the shifts in emission maximum have revealed that the probe **1** with the lowest number of double bonds identifies selectively all three biothiols in methanol. Based on it, fluorescent cysteine probe **1a** was prepared and it showed the highest fluorescence intensity which was 6.5 times higher than that of the initial probe in dimethyl sulfoxide. The absorption maximum for the probes **2** and **3** with a longer conjugated chains of double bonds was shifted to a region of electromagnetic radiation, which is particularly attractive for identification of mercapto amino acids, i. e. 650-900 nm (Fig. 2). The probes **2** and **3** identifies selectively all three biothiols in dimethyl sulfoxide. Fluorescent cysteine probe **2a** showed even better fluorescence intensity results, which were even 9 times higher in comparison with the one for the initial probe **2**, whereas fluorescent cysteine probe **3a** fluoresced most of all and fluorescence intensity results were even 12.5 times higher in comparison with the ones for the initial probe **3**.

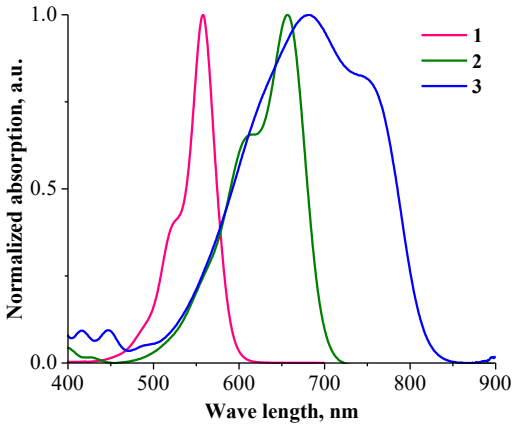

Fig. 2. Absorption spectra for probes **1**, **2** and **3**

In conclusion, the synthesized new probes can be used successfully for the selective identification of mercapto amino acids in biological samples.

[1] B. H. Northrop, S. H. Frayne, U. Choudhary, Thiol – maleimide „click“ chemistry: evaluating the influence of solvent, initiator, and thiol on the reaction mechanism, kinetics, and selectivity, Polymer Chemistry **6,** 3415-3430 (2015).

[2] V. Parthasarathy, R. Pandey, M. Stolte, et al., Combination of cyanine behaviour and giant hyperpolarizability in novel merocyanine dyes: beyond the bond length alternation (BLA) paradigm, Chemistry a European Journal **21,** 14211-14217 (2015).

CANCELLED DUE TO COVID-19

NEW FLUORESCENT EMITTERS EXHIBITING AGGREGATION INDUCED EMISSION FOR OLEDs

Adam Marek Pieczonka[1], Justyna Adamczyk[1], Lena Marciniak[2]

[1] Department of Organic and Applied Chemistry, Faculty of Chemistry, University of Lodz
[2] University of Lodz, The Bio-Med-Chem Doctoral School of the University of Lodz Institutes of the Polish Academy of Sciences
adam.pieczonka@gmail.com, adam.pieczonka@chemia.uni.lodz.pl

CANCELLED DUE TO COVID-19

Luminogenic materials with unique Aggregation Induced Emission (AIE) have attracted growing attention as materials with broad spectrum of application in various technological fields [1]. Conventional luminescent materials used in the field of organic electronics, especially in organic light emitting diodes (OLEDs), transistors, organic lasers, as well as fluorescent sensors or probes have suffered from aggregation caused quenching (ACQ) due to intermolecular interactions when their molecules are in the close proximity [1,2]. In the field of OLEDs, aggregation is inhibited e.g. by so-called host-guest systems when small-molecule emitters are dispersed in a polymer matrix [3]. It forces us to use emitters with very high quantum yields and with specified HOMO/LUMO levels to interact with the matrix [4].

In sharp contrast to destructive ACQ, aggregation-induced emission (AIE) enables active utilization of the aggregation process, instead of passively working against it. AIE refers to the group of luminogenic materials which emission is poor once they are dissolved in appropriate solvents but become significantly increased when aggregates are formed in solid state or in the thin layer. The most possible working mechanism involved in this highly unique and useful process is called restriction of intramolecular rotation (RIR) which could be achieved through bulky substitutions, metal chelation or strong hydrogen bonding [1,2].

We present the synthesis and use of new small-molecule organic compounds in the fabrication of AIE fluorescent thin layers. We have designed the target molecules to connect highly fluorescent core with long and/or branched alkyl chains (Fig. 1.). Modifications around the core of the designed systems make them applicable to the production of fluorescent thin layers which can be used in organic devices like OLEDs as well as other organic semiconducting materials. It is particularly important to obtain derivatives that will be solution processable to implement the inkjet printing techniques for the fabrication of the thin layers. For the received systems, the photophysical properties as well as the ability to produce thin films were tested.

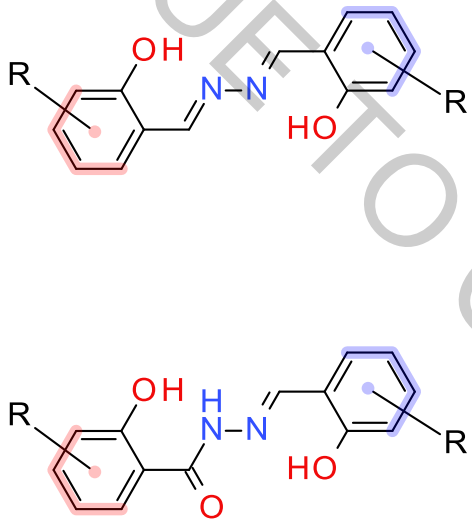

Fig. 1. Structure of new AIE compounds.

[1] Y. Hong, J. W. Y. Lam, B. Z. Tang, Aggregation-induced emission, Chemical Society Reviews **40**, 5361-5388, (2011).
[2] S. Kagatikar, D. Sunil, , Aggregation-induced emission of azines: An up-to-date review, Journal of Molecular Liquids **292**, 111371, (2019).
[3] K. Kotwica, P. Bujak, D. Wamil, A. Pieczonka, G. Wiosna-Salyga, P. A. Gunka, T. Jaroch, R. Nowakowski, B. Łuszczyńska, E. Witkowska, I. Głowacki, J. Ulański, M. Zagórska, A. Proń, Structural, Spectroscopic, Electrochemical, and Electroluminescent Properties of Tetraalkoxydinaphtophenazines: New Solution-Processable Nonlinear Azaacenes, The Journal of Physical Chemistry C **19**, 10700-10708 (2015).
[4] Ł. Skórka, P. Kurzep, G. Wiosna-Sałyga, B. Łuszczyńska, I. Wielgus, Z. Wróbel, J. Ulański, I. Kulszewicz-Bajer, New diarylaminophenyl derivatives of carbazole: Effect of substituent position on their redox, spectroscopic and electroluminescent properties, Synthetic Metals **228**, 1-8, (2017).

ANALYTE FOCUSING AND ENRICHMENT ON GAS CHROMATOGRAPHY COLUMN

Audrius Sadaunykas, Audrius Zolumskis, Evaldas Naujalis

State Research Institute Center for Physical Sciences and Technology, Metrology Department
Lukiškių str. 9, LT-01108 Vilnius, Lithuania.
audrius.sadaunykas@ftmc.lt

CANCELLED DUE TO COVID-19

The objective of this work was to design, construct and test sample focusing and concentration enrichment device for gas chromatography (GC). Gas chromatography is one of the most popular analytical methods in the world, widely used for analysis of different organic compounds. Many researchers use GC method every day; however they face problems of separation, lack of sensitivity or difficult sample preparation. There were many attempts to improve GC method and one of them was to construct different modules [1, 2], that would solve one or few of these problems. Our device is designed based on cryofocusing principles [3] and was constructed in-house. Using our prototype, we aimed to improve both sensitivity and resolution of separation using GC system.

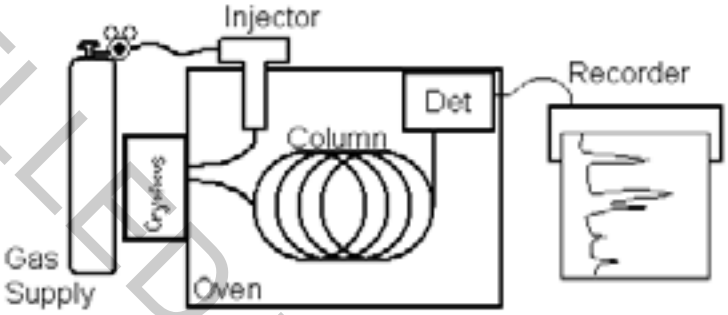

Fig. 1. Gas chromatography systems with focusing module scheme

Normally mixture of analytes is injected in gas chromatography system and then they are separated on GC column and detected using a detector. Using our prototype device, after injection analytes were stopped briefly to focus them and then continued traveling along the column to a detector. Analyte peaks became up to 37% narrower and up to two times higher just after one focusing cycle. That is significant improvement of the resolution and sensitivity of the analysis. Also this device could be used for the concentrating of the analytes on the column. Analytes moving through GC column are retained in the enrichment zone of our prototype. Consecutive injections could be made till certain amount of the analyte will be collected and then all this amount will be released to move further through the column at the same time. Number of injections correlate with the signal increase. In our testing we managed to get up to 20 times higher peak areas after 20 consecutive injections.

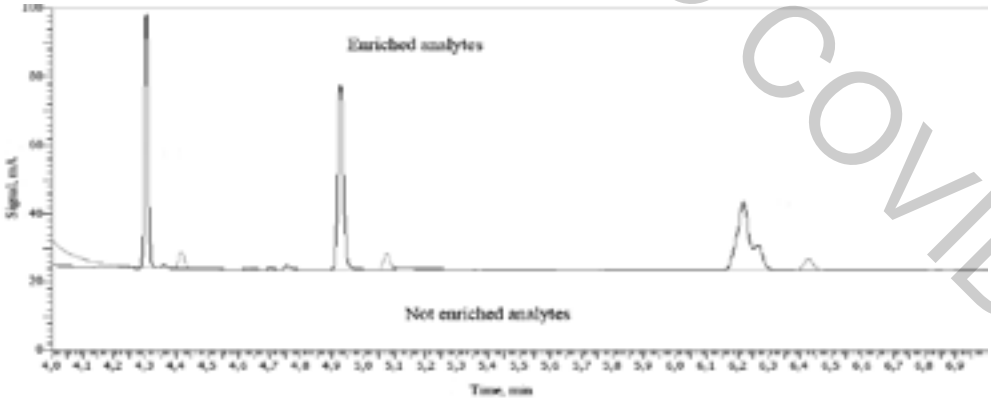

Fig. 2. Enriched (tall peaks) and standard (small peaks) chromatograms compared.

These results are just the beginning of our work in this topic and we will continue to improve this system.

[1] Wilson, R. B. *et al.* High-speed cryo-focusing injection for gas chromatography: Reduction of injection band broadening with concentration enrichment. *Talanta*, 97, 9–15, 2012
[2] Chin, *et al.* Universal Method for Online Enrichment of Target Compounds in Capillary Gas Chromatography Using In-Oven Cryotrapping. *Analytical Chemistry*, 83(17), 6485–6492, 2012
[3] Falaki, Foujan. "Sample Preparation Techniques for Gas Chromatography. *Gas Chromatography-Derivatization, Sample Preparation, Application*. IntechOpen, 2019

SYNTHESIS OF SODIUM YTTRIUM FLUORIDE VIA HYDROTHERMAL METHOD AND ITS MORPHOLOGY ANALYSIS

Ruta Juodvalkyte[1], Simas Sakirzanovas[1]

[1] Department of Applied Chemistry, Faculty of Chemistry and Geosciences, Vilnius University, Lithuania
rutajjuodvalkyte@gmail.com

$NaYF_4$ materials doped by rare-earth ions has caught scientist attention because of fluoride unique properties, such as low phonon energies, tunable crystal phase, high refractive index and chemical stability. Upconversion nano- and micro- particles doped by rare earth elements are able to convert low-energy near-infrared (NIR) photons into higher-energy visible or ultraviolet photons, this mechanism provide high excitation penetration depth in tissues and, additionally, absence of autofluorescence. Because of these characteristics, $NaYF_4$ doped by rare earth elements can be utilized in diagnostics and biomedical imaging systems [1]. Rare earth doped $NaYF_4$ can also be applied in light emitting diode (LEDs) displays, solar cells, lasers and optoelectronic devices [2].

β-phase $NaYF_4$ nanocrystals or microcrystals have been considered as better upconversion host material compared with α-phase [3]. This is the reason why the main focus was on obtaining β-phase particles. The samples were prepared via hydrothermal method, which is suitable and effective solution-based technique that can used to prepare stabile crystalline phases at considerably low temperatures. We experimentally verified the role of chelating agent, pH value and hydrothermal reaction time in the synthesis of β-$NaYF_4$.

Synthesized samples were characterized by X-ray diffraction (XRD) and scanning electron microscope (SEM) (figure 1).

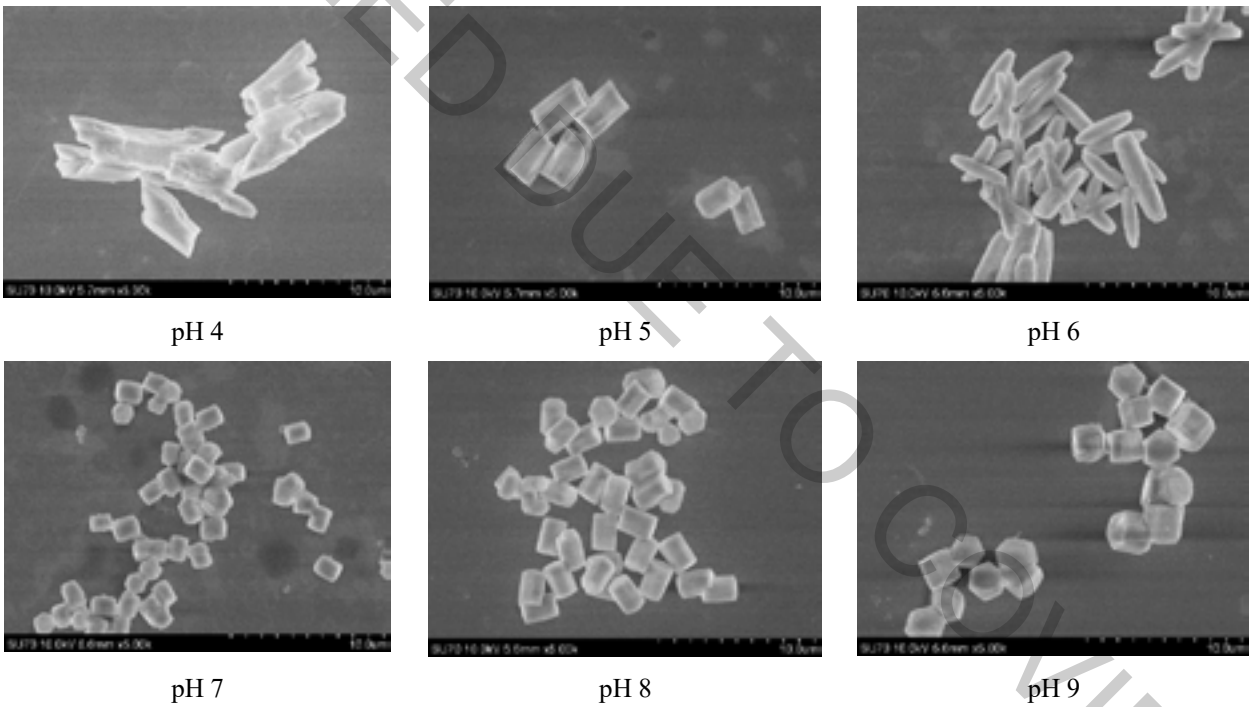

Fig. 1. SEM images of $NaYF_4$ particles synthesized by hydrothermal synthesis alternating pH values.

[1] Rafique, R., Baek, S. H., Park, C. Y., Chang, S. J., Gul, A. R., Ha, S., ... & Lee, H.. Morphological evolution of upconversion nanoparticles and their biomedical signal generation. Scientific reports, 8(1), 1-11 (2018).

[2] Pavel, E., Marinescu, V., Lungulescu, M., & Sbarcea, B. Hydrothermal synthesis of β-NaYF4: Ce, Tb crystals doped with different cerium concentrations. Materials Letters, 210, 12-15, (2018).

[3] Jiang, T., Qin, W., Di, W., Yang, R., Liu, D., Zhai, X., & Qin, G. Citric acid-assisted hydrothermal synthesis of α-NaYF 4: Yb 3+, Tm 3+ nanocrystals and their enhanced ultraviolet upconversion emissions. CrystEngComm, 14(6), 2302-2307 (2012).

CANCELLED DUE TO COVID-19

SYNTHESIS AND CHARACTERIZATION OF GADOLINIUM DOPED CERIA OXIDE CERAMIC

Giedrė Gaidamavičienė, Artūras Žalga

Faculty of Chemistry and Geosciences, Vilnius University, Naugarduko Str. 24, LT-03225 Vilnius, Lithuania
giedre.prievelyte@chf.vu.lt

The increasing ecological requirements force scientists to look for new energy conversion systems, which will either partly replace or improve the existing applications. One of the possible choices could be a solid oxide fuel cells (SOFCs) that are clean and efficient technology enabling the conversion of chemical energy to the electricity by the electrochemical reaction. In this case, the hydrogen gases are used as a fuel that is converting to the water molecules under the electrochemical oxidation. Despite the optimistic vision, this system also possesses several disadvantages such as the high cost of individual components and high operating temperature of the final electrochemical cell. According to these drawbacks, the production of solid electrolyte that operates at a lower temperature is highly desirable [1]. Nowadays, the most popular electrolytes for SOFCs are zirconia oxide (ZrO_2), yttria-stabilized zirconia (YSZ) and lanthanum based materials. However, these ceramic electrolytes require high-operating temperatures (~1000°C) to obtain high oxide-ion conductivity and this could cause seal in high temperature, interface reaction between components of SOFC, the sintering of the electrodes and more [2]. In addition, there are some requirements for SOFC electrolytes: chemical and physical stability and compatibility with other cell components, high oxygen-ion conductivity, similar thermal expansion to avoid cracking during the cell operation, dense ceramic to prevent gas mixing, low cost and other [3-4].

Solid solutions of cerium dioxide with rare earth (RE) elements (Gd, Sm, Y etc.) are promising materials for application in SOFC as electrolytes in lower temperatures. Moreover, it was also found that doping ceria dioxide with RE elements increases the concentration of oxygen vacancy due to the reduction of Ce^{4+} to Ce^{3+}. According to the literature, the best oxygen-ion conductivity could be achieved doping CeO_2 by gadolinium or samarium. Many experiments were made to find an ideal doping ratio and an appropriate ion to balance stability. Finally, it was found that the highest value of ionic conductivity could be achieved after the doping of cerium dioxide by 10 mol% of gadolinium [1, 5-6].

In this work, we present the aqueous tartaric acid assisted syntheses of Ce–Gd–O tartrate gel precursor for $Ce_{1-x}Gd_xO_{2-\delta}$ (x=0.1, 0.2, 0.3, and 0.4) ceramic. In order to obtain the dense and fully crystalline oxides, the as-prepared gels were heat-treated at the temperatures of 1,000, 1,200, 1,350 and 1,500 °C, respectively. The thermal decomposition mechanism of the as-prepared Ce–Gd–O tartrate gel precursors was investigated by thermogravimetric (TG) and differential scanning calorimetric (DSC) analysis. X-ray diffraction (XRD) analysis was performed in order to determine the crystal structure of the heat-treated ceramic materials. The microstructure and surface morphology was analyzed by scanning electron microscopy (SEM). Finally, the Fourier transform infrared spectroscopy (FT-IR) was applied for the determination of the functional group vibrations in the sample powders.

[1] A. Arabaci, M. Faruk Oksuzomer, Preparation and characterization of 10 mol% Gd doped CeO_2 (GDC) electrolyte for SOFC applications, Ceramics International **38**, 6509-6515 (2012).
[2] X. Gao, T. He and Y. Shen, Structures, electrical and thermal expansion properties of Sr-doped $La_2Mo_2O_9$ oxide-ion conductors, Journal of Alloys and Compounds **464**, 461-466 (2008).
[3] A. Boudghene Stambouli, E. Traversa, Solid oxide fuel cells (SOFCs): a review of an environmentally clean and efficient source of energy, Renewable and Sustainable Energy Reviews **6**, 433-455 (2002).
[4] S. P. S. Badwal andd K. Foger, Solid oxide electrolyte fuel cell review, Ceramics International **22**, 257-265 (1996).
[5] G. Gaidamavičienė, B. Abakevičienė, A. Žalga, Oxalic acid assisted synthesis of the gadolinium-doped ceria oxide-ion conductor as electrolyte for solid oxide fuel cells, Chemical Papers **73(4)**, 891-899 (2019).
[6] R. M. Batista, E. N. S. Muccillo, Analysis of the sintering process in gadolinia-doped ceria by thermodilatometry and correlation with microstructure evolution, Journal of Thermal Analysis and Calorimetry **132**, 851-857 (2018).

CANCELLED DUE TO COVID-19

ELECTROCHEMICALLY DEPOSTED IRON ONTO COPPER FOAM CATALYST FOR HETEROGENOUS FENTON REACTION

Modestas Vainoris[1], Natalia Tsyntsaru[1,2], Henrikas Cesiulis[1]

[1]Dept. of Physical Chemistry, Vilnius University, Vilnius, Lithuania
[2]Institute of Applied Physics, Chisinau, Moldova
m.vainoris@chgf.vu.lt

The need for clean water is ever increasing, and with limited resources of freshwater, cleaning of wastewaters is urgent issue to be solved. Textile and leather industries are ones of the most polluting ones in the world, they generate up to 200 L of wastewater per 1kg of textile. [1]

Homogenous Fenton reaction has been known since late 19th century, where mixture of iron (II) ions and hydrogen peroxide is used for degradation of various organic materials. [2] Fenton reaction offers a fast, reliable and clean way to remove all organic materials from wastewater. One of the big drawbacks of homogenous Fenton reaction is the need to remove large amounts of iron sludge after oxidation [3]. The rate and efficiency can be improved by using heterogeneous Fenton reactions, also the need to remove iron sludge can be eliminated. [3] In this study, we report an electrochemical deposition method for preparation of porous Fe/Cu foam catalyst for Fenton reaction. The efficiency of obtained catalysts has been evaluated using nitro dye - methyl orange (MO) aqueous solution.

The catalyst was deposited using potentiostatic deposition onto Cu foams. Deposited coatings morphology has been investigated using SEM with EDS module and XRD spectroscopy. Catalysts activity has been tested in 40 mg/L MO and 20 g/L Na_2SO_4 solution. Solutions pH was 3. Spectrophotometric and electrochemical impedance spectroscopy (EIS) were used for characterization and evaluation of deposited catalyst activity.

Fenton reactions rate (Eq. 1) depends on the concentration of Fe^{2+} ions, that are affected by the presence of Cu^{+} ions in the system (Eq. 2). The later ones can be obtained according to Wang [4] due to interaction of copper with H_2O_2 in the acidic media (Eq. 3). Thus, the use of copper foam has beneficial effect on heterogeneous reaction rate. Substantial increase in the reaction rate have been noticed if coatings are thinner (Fig. 1). We managed to oxidize 40 mg/L methyl orange in 8 min under optimum experimental conditions (Fig. 1).

$$Fe^{2+} + H_2O_2 \rightarrow Fe^{3+} + OH\cdot + OH^- \quad - \quad \textbf{(1)}$$

$$Fe^{3+} + Cu^{+} \rightarrow Fe^{2+} + Cu^{2+}; \quad \Delta E^0 = 0.6\ V \quad \textbf{(2)}$$

$$2Cu^0 + 2H^+ H_2O_2 \rightarrow 2Cu^{+} + 2H_2O \quad \textbf{(3)}$$

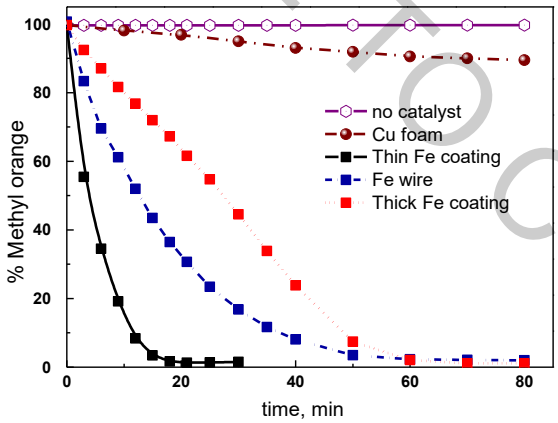

Fig. 1. Catalytic activity of different materials in degradation of methyl orange during Fenton reaction.

ACKNOWLEDGEMENTS. Authors acknowledge funding from H2020 project SMARTELECTRODES (No778357) and Research Council of Lithuania project No 09.3.3-LMT-K-712-08-0003.

[1] R Ananthashankar, A.G. Production, Characterization and Treatment of Textile Effluents: A Critical Review. *J. Chem. Eng. Process Technol.*, ***05***, 1–18, (2013).
[2] H. J. H. Fenton, "LXXIII.—oxidation of tartaric acid in presence of iron," Journal of the Chemical Society, Transactions, vol. 65, pp. 899–910, (1894).
[3] Centi, G.; Perathoner, S.; Torre, T.; Verduna, M.G. Catalytic wet oxidation with H2O2 of carboxylic acids on homogeneous and heterogeneous Fenton-type catalysts. *Catal. Today* **2000**, *55*, 61–69.
[4] J. Wang, C. Liu, L. Tong, J. Li, R. Luo, J. Qi, Y. Li, L. Wang, Iron-copper bimetallic nanoparticles supported on hollow mesoporous silica spheres: An effective heterogeneous Fenton catalyst for orange II degradation, RSC Adv. 5 (2015) 69593-69605

CANCELLED DUE TO COVID-19

SYNTHESIS AND EVALUATION OF PYRROLIDINONE-BEARING BENZENESULFONAMIDES AS HUMAN CARBONIC ANHYDRASE INHIBITORS

Benas Balandis[1], Guostė Ivanauskaitė[2], Joana Smirnovienė[2], Daumantas Matulis[2], Asta Zubrienė[2], Vytautas Mickevičius[1]

[1] Department of Organic Chemistry, Kaunas University of Technology, Lithuania
[2]Department of Biothermodynamics and Drug Design, Institute of Biotechnology, Life Sciences Center, Vilnius University, Lithuania
benas.balandis@ktu.edu

There are twelve alpha carbonic anhydrase (CA) isozymes in human that catalyze reversible hydration of CO_2 to protons and bicarbonate, a vital reaction for the respiration and transport of CO_2 between tissues, in pH regulation and homeostasis [1]. Increased expression levels of several CA isozymes are associated with numerous diseases. Currently CAs are established therapeutic targets of cancer (CA IX and CA XII), glaucoma (CA II, CA IV, CA XII), high altitude sickness (CA II) and obesity (CA VA and CA VB). Many recent studies have focused on designing and developing of inhibitors against CA IX that show potential for treating solid tumors [2,3].

In this study we synthesized pyrrolidinone-based chlorinated benzenesulfonamide derivatives (Fig. 1) and evaluated their binding toward all 12 human catalytically active CA isozymes. Ester **2** was synthesized by an esterification reaction of the acid **1** with an excess of methanol at reflux temperature in the presence of sulfuric acid as a catalyst. Reaction of ester **5** with hydrazine hydrate in propan-2-ol at reflux temperature gave hydrazide **3**.

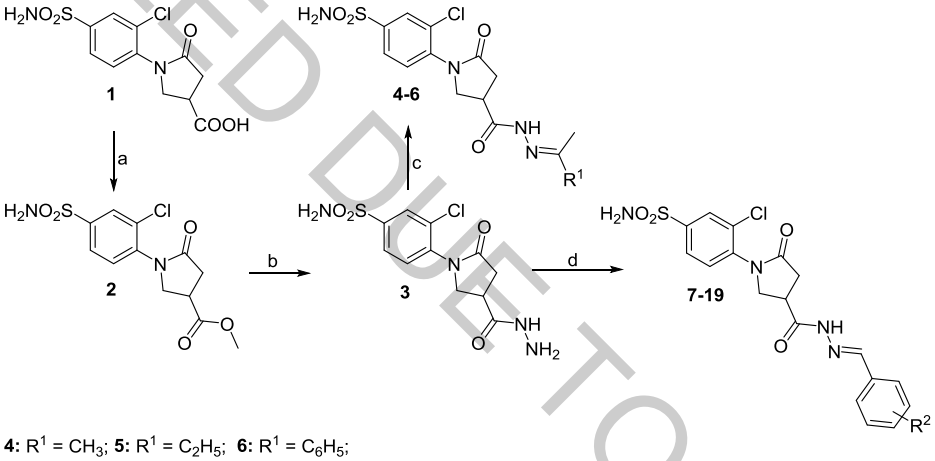

4: $R^1 = CH_3$; **5:** $R^1 = C_2H_5$; **6:** $R^1 = C_6H_5$;
7: R^2 = H; **8:** R^2 = 2-OH; **9:** R^2 = 3-OH; **10:** R^2 = 4-OH; **11:** R^2 = 2-Cl; **12:** R^2 = 3-Cl; **13:** R^2 = 4-Cl; **14:** R^2 = 4-F; **15:** R^2 = 4-OCH_3; **16:** R^2 = 2-NO_2; **17:** R^2 = 3-NO_2; **18:** R^2 = 4-NO_2; **19:** R^2 = 4-COOH;
Reaction conditions: (a) MeOH, conc. H_2SO_4, reflux, 8 h; (b) $N_2H_4 \cdot H_2O$, propan-2-ol, reflux, 5 h;
(c) corresponding ketone, propan-2-ol, reflux, 2-4 h; (d) corresponding aldehyde, propan-2-ol, reflux, 1-2 h;

Fig. 1. Synthesis of pyrrolidinone-bearing benzenesulfonamides

Hydrazide **3** reactions with corresponding ketones in propan-2-ol at reflux temperature yielded hydrazones **4**–**6**, whereas the ones with corresponding benzaldehydes provided corresponding hydrazones **7**–**19**. The structures of all synthesized compounds have been confirmed by the data of IR, ^{1}H and ^{13}C NMR spectroscopy as well as mass spectrometry data.

The binding affinity of synthesized compounds was determined by the thermal shift assay and stop-flow CO_2 hydration assay. Most of the compounds showed nanomolar binding affinities towards CA II, CA IX and CA XIV. The compounds have a potential for further development of CA inhibitors with higher selectivity for a particular CA isozyme.

[1] Aggarwal, M., Boone, C. D., et al. Structural annotation of human carbonic anhydrases. Journal of Enzyme Inhibition and Medicinal Chemistry **28**, 267–277 (2013).
[2] Mboge, M. Y., Mahon, B. P., et al. Carbonic Anhydrases: Role in pH Control and Cancer. Metabolites **8**, (2018).
[3] Tafreshi, N. K., Lloyd, M. C., et al. Carbonic Anhydrase IX as an Imaging and Therapeutic Target for Tumors and Metastases. Subcell Biochem **75**, 221–254 (2014).

CANCELLED DUE TO COVID-19

SYNTHESIS OF HYDRAZIDE HYDRAZONES WITH LUMINESCENT PROPERTIES

Lena Marciniak[1], Adam Marek Pieczonka[2], Michał Rachwalski[2]

[1] University of Lodz, The Bio-Med-Chem Doctoral School of the University of Lodz Institutes of the Polish Academy of Sciences

[2] Department of Organic and Applied Chemistry, Faculty of Chemistry, University of Lodz

lena.marciniak@onet.pl

CANCELLED DUE TO COVID-19

Preparation of organic light-emitting diodes (OLED) is one of the latest and dynamically developing techniques in organic electronics. It uses the unique properties of selected small-molecule organic compounds. Their most important feature is the occurrence of strong luminescent properties. The structure of the molecules enabling the appropriate flow of electrons in thin layers of OLED diodes [1] and a predisposition to create uniform thin layers of solids is also an important aspect during designing new molecules.

The purpose of my research was to obtain small-molecule organic compounds, derivatives of carboxylic acid hydrazides, showing luminescence in thin layer. An additional goal was also to obtain molecules with chemical structure allowing the production of uniform, thin layers, and then to use them in innovative technology to produce active layers in OLED diodes. Hydrazide hydrazones, derivatives of carboxylic acid hydrazides, e.g. salicylic acid, have an appropriate structure that allows both luminescence and the formation of thin layers of solids (Fig. 1.). The emission of these organic compounds in the solution is definitely weaker than in the solid, which indicates the presence of the effect of emission induced by aggregation of molecules called AIE (Aggregation Induced Emission) effect.

The most important issue was the obtainment of molecules with strictly defined physical and chemical properties, expanding the hydrazone core in an appropriate manner. Salicylic acid derivatives have hydroxyl groups in their structure. Thanks to them, hydrogen bonds are easily formed, which exhibit a significant impact on the luminescence as well as self-organization of molecules in thin layers.

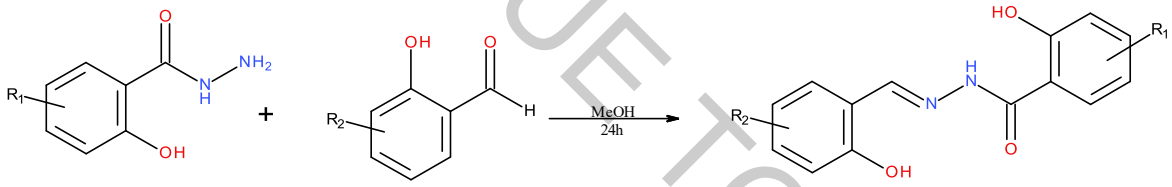

Fig. 1. General scheme of hydrazide hydrazone synthesis

[1] K. Kotwica, P. Bujak, D. Wamil, A. Pieczonka, G. Wiosna-Salyga, P. A. Gunka, T. Jaroch, R. Nowakowski, B. Łuszczyńska, E. Witkowska, I. Głowacki, J. Ulański, M. Zagórska, A. Proń, Structural, Spectroscopic, Electrochemical, and Electroluminescent Properties of Tetraalkoxydinaphtophenazines: New Solution-Processable Nonlinear Azaacenes, The Journal of Physical Chemistry C **19**, 10700-10708 (2015).

ELECTROPHILE-INITIATED CYCLIZATION REACTIONS OF 2-(3-SUBSTITUTED 2-PROPINILTHIO)-1*H*-IMIDAZOLES

Vincenta Mikulėnaitė, Ieva Karpavičienė

Department of Organic Chemistry, Faculty of Chemistry and Geosciences, Vilnius University, Lithuania
vincenta.mikulenaite@chf.stud.vu.lt

Heterocycles are of major interest in the design of biologically active molecules and advanced organic compounds. In fact, ring closure reactions, in which a new carbon-heteroatom bond is formed, are a commonly used approach in the synthesis of functionalized heterocycles [1]. Specifically, the intramolecular addition of nitrogen functionality to an alkyne is a valuable strategy. In the first attempts to obtain cyclization products, metallic catalysts and strong bases were used. Later on, the investigation of electrophile induced cyclization reactions appeared to be a favorable approach as well. This synthetic route could offer a new way to synthesize derivatives containing thio-imidazole ring system which were found to exhibit potential pharmaceutical properties [2,3]. In order to broaden the scope of the electrophilic cyclization of propargylic substrates, we investigated the pathway of the cyclization reaction between various electrophiles and two propargylic thio-imidazole substrates **1** which differ in aromaticity.

Herein, we report a synthetic methodology which, depending on the aromaticity of the substrate and the substitute of the propargylic compound, enables efficient access to the construction of five- or six- membered heterocyclic rings *via* intramolecular ring closure reactions.

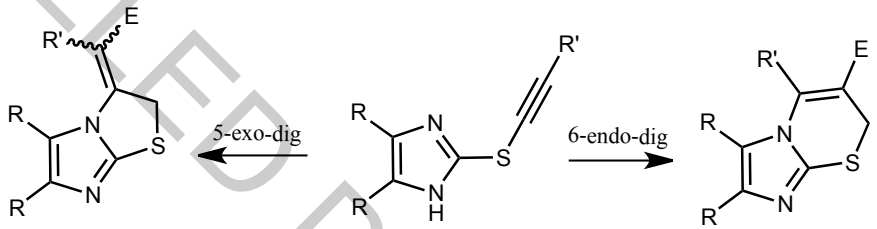

1

R= H, Ph
R'= H, Et, 4-MeC$_6$H$_4$
E= I, Br, PhSe

Fig. 1. Possible pathways of electrophilic cyclization of propargylic compound **1.**

[1] French, J. M.; Diver, S. T. J. *Org. Chem*. 2014, 79, 5569−5585.
[2] K.A. Al-Rashood, H. A. Abdel-Aziz *Molecules* 2010, 15, 3775-3815.
[3] Su Y. Kim. S. H. Lee, J. S. Shin, D. Lee, T. Lee, K. Ch. Park, K. H. Min, DS. Kim, *Die Pharmazie*, 2014, 69, 5, 353-357.

CANCELLED DUE TO COVID-19

ELECTROCHEMICAL FABRICATION OF $(Bi_2)_m(Bi_2Te_3)_n$ THIN FILMS WITH CONTROLLABLE BISMUTH CONTENT

Aliaksei Bakavets[1,2*], Yauhen Aniskevich[1,2], Genady Ragoisha[1], Henrikas Cesiulis[3], Natalia Tsyntsaru[3], Eugene Streltsov[2]

[1]Research Institute for Physical Chemical Problems, Belarusian State University, Minsk, 220006, Belarus
[2]Chemistry Department, Belarusian State University, Minsk, 220030, Belarus
[3]Department of Physical Chemistry, Faculty of Chemistry, Vilnius University, Vilnius, Lithuania
*e-mail: alexeibokovets@gmail.com

CANCELLED DUE TO COVID-19

Thermoelectric materials attract a lot of attention, especially due to waste heat conversion into electricity which is expected to reduce the contribution of anthropogenic heat in global warming. Bismuth telluride is one of the best materials available for these applications, though thermoelectric perfomance of bare bismuth telluride is not sufficient for the waste heat conversion on a large scale.

To increase the overall performance of a thermoelectric material, its thermal conductivity should be reduced. Although it is hard to suppress electronic heat transport while maintaining a high power factor, lattice thermal conductivity can be reduced without any fallout. Formation of Bi_2Te_3-based superlattices has proven to be useful as a way to reduce the lattice thermal conductivity. We have developed the electrochemical pulse potential controlled deposition of $(Bi_2)_m(Bi_2Te_3)_n$ superlattices with controllable Bi-content [1]. The superlattice structure of the deposits was proved via XRD analysis, XPS analysis, and TEM. The composition is controlled by the ratio of Bi^{3+} and TeO_2 precursor concentrations in the electrolyte. Moreover, we have shown that bismuth interlayers can be removed from the superlattice structure by selective anodic oxidation, with the oxidation resulting in the product corresponding to Bi_2Te_3 by stoichiometry but having an expanded crystal structure. These results clear the way for new synthetic strategies of high performance Bi_2Te_3-based thermoelectric materials preparation.

We also consider effect of pulse deposition parameters, electrolyte composition, pretreatment of substrate on the nucleation and growth of the superlattice structure, morphology and uniformity of the deposit. Characterization of the effects helps to find optimal conditions for preparation of uniform films for thermoelectric applications.

Acknowledgment: This research has received funding from Horizon 2020 research and innovation programme under MSCA-RISE-2017 grant agreement No. 778357.

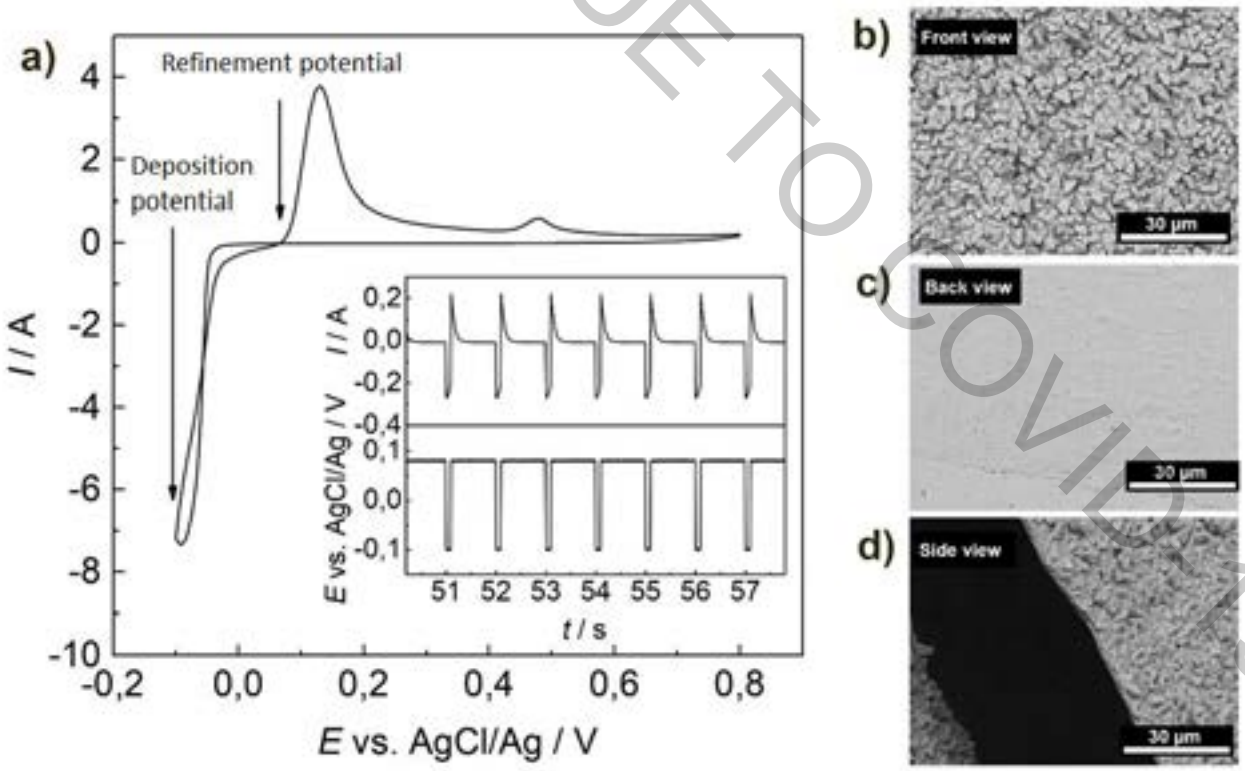

Fig. 1. (a) Typical cyclic voltammetry profile of $(Bi_2)_m(Bi_2Te_3)_n$ electrodeposition and pulse deposition profile (in the insert), (b-d) SEM images of $(Bi_2)_m(Bi_2Te_3)_n$ electrodeposited thin film.

[1] A. Bakavets et al. Journal of Power Sources **450** (2020) 227605.

SYNTHESIS AND INVESTIGATION OF ELECTRON TRANSPORTING ORGANIC SEMICONDUCTORS CONTAINING ANCHORING FRAGMENTS

Lauryna Monika Svirskaitė, Ernestas Kasparavičius, Tadas Malinauskas

Faculty of Chemical Technology, Kaunas University of Technology, Radvilėnų pl. 19, Kaunas
lauryna.svirskaite@ktu.edu

In the last few decades, rapid increase in energy consumption contributes to the climate change. Limited reserves of fossil fuels are demanding more research on sustainable and renewable energy sources. Solar photovoltaic technologies are considered as clean source of energy, as they replenish themselves naturally without additional depletion of earth resources. Increased usage of solar energy could provide opportunity for mitigation of greenhouse gas emissions and reducing global warming [1].

Perovskite solar cells (PSCs) are considered as potential candidates for next-generation energy harvesting devices, due to their low cost, simple fabrication process and high power conversion efficiency. PSCs consist of active perovskite layer which is sandwiched between hole-transporting layer (HTL) and electron-transporting layer (ETL). The basic functions of the transporting layers are to lower bandgap differences between each semiconductor and perovskite layers, to extract photo-generated charges from the perovskite and prevent their recombination. Yet, the most challenging issue in PSCs is the long-term stability. For example, dopants, such as LiTFSI and *tert*-butylpyridine (t-BP), are significant additives, used to increase conductivity of HTMs and power conversion efficiency of PSCs. However, due to the hygroscopic nature of LiTFSI and relatively low boiling point of t-BP, aswell as possible formation of pyridinated derivatives, both mentioned dopants accelerate the degradation of whole device in general and perovskite light absorber in particular [2,3].

The widely used electron transporting layer in inverted perovskite solar cells are fullerenes and their modified soluble derivatives (e.g. PCBM). Unfortunately, these compounds show some disadvantages such as low solubility of non-modified fullerenes, which limits their application, meanwhile modified fullerenes are relatively expensive [4].

In the past few years scientists were searching for new non-fullerene semiconductors, which could replace fullerene derivatives and improve stability of the perovskite. Naphthalene diimide based electron transporting materials have received a lot of attention due to the simple „one-pot" synthesis, solubility in different organic solvents, good thermal stability, high electron mobility and possibility to be used as self-assembled monolayer compounds by attaching corresponding anchoring functional groups [5,6].

In this work new 1,4,5,8-naphthalenetetracarboxylic diimide semiconductors containing anchoring groups were synthesized. These fragments were used in order to form monolayer of synthesized compounds on top of the perovskite surface.

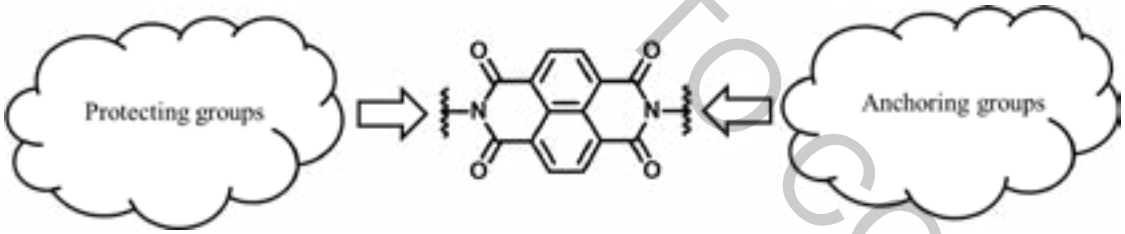

Fig. 1. General structure of synthesized compounds

Studies have revealed that these compounds can be applied as electron transporting materials in the PSCs with inverted architecture. From the obtained results it was determined that anchoring groups can form bonds with the surface of perovskite. Preliminary investigation of synthesized electron transporting materials have shown beneficial optical and thermal properties as well as ability to reduce degradation of perovskite.

[1] S. Asumadu-Sarkodie, P. A Owusu, et al., A review of renewable energy sources, sustainability issues and climate change mitigation, Cogent Engineering, 3: 1167990 (2016).
[2] S. Wang, Z. Huang, et. Al., Unveiling the Role of tBP-LiTFSI Complexes in Perovskite Solar Cells. *J. Am. Chem. Soc.* 2018, 140, 48, 16720-16730.
[3] D. Zhou, T. Zhou, et al., Perovskite-Based Solar Cells: Materials, Methods, and Future Perspectives, Journal of Nanomaterials, 1-15 (2018).
[4] R. Wang, M. Mujahid, et. al, A Review of Perovskites Solar Cell Stability, Advanced Functional Materials, 1808843 (2019).
[5] A. A. Said, J. Xie, et al., Recent Progress in Organic Electron Transport Materials in Inverted Perovskite Solar Cells, Small, 15, 1900854 (2019).
[6] L. Li, Y. Wu, et al., Self-assembled naphthalimide derivatives as an efficient and low-cost electron extraction layer for n-i-p perovskite solar cells, Chemical Communications, 55, 13239-13242 (2019).

CREATED DUE TO COVID-19

INVESTIGATION OF ELECTROPHYLIC CYCLIZATION REACTIONS OF BENZIMIDAZOL-2-YL ALKYNES

Indrė Misiūnaitė, Justas Pošiūnas, Rita Bukšnaitienė, Ieva Karpavičienė

Faculty of Chemistry and Geosciences, Vilnius University, Naugarduko g. 24, LT-03225, Vilnius, Lithuania
Indre.Misiunaite@gmail.com

The synthesis of heterocycles has always been an important process in organic synthesis. A variety of synthetic approaches to the heterocyclic ring structures can be found in literature [1]. Quite common way to obtain heterocycles from alkynes is *via* cyclization reactions catalyzed by transition metals [2]. On the other hand, in recent years electrophilic initiated cyclization reactions are becoming more popular [3]. Furthermore, there are no articles about reactivity and electrophile promoted cyclizations of benzimidazol-2-yl alkynes. Consequently to this we decided to synthesize various benzimidazol-2-yl alkynes containing heteroatoms.

For this research 2-(3-substituted prop-2-ynylthio)benzimidazoles were selected as model reactants in investigation of electrophile induced cyclization reactions. It was found that cyclization went through 6-*exo*-dig path with chosen electrophiles. While, cyclizations with N-(substituted-2-ynyl)-1H-benzo[d]imidazol-2-amines or 2-(pent-2-ynylthio)-1H-benzo[d]imidazoles went through 5-*exo*-dig or 6-*endo*-dig path, depending on the substituent R. More details about selectivity, scope, and limitations of the reaction will be discussed in presentation.

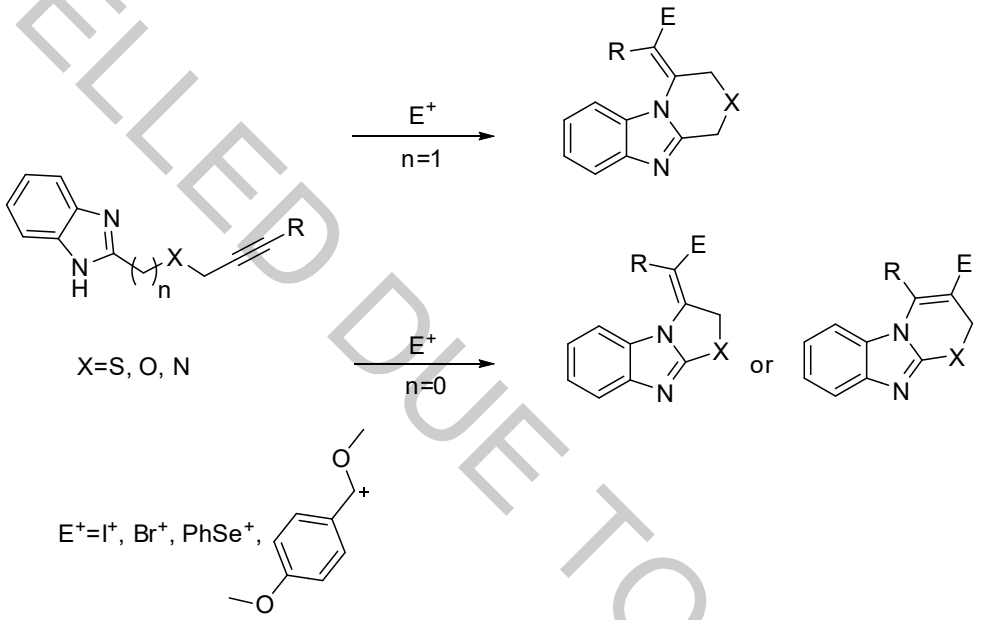

Fig. 1. General scheme of reactions

This research is funded by the European Social Fund under the No 09.3.3-LMT-K-712“ Development of Competences of Scientists, other Researchers and Students through Practical Research Activities” measure.

[1] Chem. Rev. **104**, Issue 5 (2004).

[2] (a), Y. Yamamoto, I.D. Gridnev, , N.T. Patil, T. Jin, Alkyne activation with Brønsted acids, iodine, or gold complexes, and its fate leading to synthetic application, Chem. Commun. 5075-5087 (2009). (b), I. Nakamura, Y. Yamamoto, Transition-Metal-Catalyzed Reactions in Heterocyclic Synthesis, Chem. Rev. **104**, 2127-2198 (2004).

[3] B. Godoi, R.F. Schumacher, G. Zeni, Synthesis of Heterocycles via Electrophilic Cyclization of Alkynes Containing Heteroatom, Chem. Rev. **111**, 2937-2980 (2011).

CANCELLED DUE TO COVID-19

CHARACTERIZATION OF AEROSOL PARTICLES IN FOREST ENVIRONMENT USING AN AEROSOL CHEMICAL SPECIATION MONITOR

Viktorija Padolskytė[1,2], Vadimas Dudoitis[2], Vidmantas Ulevičius[2]

[1] Faculty of Physics, Vilnius University, Vilnius, Lithuania
[2] Center for Physical Sciences and Technology, Vilnius, Lithuania
viktorija.padolskyte@ff.stud.vu.lt

Atmospheric aerosol particles have a significant impact on local and global climate and on human health. The studies show that emissions of volatile organic compounds from which aerosol particles are formed are an order of magnitude higher from biogenic sources than anthropogenic [1]. Therefore, organic aerosol makes up a large fraction (20 to 90%) of the submicron particulate mass [2]. To estimate aerosol impact on climate and human health there is a need for identification and evaluation of aerosol sources.

In this study, an aerosol chemical speciation monitor (ACSM) [3] was used to characterize chemical composition of submicron non-refractory PM_1 (NR-PM_1) aerosol particles. The composition was measured from April to September 2018 at the forest site at the Aukštaitija Integrated Monitoring Station in Rūgšteliškis, eastern part of Lithuania (55.46N; 26.00E). The measurement site is characterized as rural, more than 80% of its area is covered by coniferous trees.

Concentration of five aerosol components (organics, sulphate, ammonium, nitrate and chloride) was evaluated. The contribution of organics to NR-PM_1 was dominant and reached 73.5% of the total loading. The sulphate concentration reached 13.7% and was the second largest aerosol component in the forest environment. Submicron forest organic aerosol mass (SFOM) evaluation was also performed. SFOM data was calculated from the concentration of organics using several criteria [1]. Firstly, to eliminate anthropogenic contribution of sulphate from the data set, the time periods with the ratio of organics/(organics + sulphate) > 0.7 were used. Secondly, the time periods corresponding to the SFOM data with average wind speed greater than 1 m s^{-1} and solar radiation greater than 400 W m^{-2} were selected [4]. SFOM concentration correlation of 0.63 and 0.40 with temperature was observed in summer and spring, respectively (Fig. 1). In this study, the anthropogenic sulphate aerosol source apportionment was performed using HYSPLIT air mass backward trajectories. An anthropogenic pollution source originating from the West was related to the Klaipėda city port activity.

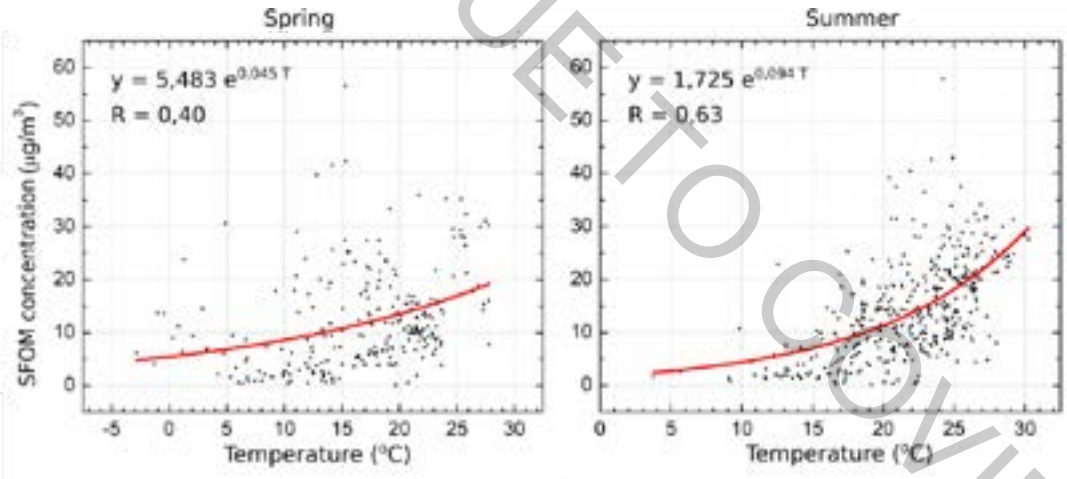

Fig. 1. SFOM concentration dependency on temperature in spring and summer.

[1] W. R. Leaitch *et. al.*, Temperature response of the submicron organic aerosol from temperate forests, Atmospheric environment, **45**, 6696–6704 (2011).
[2] J. L. Jimenez *et al.*, Evolution of Organic Aerosols in the Atmosphere, Science, **326 (5959)**, 1525–1529 (2009).
[3] N. L. Ng *et. al.*, An Aerosol Chemical Speciation Monitor (ACSM) for Routine Monitoring of the Composition and Mass Concentrations of Ambient Aerosol, Aerosol Science and Technology, **45 (7)**, 780–794 (2011).
[4] J. Pauraite *et. al.*, Characterization of aerosol mass spectra responses to temperature over a forest site in Lithuania, Journal of Aerosol Science, **133**, 56–64 (2019).

CANCELLED DUE TO COVID-19

THE SYNTHESIS OF FLUORINATED BENZENESULFONAMIDES BEARING SPECIFIC FUNCTIONAL GROUP AS INHIBITORS OF HUMAN CARBONIC ANHYDRASES

Aivaras Vaškevičius, Denis Baronas, Asta Zubrienė, Daumantas Matulis, Virginija Dudutienė

Department of Biothermodynamics and Drug Design, Institute of Biotechnology, Life Sciences Center, Vilnius University, Lithuania
aivarasvaskevicius@yahoo.com

Carbonic anhydrases (CAs) are family of zinc metaloenzymes that catalyze the reversible hydration of CO_2, maintaining various physiological functions in different species of organisms. There are twelve catalytically active CA isoforms in human body. Their overexpression causes numerous diseases including cancer. Isoform CA IX is overexpressed in numerous hypoxic tumors and is thought to be a good target for anticancer drug development. [1]. The most widely known CA inhibitors bear the benzenesulfonamide moiety and a number of drugs used in clinic bear this functional group.

Our research group has successfully designed compounds that inhibit CA IX, with high affinity and selectivity over other CA isoforms. One of them, 3-(cyclooctylamino)-2,5,6-trifluoro-4-[(2-hydroxyethyl)sulfonyl]benzenesulfonamide (VD11-4-2), exhibited subnanomolar affinity for CA IX (K_d = 0.05 nM) [2]. Recently it was discovered that the modification of the *para* tail of VD11-4-2 led to the compound with even higher binding affinity towards CA IX, implying that the tail group made additional contacts with the residues of CA.

The aim of this study is to determine the importance of various moieties for the high affinity towards CA isoforms. For this purpose, we synthesized a series of compounds with modified *para* substituent and sulfonamide group (Fig. 1). Various modifications done to *para* substituent revealed that only benzensulfonamides with specific sulfur oxidation state, particular tail length and exact group significantly increase binding affinity towards CAs.

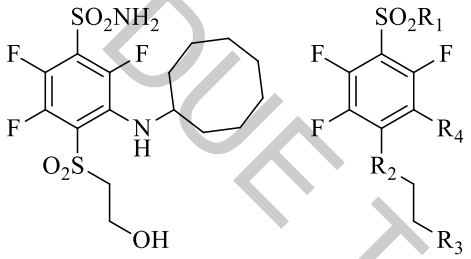

VD11-4-2

Fig. 1. Compound VD 11-4-2 and schematic representation of modification sites on benzensulfonamide scaffold.

[1] M.Y. Mboge et al. Carbonic Anhydrases: Role in pH Control and Cancer. *Metabolites*. 2018;8(1):19.
[2] V. Dudutienė et al. Discovery and characterization of novel selective inhibitors of carbonic anhydrase IX. J. Med Chem. 2014, 57, 9435

CANCELLED DUE TO COVID-19

DESIGN, PREPARATION AND STUDIES OF NAPHTHALIMIDE MATERIALS

Naveen Masimukku[1], Dalius Gudeika[1], Dmytro Volyniuk[1], Juozas Vidas Grazulevicius[1]

[1]Kaunas University of Technology, Department of Polymer Chemistry and technology,
Radvilenu plentas 19, LT-50254, Kaunas, Lithuania
naveen.masimukku@ktu.edu

Development of orange red thermally-activated-delayed-fluorescence (TADF) emitters has been lagging behind when compared with blue and green fluorophores. TADF occurs due to reverse intersystem crossing. It is possible when the energy difference between excited singlet (S_1) and triplet (T_1) energy levels is very low [1]. External quantum effiencies (EQEs) of TADF OLEDs have been rapidly boosting in past few years The most efficient red TADF-OLED reported to date, based on a heptaazaphenalene derivative, has a state-of-the-art EQE of 17.5% with an EL emission maximum (λ_{EL}) at ≈610 nm and CIE coordinates of (0.60, 0.40). However, there is still much room for improving the overall performance due to poor color purity and significant roll-off at high current density. Thus, further developing high-performance pure-red TADF materials and their devices with CIE coordinates close to the National Television System Committee (NTSC) standard red (0.67, 0.33) is a key challenge for OLED technology. However, the highest EQEs of orange–red TADF OLEDs are significantly lower compared to those of blue and green TADF OLEDs [2].

Four 1,8-naphthalimide based compounds were synthesized. The synthesis of these compounds was carried out in three steps. It included bromination, imidazation and Buchwald-Hartwig coupling. The structures of the synthesized compounds were confirmed by nuclear magnetic resonance spectroscopy and mass spectrometry. Photophysical, electrochemical, thermal properties and performance in OLEDs will be reported.

Acknowledgements

This project has received funding from the Research Council of Lithuania agreement No [S-LU-20-3].

[1] Jia-Xiong. C, Wen-Wen. T, Ya-Fang. X, Kai. W et al., Efficient Orange-Red Thermally Activated Delayed Fluorescence Emitters Feasible for Both Thermal Evaporation and Solution Process, ACS Applied Materials & Interfaces **11(32)**, 29086-29093 (2019).
[2] You-Jun. Y, Xun. T, Ting. G, Yi. Y, Zuo-Quan. J, Liang-Sheng. L, Alleviating Efficiency Roll-Off of Hybrid Single-Emitting Layer WOLED Utilizing Bipolar TADF Material as Host and Emitter, Organic Electronics **73**, 240-246 (2019).

CANCELLED DUE TO COVID-19

DETERMINATION OF THE CHEMICAL COMPOSITION OF USED COFFEE GROUNDS

Dovilė Ragauskaitė, Rasa Šlinkšienė

Department of Physical and Inorganic Chemistry, Kaunas University of Technology, Lithuania
dovile.ragauskaite@ktu.lt

One of the world's most consumed beverage is coffee. Over 2.25 billion cups of coffee are prepared per day. It takes about 11 grams of fresh ground coffee to make one cup. As a result, 24750 tons of ground coffee becomes a waste. Most of used coffee grounds are thrown away as a general waste. Because of the moisture that comes within, grounds are starting to rot in a landfill. As a consequence, they emit a greenhouse gas – methane [1]. The growing awareness of environmental protection encourages to recycle and design new zero waste technologies. Dried coffee grounds are natural, not harmful to the environment resource, which can be applied in many other fields. For example dried coffee grounds can be used as a source of thermal energy, because of the calorific value (100 kg coffee grounds produce 4600 MJ) [2]. Moreover, spent coffee grounds can be used as bio-fuel, water filter or even as an abrasive [3, 4]. Literature sources claim that used coffee grounds are very beneficial for soil and plants in particular. It can be used as a mulch or even a fertilizer [5]. The main purpose of this thesis is to analyze chemical composition of spent coffee grounds and evaluate its application in fertilizers industry. Four types of well-known coffee brands were used in this research. Spent coffee grounds were processed with hot water and concentrated sulfuric acid. Nitrogen content in spent coffee grounds was determined by Kjeldahl method, potassium by using flame photometer. UV/Vis spectrophotometer was used to measure phosphorus concentration. Concentrations of microelements and heavy metals were determined by using atomic absorption spectroscopy (AAS). Chemical composition of spent coffee grounds is shown in the table.

Table MN*, ME* and other elements concentrations in spent coffee grounds processed with hot water and concentrated sulfuric acid.

Element	Processed with hot water, %				Processed with concentrated sulfuric acid, %			
	Coffee brand							
	Jacobs	Paulig	Lavazza	Caif	Jacobs	Paulig	Lavazza	Caif
N	1.55	2.55	1.99	0.98	2.26	2.52	2.11	2.09
K_2O	0.59	0.67	0.59	0.51	2.87	2.17	2.07	2.17
P_2O_5	0.46	0.68	0.54	0.45	2.53	2.40	1.50	1.76
Fe	–	–	–	–	0.010	0.010	0.0095	0.0177
Mn	–	–	0.00005	–	0.0016	0.0014	0.0016	0.0017
Cu	–	–	–	–	0.00063	0.00068	–	–
Cr	–	–	–	–	0.00073	0.00080	0.00072	0.0004
Ni	–	–	–	–	–	–	–	–
Zn	–	–	–	–	0.0030	0.0073	0.0024	0.0038
Pb	0.00054	0.00038	–	0.00063	0.00078	0.00068	0.00063	0.00064

*MN – Macronutrients; ME – Microelements

Results show that concentration of elements in spent coffee grounds depends on how they were processed. Grounds processed with hot water contain lower concentration of macronutrients than with concentrated sulfuric acid. Except "Paulig" coffee brand, in which concentration of nitrogen processed both ways is almost the same (2.52 – 2.55 %). K_2O and P_2O_5 concentrations in grounds processed with hot water are almost four times lower than processed with sulfuric acid. Concentrations of microelements (Fe, Mn, Cu, Zn) in spent coffee grounds processed with hot water are very low or below analyzer's sensitivity threshold. However, there is no significant concentration difference in grounds processed with sulfuric acid. It is essential to mention that spent coffee grounds contain heavy metals such as chromium (0.004 – 0.0008 %) and lead (0.00063 – 0.00078 %).

Carbon content has been determined by using dichromate oxidation method with concentrated sulfuric acid and results vary between 3.31 – 3.44 %. Moreover, thermogravimetric analysis (TGA) and differential scanning calorimetry (DSC) were used to determine thermal stability and total weight loss of used coffee grounds. The functional groups in spent coffee grounds were identified with Fourier – transform infrared spectroscopy (FTIR). X – Ray Diffraction (XRD) results show that spent coffee grounds are amorphous compound.

[1] https://www.bio-bean.com/news-post/the-significant-value-of-spent-coffee-grounds
[2] https://wood-pellet-line.com/recycling-coffee-grounds-into-biomass-pellets-for-home-heating/
[3] https://newatlas.com/coffee-grounds-biofuel/49473/
[4] https://www.popsci.com/foam-made-from-coffee-can-clean-contaminated water
[5] https://www.gardena.com/lt/sodo-gyvenimas/sodo-zurnalas/paprastumas-is-gamtos-pasigaminkite-trasu/

CANCELLED DUE TO COVID-19

EVALUATION OF ELECTROCHROMIC PROPERTIES OF POLYPYRROLE FILMS MODIFIED BY PHENOTHIAZINE DERIVATIVES

Raimonda Bogužaitė[1], Vilma Ratautaitė[1], Arūnas Ramanavičius[1,2]

[1] Center for Physical Sciences and Technology, Department of Functional Materials and Electronics, Laboratory of Nanotechnology, Sauletekio av. 3, Vilnius LT-10257, Lithuania
[2] Vilnius University, Faculty of Chemistry and Geosciences, Institute of Chemistry, Naugarduko str. 24, LT-03225 Vilnius
raimonda.boguzaite@gmail.com

Electrochromism is the phenomenon, where the color of a material changes by applying a voltage [1]. This feature is very important for a wide range of materials such as smart windows, screens, thermal modulators and others [1]. Electrochromic properties are characteristic for some metal oxides and also some organic materials such as polymers too [2]. Polymers have a wide range of possibilities for both synthesis and application, and therefore can be used in the production of electrochromic materials [3]. Moreover, polymerization may involve phenothiazine derivatives that are biologically active [4]. Phenothiazine derivatives can be combined with other polymers, for instance pyrrole, in order to create electrochromic films with better properties [5, 6].

The aim of this research was to investigate three different syntheses of films based on polypyrrole and three phenothiazine derivatives - methylene blue, azure A, thionine. The conditions of these films where investigated and analyzed by different methods. Films were synthesized on indium tin oxide coated glass electrode by cyclic voltammetry (CV) method at scan rate of 50 mV/s between −0,2 and +1 V for 25 cycles, step potential 2,44 mV. The obtained films were analyzed by cyclic voltamperometry, chronamperometry, AFM methods. The surface morphology of the coatings was determined by AFM and it was found that the thickness of the surface irregularities ranges from 1 to 3 μm. The investigated polymeric coatings exhibited electrochromic properties (color change in different media), reacted to pH changes, ascorbic acid concentration. It is contemplated that coatings of pyrrole and methylene blue or thionine may also be used for ascorbic acid detection.

References

[1] C. G. Granqvist, Oxide electrochromics: An introduction to devices and materials, Sol. Energy Mater. Sol. Cells, 99, 1–13 (2012).
[2] Avni A. Argun, Pierre-Henri Aubert, Barry C. Thompson and and J. R. R. Irina Schwendeman, Carleton L. Gaupp, Jungseek Hwang, Nicholas J. Pinto, David B. Tanner, Alan G. MacDiarmid, Multicolored Electrochromism in Polymers: Structures and Devices, Chemistry of Materials, 16, 4401–4412 (2004)
[3] K. Hyodo, "Electrochromism of conducting polymers," Electrochim. Acta, 39, 265–272 (1994).
[4] L. G. L.T. Kubota, "Electrochemical Study of Flavins, Phenazines, Phenoxazines and Phenothiazines Immobilized on Zirconium Phosphate," J. Electroanal. Chem., 431, 23–27 (1999).
[5] B. Liu, H. Cang, L. Cui, and H. Zhang, "Electrochemical polymerization of methylene blue on glassy carbon electrode," Int. J. Electrochem. Sci., 12, 9907–9913 (2017).
[6] R. M. Ion, F. Scarlat, F. Scarlat, and V. I. R. Niculescu, "Methylene - Blue modified polypyrrole film electrode for optoelectronic applications," J. Optoelectron. Adv. Mater., 5, 109–115 (2003).

CANCELLED DUE TO COVID-19

SOURCE APPORTIONMENT AND OPTICAL PROPERTIES OF CARBONACEOUS AEROSOL PARTICLES

Agnė Minderytė[1,2], Julija Pauraitė[1], Steigvilė Byčenkienė[1*]

[1]Center for Physical Sciences and Technology, Saulėtekio av. 3, LT-10257 Vilnius, Lithuania
[2]Institute of Chemistry, Vilnius University, Naugarduko st. 24, LT-03225 Vilnius, Lithuania
agne.minderyte@ftmc.lt

CANCELLED DUE TO COVID-19

As the consequences of climate change are becoming more visible and difficult to manage, the importance of understanding the influence of composition and aging processes of atmospheric aerosols on climate and air quality is crucial. The impact of aerosol particles on climate and ecosystems comes from the ability to scatter or absorb solar radiation and alter optical properties of clouds. The interaction of light and the particle is strongly dependent on the chemical composition of aerosol particles. One of the most abundant light-absorbing components of atmospheric aerosols emerging from fossil fuel combustion and biomass burning in urban areas is black carbon (BC) which is strongly associated with air pollution and climate change. Its significance as a short-lived climate forcer was acknowledged in special report *Global Warming of 1.5 ℃* by IPCC [1]. And yet, the net impact of BC is still unknown as it can influence climate through multiple mechanisms [2].While the importance of BC light absorption to atmospheric radiative balance is widely known, the input of colored organic aerosol (OA) (known as light absorbing brown carbon (BrC)) is often downgraded. In fact, recent studies demonstrated that BrC accounts for 20-40% of the total absorption by carbonaceous aerosols and causes radiative effects of +0.1 to +0.6 W/m^2 in global scale [3].

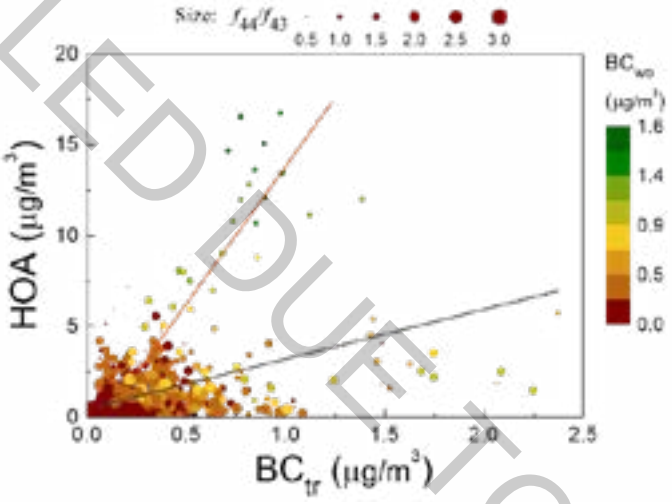

Figure 1 The relationship between HOA, BCwb and BCtr mass concentrations with PMF analysis findings.

An Aerosol Chemical Speciation Monitor (ACSM) and a 7-wavelength Aethalometer were deployed in Vilnius (urban background site) in October 2014 – April 2015. The aim of this study is to perform a systematic source apportionment for OA and BC by examining dynamics of mass concentration and optical properties as well as BrC absorption coefficient alteration during heating and non-heating seasons. In order to separate BC_{tr} (originated from traffic emissions) and BC_{wb} (originated from biomass burning) the most suitable values of AAE (absorption Angstrom exponent) were selected (0.9 and 2.09), respectively. It has been found that during heating season contribution of BCwb to total BC was 55%. OA source apportionment analysis (PMF) revealed four main sources: hydrocarbon-like OA (HOA), local OA (LOA), biomass burning OA (BBOA) and oxygenated OA (OOA). Diurnal analysis showed that HOA mass concentration variation corresponds well with the traffic rush hours. However, low correlation was found between HOA and BC_{tr} mass concentrations, indicating that HOA could originate not only from fossil fuel combustion (Figure 1). The results of this study will provide additional insights into forecasting the radiative forcing in local and global scale.

[1] V. Masson-Delmotte *et al.*, "Global Warming of 1.5 °C. An IPCC special report on the impacts of global warming of 1.5 °C above pre-industrial levels and related global greenhouse gas emission pathways, in the context of strengthening the global response to the threat of climate chang," 2018.

[2] J. Schacht *et al.*, "The importance of the representation of air pollution emissions for the modeled distribution and radiative effects of black carbon in the Arctic," *Atmos. Chem. Phys. Discuss.*, pp. 1–39, 2019.

[3] Q. Wang *et al.*, "High Contribution of Secondary Brown Carbon to Aerosol Light Absorption in the Southeastern Margin of Tibetan Plateau," *Geophys. Res. Lett.*, vol. 46, no. 9, pp. 4962–4970, 2019.

THE REGIOSELECTIVITY OF ASYMMETRIC OXIRANE RING-OPENING BY BENZOATE ANION

Evgeniia Bakhalova[1], Yulia Bespalko[2], Elena Shved[1]

[1] Department of Chemistry, Biology and Biotechnologies, Vasyl' Stus Donetsk National University, Vinnytsia, Ukraine
[2] Department of Chemistry, University of Leuven, Belgium
je.bahalova@donnu.edu.ua

CANCELLED DUE TO COVID-19

The reaction of oxiranes with proton-donor nucleophilic reagents in the presence of bases is important both for the development of theoretical concepts regarding the reactivity of organic compounds and reaction mechanisms, and for wide practical application, in particular, in the chemistry of polymers. The asymmetric oxirane ring-opening gives "normal"(I) and "abnormal"(II) products. Only product (I) is used for synthesis of epoxy resins.

In order to study reaction regioselectivity of the oxirane ring opening by the benzoate-anion of "2-(chloromethyl)oxirane – benzoate anion" system a quantum-chemical modeling was utilized [1]. Transition state Z- and E- equilibrium configurations on the reaction path were evaluated for the backside and frontside attack by nucleophile on primary (α) and secondary (β) carbon atoms of 2-(chloromethyl)oxirane. Geometric and activation parameters of possible transition states were established for potential ring-opening ways. Via the values of the fraction of bond formation / cleavage it was shown that transitional states belong to dissociative. The study of stereo- and regioselectivity in the "2-(chloromethyl)oxirane – benzoate anion" reaction system by quantum chemistry revealed that the oxirane ring opening in (α) -carbon is energetically favorable (TS2, Fig. 2). It has been established that using of the benzoate anion as a nucleophile provides the S_N2 mechanism contribution increase and the "boundary" S_N2 mechanism contribution decrease, which leads to the reaction stereoselectivity and regioselectivity increase. The possible directions of nucleophilic attack during the oxirane ring-opening are shown schematically in Fig. 3: backside and/or front attack, and the relative position of benzoate anion and chloromethyl group (Z- and E-configurations).

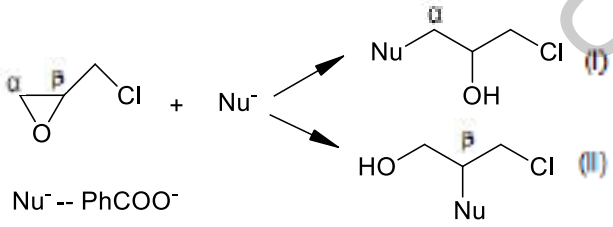

Fig. 1. The oxirane ring opening by benzoate anion

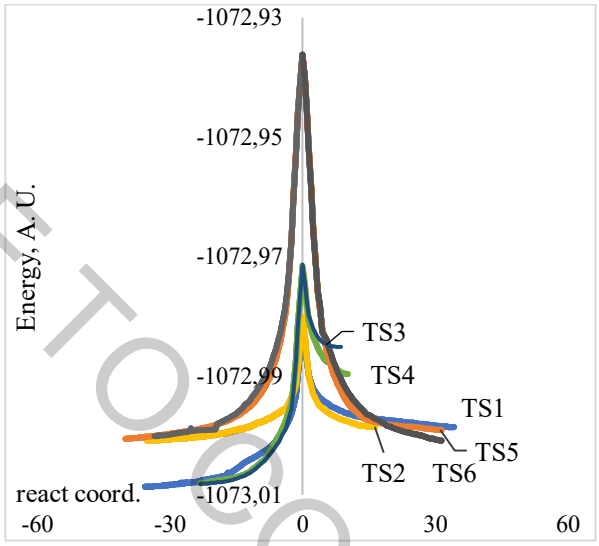

Fig. 2. Energy diagrams of the oxirane ring-opening by benzoate anion passed through TS1-TS6 for the gas phase

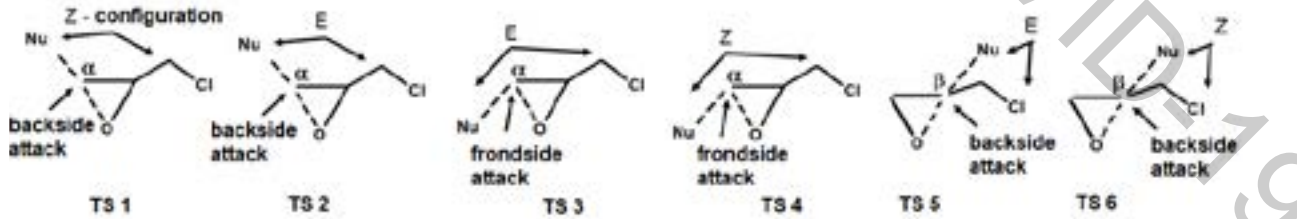

Fig. 3. Transitional state structures for different directions of nucleophilic attack during the oxirane-ring opening

This statement is confirmed by experimental data [2]. Interaction of 2-(chloromethyl)oxirane with benzoic acid and 3-nitrobenzoic acid (catalyst - tetraethylammonium bromide, N,N-dimethylaniline) results in ca. 89 and 92% of the nomalous product (I) yield.

[1] E. A. Bakhalova, Y. M. Bespalko, E. M. Shved Modelyuvannya povedinky benzoaktyvnykh tetraalkilamoniyu v reaktsiyakh rozkryttya oksyranovoho tsyklu 2- (khlormetyl) oksydu karbonovykh kysloty. Bulletin of Dnipropetrovsk university. Series Chemistry, 25(2), 65-72 (2017).
[2] M.A. Sinel'nikova, E.N. Shved, Regioselectivity of the Acidolysis of 2-(Chloromethyl)oxirane with Aromatic Acids in the Presence of Organic Bases. Russian Journal of Organic Chemistry, 50(3), 332–336 (2014).

USE OF WOOD ASH IN THE FOREST AND ITS EFFECT ON THE CHEMICAL ELEMENT FLOW IN BLUEBERRIES *(VACCINIUM MYRTILLUS L.)*

Vitālijs Lazarenko[1], Vita Rudoviča[1], Arturs Vīksna[1], Māris Bērtiņš[1], Zaiga Anna Zvaigzne[2], Modris Okmanis[2]

[1]University of Latvia, Faculty of Chemistry, Jelgavas iela 1, Riga, Latvia
[2]Latvian State Forest Research Institute "Silava", Rīgas iela 111, Salaspils, Latvia
vitalijs.lazarenko@lu.lv

CANCELLED DUE TO COVID-19

Wood ash is a biological residue produced by the combustion of wood or their products (chips, sawdust, etc.). Fertilizing is one of the main ways for using wood ash because it contains high amount of nutrients that are necessary for the development of plants and trees. Using wood ash as a fertilizer allows to solve following problems – ensures efficient utilization and disposal of wood ash from industrial areas and prevents valuable nutrients from being wasted.

Several studies have proved that fertilization with wood ash affects only topsoil. Also, wood ash can contain high amount of heavy metallic elements and metalloids such as Cd, As and Pb which can cause poisoning of a plant.

One of the main goals of the policy in Latvia is to preserve and increase the amount of forest land areas. After deforestation processes soil buffer capacity and nutrient reserves reduces what causes soil acidification and deterioration of growing conditions. To avoid these adverse processes and improve forest growth condition, wood ash is used as a fertilizer.

The wild-growing blueberries *(Vaccinium myrtillus L.)* is one of the most popular berries which are located in Europe, North America and Asia. They are deciduous species as they shed leaves during fall seasons preparing for winter. In some studies blueberries are used as a model species for forest ecosystem monitoring as they are sensitive to environmental changes (temperature, humidity, soil chemical composition, etc.).

The aim of our research was to analyse the flow of chemical elements in blueberries in the forest areas which was fertilized with wood ash.

For research were chosen two pine forest areas which was fertilized with fly and bottom wood ash. Approximately 3 tons per hectare. In order to evaluate the impact of wood ash on the forest, two different types of plots were selected in each area – fertilized and control.

Blueberry samples were dried till air-dry condition and digested in the mixture of HNO_3:H_2O_2 (6:2) using the closed microwave digestion system. The chemical element concentration was determined by ICP-MS.

The distribution of wood ash in the forest area did not change the macro and micro element content of blueberry berries.

The research results show that in the area which was fertilized with fly wood ash there is observable trend that in the fertilized sampling plots rare earth element content in blueberry roots are ~2-5 times higher than in the plant root system of control plots.

Calculated transfer factor values indicate that content of micro and rare earth elements accumulates in the root system of blueberry plants.

This work was supported by Short term scientific mission organized in scope of project "Research program on improve of forest growth conditions 2016-2021".

LEMON JUICE AS PYRAZOLE REACTION MEDIUM

Daria Łuczak[1], Adam Marek Pieczonka[1]

[1]Department of Organic and Applied Chemistry, Faculty of Chemistry, University of Łódź, Tamka 12, 91-403 Łódź, Poland
e-mail: daria.luczak@op.pl

Lemons are among the world's most popular citrus fruits. Lemons contain many plant compounts, minerals and essential oils additionally they are a great source of vitamin C and fiber. Lemon juice can be used in various fields: medical, cosmetic, food, chemical, etc. Additionally, reactions in lemon juice are an interesting subject in green chemistry.

Pyrazoles are an interesting class of five-membered heterocyclic compounds which show diverse activities (biological activities, ligands in cross-coupling reactions and optical sensors) [1]. Among them tetraarylpyrazoles exhibit luminescence properties [2]. There are several methods for the synthesis of pyrazoles, such as: reaction of chalcones and hydrazines, coupling of hydrazine, aldehyde and ethyl acetoacetate but these reactions are often performed at elevated temperature in organic solvents, and in the presence of different harmful catalysts [3].

Reactions using lemon juice as medium are eco-frendly. In our research we used lemon juice as a medium in the synthesis of N-acyl substituted 3,5-dimetylpyrazoles with luminescent properties (Fig. 1). Different aromatic carbohydrazides were transformed into expected pyrazole derivatives with high yields. Pyrazoles with large aromatic substituents have luminescent properties in solution as well as in the solid state.

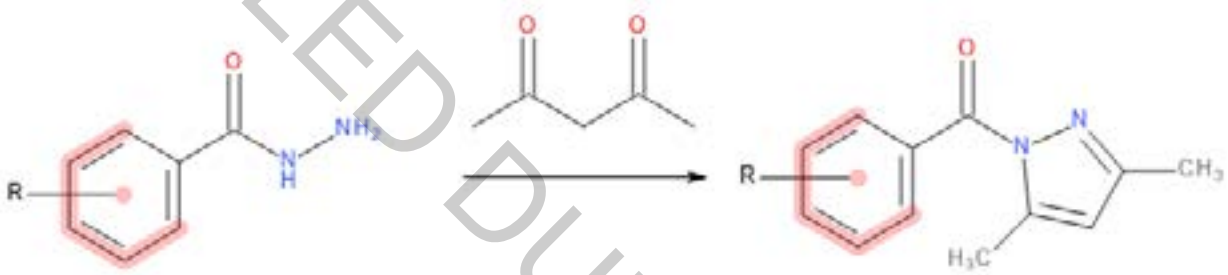

Fig. 1. General procedures for systhesis of pyrazole derivatives.

CANCELLED DUE TO COVID-19

[1] B. R. Vaddula, R. S. Varma, J. Leazer, Mising with microwaves: solvent-free and catalyst-free synthesis of pyrazoles and diazepines, Tetrahedron Letters **54**, 1538-1541 (2013).
[2] S. Mukherjee, P. S. Salini, A. Srinivasan, S. Peruncheralathan, AIEE phenomenon: tetraarys vs. triaryl pyrazoles, Chem. Commun **51**, 17148 (2015).
[3] V. Milovanović, Z. D. Petrović, S. Novakowić, G. A. Bogdanović, D/ Simijonović, V. P. Petrović, Structural characterization of benzoyl-1H-pyrazole derivatives obtained in lemon juice medium: Experimental and theoretical approach, Journal of Molecular Structure **1195**, 85-94 (2019).

SINGLE SCATTERING ALBEDO DEPENDENCE ON AEROSOL SIZE AND CHEMICAL COMPOSITION

Julija Pauraitė, Steigvilė Byčenkienė, Kristina Plauškaitė and Vidmantas Ulevicius

[1] Center for Physical Sciences and Technology, Vilnius, Lithuania
julija.pauraite@ftmc.lt

Atmospheric aerosols can significantly influence local and global climate. The impact of particles depends on their chemical composition and physical properties (such as optics). The the light absorption and light scattering are two main interaction processes in the atmosphere between aerosol particles and solar radiation. Large uncertainties in estimating the aerosol radiative forcing [1] urge a better understanding of optical processes in the atmosphere. Single scattering albedo (SSA) is the essential parameter of aerosol optical properties, which enables investigation of total aerosol radiative forcing effect. Therefore, SSA is a key input parameter in climate models.

We investigated aerosol optical properties during domestic heating season in Preila (rural-coastal background site). During measurement campaign in December 2017 – March 2018, we deployed an Aerosol Chemical Speciation Monitor (ACSM), a 7-wavelength Aethalometer and an integrating Nephelometer (TSI). Additional measurements included the meteorological parameters (temperature, relative humidity, solar radiation and wind speed). Absorption Angström exponent (AAE), scattering Angström exponent (SAE) and SSA were calculated. Furthermore, absorption due to coloured organics known as brown carbon (BrC) was evaluated.

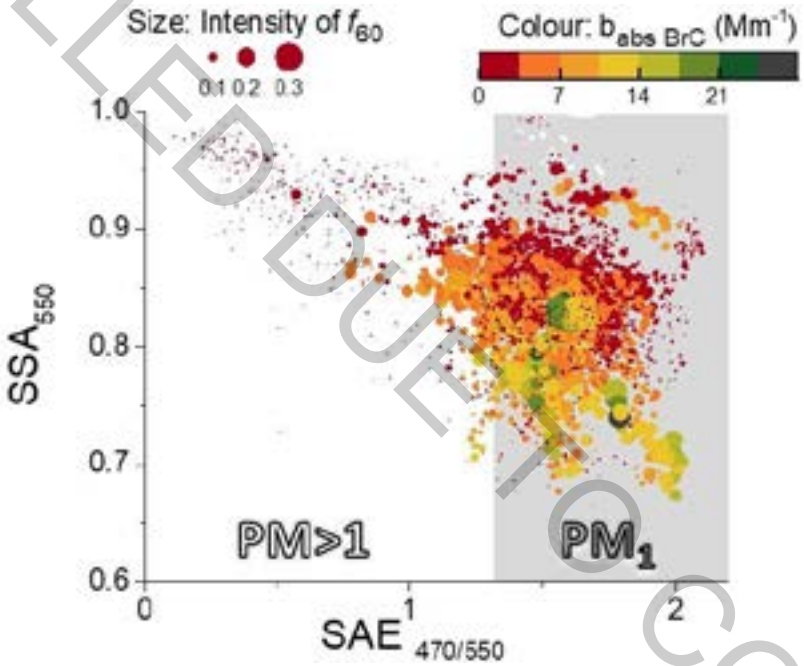

Fig. 1. SSA at 550 nm for all measurement period versus SAE at 470 and 550 nm. Size range stands for intensity of the signal f_{60}. Absorption coefficient of BrC depicted in colour scale. Division by sizes suggested by Cappa et al., 2016[2].

As can be seen in Fig. 1, SSA shows a strong dependence on both size and chemical composition. The lowest SSA values were reached when PM_1 fraction was dominating. Furthermore, decrease in SSA could be associated with higher f_{60} together with higher absorption coefficient of BrC. These results indicate fresh combustion products contribute to the atmospheric heating the most while with aging and bleaching processes the capability to heat decreases. These results will benefit in understanding the SSA sensitivity towards different atmospheric processes and to the broad extend will provide knowledge for modelling of atmospheric radiative balance.

This work was supported by by the COST Action CA16109 COLOSSAL (Chemical On-Line cOmpo- Sition and Source Apportionment of fine aerosoL).

[1] P. Forster et al., Changes in Atmospheric Constituents and in Radiative Forcing, Condensed Matter and Materials Physics, **77**, 129-234 (2008).
[2] C. D. Cappa et al., Understanding the optical properties of ambient sub- and supermicron particulate matter: results from the CARES 2010 field study in northern California, Atmospheric Chemistry and Physics, **16**, 6511–6535 (2016).

CANCELLED DUE TO COVID-19

SYNTHESIS AND INVESTIGATION OF ORGANIC SEMICONDUCTORS FOR TADF OLEDs

Kestutis Dabrovolskas, Dalius Gudeika

Kaunas University of Technology, Department of Polymer Chemistry and Technology, Lithuania Radvilėnų plentas 19, LT-50254, Kaunas Lithuania
kestutis.dabrovolskas@ktu.edu

Over the years organic light-emitting diodes (OLEDs) have shown a wide variety of excellent properties, such as energy consumption, flexibility, light weight etc. Therefore, they have become a highly promising technology for flat panel displays [1]. Seeing that first-generation materials for OLEDs are fluorescent and have greatly limited efficiency up to 25% [2] and on the other hand second-generation OLEDs use phosphorescent materials that can achieve almost 100% but require expensive heavy metals such as platinum and iridium [3]. In response to these issues the search for efficient and cheap luminescent materials lead to purely organic materials with thermally activated delayed fluorescence (TADF) [4]. OLEDs based on such emitters enable the possibility to harvest both triplet and singlet excitons, duo to very low energy gap (ΔE_{ST}), theoretically granting internal quantum efficiencies of up to 100% of the devices [5].

In this work synthesized compounds and their thermal, electrochemical, photophysical, electrochemical, photoelectrical properties as well as device characterization is going to be presented.

Acknowledgement. This project has received funding from the Research Council of Lithuania (LMTLT), agreement No [S-LU-20-3].

[1] Zhang. P, et al., New Aggregation-Induced Delayed Fluorescence Luminogens With Through-Space Charge Transfer for Efficient Non-doped OLEDs, Front. Chem. **7:199**, 1-11 (2019).
[2] C. W. Tang, S. A. VanSlyke, Organic electroluminescent diodes, Appl. Phys. Lett. **51**, 913 (1987).
[3] B. Minaev, et al., Principles of phosphorescent organic light emitting devices, Phys. Chem. Chem. Phys. **16**, 1719–1758 (2014).
[4] H. Wang, et al., Novel thermally activated delayed fluorescence materials-thioxanthone derivatives and their applications for highly efficient OLEDs, *Adv. Mater. Weinheim.* **26**, 5198–5204 (2014).
[5] H. Kaji, et al, Purely organic electroluminescent material realizing 100% conversion from electricity to light, *Nat. Commun.* **6**, 8476 (2015).

CANCELLED DUE TO COVID-19

HYDRO(SOLVO)THERMAL SYNTHESIS OF $NaTi_2(PO_4)_3$ AS ANODE MATERIAL FOR NA-ION BATTERIES

Gintarė Plečkaitytė[1], Jurgis Pilipavičius[1], Milda Petrulevičienė[1], Jurga Juodkazytė[1], Linas Vilčiauskas[1]

[1] Center for Physical Sciences and Technology, Saulėtekio al. 3, LT-10257 Vilnius, Lithuania
gintare.pleckaityte@ftmc.lt

Electrochemical batteries are deemed to be one of the most attractive alternatives for electrical energy storage, covering the widest available power and energy range as well as having superior round-trip energy efficiencies, low environmental footprint, and easy scalability. Li-ion batteries are more and more widely used as rechargeable power sources, owning to their high energy and power density. However, the high cost of Li and necessary transition metals as well as safety issues related to the use of highly flammable electrolytes have pushed towards the search for alternatives. Na-ion batteries and especially their aqueous variants are attracting particular attention as potential candidates for large-scale energy storage because of the accessible and unlimited Na resources and elimination of certain rare transition metals. Moreover, the aqueous aspect makes them significantly safer, non-flammable, low cost and environmentally friendly in comparison to the current Li-ion technology [1-3]. NASICON (Na SuperIonic Conductor) type compounds have been intensively investigated as promising cathodes and anodes for Na-ion batteries due to their open framework structure which enables fast Na ionic conduction and provides superior electrochemical durability [4].

The aim of this work is to find new materials based on such phosphate frameworks suitable for application as novel battery electrode materials, optimize their properties, morphology and composite microstructure for the use in aqueous Na-ion battery cells [5]. Pure phase NASICON-type $NaTi_2(PO_4)_3$ material is synthesized by hydro(solvo)thermal synthesis method by varying a number of parameters such as solvent (ethylene glycol, ethanol, water), temperature (140-200°C) and synthesis time. The structure and morphology of prepared materials are characterized by X-Ray Diffraction and Scanning Electron Microscopy. The electrochemical properties of prepared $NaTi_2(PO_4)_3$ based electrodes are investigated by Cyclic voltammetry and Charge/Discharge galvanostatic cycling in the three-electrode bottom mount flat sample beaker cells. The results (Fig. 1) show that truly nanostructured pure phase $NaTi_2(PO_4)_3$ and carbon composites could be obtained using the hydro(solvo)thermal methods showing superior electrochemical response.

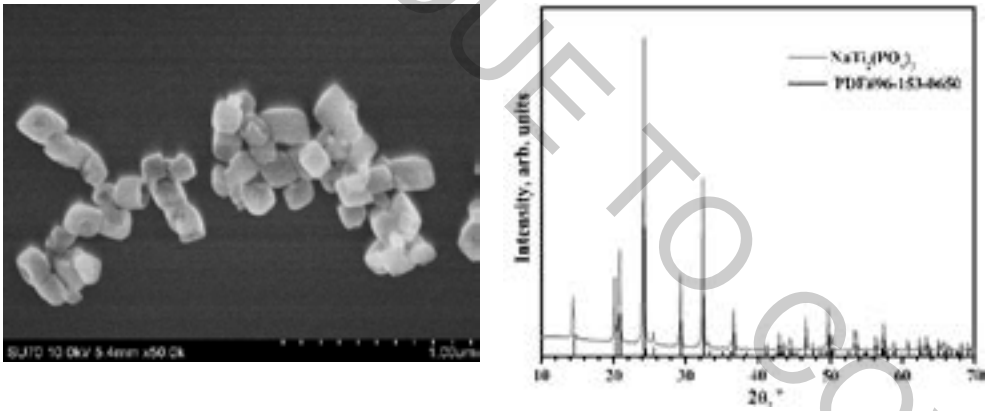

Fig. 1. SEM image (left) and XRD pattern (right) of $NaTi_2(PO_4)_3$.

Acknowledgements:
This project has received funding from the European Regional Development Fund (Project No. 01.2.2-LMT-K-718-02-0005) under grant agreement with the Research Council of Lithuania (LMTLT).

[1] X. Pu, H. Wang, D. Zhao, H. Yang, X. Ai, S. Cao, Z. Chen, Y. Cao, Recent Progress in Rechargeable Sodium-Ion Batteries: toward High-Power Applications, Small 15, 1805427 (2019).
[2] P. K. Nayak, L. Yang, W. Brehm, P. Adelhelm, From Lithium-Ion to Sodium-Ion Batteries: Advantages, Challenges and Surprises, Angew. Chem. Int. Ed. 57, 102 –120 (2018).
[3] H. Kim, H. Kim, Z. Ding, M. Hwan Lee, K. Lim, G. Yoon, K. Kang, Recent Progress in Electrode Materials for Sodium-Ion Batteries, Adv. Energy Mater., 1600943 (2016).
[4] C. Masquelier, L. Croguennec, Polyanionic (Phosphates, Silicates, Sulfates) Frameworks as Electrode Materials for Rechargeable Li (or Na) Batteries, Chem. Rev. 113, 8, 6552-6591 (2013).
[5] M. Wu, W. Ni, J. Hu, J. Ma, NASICON-Structured $NaTi_2(PO_4)_3$ for Sustainable Energy Storage, Nano-Micro Letters 11, 44 (2019).

CANCELLED DUE TO COVID-19

HYDROGEL BASED MICRO AG/AGCL REFERENCE ELECTRODES. QUICK PROTOTYPING OF REFERENCE ELECTRODES

Eivydas Andriukonis[1,2], Marius Butkevicius[3]

[1]Faculty of Chemistry and Geosciences, Department of Physical Chemistry, Vilnius University, Vilnius, Lithuania.
[2]Laboratory of Nanotechnology, Center for Physical Sciences and Technology, Vilnius, Lithuania.
[3]Institute of Biochemistry, Life Sciences Center, Vilnius University, Vilnius, Lithuania.
eivydas.andriukonis@ftmc.lt

Electrochemical measurements are based on the control or observation of potential at the working electrode, for that purpose an electrode of constant potential is needed. Reference electrode (RE) has a fixed potential and this potential does not change as current flows through it. One of the most popular RE is Ag/AgCl electrode. Ag/AgCl RE is often used for electrochemical measurements due to simplicity, inexpensive design, and nontoxic components. These RE are commercially available in various shapes, sizes, junctions and other parameters. However when developing an electrochemical device prototypes there can rise necessity to make unconventional shape or size RE.

Here we explore applicability of RE membrane preparation from polyacrylamide hydrogel. During experimenting we observed almost excellent electrochemical performance of "in house" made RE compared with several commercially available ones. The electrode potential difference was 40 mV versus the calomel electrode and 7 mV versus the commercial Ag/AgCl electrode. On the other hand polyacrylamide membranes have porous micro/nano structure with varying pore sizes, which was observed with scanning electron microscopy. Observed porous structure does not permit leakage of inner chloride ions, as chloride flux was evaluated. Permeability to chloride ions doesn't make polyacrylamide hydrogel an ideal membrane in long term experiments. Though as membranes are quickly and easily prepared it is ideal candidate for quick electrochemical system designing and testing even possible application in disposable one time use devices.

CANCELLED DUE TO COVID-19

HIGHLY DIASTEREOSELECTIVE SYNTHESIS OF POLYCYCLIC ALCOHOLS VIA ANIONIC CASCADE CYCLIZATION

Arminas Jurys[1], Tomas Javorskis[1,2], Ieva Karpavičienė[1], Gustautas Snarskis[2], Rita Bukšnaitienė[1], Edvinas Orentas[1]*

[1] Department of Organic Chemistry, Vilnius University, Lithuania
[2] Department of Nanoengineering, Center for Physical Sciences and Technology, Lithuania
arminas.jurys@chgf.vu.lt

CANCELLED DUE TO COVID-19

Polycyclic molecular architectures are the hallmark of many important bioactive natural products. The structural complexity of such compounds often represents a formidable challenge in their synthesis and requires multistep tedious procedures to ensure the correct installation of all stereogenic centers. On the other hand, cascade cyclization reactions where one step occurs after another along a well-defined sequence of events allows an access to complex polycyclic scaffolds in one-pot operation. The cation initiated cyclization cascades of unsaturated substrates are well known and widely utilized in both biological and synthetic setups, however, the corresponding anionic reactions are much less explored.

Herein we report a hitherto unknown cascade cyclization reaction representing the first example of formal [2+2] cycloaddition reaction between ketone enolates and allenes. The careful choice of base enables a well-orchestrated synthetic sequence via *in situ* formation of allene from the corresponding propargylic ethers. Subsequent addition of ketone enolate results in the formation of anionic intermediate which after intramolecular addition to carbonyl group affords unique polycyclic scaffold comprising of fused six-, five- and four-membered rings. The reaction is fully diastereoselective and allows the assembly of otherwise hardly accessible compounds possessing four consecutive quaternary carbons.

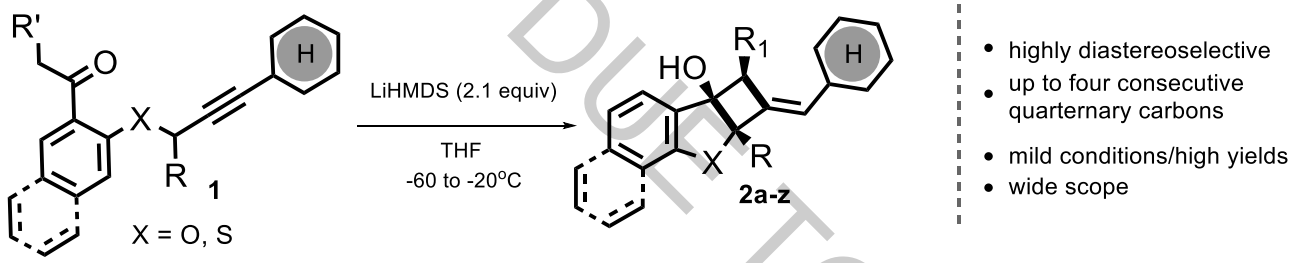

Fig. 1. Anionic cascade cyclization initiated by an addition of enolate to *in situ* formed allene.

OPTICAL AND ELECTROCHEMICAL DETECTION OF UREA BY USING PRUSSIAN BLUE MODIFIED ELECTRODES

Gabija Kavaliauskaitė[1], Povilas Virbickas[1], Giedrė Medvikytė[1], Aušra Valiūnienė[1]

[1]Department of Physical Chemistry, Faculty of Chemistry and Geosciences, Vilnius University, Vilnius, Lithuania
kav.gabija@gmail.com

Carbamide ($CO(NH_2)_2$), better knonwn as urea, is an organic amide, which is the final product of protein degradation in the human body. High carbamide levels in blood or body fluids can be associated with kidney failure or liver malfunction [1]. This medical reason is very important cause for finding new, fast and inexpensive methods for urea detection. Iron hexacyanoferrate (Prussian blue (PB)) is an inorganic, electrochromic compound, which is selective for several monovalent ions (Cs^+, Rb^+, K^+ and NH_4^+). These ions (Cs^+, Rb^+, K^+ and NH_4^+) is incorporated in the crystal lattice of PB when PB is electrochemically reduced in Cs^+, Rb^+, K^+ or NH_4^+ ions containing solution [2]. Moreover, the concentration of PB reduction promoting ions (Cs^+, Rb^+, K^+ and NH_4^+) affects the reduction potential of PB. For this reason, PB can be used as a signal transducer in optical and electrochemical analytical systems, such as electrochemical ion sensors [3].

In this research concentration of urea was evaluated due to electrochromic PB selectivity to ammonium ions: the addition of ammonium ions into the electrochemical cell causes the increase of PB reduction potential (Fig. 1 A). Therefore, when the constant electric potential (0.2 V *vs* Ag|AgCl|KCl_{sat}) is applied to the PB coating, the increase of ammonium ions concentration causes the reduction of PB into the colorless form (Prussian white (PW)) (Fig. 1 B). During this experiment, ammonium ions were generated in the electrochemical cell by applying enzymatic urea hydrolysis (Fig. 1 B) or electrochemical oxidation of urea (Fig. 1 A). In both cases, concentration of ammonium ions was proportional to the concentration of urea.

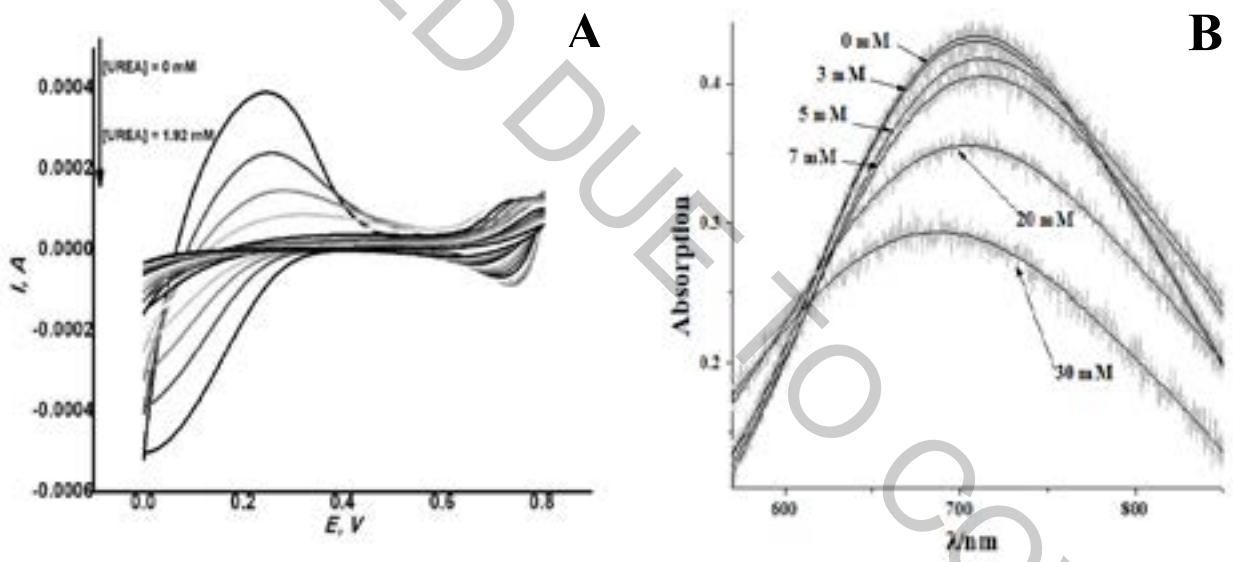

Fig. 1 Prussian Blue modified electrode electrochemical (A) and optical (B) signal dependence on urea concentration.

This project has partly received funding from European Social Fund (project No [09.3.3-LMT-K-712-16-0278]) under grant agreement with the Research Council of Lithuania (LMTLT).

[1] C.S. Pundir, S. Jakhar, N. Vinay, Determination of urea with special emphasis on biosensors: A review, Biosens. Bioelectron. 123, p. 36 – 50 (2019).
[2] A.A. Karyakin, E.E. Karyakina, L. Gorton, On the mechanism of H2O2 reduction at Prussian blue modified electrodes, Electrochem. Commun. 1, p. 78 – 82 (1999).
[3] Arkady A. Karyakin, Prussian Blue and Its Analogues: Electrochemistry and Analytical Applications, Electroanalysis 13, No. 10, p. 813 – 819 (2001).

CANCELLED DUE TO COVID-19

SCANNING ELECTROCHEMICAL MICROSCOPY APPLICATION FOR HYBRID PHOSPHOLIPID BILAYER INVESTIGATION AND MODIFICATION

Margarita Poderyte, Inga Gabriunaite, Ausra Valiuniene

Faculty of Chemistry and Geosciences, Vilnius University, Naugarduko str. 24, Vilnius, Lithuania
margarita.poderyte@chgf.stud.vu.lt

Essential part of every living cell is its plasma membrane. Not only it surrounds the cell, but also controls materials transportation and is involved in transmitting a signal coming from the environment [1]. Due to the complex structure of biological membranes, various cell membrane-modeling derivatives have been developed. Solid supported bilayer phospholipid membranes are used as stable phospholipid membranes models for investigating various biologically relevant processes since it exhibits most of the bilayer properties and are quite easy to produce [2]. Widely investigated membrane property is selective permeability, which can be modified. One of the ways to achieve this is electroporation - a physical method in which cells are subjected to an electrical impulse. This results in the formation of pores in the phospholipid layer [3]. Although electroporation is already used in practice (electrochemotherapy, genetic engineering, food industry), certain studies on the size of the pores formed and the time of pore closure are still relevant [4]. By being able to control these process parameters, the phenomenon of electroporation could be applied more extensively and efficiently.

In this work a glass plate coated with a layer of tin oxide doped with fluorine atoms (FTO) was used as a substrate for self-assembled monolayer (SAM) and phospholipid bilayer membrane (BLM) formation. Octadecyl trichloro silane (OTS) was used to form SAM. The hybrid phospholipid bilayer membrane was prepared using the vesicle fusion method from 1,2-dioleoyl-sn-glycero-3-phosphocholine (DOPC) and cholesterol in phosphate buffer solution (PBS).

In the present research scanning electrochemical microscope (SECM) was applied to investigate hybrid phospholipid bilayer (BLM) surface properties and modify it with electric impulse. Measurements with SECM are widely used in researching or modifying biological systems since it is carried out in a liquid medium that can be easily biocompatible. The SECM signal is a Faradaic current flowing through an ultra-microelectrode (UME) which radius can range from several nm to 25 μm. UME can be moved in space in x, y and z directions which allows to scan the surface and depict it [5]. Through targeted feedback mode approach experiments, SECM was applied to locally detect membrane surface, electroporate it and capture the changes. Reversible and irreversible electroporation was achieved by varying different aspects of method: UME potential vs Ag/AgCl/KClsat, electric impulse time and electrode height above the surface. Since the pores are formed directly below UME (working electrode), with SECM it becomes possible to perform locally targeted electroporation. It has been found that in order to obtain reversible electroporation, it is necessary to leave the system for a certain time period without giving it any potential. It is also assumed that the size of the resulting pores formed should depend on the size of the UME used.

These experiments lead to a promising expectation that SECM has a great potential in controlling electroporation phenomenon.

[1] Chance, B., Mueller, P., De Vault, D., & Powers, L. (1980). Biological membranes. Physics Today, 33(10), 32–38.
[2] Gabriunaite, I., Valiūnienė, A., & Valincius, G. (2018). Formation and properties of phospholipid bilayers on fluorine doped tin oxide electrodes. Electrochimica Acta, 283, 1351–1358.
[3] Tarek, M. (2005). Membrane electroporation: A molecular dynamics simulation. Biophysical Journal, 88(6), 4045–4053.
[4] Kandušer M., Miklavčič D. (2009) Electroporation in Biological Cell and Tissue: An Overview. In: Electrotechnologies for Extraction from Food Plants and Biomaterials. Food Engineering Series. Springer, New York, NY
[5] Daniel, M. (2012). Micro- and Nanopatterning Using Scanning Electrochemical Microscopy. Scanning Electrochemical Microscopy, Second Edition, 489–524.

CANCELLED DUE TO COVID-19

THE INFLUENCE OF GROWTH RATE AND SUBSTRATES' THERMAL EXPANSION COEFFICIENT ON PROPERTIES OF NANOCRYSTALLINE La-Sr-Mn-Co-O FILMS

Milita Vagner[1,2], Karolis Motiejuitis[1], Valentina Plaušinaitienė[1,2]

[1] Institute of Chemistry, Faculty of Chemistry and Geosciences, Vilnius University, LT- 03225 Vilnius, Lithuania
[2] Department of Functional Materials and Electronucs, Center for Physical Sciences and Technology, LT-10257 Vilnius, Lithuania
milita.vagner@chgf.vu.lt

CANCELLED DUE TO COVID-19

Thin polycrystalline manganite-cobaltite (LSMCO) films are interesting for their magnetoresistive (MR) properties and current application as room temperature B-scalar magnetic field sensors. Further research activities were performed in order to enable application of nanostructured LSMCO films in weak magnetic field sensing. In previous research it was determined the dependence of MR and electrical properties on Co content and on intrinsic tensile strain in the LSMCO films [1]. On the other hand, the tensile strain is largely influenced by the thermal expansion coefficient of the used substrates and the thin film growth rate [2].

In the present research the strain influence on the properties of nanostructured LSMCO films is investigated. Therefore, pulsed-injection metalorganic chemical vapor deposition (PI-MOCVD) method was used for the deposition of nanostructured $La_{0,81}Sr_{0,19}Mn_{1,09}Co_{0,06}O_3$ on substrates with different thermal expansions coefficients: polycrystalline Al_2O_3 (7.6 x 10^{-6} K^{-1}), x-cut $LiTaO_3$ (LTO_x) (16.1 x 10^{-6} / K^{-1}) and Zerodur® (0.5 x 10^{-6} / K^{-1}). Furthermore, the growth rate influence was investigated by growing 400 nm thick LSMCO films at different deposition rates at the growth temperature of 600 °C.

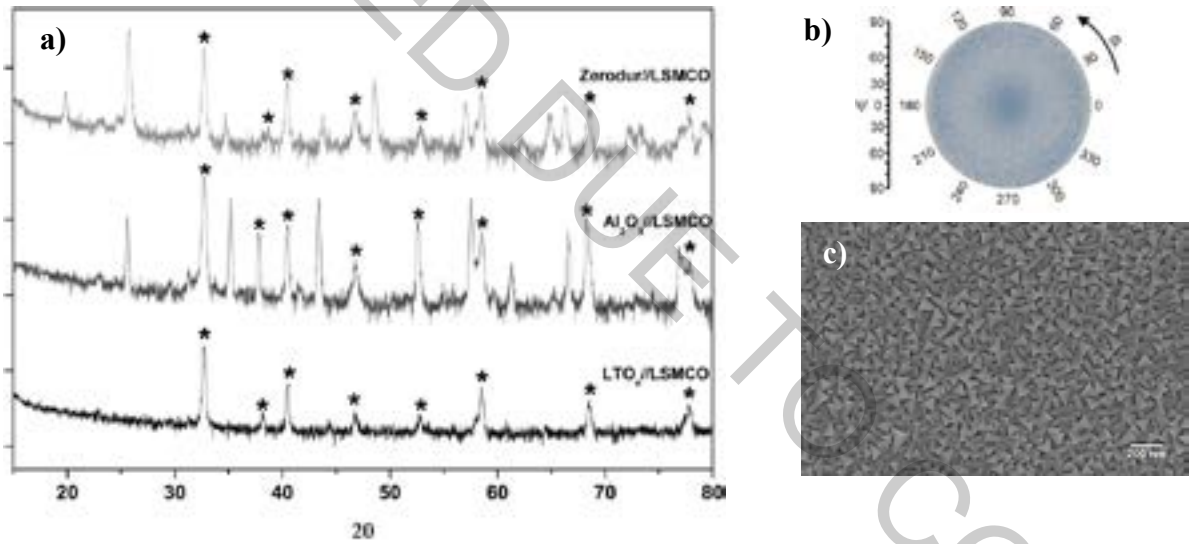

Fig 1. a) Grazing incidence diffractograms of LSMCO thin films grown on different substrates, where stars indicate characteristic reflection peaks of LSMCO; b) Characteristic (111) pole figure of polycrystalline LSMCO on Al_2O_3 substrate; c) Characteristic scanning electron microscope (SEM) image of nanostructured LSMCO films.

Despite the difference in thermal expansion coefficients of the substrates, all grown LSMCO films were polycrystalline (Fig. 1a). The characteristic (111) pole figure (Fig. 1b) as well as SEM images (Fig. 1c) confirmed the nanostructured behavior of LSMCO films with the average grain size below 100 nm.

[1] Vagner, M., et al. (2020). "PI-MOCVD technology of (La, Sr)(Mn, Co)O3: From epitaxial to nanostructured films." Surface and Coatings Technology **385**: 125287.
[2] G. Abadias, et al. (2018). "Review article: Stress in thin films and coatings: Current status, challenges, and prospects". J. Vac. Sci. Technol. A **36**: 020801.

MODELING BETA-CAROTENE INTERNAL CONVERSION IN THERMAL ENVIRONMENT USING DIRAC-FRENKEL VARIATIONAL METHOD

Mantas Jakučionis[1], Darius Abramavičius[1]

[1] Institute of Chemical Physics, Vilnius University, Lithuania
mantas.jakucionis@ff.vu.lt

Theoretical description of molecular excitation dynamics is a complex quantum mechanical problem, because interactions between all constituent parts of a molecule have to be considered at an *ab-initio* level. Therefore, complex quantum chemistry methods exist, which are capable of computing molecular excited state energy levels, transition dipole moments, vibrational mode frequencies, oscillation strengths and other microscopic molecule properties.

Meanwhile, the problem of excitation energy relaxation involves degrees of freedom (DOF) beyond an isolated molecule, requiring to treat the thermal fluctuations of molecule environment, which are an essential aspect of thermodynamically correct excitation energy relaxation modeling. Due to, e.g., internal conversion (IC), a big portion of excitation energy is quickly transformed into molecular vibrational energy (heat), which ought to redistribute among all vibrational DOFs, including those of environment, and, eventually, thermodynamic equilibrium should be restored. Thermal energy redistribution (TER) processes are important in both natural complexes and artificial structures, but due to a large number of interacting DOFs, modeling becomes a challenge. It has been recently demonstrated that this approximation is not accurate for carotenoids and TER processes have to be considered simultaneously [1].

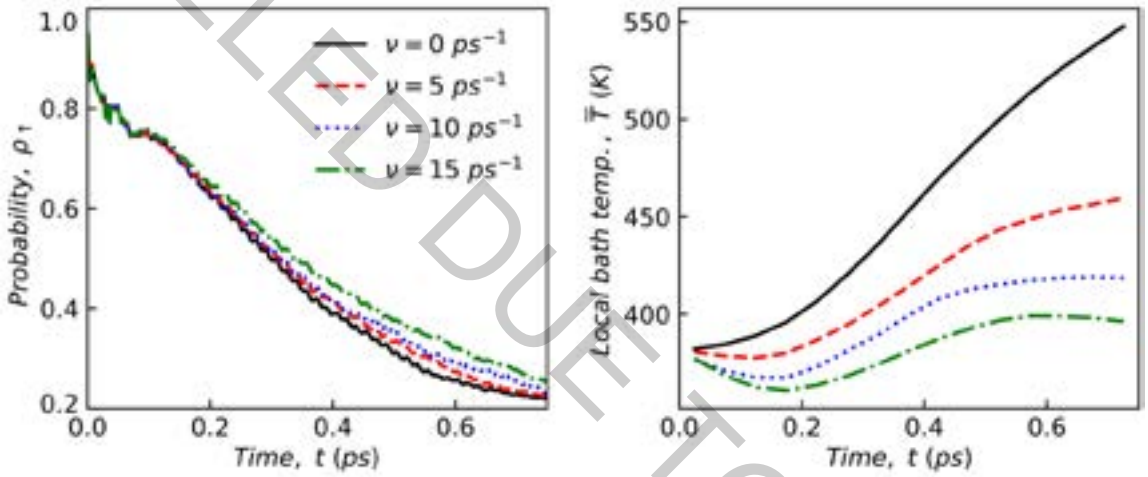

Fig. 1. Model beta-carotene S2 state occupation probability and the local bath temperature dynamics dependence on the thermalization rate ν.

We have created a general purpose molecular IC model where molecular DOFs are treated exactly, while states of environment vibrational DOFs are represented by a superposition of Davydov D2 Ansätze (sD2). A set of equations was derived to calculate the model time evolution. Also, algorithms for considering environment DOFs at a finite temperature and their thermalization, when using the sD2 ansatz, were proposed.

To validate the algorithms, we have considered a model system and have shown that they are capable of maintaining environment DOFs at a finite temperature, even when environment is under the influence of a molecule. Simulations of beta-carotene S2→S1 IC transition with simultaneous TER processes revealed that beta-carotene IC occurs faster, when the nearest environment temperature increases. Also, that the impact of beta-carotene nearest environment representation by a sD2 wavefunction is minimal.

[1] V. Balevičius Jr. et al., The full dynamics of energy relaxation in large organic molecules: from photo-excitation to solvent heating, Chemical Science **10**, 4792-4804 (2019).

CANCELLED DUE TO COVID-19

AZIRIDINE/PALLADIUM COMPLEXES IN THE SYNTHESIS OF LUMINOPHORES

Dominika Lubikowska[1], Stanisław Leśniak, Adam Marek Pieczonka

[1] Department of Organic Chemistry, University of Lodz, Poland
dominika.lubikowska@gmail.com

Chiral, optically pure aziridine derivatives are commonly used compounds as a chiral shift reagents [1], ligands or organocatalysts in stereocontrolled synthesis [2], or as a biologically active compounds eg. antibacterial agents [3]. Aziridine ring in the combination with second electron donating group can act as very efficient catalyst. Insertion of diphenylphosphine subunit into aziridine containing system will allow to use such compounds as a ligands in palladium catalyzed reactions like Suzuki reaction.

In the presented project a new group of aziridine derivatives bearing phosphine subunit were obtained in relatively simple synthesis. All new compounds were tested as a ligands in Suzuki-Miyaura reaction of different boronic acids with bromosalicylicaldehyde (Fig. 1.). Products of the presented Suzuki couplings are a starting materials in the synthesis of diverse small-molecule organic compounds exhibiting strong luminescent properties.

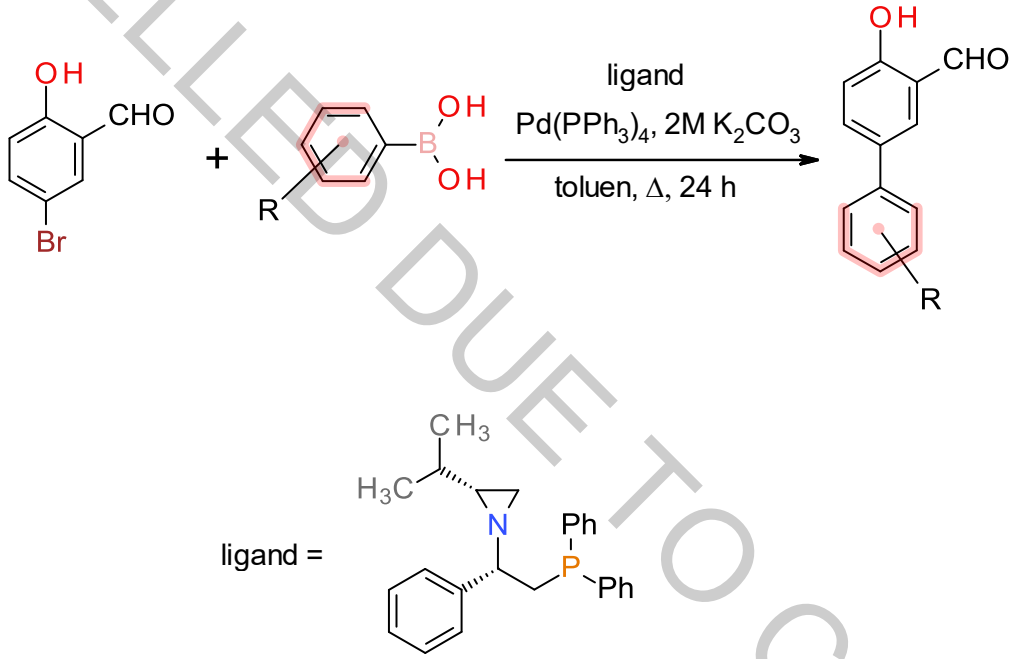

Fig. 1. Suzuki reaction in the presence of aziridine ligands.

[1] A. M. Pieczonka, S. Leśniak, M. Rachwalski, Tetrahedron **74**, 1571–1579, (2018).
[2] A. M. Pieczonka, S. Leśniak, S. Jarzyński, M. Rachwalski, Tetrahedron: Asymmetry **26**, 148-151, (2015).
[3] A. Kowalczyk, A. M. Pieczonka, M. Rachwalski, S. Leśniak, P. Stączek, Molecules **23**, 45, (2018).

CANCELLED DUE TO COVID-19

INVESTIGATION OF 2-((SUBSTITUTED IMINO)METHYL)PHENOLS 1,3-CYCLOADDITION REACTIONS

Paulina Kaziukonytė[1], Inga Valionytė[2], Algirdas Brukštus[1]

[1] Faculty of Chemistry and Geosciences, Vilnius University, Lithuania
[2] Faculty of Medicine, Vilnius University, Lithuania
paulina.kaziukonyte@chgf.vu.lt

Hsp90 (heat shock protein) – chaperone protein, responsible for folding and stabilization of client proteins. Although it is important in normal cell regulation processes, the amount of Hsp90 is significantly larger in malignant cells. Continuing our research on potential Hsp90 inhibitors [1], we decided to synthesize compounds, containing two known pharmacophores – 4-isopropyl-1,3-diol fragment, affined to Hsp90 binding center, and imidazole ring, which has antimicrobial, antiviral and anticancer properties [2]. In our efforts to obtain 4-isopropyl-6-(1-(4-methoxyphenyl)-1*H*-imidazol-5-yl)benzene-1,3-diol (**4**, fig. 1) by van Leusen imidazole synthesis [3] we isolated unexpected by-product **5** with condensed heterocyclic system never described in literature.

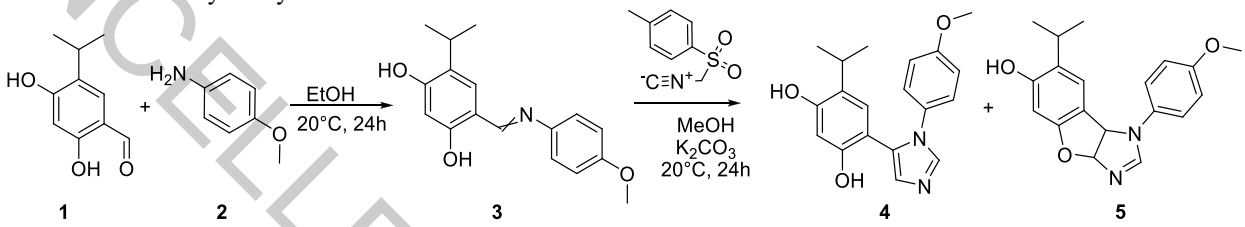

Fig. 1. Synthesis of 4-isopropyl-6-(1-(4-methoxyphenyl)-1*H*-imidazol-5-yl)benzene-1,3-diol.

In order to investigate the formation of 3a,8b-dihydro-1*H*-benzofuro[3,2-*d*]imidazole fragment we decided to explore other imines with *ortho*-hydroxysubstituted aromatic rings. Firstly, we optimized conditions of the reaction with toluenesulfonylmethyl isocyanide (TosMIC). Best solvent proved to be polar protic methanol. Organic bases such as triethylamine and pyridine did not favor the reaction and inorganic base K_2CO_3 gave the best total yield as well as the best yield of compound with fused three-ring moiety. Secondly, we decided to investigate the impact of various substitutes R and R' (fig. 2). We prepared different Shiff's bases (**6a-o**) according to known procedures. Then imines reacted with TosMIC and K_2CO_3 in methanol to give compounds **7a-o** and **8a-o**. Further results will be discussed in the poster presentation.

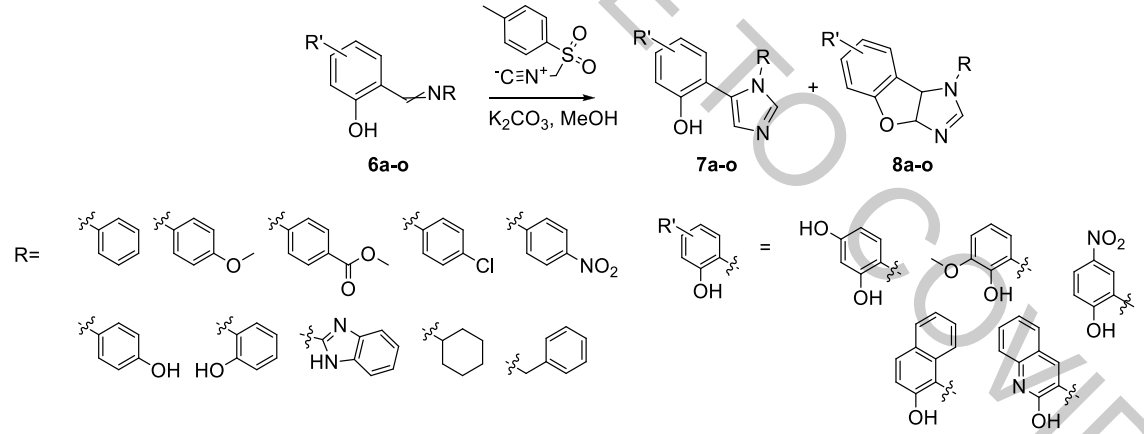

Fig. 2. Investigation of 1,3-cycloaddition reactions.

[1] E. Kazlauskas, A. Brukštus, H. Petrikas, V. Petrikaitė, I. Čikotienė, D. Matulis, Improving the Hsp90 inhibitors containing 4-(2,4-dihydroxyphenyl)-1,2,3-thiadiazole scaffold: synthesis, affinity and effect on cancer cells, Anticancer Agents Med Chem **17** (11), 1593-1603 (2017).
[2] N. Shalmali, R. Ali, S. Bawa, Imidazole: an essential edifice for the identification of new lead compounds and drug development, Mini-Reviews in Medicinal Chemistry **18** (2), 142-163 (2018).
[3] A. M. Van Leusen, J. Wildeman, O. H. Oldenziel, Chemistry of sulfonylmethyl isocyanides. 12. Base-induced cycloaddition of sulfonylmethyl isocyanides to carbon,nitrogen double bonds. Synthesis of 1,5-disubstituted and 1,4,5-trisubstituted imidazoles from aldimines and imidoyl chlorides, J Org Chem **42**, 1153-1159 (1977).

CANCELLED DUE TO COVID-19

PREDICTION OF SOLID SOLUTION FORMATION AMONG CHEMICALLY SIMILAR MOLECULES USING CALCULATION OF LATTICE AND INTERMOLECULAR INTERACTION ENERGY

Kristaps Saršūns[a], Agris Bērziņš[a]

[a] Faculty of Chemistry, University of Latvia, Jelgavas street 1, Riga, Latvia
kristaps.sarsuns@lu.lv

CANCELLED DUE TO COVID-19

Organic solids are able to form very wide range of crystalline structures of different compositions – including polymorphs, solvates, co-crystals and solid solutions (**SS**). In last decade, research of solid solutions has increased significantly and has become common in crystal engineering. While analysing solid solutions and their molecular packing, more attention is paid to structural aspects that promote and are responsible for the formation of solid solutions in two-component systems [1]. Both geometric and chemical aspects, such as molecule dimensions, symmetry, and intermolecular interactions, are important in understanding solid-state properties of all these phases [1, 2].

Several 2-substituted 4-nitrobenzoic acid (**NBA**) derivatives (**Fig.1**) were selected as model compounds because of their availability and chemically similar structures, in which the different group/atom (**R**) does not significantly affect the dominant intermolecular interactions [2].

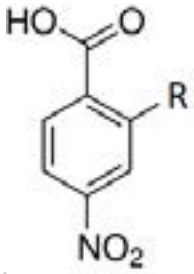

R = halogen atom (-Cl), hydroxyl group (-OH) or methyl group (-CH_3)

Fig.1. Molecular structure of 2-substituted 4-nitrobenzoic acid

Quantum chemical calculations for lattice and intermolecular interaction energy were carried out to identify possible factors, which could be used in prediction of the formation of solid solutions in binary systems of chemically similar molecules, in this case - various nitrobenzoic acid derivatives [2, 3]. While crystallization experiments were used to determine the experimental information (**Table 1**) about formation of solid solutions. Obtained crystalline phases were characterized by combined use of powder X-ray diffraction (**PXRD**) and differential scanning calorimetry (**DSC**) [3].

Table 1. Experimentally obtained crystalline phases from different nitrobenzoic acid mixtures

Substance ratio / %	Series of nitrobenzoic acid derivatives		
	$2OH4NBA_{100-x}2C4NBA_x$	$2CH_34NBA_{100-x}2C4NBA_x$	$2OH4NBA_{100-x}2CH_34NBA_x$
0:100	$^{2C4NBA}I$	$^{2C4NBA}I$	$^{2CH34NBA}I$
10:90	**Mixture**	**Mixture**	$SS^{2CH34NBA}I$
25:75	**Mixture**	$SS^{2CH34NBA}I$	**Mixture**
30:70	$SS^{2OH4NBA}I$	$SS^{2CH34NBA}I$	**Mixture**
50:50	$SS^{2OH4NBA}I$	$SS^{2CH34NBA}I$	**Mixture**
70:30	$SS^{2OH4NBA}I$	$SS^{2CH34NBA}I$	$SS^{2OH4NBA}I$
75:25	$SS^{2OH4NBA}I$	$SS^{2CH34NBA}I$	$SS^{2OH4NBA}I$
90:10	$SS^{2OH4NBA}I$	$SS^{2CH34NBA}I$	$SS^{2OH4NBA}I$
100:0	$^{2OH4NBA}I$	$^{2CH34NBA}I$	$^{2OH4NBA}I$

2OH4NBA – 2-hydroxy-4-nitrobenzoic acid, 2C4NBA – 2-chloro-4-nitrobenzoic acid, $2CH_34NBA$ – 2-methyl-4-nitrobenzoic acid, I – polymorph, SS – solid solution.

Acknowledgements

This research has been supported by the Latvian Council of Science, project "Crystal engineering of pharmaceutical multicomponent phases for more efficient crystalline phase design", project No. lzp-2018/1-0312.

[1] Lusi, M. *Crystal Growth & Design*, **2018**, *18(6)*, 3704-3712.
[2] Corpinot, M. K., Guo, R., Tocher, D. A., Buanz, A. B. M., Gaisford, S., Price, S. L., Bučar, D. K. *Cryst. Growth Des.*, **2017**, *17*, 827−833.
[3] Romasanta, A. K. S., Braga, D., Duarte, M. T., Grepioni, F. *CrystEngComm.*, **2017**, *19*, 653-660.

KINETICS OF ELECTROSTATIC SELF-ASSEMBLY OF SILVER NANOPLATES ON THIN POLYELECTROLYTE FILMS

Pavel Malakhovsky[1], Dzmitry Murauski, Egor Minakov, Mikhail Artemyev[1]

[1] Research Institute for Physical Chemcal Problems, Belarusian State University, Belarus
malakhpo@bsu.by

Silver nanoplates (AgNPls) are widely utilized in biosensing due to sensitivity of localized surface plasmon resonance (LSPR) frequency to ligand environment of AgNPls [1]. Recently we have developed a technique to obtain monolayers of laterally-oriented AgNPls through electrostatic self-assembly on the surface of thin (~20 nm) film of copolymer containing tertiary amino groups (TAGs) [2]. This method allows simultaneous optical spectroscopic and TEM- investigation of as-deposited AgNPls. The aim of current work is to determine kinetic parameters of deposition of AgNPls onto thin polymer films and their arrangement on it.

Syntheses of AgNPls, poly(ethylmethacrylate)-based copolymers with 10, 25 and 50 mol. % TAGs, thin film fabrication and functionalization of AgNPls with 11-mercaptoundecanoic acid (MUA) were described in our previous work [2].We immersed thin film of copolymer with 25% TAGs in aqueous colloidal solution of MUA-functionalized AgNPls with different optical density (2, 5 and 10 at optical path length 1 cm at LSPR peak) at pH 6.6 for 6 hours with periodical removing of the film from colloidal solution in order to conduct optical measurements. We also performed three additional experiments– using copolymers with 10 and 50% TAGs at pH 6.6 and with 25% TAGs at pH 8.5.

Inductively coupled plasma atomic emission spectroscopic and transmission electron microscopic (TEM) studies revealed that AgNPls have molar extinction coefficient 5.2×10^9 $M^{-1}cm^{-1}$ on thin polymer film with optical density (OD) 0.19 at LSPR peak. Using this molar extinction coefficient, we transformed optical data to surface concentration of AgNPls on kinetic curves. The figure 1, (a) represents a TEM image of as-deposited AgNPls monolayer with OD 0.216. Point pattern analysis of AgNPls' positions by nearest neighbor analysis (NNA) shows that they are arranged chaotically.

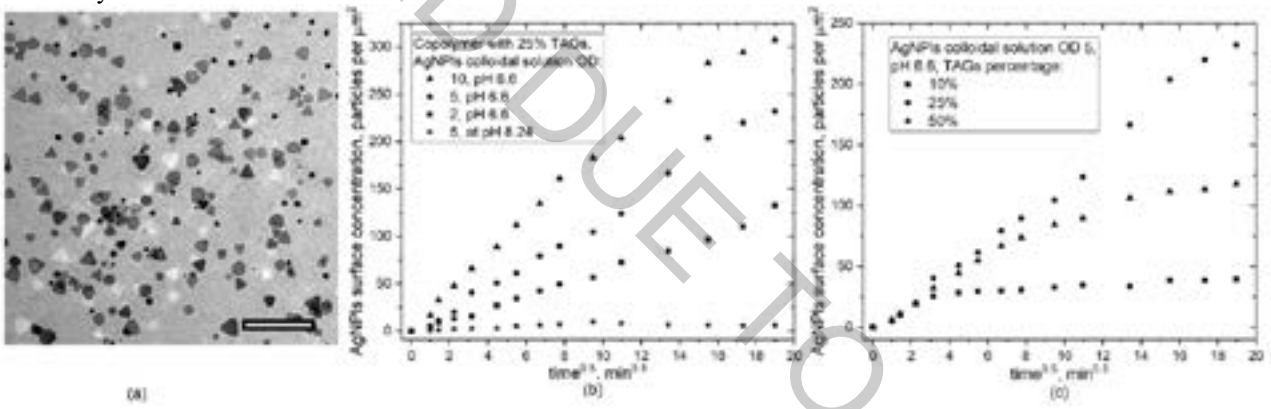

Fig 1. (a) TEM image of AgNPls electrostatic-assembled monolayer, scale bar is 250 nm; (b), (c) time-dependence of AgNPls surface concentration under specified conditions.

The Fig. 1, (b) shows the graphs of the average surface concentration of AgNPls (particles per square micrometer) on polymer film versus the square root of the immersion time obtained from AgNPls colloidal solutions with alternate optical densities. The linear relation between these parameters indicates that the most probable mechanism of deposition is random sequential adsorption, which was observed in nanoparticles deposition process recently [3]. Our calculations also revealed the linear relation between slopes of the graphs and the optical density of the AgNPls colloidal solution. This is also in good accordance with chosen model.

The dependence of AgNPls surface concentration on the TAGs percentage is more complex. After 10 min (about 3,5 $min^{0.5}$) of deposition time kinetic curve for film of copolymer with 10% TAGs goes to saturation. NNA shows that the two-dimensional ordering of the AgNPls on the surface of polymer film markedly improves. Kinetic curve for film of copolymer with 50% goes to saturation, but much slower. With an increase in pH from 6.6 to 8.24 self-assembly of AgNPls becomes very low. We associate that fact with a decrease in TAGs partial charges at high pH.

We acknowledge the financial support from Chemreagents Program. Mikhail Artemyev acknowledges partial financial support from BRFFI grant X18P-173.

[1] M. Rycenga, C. M. Cobley, J. Zeng et al. Controlling the synthesis and assembly of silver nanostructures for plasmonic applications. Chem. Rev. **111(6),** 3669-3712 (2011).

[2] P. Malakhovsky, M. Artemyev. Optical properties of laterally oriented self-assembled monolayers of silver nanoplatelets on cationic polymers. Int. J. of Nanosci.: Short reviews **18(3&4)**, 1940050 (2019).

[3] M. Dąbkowska, Z. Adamczyk, M. Kujda. Mechanism of HSA adsorption on mica determined by streaming potential, AFM and XPS measurements. Colloids Surf. B Biointerfaces **1(101)**, 442-449 (2013).

CREATED DUE TO COVID-19

INHIBITION OF ALUMINUM CURRENT COLLECTOR CORROSION IN AQUEOUS NA-ION BATTERY

Davit Tediashvili[1,2], Linas Vilčiauskas[2]

[1] Institute of Chemistry, Faculty of Chemistry and Geosciences, Vilnius University, Lithuania
[2] Center for Physical Sciences and Technology, Saulėtekio al. 3, LT-10257 Vilnius, Lithuania
davit.tediashvili@chgf.stud.vu.lt

Rechargeable lithium-ion batteries with organic electrolytes are widely used as commercial energy storage devices. They have many attractive properties, such as high efficiency, energy density and stability. However, as the energy demand increases, growing prices on scarce lithium resources also increase, making lithium-ion batteries less attractive. On the other hand, sodium is the 6th most abundant element in earth's crust. Another big issue of commercial batteries remains the usage of organic solvents, which increase production cost and raise safety concerns. This problem can be solved by replacing organic solvents with aqueous electrolytes. Traditionally, usage of aqueous electrolytes in batteries was limited by narrow potential window of operation, beyond which water decomposes. However, recently developed water-in-salt electrolytes can expand this potential window [1], making aqueous electrolytes a viable alternative. One of the other factors, which affects the long-term performance of aqueous batteries, is the corrosion of current collectors. Aluminum current collectors offer many advantages, such as low density and cost, good conductivity and easy manufacturing. However, the long-term corrosion problem of aluminum in aqueous electrolytes remains a major problem.

This study addressed the problem of the aluminum current collector corrosion. Naturally, aluminum is covered with a thin oxide layer, making it relatively stable. However, depending on the electrolyte pH and electrode potential, this layer can be damaged, causing rapid corrosion, which leads to poor electrode performance and capacity fade. Previously, it has been shown that chromate conversion coatings (CCC) can successfully passivate aluminum's surface with negligible increase in electrical resistance [3,4]. In this work, corrosion properties of pristine, CCC and non-chromate conversion passivated (Iridite NCP™) aluminum current collectors were studied by cyclic (CV) and linear sweep voltammetry (LSV) at various pH values. Tafel analysis of studied samples revealed that CCC shows the lowest corrosion current density, indicating its superior resistance, while pristine aluminum and NCP foil exhibit similar behavior. Alongside surface passivating coatings, different electrolyte additives are explored as potential corrosion inhibitors. For example, CVs recorded in electrolyte containing 0.1M sodium phosphate show sharp drop in current density after the first CV scan for all of the studied samples. NASICON-structured $NaTi_2(PO_4)_3$ (NTP) electrodes cast on aluminum foil also perform better (show higher capacity) when phosphate is present in the electrolyte. Overall, results indicate that electrolyte additives, as well as passivating coatings can be used to suppress the aluminum current collector corrosion in aqueous batteries, leading to enhanced performance and making aqueous batteries a viable alternative to organic ones.

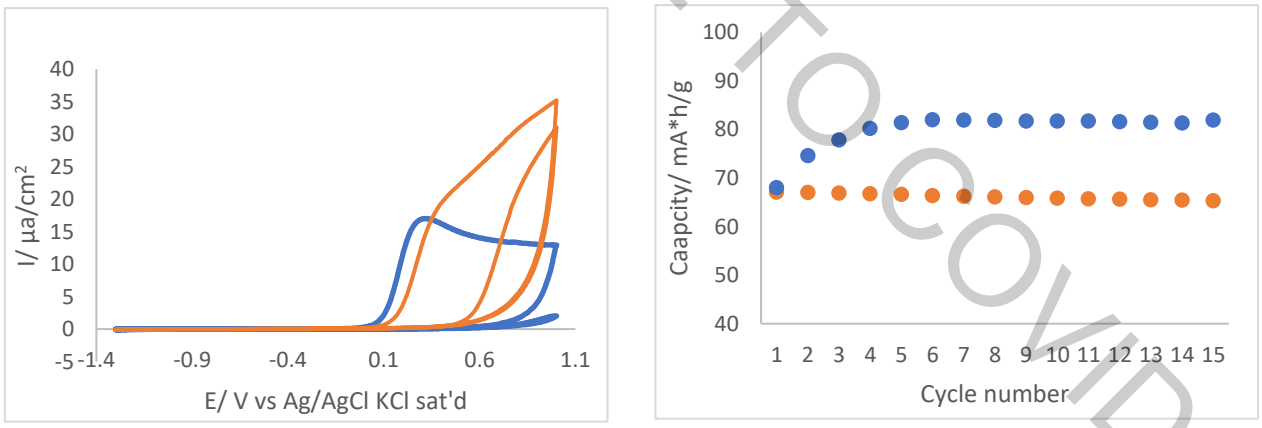

Fig 1. First two CV scans on aluminum foil(left) and galvanostatic cycling of NTP (right) in 1M Na_2SO_4(yellow) and 0.85M Na_2SO_4 + 0.1M Na_3PO_4(blue) electrolytes

Acknowledgements:
This project has received funding from the European Regional Development Fund (Project No. 01.2.2-LMT-K-718-02-0005) under grant agreement with the Research Council of Lithuania (LMTLT).

[1] L. Suo et al., "Water-in-salt" electrolyte enables high-voltage aqueous lithium-ion chemistries, Science **350**, 938-943 (2015)
[2] X. Wang et al., Inhibition of anodic corrosion of aluminum cathode current collector on recharging in lithium imide electrolytes, Electrochimica Acta **45**, 2677-2684 (2000)
[3] N. Piao et al., Corrosion resistance mechanism of chromate conversion coated aluminum current collector in lithium-ion batteries, Corrosion science **158**, 108100 (2019).
[4] S. Gheyani et al., Chromate conversion coated aluminum as a lightweight and corrosion-resistant current collector for aqueous lithium-ion batteries. Journal of Materials Chemistry A **4**, 395-399 (2016).

ONLY FOR REFERENCE TO COVID-19

HYDROGEN PRODUCTION FROM WATER SPLITTING USING PEROVSKITE NANOPARTICLES

Dovydas Vdovinskis[1], Aldona Balčiūnaitė[2], Loreta Tamašauskaitė-Tamašiūnaitė[2], Eugenijus Norkus[2]

[1] Faculty of Chemistry and Geosciences, Vilnius university, Naugarduko 24, LT-03225, Vilnius, Lithuania
[2] Department of Catalysis, Center for Physical Sciences and Technology, Saulėtekio Ave. 3, LT-10257, Vilnius, Lithuania
dovydas.vdovinskis@chgf.stud.vu.lt

CANCELLED DUE TO COVID-19

In the recent decades the use of fuel has grown drastically, which leads to the unavoidable truth that one day our planet will eventually run out of fossil fuels. This raises an important task to find an alternative to fossil fuels and to start using renewable energy or different fuels. One of the most commonly used renewable energy sources is fuel cells that directly convert the chemical reaction energy into electricity. Hydrogen, which can be produced from water, is applicable in such fuel cells.

In this work, the production of hydrogen from water splitting reaction is analyzed using different perovskite nanoparticles, which were prepared by a rapid microwave heating method. All syntheses of four different catalysts consist of $Co(NO_3)_2*6H_2O$ and $FeSO_4*7H_2O$ reagents with two of them being dissolved in water and the other two in ethylene glycol. Also, N-doped carbon material was added in those reaction mixtures with different dissolvents. The synthesis was carried out at a temperature of 150 ºC for 30 min. The morphology and composition of synthesized nanoparticles were examined using Scanning Electron Microscopy (SEM), X-Ray Diffraction (XRD) and Inductively Coupled Plasma Optical Emission Spectroscopy (ICP-OES). The electroactivity of synthesized catalysts for the hydrogen evolution reaction (HER) was examined using cyclic voltammetry and linear sweep voltammetry at different temperatures in a KOH electrolyte. It was found that the $FeCoO_3$ and $FeCoO_3$/C exhibit an electroactivity for a hydrogen evolution due to the increase in current starting at about 1,4 V potential. The increase in temperature results in higher electroactivity of hydrogen evolution.

LONG-TERM ^{14}C ACTIVITY MEASUREMENTS IN TREE RINGS NEAR IGNALINA NUCLEAR POWER PLANT: HOW IT HELPS TO INCREASE SAFETY OF OUR ENVIRONMENT

Algirdas Pabedinskas, Dominykas Žiemys, Evaldas Maceika, Žilvinas Ežerinskis, Justina Šapolaitė, Laurynas Butkus, Laurynas Bučinskas, Vidmantas Remeikis.

Nuclear research department, Center for physical science and technology, Lithuania
algirdas.pabedinskas@ftmc.lt

Atmospheric ^{14}C is produced by natural process of cosmic radiation interaction with Earth atmosphere as well as by anthropogenic human activities [1]. Almost double concentration of the anthropogenic radiocarbon appeared in atmosphere as a result of intensive nuclear weapon testing back in 1960's. After moratorium of the tests, introduced since 1963, the ^{14}C activity in global atmosphere is declining. However, considerable amounts of ^{14}C in the nuclear reactors is generated by neutron radiation interaction with ^{17}O, ^{14}N and ^{13}C. It accumulates in reactor vessel components, coolant and cleaning systems, and is partly released into environment mainly in a form of $^{14}CO_2$ and $^{14}CH_4$. RBMK-1500 type graphite moderator reactors were exploited at Ignalina NPP (Lithuania): Unit 1 - 1983-2004; Unit 2 - 1987-2009. Over decades $^{14}CO_2$ gas releases from NPP accumulates in local biosphere by photosynthesis, while increasing overall radiation background.

In order to examine the temporal variations and dilution pecularities of the released radiocarbon gaseus efluents from Ignalina NPP, there were extracted 9 pine tree cores around the INPP which were separated to 410 tree ring samples (time span 1980-2017) to determine the overall increase of radiocarbon concentration in NPP surroundings as compare to 3 tree cores from background rural area at Vaikšteniai. Paired tree core samples, taken at the unidirectional samling sites (located to the south direction form INPP at the 1.8 and 5.1 km, to the west direction at the 2.6 and 4 km, and to the north-east direction at 1.9 and 6.6 km), were examined in detailes by considering meteorological data records from the Ignalina NPP local meteorological station (2004-2015) in order to trace atmosferic dilution effectivenes of ^{14}C released from the 150 m heigth INPP ventilation stacks.

Samples were physically and chemically (BABAB) prepared [2], graphitized with AGE-3 (IonPlus AG) coupled with elemental analyzer (Vario Isotope Select, Elementar, GmbH) [3] and measured at Vilnius Radiocarbon SSAMS (NEC, USA) facility [4].

The results showed pronounced increase of ^{14}C up to 17.8 pMC in the tree rings during INPP exploitation as well during decommission periods. Year-by-year tree rings ^{14}C concentration data analysis of unidirectional samples revealed high variation of the atmospheric dilution conditions, which resulted in average about 30% variation of dilution effectiveness peeking up to about 300% for some years. This database of local radiocarbon activity variations could be used to reconstruct a history of unknow events in Ignalina NPP.

[1] B. Bolin, E. T. Degens, S. Kempe et al. Global carbon cycle: SCOPE 13, John Wiley and Sons, New York (1979).
[2] M. Nemec, L. Wacker, I. Hajdas, H. Gäggeler, Alternative Methods for Cellulose Preparation for AMS Measurement, Radiocarbon, 52, 1358–1370 (2010).
[3] L. Wacker, M. Němec, J. Bourquin, A revolutionary graphitisation system: Fully automated, compact and simple, Nuclear Instruments and Methods in Physics Research 268, 931-934 (2010)
[4] G. Skog, The single stage AMS machine at Lund University: Status report, Nuclear Instruments and Methods in Physics Research 259, 1–6 (2007).

CANCELLED DUE TO COVID-19

SYNTHESIS, CHARACTERISATION AND INVESTIGATION OF NITROGEN-DOPED CARBON SUPPORTED MN-CO NANOPARTICLES

Eivilė Budrytė, Aldona Balčiūnaitė, Jūratė Vaičiūnienė, Gediminas Niaura, Sandra Stanionytė, Loreta Tamašauskaitė-Tamašiūnaitė, Eugenijus Norkus

Department of Catalysis, Center for Physical Sciences and Technology, Sauletekio Ave. 3, LT-10257, Vilnius, Lithuania
aldona.balciunaite@ftmc.lt

CANCELLED DUE TO COVID-19

The development and investigation of various materials used in fuel cells, as renewable energy source, is a major challenge among the scientific community In this study, nitrogen-doped carbon (N-doped C), that has graphene-like structure, has been chosen as a support for the deposition of Mn-Co nanoparticles (Mn-CoNPs) using microwave heating method with the aim to use them as anode material for direct hydrazine fuel cells (DHFCs), likewise, identify its features as supercapacitor. For comparison, pure CoNPs/N-doped C and MnNPs/N-doped C catalysts have been synthesized under identical conditions.

The structure, morphology, and composition of nanocomposites have been characterized using Transmission Electron Microscopy (TEM), Raman Spectroscopy, X-ray Photoelectron Spectroscopy (XPS) and Inductively Coupled Plasma Optical Emission Spectroscopy (ICP-OES). Moreover, electrochemical performance has been investigated by cyclic voltammetry (CV) in a 1 M Na_2SO_4 solution at the scan rates of 1, 5, 10, 20, 100 and 150 mV s^{-1}. Cyclic voltammograms on the prepared catalyst were also recorded in a 0.05 M N_2H_4 + 1 M NaOH solution at a potential scan rate of 10 mV s^{-1}.

It has been determined that Mn-CoNPs/N-doped C, CoNPs/N-doped C, and MnNPs/N-doped C catalysts show an enhanced electrocatalytic activity towards the oxidation of hydrazine in an alkaline medium and it is controlled by the diffusion processes. What is more, it was found that the specific capacitance (C_s) value for the Mn-CoNPs/N-doped C nanocomposite in a 1 M Na_2SO_4 solution was equal to 497.5 F g^{-1} at a scan rate of 1 mV s^{-1} and decreased to 254.4 F g^{-1} at a scan rate of 150 mV s^{-1}. The Mn-CoNPs/N-doped C catalyst preserves 51.1 % of its specific capacitance as the scan rate increases from 1 mV s^{-1} to 150 mV s^{-1}. The obtained results confirmed the good performance of the prepared Mn-CoNPs/N-doped C nanocomposite as the electrode material for supercapacitors application.

SYNTHESIS AND INVESTIGATION OF THE CARBAZOLE BASED PHOSPHONIC ACIDS WITH DIFFERENT ALIPHATIC LINKERS

Aida Drevilkauskaitė, Artiom Magomedov, Ernestas Kasparavičius, Tadas Malinauskas, Vytautas Getautis

Department of Organic Chemistry, Kaunas University of Technology, Lithuania
aida.drevilkauskaite@ktu.edu

Over the last decade, perovskite solar cells (PSCs) have attracted major interest from scientists and industry. It can be attributed to the simple fabrication process and low consumption of materials. In particular, the formation of the functional layers can be achieved without the use of high temperatures via solution processes. To maximize the performance of the final device, it is very important to optimize every individual layer. For example, hole transporting material (HTM) needs to ensure high selectivity to the holes, while simultaneously passivating interface with a perovskite absorber layer.

To ensure a successful transition to the market, apart from efficiency and price, another important parameter is the stability of the devices. In recent work, HTM layer is often described as the weakest link of the PSC, due to the extensive use of the dopants [1]. Therefore, it is important to look for an alternative, dopant-free HTMs, that does not require the use of the dopants.

Recently, as an alternative to the traditional HTMs, hole-selective monolayers were introduced into PSCs with the p-i-n configuration [2]. In this case, instead of a spin-coating, a simple and scalable dipping method can be used. This alternative method is giving several important advantages, i.e. low material consumption, ability to form a layer on the rough surfaces, minimal parasitic absorption, etc. The highest efficiency of 20.8% was achieved with carbazole based phosphonic acid, called 2PACz (Fig. 1. n=2). In this material, carbazole moiety is ensuring high selectivity for holes, while phosphonic acid anchoring group is providing good binding with indium tin oxide surface. Seeing a high potential of monolayer HTMs, further structure optimization was performed.

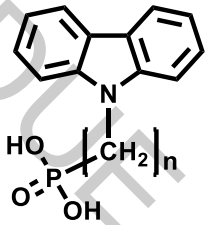

Fig. 1. The general structure of the **nPACz** materials, where n=2, 3, 4, 5, 6.

In this work, a series of new carbazole based phosphonic acids with different aliphatic chain linkers were synthesized (Fig. 1.) It is expected, that longer aliphatic chains could improve the ordering of the monolayer film, however, at the cost of reduced ability to transport charges. To achieve that, the carbazole starting material was alkylated with dibromoalkanes to give intermediate compounds with an aliphatic bromide functional group. In the following step, it was transformed into phosphonic acid ethyl ester, by means of Arbuzov reaction. Finally, ester cleavage was performed using reaction with bromotrimethylsilane, with the subsequent hydrolysis, to give a final compounds **nPACz**. The structures of the synthesized materials were confirmed by ^{1}H and ^{13}C NMR spectroscopy. In future research, the synthesized materials are planned to be tested in photovoltaic devices.

[1] A.K. Jena, A. Kulkarni, T. Miyasaka Halide Perovskite Photovoltaics: Background, Status, and Future Prospects. Chemical Reviews, ACS 119(5), 3036–3103 (2019)

[2] A. Al-Ashouri, A. Magomedov, M. Roß, et al. Conformal monolayer contacts with lossless interfaces for perovskite single junction and monolithic tandem solar cells. Energy & Environmental Science, 12(11), 3356–3369. (2019)

CANCELLED DUE TO COVID-19

INVESTIGATION OF THIN PEROVSKITE La:$BaSnO_3$ FILMS' PROPERTIES USING DIFFERENT SUBSTRATES

Tomas Murauskas[1], Mantvydas Levulis[1], Virgaudas Kubilius[1], Valentina Plaušinaitienė[1]

[1] Department of Inorganic Chemistry, Vilnius University, Lithuania
tomas.murauskas@chf.vu.lt

Wide bandgap La-doped $BaSnO_3$ (LBSO) has attracted increasing attention as one of the transparent conducting perovskite semiconductors as its bulk single-crystal carrier mobility reached 320 $cm^2\ V^{-1}s^{-1}$ with a high carrier concentration ($10^{20}\ cm^{-3}$) at room temperature [1]. Many researchers have fabricated LBSO epitaxial films thus far, but the obtainable carrier mobility is substantially low compared to that of single crystals due to the formation of the lattice/structural and/or nonstoichiometric defects. Thin film electrical properties (mainly carrier mobility) are highly dependent on film morphology, structure and inherently to the selected substrate lattice mismatch. Therefore, in this work thin La-doped $BaSnO_3$ films have been deposited using pulsed injection metal organic chemical vapor deposition (PI-MOCVD) method on multiple substrates and using different stoichiometric ratios of Sn/(Ba+La). In order to investigate different film/substrate lattice mismatch related to stoichiometry on LBSO properties, pseudocubic $LaAlO_3$, cubic $SrTiO_3$ and cubic MgO substrates were selected respectively.

Surface morphology of LBSO films obtained using the same metalorganic vapor phase composition was highly dependent on the selected substrate (Fig. 1). Here we report different thin film stoichiometry ratios related to most homogeneous surface structure. Optimal thin films stoichiometry has been determined to achieve the most homogeneous surface structure on each substrate at specific Sn/(Ba+La) ratio of the film. La-doped film carrier mobility and carrier concentration were determined using Hall measurements. Largest mobility values were achieved on $SrTiO_3$ substrates.

Fig. 1. Scanning electron microscopy (SEM) image of characteristic surface of near-stoichiometric LBSO films deposited on different substrates: a) $LaAlO_3$, b) $SrTiO_3$, c) MgO.

CANCELLED DUE TO COVID-19

[1] William Shepherd et al., Accurate control of stoichiometry and doping in barium stannate perovskite oxide nanoparticles, Chemical Communications **55** (79) 11880-11883, (2019).

MODIFICATION OF THE METHOD FOR PREPARING OLIGOMERS FROM HIGH MOLECULAR WEIGHT CHITOSAN

Yauheni Malich[1], Anastasiya Kanunnikava[1,2], Ilya Novikov[1]

[1]Chemistry Department, Belarusian State University, Minsk, 220030, Belarus
[2]Research Institute for Physical Chemical Problems of the Belarusian State University, Minsk, 220006, Belarus
malich.eugene@gmail.com

Chitosan is a natural polymer with huge structural possibilities for chemical modifications to generate novel properties for the application in different spheres, especially in biomedical and pharmaceutical ones. The biomedical utilization of high molecular weight chitosan is restricted by its water insolubility. Nevertheless, its biocompatibility, biodegradability, and non-toxicity combined with its antimicrobial activity and low immunogenicity point to reveal the immense potential for future development. Low molecular weight chitosan and, especially chitosan oligomers do not only have the same beneficial biological features as high molecular weight chitosan, but their solubility in water makes them the attractive pharmaceutical ingredients [1,2].

Chitosan is a random linear copolymer of (1-4)-linked 2-acetamido-2-deoxy-β-D-glucan (GlcNAc) and 2-amino-2-deoxy-β-D-glucan (GlcN) units in varying proportions. It is usually obtained by degradation and deacetylation of natural polymer chitin found in the exoskeletons of insects, the cell walls of fungi, and certain hard structures in invertebrates and fish. For example, chitin is the main building component of crustacean shells [3].

Traditionally, low molecular weight chitosan is synthesized by different enzymatic and chemical depolymerization methods. The enzymatic methods are based on the usage of specific enzymes. Although they were found to be efficient in the depolymerization of chitosan, their usage is restricted by the cost of these enzymes and their availability. Moreover, this method can not be applied on a broad scale in the industry [1]. The objective of this study was to perform an experiment in a way it can be represented as commercially available.

One of the most reliable ways to obtain chitosan oligomers is acid hydrolysis by hydrochloric acid. Our procedure is distinguished by the usage of a cheap ion exchange resin to remove chloride ion from the solution instead of the ultrafiltration cell. We based our research on the famous data [4]. Acid hydrolysis of chitosan was performed by mixing chitosan with concentrated HCl in a glass reactor. The suspension was stirred for a while in the thermostated bath. Then the mixture was cooled by cold water. The obtained solution was evaporated under vacuum, the residue was dissolved in water, and evaporated again. This stage was performed repeatedly to remove most of the HCl used for synthesis. After the evaporating, the products were dissolved in water one more time and the pH of the obtained solution was adjusted by the ion exchange resin that is capable of replacing chloride anions by hydroxide ions in the solution. After passing the solution through the ion-exchange resin, high molecular weight chitosan precipitated. Then it was filtered and concentrated under vacuum. The obtained solution was treated by isopropanol. The salt remained in the aqueous phase, while low molecular chitosan precipitated. This two-phase system was separated by filtration through a glass filter. The obtained solution was evaporated to dryness under vacuum and partially dissolved in isopropanol. The solubility of chitosan oligomers in isopropanol allowed to extract it from by-products. The resulting solution was evaporated under vacuum to obtain chitosan oligomers.

The determination of the molecular weight of the obtained samples was measured by viscosity measurement using an Ubbleohde capillary viscometer. Molecular weights were calculated using the classic Mark-Houwink equation, Eq. (1):

$$[\eta] = k \times M^{\alpha} \quad (1)$$

The main advantage of our method is that we have not used any specific and expensive equipment and compounds that were used to treat our products are widely used. Nevertheless, the obtained low molecular weights chitosan and oligomeric chitosan are water-soluble. The optimized procedure can be considered as cost-effective, practical, and potentially suitable for the industrial production of low molecular weight chitosan

[1] Aljbour, N. D., Beg, M. D. H. & Gimbun, J. Acid Hydrolysis of Chitosan to Oligomers Using Hydrochloric Acid. Chem. Eng. Technol. 42, 1741–1746 (2019).
[2] Pillai, C. K. S., Paul, W. & Sharma, C. P. Chitin and chitosan polymers: Chemistry, solubility and fiber formation. Progress in Polymer Science (Oxford) 34, 641–678 (2009).
[3] Ibrahim, K. et al. Preparation of Chito-Oligomers by Hydrolysis of Chitosan in the Presence of Zeolite as Adsorbent. Mar. Drugs 14, 43 (2016).
[4] Trombotto, S., Ladavière, C., Delolme, F. & Domard, A. Chemical Preparation and Structural Characterization of a Homogeneous Series of Chitin/Chitosan Oligomers. Biomacromolecules 9, 1731–1738 (2008).

ORIGINAL PAPER COVID-19

THE RESEARCH OF PHOTOOXIDATIVE REACTIONS OF TETRAPYRROLE COMPOUNDS USING EPR SPECTROSCOPY

Edvinas Petraitis[1], Paulius Janaščius[2], Arūnas Maršalka[1], Saulius Bagdonas[2]

[1] Institute of Chemical Physics and [2] Laser Reseach Center
Faculty of Physics, Vilnius University, Lithuania
edvinaspetraitis97@gmail.com

Photosensitized tumor therapy is one of the most perspective methods to treat and diagnose oncological diseases. With the help of tetrapyrrolic compounds as photosensitizers and their retention of tumor tissues, it is possible to diagnose cancer in the early stages. In many cases of oncological diseases, this is the most important condition to successfully treat it. Photosensitizer is excited by the light after it accumulates in the tumor tissue and then can be used to localize cancer through the process of fluorescence. Moreover, singlet oxygen, which actively reacts with surrounding molecules that are in tumor tissues and damages them, is generated after the excitation of the tetrapyrrolic compounds [1].

Two tetrapyrrole compounds that initiate photooxidative reactions via singlet oxygen pathway were studied in this work: protoporphyrin IX (PPIX) and hematoporphyrin dimethyl ester (Hp-DME). A greenlight (532 nm) laser and a (405 nm) light emitting diode were chosen to excite the photosensitizers, the samples were dissolved in aqueous buffer solution (pH 7) with ascorbic acid and the spectroscopic data were registered using a EPR spectrometer "Bruker ELSYS E 580" and an absorption spectrometer "AvaSpec 2048".

Stock solutions were prepared with 10^{-3} – 10^{-4} mol/L concentration PPIX and Hp-DME. During the experiment, the acidity and concentration were varied in accordance with experimental needs.

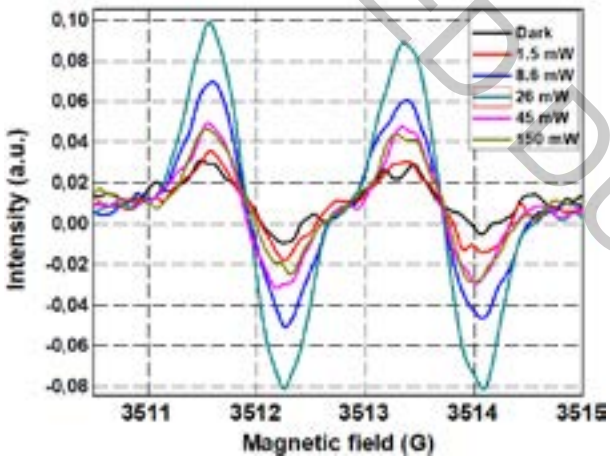

Fig. 1. Variation of EPR spectra of an ascorbate radical, depending on the intensity of laser light. Registration parameters were set to: Modulation Amplitude 0.80 G, Modulation Frequency 100 kHz, Number of Scans 7, Waveband X 9.8 GHz.

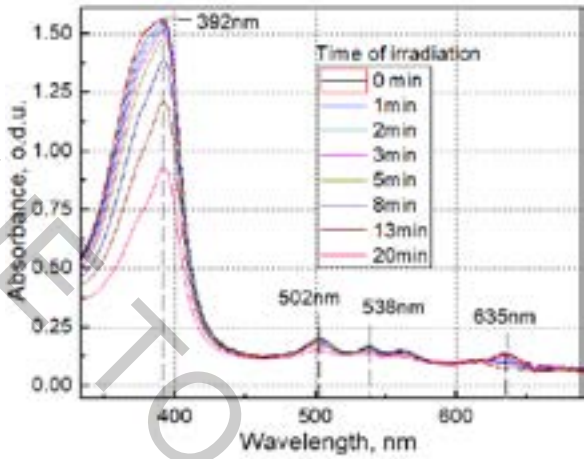

Fig. 2. Changes in Hp-DME absorbance spectra a pH 7 buffer, depending on the duration of diode generated light constant irradiation.

Nonlinear dependence of ascorbate radical generation on the intensity of laser radiation was registered during the examination of PPIX by applying EPR spectrometry. The amount of ascorbate radical increased while the intensity of the laser was increasing from 1.5 mW to 26 mW (Fig. 1). The registered amount of radicals started to decrease when the radiation intensity increased furthermore. Absorbance spectra of Hp-DME showed that the intensity of peaks decreased depending on the duration of irradiation (Fig. 2).

The relationship between EPR and absorbance spectra of PPIX and Hp-DME and their dependencies on acidity, concentration of antioxidants and, the intensity of various excitation sources will be presented and discussed.

[1] Rotomskis R., Streckytė G., Griciūtė L. „Fotosensibilizuota navikų terapija: pirminiai vyksmai." Vilnius: „Lietuvos mokslo" redakcija. 2002.

CANCELLED DUE TO COVID-19

APPLICATION OF INTENSITY MODULATED PHOTOCURRENT SPECTROSCOPY FOR PHOTOACTIVE MATERIAL CHARACTERIZATION

Ramūnas Levinas[1], Natalia Tsyntsaru[1,2], Henrikas Cesiulis[1]

[1] Faculty of Chemistry and Geosciences, Department of Physical Chemistry, Vilnius University, Lithuania
[2] Institute of applied physics of ASM, Moldova
ramunas.levinas@chf.vu.lt

Unlike in *Electrochemical Impedance Spectroscopy* (**EIS**), where the applied perturbation is commonly on the electrode potential, the *Intensity Modulated Photocurrent Spectroscopy* (**IMPS**) method works by modulating the illumination intensity by a pre-set amplitude (usually ~ 10% of total intensity) and frequency. For sufficiently photoactive materials, this results in a sinusoidal photocurrent response. Thus, as with EIS, by applying a transfer function the experimental parameters can be projected onto a complex plane as an IMPS spectrum. These spectra can then, in turn, be compared or interpreted to obtain key parameters of the material under investigation: charge transfer and carrier-hole recombination rate constants.

In this study we have prepared WO_3 films by electrodeposition from a peroxide-containing solution, at a potential of -0.45 V vs SCE, for different times. Another series of WO_3 films was prepared, but with incorporating TiO_2 nanoparticles during electrodeposition. All films were annealed at 450°C for 2 hours. The IMPS spectra were measured in 0.5M Na_2SO_4, under 100 W m^{-2} illumination intensity (365nm wavelength source), from 10 KHz to 0.1 Hz. Several differences were observed (see Fig. 1). Most notably the low-frequency intercept with the x-axis shifted closer towards 0 with the addition of TiO_2, which signifies a change in the recombination or charge transfer kinetics.

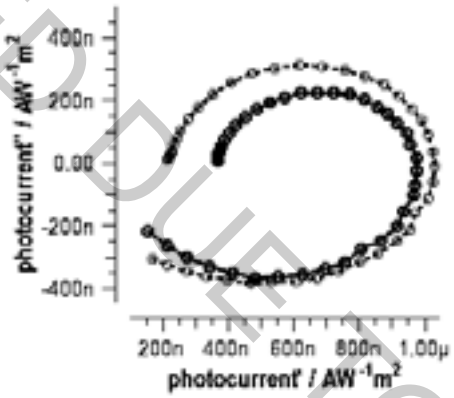

Fig. 1. IMPS spectra of WO_3 and WO_3 with TiO_2 films, electrodeposited for 10 minutes. Bias potential 1.0V vs Ag/AgCl.

Acknowledgement: authors acknowledge funding from H2020 project SMARTELECTRODES (No.778357) and by Research Council of Lithuania No 09.3.3-LMT-K-712-08-0003.

CANCELLED DUE TO COVID-19

IN SILICO STUDY OF L-GLUTAMIC ACID AND L-GLUTAMINE FRAGMENTATION BY LOW ENERGY ELECTRONS

Laura Baliulyte[1], Jelena Tamuliene[2]

[1]Institute of Biosciences, Life sciences center, Vilnius University, Vilnius, Lithuania
[2]Institute of Theoretical Physics and Astronomy, Vilnius University, Vilnius, Lithuania
baliulyte.laura@gmail.com

Low-energy electrons are produced due to the interaction of X- and ϒ-rays with biomolecules. These low-energy electrons induce the damage of bioorganic molecules including amino acids e.g. L-glutamic acid (Glu) and L-glutamine (Gln).

It is well know that, L-glutamic acid is the most abundant intracellular amino acid (concentrations 2-20 mM) whereas L-glutamine is the most prevalent extracellular amino acid (concentration 0.7 mM) [1]. Furthermore, the mass of these amino acids is very similar- Glu (m=147 Da), whereas Gln (m=146 Da). While side chains of these amino acids are quite different: L-glutamic acid R is $(CH_2)_2$–COOH, whereas L-glutamine- $(CH_2)_2$-$CO(NH_2)$. According to our knowledge, there is no data about Glu and Gln fragmentation similarities and differences.

The aim of our study is to determine whether the chemical composition and appearance energies of same mass fragments, which are produced during the fragmentation of Glu and Gln by low energy electrons, are different.

We used Gaussian 09 Rev D.01 program. Structures and fragments of the L-glutamic acid and L-glutamine molecules were studied by B3LYP with cc-pVTZ. Fragments were selected on the basis of the experimental mass spectrometry data. We used L-glutamic acid and L-glutamine positively charged fragments mass spectrum measured by our colleagues (L. Romanova, V. Vukstich, A. Papp and A. Snegursky) [2] and data from the NIST database [3]. Peaks at masses m/z=28, 41, 56 and 84 are most intensive in Glu and Gln mass spectrums. Moreover, their intensities are similar.

Our research indicate that CH_2N^+ (m/z=28) and $C_3H_5^+$ (m/z=41) cations could be produced during fragmentation of both Glu and Gln, while $C_3H_6N^+$ (m/z=56) and $C_4H_6NO^+$(m/z=84) could only be produced during fragmentation of Glu, $C_2H_2NO^+$(m/z=56) and $C_4H_8N^+$(m/z=84)- only during fragmentation of Gln.

Acknowledgment

The authors are thankful for the high performance computing resources provided by the Information Technology Open Access Center of Vilnius University.

[1] P. Newsholme, J. Procopio et al., Glutamine and glutamate— their central role in cell metabolism and function, Cell Biochem. Funct. **21**, 1–9 (2003).
[2] J. Tamuliene, L. Romanova et al., The impact of low-energy ionizing radiation on glutamine, Int. J Mass Spectrom. **444** (2019).
[3] https://webbook.nist.gov/chemistry/

CANCELLED DUE TO COVID-19

THE SEARCH FOR NEW ORGANIC SEMI-CONDUCTORS WITH EFFICIENT HOLE TRANSFERING PROPERTIES

Tadas Žutautas[1], Audrius Bučinskas[1]

[1] Faculty of Chemical Technology, Kaunas University of Technology, Lithuania
tadas.zutautas@ktu.edu

Since the first industrial revolution, humanity‘s demand for energy increased rapidly. Furthermore, the growing need for fossil fuels brought the issues related with global climate change. No wonder that during several decades scientific community has been working on the search of alternative energy sources and different approaches to optimize household energy consumptions. Compared to widespread incandescent and fluorescent light bulbs efficient light emitting diodes (LED) brought huge impact to the sphere of interiors and exteriors illumination. In spite of of toxic metals (cadmium, indium, gallium) and their compounds used for massive production of inorganic LEDs devices possess mechanical fragility and high utilization cost. Recently, as an alternative to LEDs, the interest of organic light emitting diodes (OLEDs) in the global market is growing rapidly. Taking into account alternative energy sources, the considerable increase of power conversion efficiency (~25 %) of perovskite solar cells (PSC) have made them very attractive to the photovoltaic (PV) community, as well.[1] In both types of devices the structure is built using more than three electroactive organic layers packed between two electrodes. Each layer possess their own specific function. For example, in OLEDs the purpose of hole transporting layer is to ensure the efficient transportation of holes to light emitting layer and blocking of electrons, which are passing the emission layer from cathode. In case of organic perovskite solar cells, despite of reduction of recombination processes and increment of the light absorption the main role of hole-transporting layer is smooth transportation of holes to the electrode. Therefore, the efficiency of OLEDs and PSCs depends not only on the efficient formation/dissociation of the excitons, but on balanced charge transportation, as well. By focusing our attention on hole transporting materials, we found that in solar cells[2] and organic light emitting diodes[3] triphenylamine and carbazole derivative - TCTA, 4,4’,4’’-tri(carbazol-9-yl)triphenylamine - is widely used.

Our work aim is to synthesize three new hole transporting materials modifying the TCTA compound through carbazole moiety by:
- replacing the 2nd and 7th position hydrogens with methoxy- groups.
- replacing the 3rd and 6th position hydrogens in the carbazole molecules with methoxy- groups.
- replacing the 2nd and 7th position hydrogens in the carbazole molecules with methoxy- groups and 3rd and 6th position hydrogens with tretbutyl- derivatives.

We believe that the addition of methoxy groups could increase the number of intermolecular bonding (hydrogen bonds) which should improve the morphological characteristics and charge transporting properties in the layer. Furthermore, by replacing the active C-3 and C-6 hydrogen atoms in the carbazole fragment with alkyl-derivatives, we hope to improve the electrochemical stability of the compounds. The main aspects of the synthesis and characterization of new compounds as well as comparative study of their photophysical, optical, thermal, electrochemical, charge transporting properties will be reported in the presentation.

CANCELLED DUE TO COVID-19

[1][Best Research-Cell Efficiencies. 2019; https://www.nrel.gov/pv/assets/pdfs/best-reserch-cell-efficiencies.20190923.pdf
[2] Dänekamp, B., et al. Journal of Materials Chemistry C, 7(3), 523–527. https://doi.org/10.1039/C8TC05372C 2019, the effectivness of the device reaches 14 %)
[3] Ràfols-Ribé, J., et al. Science Advances, 4(5), eaar8332. https://doi.org/10.1126/sciadv.aar8332, 2018, the effectivness of the device reaches 24 %

SYNTHESIS AND OPTICAL PROPERTIES OF Er^{3+}, Yb^{3+} AND Nd^{3+} DOPED Y_2BaZnO_5

Lukas Šerpytis[1], Simas Šakirzanovas[1]

[1]Department of Applied Chemistry, Faculty of Chemistry and Geosience, Vilnius University, Lithuania
lukas.serpytis95@gmail.com

CANCELLED DUE TO COVID-19

Upconverting phosphor materials are attracting considerable attention for their possible applications in solar cells with improved efficiency or as safety ink, nanomaterials for bio-imaging, lasers and novel display technologies [3]. Upconversion materials consists of inorganic host lattice doped with lanthanide ions, can convert low-energy incident radiation into higher energy emitted radiation. Upconversion refers to non-linear optical processes characterized by the successive absorption of two or more excitation photons via intermediate long-lived energy states followed by the emission of a shorter wavelength photon than the excitation [1]. Up to now, reported upconversion efficiencies have been relatively low, excitation thresholds quite high, and the investigated phosphors (generally fluorides) often presented poor chemical stability (hygroscopy), limiting their industrial applicability [2]. Y_2BaZnO_5 can be an excellent host material for doping with lanthanide ions. It has good chemical, physical properties and is stable at high temperature [3,4].

In this work, Er^{3+}, Yb^{3+} and Nd^{3+} co-doped orthorombic Y_2BaZnO_5 phosfors were synthesized via high temperature solid-state method. Pure phase Y_2BaZnO_5 synthesized by 4 stages of heating. A variety of dopants, including Er^{3+}, Yb^{3+} and Nd^{3+}, were embedded in the host lattice, resulting in bright red and green light emissions under 980 nm excitation and at relatively low excitation powers. Thermal stability of synthesised Y_2BaZnO_5 were measured by X-ray diffraction after heating sample at high temperatures for 24 hours. There was no other phases after heating the same Y_2BaZnO_5 sample at 300 °C, 600 °C and 950 °C for 24 hours in all temperatures.

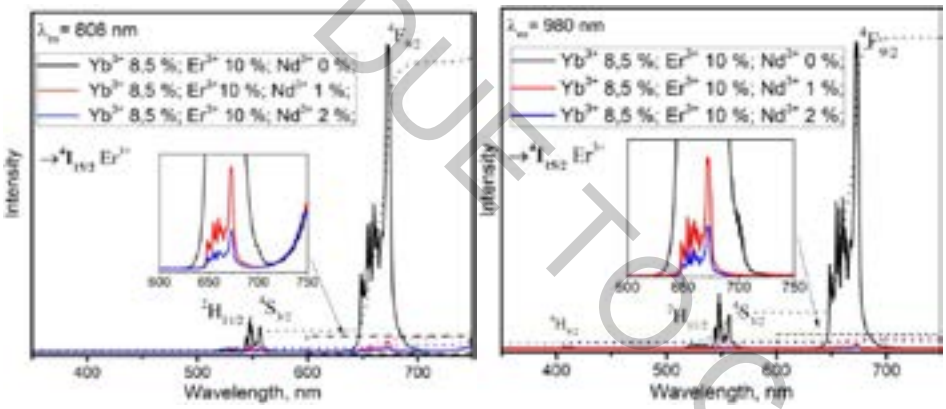

Fig. 1 Y_2BaZnO_5 co-doped with Er^{3+}, Yb^{3+} and Nd^{3+} apconversion emision spectra with different exitation wavelength a) 808 nm and b) 980 nm.

[1] Zhou, B.; et al. Nature Nanotechnology 10: 924–936 (2015).
[2] L. Y. Ang, M. E. Lim, L. C. Ong, Y. Zhang, Nanomedicine, 6, 2011, p. 1273 – 1288.
[3] I. Etchart, Metal Oxides for Efficient Infrared to Visible Upconversion, Summary of doctoral dissertation, University of Cambridge, Cambridge, 2010.
[4]V. Kumar, S. Som, S. Dutta, H. C. Swart, Proceedings of SAIP, 2015, p. 255 – 260.

COMPUTATIONAL AND EXPERIMENTAL VIBRATIONAL STUDY OF 1-CHLOROMETHYL-1-FLUOROSILACYCLOHEXANE CONFORMATIONS AND ITS REARRANGEMENTS

Joanna Stocka[1], Rasa Platakytė[1], Justinas Čeponkus[1], Valdas Šablinskas[1], Gamil A. Guirgis[2], Paweł Rodziewicz[3]

[1] Chemical Physics Institute, Vilnius University, Saulėtekio al. 3, 10257 Vilnius, Lithuania
[2] Department of Chemistry and Biochemistry, College of Charleston, Charleston, SC 29424, USA
[3] Institute of Chemistry, Jan Kochanowski University, 15G Świętokrzyska St., 25-406, Kielce, Poland
joana.stocka@gmail.com

CANCELLED DUE TO COVID-19

Organosilicon compounds are rather attractive in the field of surface science. Cyclic hydrocarbon films have good surface adhesion properties which are mostly related to a π electron orbital[1]. Substituting one carbon atom in the ring with a silicon atom enhances adhesion since it acts as hydrolytically sensitive center that can react with inorganic substrates such as glass to form stable covalent bonds[2]. 1-chloromethyl-1-fluorosilacyclohexane is a newly synthesized cyclic organic compound with unknown structural parameters and conformational diversity.

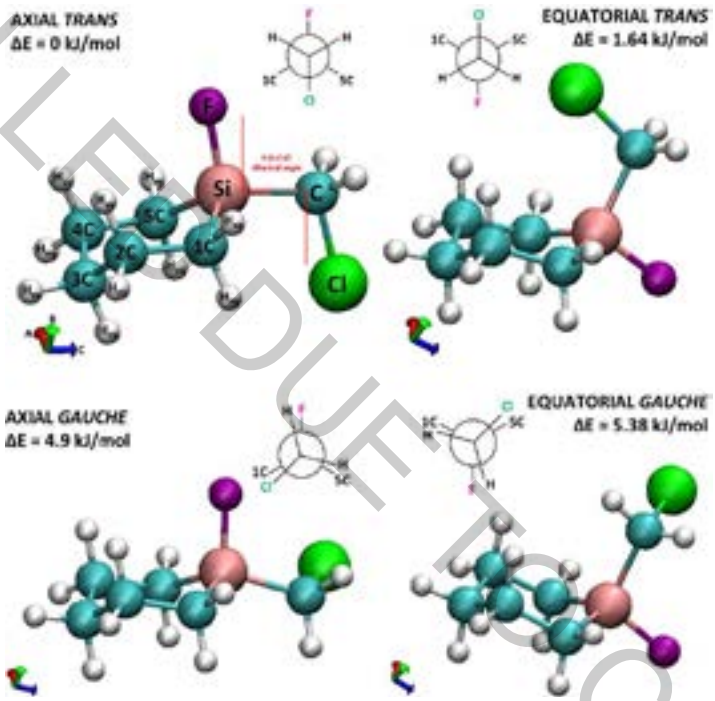

Fig. 1. Structures of four lowest energy conformers of 1-chloromethyl-1-fluorosilacyclohexane and the respective DFT/B3LYP relative energies. The F-Si-C-Cl dihedral angle change is shown as Newman projection. Internal axes are marked as: A (red), B (green), C (blue).

Several different vibrational spectroscopy methods were employed to analyze the properties of this molecule. Infrared and Raman spectra were recorded for the sample in liquid phase. Additionally, IR absorption spectra were registered in gaseous phase and as low temperature solid with the molecules isolated in argon and nitrogen matrices. In order to control thermodynamic equilibrium between the conformers hot nozzle technique was used during the deposition of the gaseous matrix mixture.. DFT calculations were performed utilizing B3LYP functional and augmented Dunning correlation-consistent valence double zeta basis set. The 1-fluoro-1-chlormethyl-silacyclohexane molecule can reveal twelve conformations out of which the chair-axial-trans one has the lowest energy. However, there are also three two more chair type conformers that are stable enough to possibly be observed in experimental spectra.

[1] H. Butt, K Graf, M. Kappl, Physics and Chemistry of Interfaces, Wiley, 2003
[2] J. Ceponkus, V. Sablinskas, V.Aleksa, M.Pucetaite, R.Platakyte, C.W.Reed, C.Cotter, G.Guirgis, Vibrational Spectroscopy, 81, 136-143, 2015

SYNTHESIS OF NONSYMMETRICAL 1,3,4-OXADIAZOLES NEW SMALL-MOLECULE METRIALS FOR OLED DIODES

Patrycja Szamweber[1], Adam Marek Pieczonka[1]

[1] Department of Organic Chemistry, University of Lodz, Poland
patrycjaszamweber@gmail.com

Over the past several years, there has been a growing interest in chemical compounds belonging to the 1,3,4-oxadiazole group. It finds diverse range of applications in analysis and pharmacy as well as agriculture and restructuring [1]. Their photoluminescent properties deserve attention because of an extended aromatic system formed around 1,3,4-oxadiazole. Presence of a diazole fragment in the heterocyclic rings of 1,3,4-oxadiazoles acts as electron withdrawing group, that may be found in various linear conductive systems [2]. The appearance of aforementioned fragment greatly enhances quantum yield of fluorescence and stability of the received products. Small-molecule compounds belonging to 1,3,4-oxadiazoles are semiconducting materials often used in active layers of OLED devices.

The aim of my study was to obtain nonsymmetrical 1,3,4-oxadiazoles with strong luminescent properties in solutions as well as in the solid state. Strictly reaction of benzoic acid derivatives with differently substituted benzohydrazides allowed to obtain expected 1,3,4-oxadiazoles (Fig. 1.) [3]. All new 1,3,4-oxadiazole derivatives obtained in this project exhibited significant luminescence. I used an easy and tunable deposition method as a drop-casting – to observed abilities of particles to self-organize in process of creating polycrystalline layers. Furthermore, I have carried out analysis of surface morphology of thin layers utilizing a microscope.

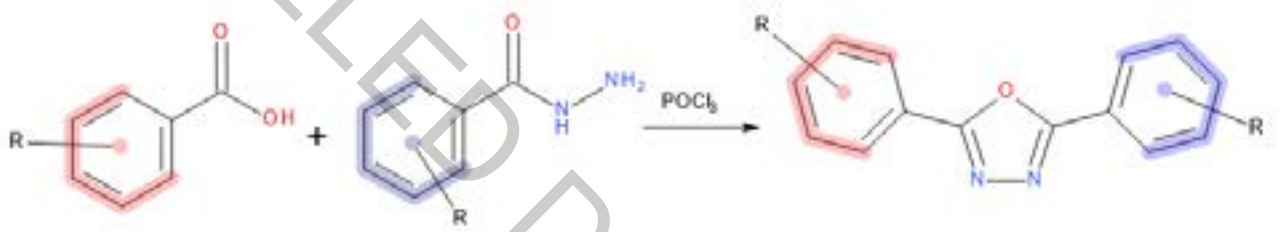

Fig. 1. General procedure for synthesis of 1,3,4-oxadiazoles.

CANCELLED DUE TO COVID-19

[1] K. Jasiak, A Kudelko, W. Zieliński, N. Kuźnik, Study on DDQ-promoted synthesis of 2,5disubstituted 1,3,4-oxadiazoles from acid hydrazides and aldehydes, Arkivoc **ii**, 88, (2017).
[2] M. Wróblowska, A. Kudelko, N. Kuźnik, K. Łaba, M. Łapkowski, Synthesis of Extended 1,3,4-Oxadiazole and 1,3,4-Thiadiazole Derivatives in the Suzuki Cross-coupling Reactions, J. Heterocyclic Chem. **54**, 1550-1557, (2017).
[3] Z. Wang, H. Zhang, B. J. Killian, F. Jabeen, G. G. Pillai, H. M. Berman, M. Mathelier, A. J. Sibble, J. Yeung, W. Zhou, P. J. Steel, C. D. Hall, A. R. Katritzky, Synthesis, Characterization and Energetic Properties of 1,3,4-Oxadiazoles, Eur. J. Org. Chem., 5183–5188, (2015).

THEORETICAL AND EXPERIMENTAL STUDY OF THE BEHAVIOR OF E^+–Nu^- SALTS IN THE NUCLEOPHILIC RING OPENING REACTION OF 2-(CHLOROMETHYL)OXIRANE

Kseniia Yutilova[1], Elena Shved[1], Yuliia Bespalko[2]

[1] Faculty of Chemistry, Biology and Biotechnologies, Vasyl' Stus Donetsk National University, Ukraine
[2] Department of Chemistry, University of Leuven, Belgium
k.iutilova@donnu.edu.ua

CANCELLED DUE TO COVID-19

Oxiranes are widely used as universal synthons and intermediates in organic synthesis. Asymmetric oxiranes, amongst them 2-(chloromethyl)oxirane (epichlorohydrin, ECH), have a high synthetic potential [1]. The strained three-membered ECH cycle is easily opened under the attack of proton-donating nucleophilic reagents E^+–Nu^-, such as carboxylic acids (Fig. 1), alcohols, phenols, salts, forming two products of "normal" and "abnormal" ring opening.

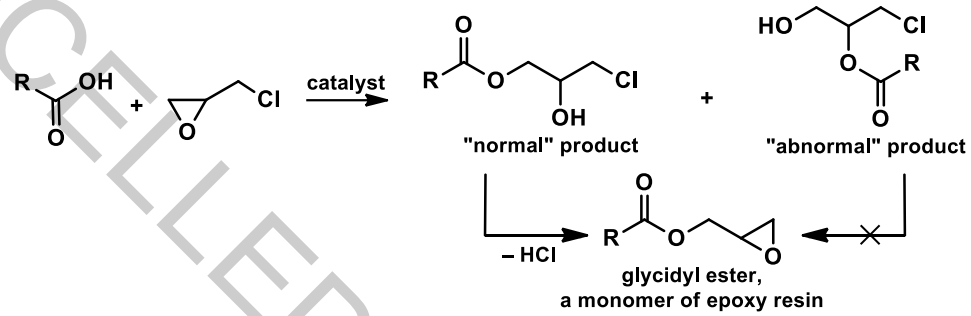

Fig. 1. Ring-opening reaction of 2-(chloromethyl)oxirane with carboxylic acids.

However, only a "normal" product is able to convert to glycidyl esters used in the synthesis of epoxy resins. Therefore, the study of factors affecting the rate and regioselectivity of reaction is important for the targeted oxirane ring opening. As shown by previous studies [2], one of the factors contributing to an increase in the rate of ECH acidolysis is the electrophilic activation of oxirane ring opening (Fig. 2, pathway B) with proton-donating reagents.

Modelling of the oxirane ring opening with E^+–Nu^- reagents, where the proton acts as an electrophile, does not allow localization of transition states on the reaction path, and leads directly to the product. In order to study the effect of the nature of the electrophile in E^+–Nu^- particles, there are promising models involving alkali metal cations as counterions for attacking nucleophiles. This approach allows studying not only the effect of the electrophilic activation on the rate and regioselectivity of the ring opening, but also assessing the impact of the cation volume on the efficiency of activation.

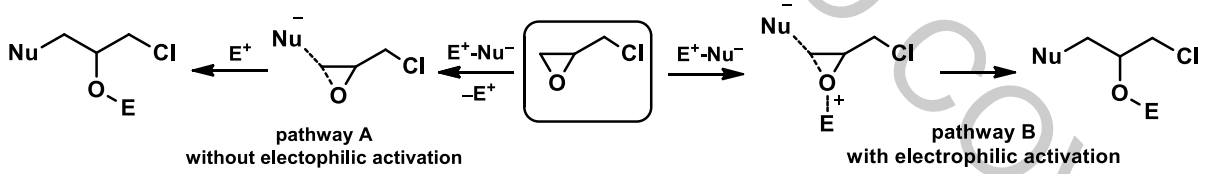

Fig. 2. Nucleophilic ring-opening reaction of 2-(chloromethyl)oxirane without (A) and with (B) electrophilic activation.

The aim of the study is to investigate the oxirane ring opening reaction of 2-(chloromethyl)oxirane by methods of quantum chemical modelling with alkali metal salts MX (M = Li^+, Na^+, K^+; X = Br^-, CH_3COO^-) and the subsequent experimental study of acetolysis of 2-(chloromethyl)oxirane in the presence of tetraalkylammonium halides R_4NX: tetraethylammonium bromide, tetraethylammonium iodide, tetra-*n*-butylammonium iodide. The computation was performed using the density functional theory (DFT) method with the B3LYP basic set. Acetolysis of ECH was studied at 333 K in a binary solvent ECH : tetrahydrofuran (50% vol.).

The studies showed that for both tetraalkylammonium and alkali metal salts, the kinetic behavior changes in the same manner, which indicates the same mechanism for the catalysis of 2-(chloromethyl)oxirane acetolysis with R_4NX and MX. It was found that the catalytic activity of R_4NX and MX increases with an increase in the nucleophilicity and electrophilicity of ions. The regioselectivity of the ECH ring opening by E^+–Nu^- particles rises with an increase in the nucleophilicity of the anion and a decrease in the cation volume. The data obtained are important both for the targeted synthesis of epoxides and for studying the mechanism of nucleophilic oxirane ring opening.

[1] G. S. Singh, K. Mollet, M. D'Hooghe et al., Epihalohydrins in organic synthesis, Chem. Rev. **113**, 1441-1498 (2013).
[2] K. Yutilova, Y. Bespal'ko, E. Shved, A Computational Study of 2-(chloromethyl)oxirane Ring Opening by Bromide and Acetate Anions Considering Electrophilic Activation with Cations of Alkali Metals, Croat. Chem. Acta **92**, 1-11 (2019).

CYTOCHROME P450 7B1 F470I MUTATION AFFECTS ON LIGAND BINDING PROPERTIES

Yaraslau Dzichenka[1], Eugene Hudny[1,2],

[1] Institute of Bioorganic Chemistry, National Academy of Sciences, Belarus
[2] Department of Biology, Belarusian State University, Belarus
dichenko@iboch.by

Human steroid 7α-hydroxylase (CYP7B1, EC 1.14.13.100) is a microsomal liver enzyme, which takes part in the biosynthesis of intermediate bile acid products. In addition to liver cells. Human cells of the testes, ovary, kidneys and small intestine, prostate gland, large intestine and brain express CYP7B1 [1]. CYP7B1 hydroxylates various oxysterols and neurosteroids, for example DHEA (dehydroepiandrosterone), EPIA (epiandrosterone) [2, 3]. CYP7B1 dysfunction in the human body is associated with the development of a neurodegenerative disease with spastic paraplegia type 5a and osteoarthritis. However, the molecular mechanisms of these diseases are not fully understood due to lacking of information about chemical and physical properties of mutant form of the enzyme.

The aim of this work was to characterize the chemical and physical properties of the mutant form of CYP7B1 with the amino acid substitution Phe470Ile, associated with spastic paraplegia type 5a. For this, we screened the ligands of the active center of the mutant protein form and compared it with the existing data for the wild type. Screening was performed using spectrophotometric titration. To assess the ability of a potential ligand to bind to a protein, we used the constant of dissociation (K_d) of enzyme-ligand complex. There was found that five new ligands bind with protein mutant (Fig. 1): 5β–androstane–17–one, 5β– androstane –3β–ol–16–one, 5α– androstane–3–one, 5–androstane–3β, 17α-diol, 5–androstane–3β–ol–16–one, in contrast to the wild type.

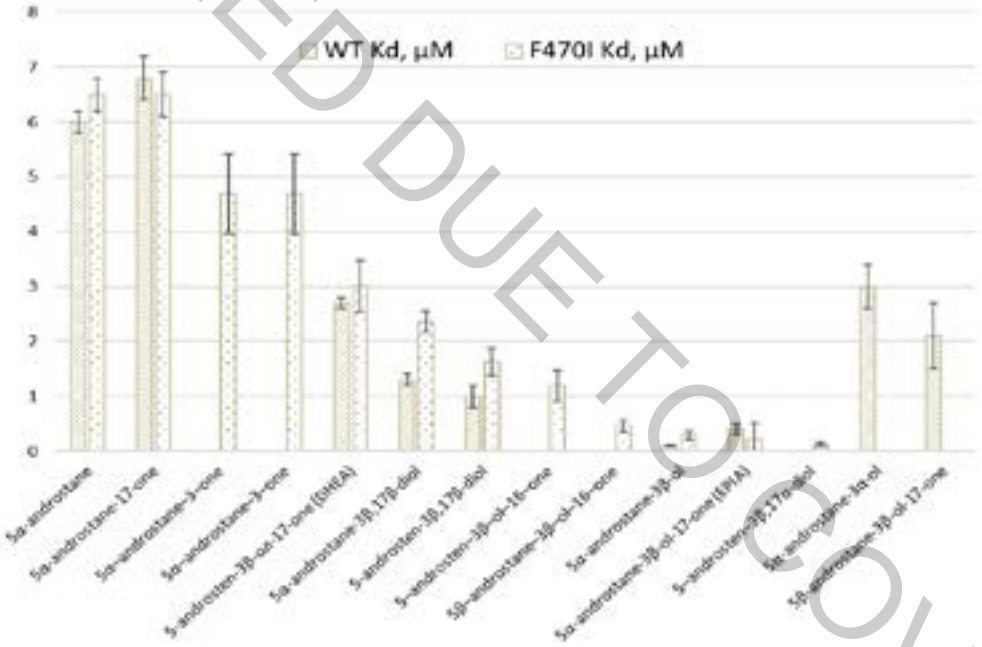

Fig. 1. The calculated value of the dissociation constant (Kd) of the ligand-enzyme complex for CYP7B1 (WT) and CYP7B1_Phe470Ile (F470I).

The data obtained indicate that the enzyme retains the ability to bind steroids and their derivatives, but the substrate profile for binding changes. The results of accelerated molecular dynamics that we have published previously indirectly indicate changes in the structure of the active center of the mutant protein that can explain the change in the ligand profile [4]. However, for an accurate and complete understanding of the changes caused by the Phe470Ile mutation, further experiments are required both *in silico* and *in vitro*.

[1] S. Steckelbroeck et al, Characterization of the dehydroepiandrosterone (DHEA) metabolism via oxysterol 7alpha-hydroxylase and 17-ketosteroid reductase activity in the human brain, J. Neurochem. 83 (3), 713-726 (2002).
[2] A.R. Stiles et al, CYP7B1: one cytochrome P450, two human genetic diseases, and multiple physiological functions, J. Biol. Chem.284(42), 28485-28489 (2009).
[3] Y. Akwa et al, Neurosteroid metabolism. 7 alpha-Hydroxylation of dehydroepiandrosterone and pregnenolone by rat brain microsomes, Biochem. J. 288(3), 959-964 (1992)
[4] Dzichenka, Y. V. Cytochrome P450 7B1 F470I mutation affects on protein structure stability / Y. Dzichenka, E. Gudnyy, S. Smolskaya // The 61th Scientific Conference for Young Scientists of Physics and Natural Sciences Open Readings 2018, Vilnius, Lithuania, March 20-23, 2018. / Vilnius University ; – Vilnius, 2018. – P. 302.

CANCELLED DUE TO COVID-19

COMPOSITION OF Ag-In-Se LAYERS DEPOSITED ON PES/PVC SURFACE

Lina Jatautė[1*], Valentina Krylova[1], Nijolė Dukštienė[1], Martynas Lelis[2]

[1]Department of Physical and Inorganic Chemistry, Kaunas University of Technology, Lithuania
[2]Lithuanian Energy Institute, Lithuania
lina.sciupakovaite@ktu.edu

CANCELLED DUE TO COVID-19

Different international directives on the energy performance of buildings stipulate that in a near future all new buildings must be nearly zero-energy buildings [1]. As architectural textiles are usually used to cover extensive out door parts of buildings, the development of the functional properties of these substances by integrating element modules converting solar energy into electricity is a highly promising activity allowing profitable use of the available space and the construction of energetically efficient buildings. The Ag-In-Se materials, especially the ternary compound $AgInSe_2$ has become a candidate as an absorbing layer for solar cells technologies because of its high absorption coefficient [2], good radiation stability [3] and the value of band gap energy ranging from 0.8 to 2.73 [4].

In this work, PES/PVC-Ag-In-Se composites obtained at room temperature by three-step assembly synthesis route. Firstly, for change physical surface properties the PES/PVC mechanical roughened and treated with etching solution. In the second step, a chemical bath deposition method employed for preparation of PES/PVC-Se precursors at room temperature using H_2SeO_3 and Na_2SO_3 solutions. Further, this PES/PVC-Se serves as proxies for silver-indium selenide formation. The formation of silver-indium selenide was attained by exposing the PES/PVC-Se precursors into an $AgNO_3$ and $In(NO_3)_3$ solutions for different time. The reaction system depends on the heterogeneous reaction between Ag^+ and In^{3+} ions and Se on PES/PVC surface. The obtained composites were characterized by X- ray photoelectron spectroscopy (XPS) and X-ray fluorescence analysis (XRF).

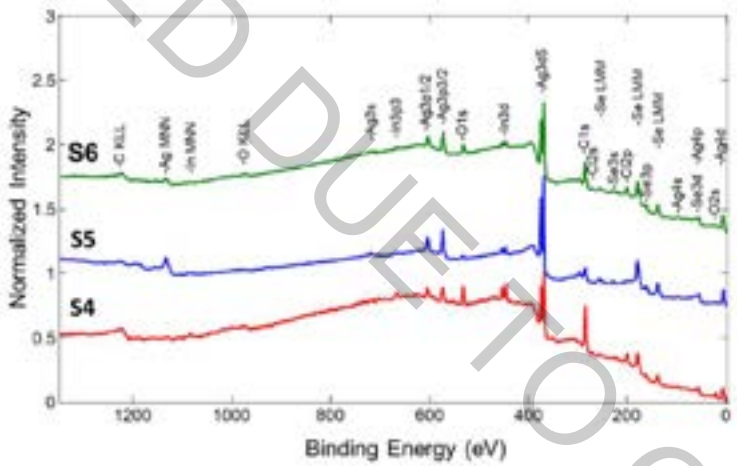

Fig. 1. XPS survey spectra of samples S4, S5 and S6

As expected XPS data indicated presence of Ag, Se and In.

Table 1. Elemental composition of the samples based on XRF data.

Sample	Elemental concentration, at. %						
	Ag	In	Se	Cl	Ti	Ca	Other (C, H, O, Si, Al…)
Pre-treated PES/PVC	0.00	0.00	0.00	48.10	5.86	4.42	41.62
S4	0.84	0.06	0.59	48.60	5.22	2.29	42.40
S5	1.10	0.09	0.68	43.90	4.77	2.02	47.44
S6	1.30	0.15	1.45	45.90	4.38	1.75	45.07

With increasing deposition time of the Ag-In-Se layers, the atomic percentages of the Ag, In and Se increases.

[1] A.L. Martinez, A. Menendez, P. Sanchez, et al., Solar photovoltaic technology on rough low carbon steel substrates for building integrated photovoltaics: A complete fabrication sequence, Sol. Energy **124**, 216-226 (2016).
[2] D. Pathak, R.K. Bedi, D. Kaur, Growth of $AgInSe_2$ on Si(100) substrate by thermal evaporation technique, J. Appl. Phys. **95**, 843-847 (2009).
[3] J.J. Loferski, Stoichiometric effects on the properties of Cu based chalcopyrite I-III-VI_2 semiconductor thin films, Mater. Si. Eng. B **13(4)**, 271-277 (1992).
[4] M. Kaleli, T. Colakoglu, M. Parlak, Production and characterization of layer-by-layer sputtered single-phase $AgInSe_2$ thin film by thermal selenization, Appl. Surf. Sci. **286**, 171-176 (2013).

SYNTHESIS OF NEW 1- (4-OXOTHIAZOLIN-2-IL) PYRAZOLINES BASED ON CHALCONS

Dmytro Smychko[1,2], Olena Shvets[1], Olga Bui[2], Volodymyr Vakula[2]

[1] V. N. Karazin Kharkiv National University, Ukraine
[2] State Institution "Institute of Endocrine Pathology Problems of the National Academy of Medical Sciences of Ukraine, Kharkov, Ukraine
smychko.dima@gmail.com

Heterocyclic compounds are a combination of pyrazoline and thiazoline fragments, are privileged structures - objects of study of medical chemistry due to a wide range of pharmacological properties. It was established that such compounds exhibit high antitumor, anti-inflammatory, antiviral, antimicrobial activity.

The synthesis of intermediate N-thiocarbamoylpyrazolines **1** was carried out by the cyclization reaction of the corresponding substituted chalcones with thiosemicarbazide by boiling in alcohol in an alkaline medium. Boiling in acetic acid recommended in some sources leads to worse results. For the formation of a thiazoline cycle based on 1, the use of chloroacetic acid and its derivatives has been proposed in the literature [1, 2].

We have shown that such heterocyclization using iodoacetamide occurs under mild conditions and with high yields.

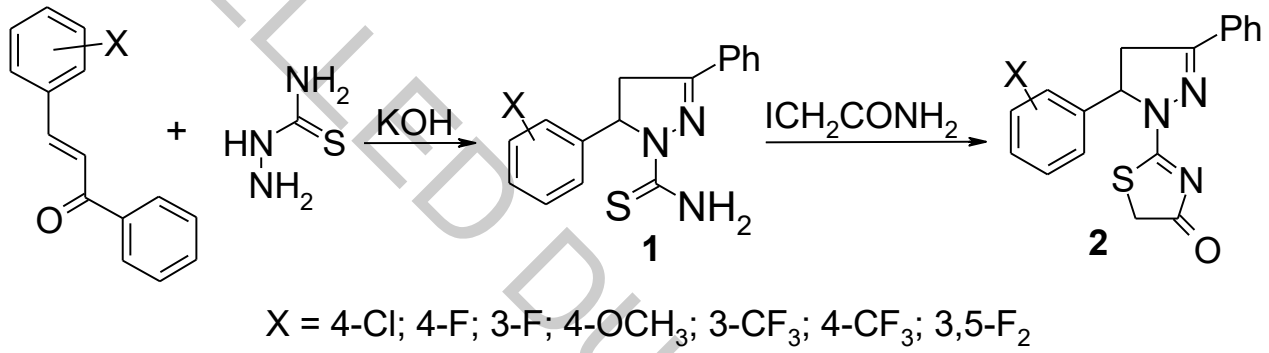

Fig.1. Scheme of synthesis of 1- (4-Oxothiazolin-2-il) pyrazolines

The reaction process and the purity of the obtained products were monitored by TLC (silica gel, eluent chloroform - ethanol, 24: 1). The structure of the obtained compounds was proved using 1H-NMR, IR and mass spectroscopy.

It is supposed to test some of the obtained compounds using models of such endocrinopathies as type 2 diabetes mellitus and hyperthyroidism in animals.

[1] El-Enany M. M. et al. Synthesis and antimicrobial activity of some 3, 5-diaryl-4, 5- dihydropyrazole derivatives //Oriental Journal of Chemistry. – 2010. – Vol. 26. – №. 4. – P. 1265.

[2] Havrylyuk D. et al. Synthesis and Anticancer and Antiviral Activities of New 2-Pyrazoline-Substituted 4-Thiazolidinones //Journal of Heterocyclic Chemistry. – 2013. – Vol. 50. – №. S1. – P. E55-E62.

CANCELLED DUE TO COVID-19

SYNTHESIS AND ANALYSIS OF TUNGSTEN OXIDE THIN FILMS FORMED BY MAGNETRON SPUTTERING

Karolis Treinys[1], Vilma Ratautaitė[2], Simonas Ramanavičius[2], Andrius Maneikis[2], Urtė Samukaitė-Bubnienė[1,2], Povilas Genys[1], Arūnas Ramanavičius[1,2]

[1] Vilnius University, Faculty of Chemistry and Geosciences, Institute of Chemistry, Department of Physical Chemisty, Vilnius LT-03225, Lithuania
[2] State Research Institute "Center for Physical Sciences and Technology", Vilnius LT-10257, Lithuania
karolis.treinys@chf.stud.vu.lt

CANCELLED DUE TO COVID-19

Tungsten oxide (WO_x) films are interesting due to their properties in many fields of research: catalytic properties, electro-chromism and potential usage in gas sensing [1, 2]. There are many possible techniques for making WO_x thin films. One of them is magnetron-sputtering technique [3]. The aim of this research was to prepare WO_x structures and to study dependency of its properties from the thin films thickness and substrate temperature.

In this work WO_x films thickness in a range from 50 to 400 nm were deposited by magnetron-sputtering technique on a silicon substrate at different temperatures: 200, 400 and 600 °C. It was investigated how such parameters as the layer thickness and substrate temperature during deposition affects WO_x crystal structure and band-gap width. It was also tested how the conductivity of these samples depends on the adsorption of various analytes. This was done to determine the best working configuration for further experiments and analysis.

Surfaces of prepared samples were investigated by using scanning electron microscopy, crystal phase composition by using X-Ray diffraction measurements and band-gaps were calculated by using ellipsometry measurements data.

[1] Rhushikesh Godbolea, V.P. Godboleb, Sunita Bhagwat, Surface morphology dependent tungsten oxide thin films as toxic gas sensor, *Materials Science in Semiconductor Processing* 63, (2017), 212-219
[2] C. Dong, R. Zhao, L. Yao, Y. Ran, X. Zhang, Y. Wang, A review on WO_3 based gas sensors: Morphology control and enhanced sensing properties, *Journal of Alloys and Compounds* 850, (2019), doi: https://doi.org/10.1016/j.jallcom.2019.153194
[3] Vyomesh R. Buch --- Dongmei Dong, Structural, Optical and Electrochromic Property of WO3: MoO3 Thin Film Prepared by RF Magnetron Sputtering Technique, *Journal of Asian Scientific Research* 9, (2019), 65-70.

DETECTOR FOR LUMINOSITY MEASUREMENT AT HIGH ENERGY PHYSICS EXPERIMENTS

Sergey Barsuk[1], Leonid Burmistrov[1], Veronique Puill[1], Patrick Robbe[1]
Oleg Bezshyyko[2], Larisa Golinka-Bezshyyko[2], Vladyslav Orlov[2], Vsevolod Yeroshenko[2],

[1]Laboratoire de l'Accélérateur Linéaire, Orsay, France
[2]Taras Shevchenko National University of Kyiv, Kyiv, Ukraine
orlov.vlad.serg@cern.ch

CANCELLED DUE TO COVID-19

Luminosity measurement detector is a project of fast backward Cherenkov veto counter for both online and offline analysis applied for operation in p-p collisions, beam-gas and heavy ion modes. We performed Geant4 simulation of the quartz detector using events generated by Pythia8 in order to study various options to optimize luminosity measurement precision. Both empty event and hit counting approaches were considered. Several different geometries and configurations were proposed and simulated using GEANT4 framework. Detector structure optimization options were studied and a splitting approach was introduced providing an operation flexibility in a wide range of luminosity.

Main goal of this project is to develop a robust detector system that can provide accurate measurements of luminosity in radiation intensive environment. Increasing of luminosity and detection accuracy causes the need to review the triggers and the priority of different data streams. Thus, past luminosity control methods become obsolete and there is a need for the introduction of a new system for luminosity measurement and beam quality monitoring during the physics data taking.

A quartz Cherenkov detector was proposed for this purpose. It faces the following tasks:

- beam quality control for the high-luminosity hadron collider operation;
- luminosity measurement offline and real-time on a time scale of 10-100 ms;
- veto to determine luminosity for the heavy ion programme.

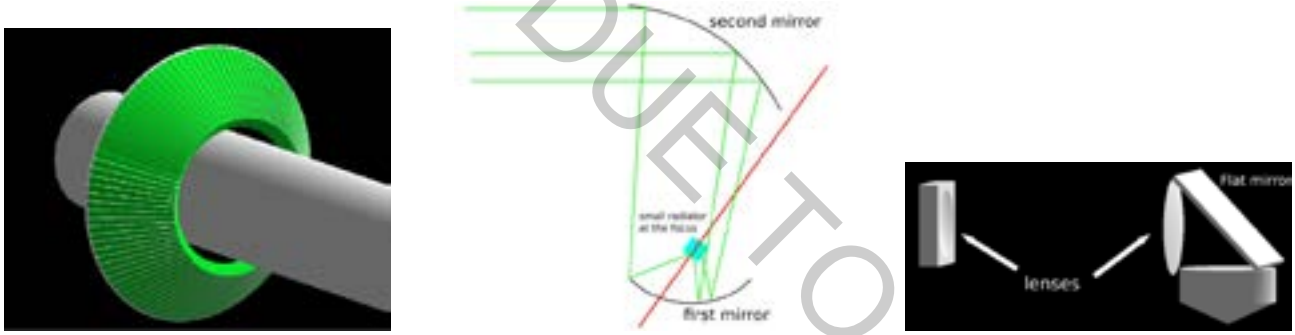

Fig. 1. Some of the geometries that were studied. Trapezoidal quartz bars tilted at an angle (left), two parbolic mirrors that deflect and focus ligh (center), quartz cone with mirror surface and focusing lenses (right)

In order to determine the optimal detector design, several geometries were simulated using Geant4 framework. Simplified material arrangement is included into the simulation to estimate the performance. This different methods were then tested at the DESY beamtest facility, using 5.6 GeV electron beam.

[1] Simulation of the Quartz Detector for Luminosity Measurement at LHCb upgrade, WDS'19 Proceedings of Contributed Papers - Physics, f9, pp. 189–192 (ISBN 978-80-7378-409-6)
[2] LHCb collaboration, The LHCb Detector at the LHC, JINST, 3, S08005, 2008.
[3] LHCb collaboration, Absolute luminosity measurements with the LHCb detector at the LHC, JINST, 7, P01010, 2012.
[4] Balagura, V., Analysis methods for luminosity data, CERN-LHCb-INT-2009-001, 2009.

GOLD PATTERNS ON *n*-SILICON SURFACE FOR SENSORIC APPLICATION

Victoria Bundyukova, Dzmitry Yakimchuk, Vladislav Prigodich

Scientific-Practical Materials Research Centre of the NAS of Belarus, 220072 Minsk, Belarus
victoria.bundyukova@gmail.com

Silicon as a widely used semiconductor material, is used to a wide range of scientific and engineering applications, such as photovoltaic, nanoelectronic, sensitive biosensor devices, etc [1], [2]. The possibility of modifying silicon with various metals allows it to be used as the basis for sensor devices. Numerous works describe the method of electrodeposition of noble metals on the silicon surface to form a microrod array [3], [4]. However, this one has various limitations, including the size of the formed nanoparticles and morphology, the unevenness of the coating thickness, etc [5].

In this work, a galvanic deposition method was used to obtained gold nano patterns on a silicon surface of n-types from a salt of AuCl3 · (H2O) in aqueous solution at various temperatures. The concentration of gold ions in the initial solution was 0.01 M with the subsequent addition of 5 M HF acid in a 1:1 ratio. The morphological and structural properties of the resulting structures were studied depending on the temperature of the gold solution.

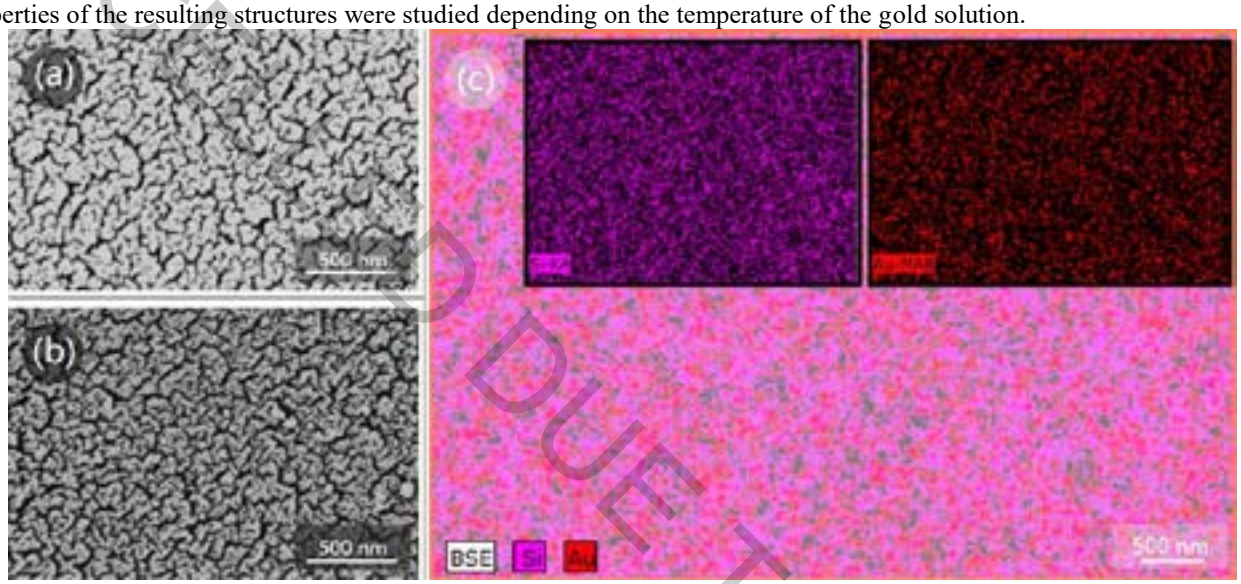

Fig. 1. SEM images of gold NSs on Si template deposited from $AuCl_3$ solution at different temperatures: (a) – 25ºC; (b) – 50 ºC; (c) – EDX-map corresponding to the SEM image (a).

The obtained gold nanopatterns demonstrated the potential use for Raman signal amplification on a reference analyte Rhodamine 6G with a concentration of 10^{-6} M. Thus, there is a possibility of using gold nanotracks as SERS-active surfaces for sensors.

The authors acknowledge the support of the work in frames of H2020 - MSCA - RISE2017 - 778308 - SPINMULTIFILM Project, the Scientific-technical ‘program Technology-SG’ [project number 3.1.5.1].

[1] Wang, Y., Lu, N., Wang, W., Liu, L., Feng, L., Zeng, Z., … Chi, L. (2013). Highly effective and reproducible surface-enhanced Raman scattering substrates based on Ag pyramidal arrays. Nano Research, 6(3), 159–166.
[2] Tripathy, A., Sen, P., Su, B., & Briscoe, W. H. (2017). Natural and bioinspired nanostructured bactericidal surfaces. Advances in Colloid and Interface Science, 248, 85–104.
[3] Fukami, K., Kobayashi, K., Matsumoto, T., Kawamura, Y. L., Sakka, T., & Ogata, Y. H. (2008). Electrodeposition of Noble Metals into Ordered Macropores in p-Type Silicon. Journal of The Electrochemical Society, 155(6), D443.
[4] Ogata, Y., Kobayashi, K., & Motoyama, M. (2006). Electrochemical metal deposition on silicon. Current Opinion in Solid State and Materials Science, 10(3-4), 163–172.
[5] Tonelli, D., Scavetta, E., & Gualandi, I. (2019). Electrochemical Deposition of Nanomaterials for Electrochemical Sensing. Sensors, 19(5), 1186.

CANCELLED DUE TO COVID-19

MODELING OF LOW-TEMPERATURE TORSIONAL SPECTRA OF THE DOOOH AND DOOOD MOLECULES

Alexandr Vasilevsky[1], Anna Kozhevnikova[1], Viktoryia Zhautok[1], Alex Malevich[1], George Pitsevich[1], Valdas Sablinskas[2]

[1]Belarusian State University, Minsk, Belarus
[2]Vilnius University, Vilnius, Lithuania
zheltokvika@gmail.com

CANCELLED DUE TO COVID-19

Large amplitude motions (LAM) in molecules and complexes had been attracting the attention of the researchers for a long time. At the same time, the technique of analysis of such vibrations was constantly improved. Torsional vibrations in molecules undoubtedly belong to the LAM. Recently [1] we have analyzed torsional vibrations in the hydrogen trioxide (HOOOH) molecule. The purpose of this study is getting the torsional spectra of DOOOH and DOOOD molecules. There are at least two reasons to analyze the torsional spectra of these molecules. First of all, it is reasonable to expect that replacing the hydrogen atoms with deuterium ones should lead to a decrease of all tunneling frequencies. Secondly, replacing only one hydrogen atom with deuterium in DOOOH molecule should lead to the changing of the symmetry properties in comparison with those for HOOOH and DOOOD molecules. Actually, assuming tunneling is prohibited, the DOOOH molecule will have no symmetry elements. However, since tunneling still takes place DOOOH molecule belongs to the $C_S(M)$ molecular symmetry group which is isomorph to the C_S point group symmetry. This fact changes the restrictions on the transition between torsional levels what affects the form of the spectrum. The values of the kinematic coefficients are changing for both considered molecules too.

To find the splitting of the torsional energy levels due to tunneling the stationary vibrational Schrödinger of the following form

$$\left[-F_{\gamma\gamma}(\gamma,\varphi)\frac{\partial^2}{\partial\gamma^2} - G_{\varphi\varphi}(\gamma,\varphi)\frac{\partial^2}{\partial\varphi^2} - S_{\gamma\varphi}(\gamma,\varphi)\frac{\partial^2}{\partial\gamma\partial\varphi} + U(\gamma,\varphi)\right]\Psi(\gamma,\varphi) = E\Psi(\gamma,\varphi);$$

was solved using the Fourier method. Here $F_{\gamma\gamma}(\gamma, \varphi)$, $G_{\varphi\varphi}(\gamma, \varphi)$ are the kinematics coefficients for the O-H, O-D groups, $S_{\gamma\varphi}(\gamma, \varphi)$ - kinematics coefficients for the interaction between O-H, O-D groups, and $U(\gamma, \varphi)$ - potential energy. The calculated values of the tunneling frequencies in the ground states of the DOOOH and DOOOD are equal to $2.22\cdot10^{-10}$ and $6.67\cdot10^{-11}$ cm^{-1} respectively, what is less than in the case of HOOOH molecule. Some information about calculated values of torsional states energies of the DOOOH molecule represented in Table 1.

Table. 1. The calculated at MP2/cc-pVQZ level of theory values of torsional states energies of the DOOOH molecule and their assignments.

	DOOOH					
Energy level number	Confomation	Energy[cm^{-1}]	Energy splitting [cm^{-1}]	n_{OH}	n_{OD}	Symmetry species
1	trans	0	$2.22\cdot10^{-10}$	0	0	A'
2	trans	$2.22\cdot10^{-10}$		0	0	A''
3	trans	286.625	$1.93\cdot10^{-11}$	0	1	A'
4	trans	286.625		0	1	A''
5	trans	378.873	$5.50\cdot10^{-10}$	1	0	A'
6	trans	378.873		1	0	A''
7	trans	559.773	$1.49\cdot10^{-10}$	0	2	A'
8	trans	559.773		0	2	A''
9	trans	666.981	$2.54\cdot10^{-10}$	1	1	A'
10	trans	666.981		1	1	A''
11	trans	730.245	$2.26\cdot10^{-9}$	2	0	A'
12	trans	730.245		2	0	A''

Based on calculated data the low-temperature torsional spectra of the DOOOH and DOOOD were predicted too.

[1] G.A. Pitsevich, A.E. Malevich, U.U. Sapeshka, Chem.Phys., 530 (2020) 110633.

NUMERICAL SIMULATION OF QUANTUM EFFECTS DUE TO INTERNAL ROTATION IN A HYDROGEN PEROXIDE MOLECULE

Artem Shlyk[1], Sergei Yanushkevich[1], Darya Kisuryna[1], Alex Malevich[1], George Pitsevich[1], Vitas Balevicius[2]

[1]Belarusian State University, Minsk, Belarus
[2]Vilnius University, Vilnius, Lithuania
kisurinadasha@gmail.com

CANCELLED DUE TO COVID-19

Hydrogen peroxide molecule (HOOH) is a simplest object with internal rotation around O-O bond. It plays an important role in the Earth atmospheric phenomena, was found in cosmic space and has an application in a number of industrial processes. In the equilibrium configuration H_2O_2 molecule exists in the gosh- conformation. During internal rotation molecule goes through the low trans-barrier and the high cis-barrier. Splitting of the torsional levels of energy due to the tunneling through trans- barrier was experimentally confirmed, while tunneling through the cis-barrier is still not experimentally detected. We have calculated 1D potential energy curve and kinematic coefficients as functions of the torsional angle γ at the MP2/acc-pVQZ level of theory. To estimate the energies splitting through cis-barrier the torsional coordinate range was doubly increased ($0° \le \gamma \le 720°$). Then the stationary Schrödinger equation of the following form

$$F(\gamma)\frac{\partial^2\Psi}{\partial\gamma^2}+U(\gamma)\Psi=E\Psi,$$

where F(γ) is kinematic coefficient and U(γ) is potential function, was numerically solved using DVR method. It was found that the calculated splitting of the ground state due to tunneling through the cis- barrier is close to zero ($3.21\cdot10^{-12}$ cm^{-1}), while the calculated splitting through the trans-barrier (12.51 cm^{-1}) is very close to the experimental value (11.43 cm^{-1}). As one can see from Fig.1a in the ground state the wave function is localized in one half of the full region of γ variation.

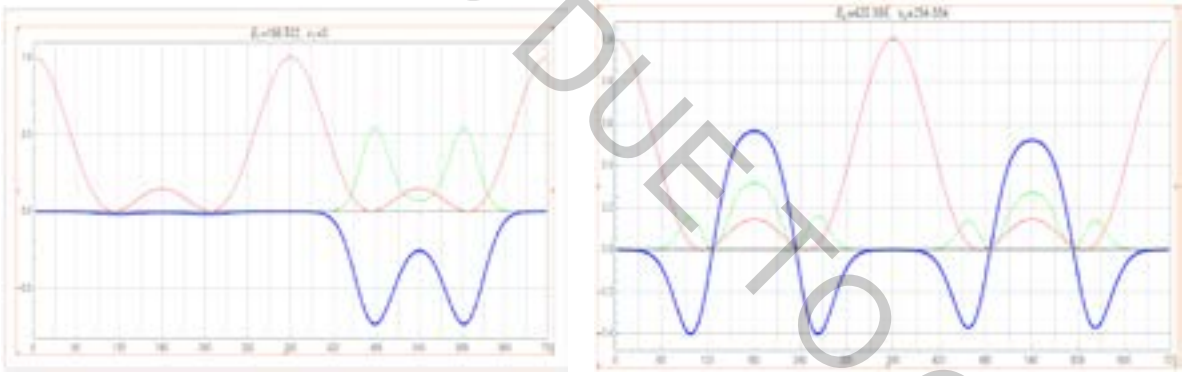

a) b)

Fig. 1. U(γ) - red curve, Ψ(γ) - blue curve, $\Psi^2(\gamma)$ - green curve calculated at MP2/acc-pVQZ level of theory for different energy levels.

It means tunneling through cis-barrier in this case rather absent. Different situation appears for the sixth torsional energy level (see Fig.1b). The wave function is delocalized in full region of γ variation. And it means the tunneling has place in this case even though the value of the tunneling frequency does not increase significantly ($6.31\cdot10^{-11}$ cm^{-1}).

To analyze some time depended quantum effects due to internal rotation in hydroxyl peroxide molecule the following time-depended Schrödinger equation was solved numerically using DVR method:

$$B_0\frac{\partial\Psi(\gamma,t)}{\partial t}+F(\gamma)\frac{\partial^2\Psi(\gamma,t)}{\partial\gamma^2}+(U(\gamma)+D(\gamma)\cdot\Theta(t)-E)\Psi(\gamma,t)=0$$

where D(γ) is a dipole momentum operator, Θ(t) is oscillating electric field of the incident light, B_0 – constant which value depends on time scale. We have found the energy fluctuations due to Heisenberg uncertainty relation when time-dependent perturbation is absent and wave function time dependence in the opposite case.

GROUP-THEORETICAL ANALYSIS OF THE TORSIONAL VIBRATIONS IN NON-RIGID MOLECULES HXYXH TYPE

Alexandr Vasilevich[1], Andrei Ostyakov[1], Aryna Khrapunova[1], Alex Malevich[1], George Pitsevich[1], Valdas Sablinskas[2]

[1]Belarusian State University, Minsk, Belarus
[2]Vilnius University, Vilnius, Lithuania
arishka102000@gmail.com

CANCELLED DUE TO COVID-19

Here we present a very interesting group of molecules whose structure can be described by following general formula HXYXH. Different molecules appear if we connect in different combinations X=O, S, Se and Y=CH_2, O, S, Se. Recently torsional spectra of the $HOCH_2OH$ and HOOOH molecules were studied [1,2]. All of these molecules have common structural properties. They all have two equivalent internal tops (hydroxyl groups) and have two stable conformations (trans- and cis-). Usually, the first conformer is energetically preferable than the second. Both conformers can exist in two configurationally-equivalent states as it is shown in Fig.1 for the HSSSH molecule.

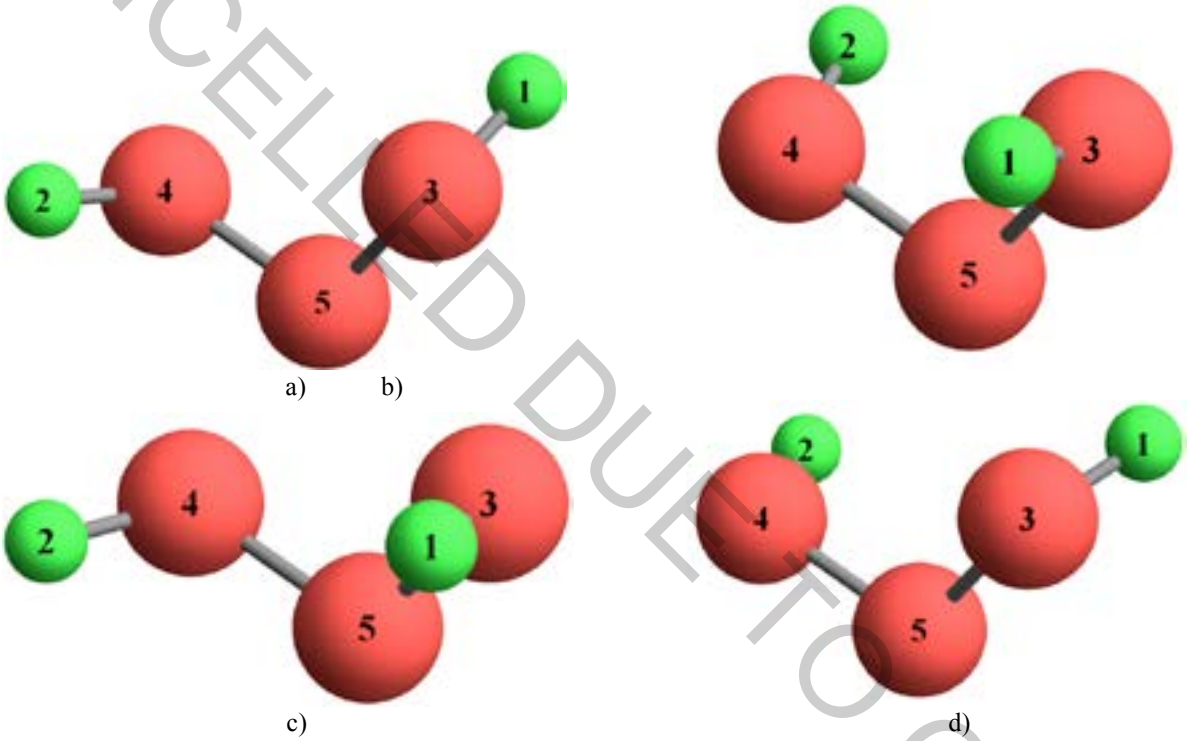

Fig. 1. Trans- (a, b) and cis- (c, d) conformers of the HSSSH molecule.

As we are dealing with non-rigid molecules to classify torsional states we have to use molecular symmetry groups. Even though different molecules from the analyzed group have different symmetry elements, all molecules belong to $C_{2V}(M)$ molecular symmetry group which is isomorph to C_{2V} point symmetry group. It means that all torsional states of any molecule from HXYXH group belong to one of A_1, A_2, B_1, B_2 symmetry species. It is obvious if we consider trans- and cis-conformers of any molecule like a rigid object, their configurations will belong to C_2 and C_S point groups respectively. It is interesting and important to find the correlation between irreducible representations of C_2, C_S point symmetry groups and $C_{2V}(M)$ molecular symmetry group. The performed analysis has showed that A and B irreducible representations of C_2 point group split into A_1, A_2 and B_1, B_2 irreducible representations of the $C_{2V}(M)$ molecular symmetry group respectively, while A' and A'' irreducible representations of C_S point group split into A_1, B_2 and A_2, B_1 irreducible representations of $C_{2V}(M)$ molecular symmetry group respectively. In addition, symmetry properties of the 2D PES, 2D dipole momentum components, 2D kinematic coefficients and torsional coordinates were analyzed too and will be discussed.

[1] G.A. Pitsevich, A.Ye. Malevich, V.V. Sapeshko, J.Mol.Spectr., 360 (2019) 31-38
[2] G.A. Pitsevich, A.E. Malevich, U.U. Sapeshka, Chem.Phys., 530 (2020) 110633.

STRUCTURAL AND SPECTRAL PROPERTIES OF THE (*Z*)-3-(ADAMANTAN-1-YL)-1-(3-CHLOROPHENYL)-*S*-BENZYLISOTHIOUREA

Darya Meniailava[1], Ulada Vysotskaya[1], Aliaksandr Ruskikh[1], Anna Matsukovich[2], Maksim Shundalau[1]

[1] Faculty of Physics, Belarusian State University, Belarus
[2] B.I. Stepanov Institute of Physics, National Academy of Science of Belarus, Belarus
vladavysotskaya@mail.ru

CANCELLED DUE TO COVID-19

Complex organic molecules including an adamantyl fragment in their structure are used as the basis for antiviral and antibacterial agents. They also possess antimicrobial, anti-inflammatory and anti-proliferative activities [1]. Such molecules usually have a complex spatial structure, may have a number of equilibrium configurations, which complicates the prediction and interpretation of the spectral characteristics of such molecular systems.

In this study the structural, spectral, and energy characteristics of (*Z*)-3-(adamantan-1-yl)-1-(3-chlorophenyl)-*S*-benzylisothiourea are presented. The calculations of structural characteristics were performed within the framework of the Density Functional Theory (DFT) by using B3LYP functional and cc-pVTZ basis set. These calculations showed the existence of four stable conformers arising from the rotations around S–C and N–C single bonds with 0 (Fig. 1*a*), 103, 289, and 1341 cm^{-1} relative energies. The results of the current calculations are confirmed by X-ray analysis performed for the crystalline phase earlier [2].

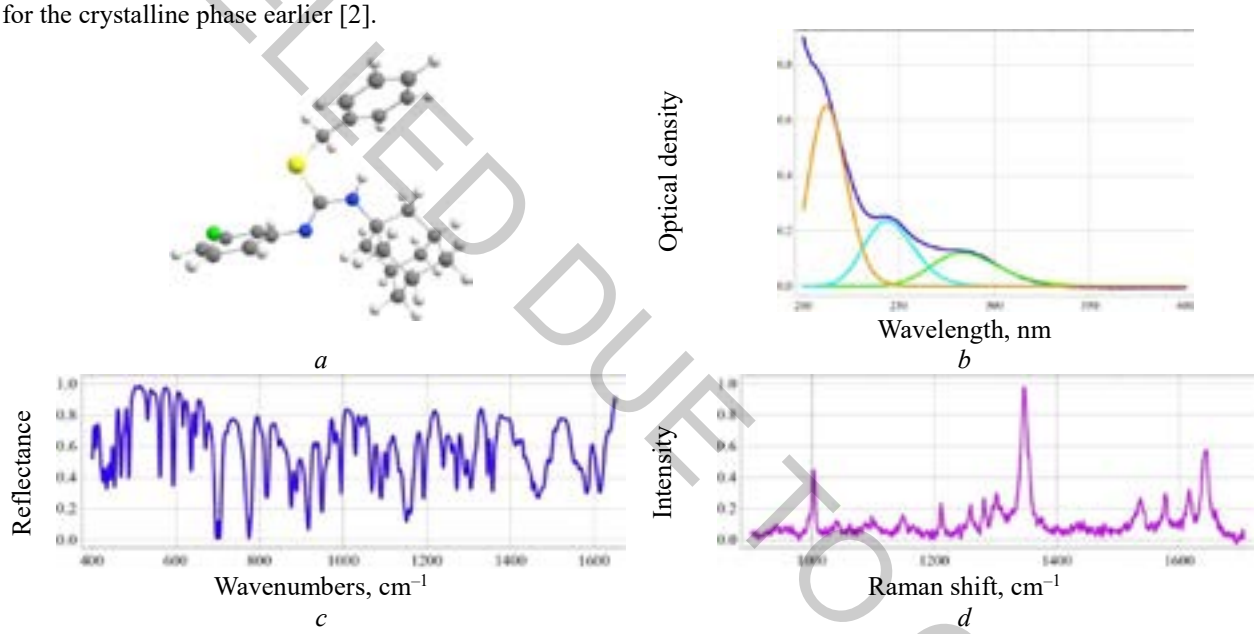

a *b* *c* *d*

Fig. 1. The structure of the most stable conformer of the title compound (*a*), the experimental UV/Vis with the Gaussian deconvolution (*b*), FT-IR (*c*), and Raman (*d*) spectra of the title compound.

The FT-IR (reflection mode, Fig. 1*c*) and Raman scattering (Fig. 1*d*) spectra of the compound for the crystalline phase were measured in the ranges of 4000–400 and 3200–150 cm^{-1}, respectively. The vibrational IR and Raman spectra were also predicted for all conformers at the B3LYP/cc-pVTZ level of theory in the harmonic approximation. According to the results obtained, the assignment of the frequencies of the calculated spectra differs for each of the conformers and the difference is most noticeable in the low-frequency region. The experimental spectra were completely interpreted by using the results of our calculations.

The UV/Vis spectrum of the solution of the compound in ethanol (Fig. 1*b*) was measured in the range of 400–200 nm. The spectrum of electronic absorption turns out to be complicated with three maxima observed. For interpreting the experimental spectrum the calculations for all conformers at the Time-Dependent DFT (TDDFT) and Multi-Reference Perturbation Theory (MRPT) levels of theory were performed. The results of the MRPT calculations with taking into account Boltzman distribution for the conformers qualitatively and quantitatively fully reproduce the experimental spectrum. The results of the calculations performed within the framework of TDDFT completely diverge with the experimental data, which shows the inapplicability of this approximation for the molecular system under study. It is highly probable that this is a consequence of the intramolecular charge transfer.

This work was supported by Belarusian Republican Foundation for Fundamental Research (project No. F18MS-046).

[1] G. Ali Mansoori, P.L. Barros de Araujo, E. Silvano de Araujo. Diamondoid Molecules: With Applications in Biomedicine, Materials Science, Nanotechnology & Petroleum Science, Hackensack, World Scientific Publishing, 2012.

[2] A. A El-Emam, F.A. Al-Omary, L. S. Al-Rasheed et al., Crystal structure of (Z)-3-(adamantan-1-yl)-1-(3-chlorophenyl)-S-benzylisothiourea, $C_{24}H_{27}ClN_2S$, Zeitschrift für Kristallographie-New Crystal Structures, **232**(3), 453-456 (2017).

PHOTOPHYSICAL PROPERTIES OF THIOPHENE-SUBSTITUTED BODIPY MOLECULAR ROTORS

Karolina Maleckaitė[1], Jelena Dodonova[2], Sigitas Tumkevičius[2], Aurimas Vyšniauskas[1]

[1] Center for Physical Sciences and Technology, Saulėtekio av. 3, Vilnius, Lithuania
[2] Institute of Chemistry, Faculty of Chemistry and Geosciences, Vilnius University, Naugarduko str. 24, Vilnius, Lithuania
karolina.maleckaite@ftmc.lt

Imaging viscosity at a microscopic scale can provide information about the diffusion controlled processes in biosystems. The changes in viscosity can be an indicator of the development of atherosclerosis, diabetes, and Alzheimer's disease [1]. One of the easiest ways to image viscosity is provided by viscosity-sensitive fluorophores termed 'molecular rotors'. These fluorophores have been used in various microscopic samples, such as polymers, aerosols, model lipid bilayers, and live cells. Molecular rotors mechanism is based on a change in fluorescence signal, which arises from the competition between fluorescence and intramolecular rotation. Rotation of the molecule changes the nature of the electronically excited state leading to faster relaxation. Therefore, in a high viscosity environment the molecule stays in fluorescent state longer resulting in longer fluorescence lifetime [1].

One of the most promising molecular rotors are based on phenyl substituted boron-dipyrromethene (BODIPY) structure (Fig. 1A). These derivatives have been paid much attention because of their easy functionalization, high molar extinction coefficients, and photostability. The most widely used variations are substituted with $-OC_{10}H_{21}$ and $-OC_{12}H_{25}$ [1]. Unfortunately, a great drawback of these molecules is a green fluorescence [1]. It is well known, that red and infrared wavelengths are more biocompatible because longer waves can be used in thicker biological samples, where light scattering is an issue [2]. It is possible to achieve longer wavelengths by adding thiophene group moieties, which increases conjugated system and shows a larger Stokes shift. [3] Furthermore, recently it was showed that connecting an additional nitro group to a BODIPY core improves its viscosity sensing abilities [2].

In this work, we investigate two thiophene-substituted BODIPY molecular rotors with (**BP-N**) and without (**BP-T**) $-NO_2$ group (Fig. 1B). In this case, adding thiophene moieties in 2- and 6- BODIPY positions increases molecule's conjugation and redshifts fluorescent spectra to more biologically-friendly wavelengths. Moreover, a recent research has showed that attached thiophene moieties to the BODIPY core can rotate and this suggests that these derivatives could be sensitive to viscosity [3].

The investigation consists of absorption and fluorescence spectra measurements, as well as fluorescence lifetime evaluation in many different solvents. Dependencies regarding increasing solvent polarity, viscosity, and temperature were investigated. Spectrometry results showed that connecting a nitro group shifts absorbance and fluorescence spectra to lower energies. Moreover, it increases the Stokes shift and shortens the fluorescence lifetime (Fig. 1C).

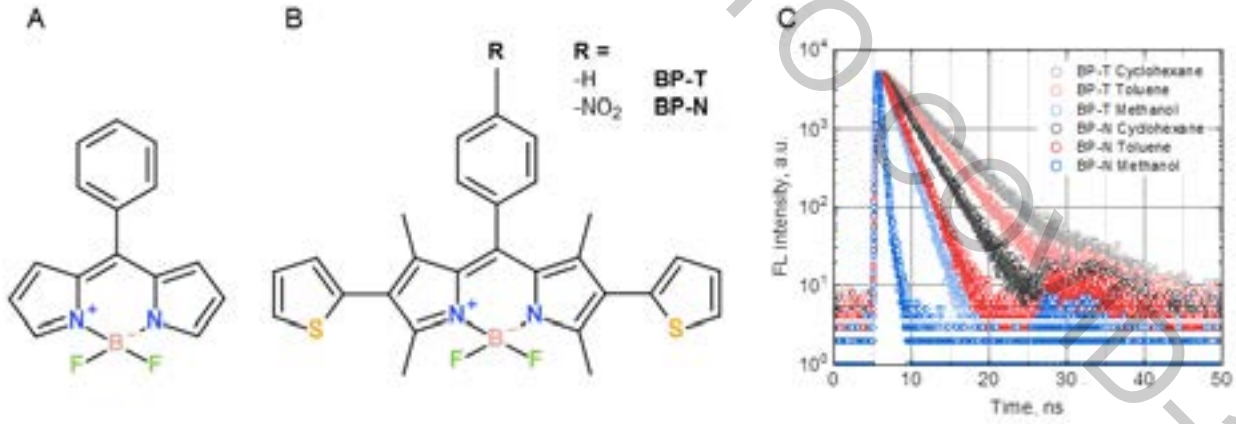

Fig. 1. The molecular structures of the widely used phenyl substituted BODIPY (A) and molecular rotors examined in this work (B). Fluorescent lifetimes of **BP-T** and **BP-N** in different solvents (C).

[1] M. K. Kuimova, "Mapping viscosity in cells using molecular rotors," Phys. Chem. Chem. Phys. vol 14, no 37, p. 12671, 2012.
[2] S. Toliautas et al., "Enhancing the Viscosity-Sensitive Range of a BODIPY Molecular Rotor by Two Orders of Magnitude", Chemistry A European Journal, vol. 25, 44, p. 10342-10349, 2019.
[3] Y. Chen et al., "Geometry Relaxation-Induced Large Stokes Shift in Red-Emitting Borondipyrromethenes (BODIPY) and Applications in Fluorescent Thiol Probes", J. Org. Chem. vol. 77, 5, p. 2192-2206, 2012.

CANCELLED DUE TO COVID-19

STUDY OF URINARY BLADDER CANCER BY MEANS OF SURFACE ENHANCED RAMAN SCATTERING SPECTROSCOPY

Edvinas Zacharovas[1], Martynas Velička[1], Gediminas Platkevičius[2], Arūnas Želvys[2], Valdas Šablinskas[1]

[1]Institute of Chemical Physics, Faculty of Physics, Vilnius University, Lithuania
[2]Clinic of Gastroenterology, Nephrourology and Surgery, Institute of Clinical Medicine, Faculty of Medicine, Vilnius University, Lithuania
edvinas.zacharovas@ff.stud.vu.lt

CONFERENCE PROCEEDINGS

Urinary bladder cancer is the 10th most diagnosed form of cancer in Lithuania and worldwide. This type of cancer affects about 4 times more men than women. By 2030, the number of new bladder cancer cases in Lithuania is expected to increase by 16 % for men and 62 % for women [1]. Cystoscopy (bladder endoscopy) with the following biopsy of the suspicious areas of the bladder and cytological examination of the bladder washouts are the most commonly used methods in the diagnosis of bladder cancer [2]. Histological examination of bladder tissue today is the golden standard for diagnosing bladder cancer but it is an invasive, time consuming procedure. Furthermore, cytological examination is effective for the diagnosis of tumors with a high degree of differentiation, but have low susceptibility to the most common tumors of low malignancy and early stage. As a result, bladder surgery makes it difficult to determine the exact limits of tumor expansion intraoperatively. Effective identification of bladder and other cancers of the urinary system and the establishment of clear boundaries between healthy and tumor tissue require new reliable diagnostic techniques that enable rapid and accurate characterization of samples.

Tumor growth and metastasis lead to changes in the concentration of certain molecules in the body. These changes can be monitored by quantitative and qualitative analysis of biological fluids. One such fluid whose changes in composition are associated with metabolism of cancer is the extracellular fluid [3]. It involves the supply of nutrients essential for cellular metabolism and the removal of metabolites from them. The extracellular fluid layers are formed by smearing the tissue sample across the specimen holder. Single tissue cells may also be found in the layer of extracellular fluid formed in this way. For this reason, extracellular fluid assays provide information not only on the changes in the metabolism of the tissue cells, but also on the morphological differences between the cells themselves.

Molecular vibrational spectroscopy techniques are well-suited for detecting changes in molecule concentration which are caused by cancer activity. The aim of this work was to investigate the applicability of the surface enhanced Raman scattering (SERS) spectroscopy for the detection of cancerous urinary bladder tissue. By using this non-destructive method, the Raman scattering signal is enhanced when the analyte molecules approach the metal-dielectric phase boundary or adsorb on the metal surface. Colloidal solutions of noble metal nanoparticles are commonly used to form SERS active surfaces (Fig. 1 A). The effectiveness of these layers depends on the size, shape, concentration, type of the metal and other factors. Optimization of the synthesis of colloidal solution is an important process that can improve the quality of SERS research. Thus, the application of SERS spectroscopy for the analysis of biological tissue and extracellular fluid could have a direct application in the diagnosis of oncological diseases (Fig. 1 B).

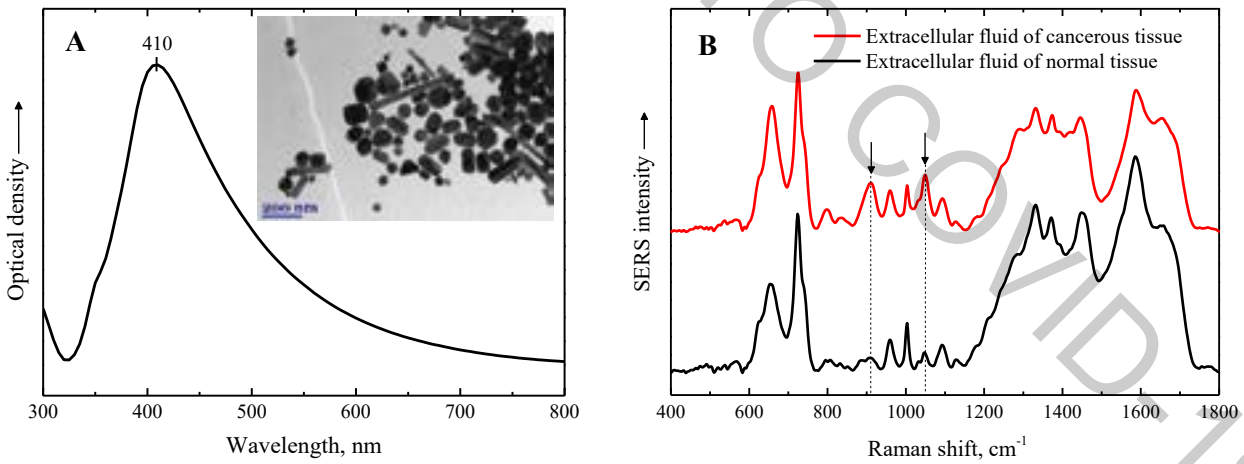

Fig. 1. Absorbance spectra of colloidal solution of silver nanoparticles (A) and SERS spectra of extracellular fluid of cancerous and normal tissue (B).

[1] M. C. S. Wong, F. D. H. Fung et al., The global epidemiology of bladder cancer: a joinpoint regression analysis of its incidence and mortality trends and projections, Scientific Reports, 8(1), 1-12 (2018).
[2] C.-Z. Zhu, H.-N. Ting, K.-H. Ng et al., A review on the accurancy of bladder cancer detection methods, Journal of Cancer, 10(17), 4038-4044 (2019).
[3] H. Wiig et al., Interstitial fluid: the overlooked component of the tumor microenvironment?, Fibrogenesis & Tissue Repair, 3(12), 1-11 (2010).

IDENTIFICATION OF THE PATHOGENIC FUNGI AND BACTERIA. THEIR LIFE-CYCLE STUDY USING INFRARED SPECTROSCOPY

Gerda Mickūnaitė[1], Rimantė Bandzevičiūtė[1], Justinas Čeponkus[1], Eglė Lastauskienė[2], Renata Gudiukaitė[2], Valdas Šablinskas[1]

[1]Chemical Physics Institute, Faculty of Physics, Vilnius University, Saulėtekio Av. 3, LT-10257 Vilnius, Lithuania
[2]Institute of Biosciences, Life Sciences Center, Vilnius University, Saulėtekio Av. 7, LT-10257 Vilnius, Lithuania
gerda.mickunaite@ff.vu.lt

CANCELLED DUE TO COVID-19

Nowadays, a variety of methods that can be applied for identification of different species of pathogenic fungi and bacteria are currently being sought and tested. Bacteria and fungi can cause infectious diseases, so it is important not only to identify them early but also to accurately determine their species. The early identification of fungi and bacteria in the organism can prevent a patient from negative consequences and it can help while prescribing antibiotic therapy, because antibiotics have no effect on fungi while some bacterial species can develop antibiotic resistance. Identification of fungi and bacteria is also important in food quality control, pharmaceutical and cosmetic manufacturing processes to ensure that the final product is not contaminated [1-3].

In this work, the method of an attenuated total reflection of infrared radiation (ATR IR) spectroscopy was applied for the analysis. ATR IR absorption spectra of 56 samples of different bacteria (20 samples, 9 different species) and fungi (36 samples, 5 different species) were analyzed. After spectral analysis, the main spectral differences that allow separating bacteria from fungi were observed in 1183-930 cm^{-1} spectral range (Fig. 1. (a)). The spectral bands which are observed in this range, varies depending on the fungi and bacteria species, and can be attributed to glycogen, amino acids and phosphates.

To assist the identification of bacteria and fungi from ATR IR spectra, cluster analysis was performed. Cluster analysis was performed using the Ward Algorithm, selecting the 1718-935 cm^{-1} spectral range and applying the first derivative and vector normalization preprocessing. Fungi and bacteria were separated into two clusters with 100 % accuracy.

Fungi life-cycle analysis was carried out by performing cluster analysis, of spectra of normal, thermally damaged and damaged by UV light *Candida lusitaniae* fungi (Fig. 1. (b)). Cluster analysis was performed in 1725-1488 cm^{-1} spectral range using the Ward algorithm. Cluster analysis of *C. lusitaniae* showed that normal, damaged by UV light and thermal shock fungi can be separated with 100% accuracy.

In conclusion, it can be stated that infrared spectroscopy is a suitable method for the identification of bacteria and fungi. More detailed studies with a larger number of the samples would let to apply infrared spectroscopy not only in *ex vivo* but in medical *in vivo* studies.

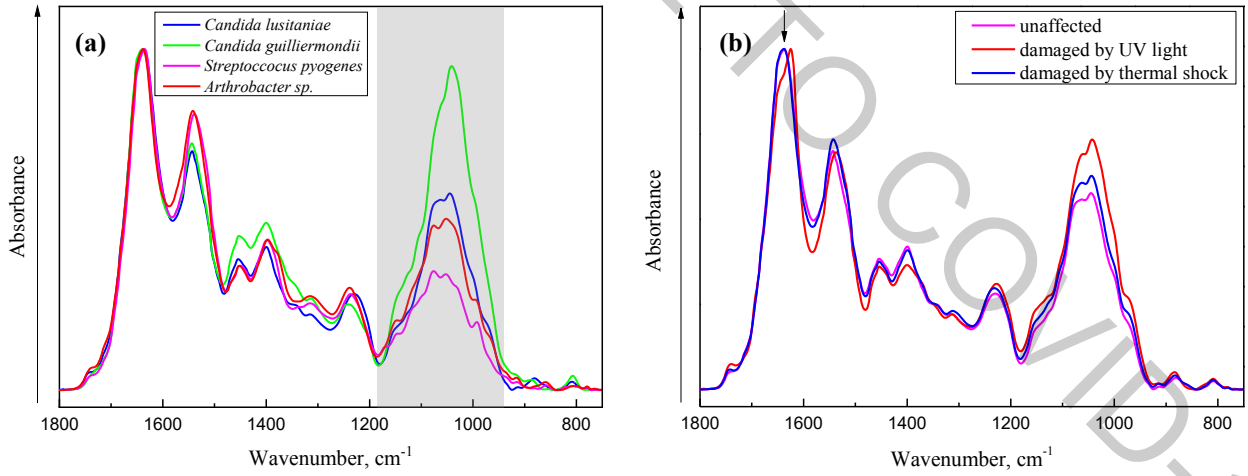

Fig. 1. ATR IR absorption spectra of: (a) different types of bacteria and fungi, (b) normal, damaged by thermal shock and UV light fungi.

Aknowledgement. This research is funded by the European Social Fund under the No 09.3.3.-LMT-K-712-16-0174 "Development of Competences of Scientists, other Researchers and Students through Practical Research Activities" measure.

[1] M. Harz et al., Vibrational Spectroscopy – A Powerful Tool for the Rapid Identification of Microbial Cells at the Single Cell Level, Cytometry **75A**, 104-113 (2009)
[2] C. Spampinato et al., Candida infections, causes, targets, and resistance mechanisms: traditional and alternative antifungal agents, Biomed Res Int. **2013**, 1-13 (2013)
[3] Erin A. Almand et al., Virus-Bacteria Interactions: An Emerging Topic in Human Infection, Viruses **9**, 1-10 (2017)

IDENTIFICATION OF PANCREATIC CANCER BY FIBER BASED ATR IR SPECTROSCOPY

Rimantė Bandzevičiūtė[1], Justinas Čeponkus[1], Valdas Šablinskas[1], Christian Teske[2], Gerald Steiner[3]

[1] Chemical Physics Institute, Faculty of Physics, Vilnius University, Saulėtekio Av. 3, LT-10257 Vilnius, Lithuania
[2] Department for Visceral, Thoracic and Vascular Surgery (VTG), University Hospital Carl Gustav Carus Dresden, Dresden University of Technology, Fetscherstr. 74, 01037 Dresden, Germany
[3]Clinical Sensoring and Monitoring, Faculty of Medicine Carl Gustav Carus, Dresden University of Technology, Fetscherstr. 13, 01307 Dresden, Germany
rimante.bandzeviciute@ff.vu.lt

CANCELLED DUE TO COVID-19

Pancreatic cancer has one of the highest mortality rates [1]. Pancreatic tumors tend to spread. Usually it spreads to liver, also it can metastasize to lymph nodes, lungs or other more distal organs. If a tumor is resectable, the standard treatment applied for pancreatic tumors is a surgery followed by chemotherapy. During the surgery, one of the most important factors for successful treatment is determination of the exact margin between normal and tumorous tissues. In order to avoid recurrence of the disease, all of the malignant cells have to be removed. On the other hand, it is important to leave as much as possible of the healthy tissue to safe vital functions of the organ. A method for real time identification of a tumor, usable directly during the surgery is needed.

During the last decades, various methods of vibrational spectroscopy were applied for biological tissue examination [2]. In case of conventional spectroscopic experiment, the sample has to be transferred to the device, the examination of tissue is limited by size and preparation of the sample. All these factors restrict the use of the methods for clinical application. Using the technique of attenuated total reflection of infrared radiation (ATR IR), the sample can be examined in native conditions without any special sample preparation. The use of optical fibers enables to perform measurements *in situ* or *in vivo* conditions, this is important during live surgery.

In this study, we used ATR fiber probe coupled with portable standard FT-IR spectrometer. The compact size of the device allows to perform the measurements in the operating room. Spectra of the tissue can be collected in a few minutes.

During the study, cases of 25 patients with pancreas pathology including pancreatic ductal adenocarcinoma, neuroendocrine carcinoma, cystic, metastatic tumors and pancreatitis were investigated. ATR IR absorption spectra of normal and tumorous (pancreatic ductal adenocarcinoma - PDAC) tissue are presented in Fig. 1. The most significant differences between normal and cancerous tissues are observed for the bands at 1034,1207 and 1339 cm^{-1}. The increased intensity of these spectral bands in tumorous tissue indicates altered levels of collagen in the tissue. The amount of collagen in PDAC tissue increases due to the desmoplasia which is a common feature of PDAC tumors. During this desmoplastic reaction fibroblast cells secrete more fibrous proteins (collagen) in the extracellular matrix of the tissue. Established spectral markers for tumorous pancreatic tissue indicates that applied technique is appropriate for malignant pancreatic tissue identification.

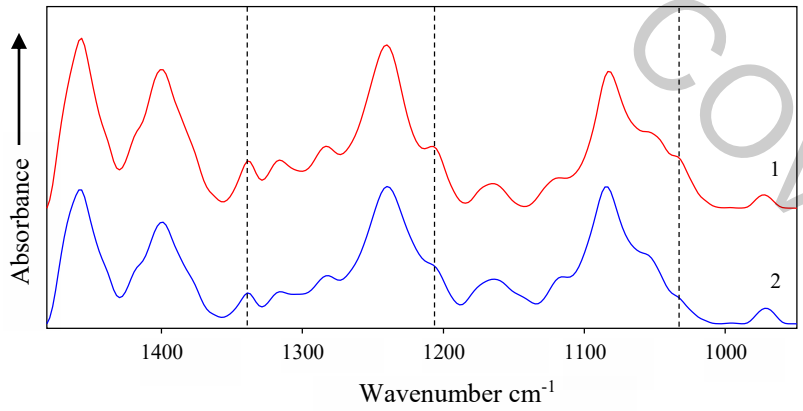

Fig. 1. Averaged ATR IR absorption spectra of PDAC (1) and normal (2) pancreas tissue of 25 patients.

[1] M. Orth, P. Metzger, S. Gerum, et al., Pancreatic ductal adenocarcinoma: biological hallmarks, current status, and future perspectives of combined modality treatment approaches. Radiat Oncol **14**, 141 (2019)
[2] G. Bellisola, C. Sorio, Infrared spectroscopy and microscopy in cancer research and diagnosis, AM J CANCER RES **2**, 1 (2012)

UNSATURATED POLYESTERS FOR BIO-TISSUE: EFFECT OF PDMS AND MULTIFUNCTIONAL HYDROXY COMPOUNDS ON STRUCTURE AND PROPERTIES

Sonata Gailiūnaitė[1], Saulutė Budrienė[1]

[1] Faculty of Chemistry and Geosciences, Department of Polymer Chemistry, Vilnius University, Vilnius, Lithuania
sonata.gailiunaite@chgf.stud.vu.lt

Tissue engineering combines the principles of material synthesis and cell transplantation to create replacement for damaged tissues or promote their regeneration. This field of science began to develop rapidly because of a critical gap between the number of patients on the organ transplant list and donors. Successful artificial tissue formation is highly dependent on the choice of biomaterials for the artificial carcass, and may therefore be one of the key aspects of successful application. [1]. The cells will reproduce and functionalize on frame, so the materials chosen for it should be biocompatible, also it must have mechanical strength, be flexible, biodegradable and non-toxic [2].

Biodegradable polymers have the advantage over ceramic and metal based biomaterials because, depending on the synthesis conditions and used materials, materials with various mechanical, physical and chemical properties can be obtained. Also, polymeric biomaterials are already widely used in the regeneration of muscle, cardiovascular and skin tissues. [3].

Aliphatic polyesters have recently been highlighted for their potential applications in biomedicine due to their degradability and biocompatibility. They undergo hydrolysis in aqueous media to non-toxic oligomers or monomers containing carboxy and hydroxy groups. This is very important because the polyester loses its place in proliferating cells and the degraded products are eliminated from the organism [3]. Most polyesters are elastic materials that are biocompatible and easy to synthesize. For these reasons, polyesters would be a great alternative to fabricate artificial carcass for tissue engineering [4].

The aim of this work was to obtain biocompatible and biodegradable films from polyesters modified with hydroxyl terminated PDMS. Polyester films were synthesized from maleic anhydride, azelaic acid, diethylene glycol/sorbitol/ polyethylene glycol and were chemically modified with hydroxyl terminated PDMS, at various initial molar ratios. Glycidyl methacrylate and/or buthyl methacrylate at various initial molar ratios were used as curing agents to obtain UV-curable films. The films were tested for swelling and solubility in hexane, ethanol and water. To investigate the hydrophilicity of films, a study of humidification angle was performed. The strength of the films was also measured by tensile test.

Acknowledgements

This research was funded by the European Social Fund under the No. 09.3.3-LMT-K-712 "Development of Competences of Scientists, other Researchers and Students through Practical Research Activities" measure (grant No. 09.3.3.-LMT-K-712-16-0270).

[1] Turksen et al., *Cell Biology and Translational Medicine, Volume 4* (Trans. Springer International Publishing, Switzerland, 2018).
[2] C. Yu et. al., Scanningless and continuous 3D bioprinting of human tissues with decellularized extracellular matrix, Biomaterials **194**, 1-13 (2019).
[3] H. T. Weng et. al., Mechanical and thermal properties of biodegradable hydroxyapatite/poly(sorbitol sebacate malate) composites, Songklanakarin Journal of Science and Technology **35(1)**, 57-61 (2013).
[4] H. Ye et. al., Polyester elastomers for soft tissue engineering, Chem. Soc. Rev. **47**, 4545-4580 (2018).

CANCELLED DUE TO COVID-19

SPECTROSCOPIC PROPERTIES AND ACTIVITY OF GLUCOSE OXIDASE

Rugilė Lukaševičiūtė[1], Renata Karpič[2]

[1] Faculty of Chemistry and Geosciences, Vilnius University, Lithuania
[2] Department of Molecular Compound Physics, Center for Physical Sciences and Technology, Lithuania
rugile.lukaseviciute@chf.stud.vu.lt

Usage of biosensing systems is the promising, rapid and accurate method for detection and analysis of various compounds concentration. Nowadays the best-known and the most common biosensors are amperometric glucose biosensors. They can detect blood's free glucose in a short amount of time – it is very important for people with diabetes. The active part of the biosensor is glucose oxidase (GOx) enzyme immobilized on the surface of the electrode [1-3]. In order to create a non-invasive biosensor based on GOx, it is necessary to understand the properties of this enzyme related to the influence of the surrounding environment.

The purpose of this research was to evaluate absorption and fluorescence spectra changes and to associate them with changes of GOx activity.

During this work, the changes of the spectroscopic properties of GOx and flavin adenine dinucleotide (FAD) were investigated in three different cocentration citrate-phosphate buffering solutions with pH values in the range [3 ÷ 8]. During the study, changes in stationary absorption, fluorescence spectra, and fluorescence emission kinetics were observed during the 16-days period. The activity of the GOx enzyme was determined in two different ways – Spectrophotometric Benzoquinone method and Colorimetric method.

GOx enzyme selectively catalyzes the oxidation of D-glucose. Products of the reaction change the stability of the solution system. This leads to changes of GOx spectroscopic properties, which are associated with changes in the structure of the enzyme, during which the FAD is more quickly released from the active center of the enzyme [3].

During this study, we found that GOx enzyme fluorescence band at 530 nm belongs to coenzyme FAD fluorescence. In 16 days measurement period, the increase of GOx fluorescence, which is due to the fact that the enzyme has changed its structure and denatured, was visible.

[1] S. Ferri, K. Kojima ir K. Sode, „Review of Glucose Oxidases and Glucose Dehydrogenases: A Bird's Eye View of Glucose Sensing Enzymes," Journal of Diabetes Science and Technology, t. 5, 2011.
[2] F. Su, L. Zhang, X. Kong, F.Lee, Y. Tian ir D. R. Meldruma, „Ratiometric glucose sensing based on fluorescent oxygen films and glucose oxidase," Sensing and Bio-Sensing Researc, pp. 1-6, 2017.
[3] E. H. Yoo ir S. Y. Le, „Glucose Biosensors: An Overview of Use in Clinical Practice," *Sensors*, pp. 4558-4576, 2010.

CANCELLED DUE TO COVID-19

STUDY OF ACETYLSALICYLIC ACID MOLECULES BY THE MEANS OF MATRIX ISOLATION

Domantas Česnys[1], Rasa Platakytė[1], Justinas Čeponkus[1], Claudine Crepin[2]

[1]Institute of Chemical Physics, Faculty of Physics, Vilnius University, Lithuania
[2]Institut des Sciences Moléculaires d'Orsay, Université Paris-Sud, Orsay, France
domantascesnys@gmail.com

CANCELLED DUE TO COVID-19

Acetylsalicylic acid (ASA) is a key ingredient in anti-inflammatory pain relief medicine. It is critical to analyze structure of this molecule as it can have various conformational isomers with varying properties. The molecular structure can be studied using matrix isolation method which allows sample molecules to be trapped in noble gas matrix. The inert environment and low temperatures help prevent interactions between sample molecules and their environment. The registered spectra exhibit narrow bands from which specific information about molecular structure and its changes can be derived.

In this work, powder samples of ASA were heated to approximately 308 K temperature as the vapor pressure is too low to get a good gas phase sample otherwise. The sample-argon gas mixture was deposited on a CsI plate cooled by closed-cycle helium-refrigeration cryostat to 10 K temperature. FTIR spectrometer was used to register IR spectra of the isolated molecules. DFT calculations of molecules with the B3LYP/6-311++G (3df, 3pd) basis set were performed in order to get theoretically calculated spectra.

The isolated ASA molecule spectrum is compared with ATR (attenuated total reflection) and theoretically calculated spectra of the same molecule. ATR spectrum has naturally broad bands but it is enough to confirm that matrix isolation spectrum (fig. 1b) is needed of ASA. Although most of the peaks of spectrum correspond theoretically calculated ones, there are unassigned bands which could mean that more than one conformer may be found in argon matrix.

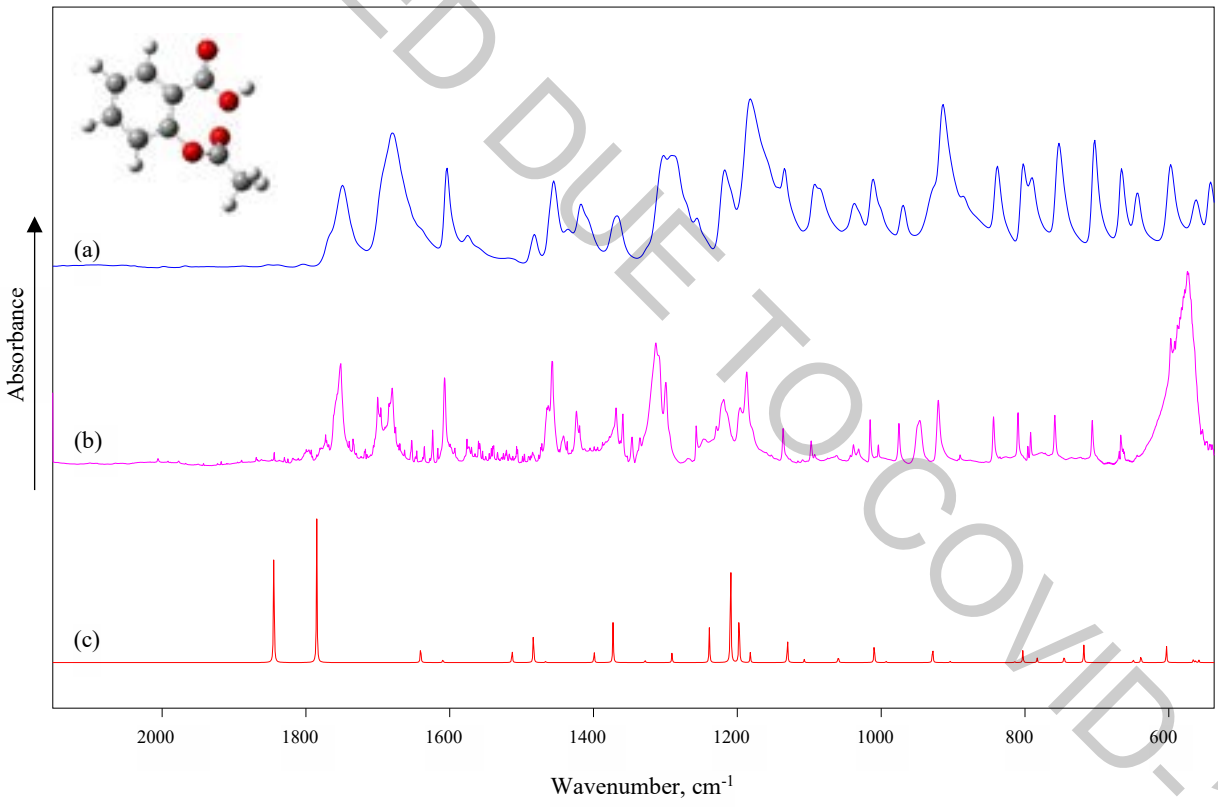

Fig. 1. Spectra of acetylsalicylic acid: (a) ATR spectrum, (b) spectrum of ASA isolated in argon matrix at 10 K, (c) theoretically calculated spectra (B3LYP 6-311++G(3df,3pd)).

Acknowledgements

This work was supported by bilateral Lithuanian-French agreement Gilibert (P-LZ-1/2019/). Computations were performed on resources at the High Performance Computing Center "HPC Sauletekis" in Vilnius University Faculty of Physics.

APPLICATION OF AM and PU ISOTOPES TO TRACE SEDIMENT REDISTRIBUTION IN THE BALTIC SEA

Romanenko Vitaliy[1], Lujanienė Galina[1], Šemčuk Sergej[1], Jonas Mažeika[2], Olga Jevanova[2], Ezhova Elena[3], Garnaga-Budrė Galina[4], Povinec Pavel[5]

[1] SRI Center for Physical Sciences and Technology, Lithuania
[2] SRI Nature Research Centre, Vilnius, Lithuania
[3]P.P. Shirshov Institute of Oceanology RAS, Moscow, Russia
[4]Environmental Protection Agency, Klaipėda, Lithuania
[5]Comenius University, Faculty of Mathematics, Physics and Informatics, Bratislava, Slovakia
Vitaliy.romanenko@ftmc.lt

CANCELLED BEFORE ECORAD 19

The Baltic Sea is under high anthropogenic pressure due to the impact of the coastal territories of densely populated nine countries. It is generally accepted that the main sources of radionuclides in the Baltic Sea are global fallout after nuclear weapons tests, pollution after the Chernobyl accident and releases from European nuclear facilities. Although the radiological situation in the Baltic Sea is constantly monitored, there is a lack of data on actinide contamination, which is most likely associated with difficulties in determination. Besides, recent studies of the plutonium isotopic composition in bottom sediments have revealed unclear sources of pollution. Currently, monitoring the radiological situation is also of particular importance due to the operation and construction of new nuclear plants.

Most of the information about contamination of bottom sediments deals with ^{137}Cs and ^{90}Sr, while less attention is paid to Pu isotopes. The possible application of radionuclides to trace the spread of pollutants in the Baltic has been discussed in recent publications [1-3]. However, the current state of knowledge in this area is still insufficient to conduct tracer research. The most promising indicator for studying redistribution of sediments and assessing the pollution sources are Pu isotopes [4], due to their long half-life compared to ^{137}Cs. ^{241}Am can also serve as an indicator, but there is a significant lack of information about its activity concentrations and behavior in the Baltic Sea [2].

This study aims to assess the concentrations of ^{137}Cs, ^{241}Am and ^{239,240}Pu ^{240}Pu as well as radionuclide and ^{240}Pu/^{239}Pu atom ratio in the bottom sediments of the Baltic Sea with a view of applying these data in tracer studies. A sampling of bottom sediments was carried out by *the* Environmental Protection Agency (Klaipėda, Lithuania) and by P.P. Shirshov Institute of Oceanology RAS (Moscow, Russia). Bottom sediment samples of the surface layer of 0–5 cm were taken from a depth of 43–220 m using a Van Veen Grab Sampler. The location of the sampling station is shown in the figure (Fig. 1.). ^{137}Cs activities were measured with HPGe detectors (resolution 1.8 keV (FWHM) at 1.33 MeV and efficiency 42%). Samples were ashed at 550ºC and then dissolved in strong acids. The TOPO/cyclohexane extraction and radiochemical purification using UTEVA, TRU and TEVA resins (100-150 mm) were used for separation of Am and Pu isotopes. ^{242}Pu and ^{243}Am (AEA Technology UK, Isotrak, QSA Amersham international, PRP10020 and ATP10020) were used as yield tracers. Plutonium and Am after purification were electroplated onto stainless steel disks and measured using an alpha-spectrometry system with passivated implanted planar silicon (PIPS) detectors, 450 mm^2 active area (AMETEK, Oak Ridge, Tenn, USA). The Pu isotope ratios after additional purification were determined by the AMS.

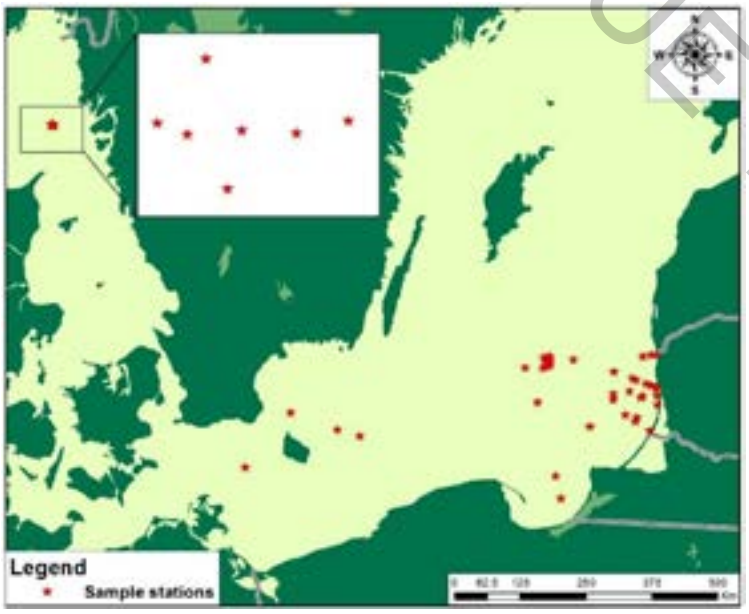

Fig. 1. The area of sampling.

The preliminary results indicated that activity concentration of ^{137}Cs, ^{241}Am and ^{239,240}Pu in studied samples ranged from 1.9 to 220 Bq/kg, from 0.02 to 0.13 Bq/kg and 0.02 to 3.03 Bq/kg, respectively. The obtained results will be used in tracer studies.

[1] Mattila, J., Kankaanpää, H., & Ilus, E. (2006)., Boreal Env. Res. Vol. 11, 95–107.
[2] G. Lujaniene, Remeikaite, N., & Semcuk, S. (2014). J. Environ Radioact. 127, 40–49.
[3] Dagmara I. Struminska-Parulska (2014). Mar. Pol Bull. 89, 12–15.
[4] Lal, R., Fifield, L. K., Tims, S. G., Wasson, R. J., & Howe, D. (2020). J. Environ Radioact. 178-179 (2017) 394-403.

DISPERSION RELATION ANALYSIS OF BLOCH SURFACE WAVES AND SURFACE PLASMON POLARITONS USING TOTAL INTERNAL REFLECTION ELLIPSOMETRY

Vaida Grasyte[1], Ernesta Buzavaite-Verteliene[1], Zigmas Balevicius[1]

[1] Plasmonics and nanophotonics lab., Department of Laser technologies, State Research Institute Center for Physical Sciences and Technology, Lithuania
vaida.grasyte@ff.stud.vu.lt

CANCELLED DUE TO COVID-19

Electromagnetic surface waves (SW) have been extensively used for various optical sensing. One of the most commonly known and used SWs is the surface plasmon polariton (SPPs) propagating at metal dielectric interface. Surface plasmon polaritons are widely used in optical sensors such as biosensor application [1, 2] due to high sensitivity of such type SW. Some proteins are not biocompatible with metal surfaces, therefore alternative methods are developed. Here comes handy another type of surface waves - Bloch surface wave (BSW) generated at the interface of periodic dielectric structure (photonic crystal) and surrounding media (dielectric) [3]. Bloch surface waves can be tuned in wide spectral range by adjusting the materials and period of the photonic crystal (PC). Due to low losses in the dielectrics the BSW can propagate for long distances. Another advantage of BSW is that it can be excited in both TE and TM polarization, thus allowing us to investigate changes of polarization states. Since there are not many techniques allowing us to investigate polarization and phase changes, we use spectroscopic ellipsometry measuring technique. In order to excite SPP or BSW a glass prism or grating as a coupler to achieve conditions of total internal reflection (TIR) is used. TIR configuration is commonly used in biosensing application as it allows to measure protein interaction without light propagation through liquids, removing additional noise from the system. By combining advantages of TIR and spectroscopic ellipsometry with ability to simultaneously measure the amplitude and phase changes, we get total internal reflection ellipsometry (TIRE) technique.

The aim of this study was to investigate the optical dispersion relations of SPPs and BSWs resonances and analyze their sensitivity to the refractive index changes of ambient medium. The total internal reflection ellipsometry (TIRE) method was employed for excitation and study of SPP and BSW dispersion curves [4]. For excitation of SPP a model consisted of BK-7 glass substrate, 1 nm Cr and 45 nm Au layers was used. Meanwhile, for the BSWs generation a BK-7 glass substrate with PC consisting of 6 bilayers of TiO_2 (60nm) and SiO_2 (110 nm) with single 30 nm TiO_2 layer on top model was used. In this study we present numerical calculations of SPPs and BSWs dispersion relations, the differences of dispersion curves due to changes of refractive index of the medium and sensitivity of ellipsometric parameters Ψ and Δ of such optical sensors. The evaluation showed that SPP was more sensitive in resonance wavelength displacement $\delta\lambda$/RIU (refractive index unit) than BSW. As BSW had a higher sensitivity $\delta\Psi$/RIU and $\delta\Delta$/RIU for ellipsometric parameters Ψ and Δ rather than SPP.

[1] I. Baleviciute, Z. Balevicius, A. Makaraviciute et. al., Study of antibody/antigen binding kinetics by total internal reflection ellipsometry, *Biosensors and Bioelectronics* **39**, 170-176 (2013).
[2] L. Wu, H. S. Chu et al., Highly sensitive graphene biosensors based on surface plasmon resonance, *Optics Express* **18**, 14395-14400 (2010).
[3] P. Yeh, A. Yariv, and C.-S. Hong, Electromagnetic propagation in periodic stratified media I General theory*, *Journal of the Optical Society of America* **67**, 423-438 (1977).
[4] Z. Balevicius and A. Baskys, Optical Dispersions of Bloch Surface Waves and Surface Plasmon Polaritons: Towards Advanced Biosensors, *Materials* **12**, 1-10 (2019).

EVALUATION OF THE DOSE ACCUMULATION COEFFICIENT BY *IN SILICO* MODELLING OF THE X-RAY DIAGNOSTICS OF THE RIB THORAX

Dzmitry Kacharhin[1]

[1] Department of Nuclear Physics, Belarusian State University, Belarus
dmitriyrbu@gmail.com

Procedure of the X-ray diagnostics have an essential role in fields of epidemiology, traumatology and oncology. Doctors at mentioned areas often use it for the diagnosis and visual presentation of the disease picture. In order to minimize harmful affection on patients it's necessary to most accurately account contribution of the X-ray dose received during medical procedures to annual dose of radiation.

During radiological procedure on patient one can estimate whether a used radiation dose is critically high for a current procedure under normal conditions. A parameter called *diagnostic reference level* DRL is used for that estimation. Equivalent parameter to the DRL is the *dose accumulation coefficient* D_{acc} which characterizes the ratio of energy obtained from the both reflected and direct radiation to energy of the direct one. The D_{acc} is used in order to measure level of affection on the patient as a dose obtained at the patient effective surface during the X-ray research procedure.

This *in silico* research studies influence of the X-ray machine parameters and the absorbing body properties on the dose accumulation coefficient D_{acc} in the case of the X-ray diagnostics of a rib thorax.

A model of the X-ray diagnostics includes the X-ray machine model, the absorbing body model and the detector plate model. Geometrically the model of the X-ray diagnostics consist of a point X-ray source (the X-ray machine model) that placed in front of a circular cylinder filled with water (the patient model), right behind the cylinder is placed an air plate (the detector plate model). The cylinder and the detector plate are placed on the axis of the beam from the source.

In this approach used a model of the static X-ray machine, which includes an X-ray source, an energy spectrum smoothing filter and a collimation system.

The patient model parameters like height and radius of the cylinder are depend on the age of the patient being examined. Thus, for each patient a refinement is made to the value of the coefficient D_{acc} by approaching the source and changing the radiation field. The parameters of the cylinder are taken on the basis of the tables of mass and growth of patients given in the ICRP-89.

The radiation detector model has linear dimensions of 5x5 cm and a thickness of 1 mm. The material of the detector plate is air under normal conditions. The detector is placed as close as possible to the cylinder. So, the distance from the detector to the source depends just on the radius of the cylinder. In addition, another case of detector geometry is a set of detectors located on the beam axis, placed at equal intervals from the cylinder. That configuration allows to determine the rate of decline of the dose accumulation coefficient D_{acc} with the distance.

List of parameters that was changing in the research:

- Voltage of the X-ray tube (kV)
- Voltage ripple (%)
- Effective patient body thickness (mm)
- Patient age (years)
- Smoothing filter depth (mm)

In this approach data for X-ray energy spectra from the source was taking from TASMIP [2], and include dependents from aluminum filter, voltage and voltage ripple. Monte-Carlo modelling used for computation energy, that was delivered to detector by gamma-quanta. Results of the *in silico* experiments:

1. In this work, more than 500 values for the were calculated for various exposure parameters.
2. The contribution of the smoothing filter depth to the coefficient value is 9% when considering ripple at 10% and its absence. Thus, it should be born in mind that when using filters of various thicknesses, a noticeable increase in the dose accumulation coefficient occurs.
3. The contribution of the effective patient body thickness to the coefficient value is 0.8% when considering ripple at 10% and its absence.
4. The dose accumulation coefficient increases with increasing voltage. An increase in the coefficient values with an increase in thickness is 4–4.7% for various stresses.
5. The difference in the value of the coefficient for the ages of 15 and 18 years depending on gender varies from 0.5% to 3.5% depending on changes in various parameters of the radiographic procedure.

Results of this work can be used to assess the success of lung radiography. The obtained results allow to determine the input dose on the surface for most types of patients, and the effect on these values of such characteristics of the X-ray tube as the values of the anode voltage, the smoothing filter thickness and the voltage ripple.

[1] ICRP 89
[2] John M. Boone J. Anthony Seibert TASMIP USA, 1997.

CANCELLED DUE TO COVID-19

ANALYSIS OF VERY LARGE HAIL AND TORNADOS IN LITHUANIA IN THE PERIOD 1961–2019

Izolda Marcinonienė

Vilnius University Faculty of Chemistry and Geosciences
izolda.marcinoniene@chgf.vu.lt

Global climate change creates unprecedented local consequences the world over and in Europe as well. The problem makes meteorologists turn from discussions to deep research and take action to combat this problem. The recurrence of heat waves and powerful summer storms have a significant influence on the weather situation in the Baltic region as well (Fig. 1). The main purpose of this presentation is a quantitative analysis along with qualitative study of two hazardous meteorological phenomena in Lithuania – very large hail (hailstone diameter ≥20 mm) and strong tornados (wind gusts ≥28 m/s). According to national criteria for severe weather, they are considered as disastrous meteorological phenomenon potentially devastating for aviation, agriculture and constructions. All data since 1962 have been collected from archives of Lithuanian Hydrometeorological Service.

During the long 58 years period 86 cases of very large hail have been registered in 123 places and 27 tornados cases in 33 places of the country. In fact, about 1 tornado per 2 years and ~2 large hail cases per year registered in the country. Considering to their locality, the real number of occurrences is higher than the observed figure. However due to new technology the information on these phenomena is more and more frequent and exact nowadays. The question, if the density of population influences the number of cases observed, could be rose up as well.

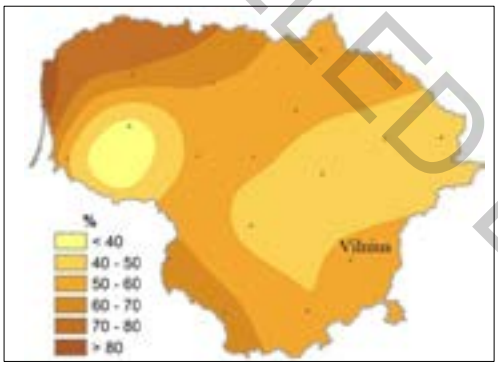

Fig. 1. Icrease of days (%) with Temp Max ≥25 °C in Lithuania, according to the trend 1961–2018

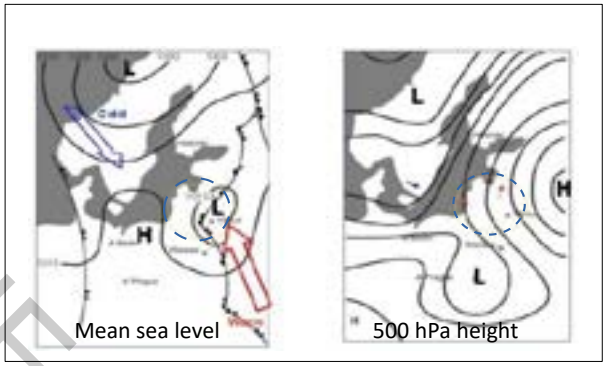

Fig. 2.Typical severe weather patern in Lithuania

In most cases, especially intense convection develops in situation when cold front from the western or southwestern part of Lithuania approaches the eastern one which is more frequently occupied by hot and wet tropical air mass (50 % of tornados and 40 % of hail cases, Fig. 2). In some events mesocyclones develop and they could be detected on radar reflective image as a "hook echo" – it shows the initial stage of mesocyclone that is in tornadic mode. Later this „hook" could be seen as this supercell is in great rotation and tornado occurs. Usage of special meteorological satellite product "sandwich" helps to monitor the development of mesoscale convective system. The convergence at the surface and strong upward of hot and humidit air masss in these mesocyclones associated with divergence at cold dry higher levels is the main reason of powerful discharge of the energy of instability. Obviously, the S/SW/SE flows dominate in 44% of hail and 55 % of tornado cases. The increment of days with tropical air mass in northern countries could be attributed to climate change.

Over 70 % cases of large hail occur due to the passage of atmospheric fronts and 61 % of these fronts move in deep cyclonic lows. In contrary, there exists a distinction between two basic synoptic situations leading to the development of tornados: the lines of convergence/instability in the tropical air mass (close to 50 % of cases) and the areas of mesoscale convective systems which develop on cold-front wave tops (~30 % of all tornadoes cases) and only 3 tornadoes cases were associated with front of occlusion.

Detection of climate change impact on severe weather events in Lithuania is an additional purpose of this paper. The influence of the North Atlantic Oscilliation (NAO) on disastrous meteorological phenomenon has been analyzed and results will be presented. Data have been taken from NOAA's Climate Prediction Center (USA).

The poster demonstrates both phenomena using the charts of distribution over Lithuania, diagrams and histograms as well as impact. Additionally, this paper widely illustrates the distinct spread of very large hail and tornados by daytime and by seasons and the prevailing size of hailstones or wind speed of tornados.

CANCELLED DUE TO COVID-19

EFFICIENT NON-DOPED OLEDS BASED ON MULTI-CARBAZOLE DERIVATIVES SUBSTITUTED BY DIFFERENT ACCEPTORS

Malek Mahmoudi[1*], Dalius Gudeika[1,2], Dmytro Volniuk[1], Jouzas V. Grazulevicius[1]

[1] Department of Polymer Chemistry and Technology, Kaunas University of Technology, Radvilenu pl. 19, LT-50254, Kaunas, Lithuania

[2] Institute of Solid State Physics, University of Latvia, Kengaraga st. 8, LV-1063, Riga, Latvia

malek.mahmoudi@ktu.edu

From the standpoint of fabrication technology, doping-free organic light-emitting diodes (OLEDs) are more appealing than the doped ones [1]. Recently, 21% external quantum efficiency was archived for non-doped solution-processed sky-blue thermally activated delayed fluorescence OLEDs using multi-donor/acceptor emitter with through-space/-bond charge transfer [2].

To further understand impact of acceptor substitution patterns of multi-donor/acceptor emitters, five multi-carbazole derivatives were substituted by different acceptors in this study. Non-doped films of those derivatives were characterized by blue/sky-blue emission with PL spectra having maximum wavelengths in the range from 473 to 512 nm. Their emission was attributed to efficient thermally activated delayed fluorescence (TADF) due to their triplet-singlet energy splitting lower than 0.2 eV. TADF properties for the developed compounds were additionally proved by time-resolved spectroscopy. High photoluminescence quantum yield values achieving of 77 % and 34.3 % were recorded for the studied compounds in deoxygenated toluene and solid films, respectively. Ionization potentials of those materials were found in the range from 5.39 to 5.9 eV for solid samples by photoelectron emission method in air.

Electroluminescent characteristics of the studied compounds were tested in non-doped TADF OLEDs (marcked as device A-E) using them as emitters. The fabricated devices were characterized by blue/sky-blue electroluminescence with CIE1931 coordinates of (0.201,0.432), (0.232,0.339), (0.174, 0.265), (0.177, 0.267) and (0.173, 0.305) (Figure 1). In the best case using a multi-carbazole derivative substituted by two CN-moieties, devices showed maximum luminance of 36000 cd m^{-2}, current efficiency of 19.5 cd/A, power efficiency of 6.1 lm/W and external quantum efficiency of 7.3%.

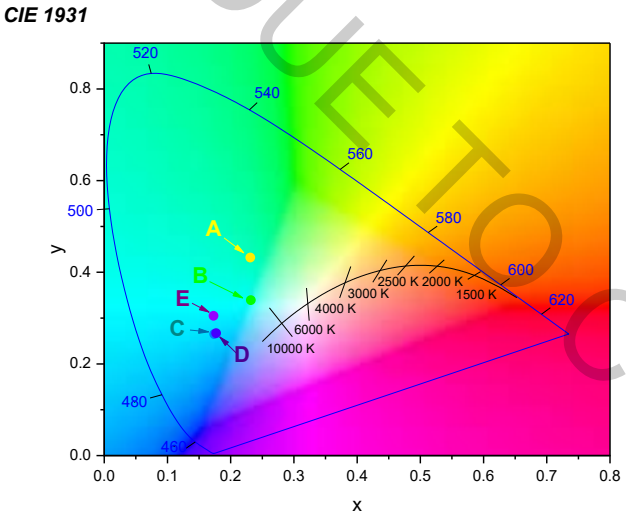

Fig. 1. CIE1931 coordinates of the studied devices.

Acknowledgements

This work was supported by the project of scientific co-operation program between Lithuania and Ukraine "Development of highly efficient white light-emitting diodes utilizing organic emitters with exciplex and thermaly-assisted fluorescence for lighting applications (LUW)" (grant No. S-LU-20-9).

[1] D. A. Islam, Q.Wang et al., Efficient non-doped deep blue organic light emitting diodes with high external quantum efficiency and a low efficiency roll-off based on donor-acceptor molecules, Dyes and Pigments **142**, 499-506(2017)

[2] X. Zheng, R. Huang et al., Achieving 21% external quantum efficiency for non-doped solution-processed sky-blue thermally activated delayed fluorescence OLEDs by means of multi-donor/acceptor emitter with through-space/-bond charge transfer, Advanced Science, just accepted article, DOI: 10.1002/advs.201902087 (2020)

CANCELLED DUE TO COVID-19

SPECTRAL ANALYSIS OF AIR PLASMA JETS AT ATMOSPHERIC PRESSURE

Alena Vabishchevich[1], Aliaksandra Kazak[1], Olga Emeliyanova[2], Goran Sretenovich[3]

[1] Institute of Physics of the National academy of sciences of Belarus, Minsk, Belarus
[2] Republican unitary enterprise Scientific Practical Centre of Hygiene, Minsk, Belarus
[3] University of Belgrade, Faculty of Physics, Belgrade, Serbia
elena199713.elena@mail.ru

CANNOT BE DUPLICATED

Atmospheric pressure plasma jets are widely studied due to their prospective capabilities to be used in plasma medicine technologies [1]. Basic applications of atmospheric pressure plasma jets are linked with that they can transfer numerous chemical and biological active species from a discharge region to a treated object. A bactericidal number of active species (reactive oxygen and nitrogen species or RONS) is efficiently generated in the case of using air as a feeding gas. [1-2].

This paper presents the results of studies of air plasma jets by atmospheric pressure glow microdischarge (APGμD) and dielectric-barrier discharge (DBD) and their spectral analysis. The electrical circuit for the generation of APGμD on direct current and the discharge chamber is show in [3]. The electrical circuit for generating a DBD jet and a discharge chamber is presented in [4]. The discharges and plasma jets formed on their basis were investigated using emission and absorption spectroscopy methods.

It has been shown by emission spectroscopy that the presence of the NO, OH, N_2 (2+), N_2 (1+), N_2, OI bands is characteristic of the APGμD spectrum (Fig. 1a), the main difference between the discharge spectrum and the jet spectrum is the presence of a band NO_2 spectrum due to the three-particle chemiluminescent reaction $NO + O_2 + M \rightarrow NO_2 + M$. The characteristic DBD spectrum (Fig. 1b) includes OH, N_2 (2+), N_2 (1+), N_2, and the discharge has such a low luminescence intensity that the resulting plasma jet does not emit in the range of 200-900 nm.

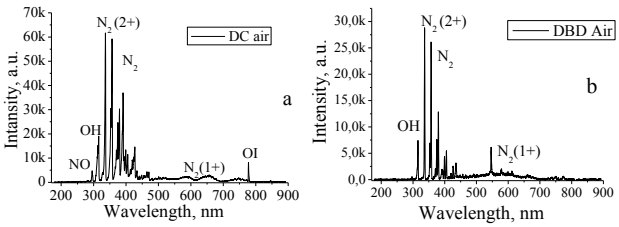

Fig. 1 –Discharge spectrum APGμD (a) and DBD (b)

Using FT-IR spectroscopy was shown that, in the range of 600–4000 cm^{-1}, APGμD jet in air are characterized by the presence of NO, NO_2, HNO_2, N_2O bands (Fig. 2a), while DBD jets in air are characterized by the presence of O_3 and N_2O bands (Fig. 2b). The concentration distribution along the axis of the jet is shown in Fig. 2c and 2d. In treatment zone of microorganisms (4 cm from the anode), the concentrations of RONS are: NO – 35 ppm, NO_2 – 20 ppm, HNO_2 – 9 ppm (for APGμD jet), O_3 – 2 ppm (for DBD jet). The concentration of the N_2O molecule is about 1 ppm for both cases.

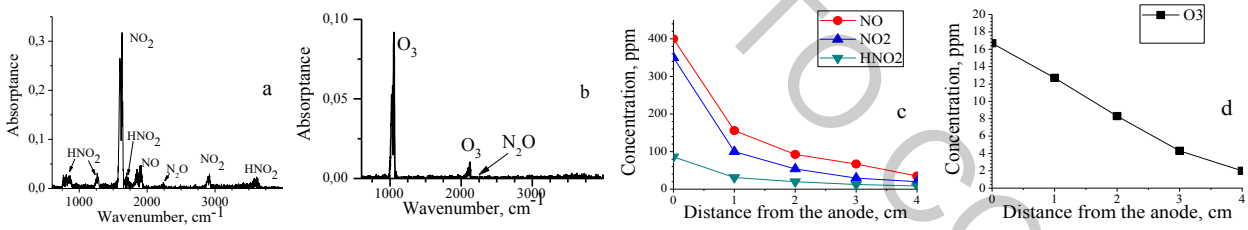

Fig. 2 – Absorption spectra APGμD (a) and DBD (b) air plasma jets, distribution of concentrations of bioactive components along the axis of the plasma jets (c, d)

The inactivation ability of the obtained plasma jets was studied by determining the diameter of the zones of inhibition. For this, a culture of *S. aureus* and *E. coli* was seeded in Petri dishes with an initial concentration of 10^5 CFU/ml, after which treatment with both plasma jets was carried out at different exposure times. During an exposure of 10 minutes on *S.aureus*, it was noted that for DBD jets in plasma, *S.aureus* inactivation is faster (10^1 CFU/ml left in 7 minutes of treatment) than for APGμD jets in plasma (10^1 CFU/ml left in 10 minutes of treatment). The opposite situation was observed for *E. coli*, in this case it is most efficient to use the APGμD air plasma jet.

This make it possible to more efficiently select the conditions for the generation of the required composition of bactericidal components for a specific problem.

The work is partially supported by the grant of BRFFR F19RM-018.

[1] A. Fridman, G. Friedman, *Plasma Medicine.*, p. 526 , (Wiley, New Delhi, 2013).

[2] J Winter, R Brandenburg and K-D Weltmann, Atmospheric pressure plasma jets: an overview of devices and new directions, Plasma Sources Sci. Technol. 24, 064001 (2015).

[3] V.I. Arkhipenko et al., Mechanisms underlying the formation of inactivation components of an air DC plasma jet, High Temp. Mater. Process. 22 (4), 273–278 (2018).

[4] Sretenović, G. B., et al., Spatio-temporally resolved electric field measurements in helium plasma jet, J. Phys. D: Appl. Phys. 47, 102001 (2014).

SYNTHESIS AND CHARACTERISATION OF GLASSY AND NANOCRYSTALLINE ANALOGUES OF LiFePO4 OLIVINES

Krzysztof Gadomski[1], Tomasz K. Pietrzak[1]

[1] Faculty of Physics, Warsaw University of Technology, Koszykowa 75, 00-662 Warsaw, Poland
krzysztof.gadomski2.stud@pw.edu.pl

Low electronic conductivity of cathode materials for the next generation of Li-ion batteries is a serious factor limiting their electrochemical performance. Thermal nanocrystallization of glassy analogues of selected cathode materials for Li-ion batteries is a powerful but relatively simple method to prepare highly-conducting nanomaterials. In previous paper [1], properties of nanocrystallised $LiFePO_4$ with small amounts of vanadium, prepared with this method, were described. Vanadium was used to facilitate glass formation of priscine samples. Subsequently, the research was carried out to prepare and explore properties of nanocrystallised $LiFePO_4$ without addition of vanadium, and the preliminary results of this research are presented here.

Objective of this paper was to develop the idea of thermal nanocrystallisation through systematic research on optimal conditions of obtaining amorphous $LiFePO_4$. Syntheses of samples were carried out with twin rollers method [2] and with different process conditions. After synthesis, samples were analysed with differential thermal analysis (identify temperature of glass transition and temperature of crystallization), X-ray diffractometry (verify amorphousness of samples and study process of (nano)crystallization) and impedance spectroscopy (determine electrical conductivity).

First results of X-ray diffractometry (Fig. 1) showed that different conditions of synthesis (i.e. rotation speed of the rollers) has effect of content of amorphous phase in samples.

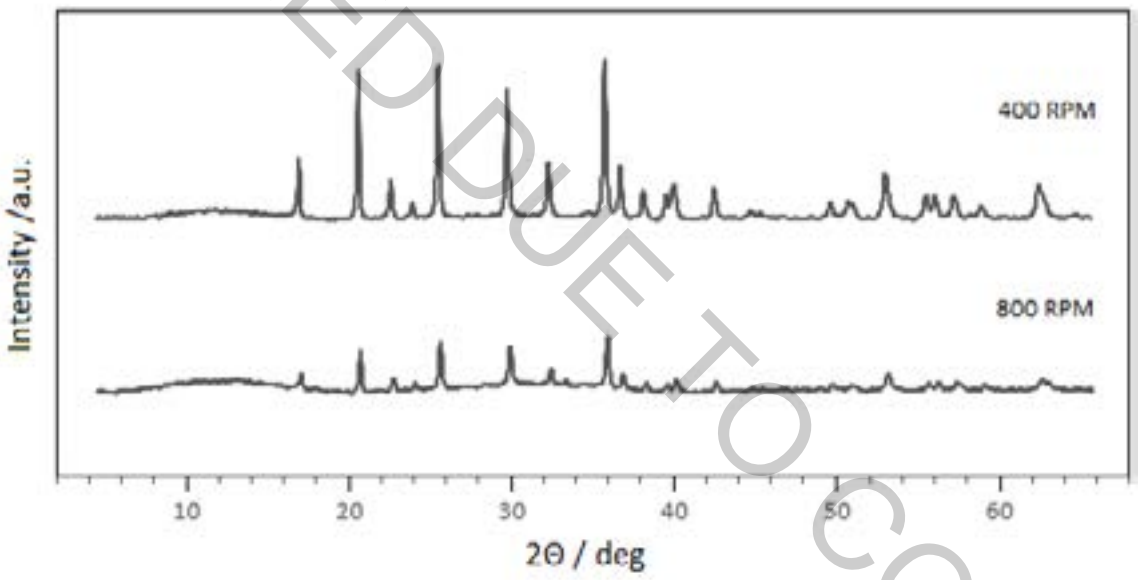

Fig. 1. X-ray patterns of the material under study. Sample whose start conditions was 800 RPM of the rollers is more amorphous than sample which rotation speed of the rollers was 400 RPM in the same synthesis temperature.

[1] J. E. Garbarczyk, T.K. Pietrzak, M. Wasiucionek, A. Kaleta, A. Dorau, J.L. Nowiński *High electronic conductivity in nanostructured materials based on lithium-iron-vanade-phospate glasses.* Solid State Ionics 272 (2015) 53-59

[2] J. T.K. Pietrzak, M. Maciaszek, J.L. Nowiński, W. Ślubowska, S. Ferrari, P. Mustarelli, M. Wasiucionek, M. Wzorek, J.E. Garbarczyk *Electrical properties of V_2O_5 nanomaterials prepared by twin rollers technique.* Solid State Ionics 225 (2012), 658-662

CANCELLED DUE TO COVID-19

EVALUATION OF THE DOSE ACCUMULATION COEFFICIENT BY *IN SILICO* MODELLING OF THE X-RAY DIAGNOSTICS OF THE RIB THORAX

Dzmitry Kacharhin[1]

[1] Department of Nuclear Physics, Belarusian State University, Belarus
dmitriyrbu@gmail.com

Procedure of the X-ray diagnostics have an essential role in fields of epidemiology, traumatology and oncology. Doctors at mentioned areas often use it for the diagnosis and visual presentation of the disease picture. In order to minimize harmful affection on patients it's necessary to most accurately account contribution of the X-ray dose received during medical procedures to annual dose of radiation.

During radiological procedure on patient one can estimate whether a used radiation dose is critically high for a current procedure under normal conditions. A parameter called *diagnostic reference level* DRL is used for that estimation. Equivalent parameter to the DRL is the *dose accumulation coefficient* D_{acc} which characterizes the ratio of energy obtained from the both reflected and direct radiation to energy of the direct one. The D_{acc} is used in order to measure level of affection on the patient as a dose obtained at the patient effective surface during the X-ray research procedure.

This *in silico* research studies influence of the X-ray machine parameters and the absorbing body properties on the dose accumulation coefficient D_{acc} in the case of the X-ray diagnostics of a rib thorax.

A model of the X-ray diagnostics includes the X-ray machine model, the absorbing body model and the detector plate model. Geometrically the model of the X-ray diagnostics consist of a point X-ray source (the X-ray machine model) that placed in front of a circular cylinder filled with water (the patient model), right behind the cylinder is placed an air plate (the detector plate model). The cylinder and the detector plate are placed on the axis of the beam from the source.

In this approach used a model of the static X-ray machine, which includes an X-ray source, an energy spectrum smoothing filter and a collimation system.

The patient model parameters like height and radius of the cylinder are depend on the age of the patient being examined. Thus, for each patient a refinement is made to the value of the coefficient D_{acc} by approaching the source and changing the radiation field. The parameters of the cylinder are taken on the basis of the tables of mass and growth of patients given in the ICRP-89.

The radiation detector model has linear dimensions of 5x5 cm and a thickness of 1 mm. The material of the detector plate is air under normal conditions. The detector is placed as close as possible to the cylinder. So, the distance from the detector to the source depends just on the radius of the cylinder. In addition, another case of detector geometry is a set of detectors located on the beam axis, placed at equal intervals from the cylinder. That configuration allows to determine the rate of decline of the dose accumulation coefficient D_{acc} with the distance.

List of parameters that was changing in the research:

- Voltage of the X-ray tube (kV)
- Voltage ripple (%)
- Effective patient body thickness (mm)
- Patient age (years)
- Smoothing filter depth (mm)

In this approach data for X-ray energy spectra from the source was taking from TASMIP [2], and include dependents from aluminum filter, voltage and voltage ripple. Monte-Carlo modelling used for computation energy, that was delivered to detector by gamma-quanta. Results of the *in silico* experiments:

1. In this work, more than 500 values for the were calculated for various exposure parameters.
2. The contribution of the smoothing filter depth to the coefficient value is 9% when considering ripple at 10% and its absence. Thus, it should be born in mind that when using filters of various thicknesses, a noticeable increase in the dose accumulation coefficient occurs.
3. The contribution of the effective patient body thickness to the coefficient value is 0.8% when considering ripple at 10% and its absence.
4. The dose accumulation coefficient increases with increasing voltage. An increase in the coefficient values with an increase in thickness is 4–4.7% for various stresses.
5. The difference in the value of the coefficient for the ages of 15 and 18 years depending on gender varies from 0.5% to 3.5% depending on changes in various parameters of the radiographic procedure.

Results of this work can be used to assess the success of lung radiography. The obtained results allow to determine the input dose on the surface for most types of patients, and the effect on these values of such characteristics of the X-ray tube as the values of the anode voltage, the smoothing filter thickness and the voltage ripple.

[1] ICRP 89
[2] John M. Boone J. Anthony Seibert TASMIP USA, 1997.

CANCELLED DUE TO COVID-19

PHOTOMETRIC PROPERTIES OF STAR CLUSTERS IN THE ANDROMEDA GALAXY

Eimantas Kriščiūnas[1,2], Rima Stonkutė[1,2]

[1]Vilnius University Observatory, Saulėtekio av. 3, LT-10257 Vilnius, Lithuania
[2]Center for Physical Sciences and Technology, Saulėtekio av. 3, LT-10257 Vilnius, Lithuania
eimantas.krisciunas@ff.stud.vu.lt

The Panchromatic Hubble Andromeda Treasury (PHAT) survey is a Hubble Space Telescope (HST) multi-cycle program which obtained images of one third of the Andromeda (M31) disk in six filter passbands, ranging from near-ultraviolet to near-infrared wavelengths. High spatial resolution of HST has allowed to identify thousands of new clusters that were previously inaccessible with existing ground-based surveys. All of the detected clusters were sorted out into three categories: star cluster, galaxy, and ancillary [1].

The aim of this study is to analyse properties of all detected star cluster candidates in the Andromeda galaxy. Age, mass, and extinction parameters were estimated using a probabilistic technique, which accounts for stochastic effects in star clusters. For some objects derived parameters were degenerate, thus we separated clusters into three groups according to photometric uncertainties (see Fig. 1b). Example of mass parameter distribution is shown in Fig. 1a. We have demonstrated that objects from the ancillary catalogue are less massive and dimmer comparing to star clusters from the main catalogue. Therefore, we significantly supplemented the star cluster catalogue of the Andromeda galaxy.

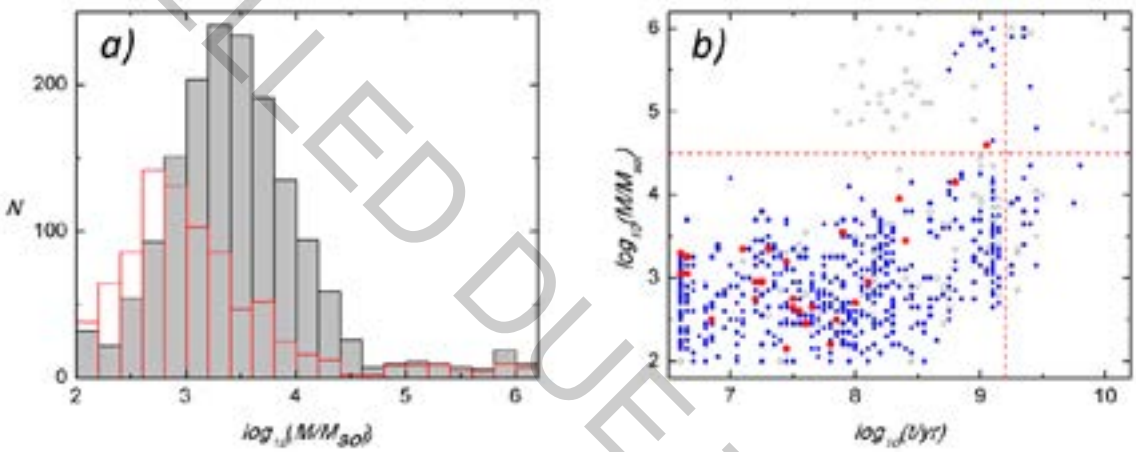

Fig. 1. a) Mass distributions of formerly known (grey bins) and newly included into the catalogue (red lines) star clusters. b) Age versus mass of new star clusters. Red dots mark star clusters of the "Group 1" 26 objects ($\sigma_{F275W,\ F336W} < 0.15$ mag, $\sigma_{F475W,\ F814W} < 0.1$ mag, $\sigma_{F110W,\ F160W} < 0.2$ mag); blue dots – "Group 2" 665 objects ($0.1 < \sigma_{F475W} < 0.2$ mag); open circles – "Group 3" 165 objects with the lowest photometric accuracy. Two red dashed lines mark limits of reliable mass ($\log_{10}M > 4.5\ M_{sol}$) and age ($\log_{10}t > 9.2$) determination.

[1] L. C. Johnson, A. C. Seth, J. J. Dalcanton et al., PHAT stellar cluster survey II. Andromeda Project cluster catalog, Astrophysical Journal, 802:127 (22pp), 2015

CANCELLED DUE TO COVID-19

STANDING WAVES IN GENERAL RELATIVITY

Sebastian J. Szybka[1,3], Adam Cieślik[2,3]

[1] Astronomical Observatory, Jagiellonian University
[2] Institute of Physics, Jagiellonian University
[3] Copernicus Center for Interdisciplinary Studies
adam.cieslik@student.uj.edu.pl

In the mid-thirties, Albert Einstein and Nathan Rosen undertook an attempt to find exact wave solutions of equations of Einstein's theory of gravity [1]. They found physically satisfying cylindrical waves.

Almost two decades ago Hans Stephani formulated a question [2]: *Are there standing gravitational wave solutions of vacuum Einstein's equations?* Stephani suggested to look for exact solutions such that [2]: (i) the constitutive parts of the metric functions should depend on the timelike coordinate only through a periodic factor, and they should also depend on spacelike coordinates; (ii) the time average of some of the metric functions should vanish; in particular, the analogue of the Poynting vector (if there is any) should be divergencefree and the time average of the spatial components should be zero.

These criteria may raise ambiguities. We propose a covariant definition of standing gravitational wave which can solve these issues.

[1] A. Einstein and N. Rosen: *On gravitational waves*. Journal of the Franklin Institute, 223:43-54, 1937.
[2] H. Stephani: *Some remarks on standing gravitational waves*. General Relativity and Gravitation, 35:467, 2003.

CANCELLED DUE TO COVID-19

ON A GENERALIZED BIRTH AND DEATH MODEL APPLIED TO A POINT NUCLEAR REACTOR THEORY

Maksim Kravchenko[1], Tamara Korbut[1], Eduard Rudak[1], Andrey Petrovski[1], Maria Bobkova[1]

[1]Laboratory of Nuclear Reactor Physics, Scientific Institution "JIPNR – Sosny", Misnsk, Belarus
m.kravch@sosny.bas-net.by

The operation of a nuclear reactor is caused, first of all, by the interaction of neutrons with a breeding medium - nuclear fuel. The course of these processes is determined by the neutron space-, energy- and time- distribution. The neutron distribution can be obtained by numerically solving the transport equation by substituting a complete set of reaction cross sections. This approach is widely described in the literature on nuclear reactors [1]. Obtaining such a solution is provided by Monte Carlo methods using computational codes and computer clusters. Capabilities of such methods are often limited only by solving homogeneous and stationary heterogeneous neutron transfer equations, which is sufficient to obtain results consistent with experiment. On the other hand, the methods and mathematical apparatus used in such codes are often hidden from the end user. This fact does not allow the user to track the calculation process and conduct its physical interpretation.

The approach proposed in current work is aimed at developing analytical methods for the analysis of nuclear reactor parameters. The approach is based on the general theory of probability mathematical apparatus. It was proposed to use a mathematical model of birth and death for this purpose [2, 3].

The model is based on the problem of the time-dependent process prediction. Prediction of values X_{n+r} in terms of $X_n, X_{n-1}, ...$ comes to the estimate of the quantity $[H(X_{n+r})|X_n, X_{n-1}, ...]$ for any function of interest H. According to the Chapman–Kolmogorov theorem [4] for Markov process, where X_n can be only countable, the following equation can be obtained:

$$E[H(X_n|X_m)] = E[E(H(X_n)|X_r)|X_m]. \tag{1}$$

Through the mathematical operations and inferences one can derive a simple solution for a Kolmogorov differential equations in application to the nuclear reactor. The main parameter to analysis in this case will be the average number of neutrons in the breeding medium of reactor core. The expression for estimating he average number of neutrons in a system is

$$\frac{M(t)}{dt} = [\lambda(t) - \mu(t)]M(t) + a(t) + b(t). \tag{2}$$

General solution for the Eq.(2) is well known. When the "breeding medium + neutron" system is being considered the more specific solution must be found taking into account parameters of the certain reactor core. Such a type of solution is shown in current work. Also the analytical equations for estimating main parameters of nuclear reactor (K_{eff}, ρ and etc.) were obtained from this solution.

[1] J. Duderstadt, L. Hamilton, *Nuclear Reactor Analysis*, (Wiley, NY, 1976)
[2] T. N. Korbut, Ed. A. Rudak, O. A. Yachnik, Birth-Death model adaptation for description of time evolution of the neutron + subritical multiplying medium system, LXIV International conference "NUCLEUS 2014", BSU, Minsk, 256 (2014).
[3] M. O. Kravchenko, T. N. Korbut et al., Analytical description of thermal point-reactor parameters within particles birth and death model, JP: Conf. Ser. **1133**, ISSN 17426596, (2018)
[4] M. Sheldon, *Introduction to Probability Models, (11th ed.)*. (Elsevier Inc., 2014)

CANCELLED DUE TO COVID-19

HYADES STAR CLUSTER AND THE NEW COMETS

Maria Sizova[1], Ekaterina Postnikova[2], Natalia Chupina[2], Sergey Vereshchagin[2]

[1] Department of Solar system research, Institute of Astronomy, Russian Academy of Sciences, Russia, Moscow
[2] Department of physics of stellar systems, Institute of Astronomy, Russian Academy of Sciences, Russia, Moscow
sizova@inasan.ru

We examined the influence of the Hyades star cluster on the possibility of the appearance of long-period comets in the Solar system. It is known that the Hyades cluster is extended along the spatial orbit on tens of parsecs. To our estimations, 0.85 million years ago, there was a close approach of the cluster to the Sun of 24.8 pc. The approach of one of the cluster stars to the Sun at the minimally known distance of about 6.9 pc was 1.6 million years ago according to catalogue presented in [1] and 2.1 pc 1.5 million years ago according to [2]. The main part of the cluster was close to the Sun from 1 to 2 million years ago (all simulations performed using [3]). Such proximity is not essential for the impact on the dynamics of small bodies in the external part of the Oort cloud, although the view may change after additional study of the cluster structure. Possible orbits perihelion displacements of the small bodies of the outer part of the Oort cloud move some of them in observable comets region.

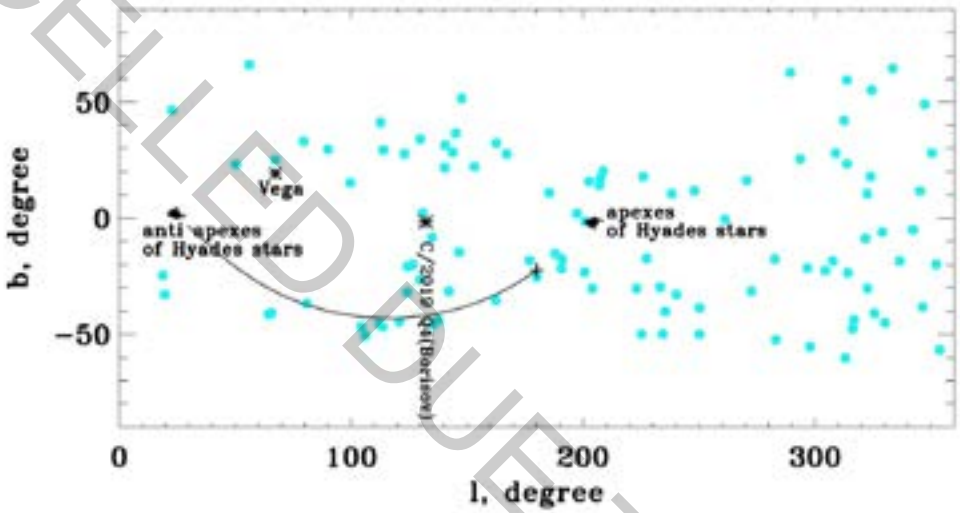

Fig. 1. LB-diagram. The track (in black dotted lines) indicates the displacement of the Hyades cluster center 3 million years ago. Areas of the apex and anti-apex of Hyades are signed. The red lines show the position of a new comets region with a binding energy of $30 < x < 60$ and orbital inclinations close to 103° (the appearance of these comets could have caused by hypothetical massive Sun satellite of located inside the Oort cloud). Comet positions according to the table ([4]) (Appendix B).

Could such a rapprochement between the Sun and Hyades cluster affect the orbit parameter change of many small bodies from the Oort cloud? Only under certain conditions. Analytical estimations gives us cluster perturbation velocity $\Delta V = 0.01 m \cdot s^{-1}$, using equation 1, where $M_{Hyades} = 435 M\odot$ [5] considering 1.15 mass increment [6] because of 20% unresolved binaries, $r_{comet} = 0.5$pc for Outer Oort cloud comets and $V, d_{close\ approach}$ is a Hyades cluster velocity and close approach distance.

$$\Delta V = \frac{2 \cdot G \cdot M_{Hyades} \cdot r_{comet}}{V \cdot d^2_{close\ approach}} \quad (1)$$

Note that perihelion perturbation can be $\Delta q = 1$ AU (while Galactic tidal gives 10 AU), and Hyades passed "under" the Solar system in the galactic disk, which increasing perturbations, so one should note such influences.

[1] Meingast, S. and Alves, J. VizieR Online Data Catalog: Hyades tidal tails with Gaia DR2, VizieR Online Data Catalog **J/A+A/621/L3**, (2019).
[2] Lodieu, N et. al, VizieR Online Data Catalog: A 3D view of the Hyades population, VizieR Online Data Catalog **J/A+A/623/A35**, (2019).
[3] Bovy, Jo, galpy A python Library for Galactic Dynamics, Astrophysical Journal **216**, 29 (2015).
[4] Matese, John J. and Whitmire, Daniel P. Persistent evidence of a jovian mass solar companion in the Oort cloud, Icarus **211**, 926-938 (2011).
[5] Roser, S. et.al, A deep all-sky census of the Hyades, Astronomy and Astrophysics **531**, A92 (2011).
[6] Seleznev, A. F. et.al, An Influence of Unresolved Binaries on the Open Cluster Mass Estimate, Modern Star Astronomy **1**, 280-283 (2018).

CANCELLED DUE TO COVID-19

COMPUTER MODELLING OF WGM MICRORESONATORS WITH A ZINC OXIDE NANOLAYER USING COMSOL MULTIPHYSICS SOFTWARE

Kristians Draguns, Karlis Grundsteins, Inga Brice, Janis Alnis, Aigars Atvars

Institute of Atomic Physics and Spectroscopy, University of Latvia, Latvia
kristians.draguns@gmail.com

CANCELLED DUE TO COVID-19

The WGM (whispering gallery mode) microresonators are spherical or cylindrical optical structures where light can "rotate" inside due to total internal reflection. When an integer number of light waves fits into the perimeter of the microresonator, constructive interference takes place and resonance occurs. It`s described by Eq. (1), where n is the refractive index:

$$N\lambda = 2\pi Rn, \quad (1)$$

The quality factors of WGM microresonators are very high ~10^6, so the resonant frequency is narrow, which is good for using a laser and having a precise measurement. The WGM microresonators are sometimes called the morphologically dependant resonators because the resonant frequency is dependent on the form of the microresonator. Small changes in the environment are picked up by microresonators changing their radius or refractive index, thus changing the resonant frequency. This allows WGM microresonators to be used as sensors.

Sometimes it`s good to coat the microresonator with an extra layer, for example, a zinc oxide layer. This layer helps to later stick antigens for biosensing. The effects of adding this extra layer can be simulated using COMSOL Multiphysics software. The extra layer changes how close to the surface the light is propagating and ads extra modes. Various methods are used for exploration of this topic such as using random functions to better describe the roughness of the surface, witch in micro and nanoscale makes a difference.

A CASE STUDY OF A SYNESTHETIC APPLYING NEURAL NETWORKS

Raminta Bartuliene[1], Ruta Narvilaite[1], Gustavas Davidavicius[1], Ausra Saudargiene[1,2], Sarunas Asmantas[1], Saulius Satkauskas[1]

[1] Department of Informatics, Vytautas Magnus University, Kaunas, Lithuania
[2] Neuroscience Institute, Lithuanian University of Health Sciences, Kaunas, Lithuania
raminta.bartuliene@vdu.lt

Synesthesia is a perceptual phenomenon in which one type of sensory stimulus automatically and involuntarily evokes another type of sensory sensation. There are many forms of synesthesia: sound-to-colour synesthesia, mirror-touch synesthesia, grapheme-colour, lexical-gustatory and many more. This study focuses on a case of chromesthesia. Chromesthesia is a type of synesthesia in which heard sounds evoke colour sensation. The study aims to distinguish evoked colours based on voice features.

The research subject was a female with visual deficiency. She claims that the grey silhouette of a person develops a colour after communicating with them. 39 participants (19 male and 20 female) attended in the study. Participants' voices were recorded with two-channel audio recording equipment and the colour which was seen by the research subject was registered. For audio analysis, our team extracted voice features using pyAudioAnalysis Python module. We extracted 68 auditory signal features: averages and standard deviations of Zero crossing rate, Energy, Entropy of Energy, Spectral Centroid, Spectral Spread, Spectral Entropy, Spectral Flux, Spectral Rolloff, 13 Mel Frequency Cepstral Coefficients, 12 Chroma Vectors, Chroma Deviation in 20 windows of 25ms length. For colour classification, we designed and trained a Multilayer Perceptron (MLP) neural network using Keras Python module. The MLP was constructed with 1 input layer (68 input neurons, activation - ReLU), 3 hidden layers (with 50-30-20 neurons in respective layers, activation - ReLU) and 1 output layer (1 output neuron, activation - sigmoid). To train the error backpropagation method with binary cross-entropy loss function was used. The MLP neural network was trained with data from 2 colour classes: pink and white females (6 pink and 5 white subjects). We dedicated 15% of the data for model testing. The rest of the data was split into training (80%) and validation (20%) sets.

The dominant registered colours of study participants were white (5) and pink (6) for females and blue (7) and black (3). There was also 12 multi-colour samples and the rest were 1-2 samples per colour.

White and pink females were classified with the accuracy of 93% by the neural network. F1 scores were 0.90 for the class of white-colour subjects and 0.95 for the class of pink-colour subjects.

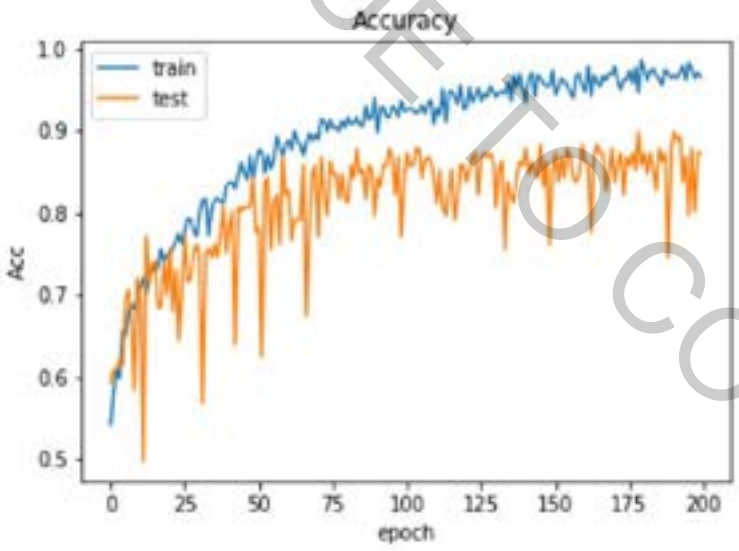

Fig. 1. The classification accuracy of the MLP model over 200 epochs.

After the study, we can claim that in this case, the evoked colour depends on the features extracted from recorded voice clips. Different classes were classified successfully using the MLP neural network. For better results, we need to do feature selection to remove irrelevant features. Our next goal is to design and train a neural network, that successfully classifies all participant colours and to determine which extracted features are key in evoking different colour sensation. For that purpose, collection of more voice data may be required.

CANCELLED DUE TO COVID-19

CLASSIFICATION OF SUPERPIXELS FOR TUMOR SEGMENTATION ON IMMUNOHISTOCHEMISTRY IMAGES

Yauheniya Lisitsa, Victor Skakun

Faculty of Radiophysics and Computer Technologies, Belarusian State University, Republic of Belarus
lisitsa@bsu.by

The breast cancer is the most common invasive cancer in women [1]. Immunohistochemistry (IHC) is widely exploited at biological researches and medical treatments of cancer diseases. It is based specific markers, which are able to label aimed proteins and to color them [2]. Hematoxylin and eosin stain (H&E) is one of the most popular technologies for tissue staining in histology [3].

The superpixels with simple linear iterative clustering (SLIC) are used to segment different kinds of images. For example, the algorithm based on SLIC determines cellular structures in high-dimensional histopathological images of renal cell carcinoma [4]. It shows sufficient results for x-ray image segmentation [5, 6]. The random forest classification is the robust method of classification [7], which is used for different classification tasks such as non-small cell lung cancer classification [8] and dose-response prediction [9]. The aim of our work is to develop the algorithm of tumor segmentation based on superpixels and random forest classification to process images of breast cancer.

We studied the immunohistochemical image of breast cancer cells (Fig.1A), which were received by transmitted light microscope. The images are stained by H&E. The acquisition is received by Leica recording system with a DFC 420 C camera, DM5000B lens and by using LEAD Technologies Inc. V1.01 software. The image resolution is 300 pixels per inch, shutter speed is 1/12 second, image size is 2592 by 1944 pixels, color depth is 24 bits.

The first part of our algorithm is the superpixels segmentation by SLIC model. The main parameter for segmentation is average superpixels size, which default value is 50 pixels. The number of iterations for SLIC method is 10.

The second part of the algorithm is classification by random forest. The successful classification was received with the following parameters: the number of trees in the forest is 50, the nodes are expanded until all leaves are pure or until all leaves contain less than 2 samples. Each superpixel is described by 400 features, which are received as intensities (red, green and blue channels) of neighboring pixels of the superpixel center in the surrounding area at 20 pixels. The random forest was trained by the set of 29670 objects collected from three images. Each object was a pixels described by the neighboring pixels as it described above.

The fig.1D shows our results of tumor segmentation. The segmentation error is 6.3%. It is caused by misclassified superpixels, because the shape of the superpixels overcomes the linear size of cells. In order to reduce the segmentation error it is suggested to use smaller superpixel size. However, in this case it will cause incorrect edge detection of tumor edges. If the average superpixel size is 25, the segmentation error is 5.2%.

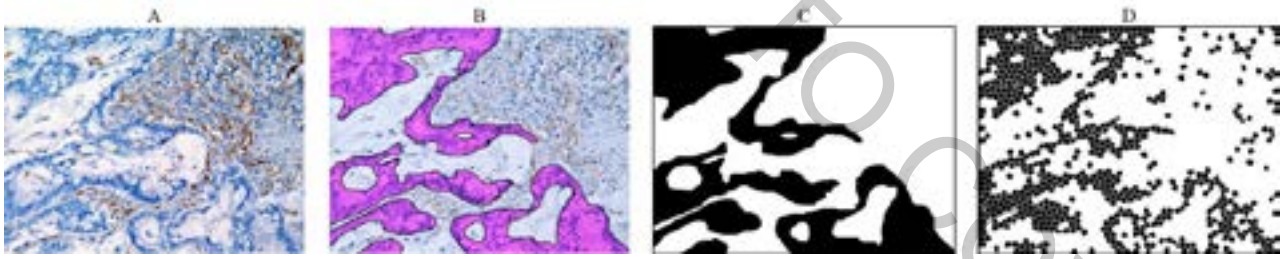

Fig. 1. Tumor segmentation on immunohistochemistry images. A) Original image B) Tumor mask received by expert C) Binary tumor mask received from C D) Segmented mask after superpixels classification

The accuracy of segmentation also depends on the quality of the random forest teaching; therefore, the method robustness can be improved by using more diverse set of data.

[1] A. Albayrak, G. Bilgin, Breast Cancer Epidemiology, Presse Med, **48(10)**, 1076-1084 (2019).
[2] N. Sukswai, J. D Khoury, Immunohistochemistry Innovations for Diagnosis and Tissue-Based Biomarker Detection, Curr Hematol Malig Rep, **14(5)**, 368-375 (2019)
[3] A. Grosset, K. Loayza-Vega, É. Grangeret et al., Hematoxylin and Eosin Counterstaining Protocol for Immunohistochemistry Interpretation and Diagnosis, Appl Immunohistochem Mol Morphol, **27 (7)**, 558-563 (2019)
[4] H. Sancho-Garnier, M. Colonna, Automatic cell segmentation in histopathological images via two-staged superpixel-based algorithms, Med Biol Eng Comput, **57(3)**, 653-665 (2019).
[5] J. Chu, H. Min, L. Liu, W. Lu, A novel computer aided breast mass detection scheme based on morphological enhancement and SLIC superpixel segmentation, Med Phys, **42(7)**, 3859-3869 (2015).
[6] L. Yao, S. Muhammad, A novel technique for analysing histogram equalized medical images using superpixels, Comput Assist Surg (Abingdon) **24(sup1)**, 53-61 (2019).
[7] L. Bierman. Random Forest. Mach. Learn., **45(1)**, 5-32 (2001)
[8] C. Guoliang Luo, Y. Zhu, R. Wang et al., Wang, Random Forest-Based Classsification and Analysis of Hemiplegia Gait Using Low-Cost Depth, Med Biol Eng Comput [Online ahead of print], (2019)
[9] R. Rahman, S. Dhruba, S. Ghosh et al., Functional Random Forest With Applications in Dose-Response Predictions, Sci Rep, **9(1)**, 1628 (2019)

CREATED DUE TO COVID-19

THE HYDROGEN BOND NETWORK TOPOLOGY OF PHOSPHORIC ACID AND WATER SYSTEMS

Austėja Mikalčiūtė[1], Linas Vilčiauskas[1]

[1]Institute of Chemistry, Faculty of Chemistry and Geosciences, Vilnius University, Lithuania
austeja.mikalciute@chf.stud.vu.lt

Hydrogen bonding is one of the most important intermolecular interactions in chemical and biological systems playing a vital role in their structure, function and dynamics. Long-range proton transport is directly related to the structure and dynamics of hydrogen bonds and the way they arrange themselves into extended networks. Pure phosphoric acid (H_3PO_4) is the best intrinsic proton conductor known to science, having a high density of highly mobile charge carriers. The phosphoric acid and water mixtures represent a special case in the field of proton conducting materials: at low acid concentrations the system behaves like a typical dilute aqueous solution – proton conductivity is caused by excess H^+ aqueous diffusion, but in concentrated solutions with higher acid contents, the conduction is increasingly determined by proton structural diffusion [1].

We present a theoretical study of H_3PO_4-H_2O systems, which shows a connection between structural and dynamical properties and hydrogen bond (HB) network topology. Wide range of phosphoric acid-water systems were simulated using GROMACS molecular dynamics (MD) package, using Generalized Amber Force Field (GAFF) for phosphoric acid and flexible SPC/E model for water. From MD simulation data diffusivities, diffusion activation energies, radial distribution function (RDF) and free Helmholtz energy surfaces from combined radial-angular distribution functions (CDF) were calculated. Diffusivities for both phosphoric acid and water show a non-linear tendency to increase in systems with larger molar fraction of water in agreement with experimental data [2]. HB was defined as a contour passing through the saddle point and surrounding the local minima on the Helmholtz free energy surface calculated from the CDFs as defined by Kumar et al. [3]. Then each molecule was represented as a node and a hydrogen bond between them as an undirected, unweighted edge in a graph [4]. A number of network properties such as average shortest path length and average clustering coefficient were calculated for this HB network using Python *NetworkX* package. These network theoretical properties show similar tendencies to the macroscopic ones: clustering coefficient of a system decreases and shortest path length increases non-linearly, when the molar fraction of H_2O increases. Therefore, these results show that there is relation between structural and dynamical properties in H_3PO_4-H_2O systems and hydrogen bond network topology. There is a strong indication that phosphoric acid tends to form very tight HB networks having the small-world property (high clustering coefficient and low average shortest path length), whereas water is forming the usual random network (low clustering coefficient). These observations might hold key in explaining proton transport mechanism in many condensed matter systems.

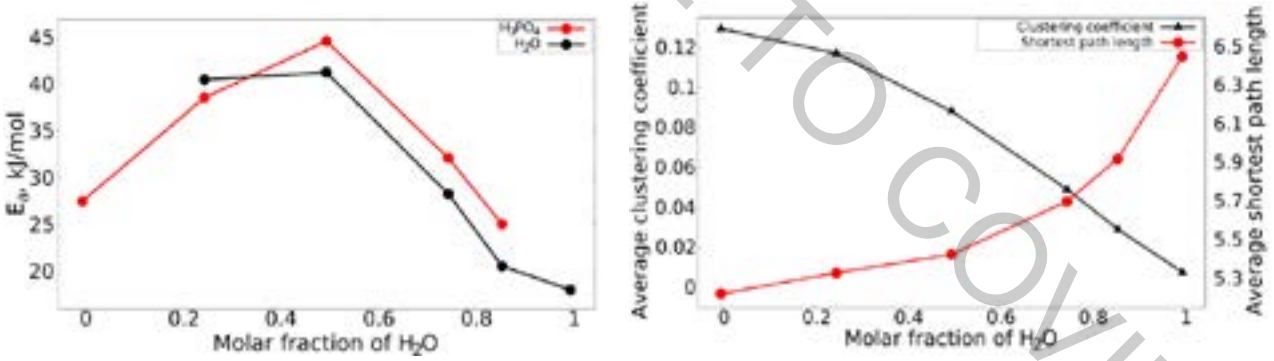

a **b**

Fig. 1. a) Diffusion activation energy versus molar fraction of H_2O in the system b) average shortest path length and average clustering coefficient versus molar fraction of H_2O in the system.

[1] Vilčiauskas, L. et al. (2012). The mechanism of proton conduction in phosphoric acid. Nature Chemistry, 4, 461-466.
[2] Melchior, J.P., Kreuer, K. D., Maier J., (2016) Proton conduction mechanisms in the phosphoric acid-water system ($H_4P_2O_7$-$H_3PO_4 \cdot 2H_2O$): a ^1H, ^{31}P and ^{17}O PFG-NMR and conductivity study. Physical Chemistry Chemical Physics, 19, 587-600.
[3] Kumar, R. et al. (2007). Hydrogen bonding definitions and dynamics in liquid water. The Journal of Chemical Physics, 126(20), 204107.
[4] Ramirez, B.V. et al. (2018). Water phase transitions from the perspective of hydrogen-bond network analysis. Physical Chemistry Chemical Physics, 20(44), 28308-28318.

CANCELLED DUE TO COVID-19

NEW STUDIES ON PETROPHYSICAL PROPERTIES OF SHALES FOR POTENTIAL GAS EXPLORATION

Saulius Lozovskis[1], Saulius Šliaupa[2], Jurga Lazauskienė[1], Rasa Šliaupienė[2]

[1] Department of Chemistry and Geosciences, Vilnius University,Vilnius, Lithuania
[2] Institute of Geology and Geography, Nature Research Centre, Vilnius, Lithuania
saulius.lozovskis@gf.vu.lt

The Baltic sedimentary basin has several organic rich shale formations that are identified in the sedimentary pile, related to the Cambrian, Ordovician and Silurian systems that provide some prospects for exploration of the unconventional hydrocarbons. Unconventional hydrocarbon topic is very important in energy resource branch. In Lithuania The Lower Silurian shale succession is considered the most perspective in terms of oil and gas potential due to high organic matter content and considerable thickness. However, there is only scarce data on other key shale parameters that are important in determining the reservoir quality of the Silurian shale package. The present study is focused on characterisation of new petrophysical properties of the Lower Silurian shales in west and central Lithuania.

In this work we focused on the whole rock cation exchange capacity (CEC), the relative sensitivity of a rock sample to fluids by adopting the capillary suction time (CST) method and the stability characteristics using Roller oven equipment to conduct the stability tests. These properties are very important in evaluating economical capabilities of the potential exploration.

Free gas can be produced immediately, while pressure decline by dewatering of shales is needed to exploit adsorbed gas in wells. The adsorption capacity of gas primarily depends on the content and mineral composition of clays, which is sensitive to the burial history of the basin. Smectite is characterised by the highest absorbed gas capacity, whereas illite has a lower adsorption capacity and kaolinite is characterised by the lowest adsorption capacity [1]. The measured Cation Exchange Capacity (CEC) values of the Lower Saurian shales vary from 0.2 to 8.8 meq/100g. Results of this study suggests that organic matter has a primary impact on the CEC in the studied samples.

Clays dispersed from shales have varying swelling capacity that can lead to difficulties in fractured system operation. Two mechanisms are responsible for clay swelling, namely surface hydration and osmotic swelling. Surface hydration has relatively little effect on clay swelling compared to osmotic process. It occurs when the concentration of ions at the fracture surface is higher than that of the back-flush fluid. Accordingly, osmotic swelling could be reduced if the concentration of acids in the working fluid is higher than that in the shale [2]. The capillary suction time (CST) method predicts the behaviour of the shale zone during drilling. The measured CST ratio values are rather low and are in accordance to the mineral composition of the Lower Silurian shales: predominating illite has a low swelling capacity, while kaolinite and chlorite do not swell to an appreciable extent. A 7 %KCl solution in water was found to be the most suitable for controlling reactive clay.

The Roller oven shale stability test is commonly carried out to evaluate rock erodibility. The Lower Silurian shales samples show different resistance to erosion. All analysed samples demonstrate a moderate erodibility with water additive combinations. A 7%KCl solution shows the best effect on retaining the erosion. The obtained analytic results are in accordance to published results indicating that K^+ ions added to the water-base mud effectively inhibit the clay from dispersing [3].

This study presents key petrophysical properties of shales that are important for the prognosis of reservoir performance during hydrofracturing and shale oil/gas exploitation.

[1] D.J.K. Ross, R. M Bustin, The importance of shale composition and pore structure upon gas storage potential of shale gas reservoirs. Marine and Petroleum Geology, **26,** 916–927 (2009).
[2] N. Van Olphen, An Introduction to Clay Colloid Chemistry for Clay Technologists, and Soil Scientists. John Wiley and Sons (1963).
[3] J. Hallman, Potassium Formate Improves Shale Stability and Productivity in Underbalanced Drilling Operations, Paper # 2003-028 presented at the CADE / CAODC Drilling Conference,October 2003, Calgary, Alberta, Canada.

CANCELLED DUE TO COVID-19

ACRYLATED GLYCEROL-BASED PHOTOCROSS-LINKED POLYMERS

Tautvydas Brazaitis, Sigita Kasetaite, Jolita Ostrauskaite

Department of Polymer Chemistry and Technology, Kaunas University of Technology
sigita.kasetaite@ktu.lt

The availability of petroleum-based resources has decreased significantly with the increase of worldwide demand for energy. Indeed, the depletion of fossil reserves associated with serious ecological problems related to greenhouse gas emissions forced researchers to develop new polymeric materials based on renewable and sustainable sources. Glycerol, as a by-product of the biodiesel production process, is a highly available commercial compound in recent times [1] and can be chemically transformed into high added-value chemical products [2]. Photopolymerization is nowadays a high-performance technology for the synthesis of polymer materials in various industrial fields such as coatings, dental resins, automotive, holographic data storage, stereolithography, etc. [3]. Several advantages over the thermally-induced polymerization process make photopolymerization an eco-friendly technology with time, money and energy savings, waste reduction, absence of solvent, etc. [4].

After considering the advantages of glycerol and photopolymerization, it was decided to synthesize novel acrylated glycerol-based photocross-linked polymers. In this study, the cross-linked polymers were obtained by photopolymerization of 2,3-dihydroxypropylmethacrylate (GM), glycerol dimethacrylate (mixture of isomers) (GDM), and glycerol trimethacrylate (GTM), using ethyl (2,4,6-trimethylbenzoyl) phenyl phosphinate as photoinitiator (TPOL). The chemical structure of polymers was confirmed by FT-IR spectroscopy. The amount of insoluble polymer fraction was determined by Soxhlet extraction. The reaction process was studied by the real-time photorheometry. The obtained polymers were characterized by differential scanning calorimetry, thermogravimetry, and mechanical testing.

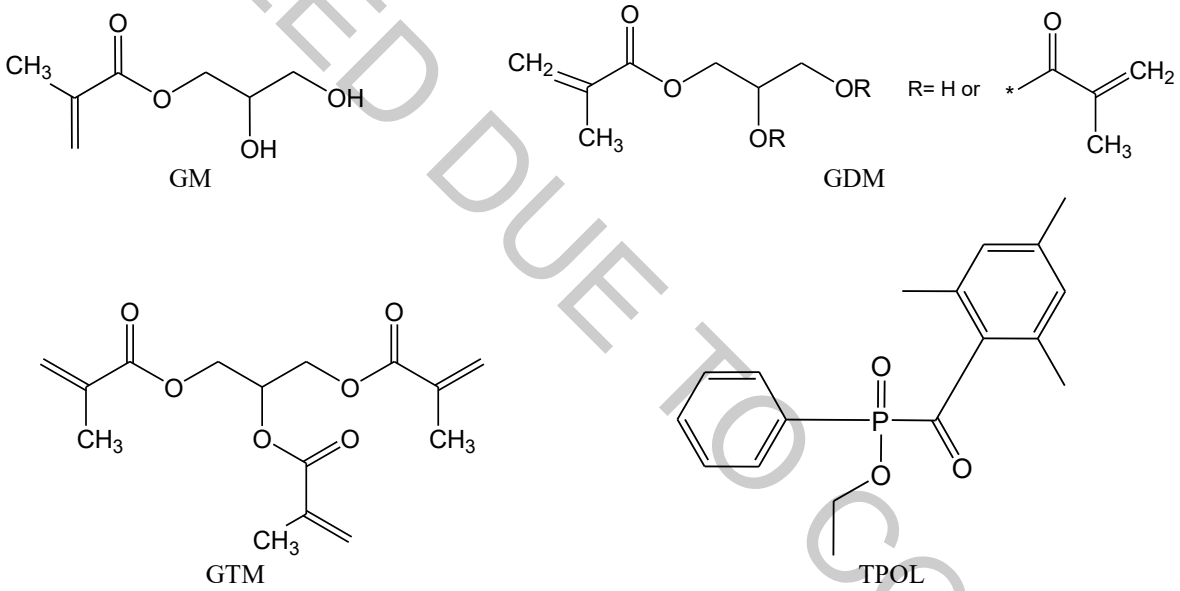

Fig. 1. Chemical structure of monomers and photoinitiator used in this study.

The addition of photoinitiator into the compositions reduced reaction duration and improved the rheological, thermal, and mechanical properties of the resulting polymers due to the increased cross-linking density. The rheological properties of polymers were improved by increase of the amount of acrylgroup in the compositions.

Acknowledgement. Financial support from the EU ERDF through INTERREG BSR Programme (ECOLABNET project #R077) is gratefully acknowledged.

[1] M. Anitha, S. K. Kamarudin, N. T. Kofli, The potential of glycerol as a value-added commodity, Chem. Eng. J. **295**, 119-130 (2016).
[2] Y. Zheng, X. Chen, Y. Shen, Commodity chemicals derived from glycerol, an important biorefinery feedstock, Chem. Rev. **108**, 5253-5277 (2008).
[3] J. Christmann, C. Ley, X. Allonas, A. Ibrahim, C. Croutxé-Barghorn, Experimental and theoretical investigations of free radical photopolymerization: Inhibition and termination reactions, Polymer **160**, 254-264 (2020).
[4] Y. Yagci, S. Jockusch, N. J. Turro, Photoinitiated polymerization: advances, challenges, and opportunities, Macromolecules **43**, 6245-6260 (2010).

CANCELLED DUE TO COVID-19

SYNTHESIS AND INVESTIGATION OF POLYMERS COMPOSED OF BIOBASED METHACRYLATES

Vidmantas Klimaitis, Migle Lebedevaite*, Jolita Ostrauskaite

Department of Polymer Chemistry and Technology, Kaunas University of Technology, Radvilenu Rd. 19, LT-50254 Kaunas, Lithuania
migle.lebedevaite@ktu.lt

The (meth)acrylate systems are easily and promptly polymerizable materials which undergo radical chain-growth polymerization during photocross-linking forming a cross-linked network [1]. Due to this (meth)acrylate feature they are used in optical 3D printing, acrylic paints, organic glass, acrylic fiber and etc. The most widely used (meth)acrylates are petroleum-derived and, because of decreasing petroleum recourses, it became crucial to search for alternative materials such as renewable resources [2]. The biobased (meth)acrylates could be obtained from wood, vegetable oils, animal fat, and other natural feedstock.

Isoboronyl methacrylate (IBOMA) is a 71% biobased monomer coming from pine resin, having the homopolymer T_g of 150 °C, and being suitable as a hard monomer. The IBOMA monomers are produced from camphene through the reaction with (meth)acrylic acid [3]. Methacrylated fatty acids as soft monomers could be used in order to increase the elasticity of IBOMA polymers. Dodecyl methacrylate (C13-MA) and hexadecyl methacrylate (C17-MA) are obtained from fatty acids derived from triglycerides that were extracted from vegetable oils and subsequently hydrolysed [4].

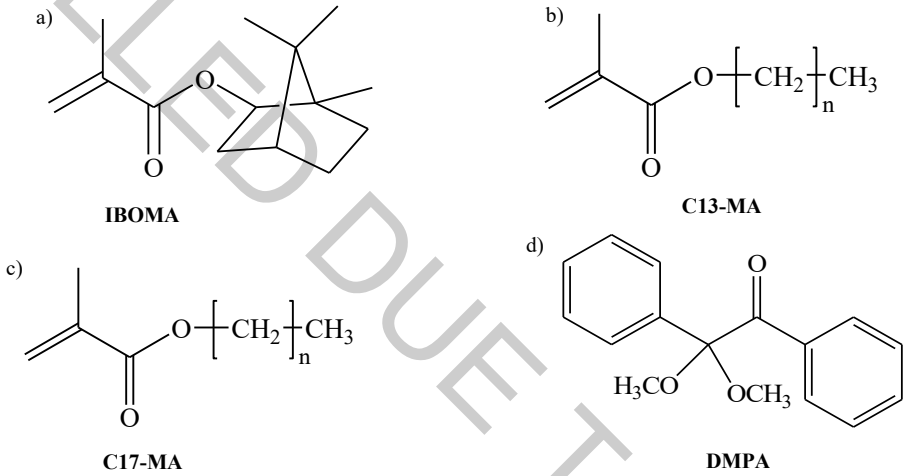

Fig. 1. Chemical structure of isoboronyl methacrylate (a), dodecyl methacrylate (b), hexadecyl methacrylate (c), and 2,2-dimethoxy-2-phenylacetophenone (d)

In this study, biobased IBOMA was photocross-linked with biobased C13-MA and C17-MA. 2,2-Dimethoxy-2-phenylacetophenone (DMPA) was used as photoinitiator. The investigation of photocross-linking kinetics was carried out with MCR302 rheometer from Anton Paar equipped with plate/plate measuring system. The insoluble fraction of the cross-linked polymers was determined by Soxhlet extraction. Mechanical testing of the cross-linked polymer specimens was performed by tensile test on a Testometric M500-50CT.

It was determined that pure IBOMA undergo the photocross-linking reaction the fastest forming a hard highly cross-linked polymer, though C13-MA and C17-MA formed gel-like soft polymers. The photocross-linking of the mixtures with higher amount of IBOMA was the faster and more cross-linked polymers with better mechanical properties were formed.

Acknowledgments: Financial support from the EU ERDF, through the INTERREG BSR Programme (ECOLABNET project #R077) is gratefully acknowledged.

[1] Ligon-Auer, Samuel Clark, et al. "Toughening of photo-curable polymer networks: a review." Polymer Chemistry 7.2 (2016): 257-286.
[2] Lebedevaite, Migle, et al. "Photoinitiator free resins composed of plant-derived monomers for the optical μ-3D printing of thermosets." Polymers 11.1 (2019): 116.
[3] Badía, Adrián, et al. "High biobased content latexes for development of sustainable pressure sensitive adhesives." Industrial & Engineering Chemistry Research 57.43 (2018): 14509-14516.
[4] Cousinet, Sylvain, et al. "Toward replacement of styrene by bio-based methacrylates in unsaturated polyester resins." European Polymer Journal 67 (2015): 539-550.

CANCELLED DUE TO COVID-19

HIGH-TEMPERATURE SYNTHESIS, STRUCTURAL AND LUMINESCENT PROPERTIES OF Mn-DOPED α-TRICALCIUM PHOSPHATE

Lauryna Sinusaite[1], Diana Griesiute[1], Andris Antuzevics[2], Arturas Katelnikovas[1], Aleksej Zarkov[1]

[1]Institute of Chemistry, Vilnius University, Naugarduko st. 24, LT-03225, Vilnius, Lithuania
[2]Institute of Solid State Physiscs, University of Latvia, Kengaraga st. 8, LV-1063 Riga, Latvia
lauryna.sinusaite@gmail.com

Tricalcium phosphate polymorphs (α- and β-TCP) are alloplastic bone substitutes that belong to the class of calcium phosphate ceramics (CPCs). Due to their injectability, nontoxicity, bioactivity, osteoconductivity and biocompatibility, CPCs are promising biomaterials for bone tissue engineering applications and are commonly used as scaffolds and carriers to deliver stem cells, drugs and growth factors [1, 2]. α- and β-TCP possess same chemical composition, but due to having different structure, density and solubility, more reactive α-TCP is usually used as powder component of various bone cements while β-TCP – as biodegradable ceramics. The main advantages of α -TCP are that it can be used on its own and under physiological conditions with minimal heat release (meaning having no damage to human organism) it hydrates and sets into the biggest mineral component of natural bone – calcium deficient hydroxyapatite (CDHAp) [3].

Partial substitution of Ca ions by other biologically active cations is assumed to be a promising tool to superior biological properties of synthetic CPs. It is well known that presence of foreign ions in CP matrix can modify significantly physicochemical, mechanical and anti-bacterial properties of materials, to promote changes in morphology, solubility and kinetics of ion release. Additionally, doping elements open new possibilities for application of CPs as multifunctional materials. Optically active and paramagnetic ions make it possible to use these materials for bioimaging applications including fluorescence, magnetic resonance or multimodal imaging.

Manganese is an essential element in human organism that plays important role for normal bone formation and development. Studies have revealed that Mn^{2+} enhances the ligand binding affinity of integrin, activates cell adhesion and increases osteoblast adhesion. However, high levels of Mn^{2+} in human body may cause neurological disorder – manganism [4, 5]. At the same time, Mn is also known for its optical properties and was incorporated into different hosts for the preparation of luminescent materials. Mn^{2+}-doped materials after excitation can exhibit broad band emission in the red region and therefore can be used as photoluminescent materials [6].

The main aim of this study was to investigate feasibility of the synthesis of Mn-doped α-TCP and to study its photoluminescent and structural properties. In order to do that, a series of α-TCP powders doped with different amounts of Mn^{2+} ions (from 0.2 to 1.0 mol%) were synthesized by wet precipitation method followed by high temperature synthesis using $Ca(NO_3)_2 \cdot 4H_2O$, $Mn(NO_3)_2 \cdot 4H_2O$ and $(NH_4)_2HPO_4$ as starting materials. Metals to phosphorous ratio was kept 1.5. Obtained precipitates were vacuum filtered, washed with deionized water and ethanol afterwards dried in oven at 50 °C overnight and annealed at 1250 °C. Thermal quenching was used in order to stabilize α-TCP structure.

The crystal structure and purity were evaluated by X-ray powder diffraction (XRD), electron paramagnetic resonance (EPR) and Fourier-transform infrared (FTIR) spectroscopy. Scanning electron microscopy (SEM) was used to determine the morphological features of the synthesized products. Optical properties of the synthesized specimens were investigated in terms of photoluminescence (PL), excitation and emission spectra were recorded. ICP-OES analysis was performed in order to determine elemental composition of the products.

The results of XRD, FTIR and elemental analysis confirmed that proposed synthetic approach is suitable for the synthesis of Mn-doped TCP with a good phase purity and controllable chemical composition. It was demonstrated that Mn-containing powders under excitation at 408 nm revealed red emission centered at 630 nm. Emission intensity was found to be dependent on concentration of Mn^{2+} ions.

[1] H. Xu, P. Wang, L. Wang et al, Calcium phosphate cements for bone engineering and their biological properties, Bone Research **5**, 17056 (2017).
[2] A. Lasckus, J. Kolmas, Ionic Substitutions in Non-ApatiticCalcium Phosphates, International Journal of Molecular Sciences **18**, 2542 (2017).
[3] R. G. Carrodeguas, S. De Aza, α-Tricalcium phosphate: Synthesis, properties and biomedical applications, Acta Biomaterialia **7**, 3536-3546 (2011).
[4] T. Wu, H. Shid, Y. Liang et al, Improving osteogenesis of calcium phosphate bone cement by incorporating with manganese doped β-tricalcium phosphate, Materials Science & Engineering C **109**, 110481 (2020).
[5] R. Singh, M. Srivastava, N. K. Prasad, Structural analysis and magnetic induced hyperthermia of Fe^{3+} and Mn^{2+} substituted β-$Ca_3(PO_4)_2$, New Journal of Chemistry **41**(21), 12879-12891 (2017).
[6] Q. Zhou, L. Dolgov, A. M. Srivastava et al, Mn^{2+} and Mn^{4+} red phosphors: synthesis, luminescence and applications in WLEDs. A review, Journal of Materials Chemistry C **6**, 2652 (2018).

CANCELLED DUE TO COVID-19

RESEARCH ON ADHESION OF PASTEURIZED ADHESIVE LABELS

Asta Kabelkaite-Lukosevice[1], Ilona Kapociute[1], Ingrida Venyte[1], Laura Gegeckiene[1], Georgij Petriaszwili[2]

[1] Department of Production Engineering, Kaunas University of Technology, Lithuania
[2] Department of Printing Technologies, Warsaw University of Technology, Poland
asta.kabelkaite@ktu.lt

CANCELLED DUE TO COVID-19

In food packaging production are various problems.For marking of pasteurized packaging often is used adhesive labels. So the adhesion of the adhesive labels to the surface is very important.This is important because the growth in consumption, food products are produced ahead of time, packed in film, frozen and pasteurized when needed, not only with the package but also with an informative label.Insufficient adhesion of the layers may impair the performance of the product. The adhesion strength may vary due to the properties of the raw material used, the adhesion strength of the raw materials, the technological processes as well as the operating parameters (temperature, fat, etc.). Because digital printing is currently used for printing smaller quantities of adhesive labels, it is important to investigate how the pasteurization process influenced the quality of the labels. There is not much research about labels resistance pasteurization printed in flexography, investigate the influence of pasteurization on adhesive labels printed with flexographic and digital printing [1-2].

He study uses two polymer films:

- PP GW TC60/UNIV RP37 – is a white, glossy, biaxially oriented, activated, top-coated polypropylene film. Multipurpose white, pearlescent film for adhesive labels, where good water, chemical, and oil resistance is needed. The grammar is 61 g / m^2, the thickness –133 μm. Suitable for flexography, screen and offset printing method.
- RAFLACOAT PLUS PEFC/ SPEC S2045 - is a white woodfree machine coated mid-gloss paper. Suitable for flexography, offset, rotogravure, screen, and hot foil. The grammar is 80 g / m^2, the thickness –69 μm. SPEC S2045 a rubber-based, permanent adhesive.

For the study, the labels were printed on a flexographic printing press Gallus EM 280 and a digital printing press HP Indigo WS6800. 20 specimens were used for testing, 10 printing flexographic printing and 10 printing digital printing (electrographically). Digital printing uses Indigo inks, which consist of electrically charged particles, a true ink suspended in a non-conductive carrier fluid (ElectroInk). Digital printed labels have been varnished to withstand temperatures of 100 ° C according to the supplier's specifications. Flexographic printing labels were printed using UV ink and UV protective varnish (YL-7G100-K058).

The classic pasteurization (heat treatment) method is based on heating the products to a temperature above 60 ° C but not exceeding 100 ° C. The samples were heated at 90 ° C for 60 minutes in a closed container. For thermal simulation was used equipment BINDER BD 56.

The peel force test is intended to measure the material's strength. Labels have adhered to polymeric packaging (pet+pe/evoh/pe) for food contact. The Thwing-Albert FP-2255 was used for experiments. The specimen is placed between the two grippers of the device. The grippers are pulled apart at a constant speed. The force required to break the barrier is equal to the adhesion strength. When the device is switched on, the force required to peel 1.5 cm wide by 1.0 cm long pull at a constant speed of 15 cm/min is recorded. [3]

[1] D.Kazlauskas, J. Sidaravičius, Investigation into the Quality of Thermally Treated Package Lamination.Mechanics, material science, industrial engineering and management, Vol. 2. No. 4, 5-9 (2010)
[2] S. Grigaliūnienė, D. Abazoriūtė, M.Kulišauskaitė, A. Ziminskaitė, J. Sidaravičius, J. Turla, V. Mechanical properties of flexographic prints. Science – Future of Lithuania, *5*(6), 583-586(2013).https://doi.org/10.3846/mla.2013.92
[3] FINAT method. A. Jack, FINAT Technical Handbook 6th edition, Barry, UK, 2001.

MODELING OF THE INFLUENCE OF CH_4 FRACTION GAS ON OXYGEN ION DIFFUSION IN ELECTROLYTE IN SINGLE-CHAMBER SOLID OXIDE FUEL CELLS

Paulius Andriūnas[1], Arvaidas Galdikas[1*]

[1] Department of Physics, Kaunas University of Technology, Studentų g. 50, 51368 Kaunas, Lithuania
paulius.andriunas@ktu.edu

A fuel cell is a device that generates an electric current between two electrodes through an electrochemical reaction. They undergo oxygen reduction at the cathode, and at the anode fuel oxidation and the resulting ions travel through the electrolyte. Solid oxide fuel cells (SOFC) are characterized by the use of oxygen-transported oxide as an electrolyte, the advantages of which are high efficiency, fuel flexibility, relatively inexpensive materials due to high operating temperature. However, these elements also have drawbacks, such as high operating temperatures, which reduce the durability of the element and make it difficult to seal the element between the two chambers [1].

A single-chamber solid oxide fuel cell (SC-SOFC) can eliminate some of the disadvantages mentioned, such as the cell's tightness due to its interesting structure. The SC-SOFC structure is made up of a single chamber traveling through a mixture of oxidizer and fuel. This chamber contains cathodes and anodes exposed to the same gas mixture, which makes it easier to seal the element [2]. However, this gas mixing has its own drawbacks, like parasitic combustion at the electrodes, which can raise the temperature, reduce the efficiency of the element or reduce the power density [3]. The work also showed that the constituent of the supplied mixture has a significant effect on the performance of SC-SOFC, and by choosing the right mixture, higher power can be obtained [4].

The aim of this work is to develop mathematical models and algorithm to simulate the kinetics of SC-SOFC mass transfer and catalytic processes and to predict how the optimal amount of CH_4 gas in the mixture changes by changing the reaction rate constant of the cathode and anode.

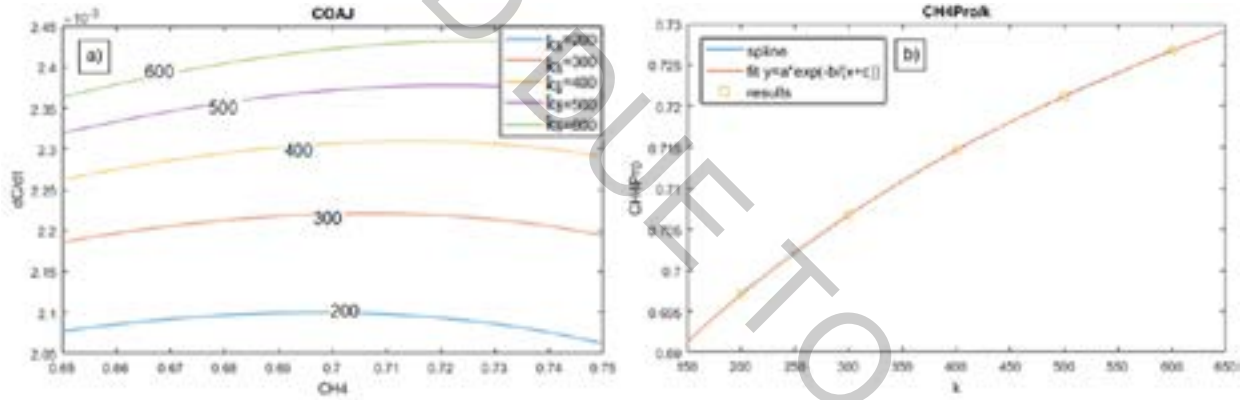

Fig. 1. a) The dependence of the oxygen ion diffusion rate at the anode on the CH_4 fraction change in the gas mixture with the change of H_2O production rate b) Dependence of optimal CH_4 fraction on reaction rate constant k_5 (or temperature) a = 0.79, b = 104.7, c = 621.51.

Using the resulting graphs, a mathematical formula was found that predicts the optimal proportion of CH_4 in the gas mixture depending on the rate constant of the reactions. Eq. (1):

$$y = ae^{-\frac{b}{x+c}} \tag{1}$$

From the results, it has been observed that as the rate constant of the cathode or anode increases, the CH_4 fraction in the gas mixture must also be increased to obtain the highest diffusion rate. However, from the rate constant of the reaction to the cathode, it has also been observed that with the decrease of the methane fraction, it is preferable to use cathodes with a slower rate of oxygen decomposition.

[1] YANO, M., TOMITA, A., SANO, M. and HIBINO, T. Recent Advances in Single-Chamber Solid Oxide Fuel Cells: A Review. Solid State Ionics 177 (2007) 3351–3359

[2] LEE, D., AHN, S., KIM, J. and MOON, J. Influence of Water Vapor on Performance of Co-Planar Single Chamber Solid Oxide Fuel Cells. Journal of Power Sources 195 (2010) 6504–6509

[3] YIN, J., et al. Anode-Supported Single-Chamber Solid Oxide Fuel Cell Based on Cobalt-Free Composite Cathode of Nd0.5Sr0.5Fe0.8Cu0.2O3−δ–Sm0.2Ce0.8O1.9 at Intermediate Temperatures. Journal of Power Sources 286 (2015) 217-223

[4] YANG, G., et al. Single-Chamber Solid Oxide Fuel Cells with Nanocatalyst-Modified Anodes Capable of in Situ Activation. Journal of Power Sources 264 (2014) 220-228

CREATED DUE TO COVID 19

LATTICE DISTORTION MODEL ANALYSIS SIMULATING POISSON'S RATIO ON CRYSTALLINE MATERIALS OF BCC-LATTICES

Tomas Vaitkūnas[1], Audrius Jutas[1*]

[1] Department of Mechanical Engineering and Design, Kaunas University of Technology, Lithuania
tomas.vaitkunas@ktu.edu

CANCELLED DUE TO COVID-19

We offered a lattice distortion model [1] which describes the complex behavior of atomic systems aligned by different spatial angles in neighbor microstructures. Poisson's ratio value of crystalline material ν_{sim} can be simulated without doing any experiment and expressed as average value of all groups' of materials lattices oriented at different angles interacting together during *l* number of peaks:

$$\nu_{sim} = \frac{1}{l}\left(\frac{1}{l}\sum_{k=1}^{l}\nu_{\max k} + \frac{1}{l-1}\sum_{k=2}^{l}\nu_{\max k} + \ldots + \nu_{\max l}\right); \quad (1)$$

where $\nu = \frac{1}{N}\sum_{i=1}^{N}\sum_{j=1}^{n}\frac{\nu_j}{n}$ is Poisson's ratio values of *n* lattices' groups interacting together, $\nu_j = -\frac{\varepsilon_{yj}}{\varepsilon_{xj}}$ is Poisson's ratio values of *j* group of lattices in the model, N is number of interactions in model, $\varepsilon_{xj}\left(d_{xj}, \alpha_{xj}, C\right)$ and $\varepsilon_{yj}\left(d_{yj}, \alpha_{yj}\right)$ is longitudinal and transverse deformation, C is coefficient of deformation intensity $1/\xi \le C \le 1/\xi^2$ while ξ is parameter which shows an intensity of one atom inertia to another according to the movement direction and depends on deformation level $(0 < \xi \le 1)$.

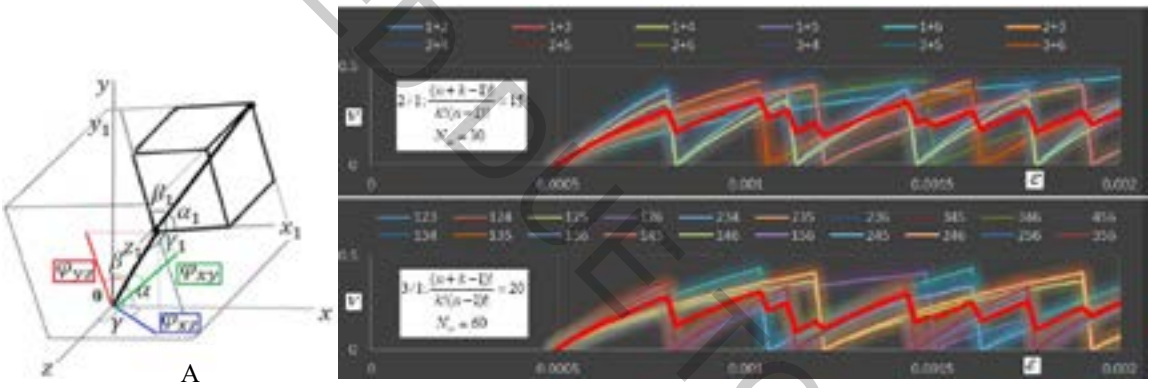

Fig. 1. Crystalline materials lattice distortion model: principles and stability. A is the aligned BBC-lattice in both global and local coordinate systems. The angles α, β, γ are used in equations of tangent plane going at any single point of the outside surface of the unit sphere and for an evaluation of Burger's vectors <XYZ> [2]. **B** shows simulated Poisson's ratio values of Iron when two groups of lattices interacting together (*n* = 2). In **C** Poisson's ratio values of Iron when three groups of lattices interacting together (*n* = 3) are given. Differences between results given in **B** and **C** pictures are not greater than 3 %. This fact confirms high model stability with different lattices interaction mechanisms.

Some corrections of this model can be done by evaluating the electron sublayers configuration in the lattice:

$$\nu = \nu_{sim} \cdot \left(1 + f_1\left(\sum x / \sum Y\right)\right); \quad (2)$$

where ν_{sim} is simulated Poisson's ratio value according to the equation (1), f_1 is weight function, $\sum x$ is sum of electrons in atom sublayers by their filling and $\sum Y$ is sum of electrons in the sublayer to be filled.

The model improvement from the perspective of sublayer filling by electrons increased proximity of simulated Poisson's ratio values to experimental by 53 %. In present study, the multiparametric atomistic model of crystalline materials is shown as a maturing and perspective tool in solid state physics and materials science. It can be used for the fine investigations of atomic states descriptive elastic characteristics of solid and comprehensive transformational evolution between differently aligned atomic systems and neighbor grains of microstructure. For the quantitative analysis, further studies are directed to creation of exact models for other crystalline materials having BCC-lattice.

[1] Vaitkūnas, T, and Jutas, A. "Lattice Distortion Model and Probabilistic Analysis Simulating Elastic Behavior of Crystalline Materials" 16th International Conference of Young Scientists on Energy Issues, (CYSENI 2019), 23-24 May 2019, Kaunas, Lithuania (2019): 390-98. Web.

[2] D. Raabe, M. Sachtleber, Z. Zhao, F. Roters, S. Zaefferer, Micromechanical and macromechanical effects in grain scale polycrystal plasticity experimentation and simulation Acta Materialia 17, pp. 3433-3441 (2001)

ANALYSIS OF THE NA-MN-TI-PO4 PHASE DIAGRAM USING FIRST-PRINCIPLES CALCULATIONS

Gustautas Snarskis[1], Linas Vilčiauskas[2]

[1]Faculty of Physics, Vilnius University, Vilnius, Lithuania
[2]Institute of Chemistry, Vilnius University, Saulėtekio al. 3, LT-10257 Vilnius, Lithuania
gustautass@gmail.com

CANCELLED DUE TO COVID-19

The development of electrochemical rechargeable batteries is one of the current most important topics in science and technology. Although, lithium-ion batteries are becoming the leading technology, it faces a number of problems like safety and rare and expensive (cobalt, lithium) raw materials needed for production. Sodium-ion batteries are a viable alternative in applications where particularly high energy densities are not required and may be based on inexpensive and widespread materials [**?**]. Natrium SuperIonic Conductor (NASICON) framework compounds having the general formula of $Me'_xMe''_y(PO_4)_3$ (Me' = Na, Li, Me'' = Ti, V, Zr, Mn, Sc, Fe, etc.) are currently attracting massive attention from battery research community [**?**].

In this work a part of the Na-Mn-Ti-PO_4 phase diagram (Fig. **??**) corresponding to Mn solid solutions of different concentration in the NTP-123 system $Na_{(1+2x)}Mn_xTi_{(2-x)}(PO_4)_3$, where $x = 0.25; 0.5; 0.75; 1.0; 1.25; 1.5$, was constructed using periodic density function theory calculations and comparing the stability of these systems with the vertices of the ternary phase diagram taken as $NaTi_2(PO_4)_3$, Na_3PO_4 and $NaMnPO_4$. Calculations anticipate solid solutions to be stable at concentrations from $x = 0.5$ to $x = 1.5$, with $x = 1$ being the most stable, and $x = 0.5$ corresponding to the edge of the miscibility gap. The latter was shown to be stabilized by configurational entropy which was evaluated using a Cluster Expansion Approach together with Monte Carlo simulations [**?**].

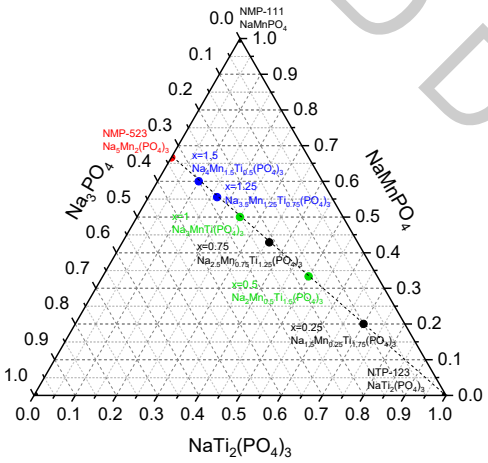

Fig. 1. Ternary phase diagram marked with calculated points corresponding to different concentrations.

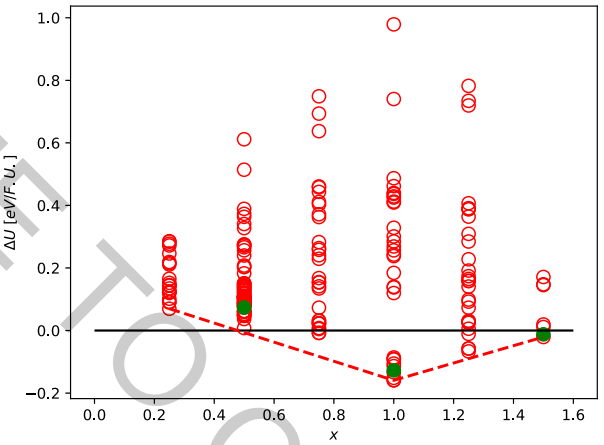

Fig. 2. Convex hull of $Na_{(1+2x)}Mn_xTi_{(2-x)}(PO_4)_3$. Red circles - PBE (GGA) formation energies, green dots - B1WC (Hybrid) formation energies.

Acknowledgements:
This project has received funding from from the European Social Fund according to the 2014–2020 Operational Programme for the European Union Funds' Investments under activity *Improvement of researchers' qualification by implementing world-class R&D projects* measure *Development of Competences of Scientists, Other Researchers And Students Through Practical Research Activities* under grant agreement with the Research Council of Lithuania (LMTLT). (Project No. 09.3.3-LMT-K-712-16-0156).

[1] Nayak, P. K.; Yang, L.; Brehm, W.; Adelhelm, P. From lithium-ion to sodium-ion batteries: advantages, challenges, and surprises. Angew. Chem.-Int. Edit. 2018, 57, 102-120.
[2] Jian, Z.; Hu, Y.-S.; Ji, X.; Chen, W. NASICON-structured materials for energy storage. Adv. Mater. 2017, 29, 1601925.
[3] Puchala, B.; Van der Ven, A. Thermodynamics of the Zr-O system from first-principles calculations. Phys. Rev. B 2013, 88, 094108.

THEORETICAL PREDICTION OF Sb_2Se_3 GROWTH MORPHOLOGY AND ORIENTATION ON MUSCOVITE MICA SUBSTRATES

Martynas Bertašius[1], Rokas Kondrotas[1]

1-Department of Characterisation of Materials Structure, Center for Physical Sciences and Technology (FTMC), Saulėtekio av. 3, LT-10257 Vilnius, Lithuania
martynas.bertasius@ftmc.lt

CANCELLED DUE TO COVID-19

Ever since the first demonstration in 2004, van der Waals heterostructures have received considerable attention due to their unique interlayer coupling and optoelectronic properties. Therefore, such heterostructures can benefit the performance of photodetectors, solar cells or other optoelectronic devices by reducing surface recombination velocity. Sb_2Se_3 is a quasi-one-dimensional material that can form van der Waals heterostructures on other low dimensional or three-dimensional substrates and has been shown to exhibit excellent optoelectronic properties [1, 2]. However, despite few experimental works, the growth mechanism of Sb_2Se_3 on low dimensional substrates is elusive.

Under equilibrium conditions, the growth of low dimensional materials is governed by van der Waals epitaxy. As in classical epitaxy, the growing layer adopts specific orientation to minimize lattice mismatch. The structure of Sb_2Se_3 resembles that of the molecular crystal, therefore the epitaxial relationship on the specific substrate can be estimated through relatively simple algorithm [3]. Therefore, in this work, we aim to predict the orientation of low dimensional materials grown on the specific substrate.

As a case study, we chose to examine epitaxial relation of Sb_2Se_3 and muscovite mica. The determination of the optimum overlayer orientation was accomplished using a simple geometric lattice misfit modelling algorithm that calculates a "dimensionless potential":

$$\frac{V}{V_0} = \left(1 - \frac{\sin(M\pi p_x)\sin(N\pi q_x)}{2MN\sin(\pi p_x)\sin(\pi q_x)} - \frac{\sin(M\pi q_y)\sin(N\pi p_y)}{2MN\sin(\pi q_y)\sin(\pi p_y)}\right); \quad (1)$$

Here the integer numbers M and N define the size of the overlayer, and the values of $p_{x,y}$ and $q_{x,y}$ are defined by a transformation matrix that relates the overlayer lattice vectors $b_{1,2}$ to the lattice vectors of the substrate $a_{1,2}$ [3]. For muscovite mica substrate, the values were taken a_1=5.18Å and a_2=8.99Å with a perpendicular angle, and for Sb_2Se_3 various orientations of the layers and vectors' $b_{1,2}$ lengths were taken for the calculations.

Out of 10 tested planes with miller indices of (hk0), where h varied in 1 to 3 and k in 1 to 5 range, the (120) indicated the point-on-line coincidence at azimuthal angle at θ~90 and 270 deg. A fair agreement was found with experimental results available in the literature. The existence of lattice coincidence verify that molecular crystal lattice misfit modelling algorithm can be suitable for prediction of Sb_2Se_3 morphology and orientation, and could be helpful in van der Waals epitaxial growth of 1D/2D p-n heterostructures optimization and selection of the substrates.

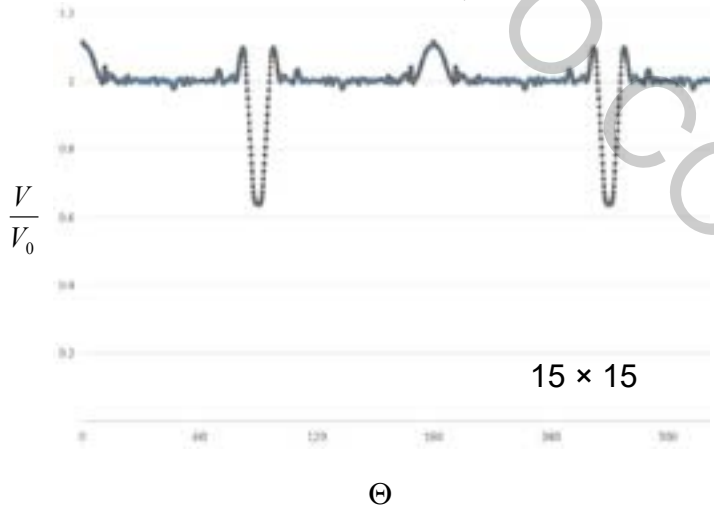

Fig. 1. Dependence of V/V_0 on azimuthal angle Θ for the (120) orientation for Sb_2Se_3 layer with b_1=3.962Å, b_2=26.051Å on muscovite mica substrate with a_1=5.18Å and a_2=8.99Å. Overlayer size M×N for the calculation is 15×15.

[1] Sun, G., Li, B., Li, J. et al. Nano Res. (2019) 12: 1139. https://doi.org/10.1007/s12274-019-2364-1
[2] Ma Z, Chai S, Feng Q, Li L, Li X, Huang L, Liu D, Sun J, Jiang R, Zhai T, Xu H. ,Small. 2019 Mar;15(9):e1805307. doi:10.1002/smll.201805307
[3] Julie A. Last, Daniel E. Hooks, Andrew C. Hillier, and Michael D. Ward, *The Physicochemical Origins of Coincident Epitaxy in Molecular Overlayers: Lattice Modeling vs Potential Energy Calculations*, J. Phys. Chem. B **1999**, 103, 6723-6733 (1999)

MICROSTRUCTURAL ANALYSIS OF ADDITIVELY MANUFACTURED STAINLESS STEEL PARTS

Ada Steponavičiūtė, Genrik Mordas, Karolis Stravinskas, Aušra Selskienė

Department of Laser Technologies, Center for Physical Sciences and Technology, Lithuania
ada.steponaviciute@ftmc.lt

Additive manufacturing (AM) is a manufacturing technology used for 3D object production which opens a pathway to fabricate complex parts due to the high geometrical flexibility of the technology [1]. Direct Metal Laser Sintering (DMLS) is one of the most widely applied metal AM technologies, where, in a layer-by-layer fashion, bulk parts are created by selective sintering and consolidation of thin powder layers using a laser beam [2]. DMLS can be used for part fabrication using different metals and their alloys. Although iron and its alloys have been used in conventional manufacturing for a long time and the most advantages and disadvantages of these materials are well known, using them in additive manufacturing to achieve high quality still can be problematic. In DMLS, the main challenge is to understand the influence of energy density on porosity, microstructure and mechanical properties of a manufactured part.

In this study, test specimens were produced from 17-4PH stainless steel using different sets of build parameters on the EOSINT M280 machine. Cross-sectional microstructure of the manufactured specimens was investigated using scanning electron microscopy (SEM) and optical microscopy in order to determine the relation between porosity and energy density applied during the printing process. Defects visible in cross-sections were evaluated with help of image processing software, which showed the amount of pores present in specimens, depending on various energy density values.

Energy density values vary throughout the experiment and there is a visible decrease in the amount of defects, the higher the energy density is. All manufactured stainless steel parts could be divided into three different types depending on their cross-sectional microstructure: 15-32 J/mm^3 (I), 32-48 J/mm^3 (II) and 48-65 J/mm^3 (III), The zones and optical micrographs corresponding to each of them are shown in Fig.1. All defects compiled take up 16,5-17,5% of the area in I, 5-7% in II and less than 0,5% in III.

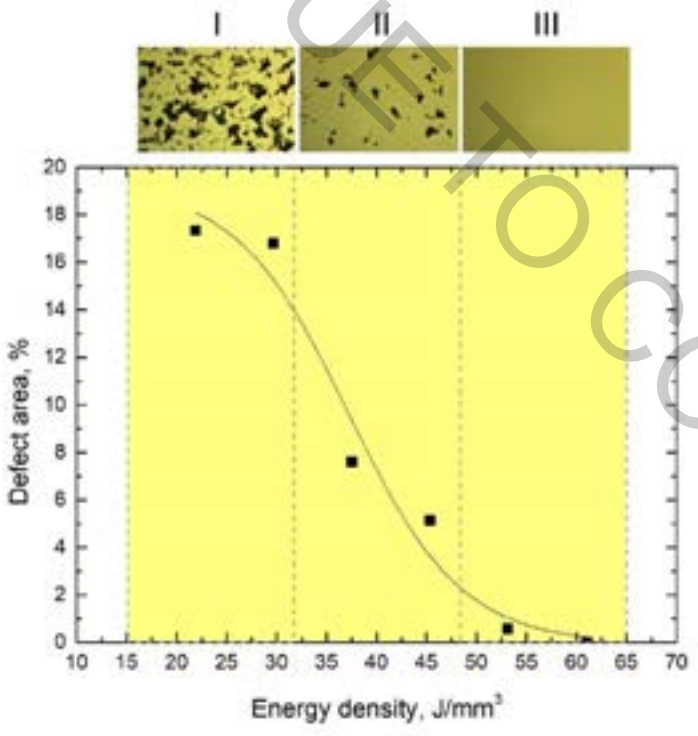

Fig. 1. Microstructural evolution of additively manufactured parts

[1] L. Hitzler, M. Merkel et al., A Review of Metal Fabricated with Laser- and Powder-Bed Based Additive Manufacturing Techniques: Process, Nomenclature, Materials, Achievable Properties, and its Utilization in the Medical Sector, Advanced Engineering Materials Volume 20, Issue 5 (2018).
[2] B. Song, S. Dong et al., Microstructure and tensile properties of iron parts fabricated by selective laser melting, Optics & Laser Technology 56, 451-460 (2014).

CANCELLED DUE TO COVID-19

SYNTHESIS AND INVESTIGATION OF XANTHENONE BASED OLED EMITTERS EXHIBITING BOTH AIEE AND TADF

Sohrab Nasiri [1*], Simas Macionis [1], Dalius Gudeika [1], Dmytro Volyniuk [1], Juozas V. Grazulevicius [1]

[1] Department of Polymer Chemistry and Technology, Kaunas University of Technology, Radvilenu pl. 19, LT-50254, Kaunas, Lithuania
sohrab.nasiri@ktu.edu

new donor-acceptor compounds were designed, synthesized and investigated by theoretical and experimental approaches aiming to estimate effect of the structure of a donor on the properties of potential OLED emitters. Because of the different electron-donating abilities of the nitrogen-containing heterocycles, derivatives of xanthenone containing di-tert-butyl-carbazolyl, di-tert-butyl-acridanyl, di-tert-butyl-phenothiazinyl and penoxazinyl moieties exhibited different photophysical behavior. Because of big dihedral angles between the donors and acceptor as well as because of possibility of rotation around N-C bond, the designed compounds were characterized by thermally activated delayed fluorescence and aggregation induced emission enhancement effect. Twice higher photoluminescence quantum yields reaching 38% in doped films were obtained for compounds containing di-tert-butyl-carbazolyl and di-tert-butyl-acridanyl moieties as compared to those observed for compounds with the donors containing S and O heteroatoms. Strong effect of the donor substituents on charge injection (ionization potentials were in the range of 5.67-5.96 eV) and charge-transporting properties (hole and electron mobilities were in a wide range from 6.3×10^{-8} to 6.3×10^{-4} $cm^2V^{-1}s^{-1}$ at electric field of 2.5×10^5 $V\cdot cm^{-1}$) was detected. The differently substituted compounds were utilized as emitters in OLEDs. Higher maximum values of brightness (up to 20900 cdm-2) were observed for OLEDs based on emitters with nitrogen containing donors relative to estimated for OLEDs based on emitters containing di-tert-butyl-phenothiazinyl and penoxazinyl moieties. Energy diagram and EL spectra of OLEDs submitted at Figure 1.

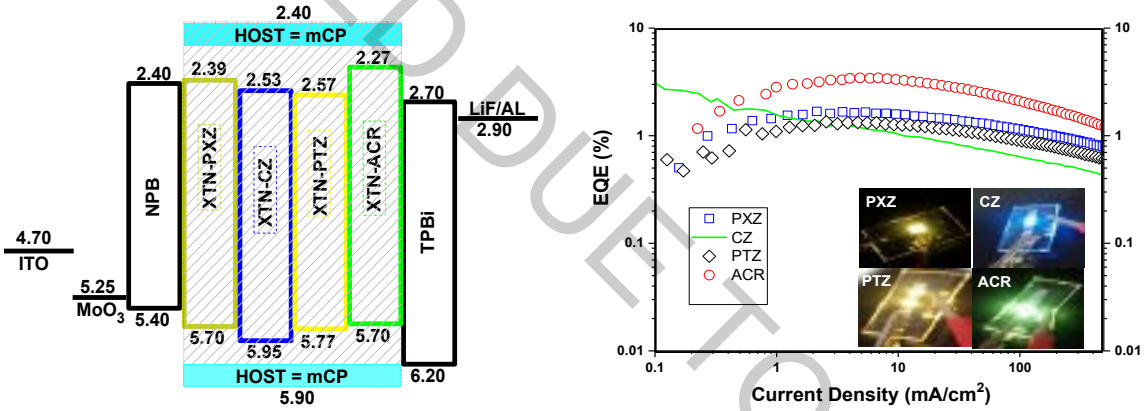

(a) (b)

Fig. 1. (a) Energy diagram and (b) EL spectra of devices

The radiation transition rates of the doped films of the compounds were calculated using the formula [1].

$$k_{PF} = \frac{\eta_{PF}}{\tau_{PF}} \quad (1)$$

$$k_{ISC} = \frac{\eta_{DF}}{\eta_{PF}+\eta_{DF}} k_{PF} \quad (2)$$

$$k_{DF} = \frac{\eta_{DF}}{\tau_{DF}} \quad (3)$$

$$k_{RISC} = \frac{\eta_{DF}}{\eta_{PF}} \cdot \frac{k_{PF}.k_{DF}}{k_{ISC}} \quad (4)$$

where k_{PF}, k_{DF}, k_{ISC}, and k_{RISC} are rate constants of prompt and delayed components, intersystem crossing (ISC) and RISC processes, respectively; η_{PF} and η_{DF} are prompt and delayed PLQYs distinguished from the total PLQY by comparing the integrated intensity of the prompt and delayed components. k_{ISC} and k_{RISC} values of compound XTN-ACR were reported 1.15×10^6 s^{-1} and 0.8×10^5 s^{-1} respectively.

[1] C. Han, Z. Zhang, D. Ding, et al., Dipole-dipole interaction management for efficient blue thermally activated delayed fluorescence diodes. Chem, **4**, 2154-2167 (2018).

ACCEPTED DUE TO COVID-19

SCANNING BEHAVIOR IN ULTRASONIC NDE OF T-SHAPED CFRP COMPONENT

Khaja Naib Rasool Shaik[1], Gopi Kompelli[2], Hari Prasanna Manimaran[1], Dr. Elena Jasiūnienė[3]

[1] Department of Aeronautical Engineering, Kaunas University of Technology, Studentų 56, Kaunas, Lithuania
[2] Department of Vehicle Engineering, Kaunas University of Technology, Studentų 56, Kaunas, Lithuania
[3] Prof. K. Baršauskas Ultrasound Research Institute, Kaunas University of Technology, Kaunas, Lithuania
Khaja.shaik@ktu.edu

CANCELLED DUE TO COVID-19

The composite materials are used in the structural applications and components of aircraft. In all aircraft applications, the composite materials are highly using because of its lightweight and high strength properties [1]. Aircraft structures consist of numerous joints such as T-Joint, U- Joint, V-Joint, Lap joint and Butt Joint, etc. T-Joints are can found in aircraft wing structures, whereas bulkhead to the skin, rib to the skin, and spar to skin interfaces [2].

The work aims to investigate the better scanning techniques and possibilities to detect the position and size of the defects in the CFRP T-Shape component. The 3D model of the CFRP T-Shape component having 6 side-drilled holes is designed with 3mm and 6mm diameter in the CIVA Software. The side-drilled holes are placed in three different depths: close to the upper surface, in the center and close to lower surface with different sizes and thickness as shown in Fig 1. Firstly, focused scanning process performed with 10 MHz frequency to show good quality of scanning. In the focused scanning process, a single point focus used as transmission. In the focused scanning, the quality of scanning is better to find the position,depth and size of the side-drilled holes.

The next step is linear and sectorial scanning for size measurement. In the linear scanning inspection process, it is difficult to get the back wall reflections from side-drilled holes because of its circular shape and also in linear scanning process its difficult to measure the daimeter of the holes because the ultrasonic waves refelct only from top surface of the side-drilled holes. So, by these difficulties sectorial scanning is chosen to make better results. In the sectorial scanning process, the initial and final angle will be -45^0 and 45^0 and ultrasonic waves can reflect from half of the side-drilled holes because of the inspection angles and it is easy to measure the size. From the sectorial scanning results, the segmentation process is used to measure the size of the side-drilled holes. Segmentation is a procedure to use the simulation data to compute the segments that show the various echoes. In the segmentation process, different dB values are used for the 3mm and 6mm side-drilled holes for size measurement. The sectorial scanning results are obtained shown in below Fig 2.

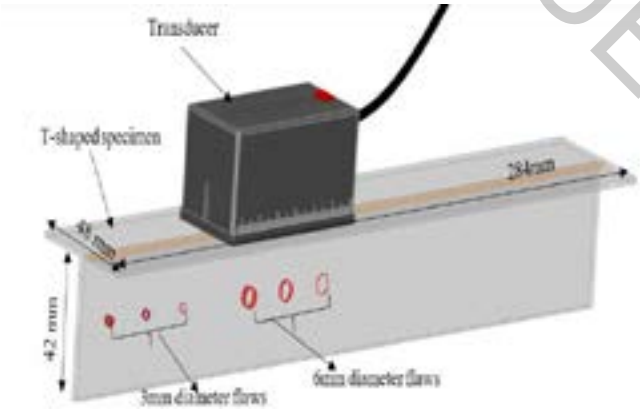

Fig. 1. 3D Model in CIVA Software

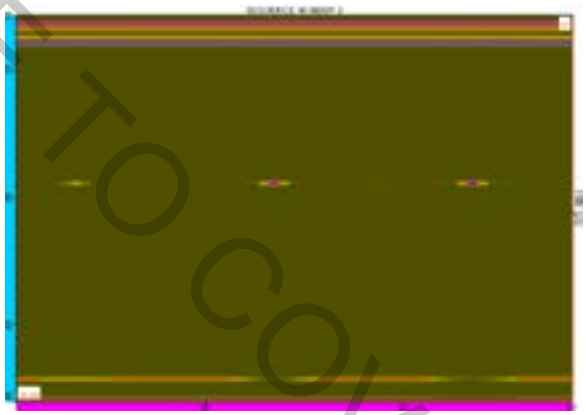

Fig. 2. B-Scan results for side drilled holes.

The results conclude that the CIVA Software can be used for modelling of all the types of scanning techniques and size measurements. The focus scanning technique gives better scanning quality results to find the position, depth and size of side-drilled holes. In linear and sectorial scanning techniques, the sectorial scanning is suitable to make proper results in the segmentation process to measure the size of the side-drilled holes. From the segmentation results, the flaw size is 3mm for small side drilled holes at -12dB in sectorial scanning but for 6mm side drilled holes, the result obtained in both linear and sectorial scanning at -12dB. So, from all the above results and discussion 3mm side drilled is difficult to find in linear scanning because of its size.

[1] Michael May, Georg Ganzenmüller, Johannes Wolfrum, Sebastian Heimbs, Analysis of composite T-joint designs for enhanced resistance to hydrodynamic ram, Composite structures, Volume 125, July 2015, Pages 188-194.
[2]] K.N. Arunkumar, N. Lohith and B.B. Ganesha, Effect of ribs and stringer spacings on the weight of aircraft composite structures, ARPN Journal of Engineering and Applied Sciences, Vol. 9, No. 4, April 2014.

SURFACE MODIFICATION OF 3D PRINTED TRABECULAR TITANIUM ALLOY STRUCTURE

Sandra Navickytė[1,2], Skirmantas Norkus[2], Brigita Abakevičienė[1]

[1] Department of Physics, Kaunas University of Technology, Studentu str. 50, LT-51368, Kaunas, Lithuania
[2] Ortho Baltic, Taikos ave. 131A, LT-51124, Kaunas, Lithuania
Sandra.navickyte@ktu.edu

Additive manufacturing by direct metal laser sintering allows to produce implants with trabecular structure [1]. Metal trabecular structure mimics the internal structure of the bone. By adjusting the porosity and surface of trabecular structure, partial or complete bone structure may be restored [2]. Ti-6Al-4V alloy trabecular structure specimens were produced using direct metal laser sintering (DMLS). After manufacturing and annealing specimens, the chemical etching processes were done to modify the micro-roughness of the titanium alloy surface. The topography of the surfaces was investigated using scanning electron microscope (SEM). Chemical composition was done using X-ray photoelectron spectroscopy (XPS). Porosity was set using micro-computer tomography. SEM analysis showed that the surface topography consists of a macro- and microroughness. The results of micro-computer tomography showed of specimen's porosity. This study showed that alkali and acid etching technologies allow to control roughness, topography, chemical composition and cells adhesion of additively manufactured Ti-6Al-4V alloy trabecular structure surface.

[1] W.-S Lin., T. L. Starr et al. Additive Manufacturing Technology (Direct Metal Laser Sintering) as a Novel Approach to Fabricate Functionally Graded Titanium Implants: Preliminary Investigation of Fabrication Parameters.1490-1495 (2013).
[2] L. Yuan, S. Ding, C. Wen. Additive manufacturing technology for porous metal implant applications and triple minimal surface structures: A review. Nature: **4**, 56-70 (2019).

CANCELLED DUE TO COVID-19

PHOTORHEOMETRICAL STUDY OF ACRYLATED VANILLIN-BASED RESINS

Greta Motiekaitytė[1], Auksė Navaruckienė[1], Jolita Ostrauskaitė[1]

[1] Department of Polymer Chemistry and Technology, Kaunas University of Technology, Radvilenu Rd. 19, LT-50254 Kaunas, Lithuania
greta.motiekaityte@ktu.edu

Photopolymerization is the rapid formation of cross-linked polymers from monomers under the influence of the light. Photopolymerization can be initiated by UV-, visible- and rarely by IR-light [1]. In the last years vanillin and its derivatives were used in polymer synthesis as their aromatic resins provide high rigidity and thermal stability of the resulting polymers [2].

In this study two commercially available vanillin derivatives, vanillin dimethacrylate (VDM) and vanillin diacrylate (VD), were tested in thiol-ene photocurable systems with 1.3-benzenedithiol (1.3BDT) and without 1.3BDT. Phenylbis(2.4.6-trimethylbenzoyl)phosphine oxide (BAPO) was selected as photoinitiator and dichloromethane (DCM) was used as solvent.

Real-time photorheometry was used to monitor the evolution of thiol-ene and free-radical photocross-linking process. As an example, the dependencies of storage modulus G', loss modulus G", loss factor tanδ, and complex viscosity η* of the resin VD/3BAPO on irradiation time are presented in Fig. 1. When irradiation of the resin started, the values of storage modulus G', loss modulus G", and complex viscosity η* started to increase indicating the beginning of the cross-linking process. The onset of gelation process is described as the gel point (t_{gel}), i.e. the point at which G' and G" modulus curves intersect [3]. As the irradiation of the resin proceeded with time, the values of G', G" modulus, and η* continued to increase due to the gel aging and settled down into a steady-state indicating the end of the cross-linking process. All vanillin-based resins investigated in this study showed the similar behaviours.

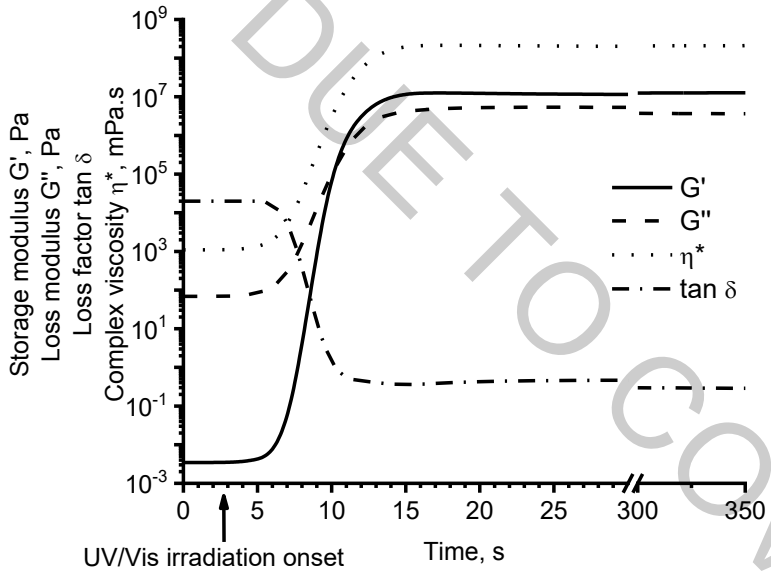

Fig. 1. Dependencies of storage modulus G', loss modulus G", loss factor tan δ, and complex viscosity η* of the resin VD/3BAPO on irradiation time.

Real time photorheometrical studies showed that in most cases the addition of solvent and 1.3BDT slowed down the photopolymerization process and thus the less rigid polymers were obtained.

Acknowledgements. This research was funded by the European Social Fund under the measure No. 09.3.3-LMT-K-712 "Development of Competences of Scientists, other Researchers and Students through Practical Research Activities" and EU ERDF, through the INTERREG BSR Programme, (ECOLABNET project #R077).

[1] X. Zhu, Q, Niu, Y. Xu et al., From small molecules to polymer fibers: Photopolymerization with electrospinning on the fly, Photoch. Photobio. A **353**, 101-107 (2018)
[2] J.F. Stanzione, J.P. Sadler, J.J. La Scala et al., Vanillin-based resin for use in composite applications, Green. Chem. **14**, 2346-2352 (2012)
[3] T. G. Mezger, *The Rheology Handbook, 3rd ed.* (Vincentz Network, Hanover, 2011)

CANCELLED DUE TO COVID-19

NEW TYPE OF METAL PARTICLE DOSING, TRANSPORTATION AND POSITIONING SYSTEM

Karolis Stravinskas[1], Sergejus Borodinas[2], Ada Steponavičiūtė[1], Genrik Mordas[1]

[1] Department of Laser Technologies, Center for Physical Sciences and Technology, Lithuania
[2] Faculty of Civil Engineering, Vilnius Gediminas Technical University, Lithuania
karolis.stravinskas@ftmc.lt

CANCELLED DUE TO COVID-19

Laser metal deposition (LMD) technology is an additive manufacturing technique, which allows producing metal parts characterized by good metallurgical properties using an extremely low consumption of the metal powder. Therefore, LMD has been of most interest in high value added applications such as in aerospace and medicine which can afford this developing process as a whole, in spite of the criticality of performance and acceptance criteria in these industry sectors [1].

However, one of the major disadvantages of this process is the relatively low melt pool resolution and repeatability of particle tracing which have impact on the surface roughness. Although surface roughness can be improved using melt pool and layer thickness, but this has an impact on a slow production turnaround. Relatively low efficiency of the trapped powder, which can be less than 5% in some cases, is an additional drawback of this technology in our days. The main goal is to design a novel high definition (HD) Head for LMD process with low particle dispersion.

Our proposed HD-Head consists of an ultrasonic actuator of tulip type, a mixing chamber and an outlet tube. The ultrasonic actuator generates the acoustic pressure field in local volume zone (Fig. 1a). Special geometry of the mixing chamber creates aerodynamic conditions for tornado appliers (Fig. 1b). The tornado allows transporting particles from the walls of the actuator to the centerline of the HD-Head. The centerline of the HD-Head contains the highest particle concentration; thus the outlet tube is positioned in this area. Collected particles pass though the outlet tube and enter the de Laval tube, where they are accelerated and form a precise particle beam with low dispersion. Analysis of the novel dosing, transportation and positioning system for LMD process was conducted using COMSOL Multiphysics software.

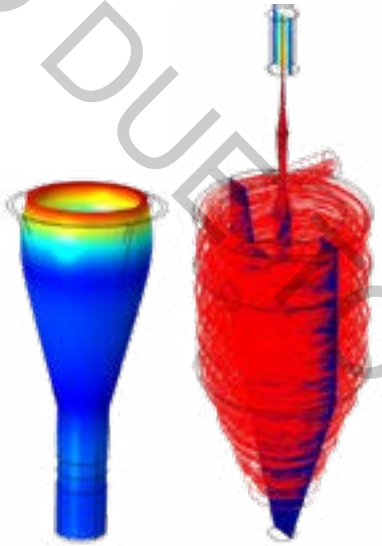

a) b)

Fig. 1. Microstructural evolution of additively manufactured parts

[1] C. Selcuk, S. Bond, P. Woollin, Joining processes for powder metallurgy parts: a review, Powder Metallurgy, 53:1, 7-11 (2010).

NANOCOMPOSITE BROADBAND DIELETRIC SPECTROSCOPY

Rytis Šalaševičius[1], Sergejus Balčiūnas[1], Jūras Banys[1], Satoshi Wada[2]

[1] Department of Physics, University of Vilnius, Lithuania
[2] Interdisciplinary Graduate School of Medicine and Engineering, University of Yamanashi, Japan
Rytis.salasevicius@ff.stud.vu.lt

For the last few decades there has been a growing interest in applicable lead-free materials [1]. Due to environmental concerns the lead-free piezoelectric material research has grown significantly. As most commercially viable piezoelectric materials with lead have great piezoelectric constant and can operate in a broad temperature range, the aim of this research is to improve dielectric and piezoelectric properties in lead free solid solutions.

Nanocomposite ceramics have been making a breakthrough in search for piezoelectric materials. In this case the material is a "core-shell" type nanocomposite ceramic that consists of a BT-BMT crystallites cores which are coated in a BT shell.

BT-BMT/BT "core/shell" composites were prepared in two steps: the BT-BMT solid solution core was mixed with TiO_2 crystallites in a high pressure compressor into cylindrical shape pellets [2], [3] and then submerged into barium hydroxide solution at 175 ˚C for solvothermal solidification [4], [5].

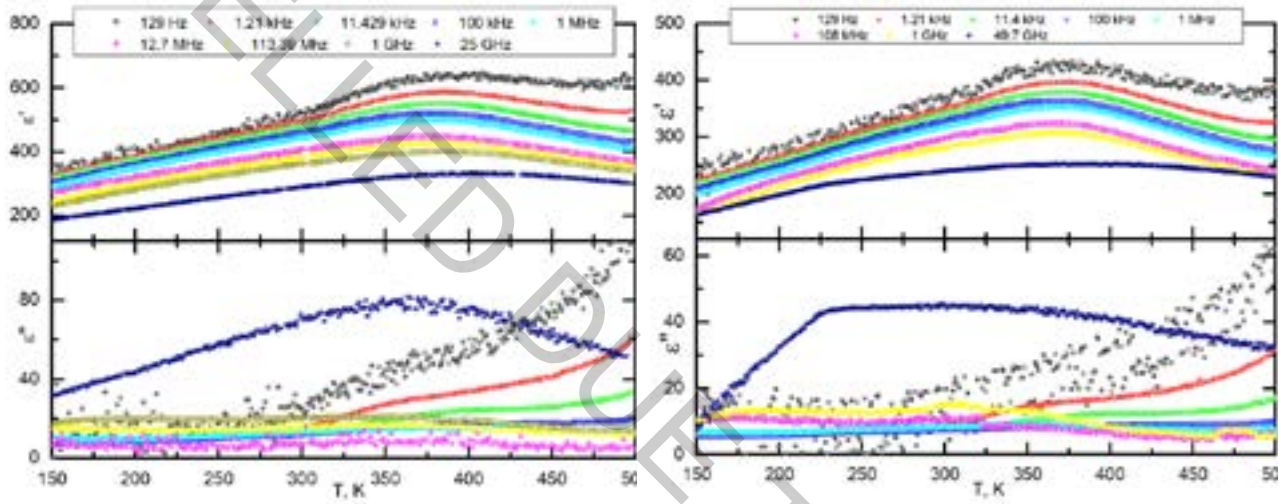

Fig. 1. Dielectric permittivity dependence of 0.6BT-0.4BMT/BT (left) and 0.7BT-0.3BMT/BT (right) "core/shell" over a broad temperature and frequency range.

In figure 1 we can observe an complex dielectric permittivity of (1-x)BT-xBMT/BT where x=0.4 (left) and x=0.3 (right) "core/shell" solid solutions an anomalous dielectric constant close to 395 K temperature in x=0.4 ceramic can be seen. Adding a little bit of BT x=0.3 into the system shifts the anomaly toward lower temperature range by 20 K. This dielectric constant peak could be linked to a structural phase transition.

The dielectric constant dependence of temperature seems similar in both solid solutions. The value of dielectric constant is lower, however there seems to be an increase of dielectric permittivity in lower frequencies and high temperatures.

In the poster presentation further investigation would be presented as the 0,6BT-0,4BMT/BT solid solution would be compared to 0,7BT-0,3BMT/BT composite.

[1] E. U. Council, "Directive 2002/95/EC of the European parliament and of the council." eur-lex.europa.eu, 2003.
[2] C. Chen, J. Cheng, S. Yu, L. Che, and Z. Meng, "Hydrothermal synthesis of perovskite bismuth ferrite crystallites," J. Cryst. Growth, vol. 291, no. 1, pp. 135–139, 2006.
[3] Y. Wang et al., "Mineralizer-Assisted Hydrothermal Synthesis and Characterization of BiFeO3 Nanoparticles," J. Am. Ceram. Soc., vol. 90, no. 8, pp. 2615–2617, 2007.
[4] Y. Hirose, S. Ueno, K. Nakashima, and S. Wada, "Fabrication of BaTiO3/BiFeO3 Nano-complex Ceramics by Hydrothermal Method," Trans. Mater. Res. Soc. Jpn., vol.
[5] Y. Hirose, S. Ueno, K. Nakashima, and S. Wada, "Preparation of BaTiO3 Nanostructured Ceramics by Solvothermal Solidification Method," Trans. Mater. Res. Soc. Jpn., vol. 40, no. 3, pp. 239–242, 2015.

CANCELLED DUE TO COVID-19

RESEARCH OF THE HORIZONTAL PENDULUM BASE HARVESTER FOR LOW ENERGY DENSITY SYSTEMS

Viktor Kovalevskyi, Darius Viržonis, Vytautas Bučinskas, Rimgaudas Urbonas, Sigitas Petkevičius, Inga Morkvėnaitė –Vilkončienė, Andrius Dzedzickis

Department of Mechatronics, Robotics and Digital Manufacturing, Vilnius Gediminas Technical University, Lithuania
viktor.kovalevskyi@vgtu.lt

CANCELLED DUE TO COVID-19

A proposed energy harvesting system intended to convert ambient mechanical vibration into electrical energy to power autonomous low power electronic systems [1]. The device operation is based on non-holonomic vibration system, called horizontal pendulum. This design allows developing a system without natural frequency and having possibility to excite from chaotic vibrations. Harvester uses swinging type generator with permanent magnets and built using 3-phase system followed by rectifier and energy collection system. Experimental research performed on original setup, which consists from horizontal pendulum, supported by spring and swinging rotor generator. Both elements were modelled in advance using finite element method (FEM) modelling features.

The purpose of the experimental research was to evaluate possibilities for horizontal pendulum swinging system and swinging rotor generator amount of energy from mechanical vibrations. Also the main parameters of an electrical part should be determined to be able to make a prototype for further research. We have created the first prototype of the harvester Fig. 1 and performed initial measurements.

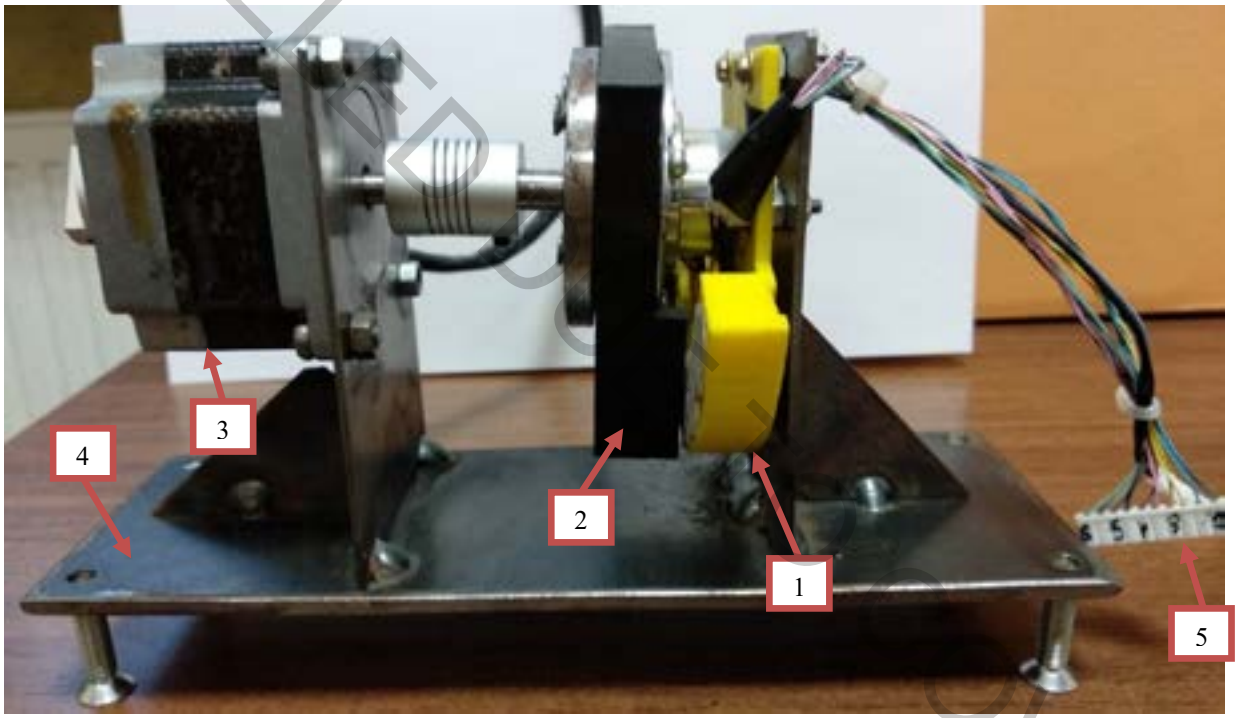

Fig. 1 Experimental setup: 1) coil holder; 2) magnet holder; 3) stepper motor; 4) device frame; 5) coil's output wires

The results of the experiments allowed us to find better design of the coil and magnetic chain. Experimental research obtained the highest voltage was generated with coil, containing 2000 windings of 0.12 mm diameter copper wire. Magnetic chain with internal core of ferromagnetic steel showed better results than internal and external core. Low frequency vibrations of 2 Hz generate enough power for desired application and using moderate mechanical resistance for horizontal pendulum harvester. The results obtained using 4 mm diameter core. The coil with the outside metal core or outside and inside core was less efficient in the sense of mechanic energy transformation into electric energy.

Acknowledgement:
This research was funded by the European Social Fund under the No. 09.3.3.-LMT-K-712-16-0209.

[1] K. J. Åström, K. Furuta, Swinging up a pendulum by energy control, Automatica 36(2), 287-295 (2000).
[2] S. Meninger, J. O. Mur-Miranda, R. Amirtharajah, et al., Vibration-to-electric energy conversion, IEEE Transactions on Very Large Scale Integration (VLSI) Systems 9(1), 64-76 (2001).

INVESTIGATION OF CHAOTIC LOW FREQUENCY VIBRATIONS TRANSFORMATION EFFICIENCY OF HORIZONTAL PENDULUM BASE HARVESTER

Viktor Kovalevskyi, Darius Viržonis, Vytautas Bučinskas, Rimgaudas Urbonas, Sigitas Petkevičius, Inga Morkvėnaitė –Vilkončienė, Andrius Dzedzickis

Department of Mechatronics, Robotics and Digital Manufacturing, Vilnius Gediminas Technical University, Lithuania
viktor.kovalevskyi@vgtu.lt

CANCELLED DUE TO COVID-19

Powering of devices with low energy consumption became actual task in the eras when mechatronic equipment flooded industry and daily life. Remote located sensors typically powered using batteries or with permanent line, existing devices often can be powered from environment energy like vibration, wind or sunshine [1,2]. Generation or harvesting of electric energy as process is usually known, but harvesting of it from low-density sources has some specific problems. Energy generation for chaotic vibration source has even more problems, therefore special mechanical vibration element necessary.

Implementation of horizontal pendulum as mechanical part of the harvester allows retrieving energy from vibrating object due to excitation without prevailing frequency allows gaining energy from chaotic vibration of the bridge span. An effect of damping reduces amplitude and as result - the generated amount of energy (Fig. 1).

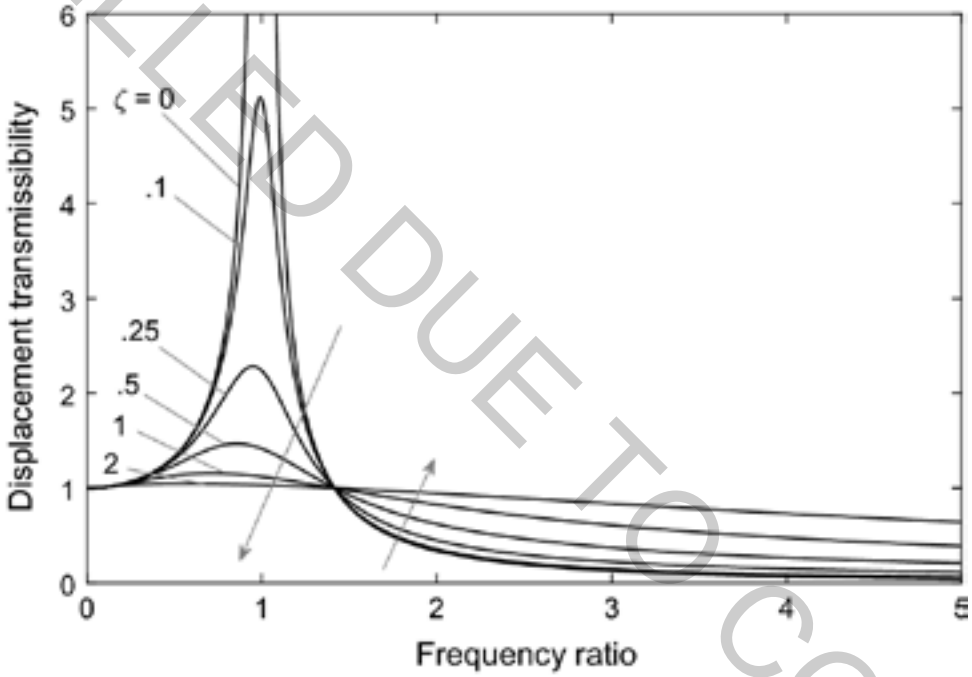

Fig. 1 Transmissibility in a one-degree-of-freedom system [3].

An efficiency equation is presented below and shows the ratio between the input energy (in current case energy of vibrations) and generated energy Eq. 1:

$$\text{Energy efficiency} = \frac{\text{Useful output energy}}{\text{Total input energy}} \quad (1)$$

The purpose of the research is to investigate the efficiency of the harvester prototype measuring the amount of energy needed for system to vibrate with desired frequency and comparing it with the energy output. Resultant graph will show the ratio and the efficiency of the created prototype will be evaluated comparing with other existing similar devices.

Acknowledgement:
This research was funded by the European Social Fund under the No. 09.3.3.-LMT-K-712-16-0209.

[1] V. Bučinskas, A. Dzedzickis, N. Šešok et al., Two-axis mechanical vibration harvester, Dynamical systems, Mechatronics and Life Sciences, Lodz, Poland, 99-110 (2015).
[2] N. G. Elvin, A. A. Elvin, An experimentally validated electromagnetic energy harvester, Journal of Sound and Vibration **330(10)**, 2314-2324 (2011).
[3] L. Marino, A. Cicirello, D. A. Hills, Displacement transmissibility of a Coulomb friction oscillator subject to joined base-wall motion, Nonlinear Dynamics **98**, 2596-2612(2019).

GRAPHENE FORMATION THROUGH CARBON SEGREGATION ON AMORPHOUS CARBON AND TRANSITION METAL COMPOSITES

Paulius Dolmantas[1,2*], Andrius Vasiliauskas[1], Šarūnas Meškinis[1]

[1] Institute of Materials Science of Kaunas University of Technology, K. Baršausko st. 59, LT-51423 Kaunas, Lithuania
[2] Department of Physics, Faculty of Mathematics and Natural Sciences, Kaunas University of Technology, Studentų st. 50, LT-51368, Kaunas, Lithuania
Paulius.Dolmantas@ktu.edu

Graphene is notorious two-dimensional material, consisting of one or a few layers of sp^2 bonded carbon atoms distributed in honeycomb crystal lattice. Unique properties of graphene such as high electron and hole mobility, thermal conductivity, mechanical resistance, tunable bandgap and more makes it focus of both fundamental and applied scientific research [1], [2]. While mechanically exfoliated graphene exhibits best performance when incorporated in devices, this type of graphene is hardly obtainable in large areas and mass quantities [3]. Moreover, device fabrication requires transfer step during which graphene is contaminated by adsorbents, wrinkles and potentially cracks [4].

In present work, few layer graphene is produced by annealing amorphous carbon – nickel (a-C:Ni) and amorphous carbon – cobalt (a-C:Co) thin film composites, deposited by magnetron co-sputtering. Relative carbon and transition metal concentrations and film thicknesses were varied to find optimal sputtering conditions for graphene formation. Raman spectroscopy as well as X-ray diffractometry and X-ray photoelectron spectroscopy were used to characterize graphene and film phase. Residual metal was treated with appropriate etchants (ceric ammonium nitrate for nickel composites and chloric acid for cobalt composites). From fig. 1 it is evident that few-layer graphene formed on both post-annealed a-C:Ni and a-C:Co films. However, cobalt composites exhibit less defects (lower D band) and smaller number of layers (higher I_{2D}/I_G ratio).

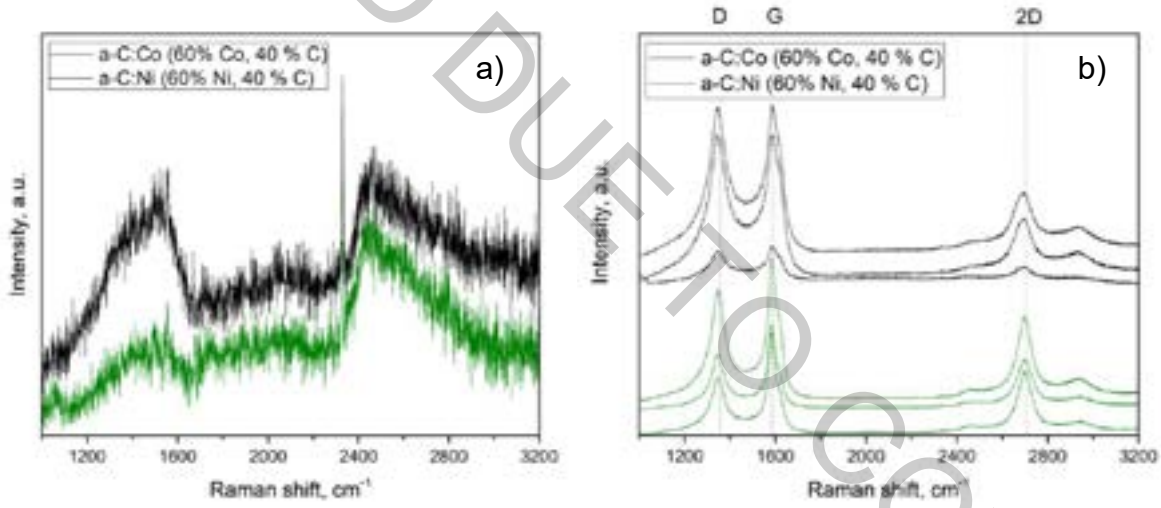

Fig. 1. Raman spectra of a-C:Co and a-C:Ni films: a) before annealing, b) after annealing at 800 °C, Ar, t = 30 min

These results are promising as graphene formed through a-C:Co composite carbon segregation process can be used for graphene-silicon Schottky diode production.

[1] C. Soldano, A. Mahmood, and E. Dujardin, 'Production, properties and potential of graphene', *Carbon N. Y.*, vol. 48, no. 8, p. 21, 2010.
[2] Y. Zhang *et al.*, 'Direct observation of a widely tunable bandgap in bilayer graphene', *Nature*, 2009.
[3] B. Jayasena and S. N. Melkote, 'An Investigation of PDMS Stamp Assisted Mechanical Exfoliation of Large Area Graphene', *Procedia Manuf.*, 2015.
[4] W. S. Leong *et al.*, 'Paraffin-enabled graphene transfer', *Nat. Commun.*, vol. 10, no. 1, p. 867, Dec. 2019.

CANCELLED DUE TO COVID-19

POROUS PERIODICAL SILICON STRUCTURE AS SUBSTRATE FOR SERS APPLICATION

Augusto Jesus Hernandez Lombardini[1*], Nadzeya Khinevich[1*], Nikita Grevtsov[2], Alex Burko[2], Hanna Banadrenka[2], Tomas Tamulevičius[1, 3], Sigitas Tamulevičius[1, 3]

[1] Institute of Materials Science, Kaunas University of Technology, Kaunas, Lithuania
[2] Applied plasmonic Laboratory, Belarusian State University of Informatics and Radioelectronics, Minsk, Belarus
[3]Department of Physics, Kaunas University of Technology, Kaunas, Lithuania
augusto.hernandez@ktu.edu, nadzeya.khinevich@ktu.edu

Raman scattering spectroscopy is widely used for different applications that include chemistry, material science, medicine and biomedical sensing [1]. Since the discovery of the surface-enhanced Raman scattering (SERS) effect scientists have started to produce specialized substrates suitable for detection and study of extremely low concentrations of biomolecules by SERS spectroscopy. Most commonly, SERS-active substrates incorporate nanoscale noble metal particles of various shapes in colloidal solutions or placed on glass and silicon substrates. Certain plasmonic nanoparticle arrangements on the diffraction gratings have demonstrated an increase in the Raman signal enhancement up to a four-time [2].

In this work, we demonstrate a highly efficient combination of silver nanoparticles (AgNPs), porous silicon (PS) and diffraction grating for SERS application. Diffraction grating of 6-15 μm pitch was produced in n-type silicon wafer substrates by Yb:KGW femtosecond laser ablation. Different quality periodical lines in silicon where achieved varying the pulse densities and energies per pulse. Afterwards, the diffraction gratings were porosified by the electrochemical etching in an electrolyte based on a hydrofluoric acid. Silver colloids were synthesized following the Turkevich protocol [3] and exhibited a localized surface plasmon resonance related absorbance band in the blue range of the visible spectrum. Ag NPs were adsorbed on top of the PS grooves by exposing them to the colloid solutions for 1 hour. The same process was carried out for 3 days for periodical grooves formed on monocrystalline silicon wafers.

Morphologies of the produced structures were studied by scanning electron microscopy. Dependence of the resulting grooves' width on the number of applied laser processing parameters was determined. Major differences of the AgNPs deposition density on PS and monocrystalline silicon diffraction gratings were observed. SERS activity was evaluated using 3D scanning confocal Raman spectroscopy with a 633 nm laser and using Rhodamine 6G (R6G) as the test analyte.

AgNP-covered PS diffraction gratings demonstrated expressed SERS signal of R6G. The enhanced of Raman scattering signal is two times higher in the grooves compared to the ridge of the investigated periodical structures (see Fig. 1). In contrary, pristine Ag NP-covered silicon diffraction grating was not demonstrating any useful signal enhancement.

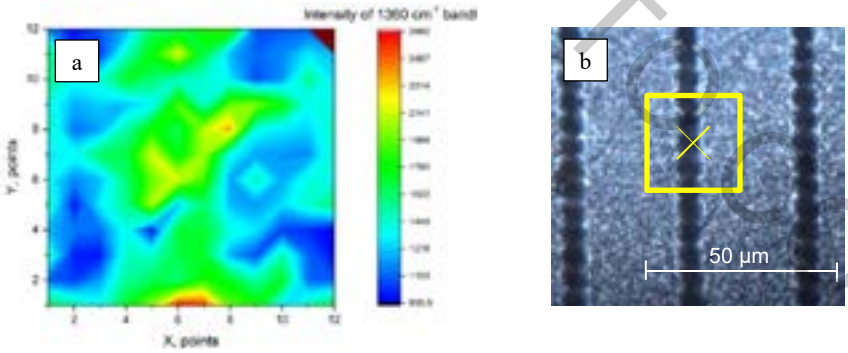

Fig. 1. Distribution map of the SERS-signal intensity of the 1360 cm^{-1} band in the SERS spectra of R6G (a) and surface image (b) of the sample with the identified area of investigation.

In summary, new type of SERS substrates based on the AgNPs in diffraction gratings of porous silicon were demonstrated. The preliminary results of the enhancement of Raman scattering are promising towards development of methods for highly sensitive detection of organic compounds.

This research was funded by the European Social Fund under the No. 09.3.3-LMT-K-712 "Development of Competences of Scientists, other Researchers and Students through Practical Research Activities" measure.

[1] Schrader, Bernhard, ed. *Infrared and Raman spectroscopy: methods and applications (*John Wiley & Sons, 2008).
[2] J. Wang, Z. Jia, and C. Lv, "Enhanced Raman scattering in porous silicon grating," Opt. Express **26 (6)**, 6507 (2018).
[3] Mazzonello, A. Valdramidis, V. "Synthesis and characterization of silver nanoparticles", International Journal of Engineering Research **7 (3)**, 41 (2017).

CANCELLED DUE TO COVID-19

CHANGES OF ELECTRIC AND MAGNETOTRANSPORT PROPERTIES OF δ-LAYERS DUE TO SWIFT HEAVY IONS IRRADIATION

Alexander K. Fedotov[2], Uladzislaw E. Gumiennik[1,2] , Dmitry V. Yurasov[3,4], Alexey V. Novikov[3,4], Pavel Yu. Apel[5,6]

[1] Belarusian State University, Praspiekt Niezaliežnasci 2, 220030 Minsk, Belarus
[2] Institute for Nuclear Problems, Belarusian State University, Babrujskaja Str. 11, 220030 Minsk, Belarus
[3] Institute for Physics of Microstructures, Russian Academy of Sciences, 603950 Nizhny Novgorod, Russia
[4] Lobachevsky State University of Nizhny Novgorod, 603950 Nizhny Novgorod, Russia
[5] Joint Institute for Nuclear Research, 6 Joliot-Curie Str., 141980 Dubna, Russia
[6] Dubna State University, 19 Universitetskaya Str., 141982 Dubna, Russia
gumennik@bsu.by

CANCELLED DUE TO COVID-19

Dopant distribution profiles in semiconductors (known as δ-layers) are the subject of interest for fabricating nanoscale electronic devices as well as for the study of carrier transport in low-dimensional structures [1]. *Sb* δ-doping of *Si* by molecular beam epitaxy (MBE) has received much attention in view of their application in such devices as tunnel diodes and heterojunction bipolar transistors. The creation of sharp *n*-type dopant profiles in *Si* during MBE growth is challenging due to the pronounced surface segregation of the mostly used dopants like *Sb*, *P* and *As*.

The δ-doped layer was formed using the selective doping technique described in [2] and the growth procedure is described in brief below. After standard cleaning of *Si* substrate a 100 *nm* thick *Si* buffer layer was deposited at 550 in order to obtain an atomically flat *Si* surface. Then temperature was dropped down to 350^oC and a certain amount of *Sb* was deposited and then capped by a 2 *nm* thick *Si* layer at such a low temperature. This allowed us to obtain a sharp rise in doping concentration. In order to obtain a sharp drop in *Sb* bulk concentration the growth was inter-rupted, temperature was raised up to 535^oC and a 75 *nm* thick *Si* capping layer was deposited at this temperature. Due to the very high value of segregation ratio at 535 [2], the *Sb* incorporation is negligible that allowed obtaining the sharp decrease in *Sb* bulk concentration.

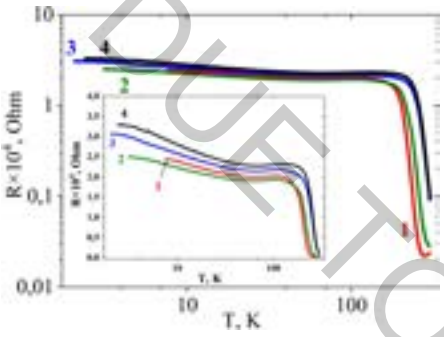

Fig. 1. Resistance $R_{Sq}(T)$ before (1) and after SHI irradiation D: $1{\cdot}10^8$ (2), $1{\cdot}10^9$ (3), $1{\cdot}10^{10}$ (4) and $5{\cdot}10^{10}$ ion/cm^2 (5).

Temperature and magnetic field dependences of the electrical resistance$R(T,B)$ in the temperature range of $2 < T < 300$ K and magnetic induction $B{\leq}8T$ before and after the SHI irradiations were measured. After initial electric characterization, the samples were irradiated with the fluence of $D = 1{\times}10^8$ ion/cm^2 at room temperature by 167 MeV Xe^{+26} ions at the IC-100 cyclotron at FLNR JINR, Dubna (Russia). This procedure is repeated two more times with $D = 1{\times}10^{10}$ cm^{-2}, $5{\times}10^{10}$ cm^{-2}. The ion beam homogeneity to 5 % on irradiating specimen surface has been reached using the beam scanning in horizontal and vertical directions. Average Xe ion flux was about $5{\times}10^7$ $cm^{-2}s^{-1}$ thus excluding any target heating.

Electron transport in $Si < Sb > \delta$-layer grown by MBE was studied in detail at temperatures lower than 15 K and in magnetic fields B up to 8 T before and after three acts of the 167 MeV Xe^{+26} ion irradiation with ion fluence $1{\times}10^8$ cm^{-2}, $1{\times}10^{10}$ cm^{-2}, $5{\times}10^{10}$ cm^{-2}. It was shown that the low temperature conductivity in δ-layer is described by the theory of 2D quantum corrections to conductivity in the case of weak localization Eq. 1.

$$MR = \frac{\Delta R_{sqr}(B,T)}{R_{sqr}(B,T)} = R_{sqr}(B,T)\frac{e^2}{2\pi\hbar}\left\{\psi\left[\frac{1}{2}+\frac{B_i}{B}\right] - ln\left[\frac{B}{B_i}\right]\right\}. \quad (1)$$

where R_{sqr} - sheet resistance, B - magnetic induction, ψ - digamma function, $B_i = \frac{\hbar}{4eD_d\tau_{Th}} = \frac{\hbar}{4eL_{Th}}$, D_d - diffusion coefficient of carriers, τ_{Th} - the phase failure, L_{Th} - Thouless length.

In so doing, SHI irradiation results in decrease of Thouless length from 14.08 to 5.17 *nm*.

[1] Y. Imry, Nanostructures and Mesoscopic Systems, (Academic, New York, USA 1992).
[2] D.V. Yurasov et al., Usage of antimony segregation for selective doping of Si in molecular beam epitaxy, J. Appl. Phys. *109*, 113533 (2011).

REACTIVE MAGNETRON SPUTTERING OF ALUMINIUM OXYNITRIDE FILMS FOR OPTICAL COATINGS APPLICATIONS

Naglis Kyžas[1], Alexandr Belosludtsev[1], Algirdas Selskis[1]

[1]Center for Physical Sciences and Technology, Lithuania
naglis.kyzas@ftmc.lt

Reactive Magnetron Sputtering (RMS) is a Physical Vapor Deposition (PVD) technology used widely in both scientific investigation and commercial coating production. The RMS processes without appropriate process control can be accompanied by problems, such as uncontrolled transition to a fully poisoned target state (with a significant drop in deposition rate), process drift, arcing, poor run-to-run repeatability. Those are main limiting factors to use RMS technology in deposition of high quality optical coatings for precise laser optics.

Previously, in our laboratory RMS of metallic Hf, Zr, Nb and Sc targets, showed unique possibilities to control deposition process by combined different feed-back signals, leading high refractive index and low loss HfO_2, ZrO_2, Nb_2O_5 and Sc_2O_3 film deposition, suitable for laser optics application [1].

Oxynitrides are materials with yet unexplored physical and functional properties with great potential for industrial applications [2]. With one metal target in various gas mixture it is possible effectively control oxynitride film composition and properties. In optical applications, oxynitride materials might be used, for example, as selective absorber, for antireflective coating for solar cells, rugate, edge filters and sensors.

In this research [3], investigation of aluminum oxynitride films deposition using one metallic target in various gas mixtures was done. The optimized preparation conditions for such RMS process were found. Non-optimized conditions led to sputtering target poisoning or under stoichiometric films formation. Dependence between gas composition and changes of nitrogen concentration in the film and their properties was investigated. The possibility of using oxynitride films for antireflective coatings (AR) deposition was shown. Such coatings were compared with the traditional ones that consist of high refractive index – low refractive index layers combination. Oxynitrides films allow producing AR coating in less number of layers. Moreover, this coatings might be made in a form of quasi-continuous coating with less deposition time and reduced stress in comparison to traditional approach.

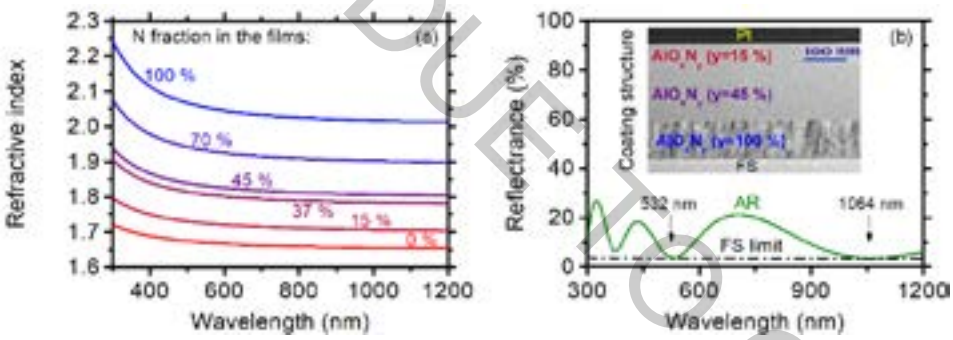

Fig. 1. Refractive index of aluminium oxynitrides prepared with various nitrogen fraction in the films (a) and reflectance spectra with the AR coating structure (b).

[1] A. Belosludtsev, K. Juškevičius, L. Ceizaris et al., Correlation between stoichiometry and properties of scandium oxide films prepared by reactive magnetron sputtering, Applied Surface Science **427**, 312-318 (2018).
[2] F. Vaz, N. Martin, M. Fenker, eds., Metallic Oxynitride Thin Films by Reactive Sputtering and Related Deposition Methods: Process, Properties and Applications, Bentham Science Publishers (2013).
[3] A Belosludtsev, N. Kyžas, A. Selskis et al., Design, preparation and characterization of antireflective coatings using oxynitride films, Optical Materials **98**, 109430 (2019).

CORRECTED PUBLICATION COVID-19

INFLUENCE OF CATALYST ON SYNTHESIS AND PROPERTIES OF STARCH ACETATE

Ugne Naruseviciute, Laura Peciulyte

Department of Polymer Chemistry and Technology, Kaunas University of Technology
ugne.naruseviciute@ktu.edu

Starch acetate based on a sustainable native polymer can be used as a thermoplastic substance for replacement nondegradable plastic products. The acetylation of potato starch with acetic anhydride and sodium hydroxide/ calcium oxide as catalysts was investigated in this work. Low and high temperature starch acetylation reactions were carried out at 45°C and 123°C, respectively, by using Mark and Mehltretter method [1] with some modifications (see Fig. 1.).

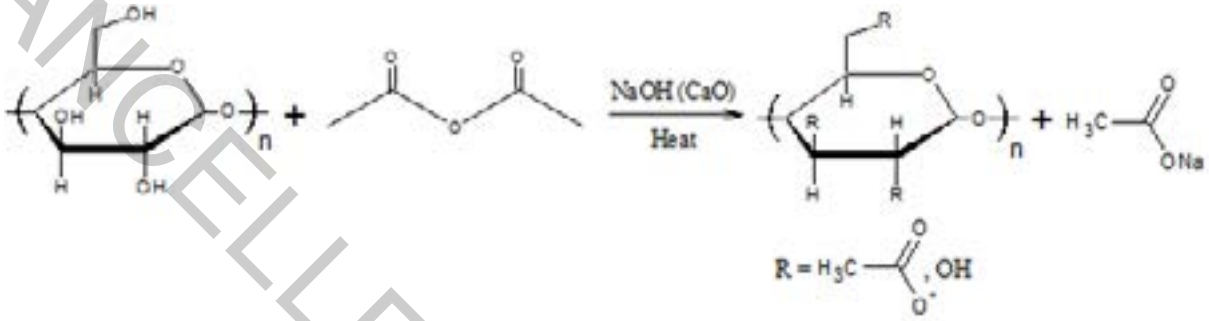

Fig. 1. Reaction scheme of starch acetylation

The effects of process variables such as temperature (45 and 123 °C), NaOH and CaO to starch ratio (0–2.75 mol/mol AGU) and reaction time (1–40 hours) on the degree of substitution (DS) of acetyl groups were investigated (Table 1). At these conditions, acetylated potato starches with DS values ranging from 0.22 to 1.10 were obtained.

Table 1. Influence of reaction parameters on DS of acetylated starch

Sample No.	Starch: NaOH: CaO:Acetic anhydride molar ratio	T, °C	Time, h	DS
1	1: 0.04: 0: 3	45	16	0.30
2	1: 0.04: 0: 3	45	40	0.26
3	1: 0.08: 0: 3	45	16	0.30
4	1: 0.08: 0: 3	45	40	0.31
5	1: 0.04: 0.04: 3	45	16	0.22
6	1: 0.04: 0.04: 3	45	40	0.35
7	1: 0.08: 0.04: 3	45	16	0.26
8	1: 0.08: 0.04: 3	45	40	0.30
9	1: 2.75: 0: 3	123	1	0.50
10	1: 2.75: 0: 3	123	2	0.70
11	1: 2.75: 0.04: 3	123	1	0.80
12	1: 2.75: 0.04: 3	123	2	1.10

It was determined that at low temperature reaction conditions the DS of the obtained products was affected to higher degree by NaOH content than CaO content. The DS of the samples prepared at 123 °C was higher than that of the samples obtained at 45 °C. CaO had significant influence on DS only at high temperature conditions. Moreover, the DS of acetylated starch obtained at high temperature conditions by using CaO was higher than that synthesized without CaO. Obtained acetylated starches were characterized by infrared spectroscopy, microscopy and thermal analysis.

[1] Y. Xu, V. Miladinov and A. Hanna, Synthesis and Characterization of Starch Acetates with High Substitution, Cereal Chemistry, 735-740 (2004).

CANCELLED DUE TO COVID-19

POLYMER SYSTEM FOR DECONTAMINATION OF PHOSPHORORGANIC TOXIC SUBSTANCES

Serhii Mazura[1], Volodymyr Bessarabov[1], Liubov Vakhitova[2]

[1] Department of Industrial Pharmacy, Kyiv National University of Technologies and Design, Ukraine
[2] Department of Research of Nucleophilic Reactions, L. M. Litvinenko Institute of Physical-Organic Chemistry and Coal Chemistry National Academy of Sciences of Ukraine, Ukraine
s.mazura@kyivpharma.eu

CANCELLED DUE TO COVID-19

Particularly hazardous substances of organophosphorus (OP) nature are very dangerous for human health and the environment. Many pesticide active constituents used in agriculture (paraoxon, methyl parathion, glyphosate, chlorophos), as well as chemical weapons and active pharmaceutical ingredients, are known or possible carcinogens, produce acute or chronic toxic effects, suppress immunity, cause disorders of the endocrine, central and peripheral nervous systems [1]. There is also evidence that OP have a negative effect on reproductive function, are teratogens, and pose an increased risk to children [2]. That is why one of the priorities of the chemical industry of Ukraine and the EU in general is the search for systems of OP decontamination and elimination of consequences of their action.

An effective method of OP destruction is alkaline hydrolysis in the presence of peroxide anion (HOO^-) [3]. Hydrogen peroxide (H_2O_2) was selected as the donor of these anions.

In this work, a decontamination composition with special rheological properties is developed, which makes it easy to apply to the skin and reduces the irritating effect of alkali. It is a highly alkaline solution (pH 13.0) of sodium hydroxide (NaOH) and H_2O_2. A pharmaceutically acceptable polymer (POL) was used to provide rheological properties.

Kinetic studies of the rate of decay of paraoxon by spectrophotometric method were also performed. Several systems were investigated: aqueous NaOH solutions with different hydrogen indexes (12.7 - 13.0) to determine the optimum pH at which the reaction rate is the highest; NaOH solution (pH 13.0) with POL; a solution of NaOH (pH 13.0) with H_2O_2; NaOH solution (pH 13.0) with H_2O_2 and POL (Fig. 1).

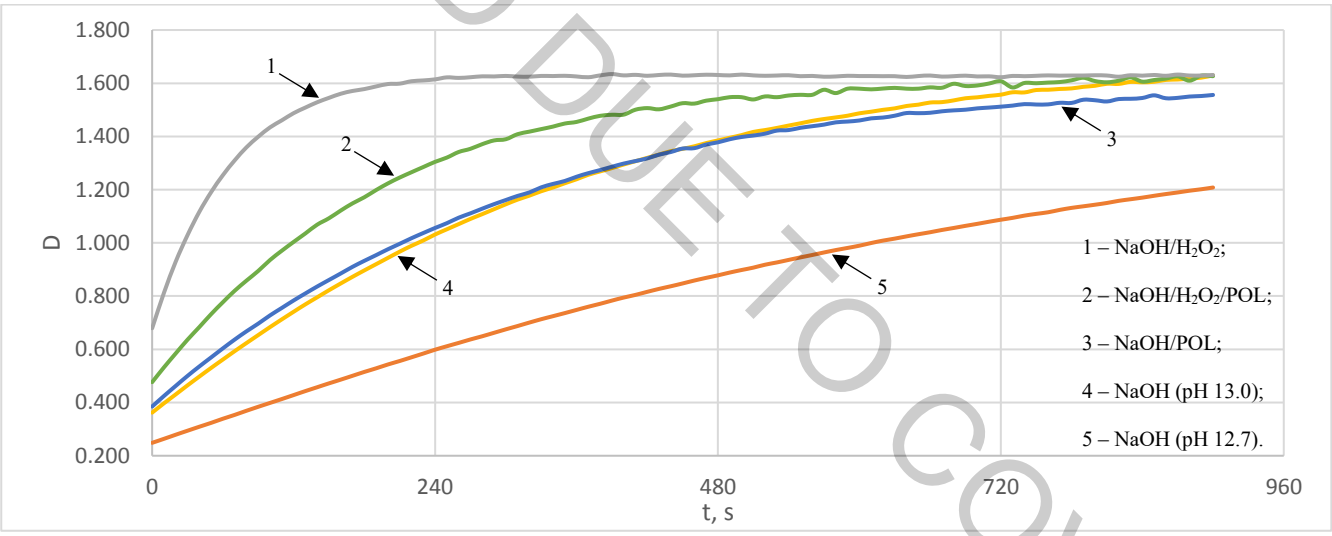

Fig. 1. Kinetics of decomposition of paraoxon depending on the composition of decontamination systems

As a conclusion, the reaction rate is directly proportional to the pH, so the most alkaline solution (pH 13.0) should be used (curves 4, 5). In a system with aqueous NaOH solution, POL does not affect the decontamination rate (curves 3, 4). Addition H_2O_2 to the system increases the reaction rate (curve 1). The POL system exhibits greater stability over time, but a lower reaction rate during the first decontamination time (curve 2). In our composition, POL exhibits stabilizing properties, which has been demonstrated by reproducibility of results over several weeks.

[1] G. Liu, Q. Tang, Y. Zhou, X. Cao, J. Zhao, D. Zhu, Photo-induced phosphate released from organic phosphorus degradation in deionized and natural water, Photochemical & Photobiological Sciences Vol. 16, Issue 4, 467–475 (2017). doi: 10.1039/c6pp00313c
[2] J. Martin- Reina, J. A. Duarte, L. Cerrillos, J. D. Bautista, M. M. Soliman, Insecticide Reproductive Toxicity Profile: Organophosphate, Carbamate and Pyrethroids, Journal of Toxins Vol. 4, Issue 1, 01–07 (2017). doi: 10.13188/2328-1723.1000019
[3] L. Vakhitova, V. Bessarabov, N. Taran, G. Kuzmina, G. Zagoriy, O. Baula, A. Popov, Decontamination of methyl parathion in activated nucleophilic systems based on carbamide peroxisolvate, Eastern-European Journal of Enterprise Technologies Vol. 6, 10 (90), 31-37 (2017). doi: 10.15587/1729-4061.2017.119495

SUPPRESSED CONCENTRATION QUENCHING BY 3,5-DI-TERT-BUTYL-PHENYL SUBSTITUTION IN RUBRENE FOR SOLID-STATE PHOTON UPCONVERSION

Manvydas Dapkevičius[1], Edvinas Radiunas[1], Steponas Raišys[1], Augustina Jozeliūnaitė[2], Tomas Javorskis[2], Ugnė Šinkevičiūtė[2], Edvinas Orentas[2], Saulius Juršėnas[1], Karolis Kazlauskas[1]

[1]Institute of Photonics and Nanotechnology, Vilnius University, Lithuania
[2]Department of Organic Chemistry, Vilnius University, Lithuania
manvydas.dapkevicius@ff.vu.lt

Photon upconversion (UC) through triplet-triplet annihilation is a phenomenon that can be used to increase solar cell efficiency,[1] activation of drugs inside organic tissue,[2] bio-imaging[3] and others[4]. Rubrene is an excellent material for near-infrared to visible UC, since it features efficient photoluminescence (PL) in isolated phase with PL quantum yield (QY) of 100%. High PLQY enables efficient UC in solutions, but for practical applications, the solid-state UC is of higher interest. However, rubrene suffers from aggregation induced PL quenching, which hampers UC performance in the solid-state. Therefore, to diminish concentration quenching in the solid films the chemical modification of the rubrene is necessary to attain higher UCQY.

In this work, optical properties of new rubrene-based derivatives with 3,5-di-tert-butyl-phenyl substituents are reported (Fig. 1). Photophysical properties of the rubrene compounds in solid polystyrene (PS) doped films were assessed by measuring PL spectra and PLQY. In addition, sensitized UC films with high emitter concentrations were prepared and UCQY were measured. Due to sensitivity of the rubrene to oxygen, sample series were prepared in N_2 environment (O_2 and H_2O < 0.1 ppm) and encapsulated between two glass slides using epoxy glue. To assess the degree of aggregation, rubrene derivatives were dispersed in PS matrix with increasing its concentration and PLQY was determined using integrating sphere (Fig. 1).

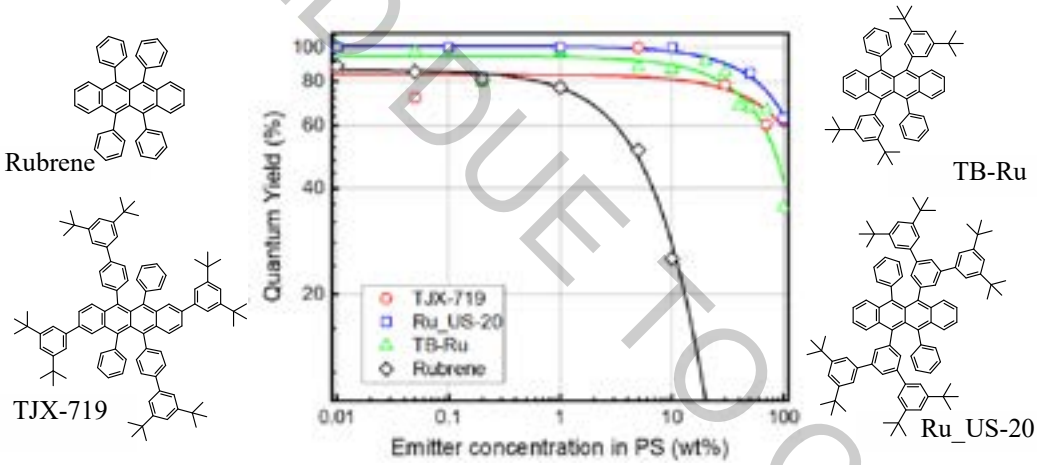

Fig. 1. Chemical structure of rubrene derivatives and PLQY dependence on emitter concentration in PS.

Experimental results indicate that the lowest absorption peak depends on the position of the substituents attached. Absorption band of the TJX-719 it is redshifted, while for Ru_US-20 is blue shifted as compared to unsubstituted rubrene. Absorption spectrum of TB-Ru is virtually unchanged as compared to rubrene. Generally, quantum yields of rubrene derivatives were found to be high (close to 100%) at low emitter content in the PS matrix. However, PLQY of the rubrene films experienced rapid drop with increasing emitter concentration already above 1 wt%, whereas 3,5-di-tert-butyl-phenyl substituted rubrene derivatives showed persistently high PLQY up to 30 wt% and only above this concentration slight decrease of PLQY was observed. In the neat rubrene film (at 100 wt% of emitter) PLQY drastically decreased down to 1.5%, which is ascribed to the formation of crystalline aggregates facilitating singlet fission.

4-fold higher UCQY were attained in the sensitized TB-Ru PS films as compared with rubrene due to reduced concentration quenching, however higher number of substituents in TJX-719 and Ru_US-20 resulted in reduced triplet exciton transfer rate and consequently lower UCQY.

[1] A. Nattestad, Y.-Y. Cheng, R.-W. MacQueen, et al., Dye-sensitized solar cell with integrated triplet–triplet annihilation upconversion system, J. Phys. Chem. Lett. **4**, 2073-2078 (2013).
[2] S.-H.-C. Askes, M.-S. Meijer, T. Bouwens, et al., Red light activation of Ru(II) polypyridyl prodrugs via triplet-triplet annihilation upconversion: feasibility in air and through meat, Molecules **21**, 1460 (2016).
[3] F. Liu, T. Yang, W. Feng, F. Li, et al., Blue-emissive upconversion nanoparticles for low-power-excited bioimaging in vivo, J. Am. Chem. Soc. **134**, 5390-5397 (2012).
[4] J. Zhou, Q. Liu, W. Feng, et al., Upconversion luminescent materials: advances and applications, Chem. Rev. **115**, 395-465 (2014).

CANCELLED DUE TO COVID-19

TERT-BUTYL-PHENYL RUBRENE EMITTER FOR TRIPLET-TRIPLET ANNIHILATION MEDIATED NIR-TO-VISIBLE PHOTON UPCONVERSION

Lukas Naimovičius[1], Edvinas Radiunas[1], Karolis Kazlauskas[1], Steponas Raišys[1], Augustina Jozeliūnaitė[2], Tomas Jarovskis[2], Ugnė Šinkevičiūtė[2], Edvinas Orentas[2]

[1]Institute of Photonics and Nanotechnology, Vilnius University, Lithuania
[2]Department of Organic Chemistry, Vilnius University, Lithuania
lukas.naimovicius@ff.stud.vu.lt

CANCELLED DUE TO COVID-19

Triplet-triplet annihilation (TTA) mediated NIR-to-visible photon upconversion (UC) has made a significant breakthrough in the field of photonics in recent years. [1] TTA-UC has promising applications in photovoltaic, photocatalysis, night vision and bio-imaging devices, among others. [2] UC systems are typically composed of a sensitizer and emitter. Sensitizer is responsible for absorption and triplet generation whereas emitter accumulates triplets and undergoes TTA. However, several challenges related to poor sensitizer absorption in the NIR range and low UC quantum yield are yet to be overcome. Rubrene (Rub) is widely used emitter (annihilator) in NIR-to-visible UC, although its tendency to aggregate at high concentrations severely limits TTA-UC performance. Thus, alteration of Rub molecular structure to suppress aggregation is one of the prime tasks.

The research focus of this work is laid on the examination of an impact of tert-butyl-phenyl (tbp) moieties on the concentration quenching as well as other photophysical parameters of annihilator for boosting UC quantum yield. To this end, photophysical properties of tbp-Rub emitter including absorption, emission, excited state lifetime and quantum yield were thoroughly assessed. Absorption spectrum of dilute toluene solution (10^{-5} M) of tbp-Rub exhibited vibronic structure with the peaks centered at 463 nm, 492 nm and 527 nm whereas fluorescence (similar to unmodified Rub) was peaking at 560 nm. Fluorescence quantum yield measurements carried out by using integrated sphere have shown that tbp-Rub in the isolated form is nearly 100% efficient. For UC measurements sample solutions and films with different concentration of emitter and phthalocyanine (PdPc) sensitizer in the polystyrene matrix were prepared in nitrogen glovebox (O_2 and H_2O concentration <0.1 ppm). Furthermore, UC intensity dependence from excitation power density was investigated and the threshold for TTA-UC was estimated to be 40 W/cm^2. Being considerably higher as compared to the threshold of unmodified Rub UC system (~2 W/cm^2), it demonstrates the negative impact of alkyl moieties in Rub on the performance of UC solutions.

In summary, although the introduction of tbp spacers into Rub enabled to suppress aggregation and enhance fluorescence yield, this substantially increased UC threshold making tbp-Rub emitter less suitable for practical NIR-to-visible UC applications.

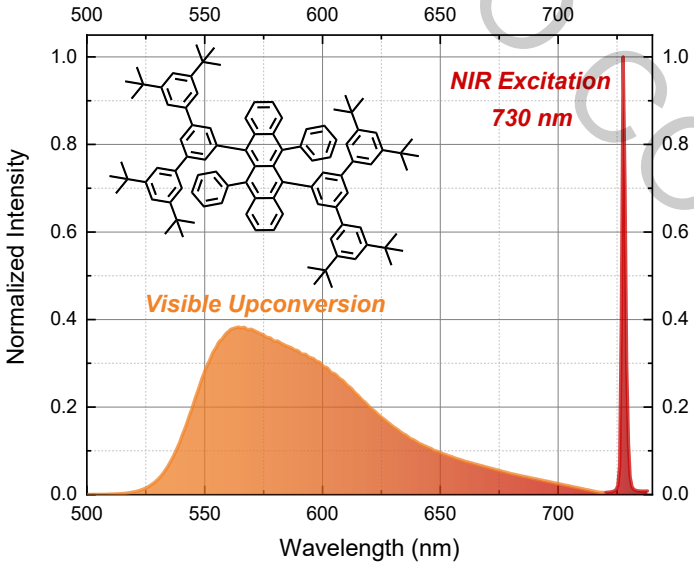

Fig. 1 NIR-to visible photon UC spectrum of PdPc-sensitized tbp-Rub system.

[1] M. Wu et al., "Solid-state infrared-to-visible upconversion sensitized by colloidal nanocrystals," Nat. Photonics, vol. 10, no. 1, pp. 31–34, (2016)
[2] J. Zhou et al., "Upconversion luminescent materials: Advances and applications," Chem. Rev., vol. 115, no. 1, pp. 395–465, (2015)

TRIPHENYLAMINE- AND CARBAZOLE-BASED COMPOUNDS EXHIBITING DELAYED FLUORESCENCE

Uliana Tsiko, Galyna Sych, Yan Danyliv, Iryna Hladka, Juozas Vidas Grazulevicius

Department of Polymer Chemistry and Technology, Kaunas University of Technology, Lithuania
ulyana.ziko@gmail.com

Organic electroactive materials are widely used in organic optoelectronic devices. Organic semiconductors with donor-acceptor structures are widely applied in organic light diodes (OLEDs) [1]. Compounds exhibiting thermally activated delayed fluorescence in solid state are ideal emitters for implementation in non-doped OLEDs [2].

The compounds containing pyrimidine electron-withdrawing moiety and electron-donating moieties such as triphenylamine and carbazole were synthesized and investigated (Fig1.).

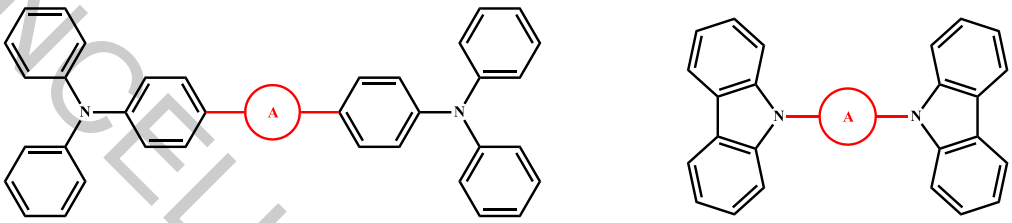

1 **2**

Fig. 1. General structures of triphenylamine- and carbazole based compounds

The toluene solution of compound **1** containing triphenylamino moiety demonstrated sky-blue emission with photoluminescence intensity maximum centered at 486 nm while this compound in solid state exhibited emission with the intensity maximum at 506 nm (Table 1.). The toluene solution of compound **2** emitted light in blue region with emission maximum at 466 nm and the film of the compound with carbazole units exhibited emission in sky-blue region with maximum at 488 nm. The compound containing triphenylamine moieties demonstrated high photoluminescence quantum yield of 45 % in solid state and in toluene solutions (83 %). Compound **2** exhibited lower value of photoluminescence quantum yields of 33 % and 2 % in solid state and toluene solutions respectively. Both the compounds showed thermally activated delayed fluorescence.

Table 1. Photophysical characteristics of compounds **1** and **2**

Compounds	λ^{Tol}_{PL}, nm	λ^{film}_{PL}, nm	Φ^{Tol}_{PL}, %	Φ^{film}_{PL}, %
1	486	506	83	45
2	466	488	2	33

[1] Goushi K., Yoshida K., Sato K. et. al., Organic light-emitting diodes employing efficient reverse intersystem crossing for triplet-to-singlet state conversion, Nat. Photonics **6**, 253–258 (2012).
[2] Guo J., Li X.-L. Nie H. et. al., Achieving High-Performance Nondoped OLEDs with Extremely Small Efficiency Roll-Off by Combining Aggregation-Induced Emission and Thermally Activated Delayed Fluorescence. Adv. Funct. Mater. **27**, 1606458 (2017).

CANCELLED DUE TO COVID-19

UV STABILITY OF THERMOCHROMIC MICROCAPSULES FOR SMART POLYMER COMPOSITE STRUCTURES

Olga Bulderberga, Edvins Druska, Andrey Aniskevich

Institute for Mechanics of Materials, University of Latvia, Latvia
edvinsdruska@inbox.lv

By incorporation of stimuli-responsive microcapsules into a composite structure, the application possibilities of its could be extended. Such a smart structure is not only a part of the construction but also implements an integrated function of sensors. Encapsulated thermochromic dyes could be relatively simply mixed into a polymer structure and they can perform the function of detecting an increase in ambient temperature where it is important for the structure as a whole. The ability of thermochromic material to alter its light absorption and emission parameters upon the crystalline phase (liquid crystal dye) or chemical form (leuco dye) change induced by a change in temperature is applied. A dramatic visual colour change of the material will occur when the temperature reaches a certain threshold value set by the thermochromic material manufacturing process. Dyes are known victims of intense ultraviolet degradation in the form of colour fade and colour change due to chromophore chemical bond damage. Despite the fact that the thermochromic dye is encapsulated to protect it from the effects of environmental factors, even encapsulated it still remains sensitive to UV. Thermochromic microcapsule colours are visible with the naked eye due to their capsule shells being transparent, exposing the thermochromic core and letting light interact with chromophores through absorption and emission. This naturally raises the question of whether these microcapsules are viable for use under direct sunlight as ultraviolet radiation is part of the total terrestrial insolation spectrum.

The aim of the work is to evaluate the effect of UV light on the service-life of thermochromic microcapsules. To achieve the aim several tasks were outlined:

1. Define the method of colour change control and quantitative evaluation.
2. Experimentally define colour changes of thermochromic microcapsules integrated into the polymer structure under UV exposure.
3. Define the critical time of UV exposure for thermochromic microcapsules integrated into the polymer structure.

Thermochromic microcapsules with a colour change at temperatures 31, 40, and 50 °C were mixed into acrylic paint as a polymer matrix. Samples as thin films were prepared. Samples were exposed by UV (radiation energy 24.6 W for wavelength 240 - 320 nm) for the time interval from some minutes to 72 hours. The difference in colour change, as well as the ability to change colour after the increase of temperature, was evaluated vs. the time of UV exposure. The trend of experimental results indicates that there is a certain time of UV exposure where thermochromic pigment in microcapsules has degraded to the point of not showing the colour difference after the increase of temperature.

Colour change of samples was evaluated by images made in the photo light box (thus excluding the influence of ambient lighting in the room) and treated in Adobe® Photoshop® software. Images were converted to grayscale and Info tool was used to obtain K value from grayscale images. K is a value in 8 bit CMYK colour scheme graded from white (255 = 0%) to black (0 = 100%) in percent.

In the result of the work it was defined that for microcapsules with different colour change temperatures, time of UV exposure leading to pigment degradation is not the same. The pigments in microcapsules used for colour change at 40 °C, and 50 °C are more stable to UV compared to the pigment used for colour change at 30 °C.

CANCELLED DUE TO COVID-19

PRODUCTION OF VARIOUS SIZE ORGANIC PHOTOVOLTAIC CELLS WITH P3HT:PC61BM AS AN ACTIVE LAYER

Dominik Suwala[1], Grzegorz Wryk[2],
Aleksandra Szymanska[3], Krzysztof Domanski[4],
Alicja Kalucka, Ola Bednarczyk, Dana Binczuk
Wojciech Mech, Adam Wincukiewicz, Maciej Krajewski,
Joanna Sitnicka, Krzysztof P. Korona, Maria Kaminska

Faculty of Physics, University of Warsaw, Pasteura 5 st. 02-093, Warsaw
[1]d.suwala@student.uw.edu.pl, [2]g.wryk@student.uw.edu.pl,
[3] a.szymanska40@student.uw.edu.pl, [4]k.domanski5@student.uw.edu.pl

CANCELLED DUE TO COVID-19

Due to climate changes and increasing global warming developing effective renewable energy sources is crucial. Organic photovoltaics (OPV), although demonstrate much lower efficiencies than its inorganic counterparts, still provide unique possibilities. They are much cheaper than silicon cells and moreover, can be deposited on flexible substrates, which opens potential for new niches such as wearable electronics and building incorporated panels.

Although promising, OPV suffers from relatively low efficiencies (c.a. $5-7\%$) that for time being are the main obstacle in the way for further commercialization. The two major reasons behind this behavior are short exciton diffusion lengths and very low carrier mobility in an active layer.

In this work we present organic solar cell structures with P3HT:PC61BM mixture in weight ratio 1:0.6 as the active layer. P3HT (Poly(3-hexylthiophene-2,5-diyl)) is a conductive polymer with absorption edge in the visible region working as an electron donor. PC61BM is a C_{60} fullerene derivative working as an acceptor. In our research we focus on the optimization of the deposition parameters, i.e. active layer annealing temperature, spin coating rotation speed and used solvents. Also, to test scalability of our method we prepare the cells onto indium-tin oxide substrates with two, substantially different sizes: 3 cm^2 and 25 cm^2.

As the result we present absorption spectra of the P3HT and PC61BM. Regarding solar cells, I-V characteristics, photocurrent and external quantum efficiency measurements will be discussed.

EFFECT OF ANNEALING ON EXCITED STATES RELAXATION IN FPMAI/$MAPBI_3$ PEROVSKITE NANOPARTICLES

Laurynas Endriukaitis[1], Andrius Devižis[2]

[1] Institute of Photonics and Nanotechnology, Faculty of Physics, Vilnius University, Lithuania
[2] Department of Molecular Compound Physics, Center for Physical Sciences and Technology, Vilnius, Lithuania
Laurynas.endriukaitis@gmail.com

Organic – inorganic hybrid perovskites have emerged as low cost semiconducting materials with promising optoelectronic properties which can be used to create photovoltaic cells, perovskite light-emitting diodes (PeLEDs) and lasers [1]. It was observed that external quantum efficiency of electroluminescence of PeLEDs based on $CH_3NH_3PbI_3$ ($MAPbI_3$) perovskite with addition of 4-fluorobenzylammonium iodide (FPMAI) changes upon annealing. As photovoltaic cells and lasers can reach high temperatures it is important to understand exactly what effect does annealing have.

In order to elucidate the factors that play a role in appearing differences between two $MAPbI_3$/FPMAI samples, one of which was annealed, the pump – probe optical spectroscopy was used. When various pump impulse intensities were applied in pump – probe experiment, no significant differences between samples were observed. Although, when pump impulse intensity was a constant and temperature of samples was varied in 293 K – 10K range, a major difference in charge carrier recombination time was noticed according to the dynamics of ground state bleaching detected at the wavelength of 750 nm. Moreover, not annealed sample had extra regions of absorption at wavelength interval of 600 – 650 nm. These differences might occur because sample with no annealing is made of heterogeneous crystallites. There are small regions inside crystallite with different energies. When perovskite is annealed, these regions are eliminated and crystallites become homogeneous.

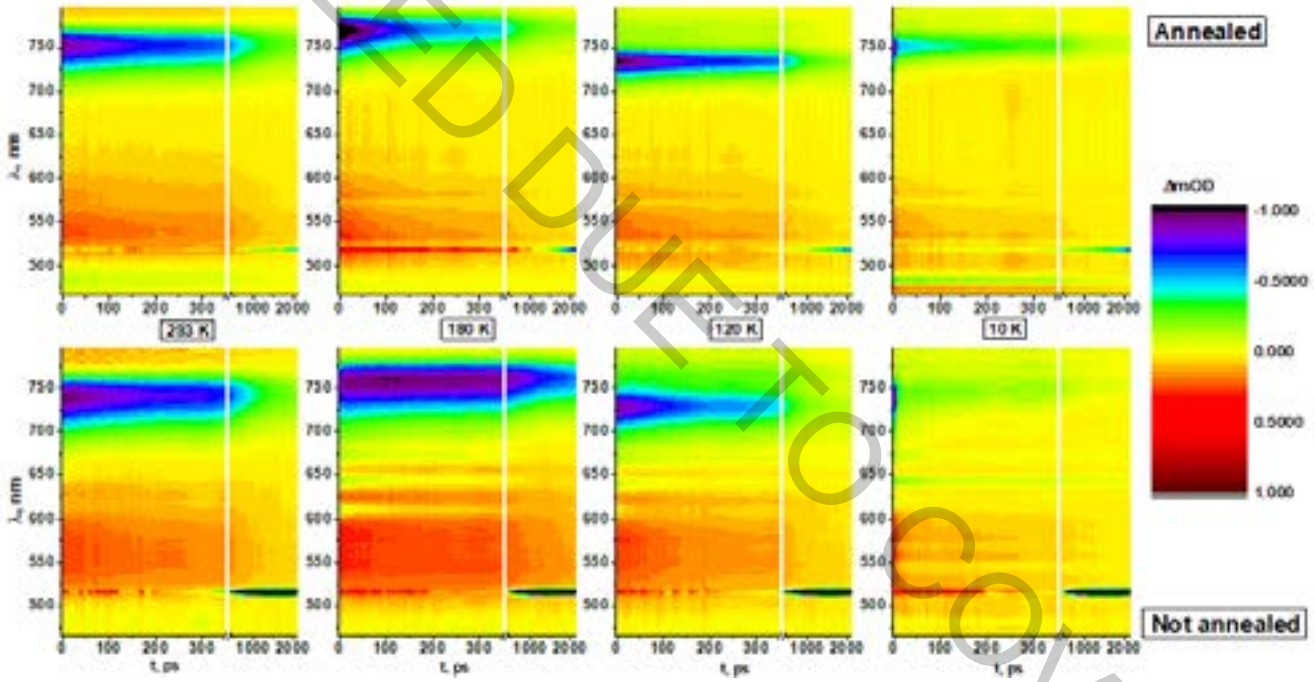

Fig. 1. Transient absorption of annealed and not annealed $MAPbI_3$ /FPMAI films at different temperatures. Excitation wavelength 515 nm.

[1] Zhao L, Rolston N, Lee KM, Zhao X, Reyes-Martinez MA, Tran NL, et al. Influence of Bulky Organo-Ammonium Halide Additive Choice on the Flexibility and Efficiency of Perovskite Light-Emitting Devices. Advanced Functional Materials. 2018;28(31):1802060.

CANCELLED DUE TO COVID-19

SIMPLY DESIGNED HOLE TRANSPORTING MATERIALS FOR EFFICIENT PEROVSKITE SOLAR CELLS

Ranush Durgaryan, Yan Danyliv, Dmitriy Volyniuk, Juozas Vidas Gražulevičius

Department of Polymer Chemistry and Technology, Kaunas University of Technology, Kaunas, Lithuania
E-mail: hranushdurgaryan@gmail.com

The application of solar cells is one of the most promising solutions for satisfying the ever-increasing global energy demand [1]. Recently, perovskite solar cells (PSC) are gathering attention and have emerged as an extremely promising photovoltaic technology due to their remarkable photovoltaic performance and potentially low production cost [2,3]. Hole- and electron- transporting materials are important constituents of PSCs as they selectively transport charges within the device, influence photovoltaic properties, affect device stability and also influence its cost [4].

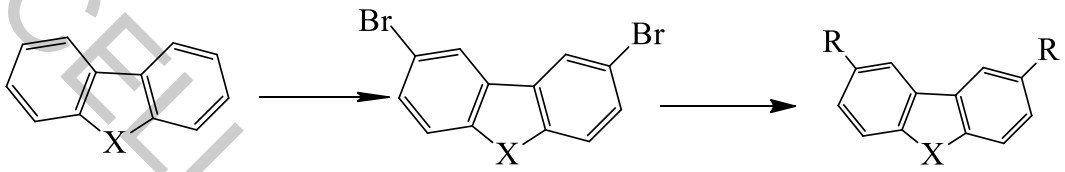

X=O,S R=OMe- ,tBu-,(4-MeOPh$_2$)N-

Scheme 1. General structures of the compounds with potential application as HTMs

The aim of this work was the search for new inexpensive and easily synthesizable hole-transporting materials based on carbazole, dibenzofuran or dibenzothiophene heterocyclic core, intended for applications in organic light-emitting diodes and perovskite solar cells. Hole-transporting materials were obtained by two-step synthesis with using of palladium-catalyzed Buchwald-Hartwig reaction. The structures of the obtained compounds were confirmed by NMR spectroscopy (^{1}H, ^{13}C) and mass spectrometry. Additionally, photophysical, electrochemical, thermal properties of all compounds were measured.

---

[1]. Polman A, Knight M, Garnett E C, et al. Photovoltaic materials: present efficiencies and future challenges. Science, 2016 352(6283):307
[2]. Zhou H P, Chen Q, Li G, et al. Interface engineering of highly efficient perovskite solar cells. Science, 201
[3]. Yang W S, Noh J H, Jeon N J, et al. High-performance photovoltaic perovskite layers fabricated through intramolecular exchange. Science, 2015, 348(6240): 1234
[4]. Zinab H. Bakra, Qamar Walia, Azhar Fakharuddinc, Lukas Schmidt-Mendec, Thomas M. Browne, Rajan Josea, Nano Energy 34 (2017) 271-305

CANCELLED DUE TO COVID-19

HOLES‘ MOBILITY PROPERTIES OF PCPDTBT THIN FILM HYBRID TRANSISTORS

Andrius Aukštuolis[1], Nerijus Nekrašas[1], Kristijonas Genevičius[1], Jūratė Jonikaitė-Švėgždienė[2], Giedrius Juška[1]

[1] Vilnius University, Faculty of Physics, Institute of Chemical Physics, Vilnius, Lithuania
[2] Vilnius University, Faculty of Chemistry and Geosciences, Institute of Chemistry, Vilnius, Lithuania
andrius.aukstuolis@ff.vu.lt

In the organic semiconductors devices morphology, temperature and charge carriers movement are tightly linked together. The change in the temperature of the active layer can affect charge carriers transport but it can also significantly change the morphology of the organic layer. In this work we investigated holes' mobility in the hybrid field effect transistor structures with an active layer of PCPDTBT on SiO_2/Si substrates. Holes' mobility and its dependence on the temperature was measured by i-CELIV [1] and current transient [2] methods. The combination of both techniques allowed us to investigate properties of holes transport in different directions in the layer (perpendicular and parallel to the SiO_2/Si substrate). Differential scanning calorimetry (DSC) measurements in the same temperature range were performed to investigate and explain morphological changes in the active layer of the field effect transistor structure.

[1] G. Juška, N. Nekrašas, K. Genevičius, Investigation of charge carriers transport from extraction current transients of injected charge carriers, Journal of Non-Crystalline Solids 358 (2012) 748–750, https://doi:10.1016/j.jnoncrysol.2011.12.016.
[2] G. Juška, N. Nekrašas,K. Genevičius and A. Pivrikas, Current transients in organic field effect transistors, APPLIED PHYSICS LETTERS 102, (2013) 163306, https://dx.doi.org/10.1063/1.4803054.

CANCELLED DUE TO COVID-19

SUBSTRATE BIAS VOLTAGE EFFECT ON AMORPHOUS CARBON FILM GROWTH RATE AND OPTICAL PROPERTIES

Gytis Vėjelis[1,2], Vilius Dovydaitis[2]

[1] Kaunas University of Technology Gymnasium, Lithuania
[2] Department of Physics, Kaunas University of Technology, Lithuania
gytis334@gmail.com

CANCELLED DUE TO COVID-19

Diamond like amorphous carbon (DLC) thin films are universally used as a protective layer in: optics, medical industry, electro-mechanical devices and elsewhere. It is well known that amorphous carbon consists of sp^3 and sp^2 bonds. Diamond-like properties are achieved when sp^3 bonds are dominant in the thin film, while sp^2 bonds are responsible for graphite-like properties. Therefore, sp^3/sp^2 ratio determines the characteristics of amorphous carbon layer. Differentiation between distinct properties and the optimal magnetron sputtering deposition parameters (working pressure, temperature, bias voltage, sputtering current/power) for film growth proves to be immensely pragmatic. Extensive research has been conducted on DLC's [1], nonetheless the substrate bias dependence on optical properties is yet to be thoroughly evaluated. There are some disagreement on the substrate bias voltage influence on carbon film deposition rate [2, 3]. Thus, the aim of this research was to determine the substrate bias voltage effect on growth rate and optical properties of DLC films.

n – type silicon wafers (1 cm x 1 cm) and glass substrates (1 cm x 2 cm) were coated using magnetron sputtering. Films were grown for 40 minutes, while the working pressure was held constant at 2 Pa. Discharge current was: 0,5 A, 1 A, 1,5 A, substrate bias: 0 V, -50 V, -100 V and -200 V. Every possible combination was analyzed, in total producing 12 unique series. The temperature of the substrate at the end of the sputtering process was monitored using thermocouple, along with substrate ion current. In addition, ellipsometer, micro-interferometer and UV-vis were utilized to analyze the complex reflective index, the transmittance and thickness of the aforementioned films.

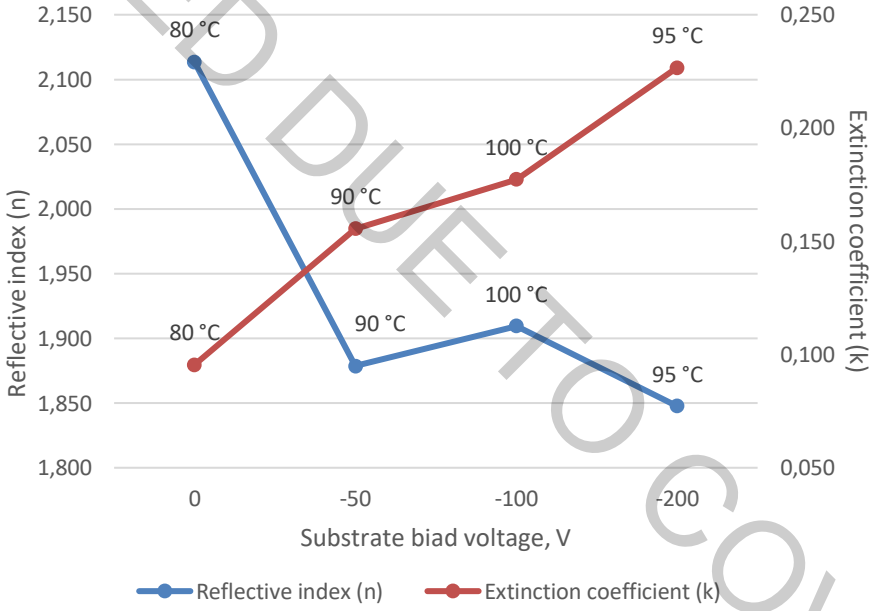

Fig. 1. Reflective index and extinction coefficient dependence on substrate bias voltage (discharge current: 0,5 A).

After methodical measurements it was noticed that by lowering substrate bias and increasing discharge current the reflective index deteriorate from 2,11 to 1,66, extinction coefficient went up from 0,10 to 0,49, while transmittance subsided. Furthermore, the film thickness escalated from 150,08 nm to 552,86 nm, consequently affecting the growth rate from 3,75 to 13,82 nm/min. The substrate bias changing from 0 V to -200 V enhanced the ion bombardment, hence increasing the substrate temperature and reconstructing sp^3 to sp^2 bonds and causing graphitization of the films.

q

[1] J. Robertson, Diamond-like amorphous carbon, Materials Science and Engineering R **37**, 129-281 (2002).
[2] I. Ahmad, S. S. Roy, P. D. Maguire, Effect of substrate bias voltage and substrate on the structural properties of amorphous carbon films deposited by unbalanced magnetron sputtering, Thin Solid Films **482**, 45-49 (2005).
[3] H.Y. Dai, Y.Q. Wang, X.R. Cheng et al., Characterization and properties of amorphous carbon coatings prepared by middle frequency pulsed unbalanced magnetron sputtering at different substrate bias, Applied Surface Science **258**, 5462–5466 (2012).

GALVO-SCANNER LASER PULSE DELIVERY TECHNIQUES FOR ELECROLESS COPPER DEPOSITION ON PC-ABS.

Vytautas Vosylius[1], Karolis Ratautas[1], Inga Andriulionytė[1], Aldona Jagminienė[2], Ina Stankevičienė[2] , Eugenijus Norkus[2], Gediminas Račiukaitis[1].

[1] Laser research department, Center for physical science and technology (FTMC), Lithuania
[2]Department of chemical catalysis, Center for physical science and technology (FTMC), Lithuania
Vytautas.vosylius@ftmc.lt

Advanced process for electric circuit traces formation on flexible and 3D shaped dielectrics is presented. The Selective Surface Activation Induced by a Laser (SSAIL) method is a promising technology [1], consists of 3 main steps: 1. Laser modification of the surface. 2. Chemical activation of modified area. 3. Electroless copper deposition on activated area. The process can be exceptionally applied on standard commercial dielectric materials such as various plastics, ceramics, glasses, and polymeric films.

The aim of research was to try different laser writing techniques and find best parameters for rapid and high quality electric circuit traces formation. Sheet resistance, optical, and scanning electron microscopy measurements were applied for investigate the optimal processing parameters. In the experiment an ultrashort pulsed laser and a galvanometric scanner for fast and precise pulse delivery on surface were used. Laser writing technique by skipping pulses is presented.

[1] K. Ratautas, et al, *Laser-assisted selective copper deposition on commercial PA6 by catalytic electroless plating – process and activation mechanism* (Appl Surf Sci, 470 (2019), pp. 405-410).

CANCELLED DUE TO COVID-19

NETWORK OF SURFACE ACOUSTIC WAVE SENSORS WITH WIDE-BAND HYPERBOLICALLY FREQUENCY-MODULATED TECHNOLOGY

Dmitrij Smirnov[1], Andrius Bartašiūnas[1], Rimantas Miškinis[1], Emilis Urba[1*], Victor Plessky[2]

[1] Department of Metrology, Center for Physical Sciences and Technology, Lithuania
[2] Resonant Trade SA, Switzerland
dmitrij.smirnov@ftmc.lt

CANCELLED DUE TO COVID-19

Developing the technology had been prompted by the fact that hyperbolically frequency-modulated signals are used in nature, e. g., by some of the species of dolphins and bats who use such a modulation for echo-location. Application of the technology in surface acoustic wave (SAW) sensors allows achieving their operation in a wide range of temperatures, which would be difficult to achieve by using other wide-band frequency modulations, e. g., linear [1]. To demonstrate that, a surface acoustic wave temperature sensor with the SAW reflecting gratings designed for operation with HFM signals was fabricated. The operating principle of the sensor is illustrated in Fig. 1.

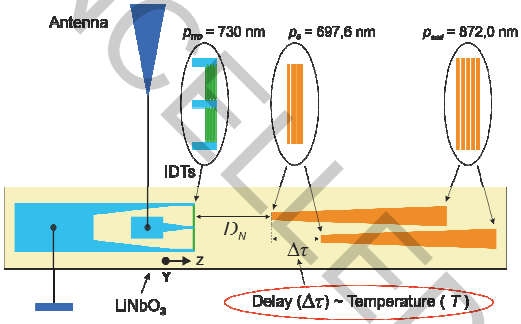

Fig. 1. Design of SAW sensors

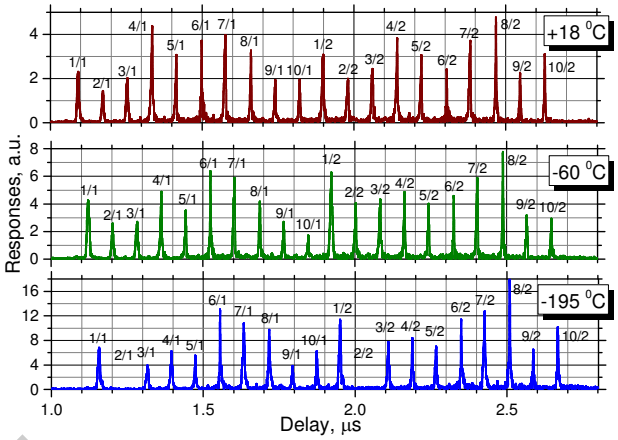

Fig. 2. Response of the network of 10 sensors at different temperatures. The peaks are denoted by *N*/*M*, where *N* is the number of sensor, and *M* is the number of its response

The temperature response is obtained from the times of the SAW propagation in the sensors. The device was fabricated by forming two pairs of identical aluminum interdigital transducers and etched-groove reflectors in parallel acoustic channels on a YZ-cut lithium niobate ($LiNbO_3$) substrate. The sensors were remotely (via antennas) interrogated by a reader ("Hybrid SAW Reader" by RSSI GmbH) in the frequency range of (2 – 2.5) GHz. Echo-responses were post-processed using a numerical matched-to-signal filter to obtain the compressed time responses. The difference $\Delta\tau$ between the peaks of the time response was proportional to the deviation of the sensor temperature; the proportionality was determined by thermal properties of $LiNbO_3$.

To demonstrate operation of sensors network and its measurement characteristics, a set of surface acoustic wave temperature sensors with the SAW reflecting gratings designed for operation with HFM signals was fabricated. The design of a SAW sensor is illustrated in Fig. 1.

The results obtained imply that the sensor properly operated remotely in the temperature range from -150 °C to +140 °C, allowing determining the temperature with the uncertainty of 50 mK (0.05 °C) [2].

Combining several sensors in a network allows obtaining simultaneously temperature responses from different sites. Initial delay of each sensor is different. The difference allows distinguishing between responses coming from different sensors. Response of the network of 10 sensors at different temperatures is depicted in Fig. 2. The temperature of each sensor is determined from the abovementioned difference $\Delta\tau$ between the peaks of time responses.

This work was carried out in the frame of the Swiss-Lithuanian Eurostars Project No. E!10640 UWB_SENS.

[1] V. Plessky, M. Lamothe, Hyperbolically frequency modulated transducer in SAW sensors and tags, Electronics Letters **49** (24), 1503-1504 (2013).
[2] S. Yandrapalli, R. Miskinis, D. Smirnov, V. Plessky, A. Shimko, Ultra-Wide-Band SAW Sensor with HFM Etched Reflectors, 2018 IEEE International Ultrasonics Symposium, DOI: 10.1109/ULTSYM.2018.8580225.

ARSENIC DETECTION BY GOLD COBALT/COPPER ELECTRODE IN AQUEOUS MEDIA

Kristina Radinović[1], Jadranka Milikić[1*], Aldona Balčiūnaitė[2], Zita Sukackienė[2], Loreta Tamašauskaitė-Tamašiūnaitė[2] and Biljana Šljukić[1]

[1] Faculty of Physical Chemistry, University of Belgrade, Studentski trg 12-16, 11158 Belgrade, Serbia
[2] Department of Catalysis, Center for Physical Sciences and Technology, Saulėtekio Ave. 3, LT-10257, Vilnius, Lithuania
*jadranka@ffh.bg.ac.rs

CANCELLED DUE TO COVID-19

Arsenic has five different oxidation states −3, 0, +3, and +5. In the natural water As usually exists in arsenite (As(III)), and arsenate (As(V)) as inorganic forms. Arsenic can also exist as organic dimethylarsinic and monomethylarsonic acids. Drinking arsenic-polluted water can cause serious health problems like irregular heartbeat, atherosclerosis and skin cancers [1]. It is very important to note that arsenite is more toxic than arsenate, the same as inorganic arsenic is more toxic than the organic arsenic forms [2]. Arsenic can be determined by several analytical methods including atomic absorptions spectroscopy (AAS), inductively coupled plasma – atomic emission spectrometry (ICP-AES), inductively coupled plasma – mass spectrometry (ICP-MS), etc. [3]. Analysis using these methods takes a lot of time and it is expensive, therefore electrochemical methods could be a good replacement as cheap, fast and easy methods for arsenic detection.

Herein, three different gold cobalt/copper (AuCo/Cu) electrodes were prepared by electroless deposition of Co on Cu surface, followed by Au nanoparticles deposition on the prepared Co/Cu electrodes by galvanic displacement using three different deposition times (30, 60 and 300 s).

Au loading was determined by energy-dispersive X-ray spectroscopy (EDX) analysis for all three electrodes and it was found to be 5.8, 7.1 and 15.3 μg cm^{-2} for AuCo/Cu(30s), AuCo/Cu(60s) and AuCo/Cu(300s), respectively.

Next, these electrodes were tested in 1 mM $NaAsO_2$ in $NaHCO_3$ + Na_2CO_3 buffer by anodic stripping voltammetry (ASV) in potential range from -0.7 V to -0.2 V vs. SCE at a scan rate of 50 mV s^{-1}. Arsenic determination by ASV method proceeds in two steps where As(III) is reduced to As(0) as the adsorbed form on the electrode surface and then oxidized to As(III) form that diffuses into the solution, scheme 1.

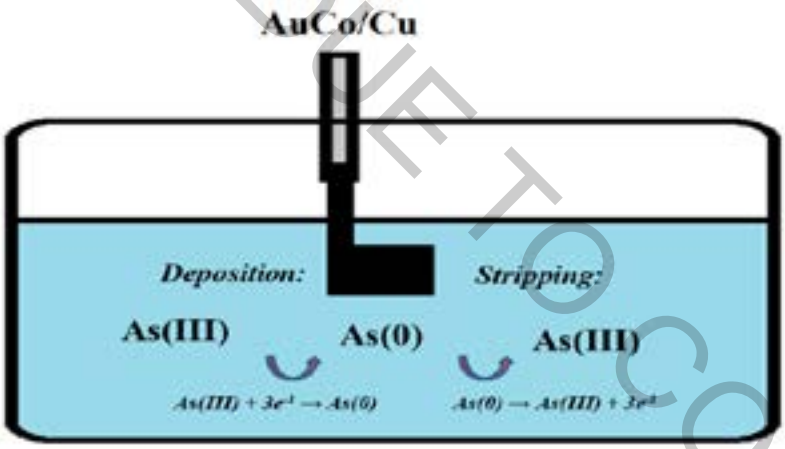

Scheme 1. Schematic representation of arsenic ions sensing at AuCo/Cu electrodes by anodic stripping voltammetry.

Cyclic voltammogram (CVs) of AuCo/Cu(30s) electrode reveals activity for detection of As(III) in 1 mM $NaAsO_2$ solution. Namely, AuCo/Cu gave a well-defined peak corresposning to As electrooxidation. The peak current density amounted to1.73 mA cm^{-2} at -0.4 V , while it was only 0.15 mA cm^{-2} at the same potential in the absence of As ions in the solution. The influence of experimental conditions on arsenic detection was tested by recording CVs at different deposition potential (E_d) and different deposition time (t_d).

The real water sample was diluted with $NaHCO_3$ + Na_2CO_3 buffer (sample: buffer 75:25 vol.% ratio) and used for arsenic determination. AuCo/Cu(30s) electrode shows a well-defined arsenic oxidation peak in the real sample.

Within this work, AuCo/Cu(30s) electrode with only 5.8 μg cm^{-2} of Au showed good activity for arsenic detection in the real sample and in 1 mM $NaAsO_2$ with $NaHCO_3$ + Na_2CO_3 buffer. This electrode is prepared by the simple and fast method, and it could be a potentially good sensor for arsenic detection in aqueous media.

[1] Y.G. Zhu, P.N. Williams, A.A. Meharg, Exposure to inorganic arsenic from rice: A global health issue?, Environmental Pollution **154,** 169–171 (2008).

[2] A. Giacomino, O. Abollino, M. Lazzara, M. Malandrino, E. Mentasti, Determination of As(III) by anodic stripping voltammetry using a lateral gold electrode: Experimental conditions, electron transfer and monitoring of electrode surface, Talanta **83**, 1428–1435 (2011).

[3] M. Yang, Z. Guo, L.N. Li, et al. Electrochemical determination of arsenic(III) with ultra-high anti-interference performance using Au-Cu bimetallic nanoparticles, Sensors and Actuators, B: Chemical. **231**, 70–78 (2016).

RAMAN SPECTROSCOPY ANALYSIS OF FS LASER INDUCED STRUCTURAL DAMAGE ON SODA-LIME GLASS

Laura Tauraitė[1], Erminas Kozlovskis[1], Antanas Urbas[1,2], Sergejus Orlovas[1], Ilja Ignatjev[1]

[1] Center of Physical Sciences and Technology, Industrial Laboratory for Photonic Technologies, Lithuania
[2] Altechna R&D Ltd, Lithuania
Erminas.Kozlovskis@ff.stud.vu.lt

CANCELLED DUE TO COVID-19

Selective etching is an important process in electronic and medicinal instrument manufacturing. However, it is a time-consuming process thus reducing manufacturing speed. It is known that chemical etching rate (using potassium hydroxide KOH) of corona-charge treated domain of the soda-lime glass substrate is 1.6 times higher than that of normal glass [1]. Furthermore, it was observed that chemical etching rate (using potassium hydroxide KOH) of fs laser induced damage areas of soda-lime glass is up to 1000 times higher. The purpose of this study is to analyse structural changes of soda-lime glass when affected by fs laser pulses.

Soda-lime glass is composed of silicon dioxide (SiO_2), sodium carbonate (Na_2CO_3) and calcium oxide (CaO) compounds. The structural network is formed by silicon and oxygen compounds in the shape of tetrahedrons, also known as Q species. Q species are connected by bridging oxygen atoms (Fig. 1). Alkali and alkaline earth elements work as network modifiers, consequently changing physical and chemical properties of the glass.

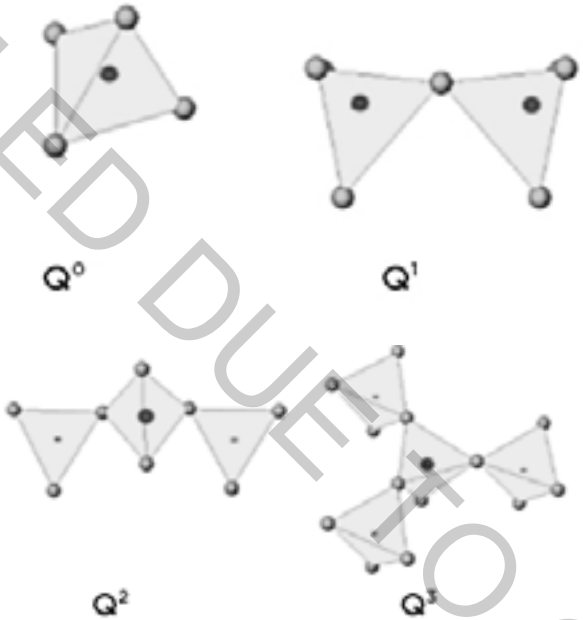

Fig. 1. Visualisation of Q group compounds

In this study, soda-lime glass samples were affected by a 1030 nm wavelength Bessel beam. Damaged samples were analyzed with Raman spectroscopy. This method was chosen because Raman shift values of Q species compounds are precisely known and do not depend on alkali metal compounds in the glass structure [2].

In this research, Raman spectroscopy was done with a 532 nm wavelength excitation beam. By analysing the measured spectra, structural differences between damaged and normal glass can be determined.

Analysis of the Raman spectra showed there was a noticeable difference in the quantity of Q^4 and Q^2 species compounds in the damaged glass compared to normal glass.

[1] Daisuke Sakai *et al* 2013 *Jpn. J. Appl. Phys.* **52** 036701.
[2] G.S. Henderson, H.W. Nesbitt, G.M. Bancroft, *Some Interesting Observations on Oxygen Environments in Silicate Glasses with Implications for the Fitting of the High Frequency Raman Envelope* (Cargese, France, 2017).

ANISOTROPIC THIN FILMS BASED POLARIZING COATINGS FOR HIGH POWER LASERS

Lukas Ramalis, Lina Grinevičiūtė, Rytis Buzelis and Tomas Tolenis

State Research Institute Center for Physical Sciences and Technology,
Savanorių ave, 231, LT-02300, Vilnius, Lithuania
Lukas.ramalis@ftmc.lt

Optical components are the main parts in laser systems and used for controlling the properties of the beam. Present innovative optical devices feature integrated laser systems capable of high power and precision. Applications are in a variety of areas such as material processing (cutting, drilling), medicine, communications technology, etc. In order to apply laser systems in everyday life more, the system dimensions should be reduced by replacing existing optical components with more compact elements. In solid state laser system, isotropic crystal generates unpolarized light beam, thus additional polarizer must be placed. Therefore, unique solutions are required for optical components, such as polarizers.

Anisotropic sculptured multilayer coating deposition directly on existing elements in the microlaser system (mirrors, nonlinear crystals, etc.) could be used to select the polarization of laser light flux. Forming such multilayer structure allows generation of desired polarization, while depolarization beam is sent from the resonator. Unfortunately, standard isotropic multilayer coatings do not have birefringence and can separate the polarized light only at large angles (e.g. Brewster angle). Columnar structure in dielectric coating (Fig. 1) induces birefringence and spectral performance of the total coating is different for perpendicular polarizations as a consequence [1].

In present work, glancing angle deposition method is used to induce the self–shadowing effect [2] and form nano-structured multilayer anisotropic coatings [3]. Using physical vapor deposition method and changing the angle of a substrate, different refractive index of anisotropic layers may be achieved. Combining the layers which have similar refractive indexes in one direction (horizontal axis) and different in other direction (vertical axis), high transmission can be achieved for one polarization while Bragg mirror can be formed for the perpendicular polarization (Fig. 2).

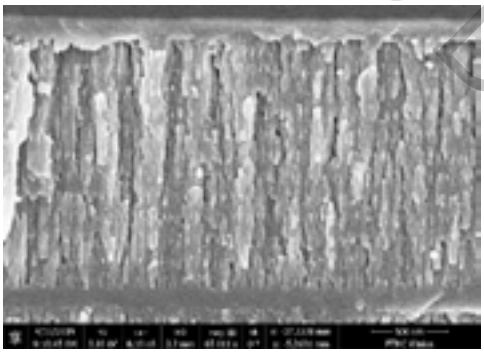

Fig. 1. SEM image of the cross-section of all-silica polarizer.

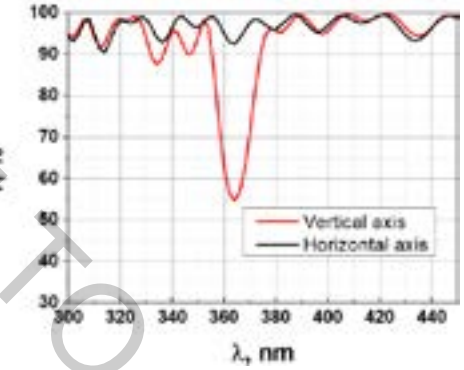

Fig. 2. Transmittance for different directions: vertical axis and horizontal axis.

Investigation of optical and structural properties indicates the possibility to form the all-silica polarizers for zero angle of incidence. Such optical elements exhibit superior optical performance: high resistivity to laser radiation, low optical losses and can be coated on crystal substrates.

[1] A. Lakhtakia and R. Messier. Sculptured thin films: nanoengineered morphology and optics. Bellingham, Wash: SPIE Press, (2005).

[2] Hodgkinson, I. & Wu and Q. H. Serial bideposition of anisotropic thin films with enhanced linear birefringence. Appl. Opt. 38, 3621–3625 (1999).

[3] L. Grinevičiūtė et al., Highly resistant zero-order waveplates based on all-silica multilayer coatings. Physica Status Solidi A, Vol 214, 1-8 (2017).

CANCELLED DUE TO COVID-19

INFLUENCE OF ELECTROLYTE COMPOSITION ON PHYSICAL PROPERTIES OF COPPER (I) OXIDE THIN FILMS

Anton Sikorski[1*], Evgeny Bondarenko[2], Natallia Mahon[1],
Olga V. Korolik[1], Tomas Ingr[3], Denis Esipenko[4]

[1] Energy Physics Department, Belarusian State University, Republic of Belarus
[2] Department of Electrochemistry, Belarusian State University, Republic of Belarus
[3] Department of Experimental Physics, Palacky University, Czech Republic
[4] Department of Solid-State Physics, Belarusian State University, Republic of Belarus
mr.a.i.sikorski@gmail.com

At the present time, the problem of making cheap and affordable alternative energy sources is more urgent than ever. Copper (I) oxide is characterized by band gap energy appropriate for solar energy conversion with theoretical limit of photocurrent density of 14.7 mA/cm^2 under AM1.5 illumination [1]. Also Cu_2O is available, low toxic, and can be prepared with simple methods [2]. This material can be used for hydrogen production, as a photocatalyst for waste water treatment and in photovoltaics devices [3, 4].

One of the most convenient and available method for synthesis of Cu_2O thin films is the electrochemical deposition from solution containing copper complexes (lactate, citrate, etc.) [5]. The lactate based solutions are not convenient for the electrodeposition of Cu_2O films due to difficulties in purification of lactic acid [6]. On the other hand, the citrate solutions have strong tendency to hydrolysis and thus are also uncomfortable in use [7].

We suggest a simple method for electrochemical deposition of Cu_2O thin films using aqueous copper tartrate solution. As a copper source, we used the different copper salts with SO_4^{2-}, Cl^-, NO_3^-. The goal of our work was to investigate the influence of these anions on the morphology, structural and optical properties of the Cu_2O thin films electrodeposited using the method developed by us.

X-ray diffraction demonstrated that all electrodeposited films do not contain any phases except Cu_2O. Single phase composition of the films is in agreement with their Raman spectra, which contain only peaks inherent to Cu_2O. The films deposited from sulfate and nitrate solutions display the similar X-ray diffraction patterns with pronounced (111) texture, whereas the films prepared from Cl^- containing solutions are not textured.

The scanning electron microscopy revealed the cubic shape of the crystals in the case of SO_4^{2-} and NO_3^-. The films have a thickness about 1 μm and do not contain any visible defects. For the Cu_2O thin films electrodeposited from chloride-containing solution, the primary shape of crystals is octahedral, and the substrate is not covered completely by the Cu_2O.

Photoluminescence spectra of all electrodeposited Cu_2O films demonstrate week band at ≈0.63 μm related to phonon-assisted exciton radiative recombination, as well as pronounced band at longer wavelength, which corresponds to oxygen vacancy. While intensity of this band is comparable for all samples, there is its remarkable red shift (from 0.77 to 0.82 μm) in the case of Cl^- anions.

Based on the obtained data, one can conclude strong influence of anions, especially Cl^-, on the formation of copper oxide (I) thin films. Thus, the copper tartrate complexes solution with different anions (SO_4^{2-}, Cl^-, NO_3^-) could be used for electrodeposition of Cu_2O thin films with desired texture, surface morphology and photoluminescence properties.

[1] P. Wang., Anodized Cuprous Oxide Photocathodes for Solar Energy Conversion, 14-17 (2015).
[2] B. M. Başol, Application of electrochemical deposition techniques to thin film solar cell processing, Proceedings of the SPIE, **8110**, 3-4 (2011).
[3] C. G. Morales-Guio, S. D. Tilley, Hydrogen evolution from a copper (I) oxide photocathode coated with an amorphous molybdenum sulphide catalyst, Nat. Commun., **5:3059**, 1-7 (2014).
[4] Y. Abdu, A.O. Musa, Copper (I) oxide (Cu2O) based solar cells, Bayero Journal of Pure and Applied Sciences, **2**, 8 - 12 (2009).
[5] M. B. Gawande, Cu and Cu-Based Nanoparticles: Synthesis and Applications in Catalysis, Chem. Rev., **116**, 3722-3811 (2016).
[6] A. Komesu, M. R. Wolf Maciel, R. Maciel Filho, Separation and purification technologies for lactic acid, BioRes., **12**, 6885-6901 (2017).
[7] H. Poerwono, H. G. Brittain, Analytical Profiles of Drug Substances and Excipients, 28, 1st Edition (2001)

CANCELLED DUE TO COVID-19

DIELECTRIC ANISOTROPY OF METHYLAMMONIUM LEAD IODIDE

Diana Pavlovaitė[1], Sergejus Balčiūnas[1], Šarūnas Svirskas[1], Mirosław Mączka[2], Jūras Banys[1]

[1] Faculty of Physics, Vilnius University, Sauletekio av. 9, LT-10222 Vilnius, Lithuania
[2]Institute of Low Temperature and Structure Research, Polish Academy of Sciences, P.O. Box-1410, PL-50-950 Wroclaw 2, Poland
diana.pavlovaite@ff.stud.vu.lt

In recent years, perovskite methylammonium lead halides $CH_3NH_3PbX_3$ (where X = I, Br, Cl) have gained notable attention of the scientific community as they show properties appropriate in the making of efficient and affordable solar cells. The key factor for this valuable use is the power conversion efficiency (PCE) which was recently improved to exceed 20 % [1]. For this particular reason perovskite solar cells based on $MAPBI_3$ are challenging existing silicon-based solar cell technology with their simple solution process and low costs. In this research MAPBI3 crystals were studied along different crystallographic directions in 150-300 K temperature range and 100Hz – 1 MHz frequency region.

Figure 1 shows the temperature dependences of the dielectric permittivity measured upon cooling at 1 MHz. The real part of dielectric permittivity experiences a gradual increase and in 162 K step- like anomaly can be observed. This behavior corresponds to the tetragonal-to-orthorombic phase transition. [2].There seems to be a slight difference in dielectric properties whilst measuring in one particular direction.

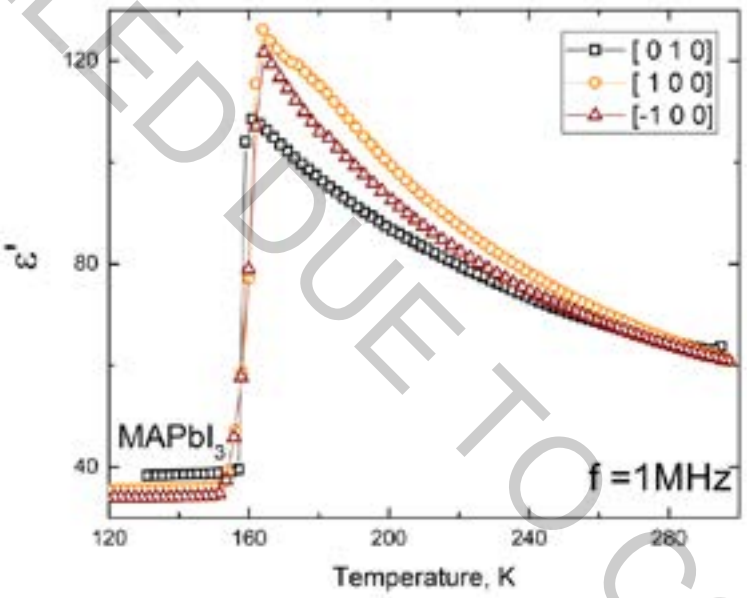

Fig 1. Temperature dependences of the real part of the dielectric permittivity of CH3NH3PbI3 single crystals in different crystallographic directions measured at a frequency of 1 MHz.

[1] N. J. Jeon *et al.*, "Compositional engineering of perovskite materials for high-performance solar cells," *Nature*, vol. 517, no. 7535, pp. 476–480, 2015.

[2] I. Anusca *et al.*, "Dielectric Response: Answer to Many Questions in the Methylammonium Lead Halide Solar Cell Absorbers," *Adv. Energy Mater.*, vol. 7, no. 19, pp. 1–12, 2017.

CANCELLED DUE TO COVID-19

INFLUENCE OF DEPOSITION PARAMETERS ON PROPERTIES OF POLY CRYSTALLINE DIAMOND FILMS

Tomas Grigaitis, Andrius Aukštuolis

Institute of Chemical Physics, Vilnius University, Lithuania
tomas.grigaitis@ff.vu.lt

Diamond is well known for its mechanical, thermal, chemical, and electrical properties. Also, diamond is a wide band gap material with low atomic number and exhibits very high radiation resistance even to the strong flux of high energy particles in detectors [1], therefore, diamond is a perfect candidate for beta voltaic batteries application [2]

In this work diamond films were deposited using a hot wire chemical vapour deposition (HW-CVD) reactor. Methane, hydrogen and argon gases with a different gas flow ratios were used for diamond deposition. The Raman peak at 1332 cm^{-1} was the evidence for the presence of diamond phase in the deposited layer. From AFM analysis it was found that decreasing the methane gas flow leads to lower deposition rate and lower surface roughness. Also, the depositions were carried out at different pressure in the range of 5 – 20 Torr with the fixed gas flow. It was concluded that the highest deposition rate with the most pronounced first-order diamond Raman peak were achieved at 10 Torr pressure using 2% methane and 98 % hydrogen gas mixture.

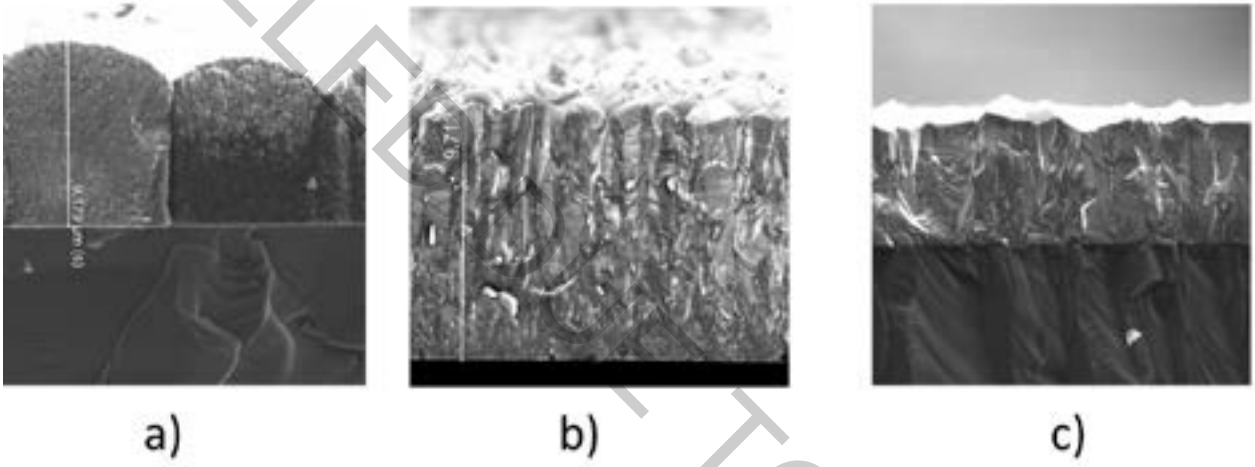

Fig. 1.Deposited diamond films on silicon substrate at different H_2 gas flow: a) 50 sccm b) 100 sccm c) 150 sccm. Pressure - 10 Torr pressure, heater temperature - 1023 K, CH_4 gas flow - 2 sccm.

[1] V. Bormashov, S. Troschiev, A. Volkov, S. Tarelkin, E. Korostylev, A. Golovanov, M. Kuznetsov, D. Teteruk, N. Kornilov, S. Terentiev, S. Buga, V. Blank, Development of nuclear microbattery prototype based on Schottky barrier diamond diodes, Physica Status Solidi (a). 212 (2015) 2539–2547.

[2] Y. M. Liu, J. B. Lu, X. Xu, R. He, Ren-Zhou Zheng, G. D. Wei, Theoretical Prediction of Diamond Betavoltaic Batteries Performance Using 63 Ni, Chin. Phys. Lett. 35 (2018) 072301.

CANCELLED DUE TO COVID-19

A study of supervised combined neural-network-based ultrasonic method for reconstruction of spatial distribution of material properties

Paulius Dapkus[1], Liudas Mažeika[2]

[1] Ultrasound Institute, Kaunas University of Technology, Studentu str. 50, Kaunas LT-51368, Lithuania
paulius.dapkus@ktu.lt

CANCELLED DUE TO COVID-19

The general objective of this research is non-destructive assessment of the grain size in the metals. The authors propose fresh attempt at applying neural network technology to achieve this goal by application of the neural-network for analysis of the ultrasonic structural noise. It was assumed that the signals of ultrasonic structural noise are measured at several frequencies. To address structural noise issues, a convolutional neural network is designed to process ultrasonic sensor data, to learn structural noise features and to achieve direct grain size estimation simultaneously. To ensure minimum data gathering of metal samples the design focuses on neural network with concept of semantic instance segmentation, for data extrapolation. Experimental results show that proposed methods as semantic instance segmentation with combined convolutional and fully connected dense neural networks with classifiers, outperform the others single neural networks with original samples with high SN data.

This study introduces a new approach to grain size estimation using neural networks with adapted architecture. Proposed feature learning model for metal object grain size prediction shown in Fig. 1.

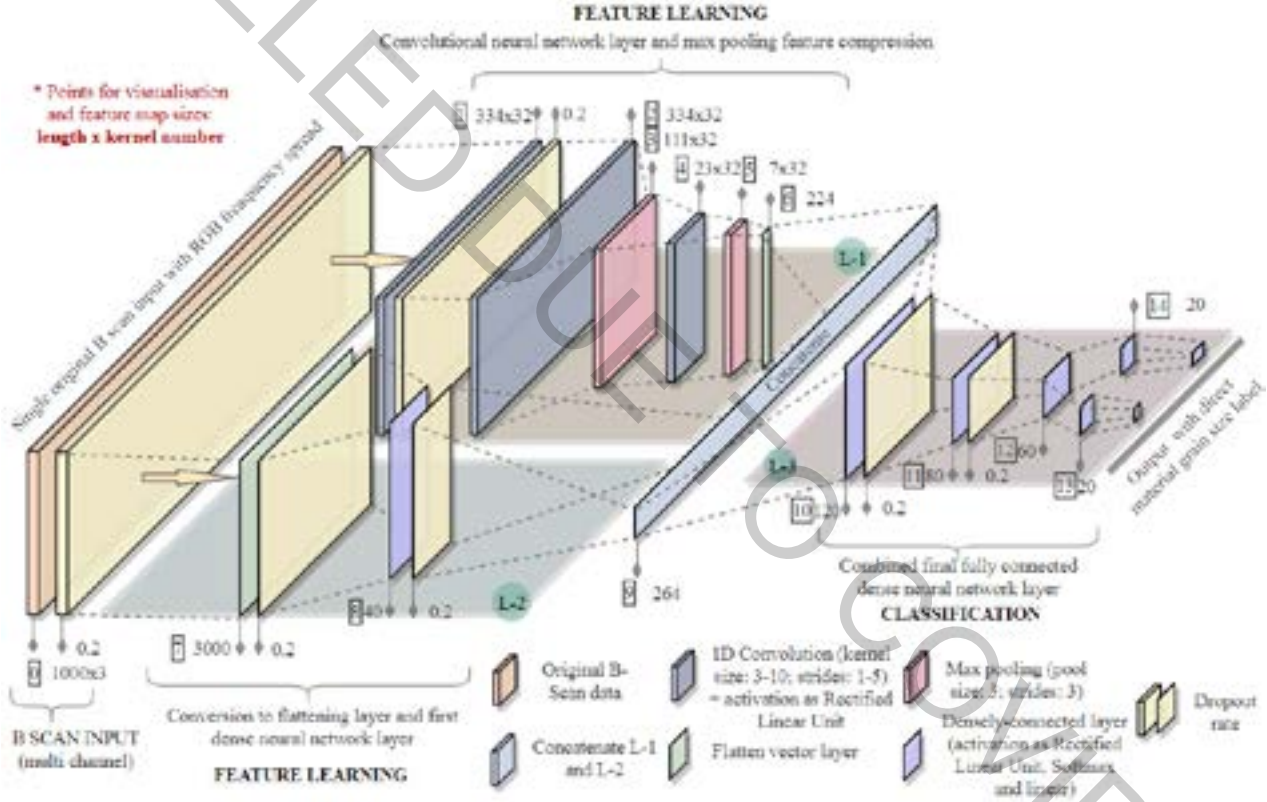

Fig. 1. Architecture of grain size in metals detection method shape. Using multiple spreaded neural networks - Convolutional neural networks and Dens fully connected neural networks

To solve grain size estimation problem, this presentation will provide visualization of hidden layers in the network by maximizing the activation of the target layer on the input. The final neural layers of the network which plays a big role as band-pass filters that focus on the structure's natural frequencies. Multi-band filters which can be found in the middle layers. Learning process that the network has independently learned the concept of structural mode.

[1] Blachowski, B., An, Y., Spencer, B. F. & Ou, J. (2017), Axial strain accelerations approach for damage localization in statically determinate truss structures, Computer-Aided Civil & Infrastructure Engineering, 32(4), 304–18.

[2] Amezquita-Sanchez, J. & Adeli, H. (2015), Feature extraction and classification techniques for health monitoring of structures, Scientia Iranica. Transaction A, Civil Engineering, 22(6), 1931.

[3] Cha, Y.-J., Choi, W. & Buyukozturk, O. (2017), Deep learning-based crack damage detection using convolutional neural network,Computer-Aided Civil & Infrastructure Engineering,32(3), 2013–14.

ANALYSIS OF LASERS DIODES BASED ON INGAN / GAN

Agnieszka Anna Wiciak[1,2], Veit Hoffmann[2], Sven Einfeld[2]

[1]Faculty of Technical Physics, Poznan University of Technology, Poznań, Poland
[2]Ferdinand-Braun-Institut Leibniz-Institut für Höchstfrequenztechnik, Berlin, Germany
Agnieszka.wiciak@student.put.poznan.pl

Blue-violet laser diodes (LD) available based on InGaN quantum studies (MQW) were first introduced by Nakamura and colleagues over a decade ago. Currently, they are widely used in many applications such as high-performance optical data collection systems or optical spectroscopy. LD emitting in the blue-green wavelength range also attract attention as a light source for full-color displays and laser projectors. However, many applications are still limited by the low output power involved (for example, laser displays). Key parameters that increase LD output power Configuration on nitrides at reasonable operating voltages are lowered external quantum yields. These parameters strongly depend on the structural best ranges of the InGaN MQW (AR) region. Emissions at such wavelengths require large molar fractions in quantum studies of indual nitride (InGaN) (QW), which results in strong piezoelectric fields due to the high deformation and piezoelectric properties of materials (Al, In, Ga) N. Under conditions of low excitation of separate piezoelectric fields electrons and holes in QW, and therefore significantly reduces the strength of the oscillator. Moreover, the emission will be shifted towards longer waves as a result of closed quantum closure (QCSE). For devices used at high excitation, material increase consists due to degradation in the quality of the crystal in the active layer with an increase in In in QWs. Because the two wave functions overlap and the quality of the QW material may depend on the QW width (dQW), this parameter has a big impact on the device performance. Waveguide structures (WG) emitting light with a wavelength of about 420nm made of InAlGaN / GaN were analyzed by photoluminescence (PL) and photoconductive (PC) spectroscopy using a scanning optical microscope near field (NSOM) for excitation and detection.

CANCELLED DUE TO COVID-19

TUNING OF PHOTOELECTROCHEMICAL ACTIVITY OF NANOSTRUCTURED WO_3 FILMS THROUGH MODIFICATION OF SOL-GEL SYNTHESIS PROCEDURE

Maliha Parvin, Milda Petrulevičienė, Irena Savickaja, Benjaminas Šebeka, Arnas Naujokaitis, Vidas Pakštas, Jurga Juodkazytė

Center for Physical Sciences and Technology, Saulėtekio av. 3, Vilnius 10257, Lithuania
maliha.parvin@ftmc.lt

Photoelectrochemical (PEC) water splitting has been considered as one of the most promising technologies in clean and renewable energy production. Numerous semiconductor materials have been intensively studied as photoelectrodes in PEC systems. Among them tungsten trioxide (WO_3) nanomaterials have received considerable attention due to the ability of capturing 12% of the solar illumination with band gap energy of around 2.5-2.7 eV, high crystallinity, porosity, moderate hole diffusion length, good chemical stability, low cost and low toxicity [1-3].

In this study, nanostructured layers of WO_3 on fluorine-doped tin oxide (FTO) substrate were formed by sol-gel method. Six different reductants have been used to investigate their influence on photoelectrochemical activity and properties of WO_3 photoanodes. Peroxytungstic acid (PTA) was synthesized using sodium tungstate (Na_2WO_4 x $2H_2O$), HCl and H_2O_2 as precursors and $(NH_4)_2C_2O_4$ as capping agent. Subsequently, methanol, ethanol, propanol, isopropanol, butanol or acetic acid was added separately as reductant, which slowly and controllably reduced peroxotungstates to form uniform and ordered $WO_3 \cdot H_2O$ films on FTO under soft water bath conditions at 85°C. After coating procedure, samples were annealed at 500 °C for 2 h with heating rate of 1°C/min to obtain a crystalline nanostructured WO_3 films and to remove residual carbon. The crystallographic structure of the calcined WO_3 films was characterized by X-ray diffraction (XRD) and photoelectrochemical behaviour of the samples was investigated by cyclic voltammetry (CV) (Fig. 1).

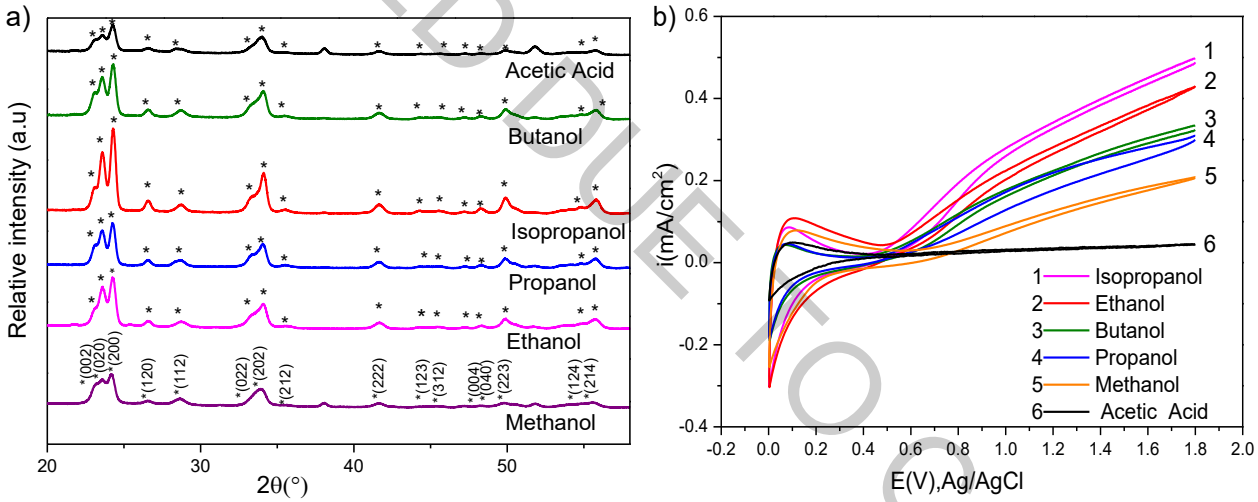

Fig. 1. a) XRD spectra of sol-gel derived WO_3 films formed using different reductants, b) cyclic voltammograms of the same films in 0.5 M H_2SO_4 solution, potential scan rate of 50 mV s^{-1}, intensity of illumination ~ 100 mW cm^{-2}

Fig.1(a) shows the XRD patterns of six WO_3 samples using six different reductants. Notably, all the samples have the same peaks at 23.13°, 23.56°, 24.33°, 26.5°,28.6°,34.09°,41.65°, 44.38°, 45.5°,47.18°, 48.15°, 49.88°, 54.73°, 55.83° corresponding to (002), (020), (200), (120), (112), (202), (222), (123), (312), (004), (040), (223), (124), (124) reflections of monoclinic WO_3 structure (COD Entry. 96-210-6383). WO_3 films formed with isopropanol as a reductant shows the most intensive peaks in the whole range of 2θ which is attributed to the highest crystallinity.

Cyclic voltammograms of FTO/WO_3 photoanodes recorded in 0.5 M H_2SO_4 under illumination represent typical response of WO_3. Using isopropanol as a reductant in the reported synthesis has been found to be the most effective route to increase the photoelectrochemical activity of WO_3 photoanodes, as these films showed the highest photocurrent density at 1.8 V vs Ag/AgCl among the tested samples. Photoelectrochemical activity of FTO/WO_3 electrodes prepared with six different reductants decreased in the following order: isopropanol > ethanol >butanol > propanol > methanol > acetic acid.

Correlation between PEC activity and morphology, structure, phase composition of sol-gel derived WO_3 films will be elaborated at the conference.

[1] T. Zhang, Z. Zhu, H. Chen, Y. Bai, S. Xiao, X. Zheng, & S. Yang, Iron-doping-enhanced photoelectrochemical water splitting performance of nanostructured WO_3: a combined experimental and theoretical study, Nanoscale **7**, 2933-2940(2015)
[2] R. Zhang, F. Ning, S. Xu, L. Zhou, M. Shao and M. Wei, Oxygen vacancy engineering of WO_3 toward largely enhanced photoelectrochemical water splitting, Electrochim. Acta. **274**, 217-223 (2018).
[3] J. Joy, J. Mathew, and S. C. George, Nanomaterials for photoelectrochemical water splitting–review, Int. J. Hydrogen Energy. **43,** 4804-4817(2018).

CANCELLED DUE TO COVID-19

STRESS-STRAIN STATE AND DAMAGED VOLUME IN CONTACT AREA OF CAR TIRE–ASPHALT CONCRETE SYSTEM UNDER VARIOUS LOADS

Gleb Gribovskii

Department of Theoretical and Applied Mechanics, Belarusian State University, Belarus
mmf.gribovskiy@gmail.com

Computer finite-elements models for describing the 3D stress-strain state of an active system "car tire–asphalt concrete" have great practical importance for road and tire industry. Also important challenge for road services and tires manufacturers is the assessment of volume damageability and wear of the tire tread and the asphalt pavement, which work in conditions of contact, mechanical and sliding fatigue. Today, there are many works dedicated to analytical and FEM simulation of the "car tire–asphalt concrete" separate system components. However, the problem of estimating 3D stress-strain state and the state of the volumetric damageability in contact interactions of asphalt and multicomponent tire with rib pattern is still not fully investigated.

In this investigate simultaneous contact interactions of the full multielement system "car tire–asphalt concrete", loaded by the various tire inner pressure P_S (from 0.65 to 0.85 MPa) and radial load F_H (from 6 to 10 kN) on rim were modelled using finite-element method [1,2]. The main goal of this work is determine and analyze 3D stress-strain state of the whole system and the state of volumetric damageability by maximum stress intensity σ_{int}^{max} and damaged volume V_{int} in contact interaction area of tire and asphalt concrete, where maximum stresses occur: 1) asphalt concrete, 2) tire tread and 3) rubber under radial ply [2]. Calculation of damaged volume V_{int} is based on the model of deformable solid mechanics [3]. According to this model damaged volume V_{int} is the volume where acting stresses σ_{int} are greater than limiting stress $\sigma_{int}^{(lim)}$. Allowable limit stress by stress intensity $\sigma_{int}^{(lim)}$ for friction fatigue in contact zone of tire and asphalt is 0.5 MPa and for others rubber parts of tire is 1 MPa which work in conditions of mechanical fatigue.

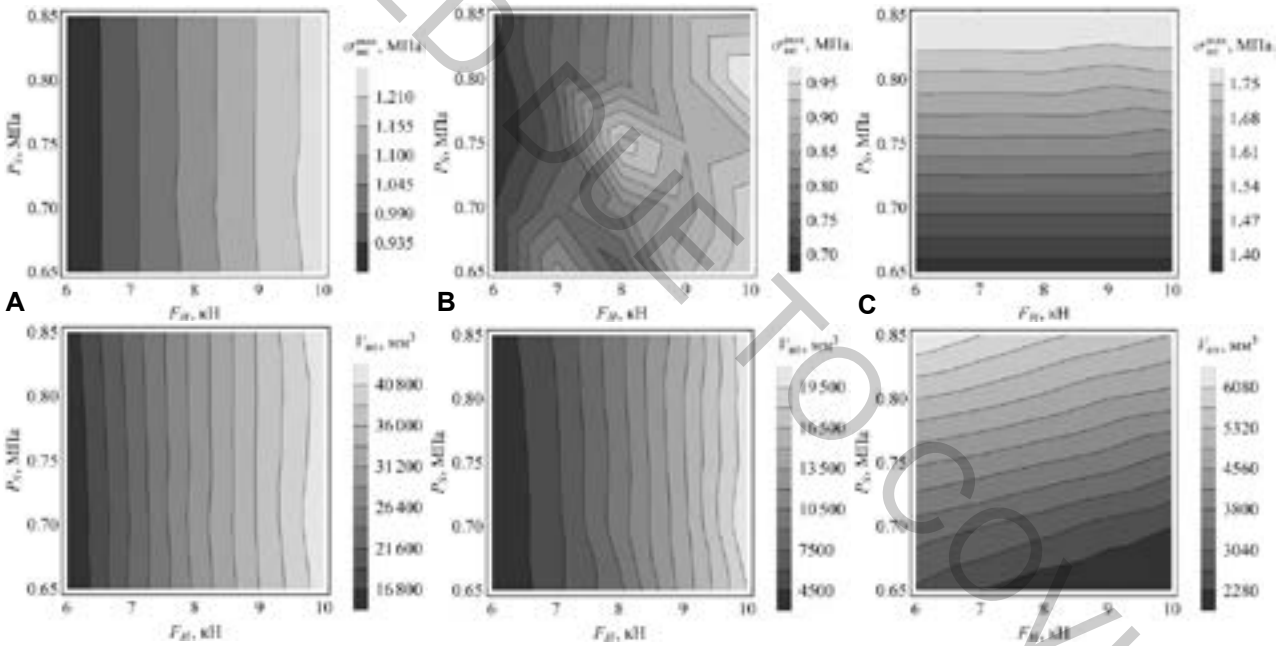

Fig. 1. Values of σ_{int}^{max} (top) and V_{int} (bottom) by F_H and P_S in tread (A), asphalt (B) and rubber under radial ply (C)

Values of σ_{int}^{max} and V_{int} in tire tread (fig. 1-a) increased to 1.4 and 2.7–3 times when the F_H is increased from 6 to 10 kN and increased slightly when P_S is increased from 0.65 to 0.85 MPa.

Values of σ_{int}^{max} in asphalt (fig. 1-b) increased to 1.28¬1.46 times when the F_H is increased and σ_{int}^{max} changed nonlinearly to 3–27% without an explicit dependency with local minimum and maximum when the P_S is increased. At the same time V_{int} increased to 6–7.5 times when F_H is increased and V_{int} increased to 3–27% when P_S is increased. At this case system stress-strain analysis by V_{in} is easier than by σ_{int}^{max} and allows to smooth features of FEM calculations.

Values of σ_{int}^{max} in rubber under radial ply (fig 1-c) changed slightly when F_H is increased, however, V_{in} decreased to 17–34%. At the same time σ_{int}^{max} and V_{int} in rubber under radial ply increased to 1.3 and 2.4–3.1 times when P_S is increased. This case shown us much more influence P_S on system stress-strain state at analysis by V_{int} than by σ_{int}^{max}

[1] S. S. Sherbakov, G. V. Gribovskiy, Stress-strain state of multicomponent «rim–tire–asphalt-concrete» system for different values of radial load on the rim and internal pressure in the tire, International Scientific and Technical Collection Theoretical and Applied Mechanics 34, 307 – 313 (2019).
[2] G. V. Gribovskii, Damageability in contact area of tire and asphalt concrete under various loads, 62nd scientific conference for young students of physics and natural sciences Open Readings 2019, Vilnius University, 311 (2019).
[3] L.A. Sosnovskiy, S.S. Sherbakov, Mechanothermodynamics (Springer, 2016).

CANCELLED DUE TO COVID-19

PHYSICO-CHEMICAL ASPECTS OF ULTRASONIC METAL NANOSTRUCTURING

Nadzeya Brezhneva[1,2*], Sviatlana A. Ulasevich[2], Nikolai V. Dezhkunov[3], Ekaterina V. Skorb[2]

[1] Chemistry Faculty, Belarusian State University, Minsk, Belarus
[2] ITMO University, Saint-Petersburg, Russia
[3] Department of Research and Development, Belarusian State University of Informatics and Radioelectronics, Minsk, Belarus
brezhNY@bsu.by

Nowadays ultrasound appears to be a convenient, safe and time-effective method of solid nanostructuring for materials science and engineering applications. Passing of ultrasonic (US) waves through the liquid results in the formation of cavitation bubbles that can grow either linearly and provide stable cavitation or nonlinearly (attributed to transient cavitation) and collapse creating the local areas with extremely high temperatures and pressures (up to 10000 K and 1000 atm [1]). Such non-equilibrium conditions can provide the possibility of the potential application of ultrasound for surface oxidation for the formation of oxide/hydroxide structures with highly developed porous surface, metastable phases that could not be formed in the absence of ultrasound (*e.g.* in the cases of conventional heat treatment).

Herein, we investigated the aspects of (i) ultrasonic structuring of metals with different chemical activity in various liquids (water, ethanol, ethylene glycol) by means of the cavitation bubbles collapse as well as (ii) the influence of the chemical activity of metal and the formed products on the cavitation activity development.

US treatment of highly reactive metals (magnesium, aluminum, zinc) in water is characterized by the oxidation of metal surface, leading to the transformation of the porous structure in accordance with the duration of US treatment. These processes denote the formation of hydroxide phases and highly developed surface area with the formation of metal sponges [2]. Metals with less chemical activity (*e.g.* titanium) are characterized by the transformations of the surface layer leading to the formation of defective structure [3]. Noble metals such as gold, silver and platinum are not modified during ultrasonic treatment in water [4].

US treatment in non-aqueous media (ethanol, ethylene glycol) showed the tendency to suppress the oxidation of metal surfaces with different reactivity (for reactive magnesium as well as for the high resistant titanium) resulted from the scavenging of the reactive oxygen species by the molecules of ethanol and ethylene glycol [5].

The sonochemical treatment of metal particles is characterized by the oscillations of the crystallite sizes [6] which can be explained by the two opposite processes – recrystallization and growth of the crystallites by means of atomic diffusion. These processes are the sequence of the formation of local high temperatures and pressures occurred after the formation of "hot spots". These phenomenon depends on the nature of the used liquid dispersed medium (*e.g.* heat capacity, vapor pressure *etc.*), duration of treatment.

For the porous structure preparation for high resistant metal (*e.g.* titanium that is widely exploited in engineering, shipbuilding, biomedicine) the use of medium with higher chemical etching property should be used. In our case we used aqueous alkaline solutions [3]. However, concerning the biomedical applications, titanium implants coated with native oxide layer is regarded as a bio-inert material still possibly leading to high risks of inflammation or abruption inside the organism. Thus, it is necessary to obtain the biocompatible coating with appropriate porous structure, roughness and adhesion. For this reason, US treatment of titanium in alkaline solutions leads to the formation of porous layer based on metal foam with incorporation of titania and sodium titanates [3]. Besides demonstrating good biocompatibility properties, these coatings also possess the photocurrent under 405 nm irradiation [7].

Concerning the study of the evolution of cavitation activity during sonochemical treatment of metal particles, we found out that during US treatment of reactive magnesium particles, the released hydrogen gas is involved in the development of cavitation bubbles. The cavitation bubbles activity is characterized by the complicated behavior, starting from the nucleation of the bubbles, their consequent growth by several mechanisms, fragmentation, reaching the critical value with further collapse. In addition, in the conditions of ultrasonic treatment magnesium particles are characterized not only by the formation of porous hydroxide layer but also the presence of magnesium hydride which was not formed in the absence of ultrasound. On the examples of other metals with lower chemical activity, it has been demonstrated that the ability of metal to produce hydrogen plays an essential role in the development of cavitation activity.

[1] K. S. Suslick, Sonochemistry, Science **247**, 1439-1445 (1990).
[2] E. V. Skorb, D. Fix, D.G. Shchukin, H. Möhwald, D. V. Sviridov, R. Mousa, N. Wanderka, J. Schäferhans, N. Pazos-Pérez, A. Fery, D. V. Andreeva, Sonochemical formation of metal sponges, Nanoscale **3**, 985-993 (2011).
[3] Y. Zhukova, S. A. Ulasevich, J. Dunlop, P. Fratzl, H. Möhwald, E. V. Skorb, Ultrasound-driven titanium modification with formation of titania based nanofoam surfaces, Ultrason. Sonochem. **36**, 146-154 (2017).
[4] E. V. Skorb, H. Möhwald, Ultrasonic approach for surface nanostructuring, Ultrason. Sonochem. **29**, 589-603 (2017).
[5] P. V. Cherepanov, I. Melnyk, D. V. Andreeva, Effect of high intensity ultrasound on Al_3Ni_2, Al_3Ni crystallite size in binary AlNi (50 wt% of Ni) alloy, Ultrason. Sonochem. **23**, 26-30 (2015).
[6] A. Kollath, N. Brezhneva, E. V. Skorb, E. V., Andreeva, Microbubbles trigger oscillation of crystal size in solids, Phys. Chem. Chem. Phys. **19**, 6286-6291 (2017).
[7] D. V. Andreeva, A. Kollath, N. Brezhneva, D. V. Sviridov, B. J. Cafferty, H. Möhwald, E. V. Skorb, Using a chitosan nanolayer as an efficient pH buffer to protect pH-sensitive supramolecular assemblies, Phys. Chem. Chem. Phys. **19**, 23843-23848 (2017).

CHEMISTRY OF ICSOMR 19

PHASE COMPOSITION AND PROPERTIES OF ZnO-METAL OXIDES CERAMICS

Aliaksei Pashkevich[1,2], Alexander K. Fedotov[1], Krystsina Kirylchyk[3], Viktoryia Halauchuk[2]

[1]Institute for Nuclear Problems of Belarusian State University, Republic of Belarus
[2]Faculty of Physics, Belarusian State University, Republic of Belarus
[3]A.V. Luikov Heat and Mass Transfer Institute of NAS of Belarus, Republic of Belarus
alexei.paschckevich@yandex.by

CANCELLED DUE TO COVID-19

Nowadays, great attention is paid to the search for new materials based on wide-gap oxides, as well as to studying their structure and properties for the purpose of application in various areas of the radioengineering, electronics and optoelectronics [1, 2]. However, the influence of doping on electric properties of such widely known oxide as ZnO, obtained by ceramic technologies, are not fully understood. The aim of this work is to study interconnection between electric properties (resistivity, Seebeck effect) and phase structure of doped ZnO-based ceramics.

In the ceramics studied, we used powder mixtures (MO)-(ZnO) with different its relations, where MO = Al_2O_3, NiO, TiO_2, CoO, after uniaxial pressing and one-step annealing for 3 hours at 1200 °C. The intial powders were either commercial or prepared by technology of sol-gel synthesis.

It was revealed that, when using the sol-gel synthesis for preparation of initial powders, the size of the microparticles in the ZnO–based ceramics decreases slightly after annealing. As is seen from Fig. 1a, additions of MO powders did not change wurtzite type of crystal lattice in ZnO-based solid solutions but forms after annealing new extra phases of ganite $ZnAl_2O_4$ [3] and zinc orthotitanate Zn_2TiO_4 [4] with spinel structure for MO = Al_2O_3, TiO_2. At the same time, addition of CoO did not result in the formation of extra phases.

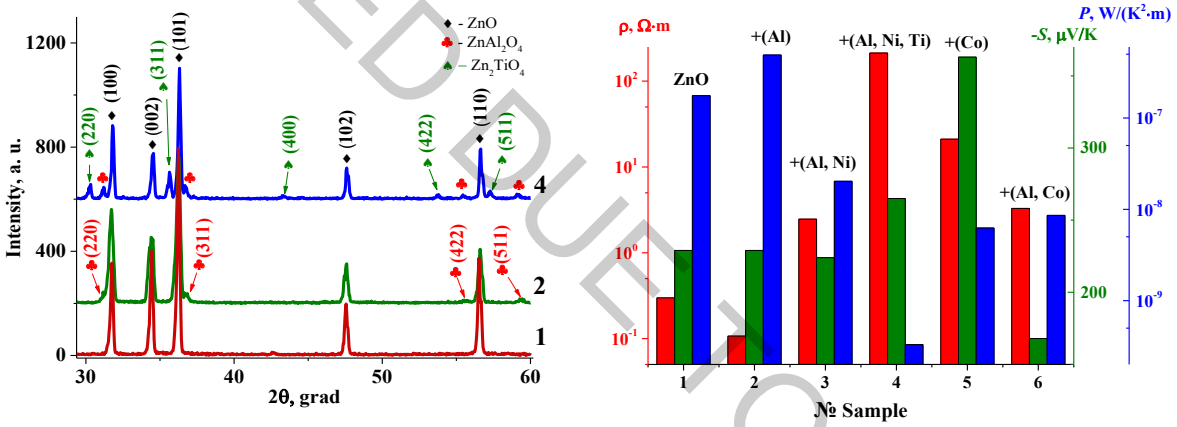

(a) (b)

Fig. 1. XRD pattern (a) and histogram (b) of electrical resistivity, Seebeck coefficient and power factor at 300 K in ceramic samples: 1 – undoped ZnO; 2 - $(ZnO)_{97}(Al_2O_3)_3$; 3 - $(ZnO)_{96,5}(Al_2O_3)_3(NiO)_{0,5}$; 4 - $(ZnO)_{77,5}(TiO_2)_{19,3}(Al_2O_3)_{2,8}(NiO)_{0,4}$; 5 - $(CoO)_{50}(ZnO)_{50}$; 6 - $(ZnO)_{96,5}(Al_2O_3)_3(50CoO{\cdot}50ZnO)_{0,5}$.

In the annealed ceramics with 50 wt. % CoO (sample 5 in Fig. 1b) resulted in increase of Seebeck coefficient *S* although simultaneous addition of small amounts of CoO and Al_2O_3 (sample 6 in fig. 1b) oppositely suppressed S values 4 times and increased resistivity twice. Addition of 3 wt. % of Al_2O_3 decreased resistivity 4 times and practically did not change *S* (sample 2 in Fig. 1b). At the same time, additions of app. 19 wt.% of TiO_2 simultaneously with Al_2O_3 (2,8 wt. %) and NiO (0,4 wt. %) strongly increased resistivity, but only slightly changed *S* values (samples 3 and 4 in Fig. 1b). As is seen, the electrical resistivity ρ increases with the addition of cobalt, titanium and nickel oxides, which negatively affects the value of the power factor *P* due to dielectric properties of metal oxides [5].

[1] Ayman Sawalha, M.Abu-Abdeen, A. Sedky, Electrical conductivity study in pure and doped ZnO ceramic system, Physica B **404** (2009).
[2] A.S. Fedotov, V. Shepelevich, S. Poznyak et al., Simulation of polycrystalline bismuth films Seebeck coefficient based on experimental texture identification, Materials Chemistry and Physics **177**, 413 – 416, (2016).
[3] Wang S.-F, A comparative study of ZnAl2O4 nanoparticles synthesized from different aluminum salts for use as fluorescence materials, J. Scientific Reports 5, **12849,** 1-12, (2015).
[4] Budigi Lokesh, Nasina Madhusudhana Rao; Shaik Kaleemulla et al., Freeze-drying synthesis and characterisation of Na composites of ZnO, TiO_2 and $ZnTiO_3$ semiconductor oxides, Chemical Papers, 1481-1490, (2015).
[5] B.I. Shklovskii, A.L. Efros, *Electronic Properties of Doped Semiconductors* (Berlin, Springer, 1984).

ENERGY GENERATION FROM VEHICLE VIBRATIONS USING SMART DAMPER

Tadas Lenkutis[1], Andrius Dzedzickis[1], Barbora Kačinskaitė[1], Dainius Kunkis[1], Vytautas Bučinskas[1]

[1] Department of Mechatronics, robotics and digital manufacturing, Vilnius Gediminas technical university
tadas.lenkutis@vgtu.lt

CANCELLED DUE TO COVID-19

Vibrations energy is one of the biggest unused energy sources in nowadays engineering. This happens, because collecting energy from vibrations is uncommon task and requires non-standard solutions. This paper presents shock absorber construction that has implemented energy generation function and can fulfill vibrations energy generation task.

Vibrations in vehicle appears then vehicle tire contacts road [1]. More then 100 years these vibrations were named as harmful and only solution to avoid them was to absorb the energy and dissipate it as heat. Possibility to collect vibrations energy can lower travel energy costs from 2 % to 10 %, depending on vehicle type [2]. The biggest challenge is to convert energy only few shock absorbers types prevails in researches: Mechanical shock absorbers, where linear movement is changed to rotary by pinion gear [3] and Magnetic absorbers [4].

Our proposed solution is shock absorber with magneto-rheological fluid. Magneto-rheological fluid also known as smart fluid consists of two main elements: oil and magnetic parts. The main feature of smart fluid is that then magnetic field is applied the magnetic parts in fluid organizes and fluid gets thicker. In our case the smart fluid performs three tasks: holds permanent magnetic field for energy generation, lubricates the system and allows to change shock absorbers damping coefficient.

For experimental research were created prototype of shock absorber, which is shown in fig. 1 A. where: 1 – frame; 2 – solenoid coil; 3 – piston stem for force application; 4 – piston; 5 – smart fluid; 6 – fixing eye; 7 – compensating spring; 8 – air piston. This prototype was created for generated energy size determination. Experiments were performed using test rig SPA PSD 2004. Prototype was tested in various regimes applying two different excitation amplitudes: 25 mm and 50mm and frequencies: 1 Hz, 2 Hz, 3 Hz, 4 Hz, 5 Hz, 5,5 Hz, 6 Hz, 6,5 Hz, 7 Hz, 7,5 Hz. Generated voltage was measured in two coils (1st and 3rd from top) obtained results are shown in fig. 1 B.

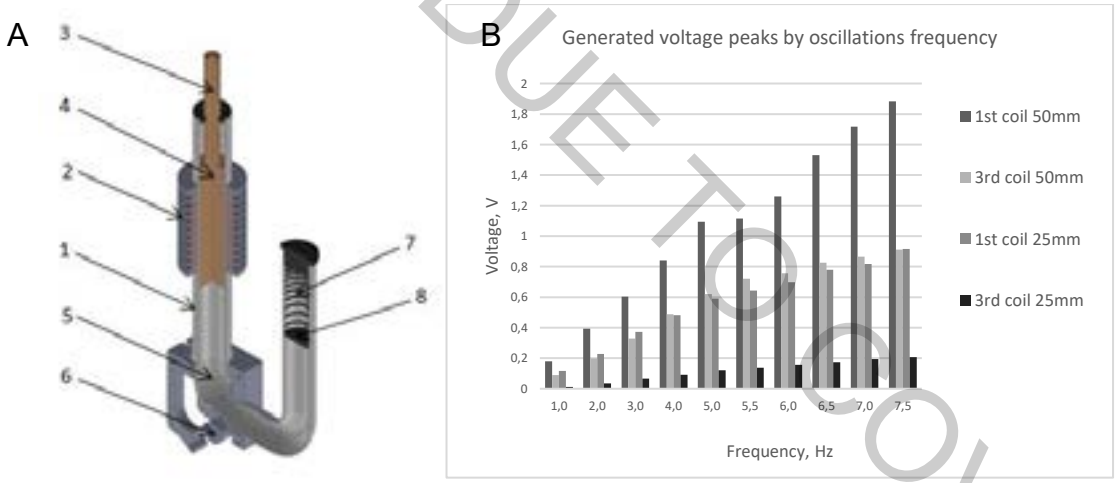

Fig. 1. A- Experiments prototype, B – Energy generation results.

Performed experimental research revealed many interesting effects of implementing such design of the shock absorber. Firstly, this type of liquid core generator can operate and it is really functional. Secondly, obtained voltages are enough high, and this proves that amount of energy harvested from vehicle vibrations is significant and can be used for a variety of purposes, for example powering sensors in autonomous vehicles. In the other hand, many features of this type of electric machines are unknown and need to be further researched.

[1] A. Kumar, A. Dwivedi, H. Jaiswal, and P. P. Patil, "Material-Based Vibration Characteristic Analysis of Heavy Vehicle Transmission Gearbox Casing Using Finite Element Analysis ", Intelligent Computing, Communication and Devices, Springer pp. 527-533, 2015.
[2] M. A. Abdelkareem, L. Xu, M. K. A. Ali, A. Elagouz, J. Mi, S. Guo and L. Zuo, "Vibration energy harvesting in automotive suspension system: A detailed review", Applied energy, vol. 229, pp. 672-699, 2018.
[3] Z. Li, L. Zuo, G. Luhrs, L. Lin and Y. X. Qin, "Electromagnetic energy-harvesting shock absorbers: design, modeling, and road tests". IEEE Transactions on vehicular technology, vol. 62, no. 3, pp. 1065-1074, 2012.
[4] B. Sapiński, "Energy-harvesting linear MR damper: prototyping and testing", Smart Materials and Structures, vol. 23 no. 3, 2014.

AN EXPERIEMENTAL STUDY OF ALUMINIUM (AL) INCORPORATED DIAMOND LIKE CARBON (DLC) THIN FILMS

Kanak Kalita[1], Ranjan Kumar Ghadai[2]

[1] Department of Mechanical Engineering, Vel Tech Rangarajan Dr.Sagunthala R&D Institute of Science and Technology, Avadi, Chennai, India
[2]Department of Mechanical Engineering, Sikkim Manipal Institute of Technology, Sikkim Manipal University, Majitar, Rangpo-East Sikkim, 737136, India
kanakkalita02@gmail.com

In the present work Aluminium (Al) incorporated Diamond like Carbon (DLC) thin films have been synthesized over Si(100) substrate using Atmospheric pressure chemical vapour deposition (APCVD) technique with variation in deposition temperature and keeping the N_2 flow rate constant. The morphology, corrosion behavior and mechanical properties of the thin films were characterized by Scanning Electron Microscope (SEM), Atomic force microscopy (AFM), corrosion test and nano-Indentation. SEM results revealed the smooth surface morphology of the coatings grown at different process temperatures. The surface roughness of the Al-DLC coatings was observed in the range of 20µm to 36µm and it is found to be increased with increasing in the deposition temperature. The corrosion resistance of the coating found to be decreased with increase in the deposition temperature and this could be due higher randomness of gaseous molecules at high temperatures. The nano indentation result revealed that the coating Hardness (H) and Young's Modulus (E) were increased with increasing the deposition temperature. The parameters H/E and H_3/E_2 indicated the elastic–plastic property exhibited by the coating and it also provides the wear properties of the films. The residual stresses have been calculated by using Stoney's equation and it is observed that residual stress of the film decreases with the increase of deposition temperature.

The SEM images of the Al-DLC coated samples prepared at different CVD process temperature has been shown in Fig. 1. The SEM images revealed a smooth coating for all the samples grown at different process temperatures. However, through SEM technique no particular pattern of the grains was observed. The morphology of the coating prepared at 920 ℃ showed white colour spot over the surface. This spot may be attributed to white agglomerated particles that could have deposited at the time of deposition due to partial melting and evaporation of the powder particles. The coatings were observed with negligible pores and inclusions. In past research works it is reported that the morphology of the coatings greatly depends upon atom diffusion, deposition and etching effect [1, 2]. The proper estimation of grain size or particle size the coatings were further characterized by AFM technique. The composition of various elements of Al-DLC coatings prepared under various process temperatures has been presented in Table 1. EDS result revealed that with increase in process temperature from 800 ℃ to 920 ℃ the atomic % of carbon increases and aluminium decreased.

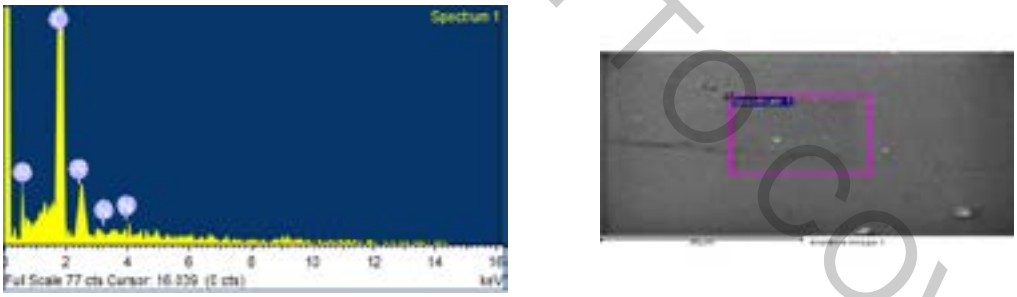

Fig. 1 EDS analysis of Al-DLC coating grown at 800 ℃ using APCVD.

Table 1. Composition of various elements of Al-DLC thin film estimated from EDS technique.

Sample No	% of Carbon	% of Al	% of Nitrogen
Al-DLC 800	90.46	9.12	0.42
Al-DLC 840	91.26	8.18	0.56
Al-DLC 880	91.61	8.03	0.36
Al-DLC 920	90.31	9.16	0.53

[1] Sun, Z. J. Non-Cryst. Solids, 261, no. 1-3, 211-217, (2000).
[2] J. H. Liang, M. H. Chen, W. F. Tsai, S. C. Lee, C. F. Ai. Nucl. Instrum. Methods Phys. Res., Sect. B 257, 1-2, 696-701, 2007.K. Melcher, L.-M. Ng, E. Zhou et al., A gate-latch-lock mechanism for hormone signaling by abscisic acid receptors, Nature 462, 602-608 (1990).

CRORRESPONDENCE TO COVID-19

GRAPHENE OXIDE CHITOSAN COPPER PLATINUM NANO COMPOSITE THIN FILMS FOR ANTI-BACTERIAL APPLICATIONS

Edith Flora Joel[1], Galina Lujanienė[1], Ieva Uogintė[1], Sandra Stanionytė[1], Martynas Skapas[1], Loreta Leviskaitė[2]

[1] SRI Center for Physical Sciences and Technology, Lithuania
[2] SRI Nature Research Centre, Vilnius, Lithuania
edith.joel@ftmc.lt

CANCELLED DUE TO COVID-19

The irreversible attachment to and on the surface of the microorganisms and the formation of an extracellular matrix improves the ability of cell growth and the gene transcription, eliminates their response to antimicrobial components. Developing ideas about biofilm has a great impact on public health, based on the role of several infectious diseases and various device-related problems [1]. The problem with antibacterial coatings and thin films is resistance to clinical drugs [2]. The progress in the new developments associated with metal nano-composites particles demonstrates a growing potential in infection control of bacteria and demanded to prevent biofilm formation. This work shows the synthesis and the antimicrobial activity of chitosan capped metal inorganic nano-particles, which have been expected to have strong antimicrobial effects in the clinical field. Chitosan nanoparticles having an extensive spectrum of antibacterial characteristics and are used to improve the antiseptic characters of inorganic nanoparticles toward biofilms. In addition to Chitosan (CS) nanomaterials, Copper (Cu), copper oxide (CuO), Graphene oxide (GO), Platinum (Pt) which are claimed to have high antimicrobial activity on bacteria [3–5]. In this study the chitosan copper oxide, chitosan capped copper, chitosan-graphene oxide-platinum and chitosan-graphene oxide-platinum-copper nano-materials were synthesized using various chemistry methods and applied to make thin films by a cast solution method; since the combination of nano-materials is also considered to have noticeable inhibitory effects on the bacteria [6].

The Copper nanoparticles are claimed to have greater toxicity to the bacteria than Copper Oxide, they are kept as a control for composites thin films in the study [3]. Copper and Platinum have been well known as efficient antibacterial materials, along with graphene oxide that has destructive interactions with microbes when the problem of biofilm is encountered. The amount of Copper introduced into nanomaterial can be an important factor effecting in the antibacterial properties. Physical Characteristics, as well as microbial properties of the developed materials in the thin film, were studied and characterized by the Transmission Electron Microscope (TEM), X-Ray Diffraction (XRD). The antibacterial effects of chitosan-nanocomposite thin films against bacteria were examined by film attachment method and zone inhibition method. The bactericidal activity was studied was estimated by the relative number of bacterial colonies survived calculated from the number of viable colonies. The possible applications include wound dressing, food packaging, anti-biofilm coating, etc.

[1] Flemming, H., Wingender, J., Szewzyk, U. et al. Biofilms: an emergent form of bacterial life. Nat Rev Microbiol **14**, 563–575 (2016). https://doi.org/10.1038/nrmicro.2016.94

[2] Dufrêne, Y.F., Persat, A. Mechanomicrobiology: how bacteria sense and respond to forces. Nat Rev Microbiol (2020). https://doi.org/10.1038/s41579-019-0314-2

[3] Akhavan, O., Ghaderi, E. Cu and CuO nanoparticles immobilized by silica thin films as antibacterial materials and photocatalysts. Surface and Coatings Technology, **205(1)**, 219–223 (2010). doi:10.1016/j.surfcoat.2010.06.036

[4] Ayaz Ahmed, K. B., Raman, T., Anbazhagan, V. Platinum nanoparticles inhibit bacteria proliferation and rescue zebrafish from bacterial infection. RSC Advances, **6(50)**, 44415–44424 (2016). doi:10.1039/c6ra03732a

[5] Li, J., Wang, G., Zhu, H. et al. Antibacterial activity of large-area monolayer graphene film manipulated by charge transfer. Sci Rep **4**, 4359 (2015). https://doi.org/10.1038/srep04359

[6] Liu, Y., Padmanabhan, J., Cheung, B. et al. Combinatorial development of antibacterial Zr-Cu-Al-Ag thin film metallic glasses. Sci Rep **6**, 26950 (2016). https://doi.org/10.1038/srep26950

SUBSTRATE IMPACT ON THE STRUCTURE AND ELECTROCATALYST PROPERTIES OF MOLYBDENUM DISULFIDE FOR HER FROM WATER

Paulius Gaigalas[1], Arūnas Jagminas[1], Arnas Naujokaitis[1], Simonas Ramanavičius[1], Marija Kurtinaitienė[1], Rolandas Trusovas[1]

[1] State Research Institute Center for Physical Sciences and Technology, Saulėtekio ave. 3, LT-10257, Vilnius, Lithuania
paulius.gaigalas@ftmc.lt

In order to replace highly effective but costly platinum and rhodium electrocatalysts for hydrogen evolution reaction (HER), nanostructured materials are attracting attention [1] as a possible cost-effective candidate to replace the noble metal electrocatalysts and facilitate the process of water splitting for hydrogen gas production.

In this study, nanostructured MoS_2 films were designed on Mo, Ti, Si/SiO_2 and Al substrates in attempt to show the influence of substrates on MoS_2 nanoplatelet formation. MoS_2 nanostructures at various substrates were fabricated *via* hydrothermal synthesis using a Teflon-lined steel autoclave and a synthesis solution containing thiourea, $(NH_2)_2CS$, ammonium heptamolybdate and aniline, $C_6H_5NH_2$. The synthesis reaction was conducted at 220 ± 2 °C for 5 to 15 h.

The obtained nanostructures were examined using SEM. These images (Fig. 1) outline that with the exception of films grown on Si/SiO_2 substrate (Fig. 1a), obtained films are of nanosheet morphology (Fig. 1b), however, a gap between the deposited films and Ti and Al substrates are observed (Fig. 1c, d). These substrates are therefore not viable for electrocatalyst fabrication. In contrast, the films fabricated onto the Mo substrate are thicker and better attached to the substrate, as seen in the SEM image (Fig. 1e).

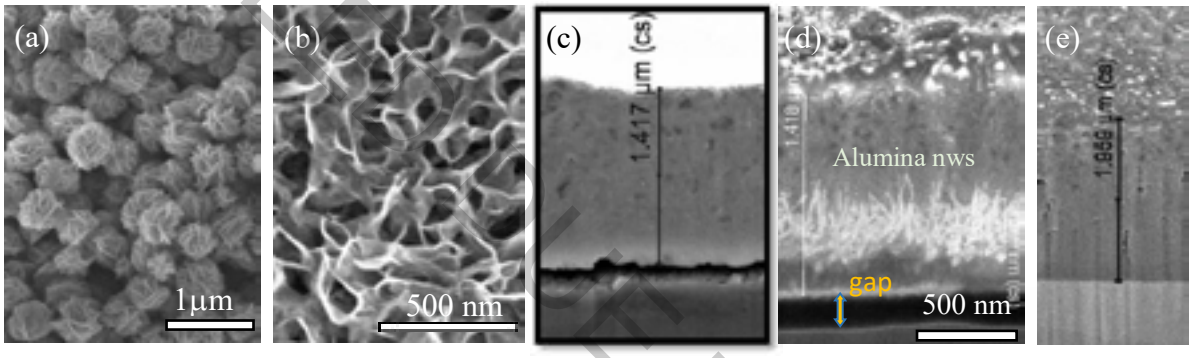

Fig. 1. Top-side (a, b) and cross-sectional (c, d, e) SEM views of MoS_2 films fabricated onto the Si/SiO_2 (a), Ti (b, c), Al (d) and Mo (e) substrates *via* hydrothermal synthesis in the solution containing (in mmol L^{-1}): 5 ammonium heptamolybdate, 90 thiourea and 25 aniline at 220 °C for 10 h.

Since MoS_2 nanoplatelet films on the Ti substrates were found to be unstable over a long period of HER time, these films were also fabricated onto anodized Ti substrates. MoS_2 films deposited on anodized Ti substrates were similar to the ones depicted previously (Fig. 1b), differing in that MoS_2 was deposited not solely onto the surface, but also filled titanium nanotubes, inter-tube gaps and cracks, which were formed during the anodizing process. Therefore, these fabricated electocatalysts exhibited much higher HER activity and greatly increased HER stability in acidic solution.

In order to increase both activity and stability of fabricated electrocatalysts, improvements of deposited films as well as anodizing process of Ti substrates are considered.

[1] L. Yang, W. Zhou, D. Hou, K. Zhai, G. Li, Z. Tang, L. Li, S. Chen, Porous metallic MoO_2-supported MoS_2 nanosheets for enhanced electrocatalytic activity in the hydrogen evolution reaction. Nanoscale 7 (2015) 5203-5208.

CANCELLED DUE TO COVID-19

MATHEMATICAL ANALYSIS OF POROSITY IN NANOFIBERS

Virginija Kleivaitė[1], Rimvydas Milašius[1]

Faculty of Mechanical Engineering and Design, Kaunas University of Technology, Lithuania
virginija.kleivaite@ktu.edu

Electrospun nanofibers incorporated with antimicrobial agents have been produced with antimicrobial capability against a wide range of microorganisms. The morphologies and performance of antimicrobial electrospun nanofibers are emphasized and specific attention is given to future application of electrospun nanofibers with antimicrobial capability. The porosity of the structure of the nanofibers is not evaluated, although it can be considered as a structural imbalance. Many people may ask for materials containing barrier properties such as to prevent any harmful effects on the human body, and because of this there are many additional substances that can have an antibacterial effect and can easily get into the structure, but there are many people who are allergic to such substances as silver or zinc. Therefore, it is necessary to block the path to the bacteria without additional added substances.

Nanofiber web structures formed by electrospinning are influenced by many factors. Analyzing the various literature sources about the electrospinning process, the authors‘ opinion often differs, due to the influence of various parameters on porosity of nanofibers. Analyzing the SEM images of the webs formed during the research, it was observed that the web is formed by pores of different sizes [1-2].

Analysis of 4 series of measurements shows that the character of distribution in all cases was obtained very similarly – the average value in all cases was obtained in the column of modal value of distribution, i.e. at 100-200 nm. All distributions have the similar positively skew and the coefficient of asymmetry A, which evaluates the skewness of distribution, was obtained in the range of 1.4. Such not low skew shows an important difference from classical normal Gausian distribution. It means that we cannot use classical statistical evaluation of obtained distributions and cannot predict the highest value of possible pore size without additional analysis of distribution.

The highest differences were obtained in the maximum pore of all measurements of 4 series – twice it was obtained that maximum pore is in the range 500-600 nm, once in the range 400-500 nm, and once in the range (for example Fig. 1) of 600-700 nm. It means that sometimes in electrospun web we can find the pore whose range is not similar to other series of measurements. This phenomenon creates a big difficulty for maximum porosity of all web evaluation. On the other hand, only once it was found that a pore of web is much higher than in other series – only one pore had the diameter higher than 600 nm, i.e., it had 667 nm, and the next after maximum pore was similar to the cases of maximum pore of series No.2 and No.4, i.e., the diameters were in the range of 580 nm. The difference between the maximum pore and the second one is not very high – only 13% in all series of measurements [3].

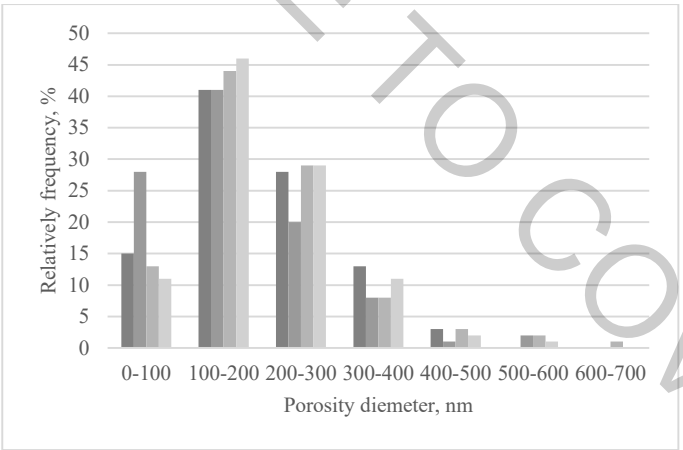

Fig. 1. SEM image of maximum pore size

[1] Malašauskiene J., Milašius R., Mathematical Analysis of the Diameter Distribution of Electrospun Nanofibres. Fibres & Textiles in Eastern Europe, Vol. 18, No. 6 (83) p. 45-48, 2010.
[2] Kleivaitė V., Milašius R., Electrospinning – 100 Years of investigations and still open questions of web structure estimination. Autex Reasearch Journal, Vol. 18, No 4, December 2018.
[3] Kleivaitė V., Milašius R., Investigation of electrospun web porosity and its statistical evaluation. The Journal of the Textile Institute, July 2019.

CANCELLED DUE TO COVID-19

ELECTROCATALYTIC ACTIVITY OF TITANIA NANOTUBULAR LAYERS DECORATED BY GOLD NANOPARTICLES IN OXYGEN ELECTROREDUCTION

Hanna Maltanava[1], Semyon Mazheika[2], Evgeni Ovodok[1], Sergei Voitekhovich[1], Tatyana Gaevskaya[1], Sergey Poznyak[1]

[1]Research Institute for Physical Chemical Problems, Belarusian State University, Belarus
[2] Department of Chemistry, Belarusian State University, Belarus
maltanava@bsu.by

CREATED DUE TO COVID-19

The tremendous research efforts have been devoted to the oxygen electroreduction reaction (ORR), particularly with respect to potential application for fuel cells. The progress in fabrication of different anion-exchange membrane including hydroxyl-conducting polymer membrane has driven interest to Alkaline Fuel Cells [1]. The great deal of attention has been focused on development of suitable alternative electrocatalysts efficient enough in alkaline medium to replace platinum group metals. Thus, the systems based on gold nanoparticles (Au NPs) capable to ORR in alkaline medium have aroused interest as potential electrocatalyst for ORR [1]. Herein, we investigated the activity of 2 nm and 5 nm Au NPs deposited onto titania nanotubes (TNT) towards the ORR.

Tinania nanotubes were produced by two-stage anodization of Ti in ethylene glycol electrolyte containing 0.75 wt.% NH_4F and 2 vol.% H_2O. In order to obtain crystalline structure of anatase, the TiO_2 nanotubes were annealed at 450 °C for 3 h in air. Colloidal Au NPs with an average diameter of 5 nm and 2 nm were fabricated via methods described in [2, 3]. To study the influence of Au NPs loading on the activity of Au-TNT systems in ORR, different amount of Au NPs (0.75÷3 μg/cm^2) was deposited from sol onto TNT electrodes. Electrocatalytic activity of Au−TNT toward ORR was examined by cyclic voltammetry (CV) using an Autolab potentiostat in a 0.1 M KOH solution saturated with oxygen. The electrode potentials are referred with respect to a Hg/HgO (1 M KOH) reference electrode.

The annealed TNT samples have well-aligned nanotubular structure with a relatively narrow distribution of the inner diameter (60±5 nm) and the wall thickness (12±2 nm) of vertical nanotubes having a length of 10±1 μm. The Au NPs deposited on TNT are well separated and distributed both on the upper and on the inner side of the nanotubes.

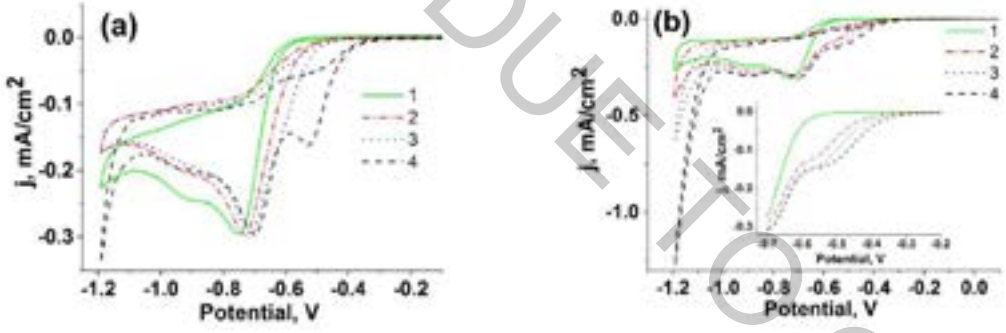

Fig. 1. Cyclic voltammograms of ORR on TNT decorated by 5 nm (a) and 2 nm Au NPs (b) (1 – bare TiO_2; 2 – TiO_2-0.75 μg/cm^2 Au; 3 – TiO_2-1.5 μg/cm^2 Au; 4 – TiO_2-3 μg/cm^2 Au)

Oxygen electroreduction at the bare TNT electrodes demonstrates a cathodic wave at potentials more negative than –0.65 V. Deposition of Au NPs onto TNT leads to a decrease of overpotential toward ORR. Moreover, the behavior of Au−TNT systems depends on the surface concentration and the size of deposited Au NPs. In the case of 5 nm Au NPs, an increase of the amount of Au NPs from 0.75 to 3 μg/cm^2 reduces the overvoltage of ORR by 0.1 V at a current density of 100 μA/cm^2 (Fig. 1a). It is worth mentioning that the waves from Au NPs for the Au-modified systems containing 0.75 μg/cm^2 and 1.5 μg/cm^2 of Au NPs are superimposed on the ORR wave from TiO_2, and their position cannot be determined unambiguously. For the TNT loaded with 3 μg/cm^2 Au NPs, a clearly distinguishable additional wave, which can be related to ORR on Au surface, appears at less negative potentials. In case of 2 nm Au NPs, the additional Au-catalyzed wave is formed, already starting from 0.75 μg/cm^2 of Au NPs (Fig. 2b). A 2- and 4-fold increase in the amount of deposited Au NPs leads to a decrease in the ORR overvoltage by 30 and 60 mV, respectively (Fig. 2b, insert). In general, the electrocatalytic activity of 2 nm Au NPs is slightly higher than those of 5 nm. When the Au NPs size reduces from 5 nm to 2 nm, provided that the amount of Au NPs is the same, half-wave potential of ORR on the gold surface is shifted by 10÷20 mV to the positive direction.

Thus, the ORR overvoltage of Au−TNT system depends on the size and concentration of Au NPs. A decrease of Au NPs size from 5 nm to 2 nm and an increase in the amount of nanoparticles leads to increasing the activity of Au−TNT systems in the process of O_2 electroreduction.

[1] G. Merle, M. Wessling, K. Nijmeijer, Anion exchange membranes for alkaline fuel cells: a review, J. Membr. Sci. **377,** 1–35 (2011).
[2] H. Maltanava, S. Poznyak, M. Starykevich, M. Ivanovskaya, Electrocatalytic activity of Au nanoparticles onto TiO_2 nanotubular layers in oxygen electroreduction reaction: size and support effects, Electrochim. Acta. **222**, 1013–1020 (2016).
[3] S. V. Voitekhovich, A. Wolf, C. Guhrenz et al., 5-(2-Mercaptoethyl)-1H-tetrazole: Facile Synthesis and Application for the Preparation of Water Soluble Nanocrystals and Their Gels, Chem. - A Eur. J. **22**, 14746–14752 (2016).

WATER-SOLUBLE SEMICONDUCTOR CORE-SHELL NANOCRYSTALS WITH CONTROLLED SURFACE CHARGE

Aliaksandra Radchanka[1], Varvara Hrybouskaya[2]

[1] Institute for Physical Chemical Research, Belarusian State University, Belarus
[2]Belarusian State University, Chemistry Department, Belarus
aleksandraradchenko10@gmail.com

Highly luminescent quantum dots (QDs) are generally made using high-temperature syntheses in organic solvents. Core-shell QDs (e.g. CdSe/ZnS) possess high photostability and quantum yield, broad absorption, and narrow emission peaks and have found wide application in biological and biomedical applications [1]. Since QDs synthesized in organic media are highly hydrophobic, and biological applications require water-soluble QDs. Among others, the encapsulation of QDs with amphiphilic polymer has proven to be the most effective approach that allows preparing colloidal stable water-soluble QDs with low hydrodynamic size and preserve their unique optical properties [2]. Additionally, chemical modification of the polymeric shell with various functional groups enables control of the surface charge and hydrodynamic size of QDs.

The purpose of this work was to create a new approach to modify poly(maleic anhydride-*alt*-1-tetradecene) (PMAT) with various functional groups which is then used for the encapsulation of CdSe/ZnS core-shell QDs. Also, we studied variations in the surface charge with respect to pH and a type of functional group embedded into the polymer.

The idea was to modify PMAT with molecules with various functional groups to create a polymeric shell of QDS with a different sign of surface charge, its magnitude, and its relation to the pH of the media. Chemical modification of PMAT was performed according to the procedure that involved the reaction of PMAT in organic solution with bi-functional molecules, containing both primary NH_2-group and different charged groups (sulfonate, sulfate, phosphate, phosphonate and quaternary ammonium groups). After chemical modification of PMAT with selected agents hydrophobic CdSe/ZnS core-shell QDs were encapsulated by modified PMAT according to the standard protocol [3]. Encapsulated QDs were dissolved in different 0.01 M buffer solutions with the pH ranging from 4.5 to 9.5. ξ-potential and hydrodynamic size of water-soluble QDs were measured with the dynamic light scattering analyzer Malvern Zetasizer NanoZS90.

Encapsulated with PMAT 100% modified with phosphonic and sulfonic groups QDs results in a ξ-potential of approximately - 38 mV (Fig. 1, A). Embedding of phosphate and sulfate groups into the PMAT leads to a ξ-potential around to -23 mV. Sulfate- and sulfonate-modified PMAT shows almost constant ξ-potential value in overall pH range, while phosphate, phosphonate, and carboxylic groups show on the surface of QDs leads to increase the negative value in basic buffers due to weak acidity for their monomolecular inorganic analogs.

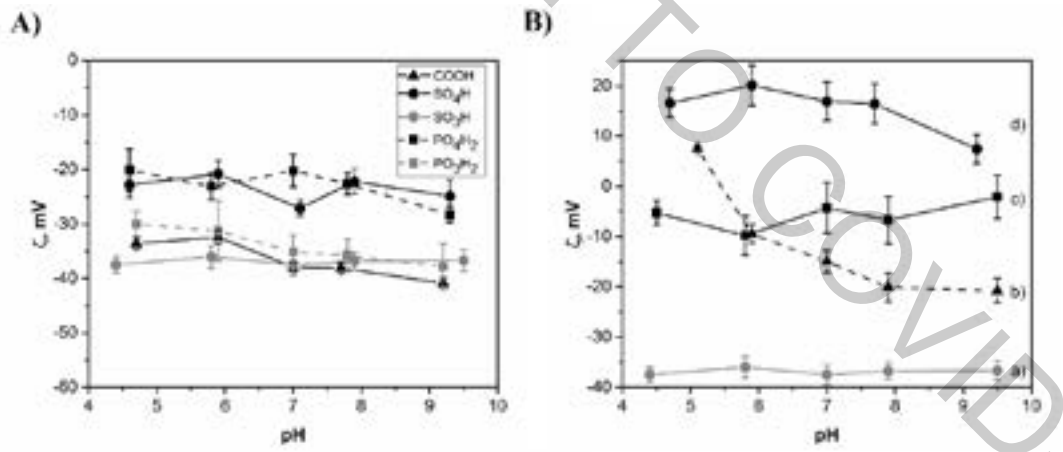

Fig. 1. A) Influence of pH on the ζ-potential of QDs encapsulated with PMAT with negatively-charged functional groups. B) pH-dependence of ζ-potential of QDs encapsulated with PMAT with different modifiers: a) 100% of taurine; b) 50% (2-aminoethyl)trimethylammonium chloride; c) 50% of (2-aminoethyl)trimethylammonium chloride and 50% of taurine; d) 100% of (2-aminoethyl)trimethylammonium chloride.

Modification of PMAT with 100% of (2-aminoethyl)trimethylammonium chloride results in a constant positive ξ-potential of encapsulated QDs around +17 mV in the biological pH range of 5-8, then it drops at pH above 8 (Fig. 1, B-d). Partial, 50 % modification of PMAT with quaternary ammonium groups gives encapsulated QDs with pH-dependent ξ-potential. At acidic pH, ζ-potential is +13 mV, while in basic solutions zeta potential drops down to 20 mV passing through zero. Therefore, we can change ξ-potential of our QDs by varying the pH of a solution.

[1] N. Tomczak, R. Liu, J. G. Vansco, Nanoscale **5**, 12018 (2013).
[2] E. Petryaeva, W. Russ Algar, and I.L. Medintz. Appl. Spectrosc. **67**, 216 (2013).
[3] Fedosyuk, A., Radchanka, A., Antanovich, A., Prudnikau, A., Kvach, M., Shmanai, V., Artemyev, M. Langmuir **32**, 1955 (2016).

CANCELLED DUE TO COVID-19

ULTRAFAST PLASMON RELAXATION DYNAMICS OF LASER AFFECTED SILVER NANOPARTICLES

Gerda Klimaitė[1], Domantas Peckus[2], Mantas Mikalkevičius[1,2], Asta Tamulevičienė[1,2], Tomas Tamulevičius[1,2], Sigitas Tamulevičius[1,2]

[1]Department of Physics, Kaunas University of Technology, Studentų St. 50, LT-51368 Kaunas, Lithuania
[2]Institute of Materials Science, Kaunas University of Technology, K. Baršausko St. 59, LT-51423 Kaunas, Lithuania
gerda.klimaite@ktu.edu

Silver nanoparticles (Ag NPs) have become attractive for various electrooptical applications because of their plasmonic properties. These properties originate from the excitation of oscillations of free surface electrons, a phenomenon in nanosized plasmonic metals known as *Localized Surface Plasmon Resonance* (LSPR) [1]. Metal NPs with unique optical properties can be created by varying size and shape of NPs therefore better control of these parameters could lead to more advanced applications [1].

The purpose of this work was to modify chemically synthesized Ag NPs using ultrafast laser pulses and analyze the dynamics of ultrafast relaxation processes after the modification. Ag NPs were synthesized employing polyol synthesis method using 1,5-pentanediol as reaction medium, silver nitrate $AgNO_3$ as precursor and PVP as capping agent [2]. Synthesized nanoparticles had broad size distribution and cube like shape where the length of cube edge was ranging from few nanometers up to 60 nm. The application of ultrashort laser pulses was used in order to change the size distribution expecting it will become narrower.

The modification of colloidal solutions was performed with femtosecond Yb:KGW laser (290 fs pulse duration, 1030 nm wavelength, 40 kHz repetition rate, 4 W power) Steady-state absorption measurements were performed with an UV-VIS spectrometer (Avantes) in a range of 200 – 1000 nm (Fig. 1 a). Ultrafast transient absorption spectroscopy (TAS) technique was used to measure ultrafast plasmon relaxation dynamics in Ag NPs. The size distribution of Ag NPs was determined from SEM micrographs using "ImageJ" software (Fig. 1 b, c).

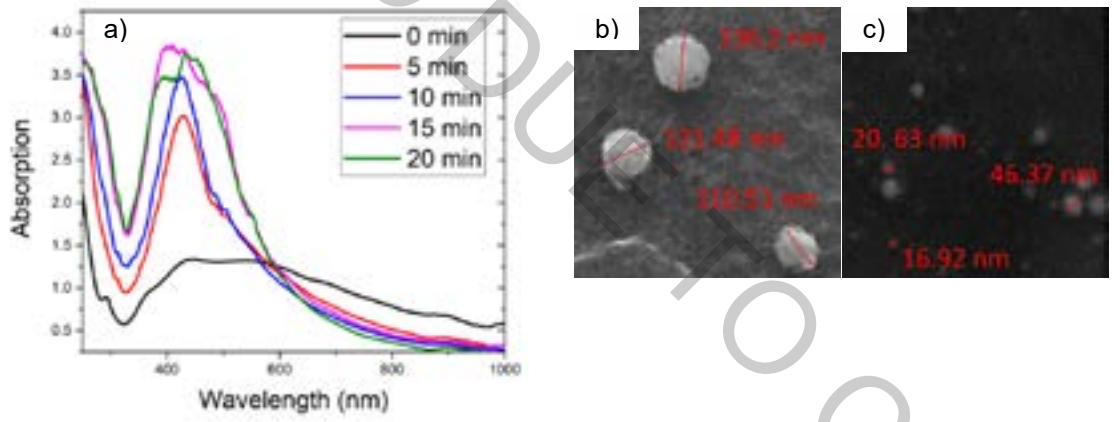

Fig. 1. a) Absorption of synthesized (black curve, 0 min) and modified colloidal solutions, b) SEM micrographs after 5 min irradiation; c) SEM micrographs after 20 min irradiation.

The Ag NPs affected with femtosecond laser pulses for 0, 5, 10, 15 and 20 min were analyzed by TAS, UV/VIS steady-state absorption spectrometer and SEM. TAS spectra have not shown a clear dependence on laser irradiation time of Ag NPs samples. However, it has an influence on decay times of TAS signal relaxation. The deeper analysis of absorption graphs (Fig. 1 a) and SEM micrographs (Fig. 1 b and c) revealed that the absorption spectrum of the laser affected Ag NPs was shifted into shorter wavelengths area and the peak width was reduced in comparison to primary Ag NPs sample. The irradiation with ultrashort laser pulses resulted in the change of nanoparticle shape into spherical. Depending on the irradiation time average Ag NPs diameter varies from 130.38 nm (5 min) to 40.64 nm (20 min).

Acknowledgement: This research was funded by the European Social Fund under the No. 09.3.3-LMT-K-712 "Development of Competences of Scientists, other Researchers and Students through Practical Research Activities" measure, grant No. 09.3.3-LMT-K-712-16-0197.

[1] E. Martinsson, et al., Substrate Effect on the Refractive Index Sensitivity of Silver Nanoparticles. The Journal of Physical Chemistry C, 118, 24680-24687 (2014).
[2] D. Peckus, et al., Hot Electron Emission Can Lead to Damping of Optomechanical Modes in Core-Shell Ag@TiO2 Nanocubes, J.Phys.Chem.C, 121, 24159-24167 (2017)

CHEMFED DUBLIN COVID-19

PHOTOELECTRIC ACTIVITY OF GRAPHENE/BACTERIAL REACTION CENTER NANOCOMPOSITE

Greta Urbonaitė[1*], Tibor Szabo[2], Radmila Panajotović[3], Jasna Vujin[3], Tijana Tomašević-Ilić[3], Ieva Bagdanavičiūtė[4], Richard Cseko[2], Klara Hernadi[5], Gyorgy Varof[6] and Laszlo Nagy[2]

[1] Faculty of Mathematics and Natural Sciences, Kaunas University of Technology, Lithuania
[2]Institute of Medical Physics and Informatics, University of Szeged, Hungary
[3]Institute of Physics, University of Belgrade, Belgrade, Serbia
[4]Faculty of Chemical Technology, Kaunas University of Technology, Lithuania
[5]Department of Applied and Environmental Chemistry, University of Szeged
[6]Institute of Biophysics, Biological Research Center, Szeged, Hungary

urbonaiteeg@gmail.com

CANCELLED DUE TO COVID-19

This work presents a research with one of the most important proteins for the light energy conversion, called the photosynthetic reaction center (RC) proteins [1]. They are the complexes of proteins, functional cofactors, pigments and redox active chromophores performing energy collection and primary electron transfer processes [2]. It has been indicated, that the biological activity of the RC proteins can be partly maintained by bonding them to nanostructures [3]. Here, the RC proteins were purified from *Rhodobacter (Rb.) sphaeroides* 2.4.1. purple bacterium (Fig. 1) and deposited on the graphene layer prepared by liquid exfoliation and light-induced resistance change was measured.

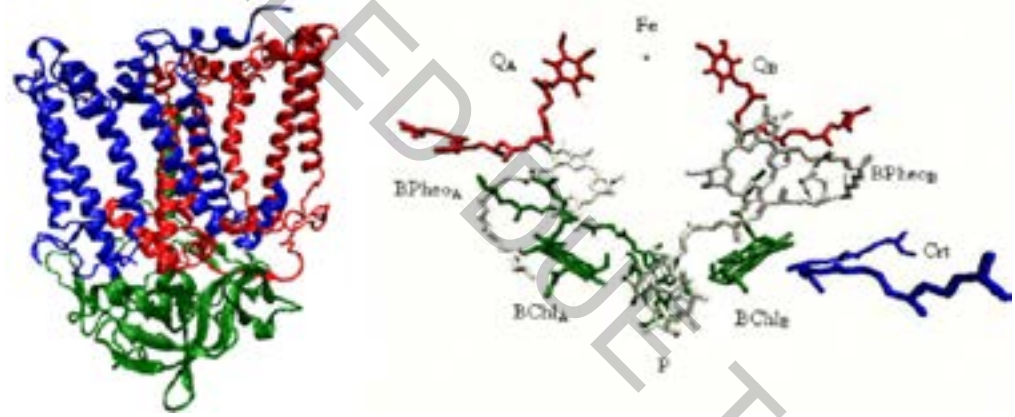

Fig. 1. The molecular model of photosynthetic reaction centre of *Rb. sphaeroides*. Left: three subunits (H-green, L-blue and M-red) of the protein. Right: redox active cofactors that are carrying the electron transfer [4].

The photosynthetic reaction center is able to perform photoactivity when deposited on graphene even in dried form. By measuring the temperature dependence of the resistance change of the bare and RC functionalized graphene and compared with the one inactivated by protein unfolding two effects were possible to separate. One of them is the resistance change due to the temperature effect. The other one clearly indicates a possible electric/electronic interaction between the charge flow in the graphene and the light-induced charge pair within the protein, which is, essentially, different in the open (dark, PBPheo) and closed (light, P^+BPheo^-) states. These results provide useful information for designing hybrid bio-photonic devices which are able to absorb and convert light energy.

[1] T. Szabó, M. Magyar, K. Hajdu, M. Dorogi, E. Nyerki, T. Tóth, M. Lingvay, G. Garab, K. Hernádi and L. Nagy, Structural and Functional Hierarchy in Photosynthetic Energy Conversion—from Molecules to Nanostructures, Nanoscale Research Letters, 10, 1-12 (2015).
[2] G. D. Scholes. G. R Fleming, A. Olaya-Castro and R. van Grondelle, Lessons from nature about solar light harvesting. Nature Chemistry, 3, 763-774 (2011).
[3] K. Hajdu, T. Szabó, A. E. Sarrai, L. Rinyu and L. Nagy, Functional Nanohybrid Materials from Photosynthetic Reaction Center Proteins, International Journal of Photoenergy, 2017, 14 (2017).
[4] L. Nagy, K. Hajdu, B. Fisher, K. Hernandi, K. Nagy and J. Vincze, Photosynthetic reaction centres-from basic research to application possibilities, Notulae Scientia Biologicae,. 2, 7-13 (2010).

DEVELOPMENT OF CLAY-BASED NANOCOMPOSITE MATERIALS

Raman Novikau[1], Galina Lujanienė[1*], Kęstutis Mažeika[2], Sergej Šemčuk[1*]

[1] Department of Environmental Research, Center for Physical Sciences and Technology, Lithuania
[2]Department of Nuclear Research, Center for Physical Sciences and Technology, Lithuania
novikaur95@gmail.com

Nowadays, the main sources of environmental pollution are waste products of the various kinds of industrial enterprises. In this regard, the development of biocompatible adsorbents, the use of which would be aimed at wastewater treatment to remove potential pollutants: organic and inorganic, to minimize their environmental impact, is relevant [1, 2].

The use of clay as an adsorbent is due to the peculiarities of its structure, as well as its economic availability and ubiquity, the tendency to use clay has undergone several changes, from its pure use to modifications and combination with other adsorbents, obtaining composite materials, as well as by combining various methods for obtaining new composites [3, 4].

The problem of using most of these composites is due to low and/or medium biocompatibility, as well as the possibility of secondary environmental pollution.

The study aimed to develop a nanocomposite of clay – graphene oxide – magnetite/maghemite, obtained by different synthesis methods.

Graphene oxide was obtained by the Hammers method. Magnetite/maghemite based nanocomposite were synthesized in a solution containing graphene oxide by a liquid-phase method based on the coprecipitation of salts of ferrous and ferric iron with aqueous ammonia.

Then, the obtained graphene oxide – magnetite/maghemite nanocomposites and clay were dispersed in water in an ultrasonic bath for 8 hours. The Triassic clay from Šaltiškiai quarry located in the North of Lithuania was used in this study. The mass ratio of clay:graphene oxide – magnetite, were as follows: 1:1; 1:0.75; 1:0.5; 1:0.25.

The second synthesis method was based on the fact that the clay – graphene oxide nanocomposite was first obtained by dispersing graphene oxide in water for 2 hours, followed by the addition of clay, and dispersed for another 30 minutes on an ultrasonic bath, then stirred for 30 minutes on a magnetic stirrer while heating, the resulting nanocomposite was dried, then separately prepared magnetite was added to it, dispersed in water on an ultrasonic bath for an hour, mass ratios were of 10:1 and 1.5:1 (magnetite:graphene oxide – clay).

The resulting nanocomposites respond well to the influence of a magnetic field, and they were also evaluated using X-ray diffraction (XRD) and Mössbauer spectroscopy. This is the first stage of our research; the second stage will be aimed at studying the adsorption characteristics of the obtained nanocomposite.

---

[1] M.N. Rashed, Adsorption technique for the removal of organic pollutants from water and wastewater, Organic Pollutants – Monitoring, Risk and Treatment, 167-179 (2013).
[2] X. Mao, R. Jiang et al., Use of surfactants for the remediation of contaminated soils: a review, Journal of Hazardous Materials Mater **285**, 419-435 (2015).
[3] H. Han, M. Rafiq et al., A critical review of clay-based composites with enhanced adsorption performance for metal and organic pollutants, Journal of hazardous materials **369**, 780-796 (2019).
[4] A. Awad, S. Shaikh et al. Adsorption of organic pollutants by natural and modified clays: a comprehensive review. Separation and Purification Technology **228**, 1-39 (2019).

CANCELLED DUE TO COVID-19

DEPOSITION OF MULTILAYER OPTICAL COATINGS ON CORRUGATED SURFACES

Julianija Nikitina[1,2*], Tomas Tolenis[1], Lina Grinevičiūtė[1]

[1] Center for physical sciences and technology, Savanorių ave. 231, LT-02300 Vilnius, Lithuania
[2] Department of Physics, Vilnius University, Saulėtekio ave. 9, LT-10222, Vilnius, Lithuania
[*]julianija.nikitina@ff.stud.vu.lt

During recent decades, thin film coating technology has experienced significant development, providing high quality laser optics with desired functionalities, like optical filters, high-reflection mirrors etc. Fabrication processes of such optical elements usually consider multilayer interference coatings deposition on initially flat substrates, thus creating refractive index modulation in one direction, as in case of 1-dimentional photonic crystal. Meanwhile, the evolving nanophotonics field requires more complex and novel optical elements with 2D or even 3D periodicity of refractive index [1]. Unfortunately, state-of-the-art fabrication technologies, even like direct laser writing, are not suitable in this case due to restricted control over the formation of the structure at nanoscale.

Present work proposes an alternative fabrication process – deposition of multilayer optical coatings on modulated surfaces employing PVD technologies together with glancing angle deposition (GLAD) method. GLAD allows to form the so called sculptured thin films by directing vapor flux towards the substrate at oblique angle. This feature potentially may help to conformally cover non-flat surfaces and maintain initial structure modulation throughout the film thickness, which is crucial considering optical elements with 2D or 3D periodicity of refractive index. In this case several variables appear: substrate relative orientation during the deposition process and the angle θ subtended between the substrate normal and the incident vapor flux. It is important to evaluate the dependence of final structure on these values. Primary numerical simulations were performed employing NASCAM (NAno SCAle Modeling) software based on kinetic Monte Carlo algorithm [2]. This software does not take into account the vibrational movement of atoms or interatomic interactions, hence allows to investigate time evolution of relatively large systems containing millions of atoms. As an example, in Fig. 1 are shown 10 alternating layers of SiO_2 and Al_2O_3 coating evolution in different cases: (a) multilayer structure on flat surface creates refractive index modulation in one direction and it can be easily deposited employing conventional PVD technologies. Although layers deposition on modulated surfaces can face several problems, like cracks formation along film thickness (Fig.1 (b) and (c)) or modulation extinction after several layers (Fig.1 (c)).

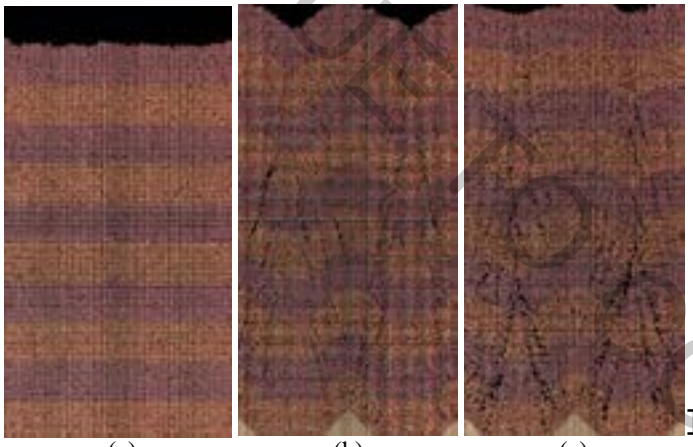

(a) (b) (c)

Fig. 1. Simulations performed by NASCAM software for 10 alternating layers of SiO_2 and Al_2O_3 deposited: (a) on flat substrate at θ=0º angle; (b) on grating at θ=30º while the plane between the vapor flux and normal of the surface is parallel and (c) perpendicular to grating lines orientation.

The aim of this research is to simulate and evaluate the growth mechanism of multilayer optical coatings on modulated surfaces and compare theoretical results with experimental measurements. Experimental part was performed with different PVD technologies, as ion beam sputtering, electron beam evaporation and with GLAD method, to evaluate their ability to conformally cover modulated surfaces.

[1] L. Grineviciute, C. Babayigit, D. Gailevičius, E. Bor, M. Turduev, V. Purlys, T. Tolenis, H. Kurt, and K. Staliunas. "Angular filtering by Bragg photonic microstructures fabricated by physical vapour deposition." Appl Surf Sci., 481, pp. 353 – 359 (2019)
[2] Moskovkin, P., & Lucas, S. Computer simulations of the early-stage growth of Ge clusters at elevated temperatures on patterned Si substrate using the kinetic Monte Carlo method. Thin solid films, 536, 313-317 (2013)

CANCELLED DUE TO COVID-19

STUDY OF THE TEMPERATURE INFLUENCE ON THE GEOMETRY OF THE SILVER NANOPARTICLES DURING POLYOL SYNTHESIS

Simona Vyčaitė[1], Asta Tamulevičienė[1,2]

[1] Department of Physics, Kaunas University of Technology, Lithuania
[2] Institute of Materials Science, Kaunas University of Technology, Lithuania
simona.vycaite@ktu.edu

CANCELLED DUE TO COVID-19

Metal nanoparticles with different sizes and shapes have broad spectrum of application including localized surface plasmon resonance (LSPR), surface enhanced Raman scattering (SERS) [1], sensors, optical probes, catalysts [2]. The polyol synthesis route allows to obtain nanoparticles of various shapes and sizes. Size and shape of the nanoparticles mainly depends on the synthesis temperature, precursors, synthesis time [2,3].

Polyol synthesis is simple chemical reduction method where the medium of reaction is multivalent alcohols [4]. The main advantage of this synthesis is that variety of polyols can be used and simplicity - it does not require very expensive materials to obtain particles of normative size by chemical reduction in a short time.

In this research, polyol synthesis was used to synthesize silver nanostructures. The precursor was silver nitrate, copper chloride was used as etchant and polyvinylpyrrolidone – as capping agent. All reagents were dissolved in 1,5 – pentanediol. The reaction took place in a heated vial with 1,5-pentanediol repeatedly injecting AgNO3 and PVP solutions. These two solutions were injected repeatedly in a hot flask with 1,5-pentanediol. The process took about 15 minutes in average until the solution in reaction flask became opaque. The final solution was left to cool down in a room temperature and optical properties were measured (Avantes, 190-1100 nm, resolution 1.4 nm). The influence of synthesis temperature to the yield and geometry of nanoparticles was investigated in a range of 125 – 155°C.

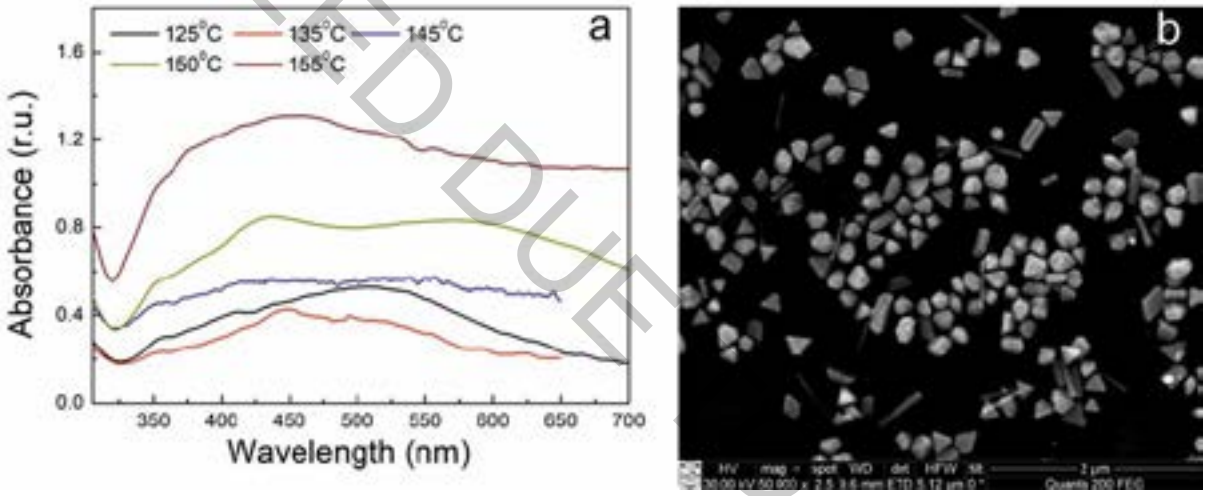

Fig. 1. UV-VIS spectra of nanoparticle solutions synthesized at different temperatures (a) and corresponding SEM image of nanoparticles synthesized at 155°C

The effect of the temperature on the optical properties of colloidal solution is shown in Fig. 1 (a). It was found that in all used temperature range, silver nanostructures were formed as characteristic surface plasmon peak was observed. Only at 145°C temperature the peak is not so well expressed (due to broad size distribution). From the absorption spectra of the nanoparticles synthesized at 125 ^{0}C and 150 ^{0}C two main peaks were identified – at the 420 nm and 510 – 600 nm with shoulder at 350 nm. That is an indication of synthesized particles with sharp edges [5]. Analysis with SEM has proved our conclusion from UV-VIS spectra (Fig. 1 (b)). From the SEM image one can see that there are different shape particles and some of those are single crystalline particles and some – multiply twinned.

[1] X. Luo, Y. Shen, D. Yang et al., Morphology control of silver nano-crystals through a polyol synthesis, Elsevier, Solid State Sciences **13**, 1719-1723 (2011).
[2] C. L. Keat, A. Aziz et.al., Biosynthesis of nanoparticles and silver nanoparticles, Bioresources and Bioprocessing, 2:47 (2015).
[3] B. Khodashenas, H. R.Ghorbani, Synthesis of silver nanoparticles with different shapes, Arabian Journal of Chemistry, Vol. **12**, Issue 8, 1823-1838 (2019).
[4] Zhang, A.-Q., Qian, D.-J., & Chen, M. (2013). Simulated optical properties of noble metallic nanopolyhedra with different shapes and structures. The European Physical Journal D, 67 (11).
[5] M. B. Cortie, F. Liu, M.D. Arnold, et al., Multimode Resonances in Silver Nanocuboids, Langmuir, **28**, 9103-9112 (2012).

CONTROL OF THE STAINLESS STEEL WETTABILITY VIA FEMTOSECOND LASER-INDUCED PERIODIC STRUCTURES AND DEPOSITION OF AMORPHOUS DIAMOND LIKE CARBON THIN FILMS

Mantas Mikalkevičius[1], Mindaugas Juodėnas[1], Tomas Tamulevičius[1,2], Saulius Burinskas[1], Asta Tamulevičienė[1,2]

[1]Institute of Materials Science of Kaunas University of Technology, K. Baršausko Str. 59, LT-51423, Kaunas, Lithuania
[2]Department of Physics of Kaunas University of Technology, Studentų Str. 50, LT-51368, Kaunas, Lithuania
mantas.mikalkevicius@ktu.edu

Next generation digital flowmeter devices employ ultrasound methods for precise gauging of liquid flow. Stainless steel mirrors that reflect the ultrasound waves ensure corrosion resistance but the permanent contact with domestic water with a high mineral content leads to biofouling which inevitably changes the performance of such smart devices. Processing of solids near their ablation threshold by high intensity polarized laser irradiation may lead to the development of regular nanoscale structures known as Laser-induced Periodic Surface Structures (LIPSS). Applying LIPSS to a surface can lead to numerous applications of surface functionalization such as improved wetting performance [1] and anti-bacterial activity [2]. On top of that, it can be additionally controlled by employing hydrophobic amorphous diamond like carbon (DLC) films, which could also aid to preserve the laser induced nanostructures under constant water flow in the long term.

In this work, the fundamental harmonic (1030 nm) of a linearly polarized Yb:KGW femtosecond laser beam was scanned over the surface of a stainless steel mirror while varying the pulse energy and laser spot overlap. Amorphous DLC films were deposited on virgin and laser treated stainless steel surfaces by employing the direct ion beam synthesis from a hexamethyldisiloxane precursor. Wettability of the surfaces was evaluated using sessile drop method where 1 µl volume droplets of water were dispensed on the pristine and differently treated surfaces. Optical microscope images of the laser treated and later on DLC coated samples are depicted in Fig. 1.

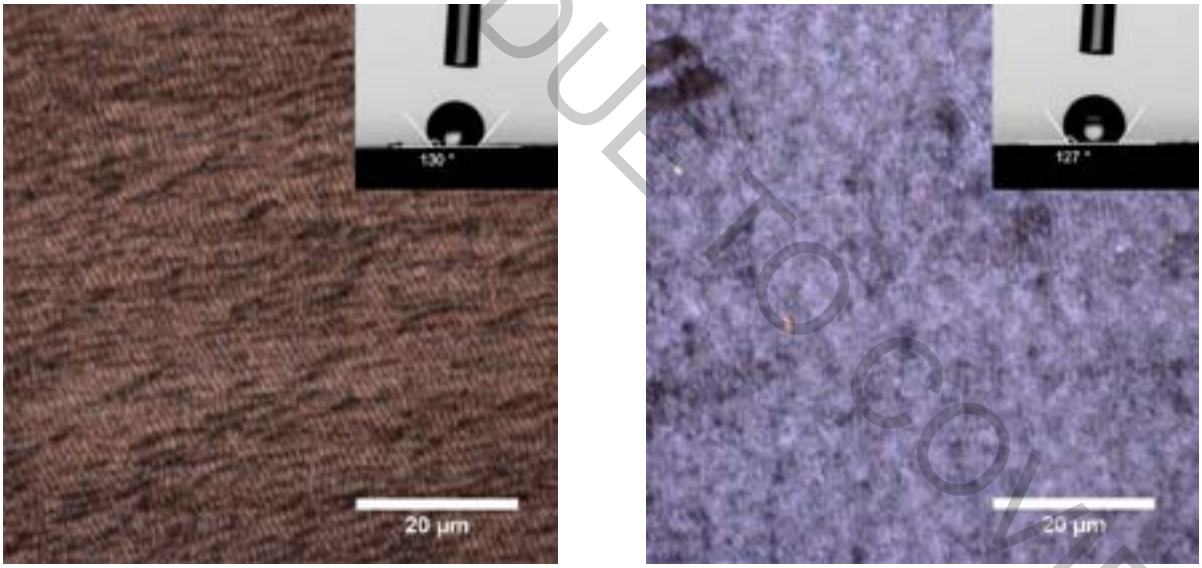

Fig. 1. Stainless steel surface micrographs after (a) laser treatment and (b) application of the DLC thin film. The inset depicts the water contact angles.

The laser treatment conditions that ensured a contact angle of 130° for deionized water close to the laser ablation threshold were obtained. Amorphous DLC films increased the water contact angle of pristine stainless steel surface by 40° while in the case of laser treated surface it remained constant. The anti-biofouling properties of treated surfaces were investigated in a custom-built setup that simulates tap water flow in a domestic system.

This research was funded by the European Social Fund under the No. 09.3.3-LMT-K-712 “Development of Competences of Scientists, other Researchers and Students through Practical Research Activities” measure.

[1] Van Driel, H. M., Sipe, J. E., and Young, J. F., *Laser-induced periodic surface structure on solids: a universal phenomenon,* Physical Review Letters 49(26), 1955–1958 (1982). https://doi.org/10.1103/PhysRevLett.49.1955
[2] Lutey, A. H., Gemini, L., Romoli, L., Lazzini, G., Fuso, F., Faucon, M., and Kling, R., *Towards laser-textured antibacterial surfaces*, Scientific Reports 8(1), 1–10 (2018). https://doi.org/10.1038/s41598-018-28454-2

CANCELLED DUE TO COVID-19

EFFECTS OF THERMAL ANNEALING ON GRAPHENE STRUCTURE DIRECTLY SYNTHESISED ON SI(100) SUBSTRATE

Šarūnas Jankauskas[1], Rimantas Gudaitis[1], Andrius Vasiliauskas[1], Šarūnas Meškinis[1]

[1] Institute of Materials Science of Kaunas University of Technology, Lithuania
sarunas.jankauskas@ktu.lt

In recent years, graphene has become one the most studied nanomaterials due to its intrinsic optical, mechanical, thermal and electronic properties. This proposes many possibilities for creation of novel graphene based optoelectronic devices [1] which encompass all the previously mentioned qualities. To achieve correct geometry, thickness and most importantly large surface area of graphene sheets, microwave plasma enhanced chemical vapor deposition (MW-PECVD) is known as a feasible method for direct growth of graphene on desired substrates. However, despite decreased production times and the ability to ensure correct growth dynamics, MW-PECVD has a huge negative impact on graphitic structures – defect density tends to be noticeably higher compared to graphene synthesized using other techniques [2].

To tackle this issue thermal annealing is rather straight forward method, which usually increases the overall quality of graphene by reducing the number of defects and other structural deformations, however there are other predominant effects, such as doping and strain effects, which could damage the sample [3]. To investigate these structural changes, Raman spectroscopy is a useful technique to determine changes in graphene quality. By comparing I_{2D}/I_G we can establish if the deformations are compressive of tensile and I_D/I_G is used for direct defective site related behavior.

In this work, four graphene samples were grown on Si(100) substrate, using MW-PECVD system (IPLAS Innovative Plasma Systems GmbH). Thermal annealing of samples was accomplished accordingly: in 200-800°C Ar environment, in 300-400°C N_2 environment and using 300°C in vacuum. All annealing's were performed for 30 min. The characterization of graphene samples was carried out using Raman spectrometer (Renishaw inVia, 532 nm) by analyzing changes in D, 2D and G bands.

After annealing in Ar environment at temperatures, lower than 800°C, I_{2D}/I_G ratio changed from 1.04 to 0.47 and I_D/I_G ratio changed from 1.3 to 1.45, suggesting appearance of additional deformations. Annealing in N_2 environment, I_{2D}/I_G changed from 1.6 to 0.62 and I_D/I_G from 1.56 to 2.02 hinting a huge increase in defective sites and strain development. After investigating changes in Raman spectrum after annealing in vacuum we have found out that I_{2D}/I_G changed from 0.61 to 0.23 and I_D/I_G from 1.53 to 1.71, showing that the dominant effect is rather defect formation than reduction, however values indicate a large number of layers, which could lead to inconclusive estimations.

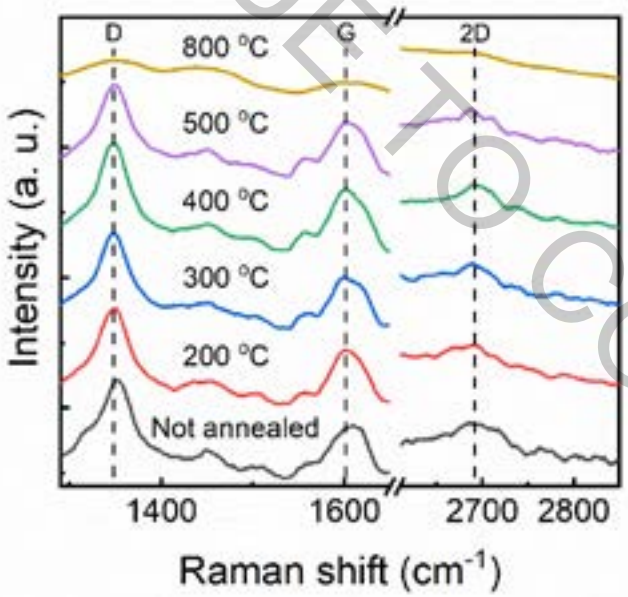

Fig. 1. Raman spectra of graphene sample before and after thermal annealing in argon environment.

Acknowledgements. This research was partially funded by the European Social Fund under the No 09.3.3-LMT-K-712 "Development of Competences of Scientists, other Researchers and Students through Practical Research Activities" measure.

[1] W. Choi et al., Synthesis of Graphene and Its Applications: A Review, Critical Reviews in Solid State and Materials Sciences **35(1)**, 52-71 (2010).
[2] S. Zheng et al., Metal-catalyst-free growth of graphene on insulating substrates by ammonia-assisted microwave plasma-enhanced chemical vapor deposition, RSC Advances **7(53)**, 33185–33193 (2017).
[3] M. Alyobi et al., Effects of Thermal Annealing on the Properties of Mechanically Exfoliated Suspended and On-Substrate Few-Layer Graphene, Crystals **7(11)**, 349 (2017).

ARTICLE DUE TO COVID-19

OUTPUT CHARACTERISTICS OF THE EXPERIMENTAL PHOTOACOUSTIC TRANSDUCER WITH SILVER NANOPARTICLES AT OPTICAL FIBER EDGE

Alena Mikitchuk[1], Konstantin Kozadaev[1], Elizaveta Girshova[2], Liubou Hauryk[1], Uladzislau Dolnikau[1], Anton Talkachov[3]

[1] Department of Radiophysics and Computer Technology, Belarusian State University, Belarus
[2] Department of Nanophotonic, St. Petersburg Academic University, Russia
[3] Department of Physics and Information Technologies, Gomel State University, Belarus
m.helenay@yandex.by

CANCELLED DUE TO COVID-19

There are a number of methods of non-destructive testing, which are suitable for breakdown diagnostics of technical equipment, industrial machines and mechanisms, as well as eliminate defects in products manufactured. One of the main approaches is the usage of ultrasound signals as a diagnostic tool. Compared with other methods of non-destructive testing, this method has a set of important advantages: high sensitivity; low cost; safety for humans (unlike X-ray inspection); possibility of non-destructive testing without interruption of technological process; possibility to control wide range of materials. Conventional piezoelectric electro-acoustic transducers are characterized by high supply voltages, large size and high weight, high electromagnetic interference susceptibility, relatively narrow operation bandwidth []. Photoacoustic transducers are very attractive alternative to electro-acoustic transducers. In photoacoustic transducers, absorber is heated and cooled, leading to mechanical deformations, which cause cycles of pressure, or, in the other words, acoustic waves in ambient surrounding [1].

This paper describes the output characteristics of the experimental fiber-optic photoacoustic transducer with a monolayer of silver nanoparticles, previously created by the authors [2,3]. Silver nanoparticles monolayer has been deposited on the optical fiber edge using pulsed laser deposition method [3]. The average diameter of the nanoparticles is 35 nm, the mean square size dispersion is 12 nm, the density of the filling of the substrate with nanoparticles is 3.8% [4]. The photoacoustic response is observed in the frequency range of 10–18 MHz and its level is more than 12 dB higher than setup noise floor (fig. 1, left). There is no observable effect of 1 hour operation on the surface nanostructure microscopic parameters (fig. 1, right). This fact makes it possible to use such transducers as part of high-resolution technical diagnostic and non-destructive testing systems.

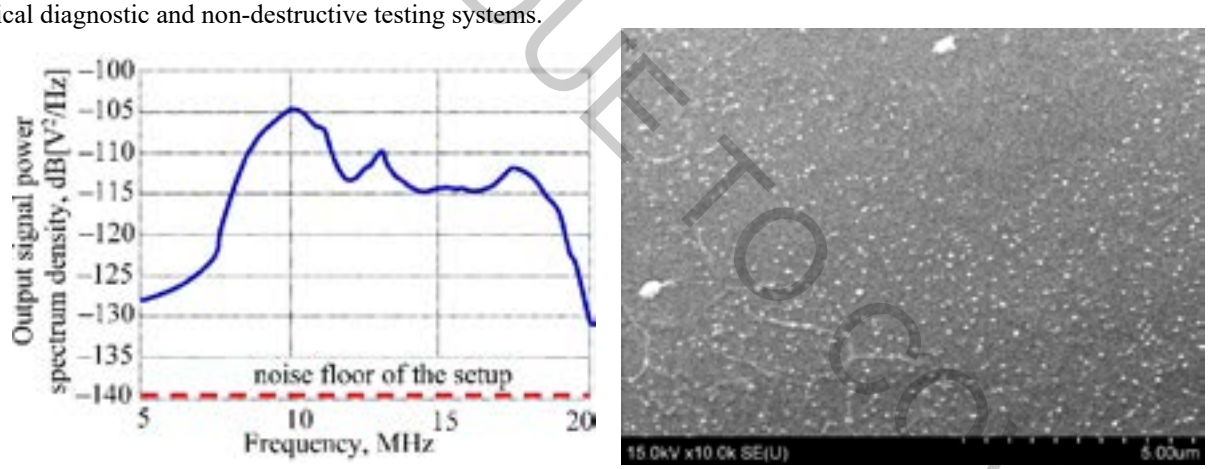

Fig. 1. Left: frequency dependence of the power spectral density of the output acoustic signal from experimental fiber-optic photoacoustic transducer; right: microphoto of photoacoustic transducer surface with monolayer of silver nanoparticles before measurement of acoustic signal (obtained with scanning electron microscope Hitachi S-4800).

Thus, experimental fiber-optic photoacoustic converter (based on Ag nanoparticle monolayer with a gamma distribution of nanoparticles in size, diameter of 35 nm and a size dispersion of 12 nm formed at the edge of the optical fiber) it is possible to obtain reliable ultrasound generation in water in the frequency range of 10 – 18 MHz using a laser diode with fiber-optic pigtail and peak power of 40 mW.

The work is supported by grant "BRFFR-RFBR M-2019" № F19RM-006 “Study of 2D plasmonic nanostructures for photoacoustic transducers”. This work is also a part of the PhD thesis of Alena Mikitchuk.

[1] A.P. Mikitchuk, K.V Kozadaev, Simulation of the optical properties of surface nanostructures for photoacoustic converters, Quantum Electronics **48**(7), 630-636 (2018).
[2] A.P. Mikitchuk, K.V Kozadaev, Photoacoustic generation with surface noble metal nanostructures, Semiconductors **52** (14), 1839-1842 (2018).
[3] V.K. Goncharov, K.V. Kozadaev, A.P. Mikitchuk et al., Synthesis, structural and spectral properties of surface noble metal nanostructures for fiber-optic photoacoustic generation, Semiconductors **53** (14), 1950-1953 (2019).
[4] A.P. Mikitchuk, K.V Kozadaev, Characteristics of fiber-optic photoacoustic transducers with monolayer of metal nanoparticles for systems of technical diagnostics, Journal of the Belarusian State University. Physics **1**, 4-15 (2020).

MODELING THE OPTICAL PROPERTIES OF AG AND AU NANOPARTICLES ON THE BUTT OF AN OPTICAL FIBER FOR A COMPACT ULTRASONIC EMITTER

Liubou Hauryk[1], Anton Talkachov[2], Alena Mikitchuk[1],
Uladzislau Dolnikau[1], Elizaveta Girshova[3]

[1] Department of Radiophysics and Computer Technology, Belarusian State University, Belarus
[2] Department of Physics and Information Technologies, Gomel State University, Belarus
[3] Department of Nanophotonic, St.Petersburg Academic University, Russia
Luba-gavrik@yandex.ru

CANCELLED DUE TO COVID-19

Ultrasound is essential for biological research to create targeted mutations in plant breeding, to break cell membranes and destroy intracellular structures [1]. Ultrasound is commonly used for a therapy and a diagnosis in medicine.

Compact ultrasonic emitters are necessary today. In this article, such emitters are designed. A compact ultrasonic emitter consists of an optical fiber and a layer of nanoparticles deposited on its edge. Emitter under study is characterized by wide range of possible ultrasonic signals for various media, in particular for biological fluids. Compact ultrasonic emitters have benefits of compact size, low weight, high resistance to electromagnetic interference, mechanical flexibility and high chemical resistance.

The ultrasound emission is based on surface plasmon resonance effect. Modulated laser signal passes through optical fiber and it is absorbed by metal nanoparticles at the fiber edge. Due to thermal expansion, nanoparticle re-radiates mechanical oscillations [2]. Results of optical properties computer modelling are presented in this article for nanostructures with metal nanoparticles at the optical fiber edge fiber in various media such as air, water and biological fluids (including blood). The purpose of the work is to find the optimal parameters for the compact ultrasound emitter to increase the efficiency of ultrasound generation. The absorption of modulated optical signal by nanoparticles should be maximazed [3]. Hence, nanoparticles radii and the media should be chosen according to the condition above. The simulation was performed with the MiePlot package for gold and silver nanoparticles with radii from 5 nm to 50 nm and medium with a refractive index ranging from 1.2 to 1.6.

To provide quick simulation, an effective refractive index for both media and substrate (optical fiber) is used. The effective refractive index is equal to arithmetic average of the refractive index of the media and substrate. This approach allows to perform express diagnostics of optical spectra.

Therefore, the absorption coefficient is maximum for silver nanoparticles with radius of 10 nm at a wavelength of 410 nm in media with effective refractive index of n = 1.52. As for gold nanoparticles, the absorption maximum is reached in the same medium at wavelength of 548 nm for radius of 25 nm. In conclusion, silver nanoparticles have four times the absorption coefficient as big as the absorption coefficient in gold nanoparticles under the same conditions. It was found that increase of the refractive index of the medium leads to a rise of the maximum value of the absorption coefficient. Its peak position also shifts towards to longer wavelengths. The shift is 10 nm for nanoparticles with a radius of 50 nm compared to nanoparticles with radius of 10 nm.

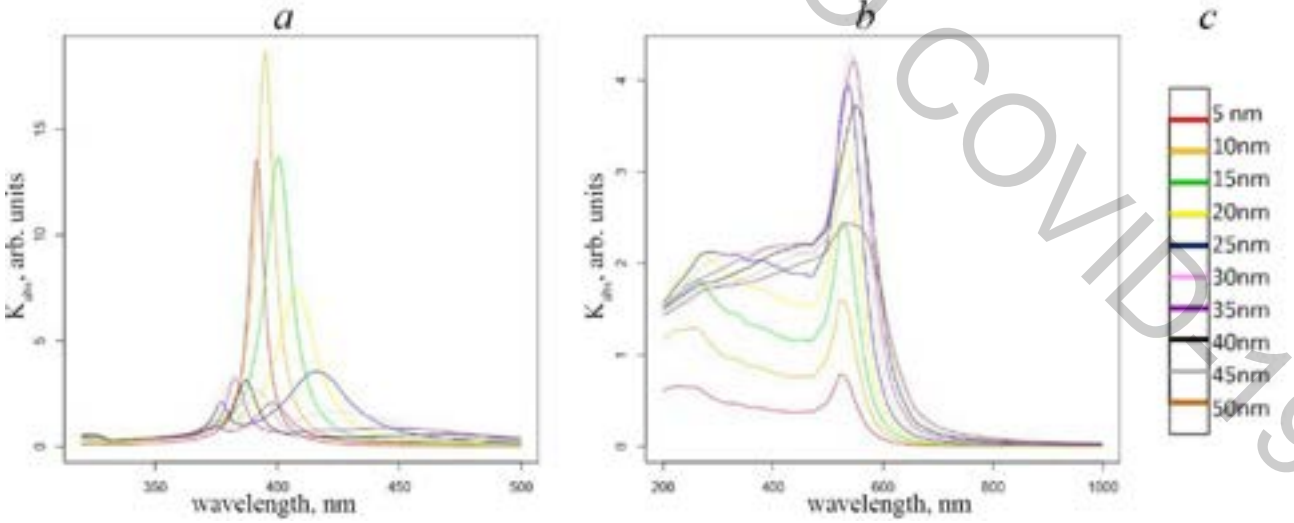

Fig. 1. Absorption coefficient of the nanostructure at the edge of the optical fiber in the wavelength range from 200 nm to 1000 nm, depending on the radius of the nanoparticles and the medium of the nanostructure a) based on Ag; b) based on Au; c) graphs legend.

[1] *Handbook of Technical Diagnostics,* Ed. by H. Czichos (Springer, New York, 2013).
[2] A.P. Mikitchuk, K.V Kozadaev, Simulation of the optical properties of surface nanostructures for photoacoustic converters, Quantum Electronics **48**(7), 630-636 (2018).
[3] A.P. Mikitchuk, K.V Kozadaev, Photoacoustic generation with surface noble metal nanostructures, Semiconductors **52** (14), 1839-1842 (2018).

PREPARATION OF NANOSIZED SULFUR PARTICLES

Magdalena Bartolewska [1], Maciej Mazur [2]

[1] Faculty of Physics, University of Warsaw, Pasteura 5, 02-093, Warszawa, Poland
[2] Faculty of Chemistry, University of Warsaw, Pasteura 1, 02-093, Warszawa, Poland
m.bartolewska@gmail.com

Sulfur is a widely used chemical element for a variety of application such as fertilizers, pharmaceuticals, antimicrobial agents, insecticides, fumigants, etc. Moreover, the nanosized sulfur particles are applicable in pharmaceuticals or as components of lithium ion batteries. In this work the sulfur nanoparticles (S-NPs) were prepared employing the disproportionation reaction of sodium thiosulphate in the presence of hydrochloric acid. The size of the S-NPs was controlled by changing the reaction parameters like temperature or the type of the stabilizer (PVP, PVA, Chitosan, sulforaphane).

The resulting structures have been examined with a range of physicochemical methods including dynamic light scattering, electron microscopy and spectroscopic techniques. It has been shown that the addition of the stabilizers to the reaction significantly reduces the particle size. The size of the particles can be also controlled by changing the temperature of the reaction.

The sulfur particles appear as a new promising material for medical applications like drug delivery or diagnostics.

CANCELLED DUE TO COVID-19

PROTEIN IMMOBILIZATION ON SURFACE OF ZnO NANOSTRUCTURES FOR OPTICAL BIOSENSOR DESIGN

Eimantas Bucmys[1], Anton Popov[1], Auguste Adamonyte[1], Ieva Plikusiene[1,2]

[1] NanoTechnas – Center of Nanotechnology and Materials Science, Faculty of Chemistry and Geosciences, Vilnius University, Lithuania

[2]Department of Physical Chemistry, Faculty of Chemistry and Geosciences, Vilnius University, Lithuania

ebucmys@gmail.com

Optical biosensors exhibit good performance in detecting biological systems and promote significant advances due to high sensitivity, immunity to external disturbance, stability, and low noise [1]. Photoluminescence (PL) from nanomaterials is a suitable and simple method for detection of various analytes. One of the most interesting metal oxide materials is ZnO with a wide band gap (3.37 eV), high isoelectric point (pH 9–9.5) and intense room temperature photoluminescence [2]. Zinc oxide nanostructures have also shown beneficial physico-chemical properties for use in bioanalysis as transducers due to their biocompatibility, high surface/volume ratio and surface tailoring ability which allows for various types of biomolecules to be immobilized [3]. In this work polyacrylonitrile (PAN) nanofibers synthesized by electrospinning and modified by ZnO using ALD technique [4] were used as a substrate for protein immobilization.

The main aim of this study was to choose the optimal method of protein immobilization on the surface of polyacrylonitrile PAN/ZnO nanostructures for optical biosensor design. Several strategies for the modification of PAN/ZnO samples were chosen. The PAN/ZnO nanostructures were modified by silanization using (3-aminopropyl)triethoxysilane (APTES) or (3-mercaptopropyl)triethoxysilane (MPTES). Other samples were modified by formation of Au nanostructures on the surface of ZnO using UV irradiation. Self-assembled monolayer (SAM) of 11-mercaptoundecanoic acid was subsequently formed on the surface of Au nanostructures. FTIR analysis was used to confirm successful silanization and SAM formation. Finally, antibodies labelled with the enzyme horseradish peroxidase (HRP) were covalently immobilized on the modified PAN/ZnO surfaces *via* their carboxyl groups. Immobilization of antibodies was evaluated using the enzymatic reaction between HRP and 3,3′,5,5′-tetramethylbenzidine which results in colour change of solution. Moreover, an optical system of PL detection was carried out for antibodies immobilization control. ZnO nanostructures were excited by LED (λ = 325 nm) and PL spectra were collected by fiber optic spectrometer QEPro from Ocean Optics.

Acknowledgements

This project has received funding from European Social Fund (project No 09.3.3.-LMT-K-712-16-0163) under grant agreement with the Research Council of Lithuania (LMTLT).

[1] C. Chen, J. Wang, Optical biosensors: an exhaustive and comprehensive review, Analyst, 2020.

[2] A. Tereshchenko, M. Bechelany, R. Viter, V. Khranovskyy, V. Smyntyna, N. Starodub, & R. Yakimova, Optical biosensors based on ZnO nanostructures: advantages and perspectives. A review. Sensors and Actuators B: Chemical, 229, 664–677 (2016).

[3] J. Zhou, N. Xu, Z. L. Wang: Dissolving Behavior and Stability of ZnO Wires in Biofluids: A Study on Biodegradability and Biocompatibility of ZnO Nanostructures, Adv Mater 18, 2432–2435 (2006).

[4] I. Iatsunskyi, A. Vasylenko, R. Viter, M. Kempiński, G. Nowaczyk, S. Jurga, M. Bechelany, Tailoring of the electronic properties of ZnO-polyacrylonitrile nanofibers: Experiment and theory, Applied Surface Science, Volume 411, 494-501 (2017).

CANCELLED DUE TO COVID-19

CERIUM DOPED ZINC OXIDE NANOSTRUCTURES OBTAINED BY MICROWAVE ASSISTED METHOD WITH THE USE OF AMINO-GROUP CONTAINING PRECURSORS

Aleksandra Shulga[1], Leonid Butusov[1,2], Galina Chudinova[2,3], Tatiana Sheshko[1], Vladimir Kopylov[1]

[1]Department of Physical and Colloidal Chemistry, RUDN University, Russia
[2] Carbon Nanophotonics laboratory A.M. Prokhorov Institute of General Physics RAS, Russia
[3] Department of laser micro-and nanotechnologies, National Research Nuclear University "MEPhI", Russia,
aleksandra-box@mail.ru

The study considers the use of amino group containing precursors in microwave synthesis of cerium doped zinc oxide nanoparticles. At the moment precursors have become an integral part of the synthesis of various nanoparticles, because of their small quantity can significantly reduce particle aggregation and a decrease in the amorphous component of the synthesis product [1].

Using cerium doped zinc oxide as an example, we examined the effect of aliphatic and polycyclic amines as precursors - isopropylethylenediamine and urotropine and studied by X-ray diffraction analysis, fluorescence spectroscopy and scanning electron microscopy. A relationship between the sizes of nanoparticles and their crystallinity with the number of nitrogen atoms of the precursor molecules has been established [5].

Thus, urotropine containing 4 nitrogen atoms allowed us to obtain particles of 48 nm size and the crystallinity was 87.5%, while for particles obtained with a precursor containing 2 nitrogen atoms - isopropylene ethylenediamine it was 56 nm with a crystallinity of 85.5%.

The most important difference in the synthesis of results is found in the size of aggregates (Fig.1).

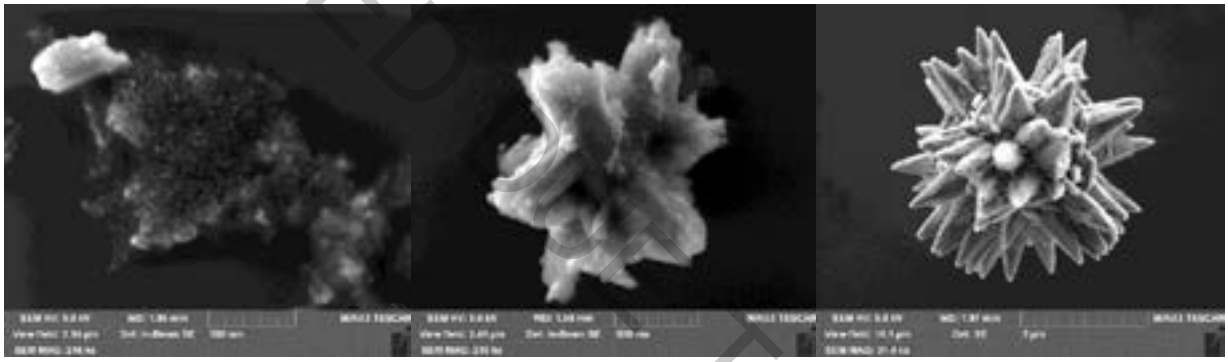

Fig. 1. From left to right: cluster of nanoparticles, aggregates for urotropine precursor

We found that the biggest agregates for urotropine are about 1.5 μm and 8 μm for isopropylene ethylenediamine which implies a more efficient growth when using an aliphatic compound. At the same time this effect is not observed for precursors based on glycols.

Acknowledgements.
This publication was prepared with the support of the “RUDN University Program 5-100”.

[1] Shulga A., Butusov L.A., Boruleva E.A., Chudinova G.K., Sheshko T.F, Kurilkin V.V, Kochneva M.V., FLUORESCENT PROPERTIES OF GD-DOPED ZNO NANONPOROUS NETWORKS & ITS APPLICATION IN OPTICAL BIOSENSING, IOP Conf. Series: Journal of Physics: Conf. Series 1092 (2018)

[2] Lorena Portela Brazuna, Thiago Galeote Tabuti, Adrielle de Paula Silva, Dayane Batista Tada, Ma rio Jose Politi, Rebeca Bacani, Eduardo Rezende Triboni. New Journal of Chemistry (2019)

CANCELLED DUE TO COVID-19

SYNTHESIS OF GOLD COATED MAGNETIC NANOPARTICLES AND MODIFICATION WITH ANTIBODIES AT OPTIMAL CONDITIONS

Ema Baliūnaitė[1], Ernesta Lubinaitė[1], Almira Ramanavičienė[1]

[1] NanoTechnas – Center of Nanotechnology and Materials Science, Faculty of Chemistry and Geosciences, Vilnius University, Lithuania
emabaliunaite@gmail.com

Nowadays gold nanoparticles are widely used in many areas such as electronics, photonics, catalysis, chemical and biochemical sensing. These nanoparticles are biocompatible, have unique optical and electromagnetic properties, good conductivity, and can be easily functionalised and modified with biomolecules. Gold coated magnetic nanoparticles (Au-MNPs), besides the above-mentioned properties characteristic to gold nanoparticles, interact with magnetic fields and their position in space can be controlled with the use of magnets. This property can be successfully applied for the collection and bio-separation of nanoparticles after each step of modification [1-3]. The use of Au-MNPs is advantageous for the development of electrochemical and optical biosensors and immunosensors. The existing scientific data does not allow us to select the most efficient concentration of immobilized antibodies and the optimal conditions for effective modification of nanoparticles in order to develop a sensitive immunoassay or immunosensor [4].

The main aim of this study was to synthesise Au-MNPs by reducing Au^{3+} with hydroxylamine hydrochloride in the presence of cetrimonium bromide (CTAB), to determine their size and to select the optimal conditions for Au-MNP modification by antibodies, finding the lowest sufficient antibody concentration for the selective and sensitive detection of analyte. In this work sodium borohydride was used for the reduction of CTAB present on the surface of nanoparticles [5]. Then different antibody concentrations and various methods (adsorption, covalent immobilization and others) were used for modification of Au-MNPs. The Au-MNPs before and after modification were characterized spectroscopically, using transmission electron microscopy and gel electrophoresis.

Acknowledgements

This project has received funding from European Social Fund (project No 09.3.3.-LMT-K-712-16-0170) under grant agreement with the Research Council of Lithuania (LMTLT).

[1] J. Zhao, A.O. Pinchuk, et al., Methods for describing the electromagnetic properties of silver and gold nanoparticles, Accounts of Chemical Research **41**, 1710-1720 (2008).

[2] P.K. Jain, X. Huang, et al. Review of some interesting surface plasmon resonance-enhanced properties of noble metal nanoparticles and their applications to biosystems, Plasmonics **2**, 107-118 (2007).

[3] S.S. Moraes, R. Tavallaie, et al., Gold coated magnetic nanoparticles: from preparation to surface modification for analytical and biomedical applications, Chemical Communication **48**, 7528-7540 (2016).

[4] N.A. Byzova, I.V. Safenkova et al., Less is more: A comparison of antibody-gold nanoparticle conjugates of different ratios, Bioconjugate Chemistry **28**, 2737-2746 (2017).

[5] J. He, S. Unser, I. Bruzas et al., The facile removal of CTAB from the surface of gold nanorods, Colloids and Surfaces B: Biointerfaces **163**, 140-145 (2018).

CANCELLED DUE TO COVID-19

SURFACE MODIFICATION AND STABILIZATION OF UPCONVERTING $NaGdF_4:Yb^{3+}/Er^{3+}$ NANOPARTICLES IN AQUEOUS MEDIA USING ANIONIC BRUSH-TYPE PLYELECTROLYTES

Gabija Grudzinskaite[1], Vaidas Klimkevicius[1], Simas Sakirzanovas[1]

[1] Institute of chemistry, Vilnius University, Vilnius, Lithuania
gabija.grudzinskaite@chgf.stud.vu.lt

In recent years, the up-converting nanoparticles (UCNPs) have a tremendous scientific interest. Due to combined properties such as magnetic, optical stability, low toxicity, these particles have application possibilities in multiple fields: drug delivery, bio-sensing, nanophotonics, nanoelectronics and many more. However, the versatile applicability of particles usually is limited by poor colloidal stability, especially in aqueous media. The preparation of stable nanoparticle dispersion is one of the major challenge restricting wide and easy usage in research and modern technology. Several approaches including surface ligand exchange, ligand removal, ligand oxidation, silanization, and amphiphilic polymer [1] coating have been developed in order to transfer stable nanoparticles into aqueous biological medium, however the universal method to obtain stable coloids is not found yet. Taking into account all applied materials in colloidal stabilization, the non-linear structure (brush-type) polyelectrolytes have highest potential to be developed as super dispersants for UPNPs, because of the ability to modify surfaces creating steric barriers, preventing particles to form agglomerates.

In this work the focus was on study of core $NaGdF_4:Yb^{3+}/Er^{3+}$ up-converting nanoparticles synthesis and demonstration of effective surface modification method for stabilization using anionic brush-type p(MAA-*stat*-PEO_9MEMA) polyelectrolytes. The β-$NaGdF_4:Yb^{3+}/Er^{3+}$ nanoparticles with distinct diameter of around 12 nm were synthesized via thermal decomposition method, following published procedure with minor adjustments [2]. The exact diameter and crystal structure of synthesized core particles were determined using scanning electron microscopy (SEM) and powder X-ray diffraction (XRD). The surface modification procedure was carried out in two steps: 1) the oleic acid ligands were removed from the surface of NPs; 2) the anionic brush-type p(MAA-*stat*-PEO_9MEMA) were applied onto "uncoated" NPs.

The colloidal stability of "uncoated" particles and particles modified with anionic brush-type polyelectrolytes were initially studied and compared. First, the isoelectric point of "uncoated" $NaGdF_4:Yb^{3+}/Er^{3+}$ nanoparticles in aqueous dispersion were determined by measuring zeta potentials under various pH. The particles size distribution (PSD) in colloidal systems at each pH were determined by dynamic light scattering (DLS). The pH value, where surface charge of $NaGdF_4:Yb^{3+}/Er^{3+}$ particles is positively expressed was chosen, and the effect of polyeletrolyte concentration on particle surface potential change and colloidal stability was evaluated. The stability of both "uncoated" and modified particles under biological pH range (pH = 7.4) was evaluated and compared.

Fig.1. β-$NaGdF_4:Yb^{3+}/Er^{3+}$ surface modification steps: removal of hydrophobic oleic acid ligands (a); nanoparticle surface modification using anionic brush-type p(MAA-*stat*-PEO_9MEMA) polyelectrolytes (b).

[1] Liu, Y.; Tu, D.; Zhu, H.; Li, R.; Luo, W.; Chen, X. *Adv. Mater.* 2010, *22,* 3266. doi:10.1002/adma.201000128;
[2] Cheng, L.; Yang, K.; Zhang, S.; Shao, M.; Lee, S.; Liu, Z. *Nano Res.*2010**,** *3,* 722–732. doi:10.1007/s12274-010-0036

CHEMISTRY TO COVID-19

CADMIUM CHALCOGENIDE NANOPLATELETS FOR CELL LABELING AND VISUALIZATION WITH TWO-PHOTON EXCITATION

Andrey Iodchik[1], Aliaksandra Radchanka[1], Tatsiana Terpinskaya[2], Tatjana Balashevich[2], Tatsiana Yanchanka[2], Palukoshka Alena[2], Svetlana Sizova[3], Vladimir Oleinikov[3], Alexei Feofanov[3, 4], Mikhail Artemyev[1*]

[1] Research Institute for Physical Chemical Problems of the Belarusian State University, Minsk 220006, Belarus
[2] Institute of Physiology, National Academy of Science of Belarus, Minsk 220072, Belarus
[3] Shemyakin-Ovchinnikov Institute of Bioorganic Chemistry Russian Academy of Science, Moscow 117997, Russia
[4] Biological Faculty, Lomonosov Moscow State University, 119992, Moscow, Russia
iodchik98@mail.ru

Luminescent semiconductor nanocrystals known as quantum dots (QDs) have widely been used in various biological assays: bioimaging, cell functioning, and intercellular interactions. [1] However, their 2D analogous – semiconductor nanoplatelets (NPls) - could be even more perspective in those applications. Having larger two-photon cross section comparing to both quantum dots and traditional organic fluorophores, they may be used as highly efficient fluorescent labels in biomedicine.

In frame of earlier established one order of magnitude larger two-photon absorption coefficient for CdSe nanoplatelets as compared to quantum dots we examined their efficiency for cell labeling and visualization with two-photon fluorescence microscopy. In order to do that we synthesized CdSSe/ZnCdS core-shell nanoplatelets and CdSe/ZnS quantum dots, both emitting at 585 nm. Those nanoparticles were then encapsulated with amphiphilic polymeric shell, having on their surface zwitter-ionic pairs and slightly positive zeta potential. That value is required for better penetration of charged nanoparticles in cells. [2] Glioma C6 cells incubated either with nanoplatelets or quantum dots demonstrated nearly equal uptake efficiency in the flow cytometry despite of sufficiently different dimensions of these two types of nanoparticles. Two-photon confocal fluorescence microscopy revealed ca. order of magnitude larger fluorescence response from nanoplatelets taking into account difference in concentration of nanoplatelets and quantum dots uptaken by cells.

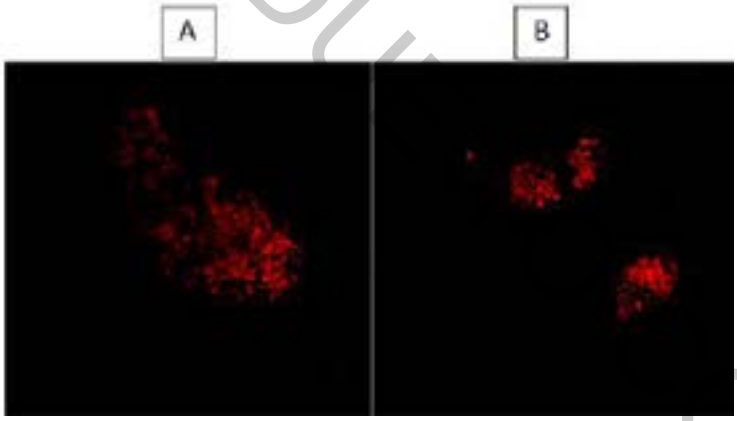

Fig. 1. Photoluminescence images of glioma C6 cells labeled with NPls (A) and QDs (B).

Our experiment confirms much higher labeling efficiency by nanoplatelets toward their visualization through two - photon fluorescence relatively to quantum dots which opens the door to use them as highly efficient fluorescent labels in biomedicine.

This work was supported by the RFBR grant 18-54-00033, BRFFI grant X18P-173 and CHEMREAGENT program

[1] N. Tomczak, R. Liu, J. G. Vansco, Nanoscale 5, 12018 (2013).
[2] A. Radchanka, T. Terpinskaya, T. Balashevich, T. Yanchanka, M. Artemyev, Luminescent quantum dots encapsulated by zwitterionic amphiphilic polymer: calcium-dependent interaction with cells, 62d scientific conference for students of physics and natural sciences Open Readings 2019, ISBN 978-609-07-0137-9, Vilnius University, 253 (2019).

CANCELLED DUE TO COVID-19

SYNTHESIS AND INVESTIGATION OF YTTRIUM IRON GARNET, YTTRIUM AND TERBIUM IRON PEROVSKITE NANOTUBES

Justinas Januškevičius*, Živilė Stankevičiūtė, Aldona Beganskienė, Aivaras Kareiva

Faculty of Chemistry and Geosciences, Vilnius University, Lithuania
januskevicius.justinas@gmail.com

Various garnet and perovskite structures have garnered a lot of interest in the scientific community lately. This is mainly due to their applicability in a wide variety of fields and often interesting properties. Some garnets, for example, show a lot of promise as potential magneto-optical materials [1], while perovskites are considered some of the most versatile structures in general [2, 3], finding use as superconductors [4], potential multiferroics [5] and sensors [6] among many others. However, there are numerous problems that still need to be solved in order to reach more mainstream technological use for these materials. One of these drawbacks is synthesis – often complex and expensive procedures are involved in the synthesis of these structures [7]. Finding simpler synthesis and structurization methods, therefore, is very important.

In this study, the precursor solutions were prepared by dissolving stoichiometric amounts yttrium (or terbium) nitrate and iron nitrate in distilled water, then adding ethylene glycol as a complexing agent. Some of this solution was then used to create nanotubes. This was achieved by using polycarbonate membranes with a pore diameter of 0.2 μm. The membranes were submerged in the solutions and soaked for about 1 minute, carefully moving them about, after which they were removed (excess liquid absorbed with paper), then left to dry for 10 minutes. This procedure was repeated 5 times, to achieve a good filling of the pores. The prepared wet membranes were placed on silicon, then sintered at two different temperatures – 550°C and 800°C. X-ray diffraction analysis and scanning electron microscopy was then used to identify the crystal structure and the parameters of the nanotubes. The results obtained showed that nanotube structure was formed.

Acknowledgements
This work was supported by a Research grant BUNACOMP (No. S-MIP-19-9) from the Research Council of Lithuania.

[1] Š. Višňovský, "Magnetooptics in Cylindrical Structures," *Applied Sciences*, vol. 8, no. 12, p. 2547, Dec. 2018.
[2] S. Mitra "ABX3, Perovskite-ilmenite structure," *Developments in Geochemistry,* vol. 9, *High-Pressure Geochemistry and Mineral Physics*, chapter 10, pp. 711–792, Jan. 2004.
[3] R. E. Schaak and T. E. Mallouk, "Perovskites by design: A toolbox of solid-state reactions," *Chemistry of Materials*. 2002.
[4] L. F. Schneemeyer, J. V. Waszczak, S. M. Zahorak, R. B. van Dover, and T. Siegrist, "Superconductivity in rare earth cuprate perovskites," *Materials Research Bulletin*, vol. 22, no. 11, pp. 1467–1473, Nov. 1987.
[5] P. Barone and S. Picozzi, "Multiferroics: theory, mechanisms, and materials," *Science and Technology of Atomic, Molecular, Condensed Matter & Biological Systems*, vol. 2, pp. 129–161, Jan. 2012.
[6] E. A. R. Assirey, "Perovskite synthesis, properties and their related biochemical and industrial application," *Saudi Pharmaceutical Journal*, vol. 27, no. 6, pp. 817–829, Sep. 2019.
[7] X. Wu, K. Huang, L. Yuan, and S. Feng, "Fabrication of ultralong perovskite structure nanotubes," *RSC Advances*, 2018.

CANCELLED DUE TO COVID-19

TUNABILITY OF OPTICAL PROPERTIES OF WATER-SOLUBLE SEMICONDUCTOR NANOCRYSTALS VIA ZETA-POTENTIAL

Aliaksandra Radchanka[1], Alexander W. Achtstein[2], Mikhail V. Artemyev[*,1]

[1]Institute for Physical Chemical Problems, Belarusian State University, Belarus
[2]Institute of Optics and Atomic Physics, Technical University of Berlin, Germany
aleksandraradchenko10@gmail.com

CANCELLED DUE TO COVID-19

Tunable optical properties combined with size control are the key characteristics of semiconductor nanocrystals (NCs), or quantum dots (QDs), due to a wide spectrum of possible applications of these phenomena in light-harvesting systems, photovoltaics, biosensing, and bioimaging [1]. Encapsulation with an amphiphilic polymer of hydrophobic QDs is proven an effective solubilization technique since NCs preserves small hydrodynamic size and relatively high quantum yield (QY). To improve colloidal stability, biocompatibility, and increase a non-specific interaction with cellular membranes the surface of QDs is modified with various molecules leading to change of zeta-potential (ξ) [2].

This work aimed to investigate the dependence of the optical characteristics of water-soluble QDs with the sign and magnitude of their surface charge and propose the physical model for describing obtained dependencies.

The idea of the experiment was to modify poly(maleic anhydride-*alt*-1-tetradecene) (PMAT) with derivatives with different functional groups of encapsulated QDs. The nature of functional groups determines the sign of surface charge, while the ratio of them influences the magnitude of ξ-potential. Further, the optical characteristics such as quantum yield, emission wavelength, and luminescence lifetime were measured as a function of ξ-potential.

Chemical modification of PMAT was performed according to the standard carbodiimide procedure. ξ-potential and hydrodynamic size of water-soluble QDs were measured with the dynamic light scattering analyzer Malvern Zetasizer NanoZS90. QY was measured relative to rhodamine 6G (95% in ethanol). Photoluminescence (PL) decay times were measured with PicoQuant Microtime200 fluorescence lifetime imaging confocal microscopy system.

According to the obtained results, QY of water-soluble QDs has the highest value when ξ-potential approaches zero. QY is not influenced by the nature of the functional group on the surface only by ξ-potential.

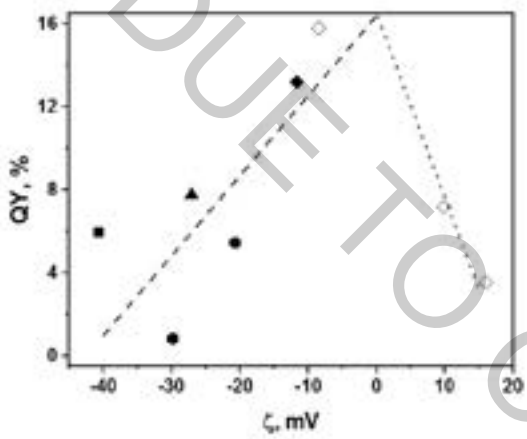

Fig. 1. QY dependency on zeta-potential of QDs with different functional groups on the surface: square – COOH, triangle – PO_3H_2, round – OPO_3H_2, hexagon – SO_3H, colored diamond – SO_4H, bare diamonds – quaternary ammonia.

Table 1. Summary of measured fluorescence lifetime and QY.

ζ-potential, mV	QY, %	τ_1, ns	A_1	τ_2, ns	A_2	$\langle\tau\rangle$, ns
-39.8	6.0	7.6	0.507	29.8	0.493	18.5
-4.3	18.2	10.8	0.462	32.5	0.538	22.5
+16.0	3.5	4.3	0.553	17.5	0.447	10.2

Highly positive or negative ξ-potentials result in similar radiative rates, while nonradiative rates increase by a factor of two. The increase of the QY near-zero ξ-potential is due to an increase of the radiative rate and less via decrease of nonradiative rates via e.g. better passivation of NCs if there is only a weak ionic double layer formed. The reason is that the free charge carriers around the QDs screen the exciton in the QDs strongly. If the screening is enhanced the exciton binding energy lowers [3].

[1] N. Tomczak, R. Liu, J. G. Vansco, Nanoscale **5**, 12018 (2013).
[2] E. A. Petrova, T. I. Terpinskaya, A. A. Fedosyuk, A. V. Radchanka, A. V. Antanovich, A. V. Prudnikau, M. V. Artemyev, Journal of Belarusian State University **2**, 3 (2018).
[3] A.W. Achtstein, A. Schliwa, A. Prudnikau, M. Hardzei, M.V. Artemyev, C. Thomsen, U. Woggon, Nano Lett. **12**, 6, 3151-3157 (2012).

DISCLOCATION-INDUCED STRAIN EFFECTS ON OPTICAL PROPERTIES OF CARBON DIMER DEFECTS IN HEXAGONAL BORON NITRIDE

Vytautas Žalandauskas[1,2], Mažena Mackoit-Sinkevičienė[1,2], Audrius Alkauskas[1,3]

[1]Department of Fundamental Research, State research institute Center for Physical Sciences and Technology, Lithuania
[2]Faculty of Physics, Vilnius University, Lithuania
[3]Department of Physics, Kaunas University of Technology, Lithuania
vytautas.zalandauskas@ftmc.lt

Layered van der Waals crystals are attracting a lot of attention due to their unique chemical and physical properties. Hexagonal boron nitride (hBN) has one of the largest bandgaps ($\sim$ 6 eV) among III-V compounds and possesses a honeycomb lattice structure akin to graphene. The discovery of quantum emission in hBN opens potential applications in quantum sensing and quantum communication [1].

Native point defects and impurities have been extensively studied using quantum chemistry calculations to determine the potential candidates of observed quantum emission [2]. Recently carbon dimer defect (C_BC_N) was proposed to give rise to ubiquitous narrow luminescence band with a zero-phonon line (ZPL) of 4.09 eV [3]. Some experiments indicate that the observed luminescence may come from point defects located near line defects like grain boundaries and dislocations which are ubiquitous in CVD-grown hBN crystals. Furthermore, the unusually high stretchability of 2D materials allows for effective strain engineering of physical and optical properties. Thus the investigation of photostability of discovered quantum emitters on applied strain is of great importance.

In this work, we discuss the impact of strain on optical properties of C_BC_N defect in hBN. Extended Tersoff potential for boron nitride systems was used to model hBN monolayers of various sizes and dislocation lengths [4]. Energy minimization calculations using the molecular dynamics package LAMMPS were performed to obtain optimized geometries. Dislocation induced strains were computed using discretisation of the deformation gradient operator. *Ab-initio* calculations were performed to determine the effect of strains on optical properties of C_BC_N defect.

We have shown that regardless of dislocation length and density, dislocation induced strains are most pronounced in the close vicinity of dislocations (up to $\sim$ 40 lattice constants). Dislocation-induced strains give rise to strong change in ZPL energy by changing orbital overlaps between initial and final states. The observable large redshift in the ZPL of the quantum emission of C_BC_N is expressed as $E_{ZPL} - \Delta E(\varepsilon_{xx/yy})$, where $\Delta E(\varepsilon_{xx/yy})$ is ZPL-strain coupling parameter for C_BC_N in hBN, which was determined in this work. We find that strain can modify emission energy of the carbon dimer defect by up to 300 meV.

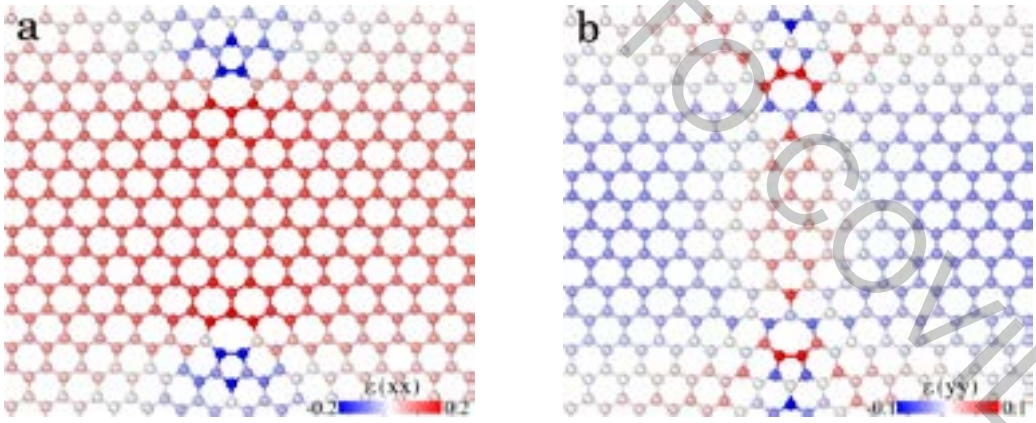

Fig. 1. Calculated ε_{xx} (a) and ε_{yy} (b) strain maps in flat hBN monolayer.

[1] R. Bourrellier, S. Meuret, A. Tararan, O. Stphan, M. Kociak, L. H. Tizei, and A. Zobelli, Nano Lett. **16**, 4317 (2016).
[2] L. Weston, D. Wickramaratne, M. Mackoit, A. Alkauskas, and C. G. Van de Walle, Phys. Rev. B **97**, 214104 (2018).
[3] M. Mackoit-Sinkevičienė, M. Maciaszek, C. G. Van de Walle, and A. Alkauskas, Appl. Phys. Lett. **115**, 212101 (2019).
[4] J. H. Los, J. M. H. Kroes, K. Albe, R. M. Gordillo, M. I. Katsnelson, and A. Fasolino Phys. Rev. B **96**, 184108 (2017).

CANCELLED DUE TO COVID-19

NUCLEAR SPIN POLARIZATION OF NV CENTERS IN DIAMOND

Laima Busaite, Reinis Lazda, Florian Gahbauer, Andris Berzins, Ruvin Ferber, Marcis Auzinsh

Laser Centre, University of Latvia, Latvia
laima.busaite@lu.lv

Nuclear spins usually exhibit long coherence times, so they are attractive for aplications in quantum information science. Electronic spin is used as an intermediary to access nuclear spins in solid state or atomic systems. In atomic systems nuclear spin can be optically prepared and near-perfectly isolated. However in nanoscale solid-state systems spins can be coupled and manipulated on fast time scales. Atomlike defects, such as Nitrogen - Vacancy center offer an interpolation between these approaches.

Due to different inter-system relaxation rates of magnetic sublevels on NV center excited state triplet, electronic spin an be optically polarized to $m_s = 0$ sublevel. Nuclear spin of ^{14}N of NV center is polarized due to hyperfine interaction. At magnetic field close to excited state level anti-crossing (ESLAC), the level pairs $|0,0\rangle$, $|-1,1\rangle$ and $|0,-1\rangle$, $|-1,0\rangle$ are mixed and after few cycles, the NV center gets polarized to $|0,1\rangle$, which stays unmixed (Figure 1 left).

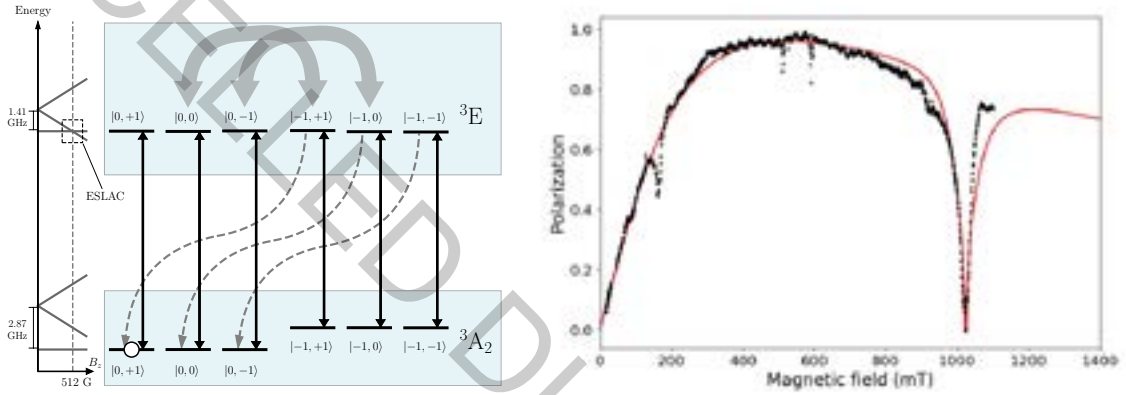

Fig. 1. Left: Nuclear spin polarization process at ESLAC. Right: Magnetic dependence of nuclear spin polarization. Black dots are experimental results, red line comes from theoretical model.The angle between magnetic field and NV axis was determined to be $\theta = 0.18°$.

Experimentally the nuclear spin polarization of ^{14}N was determined by fitting optically detectable magnetic resonance (ODMR) signals with multiple resonance curve [1]. The theoretical model was based on Lindblad equation for density matrix ρ:

$$\frac{\partial \rho}{\partial t} = -\frac{i}{\hbar}\left[\hat{H}, \rho\right] + \hat{L}\rho = 0, \tag{1}$$

where $\hat{H}$ is system Hamiltonian and $\hat{L}$ is Lindblad superoperator which is used to describe depopulation and decoherence processes of the NV center electron spin and ^{14}N nuclear spin.

We observed that ^{14}N nuclear spin polarization around ground state level anti-crossing (GSLAC) at 1025 G is very sensitive to magnetic field angle, even an angle as small as $\theta = 0.05°$ destroyed nuclear spin polarization at GSLAC. However the ODMR signals at GSLAC could be used to precisely determine the angle between magnetic field and NV axis.

The experimental and theoretical polarization match very well for a wide range of magnetic field (Figure 1 right), verifying that both fitting procedure and theoretical model describe nuclear spin polarization accurately.

[1] M. Auzinsh, A. Berzins, D. Budker, L. Busaite, R. Ferber, F. Gahbauer, R. Lazda, A. Wickenbrock, and H. Zheng. Hyperfine level structure in nitrogen-vacancy centers near the ground-state level anticrossing. *Physical Review B*, 100(7), 2019

CANCELLED DUE TO COVID-19

SYMMETRY BASED MODELING THE FUNCTIONING OF POLAR BROWNIAN ROTOR

Nastassia Savina, Irina Shapochkina

Department of Physics, Belarusian State University, Belarus
sadfiz@mail.ru

This work is devoted to the theoretical analysis of Brownian motors (ratchets), which are the systems that can demonstrate directional motion of nanoparticles as a result of rectification of nonequilibrium unbiased fluctuations of various nature in the absence of static forces and concentration gradients [1]. This effect is observed in a large variety of biological and artificial systems [2]. Molecular Brownian rotors (rotating Brownian ratchets) can manifest repetitive unidirectional rotational movement.

Our study is based on the description presented in [3], where the theory of the azimuthal jumping motion of an adsorbed polar molecule in a periodic *n*-well potential has been developed. It was shown that, for a symmetric potential of hindered rotation, unidirectional rotation a Brownian dipole rotator is possible only at both *n*=2 and simultaneous modulation of the minima and maxima of the potential by an external alternating electric field.

Our aim was to study the influence of temperature, fluctuation frequency and symmetries of the spatial and temporal dependences of the particle potential energy on the behavior of the average angular velocity of Brownian dipole rotator with the potential energy of the following form [4]:

$$U(\varphi,t)=\frac{1}{2}u[1-cos2(\varphi-\Phi)]-\mu E(t)\cos(\varphi-\varphi_0) \quad (1)$$

Here μ is the rotor dipole moment, u is the barrier of the hindered rotation, Φ and φ_0 are the phase shifts of the stationary and fluctuating parts of the potential.

System (1) is an example of a ratchet system with an additive-multiplicative form of the particle potential energy,

$$U(x,t)=\ u(x)+\ \sigma(t)w(x), \quad (2)$$

(if we put $\varphi=2\pi x/L$, $\Phi=2\pi\lambda$, and $\varphi_0=2\pi\lambda_0$) for which a number of effective theoretical approaches are developed [6]. In the high-temperature approximation, the average Brownian rotor velocity is calculated as [4,5]:

$$\langle v\rangle=k_1D\widetilde{\psi_2}\beta^3w^2\frac{u}{4}\sin 4\pi(\lambda-\lambda_0) \quad (3)$$

where k_1 is the wave number, D is the diffusion coefficient, β is the inverse thermal energy, $\widetilde{\psi_2}\equiv Dk_1^2\psi_2(Dk_1^2,Dk_1^2)$ is the dimensionless function (Eq. (15) in [4]), w is the amplitude of $w(x)$.

Symmetry-conditioned effects were analyzed within the approach suggested in [7], which showed that for a system (2) with a-symmetric forces $f(x)=-u'(x)$, $g(x)=-w'(x)$, with symmetry centers $x_a^{(f)}$ and $x_a^{(g)}$, respectively, $f\left(x+x_a^{(f)}\right)=-f(-x+x_a^{(f)})$ and $g\left(x+x_a^{(g)}\right)=-g(-x+x_a^{(g)})$, the following property takes place [7]:

$$v\{f_a(x)+g_a(x)\sigma(t)\}=-v\left\{f_a\left(x+2x_a^{(f)}-2x_a^{(g)}\right)+g_a(x)\sigma(t)\right\} \quad (4)$$

Thus, at $x_a^{(f)}\neq x_a^{(g)}$, the total force is not a-symmetric, and, hence, the ratchet effect may exist even for symmetric $u(x)$ and $w(x)$. This approach was used for analyzing the high-temperature Brownian rotor with the potential energy (1). The results were compared with the analysis in [3] and [5].

Theoretical analysis outside the high-temperature approximation required numerical solution of equations for the Green function of diffusion in the stationary part of the potential profile [6], $u(x)$, and numerical calculating of a double integral.

The frequency and temperature dependencies of the average rotor velocity have been obtained and interpreted, as well as the influence of the geometrical parameters of the system on the regime of particle motion (in particular, on existence of stopping points) has been studied. Symmetry analysis yielded conclusions on the orientations of the external electric field permitted for the appearance of directed rotation.

[1] P. Reimann, Brownian motors: noisy transport far from equilibrium, Phys. Rep. **361,** 57-265 (2002).
[2] B Lau et al., An introduction to ratchets in chemistry and biology, Mater. Horiz. **4**, 310-318 (2017).
[3] V. M. Rozenbaum, O. Ye. Vovchenko, T. Ye. Korochkova, Brownian dipole rotator in alternating electric field, Phys. Rew. **77**, 061111 (2008).
[4] V. M. Rozenbaum, I. V. Shapochkina, Y. Teranishi, L. I. Trakhtenberg, High-temperature ratchets driven by deterministic and stochastic fluctuations, Phys. Rew. **99**, 012103 (2019).
[5] O. Ye. Tsomyk, T. Ye. Korochkova, V. M. Rozenbaum, Molecular rotor as a high-temperature Brownian motor, CPTS, **7** (4), 444-452 (2016).
[6] V. M. Rozenbaum, I. V. Shapochkina, L. I. Trakhtenberg, Green's function method in the theory of Brownian motors, Physics Uspekhi **62** (5), 496-509 (2019).
[7] V. M. Rozenbaum, I. V. Shapochkina, Y. Teranishi, L. I. Trakhtenberg, Symmetry of deterministic ratchets, Phys. Rew. **100**, 022115 (2019).

CANCELLED DUE TO COVID-19

THE FORMATION OF FILMS OF ANODIC TITANIUM OXIDE AND THEIR USE IN MAXILLOFACIAL SURGERY

Lizaveta Hvazdouskaya, Sergei Lazarouk

Lab "Electrochemical nano-structure materials", Micro- & Nanoelectronics Department,
Belarusian State University of Informatics and Radioelectronics, Minsk, Belarus
elizaber@yandex.ru

Anodic titanium oxide is widely used in electronics. The first applications of valve metal oxides, in particular titanium oxide, are associated with the manufacture of capacitor dielectrics [1]. In recent years, interest in titanium oxide has increased due to its use in the production of memristors [2] and photoelectric converters [3, 4]. In addition, such films are used in medicine as coatings for titanium implants [5-7].

In this work, we studied the process of creation of anodic titanium oxide, the optical properties of the formed films, examined the options for using such films in maxillofacial surgery, in particular for visualization and hiding of titanium objects.

In the process of research, thick anodic oxide films were formed at voltages from 10 to 200 V. The thicknesses of the formed films were determined by the Newton color shade method. It should be noted that by varying the voltage in the range from 10 to 200 V, barrier oxide films with a thickness of 30 to 300 nm can be grown. In this case, the color of the formed films covers the entire color range of the visible spectrum from violet to red.

Of particular interest are films of red, blue and green, because combining these color shades you can get any color of the visible range. It should be noted, that films of dark and flesh tones are used for staining titanium medical implants used in maxillofacial surgery.

The studied films can also be used to create anti-reflective coatings for solar cells. By setting the required reflection and transmission spectra, one can use the useful part of the solar spectrum for the generation of electric energy. Also, titanium oxide is optically active, which allows the use of this oxide to purify water and air from organic contaminants.

Titanium implants, with titanium oxide films deposited on their surface, are widely used in medicine. In particular, the processing of the titanium surface is carried out in order to control the process of bone tissue regeneration on titanium structures used in the process of surgical treatment.

It is possible to use titanium implants with painted surfaces in order to visualize and hide objects in maxillofacial surgery. Since biological tissues have different optical permeabilities depending on the structure, the painted titanium surface can be visualized by exposure to visible light, which has positive and negative sides with different methods of implantation of titanium structures. Visualization of implants is due to the different optical permeability of biological tissues and the thickness of their layer. Metal structures (osseous plates and screws) during surgical interventions for traumatic injuries of the maxillofacial region can be removed after performing their functions according to indications after 10-12 months. At the same time, the cross-tissue visualization of a titanium object painted in dark colors makes it possible to determine the exact location of the titanium implant, reduce the time of surgery and minimize surgical injury.

Titanium implants for reconstruction of the bones of the facial skeleton and contour plastic suggest a constant presence in the body. In such cases, it is necessary to ensure the visualization of the implantable mounting plates. Accordingly, it becomes necessary to use implants with a surface painted in colors close to the color of biological tissues and possessing antireflection properties. Such implants are especially useful in areas with minimal thickness of soft tissues: the orbit, the back of the nose, and the oral cavity. Depending on the location and for the purpose of devising the implantable mounting plates, preference is given to yellow, pink, beige (flesh-colored) implantations. An analysis of the data obtained during the study confirms that films of anodic titanium oxide are able to fully provide the required properties for implants, which makes the use of these films promising in maxillofacial surgery.

Thus, the studies showed that oxide films with color shades covering the entire visible range from red to violet can be formed on the titanium surface using electrochemical anodization. The thickness of the studied oxides varies from 30 to 284 nm directly proportional to the anode voltage. The formed anode oxide films can be used as antireflection coatings for solar cells, as well as for staining metal implants used in maxillofacial surgery.

[1] L. Joung, *Anodic oxide films* (Energy, Leningrad, USSR, 1967).
[2] D. B. Strukov, G. S. Snider, D. R Stewart et al., The missing memristor found, Nature **453,** 80-83 (2008).
[3] U. Bach, D. Lupo, P. Comte et al., Solid-state dye-sensitized mesoporous TiO_2 solar cells with high photon-to-electron conversion efficiencies, Nature **395,** 583-585 (1998).
[4] K. Liang, B. K. Tay, O. V. Kupreeva et al., Fabrication of double-walled titania nanotubes and their photocatalytic activity, ACS Sustainable Chem. Eng. **2(4),** 991-995 (2014).
[5] S. Guizzardi, C. Galli, D. Martini et al., Different titanium surface treatment influences human mandibular osteoblast response, J Periodontol. **75(2),** 273-282 (2004).
[6] J. C. Keller, G. B. Schneider, C. M. Stanford et al., Effects of implant microtopography on osteoblast cell attachment, Implant Dent. **12,** 175-181 (2003).
[7] S. Lazaruk, O. Kupreyeva, D. Isayev et al., Influence of surface structure of titanium implants on the response from the bone tissue, Doklady BSUIR **1(95),** 100-103 (2016).

ORGELED PROOF 19

ELECTRONIC AND MAGNETIC PROPERTIES OF THE GRAPHENE-FERROMAGNET INTERFACES: *AB INITIO* SIMULATION

Dzmitry Hvazdouski, Maryia Baranava

Lab "CAD of micro- and nanoelectronic systems", Micro- & Nanoelectronics Department,
Belarusian State University of Informatics and Radioelectronics, Minsk, Belarus
gvozdovsky@bsuir.by

Graphene is a two-dimensional sheet of carbon atoms arranged in a honeycomb lattice with two crystallographically equivalent atoms (C1 and C2) in the unit cell [1, 2]. The sp^2 hybridization between one *2s* orbital and two *2p* orbitals leads to a trigonal planar structure with a formation of a σ bonds between carbon atoms that are separated by 1.42 Å. These corresponding σ bands have a filled shell and, hence, form a deep valence band. The half-filled $2p_z$ orbitals, which are perpendicular to the planar structure, form the bonding (π) and antibonding (π^*) bands in the electronic structure of graphene. The π and π^* bands touch in a single point exactly at the Fermi energy (E_F) at the corner of the hexagonal graphene's Brillouin zone (K-points). Close to this so-called Dirac point (E_D) the bands display a linear dispersion and form perfect Dirac cones [3]. Thus, undoped graphene is a semimetal ("zero-gap semiconductor"). The linear dispersion of the bands mimics the physics of quasiparticles with zero mass, so-called Dirac fermions [1 - 3].

The exceptional transport properties of graphene make it a promising material for application in microelectronics [4]. This has recently led to a revival of interest in graphene on transition metal surfaces [5, 6], as large area epitaxial graphene layers of exceptional quality can be grown, which might be an alternative to micromechanical cleavage for producing macroscopic graphene films.

The electronic interaction of graphene with a metal is both of fundamental and technologicalinterest in view of possible device applications. Graphene might be the best material for the realization of spintronic devices. Such systems usually require the effective injection of the spin-polarized electrons in the conductive channel which can be made from graphene [7]. However, prior to being able to implement graphene/ferromagnet systems in any kind of spintronic unit, a study of their electronic, magnetic, and interfacial properties has to be performed. Binding between graphene and metallic surface can be either chemical or physical in nature.

Chemical binding typically implies a strong interaction through a charge sharing between the substrate and the adsorbate, yielding modification of their electronic structures. Physisorption, on the other hand, arises due to classical electrostatic or dispersion (van der Waals) interactions.

The electronic and structural properties of the graphene-substrate system are obtained using the Perdew-Burke-Ernzerhof (PBE) functional [8]. For solving the resulting Kohn-Sham equation we have used the Vienna Ab Initio Simulation Package (VASP) [9, 10]. The plane-wave kinetic energy cutoff is set to 520 eV. The supercell used to model the graphene-metal interface is constructed from a slab of 7 layers of metal atoms with a graphene sheet adsorbed at both sides and a vacuum region of approximately 15 Å. When optimizing the geometry, the positions (z-coordinates) of the carbon atoms as well as those of the top two layers of metal atoms are allowed to relax. In the total energy calculations and during the structural relaxations the k-meshes for sampling the supercell Brillouin zone are chosen to be as dense as 21 × 21 and 11 × 11, respectively.

The electronic structure and magnetic properties of the graphene/ferromagnet interface were investigated via theoretical methods (DFT functional). The different interfaces were analyzed: graphene/Ni(111), graphene/Co(0001) . Here the electronic structure of the interface as well as the effect of induced magnetism in graphene layer were discussed. In all cases a strong modification of the electronic structure of the graphene layer and FM substrate upon graphene adsorption were detected in theoretical calculations. This modification is due to the considerable hybridization of the graphene π and FM *3d* valence band states accompanied by the partial charge transfer of spin-polarized electrons from FM onto C atoms leading to the appearance of the effective magnetic moment in the graphene layer.

[1] A. Geim, Graphene: Status and prospects, Science **324(5934),** 1530-1534 (2009).
[2] A. K. Geim, K. S. Novoselov, The rise of graphene, Nature Mater. **6,** 183-191 (2007).
[3] A. Neto, F. Guinea, N. Peres et al., The electronic properties of graphene, Rev. Mod. Phys. **81(1),** 109-162 (2009).
[4] S. V. Morozov, K. S. Novoselov, M. I. Katsnelson et al., Giant intrinsic carrier mobilities in graphene and its bilayer, Phys. Rev. Lett. **100(1),** 016602 1-4 (2008).
[5] J. Coraux, A. N'Diaye, M. Engler et al., Growth of graphene on Ir(111), New J. Phys. **11(2),** 023006 1-22 (2009).
[6] B. Wang, M. Bocquet, S. Marchini et al., Chemical origin of a graphene moire overlayer on Ru(0001), Phys. Chem. Chem. Phys. **10(24),** 3530-3534 (2008).
[7] N. Tombros, C. Jozsa, M. Popinciuc et al., Electronic spin transport and spin precession in single graphene layers at room temperature, Nature **448(7153),** 571-574 (2007).
[8] J. Perdew, K. Burke, M. Ernzerhof, Generalized gradient approximation made simple, Phys. Rev. Lett. **77(18),** 3865-3868 (1996).
[9] G. Kresse, J. Furthmuller, Efficiency of ab-initio total energy calculations for metals and semiconductors using a plane-wave basis set, Comp. Mater. Sci. **6(1),** 15-50 (1996).
[10] G. Kresse, J. Furthmuller, Efficient iterative schemes for ab initio total-energy calculations using a plane-wave basis set, Phys. Rev. B **54(16),** 11169-11186 (1996).

OPEN ACCESS PROCEEDINGS

INFLUENCE OF INSULATING SHELLS AROUND METALLIC NANOPARTICLES ON PERCOLATION THRESHOLD IN NANOCOMPOSITES

Aliaksandr V. Zaparozhtsau, Alexander S. Fedotov

Physics Faculty, Belarusian State University, Belarus
aliex.s@yandex.by

CANCELLED DUE TO COVID-19

Nanocomposite is a multiphase composite system, consisting of several materials with various structure and with a characteristic size about a nanometer. If a number of nanoparticles are located nearby, and they don't have a phase separation boundaries, they could be grouped in cluster with common properties.

Standard site percolation model assume that each vertex is conductive with a probability P_{cond} or non-conductive with probability $P_{noncond} = 1 - P_{cond}$, all edges are conductive with probability $P_{conn} = 1$ and there no phase separation boundaries. In real nanocomposites, however, there are oxide shells around metallic cores that can prevent the formation of electrical contact even if nanoparticles are close together[1]. To model such a system we augment site percolation model to consider located probability of breaking bond between particles P_{ox}, described as a result of metal core oxidation. This illustrates is a nanocomposite, consisting of conductive internal core and perforated insulating shell.

The developed model demonstrates dependency of system conductivity probability P_s as a function of two parameters $P_s = f(P_{cond}, P_{ox})$. Percolation threshold probability P_c determines depending on P_s graph view, so $P_c = f(P_{cond}, P_{ox})$ too.

Fig. 1a illustrates P_s, where each curve on a graph is $P_s = f(P_{cond})$ with different constant P_{ox} ($P_{ox} = const$).

Fig. 1b is an example of generated nanocomposite clusters, used for conductivity probability statistic.

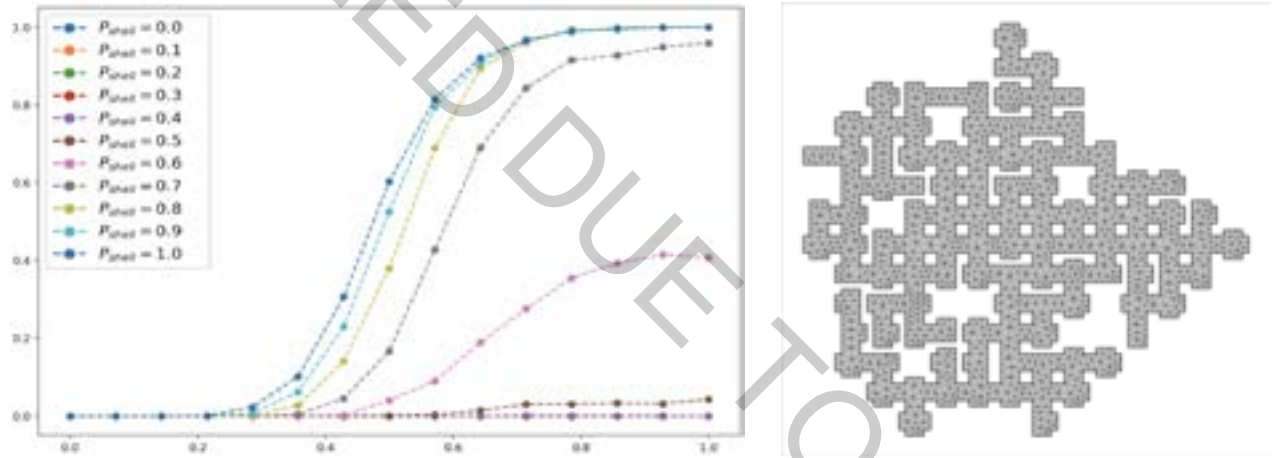

(a) Percolation function curve family

(b) Structured conductive cluster of nanocomposites

Fig. 1. Nanocomposite cluster generation results.

If $P_{cond} = 1$, this model becomes a percolation of connections only, but when $P_{conn} = 1$, it is a percolation of nodes [2]. Experiments confirm that with $P_{conn} = 1$, $P_c = 0.59$.

To generate percolation cluster could be used Hoshen-Kopelman algorithm [3]. But this algorithm could not be used for the generation of system on grid with node count $N_{node} > 1000$. To boost calculation performance, we used a corn-generation method. In the center put a conductive node (*corn*), nodes around corn marked as a possibly conductive too. Each marked node with P_{cond} became conductive or with $P_{noncond}$ marked as nonconductive. It repeats while possibly conductive node list is not empty. For each conductive node with shell conductivity probability $P_{shell} \in [0,1]$ could be added shell. Nearby nodes are connected if both have a shell from symmetrical side. If conductive cluster diameter d_{cluste} greater than environment size L_{env}, system considered conductive.

Next step will be research of conductivity of such cluster and calculation of energy flow throw shell-considered model.

[1] I. Svito, J.A. Fedotova, M. Milosavljevicc, P. Zhukowski, T.N. Koltunowicz, A. Saad, K. Kierczynski, A.K. Fedotov, Influence of sputtering atmosphere on hopping conductance in granular nanocomposite $(FeCoZr)_x(Al_2O_3)_{1-x}$, Journal of Alloys and Compounds, 1-4 (2013).

[2] Y. Tarasevich, Percolation: theory, application, algorithms. 1.1, 33-40 (2002).

[3] J. Hoshen, R. Kopelman, Percolation and cluster distribution. Cluster multiple labeling technique and critical concentration algorithm. Physical Review, **14**(8), 3438–3445(1976).

INVESTIGATION OF BIOMEDICAL AND TRIBOLOGICAL PROPERTIES OF SILICON (Si) DOPED DLC COATING

Ranjan Kumar Ghadai[1*], Soham Das[1], Ashis Sharma[1]

[1]Department of Mechanical Engineering, Sikkim Manipal Institute of Technology Sikkim Manipal University, Sikkim India
ranjan.ghadai@yahoo.com

CANCELLED DUE TO COVID-19

The use of biomaterial into the human body is the restoration of certain tribological and biological functions. The Silicon (Si) doped diamond like carbon (DLC) coating deposited over Si (100) substrates by using thermal chemical vapour deposition (CVD) technique. Four different samples were made by varying the H_2 flow rate from 30 to 90 sccm and the C_2H_2 flow rate kept constant as 9 sccm. The morphology, tribological and chemical composition of Si-DLC films were investigated by SEM, Nanoscratch and EDX respectively. From the EDX it has been observed that the Si percentage in the DLC film decreases with increase of H_2 flow rate. The average coefficient of friction (μ) were calculated from Nanoscratch and it is noted that the surface of the films is smooth at lower H_2 flow rate. The $\boldsymbol{\sigma}$ is calculated by using the Stoney equation and it is presented in equation 1.

$$\sigma = \frac{E_s}{6(1-\upsilon_s)} \times \frac{t_s^2}{t_f}\left(\frac{1}{R_2} - \frac{1}{R_1}\right) \quad (1)$$

Where t_s and t_f are the thickness of the substrate and film, respectively. R_2 is the curvature of the film and R_1 is curvature of the Si substrate before deposition of the films. The v_s and E_s are the Poisson ratio and Young modulus of the substrate. The Es and Vs for Si (100) substrate are 127 GPa and 0.27 [2]. The residual stress of the film increases with increase of H_2 flow rate which may be due to the presence of less Si at higher H_2 flow rate. It is also noted that the antibacterial properties of Si-DLC thin film increased with the Si concentration. The bio test results demonstrate that the Si-DLC films are potentially useful biomaterials having both good tribological properties and antimicrobial characteristics. Fig.1 (a) and (b) shows the Cell Viability and hemolysis of Si-DLC thin films deposited at different H_2 flow rate. In order find the hemocompatibility of Si-DLC thin film hemolysis test is performed and the hemolysis of Si doped DLC films were evaluated by performing MTT assay. In order to evaluate the cytocompatibility of the Si-DLC coating, we quantified the percentage of viable cells by the MTT cell viability assay [3].

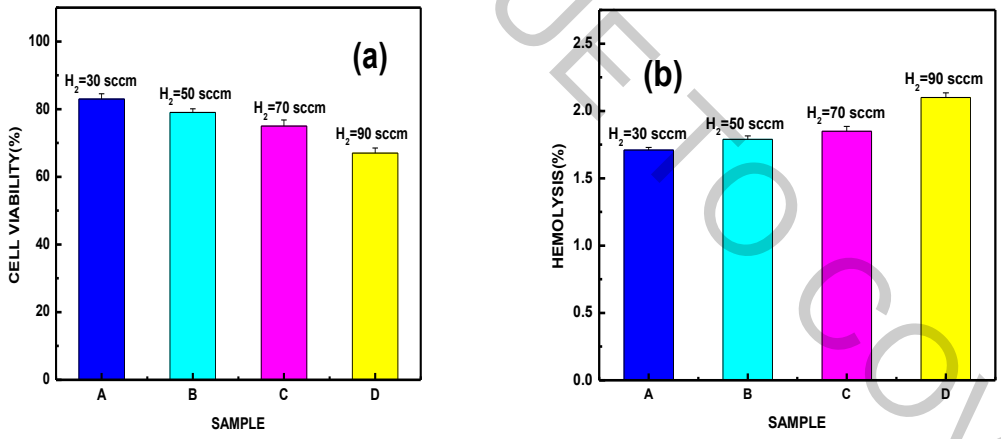

Fig. 1: Cell Viability and Hemolysis of Si-DLC thin films deposited at different temperature H_2 flow rate

From the fig. 1 (a) it is observed that the cell viability of all the Si-DLC thin film is more than 65 % and it decreases with increase in temperature. The Si-DLC thin film deposited at lower H_2 flow rate has the 83 % of cell viability which is highest among the four films. The increased cell viability could be due to the presence of Si particles in the surface of the film which facilitates efficient cellular communication and retains nutrient for longer duration. From the fig. 1(b) it is observed that the Si-DLC film deposited at lower H_2 flow rate has the lowest % of hemolysis (1.71 %) and the DLC film deposited at higher H_2 flow rate has the highest % of hemolysis (2.1 %). Thus, it is seen that higher Si content significantly reduced the hemolysis % which improves the biocompatibility of the films.

[1] H. Nakazawa, R. Kamata, S. Okuno, Deposition of silicon-doped diamond-like carbon films by plasma-enhanced chemical vapour deposition using an intermittent supply of organosilane, Diamond and Related Materials, 51 (2015) 7–13.
[2] G. C. A. M. Janssen, M. M. Abdalla, F. V. Keulen, B. R. Pujada, B. V. Venrooy, Celebrating the 100th anniversary of the Stoney equation for film stress: Developments from polycrystalline steel strips to single crystal silicon wafers, Thin Solid Films 517 (2009) 1858–1867.
[3] T. Kaur, A. Thirugnanam, Tailoring in vitro biological and mechanical properties of polyvinyl alcohol reinforced with threshold carbon nanotube concentration for improved cellular response, RSC advances, 6 (2016) 39982-39992.

TORSIONAL SPECTRUM OF THE METHYL HYDROPEROXIDE MOLECULE CALCULATED AT MP2/cc-pVQZ

Uladzimir Lazicki[1], Zlata Lepenkova[1], Darya Kisuryna[1], Alex Malevich[1], George Pitsevich[1], Vitas Balevicius[2]

[1]Belarusian State University, Minsk, Belarus
[2]Vilnius University, Vilnius, Lithuania
kisurinadasha@gmail.com

CANCELLED DUE TO COVID-19

Methyl hydroperoxide ($HOOCH_3$) is a one of the simplest molecules that have two internal tops: the hydroxyl group (OH) which can rotate around the O-O bond and the methyl group (CH_3) which can rotate around the C-O bond. This molecule was detected in the cosmic space therefore it is of interest to astrophysics. It also takes part in the Earth atmospheric phenomena as an intermediate product of the chemical reactions. $HOOCH_3$ is a non-rigit molecule. It can exist in two configurationally - equivalent states which are separated by relatively low potential barrier. To analyze the torsional spectrum of the methyl hydroperoxide (MHP) the 2D PES and 2D kinematic coefficients surface were calculated at MP2/cc-pVQZ level of theory. Two torsional angles (γ and φ) were used to specify the positions of the hydroxyl and methyl groups relative the C-O-O plane during internal rotation. When choosing the appropriate points for potential energy calculations one has to keep in mind that the C-O-O plane is a symmetry plane for any distorted configuration of the molecule. We varied the value of the γ in the range 4^0 – 356^0 with a step of 8^0. Due to φ has $2\pi/3$ period we varied the value of the φ in the range 4^0 – 56^0 with a step of 8^0. At every point of the 2D equidistant grid we performed energy optimization on all the rest internal coordinates to take into account geometry changing during internal rotation. Then the stationary vibrational Schrödinger of the following form

$$\left[-F_{\gamma\gamma}(\gamma,\varphi)\frac{\partial^2}{\partial\gamma^2} - F_{\varphi\varphi}(\gamma,\varphi)\frac{\partial^2}{\partial\varphi^2} - F_{\gamma\varphi}(\gamma,\varphi)\frac{\partial^2}{\partial\gamma\partial\varphi} + U(\gamma,\varphi)\right]\Psi(\gamma,\varphi) = E\Psi(\gamma,\varphi);$$

was solved using Fourier method. Here $F_{\gamma\gamma}(\gamma,\varphi)$, $F_{\varphi\varphi}(\gamma,\varphi)$, $F_{\gamma\varphi}(\gamma,\varphi)$ are the kinematics coefficients and $U(\gamma,\varphi)$ - potential energy. Calculated value of the tunneling frequency in the ground state is equal to 19.23 cm^{-1}. Torsional spectrum of the MHP molecule, represented on Fig.1, was calculated at 300^0 K.

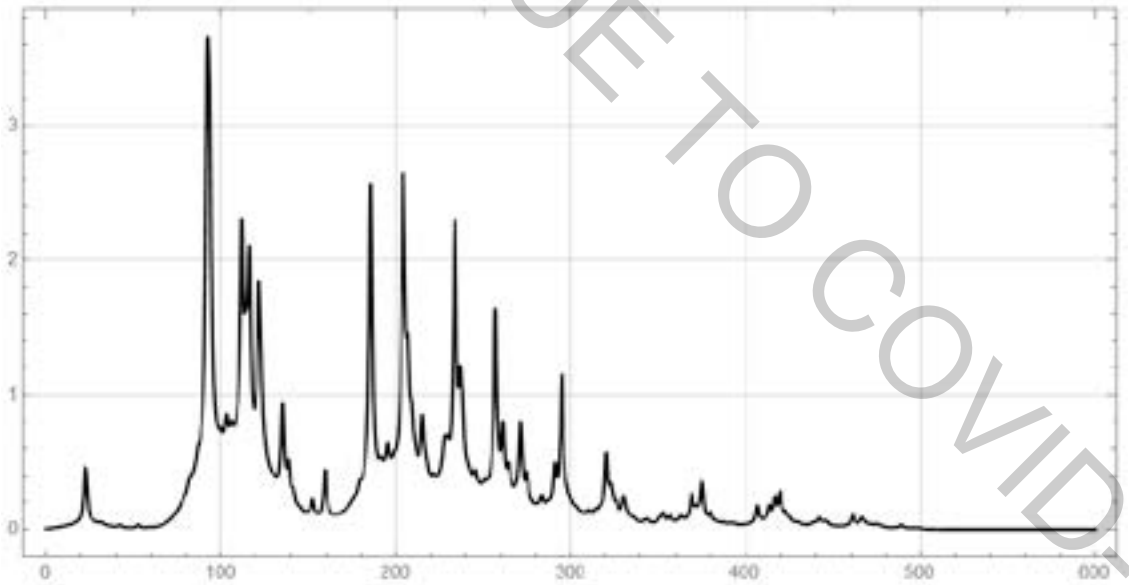

Fig. 1. Calculated at the MP2/cc-pVQZ level of theory torsional spectrum of MHP molecule at 300^0 K.

As one can see the torsional IR spectrum of the MHP molecule is rich on intensive IR bands which appears in wide spectral region. This information will be useful for the more successful search of this molecule in the cosmic space and the Earth atmosphere.

A COMPREHENSIVE BIOINFORMATION SYSTEM OF HUMAN EMOTION RECOGNITION

Siarhei Sadau, Igor Kheidorov

Department of Radio Physics and Computer Technologies, Belarusian State University, Belarus
seregasadov@gmail.com

CANCELLED DUE TO COVID-19

Most of the known computer systems which determine the emotional state of a person are based on obtaining data from a facial image in a video sequence. A more promising direction is based on the analysis of multiple streams: facial images, gestures, postures, speech and biometrical data. The proposed system allows obtaining information by analyzing facial expressions, speech and biometrical data of the object in real time.

The system (figure 1) consists of four main modules: data acquisition module, data processing module, classification module, and a data output module. Let us consider in more detail each component.

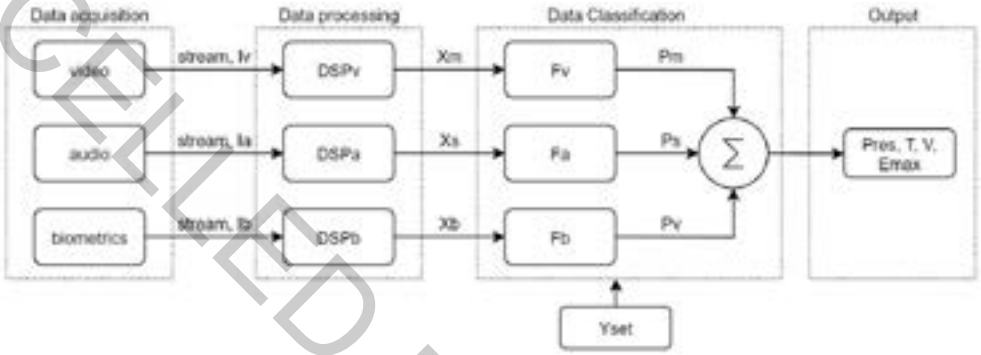

Fig 1 A model of the system

Data acquisition module

From the analyzed object the data is fed to the input of video, audio, and biometric channels. Each channel carries out a set of unique operations on the input data. The video channel performs the selection and capture of the face in the video stream, the segmentation of key areas that demonstrate muscle movement. The audio channel carries out the primary selection of the useful signal (human speech) in the audio stream. The biometric channel supplies a stream of data on skin temperature, blood pressure, and heart rate.

As a rule, the analyzed object locates in a noisy environment, therefore there is a non-zero probability of obtaining poor-quality data for each channel, up to the complete impossibility of using them. To take this feature into account, each channel must calculate its own coefficient of content relevance I_{ch} and transfer it to the processing module.

Data processing module

Such a module receives at its input previously prepared information for each of the channels and outputs normalized vectors X_{set} of data attributes at the output. Such vectors resulting from digital signal processing are unique to each non-verbal component. For example, for the mimic component, the vector contains information about the change in the location of the supporting segments on the face, which characterize the dynamics of contraction of the facial muscles. For speech - the volume, pitch and frequency response of speech.

Additional Y_{set} features to X_{set} feature vectors take into account the age, educational characteristics of a person, his gender, nationality, etc. since recent studies [1] cast doubt on the thesis of the invariance of the expression of emotions by different people.

Classification Module

The main output parameter, the P_{res} vector, reflects the probability that the non-verbal component corresponds to a certain type of emotion from a given set of considered emotions E_{set}. Functional dependencies F_{ch}: $X_{set} \rightarrow P_{ch}$, where *ch* is the corresponding non-verbal channel, the values of the feature vectors are mapped onto probability vectors P_{ch}. For such a functional display, classifiers [2], unique for each channel, which are based on a training data set, are used. Further, the output of the classifiers, P_{ch} vectors, must be normalized and summed to obtain the integral vector P_{res}.

Data output module

As a result, we can determine the parameter $E_{res} \in E_{Set}$ corresponding to the dominant type of emotion highlighted in the general set of possible emotional states

The output parameterization used also allows obtaining secondary output data - valency and tonality.

[1] Gendron M, Roberson D, van der Vyver JM, Barrett LF // Perceptions of emotion from facial expressions are not culturally universal: evidence from a remote culture, Affective Science Institute, - 2014.

[2] Soroka, A. M. Recognition of emotions in speech based on wavelet analysis with adaptable basic functions / A.M. Soroka A.V. Semenchenko, I.E. Kheidorov // Information systems and technologies: materials of the international congress on computer science.- Minsk: BSU, 2016, c.646-651.

ELECTRON IMPACT IONIZATION OF W^{5+}

Saulius Pakalka[1], Aušra Kynienė[1], Sigitas Kučas[1], Šarūnas Masys[1], Valdas Jonauskas[1]

[1]Institute of Theoretical Physics and Astronomy, Vilnius University, Lithuania
saulius.pakalka@tfai.vu.lt

Energy losses determined by radiation of impurities in various ionization stages have to be controlled for the successful ignition of a deuterium-tritium plasma in thermonuclear reactors. Ionization balance in the plasma is mainly established by electron-impact ionization and recombination processes. Such processes have to be well understood for predicting possible plasma scenarios.

The main goal of the current work is to present theoretical study of electron-impact single ionization cross sections for the W^{5+} ion. The theoretical study includes direct and indirect processes. Level-to-level calculations were performed for the $5d$ ground configuration and for several excited configurations of W^{5+}. For all contributions considered in the determination of the total single-ionization cross section, autoionization branching ratios for every level of the W^{5+} ion populated by excitation of one of the initial states were calculated accounting for Auger and radiative decays from the level.

The Flexible Atomic Code (FAC) [1], which employs the Dirac-Fock-Slater method, is used to calculate energy levels, radiative and Auger transition probabilities, and electron-impact excitation and ionization cross sections. The cross sections are obtained in the distorted wave (DW) approximation. Excitations of the $4f$, $5s$, $5p$, and $5d$ electrons from the $5d$, $6s$, $4f^{13}5d^2$, $5p^55d^2$, and $4f^{13}5d\,6s$ configurations up to the shells with $n = 12$ are taken into account in the study to ensure convergence of the EA data. Furthermore, the excitations to all subshells with orbital quantum numbers $l \leq 6$ are studied. It can be seen that there is a difference of $\sim$20% between the $n = 7$ and the $n = 12$ result at the peak of the cross section (Fig. 1). Radiative damping of the autoionizing states leads to diminishing of the total ionization cross sections by $\sim$14% at the peak.

The influence of initial- and final-state correlation on electron-impact ionization cross sections from the ground configuration is investigated. Correlation is taken care of by the implementation of configuration interaction applying suitable basis sets. The correlation effects are studied for the strongest DI channels and excitations that lead to single ionization. The configuration interaction strength (CIS) [2] is employed to determine a list of admixed configurations having the largest influence on the configuration under consideration.

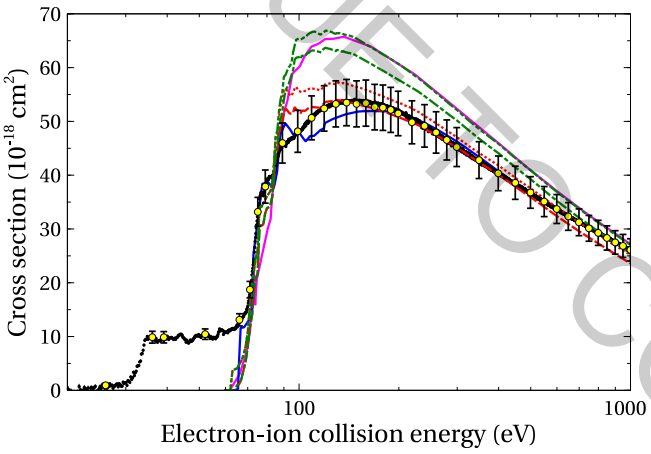

Fig. 1. (Color online) Comparison of the present experimental data to the theoretical calculations for single ionization from the ground levels of W^{5+}. Circles with light shading (yellow) and associated total error bars represent experimental absolute cross sections. The small black dots with statistical error bars of the size of the symbols are the result of the fine-step energy scan. Present theoretical results including DI and EA for excitations with $n \leq 7$ are shown by the dashed (red) line for the $5d^2D_{3/2}$ ground level and by the dotted (red) line for the $5d^2D_{5/2}$ level. The dash-dotted (green) line represents the $5d^2D_{3/2}$ cross section and the dash-dot-dotted (green) line the $5d^2D_{5/2}$ cross section which both contain EA contributions associated with excitations up to $n = 12$. The CADW results obtained by Pindzola and Griffin [3] including excitations with $n \leq 6$ are represented by the solid (blue) line that is close to the experimental data points.

[1] M.F. Gu. The flexible atomic code. Canadian Journal of Physics, 86(5):675–689, 2008.
[2] R. Karazija and Kučas. Average characteristics of the configuration interaction in atoms and their applications. J. Quant. Spectrosc. Radiat. Transf., 129:131–144, 2013.
[3] M. S. Pindzola and D. Griffin. Electron-impact ionization of tungsten ions in the configuration-average distorted-wave approximation. Physical Review A, 56(2):1654–1657, 1997.

CANCELLED DUE TO COVID-19

SIMULATION OF AN ACCELERATOR DRIVEN SYSTEM WITH DIFFERENT SPALLATION TARGETS

Aliaksandr Dubrouski, Hanna Kiyavitskaya

Belarusian State University, International Sakharov Environmental Institute, Minsk, Republic of Belarus
a1dubrovskii@gmail.com

Today, electro-nuclear systems based on high-current accelerators are considered as most promising ones for transmutation of spent nuclear fuel and energy production. The main reason is related to the usage of an accelerator as an external source which makes such systems safer to operate and easy to control the chain fission reaction.

A spallation target in Accelerator Driven system (ADS) is the main component due to generation of neutrons which then multiply in a subcritical reactor. Thus, it is necessary to calculate such characteristics as neutron yield and energy spectra, energy deposition, heating and activation of the target and production of long-lived fission fragments. These parameters can be defined using modern transport codes developed for simulation of the hadron-nucleus interactions over a wide energy range. In this work the Geant4 code was used with QGSP_BIC_HP standard physics list [1].

The model of uranium blanket with different insertions was developed to calculate the neutronics of the system. Integral data of neutron output, energy spectra and some reaction rates were calculated and compared with the experimental data [2] and the calculations with other codes [3]. The good agreement between experimental data and simulation results was obtained.

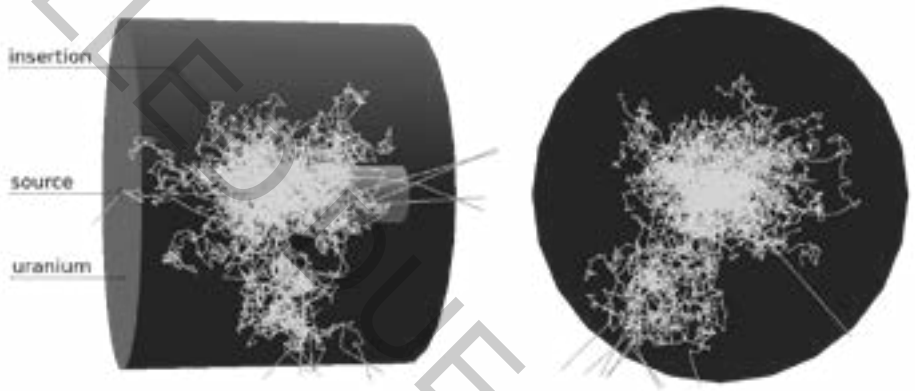

Fig. 1. Model of uranium blanket

Simulation results demonstrate that the shape of neutron spectra with increasing of proton energy does not changed. There is an increase in the reaction rates and neutron flux only. However, energy spectra are slightly different depending on the insertion material.

It is planned the investigation of the reactions of fragmentation in the spallation targets as well as the formation of fission products in more detail. The current model should be refined to reduce simulation uncertainties and for clearer understanding of the kinetics of ADS.

[1] Geant4 Use Cases – Reference Physics Lists [Electronic resource]. – Mode of access: https://Geant4.web.cern.ch/node/302 – Date of access: 01.07.2019.

[2] M. S. Zucker et al., Spallation Neutron Production Measurements, 2nd Int. Conference on Accelerator Driven Transmutation Technologies & Applications (ADTTA), Kalmar, Sweden, 3–7 Jun – 1996. – Vol.1. P. 527 – 533.

[3] O. Grudzevich, S. Yavshits, Complete files of neutron- and proton-induced nuclear data to 1 GeV for 208Pb target, 8th Int. Conference on Nuclear Data for Science and Technology, Nice, France, 22–27 April – 2007. – P. 102.

CANCELLED DUE TO COVID-19

CLARIFICATION OF ENERGY VALUE FOR THE ACTIVATION LEVEL IN THE REACTION ^{103}Rh(γ,γ')^{103m}Rh

Eduard Gohman[1], Viktor Zhaba[1]

[1] Department of Theoretical Physics, Uzhgorod National University, Uzhgorod, Ukraine
viktorzh@meta.ua

CANCELLED DUE TO COVID-19

In papers [1, 2], the dependences of the absolute yield from energies for reaction A(γ,γ')A^m on the averages (^{77}Se, ^{79}Br, ^{89}Y) and heavy (^{103}Rh, ^{111}Cd, ^{137}Ba, ^{179}Hf, ^{197}Au, ^{199}Hg) nuclei were analyzed for the presence of fractures. Fractures are the points of deviation of the energy dependence of the absolute yield from the monotonically increasing curve. These points are interpreted as individual activation levels or groups of activation levels, through which the isomers of the nucleus are populated.

The experimental data from [1] for ^{103}Rh(γ,γ')^{103m}Rh reaction were approximated by a line (Fig. 1)

$$y = a + bx. \tag{1}$$

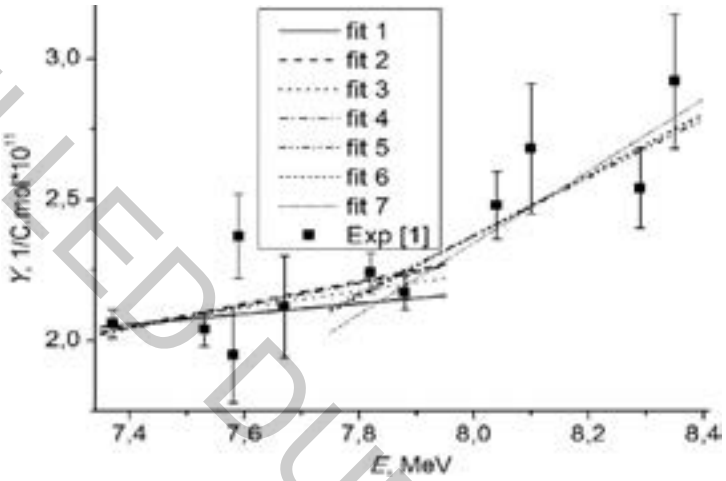

Fig. 1. Energy dependence of the absolute yield for the reaction ^{103}Rh(γ,γ')^{103m}Rh.

The "best" or "worse" approximation can be estimated by comparing the correlation coefficient R or value χ^2, and the different width of energy interval when approximating. Using the values of the parameters a and b for the approximations (step is one experimental point), it is possible to determine the intersection points x_0 for fits 1-4 and 5-7 for the energy intervals ΔE. For these purpose, we use the solution of simple linear two equations:

$$a_i + b_i x_0 = a_j + b_j x_0, \tag{2}$$

where the indexes i and j characterize fits 1-4 and 5-7 respectively. As the analysis of the obtained values x_0 shows (Table 1), the fracture of the experimental curve of reaction yield is localized in the energy interval ΔE=7.76-7.93 MeV. Given the minimum values for χ^2, the "best" approximations are fit 3 and fit 5 for the left and right arrays of energies respectively. Then the intersection point for these functions is located at energy E_a≈7.81 MeV. This value E_a corresponds to the energy of the activation level. In [2] for ^{103m}Rh, the corresponding E_a value was 7.87 MeV.

With this method, can be clarified the energy value for the activation level in the reaction (γ,γ') for others averages and heavy nuclei.

Table 1. Intersection points x_0 for approximate dependencies

fit N (ΔE in MeV)	**fit 5** (7.67-8.35)	fit 6 (7.82-8.35)	fit 7 (7.88-8.35)
fit 1 (7.37-7.67)	7.75693	7.77111	7.83524
fit 2 (7.37-7.82)	7.86915	7.87993	7.93580
fit 3 (7.37-7.88)	**7.81116**	7.82413	7.88537
fit 4 (7.37-8.04)	7.85861	7.87011	7.92806

[1] V.S. Bokhinyuk, O.G. Okunev, O.M. Parlag et al., Study of the ^{103}Rh(γ,γ')^{103m}Rh reaction, Uzhgorod Univ. Scien. Herald. Ser. Phys. **27**, 29-33 (2010).
[2] V.S. Bohinyuk, V.I. Zhaba, A.M. Parlag et al., Investigation of isomeric states in the reaction (γ,γ')^m on nuclei ^{77}Se, ^{79}Br, ^{89}Y, ^{103}Rh and ^{111}Cd, Uzhhorod Univ. Scien. Herald. Ser. Phys. **37**, 161-165 (2015).

NON-ABELIAN GEOMETRIC POTENTIALS AND SPIN-ORBIT COUPLING FOR PERIODICALLY DRIVEN SYSTEMS

Povilas Račkauskas[1], Viktor Novičenko[1], Han Pu[2], Gediminas Juzeliūnas[1]

[1]Institute of Theoretical Physics and Astronomy, Vilnius University, Lithuania
[2]Department of Physics and Astronomy, and Rice Center for Quantum Materials, Rice University, USA
povilas.rackauskas@ff.stud.vu.lt

CANCELLED DUE TO COVID-19

We demonstrate the emergence of a non-Abelian geometric potential and thus a three-dimensional (3D) spin-orbit coupling (SOC) for cold atoms without using laser beams, namely by subjecting an atom to a periodic perturbation [1]. This perturbation is taken to be the product of a fast-oscillating periodic function and a position- (and possibly time-) dependent Hermitian operator. Our analysis focuses on the case where the aforementioned Hermitian operator depends on internal states of the atom and therefore does not necessarily commute with itself at different positions. If the operator is taken to be self-commuting at different positions the system becomes equivalent to the one of the Kapitza problem [2], therefore our work can be seen as its extension. For the SOC to have a significant effect we consider a situation where the interaction amplitude is of the same order as the driving energy, and thus overcome limitations present in the previous works.

The general formalism is applied to the study of a spinful particle in a fast-oscillating spatially inhomogeneous magentic field. It is shown that a spherically symmetric magnetic field generates a fine-structure-like 3D SOC of the form $\mathbf{L}\cdot\mathbf{S}$. For large distances the coupling strength drops as $1/r^2$ and thus is long-ranged compared to the atomic fine-structure interaction. Such SOC affects the higher states of the trapped atom as well as the lower ones. It is shown that states with the same total agular momentum are nearly degenerate (Fig. 1). This degeneracy may be lifted by changing the trapping potential for the cold atoms. It is demonstrated that by introducing a specially tailored anti-trapping potential the state charecterized by the orbital quantum number $l = 1$ becomes the ground state, which is not typical for a spin-orbit coupled system and may lead to interesting many-body behavior.

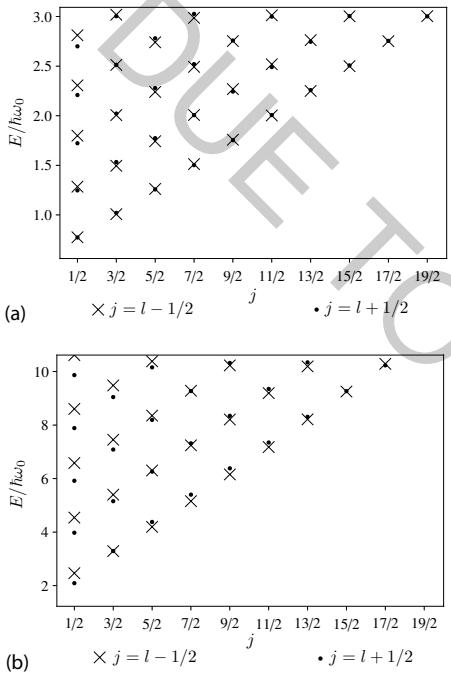

Fig. 1. Dependence of eigen-energies $E_{n_r,j,l}$ on the total angular momentum quantum number j for orbital quantum numbers $l = j \mp 1/2$ and up to five lowest radial quantum numbers n_r. Panel (a) corresponds to a softer trap $V_{ex}(r) = \frac{m\omega_0^2 r^2}{32}$ and panel (b) corresponds to a tighter trap $V_{ex}(r) = \frac{m\omega_0^2 r^2}{2}$. Energy is given in relative units charecteristic to the system.

[1] P. Račkauskas, V. Novičenko, H. Pu, G. Juzeliūnas, Non-abelian geometric potentials and spin-orbit coupling for periodically driven systems, Phys. Rev. A **100**, 063616 (2019).
[2] M. Bukov, L. D'Alessio, A. Polkovnikov, A. Green, Universal high-frequency behavior of periodically driven systems: from dynamical stabilization to Floquet engineering, Adv. Phys. **64**, 139-226 (2015).

LEARNING QUANTUM STRUCTURES IN COMPACT LOCALIZED EIGENSTATES

Giedrius Žlabys, Mantas Račiūnas, Egidijus Anisimovas

Institute of Theoretical Physics and Astronomy, Vilnius University, Saulėtekio 3, LT-10257 Vilnius, Lithuania
giedrius.zlabys@tfai.vu.lt

Application of machine learning techniques for complex quantum systems provides new numerical tools to probe quantum phenomena [1, 2]. These tools can potentially outperform traditional methods due to their high tunability and efficient information encoding. The faithful representability of many-body states by artificial neural networks (ANNs), given a sufficient number of parameters, is now becoming established as an empirical fact and is supported by analytical evidence [3]. On the other hand, the optimizability of a neural net remains an open issue: it is not *a priori* clear which models and features are well suited for machine learning techniques.

We apply ANNs to study the emergence of quantum structures in interacting bosonic systems on a lattice. We focus on the simplest one- and two-dimensional geometries that support dispersionless energy bands and the the formation of compact localized states [4] spanning just a few neighboring sites. In the presence of interactions and at suitable values of the filling, these systems demonstrate a transition to a charge density wave. Inspired by a successful machine learning treatment of the paradigmatic superfluid-Mott insulator [2] and magnetic [1] transitions, we set out to explore how successful ANNs can be in learning quantum structures defined by compact localized states. We find that while being guided only by the noisy signal of Monte-Carlo estimates of the ground-state energy, ANNs are able to learn the defining features of quantum structures with the accuracy comparable or even superior to that of ground-state energy itself.

[1] G. Carleo, M. Troyer, Solving the Quantum Many-Body Problem with Artificial Neural Networks, Science **355**, 602–606 (2017).
[2] H. Saito, Solving the Bose–Hubbard Model with Machine Learning, J. Phys. Soc. Jpn. **86**, 093001 (2017).
[3] J. Chen, S. Cheng, H. Xie, L. Wang, T. Xiang, Equivalence of restricted Boltzmann machines and tensor network states, Phys. Rev. B **97**, 085104 (2018).
[4] D. Leykam, A. Andreanov, S. Flach, Artificial flat band systems: from lattice models to experiments, Adv. Phys.: X **3**, 1473052 (2018).

CANCELLED DUE TO COVID-19

MODELING OF PUMP-PROBE SPECTRA AT HIGH EXCITATION INTENSITY IN MOLECULAR AGGREGATES

Vytautas Bubilaitis, Darius Abramavičius

Institute of Chemical Physics, Faculty of Physics, Vilnius University, Lithuania
Vytautasbubilaitis@ff.vu.lt

Polarization of an arbitrary order can be calculated by expanding density operator in powers of interaction with the excitation field[1]. The resulting optical response theory is not only useful for precise calculations, but also allows one to discover and describe various processes with the help of Feynman diagrams.

The lowest order optical signal that is generated in isotropic media is third order. At this order, the one exciton states and excited state energy transfer can be observed.

When excitation dynamics are followed at the lowest (third) power of interaction to excitation field, dependence on excitation intensity is often ignored. This dependence can be important as laser pulse intensity is one of parameters that is tuned for better signal-noise ratio. At high excitation intensity exciton-exciton annihilation (EEA)[2] takes place. EEA is the process when two molecular excitations, originating from different molecules, meet on the same molecule creating a high energy short lived state. Fast internal conversion takes place and the molecule returns back into singly excited state while the energy of the other excitation gets dissipated in its vibrational manifold. The EEA process in molecular aggregates has the effect of limiting the number of excitations, and can be used to observe exciton migration.

Nonlinear exciton equations (NEE)[3] were used for calculations of spectra. In our previous work spectra were calculated with these equations with EEA terms, but the relaxation model was too primitive and the system of equations was too small. Therefore in this work NEE system of equations is expanded beyond the third order. Secular relaxation and phenomenological EEA terms were added to the equations. Also pump-probe spectra at various excitation intensities were calculated by numerically solving NEE[4].

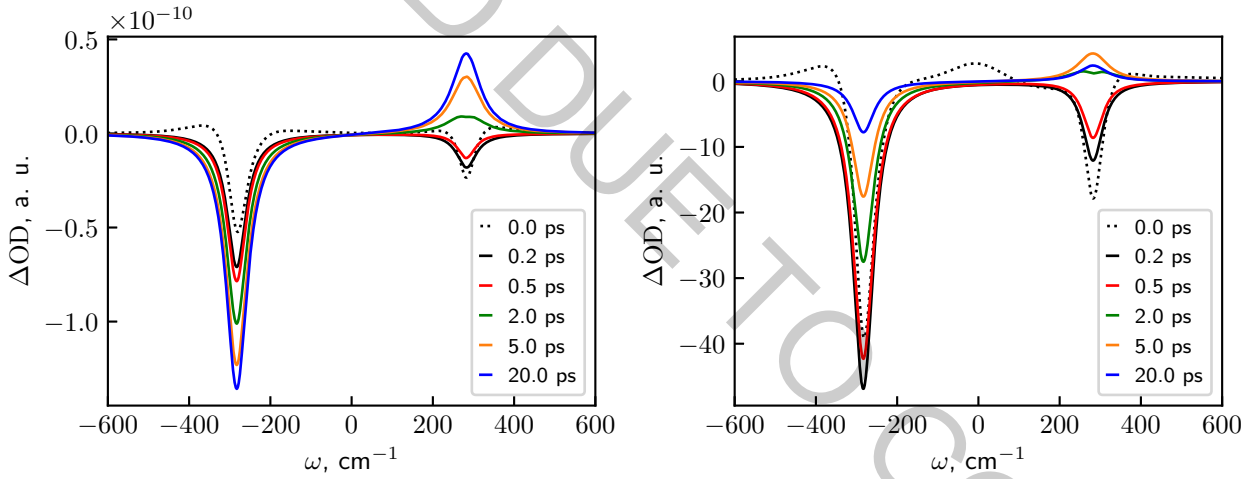

Fig. 1. Calculated Pump-probe spectra for small(left) and large(right) excitation intensity oscillator.

Calculated pump-probe spectra (Fig. 1) for molecular complex show expected relaxation and EEA dynamics: at low excitation intensity pump-probe spectra show excitation transfer, at high excitation intensity spectra amplitudes decay non-exponentially.

[1] L. Valkunas, D. Abramavicius, and T. Mančal, *Molecular Excitation Dynamics and Relaxation* (Weinheim, Germany: Wiley-VCH Verlag GmbH & Co. KGaA, 2013).
[2] J. Chmeliov, J. Narkeliunas, M. W. Graham, G. R. Fleming, and L. Valkunas, Exciton–exciton annihilation and relaxation pathways in semiconducting carbon nanotubes, Nanoscale, 2016, **8**, 1618–1626.
[3] V. Chernyak, W. M. Zhang, and S. Mukamel, Multidimensional femtosecond spectroscopies of molecular aggregates and semiconductor nanostructures: The nonlinear exciton equations, J. Chem. Phys., 1998, **109**, 9587–9601.
[4] V. Bubilaitis, J. Hauer, D. Abramavicius, Simulations of pump probe spectra of a molecular complex at high excitation intensity, Chem. Phys. 527 (2019) 110458

CANCELLED DUE TO COVID-19

ELECTRON-IMPACT DOUBLE IONIZATION OF B^+

Jurgita Koncevičiūtė[1], Valdas Jonauskas[1]

[1]Institute of Theoretical Physics and Astronomy, Vilnius University, Saulėtekio av. 3, LT-10257 Vilnius, Lithuania
jurgita.konceviciute@tfai.vu.lt

Electron-impact single and multiple ionization processes provide fundamental understanding of the electronic dynamics and structure of atoms and ions. Therefore these processes have been the focus of many theoretical and experimental studies.The study of multiple ionization processes is quite complicated as one has to deal at least with four-body Coulomb problem.

The aim of this work is to study electron-impact double ionization (DI) process of the B^+ ion. Contribution of direct and indirect processes to the total double ionization process is considered. Direct double ionization (DDI) process is investigated by applying a few-step approach [1]. This method simplifies the solution of the complex four-body Coulomb problem by treating DDI process as a sequence of two- (ionization-ionization) and three-step (excitation-ionization-ionization, and ionization-excitation-ionization) processes. This method has already been successfully applied in the study of DDI process for light ions. In addition of previously described two-step processes, in this work another two few-step processes were used to study DI of B^+ ion. Those processes include ionization-excitation process followed by further autoionization process and excitation-ionization-autoionization process. Influence of the correlation effects to the formation of the B^{3+} ion was also considered. Two limiting cases of the energy distribution of the scattered and ejected electrons are presented: scattered and ejected electrons share the excess energy (DDI^1), and one of the electrons takes all the available energy (DDI^2).

Atomic data, needed for calculation of DI cross sections, have been calculated using the Flexible Atomic Code [2], which implements the Dirac-Fock-Slater approach. Electron-impact excitation and single ionization processes were investigated using the distorted-wave (DW) approximation. For electron-impact ionization and excitation processes scaling factors [3] were introduced to diminish DW cross sections, since it is well known that DW approximation often overestimates electron-impact ionization and excitation cross sections for atoms and near neutral ions.

For DDI process, it has been shown (Fig. 1), that at the lower energies of the incident electron, the better agreement between theoretical cross sections and experimental ones is achieved in DDI^1 case. However near the ionization threshold experimental cross sections are overestimated by theoretical ones, while at higher energies DDI^1 cross sections underestimate the experimental ones. On the contrary, DDI^2 cross sections underestimate experimental ones at lower energies and overestimate at higher energies. It shows that two limiting cases of energy distribution cannot correctly describe the DDI process and some intermediate energy distribution of electrons should be taken into consideration. At the energies above the ionization threshold of the inner shell of B^+ ion good agreement with experiment is given by total DI cross sections when scattered and ejected electrons share the excess energy equally in the DDI process.

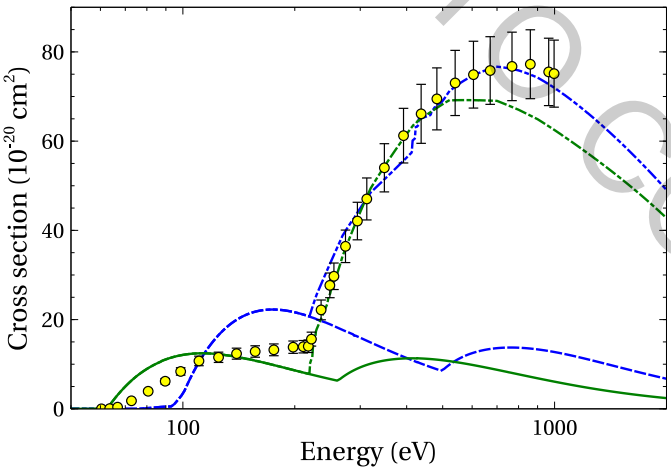

Fig. 1. Electron-impact double ionization of B^+ ion. Continuous line (green): DDI^1 cross sections; dashed line (blue): DDI^2 cross sections; dashed-dotted line (green): total DI cross sections with DDI^1; dashed-double-dotted line (blue): total DI cross sections with DDI^2; solid circle (yellow): experimental total DI cross sections [4].

[1] V. Jonauskas, A. Prancikevičius, Š. Masys et al., Electron-impact direct double ionization as a sequence of processes, Physical Review A **89**, 052714-1-052714-5 (2014).
[2] M. F. Gu, The flexible atomic code, Canadian Journal of Physics **86**, 675-689 (2008).
[3] Y.-K. Kim, Scaling of plane-wave Born cross sections for electron-impact excitation of neutral atoms, Physical Review A **64**, 032713-1-032713-10 (2001).
[4] P. Shevelko, H. Tawara, F. Scheuermann et al., Semiempirical formulae for electron-impact double-ionization cross sections of light positive ions, Journal of Physics B: Atomic, Molecular and Optical Physics **38**, 525–545 (2005).

CANCELLED DUE TO COVID-19

APPROXIMATION OF BURST DURATION'S PDFS OF BIRTH-DEATH PROCESSES

Ignas Kazakevičius[1], Vygintas Gontis[2]

[1] Institute of Theoretical Physics and Astronomy, Vilnius University, Lithuania
[2] Institute of Theoretical Physics and Astronomy, Vilnius University, Lithuania
ignas.kazakevicius93@gmail.com

CANCELLED DUE TO COVID-19

Indicator of long-range memory is considered to be a power-law power spectral density in the low frequency domain [1]. However, many different stochastic processes may have this long-range memory property. In order to identify different stochastic processes and solve previously mentioned problem we are focusing on the analysis of the stochastic processes burst and inter-burst duration's probability density functions (PDF) which can be used to determine whether a particular complex process retains the characteristics of a long-range memory in cases of different inter-burst duration's threshold limits [2].

To generate time series we used the stochastic differential equation (SDE) asymptotically describing agent-based Kirman Birth-Death process. We performed the numerical calculation of burst and inter-burst duration's PDF's dependence on the threshold value of the process. It was shown that such PDFs generated by respective SDE in general case cannot be described by analytical approximation proposed for transformations of Bessel process. However, it was shown that analytical approximation derived in this work can be used to describe the bursts PDF of Bessel process and in specific cases could be used to approximate more complex processes than Bessel process such as agent-based Birth-Death process [3].

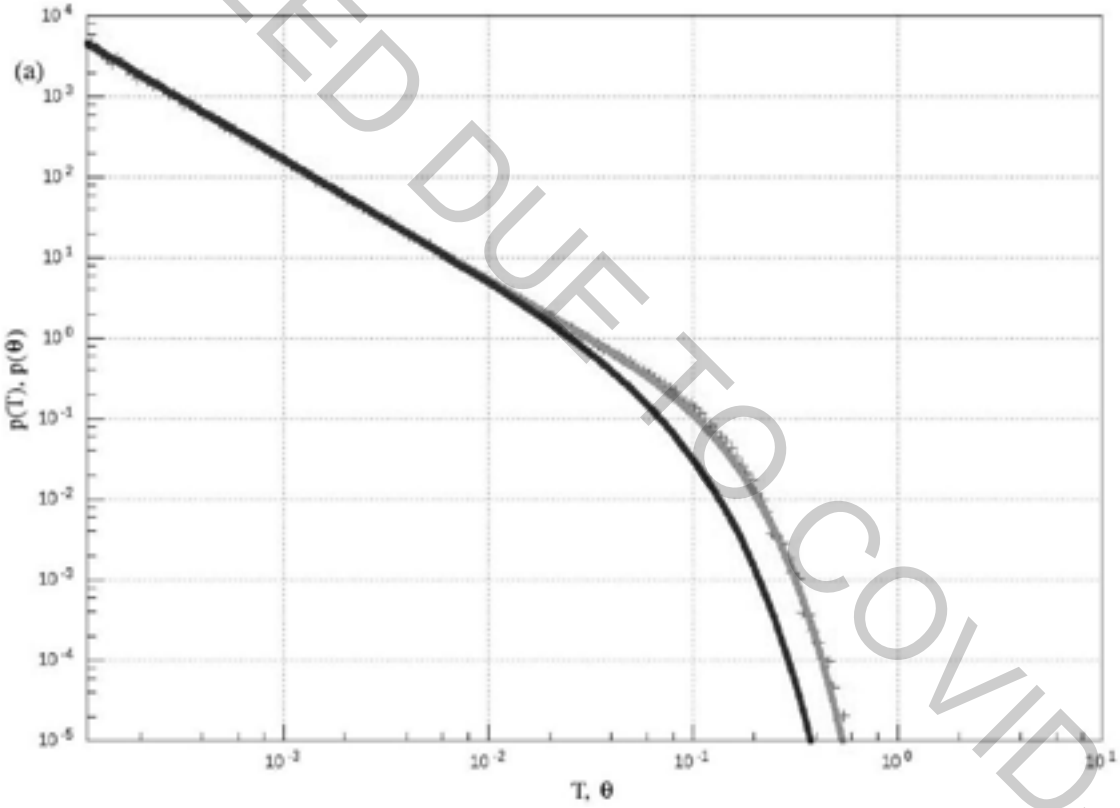

Fig. 1. Burst duration's PDFs: a) PDF calculated by solving SDE numerically (crosses), b) analytical PDF approximation [4] (black lines), c) Analytical PDF approximation in a newer work (gray lines) [3].

[1] [28] Beran J., Feng Y., Ghosh S., Kulik R. Long–Memory Processes probabilistic Properties and Statistical Methods, Spinger–Verlag Berlin Heidelberg, 2013, DOI: 10.1007/978-3-642-35512-7.
[2] V. Gontis, A. Kononovičius, Spurious Memory in Non-Equilibrium Stochastic Models of Imitative Behavior, Entropy, 19 (8), 2017, p. 387, 2017, DOI: 10.3390/e19080387.
[3] Kazakevičius I., First Passage Time of Birth-Death processes, Master Thesis, Vilnius University, 2019.
[4] Kononovičius A., Gontis V. Approximation of the First Passage Time Distribution for the Birth–Death Processes, Journal of Statistical Mechanics 2019: 073402 (2019).

RENORMALIZATION FLOW OF THE GRIMUS-NEUFELD MODEL AT ONE LOOP LEVEL

Rokas Garbačauskas[1], Thomas Gajdosik[1]

[1]Vilnius university, institute of theoretical physics and astronomy, Lithuania
rokas.garbacauskas@ff.stud.vu.lt

The Standard Model (SM) of particle physics is a very succesful theory. Taking as an input 19 (or 26 if one includes neutrino masses and their mixing angles) input parameters it produces a lot of testable predictions which up to now have withstood the experimental tests almost flawlessly. In fact some of the theoretical groundwork helped to make interesting discoveries, latest of which is the discovery of the Higgs boson.

On the other hand, the current widely accepted formulation of the SM is incomplete. For example the mechanism generating the aforementioned neutrino masses is still an open question. It has been experimentally verified in many independent experiments [1] that neutrinos can change their gauge eigenstates. This phenomenon is called neutrino oscillation. The mathematical apparatus that describes this requires that neutrinos have a mass. Many different SM additions have been proposed to accomplish this and are waiting for more experimental data to narrow down the parameter space. One such model is the Grimus-Neuefeld model (GNM) [2] which attempts to describe the two measured neutrino mass differences by an addition of an extra Higgs doublet and a sterile Majorana neutrino which via radiative mass corrections at 1 loop and the seesaw mechanism respectively do just that.

In our study we were searching for analytical expressions of the beta functions

$$\beta_\alpha = \mu \frac{d}{d\mu}\alpha. \tag{1}$$

which describe the change of the given parameters with respect to scale. Calculations involved corrections up to one loop level for some parameters essential for GNM, namely the gauge couplings of U(1) and SU(2), Yukawa couplings and the mass of the Majorana neutrino.

Achieving this required writing down the Lagrangian densities ($\mathscr{L}$) of these sectors in D dimensions in a consistent way. That is in order for the action ($S = \int d^D x \mathscr{L}$) to be dimensionless all terms of $\mathscr{L}$ have to be of mass dimension D, i. e. $[\mathscr{L}] = D$ (as usual in particle physics $\hbar = c = 1$). It is then conventional to rescale the couplings of the theory with a parameter μ ($[\mu] = 1$) in a way that the coupling itself remains a dimensionless number. For examle, in QCD $e \to \mu^{\frac{4-D}{2}} e$.

Feynman formalism was then used to write down amplitudes for events described by the parameters of interest. These amplitudes suffer from one of the issues that slowed down the advance of the mathematical apparatus behind the SM - Quantum Field Theory (QFT) - in mid XXth century: infinities emerging when evaluating integrals of some loop level corrections. The integrals generally have the form of

$$T^N_{\mu_1\ldots\mu_P}(p_1,\ldots,p_{N-1},m_0,\ldots,m_{N-1}) = \frac{(2\pi\mu)^{4-D}}{i\pi^2}\int d^D q \frac{q_{\mu 1}\cdots q_{\mu P}}{D_0 D_1 \cdots D_{N-1}}, \tag{2}$$

where D is the dimension number, N is the number of propagator factors, P is the number of the integration momenta in the numerator and

$$D_i = (q+p_i)^2 - m_i^2 + i\varepsilon,\ p_0 = 0 \text{ and } i = 1,\ldots,N-1.$$

In general these integrals diverge for $D \geq 4$ [3].

These divergences spurred the development of an entire new branch of mathematics called regularization. There are many regularization schemes but we used the most popular one - dimensional regularization - as it preserves Lorentz invariance. This approach lets the dimensionality of the problem stray from 4 by a small amount ε: $D = 4 - \varepsilon$. This allows to get analytical expression for the given integral. The divergent part is easily isolated and is written down in a counterterm Δ_α along with some constants depending on the convention and the dependance on the scale parameter. The couplings responsible for this specific interaction or field values are shifted by this counterterm. This allows to get finite values for measurable quantities as the diverging parts simply cancel out so ε can be safely sent to 0 at the end of the calculations. This also introduces the notion of running couplings as the new renormalized couplings are scale dependent. And details of this dependance are described by the beta functions eq. (1).

[1] M. G. Aartsen, M. Ackermann, J. Adams, et al., Search for nonstandard neutrino interactions with icecube deepcore, Phys. Rev. D, Apr 2018, 97, 072009

[2] Draukšas, Simonas & Dūdėnas, Vytautas & Gajdosik, Thomas & Juodagalvis, Andrius & Juodsnukis, Paulius & Jurčiukonis, Darius. (2019). The Grimus–Neufeld Model with FlexibleSUSY at One-Loop. Symmetry. 11. 1418. 10.3390/sym11111418.

[3] A. Denner, Techniques for the calculation of electroweak radiative corrections at the one-loop level and results for w-physics at lep200, 2007.

CANCELLED DUE TO COVID-19

ON-SHELL CALCULATION OF FIELD STRENGTH AND CHARGE COUNTERTERMS IN ARBITRARY COVARIANT GAUGE IN SCALAR QED

Simonas Draukšas[1], Thomas Gajdosik[1]

[1]Institute of Theoretical Physics and Astrophysics, Vilnius University, Lithuania
simonas.drauksas@ff.stud.vu.lt

Quantum Field Theory is an extremely successful framework in particle physics. For example, the Standard Model is also a QFT with specific particle content that describes our world with astonishing precision. However, in order to actually compare the theory with experiment, QFT has quite a few obstacles that have to be overcome. These obstacles manifest even in simple theories such as scalar Quantum Electrodynamics (sQED)[1]. Generally, for perturbative regimes, one draws Feynman diagrams, performs appropriate calculations and all is good at tree level. Unfortunately, already at one-loop level some calculations give infinite contributions while what we observe is manifestly finite, hence, it is needed to find a way to get rid of the infinities in a physical, technical and consistent way - it is needed to *renormalize* the theory. However, there are quite a few choices when renormalizing a theory - gauge, regulator, and subtraction scheme may all be nearly freely chosen. Some specific gauges allow to neglect entire Feynman diagrams, regulators consistently separate the infinities, and subtraction schemes define the finite parts of counterterms. In addition, there may be non-trivial relations between counterterms and even an additional type of divergences can appear, which renormalization cannot remove.

In this work, to better understand the technicalities in renormalization, we chose to compute two non-trivially related counterterms for the field strength and charge in sQED. The computation is done in arbitrary ξ gauge and in the On-Shell subtraction scheme [1] with dimensional regularization [2] in $d = 4$ dimensions.

[1] Matthew D. Schwartz, *Quantum Field Theory and the Standard Model*, Cambridge University Press, 2014, ISBN: 1107034736, 9781107034730
[2] C. G. Bollini and J. J. Giambiagi, *Dimensional renormalization: The number of dimensions as a regularizing parameter*, Il Nuovo Cimento B (1971-1996), 12.1 (1972), pp. 20-26, ISSN: 1826-9877

CANCELLED DUE TO COVID-19

SEMI-EMPIRICAL INVESTIGATIONS OF THE IONIC BISMUTH (BI II) ENERGY STRUCTURE FOR ELECTRIC QUADRUPLE MOMENT CALCULATION

Sebastian Wilman[1], Magdalena Elantkowska[1], Jarosław Ruczkowski[2]

[1] Faculty of Materials Engineering and Technical Physics, Poznan University of Technology, Poland
[2] Faculty of Control, Robotics and Electrical Engineering, Poznan University of Technology, Poland
sebastian.b.wilman@doctorate.put.poznan.pl

The history of the bismuth electric quadruple moment (Q) investigation have begun in 1960 with the R. S. Title and K. F. Smith publication titled: *The hyperfine structure of* ^{209}Bi [1]. In that paper, authors estimated the value of the bismuth electric quadruple moment as $Q = -0,360 \pm 0,001b$. Since then, the numerous amount of authors [2, 3, 4, 5], have tried to calculate the value of Q for bismuth. Unfortunately, those investigations led to the divergent results and currently there is no agreement within atomic physicists society about the bismuth quadruple moment value. Developed by us the parameterization method of the fine- (*fs*) and hyperfine structure (*hfs*)[6, 7], makes one able to calculate the electric quadruple moment. For the bismuth ion, the finally obtained values for one-body *hfs* parameters a_{6p}^{01} and b_{6p}^{02} and two-body *hfs* parameters were used to calculate the electric quadruple moment. However, to perform semi-empirical *hfs* analysis both the accurate values of hyperfine structure constants A and B and the correct fine structure eigenvectors describing electronic system of BiII are needed.

On the basis of the experimental results [8, 9, 10, 11] concerning the fine structure literature data and the hyperfine structure literature data, a parametric studies of the atomic structure for the odd and even parity configurations system of the ionic bismuth (Bi II) were performed. The present paper is the application of our many-body parametrization method allowing the analysis of complex electronic configurations system containing up to four open shells by taking into account all electromagnetic interactions expected in an atom, in accordance with the second-order perturbation theory. The above mentioned theory is described in general terms in the first work of the series under the common title *Construction of the energy matrix for complex atoms* [7].

The odd-parity configurations system contains following 81 configurations: $6p^36s$, $\sum_{n=7}^{40} 6s^26pns$, $\sum_{n=7}^{40} 6s^26pnd$, $\sum_{n=5}^{15} 6s^26png$. For the even-parity configurations system, calculations were carried out within the basis of 71 configurations: $6p^26s^2$, $\sum_{n=7}^{40} 6s^26pnp$, $\sum_{n=5}^{40} 6s^26pnf$. The *fs* analysis was performed separately for each of configuration parity. The finally obtained eigenvectors were used in *hfs* parametrization analysis. Due to the insufficient amount of the experimental data, the *hfs* calculations were performed twice: first, for each configuration parity separately and further within huge base being composed of the configurations from both parities.

For unknown electronic levels predicted values of the level energies and *hfs* constants are given, which can facilitate further experimental investigations. The value of the electric quadruple moment of bismuth nucleus was calculated and compared to the literature data.

The research will be completed in near future by data collected in similar analysis performed for the atomic bismuth system.

This research was funded by the Ministry of Science and Higher Education of the Republic of Poland.

[1] R. S. Title, K. F. Smith, The hyperfine structure of ^{209}Bi, Philosophical Magazine **5**(60), 1281–1289 (1960).
[2] J. Bieroń, P. Pyykkö, Nuclear Quadrupole Moments of Bismuth, Physical Review Letters **87**(13), (2001).
[3] J. Dembczyński, B. Arcimowicz, E. Stachowska, H. Rudnicka-Szuba, Parametrization of two-body perturbation on atomic fine and hyperfine structure. The configuration $(6p)^3$ in the bismuth atom, Zeitschrift Für Physik A Atoms and Nuclei **310**(1–2), 27–36 (1983).
[4] A. Shee, L. Visscher, T. Saue, Analytic one-electron properties at the 4-component relativistic coupled cluster level with inclusion of spin-orbit coupling, The Journal of Chemical Physics **145**(18), 184107 (2016).
[5] T. Q. Teodoro, R. L. A. Haiduke, Nuclear electric quadrupole moment of bismuth from the molecular method, Physical Review A **88**(5) (2013).
[6] J. Dembczyński, M. Elantkowska, B. Furmann, J. Ruczkowski, D. Stefańska, J. Phys. B: At. Mol. Opt. Phys. **43**, 065001 (2010).
[7] M. Elantkowska, J. Ruczkowski, J. Dembczyński, Eur. Phys. J. Plus, **130**, 14 (2015).
[8] M. Andrzejewska, F. G. Meijer, E. Stachowska, On the level system of Bi II, Journal of Physics B: Atomic, Molecular and Optical Physics **46**(20), 205003, (2013).
[9] E. Stachowska, J. Dembczyński, B. Arcimowicz, A. Kajoch, Configuration interaction effect on the hyperfine structure of the levels of the $6s6p^3$ configuration in Bi II, Zeitschrift Fr Physik D Atoms, Molecules and Clusters **7**(2), 177–183 (1987).
[10] L. Dolk, U. Litzén, G. M. Wahlgren, The laboratory analysis of Bi II and its application to the Bi-rich HgMn star HR 7775. Astronomy & Astrophysics **388**(2), 692–703 (2002).
[11] D. Grabowski, R. Drozdowski, J. Kwela, J. Heldt, Hyperfine structure and Zeeman effect studies in the 6p7p-6p7s transitions in Bi II, Zeitschrift für Physik D Atoms, Molecules and Clusters **38**(4), 289–293 (1996).

CANCELLED DUE TO COVID-19

BOSON SAMPLING WITH CONTINUOUS-WAVE DETECTION

Viktoriia Len[1], Andrii Semenov[2]

[1]Physics Department, Taras Shevchenko National University of Kyiv, Ukraine
[2]Bogolyubov Institute for Theoretical Physics, NAS of Ukraine, Kyiv, Ukraine
len.vikusik@gmail.com

Non-universal quantum computing addresses specific problems, which cannot be solved with classical computers. An example is Boson sampling, cf. Refs. [1, 2], demonstrating supremacy of quantum computations. This method is considered as highly attractive due to its clearness and possibilities of implementation with current technologies. For this scenario, the resource of quantum supremacy is the fact that phase-space quasi-probability distributions are not positive-semidefinite [3]. Boson sampling applies to computation of permanent—a matrix function defined as a sum of its so-called diagonal products [4]. This task, despite the permanent is similar to the determinant, is computationally hard for traditional classical calculations but can be successfully resolved with quantum devices.

The key element of the boson-sampling circuit is a linear multi-port interferometer. This device is associated with a set of matrices, which permanents should be evaluated. Also it includes single-photon sources and single-photon detectors. The difficulty we have to face with this scheme is the fact that realistic detectors can not discriminate adjacent photon numbers. A way to resolve this problem is the technique of so-called continuous-wave detection. Within this method one counts the pulses of photocurrent during a time interval. With an acceptable probability each pulse can be associated with one absorbed photon. However, after the pulses there exist time intervals during which detectors cannot register photons—so-called dead time. This fact may significantly destroy photocounting statistics and, as a result, lead to wrong values of permanents.

In this contribution we report about theoretical consideration of this problem. It turns out that permanents can still be successfully reconstructed from the statistics of pulses registered with the technique of continuous-wave detection. However, the standard method should be reconsidered by applying the obtained correction factors. The result can find its application for practical implementations of boson-sampling technique.

[1] S. Scheel, Permanents in linear optical networks, Acta Physica Slovaca **58**, 675 (2008).
[2] S. Aaronson,and A. Arkhipov, The computational complexity of linear optics, Theory of Computing, **9**, 143–252 (2013).
[3] F. Shahandeh, A. P. Lund, and T. C. Ralph, Quantum Correlations in Nonlocal Boson Sampling, Phys. Rev. Lett. **119**, 120502 (2017).
[4] H. Minc, Encyclopedia of mathematics and its applications, **6**, 1–2 (2013).

CANCELLED DUE TO COVID-19

NON-UNIVERSAL OPTICAL QUANTUM COMPUTING WITH ARRAY DETECTORS

Mariia Byelova[1], Andrii Semenov[2]

[1]Physics Department, Taras Shevchenko National University of Kyiv, Ukraine
[2]Bogolyubov Institute for Theoretical Physics, NAS of Ukraine, Kyiv, Ukraine
byelovam@gmail.com

Non-universal quantum computing is a powerful technique for evaluation of specific computational tasks, which cannot be solved with classical computers. Contrary to universal quantum computers, such devices are designed for dealing with a special problem or with a class of special problems. Boson sampling [1, 2] is a typical example of such a method, which can be implemented with present-available technologies. The computational task, which is resolved with such devices, consists in evaluation of permanents for matrices—a polynomial of matrix entries, similar to determinant, but without minuses. Contrary to determinants, there exist no efficient classical algorithms for calculation of permanents. An optical device, implementing boson sampling, consists of single-photon sources, multi-port linear interferometer, and single-photon detectors. A challenging task in implementation of this scheme is detectors, which can discriminate adjacent photon numbers. The problem is that standard photon diods, nano-wire detectors, etc. may detect single photons without such a discrimination. A possible way to resolve this problem consists in splitting the incoming ray into multiple components and detecting each of them with such an on/off detector. The number of detected clicks is usually associated with the number of photons. However, this statement is not really true [3]. Hence such a device may give wrong values of permanents. We report about our theoretical result, which enables to reconstruct correct values of permanents with such array detectors. The consideration is based on the true photocounting equation for this detection scheme presented in Ref. [3]. We believe that our result will find its application for practical realizations of optical non-universal quantum computers.

[1] S. Scheel, Permanents in linear optical networks, Acta Physica Slovaca **58**, 675 (2008).
[2] S. Aaronson,and A. Arkhipov, The computational complexity of linear optics, Theory of Computing, **9**, 143–252 (2013).
[3] J. Sperling, W. Vogel, and G. S. Agarwal, True photocounting statistics of multiple on-off detectors, Phys. Rev. A **85**, 023820 (2012).

CANCELLED DUE TO COVID-19

ACCURACY ASSEMENT OF REVERSE ENGINEERING PROCESS OF PLEXIGLASS STEP CYLINDER SAMPLE

Apoorva Devaraj[1], Mastan Raja Papanaboina[2], Dr. Elena Jasiūnienė[1,2]

[1]Department of Electronics Engineering, Kaunas University of Technology, Studentu St. 48, LT-51367 Kaunas, Lithuania

[2]Prof. K. Baršauskas Ultrasound Research Institute, Kaunas University of Technology, K. Barsausko St. 59, LT-51423 Kaunas, Lithuania

apoorva.devaraj@ktu.edu

Reverse engineering is one of the growing techniques which is used in almost every field now like additive manufacturing, remanufacturing of old mechanical parts or any systems, enhancing the existing system etc. During reverse engineering the accuracy of the result obtained is of most importance, because the final product is based on these results. Most of the products manufactured based on reverse engineering is used in real time applications hence its result has to be accurate [1,2]. This work is carried out to assess the factors that influence the accuracy in reverse engineering process and also to know the sources of uncertainties that influence the final results accuracy [3].

Here the reverse engineering process is done based on the computed tomography which is used to acquire the data. The process of reverse engineering includes following steps: acquisition of data, reconstruction, segmentation and conversion to 3D CAD model. The accuracy assessment starts from the initial process that is, data acquisition.

The parameters have to be optimized to obtain CT images that are free from artefacts. In the next process, reconstruction, an optimized threshold value has to be selected for proper reconstruction of CT images. During processing of the obtained CT images the surface determination has to be supervised properly to get the accurate measurement and also the mesh conversion process has to be selected in a way that is easily converted to CAD file later. Likewise the accuracy of the results of each step in reverse engineering is assessed by finding the factors that affect the accuracy. Then finally the obtained reverse engineered CAD model is compared with the pre-designed CAD model for assessment of the accuracy.

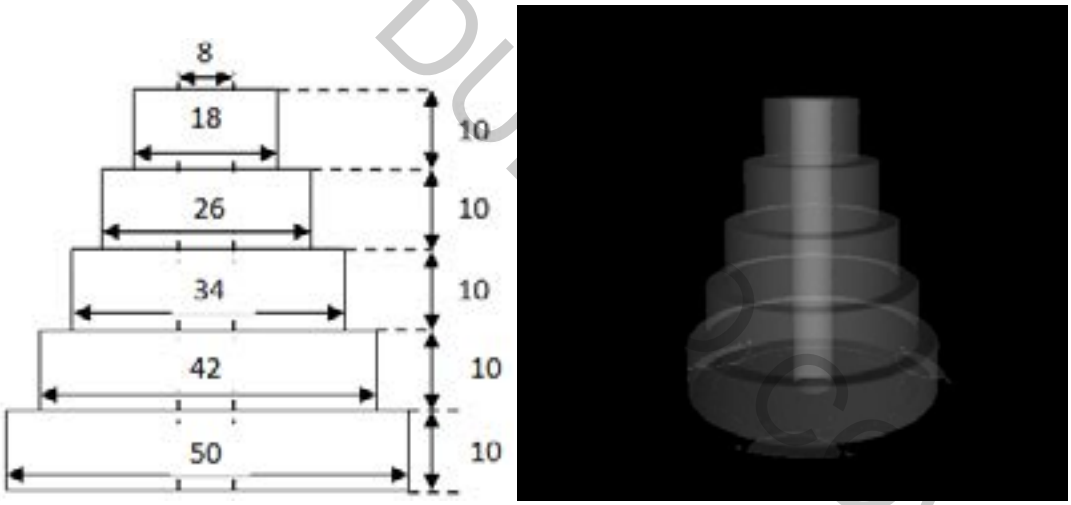

(a) (b)

Fig.**1 (a)** Measurements of Plexiglas step cylinder, **1(b)** X-Ray CT scan image of Plexiglas cylinder

[1]. Kai Schrcoder, Arno Zinke, and Reinhard Klein, “Image-Based Reverse Engineering and Visual Prototyping of Woven Cloth”, Ieee Transactions On Visualization And Computer Graphics, VOL. 21, NO. 2, February 2015.

[2]. Ruzinoor Che Mat, Shahrul Azmi, Ruslizam Daud, Abdul Nasir Zulkifli and Farzana Kabir Ahmad, “Morphological Operation on Printed Circuit Board (PCB) Reverse Engineering using MATLAB”, Fakulti of Technology Management Universiti Utara Malaysia.

[3]. Shahed E. Quadir, Junlin Chen, Domenic Forte, Navid Asadizanjani, Sina Shahbazmohamadi, Lei Wang, John Chandy, And Mark Tehranipoor, “A Survey on Chip to System Reverse Engineering”, 2016.

CANCELLED DUE TO COVID-19

DAMAGE CHARACTERIZATION ON ALUMINUM PLATE USING FINITE ELEMENT METHOD

Mastan Raja Papanaboina[1], Apoorva Devraj[2], Dr. Elena Jasiūnienė[1,2], Dr. Egidijus Zukauskas[1]

[1]Prof. K. Baršauskas Ultrasound Research Institute, Kaunas University of Technology, K. Barsausko St. 59, LT-51423 Kaunas, Lithuania

[2]Department of Electronics Engineering, Kaunas University of Technology, Studentu St. 48, LT-51367 Kaunas, Lithuania

mastan.papanaboina@ktu.edu

CANCELLED DUE TO COVID-19

The aircrafts are facing many problems during the flight due to harsh conditions at flying zone and these condition leads to create damages in aircraft components. However, NDT methods are purely determining the off-line investigations to identify the defects using complex and heavy equipment. Especially, these methods lead to time-consuming and vast labor involvement to test the large-scale structures. The conventional NDT methods need to disassemble the structures for testing which greatly increase the maintenance cost.

Structural health monitoring (SHM), the technology come out into limelight with the combination of advanced sensor technology to investigate the sample to reveal the damages [1,2]. The demand of SHM technology increasing day by day due to potential advantage of the reducing maintenance and lifecycle cost and increase of reliability and safety.

The concept initiated to give the standard damage detection scale on aluminum material. The elastic guided wave propagation and interaction on aluminum plate was modeled using Abaqus dynamic explicit solver. The simulation performed using finite element method and semi-analytical finite element technique to obtain three different modes A0, S0 and SH. The ultrasonic guided wave propagates with 200 kHz frequency and the phase velocity of A0 mode lamb wave is 1550 m/s. When there is no flaw on the plate A0 mode lamb wave propagates without distortion and dispersion curve of the of the A0 mode lamb wave overlap with scanned signal. The B-scan data obtained using 2D Fast Fourier Transformation technique and the standard dispersion curves of A0, S0 mode obtained using semi-analytical finite element method. In case of the defect in the plate at wave propagation path, the reflection, transmission and mode conversion of ultrasound wave can occur. Different type of defects can cause different type of distortion of the ultrasonic guided wave.

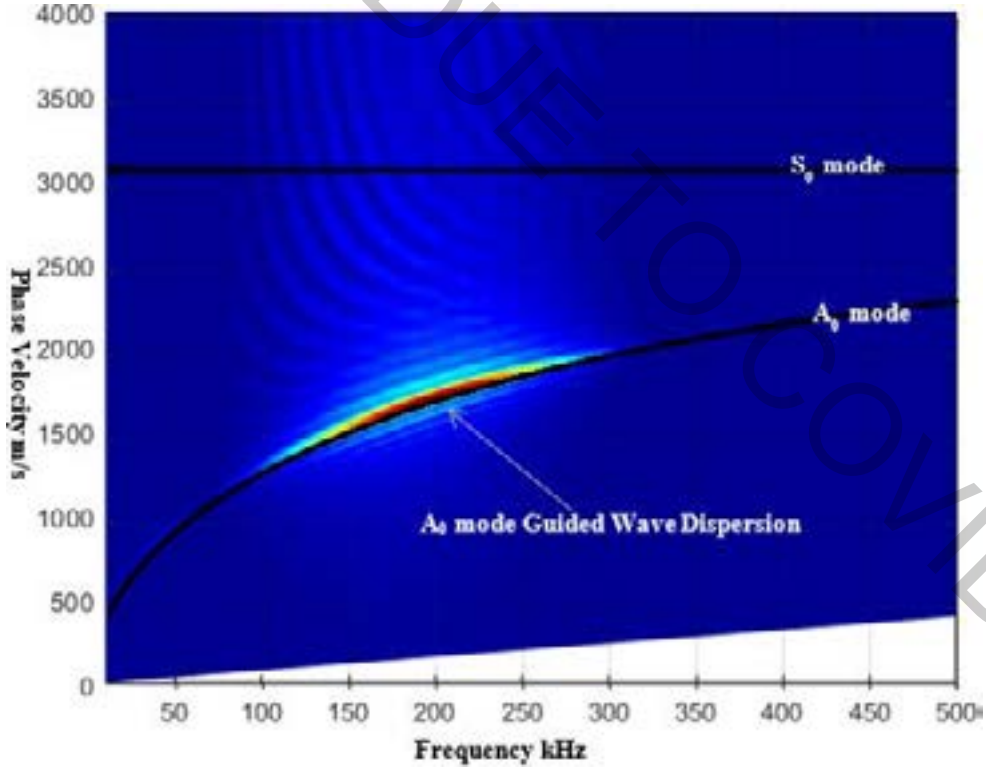

Fig.1 Comparison of the dispersion characteristics of A0 mode lamb wave using FEM and SAFE.

[1]. **Borja Hernandez Crespo, Charles R. P. Courtney, Bhavin Engineer,** Calculation of GuidedWave Dispersion Characteristics Using a Three-Transducer Measurement System, Appl. Sci. **2018**, 8, 1253; doi:10.3390/app8081253

[2] **Wenbo Duan, Xudong Niu, Tat-Hean Gan, Jamil Kanfoud and Hua-Peng Chen,** A Numerical Study on the Excitation of GuidedWaves in Rectangular Plates Using Multiple Point Sources, Metals **2017**, 7, 552; doi:10.3390/met7120552

STUDY OF STRUCTURAL PROPERTIES OF LITHIUM-IRON SILICATE (Li_2FeSiO_4) OBTAINED BY SOL-GEL METHOD

Aleksandra Cuper[1*], Przemysław P. Michalski[1], Jerzy E. Garbarczyk[1]

[1] Faculty of Physics, Warsaw University of Technology, Koszykowa 75, 00-662, Warsaw, Poland
aleksandra.cuper.stud@pw.edu.pl

In this work, structural properties of Li_2FeSiO_4 composites were studied. Lithium-iron silicate offers a promising opportunity for batteries due to its high theoretical capacity of 331 $mAh \cdot g^{-1}$. Voltage of cell consisting Li_2FeSiO_4 as a cathode is expected to be as high as 4.0–4.8 V vs Li^+/Li. Low cost and high abundance of substrates are also the advantages of this material. On the other hand, a disadvantage of Li_2FeSiO_4 is extremely low electronic conductivity of $6 \cdot 10^{-14}$ $S \cdot cm^{-1}$ [1]. Such low value may worse its electrochemical properties. Sol-gel method enables to obtain a material of high porosity and so that the both ionic and electronic conductivity may be higher [2].

In our case, the source of silicon was TEOS ($SiC_8H_{20}O_4$). TEOS was dissolved in distilled water and ethanol solution. Water solutions of lithium and iron sources (CH_3COOLi and $Fe(NO_3)_3 \cdot 9H_2O$) were added dropwise. Final solution was mixed on magnetic stirrer and temperature was rised up to 80–90°C in order to evaporate the excess of water. The pH of solution was controled by adding 2M solution of ammonia. After gelation, the obtained gel was dryed in vacuum dryer. Dense, orange-colored gels were obtained. The gels were calcined in temperatures in 600–900°C range in argon atmosphere to obtain composites.

Structural properties of composites were investigated using Panalytical Empyrean diffractometer.

[1] J. Ni, Y. Jiang, X. Bi, et al., Lithium Iron Orthosilicate Cathode: Progress and Perspectives, ACS Energy Letters **2**, 1771–1781 (2017).
[2] V. Etacheri, Sol-Gel Processed Cathode Materials for Lithium-Ion Batteries in Sol-Gel Materials for Energy, Environment and Electronic Applications (Springer, 2017).

CANCELLED DUE TO COVID-19

STUDY OF THERMAL PROPERTIES OF LITHIUM-IRON SILICATE (Li_2FeSiO_4) GELS

Klaudia Pachulska[1*], Przemysław P. Michalski[1], Jerzy E. Garbarczyk[1]

[1] Faculty of Physics, Warsaw University of Technology, Koszykowa 75, 00-662, Warsaw, Poland
klaudia.pachulska.stud@pw.edu.pl

In this work, thermal properties of Li_2FeSiO_4 were studied. Lithium-iron silicate offers a promising opportunity for batteries due to its high theoretical capacity of 331 $mAh \cdot g^{-1}$. Voltage of cell consisting Li_2FeSiO_4 as a cathode is expected to be as high as 4.0–4.8 V vs Li^+/Li. Low cost and high abundance of substrates are also the advantages of this material. On the other hand, a disadvantage of Li_2FeSiO_4 is extremely low electronic conductivity of $6 \cdot 10^{-14}$ $S \cdot cm^{-1}$ [1]. Such low value may worse its electrochemical properties. Sol-gel method enables to obtain a material of high porosity and so that the both ionic and electronic conductivity may be higher [2].

In our case, the source of silicon was TEOS ($SiC_8H_{20}O_4$). TEOS was dissolved in distilled water and ethanol solution. Water solutions of lithium and iron sources (CH_3COOLi and $Fe(NO_3)_3 \cdot 9H_2O$) were added dropwise. Final solution was mixed on magnetic stirrer and temperature was rised up to 80–90°C in order to evaporate the excess of water. The pH of solution was controled by adding 2M solution of ammonia. After gelation, the obtained gel was dryed in vacuum dryer. Dense, orange-colored gels were obtained.

Thermal properties of gels were investigated using TA Q600 thermal analyser up to 1000°C in argon atmosphere. Typical DTA/TGA curve is presented in Fig. 1. Up to 400°C, 60% of the sample mass evaporated. The evaporated gases consisted of H_2O, nitride groups and CO_2. The calcination of material took part at ca. 600°C.

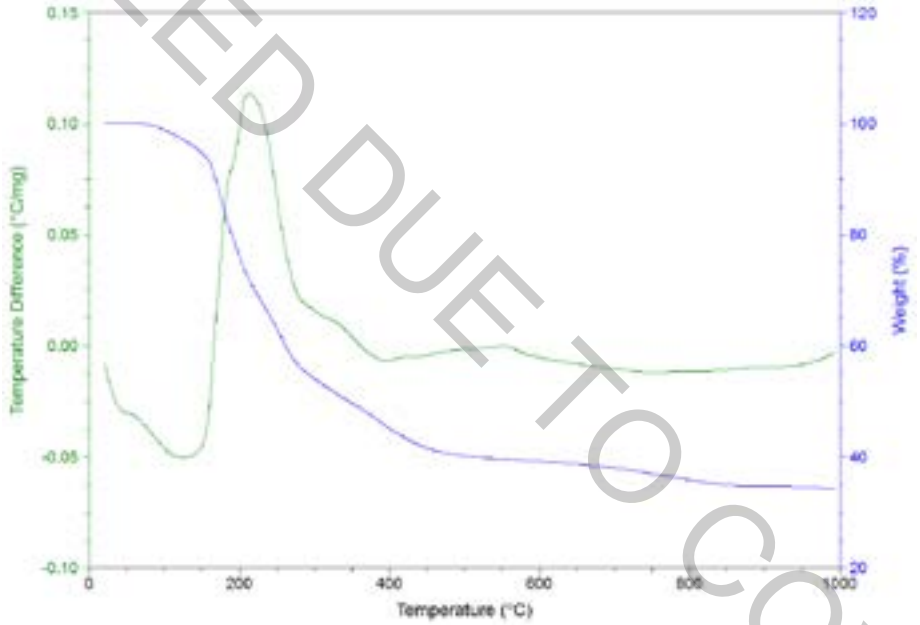

Fig. 1. Typical DTA/TGA curve for Li_2FeSiO_4 gel presented in exo up convention.

[1] J. Ni, Y. Jiang, X. Bi, et al., Lithium Iron Orthosilicate Cathode: Progress and Perspectives, ACS Energy Letters **2**, 1771–1781 (2017).
[2] V. Etacheri, Sol-Gel Processed Cathode Materials for Lithium-Ion Batteries in Sol-Gel Materials for Energy, Environment and Electronic Applications (Springer, 2017).

CANCELLED DUE TO COVID-19

SYNTHESIS OF LITHIUM-IRON SILICATE Li_2FeSiO_4 USING SOL-GEL METHOD

Maksymilian Odziemczyk[1*], Przemysław P. Michalski[1], Jerzy E. Garbarczyk[1]

[1] Faculty of Physics, Warsaw University of Technology, Koszykowa 75, 00-662, Warsaw, Poland
01133883@pw.edu.pl

The purpose of this work is synthesis of cathode material for Li-ion batteries, Li_2FeSiO_4. This material offers a promising opportunity for batteries due to its high theoretical capacity of 331 $mAh \cdot g^{-1}$. Voltage of cell consisting Li_2FeSiO_4 as a cathode is expected to be as high as 4.0–4.8 V vs Li^+/Li. Low cost and high abundance of substrates are also the advantages of this material. On the other hand, a disadvantage of Li_2FeSiO_4 is extremely low electronic conductivity of $6 \cdot 10^{-14}$ $S \cdot cm^{-1}$ [1]. Such low value may worse its electrochemical properties. Sol-gel method enables to obtain a material of high porosity and so that the both ionic and electronic conductivity may be higher [2].

In our case, the source of silicon was TEOS ($SiC_8H_{20}O_4$). TEOS was dissolved in distilled water and ethanol solution. Water solutions of lithium and iron sources (CH_3COOLi and $Fe(NO_3)_3 \cdot 9H_2O$) were added dropwise. Final solution was mixed on magnetic stirrer and temperature was rised up to 80–90°C in order to evaporate the excess of water. The pH of solution was controled by adding 2M solution of ammonia. After gelation, the obtained gel was dryed in vacuum dryer.

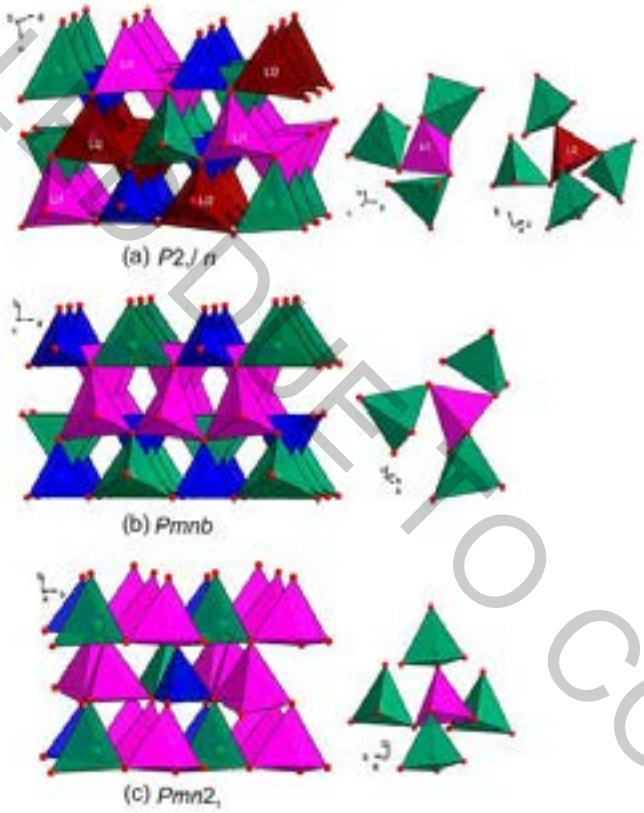

Fig. 1. Possible crystal structures of Li_2FeSiO_4: a) monoclinic, b, c) orthorhombic. Pink and brown – LiO_4 tetrahedra, blue colour – SiO_4 tetrahedra, green colour – FeO_4 tetrahedra [1].

In this poster, results of studies on pH influence on Li_2FeSiO_4 sol-gel synthesis process will be shown.

[1] J. Ni, Y. Jiang, X. Bi, et al., Lithium Iron Orthosilicate Cathode: Progress and Perspectives, ACS Energy Letters **2**, 1771–1781 (2017).
[2] V. Etacheri, Sol-Gel Processed Cathode Materials for Lithium-Ion Batteries in Sol-Gel Materials for Energy, Environment and Electronic Applications (Springer, 2017).

CANCELLED DUE TO COVID-19

STRUCTURAL PROPERTIES OF GLASS-CERAMIC COMPOSITE MATERIALS IN Bi_2O_3-Pr_2O_3 SYSTEM

Karol Olszewski, Aleksander Tecza, Paulina Kruk-Fura, Jan Jamroz

Faculty of Physics, Warsaw University of Technology, Poland
karol.olszewski.stud@pw.edu.pl

Solid oxides, characterized by high ion conductivity in intermediate temperature range ($500-700\ ^{\circ}C$), are widely investigated for potential application in fuel cells, gas detectors or gas-separating membranes. One of such materials is bismuth (III) oxide, particularly in δ-Bi_2O_3 phase, which demonstrates the highest known oside ion conductivity $\approx 1\ S/cm$, at temperature $> 730\ ^{\circ}C$. However, delta phase is only stable at narrow temperature range $(730-830\ ^{\circ}C)$ [1].

One of the methods for obtaining stable δ-Bi_2O_3 type phase at lower temperatures is to create solid state solutions of Bi_2O_3-Ln_2O_3 system, where Ln is a rare-earth metal. The radius of dopants element may determine the structure of the system. Smaller cations such as, Y^{3+}, Yb^{3+} help to stabilise fluorite type structure (δ). On the other hand the ones with similar ionic radius e.g. La^{3+}, Pr^{3+} can lead to formation of rhombohedral structure (schematically shown in fig. 1) instead [3]. What is worth noting, rhombohedral Bi_2O_3-Ln_2O_3 systems demonstrate only slightly lower ionic conductivity compared to the fluorite phase, whilst being much more stable during long-term annealing.

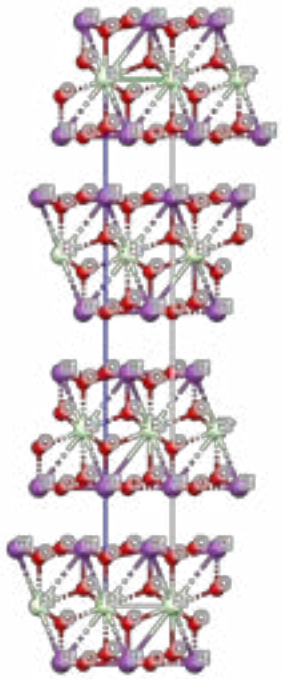

Fig. 1. Rhombohedral structure of Bi_2O_3-Pr_2O_3 generated with Mercury software [2]

Previous investigations of rhombohedral Bi_2O_3-Pr_2O_3 systems, has shown that better understanding of structural properties, particularly in the vicinity of $\beta_2 \rightarrow \beta_1$ phase transition of order-distorder type at $730\ ^{\circ}C$, provides us better understanding about stability factors of the studied materials [4]. It is also known that morphology is one of these factors, which may be modified by e.g. various methods of synthesizing those materials. Previous research has proven that using fast cooling from liquid phase techniques, like melt-quenching or twin-rollers, may result in obtaining nanomaterials or composites, of different structural properties than their polycrystalline equivalents with bigger grains [5, 6].

The aim of this work is to obtain a Bi_2O_3-Pr_2O_3 system with smaller grain size than in ceramics obtained during previous studies [4]. In particular, our aim was to synthesize glass-ceramic composites, consisting of small grains (below $100nm$), confined in glass matrix. Therefore fast-cooling techniques were applied in order to obtain glass-ceramic composites of Bi_2O_3-Pr_2O_3. X-Ray diffractometry (XRD) at room temperature (Phillips XPert Pro) was performed to investigate initial structural properties. Temperature dependent XRD measurement (Anton-Paar HTK 1200 Furnace), were conducted to observe thermal stability of as-received samples.

[1] H. A. Harwig, On the structure of bismuthsesquioxide: the α, β, γ, and δ phase, Journal of Inorganic and General Chemistry, **444**, 151–166 (1978).
[2] http://www.ccdc.cam.ac.uk/mercury/
[3] M. Drache, P. Roussel, J.P. Wignacourt, Structures and Oxide Mobility in Bi-Ln-O Materials: Heritage of Bi_2O_3 Chemical Reviews **107**, 80–96 (2007).
[4] J. Jamroz, M. Malys, F. Krok et al., The influence of defect structure changes at phase transition on electrical properties in the $Bi_{0.75}Pr_{0.25}O_{1.5}$ oxide ion conductor, To be published
[5] A.S. Kalbarczyk, Termiczne, strukturalne i elektryczne właściwości szkieł srebrowo-wanadowych otrzymywanych różnymi metodami, Rozprawa doktorska WF PW (2014).
[6] T.K. Pietrzak, J.E. Garbarczyk, M. Wasiucionek, Stabilization of the delta-Bi_2O_3-like structure down to room temperature by thermal nanocrystallization of bismuth oxide-based glasses, Solid State Ionics **323**, 78-84 (2018) .

ARTICLE DUE TO COVID-19

THERMOLUMINESCENCE OF LITHIUM FLUORIDE DOPED WITH SELECTED ELEMENTS

Michał Ołowski

[1] Department of Physics, Warsaw University of Technology, Poland
01110155@pw.edu.pl

Thermoluminescence is a process in which thermally stimulated solid emits light. This phenomenon follows the previous exposition on ionizing radiation. A thermoluminescent material absorbs some energy of radiation, which is stored by trapped electrons at imperfections in the lattice (structural defects or impurities). The emission of light is triggered by heating the material, what release the electrons from the traps. This phenomenon can be used to date materials, measurement of trap depth in materials and dosimetric applications. The goal of this study is to develop termoluminescent material based on lithium fluoride doped with selected elements and further examination of this property.

CANCELLED DUE TO COVID-19

SYNTHESIS OF VANADIUM-DOPED LITHIUM-MANGANESE BORATE BY SOL-GEL METHOD

Jakub Mrówczyński[1], Przemysław Piotr Michalski[1]

[1] Faculty of Physics, Warsaw University of Technology, Poland
jakub.mrowczynski.stud@pw.edu.pl

Nowadays, lithium-ion batteries have become very popular power sources for various devices as notebooks, mobile phones or even cars. With enormous demand for such usage, arrived a necessity for new materials and new technologies in this domain.

In this work, vanadium-doped lithium-manganese borate ($LiMn_{0.875}V_{0.05}BO_3$) was synthesised using simple sol-gel method. Lithium-manganese borate ($LiMnBO_3$) exhibits high gravimetric capacity (222 $mAh \cdot g^{-1}$) [1]. On the other hand, electronic conductivity values are only mediocre ($3.64 \cdot 10^{-7}$ $S \cdot cm^{-1}$) [2]. To handle this, the material was doped with vanadium, which can exists on a few levels of oxidation, what should improve electronic conductivity. What is more, material was synthesised using sol-gel method, what result in high porosity of resulting product. This should also have positive effect on conductivity. In this work, an impact of different pH conditions in sol-gel synthesis was studied.

We performed syntheses of gels in acidic (pH = 2.5 and pH = 3), neutral (pH = 7) and alkaline (pH = 9.5) environment. Resulting gels and composites were examined using DTA/TGA, XRD and IS methods. The results of DTA/TGA are shown in Fig. 1. We can deduce temperature of calcination for resulting material, which can be determined as temperature at which there is no further mass loss. In this case, this temperature is around 700-800°C. The results of XRD shown in Fig. 2 provide information that for pH = 7 and pH = 9.5 acquired gels have not amorphous but crystalline structure. The IS measurements showed the existence of mixed electronic-ionic conductivity in samples.

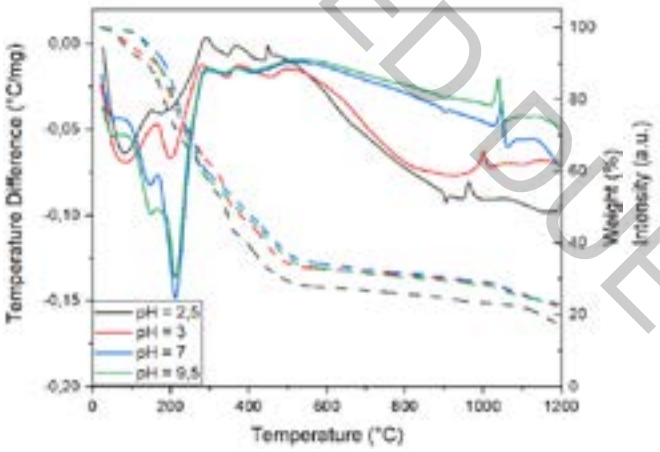

Fig. 1 DTA/TGA plot for gel samples obtained with different pH values. Full lines and dotted lines represent DTA and TGA curves, respectively.

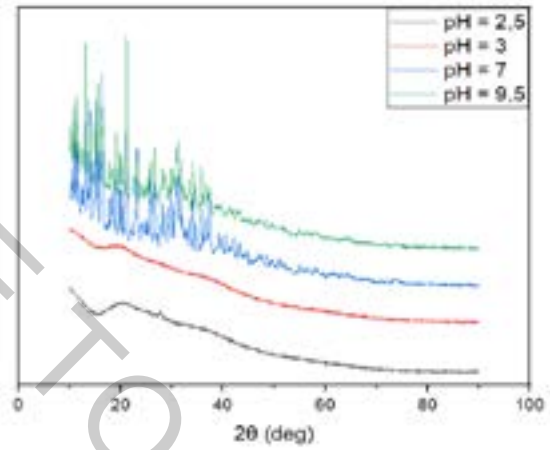

Fig. 2 XRD results for gel samples obtained with different pH values.

[1] J.C. Kim, C.J. Moore, B. Kang, G. Hautier, A. Jain, G. Ceder: Synthesis and Electrochemical Properties of Monoclinic $LiMnBO_3$ as a Li Intercalation Material. Journal of The Electrochemical Society 158 (2011) A309–A315.

[2] V. Ragupathi, M. Safiq, P. Panigrahi, T. Hussain, S. Raman, R. Ahuja, G.S. Nagarajan: Enhanced electrochemical performance of $LiMnBO_3$ with conductive glassy phase: a prospective cathode material for lithium-ion battery. Ionics 23 (2017) 1645–1653.

CANCELLED DUE TO COVID-19

INVESTIGATION OF STRUCTURAL PROPERTIES OF GLASS-CERAMIC COMOPOSITE MATERIALS Bi_2O_3-Yb_2O_3 SYSTEM

Aleksander Tecza, Karol Olszewski, Paulina Kruk-Fura, Jan Jamroz

Faculty of Physics, Warsaw University of Technology, Poland
aleksander.tecza.stud@pw.edu.pl

Materials which are oxide ion conductors, characterized by high ion conductivity in (500 – 700 °C), are widely investigated for potential application in electrochemical devices such as fuel cells, gas detectors or gas-separating membranes. Polycrystalline bismuth (III) oxide, being one of such materials, is known ionic conductor, showing polymorphic phases e. g. α, β, δ, γ. Delta phase demonstrates highest conductivity in high temperature (ca. 1 S/cm at 750 °C) amongst all known oxide ion conductors. However, it is stable only in narrow temperature range (730 – 825 °C) [1].

One of the methods to obtain stable δ-Bi_2O_3 type phase at lower temperatures can be achieved by solid solutions technique. Various metal dopands were previously applied to obtain Bi_2O_3-Ln_2O_3 systems, where Ln is rare-earth metal. One of such can be for e.g. Bi_2O_3-Yb_2O_3. Those systems, in polycrystalline form with large grains (100nm) were thoroughly investigated [2] [3]. However, morphology of those systems can be modified by e.g. various methods of synthesizing those materials. Previous research has proven that using fast cooling from liquid phase techniques, like melt-quenching or twin-rollers, may result in obtaining nanomaterials or composites, of different structural properties than their polycrystalline equivalents with bigger grains [4].

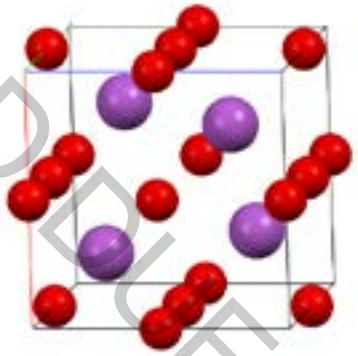

Fig. 1. Fluorite-like structure of δ-Bi_2O_3 generated with Mercury software [5]. Bigger elements represents bismuth atoms, whilst smaller are possible oxygens occupations.

The aim of this research is to obtain a Bi_2O_3-Yb_2O_3 system with morphology that have not been previously investigated. In particular, we are interested in glass-ceramic composites, consisting of small grains (below 100nm), confined in glass matrix. Investigating as synthesized materials may allow us for better understanding of fluorite phase (schematically shown in Fig. 1) of these materials. Therefore, our idea is to apply fast-cooling techniques in order to obtain glass ceramic composites of Bi_2O_3-Yb_2O_3. X-Ray diffractometry (XRD) at room temperature (Phillips XPert Pro) was performed to investigate initial structural properties. Temperature dependent XRD measurement (Anton-Paar HTK 1200 Furnace), were conducted to observe thermal stability of as-received samples.

[1] H. A. Harwig, On the structure of bismuthsesquioxide: the α, β, γ, and δ phase, Journal of Inorganic and General Chemistry, **444**, 151–166 (1978).
[2] M. Leszczynska, X. Liu, W. Wrobel et al., Total scattering analysis of cation coordination and vacancy pair distribution in Yb substituted δ-Bi_2O_3, Journal of Physics: Condensed Matter, 25, 454207 (2013)
[3] I. Abrahams et al., A Combined Total Scattering and Simulation Approach to Analyzing Defect Structure in Bi_3YO_6, Chemistry of Materials, 22, 4435–4445 (2010).
[4] T.K. Pietrzak, J.E. Garbarczyk, M. Wasiucionek, Stabilization of the delta-Bi_2O_3-like structure down to room temperature by thermal nanocrystallization of bismuth oxide-based glasses, Solid State Ionics **323**, 78-84 (2018) .
[5] http://www.ccdc.cam.ac.uk/mercury/

CANCELLED DUE TO COVID-19

STRUCTURAL AND ELECTRICAL PROPERTIES OF NANOCOMPOSITES IN Bi_2O_3–Al_2O_3–SiO_2 SYSTEM OBTAINED WITH FAST COOLING TECHNIQUE

Paulina Kruk-Fura, Tomasz K. Pietrzak, Jerzy E. Garbarczyk

Faculty of Physics, Warsaw University of Technology, Poland
paulina.kruk-fura@fizyka.pw.edu.pl

CANCELLED DUE TO COVID-19

Polycrystalline bismuth (III) oxide is very well known oxide ion conductor, which additionally occurrs in α, β, γ and δ phases (Fig. 1). Furthermore, Bi_2O_3 seems to exhibit different properties, according to its crystalline phase. Therefore, it is exceptionally interesting to study the solid state phenomena occuring. Also, these properties might enable possible practical applications in electrochemical devices like e.g. fuel cells, gas detectors, or gas-separating membranes. Especially interesting remains the δ–phase of Bi_2O_3, which exhibits the highest conductivity in high temperature range (1 S/cm at 750 °C) from among all known oxygene ion conductors. However, δ-phase is stable only in a narrow temperature range from 730 to 825 °C [1].

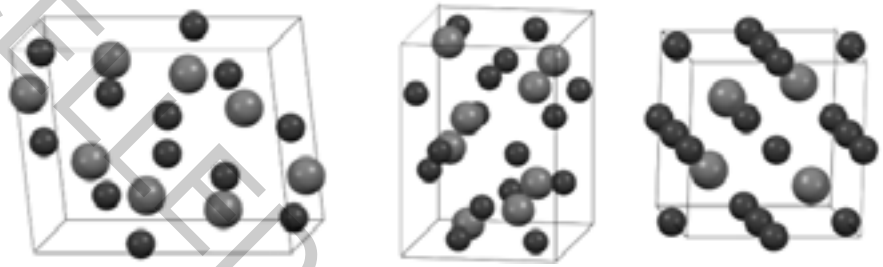

Fig. 1. Unit cells of the most important phases of bismuth (III) oxide (from left to right): ($P2_1/C$) monoclinic (α); ($P42_{1C}$) tetragonal (β); (Pn-3m) fluorite-type fcc (δ), generated by Mercury software [2] from CIFs no. 1010004, 1545547, 1010311, respectively.

δ-Bi_2O_3's unique eletrical properties has motivated many researchers to look for a method to stabilise fluorite-type structure down to lower temperature. So far the successful strategies to achieve the stabilisation of δ phase have included obtaining solid solutions of various systems (e.g. with rare-earth elements [3]) or synthesis in form of thin layers [4]. However, this is at expense of electrical conductivity value. Our approach to reach the same goal is different. It is based on previous experience with studies on various materials, e.g. V_2O_5, when using fast cooling technique, such as twin-rollers, resulted in obtaining nanocomposites [5]. Our assumption is that there might be possibility of stabilising the fluorite-like phase (δ) as nanocomposite material by combining doping and fast cooling technique. It is expected that material with such unique atomic structure would present very different structural and electrical properties compared to polycrystalline analogs.

The idea presented in this work, is to apply twin-rollers technique as one of the fast cooling techniques, in order to obtain nanocomposites in Bi_2O_3–Al_2O_3–SiO_2 system from melted batch. Additionally, we chose two particularly interesting issues to examine. Firstly, how the amount of dopands of Al_2O_3 and SiO_2, which content was controlled during synthesis, influenced the process of stabilisation of δ-like phase in studied materials. Secondly, if parameters of the synthesis affected thermal stability and electrical properites of as-received materials (and how, if so). X-ray diffraction measurements (XRD) showed that in some cases is was possible to synthesise Bi_2O_3–Al_2O_3–SiO_2 nanocomposites in the δ–like phase with twin–rollers technique. Moreover, XRD studies in function of temperature (HT–XRD) revealed that this phase remains stable up to ca. 550 °C, depending on amount of additives present in examined materials and parameters of the synthesis.

Acknowledgements: One of the Authors (Paulina Kruk-Fura) is deeply grateful to Prof. Wojciech Wrobel for scientific inspirations, fruitful discussions and helping hand with measurements and data analysis.

This work is supported by National Science Centre, Poland, Grant Preludium–14 no. 2017/27/N/ST5/01943.

[1] H. A. Harwig, On the structure of bismuthsesquioxide: the α, β, γ, and δ phase, Journal of Inorganic and General Chemistry, **444**, 151–166 (1978).
[2] http://www.ccdc.cam.ac.uk/mercury/
[3] M. Leszczynska, X. Liu, W. Wrobel et al., Oxide ion distribution, vacancy ordering and electrical behaviour in the Bi_3NbO_7–Bi_3YbO_6 pseudo-binary system, Journal of Materials Chemistry **A2**, 18624–18634 (2014).
[4] H. T. Fan, S. S. Pan, X. M. Teng et al., δ–Bi_2O_3 thin films prepared by reactive sputtering: Fabrication and characterization, Thin Solid Films **513**, 142–147 (2006).
[5] T.K. Pietrzak, M. Maciaszek, J.L. Nowiński et al., Electrical properties of V_2O_5 nanomaterials prepared by twin rollers technique, Solid State Ionics **225**, 658–662 (2012).

COMPREHENSIVE STUDY OF GLASSES AND COMPOSITES IN LITHIUM-BORATE SYSTEM

Przemysław P. Michalski[1], Agata Jarocka, Jakub S. Otrębski[1], Olivier Lafon[2,3], Julien Trébosc[2], Tomasz K. Pietrzak[1], Jan L. Nowiński [1] and Jerzy E. Garbarczyk[1]

[1]Faculty of Physics, Warsaw University of Technology, Koszykowa 75, 00-662 Warsaw, Poland
[2]University of Lille, CNRS, UMR 8181, UCCS-Unité de Catalyse et de Chimie du Solide, F-59000 Lille, France
[3]Institute Universitaire de France (IUF), 1 rue Descartes, 75231 Paris, France
przemyslaw.michalski@pw.edu.pl

CANCELLED DUE TO COVID-19

In the electrochemical energy storage field, nanomaterials have established their position as a common solution to gravimetric capacity and cyclability of a cell related problems. There is a diversity of synthesis routes to produce nanostructured materials with desirable structure and properties. Most of them usually require sophisticated devices and preparation which cannot be easily scaled to industrial needs (e.g. MBE, MOCVD) or require many time-consuming steps of synthesis in various conditions (like sol-gel method).

Some time ago, interesting compounds with the composition $LiMBO_3$ (M = Fe, Mn) have emerged as potential cathode materials for Li-ion batteries [1]. The polycrystalline samples of those have exhibited low electronic and ionic conductivity which has led to insufficient gravimetric capacity and cyclability. Herein, we present our recent results of studies on selected physical properties of $LiMBO_3$ glasses and compounds obtained by their thermal nanocrystallization. Usage of glasses may lead to some impressive results. Previously, we have successfully applied this method e.g. in case of $LiFePO_4$-like system: Li_2O–FeO–V_2O_5–P_2O_5. The heat-treated materials exhibited an advantageous microstructure and significantly enhanced electric conductivity (up to 10 orders of magnitude!) [2].

In this work, $LiFe_xMn_{1-x}BO_3$ (x = 0, 0.25, 0.5, 0.75, 1) glasses were successfully synthesized and subsequently nanocrystallized. Glasses were obtained using melt-quenching method and characterized with thermal (DTA), structural (XRD, SEM) and electrical (IS) methods. Also nuclear magnetic resonance (NMR) was used to study the local environment of lithium ions. Manganese-rich samples exhibited better glass-forming properties, but the increase of electric conductivity after nanocrystallization was modest and the final conductivity was quite low. Addition of iron led to better conductivity and higher increases after nanocrystallization, but caused worse glass-forming properties. The dependence of log(conductivity) on composition were linear (Fig. 1). These interesting results may be explained on the basis of Mott's theory of electron hopping. Also, by NMR and SEM methods, the presence of two lithium environments were proposed. The electrochemical activity of glasses and nanomaterials was also evaluated. $LiFeBO_3$ nanocomposites are able to reach gravimetric capacity of 300 $mAhg^{-1}$ under low charge/discharge currents.

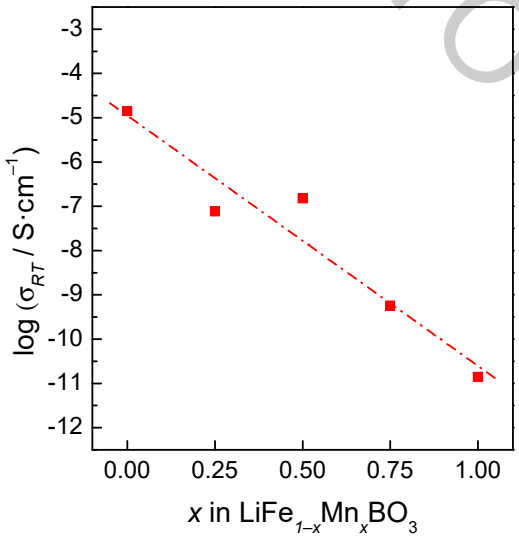

Fig. 1. Dependence of conductivity on composition x in $LiFe_xMn_{1-x}BO_3$ nanocomposites.

Acknowledgements
This project has received funding from the European Union's Horizon 2020 research and innovation program under grant agreement No 731019 (EUSMI).

[1] V. Legagneur, Y. An, A. Mosbah, R. Portal, A. Le Gal La Salle, A. Verbaere, D. Guyomard, Y. Piffard, Solid State Ionics **139** (2001) 37–46.
[2] T.K. Pietrzak, M. Wasiucionek, P.P. Michalski, A. Kaleta, J.E. Garbarczyk, Materials Science and Engineering B **213** (2016) 140–147.

TOWARDS EFFICIENT SODIUM BATTERIES: NANOCRYSTALLIZATION OF GLASSY ALLUAUDITE $Na_2Fe_2V(PO_4)_3$

Maciej Nowagiel, Tomasz K. Pietrzak

Faculty of Physics, Warsaw University of Technology, Poland
m.nowagiel@gmail.com

Application of renewable power sources carries new challenges concerning energy storage. Wind and solar plants are susceptible to atmospheric conditions. For example – wind farms produce energy only when sufficiently strong wind blows. One of the remedies to stabilize their output is utilization of battery storage stations. In this field, sodium batteries are expected to be sustainable and cheap alternative to lithium ones [1].

Alluaudites, which structure was first described by Fisher in 1955 [2], are among potential cathode materials. $Na_xMnFe_2(PO_4)_3$ attracted much interest of Trad and co-workers, since its theoretical gravimetric capacity could be close to 170 mAh/g if reversibly cycled between x = 0 and 3 [3]. Poor electrical conductivity ($\sigma(275°C) = 9.7 \cdot 10^{-7}$ S/cm [4]) is one of the main obstacles to their implementation.

Alluaudite structure can be adopted by various compounds. In our recent research, we succesfully synthesized glassy analogs of $Na_2Fe_3(PO_4)_3$, $Na_2Fe_2V(PO_4)_3$ and $Na_2FeMnV(PO_4)_3$. Thermal treatment of the samples led to nanocrystallization of alluaudite phase [5]. Previous studies on amorphous analogs of cathode materials for Li-ion batteries show significant increase of electrical conductivity as a result of their thermal nanocrystallization, due to occuring of preferable conditions for polaron hopping mechanism of conduction [6].

In this work, we decided to optimize electrical conductivity of $Na_2Fe_2V(PO_4)_3$ alluaudite-like glass by a properly planned heat-treatment. We have shown that temperature of thermal nanocrystallization is vital for enhancing its electrical properties. In preliminary measurements, we observed a significant (5 orders of magnitude) and irreversible increase of conductivity, which resulted in receiving nanomaterial with $\sigma(25°C) \approx 10^{-3}$ S/cm.

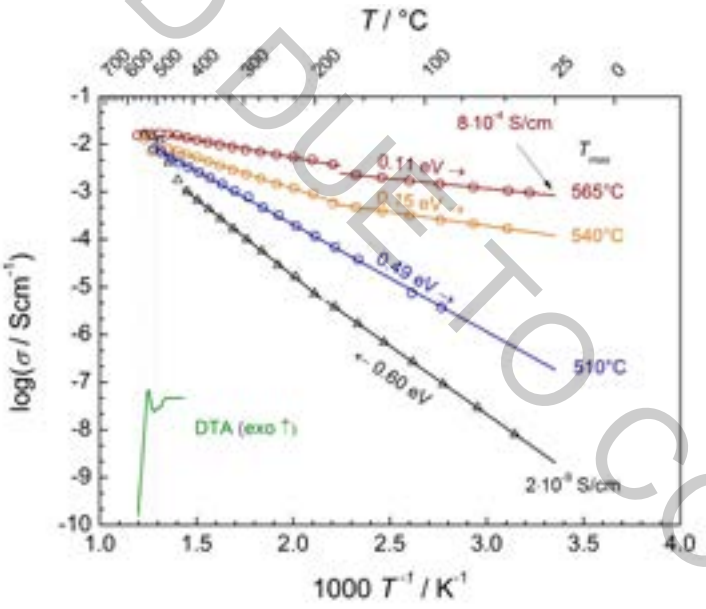

Fig. 1. Arrhenius plot for an as-prepared glassy $Na_2Fe_2V(PO_4)_3$ sample (triangles) and heated to different maximum temperatures (circles) within 510–565°C range. DTA curve is given for comparison.

[1] V. Palomares et al., Energy & Environmental Science **5** (2012), 5884–5901.
[2] D.J. Fisher, American Mineralogist **40** (1955), 1100–1109.
[3] K. Trad et al., Chemistry of Materials **22** (2010), 5554–5562.
[4] A. Daidouh et al., Solid State Sciences **4** (2002), 541–548.
[5] A.E. Chamryga et al., Journal of Non-Crystalline Solids **526** (2019), 119721.
[6] T.K. Pietrzak et al., Materials Science and Engineering **B 213** (2016), 140–147.

ORDERED DUE TO COVID-19

XPS STUDIES OF VANADIUM-DOPED LITHIUM-MANGANESE-BORATE GLASSES AND NANOCOMPOSITES

Agata Jarocka[1], Przemysław P. Michalski[1], Jacek Ryl[2], Tomasz K. Pietrzak[1], Marek Wasiucionek[1]

[1]Faculty of Physics, Warsaw University of Technology, Koszykowa 75, 00-662 Warsaw, Poland
[2]Faculty of Chemistry, Gdańsk University of Technology, Narutowicza 11/12, 80-233 Gdańsk, Poland
agata.jarocka.dokt@pw.edu.pl

CANCELLED DUE TO COVID-19

Growing demand on good quality storage systems is an extremely important global concern, e.g., for renewable energy sources – solar or wind power – when need for electricity is not that high and excess energy has to be stored. Hence comes the need for constant development of new solutions. Furthermore, similar but smaller systems are also a crucial part of every electric car. All of this has irrefutable influence on ecology and pollution reduction.

Nowadays, rapid technology development in the field of portable devices needs adjusting those devices' batteries in a way that their efficiency will improve. There is growing need for smaller, lighter and more efficient cell phones or personal computers and therefore also for batteries exhibiting improved properties. One of the factors that has significant influence on cells' parameters is the electrical conductivity of their cathode material. Therefore, scientists conduct researches on materials that potentially can be used as cathodes and search for ways to improve their conductivities.

An interesting method to improve this property is thermal nanocrystallisation of glasses developed in Solid State Ionic Division, Faculty of Physics, Warsaw University of Technology. Lithium manganese borate has found high interest in nowadays research on cathode materials for Li-ion batteries mostly due to its high theoretical gravimetric capacity of 222 mAh/g [1], which is even greater than for the widely studied phosphates. However, our research on this compound showed that final electrical conductivity after nanocrystallisation was still not sufficient enough. Basing on the studies [2] on vanadium-doped $LiFePO_4$ compound and on conclusion that even small amount of vanadium can significantly improve electrical and electrochemical properties of material, we attempted to dope aforementioned $LiMnBO_3$ with vanadium.

Glassy $LiMn_{0.925}V_{0.05}BO_3$ was successfully synthesized with use of melt-quenching process. Then, the samples were nanocrystallised in different temperatures and characterized [3]. In this work, mainly XPS (X-ray photoelectron spectroscopy) studies (Fig. 1) will be presented in order to demonstrate changes in Mn^{2+}/Mn^{3+} ions relative ratio before and after nanocrystallisation.

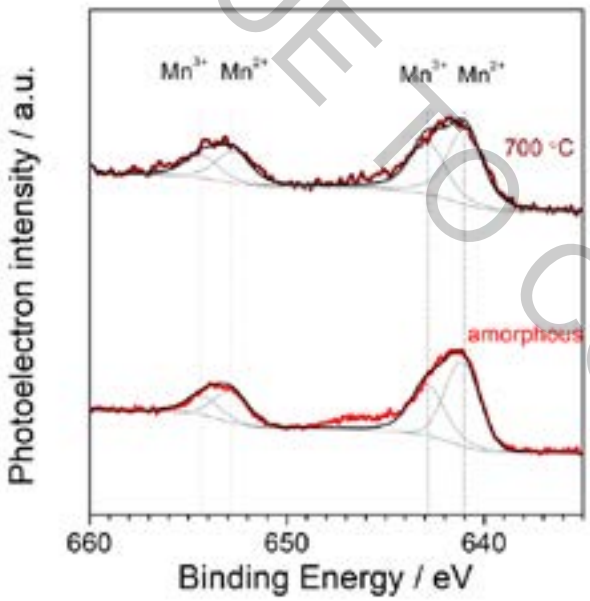

Fig. 1. High-resolution XPS spectra glassy sample and the sample crystallised at 700 °C. Fitted profiles ascribed to presence of Mn^{2+} and Mn^{3+} ions are shown as grey lines above the background.

[1] V. Legagneur, Y. An, A. Mosbah, R. Portal, A. Le Gal La Salle, A. Verbaere, D. Guyomard, Y. Piffard. Solid State Ionics 139 (2001) 37–46.
[2] F. Omenya, N.A. Chernova, S. Upreti, P.Y. Zavalij, K.-W. Nam, X.-Q. Yang, M.S. Whittingham, Chemistry of Materials 23 (2011) 4733-4740.
[3] A. Jarocka, P.P. Michalski, J. Ryl, M. Wasiucionek, J. E. Garbarczyk, T.K. Pietrzak, Ionics (2019). https://doi.org/10.1007/s11581-019-03229-5

HOLDER FOR IMPEDANCE SPECTROSCOPY MEASUREMENTS OF MIXED CONDUCTORS IN INERT ATMOSPHERE

Mateusz Samsel, Tomasz Pietrzak

Faculty of Physics, Warsaw University of Technology, Koszykowa 75, 00-662 Warsaw, Poland
mateusz.samsel.stud@pw.edu.pl

Thermal nanocrystallisation of glasses is a method of obtaining highly conductive nanomaterials by means of appropriately selected heat treatment. Works carried out in our faculty has shown that this method can lead to a giant increase in electronic conductivity of selected glassy analogues of cathode materials for lithium-ion batteries, even by 9-10 orders of magnitude [1, 2]. Recent studies of the glassy analogues of cathode materials for sodium batteries from NASICON family [3] and alludites [4] did not confirm this observation. It is believed that sodium ion conductors may react differently to the heating in air. Hence the need to investigate the change of conductivity of these materials during thermal nanocrystallization.

During this work we adapted existing systems to measure impedance in temperature function for experiments performed in the flow of inert gas (argon). This means, first of all, the construction of an hermetic measuring holder with a gas inlet and then carrying out the test measurements of impedance as a function of temperature. The mechanical drawing of the holder is shown in Fig. 1.

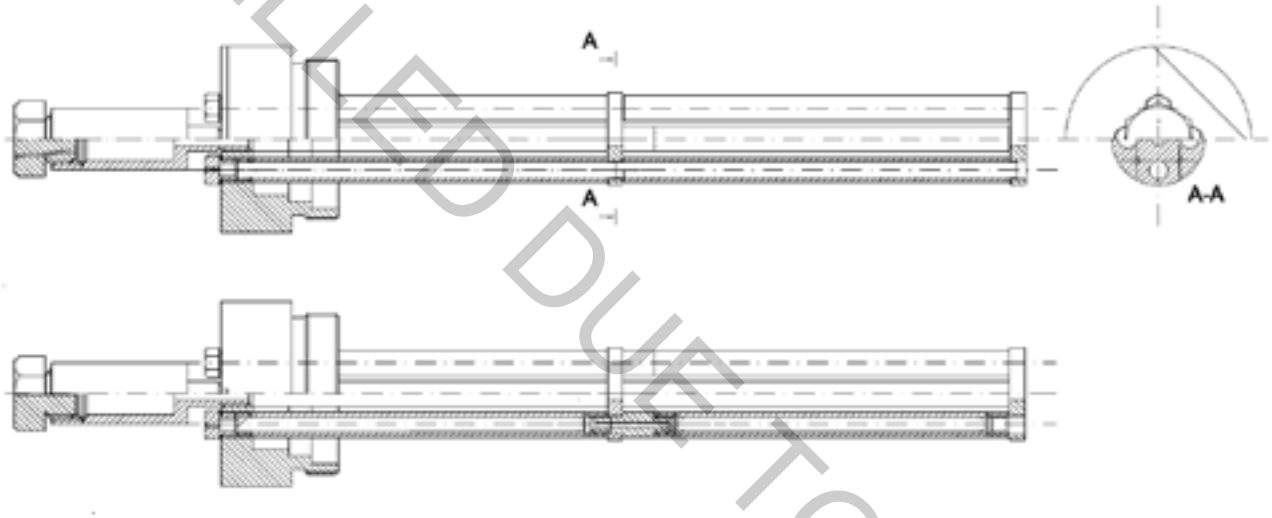

Fig. 1. The designed impedance measurement holder.

[1] T.K. Pietrzak, M. Wasiucionek, P.P. Michalski, A. Kaleta, J.E. Garbarczyk: Highly conductive cathode materials for Li-ion batteries prepared by thermal nanocrystallization of selected oxide glasses. Materials Science and Engineering B 213 (2016) 140-147.

[2] J.E. Frackiewicz, T.K. Pietrzak, M. Wasiucionek, J.E. Garbarczyk: Synthesis and Characterization of Highly-Conducting Nanocrystallized $Li(Fe_{1-x}Mn_x)_{0.88}V_{0.08}PO_4$ Cathode Materials (x = 0.25, 0.5, 0.75). ECS Transactions 80 (2017) 325-330.

[3] T.K. Pietrzak, P.E. Kruk-Fura, P.J. Mikołajczuk, J.E. Garbarczyk: Syntheses and nanocrystallization of NaF—M_2O_3—P_2O_5 NASICON-like phosphate glasses (M = V, Ti, Fe). International Journal of Applied Glass Science 11 (2020) 87-96.

[4] A.E. Chamryga, M. Nowagiel, T.K. Pietrzak: Syntheses and nanocrystallization of Na_2O-M_2O_3-P_2O_5 alluaudite-like phosphate glasses (M = V, Fe, Mn). Journal of Non-Crystalline Solids 526 (2019) 119721.

CANCELLED DUE TO COVID-19

DEVELOPMENT OF THE LASERMETALDEPOSITION TECHNOLOGY

Romuald Petkevič[1], Ada Steponavičiūtė[1], Sergejus Borodinas[2], Genrik Mordas[1]

[1]Department of Laser Technologies, Center for Physical Sciences and Technology,Lithuania
[2]Faculty of Civil Engineering, Vilnius Gediminas Technical University,Lithuania
romuald.petkevic@ftmc.lt

Since 1980, the development of additive production has begun. In recent years, several additive manufacturing technologies have been developed based on the creation of 3D objects using sequential layering processes [1]. In such processes, the layers form a homogeneous structure by consistently coating 3D objects with properly prepared materials that can sometimes be modified during the process. This creates opportunities for the production of new unexplored structured materials.

We present a development of laser metal deposition technology (LMD). This technology uses a process whereby a laser beam melts a small area of the metal surface and the metal powder nozzle deposits the metal particles at that point, creating new structures on the metal surface [2].

The main technological principle of our developed LMD system is illustrated in Fig. 1 and consists of 5 parts: (I) positioning of metal powder ultrasonic jet , (II) control system of laser, (III) suction systems for metal powder residues, (IV) printing platform with controller and (V) monitoring system. Ultrasonic jet system is used to separate metal partcles and point the powder flow towards the printing platform. Laser beam is focused and pointed to the metal powder on the printable object. Suction system helps to avoid defects in the printable object by collectng unmolten powder particles and agglomerates from the printing platform. Printing platform, where the 3D object is being produced, has threecontrolled moving axes (X, Y, Z).

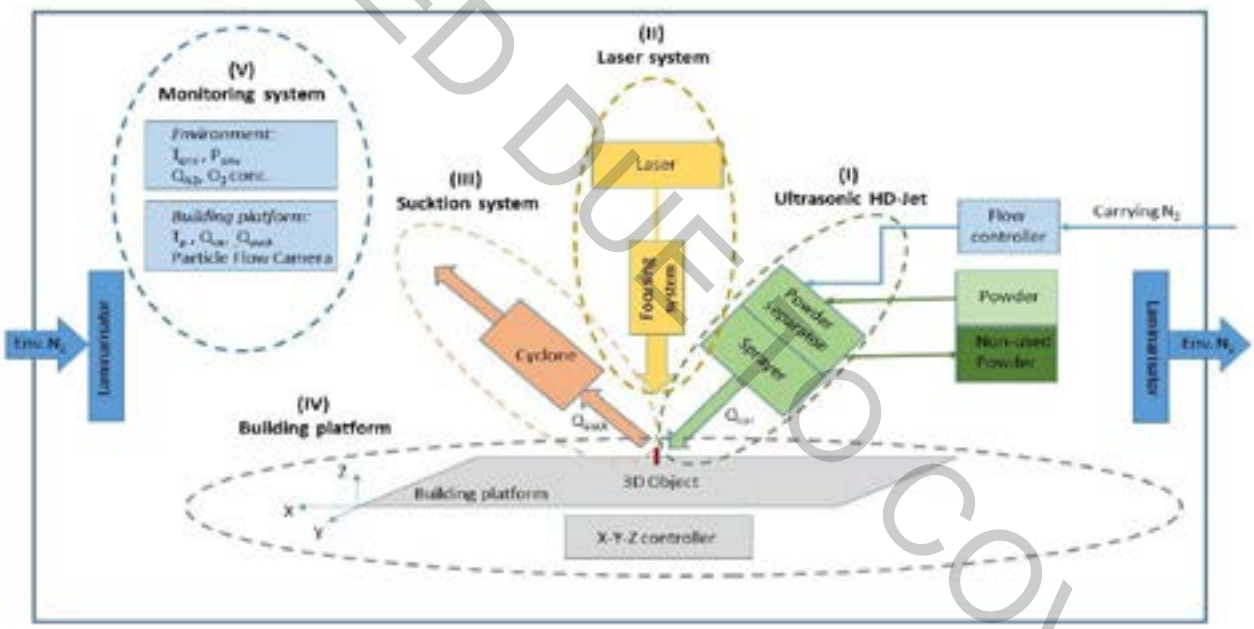

Fig. 1 Technological principle of new LMD system

The whole process of LMD system work is being observed by a monitoring system, which can determine temperature of printing platform and printable object, stability of metal particles flow density, stability of particle flow, size (diameter) of the particles, flow pressure and concentration of oxygen inside of the printing chamber.

[1] H. Assadi, H. Kreye, F. Gärtner, T. Klassen, Cold spraying — A materials perspective, Acta Mater. 116, 382–407 (2016).
[2] D. Herzog, V. Seyda, E. Wycisk, C. Emmelmann, Additive manufacturing of metals, Acta Mater. 117, 371–392 (2016).

CANCELLED DUE TO COVID-19

EFFECT OF ADDITIVES ON STRUCTURAL CHARACTERISTICS OF MCM-41-TYPE NANOPARTICLES

Roik Nadiia, Belyakova Lyudmila, Dzyazko Marina

Chuiko Institute of Surface Chemistry of NAS of Ukraine, 17 General Naumov Str., Kyiv, 03164, Ukraine
roik_nadya@ukr.net

Structural characteristics of silica materials are responsible for their physico-chemical behavior in different research fields. MCM-41-type silicas with hexagonally arranged homogeneous tunable pore channels of mesoscale size are the most promising materials in water purification, catalyst supporting, drug delivery, sensors design etc. Formation of mesoporous matrix of MCM-41 takes place at condensation of alkoxysilanes around supramolecular surfactant assemblies. Pore dimension of silica materials obtained by sol-gel synthesis can be regulated by addition of auxiliary organic compounds which change micelle configuration due to incorporation as cosurfactants or swelling agents.

In the present study, we analyzed the effect of azo dyes (ADs), alizarin yellow (AY) and methyl red (MR), as cosurfactants and their alkoxysilane derivatives as structure-forming silanes on mesostructure of silica materials prepared by base-catalyzed templated sol-gel synthesis. Potential ability of ADs to be incorporated into the long-chain alkylammonium aggregates due to arising of hydrophobic forces along with electrostatic interactions was proved by authors [1–3]. Organosilica materials with hexagonally arranged mesoporous structure were prepared by hydrothermal sol-gel condensation of tetraethyl orthosilicate and (3-aminopropyl)triethoxysilane in the presence of cetyltrimethylammonium and decyltrimethylammonium bromide as pore generating agents, ADs as cosurfactants, and their alkoxysilane derivatives as structure-forming silanes (Scheme).

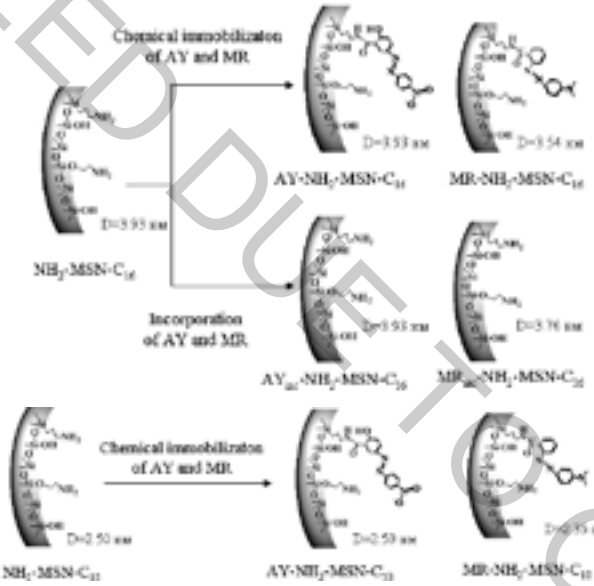

Scheme. Silica materials obtained in the presence of azo dyes and their alkoxysilane derivatives.

Mesostructure of resulting silicas was studied by low-temperature adsorption-desorption of nitrogen, x-ray diffraction analysis, and transmission electron microscopy. It was confirmed that the pore size, specific surface area and hexagonal arrangement of mesopores in synthesized silica nanoparticles were strongly affected by the AD additives. Solubilization of ADs by liquid crystal phase of long chain alkyltrimethylammonium salts and cooperative organization of dye-containing silanes with surfactants, involving penetration of aromatic groups of silanes into micelles, causes formation of more uniform mesoporous structure. As it was elucidated from the analysis of low-temperature adsorption-desorption of nitrogen, introduction of AD additives in sol-gel process results in noticeable increase of surface area, narrowing of pore size distribution and pore diameter. In accordance with the results of x-ray powder diffraction analysis, formation of silica materials which are characterized by the more distinct long-range ordering of porous structure takes place. Obviously, such changes in mesoporous structure of synthesized organosilicas are generated by penetration of hydrophobic parts of AY and MR or their alkoxysilane derivatives between chains of template micelles and drawing of silica matrix closure to the micelles core.

[1] Y.M. Cho, W.K. Lee, B.-K. Kim, Studies on the interaction of azo dyes with cationic surfactant (I), Arch. Pharm. Res. **4**, 75–84 (1981).
[2] R. Hosseinzadeh, R. Maleki, A.A. Matin, Y. Nikkhahi, Spectrophotometric study of anionic azo-dye light yellow (X6G) interaction with surfactants and its micellar solubilization in cationic surfactant micelles, Spectrochim. Acta A **69**, 1183–1187 (2008).
[3] M.F. Nazar, S.S. Shah, M.A. Khosa, Interaction of azo dye with cationic surfactant under different pH conditions, J. Surfactants Deterg. **13**, 529–537 (2010).

CANCELLED DUE TO COVID-19

ELECTROLUMINESCENT PROPERTIES OF PEROVSKITE NANOPARTICLES EMBEDDED IN A POLYMER ELECTROLYTE THIN LAYER

Sergey Anoshkin[1], Arnas Naujokaitis[2], Anatoly Pushkarev[1], Sergey Makarov[1]

[1] Department of Physics and Engineering, ITMO University, Russian Federation
[2] Center for Physical Sciences and Technology, Lithuania
sergey.anoshkin@metalab.ifmo.ru

Last decade, light-emitting diodes based on organic molecules (OLED), quantum dots (QLED), and perovskites (pero-LED) aspire to supersede well established, however, hazardous and expensive $A_{III}B_V$ technology. The outstanding performance was achieved for diodes emitting green and red light, whereas high efficiency and long-term stability of blue electroluminescent (EL) devices still remain challenging. The main drawback of organic blue light-emitting diodes stems from the bimolecular triplet-polaron annihilation (TPA). According to quantum spin statistics, singlet "bright" excitons undergoing fast radiative decay and triplet "dark" excitons experiencing non-radiative relaxation via defect states are formed with a ratio of 1:3, thus, the EL efficiency cannot exceed 25% [1]. Triplet excitons can transfer their energy to polarons that results in breaking chemical bonds in the molecules and the formation of defects which deactivate singlet excitons and decrease the EL efficiency [2].

On the contrary, cesium lead halide perovskites ($CsPbX_3$; X = Cl, Br, I) possess "bright" triplet excitons [3] which energy can be altered from 1.72 to 3.1 eV by halide anion exchange in the crystal lattice. For this reason, cesium lead mixed-halide ($Br_{3-x}Cl_x$, $1 \le x \le 3$) perovskites yielding narrow-band emission in 410−480 nm range are promising candidates for the development of blue light electroluminescent devices.

A single-layer (SL) perovskite LED includes a glass substrate with ITO conductive layer, active perovskite-polymer layer and Ga-In eutectic electrode. The active layer is deposited on substrate by spin-casting solution technique in a N_2-filled glovebox. Then, substrates with perovskite-polymer thin film are evacuated in a vacuum chamber and subsequently annealed at high temperature in air. As a result, perovskite-polymer films consisting of tightly packed grains covered with polymeric matrix is formed (Fig. 1a,b). Normal fit of the grains diameter distribution shows a maximum at 135 nm (Fig. 1c). SL-LEDs based on such films exhibit temporally stable and narrow EL peak (λ_{em} = 478 nm, FWHM = 14 nm) at bias not exceeding 3.2 V, whereas noticeable segregation occurs when applied voltage increases up to 5 V (Fig. 1d). Thereby, pure blue emission has maximum luminance of 217 cd m^{-2} at 3.2 V and the maximum value is reached for cyan light (3053 cd m^{-2}) at 5 V (Fig. 1e).

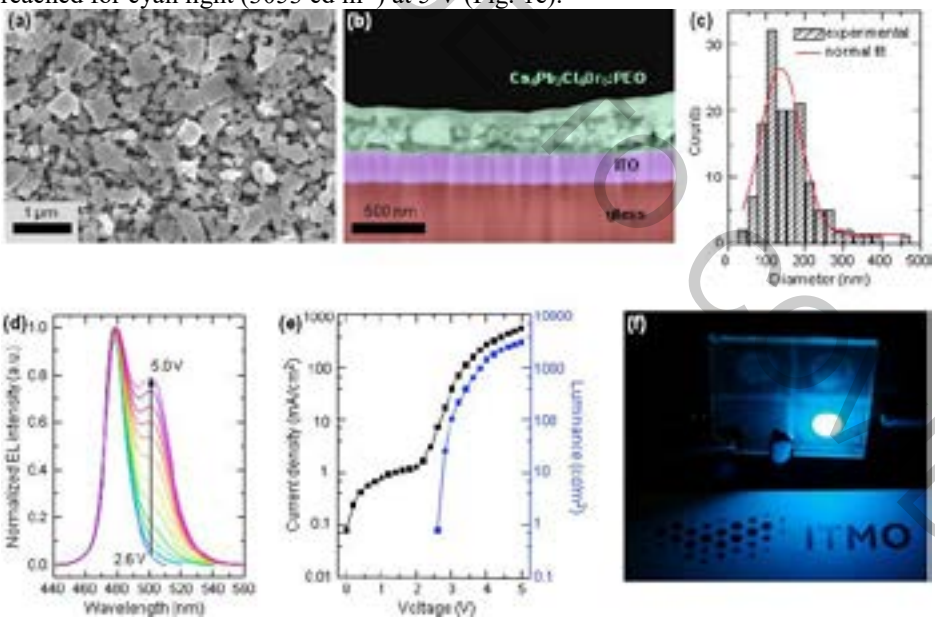

Fig. 1. (a) Top-view SEM image of $Cs_4Pb_3Cl_4Br_6$:PEO film on ITO substrate. (b) Cross-sectional SEM image. (c) Perovskite grains size distribution. (d) Normalized EL spectra of SL-LED at different bias. (e) Current density and luminance versus applied voltage curves. (f) SL-LED operating at 3.2 V illuminates logotype of ITMO University.

[1] M. Baldo, D. O'Brien et al., Excitonic singlet-triplet ratio in a semiconducting organic thin film, Phys. Rev. B **60**, 14422 (1999).
[2] S. Crooker, T. Barrick et al., Multiple temperature regimes of radiative decay in CdSe nanocrystal quantum dots: Intrinsic limits to the dark-exciton lifetime, Appl. Phys. Lett. **82**, 2793 (2003).
[3] M. Becker, R. Vaxenburg et al., Bright triplet excitons in caesium lead halide perovskites, Nature **553**, 189–193(2018).

CREATED DURING COVID-19

SWITCHING BETWEEN TADF AND RTP IN THE METHYL SUBSTITUTED PHENOTHIAZINE COMPOUNDS

Volodymyr Sendiuk[1], Tomas Serevicius[1], Rokas Skaisgiris[1], Ausra Tomkeviciene[2], Juozas Vidas Grazulevicius[2], Karolis Kazlauskas[1], Saulius Jursenas[1]

[1] Organic optoelectronic research group, Institute of Photonics and Nanotechnology, Faculty of Physics, Vilnius University, Vilnius, Lithuania
[2] Department of Polymer Chemistry and Technology, Kaunas University of Technology, Kaunas, Lithuania
volodymyr.sendiuk@ff.vu.lt

CANCELLED DUE TO COVID-19

Thermally activated delayed fluorescence (TADF) is one of the methods for harvesting luminescence from triplet states via reverse intersystem crossing (rISC) in organic molecules. [1] Donor-acceptor-donor (D-A-D) molecules have strong intramolecular charge-transfer (ICT) state and it is very important for creation of strong TADF emitter. [2] A fundamental principle of planar ICT (PICT) and twisted ICT (TICT) is demonstrated to obtain selectively either room temperature phosphorescence (RTP) or thermally activated delayed fluorescence (TADF), respectively. [3]

In this research we have TADF-based emitters of methyl-phenothiazine derivatives, because of their quasi-axial (ax) and quasi-equatorial (eq) conformers have very interesting properties especially for TADF. We used time-resolve fluorescence method to investigate the behavior of emission properties at different temperatures. We establish that different acceptors can change emitters properties from RTP to TADF.

[1] H. Uoyama, K. Goushi, K. Shizu, H. Nomura, C. Adachi, Highly efficient organic light-emitting diodes from delayed fluorescence, Nature **492**, 234-238 (2012).
[2] M. Taneda, K. Shizu, H. Tanaka, C. Adachi, High efficiency thermally activated delayed fluorescence based on 1,3,5-tris(4-(diphenylamino) phenyl)-2,4,6-tricyanobenzene. Chem. Commun. **51**, 5028–5031 (2015).
[3] C. Chen, R. Huang, A. Batsanov, P. Pander, Y. Hsu, Z. Chi, F. Dias, M. Bryce, Intramolecular charge transfer controls switching between room temperature phosphorescence and thermally activated delayed fluorescence. Angew. Chem. Int. Ed. **57**, 16407–16411 (2018).

INVESTIGATION OF ROOM-TEMPERATURE PHOSPHORESCENCE SENSITIVITY TO OXYGEN USING BENZOTRIFLUORIDE AND PHENOTHIAZINE DERIVATIVES

Karolis Leitonas[1], Rasa Keruckiene[1], Dmytro Volyniuk[1], Juozas Vidas Grazulevicius[1]

[1]Department of Polymer Chemistry and Technology, Kaunas University of Technology,
Barsausko g. 59, Kaunas, Lithuania
karolis.leitonas@ktu.edu

CANCELLED DUE TO COVID-19

Metal-free organic materials that show room-temperature phosphorescence (RTP) properties are appropriate replacements to old fashioned organometallic phosphors because of their low cost, suitable optical and environmentally friendly properties, flexible synthesis, and excellent stability. Because of many possible benefits of organic metal-free materials, molecules showing efficient RTP have huge potential for applications in different areas ranging from security, information encryption and optoelectronics to biological probes and optical sensing. [1-4]

Here we report on a pair of 2- and 4-trifluorobenzene-substituted 3,6-di-tert-butyl-phenothiazine-based derivatives which demonstrate RTP effect. Due to donor-acceptor molecular structure of the synthesized compounds, emission spectra of their solutions have single broad bands resulting from recombination of intramolecular charge transfer excitons. Under inert atmosphere dual emission was detected for solid-state samples (for pure or doped films)

Ratio of RTP to fluorescence (I_{Ph}/I_F) were more than 22 which suggesting potential application of phenothiazine-based compounds as active materials for optical sensors of oxygen. Sensitivity of compounds was tested by precise control of N_2 and O_2 gas flow ratio, they demonstrated excellent sensitivity with minimum threshold of only 0.02% O_2 in gas mixture.

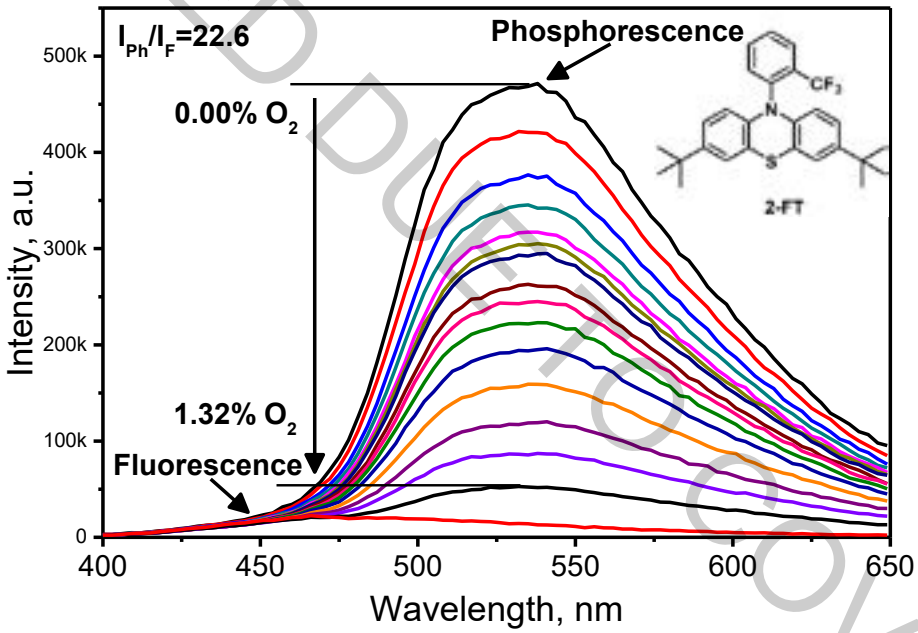

Fig. 1. Photoluminescence spectra of 2-FT in *Zeonex*® (1 wt.%) at different amounts of O_2 in environment.

Acknowledgement:

This project has received funding from European Social Fund (project No 09.3.3.-LMT-K-712-16-0009) under grant agreement with the Research Council of Lithuania.

[1] J. Yang, X. Zhen, B. Wang, X. Gao, Z. Ren, J. Wang, Y. Xie, J. Li, Q. Peng, K. Pu and Z. Li, *Nature Communications*, 2018, **9**, 840.
[2] R. Kabe, N. Notsuka, K. Yoshida and C. Adachi, *Advanced Materials*, 2016, **28**, 655–660.
[3] L. Gu, H. Shi, M. Gu, K. Ling, H. Ma, S. Cai, L. Song, C. Ma, H. Li, G. Xing, X. Hang, J. Li, Y. Gao, W. Yao, Z. Shuai, Z. An, X. Liu and W. Huang, *Angewandte Chemie International Edition*, 2018, **57**, 8425–8431.
[4] I. Sánchez-Barragán, J. M. Costa-Fernández, A. Sanz-Medel, M. Valledor and J. C. Campo, *TrAC Trends in Analytical Chemistry*, 2006, **25**, 958–967.

CONVENTIONAL AND UPCONVERSION LUMINESCENCE OF POLYMORPHOUS $BiPO_4:Yb^{3+},Tb^{3+},Eu^{3+}$ PHOSPHORS

Egle Ezerskyte, Arturas Katelnikovas

Institute of Chemistry, Faculty of Chemistry and Geosciences, Vilnius University, Lithuania
eglezerskyte@gmail.com

There are many factors contributing to the colour of both conventional and upconversion emission such as chemical composition of matrix, crystalline structure of upconverting materials, etc. Yb^{3+} ions, which are part of researched Yb-Tb-Eu system, absorbs 980 nm radiation and transfers the obtained energy to Tb^{3+} ions which then can emit green light themselves or transfer energy to Eu^{3+} ions, if they are in close vicinity, which would lead to orange/red emission of Eu^{3+} ions. Moreover, the investigated $BiPO_4:Yb^{3+},Tb^{3+},Eu^{3+}$ phosphors are able to form three different crystalline structures: trigonal, low-temperature monoclinic and high-temperature monoclinic, which also affects colour of luminescence. Thus, the purpose of this research is to produce green-to-red emitting luminescent materials by manipulating Tb^{3+}/Eu^{3+} ratio and crystalline phase of phosphor.

The investigation of structural, morphological and optical properties of the synthesized compounds was carried out by powder X-ray diffraction (XRD), scanning electron microscopy (SEM) analysis and UV-VIS-NIR spectroscopy.

$BiPO_4:Yb^{3+},Tb^{3+},Eu^{3+}$ samples with trigonal and low-temperature monoclinic crystal structure (Fig.1 (a) and (b) respectively) were synthesized via co-precipitation and high temperature solid-state reaction methods.[1,2] The XRD patterns of produced samples correspond well with the reference patterns. In addition, single phase compounds are obtained at any Tb^{3+}/Eu^{3+} ratio.

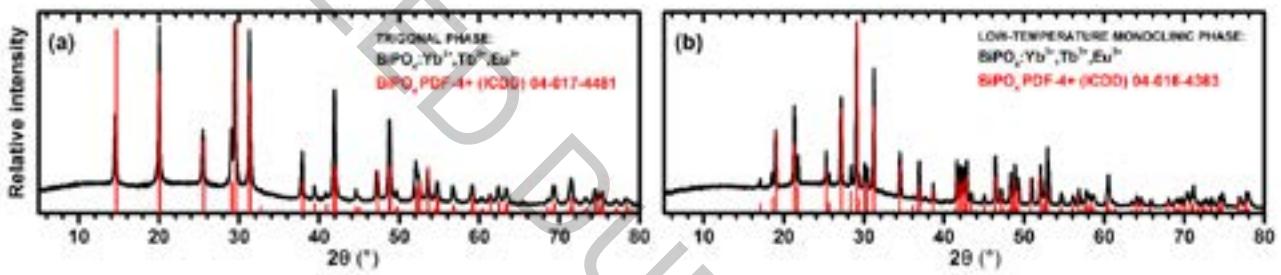

Fig. 1. XRD patterns of trigonal $BiPO_4:Yb^{3+},Tb^{3+},Eu^{3+}$ (a) and low-temperature monoclinic $BiPO_4:Yb^{3+},Tb^{3+},Eu^{3+}$ (b).

Reflection, excitation and emission spectra, decay curves, photoluminescence lifetime values, CIE 1931 colour space coordinates of $BiPO_4:Yb^{3+},Tb^{3+},Eu^{3+}$ phosphors were also investigated and will be discussed.

Acknowledgements: This project has received funding from European Social Fund (project No 09.3.3-LMT-K-712-16-0161) under grant agreement with the Research Council of Lithuania (LMTLT).

1. Achary, S.N., et al., Experimental and theoretical investigations on the polymorphism and metastability of $BiPO_4$. Dalton Transactions, 2013. 42(42): p. 14999-15015.
2. Liu, S., et al., Synthesis and luminescent properties of Eu^{3+} and Dy^{3+} doped $BiPO_4$ phosphors for near UV-based white LEDs. Journal of Materials Science: Materials in Electronics, 2013. 24(11): p. 4253-4257.

CANCELLED DUE TO COVID-19

INVESTIGATION OF PLANAR AND NANOSTRUCTURED ZnO AND Al_2O_3 APPLICATION IN BIOSERSORS DESIGN

Vincentas Mindaugas Mačiulis[1], Ieva Plikusiene[1, 2], Almira Ramanaviciene[2], Anton Popov[2], Octavio Graniel[3], Mikchael Bechelany[3], Arunas Ramanavicius[1, 2]

[1]Laboratory of Nanotechnology, State Research Institute Centre for Physical Sciences and Technology, Sauletekio ave. 3, Vilnius, Lithuania

[2]Institute of Chemistry, Faculty of Chemistry and Geosciences, Vilnius University, Naugarduko 24, Vilnius Lithuania;

[3]Institut Européen des Membranes , CNRS, France

vincentas.maciulis@ftmc.lt

In the past decade, the attention of researchers has been given to the design of new nanoscale materials with advanced properties. ZnO is known as an n-type semiconductor with good transparency, high electron mobility, wide band gap of 3.37 eV, high exciton binding energy of 60 meV, and strong luminescence at room temperature. Because of high photosensitivity, chemical stability, and nontoxicity, ZnO is a perspective material for application in UV, gas, and biological sensors [1].

Aluminum oxides exhibit such properties as biocompatibility. If Al_2O_3 is oxidised the self-organised honeycomb structure of similar diameter nanopores, which run parallel from the surface to the base of the substrate can be formed. [2]. Surface modification of this sort could lead to protein molecules being absorbed into the pAAO film nanopores.

The aim of this work was to investigate possibilities of nanostructured ZnO and Al_2O_3 application in biosensors design. The differences of binding kinetics onto planar and nanostructured ZnO layers and Al_2O_3 were obtained using spectroscopic ellipsometry (SE) method and will be presented.

Real time monitoring of proteins interaction are very important issue because information about reaction mechanisms can be evaluated. For this purpose optical methods, which are able to acquire real time measurement of molecules interaction, are contactless and do not need labeling are very suitable. In this case SE is suitable measurement technique not only because it provides earlier mentioned properties but also of ability to measure two parameters simultaneously [3].

[1] Baitimirova et al., Enhancement of Electronic and Optical Properties of ZnO/Al_2O_3 Nanolaminate Coated Electrospun Nanofibers J. Phys. Chem. C, 120, 41, 23716-23725. (2016)

[2] R. Gopikrishnan, K. Zhang, P. Ravichandran, S. Baluchamy, V. Ramesh, S. Biradar, P. Ramesh, J. Pradhan, J. C. Hall, A. K. Pradhan and G. T. Ramesh, "Synthesis, characterization and biocompatibility studies of zinc oxide (ZnO) nanorods for biomedical application", Nano-Micro Lett. 2, 31-36 (2010)

[3] Balevicius et al., "In situ study of ligand-receptor interaction by total internal reflection ellipsometry", 571, 744-748, Thin solid films (2014)

CANCELLED DUE TO COVID-19

FORMATION OF CHITOSAN AND GREEN COFFEE BEAN OR ARTICHOKE EXTRACT COMPLEXES AND THEIR ANTIFUNGAL ACTIVITY

Deimante Rosliuk[1], Dovile Liudvinaviciute[1], Anne Loron[2], Ramune Rutkaite[1], Véronique Coma[2]

[1] Department of Polymer Chemistry and Technology, Kaunas University of Technology, Lithuania
[2] University of Bordeaux, UMR 5629, CNRS, LCPO, 16 Avenue Pey Berland, 33607 Pessac, France
deimante.rosliuk@ktu.lt, dovile.liudvinaviciute@ktu.edu

Chlorogenic acid, an ester of caffeic and quinic acids, is the most abundant phenolic compound that is known to have numerous biological activities such as antioxidant, anti-inflammatory, antimicrobial and anti-proliferative. This phenolic acid as the main phenolic compound in green coffee bean (GCBE) and artichoke extract (AE) can exist in the form of three different isomers, namely, i.e. 3-O-caffeoylquinic acid, 5-O-caffeoylquinic acid and 4-O-caffeoylquinic acid [1]. However, the application of caffeoylquinic acid derivatives (CQ) is restricted because of their vulnerability to heat, oxygen, light and moisture [2]. In order to overcome these disadvantages these anionic phenolics could be immobilized on cationic polymers such as chitosan (ChS).

In the present study, the formation of water insoluble complexes between ChS and phenolic compounds such as CQ, present in GCBE and AE has been investigated. GCBE/ChS and AE/ChS complexes having 0.1786 *g* and 0.1038 *g* of adsorbed GCBE and AE per of *g* ChS, respectively, were formed and their antifungal activity against *Botrytis cinerea* and *Fusarium graminearum* has been studied.

The CQ, GCBE and AE adsorption on ChS was investigated by employing the equilibrium adsorption method, and the Langmuir adsorption model was used to describe the adsorption isotherms (Fig. 1).

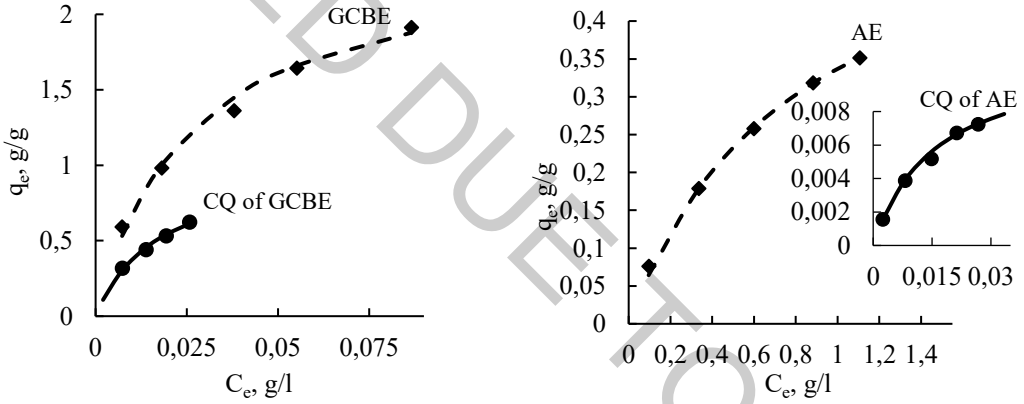

Fig. 1. Adsorption isotherms of GCBE, AE and CQ of the extracts on ChS at 30 °C temperature. Symbols represent experimental data and lines represent fitted curves of the Langmuir adsorption model.

It has been estimated by UPLC-UV method that the content of adsorbed CQ was only 1.64 % and 6.12 % of the total amount of adsorbed AE and GCBE, respectively. The obtained results indicated that not only CQ derivatives but also other phenolic compounds of natural extracts have been immobilized on ChS.

It was demonstrated by growth inhibition bioassay that GCBE/ChS and AE/ChS complexes possess some antifungal activity against *B. cinerea* and *F. graminearum* strains. AE/ChS showed higher inhibition effect on mycelial growth of *B. cinerea* and *F. graminearum* when compared to GCBE/ChS (see Table 1).

Table 1. Antifungal activity of GCBE/ChS and AE/ChS complexes against *B. cinerea* and *F. graminearum*

Sample	Inhibition of growth at day 4 (%)	
	Botrytis cinerea	*Fusarium graminearum*
AE/ChS	50.1	16.1
GCBE/ChS	37.2	5.6

Acknowledgment. The financial support of the Research Council of Lithuania for the Lithuanian-French programme "Gilibert" project No. S-LZ-19-6 is highly acknowledged.

[1] N. Nakatani, S.I. Kayano, H. Kikuzaki, K. Sumino, K. Katagiri, T. Mitani, Identification, quantitative determination, and antioxidative activities of chlorogenic acid isomers in prune (*Prunus domestica L.*), Journal of Agricultural and Food Chemistry **48** 5512-5516 (2000).
[2] B. Halliwell, Are polyphenols antioxidants or pro-oxidants? What do we learn from cell culture and in vivo studies? Archives of Biochemistry and Biophysics **476** 107-112 (2008)

CANCELLED DUE TO COVID-19

ADSORPTION OF IBUPROFEN FROM AQUEOUS MEDIUM ON CHEMICALLY MODIFIED STARCH

Paulina Andriunaite[1], Vesta Navikaite-Snipaitiene[1], Deimante Rosliuk[1]

[1] Department of Polymer Chemistry and Technology, Kaunas University of Technology, Kaunas, Lithuania
paulina.andriunaite@ktu.edu

Pharmaceutical wastewaters are very hazardous and toxic for the human and environmental life. Ibuprofen is among the most frequently reported active pharmaceutical ingredients in ambient monitoring studies and detected in drinking water at high concentrations (> 1 μg/L). This is due to its high consumption allied with the poor efficiency of conventional water treatment processes for its removal [1]. The aim of this work was to study the adsorption of ibuprofen from water on cross-linked cationic starch.

The cross-linked cationic starch (CLCS) microgranules were obtained by chemical modification of potato starch. CLCS was obtained by cross-linking starch with 0.1 mol/AGU (anhydroglucoside unit) of epichlorohydrin and cationization with 2,3-epoxypropyltrimethyammonium chloride. Degree of substitution of quaternary ammonium groups was equal to 0.33.

The ibuprofen (IBU) adsorption on CLCS microgranules was investigated by employing the equilibrium adsorption method. The Langmuir, Freundlich and Dubinin–Radushkevich adsorption models were used to describe the adsorption isotherms. The obtained isotherms of IBU adsorption on CLCS at different temperatures are presented in Fig. 1.

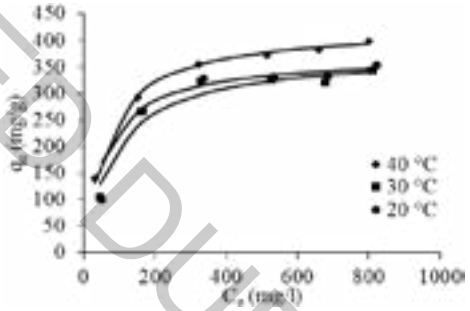

Fig. 1. Adsorption isotherms of IBU on CLCS at different temperatures. The symbols stand for experimental data whereas the lines represent the fitted curves of the Langmuir adsorption model.

According to the Langmuir adsorption model, the IBU molecules were adsorbed on the active centers i.e. quaternary ammonium groups of CLCS. Decreasing the temperature from 40 to 20 ºC the amount of the adsorbed IBU varied from 426 to 372 mg/g, respectively (Table 1). The values of Freundlich constant n_F and Dubinin–Radushkevich adsorption energy E_{DR} indicated that conditions for IBU adsorption on CLCS were favorable and the ion-exchange mechanism was predominant during adsorption.

Table 1. Adsorption models parameters for adsorption of IBU on CLCS at different temperatures

T(ºC)	**Langmuir model**		**Freundlich model**		**Dubinin-Radushkevich model**	
	Q_L *(mg/g)*	R^2	n_F	R^2	E_{DR} *(kJ/mol)*	R^2
40	426	0.9994	3.17	0.9433	12.5	0.9686
30	378	0.9953	2.55	0.8493	10.5	0.8871
20	372	0.9969	2.34	0.8471	9.8	0.8843

Table 2. Thermodynamic parameters of IBU adsorption on CLCS

T (ºC)	*ΔG (kJ/mol)*	R^2	*ΔH (kJ/mol)*	*ΔS (J/mol·K)*	R^2
40	-7.10	0.9956			
30	-3.81	0.9673	56.32	201.17	0.8693
20	-3.02	0.9727			

The thermodynamic characteristics of IBU adsorption on CLCS have been evaluated (Table 2). The negative values of ΔG indicated that adsorption of IBU onto CLCS is spontaneous. The positive values of the change in enthalpy ΔH and entropy ΔS show that adsorption of IBU on CLCS was endothermic process, and the order of the system decreases during the adsorption process.

[1] J. Martín, M. Del Mar Orta, S. Medina-Carrasco, J. L. Santos, I. Aparicio, E. Alonso., Evaluation of a modified mica and montmorillonite for the adsorption of ibuprofen from aqueous media, Applied Clay Science **171**, 29-37 (April 2019).

CANCELLED DUE TO COVID-19

IMMOBILIZATION OF CAFFEIC ACID ON CROSS-LINKED CATIONIC STARCHES WITH DIFFERENT DEGREE OF SUBSTITUTION

Diana Masiulionyte[1], Deimante Rosliuk[1], Ramune Rutkaite[1], Véronique Coma[2]

[1] Department of Polymer Chemistry and Technology, Kaunas University of Technology, Lithuania
[2]University of Bordeaux, UMR 5629, CNRS, LCPO, 16 Avenue Pey Berland, 33607 Pessac, France
diana.masiulionyte@ktu.edu

CANCELLED DUE TO COVID-19

Caffeic acid (CA) is hydroxycinnamic acid derivative, with antioxidant, anti-inflammatory, and anticancer activities. However, the application of CA is restricted because of its readily oxidation, low bioavailability, sensitivity to heat, light and moisture. In order to overcome these disadvantages this anionic phenolic compound could be immobilized on cationic polymers such as cross-linked cationic starch.

In the present study, the equilibrium adsorption of CA on cross-linked cationic starch (CCS) derivatives with different degree of substitution (DS) of quaternary ammonium groups was investigated. The Langmuir, Freundlich and Dubinin–Radushkevich adsorption models were applied to describe the adsorption isotherms of CA (Fig. 1, Table 1).

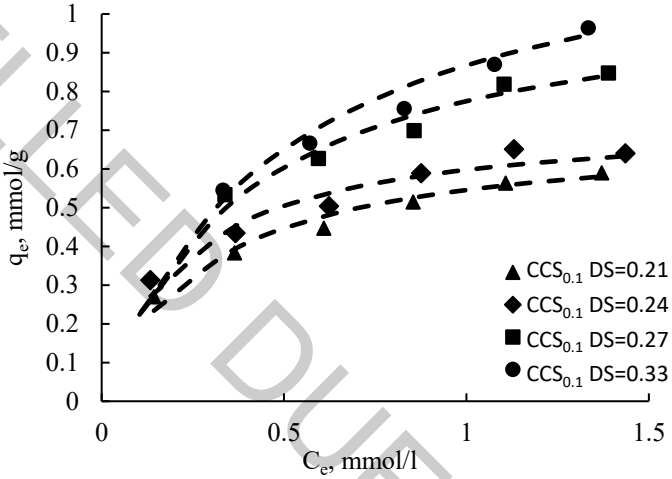

Fig. 1. Adsorption isotherms of CA on CCS with different DS at temperature of 30 °C. Symbols represent experimental data and lines represent fitted curves of the Langmuir adsorption model.

Table 1. Adsorption model parameters for adsorption of CA on CCS with different DS at temperature of 30 °C

Adsorbent	Langmuir model				Freundlich model		Dubinin-Radushkevich model	
	Q_L (mmol/g)	K_L (1/mol)	EF	R^2	n_F	R^2	E_{DR} (kJ/mol)	R^2
$CCS_{0.1}$ DS=0.21	0.70	3488	0.65	0.9918	2.85	0.9978	11.8	0.9980
$CCS_{0.1}$ DS=0.24	0.73	4368	0.61	0.9936	2.95	0.9948	12.2	0.9893
$CCS_{0.1}$ DS=0.27	1.08	2510	0.81	0.9845	3.08	0.9924	12.0	0.9863
$CCS_{0.1}$ DS=0.33	1.30	1993	0.84	0.9911	2.44	0.9984	10.7	0.9959

According to the Langmuir adsorption model, CA was adsorbed on the active centres of CCS, i.e. on the quaternary ammonium groups. The driving forces of adsorption were interactions between these groups and carboxylic groups of phenolic acid. As could be seen, with the increase of DS of CCS the values of the Langmuir sorption capacity Q_L and adsorption efficiency EF increased. Meanwhile, the calculated values of Dubinin-Radushkevich adsorption energy E_{DR} confirmed that CA was adsorbed by ion exchange mechanism and values of Freundlich constant n_F showed that conditions for CA adsorption on all CCS derivatives were favourable.

Acknowledgement. The financial support of the Research Council of Lithuania for the Lithuanian-French programme “Gilibert” project No. S-LZ-19-6 is highly acknowledged.

EPR SPECTROSCOPY OF MANGANESE DOPED $[NH_4][Zn(HCOO)_3]$ FORMATE FRAMEWORK

Marius Navickas[1], Laisvydas Giriūnas[1], Vidmantas Kalendra[1], Timur Biktagirov[2], Uwe Gerstmann[2], Wolf Gero Schmidt[2], Mirosław Mączka[3], Andreas Pöppl[4], Jūras Banys[1], Mantas Šimėnas[1]

[1]Faculty of Physics, Vilnius University, Sauletekio 9, LT-10222 Vilnius, Lithuania
[2]Department of Physics, Paderborn University, Warburger 100, D-33098 Paderborn, Germany
[3] Institute of Low Temperature and Structure Research, Polish Academy of Sciences, P.O. Box-1410, PL-50-950 Wroclaw, Poland
[4]Felix Bloch Institute for Solid State Physics, Leipzig University, Linnestrasse 5, D-04103 Leipzig, Germany
marius.navickas@ff.vu.lt

Metal-organic frameworks (MOFs) are extensively studied hybrid materials due to their potential applications in gas storage and separation systems and multiferroic memory devices [1, 2]. These coordination networks are formed from various organic linker molecules and metal centers that constitute porous structures. In the so called dense MOFs, the pore system inherently confines molecules, which are tightly bound to the framework. The most popular class of dense MOFs is metal-formate frameworks, which often exhibit interesting ferromagnetic and ferroelectric properties. These compounds consist of transition metal ions linked by formate linkers into porous frameworks, where each pore confines a molecular cation. Many members of these frameworks exhibit structural phase transitions, related to molecular cation ordering and metal-formate framework deformation. A useful method to study local changes in formate frameworks is electron paramagnetic resonance (EPR) spectroscopy.

In this work we present X-band and Q-band continuous wave (CW), pulse EPR and electron nuclear double resonance (ENDOR) study of manganese doped $[NH_4][Zn(HCOO)_3]$ (AmZnF) hybrid formate framework, which exhibits ferroelectric phase transition at 190 K. The CW EPR spectra obtained at different temperatures indicate successful substitution of the Zn^{2+} centers by paramagnetic Mn^{2+} ions allowing us to probe and characterize the structural phase transition. The obtained non-zero value of the zero-field splitting (ZFS) at low temperature shows the deformation of the MnO_6 octahedra. The temperature dependence the ZFS parameter (presented in Fig. 1.) indicates the continuous character of the phase transition. CW EPR results are supported by the density functional theory calculations.

In order to study the broader environment of the Mn^{2+} probe ion, we performed pulse EPR experiments [3]. The two and three-pulse electron spin echo envelope modulation (ESEEM) measurements data indicates the interaction between Mn^{2+} center and protons. ENDOR spectrum shows the interactions of different protons with Mn^{2+} center. The two-dimensional hyperfine sublevel correlation (HYSCORE) EPR spectrum also indicates proton interactions and demonstrates the signal of ^{13}C.

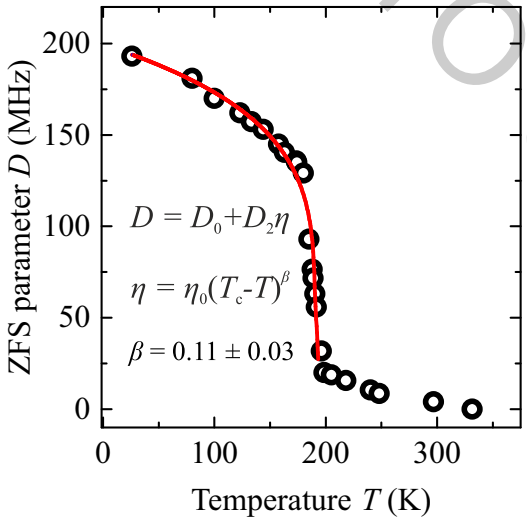

Fig. 1. Temperature dependence of the axial ZFS parameter D of the Mn^{2+} ions in AmZnF. The solid curve indicates the best fit .

[1] B. Li, H.-M. Wen, W. Zhou et al., Porous metal-organic framework for gas storage and separation: what, how and why?, The journal of physical chemistry letters **5**, 3468-3479 (2014).
[2] P. Jain, A. Stroppa, D. Nabok et al., Switchable electric polarization and ferroelectric domains in a metal–organic–framework, Npj Quantum Materials **1**, 1-6 (2016).
[3] A. Schweiger, *Principles of Pulse Electron Paramagnetic Resonance* (Oxford University Press, 2001).

CANCELLED DUE TO COVID-19

STARCH ACETATE SORBENT FOR REMOVAL OF METILPARABEN FROM WATER

Karolina Aleknaite, Deimante Rosliuk, Ugne Naruseviciute

Department of Polymer Chemistry and Technology, Kaunas University of Technology, Lithuania
karolina.aleknaite@ktu.edu

The increased contamination of aquatic environment and water resources by industrial activity became a serious threat to the sustainability of society [1, 2]. The ineffectiveness of traditional mechanical and biological water treatments to remove some specific organic compounds, such as parabens, requires to search for new ways to eliminate these contaminants.

The aim of this research was to study the binding of metilparaben to starch acetate sorbent in water.

Starch acetate (SA) microgranular sorbent (degree of substitution of acetic groups was equal to 0.34) was obtained by reacting anhydroglucoside unit of starch (AGU) with acetic anhydride (AA) using 50% aqueous NaOH as the catalyst for 4 h at 125ºC (the molar ratio AGU : AA : NaOH was 1 : 6.36 : 2.75).

The adsorption kinetics of MP on SA was investigated (Fig. 1). The adsorption kinetics showed that the adsorption equilibrium is practically achieved within 7 min. To achieve complete equilibrium, the experiment was extended to 30 min.

The metilparaben (MP) was partially removed from water by adsorption on SA microgranules. The Langmuir, Freundlich and Dubinin–Radushkevich adsorption models were applied to describe the adsorption isotherms of MP (Fig. 2, Table 1).

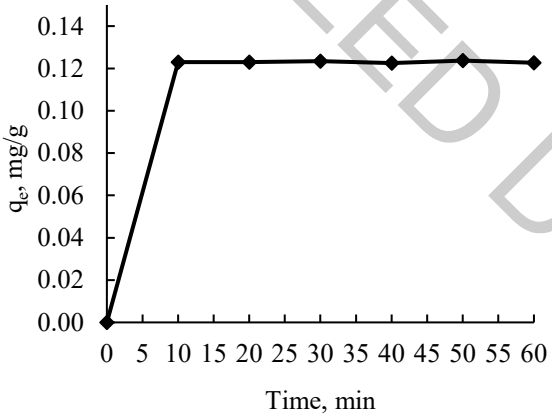

Fig. 1. The adsorption kinetics of MP on SA at temperature of 20 ºC

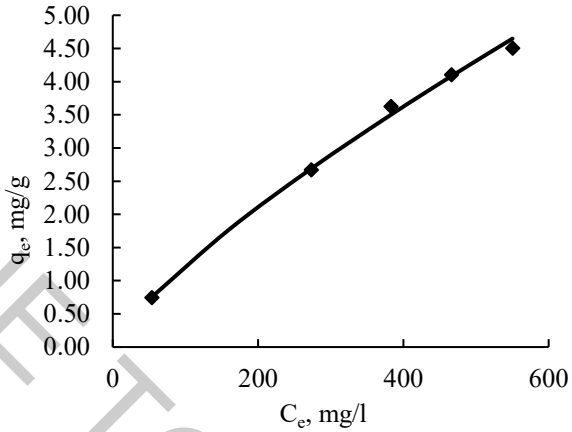

Fig. 2. Adsorption isotherm of MP on SA (DS=0.34) at temperature of 20 ºC. Symbols represent experimental data and lines represent fitted curves of the Freundlich adsorption model

Table 1. Adsorption model parameters for adsorption of MP on SA (DS=0.34) at temperature of 20 ºC

Langmuir model			Freundlich model		Dubinin-Radushkevich model	
Q_L, mg/g	K_L, 1/g	R^2	n_F	R^2	E_{DR}, kJ/mol	R^2
10.19	32791	0.9654	1.28	0.9989	7.2	0.9987

The values of $R^2 > 0.99$ support the fact that the adsorption of MP closely follows the Freundlich adsorption model. The value of the Langmuir sorption capacity Q_L showed the amount of MP adsorbed at equilibrium, i. e. 10.19 mg/g. The calculated values of Dubinin-Radushkevich adsorption energy E_{DR} indicated that MP was adsorbed due to physical forces, possible because of hydrophobic properties, and values of Freundlich constant n_F showed that conditions for MP adsorption on SA were moderately difficult.

[1] C. Haman, X. Dauchy, C. Rosin, J.-F. Munoz, Occurrence, fate and behavior of parabens in aquatic environment: A review, Water Research **68**, 1-11 (2015).

[2] Q. Mao, Q. Li, H. Li, S. Yuan, J. Zhang, Oxidative paraben removal with chlorine dioxide: Reaction kinetics and mechanism, Separation and Purification Technology **237**, 116327, (2020).

CANCELLED DUE TO COVID-19

SYNTHESIS AND APPLICATION OF UPCONVERSION MATERIALS IN ANTICOUNTERFEITING

Julija Grigorjevaite[1], Arturas Katelnikovas[1]

[1] Institute of Chemistry, Faculty of Chemistry and Geosciences, Vilnius University,
Naugarduko 24, LT-03225 Vilnius, Lithuania
julija.grigorjevaite@chf.vu.lt

CANCELLED DUE TO COVID-19

One of the most serious worldwide problems is counterfeiting. The forgery of currency, goods or important documents is a huge problem for everyone, including government bodies and big companies. The modern achievements in science and technology create new ways to overcome this serious problem [1]. One of many techniques is security printing.

Luminescent materials emitting in the visible range upon ultraviolet light excitation are used for security printing, holograms, luminescent markers and security labels. All of anti-counterfeiting techniques have advantages and limitations. From this point of view, luminescent materials improved security pigments industry due to their unique optical properties. Usually lanthanides-rich materials are used as luminescent pigments in the security printing.

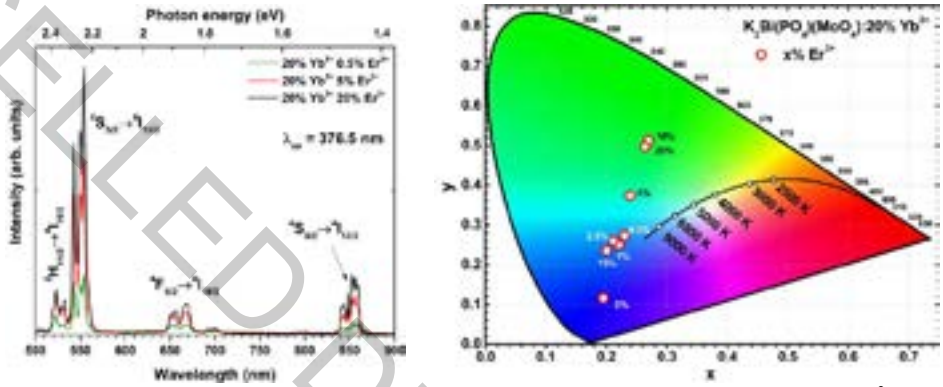

Fig. 1. Emission spectra (on the left) and colour points (on the right) of $K_2Bi(PO_4)(MoO_4)$:20%Yb^{3+} doped with 0.5%, 5% and 20% Er^{3+} under 376.5 nm excitation.

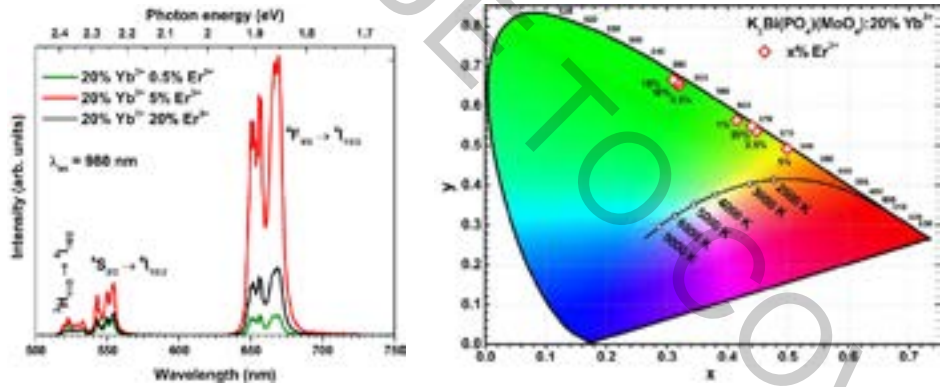

Fig. 2. Upconversion emission spectra (on the left) and colour points (on the right) of $K_2Bi(PO_4)(MoO_4)$:20%Yb^{3+} doped with 0.5%, 5% and 20%Er^{3+} under 980 nm laser excitation.

Our recent work represent new inorganic materials for anti-counterfeiting application. The synthesized $K_2Bi(PO_4)(MoO_4)$ host matrix was co-doped with 20% of Yb^{3+} and different percentage of Er^{3+}. These materials showed good colour saturation, high luminous efficacies, and good quantum efficiencies. Moreover, materials show different emission under 376.5 nm and under 980 nm laser excitation. The most intense 5% Er^{3+} doped material show green emission under UV light (see Fig. 1) meanwhile sample colour changes to orange-red under laser excitation (see Fig. 2). These features are typical for upconversion materials [2]. Characterization and investigation of the optical properties will be discussed.

This research was funded by a grant (No. D-2018-0703 “Controlling the upconversion emission by tuning band gap of the host matrix”) from the Research Council of Lithuania.

[1] Bayart, A., Szczepanski, F., Blach, J. F., Rousseau, J., Katelnikovas, A., Saitzek, S., Upconversion luminescence properties and thermal quenching mechanisms in the layered perovskite $La_{1.9}Er_{0.1}Ti_2O_7$ toward an application as optical temperature sensor, Journal Alloys and Compounds, 744, 2018, 516-527.

[2] Liu, Y., Liu, Y., Liu, G., Dong, X., Wang, J., Up/down conversion, tunable, photoluminescence and energy transfer properties of $NaLa(WO_4)_2$:Er^{3+}, Eu^{3+} phosphors, RSC Adv. 5, 2015, 97995-98003.

THE DETERMINATION OF VARIOUS BOTANICAL ORIGIN STARCH CROSSLINKING WITH EPICHLOROHYDRIN AND CROSLINKING DEGREE METHODOLOGY

Greta Čižauskaitė, Karolina Almonaitytė, Joana Bendoraitienė

Department of Polymer Chemistry and Technology, Kaunas University of Technology, Lithuania
greta.cizauskaite@ktu.edu

CANCELLED DUE TO COVID-19

Cross-linking starches most used in the paper and glue industry. Crosslinking occurs when a cross-linking agent introduces intermolecular bridges between polysaccharide macromolecules. Cross-linked starches are resistant to high temperature, low pH, and higher shear, and they also improve viscosity and textural properties of the native starch. Cross-linking granular starch reinforces hydrogen bonds holding the granule together. Various agents are used to crosslink native starch for example epichlorohydrin (EPI). The efficiency of the starch crosslinking reaction depends on the crosslinking agent concentration, temperature, reaction time, pH and botanical origin [1]. The purpose of the work was evaluate the epichlorohydrin starch cross-linking methodology, taking into account the starch botanical origin, granule size and suspension concentration, and optimize and predict the cross-linking process.

The purpose of the work potato, wheat, tapioca and corn starches was mixed by the reaction with sodium hydroxide solution and crosslinking agent EPI, whose the molar ratio of the AGU : EPI : NaOH : H_2O was 1 : 0,01 : 0,012 : 10 . The reaction mixture was maintained the temperature at 45°C for 1 h, 3 h, 5 h, 24 h, 48 h and pH 10. To end the reaction, added 1M solution of HCl to pH 5. Later reaction was filter, washed with distillation water and dried at 105°C.

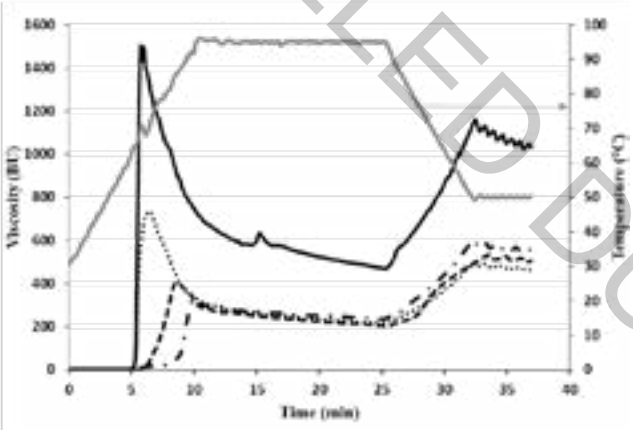

Fig. 1 Viscoamylogram of various botanical origin starch aqueous suspension (8%) of the control sample: (—) – potato starch; (---) – tapioca starch; (– – –) – corn starch; (— · — ·) – wheat starch

Table. 1. The degree of crosslinking of various botanical starch

Reaction time(h) / Starch	1	3	5	24	48
	Degree of crosslinking (%)				
Potato	-*	97.8±1.4	98.0±1.3	94.5±2.0	98.5±1.2
Wheat	23.1±3.6	74.2±4.3	89.4±3.5	94.2±1.2	92.7±1.5
Tapioca	14.9±2.4	-*	90.7±1.1	97.8±2.1	97.0±1.8
Corn	-*	83.7±2.1	97.7±1.4	96.2±2.6	97.2±2.4

* - Values are obtained by using the starch degree of determination method, which may be inappropriate for the low degree of estimation

Rheological properties and crosslinking degree of starch and cross-linked starch of different botanical origin were determined. The rheological properties - degree of cross–linking of starch different botanical origin was determined by estimating viscosity parameters of aqueous slurries (8 % starch and water suspension) of modified starches according the procedure by using a Micro Visco - Amylo - Graph® (Brabender, Germany). Controlled heating-and-cooling cycle under constant shear: heating from 30 to 95 °C at a heating rate of 6.5 °C/min. Viscoamylograph of various botanical origin starch from control sample viscosity is different as demonstrated in scheme in Fig. 1. The degree of crosslinking was estimated using the equation (1) [2] and degree of crosslinking is demonstrated in the table in Table. 1

$$Degree\ of\ crosslinking = \frac{A-B}{A} \cdot 100\% \quad (1)$$

where A is the peak viscosity in Brabender units of the control sample (0% EPI) and B is that of the crosslinked starch sample.

The degree values of crosslinking are obtained by using a cross-linking methodology which may be inappropriate to calculate the low crosslinking degree. However, the rheological properties indicate that, as the starch crosslinking reaction time increases, the crosslinking degree increases, meaning the starch paste viscosity decreases, as starch forms a crosslink starch macromolecules.

Acknowledgement. This research was funded by the European Social Fund under the measure No 09.3.3-LMT-K-712 "Development of Competences of Scientists, other Researchers and Students through Practical Research Activities"

[1] Ali S. Ayoub and Syed S. H. Rizvi (2009). An Overview on the Technology of Cross-linking of Starch for nonfood applications. Journal of Plastic Film and Sheeting. Department of Food Science, Stocking Hall, Ithaca, New York 14 853, USA,p 26-27.
[2] Joana Bendoraitiene, Edita Lekniute – Kyzike, Ramune Rutkaite (2018). Biodegradation of cross-linked and cationic starches, International Journal of Biological Macromolecules 119, 345-351.

MODIFIED STARCH SORBENTS FOR THE REMOVAL OF DICLOFENAC AND IBUPROFEN FROM WATER

Vesta Navikaite-Snipaitiene[1], Ramune Rutkaite[1], Deimante Rosliuk [1], Karolina Almonaityte[1], Vaida Vaskeliene[2], Renaldas Raisutis[2]

[1] Department of Polymer Chemistry and Technology, Kaunas University of Technology, Kaunas, Lithuania
[2] Prof. Kazimieras Barsauskas Ultrasound Research Institute, Kaunas University of Technology, Kaunas, Lithuania
vesta.navikaite@ktu.lt

CHEMIJOS DOKTORANTŪRA COVID 19

Non-steroidal anti-inflammatory drugs (NSAIDs) are widely used pharmaceuticals. These drugs treat human and animal diseases in terms of analgesic, anti-inflammatory, and antipyretic actions. Consequently, NSAIDs are among the most detected drugs in the aquatic environment. Unfortunately, traditional mechanical and biological wastewater treatment technologies are insufficient for the removal of this type of contaminants [1]. The aim of this research was to study the removal of diclofenac and ibuprofen from aqueous medium by using modified starch.

Cross-linked cationic starch (CCS) microgranular sorbent was obtained by the means of chemical and physical modification of potato starch. CCS was obtained by cross-linking potato starch with 0.1 mol/AGU (anhydroglucoside unit) of epichlorohydrin and cationizated with 2,3-epoxypropyltrimethyammonium chloride using various molar ratios of reagents. The starch derivatives with the degree of substitution of quaternary ammonium groups of 0.21, 0.33 and 0.42 were synthesized. The CCS granules were additionally treated by using ultrasonication in water (treatment conditions: 40 kHz, 300 W, 30 sec., 24±1 °C). Sorbents granules were characterized by scanning electron microscopy (see Fig.1).

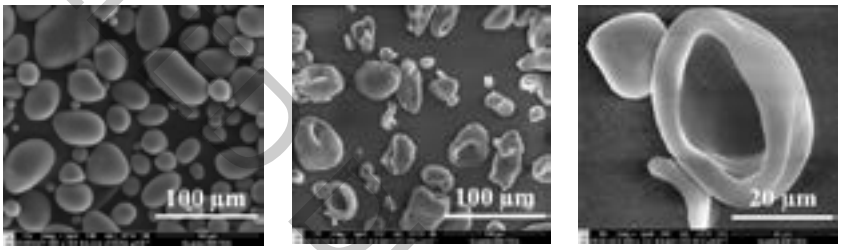

(a) (b) (c)

Fig.1. SEM micrographs of CCS/0.21 (a, ×1000) and ultrasound treated CCS/0.21 (b, ×1000; c ×5000) granules

The diclofenac or ibuprofen were partially removed from water by adsorption onto CCS or ultrasound treated CCS granules (CCSU). The Langmuir, Freundlich and Dubinin-Radushkevich adsorption models have been used to describe the equilibrium adsorption of ibuprofen or diclofenac onto CCS and CCSU. According to the Langmuir adsorption model, the diclofenac and ibuprofen were adsorbed on quaternary ammonium groups of CCS or CCSU. The sorption ability of ultrasound treated sorbent was much higher in comparison to non-treated sorbent (see Table 1). For diclofenac, the highest sorption capacity of CCS and CCSU was 614 and 787 mg/g, respectively. Meanwhile, when binding ibuprofen, the highest sorption capacity of CCS and CCSU was 345 and 579 mg/g, respectively. Consequently, the binding improvement of diclofenac and ibuprofen on ultrasound treated sorbent granules was 28 % and 68 %, respectively.

Table 1. Langmuir sorption capacity (Q_L) of CCS and CCSU by adsorbing diclofenac or ibuprofen at 30 °C temperature

Sorbent	Adsorption of diclofenac		Adsorption of ibuprofen	
	Q_L (mg/g)	R^2	Q_L (mg/g)	R^2
CCS/0.21	340	0.9999	232	0.9982
CCSU/0.21	411	0.9992	574	0.9952
CCS/0.33	629	0.9996	378	0.9916
CCSU/0.33	738	0.9998	531	0.9982
CCS/0.42	614	0.9996	345	0.9975
CCSU/0.42	787	0.9994	579	0.9958

The values of Freundlich constant (n_F=2-5) and Dubinin–Radushkevich adsorption energy (E_{DR}=9-16) indicated that conditions for diclofenac or ibuprofen adsorption on CCSU were favourable and the ion-exchange mechanism was predominant during adsorption.

Acknowledgment. This research was supported by the Research, Development and Innovation Fund of Kaunas University of Technology (project grant No. PP-91D/19).

[1] M. J. Ahmed., Adsorption of non-steroidal anti-inflammatory drugs from aqueous solution using activated carbons: Review, Journal of Environmental Management **190**, 274-282 (01 April 2017).

NMR SPECTROSCOPY OF STRUCTURAL PHASE TRANSITION IN $CH_3NH_2NH_2PbCl_3$ HYBRID PEROVSKITE

Laisvydas Giriūnas[1], Marko Bertmer[2], Mirosław Mączka[3], Jūras Banys[1], Mantas Šimėnas[1]

[1]Faculty of Physics, Vilnius University, Saulėtekio 9, LT-10222 Vilnius, Lithuania
[2]Felix Bloch Institute for Solid State Physics, Leipzig University, Linnestrasse 5, D-04103 Leipzig, Germany
[3]Institute of Low Temperature and Structure Research, Polish Academy of Sciences, P.O. Box-1410, PL-50-950 Wroclaw, Poland
laisvydas.giriunas@ff.vu.lt

CANCELLED DUE TO COVID-19

In recent years hybrid lead halide perovskites have received exceptional attention in the scientific community due to their potential application in photovoltaic devices. Solar cells based on these hybrid compounds have already reached the power conversion efficiency of more than 20%. These materials do not only have superior physical properties, but they are also higly tunable due to a variety of organic and inorganic materials that can be incorporated into such hybrid structures [1]. Hybrid lead halide perovskites are composed of lead Pb^{2+} centers joined together by halogen (Cl^-, Br^-, or I^-) anions into a porous framework. Each pore confines a single molecular cation ($CH_3NH_3^+$, $CH_3NH_2NH_2^+$, etc.). The majority of such perovskites exhibit structural phase transitions followed by the cation ordering and framework deformation [2]. Among many techniques used for characterization of crystal properties, solid-state nuclear magnetic resonance (NMR) spectroscopy is an exceptionally effective method in studying structural phase transitions and dynamics [3].

In this work we present a ^1H and ^{207}Pb NMR study of methyl-hydrazinium lead chloride $CH_3NH_2NH_2PbCl_3$ hybrid perovskite using the magic angle spinning (MAS) technique. In this crystal lead centers are linked with chlorine ions forming a three dimensional framework with two different types of $PbCl_6$ octahedra. Each pore contains a single MHy^+ cation which is bonded to the $PbCl_3^-$ framework. Upon heating this material exhibits a structural phase transition at around 340 K. ^1H NMR experiments show a broad signal which is not being affected by the phase transition. ^{207}Pb NMR measurements demonstrate two signals (see Fig. 1) which represent two differently deformed $PbCl_6$ octahedra. The temperature dependence of these spectra in Fig. 1 and their parameters define various properties of the phase transition.

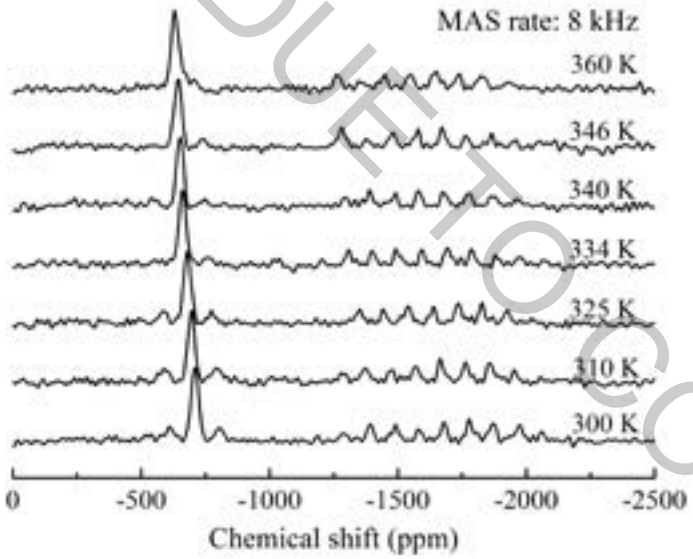

Fig. 1. Temperature dependent ^{207}Pb NMR spectra of $CH_3NH_2NH_2PbCl_3$. MAS rate was set to 8 kHz.

[1] Bryan A. Rosales *et al.*, Lead halide perovskites: Challenges and opportunities in advanced synthesis and spectroscopy, ACS Energy Letters **2**, 906-914(2017).
[2] I. Anusca *et al.*, Dielectric response: Answer to many questions in the methylammonium lead halide solar cell absorbers. Advanced Energy Materials, **7**, 1700600 (2017).
[3] C. Odin, NMR studies of Phase Transitions, Annual Reports on NMR Spectroscopy, **59**, 117-205 (2006).

EPOXY COMPOSITES LOADED WITH CARBON NANOTUBES AND GRAPHENE

Evgeni Ovodok[1], Hanna Maltanava[1], Sergey Poznyak[1], Vladimir Kurilo[2], Gediminas Monastyreckis[3], Daiva Zeleniakiene[3], Maria Omastava[4], Matej Micusik[4]

[1]Research Institute for Physical Chemical Problems, Belarusian State University, Belarus
[2]Belarusian State University, Belarus
[3]Kaunas University of Technology, Lithuania
[4]Polymer Institute, Slovak Academy of Sciences, Slovakia
ovodok@bsu.by

Addition of carbon based nanoparticles to polymers can improve thermal, mechanical, electrical properties, electromagnetic interference shielding effectiveness (EMI SE) of the composites [1]. The present work has focused on the preparation of epoxy-based composites loaded with various amounts of multiwall carbon nanotubes (MCNTs), graphene nanoparticles (GNPs), MCNTs/GNPs mixtures, and study of their electrical, mechanical properties and EMI SE in the X-band frequency range.

Epoxy resin Biresin CR122 and hardener CH122-5 were provided by SIKA. MCNTs NC7000™ having an average diameter of 9.5 nm and an average length of 1.5 μm were supplied by Nanocyl S.A. (Belgium). Elicarb® graphene epoxy dispersion was produced by Thomas Swan. The electrical conductivity of the epoxy-based composites was measured on cylindrical samples by standard two-point contact method. The EMI shielding efficiency was measured with an Agilent 8722ET transmission/reflection network analyzer at samples with thickness of 1.5 mm in the frequency range from 9 to 11 GHz. A Tinius Olsen H25KT machine equipped with a video extensometer PoE 1 was used for strain measurements.

Optical microscopy studies showed that the MCNTs or GNPs are uniformly distributed in the composites. The conductivity of free epoxy is very low (< 10^{-9} S/m). Addition of the MCNTs to the epoxy matrix leads to an increase in the composite conductivity. The conductivity rises up to 4 S/m with increasing the amount of MCNTs up to 2 wt.%. The percolation threshold for the composites filled with MCNTs is found to be 0.013 wt.%. In comparison with MCNTs, introduction of GNPs into the polymer up to 10 wt.% does not change appreciably the conductivity of the epoxy matrix. EMI shielding efficiency measurements showed that thick film composite samples with split MCNTs absorb electromagnetic waves in the range from 9 to 11 GHz when the MCNTs loading is higher than 0.05 wt.% (Figure 1a). A rise of the MCNTs content in the composite leads to an increase in the shielding efficiency by absorption and reflection (EMI SE). The value of EMI SE grows up to 13 dB when 2 wt.% of MCNTs is loaded in the composite. As compared with MCNTs, GNPs in the epoxy composites cause only slight increase in EMI SE. At the same time, addition of GNPs to the MCNTs/epoxy composites leads to an appreciable improvement of the EMI SE of the composites. Tensile strength of the free epoxy composite is 70÷80 MPa. Its value appreciably decreases with increasing the MCNTs amount (Fig. 1b). Introduction of the graphene nanoparticles up to 5 wt.% does not influence noticeably the tensile strength of the epoxy based composites (Fig. 1b). The mechanical properties of the MCNTs + GNPs composites were similar to that of the MCNTs-loaded composites without GNPs (Fig. 1b).

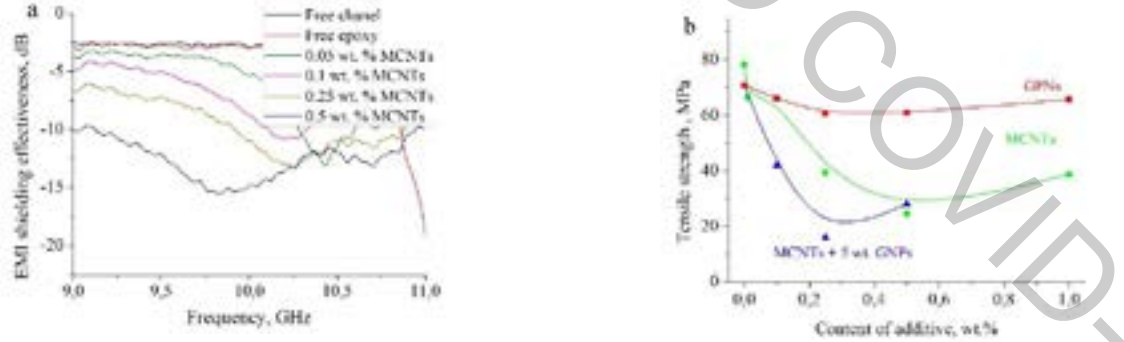

Fig. 1. EMI shielding effectiveness of the composites loaded with different amount of MCNTs (a) and dependence of tensile strength vs. concentration of additives for the epoxy composites filled by different amount of MCNTs, GNPs, MCNTs/GNPs (b)

In conlusion, the conductivity of the prepared composites is determined by the MCNTs concentration. An addition of GNPs to the MCNTs-loaded composites almost does not influence the conductivity of the composites, but improves their EMI shielding effectiveness in X-band frequency range. The MCNTs loading is found to result in the degradation of the mechanical properties of the composites, while addition of GNPs only slightly weakens the tensile strength.

Acknowledgment
This work has received funding from the European Union's Horizon 2020 research and innovation programme under the Marie Skłodowska-Curie grant agreement № 777810 and grant № APVVSK-BY-RD-19-0011.

[1] W.Bauhofer, J. Kovacs, A review and analysis of electrical percolation in carbon nanotube polymer composites, Compos Sci Technol **69**, 1486-1498 (2009).

CANCELLED DUE TO COVID-19

TAPE CASTING AND DIELECTRIC CHARACTERISTICS OF NBYT THICK FILMS

Tomas Kudrevičius[1], Artyom Plyushch[1], Šarūnas Svirskas[1], Algirdas Selskis[1], Marija Dunce[2], Eriks Birks[2], Jūras Banys[1]

[1]Faculty of Physics, Vilnius University, Sauletekio 9/3, LT10222 Vilnius, Lithuania.
[2]Institute of Solid State Physics, University of Latvia, Kengaraga st. 8, 1063, Riga, Latvia
tomas.kudrevicius@ff.stud.vu.lt

CANCELLED DUE TO COVID-19

Because of environmental regulations against high amounts of lead used in ferroelectric materials (RoHS directive in EU) a lot of studies have been done in order to find the best lead-free alternatives. $Na_{0.5}Bi_{0.5}TiO_3$ (NBT) based compositions contain quite large dielectric values and high electromechanical strain [1]. One of the most prominent techniques to create multi-layered ceramic structures is tape casting. This technology can provide high quality, large-area and thin functional materials such as ferroelectrics, piezoelectrics for multilayered capacitors [2]. Tape casting is mostly based on non-aqueous solvent but aqueous-based tape casting is also used as simple and eco-friendly method.

In this work NBT was doped with Yb (Y) and the mains task was to investigate the change of dielectric characteristics by changing bismuth concentration. There were two compositions with different bismuth concentrations: first composition had 49.82 % of bismuth and the other one had 46.79 %. Thick films were produced via an aqueous tape casting method. Dispex AA4040 was used as a surfactant and PVP solution (Luvitec K 90 Pulver) as a binder. Both chemicals were provided by BASF. Two step 500 ºC and 1200 ºC (2 h) thermal treatment on platinum substrate followed the casting and drying. Resulting films were of 170 um thickness. Dielectric properties were measured at a temperature range 30 K - 750 K on cooling with a rate of 1 K/min. Also, electromechanical properties were investigated using commercial aixaCCT TF 2000 analyzer.

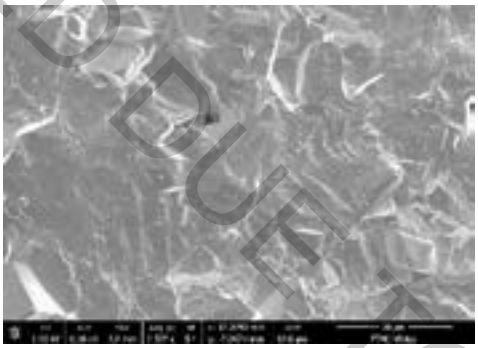

Fig 1. Scanning electron microscopy of $Na_{0.5}Bi_{0.49}Yb_{0.01}TiO_3$

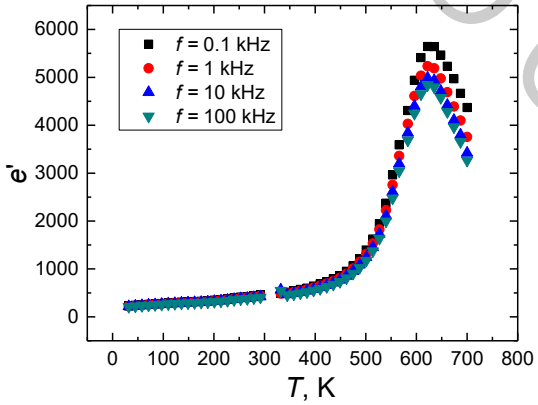

Fig 2. Temperature dependence of dielectric permittivity of $Na_{0.5}Bi_{0.49}Yb_{0.01}TiO_3$ concentration

Fig. 1 shows SEM image of NBYT thick film with 49.82 % of bismuth. This image shows that film is quite dense because there are just a few pores on surface. Fig. 2 shows temperature dependence of dielectric permittivity of concentration which has 49.82 % of bismuth. From this dependence it could be determined that phase transition occurs at a temperature of 630 K. This phase transition is from paraelectric phase to ferroelectric. No other dielectric anomalies were observed at lower temperatures.

[1] V. V. Shvartsman et al., "Lead-Free Relaxor Ferroelectrics," *Journal of the American Ceramic Society*, vol. 95, no. 1, pp. 1–26, Jan. 2012,
[2] M. Jabbari, R. Bulatova, A. I. Y. Tok, C. R. H. Bahl, E. Mitsoulis, and J. H. Hattel, "Ceramic tape casting: A review of current methods and trends with emphasis on rheological behaviour and flow analysis," *Materials Science and Engineering: B*, vol. 212, pp. 39–61, Oct. 2016.

SYNTHESIS AND PHOTOPHYSICAL PROPERTIES OF PHENOTHIAZINE-5,5-DIOXIDE BASED TADF DERIVATIVES

Edgaras Narbutaitis[1], Matas Gužauskas[2], Dmytro Volyniuk[1], Juozas Vidas Gražulevičius[1]

[1] Department of Polymer Chemistry and Technology, Kaunas University of Technology, Lithuania
[2]Department of Physics, Kaunas University of Technology, Lithuania
edgaras.narbutaitis@ktu.edu

In the recent decades, a significant research interest has been invested in the field of organic light-emitting diodes (OLED). While the efficiency of these devices has been greatly improved by introduction of heavy metal based phosphorescent emitters which utilize both singlet and triplet excitons, such compounds have several drawbacks [1]. While the cost and toxicity of these materials has been addressed by the introduction of all-organic thermally-activated delayed fluorescence (TADF) materials by Adachi et al. [2], blue TADF materials still exhibit quite long fluorescence decay lifetimes due to slow triplet exciton upconversion resulting in poor OLED stability.

In this work we present four novel TADF materials based on utilizing phenothiazine-5,5-dioxide as a push-pull donor moeity. The materials were synthesized in a simple and cost-effective two-step synthetic procedure consisting of nucleophilic substitution followed by oxidation. Structures of the materials were investigated by single crystal X-ray diffraction analysis. Photophysical properties of materials were investigated, the materials exhibit remarkably short (<100 ns) fluorescence lifetime decays in toluene solutions while still displaying common TADF characteristics: bathochromic shift in polar media, fluorescence intensity increase in deoxygenated solutions, low ΔE_{ST} values.

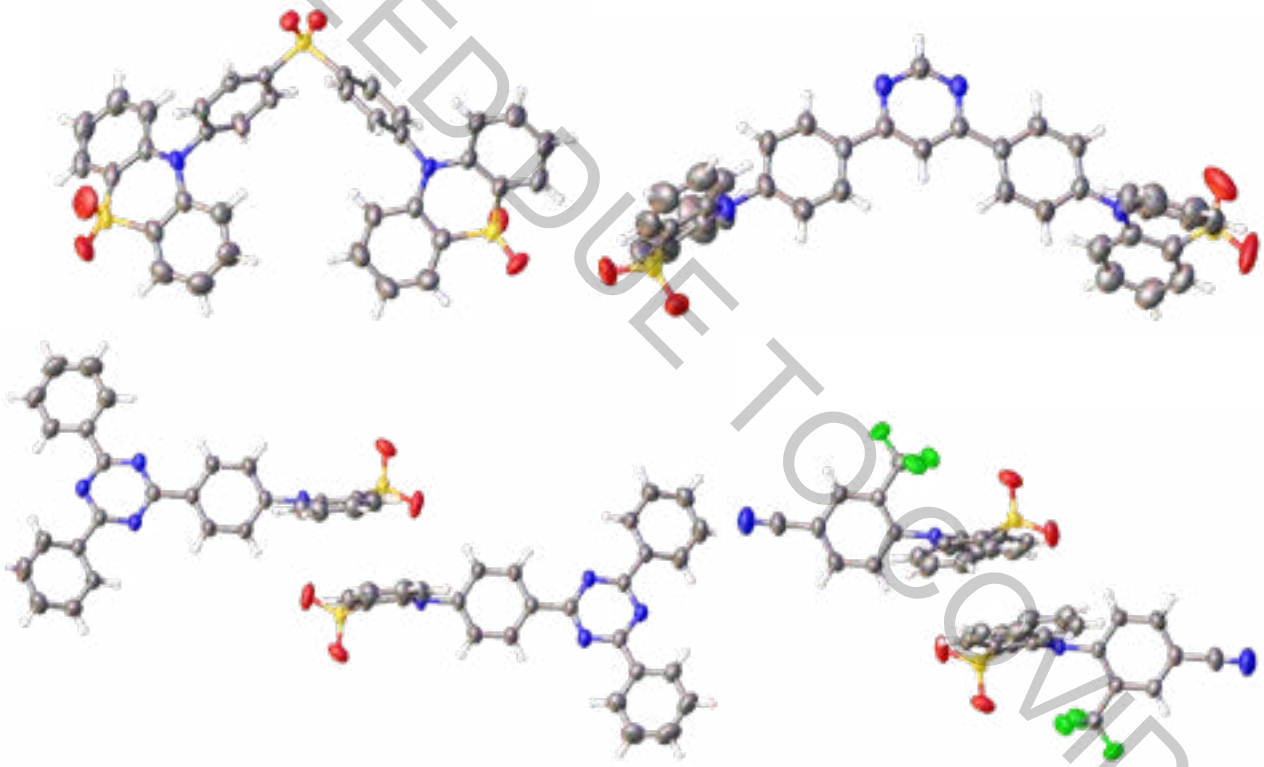

Fig. 1. ORTEP molecular structures of studied compounds, π–π intramolecular interactions displayed in relevant structures (thermal ellipsoids are shown at 50% probability level).

Acknowledgements:
This work was supported by Research Council of Lithuania (09.3.3-LMT-K-712-16-0121).

[1] L. Xiao, Z. Chen, B. Qu, J. Luo, S. Kong, Q. Gong, J. Kido, Recent Progresses on Materials for Electrophosphorescent Organic Light-Emitting Devices. Adv. Mater. 23, 926−952 (2011).
[2] H. Uoyama, K. Goushi, K. Shizu, H. Nomura, C. Adachi, Highly Efficient Organic Light-Emitting Diodes from Delayed Fluorescence. Nature 492, 234−238 (2012).

CANCELLED DUE TO COVID-19

DIELECTRIC PROPERTIES OF THE RELAXOR FERROELECTRIC $(1-x)Pb(Zn_{1/3}Nb_{2/3})O_3$- $xPbTiO_3$

Arnoldas Solovjovas[1], Šarūnas Svirskas[1], Džiugas Jablonskas[1], Shinya Tsukada[2], Seiji Kojima[3], Jūras Banys[1]

[1] Faculty of Physics, Vilnius University, Sauletekio 9/3, LT10222 Vilnius, Lithuania
[2]Faculty of Education, Shimane University, Matsue 690-8504, Japan
[3]Graduate School of Pure and Applied Sciences, University of Tsukuba, Tsukuba, Ibaraki 305-8573, Japan
Arnoldas.solovjovas@ff.vu.lt

CANCELLED DUE TO COVID-19

The history of ferroelectrics starts back in 1940s. Ferroelectric materials are known for having a high dielectric permittivity value. Usually in ferroelectrics temperature of second-order phase transition is related with maximum value of real dielectric permittivity temperature. Also, there is a related group of ferroelectrics that received special attention for the past decades due to extraordinary dielectric properties – relaxor ferroelectrics (relaxors) [1].

Compared to 'normal' ferroelectrics, relaxors have several distinctive features, which does not correspond to structural phase transition. Relaxors have a diffuse peak of dielectric permittivity. the maximum value of real (ε') and imaginary (ε'') components of the dielectric permittivity are observed at different temperature values for the different probing frequency [1],[2].

$Pb(Zn_{1/3}Nb_{2/3})O_3$ (PZN) together with $Pb(Mg_{1/3}Nb_{2/3})O_3$ (PMN) are so called canonical relaxors and play a crucial role in the field of piezoelectrics and are highly suitable for ultrasonic transducers, electromechanical actuators [3]. The main goal of our work is to investigate dielectric properties of PZN–$xPbTiO_3$(PT) single crystal along morphotropic phase boundary (MPB). In this paper four samples with different x concentrations (4.5PT, 6PT, 7PT and 12PT) were investigated.

The dielectric spectroscopy experiments were carried in two different experimental setups. The first one was done using impedance analyzer HP Agilent 4284A in the frequency range of 20 Hz to 1000 Hz. The second setup was done by measuring complex reflection coefficient using network analyzer Agilent 8714ET/ES in 1 MHz-300 MHz frequency range, while the sample is placed at the end of coaxial line.

Below in Fig. 1 you can see temperature dependence of real (ε') and imaginary (ε'') components of dielectric permittivity. The sample with 4.5PT concentration has a usual single broad peak. In 6PT and 7PT concentrations we can observe two phase transitions, because we are approaching morphotropic phase boundary. In 12PT concentration we observe a single sharp peak and a phase transformation from cubic to tetragonal phase.

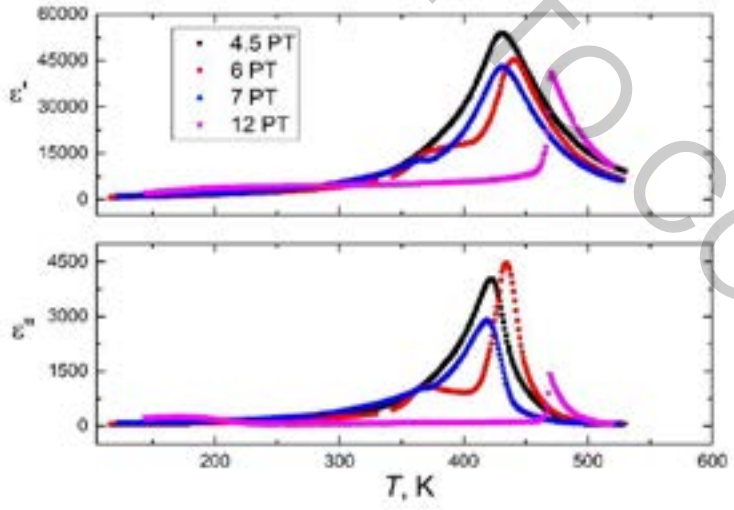

Fig. 1. Real and imaginary components of dielectric permittivity dependence to temperature

[1] A. Peliz-Barranco, F. Caldern-Piar, O. Garca-Zaldvar, and Y. Gonzlez-Abreu, "Relaxor Behaviour in Ferroelectric Ceramics," in *Advances in Ferroelectrics*, A. Peliz-Barranco, Ed. InTech, 2012

[2] C. W. Ahn *et al.*, "A brief review on relaxor ferroelectrics and selected issues in lead-free relaxors," *J. Korean Phys. Soc.*, vol. 68, no. 12, pp. 1481–1494, Jun. 2016, doi: 10.3938/jkps.68.1481

[3] K. Uchino, "The Development of Piezoelectric Materials and the New Perspective," in *Advanced Piezoelectric Materials*, Elsevier, 2017, pp. 1–92.

INVESTIGATION OF PHOTO INDUCED CONFORMATIONAL CHANGES IN ORGANIC FLUORESCENCE EMITTERS

Matas Guzauskas[1*], Edgaras Narbutaitis [2], Dmytro Volyniuk[2], Juozas Vidas Grazulevicius [2]

[1] Department of Physics, Kaunas University of Technology, Lithuania
[2] Department of Polymer Chemistry and Technology, Kaunas University of Technology, Lithuania
matas.guzauskas@ktu.lt

Nowadays organic semiconductors get a lot of interest from researchers and manufacturers because of their wide range of applicability in medicine, textile but mostly in electronics[1]. Organic light emitting diodes (OLEDs) are already used in smartphones, tablets and computers displays also for illumination[2]. Another application which gains interest is sensors with organic materials. There are publications about organic semiconductors with room temperature phosphorescence (RTP), which are used as oxygen sensing materials[3]. Still, there are endless applications for these materials, which are created every day.

In this work we present novel organic semiconductor with phenothiazine and benzophenone derivatives, EN28, and intensive photophysical investigation of it. Materials EN28 shows thermally activated delayed fluorescence, but EN28 also shows properties of ultra-violet (UV) light enhanced photoluminescence (PL) emission. PL emission of toluene solution of EN28 (emission maxima 413 nm) gets more intensive as it gets illuminated by UV light longer. Also, the PL intensity increases faster as EN28 get illuminated by more intensive UV light. The PL of more polar solutions goes from lower energy wavelength to higher energy wavelength emission (solution in DMF goes from 528 nm to 440 nm) after UV treatment (Fig. 1). The increasement of intensity and PL shift to higher energy wavelength range are explained by conformational changes in the molecule induced by UV light photons. This unique property of EN28 can be used for UV light sensing.

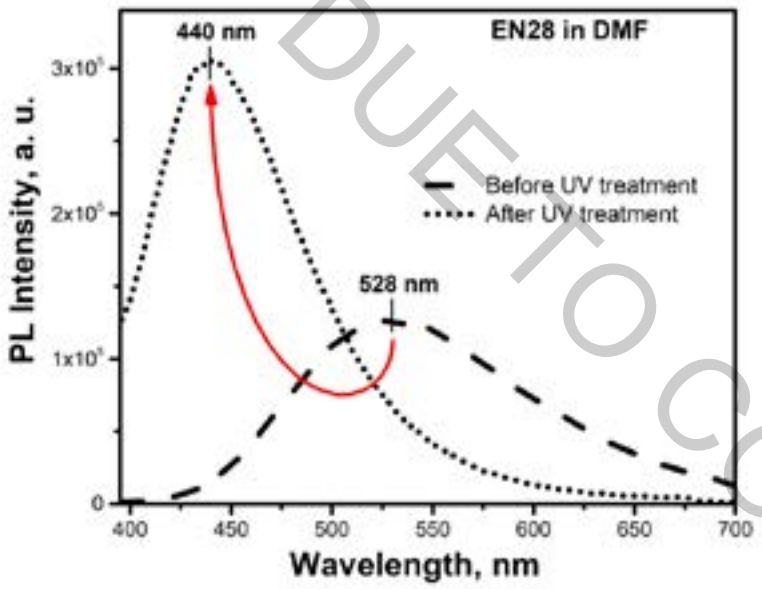

Fig. 1. The PL of DMF solution of EN28 before and after UV treatment

Acknowledgments:
This work was supported by Research Council of Lithuania (09.3.3-LMT-K-712-16-0014).

[1] "OLED Info | The OLED Experts." [Online]. Available: https://www.oled-info.com/. [Accessed: 15-May-2019].
[2] Z. Yang *et al.*, "Recent advances in organic thermally activated delayed fluorescence materials," *Chemical Society Reviews*, vol. 46, no. 3. Royal Society of Chemistry, pp. 915–1016, 07-Feb-2017.
[3] A. Tomkeviciene *et al.*, "Bipolar thianthrene derivatives exhibiting room temperature phosphorescence for oxygen sensing," *Dye. Pigment.*, vol. 170, Nov. 2019.

CANCELLED DUE TO COVID-19

THE ROLE OF EXCITONIC COUPLING IN BIFLUORENE CRYSTALS FOR LASER APPLICATIONS

Eglė Tankelevičiūtė[1], Paulius Baronas[1], Gediminas Kreiza[1], Povilas Adomėnas[1], Karolis Kazlauskas[1], Chihaya Adachi[2], and Saulius Juršėnas[1]

[1] Institute of Photonics and Nanotechnology, Vilnius University, Vilnius (Lithuania)
[2] Center for Organic Photonics and Electronics Research (OPERA), Kyushu University, Nishi (Japan)
egle.tankeleviciute@ff.stud.vu.lt

CANCELLED DUE TO COVID-19

Organic single crystals with long-range molecular order ensure high carrier mobility, enhanced photochemical and thermal stability as well as negligible light-scattering, what makes them attractive as an optical gain medium for electrically-pumped organic lasers [1]. Unfortunately, strong coulombic interactions between molecules (i.e. excitonic coupling) in crystals introduce losses degrading optical performance in crystals, hence higher lasing thresholds are observed compared to amorphous films. Bifluorene crystals were already proved as a successful gain materials [2-5]. Here, excitonic coupling in bifluorene was assessed by spectroscopic methods. Furthermore, crystal doping strategy is investigated as a method to avoid pronounced reabsorption and annihilation losses associated with J-type excitonic coupling, while taking advantage of enhanced exciton transport for efficient energy transfer (Fig. 1). Bifluorene-based derivatives linked with acetylene and ethylene rigid bridges are suitable as host and dopant system forming high-quality doped crystals. Amplified spontaneous emission (ASE) threshold down to 1.1 μJ/cm2 was enabled by minimized exciton annihilation and emission reabsorption losses.

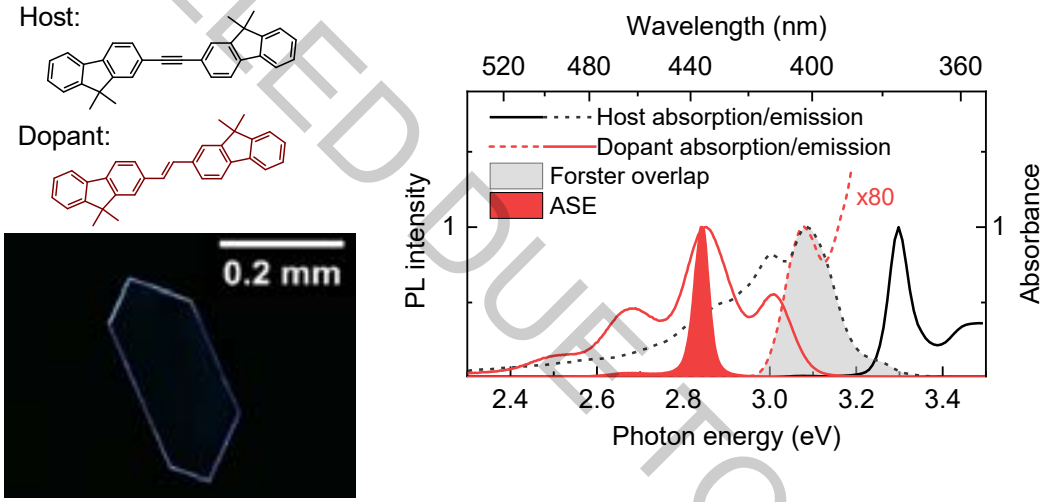

Fig. 1. Molecular composition of doped bifluorene crystals. Absorption and PL of doped crystal, spectral Förster overlap and ASE spectra are shown as colored areas.

[1] A. J. C. Kuehne, M. C. Gather, Chem. Rev. 116, 13823 (2016).
[2] G. Kreiza, et al., Adv. Optical Mater. 5, 1600823 (2016).
[3] P. Baronas, et al., Appl. Phys. Lett. 112, 033302 (2018).
[4] P. Baronas, et al., ACS Appl. Mater. Interfaces 10, 2768 (2018).
[5] P. Baronas, et al., Adv. Optical Mater. 1901670 (2019).

ANALYSIS OF MANGANESE CONTENT INFLUENCE IN NASICON-STRUCTURED $Na_{2x}Zr_{2-x}Mn_x(PO_4)_3$ PREPARED VIA SOL-GEL METHOD AND ITS USE AS A CATHODE IN AQUEOUS Na-BASED BATTERIES

Gytis Baranovas[1], Jurgis Pilipavicius[1,2], Linas Vilciauskas[1,2]

[1] Institute of Chemistry, Faculty of Chemistry and Geosciences, Vilnius University, Lithuania
[2] Department of Chemical Engineering and Technology, Institute of Chemistry, Center for Physical Sciences and Technology, Lithuania
gytisba7@gmail.com

CANCELLED DUE TO COVID-19

Lithium-ion batteries have been used for decades as high-power energy storage for portable electronic devices, not to mention their usage as a substitute power source for electric motors instead of combustion engines [1]. However, as the demand for sustainable energy all around the world increases, development of batteries based on earth-abundant materials have been getting increased attention in the recent years. In the pursuit of these new batteries, Na-based energy storage systems have been investigated as the best alternative for lithium batteries due to the high-abundance of sodium in sea water and various salt deposits as well as sodium itself being the second smallest alkali element and possessing the most beneficial electrochemical properties after lithium [1, 2]. Aqueous batteries also have gained more traction due to reduced flammability and lower price in comparison to their organic electrolyte-based counterparts [3]. Throughout the research of Na-based batteries, Na^+ cathodes consisting of polyanionic transition-metal compounds with open-frameworks structures have been investigated [4]. During this investigation rhombohedral NASICON structured $Na_3MnZr(PO_4)_3$ (NMZP) has been used as a cathode material and provided electrochemical performance greater than other manganese phosphate cathodes reported in the literature up to that point [4].

The objective of this work is to investigate Mn substitution level influence to $Na_{2x}Zr_{2-x}Mn_x(PO_4)_3$ via sol-gel method as well as investigate the structure and electrochemical properties of the obtained material for use as a cathode in aqueous Na-based batteries.

Pure NASICON-structured $Na_3MnZr(PO_4)_3$ was obtained by dissolving and mixing sodium acetate and manganese acetate in water, then adding citric acid in one beaker, dissolving ammonium dihydrogen phosphate in water in another beaker, diluting zirconium acetate in water in third beaker and then mixing all the reagents together. In order to investigate the structural shift of NMZP, sols with varying amount of Zr and Mn were performed using the same synthesis method. Obtained sols then were dried into powders and heat treated under nitrogen in 750°C and characterized by x-ray diffraction (XRD). Decreasing amount of Zn and increasing amount of Mn in the structure led to the structure changing from $NaZr_2(PO_4)_3$ (NZP) to NMZP (figure 1). Scanning electron microscope (SEM) images have shown the formation of particle clusters, with particle size being about 100-200 nm (figure 2). Nevertheless, electrochemical analysis of the material is needed to be done in order to ascertain NMZP as a viable cathode material for aqueous Na-based batteries.

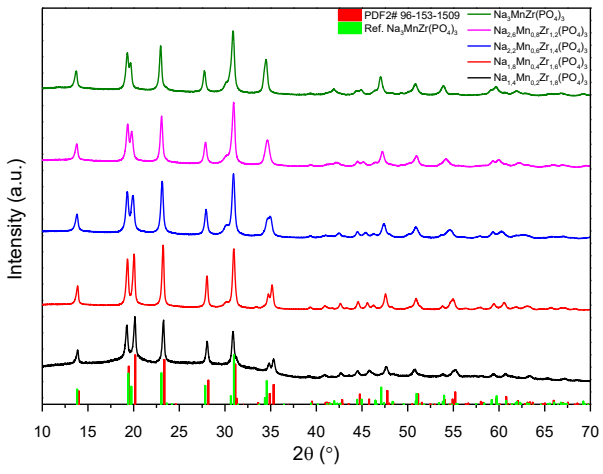

Fig. 1. XRD graph of NMZP with different amounts of Zn and Mn

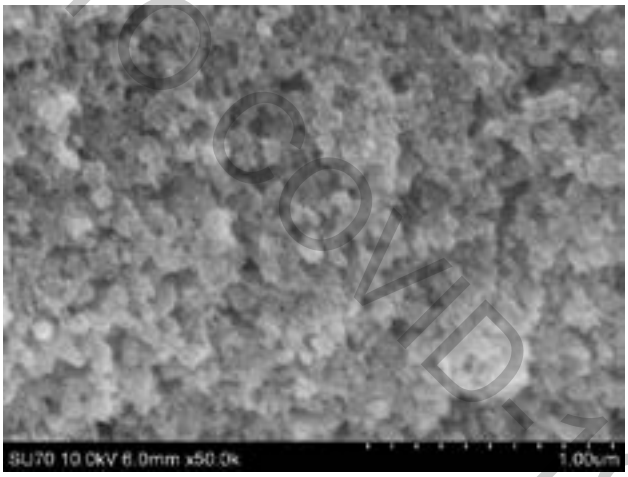

Fig. 2. SEM image of synthesized $Na_3MnZr(PO_4)_3$

[1] Dahbi, M., Yabuuchi, N., Kubota, K., Tokiwa, K., & Komaba, S. Negative electrodes for Na-ion batteries. Physical Chemistry Chemical Physics, 16(29), 15007-15028. (2014).
[2] Qian, J., Chen, Y., Wu, L., Cao, Y., Ai, X., & Yang, H. High capacity Na-storage and superior cyclability of nanocomposite Sb/C anode for Na-ion batteries. Chemical Communications, 48(56), 7070-7072. (2012).
[3] Kim, H., Hong, J., Park, K. Y., Kim, H., Kim, S. W., & Kang, K. Aqueous rechargeable Li and Na ion batteries. Chemical reviews, 114(23), 11788-11827 (2014).
[4] Gao, H., Seymour, I. D., Xin, S., Xue, L., Henkelman, G., & Goodenough, J. B. Na3MnZr(PO4)3: a high-voltage cathode for sodium batteries. Journal of the American Chemical Society, 140(51), 18192-18199 (2018).

DEEP BLUE TO BLUE TADF-OLEDs WITH LOW EFFICIENCY ROLL-OFF BASED ON NEW NAPHTHYRIDINE EMITTERS

Dovydas Banevičius[1], Gediminas Kreiza[1], Justina Jovaišaitė[1], Tomas Javorskis[2], Vytenis Vaitkevičius[2], Edvinas Orentas[2], Saulius Antanas Juršėnas[1], Karolis Kazlauskas[1]

[1] Institute of Photonics and Nanotechnology, Vilnius University, Lithuania
[2] Department of Organic Chemistry, Vilnius University, Lithuania
dovydas.banevicius@ff.vu.lt

Thermally activated delayed fluorescent (TADF) emitters are extremely attractive due to their potential to harvest all triplet excitons via reverse intersystem crossing (rISC) process into the singlet manifold thereby ensuring 100% internal quantum efficiency. [1] However, due to pronounced charge-transfer character of TADF compounds, there are difficulties in achieving deep blue emission. [2] Additionally, TADF-OLEDs suffer from early efficiency roll-off associated with high long-lived triplet exciton population. Therefore, TADF emitters with large rISC rate facilitating triplet up-conversion are required. [3]

To this end, we designed new TADF emitters based on 1,8-naphthyridine acceptor and differently substituted carbazole donor groups. Photophysical characterization of the compounds revealed high photoluminescence quantum yield (up to 86%) in mCP host with large rISC rates (up to 1.1×10^6 s^{-1}). We fabricated vacuum and solution processed TADF-OLEDs employing 7% naphthyridine-doped emissive layer. Devices exhibited deep blue to blue emission with CIE color coordinates from (0.14, 0.16), external quantum efficiency (EQE) of up to 17.6% and high brightness (up to 23000 cd/m^2). Most importantly, due to the large rISC rates TADF OLEDs demonstrated weak efficiency roll-off. EQE characteristics of the produced devices are shown in the **Fig. 1** together with their electroluminescence spectra. Obtained results indicate that 1,8-naphthyridine based emitters are promising for TADF-OLED application.

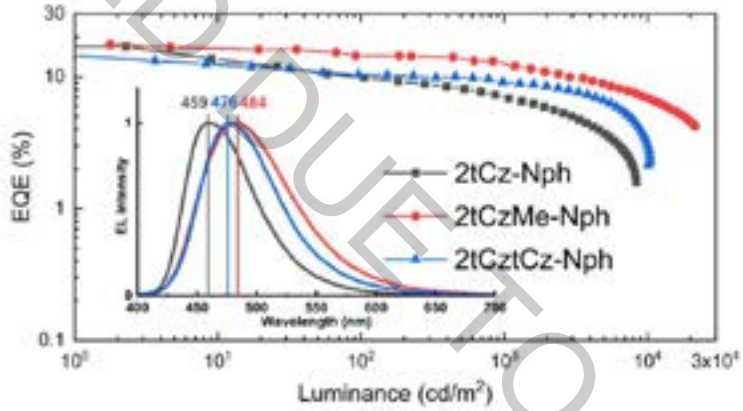

Fig. 1. External quantum efficiencies of the TADF-OLEDs fabricated employing new naphthyridine-based emitters and electroluminescence spectra of these devices (inset).

[1] H. Uoyama, K. Goushi, K. Shizu, H. Nomura, and C. Adachi, Highly efficient organic light-emitting diodes from delayed fluorescence, Nature **492**, 234 (2012).
[2] R. S. Nobuyasu, Z. Ren, G. C. Griffiths, et al., Rational Design of TADF Polymers Using a Donor–Acceptor Monomer with Enhanced TADF Efficiency Induced by the Energy Alignment of Charge Transfer and Local Triplet Excited States, Adv. Opt. Mater. **4**, 597–607 (2016).
[3] M. K. Etherington, J. Gibson, H. F. Higginbotham, et al., Revealing the spin–vibronic coupling mechanism of thermally activated delayed fluorescence, Nat. Commun. **7**, 13680 (2016).

CANCELLED DUE TO COVID-19

SYNTHESIS AND INVESTIGATION OF BENZIMIDAZOLE/*TERT*-BUTYLCARBAZOLE HYBRID BIPOLAR MATERIALS FOR HIGHLY EFFICIENT OLEDS

Simas Mačionis[1], Dalius Gudeika[1], Dmytro Volyniuk[1], Juozas Vidas Gražulevičius[1], Jiun Haw Lee[2], Tien-Lung Chiu[3]

[1] Kaunas University of Technology, Department of Polymer Chemistry and Technology, Lithuania Radvilėnų plentas 19, LT-50254, Kaunas, Lithuania
[2] Graduate Institute of Photonics and Optoelectronics, National Taiwan University, 1, Section 4, Roosevelt Road, Taipei 10617, Taiwan
[3] Department of Electrical Engineering, Yuan Ze University, 135 Yuan-Tung Road, Taoyuan 32003, Taiwan
simas.macionis@ktu.edu

CANCELLED DUE TO COVID-19

Organic light emitting diodes (OLEDs) have been a widely studied subject for past two decades and have become a staple field of research in nowdays optoelectronic technology. Despite of its high potential, OLED technology remains only partly commercialized, mainly due to short lifespan of blue OLDEs [1]. In order to achieve high efficiency in OLEDs triplet-triplet annihilation, a phenomenon accruing between phosphorescent emitters, is to be abstained from. A host matrix is needed to isolate emitters. Such host matrix materials need to meet certain prerequisites: high triplet energy, appropriate energy level complementation, appropriate charge transfer properties and high thermal stability are paramount [2].

Recently, new benzimidazole/carbazole compounds were reported, showing excellent thermal stability, and high efficiency in different color OLEDs (up to 27% external quantum yield) [3].

In this work, five new benzimidazole/*tert*-butylcarbazole compounds were synthesized and their photophysical, electrochemical and thermal properties as well as device characterization studied.

Acknowledgement. This project has received funding from the Research Council of Lithuania (LMTLT), agreement No [S-LU-20-3].

[1] Salehi, A., Fu, X., Shin, D.-H., So, F., *Adv. Funct. Mater.* 2019, 29, 1808803.
[2] R. J. Holmes, S. R. Forrest, Blue organic electrophosphorescence using exothermic host–guest energy transfer, Applied Physics Letters, 2003, 82, 15, 2422-2424.
[3] Jau-Jiun Huang, Yu-Hsiang Hung Orthogonally Substituted Benzimidazole-Carbazole Benzene AsUniversal Hosts for Phosphorescent Organic Light-Emitting Diodes, *Org. Lett.* 2016, 18, 4, 672-675

SYNTHESIS AND PROPERTIES OF QUINAZOLINE-BASED ELECTROACTIVE COMPOUNDS

Simona Vekteryte[1], Rasa Keruckiene[1], Eimantas Vijaikis[1], Matas Guzauskas[1], Juozas Vidas Grazulevicius[1]

[1]Department of Polymer Chemistry and Technology, Kaunas University of Technology, Lithuania
simona.vekteryte@ktu.edu

Electroactive organic compounds are widely used in the production of organic light emitting diodes (OLEDs). OLED technology is used to the manufacture of flexible displays, smartphones and lighting [1]. Thermally activated delayed fluorescence (TADF) materials have attracted considerable attention due to the ability to achieve 100% internal quantum efficiency [2].The TADF mechanism is only possible when the energy levels of T1 and S1 are very close to each other, so that's why endothermic reverse intersystem crossing (RISC) process can be activated by thermal motion of the atoms [3]. Because the T1 → S0 jump is forbidden, these triplet excitons are converted into singlet capable of emitting a quantum of light, thus increasing the quantum efficiency of luminescence [4]. Many studies have shown that the donor-acceptor structure is one of the best options for developing TADF emitters. Current emitters are designed based on a donor-acceptor model with high spatial separation of highest occupied molecular orbital (HOMO) and lowest unoccupied molecular orbital (LUMO) orbitals [5]

In this work, we present quinazoline-based emitters bearing donor-acceptor-donor electronic structure. Quinazoline is a planar aromatic heterocyclic compound with a fused benzene and pyrimidine ring structure. Due to its conjugated and condensed structure, the quinazoline compounds exhibit good photophysical properties [1]. The donor moieties such as ditertbutylcarbazole, ditertbutylphentiazine and ditertbutyldimethyldihidroacridine were chosen due to their their favourable HOMO orbitals delocalization and electron donating ability. The derivatives were obtained by two-step synthesis procedure (Fig. 1).

Thermal, photophysical, electrochemical and photoelectrical properties of the materials will be reported.

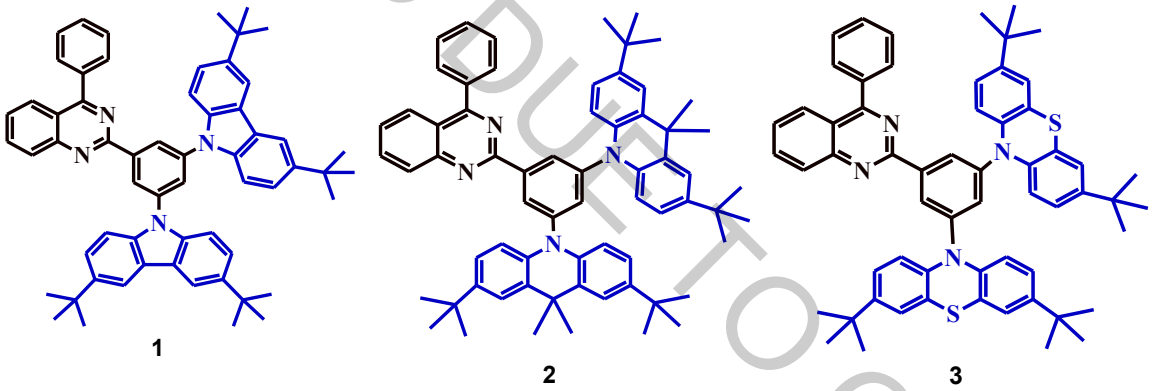

Fig. 1. The structures of the quinazoline-based derivatives

Acknowledgment. Authors acknowledge the European Union's Horizon 2020 Research and Innovation Programme under the Marie Skłodowska-Curie grant agreement No 823720.

[1] W. Qiang, F. Nannan, I. Amjad, L. Tao, H. Ling, P. Ruixiang, F. Xi, C. Liang, G. Pingqi, and G. Ziyi, Small-Molecule Emitters with High Quantum Efficiency: Mechanisms, Structures, and Applications in OLED Devices, Advanced Optical Materials **6,** 1800512 (2018).
[2] B. Li, Z. Wang, S.-J. Su, F. Guo, Y. Cao, and Y. Zhang. Quinazoline-Based Thermally Activated Delayed Fluorecence for High-Performance OLEDs with ExternalQuantum Efficiencies Exceeding 20%, Advanced Optical Materials **7**, 1801496 (2019).
[3] T. Chen, et al. Understanding the Control of Singlet-Triplet Splitting for Organic Exciton Manipulating: A Combined Theoretical and Experimental Approach. *Sci. Rep*, **5**, 10923 (2015).
[4] A. Monkman, Photophysics of thermally activated delayed fluorescence, Highly Efficient OLEDs: Materials Based on Thermally Activated Delayed Fluorescence **5**, 7931–7958 (2017).
[5] Y. Im, M. Kim, Y. J. Cho, J.-A Seo, K. S. Yook, and J. Y. Lee, Molecular Design Strategy of Organic Thermally Activated Delayed Fluorescence Emitters, Chemistry of Materials, **29**, 1946-1963 (2017).

CANCELLED DUE TO COVID-19

SYNTHESIS OF $SrAl_2O_4:Eu^{2+},Sm^{3+}$ PHOSPHORS AND THEIR SPECTROSCOPIC CHARACTERIZATION

Rugile Zilenaite[1], Egle Ezerskyte[1], David Van der Heggen[2], Philippe F. Smet[2], Arturas Katelnikovas[1], Simas Sakirzanovas[1]

[1] Institute of Chemistry, Faculty of Chemistry and Geosciences, Vilnius University, Lithuania
[2]LumiLab, Department of Solid State Sciences, Faculty of Sciences, Ghent University, Belgium
rugile.zilenaite@chf.stud.vu.lt

Usually in photoluminescent materials absorption of light brings the luminescent impurity into an excited state, which typically has a lifetime of nanoseconds up to a few milliseconds, depending on the specific electronic transition and the host-dopant interactions [1]. A persistent phosphor is a specific modification of such a photoluminescent material, where energy is stored in the so-called traps. Red and near-infrared light can be used to empty those traps, in a process called optically stimulated luminescence (OSL). The amount of emitted light is proportional to the number of trapped charges [2]. Persistent phosphors, where ambient heat is driving the release of the trapped energy, have shown their potential to be used in various glow-in-the-dark applications, ranging from emergency signage and watch dials to toys, and in light dosimetry [3,4].

The main focus of this research was to synthesize $SrAl_2O_4:Eu^{2+},Sm^{3+}$ phosphors with various concentrations of dopants using solid-state synthesis method and determine how the chemical composition of the synthesized materials affects their spectroscopic and energy storage properties (ability to accumulate energy within itself).

The obtained results show that after optimizing the amount of flux agent in solid-state synthesis, the method can be used to obtain phase pure samples. Furthermore, the afterglow of this green emitting phosphors (λ_{max} = 520 nm) goes out very quickly compared to other persistent phosphors, e.g., Eu^{2+}, Dy^{3+} doped $SrAl_2O_4$. This shows that the trapped charges are stable at room temperature. The energy accumulated in the sample can be released by irradiation with stimulation light and the intensity of the OSL was shown to depend linearly on the applied dose (Fig. 1), fulfilling a key requirement for dosimeters.

Powder X-ray diffraction, emission and excitation spectra, energy storage capacity and diffuse reflectance measurements have been recorded to characterize crystal structure and spectroscopic properties of the synthesized samples.

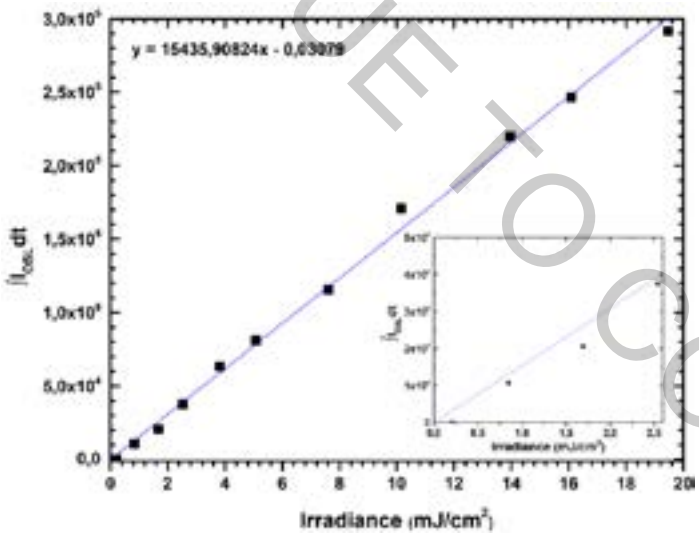

Fig. 1. Linear range of storage capacity graph of $SrAl_2O_4:1\%Eu^{2+},1\%Sm^{3+}$ sample as a function of irradiance.

CANCELLED DUE TO COVID-19

[1] P.F. Smet, K. Van den Eeckhout, O.Q. De Clercq, D. Poelman, Persistent Phosphors, 1st ed., Elsevier B.V., 2015. https://doi.org/10.1016/B978-0-444-63483-2.00001-6.
[2] D. Van der Heggen, J.J. Joos, D.C. Rodríguez Burbano, J.A. Capobianco, P.F. Smet, Counting the photons: Determining the absolute storage capacity of persistent phosphors, Materials (Basel). 10 (2017) 1–13. https://doi.org/10.3390/ma10080867.
[3] D. Van Der Heggen, J.J. Joos, P.F. Smet, Importance of Evaluating the Intensity Dependency of the Quantum Efficiency: Impact on LEDs and Persistent Phosphors, ACS Photonics. 5 (2018) 4529–4537. https://doi.org/10.1021/acsphotonics.8b00979
[4] J. Botterman, J.J. Joos, P.F. Smet, Trapping and detrapping in SrAl2O4:Eu,Dy persistent phosphors: Influence of excitation wavelength and temperature, Phys. Rev. B - Condens. Matter Mater. Phys. 90 (2014) 1–15. https://doi.org/10.1103/PhysRevB.90.085147.

EFFECT OF FLUORINE ON ELECTROACTIVE MATERIALS WITH AGGREGATION INDUCED ENHANCED EMISSION PROPERTIES

Ronit Sebastine Bernard [1], Galyna Sych [1], Sohrab Nasiri [1], Oleksandr Bezvikonnyi [1], Dmytro Volyniuk [1], Azhar Ariffin [2], Juozas V. Grazulevicius[1]

[1] Department of Polymer Chemistry and Technology, Kaunas University of Technology, Kaunas, Lithuania.
[2] Department of Chemistry, Faculty of Science, University of Malaya, 50603 Kuala Lumpur, Malaysia.
ronit.bernard@ktu.edu

Triphenylethylene (TPE) based derivatives are used to achieve aggregation induced enhanced emission (AIEE) in order to solve the problem of aggregation caused quenching (ACQ) [1]. Materials with TPE units can provide high emission efficiencies in the aggregated state that can be effectively used to fabricate efficient non-doped OLEDs [2]. The synthesized compounds were based on a donor acceptor rotor (D-A-R) molecular structure where TPE unit was used as rotor. D-A-R materials demonstrate AIEE and bipolar properties [3]. Photoluminescence decay was measured to study the fluorescence time and prompt fluorescence was observed without the delayed fluorescence, leading to the AIEE properties measurement by the mixture of THF/H_2O solution, as the H_2O concentration got increased a drastic elevation in the intensity of materials was observed proving the AIEE behaviour (Fig. 1). The best non-doped device fabricated based on the synthesized D-A-R material showed turn-on voltage of 4.2v, maximum brightness of 5700 cd/m2 and power efficiency of 3.2 lm/W.

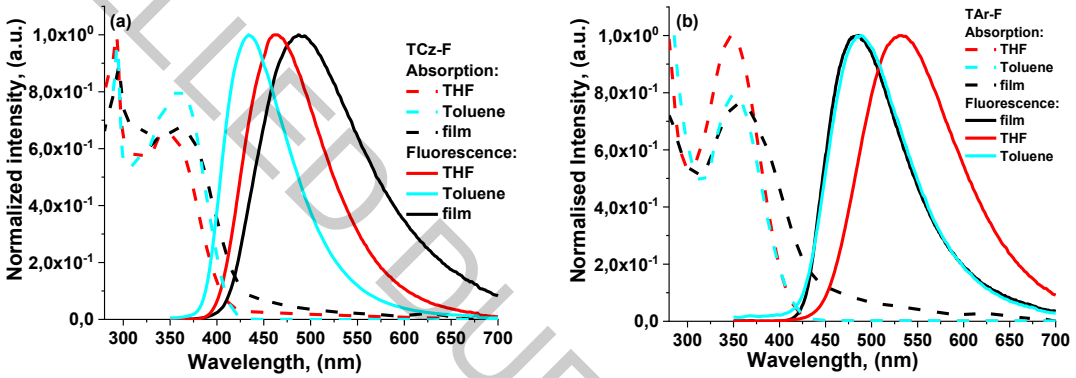

Fig. 1. Absorption and Emission spectra of compounds in different solvents and neat film (a) TCz-F, (b) TAr-F.

[1] H-T. Lin, C-L. Huang, G-S. Liou, Design, Synthesis, and Electrofluorochromism of New Triphenylamine Derivatives with AIE-Active Pendent Groups, ACS Appl. Mater. Interfaces 11, 11684−11690 (2019).

[2] J. Guo, X-L. Li, H. Nie, W. Luo, S. Gan, S. Hu, R. Hu, A. Qin, Z. Zhao, S-J. Su and B. Z. Tan, Robust luminescent small molecules with aggregation-induced delayed fluorescence for efficient solution-processed OLEDs, *Adv. Funct. Mater*27, 1606458, (2017).

[3] G. Sych, J. Simokaitiene, O. Bezvikonnyi, U. Tsiko, D. Volyniuk, D. Gudeika and J. V. Grazulevicius, Exciplex-Enhanced Singlet Emission Efficiency of Nondoped Organic Light Emitting Diodes Based on Derivatives of Tetrafluorophenylcarbazole and Tri/Tetraphenylethylene Exhibiting Aggregation-Induced Emission Enhancement**,** *J. Phys. Chem. C*,), 122, 14827 (2018).

CANCELLED DUE TO COVID-19

TADF EMISSION WAVELENGTH INSTABILITY DUE TO CONFORMATIONAL DISORDER

Rokas Skaisgiris[1], Tomas Serevičius[1], Jelena Dodonova[2], Laimis Jagintavičius[2], Jonas Bucevičius[2], Karolis Kazlauskas[1], Saulius Juršėnas[1], Sigitas Tumkevičius[2]

[1] Institute of Photonics and Nanotechnology, Faculty of Physics, Vilnius University, Lithuania
[2] Institute of Chemistry, Faculty of Chemistry and Geosciences, Vilnius University, Lithuania
rokas.skaisgiris@ff.vu.lt

CANCELLED DUE TO COVID-19

Organic light emitting diodes attracts a lot of interest due to vibrant colors, flexible, cheap and lightweight applications. However due to spin statistics 75% of electrically injected charge ends up in non-emissive "dark" triplet states. Thermally activated delayed fluorescence (TADF) is the most promising pathway for triplet harvesting since TADF compounds are cheaper and much more stable than rare-earth metals based phosphorescent emitters.

TADF molecules are usually constructed from donor (D) and acceptor (A) moieties twisted by large dihedral angles to reduce spatial overlap of HOMO–LUMO electron orbitals and minimize ΔE_{ST}, which is important to utilize non-emissive triplet states [1]. However, large steric hindrance between D and A units reduces the vibronic coupling between localized (^{3}LE) and charge transfer (^{3}CT) triplet states, which is mandatory for efficient rISC, therefore some lability of molecular core is required [2]. In dilute solutions, minor dispersion of D–A twist angles may be observed, having negligible effect on excited state relaxation. In solid films molecules are frozen in large variation of geometrical conformations with different ^{1}CT energies and ΔE_{ST} gaps, causing temporal shifts of prompt and delayed fluorescence and resulting in multiexponential emission decay with prolonged lifetime [3, 4]. The impact of conformational disorder to TADF properties in solid films, its relation to rISC rate and methods to reduce it, despite its importance, still are scarcely studied.

In this work we investigate the conformational disorder in solid films of phenothiazine-pyrimidine TADF compounds (Fig. 1) and its relation to emission properties. Compounds were designed to have different lability of molecular core and different reverse intersystem crossing (rISC) rate. Phenothiazine electron-donor unit was selected for its ability to form several conformations, increasing the number of possible molecular core arrangements in solid state. We have shown, that variations of molecular core rigidity had only minor impact on conformational disorder and emission properties, while the rISC rate was found to have the crucial importance to TADF properties. The long rISC resulted in emission wavelength redshift.

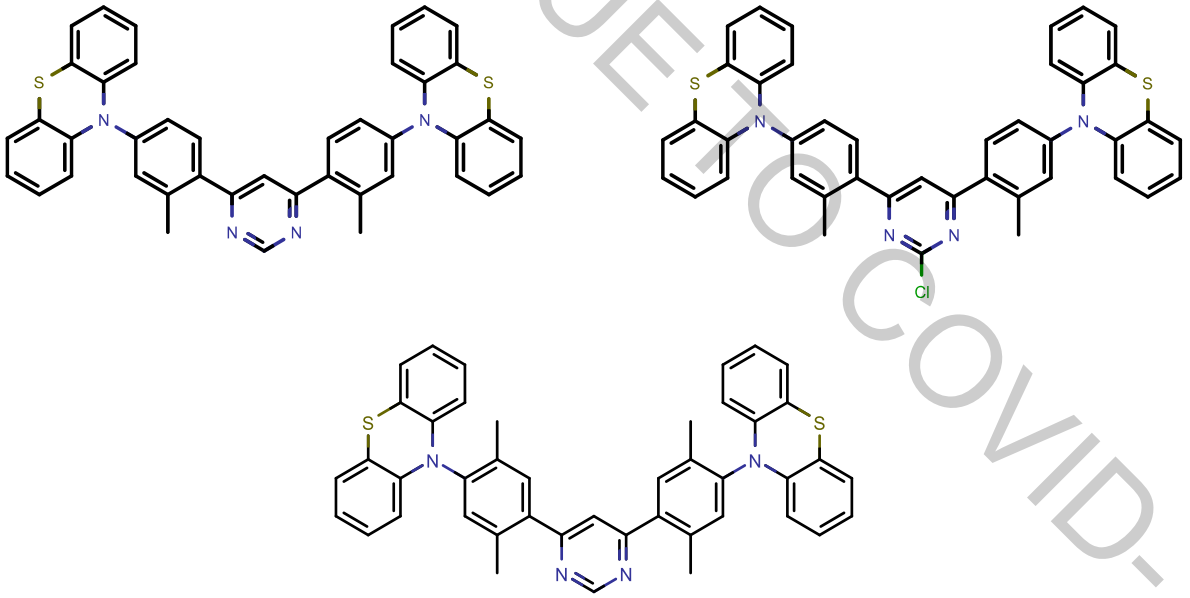

Fig. 1. Phenothiazine-pyrimidine TADF compounds analyzed in this work

[1] H. Uoyama et al., Highly efficient organic light-emitting diodes from delayed fluorescence, Nature, 2012, **492**, 234–238
[2] M. K. Etherington et al., Revealing the spin–vibronic coupling mechanism of thermally activated delayed fluorescence, Nature Communications., 2016, **7**, 13680
[3] T. Northey et al., The role of solid state solvation on the charge transfer state of a thermally activated delayed fluorescence emitter, Journal of Materials Chemistry C, 2017, **5**, 11001–11009
[4] T. Serevičius et al., Room temperature phosphorescence vs. thermally activated delayed fluorescence in carbazole–pyrimidine cored compounds, Journal of Materials Chemistry C, 2018, **6**, 11128–11136

NASICON-STRUCTURED $Na_{2x}Ti_{2-x}Mn_x(PO_4)_3$ AS AN ELECTRODE IN SYMMETRICAL SODIUM AQUEOUS BATTERY SYNTHESIZED VIA SOL-GEL METHOD

Edvinas Staišiūnas[1], Jurgis Pilipavicius[1], Linas Vilčiauskas[2]

[1] Department of Inorganic Chemistry, Faculty of Chemistry and Geosciences, Vilnius University, Lithuania
[2] Department of Applied Chemistry, Faculty of Chemistry and Geosciences, Vilnius University, Lithuania
edvinas.staisiunas@gmail.com

CANCELLED DUE TO COVID-19

Nowadays energy storage is based primarily on lithium ion batteries as Li-ion cells power everything from mobile phones to electric cars. However, the increased demand causes natural problems of increasing prices of lithium resources as well as concerns about long-term availability. One of the emerging alternatives is batteries based on sodium, which is highly abundant and cheap as well as having a redox potential only 0.3 V above of its lithium counterpart, thus a small energy loss for a cheaper alternative [1]. In recent years NASICON structures became highly investigated because of their vast ionic channels, structural stability, and the great number of sodium insertion sites. A general formula for NASICON is $A_xM_y(XO_4)_3$, in which A represents an alkali metal, M generally is a transition metal and X is a nonmetal atom, while the structure of crystalline phase is a polyanionic compound having MO_6 octahedras and XO_4 tetrahedras with vast amount of channels in between them making it possible for a quick alkali ion diffusion. Recently a new type of NASICON compound $Na_3MnTi(PO_4)_3$ (NMTP) became attractive as it contains electrochemically active Mn^{2+} and Ti^{4+} ions, allowing to construct a symmetric battery, as it can be used as both anode and cathode. Another huge advantage of this type of electrode is its theoretical oxidation reduction potential range, which is in the range of potential of either oxygen or hydrogen evolution from water, thus giving viability to use it in aqueous solution, further lowering cost and improving safety of NMTP symmetrical battery [2].

The aim of this work is to investigate NASICON structured $Na_{2x}Ti_{2-x}Mn_x(PO_4)_3$ phase formation depending on the different amounts of manganese using sol-gel method for synthesis, conjointly investigating structural properties and electrochemical behavior of the synthesized powders.

The synthesis of NASICON $Na_{2x}Ti_{2-x}Mn_x(PO_4)_3$,was made using modified sol-gel method employed by by Goodenough et al. [2]. The Sol-gel procedure involved mixing manganese acetate tetrahydrate, sodium acetate, citric acid, ammonium dihydrogen phosphate and dihyroxybis(ammonium lactato)titanium(IV) in aqueous medium. The obtained sol was dried at 100 °C. However, owing to some possible strains of crystal lattice it was not entirely possible to obtain completely pure NASICON $Na_3MnTi(PO_4)_3$, therefore an investigation of manganese insertion into NASICON $Na_2Ti(PO_4)_3$ crystal lattice was made by varying manganese amounts from 0 to 1 in final $Na_{2x}Ti_{2-x}Mn_x(PO_4)_3$ structure and calcining obtained sols in temperature ranges varying from 600 °C to 700 °C in order to attain optimal phase formation temperature of each composition. Obtained powders structure was investigated by x-ray diffractometer (XRD), size of obtained particles was characterized by scanning electron microscope (SEM). The optimal temperature for NMTP phase formation in $Na_3MnTi(PO_4)_3$ was researched to be 600 °C, which increases with decrease of manganese amount to a temperature of 700 °C in $Na_{1.4}Mn_{0.2}Ti_{1.8}(PO_4)_3$.

Furthermore, the next phase in this research will be analyzing electrochemical behavior of NMTP powders by casting electrodes and performing cyclovoltammetric and galvanostatic charge – discharge scans.

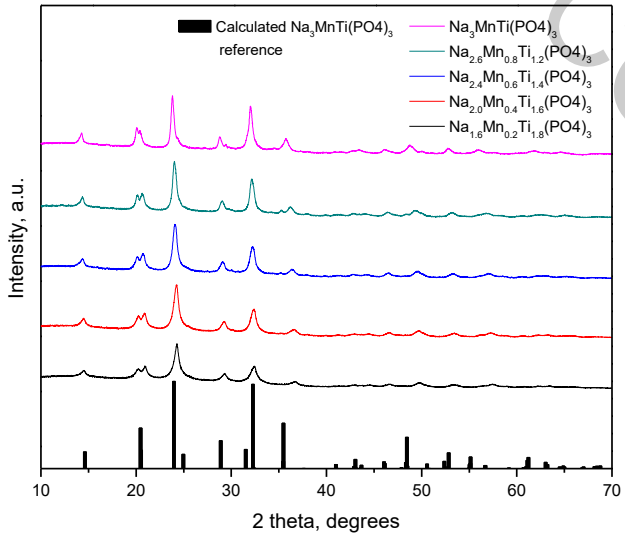

Fig. 1. XRD graph of NMTP with varying amount of manganese furnaced at 700 °C

[1] Kundu, Dipan, et al. The emerging chemistry of sodium ion batteries for electrochemical energy storage. Angewandte Chemie International Edition, 54(11), 3431-3448. (2015)
[2] Gao, Hongcai; Goodenough, John B. An Aqueous Symmetric Sodium-Ion Battery with NASICON-Structured Na3MnTi(PO4)3. Angewandte Chemie International Edition, 55(41), 12768-12772. (2016).

DESIGN, SYNTHESIS AND INVESTIGATION OF COUMARINE-BASED DERIVATIVES

Nizy Sara Samuel[1], Dalius Gudeika[2]

[1] Kaunas University of Technology, Department of Polymer Chemistry and Technology, Lithuania
Radvilėnų plentas 19, LT-50254, Kaunas, Lithuania
nizy.samuel@ktu.edu

Compounds with electroactive moieties are widely studied due to their good processability and applications in various optoelectronic devices including organic light emitting diodes [1] [2]. Their thin films on the different substrates can be fabricated by using simple techniques, i.e. casting or spin-coating from solutions. Such advantages are important in the fabrication of low cost, large area devices.

In this work, four new coumarine-based compounds were synthesized and their photophysical, electrochemical and thermal properties as well as device characterization studied.

Acknowledgement. This research was funded by a grant (No. S-LZ-19-2) from the Research Council of Lithuania.

[1] S. R. Forrest, M. E. Thompson, Organic electronics and optoelectronics, Chem. Rev. **107**, 923-1386 (2007).
[2] Y. Shirota, H. Kageyama, Charge carrier transporting molecular materials and their applications in devices, Chem. Rev. **107**, 953-1010 (2007).

CANCELLED DUE TO COVID-19

MAGNETIC PROPERTIES OF PRUSSIAN BLUE ANALOGUE $Fe_3[Cr(CN)_6]_2 \cdot nH_2O$ NANORODS OBTAINED BY ELECTRODEPOSITION METHOD

Wojciech Sas[1*], Marcin Perzanowski[1], Magdalena Fitta[1]

[1] Institute of Nuclear Physics Polish Academy of Sciences, Radzikowskiego 152, 31-342 Kraków, Poland
wojciech.sas@ifj.edu.pl

Molecular magnets are compounds assembled out of discrete building blocks, e.g. coordination complexes or organic molecules, that exhibit magnetic properties and can be treated as multifunctional materials. The continuous increase in the interest in molecular magnets can be seen in recent years. Some of them can combine multiple attractive properties, such as low density, the high magnetic moment per unit of volume, or the sensitivity for external stimuli, including temperature and pressure. Prussian blue analogues (PBAs) are one of the best-known group of molecular magnets, especially due to their functional properties (sorption capacity, photomagnetism). The numerous methods of synthesizing samples in various forms (bulk, thin films, nanoparticles) create a possibility for the interesting research, for instance, the investigation of the influence of the size reduction on their magnetic properties.

In this work, we report the synthesis and study of magnetic properties of the nanorods of PBA belonging to the system $Fe_3[Cr(CN)_6]_2 \cdot nH_2O$. The samples were prepared by template-assisted electrochemical deposition. The porous polycarbonate (PCTE) membranes covered by a thin film of Au were used as the working electrode in a three-electrode electrochemical cell. The samples were fabricated in the polycarbonate (PCTE) membranes of two different pore size: 100 and 200 nm.

The analysis of scanning electron microscope (SEM) microphotographs confirmed that nanorods of cylindrical shape with diameters of 100 and 200 nm respectively were obtained. The measurements of magnetic properties showed that obtained materials are ferromagnets with critical temperature T_c equal to 20 K. This T_c value is comparable to that observed for bulk as well as thin films. The most important result in this study is the observation of the increase of coercive filed with the reduction of nanorods diameter.

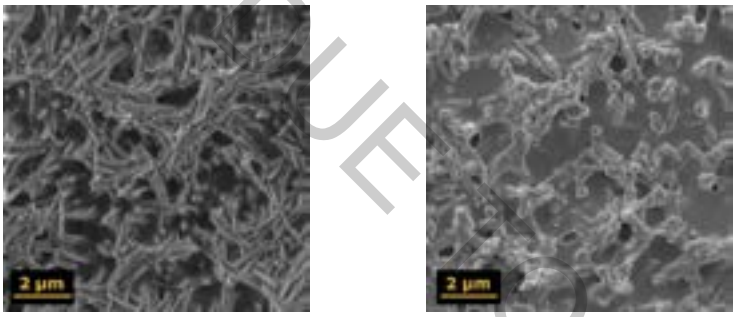

Fig. 1. Nanorods of diameter 100 nm (left) and 200 nm (right)

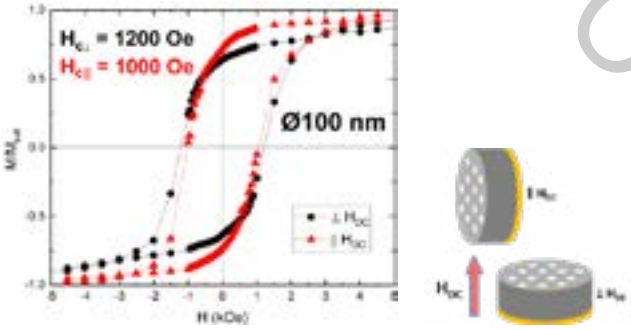

Fig. 2. Magnetic hysteresis of the sample with Ø100 nm for two different orientations with respect to the external magnetic field (explained symbolically to the right)

Acknowledgements: W.S. acknowledges the Polish National Science Centre (Grant PRELUDIUM 16: UMO-2018/31/N/ST5/03300) for financial support.

CANCELLED DUE TO COVID-19

ULTRATHIN METAL FILMS OPTICAL PROPERTIES DEPENDENCIES ON DEPOSITION PARAMETERS

Eimantas Tarailis[1,2], Audrius Valavičius[1], Mantas Drazdys[1], Darija Astrauskytė[1], Ramutis Drazdys[1]

[1] Optical coatings laboratory, Center for Physical Sciences and Technology, Savanorių ave. 231, Vilnius LT-02300, Lithuania

[2] Department of Physics, Vilnius University, Saulėtekio ave. 9, LT-10222, Vilnius, Lithuania

eimantas.tarailis@gmail.com

In recent decades optical coatings attracted a lot of scientist attention in various areas of research. Commonly the optical coatings are made of dielectric layers. To reach special optical properties multilayer stack of metallic and dielectric layer coatings are also used. However, ultrathin metallic films interaction with light exhibit uncommon optical properties. In ultrathin films of metallic copper, aluminum, gold or silver localized surface plasmon resonance occurs due to island like formation. Excitation of localized surface plasmons manifest by absorption peak in visible light. Silver distinguishes as of noble metal having the biggest extinction cross section. Because of this property such material is very attractive in optics for application in bio-sensing [1] or solar cells [2]. However, earlier research showed that ultrathin silver films are unstable in the atmosphere due to tarnishing and particles rearrangement [3]. Also, ultrathin metal films are strongly dependent on the formation condition [4]. All these effects make such layer complicate to analyze.

The aim of this work was to use atomic layer deposition (ALD) technology to stabilize island like layer in time. For this purpose ultrathin silver films were formed using thermal evaporation technology and covered by ALD. To prevent silver films from tarnishing in exposure to atmosphere alumina was used as protective layer. Thickness of silver film, temperature and vacuum in chamber was varied. After formation of full structure, optical properties were evaluated using spectrophotometer. Transmittance and reflection values were measured, and optical losses were calculated. Samples surface morphology was investigated using Atomic Force Microscope.

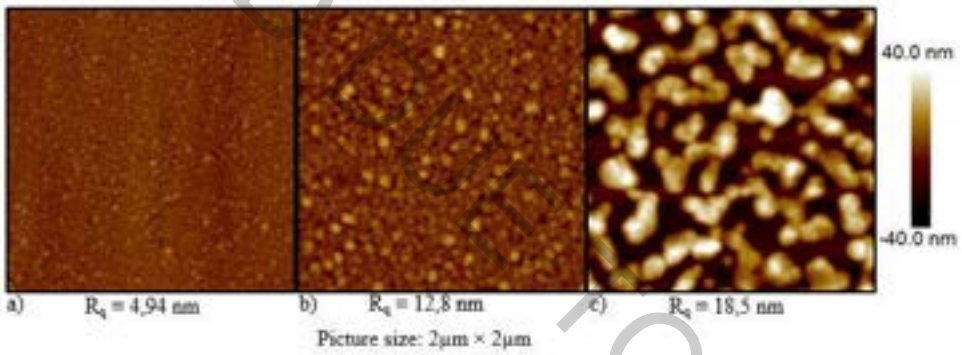

Fig. 1. Formed ultrathin silver films surface morphologies with different thicknesses: a) 7 nm; b) 10 nm; c) 14 nm

From Fig. 1 it can be seen that geometry of island-like nanoparticles changes drastically while increasing deposited amount of silver. Nanoparticles grow in size until they start to coalesce into long chain islands. Varied vacuum conditions and temperature show different influence on islands formation tendencies. More of these results will be presented at the poster session.

In summary, investigation results present the possibility to control the properties of LSPR. It shows strong dependency of LSPR on surface morphology. By varying deposition parameters absorption peak can be tuned from 400 nm to 600 nm.

[1] E. Petryayeva and U. J. Krull, "Localized surface plasmon resonance: Nanostructures, bioassays and biosensing—A review," *Anal. Chim. Acta*, vol. 706, no. 1, pp. 8–24, Nov. 2011, doi: 10.1016/j.aca.2011.08.020.

[2] S. Pillai, K. R. Catchpole, T. Trupke, and M. A. Green, "Surface plasmon enhanced silicon solar cells," *J. Appl. Phys.*, vol. 101, no. 9, p. 093105, May 2007, doi: 10.1063/1.2734885.

[3] M. D. Mcmahon, R. Lopez, H. M. Meyer, L. C. Feldman, and R. F. Haglund, "Rapid tarnishing of silver nanoparticles in ambient laboratory air," *Appl. Phys. B*, vol. 80, no. 7, pp. 915–921, Jun. 2005, doi: 10.1007/s00340-005-1793-6.

[4] M. A. Garcia, "Surface plasmons in metallic nanoparticles: fundamentals and applications," *J. Phys. Appl. Phys.*, vol. 45, no. 38, p. 389501, Sep. 2012, doi: 10.1088/0022-3727/45/38/389501.

CANCELLED DUE TO COVID-19

VORTEX TERAHERTZ WAVE GENERATION IN AIR BY FEMTOSECOND OPTICAL VORTEX PULSES

Danas Buožius[1], Julius Jokubaitis[1], Maksym Ivanov[2]

[1] Vilnius University Laser Research Center, 10 Sauletekio avenue, LT-10223 Vilnius, Lithuania
[2] Institut National de la Recherche Scientifique, 1650, Lionel-Boulet Varennes Quebec, Canada
danas.buozius@ff.vu.lt

Currently due to many applications in imaging and spectroscopy, terahertz (THz) radiation is a subject of great interest. One of the most efficient methods of creating very strong electric fields of THz radiation is using bichromatic femtosecond laser pulses consisting of the first and second harmonics (FH and SH, respectively) to create a plasma filament where THz pulses are emitted[1, 2]. In this research we conducted experiments studying properties of THz signal (modulation of intensity and azimuthal phase), emitted from laser induced plasma in air, when one or both of the pump beams were carrying an optical vortex charge. For the experiments we have used a Ti:sapphire laser system (Legend elite duo HE+, Coherent Inc.), delivering pulses with duration of 40fs (FWHM), central wavelenght of 800nm and a repetition rate of 1 kHz.

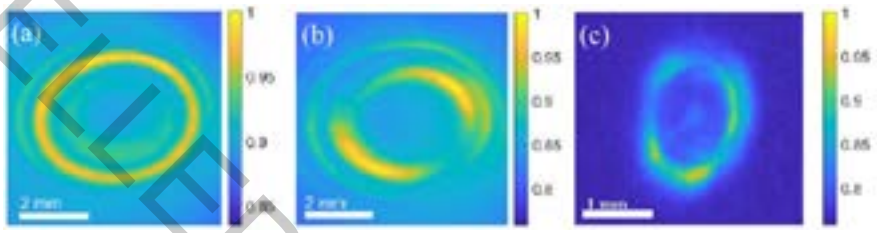

Fig. 1. Experimental images of the THz beam when it has a vortex topological charge of 0 (a), ±1 (b) and ±2 (c).

In our experiment we used two different methods for optical vortex generation. For generation of optical vortex with a topological charge of ±1 we used an s-waveplate and for generation of topological charge ±2 a nonlinear crystal was used. We used a thermographic camera to observe THz signal spatial distribution while using different combinations of topological charges of the excitation beams. It was found that when an optical vortex in a pump beam is being used, THz beam also aquires a phase modulation of a vortex. which was found by examining its intensity distributions in a collimated beam as well as focal plane of the cilindrical mirror. Moreover it was found that THz beam profile aquires different intensity modulation depending on a resulting topological charge of a THz vortex beam.

Therefore we investigated THz signal when there is an azimuthal phase modulation in one or both of pump beams. We believe that the presented investigations will open new routes towards an active control of ultra-broadband THz beam properties.

[1] Mark D. Thomson, Markus Kreß, Torsten L¨offler, and Hartmut G. Roskos, Broadband THz emission from gas plasmas induced by femtosecond optical pulses: From fundamentals to applications, Laser and photonics reviews vol. 1, no **4**, 349-368 (2007).
[2] Mark D. Thomson, Volker Blank, and Hartmut G. Roskos, Terahertz white-light pulses from an air plasma photo-induced by incommensurate two color optical fields, Optics express, vol. **18**, no. 22, 23173-23182 (2010).

CANCELLED DUE TO COVID-19

INVESTIGATION OF SCULPTURED THIN FILM GROWTH BY OPTICAL MONITORING

Gabija Petrauskaitė, Lina Grinevičiūtė, Lukas Ramalis and Tomas Tolenis

State Research Institute Center for Physical Sciences and Technology,
Savanorių ave, 231, LT-02300, Vilnius, Lithuania
gabija.petrauskaite@ftmc.lt

Thin film deposition technique is used to produce a variety of optical components which can be used in high power laser systems. In order to manufacture high quality components with high resistivity to laser damage, complex spectra and ensure process repeatability it is necessary to have accurate layer monitoring during deposition. Often used quartz monitoring is relatively accurate, however, the quality of quartz, its longevity and other factors may differ for each individual crystal, especially in higher temperature processes. Also, the quartz crystal only accounts for the number of particles deposited on it – the physical thickness. The important factor, however, is the layer's optical thickness, which also takes the refractive index into account. To enhance the accuracy, quartz monitoring is often used in conjunction with optical monitoring. The latter continuously measures the spectrum of a substrate during coating deposition process.

It is more difficult to install optical monitoring to record the growth of sculptured thin films due to constant changes in the evaporation angle between the substrate normal and evaporation angle (Fig. 1). It is important to continuously monitor the entire evaporation process at all angles since the refractive index changes with a changing angle (porosity increases with a greater angle). Therefore, a two-light-sources based monitoring system could be implemented in the vacuum chamber equipped with electron beam evaporation technology. The first experiments were performed to measure the transmission spectra of the growing thin film at 0 and 70 deg angles (Fig. 1 and 2).

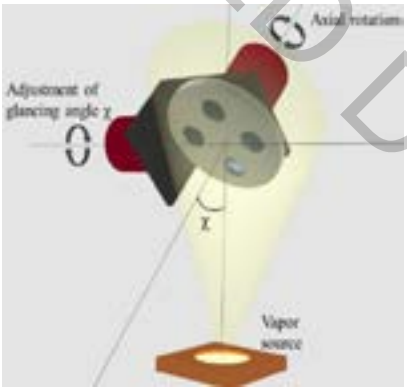

Fig. 1. Evaporation performed at an angle χ [1].

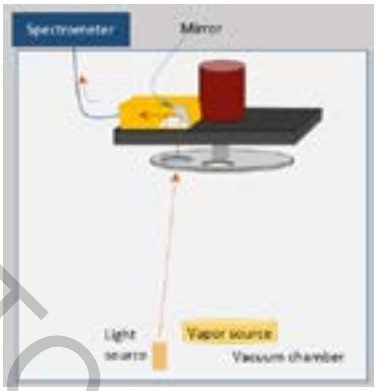

Fig. 2. Optical monitoring setup at 0deg angle with a single light source

Obtained data was used to model optical constants of the growing thin film and compared with the properties of the thin films when exposed to the atmosphere. After a multilayer mirror was deposited using quartz and optical monitoring, an error analysis was performed and indicated the weak points of quartz crystal monitoring.

Comparing the two different monitoring systems it was found that the optical monitoring recordings were more accurate on single layers, nonetheless, the recordings of multilayers still need to be improved.

[1] Grinevičiūtė, L., Andrulevičius, M., Melninkaitis, A., Buzelis, R., Selskis, A., Lazauskas, A., Tolenis, T. (2017). Highly Resistant Zero-Order Waveplates Based on All-Silica Multilayer Coatings. physica status solidi (a). 214. 1700764. 10.1002/pssa.201700764.
[2] Willey, R. R. (2006). Practical Monitoring and Control of Optical Thin Films. Willey optical, consultants.

CANCELLED DUE TO COVID-19

THE DETERMINATION OF DISPERSION AND MODELLING OF ABSORPTION DIAMOND-LIKE CARBON:SILVER NANOCOMPOSITE THIN FILMS

Justas Deveikis[1], Aušrinė Jurkevičiūtė[2], Tomas Tamulevičius[1,2], Sigitas Tamulevičius[1,2]

[1] Department of Physics, Faculty of Mathematics and Natural Sciences, Kaunas University of Technology, Studentų st. 50, LT-51368 Kaunas, Lithuania
[2] Institute of Materials Science of Kaunas University of Technology, K. Baršausko st. 59, LT-51423 Kaunas, Lithuania
justas.deveikis@ktu.edu

Diamond-like carbon (DLC) is amorphous type of carbon, in which most of the bonds between carbon atoms are sp^3 type. DLC is distinguished by its mechanical hardness, chemical inertness and optical transparency [1]. Because of these properties, DLC thin films are widely used in industry, micro-electromechanics and biomedicine. It has been observed, that DLC with embedded silver nanoparticles (DLC:Ag) changes its tribological and optical properties. The optical absorption of metallic nanoparticles embedded in the dielectric matrix shows very high visible light absorption which can be used to improve the efficiency of solar cells or make conversion from light to heat or electrical energy more effective [2].

Spectroscopic ellipsometry (SE) is an optical measurement which is used to determine the change in polarization of incident linearly polarized light upon the reflection on the sample. In this way, two parameters are measured: amplitude ratio Ψ and phase difference Δ between *s* and *p* polarized waves. It is possible to calculate the refraction index and extinction coefficient of the thin film using these parameters [3].

In this work, 2 samples of DLC:Ag with different silver atomic concentration of 14.1% (Sample 1) and 7.9% (Sample 2) were investigated employing SE. The obtained dispersion curves are shown in Fig. 1. Then these dispersion curves were used by rigorous-coupled wave analysis (RCWA) method to model the absorption of light (measured in arbitrary units) at wavelength range from 250 to 950 nm and varying the thickness of the film *d* from 10 to 200 nm at *s* and *p* polarization at a 45º angle of incidence. The results are shown in the Fig. 2

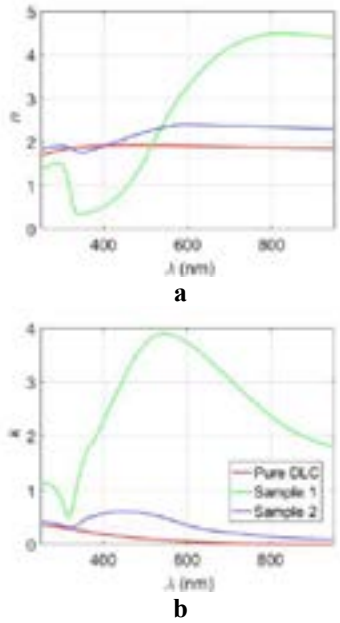

Fig. 1. The dispersion curves of investigated samples: a) refractive index *n*; b) extinction coefficient *k*.

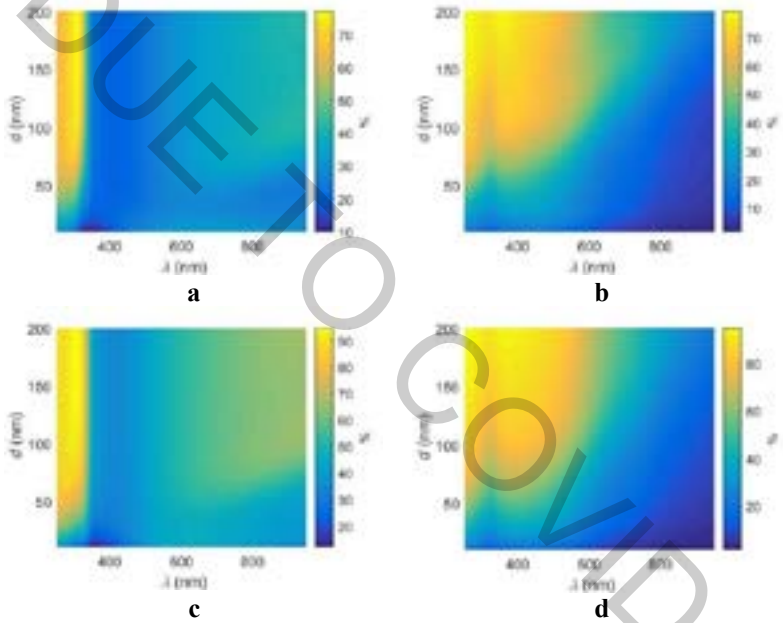

Fig. 2. The modelled absorption results at $\theta = 45^{o}$: a) of the sample 1 at *s* polarization; b) of the sample 2 at *s* polarization; c) of the sample 1 at *p* polarization; d) of the sample 2 at *p* polarization. Here *d* – the thickness of the film, λ – wavelength.

From the modelled results it is clear that at 45º angle of incidence, Sample 2 has higher light absorption in the wavelength range from 250 to 450 nm compared to Sample 1. Since the Solar cells and optical sensors have to absorb the light at wide range of angles of incidence to be efficient, the further analysis would lead to optical absorption modelling at different angles of incidence.

[1] J. Robertson, Diamond-like amorphous carbon, Mater. Sci. Eng. R. Rep. 37 (2002) 129–281.
[2] V. G. Kravets, S. Neubeck, A. N. Grigorenko, Plasmonic blackbody: Strong absorption of light by metal nanoparticles embedded in a dielectric matrix, Physical Review B 81, 165401 (2010).
[3] H. Fujiwara. Spectroscopic Ellipsometry: Principles and Applications. 2007 John Wiley & Sons, Ltd. ISBN: 978-0-470-01608-4.

CANCELLED DUE TO COVID-19

INVESTIGATION OF THERMAL EFFECTS IN POCKELS CELL WITH BBO CRYSTAL IN A HIGH AVERAGE POWER LASER SYSTEM

Jonas Banys[1], Giedrius Sinkevičius[2], Julius Vengelis[1], Rimantas Grigonis[1]

[1]Laser Research Center, Faculty of Physics, Vilnius University, Lithuania
[2]"Optolita", Mokslininkų str. 11, Vilnius, Lithuania
jonas.banys@ff.stud.vu.lt

Optical modulators are devices used to modulate a beam of light. They are used in various laser applications – regenerative amplifiers, electro-optic and acousto-optic laser beam scanners, laser-induced damage testing, laser microfabrication and modification of materials [1-2]. The most commonly used optical modulators in high-power laser systems are electro-optic modulators. They are based on the Pockels effect: when an external electric field is applied to non-centrosymmetric crystals, their refractive index changes. Consequently, a polarization change in the beam traveling through the crystal of the Pockels cell is induced, which enables the Pockels cell to be used as a voltage-controlled phase plate [3]. Beta barium borate (BBO) crystals are a widely used material for Pockels cells due to their wide transmission range, relatively high optical damage threshold and thermal stability [4-5]. However, propagation of high average power laser radiation through a Pockels cell leads to heating of the electro-optic crystal due to absorption [6]. Induced thermal load in a Pockels cell leads to thermal effects which degrade its performance, such as wave-front aberrations, stress-induced depolarization, reduced contrast ratio and thermal fracture [7]. Therefore, it is important to investigate these phenomena and determine means to reduce them.

In this work self-heating effects were investigated in a special pulse picker "MP1" which was designed and made by Lithuanian company "Optolita" and used specifically designed BBO Pockels cell with water and thermoelectric cooling. Pulse picker "MP1" can output 100 ns – 1 ms duration laser pulse trains with repetition rate of 10 Hz – 250 kHz, BBO crystal dimensions were 4x4x20 mm^3, half-wave voltage was 4.5 kV. A 15 W average power femtosecond laser system "Pharos", which was made by Lithuanian company "Light Conversion", generating 1026 nm wavelength, 609.4 kHz repetition rate and 260 fs pulses, was used as a laser source.

The dependence of the contrast ratio and crystal temperature of a BBO Pockels cell on the high-voltage control signal frequency was investigated in this study. Results show that the temperature of a BBO crystal increases with time and stabilizes after 36 minutes when no cooling was used (Fig. 1). A radial thermal gradient produces a radial strain as well as dilation of the crystal and due to stress-induced depolarization optical contrast ratio of a BBO Pockels cell decreases up to 2.13 times at the highest non-resonant high-voltage control signal frequency which in this case was 200 kHz. The results obtained show that by using water and thermoelectric cooling the temperature rise of the BBO Pockels cell crystal stabilizes much quicker (≈4 min.), the contrast ratio is 1.5 times higher with water cooling and 2 times higher with thermoelectric cooling (Fig. 2) than it was compared to case without active cooling. Thus, active cooling of the Pockels cell crystal is an efficient way to obtain the highest possible and stable optical contrast ratio.

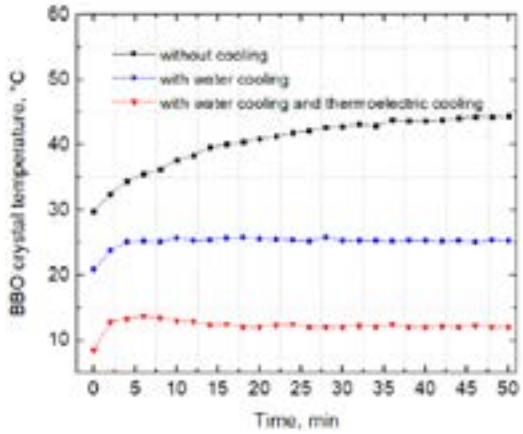

Fig. 1. BBO crystal temperature dependence over experiment time. High-voltage control signal frequency is 200 kHz, duration 1 μs.

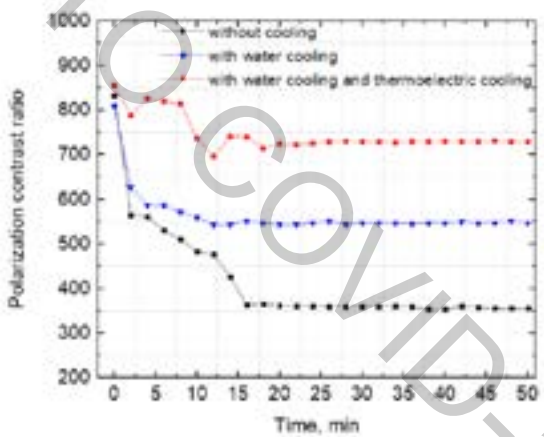

Fig. 2. BBO Pockels cell polarization contrast ratio dependence over experiment time. High-voltage control signal frequency is 200 kHz, duration 1 μs.

This study was supported by Lithuanian agency of science, innovation and technology (MITA) and performed with the partnership of "Optolita" company.

[1] S. A. Rezvani et al., Millijoule femtosecond pulses at 1937 nm from a diode-pumped ring cavity Tm:YAP regenerative amplifier," Opt. Express **26**(22), 29460–29470 (2018).
[2] C. Kerse, et al., Ablation-cooled material removal with ultrafast bursts of pulses, Nature, **537**(7618), 84-88 (2016).
[3] D. M. Robert Brunner, E. Geißler, B. Messerschmidt, A. G. Elisabeth Soergel, K. Inoue, K. Ohtaka, and K. Thyagarajan, "Advanced optical components," in *Springer Handbook of Lasers and Optics* (Springer, 2007), pp. 419–502.
[4] M. Roth, M. Tseitlin and N. Angert, Oxide crystals for electro-optic Q-switching of lasers, Phys. Chem. Glasses **31**(1), 86-95 (2005).
[5] D. Eimerl et al., Optical, mechanical, and thermal properties of barium borate, J. Appl. Phys. **62**(5), 1968-1983 (1987).
[6] I. P. Khristov, I.V. Tomov, and S.M. Saltiel, Self-heating effects in electro-optic light modulators, Opt. Quantum Electron. **15**(4), 289-295 (1983).
[7] D. Cao et al., Thermal distortion and birefringence in repetition-rate plasma electrode Pockels cell for high average power, Chin. Opt. Lett., **5**(5), 292-294 (2007).

OMICRON-LASERTECH COVID-19

INVESTIGATION OF SUPERCONTINUUM GENERATION IN POLIARIZATION-MAINTAINING PHOTONIC CRISTAL FIBER

Gabrielė Stanionytė[1], Miglė Kuliešaitė[1], Vygandas Jarutis[1], Julius Vengelis[1]

[1]Laser Research Center, Faculty of Physics, Vilnius University, Lithuania
gabriele.stanionyte@ff.stud.vu.lt

Supercontinuum generation is a nonlinear optical phenomenon when spectrum of a high intensity short pulse expands hundreds or thousands of times as it travels through a nonlinear medium [1]. One of the main applications of photonic crystal fibers (PCFs) is their usage as a nonlinear medium for supercontinuum generation, which in turn can be used in spectroscopy, frequency metrology and optical coherence tomography [2-3]. Numerous research about supercontinuum generation in PCFs have been performed, this process is not fully understood.

The goal of this research was to investigate supercontinuum generation in polarization-maintaining PCF and determine its group velocity dispersion (GVD). An optical setup for the measurements was constructed where 1030 nm wavelength, 76 MHz repetition rate and 90 fs duration pulses, generated by an Yb:KGW laser oscillator. A burst of two pulses was created using a setup consisting of a beam splitting into two parts, one of which was used as a reference pulse for cross-correlation frequency-resolved optical gating (XFROG) measurements and the other was used for pumping of supercontinuum generation in polarization-maintaining PCF. In addition, we also used a recently demonstrated technique [4] to estimate GVD of the investigated PCF using measured XFROG traces.

The results indicate that XFROG traces differ slightly when horizontal, vertical or intermediate (45°) polarization pump pulses were used: there are only slight changes in the intensity of the individual components of the supercontinuum spectra. The analysis of the XFROG traces and calculated results indicate that polarization-maintaining PCF GVD curves for the pulses of different polarizations have almost no differences. In XFROG trace we can see the bending point which corresponds to the zero group velocity dispersion wavelength (ZDW). For both horizontal and vertical polarization the ZDW wavelength is 1087.4 nm. This shows that the GVD of this polarization-maintaining PCF differs so little for the perpendicular polarization pulses, that it cannot be distinguished by the measurement technique which was used.

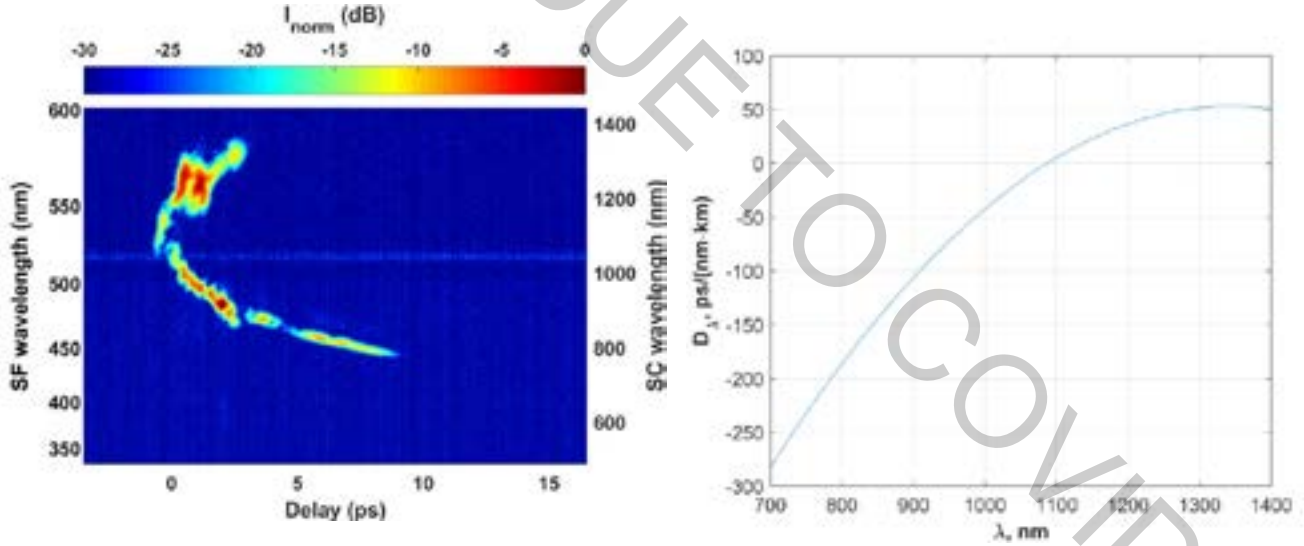

Fig. 1. Left - measured XFROG trace of supercontinuum generated in polarization-maintaining PCF. Right - calculated corresponding dispersion parameter. Pump power in this case was 0.964 W

ON HOLD DUE TO COVID-19

[1] A. Dubietis, *Netiesinė optika*, (Publisher Vilnius University, Vilnius 2011).
[2] J. C. Knight, Photonic crystal fibres, Nature, **424** (6950), 847-851 (2003).
[3] S. J. Philip. R. Russell, Photonic-Crystal Fibers, J. Lightwave Technol. **24**(12), 4729–4749 (2006).
[4] J. Vengelis, V. Jarutis, V. Sirutkaitis, Estimation of photonic fiber dispersion by means of supercontinuum generation, Opt. Lett. **42**(9), 1844-1847 (2017).

SPECTRAL CHARACTERISTICS OF TRUE-COLOR DOT-MATRIX HOLOGRAMS

Tomas Klinavičius[1], Tomas Tamulevičius[1,2]

[1] Institute of Materials Science, Kaunas University of Technology, Lithuania
[2] Department of Physics, Kaunas University of Technology, Lithuania
tomas.klinavicius@ktu.lt

Holographic security labels are worldwide used and recognized means for anti-counterfeiting applications. A common technology for realization of these labels is a dot-matrix hologram [1]. Dot-matrix holograms are usually composed of a two dimensional array of <100 μm sized spots where each spot within itself contains one (or several) diffraction gratings with a defined pitch and orientation, and the entire array is imposed on a reflective surface. The working principle of this type of hologram can be explained using conical diffraction formalism [2, 3]. It is a type of diffraction that occurs when the light incident on a diffraction grating is not perpendicular to the grooves of the diffraction grating. Selection of correct diffraction grating parameters for each hologram pixel is of paramount importance for designing such holograms. The appearance of dot-matrix holograms can be precisely modelled once their structure is given along with illumination and observation conditions [3]. Moreover, the true-color hologram appearance could be obtained that is not achievable with any digital printing technique.

This work explores determination of the dot-matrix hologram parameters necessary to ensure that the hologram originated via direct femtosecond laser interference patterning would look exactly as the selected colored object in the digital image. The proposed algorithm considers the parameters of the target hologram image itself along with its illumination and observation conditions. Fig. 1 depicts a digital image of an apple (a), rendered hologram diffraction image (b) and an actual hologram image captured with a digital camera (c). Spectral characteristics and the overall quality of the reconstructed images were evaluated.

Fig. 1. a) digital image of the hologram object, b) model of the true-color hologram diffraction image, c) photograph of the true-color hologram

[1] C. Braig, et al., An EUV beamsplitter based on conical grazing incidence diffraction, Optics Express **20**, 1825-1838 (2012).
[2] D. Pizzanelly, The development of direct-write digital holography, Technical review, Holographer.org.
[3] T. Tamulevičius, et al. Dot-matrix hologram rendering algorithm and its validation through direct laser interference patterning, Scientific Reports **8**, 14245 (2018)

CANCELLED DUE TO COVID-19

PARAMETRIC GENERATION AT 648 NM IN A LMA PHOTONIC CRYSTAL FIBER

Gustas Liaugminas[1], Julijanas Želudevičius[1], Kęstutis Regelskis[1]

[1] Department of Laser Technology, Center for Physical Sciences & Technology, Savanoriu Ave. 231, Vilnius, Lithuania
gustas.liaugminas@ftmc.lt

There is a high demand for pulsed visible spectrum coherent light sources in applications like spectroscopy, microscopy and medical therapy [1]. For all-fiber laser systems, degenerate four-wave mixing process allows conversion of two pump photons of the same wavelength into two different photons - one of longer and one of shorter wavelength than the pump photon. For this process to happen, certain phase-matching conditions should be met so that phase velocity for all four interacting waves are the same within the optical fiber. In general, three members that contribute to phase mismatch (phase velocity difference due to waveguide structure, material dispersion and non-linearities) have to cancel each other out. To fulfill such requirements for specific wavelengths, usually custom-designed optical fibers are needed. One example is photonic crystal fiber (PCF). Due to unique structure of PCF, it can have shifted dispersion curve compared to ordinary single-mode fiber. This characteristic allows all kinds of phase-matching scenarios for different types of photonic crystal fibers [2].

In this work, a solid-core commercially available photonic crystal fiber was used with a mode field diameter of 7.5 μm (1064 nm) and length of 30 cm. Pulsed fiber laser operating at 1038 nm wavelength and generating 250 ps pulses with repetition rate of 100 kHz was used as our pump source for frequency conversion. Pump pulses were amplified in two fiber amplifier stages and a Yb-doped photonic crystal fiber amplifier at the final stage. After coupling the pump pulses into our frequency conversion PCF and increasing average power to 0.18 W (pulse energy 1.8 μJ) the peak at 648 nm was registered. This wavelength matches theoretical value calculated from phase matching condition for four-wave mixing process. By increasing energy of the pump pulses, maximum of ~2.6 μJ energy pulses at 648 nm were generated with the maximum conversion efficiency of 31 %. From energy conservation law follows that maximum conversion efficiency (to signal wave at 648 nm) can be up to 80.7 %, but in reality this value is much lower due to all kinds of imperfections like temporal walk-off of the interacting wave-packets, signal wave reconversion to pump waves as well as PCF geometry variations and pump pulse parameter fluctuations.

Our results show that frequency conversion in a photonic crystal fiber remains a good method to produce short optical pulses in a visible spectral region. The results of this research is a base for further investigations to build a tunable all-fiber pulsed laser source operating in wide spectral range.

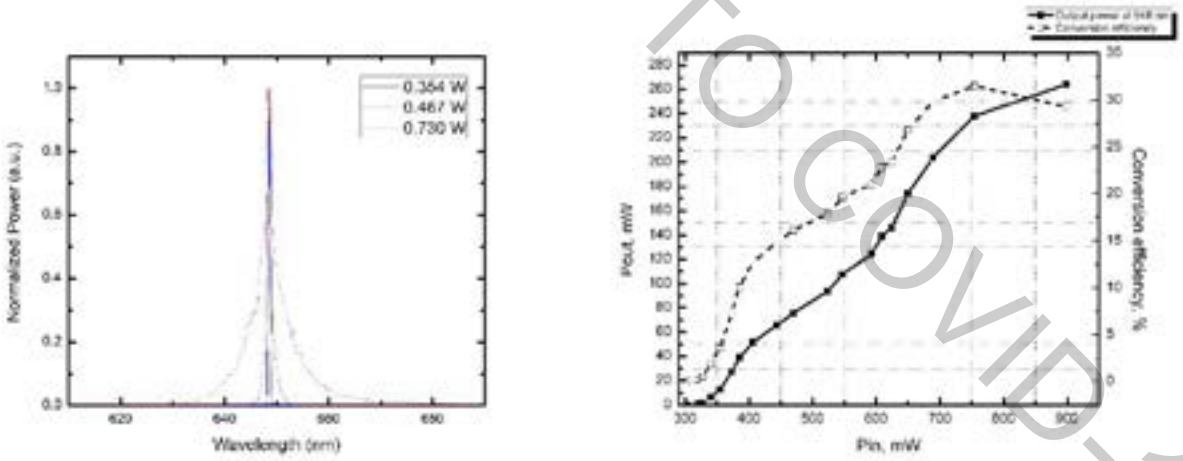

Fig. 1. Normalized spectrum of the signal wave at 648 nm (left). Average power of the signal wave and conversion efficiency vs pump power (right).

[1] C. Jauregui, A. Steinmetz, D. Nodop, J. Limpert, and A. Tunnermann, All-fiber parametric generation of sub-100ps pulses at 650nm with 9Watt average power, *Lasers, Sources, and Related Photonic Devices* (Optical Society of America, 2012).

[2] G. P. Agrawal, *Nonlinear Fiber Optics* (Academic, 2001).

CANCELLED DUE TO COVID-19

DEEP UV SUPERCONTINUUM GENERATION IN LISAF CRYSTAL USING FEMTOSECOND LASER PULSES

Agnė Šuminienė, Rosvaldas Šuminas, Vytautas Jukna, Gintaras Tamošauskas, Mikas Vengris, Audrius Dubietis

Laser Research Center, Vilnius University, Lithuania
agne.suminiene@ff.vu.lt

Ultrashort ultraviolet (UV) pulses are very desirable and widely applicable in time-resolved spectroscopy [1]. Unfortunately, supercontinuum (SC) generation in this particular spectral range is complicated due to unfavorable physical factors such as low order nonlinear absorption and high material dispersion, which increases with frequency and limits the achieved broadening of SC spectrum. Additionally, during filamentation of UV laser pulses, due to large incident photon energies, materials experience optical degradation and eventually, optical damage.

Therefore, it is more convenient to use visible or near infrared (IR) input wavelengths for UV SC generation. It was shown that alkali metal fluorides (LiF, CaF_2, MgF_2, BaF_2) produce SC spectra with blue shifts reaching below 300 nm and, in this aspect, outperform popular visible and near IR SC materials like YAG or sapphire [2,3]. However, fluorides demonstrating largest SC spectral blue shifts (LiF and CaF_2) experience other issues such as rapid color center formation and consequential SC spectral narrowing (LiF) and heat accumulation which leads to optical damage (CaF_2). These challenges encourage the search for new suitable nonlinear materials for UV SC generation. An attractive candidate is lithium strontium hexafluoraluminate ($LiSrAlF_6$, LiSAF) – a laser host crystal usually doped with chromium or cerium. Chromium doped LiSAF produces tunable laser pulses in the near IR region [4] while LiSAF doped with cerium is an appealing solid-state laser material, providing pulses in 280-320 nm range [5] and, therefore, highly resistant to intense UV irradiation. Additional LiSAF properties include a very large bandgap of 11.79 eV [6], 116 nm short-wavelength absorption edge, low refractive index and low chromatic dispersion from UV to near IR spectral range. The listed properties make LiSAF a potentially appealing material for SC generation in the UV spectral range.

In this Contribution, we present an experimental study of SC generation in an undoped 5 mm thick LiSAF crystal using UV, visible and near IR pump pulses as provided by fundamental and second harmonics of femtosecond Ti:sapphire and Yb:KGW lasers. SC spectra generated in LiSAF at respective wavelengths are depicted in Fig 1. In order to evaluate the spectral longevity of the UV SC generated in LiSAF, we investigate spectral dynamics of the blue part of the SC spectrum over time (not shown). Our measurements demonstrate that narrowing of the SC spectrum due to optical degradation of the crystal starts much earlier with pump pulses of longer wavelength. This observation is explained by the impact ionization, which increases with increasing the pump wavelength. The most stable SC generation is achieved with the shortest pump wavelength of 400 nm where LiSAF produces a 1.28 octave spanning SC spectrum with a UV cut-off at 253 nm (measured at 10^{-5} spectral intensity level) and shows no spectral degradation for two hours of operation at 500 Hz repetition rate without translating the crystal.

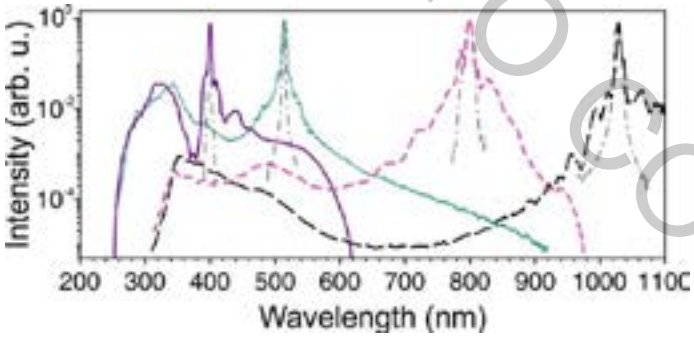

Fig. 1. Measured normalized SC spectra in LiSAF crystal pumped with 0.6 μJ, 400 nm (solid purple curve), 2 μJ, 515 nm (dotted green curve), 1.8 μJ, 800 nm (short-dashed pink curve) and 10 μJ, 1030 nm (long-dashed black curve) laser pulses. Grey dash-dotted curves represent spectra of the input pulses.

[1] N. Krebs, I. Pugliesi, J. Hauer, and E. Riedle, Two-dimensional Fourier transform spectroscopy in the ultraviolet with sub-20 fs pump pulses and 250-720 nm supercontinuum probe, New. J. Phys. **15**, 085016 (2013).
[2] R. Huber, H. Satzger, W. Zinth, and J. Wachtveitl, Noncollinear optical parametric amplifiers with output parameters improved by the applications of a white light continuum generated in CaF_2, Opt. Commun. **194**, 443-448 (2001).
[3] P. Tzankov, I. Bucharov, and T. Fiebig, Broadband optical parametric amplification in the near UV-VIS, Opt. Commun. **203**, 107-113 (2002).
[4] D. Kopf, A. Prasad, G. Zhang, M. Moser, and U. Keller, Broadly tunable femtosecond Cr:LiSAF laser, Opt. Lett. **22**, 621-623 (1997).
[5] C. D. Marshall, J. A. Speth, S. A. Payne, W. F. Krupke, G. J. Quarles, V. Castillo, and B. H. T. Chai, Ultraviolet laser emission properties of Cr^{3+}-doped $LiSrAlF_6$ and $LiCaAlF_6$, J. Opt. Soc. Am. B **11**, 2054-2065 (1994).
[6] M. V. Luong, M. J. F. Empizo, M. Cadatal-Raduban, R. Arita, Y. Minami, T. Shimizu, N. Sarukura, H. Azechi, M. H. Pham, H. D. Nguyen, Y. Kawazoe, K. G. Steenbergen, and P. Schwerdtferger, First-principles calculations of electronic and optical properties of LiCaAlF6 and LiSrAlF6 crystals as VUV to UV solid-state laser materials, Opt. Mater. **65**, 15-20 (2017).

CANCELLED DUE TO COVID-19

FORMATION OF 3D MICROSTRUCTURES IN POLYDIMETHYLSILOXANE VIA FEMTOSECOND LASER IRRADIATION

Tomas Jurkšas[1], Mindaugas Juodėnas[2], Tomas Tamulevičius[1,2], Artūras Vailionis[1,3], Sigitas Tamulevičius[1,2]

[1] Department of Physics of Kaunas University of Technology, Studentų St. 50, LT-51368, Kaunas, Lithuania
[2] Institute of Materials Science of Kaunas University of Technology, K. Baršausko St. 59, LT-51423, Kaunas, Lithuania
[3] Stanford Nano Shared Facilities, Stanford University, Stanford, CA 94305, USA
t.jurksas@ktu.edu

CANCELLED DUE TO COVID-19

Polydimethylsiloxane (PDMS) is one of the most widely used flexible polymers for various microdevices due to its physical flexibility, ease of processing, high chemical resistance, and high transmission in visible spectral region. Ultra-short femtosecond laser pulses have been shown to modify the refractive index of PDMS or even form microcavities when focused in bulk of material [1]. The formation of microcavities allows to form 3D structures in the volume of PDMS. This could be used to create 3D microchannels or optical elements inside PDMS without affecting its surface or using other, more complicated and time-consuming methods like soft lithography.

By changing pulse energy, pulse density and pulse repetition rate of the Yb:KGW femtosecond laser, we can choose between modifying PDMS refractive index or creating microcavities. Figure 1. depicts how the volume of the 3D cubes can be micromachined depending on the laser writing parameters, where cube in the bottom left corner, has the lowest pulse energy of 0.75 μJ and pulse density of 50 pulses per mm, while cube in the top right corner has the highest, i.e. 3.75 μJ and 250 pulses per mm, respectively. Three types of laser damages were identified from the bright field images of the optical microscope.

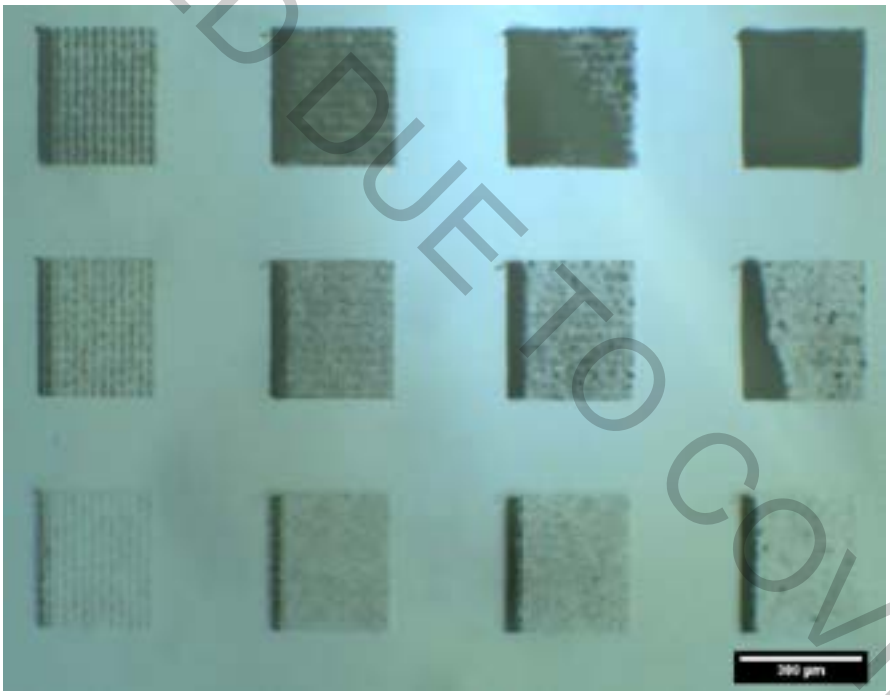

Fig. 1. Optical microscope micrographs of the 300 x 300 x 300 μm sized 3D cubes in the volume of Sylgard 184 (DowCorning) PDMS after the fs-laser treatment under different energy densities (energy increasing vertically, pulse density increasing horizontally).

X-ray microtomography was employed for the characterization of 3D microstructures. It is a non-destructive method for investigation of local density changes in the volume of materials with micrometric spatial resolution.

Acknowledgements: This research was funded by the European Social Fund under the No. 09.3.3-LMT-K-712 "Development of Competences of Scientists, other Researchers and Students through Practical Research Activities" measure, grant No. 09.3.3-LMT-K-712-16-0201.

[1] L. N. D. Kallepalli et al., Femtosecond-laser direct writing in polymers and potential applications in microfluidics and memory devices, Optical Engineering 51(7) (2012).

INVESTIGATION OF THE LASER SCRIBING CAUSED DAMAGE TO THE METAL COATING OF THE TRANSPARENT MEDIA

Evaldas Svirplys[1,2], Simonas Indrišiūnas[1],

[1] Department of Laser Technologies, Center for Physical Sciences and Technology, Lithuania
[2] Department of Optoelectronics, Center for Physical Sciences and Technology, Lithuania
evaldas.svirplys@ff.stud.vu.lt

CANCELLED DUE TO COVID-19

In recent decades laser has proven to be a versatile tool for cutting, drilling, ablating and micro-processing a variety of engineering materials [1]. Pulsed lasers provide submicrometre precision due to reduced heat diffusion related to fast laser–matter interaction, thus it is great for cutting transparent substrates with coated thin layers on them [2].

In this work we present, to our knowledge, previously little studied phenomena of laser beam causing damage to the back-side coating layer of the transparent media at the large distances from the scribe line (comparing to the laser beam spot-size). While laser scribing 1 mm thick fused silica glass with 30 nm-thick gold layer, ablated area in gold approximately 0.9 mm away and parallel to the laser beam was observed (Fig. 1).

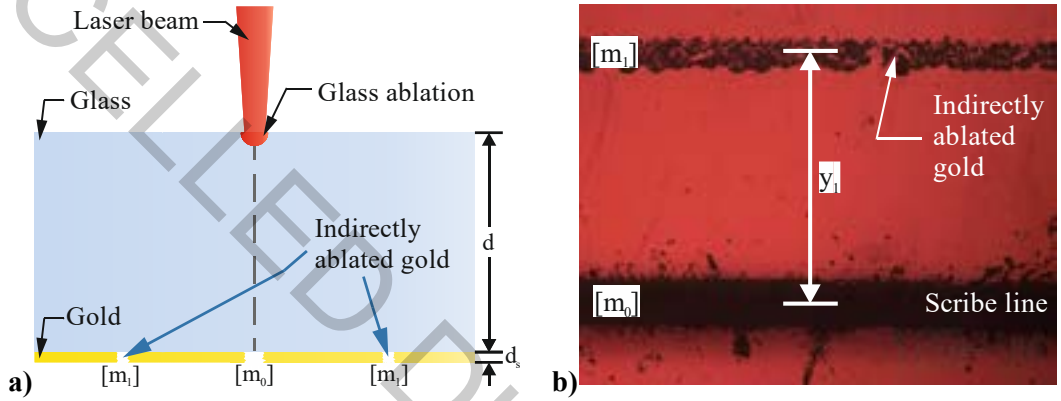

Fig. 1. (a) – Scheme of laser cutting of glass with gold thin film, deposited on the back-side, and ablated areas alongside the scribe line, (b) optical microscope image of the damage alongside the scribe line, y_1 – distance from directly and indirectly ablated lines.

In order to further investigate this phenomena picosecond pulsed laser (λ_{IH} = 1064 nm, λ_{IIH} = 532 nm) with galvanometer scanner were used. Experiments varying glass thickness, gold film thickness, laser wavelength, laser polarization and beam angle of incidence were performed (Fig. 2).

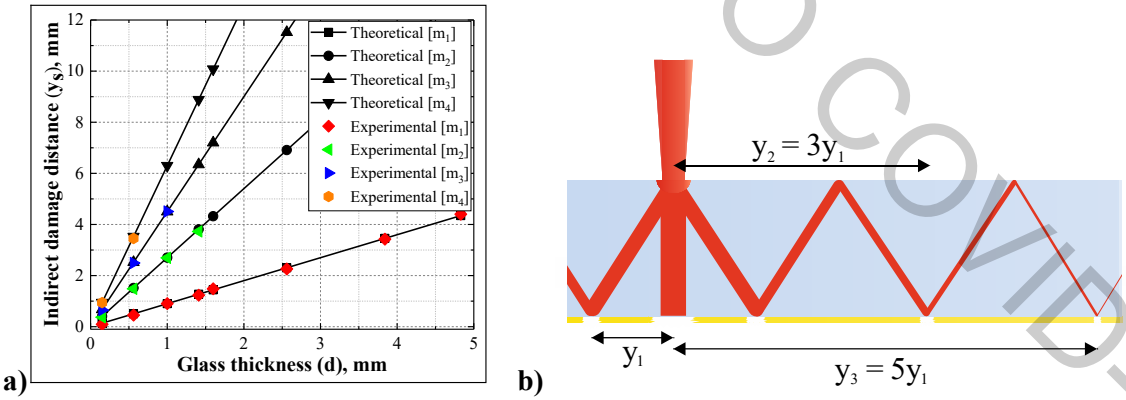

Fig. 2. (a) – Relationship between the Indirect damage distance from the center of the scribe line and glass thickness; several lines of indirect damages were seen when using glass thinner than 2 mm, (b) illustrates how these lines may be formed by diffraction and reflection.

Theoretical calculations of Fraunhofer diffraction were performed and compared with the experimental data. It was concluded, that indirect ablation of thin gold layer is due to the laser beam diffraction from the glass ablation area, where laser beam interaction with the medium reduces its transparency.

[1] G. Račiukaitis et al., Use of high repetition rate and high power lasers in microfabrication: How to keep the efficiency high?, *Journal of Laser Micro Nanoengineering* **4**(3) (2009): 186–191, doi:10.2961/jlmn.2009.03.0008.

[2] J. Hermann et al., Comparative investigation of solar cell thin film processing using nanosecond and femtosecond lasers, *J. Phys. D: Appl. Phys***39** (2006): 453–460, doi:10.1088/0022-3727/39/3/005.

WHISPERING GALLERY MODE MICRORESONATOR AS A HUMIDITY SENSOR: SENSING MECHANISMS AND APPLICATIONS

Lase Milgrave[1,2], Pauls Kristaps Reinis[2], Janis Alnis[2], Aigars Atvars[2]

[1] Department of Physics, University of Latvia, Latvia
[2] Quantum Optics Laboratory, Institute of Atomic Physics and Spectroscopy, University of Latvia, Latvia
lase.milgrave@lu.lv

CANCELLED DUE TO COVID-19

Whispering gallery mode microresonators (WGM) are widely researched due to their high quality (Q) factors and sensitivity. High Q factor is the result of the structure of the resonator: microspheres, microbottles, microbubble/capillaries, microtoroids, microrings, and microdisks. These cavities have smooth edges, they are transparent, and their refractive index is higher than that of surrounding environment, and therefore continuous total internal reflection occurs. The structures confine resonant photons for long periods of time, allowing resonant optical fields to travel inside the resonator for multiple times, which increases the sensitivity of the sensors [1]. There are many applications to WGM microresonators, such as spectroscopy and fluorescence studies, generation of frequency combs, biosensing and many others [2]. This study explores WGM microresonator as a humidity sensor, using glycerol microsphere.

Precise humidity measurements are important in various sectors: industrial processing, environmental control, automobile industry, medical field, agriculture, and general industry [3]. However, the available humidity sensors can be slow and work properly only in medium humidity levels. This study researches the precise measurements of relative humidity (RH) both in high and low humidity, which is possible using a silica microsphere dipped in pure glycerol and a tunable laser. For the experiment, glycerol was chosen due to its hygroscopicity, transparency and its stability in time and temperature. Glycerol's ability to absorb and adsorb water from the surroundings until it stabilizes is the reason shift in WGM can be observed. As glycerol absorbs water, its radius and refractive index change, resulting in a shift in resonant wavelength:

$$m\lambda = 2\pi R n_{eff}, \quad (1)$$

where m is an integer number, λ is the resonant wavelength, R is the radius and n_{eff} is the effective refractive index. It means that an integer number of wavelengths fit the optical path of the resonator [4]. In this experiment glycerol droplet of R = 0.5 mm was used. To obtain whispering gallery resonances tunable laser with wavelength 760 nm was used. Light from the laser excites the microsphere and shift in resonant frequencies was observed using an oscilloscope.

Results from this experiment are promising – glycerol as a resonator is stable both in time and temperature (no fluctuations due to change in room temperature were observed, the droplet did not evaporate or fall off the silica sphere with time), with fast reaction time, and it works in all ranges of RH. Using an oscilloscope, data was collected in the range from 55 to 65 % RH, shift in modes was observed. Results are presented in Fig. 1 where data was fitted to 5th order polynomial. However, further development of the experiment is necessary as at high humidity levels the volume of the droplet increases rapidly, and the laser beam no longer is focused in a way that excites WGM. Automated laser beam adjustment is necessary.

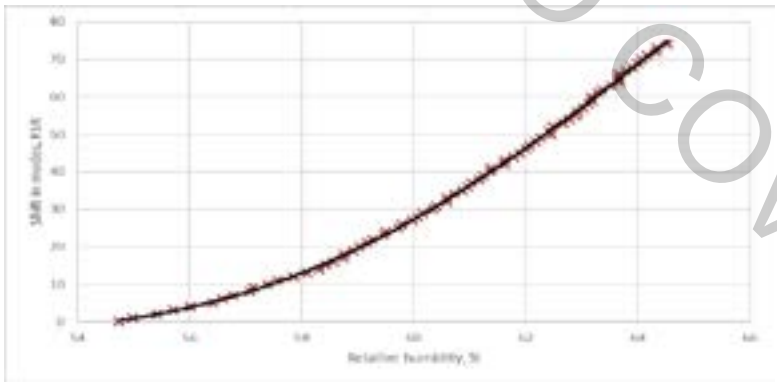

Fig. 1. Shift of WGM modes due to change in relative humidity, Shift counted in Free Spectral Range (FSR) units.

The results of this experiment show that glycerol droplet as a RH sensor is very precise, which is necessary for many industrial needs and scientific studies. Further research on this subject is necessary to test the resonator in low humidity levels, as well as test the repeatability and hysteresis of this sensor.

This study was financed by LZP project Nr.lzp-2018/1-0510 'Whispering gallery mode microresonator sensor'

[1] X. Jiang *et al.*, Whispering gallery microsensors: a review, Cornell University, arXiv:1805.00062 (2018).
[2] M. Gomilsek, Whispering gallery modes, University of Ljubljana (2011).
[3] Z. Chen, C. Lu, Humidity Sensors: A Review of Materials and Mechanisms, Sensor Letters **3,** 274-295 (2005).
[4] L. Labrador-Paez *et al*., Liquid whispering-gallery-mode resonator as a humidity sensor, Optics Express **25**, 1165-1172 (2017).

SUPERCONTINUUM GENERATION IN SAPPHIRE AND YAG: A COMPARATIVE STUDY

Vaida Marčiulionytė, Danil Bulatov, Robertas Grigutis, Nail Garejev, Gintaras Tamošauskas, Audrius Dubietis

Laser Research Center, Faculty of Physics, Vilnius University, Lithuania
vaida.marciulionyte@ff.stud.vu.lt

CANCELLED DUE TO COVID-19

Supercontinuum (SC) generation, also known as a spectral superbroadening, is an effect produced by filamentation of ultrashort laser pulses in dielectric media and resulting in a broadband radiation with high spatial and temporal coherence [1]. Thanks to these unique properties, SC finds diverse applications in spectroscopy, ultrafast nonlinear optics and photonics [2]. The most durable and reliable nonlinear materials to generate stable and reproducible SC in the visible and near-infrared spectral regions are sapphire and YAG crystals, which have high optical nonlinearity, wide band-gap, wide transmission range and high damage threshold. Many in depth studies have been conducted on SC generation in transparent bulk materials at low (1 kHz) pulse repetition rates [3,4]. Nowadays, high (hundreds of kHz or more) repetition rate lasers became available. However, no research has been done on production of SC with femtosecond lasers at high pulse repetition rates.

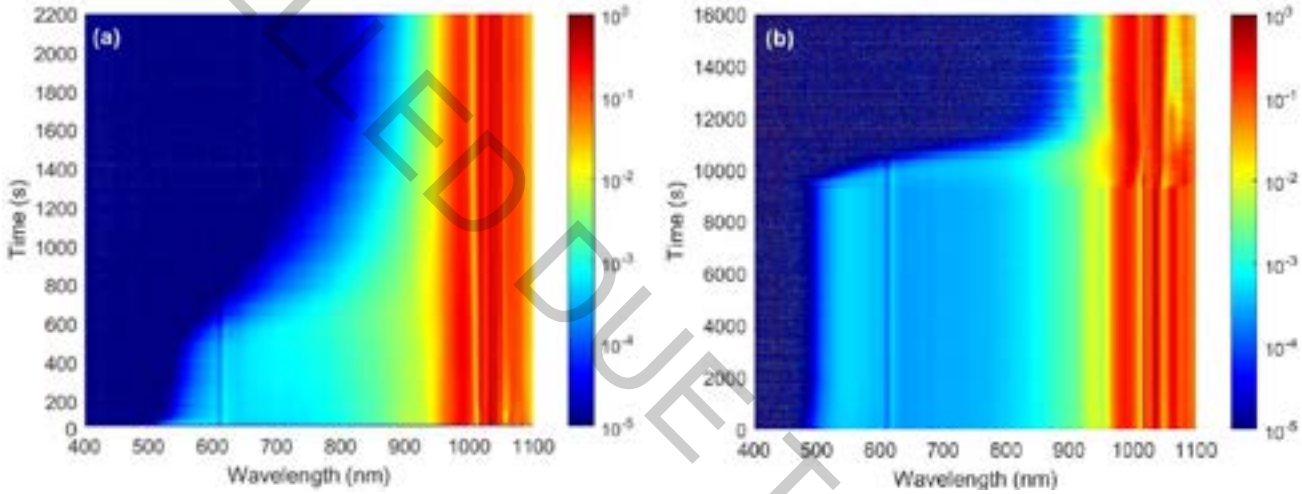

Fig. 1. The time evolutions of supercontinuum spectra in sapphire (a) and YAG (b) crystals at 200 kHz pulse repetition rate, with NA = 0.083 focusing conditions.

In this study, we experimentally investigated SC generation in sapphire and YAG crystals pumped with amplified Yb:KGW laser emitting at 1030 nm, having a pulse duration of 180 fs, and a high repetition rate of 200 kHz. The time evolution of SC spectra in tight (NA = 0.083) and loose (NA = 0.025) focusing conditions in sapphire crystal were also measured.

We observed similar SC spectral widths for both sapphire and YAG crystals ranging from visible (490 nm) to near-IR spectral range. The time evolutions of SC spectra in sapphire and YAG were investigated (Fig. 1). Our study revealed that the SC spectrum shrinks much faster in sapphire (~15 s) than in YAG (~2.5 hours) under the same experimental conditions with NA = 0.083. Our results show that production of damage-free SC in sapphire at high repetition rates could be significantly increased by choosing low NA focusing conditions. However, compared to sapphire, YAG is much more resistant even in tight focusing conditions. We believe that our findings provide insight for optimizing SC generation conditions such as beam focusing geometry and energy at high femtosecond laser pulse repetition rates, which could lead to improved system stability necessary for many practical applications.

[1] A. Dubietis, G. Tamošauskas, R. Šuminas, V. Jukna, and A. Couairon, Ultrafast supercontinuum generation in bulk condensed media, Lith. J. Phys. 57, 113–157 (2017).
[2] C. Manzoni and G. Cerullo, Design criteria for ultrafast optical parametric amplifiers, J. Opt. 18, 103501 (2016).
[3] M. Bradler, P. Baum, and E. Riedle, Femtosecond continuum generation in bulk laser host material with sub-μJ pump pulses, Appl. Phys. B 97, 561-574 (2009).
[4] A.-L. Calendron, H. Cankaya, G. Cirmi, and F. X. Kartner, White-light generation with sub-ps pulses, Opt. Express 23, 13866-13879 (2015).

WATER-ASSISTED GLASS ABLATION WITH PICOSECOND LASER

Laimis Zubauskas, Edgaras Markauskas

Center for Physical Sciences and Technology, Savanoriu Ave. 231, LT-02300, Vilnius, Lithuania
laimis.zubauskas@ftmc.com

Electronic and photonic industries demand fast and high-quality processing of glasses. Compact lasers, collimators, wave-meters and other compact systems utilize small-sized optical elements, often of a complex design. Such elements can be cut out of the standard 1 or 2-inch optical elements using laser-based technologies, such as direct laser ablation, rear side drilling and crack generation in the bulk of the material. Rear side drilling and crack generation techniques offer highest processing rates but have geometric, processing quality and technological limitations [1, 2]. Therefore, the direct ablation technique seems to be the most versatile, allowing high processing quality and cutting of complex shapes. However, the latter approach suffers from low cutting speeds [3].

Although the new ultra-short pulsed lasers offer high average power at high-pulse repetition rates allowing even faster production, the full laser potential is rarely utilized in glass cutting applications. Energy fluence, scanning speeds, pulse repetition rates and other laser parameters are limited to avoid glass overheating and generation of cracks [4, 5, 6]. Fortunately, studies have shown that laser processing speeds could be significantly increased by introducing a thin flowing water layer onto the surface of the workpiece [7, 8, 9].

In this work, a picosecond laser working at 1064 nm wavelength was used to evaluate the direct laser ablation efficiency and process quality of soda-lime, borosilicate and SF6 glasses in ambient air and water-assisted environments. Efficient ablation of the grooves and complete cutting of glass plates were investigated. Optimal laser parameters for ablation and water supply methods were defined.

Results revealed the improved ablation efficiency and glass cutting rates when the thin water layer was introduced into the laser ablation area. At optimal conditions, the glass ablation efficiency was improved 6-fold, reaching 0.18 mm^3/min/W, compared to the ablation in ambient air. Furthermore, the applied water layer reduced both the edge roughness and the chipping of glass material at the edges of the grooves (see Figure 1). Finally, optimal parameters were used to cut out optical elements of 5 mm in diameter out of the 1 mm thick mirror-coated optical glass at a cutting rate of 0.22 mm/s.

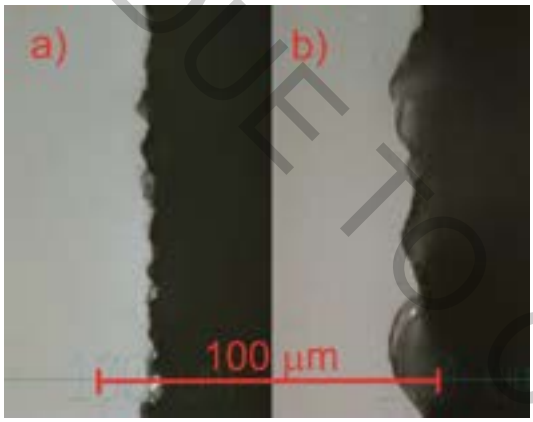

Figure 1 Images of the ablated channels in borosilicate glass in water-assisted conditions (a) and in ambient air (b) at 520 kHz pulse repetition rate.

[1] P. Gečys, J. Dudutis, and G. Račiukaitis, Nanosecond Laser Processing of Soda-Lime Glass. Journal of Laser Micro/Nanoengineering, 2015. 10(3): p. 254-258.
[2] J. Dudutis, P. Gečys, and G. Račiukaitis. Modification of glass using an axicon-generated non-symmetrical Bessel-Gaussian beam. in SPIE LASE. 2017. SPIE
[3] S. Nikumb, Q. Chen, C. Li, H. Reshef, H.Y. Zheng, H. Qiu, and D. Low, Precision glass machining, drilling and profile cutting by short pulse lasers. Thin Solid Films, 2005. 477(1): p. 216-221.\\
[4] B. N. Chicbkov, C. Momma, S. Nolte, F. yon Alvensleben, A. Tiinnermann, Femtosecond, picosecond and nanosecond laser ablation of solids, Appl. Phys., 1996. 63, 109-115.
[5] M. Sun, U. Eppelt, S. Russ, C. Hartmann, C. Siebert, J. Zhu, W. Schulz, Numerical analysis of laser ablation and damage in glass with multiple picosecond laser pulses, Optics Express, 2013. 21, 7.
[6] I. Mirza, N. M. Bulgakova, J. Tomastik, V. Michalek, O. Haderka, L. Fekete, T. Mocek, Ultrashort pulse laser ablation of dielectrics: Thresholds, mechanisms, role of breakdown, Scientific Reports, 2016. 6: Article number: 39133.
[7] J. J. J. Kaakkunen, M. Silvennoinen, K. Paivasaari, P. Vahimaa, Water-Assisted Femtosecond Laser Pulse Ablation of High Aspect Ratio Holes, Physics Procedia, 2011, 12: p. 89–93
[8] N. Krstulović, S. Shannon, R. Stefanuik, and C. Fanara, Underwater-laser drilling of aluminum. The International Journal of Advanced Manufacturing Technology, 2013. 69(5): p. 1765-1773.
[9] W. Charee and V. Tangwarodomnukun, Dynamic features of bubble induced by a nanosecond pulse laser in still and flowing water. Optics & Laser Technology, 2018. 100: p. 230-243.

CANCELLED DUE TO COVID-19

MATHEMATICAL MODELING OF COATING BASED ACHROMATIC WAVEPLATE

Ivona Juchnevičiūtė[1,2], Lina Grinevičiūtė[2], Tomas Tolenis[2]

[1] Department of Physics, Vilnius University, Lithuania
[2] Department of Laser Technologies, Center for Physical Sciences and Technology, Lithuania
ivona.juchneviciute@ff.stud.vu.lt

CANCELLED DUE TO COVID-19

The discovery and understanding of circular polarization vision in a mantis shrimp (*Stomatopod Crustacean)* [1] inspired the creation of an achromatic optical coating based quarter-wave retarder [2]. Achromatic phase retardation is exceptionally unusual optical phenomena due to the dispersion of materials. Achromatic phase retardation can be obtained in thin film optical coatings made of birefringent materials where the refractive index is different for x and y components of e-vector and it also depends on the wavelength of incident light. Thin film optical coating based waveplate is a layered structure which properties depend on multiple parameters, such as number and thickness of layers, refraction index and wavelength of light. Since the desired waveplate is achromatic, the dependence on wavelength of light must be eliminated. Selection of the correct parameters can not be done analytically but the system can be designed and parameters found by using mathematical models and numerical optimization methods.

Phase retardation can be calculated from [3]:

$$\xi = \arctan\left[\frac{-\mathrm{Im}(\eta_0 B + C)}{\mathrm{Re}(\eta_0 B + C)}\right] \tag{1}$$

Where η_0 is the admittance of incident medium and *B, C* are the parameters of thin film optical coating:

$$\begin{bmatrix} B \\ C \end{bmatrix} = \left(\prod_{r=1}^{q} \begin{bmatrix} \cos\delta_\mathrm{r} & (i\sin\delta_\mathrm{r}/\eta_\mathrm{r}) \\ i\eta_\mathrm{r}\sin\delta_\mathrm{r} & \cos\delta_\mathrm{r} \end{bmatrix}\right)\begin{bmatrix} 1 \\ \eta_\mathrm{m} \end{bmatrix} \tag{2}$$

Where the characteristic matrix of a single layer is multiplied q times, q is the number of layers in thin film optical coating. η_r is the admittance of incident medium, η_m is the admittance of substrate, phase thickness of a coating $\delta_\mathrm{r} = 2\pi nd\cos\alpha/\lambda$ where *n* is refractive index, *d* is physical thickness of a layer, α is incident angle.

But according to Herpin's theorem a symmentrical thin-film combination ABA is equivalent to a single film [4] and therefore its phase retardation can be calculated in a simple way:

$$\xi = \mathrm{q}(\gamma_\mathrm{y} - \gamma_\mathrm{x}) \tag{3}$$

Where phase thickness of a coating for one polarization:

$$\gamma = \arccos\left(\cos 2\delta_\mathrm{A}\cos\delta_\mathrm{B} - \frac{1}{2}\left(\frac{n^\mathrm{B}}{n^\mathrm{A}} - \frac{n^\mathrm{A}}{n^\mathrm{B}}\right)\sin 2\delta_\mathrm{A}\sin 2\delta_\mathrm{B}\right) \tag{4}$$

There is no need to multiply matrices q times and when more layers are added to have higher phase retardation, the multiplication of one symmetrical layer phase retardation by q is done.

By calculating all possible phase retardation values for different wavelenghts, refractive index values and physical thickness values, the best physical thickness of layers can be found by data analysis, comparing deviation and mean values of each data set. Choosing data set with lowest deviation (when phase retardation values distribute uniformly throughout the spectra and therefore waveplate is achromatic) and highest mean (desired phase retardation value can be obtained by adding less layers) best physical thickness values for achromatic waveplate can be found.

Also, using Nelder-Mead simplex algorithm lead to the same results and reduces computation time. The minima of function, where difference of phase retardation with given parameters and desired phase retardation is mathematically described, gives values of physical thickness (when refractive index values are fixed) which can be used to produce achromatic optical coating waveplate.

All aforementioned methods have been tested to create the model of an achromatic waveplate in visible regime with phase retardation equal to $\pi/2$. Several designs have been found and compared. Optimal values of refractive index and physical thickness have been computed.

[1] N. W. Roberts, T.-H. Chiou, N. J. Marshall, T. W. Cronin, *A biological quarter-wave retarder with excellent achromaticity in the visible wavelength region,* Nature Photonics (2009).
[2] Yi-Jun Jen, A. Lakhtakia, Ching-Wei Yu et al. *Biologically inspired achromatic waveplates for visible light* Nature Communications (2011).
[3] H. A. Macleod, *Thin-Film Optical Filters,* 4th edn. (CRC 2010) 55-56.
[4] L. I. Epstein, *The design of optical filters,* Journal of the Optical Society of America, vol. 42, nr 11, (1952)

GROUP DELAY DISPERSION IMPACT ON SECOND HARMONIC GENARATION WITH ULTRASHORT LASER PULSES

Raimundas Burokas[1], Pierre-Marc Dansette[1], Tadas Bartulevičius[1,2], Andrejus Michailovas[1,2]

[1] Ekspla Ltd, Savanoriu Ave. 237, LT-02300 Vilnius, Lithuania
[2] Center for Physical Sciences and Technology, Savanoriu Ave. 231, LT-02300 Vilnius, Lithuania
r.burokas@ekspla.com

Second harmonic generation is widely used technique to obtain visible light source in laser physics. There are many parameters which affect second harmonic generation (SHG) efficiency and laser beam quality, as pulse energy, beam size, pulse duration, the non-linear properties of the crystal, crystal length, group velocity mismatch between the fundamental and generated second harmonic (SH) pulses and the group delay dispersion (GDD) [1,2].

In this study we present our investigation of GDD influence to SHG efficiency and spatial beam quality parameter M^2 of SH. In the experimental system, second harmonic pulses were produced in lithium triborate (LBO) crystal using femtosecond (<300 fs) fiber laser (FemtoLux3, *Ekspla*). GDD and pulse duration was controlled with linear temperature gradient along the chirped fiber Bragg grating which was used as pulse stretcher. The measured SHG efficiency and SH beam quality parameter M^2 dependence on GDD is shown in Fig. 1. The best SHG efficiency of 61% was achieved at GDD value of zero. The efficiency of the second harmonic drops down with the variation of the positive and negative GDD. Measured beam quality parameter M^2~1.09 of the SH was close to the diffraction limit indicating excellent beam spatial properties. We observed that this dependence is asymmetric for positive and negative GDD values. SHG efficiency and SH beam quality drops sharply for positive GDD, while for negative GDD these parameters decrease more slowly. It was shown by numerical simulations that this asymmetric behavior was caused by uncompensated fourth order dispersion in the laser system or self-phase modulation in the fiber amplifier [2]. Detailed information about numerical calculations and experimental results will be presented at the conference.

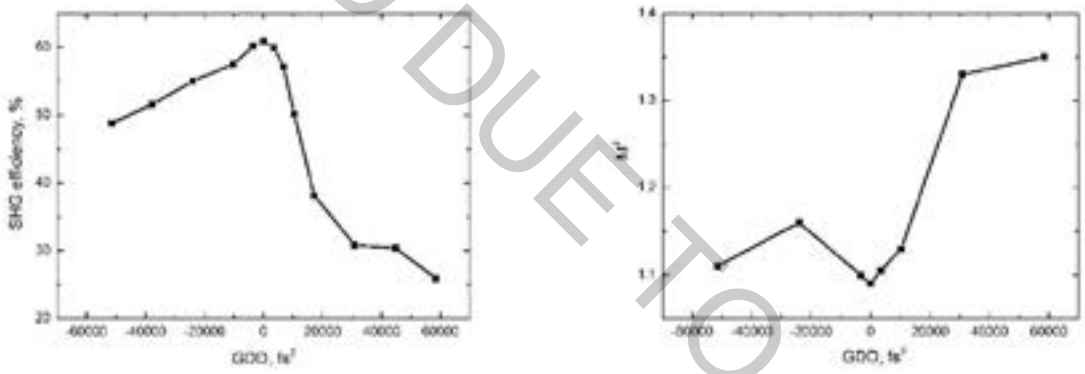

Fig. 1. The dependence of second harmonic generation (SHG) efficiency on group delay dispersion (GDD) (left) and second harmonic beam quality parameter M^2 on GDD (right).

[1] Marcinkevičius, A., Tommasini, R., Tsakiris, G. et al. Frequency doubling of multi-terawatt femtosecond pulses. Appl Phys B 79, 547–554 (2004). https://doi.org/10.1007/s00340-004-1612-5.
[2] P.-M. Dansette, R. Burokas, L. Veselis et al "Peculiarities of second harmonic generation with chirped femtosecond pulses at high conversion efficiency" Optics Communications 455 (2020) 124462. https://doi.org/10.1016/j.optcom.2019.124462.

CANCELLED DUE TO COVID-19

LABEL-FREE IMAGING OF BIOLOGICAL TISSUE USING WIDEFIELD SECOND-HARMONIC GENERATION MICROSCOPY

Danielius Samsonas[1,2], Lukas Kontenis[1,2], Mikas Vengris[1,2]

[1]Faculty of Physics, Vilnius University, Vilnius, Lithuania
[2]Light Conversion, Vilnius, Lithuania
danielius.samsonas@ff.vu.lt

Second-harmonic generation (SHG) microscopy is a nonlinear imaging technique based on the frequency-doubling of photons interacting with non-centrosymmetric structures. It enables label-free *in vivo* and *in situ* visualization of non-centrosymmetric biopolymers such as collagen in most structural tissues and myosin filaments in the sarcomeres of striated muscles. Structural label-free nonlinear imaging emerges as a successful tool for faster biomedical diagnostics, while quantitative polarimetric imaging opens up new ways for more detailed tissue characterization.

The SHG process requires hight intensity coherent light. For this reason, imaging is commonly performed by raster-scanning a tightly focused femtosecond oscillator beam and acquiring the image pixel-by-pixel using a single-element photodetector. The frame rate is thus limited by the laser scanning speed. Increasing availability of robust, affordable, high-power, femtosecond lasers operating at MHz rates has stimulated the advancement of widefield SHG microscopy. Widefield microscopy does not require scanning and therefore enables real-time imaging of large samples [1]. A high frame rate is achievable because a large imaging area is exposed to short high intensity laser pulses and the image is obtained as a single frame using a camera. It should be noted that laser parameters need to be carefully optimised because high intensity laser radiation eventually damages the sample. The signal level can also be increased by using a higher repetition rate, leading to higher average power, which eventually causes photobleaching [2].

The purpose of this work was to develop a widefield microscope and to demonstrate its performance by imaging label-free biological samples. A *PHAROS* high-repetition-rate amplified laser system was used for evaluation of the developed widefield microscope by imaging label-free rat skeletal muscle tissue (Biomax RAT901a). The laser parameters at the sample were: 1 W average power, 100 kHz repetition rate, 680 μm beam diameter ($1/e^2$), energy density of 5.5 μJ/cm^2 and a peak intensity of 19 GW/cm^2 using 290 fs pulses. We were able to produce 410 μm × 485 μm images with sub-micron resolution and with no observable damage to the sample. The image in figure 1(a,b) exhibits a periodic structure of the sarcomere anisotropic A-bands, which are clearly distinguishable from the dark isotropic I-bands due to SHG signal from myosin nanomotors. Figure 1(c) shows the SHG intensity profile of 20 sarcomeres along a myofibril, with the average sarcomere length of approximately 1 μm.

The work shows that widefield SHG microscopy provides sub-micron resolution over a large imaging area. The setup will be used to optimize novel high-repetition-rate amplified laser sources for nonlinear microscopy.

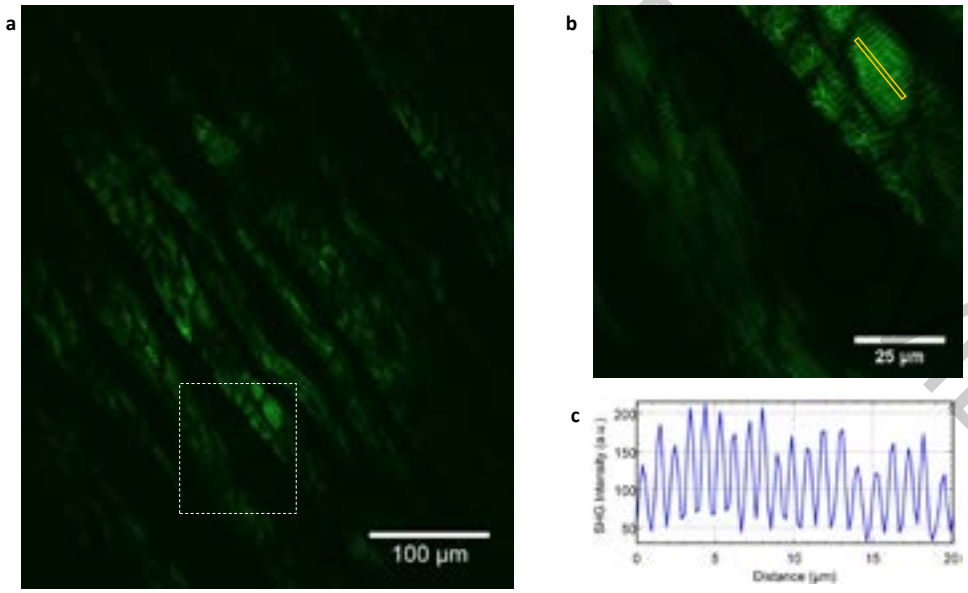

Fig. 1. Widefield SHG image of a fixed label-free rat skeletal muscle. (a) The entire 410 μm × 485 μm image area. (b) 100 μm × 100 μm cropped image area, indicated in (a) by the dashed line. (c) SHG intensity profile along the myofibrilis in the yellow rectangle.

[1] H. Zhao, R. Cisek, A. Karunendiran, D. Tokarz, B. A. Stewart, and V. Barzda, "Live imaging of contracting muscles with wide-field second harmonic generation microscopy using a high power laser," Biomedical Optics Express, vol. 10, no. 10, p. 5130, 2019.
[2] C. Macias-Romero, V. Zubkovs, S. Wang, and S. Roke, "Wide-field medium-repetition-rate multiphoton microscopy reduces photodamage of living cells," Biomedical Optics Express, vol. 7, no. 4, p. 1458, 2016.

ORIGINAL PAPER COVID-19

COHERENT RESEARCH OF METAL DEPOSITION ON D263 GLASS USING LASER PULSES AND CHEMICAL ETCHING

Kamilė Kasačiūnaitė[1,2], Antanas Urbas[1,2], Sergej Orlov[1], Ina Stankevičienė[1], Aldona Jagminienė[1]

[1] Coherent Optics Laboratory, Center for Physical Science and Technology, Vilnius, Lithuania
[2] Altechna R&D Ltd, VIlnius, Lithuania
kamile.kasaciunaite@wophotonics.com

Microelectronics has been rapidly evolving as the most in-demand field of electronics because of the ever-increasing demand for inexpensive and lightweight equipment. Materials such as silicon and copper are commonly used in manufacturing microelectronics. Therefore, direct metalization of bare glass with copper is required to reach the full potential of low-cost benefit [1]. Two step process is needed to obtain precise microstructures in glass before metal deposition: 1) create structures in glass using femtosecond laser 2) use alkali etching for via holes in the material. In this report we research a fundamental material challenge, associated with copper-to-glass adhesion.

Raman spectroscopy is a powerful method for determination of glassy material analysis. The chemical composition and structure of molecules influence the scattering and no two of the spectra being exactly similar [2]. Using Raman spectroscopy in D263 glass we indicate different chain lengths of SiO_4 tetrahedral structures. These links are specified in Q_n parameter, which describe quantity of bridging oxygens in the structure. Using laser pulses these tetrahedral chains can be contracted by creating shorter structures than the origin. Therefore, laser densified area acquires a greater reactivity to Potassium hydroxide (KOH) etchant and facile Si-O-Si cleavage [3], consequently we are observing a selective chemical etching. These two processes take place in designing desired microstructure in dielectric material.

Finally, creating laser and chemical etchant modifications in glass a selective metal deposition was witnessed. It has been a clear connection between metal deposition speed on the glass and laser pulse energy as well as chemical etching.

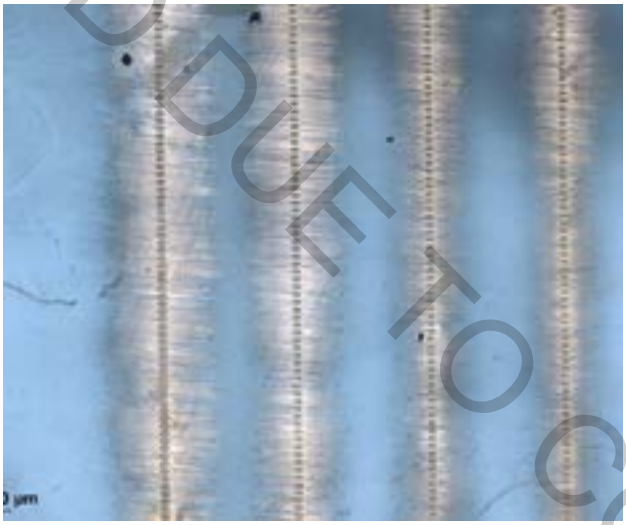

Fig. 1. Energy and copper deposition on borosilicate glass dependency. As energy from left to right decreases the amount of copper deposition decreases as well.

[1] T. Huang, V. Sandaram, P. M. Raj, H. Sharma, R. Tummala, Adhesion and Reliability of Direct Cu Metalization of Through-Package Vias in Glass Interposer, Device and Material Reliability IEEE Transaction on, vol. 17, no 4, pp. 683-691, 2017.
[2] A. K. Yadav, P. Singh, A Review of Structure of Oxide Glasses by Raman Spectroscopy, RSC Adv. **5**, 2015.
[3] S. Kiyama, S. Matsuo, S. Hashimoto, Y. Morihira, Examination of Etching Agent and Etching Mechanism on Femtosecond Laser Microfabrication of Channels Inside Vitreous Silica Substrates, J. Phys. Chem. C 2009.

CANCELLED DUE TO COVID-19

MICRO-MECHANICAL VOLTAGE ACTUATED CANTILEVER BEAM FEM ANALYSIS AND MANUFACTURE IN A FUSED QUARTZ GLASS

Dominyka Stonytė, Domas Paipulas

Laser Research Center, Faculty of Physics, Vilnius University, Lithuania
dominyka.stonyte@ff.vu.lt

Fused quartz can be modified with very intensive femtosecond laser pulses through non-linear absorption processes and the modified places can then be etched with a hydrofluoric acid [1]. Through this process we can make micro resolution complex 3d structures. A cantilever beam mechanical structure is one of the simplest and widely used in micromechanical systems. Alone it can be useful in a precise micro-movement detection, estimation of deformation of microstructures due to the applied forces, atomic microscopes, microgrippers and etc. If we selectively sputter the silver/gold contacts and apply voltage, we can then control the movement of the beam with prior to it's dependency of the applied voltage. The movement of those beams is based on a good glass tensile strength, as fused quartz can bend without causing a deformation if the bending flexure is narrow enough and the stress distribution doesn't overcome the tensile strength.

In this study we show a finite element method analysis and geometrical parameter optimization results, which were made with Comsol Multiphysics software. We also compare the manufactured voltage-actuated cantilever beam tip displacement dependencies with the modelled ones, mentioned above. We demonstrate, that the simulation results are similar to the experimental ones. We also show that the stress distribution doesn't overcome the elastic limit of the material and that there are almost no stresses outside the hinge of cantilever. The values of the eigenfrequencies are also given and the usage of the fundamental one in alternating voltage frequency is shown.

The cantilever beam which flexure hinge's width is 4 μm and length is 100 μm was manufactured with a 60 μm gap between contacts. With a 30 V voltage applied to this beam it bends 4.5 μm (tip displacement). After the geometrical parameter optimization we achieved the 11 μm stable displacement when a 23 V voltage is applied to the beam, which flexure hinge's width is 8 μm and length is 350 μm, gap between contacts is 25 μm.

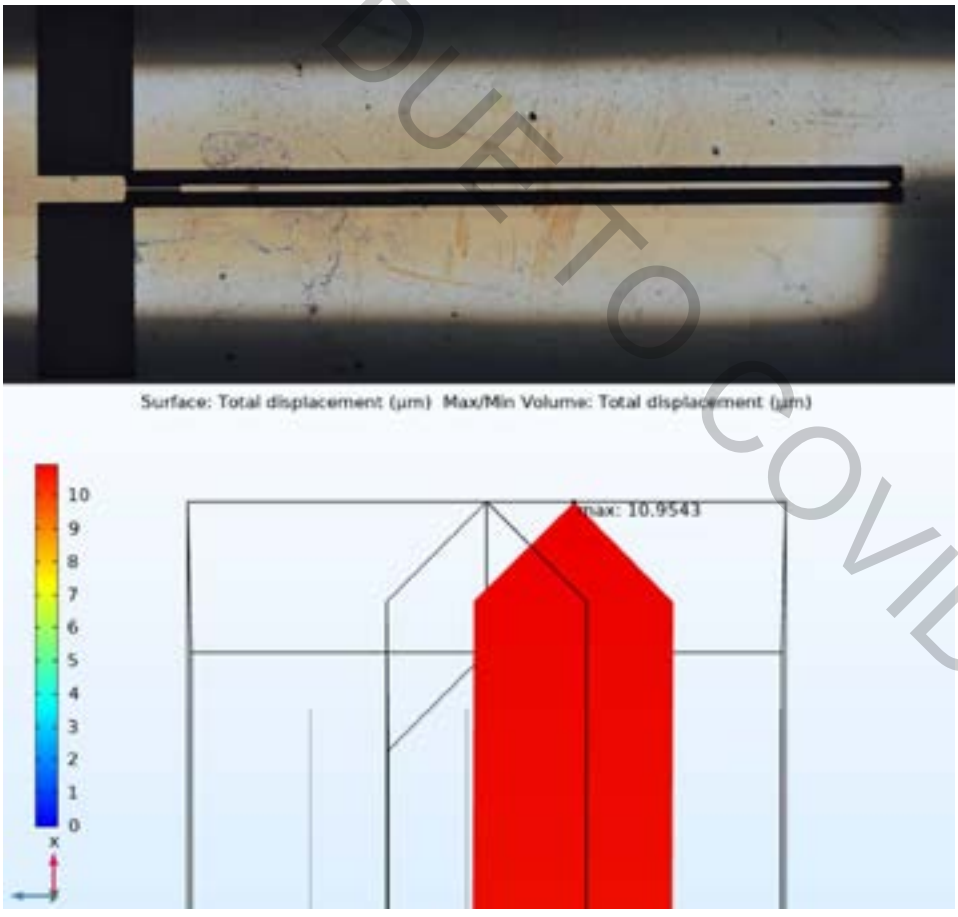

Fig. 1. The manufactured cantilever beam and the optimized beam tip displacement below.

[1] Y. Bellouard, A. A. Said, P. Bado, Integrating optics and micro-mechanics in a single substrate: a step toward monolithic integration in fused silica., Optics Express 13, 6635-6644 (2005).

CANCELLED DUE TO COVID-19

PMMA WGM microsphere resonator quality factor measurements using video recognition, temperature changes and fixed wavelenght laser

Roberts Berķis[1], Aigars Atvars[1], Inga Brice[1], Kārlis Grundšteins[1], Jānis Alnis[1]

[1] Institute of Atomic Physics and Spectroscopy of the University of Latvia, Riga, Latvia
Robertsberkis2007@inbox.lv

CANCELLED DUE TO COVID19

The whispering gallery modes (WGM) resonators are based on spherical objects, which are made from optically transparent materials, and are capable of maintaining an circling optical wave inside a sphere, using total internal reflection. If there is a light source which supplies the sphere with constant intensity, the wave moving along the perimeter of sphere starts to interfere constructively. In this case the resonance happens, which is called whispering gallery mode (WGM). When there is a change in temperature, it changes the radius of WGM resonator, and that results in change of refraction coefficient, which results in change of resonance and intensity. The current work explores the possibility of using temperature changes to measure polymethyl methacrylate (PMMA) WGM microsphere resonator quality factor (Q) and thermal expansion parameters. Different diameter and material spheres are used in the experiments for equipment testing and calibrating.

The two main parameters which determine the WGM microresonator resonance peak change with temperature are the linear thermal expansion coefficient α and the optical index of refraction change with temperature β (thermorefractive coefficient) which also changes with the wavelength of used light. The combined α and β coefficient formula could be written as Eq. (1):

$$\frac{\Delta\lambda}{\lambda} = -(\alpha + \beta)FWHM \tag{1}$$

where FWHM is the resonance full width at half maximum, measured in temperature degrees, which is obtained from the periodic resonance signals acquired by changing a temperature. Δλ / λ is the relative resonance peak shift per Kelvin. In our measurements we have a simplified case where laser wavelength is constant and resonance tuning is induced by changing temperature**.**

From the obtained traces peak width and repetition free spectral rage was measured manually and Q-factors were calculated for several different size PMMA micro resonators, see Fig. 1

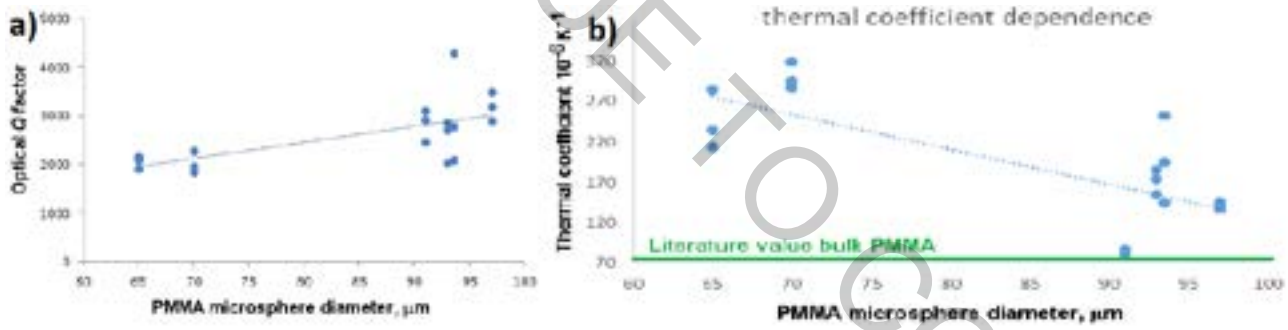

Fig. 1.a) Calculated values for Q factor of different PMMA microsphere diameters and b) thermal coefficient.

Our result show that thermal coefficient slightly increases for smaller resonators probably. For best results of thermal coefficient, would, be if the WGM micro resonator size would be around 130-140µm, where the results come close to their bulk material value of $80*10^{-6}$/K[4] .

The performed experiments show a very simplified way of measuring Q-factors for WGM micro resonators and determining thermal coefficient. This opens up a window for new measuring tool and method deign, that would be very useful for people working with WGM resonators [5]. For example a temperature sensor can be built employing the fact that different size resonators have different periodicity of resonances.

[1] M. R. Foreman, J. D. Swaim, and F. Vollmer, Whispering gallery mode sensor, Advances in Optics and Photonics 2, 168 (2015).
[2] Y. Dumeige, S. Trebaol, L. Ghisa, H. Tavernier, P. Feron, Determination of coupling regime of high-Q resonators and optical gain of highly selective amplifiers, J. Opt. Soc. Am. B 25, 2073 (2008).
[3] I. Brice, A. Pirktina, A. Ubele, K. Grundsteins, A. Atvars, R. Viter, J. Alnis, Development of optical WGM resonators for biosensors, Proceedings of SPIE 18, 105920B (2017).
[4] Z. Zhang, P. Zhao, P. Lin, F. Sun, *Thermo-optic coefficients of polymers for optical waveguide applications,* Polymer 47, 4893 (2006).
[5] A. B. Petermann, A. Varkentin, B. Roth, U. Morgner, M. Meinhardt-Wollweber, *All-polymer whispering gallery mode sensor system,*Optics Express **6**, 6052 (2016).

SUPERCONTINUUM GENERATION IN A MULTI-PLATE SYSTEM

Ramūnas Logminas[1], Arūnas Varanavičius[1]

[1]Laser Research Center, Vilnius University, Lithuania
ramunas.logminas@gmail.com

Supercontinuum which covers an optical octave is a prerequisite to single-cycle optical pulse synthesis and isolated attosecond pulse generation, also a broadband radiation with high pulse energy facilitates seeding ultrafast optical parametric amplifiers, high-speed data acquisition in optical coherence tomography as well as ultrafast, multi-dimensional molecular spectroscopy [1]. There are several ways to broaden laser pulse spectrum, for example by generating supercontinuum radiation in gaseous environment or in a bulk medium. Recent papers have shown that there is an alternative for a supercontinuum generation in a bulk medium – thin plates [2].

The main reason why primary spectrum experiencing broadening is a nonlinear phase shift, which is related to change of spectra [3]:

$$\delta w(t) = \frac{\mathrm{d}}{\mathrm{d}t} \Phi_{nl}(t) \qquad (1)$$

By replacing whole medium into separate thin plates (for example thickness of a plate is 0.1 mm) we can use higher pump power for supercontinuum generation than in case of continuous medium. Consequently, the broadband continuum pulses have much higher pulse energy, thus making this kind technique for continuum generation is more applicable. This method is rather new still requires tedious investigation to fully understand its limits and capabilities.

Thus, we have performed experiment with multi-plates setup in which we used two 0.2 mm thick and five 0.1 mm thick plates fabricated from UVFS.

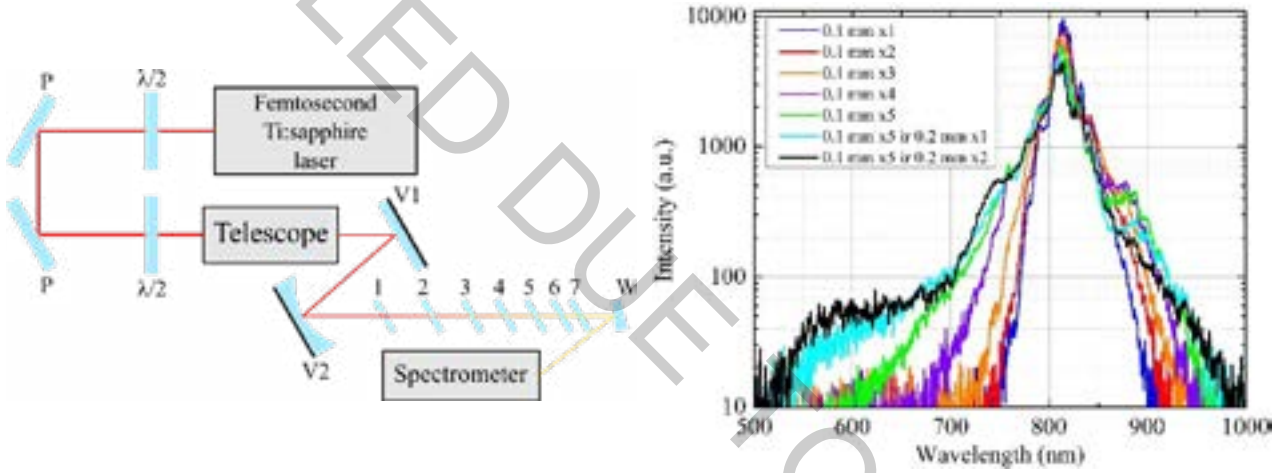

Fig. 1. In a left side: experimental setup: P – polarizer, V1 – flat mirror, V2 – concave mirror (f=750mm), 1, 2, 3 and so on – thin plates, W – wedge. In a right side: radiation spectra after each plate (plates order in experimental setup are placed in the same order as written).

Multi-plate setup was pumped by 50 fs pulses from Ti:sapphire laser and pulse energy as high as 0.5 mJ was used in experiment. The appropriate focusing conditions were achieved by using telescope. In this setup the Ti:sapphire laser pulses spectrum of 25 nm at FWHM was broadened to the spectrum covering from 500 nm to 1000 nm. The result values of spectral energy density exceed up to thousands of times those reported in literature by generating a single filament in solid media. Continuum radiation from multi-plate setup has quite high energy stability over time. Standard deviation of continuum pulses acquired during one-hour continuous operation was of order 0.02.

Presentation will include more data on energy, spectral, spatial and stability characteristics of high energy continuum produced in multi-plate setup.

[1] Y.-C. Cheng, C.-H. Lu, Y.-Y. Lin, and A. H. Kung, Supercontinuum generation in a multi-plate medium, Optical Society of America **24**, 7224-7231 (2016).
[2] C.-H. Lu, Y.-J. Tsou, H.-Y. Chen, B.-H. Chen, Y.-C. Cheng, S.-D. Yang, M.-C. Chen, C.-C. Hsu, and A. H. Kung, Generation of intense supercontinuum in condensed media, Optical Society of America **6**, 400-406 (2014).
[3] A. Dubietis, G. Tamošauskas, R. Šuminas, V. Jukna, and A. Couairon, Ultrafast supercontinuum generation in bulk condensed media (Invited Review), arXiv:1706.04356 (2017).

CANCELLED DUE TO COVID-19

CHIRALITY DRIVEN EFFECTS IN MULTIPHOTON EXCITED ORGANIC WHISPERING GALLERY MODE MICRORESONATORS

Mitetelo Nikolai[1], Popov Mikhail[1], Mamonov Evgeniy[1], Rajadurai Chandrasekar[2], Murzina Tatiana[1]

[1]Department of Physics, Quantum Electronics Division, M.V. Lomonosov Moscow State University, 119991, Moscow, Russia

[2]Functional Molecular Nano-/Micro-Solids Laboratory, School of Chemistry, University of Hyderabad, Prof C R Rao Road, Gachibowli, 500046 Hyderabad, India

nickm@shg.ru

CANCELLED DUE TO COVID-19

Miniaturization of photonic devices based on novel functional materials is one of the emerging streams of nanophotonics [1]. Organic materials are rather perspective here since they provide relatively high exciton binding energy, strong charge-transfer mediated photoluminescence (PL), efficient optical nonlinearity, tunable optical band gap and flexible device shapes compared to inorganic ones. Organic microresonators attract much attention, because they can be used in microlasers with very low excitation threshold and in sensoric applications due to strong dependence of resonant properties of cavity modes on ambient conditions. One of the most promissing methods of such microstructures fabrication is self-assembly [2]. By varying organic compound type, solvent, solution concentration and evaporation conditions structures with various shape such as spheres [2], hemispheres [2], rods [2] and so on can be obtained. It is well known that these structures can exhibit Fabry-Perot (FP) and whispering gallery (WG) cavity modes which increase field localization and lead to significant amplification of nonlinearoptical processes.

Here, 1,1'-bi-2-naphthol (Binol) is one of perspective materials capable for the formation of microspheres via self-assembling. WGMs were recently demonstrated in the single-photon PL spectrum of such structures for both enantiomers. At the same time, up to now, nonlinear-optical properties of single and coupled binol microspheres, as well as the effects accompanying multiphoton excited WGMs in them have not been studied.

For the nonlinear-optical measurements, we used the home-made multiphoton microscopy setup based on a Ti-sapphire laser (pulse duration 60 fs, repetition rate 80 MHz, mean power 3-200 mW, wavelength range = 720-890 nm) and Ytterbium-doped laser (pulse duration 200 fs, repetition rate 80 MHz, mean power 0.01-4 W, wavelength = 1050 nm) equipped with focusing and collecting objectives with NA = 0.7, which allowed to focus laser radiation in a spot with a diameter of 1 μm. The photomultiplier operating in the photon counting mode and spectrometer with a spectral resolution of 1 nm were used to detect scattered nonlinear signal.

Our studies were focused on the effective multiphoton excitation of WGMs in microspheres based on Binol (fig.1a). Microstructures shows intensive two- and three-photon photoluminescence (2PL and 3PL). Fig. 1b shows a typical 2PL spectrum of a single microsphere with narrow peaks associated with WGMs. Binol is a chiral organic compound, and it responds to left and right circular pump polarizations in different way. To study the chirality driven nonlinear optical effects in binol microspheres, we used Z-scan technique that we adapted for single microstructure measurements. It allowed us to estimate two- and three-photon absorption coefficients, for two circular pump polarizations and nonlinear circular dichroism. Its values are equals to 7.7% for two-photon response and 11% for three-photon. The self-assembly method allows for the formation of more complex microstructures such as dimers, trimers etc, which allows one to study the coupling effects in their nonlinear WGM spectra.

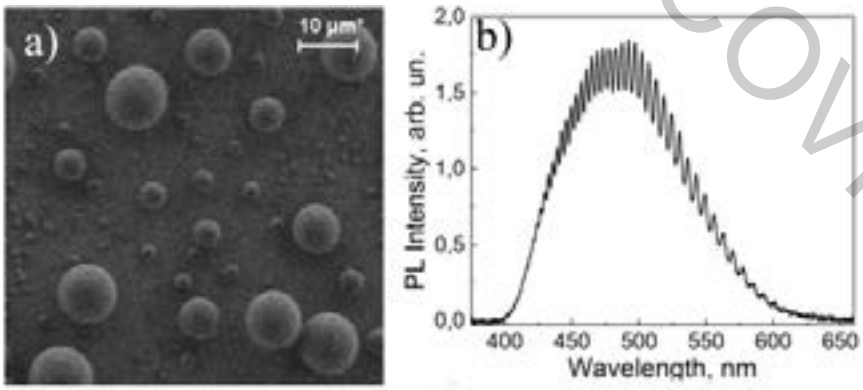

Fig. 1. a) FESEM image of array of microstructures; b) 2PL spectrum of single microsphere with WGMs.

These results make these WGM microresonators perfect candidates for the development of polarizationsensitive nonlinear-optical sensors and nanophotonic devices working with chirality-dependent signal.

[1] D. Venkatakrishnarao, R. Chandrasekar, Engineering the Self-Assembly of DCM Dyes into Whispering Gallery-Mode μ-Hemispheres and Fabry–Pèrot-Type μ-Rods for Visible–NIR (600–875 nm) Range Optical Microcavities, *Advanced Optical Materials* 4(1), 112-119 (2016).

[2] D. Venkatakrishnarao, et. al., Advanced organic and polymer whispering-gallery-mode microresonators for enhanced nonlinear optical light, *Advanced Optical Materials*, 1800343 (2018).

CASCADED NONLINEARITY INFLUENCE TO HIGH POWER FEMTOSECOND OPTICAL PARAMETRIC OSCILLATOR

Ignas Stasevičius,[1,2] G. Martynaitis[1], Mikas Vengris,[1,2]

[1]Light Conversion Ltd, Vilnius, Lithuania
[2]Vilnius University, Laser Research Centre, Vilnius, Lithuania
ignas.stasevicius@lightcon.com

Scaling the output power of femtosecond optical parametric oscillator requires full understanding of the temporal and power characteristics of the OPO radiation. In this paper, we focus on cascaded nonlinearities and their effects to pulse formation. Previous work in the field include DeSalvo *et al.* showing that cascaded $\chi^{(2)}:\chi^{(2)}$ nonlinearities induce effective $\chi^{(3)}$ nonlinearity which is proportional to the $\left(d_{eff}\right)^2/\Delta k$ [1, 2]. In this paper, we demonstrate the effect of $\chi^{(3)}$ effective nonlinearity when the resonating signal or idler is tuned from the exact phase matching - by tuning the cavity delay or by rotating the intracavity crystal. We also perform Z-scan measurements in two different nonlinear materials LBO/BBO (fig. 1) and show that this difference frequency induced effective nonlinearity cannot be explained the same way as second harmonic induced effective $\chi^{(3)}$ nonlinearity [3]. All these findings lead to an understanding of how to design a high power femtosecond optical parametric oscillator with better operation characteristics.

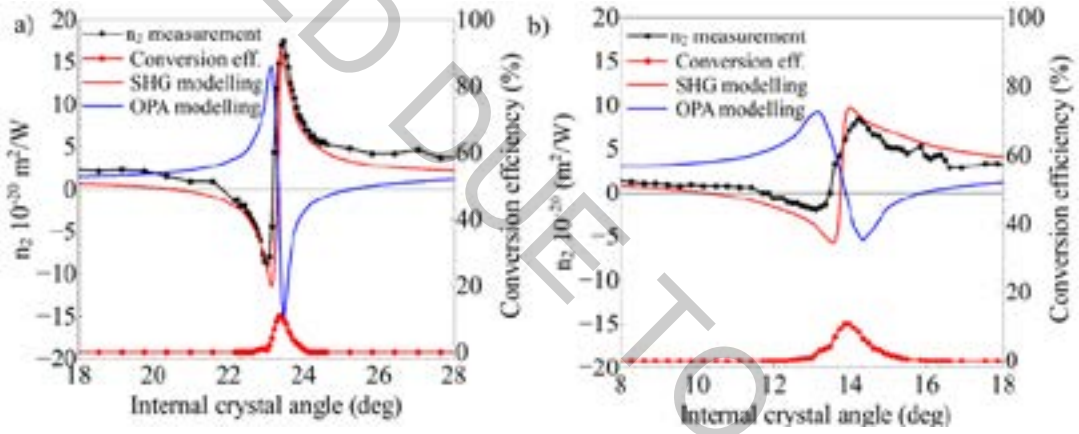

Fig 1. n_2 measurement while rotating the internal angle of the BBO crystal (panel a)) and the LBO crystal (panel b)). The measurement wavelength was 1030 nm. Black solid and symbol curve – experimental n_2 measurement; red solid and symbol curve- conversion efficiency; red solid curve – SHG simulation; blue solid curve – DFG/OPA simulation.

[1] R. DeSalvo, D. J. Hagan, M. Sheik-Bahae, G. Stegeman, W. E. Van Stryland, "Self-focusing and self-defocusing by cascaded second-order effects in KTP," Optics Letters 17, (1) 28-30 (1992).

[2] G. M. Gale, M. Cavallari, and F. Hache, "Femtosecond visible optical parametric oscillator," J. Opt. Soc. Am. B 15, (2) 702-714 (1998).

[3] C. Conti, S. Trillo, G. Gallot, G. M. Gale, P. Di Trapani, J. Kilius, A. Bramati, S. Minardi, W. Chinaglia, G. Valiulis, "Effective lensing effects in parametric frequency conversion," J. Opt. Soc. Am. B **19,** (4) 852-859 (2002).

CANCELLED DUE TO COVID-19

THE INFLUENCE OF COHERENT EFFECTS ON ANGULAR MOMENTUM DISTRIBUTION DEPENDENCE ON MAGNETIC FIELD IN ^{85}Rb: MAGNETOOPTICAL SIGNALS WITHOUT THE DOPPLER EFFECT

Artūrs Mozers, Mārcis Auzinsh, Laima Bušaite, Dace Osīte

Laser Centre, The University of Latvia, 19 Rainis Boulevard, LV-1586 Riga, Latvia
arturs.mozers@lu.lv

In the present work we show results from a theoretical investigation of angular momentum alignment-to-orientation conversion (AOC) by observing laser-induced fluorescence (LIF) signals of rubidium atoms at D1 excitation. The AOC is created by combined action of linearly polarized exciting laser radiation and an external magnetic field. This can be detected by observing circularly polarized light as circularity is direct evidence of angular momentum orientation. Due to the nonlinear dependencies of the energies of ground-state and excited-state magnetic sublevels, the angular momentum alignment, created by linearly polarized light, can be partially converted to orientation. The excitation and observation geometry for creating and observing AOC stands as follows: the magnetic field **B** defines the quantization axis and the exciting linearly polarized laser radiation **E** forms an angle of $\pi/4$ with respect to the magnetic field **B**, observation direction is in the direction perpendicular to both **E** and **B**.

The theoretical model is based on the optical Bloch equations and uses the density matrix formalism. The theoretical model takes into account all transitions, the mixing of magnetic sublevels in an external magnetic field, the coherence properties of the exciting laser radiation, and also includes averaging over the Doppler profile [1]. In the present work, however, the averaging over the Doppler profile is omitted in order to observe individual magnetic sublevel transitions, thus enabling us to understand the origins of features observed in the modelled LIF signals. We used the theoretical model to calculate two opposite circularly polarized light components (σ^+ and σ^-) and their difference. In order to explain the various effects contributing to the line shapes of these signals we manipulate our theoretical model in the following manner:

i – we switch on and off the coherent effects by setting the non-diagonal density matrix elements to zero. We do this by increasing the relaxation rate $\gamma_{\text{non-diagonal}}$ of only these elements with the ratio of $\gamma_{\text{non-diagonal}}/\gamma_{\text{diagonal}} = 10^9$ with respect to the γ_{diagonal} which is the normal transit relaxation rate experienced by diagonal elements. This allows us to observe the influence of transfer of coherences from the ground state to the excited state.

ii – we can extract additional information from the density matrix by performing the state multipole expansion. Explicitly the ρ^1_1 state multipoles – which directly indicate the orientation of the angular momentum in the transverse plane.

iii – the non-diagonal elements are attributed to the coherences between magnetic sublevels. The Δm=1 coherences are the matrix elements with indexes m, m+1 e.g. ρ_{12}. By observing the dependencies of these elements with respect to the magnetic field, we can deduce which magnetic sublevels contribute to the orientation of the angular momentum at specific magnetic field values.

A. Mozers acknowledges support from ERAF PostDoc Latvia project No. 1.1.1.2/16/117 ”Experimental and theoretical signals of ground-state angular momentum alignment-to-orientation conversion by the influence of laser radiation and external magnetic field in atomic alkali metal vapour”.

[1] M. Auzinsh et al., Nonlinear magneto-optical resonances at D1 excitation of 85Rb and 87Rb for partially resolved hyperfine F levels, Phys. Rev. A 79, 053404 (2009).

CANCELLED DUE TO COVID-19

INTENSITY DEPENDENT PROCESSES IN NONLINEAR-OPTICAL RESPONSE OF ORGANIC WGM CAVITY MICROSTRUCTURES

Popov Mikhail[1], Mitetelo Nikolai[1], Mamonov Evgeniy[1], Murzina Tatiana[1]

[1]Department of Physics, Quantum Electronics Division, M.V. Lomonosov Moscow State University, 119991, Moscow, Russia

popov@shg.ru

In the last few years, dielectric microstructures have been actively studied in order to use them in photonic devices. Organic structures have some advantages over inorganic ones due to the high tunability of their properties such as shape, size and refractive index, high luminescence yield and values of nonlinear susceptibilities. These key features bring about a wide range of photonic functions from the organic microstrucutres[1] for instance optical microresonators and light-driven single-component lasing media[2] with a possibility for tunable wavelength. In order to increase the photoluminescence (PL) efficiency, different types of optical structures are considered, including optical whispering gallery modes (WGMs) resonators.

The objects of this research are microspheres made by solvent-assisted self-assembly technique of organic dye 4-(dicyanomethylene)-2-methyl-6-(4-dimethylaminostyryl)-4Hpyran (DCM) of the typical diameter 5-10 μm (refractive index, n=1.61) on a glass substrate. Among organic dyes, DCM is a good candidate material for two-photon pumped PL devices, as it reveals high luminescent yield of nearly 0.7[3] and large two-photon absorption (TPA) cross-section.

For the NLO experiments, a two-photon confocal microscopy setup based on a femtosecond Ti:Sapphire laser operating at 810 nm wavelength is used. Fundamental radiation is focused onto a sample by objective with numerical aperture of 0.7 in a spot with a diameter of 1 μm. The spectrum of the scattered NLO signal is analyzed by a spectrometer with spectral resolution of about 1 nm.

DCM microspheres shows bright two-photon pumped PL (TPL). Typical spectrum of TPL scattered signal shown at fig. 1a. This spectrum shows pronounced peaks attributed to WGM resonances. Nature of these peaks is confirmed by the dependencies of Q-factor and free spectral range on sphere diameter. To characterize nonlinear properties of single structure TPA coefficient is measured using Z-scan method (fig. 1b) and its value is equal to 4 cm/GW. Usually Z-scan technique is applied to thin films, but here we demonstrate that it can be used for microstructures.

In order to find lasing in DCM microspheres dependence of the intensity in single resonance on the fundamental radiation intensity is measured (fig. 1c). It can be seen that there is a threshold in this dependence, where the slope value changes abruptly from 2 to 5.5, which is usually intrinsic property of lasing. DCM dye is subjected to photobleaching, which appears in a decrease of PL intensity with time under strong fundamental radiation. The effect of photobleaching on intensity dependent processes in such structures was never studied thoroughly before. We proposed simple theoretical model, which took photobleaching into account. According to this model, it is shown that photobleaching in organic microspheres leads to similar threshold dependence.

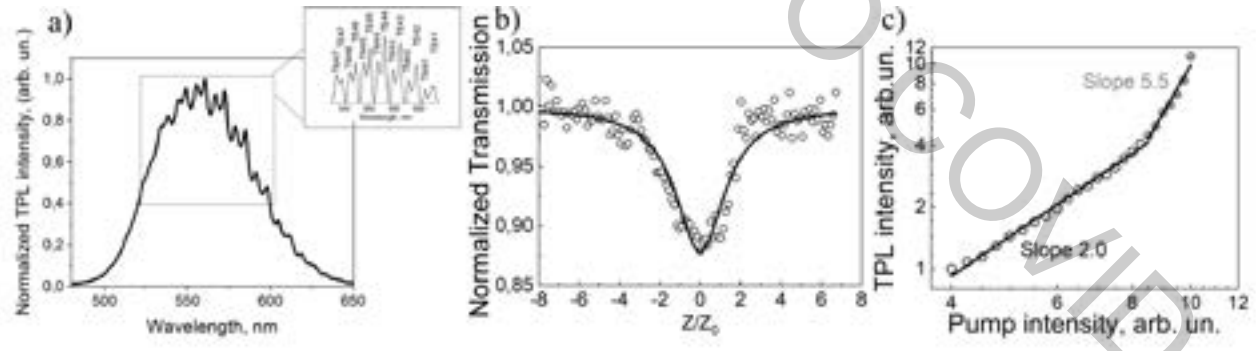

Fig. 1. a) A typical TPL spectrum, inset shows extracted WGMs spectrum with the calculated polar mode numbers; b) Normalized transmittance versus the normalized coordinate measured by the Z-scan microscopy technique; c) Typical dependences of TPL intensity on pump intensity.

Due to high field localisation, simple and low-cost production method, high quality factor and huge two-photon absorption cross-section these structures are well suitable for photonics applications.

Popov Mikhail acknowledges the financial support from the Foundation for the advancement of theoretical physics and mathematics ”BASIS”.

[1] J. Clark, G. Lanzani, Organic photonics for communications, *Nature photonics* 4(7), 438 (2010).

[2] X. Wang, Q. Liao, H. Li, S. Bai, Y. Wu, X. Lu, H. Fu, Near-infrared lasing from small-molecule organic hemispheres, *Journal of the American Chemical Society* 137(29), 9289-9295 (2015).

[3] P. R. Hammond, Laser dye DCM, its spectral properties, synthesis and comparison with other dyes in the red, *Optics Communications* 29(3), 331-333 (1979).

ONCE UPON A COVID-19

INVESTIGATION AND DEVELOPMENT OF THE SMART ILLUMINATION SYSTEM FOR ENHANCED COLOR DISCRIMINATION

Domantas Barisevičius[1], Pranciškus Vitta[1]

[1] Institute of Photonics and Nanotechnology, Faculty of Physics, Vilnius University, Lithuania
domantas.barisevicius@ff.stud.vu.lt

During medical surgeries, it is essential to provide high quality and sufficient illumination to facilitate surgeons to discern details and different tissues. According to international standard for surgery luminaires have to be powerful enough, ensure even illumination, comfortable for surgeons and not overheating the patient. Light-emitting diodes are the main choice of light sources used in surgeon lighting, but some shortcomings are still present.

Color discrimination in surgery is of high importance, but currently natural (black body radiator or sun) illumination spectra are understood to be the best for color rendering and color discrimination. Recent investigation shows that colour rendering and colour difference discrimination are not the same characteristics of white light, and some custom spectra were proposed.

In this study we present the prototype development and investigation steps of smart multi-color solid state illumination source for medical applications. In particular, optical, electrical and thermal characteristics of prototype luminaire were studied. Light spectra of the luminaire were engineered to be as close as possible to theoretically optimal solutions for enhanced colour discrimination.

We conclude, that despite the certain engineering obstacles, multicolour dynamic illumination systems have a great potential in medical applications. Furthermore, such a system could be applied in other areas where analytical properties of illumination are needed.

Fig. 1. Electronics and optics of the luminaire prototype

CANCELLED DUE TO COVID-19

LIGHT-INDUCED CURING OF $MAPbI_3$ PEROVSKITE AND ITS EFFECTS ON OPTICAL PROPERTIES

Simonas Driukas[1], Rokas Jasiūnas[1], Rokas Gegevičius[1], Vidmantas Gulbinas

[1] Center of Physical Sciences and Technology, Department of Molecular compound physics, Ultrafast Spectroscopy Laboratory, Lithuania

simonas.driukas@ftmc.lt

CANCELLED DUE TO COVID-19

During recent times the development of perovskite solar cells has flourished, as efficiencies as high as 22% was reached. This signals a potential, cheaper substitute for conventional silicon-based ones. However, many characteristics of perovskite films are still not fully understood. One of such is the photo-induced enhancing of photoluminescence (Fig. 1) and longer carrier lifetimes (Fig 2). In our study, we try to further identify the causes of such behaviour.

In $MAPbI_3$ perovskite crystal methylammonium site is surrounded by neighbouring iodide ions which are a part of corner-sharing PbI_6 octahedra. These iodide ions are known to migrate from their ground state in room temperature, creating defects in the crystal structure [1]. So far, it is proposed that light irradiation promotes recombination of iodide to its initial state, thus increasing the overall quality of the crystal [2]. To further identify these processes, we used different light soaking sources and various sample ageing conditions to determine how exactly photo-induced charges affect the migration of iodide ions and passivation of positive charge vacancies.

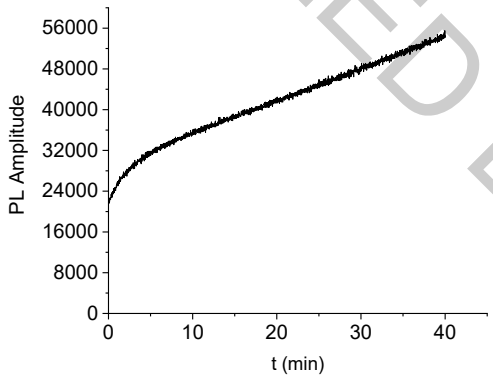

Fig. 1. PL amplitude increase during light soaking

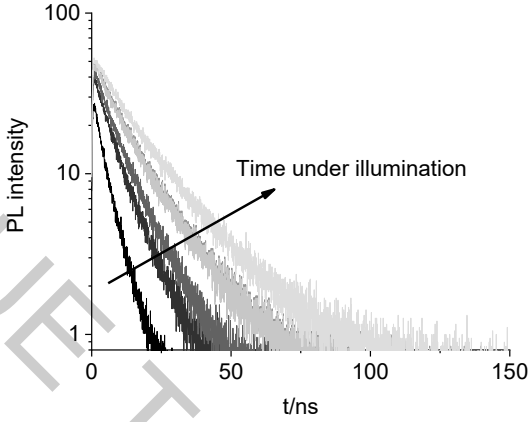

Fig. 2. PL kinetics with different light soaking times

Main experimental methods used were time-dependent PL amplitude measurements and PL kinetics via 470nm laser excitation. The samples were prepared using a solution-based spin-coating process on interdigitated combs, followed by annealing at 100C°. From our measurements, we notice that there might, in fact, be two processes that govern this behaviour, which are dependant on sample ageing conditions. One is noticeable in the first minutes of soaking while the other stays active for longer periods of time. However further research is needed and we hope to get some insight on the differences of these processes in the future.

[1] Minns, J., Zajdel, P., Chernyshov, D. et al. Structure and interstitial iodide migration in hybrid perovskite methylammonium lead iodide.
[2] Energy Environ. Sci., 2016,9, 3180-3187

DEVELOPMENT OF A PROTOTYPE ILLUMINATION SYSTEM FOR PHOTODYNAMICAL TREATMENT OF BIOLOGICAL SAMPLES

Kornelijus Raugas[1], Pranciškus Vitta[1]

[1] Institute of Photonics and Nanotechnology, Faculty of Physics, Vilnius University, Lithuania
kornelijus.raugas@ff.stud.vu.lt

Most of living creatures including bacteria are more or less sensitive to the light, especially when optically active materials like photosensitizers are present. Light photons are some of kind of energy, which can be directly transferred into the cell of molecule, and photochemical and photobiological reaction take place. Such reactions are of rising importance since in combination with natural photosensitizers they can be applied as the antimicrobial and antifungal technologies for food industry or even spacecraft environment.

However, for bio-technology development proper test equipment is needed. During the photodynamical experiments certain experimental conditions must be kept constant in order to minimize uncertainty and maintain traceability. Therefore, we report on design of smart, computer controlled illumination system. Mechanical, optical and thermal design of the prototype was designed. The system is equipped with thermal and optical feed-back loops to compensate aging and temperature caused drift of illumination intensity. The constant (ambient) temperature of the sample is controlled by continuous airflow.

We conclude, that such a illumination system (chamber) could be a useful tool for investigation of photobiological and photochemical reactions and photodynamical processes.

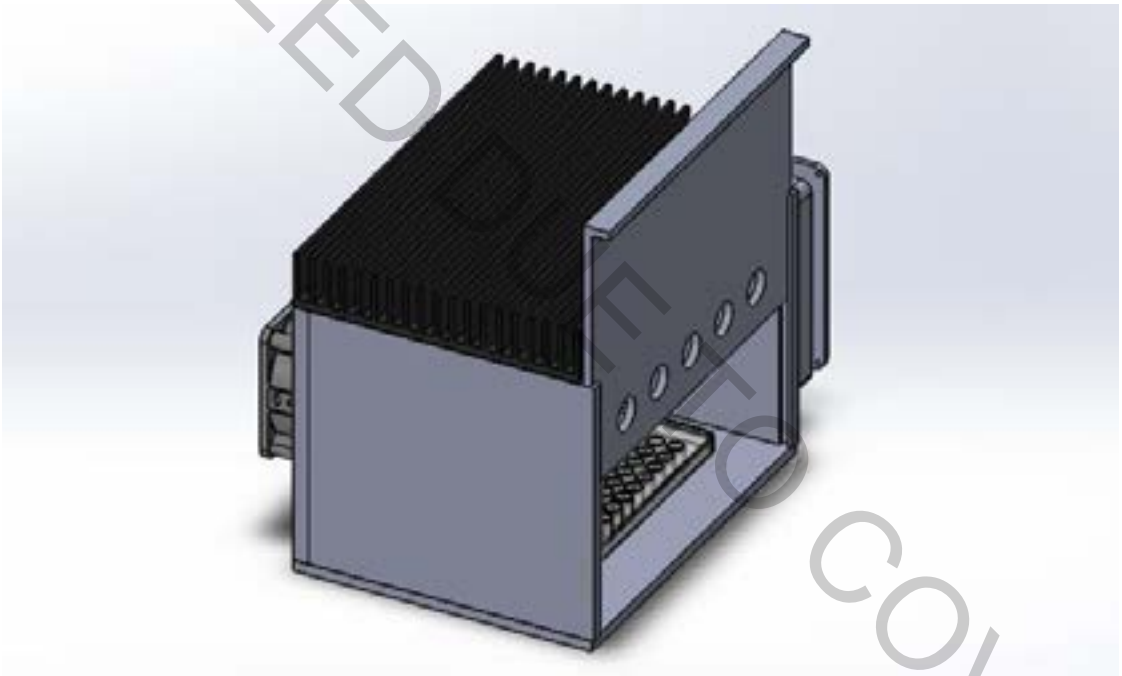

Fig. 1. Design of Prototype illumination system.

CANCELLED DUE TO COVID-19

WHISPERING GALLERY MODE HUMIDITY SENSOR: PHYSICAL PROPERTIES

Pauls Kristaps Reinis, Lase Milgrave, Aigars Atvars, Janis Alnis

Quantum Optics laboratory, Institute of Atomic Physics and Spectroscopy, University of Latvia
pr15001@edu.lu.lv

CANCELLED DUE TO COVID-19

Humidity plays an important role in many chemical and manufacturing processes as well as in human everyday life, for example air quality monitoring. Precise relative humidity (RH) measurements are also needed for various scientific studies. Currently available sensors, such as semiconductor, capacitive/resistive type sensors often have got longer response time, problems with accuracy, especially inaccurate at very low as well as very high humidity conditions. Transparent microresonator objects due to total internal reflection can trap light inside them, in such process constructive interference can occur, which is also known as whispering gallery modes (WGM). We use glycerol microdroplet WGM resonator. If relative humidity changes, refractive index and radius of the microresonator adjust to a new equilibrium condition as well and shift in resonances can be seen. Such system can be used as a high sensitivity and fast response relative humidity sensor. Comparing to silica or polymer based WGM humidity sensors [1][2] our prototype using glycerol is more sensitive to humidity, is temperature independent, and needs no fluorescent dye [3].

In this study, hygroscopic glycerol droplet (r = 0.5 mm, see **Fig. 1a**) was used as a micro resonator. Light from tunable laser was focused on the side of the droplet, constructive interference took place, whispering gallery modes were observed (see **Fig. 1b**). Benefits using tapered fiber instead of needle (for holding the droplet) such as stability, Van der Waals forces and eccentricity have been discussed. The main results show, that by increasing humidity, radius of the droplet increases. It is the main parameter influencing shift in modes. Theoretical equations were found, and they show the correlation between relative humidity and shift in resonant wavelength – by increasing humidity, resonant wavelength decreases. When relative humidity exceeds 75%, the rate of which droplet's size changes increases rapidly. Thereby, WGM humidity sensor could have extremely high precision in high humidity conditions (70-100% RH).

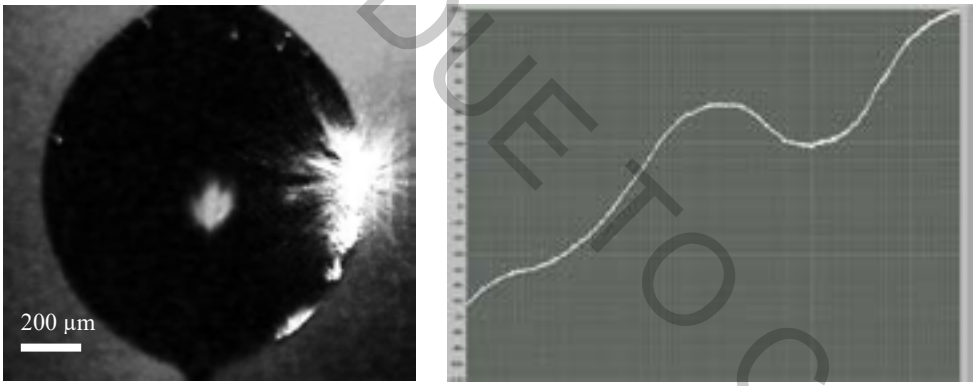

Fig. 1. (a) Glycerol droplet with laser light focused on the side of it (b) Waveform image from an oscilloscope, where WGM resonance is present, while 760 nm VSEL laser wavelength was tuned by a current ramp.

Promising liquid state WGM properties regarding polarization were observed. Depending on the place where the light was focused and the positioning of polarizer, smaller intensity modes with shorter free spectral range (FSR) were recorded. By following these drifting modes even higher sensitivity can be achieved. Our results also show that TE and TM polarization modes can be initiated in liquid state microresonators.

This study demonstrates properties of liquid state WGM resonator and discusses principles behind the prototype of optical humidity sensor. Further investigation about lifetime and work range of this type of sensor is needed. Experimental data about Q-factor degradation over time also needs to be recorded.

This study is financed by LZP project lzp-2018/1-0510 'Whispering gallery mode micro resonator sensor'

[1] Petermann AB, Hildebrandt T, Morgner U, Roth BW, Meinhardt-Wollweber M. Polymer Based Whispering Gallery Mode Humidity Sensor. *Sensors (Basel),* (2018).
[2] A. K. Mallik, G. Farrell, D. Liu, V. Kavungal, Q. Wu and Y. Semenova, "A Coated Spherical Microresonator for Measurement of Water Vapor Concentration at PPM Levels in Very Low Humidity Environments," in *Journal of Lightwave Technology* (2018).
[3] Lucía Labrador-Páez, Kevin Soler-Carracedo, Miguel Hernández-Rodríguez, Inocencio R. Martín, Tal Carmon, and Leopoldo L. Martin, "Liquid whispering-gallery-mode resonator as a humidity sensor," (2017).

SIMULATION OF SILICON-BASED BESSEL ZONE PLATES FOCUSING PERFORMANCE AT SUBTERAHERTZ RANGE

Vytautas Lukas Paukštė, Linas Minkevičius

Faculty of Physics, Vilnius University, Lithuania
Department of Optoelectronics, Center for Physical Sciences and Technology, Lithuania
vytautas.paukste@ff.stud.vu.lt

CANCELLED DUE TO COVID-19

Food, medicine and other industries require imaging systems so that they could ensure the best quality products available [1], [2]. Compact imaging systems are becoming high in demand and terahertz systems are a great example of them. These systems contain small diffractive elements that perform the same as the bulky optical lenses or mirrors [3]. Besides being compact they should have a high focusing efficiency, should be reliable, have enough focal depth to penetrate (scan) thick objects with great accuracy.

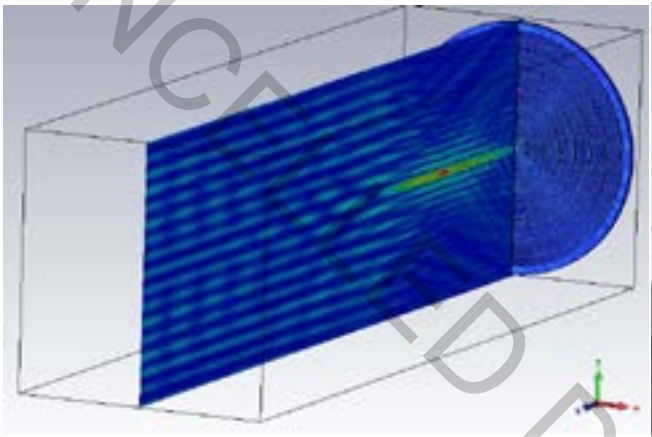

Fig. 1 Quasi- Bessel beam created by BZP with number of zones Z=7 and quantization level N=8.

Fig. 2. BZP with a quantization level of N=4 and number of zones Z=7.

In this work, we demonstrate the design and theoretical calculations of the performance of a regular axicon and Bessel zone plate (Fig. 2) which was designed for 0.6 THz frequency. „CST STUDIO SUITE“ was used for modeling of the optical elements. The axicon with a diameter of 25 mm and Bessel zone plates were designed as ideal silicon- based which had a dielectric permeability of 11.9. Using „CST STUDIO SUITE“ Time domain solver simulation option after the program made calculations we looked at the focusing performance of the axicon depending on its base angle (8°15°). With regards to the Bessel zone plate, its focusing efficiency was measured while altering two factors: number of zones, number of quantization levels. As a second task, the importance of the orientation of two separated BZP by a distance of double the focal length on the electric field distribution was calculated as well. The latter theoretical calculations ware used to see if two Bessel zone plates could in theory act as a part of a compact imaging system.

[1] G. Ok, H. J. Shin, M.-C. Lim, and S.-W. Choi, “Large-scan-area sub-terahertz imaging system for nondestructive food quality inspection,” *Food Control*, vol. 96, pp. 383–389, Feb. 2019.

[2] K. Ahi, “A method and system for enhancing the resolution of terahertz imaging,” *Measurement*, vol. 138, pp. 614–619, May 2019.

[3] L. Minkevičius *et al.*, “Terahertz multilevel phase Fresnel lenses fabricated by laser patterning of silicon,” *Opt. Lett.*, vol. 42, no. 10, p. 1875, May 2017.

NUMERICAL SIMULATION TECHNIQUES FOR THE PROCESSING OF NONLINEAR REFRACTIVE INDEX MEASUREMENTS

Gaudenis Jansonas[1], Rimantas Budriūnas[1]

[1] Laser Research Center, Faculty of Physics, Vilnius University, Lithuania
gaudenisjansonas@yahoo.com

When a material interacts with intense light its refractive index depends on the intensity of radiation. This dependency is described by a substance parameter called nonlinear refractive index (n_2). This parameter is responsible for many phenomena of nonlinear optics and in modeling such phenomena it is important to know the most precise value of n_2. Popular methods for measuring n_2, like Z-scan [1], are based on the assumption that the temporal and spatial intensity distributions of the laser radiation are in the form of a Gaussian function. In practice this is sometimes difficult to fulfill, especially in the infrared (IR) wavelength range between 2μm and 5μm, where there is a shortage of information about n_2. Therefore, a method for measuring n_2, which could include real spatial and temporal intensity distributions, is of great importance.

In this work it was chosen to measure n_2 by using an interferometer to detect a total on-axis nonlinear phase shift (B) after a sample and including measured spatial and temporal intensity distributions by numerically simulating the experiment. First, a theoretical model of a measurement was created. It was assumed that two identical linearly polarized waves with a plane wavefront are propagating at a small angle (as shown in Fig. 1). Wave1 propagates through a sample with n_2 and then is imaged on a charge-coupled device (CCD) matrix of a camera by two converging lenses of the same focal length, without any energy (E) loss and change in peak intensity. Both waves reach camera at the same time and an interference intensity pattern is formed in a form of fringes. Here B was found by fitting spatial intensity distribution (which can be any function) of wave1 to a spatial phase difference between two waves distribution (obtained from an interference pattern using Fourier transform method [2])

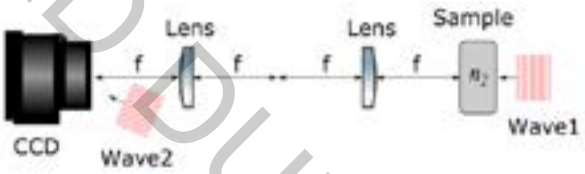

Fig. 1. Basic model of a measurement. Here f – focal length of a lens.

During numerical experimentation it was found that (because of temporal intensity modulation of a wave) this way obtained B value is less than the real value by some factor. This factor depends only on a shape of a laser pulse. Therefore, one can measure real pulse shape and then simulate the real experiment to correct the measured B values. This was demonstrated by building a real experimental setup, which realizes the model shown in Fig. 1, and measuring the n_2 of fused silica. The values of B were measured at different pulse energies. The results are shown in Fig. 2. Obtained B values were corrected according to the measured pulse shape and the n_2 was found from linearly fitted experimental data. Measured n_2 value was in good agreement with the ones given in the scientific literature.

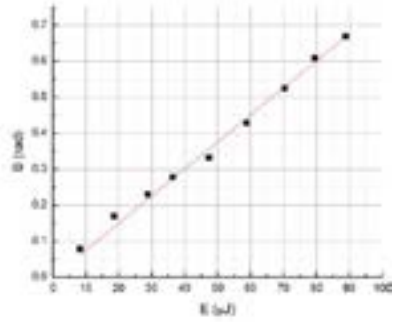

Fig. 2. Total on-axis nonlinear phase shift measuring results. Dots – experimental points, line – linear fit.

In conclusion, a method to include real temporal and spatial intensity distributions of light in n_2 measurements was successfully prepared and tested. It could be used to measure n_2 in the IR wavelength range between 2μm and 5μm, where such measurements are needed.

[1] M. Sheik-bahae, A. A. Said, and E. W. Van Stryland, "High-sensitivity, single-beam n2 measurements," Opt. Lett. **14**, 955-957 (1989).
[2] Mitsuo Takeda, Hideki Ina, and Seiji Kobayashi, "Fourier-transform method of fringe-pattern analysis for computer-based topography and interferometry," J. Opt. Soc. Am. **72**, 156-160 (1982).

CANCELLED DUE TO COVID-19

INVESTIGATION OF PHOSPHOR PHOTOLIUMINESCENCE QUANTUM EFFICIENCY

Simonas Stasiūnas[1], Greta Inkrataitė[2], Akvilė Zabiliūtė-Karaliūnė[1], Ramūnas Skaudžius[2], Pranciškus Vitta[1]

[1] Institute of Photonics and Nanotechnology, Faculty of Physics, Vilnius University
[2] Institute of Chemistry, Faculty of Chemistry and Geosciences, Vilnius University
simonas.stasiunas@ff.stud.vu.lt

Solid-state lightning has become one of the most widely used lightning options in the world. Applications that require high power density and directional beams could employ laser diodes (LD) [1]. The high light output power which exceeds that of LEDs at high current densities, are the main factors determining the future applications of LDs [2]. LEDs and LDs use phosphors to produce white light. The properties of phosphors have a large influence on the spectral characteristics of the output light. Therefore, the investigation and improvement of phosphors optical and thermal properties is one of the key points in increasing the integration of solid-state lighting in all aspects of our lives. One of the main physical properties of phosphor is photoluminescence quantum efficiency (QE).

In this work, four different condition phosphor samples were investigated: $Y_3Al_5O_{12}:Ce^{3+}$ (YAG:Ce^{3+}) powder synthesized in the laboratory, YAG:Ce^{3+} with polymer in silicone, YAG:Ce^{3+} (PhosphorTech HTY-550) in silicone and Eu doped silicate (Intematix EG3261) powder. After measuring the QE of all samples, it was observed that the excitation site in the case of phosphor powder influenced the value of QE. For example, excitation of the powder at high concentrations results in about 20% reduction in QE. The experiment compared QE of commercial phosphor and a phosphor mixed with a polymer. After analyzing the results, a tendency was observed that the phosphor converter with polymer had slightly higher QE compared to the commercial (Fig. 1). Higher QE values are likely to be caused by the phosphor grain surface defect reduction.

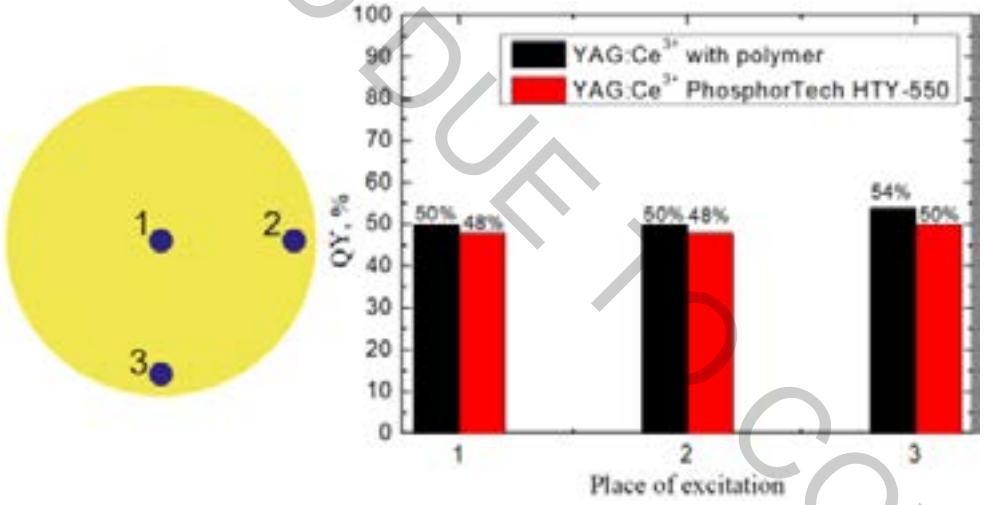

Fig.1. Dependence of QE on the excitation places.

[1]A. F. George, S. Al-waisawy, J. T. Wright, W. M. Jadwisienczak, ir F. Rahman, „Laser-driven phosphor-converted white light source for solid-state illumination“, *Appl. Opt.*, t. 55, nr. 8, p. 1899, kovo 2016, doi: 10.1364/AO.55.001899.
[2]J. J. Wierer ir J. Y. Tsao, „Advantages of III-nitride laser diodes in solid-state lighting: Advantages of III-nitride laser diodes in solid-state lighting“, *Phys. Status Solidi A*, t. 212, nr. 5, p. 980–985, geg. 2015, doi: 10.1002/pssa.201431700.

CANCELLED DUE TO COVID-19

BROADBAND CHIRPED MIRRORS FEATURING LOW GROUP DELAY DISPERSION OSCILLATIONS

Simas Melnikas, Lukas Ramalis, Simonas Kičas, Tomas Tolenis,

Optical Coatings Laboratory, Center for Physical Sciences and Technology, Lithuania
simas.melnikas@ftmc.lt

Chirped mirrors (CMs) are special type of dielectric multilayer coatings intended for stretching or compressing of ultra-short (femtosecond) laser pulses. Various types of CMs were proposed in the past: double chirped mirrors (DCMs), back side coated chirped mirrors (BASIC), complementary CM pairs, and other [1]. All of these CM configurations were implemented to reduce spectral oscillations of group delay dispersion (GDD): parameter, indicating the stretching or compressing magnitude of the mirror. Such effort allowed to compress optical pulses below 2 fs using complementary CM pair approach [1].

However, oscillation-free GDD spectral bandwidth of standard single CM is limited to half optical octave for standard coating materials [1] (e.g. $\Delta\lambda\approx200$ nm at wavelength $\lambda=800$ nm). Modifications of CM to overcome this issue require either cumbersome mechanical matching (e.g. BASIC approach) or supreme deposition accuracy (e.g. complementary CM pair approach). Recently, an easier way to expand the spectral bandwidth of CM was suggested. New type of CM was proposed and tested implementing the last ultra-low refractive index layer (e.g. $n< 1.25$ for porous SiO_2 material) to the common CM structure [2, 3]. In this way it is possible to achieve oscillation-free GDD performance from single mirror over broad optical spectrum. So far low-ripple chirped mirrors were deposited covering 240-340 nm spectral bandwidth. The purpose of this study was to extend such CM bandwidth up to 400 nm.

In this work, ion beam sputtering (IBS) technology and glancing angle deposition (GLAD) setup within electron beam evaporation coating plant were implemented to deposit chirped mirror coating (Fig.1a). 51 layers of Nb_2O_5/SiO_2 materials were deposited using IBS technology. The last (52^{nd}) layer of the coating was deposited with GLAD technology (layer consisting of vertical columns was formed) [4]. To calculate the design of the mirror, a trade-off was made between several limiting parameters of final element. Firstly, relatively high refractive index ($n\approx1.23$) was chosen for the last layer material. More porous layer would allow to further decrease theoretical GDD oscillations. However, denser layer reduces sensitivity to environmental conditions (humidity). Secondly, relatively low coating thickness (less than 5.4 µm) permitted lower reflectance (R) value, but more accurate layer thickness control and thus lower GDD oscillations.

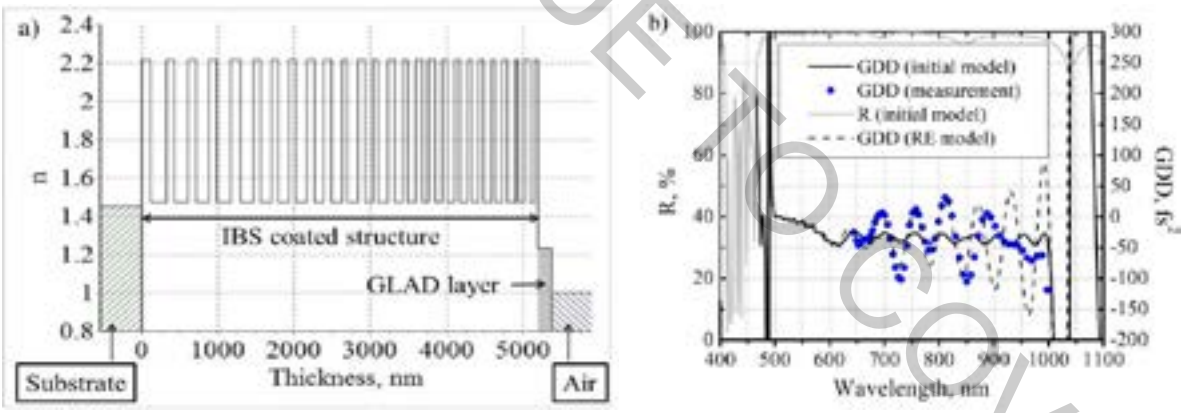

Fig. 1. Refractive index profile of chirped mirror multilayer structure: last layer ($n\approx1.23$) was deposited using GLAD technology (a); spectral parameters of chirped mirror (b).

Initial GDD measurements indicate that spectral oscillations do not exceed -35 ± 100 fs^2 limits (Fig.1b). Reverse engineering (RE) procedure of deposited layer thicknesses and refractive indices was done according to transmittance and GDD measurements. This analysis showed that roughly only one third of the increase of oscillation amplitude had been caused by IBS deposition errors. Therefore, the main source of discrepancy of spectral parameters was instability of GLAD process.

Further investigations in GLAD layer repeatability and stability will be carried out to improve CM performance.

[1] V. Pervak, O. Razskazovskaya, *et al.*, Dispersive mirror technology for ultrafast lasers in the range 220–4500 nm, Adv. Opt. Technol., **3**(1), 55-62 (2014).

[2] J. Liu, Y. Wang, *et al.*, Design, fabrication and application of dispersive mirrors with a SiO2 sculptured layer, Opt. Mater. Express, **8**(4), 836-843 (2018).

[3] P. Ma, A. Szeghalmi, *et al.*, Design and Fabrication of Single, Smooth and Broadband Chirped Mirrors with a Top Nano-Porous Layer, Optical Interference Coatings Conference (OIC) 2019, Santa Ana Pueblo, New Mexico, ThB.3, (2019).

[4] L. Grinevičiūtė, M. Andrulevičius, *et al.*, Highly Resistant Zero-Order Waveplates Based on All-Silica Multilayer Coatings, Phys. Status Solidi A, **214**(12), 1770175 (2017).

ACCEPTED DUE TO COVID-19

HEAT SOURCE DETECTION USING THE THERMOGRAPHIC METHOD FLIR ONE THERMAL CAMERA SYSTEM

Sandesh Mysore Sathyaraj[1*], Divyesh Mune Gowda[2*], Ajith Kumar Rajendra [2]

[1] Department of Electrical and Electronics Engineering,, Kaunas university Of Technology, Kaunas, Lithaunia
[2] Department of Automation, Kaunas university Of Technology, Kaunas, Lithaunia
Sandesh.mysore@ktu.edu, divyesh.mune@ktu.edu, ajith.rajendra@ktu.edu.

Abstract: Modern days any mechanical or electronic system, noticeable the energy expended eventually becomes heat[1]. Particularly the computers: the microchips in a PC move information back and forth, but in the end the electrical energy becomes heat. If we measured the heat produced and the energy consumed, we had found the balance exactly. Physicists call this principle the "Conservation of Energy". In this prospective faster, more powerful computer produce more heat than smaller, portable models. For example, a typical notebook computer, used moderately, consumes 40 watts of electricity and produces an equivalent amount of heat. A lightly used desktop machine, by comparison, uses about 100 watts. Mobile devices use far less power and produce correspondingly less heat; power consumption is limited by the small, weight-saving battery. A typical smartphone such as the iPhone 4S consumes only a few watts when making a phone call[2]. Other hand, the radiation from a component which draws more current is higher than the others. Also, the other reason is the higher internal resistance among all the thousands of circuits. So exactly speaking as long as our computer is on, heat is always generated. The following causes of more heat generation and issues .

• The Processor and Graphic card are two such components which cause the maximum heating.
• The heat these components generate is not always the same. With the increase in load (more operations to be carried out) the temperatures get higher and higher.
• Usually during gaming, the GPU has to handle lot more high-level calculations. In some cases, the temperatures of the graphic cards sore higher than that of the processor.
• Optical Disk Drives also produce large amounts of heat during reading and writing from and into CDs and DVDs respectively.
• The other sources of heat are also the LEDs. Though the amount of heat they liberate is less, it can't be neglected completely. But if this heat is not being removed fast, it could cause some serious damage to all the components inside and hence poses the ultimate threat to our computer. This are the issues in the present electrical PC systems.

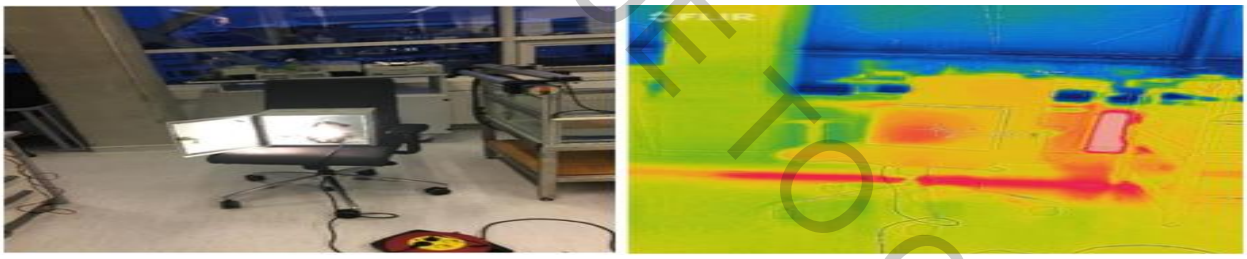

Fig. 1. Proposed heat source detection using the thermographic method Focus lamp in normal camera and FLIR ONE thermal camera system.

Considered all above issues, we proposed possibilities of heat source detection using the thermographic method[3].This method ,troubleshoot hotspots, find hidden faults, and confirm repairs quickly with the ergonomic, high-resolution. so, we can easily and comfortably diagnose electrical or mechanical issues, even in hard-to-reach areas. The proposed work ,we had the experiment with Forward-looking infrared (FLIR) camera shown in Fig. 1 and their specification. The FLIR cameras ONE Pro helps we find invisible problems faster than ever, whether we inspected electrical panels, troubleshooting mechanical systems, looking for Heating, ventilation, and air conditioning (**HVAC**) problems, or finding water damage[4]. This FLIR ONE Pro-Series camera offers 4x the native resolution of the FLIR ONE Pro LT, for sharper image clarity that's further enhanced by the revolutionary FLIR VividIR™ image processing. Measured temperatures more than 3x higher than any FLIR ONE model—up to 400°C (752°F)—with a sensitivity that detects temperature differences down to 70 mK. Packed with powerful measurement tools, the FLIR ONE Pro will work as hard as we do.

[1] Luca Scapino, Herbert A. Zondag, Johan Van Bael, Jan Diriken, Camilo C.M. Rindt,Sorption heat storage for long-term low-temperaturepplications: A review on the advancements at material and prototype scale,Applied Energy,Volume 190,2017,Pages 920-948,
[2] Kyle Forinash , Energy conservation and the first law of thermodynamics,Physics and the Environment,May,2017Pages 2-1 to 2-24
[3] L. Ferraris, E. Poskovic and F. Franchini, "Defects detection in laminated and soft magnetic composites devices with a novel thermographic method," 2017 IEEE 11th International Symposium on Diagnostics for Electrical Machines, Power Electronics and Drives (SDEMPED), Tinos, 2017, pp. 585-590.
[4] T. Malmivirta *et al*., "Hot or Not? Robust and Accurate Continuous Thermal Imaging on FLIR cameras," 2019 IEEE International Conference on Pervasive Computing and Communications PerCom, Kyoto, Japan, 2019, pp. 1-9.

CANCELLED DUE TO COVID-19

REMOTE DETECTION IN HIGH-VOLTAGE DEVICES USING THE ULTRASONIC METHOD

Sandesh Mysore Sathyaraj[1*], Divyesh Mune Gowda[2*], Ajith Kumar Rajendra [2]

[1] Department of Electrical and Electronics Engineering,, Kaunas university Of Technology, Kaunas, Lithaunia
[2] Department of Automation, Kaunas university Of Technology, Kaunas, Lithaunia
Sandesh.mysore@ktu.edu, divyesh.mune@ktu.edu, ajith.rajendra@ktu.edu.

ONSCRIPTIBUE COVID-19

Abstract: Essentially, as in generic leak detection, the area of inspection is scanned starting at a high sensitivity level. To determine the location of the emission, reduce the sensitivity and follow the sound to the loudest point. If it is not possible to remove covers, or plates or doors, scan around the seams and vent slots. For more accurate diagnosis, ultrasound spectral analysis software helps identify sound patterns related to electrical emissions through spectral (FFT) and Time Series screens. Some of the more advanced instruments have on-board sound recording while others have on-board spectral analysis screens to help provide a diagnosis on the spot. There may be instances where it is difficult to determine the type of problem heard through the headphones. In these situations, a sound recording of the condition can be made and viewed on spectral analysis software. The sounds may be heard in real time as they are viewed on an FFT or time series screen for analysis. This enables inspectors to observe subtle problems that might be missed by just viewing a screen without sound the sound sample, showing a buildup and drop off of the sound along with movement on the screen, highlighted this condition. We investigated the present paper, the potential for partial detector remote detection in high-voltage devices (2 kV and above 40 kV) using the ultrasonic method shown in Fig.1. Systems manufactures and supports ultrasound instruments used for condition monitoring and energy conservation programs. The famous Ultra probe series is the industry standard for ultrasonic inspection. These portable instruments are among other applications used to inspect, locate diagnose & trend electrical discharge on electrical apparatus. Identify early warning & locate electrical faults such as arcing, tracking and corona. Inspection results are enhanced with data management and spectral analysis software[1]. The present work analyzed using, Low voltages: The main concern in low-voltage equipment is arcing. Typically, 110-, 220-and 440-volt systems are inspected with infrared imaging and/or spot radiometers for temperature changes. Hot spots, usually an indication of resistance, can be indicative of a potential for equipment failure or it could indicate a possible fire hazard. Mid and high voltage: Higher voltages often produce more potential for equipment outage. Problems such as arcing, destructive corona or tracking (sometimes referred to as “baby arcing”) and corona as well as partial discharges and mechanical looseness all produce detectable ultrasound that warn of impending failure. Detecting these emissions is relatively easy with ultrasound[2].

Fig.1.Proposed remote detection in high-voltage devices using the ultrasonic system

This work we can online condition monitors**,** an electrical cabinet monitor is mounted on the internal side of a door or wall facing the components. Utilizing an airborne scanner, a threshold level is set. Should an event of arcing, tracking or corona occur, the sound level will be above the ambient threshold and be detected. A 4 to 20 milliamp (mA) or zero to 10 VDC output can be selected to carry the signal to an alarm mechanism or red-light alert. In addition, these units contain a heterodyned signal to provide recording capability for recordkeeping and analysis purposes. The advantage to online monitoring is obvious: it is not operator dependent and will continuously monitor. Whenever a condition occurs to produce the potential for arc flash or flashover, it will be sensed and alarmed instantly. The present Ultrasound inspection is an effective screening tool for detecting the potential for arc flash incidents. When hand-held ultrasonic instruments are used to scan enclosed electrical apparatus the procedure is fast, accurate and simple. It can help inspectors by eliminating the need for wearing cumbersome, uncomfortable PPE during a preliminary survey[3]. Online continuous monitors can alarm personnel of the presence of arcing, tracking and corona in advance of an inspection.

[1] Wang Y, Li X, Gao Y, Zhang H, Wang D, Jin B. Partial Discharge Ultrasound Detection Using the Sagnac Interferometer System. *Sensors (Basel)*. 2018;18(5):1425. Published 2018 May 4. doi:10.3390/s18051425

[2] Xu Wei ,Application research of the partial discharge automatic detection device and diagnostic method based on the ultrasonic in long distance GIL equipment ,2019 J. Phys.: Conf. Ser. 1213 052088.

[3] L. Kumpulainen, G. A. Hussain, M. Lehtonen and J. A. Kay, "Preemptive Arc Fault Detection Techniques in Switchgear and Controlgear," in *IEEE Transactions on Industry Applications*, vol. 49, no. 4, pp. 1911-1919, July-Aug. 2013.

INVESTIGATION OF LASER INDUCED DAMAGE DYNAMICS IN TRANSPARENT MEDIA AND DIELECTRIC COATING BY ULTRAFAST SPECTROSCOPY

Aivaras Pečiulis, Mikas Vengris, Linas Smalakys, Andrius Melninkaitis

Laser Research Center, Vilnius University, Lithuania
aivaras.peciulis@ff.stud.vu.lt

CANCELLED DUE TO COVID-19

Development of optical components has to keep up with constantly growing lasers' pulse peak power and radiation frequency, which mean they must have higher and higher laser induced damage threshold (LIDT). Investigating and understanding the dynamics of laser damaging would help to achieve that and avoid breach of optical elements. In this experiment, ultrafast spectroscopy methods are used to observe and analyze damage and aging processes of titanium dioxide (TiO_2) dielectric coating on BK7 optical glass bulk.

A standard pump – probe experiment was conducted to demonstrate that we can separately analyze bulk and coating of the optical element. The difference is evident in signal strength and extinction kinetics (Fig. 1(a) and (b)). Then "single-shot" method was used to detect difference transmittance spectra at the moment of excitation (*During*), after $1ms$ (*After*) and from $1ms$ to $1s$ (*Long after*) after the pump pulse. Every measurement was taken at a different location while raising beam power. Main results of TiO_2 dielectric coating investigation are shown in Fig. 2. Difference transmittance dependence on pump pulse fluence shows LIDT of the sample ($F = 0.27J/cm^2$) and the dynamics of damage.

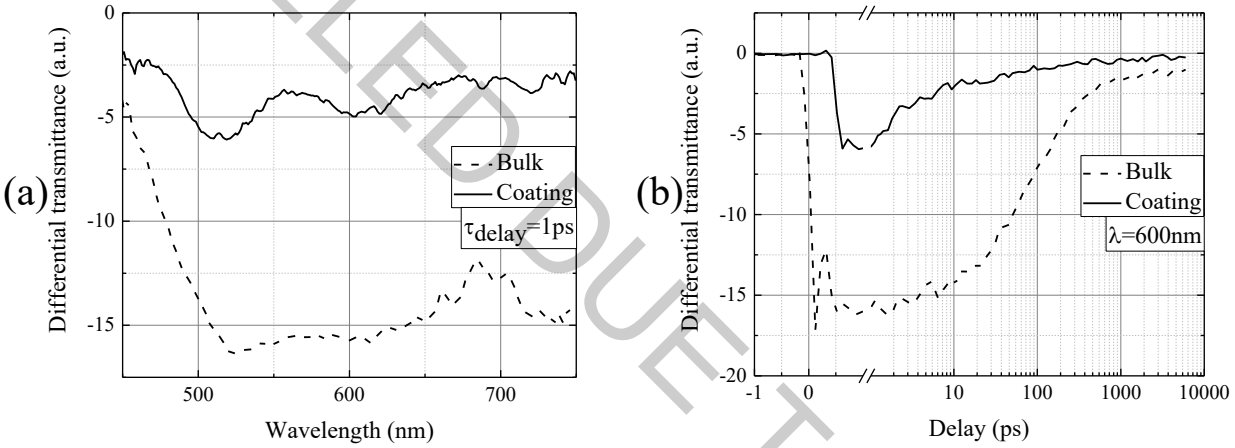

Fig. 1. Bulk and coating 's difference transmittance dependence on (a) wavelength at $\tau = 1ps$ delay and (b) delay at $\lambda = 600nm$. Excitation beam fluence $F = 0{,}07J/cm^2$.

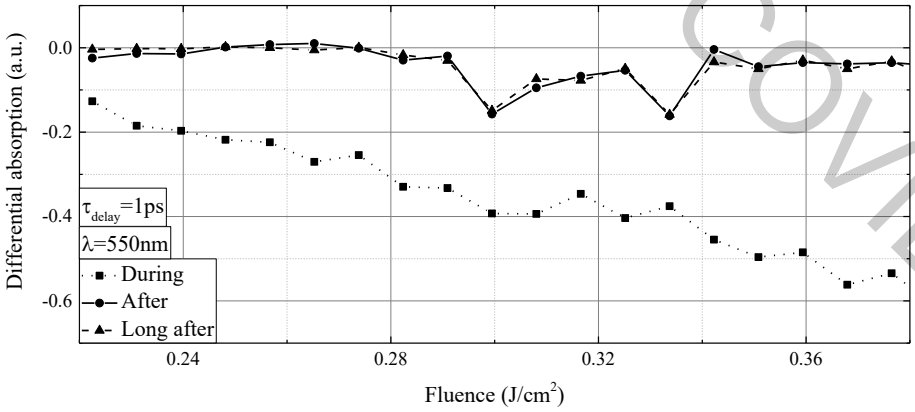

Fig. 2. TiO_2 dielectric coating differential transmittance dependence on fluence at $\tau = 1ps$ delay and $\lambda = 600nm$.

These experiments are a demonstration of laser induced damage measuring capabilities. As now we can record difference transmittance spectra in femtosecond resolution, more measurements are going to be made to determine damage mechanisms of bulk materials and coatings from their dynamics. Observing spectral similarities between different materials and coatings will help to understand the physical properties of the damage itself.

THE ORBITAL ANGULAR MOMENTUM OF LIGHT IN LASER SPECTROSCOPY

Maciej Chomski[1], Gustaw Szawioła[1], Bogusław Furmann[1]

[1] Faculty of Materials Engineering and Technical Physics, Poznan University of Technology, Poland
maciej.s.chomski@doctorate.put.poznan.pl

The states of light with non-zero value of orbital angular momentum (OAM) [1] are useful tool in numerous photonic techniques, for example optical trapping of atoms with putting them into rotational motion, optical processing of quantum information or performing optical quantum memories. One of the interesting applications of, so called, optical vortices is laser spectroscopy with breaking standard selection rules [2].

As part of this paper, the idea of an experimental system for observing quadrupole transitions in atoms, by Laser-Induced Fluorescence method in the hollow cathode discharge lamp, excited by the Laguerre-Gaussian beam (which is an example of an optical vortex) will be presented. Photons which forms classical Gaussian beam possess only Spin Angular Momentum. Because of that only dipole transitions, allowed by standard selection rules $\Delta m_j = 0, \pm 1$, can be driven by Gaussian laser light. To excite atom by the quadrupole transition the orbital component of angular momentum is required to fulfill the condition $\Delta m_j = 0, \pm 1, \pm 2$. The possibility of using a non-zero OAM for spectroscopic purpose has been demonstrated on the calcium ion in Paul's trap [3].

Progress in the construction of the experimental system for the production of optical vortices with a liquid crystal phase plate (Q-plate) and its integration with the existing hollow cathode discharge lamp system will be presented. The optical system is going to convert laser light in OAM light's states in broad visible spectral range. The generated beam in Laguerre-Gauss mode may help with studying the hyperfine structure of rare earth elements, by Laser-Induced Fluorescence method, carried out at the Division of Engineering and Quantum Metrology at the Faculty of Materials Engineering and Technical Physics of the Poznan University of Technology. The proposed modernization of the standard experimental system involved in the conducted research will allow to expand potential research possibilities.

This research was funded by the Ministry of Science and Higher Education of the Republic of Poland.

[1] S. M. Barnett, M. Babiker, M. J. Padgett, Optical orbital angular momentum, Trans. R. Soc. A **375**, 20150444 (2017).
[2] S. Franke-Arnold, Optical angular momentum and atoms, Trans. R. Soc. A **375**, 20150435 (2017).
[3] Ch. T. Schmiegelow, J. Schulz, H. Kaufmann, T. Ruster, U. G. Poschinger, F. Schmidt-Kaler, Transfer of optical orbital angular momentum to a bound electron, Nature Communications **7**, 12998 (2016).

CANCELLED DUE TO COVID-19

RADIATION INSTABILITY IN RELATIVISTIC SPLIT-CAVITY OSCILLATOR

Sergei Anishchenko, Illia Maroz, Anatoli Rouba

Research Institute for Nuclear Problems, Belarussian State University, Belarus
moroz@inp.bsu.by

In recent decades, the interest in high-power microwave (HPM) sources has been increasing. The sources are widely used in science and industry, e.g., plasma heating, high-power radars, particle acceleration, etc. Such a wide area of applications led to a large variety of HPM sources (e.g., klystron amplifiers, gyrotrons, backward wave oscillators, travelling wave tubes, transit-time oscillator, virtual cathode oscillator, etc.) that are suitable for specific purposes. Despite the great success in their development, the usage of them is often limited by a large size or low efficiency. To overcome these limitations, Barry M. Marder and his group have developed a new device called a split-cavity oscillator (SCO) [1, 2], which was further improved by others [3, 4]. The SCO consists of a cylindrical resonator with a conducting screen walls splitted by a conducting screen (Fig. 1) through which an electron beam can pass. This configuration has additional electromagnetic modes (Fig. 1) in comparison with a hollow resonator. The first theoretical consideration of the SCO in the relativistic case was carried out by V. Baryshevsky in [5].

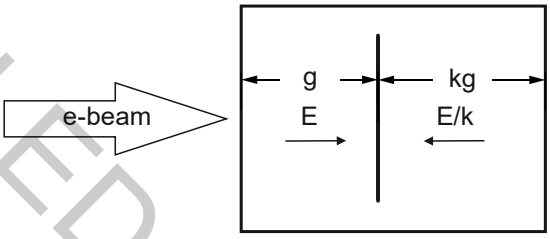

Fig. 1. Schematic representation of the asymmetric SCO, where g is the longitudinal size of a cavity, E is the electric field, k is the parameter of asymmetry.

This work is devoted to the theoretical research of the radiation instability of the electron beam in the SCO. The interaction between the electron beam and the fundamental mode was considered. Expressions of an electron energy change ΔK and a beam current modulation were obtained for the relativistic case in the asymmetric SCO. The influence of the space charge of the beam on ΔK and the beam current modulation was numerically analyzed. The rise time of the modulating electric field in the resonator was estimated. The small-signal analysis showed that the optimal configuration is symmetric (k=1, see Fig.1). Moreover, the growth of the space charge increases the energy transfer from an electron to the field (Fig.2) and almost does not affect the resonator size. The rise of the electron velocity decreases the energy transfer to the electromagnetic field (Fig.2).

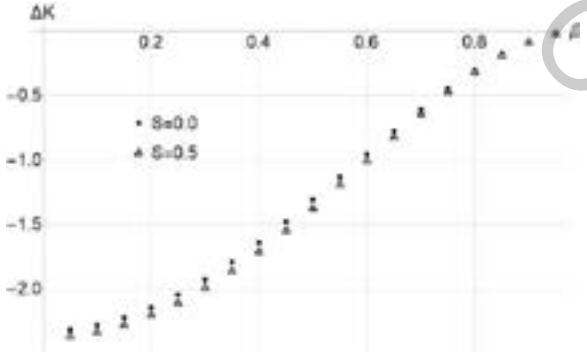

Fig. 2. Dependence of the electron energy change ΔK on electron velocity divided by the speed of light for S=0 and S=0.5, where the dimensionless parameter S describes the beam current.

[1] Barry M. Marder, M. Collins Clark, Larry D. Bacon, James M. Hoffman, Raymond W. Lemke, P. Dale Coleman, The split-cavity oscillator: a high-power E-beam modulator and microwave source, IEEE TRANSACTIONS ON PLASMA SCIENCE. – 1992. – V20, №3 – C.312–331.
[2] Raymond W. Lemke, M. Collins Clark, Barry M. Marder ,Theoretical and experimental investigation of a method for increasing the output power of a microwave tube based on the split-cavity oscillator, Journal of Applied Physics. – 1994. – V75, №10 – C.5423–5432.
[3] G.V. Sotnikov, Yu.V. Tkach, S.L. Scherbina, Eigen frequencies and field structure of axially symmetric split-cavities, Electromagnetic Phenomena. – 2008. – V8, №1(19) – c.46-61.
[4] ZHANG Yun-Jian, MA Qiao-Sheng, LUO Xiong , Study of a compact external magnetic field radial split-cavity oscillator, Chinese Physics C. – 2011. – V35, №4 – c.381-386.
[5] V.G. Baryshevsky. Relativistic split-cavity oscillator. // Research Institute for Nuclear Problems, 2014. URL: arxiv.org/abs/1402.3403 (Date of access: 29.01.2020)

CANCELLED DUE TO COVID-19

AB INITIO MULTI-REFERENCE PERTURBATION THEORY STUDY ON THE RaCl MOLECULE PROMISING FOR LASER COOLING

Yuliya Osika, Maksim Shundalau

Faculty of Physics, Belarusian State University, Belarus
yulia.osika@gmail.com

Ultracold polar molecules offer prospects for the creation of the molecular Bose-Einstein condensate with possible applications for quantum information and precision measurements [1]. One of the possibilities of obtaining molecular quantum matter with controlled properties is the transferring of the polar diatomic molecules to the ground rovibronic state by initial optical excitation into the overlying rovibronic states with specific forms of electronic terms. In this case for the high efficiency of excitation and subsequent relaxation of the molecular system the exact forms of the potential energy curves (PECs) of the combining electronic states can be obtained based on analysis and interpretation of high-resolution rovibronic spectra or cutting-edge *ab initio* calculations. The knowledge of the exact PECs also allows to define the important spectra-energetic characteristics of molecules and the macroscopic physical properties of rarefied gases.

Physical and chemical applications of ultracold molecules include ultra-high-resolution spectroscopy, few-body physics, quantum computation, molecular optics and controlled chemical processes [1]. Earlier [2] it was shown that diatomic molecules, which contain alkaline earth metal atom and halogen atom are promising for the direct laser cooling due to the matching equilibrium internuclear distances for different PECs.

In this study, *ab initio* state-of-art calculations of the low-lying doublet states of the RaCl molecule were performed for the first time (Fig. 1). The calculations at the SA-CASSCF(13,12)/XMCQDPT2 [3] level of theory were carried out in two stages taking into account static and dynamic parts of correlation energy in the range of internuclear distances from 2.26 to 12.50 Å. The PECs were analytically continued starting from 2.26 to 2.00 Å. The TZ-basis set for Cl atom and Stuttgart RSC ECP 78 for Ra atom were used in the calculations for three dissociation limits [$Ra(7s^2)$+$Cl(3p^5)$, ($Ra^+(7s)$+$Cl^-(3p^6)$, and $Ra^+(6d)$+$Cl^-(3p^6)$].

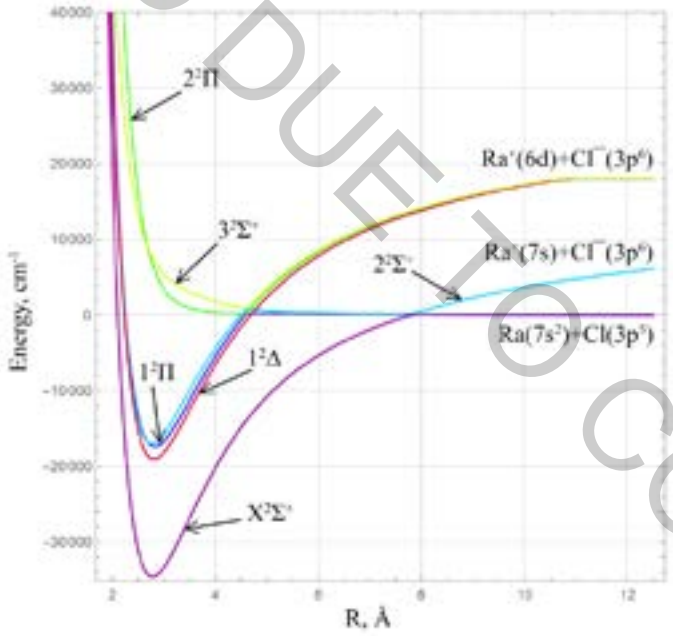

Fig. 1. The PECs of the low-lying doublet states of the RaCl molecule at the CASSCF(13,12)/XMCQDPT2 level of theory.

The results of our calculations for dissociation limits are in good agreement with energies of isolated atoms and ions. The PECs and spectroscopic parameters were obtained for the following low-lying RaCl terms: ground state $X^2\Sigma^+$ (R_e = 2.776 Å, D_e= 34605.6 cm^{-1}), and excited states $1^2\Pi$ (R_e = 2.821 Å, D_e= 17421.5 cm^{-1}), $2^2\Sigma^+$ (R_e = 2.765 Å, D_e= 17040.9 cm^{-1}), $1^2\Delta$ (R_e = 2.800 Å, D_e= 19087.6 cm^{-1}). It is worth mentioning that equilibrium internuclear distances of the ground and some excited states are close in value. The results also show that the diatomic polar molecule RaCl is a promising candidate for laser cooling and magneto-optical trapping.

[1] O. Dulieu, C. Gabbanini, The formation and interactions of cold and ultracold molecules: new challenges for interdisciplinary physics, Rep. Prog. Phys. **72**, 086401 (2009).
[2] T.A. Isaev, S. Hoekstra, R. Berger, Laser-cooled RaF as a promising candidate to measure molecular parity violation, Phys. Rev. A **82**, 052521 (2010).
[3] A.A. Granovsky, Extended multi-configuration quasi-degenerate perturbation theory: the new approach to multi-state multi-reference perturbation theory, J. Chem. Phys. **134**, 214113 (2011).

CANCELLED DUE TO COVID-19

WO_3/WO_X COMPOSITES FORMATION BY SOL-GEL METHOD

Monika Baronaitė[1], Simonas Ramanavičius[2], Milda Petrulevičienė[2], Jurga Juodkazytė[2], Asta Grigucevičienė[2], Maliha Parvin[2], Vilma Ratautaitė[2], Urte Samukaitė-Bubnienė[1], Renata Karpicz[1], Arūnas Ramanavičius[1,2]

[1] Department of Physical Chemistry, Vilnius University, Lithuania
[2] State Research Institute Center for Physical Sciences and Technology, Lithuania
monika.baronaite@chf.stud.vu.lt

Among many others non-stoichiometric metal oxides [1] tungsten oxide (WO_x) is a wide band-gap n-type transition metal oxide with wide-ranging applications. Its electronic bandgap (Eg), highly depends on oxide composition and its crystallite size [2]. These and other WO_x characteristics are applicable in many fields such as lithium-ion batteries [3], solar energy conversion system [4], catalysis [5], surface enhanced Raman spectroscopy [2], and volatile organic compounds sensors [6].

This study is focused on the synthesis of WO_3/WO_x based nanostructures by simple sol-gel synthesis seeking to prepare composites with extended characteristics in comparison with regular WO_3 structures. Different organic additives were used during the formation of these structures in order to change nanostructures morphology and other characteristics. X-ray diffraction analysis was employed to prove non-stoichiometric tungsten oxide (WO_x) structure. Scanning electron microscopy (SEM) was used to determine nanoparticles surface morphology and size distribution. Photoluminescence spectra (PL) were measured to determine structure defects.

It was determined that by applying different organic additives surface morphology and defects of WO_3/WO_x nanostructures could be controlled. By using dip-coating method samples of thin films were prepared on different substrates in search of various applications for synthesized structures.

Acknowledgement
Support by Lithuanian Research Council Project No: 09.3.3-ESFA V-711-01-0001.

[1] S. Ramanavicius, A. Tereshchenko, R. Karpicz, V. Ratautaite, U. Bubniene, A. Maneikis, A. Jagminas, A. Ramanavicius, TiO2-x/TiO2-structure based 'self-heated' sensor for the determination of some reducing gases, *Sensors* 2020, 20, 74.
[2] S. Cong, F. Geng, Z. Zhao, Tungsten Oxide Materials for Optoelectronic Applications, *Advanced Materials* 2016, 28, 10518–10528.
[3] M. Zheng, H. Tang, Q. Hu, S. Zheng, L. Li, J. Xu, H. Pang, Tungsten-Based Materials for Lithium-Ion Batteries, *Advanced Funtional Materials* 2018, 28, 1707500.
[4] N. Chandra, D. Nath, S. Yo, H. Won, J. Lee, H. Park, Nano Energy Stand-Alone Photoconversion of Carbon Dioxide on Copper Oxide Wire Arrays Powered by Tungsten Trioxide/Dye-Sensitized Solar Cell Dual Absorbers, *Nano Energy* 2016, 25, 51–59.
[5] Z. Zhao, M. Miyauchi. Nanoporous-Walled Tungsten Oxide Nanotubes as Highly ActiveVisible-Light-Driven Photocatalysts, *Angewante Chemie International Edition* 2008, 47, 7051–7055.
[6] S. Ramanavičius, M. Petrulevičienė, J. Juodkazytė, A. Grigucevičienė, A. Ramanavičius. Selectivity of tungsten oxide synthesized by sol-gel method towards some volatile organic compounds and gaseous materials in a broad range of temperatures, *Materials* 2020, 13, 523.

CANCELLED DUE TO COVID-19

EXCESS CONDUCTIVITY AND POSSIBLE PSEUDOGAP STATE IN FeSe SUPERCONDUCTORS

Eugene Petrenko[1], Andrei Solovjov[1], Lyudmila Omelchenko[1],
Elena Nazarova[2], Krastyo Buchkov[2], Krzysztof Rogacki[3]

[1] B. I. Verkin Institute for Low Temperature Physics and Engineering of National Academy of Science of Ukraine, 47 Nauki ave., 61103 Kharkov, Ukraine
[2] Georgi Nadjakov Institute of Solid State Physics, Bulgarian Academy of Sciences, 2 Tsarigradsko shosse Blvd., 1784 Sofia, Bulgaria
[3] W. Trzebiatowski Institute of Low Temperatures and Structure Research, PAS, Wroclaw, 1410 PL-50-050, Poland
petrenko@ilt.kharkov.ua

CANCELLED DUE TO COVID-19

The temperature dependence of the excess conductivity σ′(T) [1, 2] in three polycrystalline samples of the $FeSe_{0.94}$ superconductor prepared by various technologies [3] was studied. Obtained from the measurements, the temperature dependences of the parameter Δ*(T) which in cuprates is associated with a pseudogap, were analyzed in the model of local pairs. At high temperatures, all three samples exhibit a high narrow maximum Δ*(T) at T_{s1} ~ 250 K, typical of magnetic superconductors. Below T ≈ 225 K, the dependences Δ*(T) become different. In almost the entire temperature range below Ts1, sample S2, prepared by the solid-state reaction method and not containing impurities, shows Δ*(T) typical of Fe-pnictides. An exception is the interval from the temperature of the structural transition T_s = 85 K to T_c, where Δ*(T) exhibits an atypical broad maximum. An analysis of the obtained dependence suggests the discovery of a pseudogap in this $FeSe_{0.94}$ sample below T_s. Samples S1 containing 4 wt.% Ag and S3, with a nominal composition, but containing non-superconducting inclusions of the hexagonal phase, both obtained by partial melting, show identical Δ*(T), but different from S2. They reveal a number of features that correlate with temperatures at which features are observed on M(T) and the Hall coefficient $R_H(T)$ changes sign several times with decreasing T, indicating a change in the type of charge carriers in FeSe. The dependence Δ*(T) of sample S3 below Ts has practically no maximum, since non-superconducting impurities of the hexagonal phase prevent the formation of paired fermions in S3 near T_c. As a consequence, S3 has a minimum density of local pairs $\langle n_\uparrow n_\downarrow \rangle$ = 0.26, determined by comparing $\Delta^*(T_G)/\Delta_{max}$ near T_c with the Peters – Bauer theory [4], and the dependence Δ*(T) does not follow the theory. S1 has a maximal $\langle n_\uparrow n_\downarrow \rangle$ = 0.47, most likely due to the influence of Ag impurities. S2 does not contain impurities, and found $\langle n_\uparrow n_\downarrow \rangle \approx 0.3$ is the same as in $YBa_2Cu_3O_{7-\delta}$ [5]. Importantly, both dependencies Δ*(T) for S1 and S2 follow the theory in a wide temperature range.

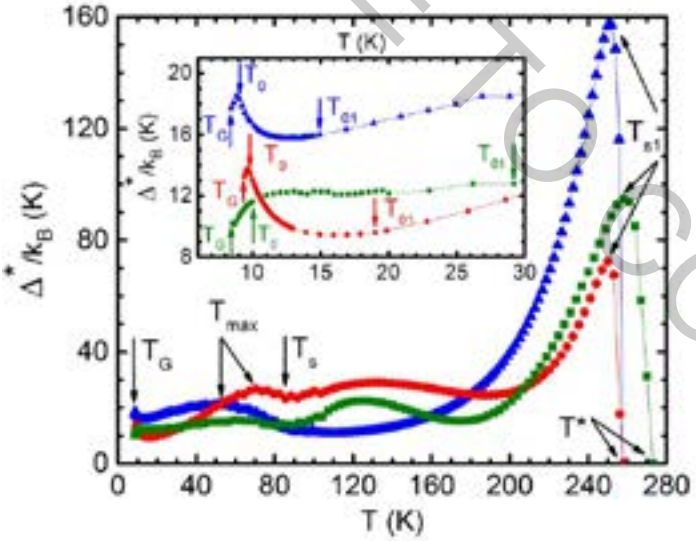

Fig. 1. Temperature dependences of possible pseudogap state Δ*(T) in three polycrystalline $FeSe_{0.94}$ samples of the $FeSe_{0.94}$ superconductor prepared by various technologies (S1 – red circles, S2 – blue triangles, S3 – green squares). Insert: The same dependence for the temperature interval $T_G < T < T_{01}$. The arrows show all characteristic temperatures. Solid lines are to guide the eye.

[1] A. L. Solovjov, in *Superconductors - Materials, Properties and Applications*, edited by A. Gabovich (InTech, Rijeka, 2012), Chap. 7, p. 137.
[2] A. L. Solovjov and V. M. Dmitriev, Low Temp. Phys. **32**, 99 (2006).
[3] E. Nazarova, N. Balchev, K. Nenkov, K. Buchkov et al. Supercond. Sci. Technol. **28**, 025013 (2015)
[4] R. Peters and J. Bauer, Phys. Rev. B **92**, 014511 (2015).
[5] A. L. Solovjov, E. V. Petrenko, L. V. Omelchenko, R. V. Vovk, I. L. Goulatis, A. Chroneos, Scientific Reports **9**, 9274 (2019).

THE INVESTIGATION OF RECOMBINATION PROCESSES BY EXTRACTION OF THE INJECTED CHARGE CARRIERS

Romualdas Jonas Čepas[1], Lukas Kukulas[1], Gytis Juška[1], Kristijonas Genevičius[1]

[1] Institute of Chemical Physics, Vilnius University, Lithuania
romualdas.cepas@ff.vu.lt

Nowadays, development of more efficient and (or) cheaper photodetectors, solar cells, photodiodes or other optoelectronic devices is associated with organic and hybrid structures. There are many photo-electric, electric and spectroscopic techniques for the study of transport and recombination in the layers of pure materials, but these techniques give only an initial understanding about the processes in multilayer structures. For example, the changes in charge carrier recombination rate in multilayered structures could vary with the morphology, formation of the interface states and changes in the charge carrier transport.

Herein we report new method for the investigation of charge transport and recombination in multilayered structures. This method is based on extraction of injected charge carriers by linearly increasing voltage (i-CELIV) [1]. In the case of double injection into a structure, consisting of hole and electron transporting layers, charge accumulates at the interface of two materials (Fig. 1) and the stationary current will be determined by recombination. In this case, the surface recombination rate can be found by measuring density of injection current j and extracted charge from the device Q[2]:

$$v = \frac{2kT\varepsilon\varepsilon_0 j}{eQ^2}, \quad (1)$$

This equation is derived by assuming that charge recombination is very weak, meaning that current flowing through the device is close to zero and charge distribution is determined by electric field and diffusion (Fig. 1b). If recombination is strong at the interface, charge carriers distribution is governed by space charge limited current (SCLC) (Fig. 1c). This method can be directly applied to dye sensitized solar cells, where the active layer is very thin. However, application of such technique in perovskite and bulk heterojunction solar cells is limited: only total recombination losses in the device can be estimated, since recombination takes place in the bulk but not at interface. In order to eliminate this drawback, the bulk heterojunctions were studied, the results were then compared with numerical calculations and other data obtained using different methodologies.

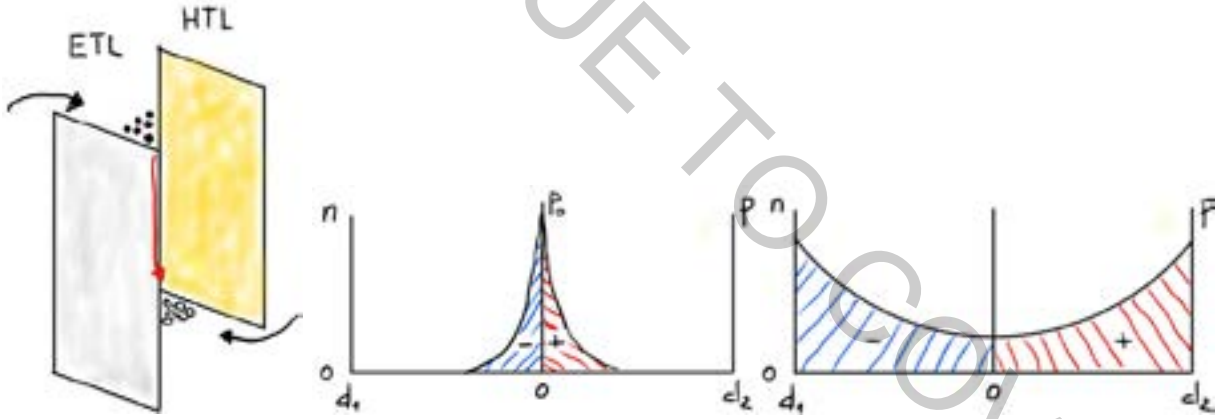

a) *b)* *c)*

Fig. 1. Energy band diagram of two-layered structure made up of electron and hole transport layers with voltage applied (a), charge distribution in case of very weak recombination (b) and in case of very strong (Langevin) recombination (c).

[1] J. Važgėla, K. Genevičius, G. Juška, i-CELIV technique for investigation of charge carriers transport properties, Chemical Physics **478**, 126-129 (2016).
[2] G. Juška, K. Genevičius, Investigation of recombination in organic heterostructures by i-CELIV, Applied Physics Letters **113**, 123301 (2018).

CANCELLED DUE TO COVID-19

IMPACT OF DIMENSIONALITY TO DIFFUSION AND RECOMBINATION PROCESSES IN LAYERED PEROVSKITES

Vaiva Soriūtė[1], Džiugas Litvinas[1], Patrik Ščajev[1], Saulius Juršėnas[1], Chuanjiang Qin[2], Takashi Fujihara[3], Toshinori Matsushima[2], Chihaya Adachi[2]

[1] Institute of Photonics and Nanotechnology, Vilnius University, Sauletekio Ave. 3, LT 10257 Vilnius, Lithuania
[2] Center for Organic Photonics and Electronics Research (OPERA), Kyushu University, 744 Motooka, Nishi, Fukuoka 819-0395, Japan
[3] Innovative Organic Device Laboratory, Institute of Systems, Information Technologies and Nanotechnologies (ISIT), Fukuoka Industry-Academia Symphonicity (FiaS), 2-110, 4-1 Kyudai-shinmachi, Nishi, Fukuoka 819-0388, Japan
vaiva.soriute@ff.stud.vu.lt

CANCELLED DUE TO COVID-19

Hybrid organic-inorganic perovskites have been gaining more attention in recent years due to their desirable properties such as a tunable bandgap, solution processability and prospects for optoelectronic applications. During last decade solar cells, LEDs, lasers [1], transistors [2] and photodetectors [3] were created from perovskites. Therefore, they require further scientific investigation in order to optimize these materials for commercialization.

The main goal of this work was to study perovskite samples $PEA_nFA_{n-1}Pb_nBr_{3n+1}$ of different dimensionality. Inside them there were increasing number of layers (N) of perovskite elementary cells sandwiched between organic ion layers. Carrier dynamics was investigated using light-induced transient grating (LITG) technique. Photoelectric parameters such as diffusion coefficient and recombination lifetime were obtained from these measurements.

Investigated layers were excited by 351 nm pulsed laser irradiation creating transient grating in the samples. Decay of this grating was observed using a probe beam of 1053 nm which was delayed by an optical delay line. Optical attenuator was employed to change the excitation energy fluence (Φ), allowing to analyze photoelectric properties of perovskite samples within the wide range of excess carrier density (10^{18} – 10^{19} cm^{-3}). Diffraction efficiency (η) decays, measured at three different grating periods Λ (Fig. 1 (a)), allowed us to extract carrier lifetime (τ_R) and diffusion coefficient (D) using Eq. (1):

$$\frac{1}{\tau_G} = \frac{1}{\tau_R} + \frac{1}{\tau_D} = \frac{1}{\tau_R} + \frac{4\pi^2 D}{\Lambda^2} \quad (1)$$

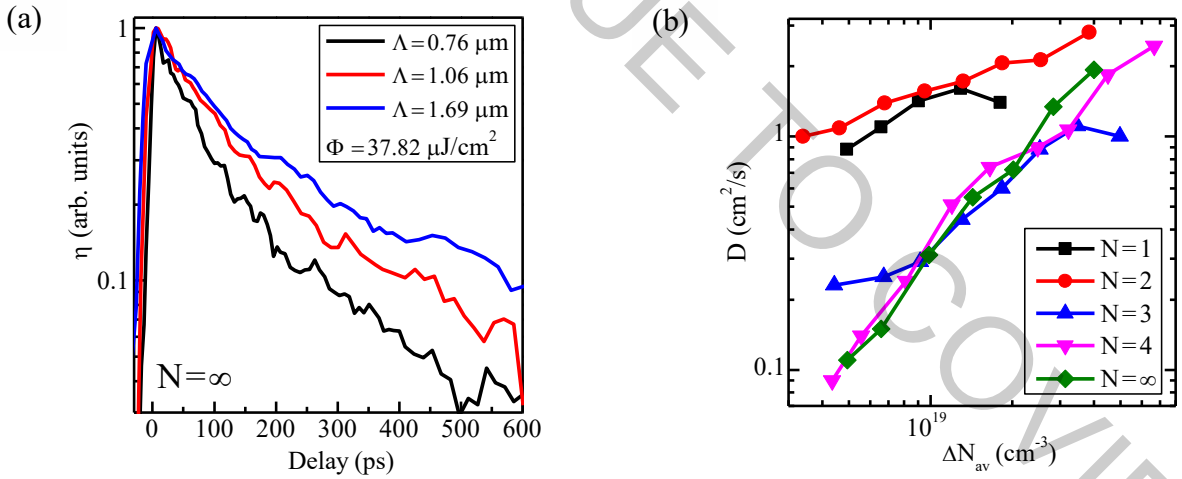

Fig. 1. (a) LITG transients measured at three different grating periods Λ. (b) Diffusion coefficient D as a functions of excess carrier density ΔN_{av}. N represents the number of perovskite layers in the sample.

In Fig. 1 (b) it can be seen that diffusion coefficient increases with excitation. Also, samples with fewer perovskite layers have a higher diffusion coefficient value which changes only slightly with increasing excitation compared to samples with higher dimensionality. This can be attributed to the carrier delocalization [4]. It is stronger in perovskite samples with more layers, therefore we see greater change in diffusion coefficient compared to their more confined counterparts. Longer carrier lifetimes in samples with higher dimensionality also can be related to stronger localization.

[1] J. R. Harwell, G. L. Whitworth, G. A. Turnbull, I. D. W. Samuel, Green perovskite distributed feedback laser. Scientific Reports **7**, 11727 (2017).
[2] Y. Gao, Z. Wei, P. Yoo, E. Shi, M. Zeller, C. Zhu, P. Liao, L. Dou, Highly stable lead-free perovskite field-effect transistors incorporating linear π conjugated organic ligands. J. Am. Chem. Soc. 141, 39, 15577-15585 (2019)
[3] S. Tong, C. Gong, C. Zhang, G. Liu, D. Zhang, C. Zhou, J. Sun, S. Xiao, J. He, Y. Gao, J. Yang, Fully-printed, flexible cesium-doped triple cation perovskite photodetector. Applied Materials Today **15**, 389–397 (2019).
[4] P. Ščajev, R. Aleksiejūnas, S. Miasojedovas, S. Nargelas, M. Inoue, C. Qin, T. Matsushima, C. Adachi, S. Juršėnas, Two regimes of carrier diffusion in vapor deposited lead-halide perovskites. J. Phys. Chem. C **121**, 21600-21609 (2017).

EXCESS CONDUCTIVITY IN MAGNETIC SUPERCONDUCTOR $Dy_{0.6}Y_{0.4}Rh_{3.85}Ru_{0.15}B_4$

Lyudmila Omelchenko, Andrei Solovjov, Eugene Petrenko, Andrei Terekhov

B.Verkin Institute for Low Temperature Physics and Engineering of NAS of Ukraine,
Nauky Ave., 47, Kharkiv 61103, Ukraine
omelchenko@ilt.kharkov.ua

Temperature dependencies of the excess conductivity σ′(T) and the possible pseudogap (PG), Δ*(T), were first studied in the magnetic superconductor $Dy_{0.6}Y_{0.4}Rh_{3.85}Ru_{0.15}B_4$. It was shown that σ′(T) near Tc well described by the 3D Aslamazov–Larkin equation, demonstrating a 3D-2D crossover with increasing temperature. Using the crossover temperature T_0, the coherence length was measured along the c axis, $\xi c(0) = (2.67 \pm 0.02)$ Å, which correlates with the literature data for strong coupling HTSCs. The pronounced effect of magnetism is found in the unusual dependence of ln σ′ on ln ε with a maximum at TFM~19 K, which is associated with the system transition to the ferromagnetic state with decreasing temperature [1].

The dependence Δ*(T) revealed a number of peculiarities typical of superconductors admit the possibility of the superconductivity - magnetism interplay. This is a high narrow maximum at T=154 K, typical of magnetic superconductors, followed by a minimum at $T_{min} \approx 95$ K. In FeSe compounds, a similar minimum corresponds to the structural phase transition from the tetra - to the ortho - phase at $T_s \sim 90$ K, [2] indicating the possibility of a similar structural transition in $Dy_{0.6}Y_{0.4}Rh_{3.85}Ru_{0.15}B_4$. Below T_{min}, Δ*(T) again increases, demonstrating a broad maximum at $T_{pair} \approx 36$ K, followed by a minimum at $T_{01} = 9.4$ K. This form of Δ*(T) is similar to the temperature dependence of the pseudogap in cuprates, which indicates the possibility of implementing the PG state in $Dy_{0.6}Y_{0.4}Rh_{3.85}Ru_{0.15}B_4$ at $T < T_{min}$, as is the case in FeSe at $T < T_s$. It was shown that, below T_{01}, Δ*(T) in $Dy_{0.6}Y_{0.4}Rh_{3.85}Ru_{0.15}B_4$ is the same as in all HTSCs with a maximum at $T \sim T_0$ and a minimum at $T=T_G$, which indicates a common behavior of both magnetic and nonmagnetic superconductors in the region of superconducting fluctuations near T_c.

Meanwhile, the analysis of Δ*(T) in $Dy_{0.6}Y_{0.4}Rh_{3.85}Ru_{0.15}B_4$ reveals a number of peculiarities. The first is an unexpectedly large value of $2\Delta^*(T_c)/k_BT_c = 7.0 \pm 0.1$. It is remarkable, however, that the same value of $2\Delta(T_c)/k_BT_c \sim 7.2$ is obtained from the Andreev spectral analysis of Au – $Dy_{0.6}Y_{0.4}Rh_{3.85}Ru_{0.15}B_4$ contacts measured in a zero magnetic field at T = 1.6 K. This result indicates a more complicated mechanism of the SC state implementation in such superconductors as compared to cuprates, especially taking into account the large intrinsic magnetic moment of Dy ions. Secondly, it is the high density of local pairs (n↑n↓) obtained by comparing the experimental values of Δ*/Δ*max with the Peters–Bauer theory. The measured (n↑n↓) (T_G) ~ 0.35 appears 1.17 times greater than (n↑n↓) (TG) obtained for optimally doped YBaCuO single crystals. This result can be explained by the fact that strong intrinsic magnetism of Dy can contribute to the increasing number of FCPs. In this regard, the role of magnetism in the SC pairing mechanism in $Dy_{0.6}Y_{0.4}Rh_{3.85}Ru_{0.15}B_4$is assumed to be very important. Furthermore, as discussed in the Introduction, the possibility of unconventional, e.g. triplet, pairing in superconductors whose strong magnetism coexists with superconductivity can also lead to the increase in (n↑n↓).

[1] A. L. Solovjov, L. V. Omelchenko, V. B. Stepanov, R. V. Vovk, H.-U. Habermeier, H. Lochmajer, P. Przyslupski, and K. Rogacki, Phys. Rev. B 94, 224505 (2016).
[2] A. L. Solovjov, L. V. Omelchenko, A. V. Terekhov, K. Rogacki, R. V. Vovk, E. P. Khlybov, and A. Chroneos, Mater. Res. Express 3, 076001 (2016).

ORDER REPRINTS DUE TO COVID-19

RECOMBINATION CHARACTERISTICS AND DEEP LEVEL SPECTRA OF GaN/Si INTERFACES

Laimonas Deveikis, Tomas Čeponis, Eugenijus Gaubas

Institute of Photonics and Nanotechnology, Vilnius University, Saulėtekio av. 3, LT-10257, Vilnius, Lithuania
laimonas.deveikis@tmi.vu.lt

GaN is a promising wide band-gap material for production of light-emitting diodes, high-electron-mobility transistors, high-frequency and high-power electronic devices, solar-blind photo-sensors and radiation tolerant particle detectors applied in high energy physics, radiation monitoring and other fields [1]. The wide band-gap of GaN determines a low leakage current. High luminescence efficiency is also an attractive characteristic of GaN in order to make the double response radiation sensors. In recent years, the formation of epitaxial GaN layers on Si substrates for various applications has gained a considerable interest due to the relatively low cost of Si substrates. In order to obtain high-quality GaN layers, the AlN buffer layer is deposited on Si beforehand. However, electrically active defects formed on the AlN/Si interface and Si surface may determine the functionality of the GaN based devices. In order to produce high-quality GaN-on Si devices, it is important to investigate the electrically active defects that are formed on the Si substrates.

The samples investigated in this work have been used as substrates for deposition of MOCVD AlN/AlGaN/GaN layers using different deposition pressure: 75 Torr (sample A) and 200 Torr (sample B). To measure recombination parameters of the interface and Si substrate, the top AlGaN/GaN layers were removed using inductively-coupled-plasma reactive ion etching (ICP-RIE) method. The recombination characteristics of the samples have been examined using a contactless technique of the microwave probed photoconductivity transients (MW-PC) by combining the bulk (λ_{ex}=1062 nm) and surface (λ_{ex}=531 nm) carrier injection regimes. The defects present in interfaces and Si substrates have been identified by deep level transient spectroscopy (DLTS) technique using junction structures formed on ICP-RIE etched samples.

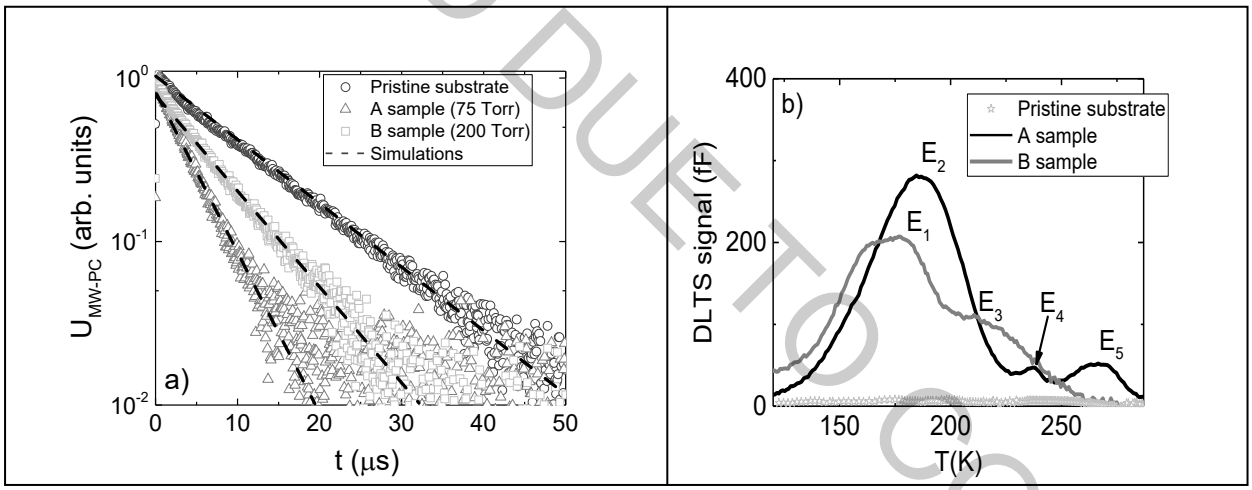

Fig. 1. (a) – Experimental (symbols) and fitted (dashed lines) MW-PC transients recorded on the pristine Si substrate and AlN/Si interfaces formed with different growth pressure. (b) – Experimental DLTS spectra with denoted spectral peaks ascribed to different energy levels associated with identified carrier traps residing in the pristine Si substrate and AlN/Si interfaces.

Analysis of the MW-PC transients allowed to determine the impact of deposition procedures of the AlN/AlGaN/GaN layers on the excess carrier lifetime. It has been found that the bulk carrier lifetime drops by the factor of 2.75 in A sample and by 1.75 in B sample relatively to the pristine Si substrates. The symmetry of the surface recombination velocities (s_0=s_d) has been revealed by measurements of s_0 and s_d on both sides of the pristine substrate by exciting the opposite surfaces with strongly absorbed light pulses. The 3.5 times higher surface recombination velocity (s_0) has been determined on the AlN/Si interface side relatively to the Si substrate (s_d) for the GaN/AlGaN/AlN/Si structures. This indicates the enhanced defect concentration introduced by formation of the AlN/Si. The DLTS spectroscopy allowed us to identify the prevailing carrier traps and to extract their concentrations in AlN/Si interfaces and pristine Si substrates. It has been inferred that the concentration of the impurities and their complexes determined for the AlN/Si interfaces substantially prevails that obtained for the pristine Si substrates. The combined analysis of the MW-PC and DLTS characteristics as well as the extracted parameters of the carrier lifetimes and trap concentrations will be discussed.

[1] S. J. Pearton, *GaN and related materials II*, (Gordon and Breach Science Publishers, Amsterdam, 2000).

ACCEPTED DUE TO COVID-19

TEMPERATURE DEPENDENT DIFFUSION COEFFICIENT, DIFFUSION LENGTH AND LIFETIME IN GeSn EPILAYER

Vaiva Soriūtė[1], Patrik Ščajev[1], Pavels Onufrijevs[2], Arturs Medvids[2], Hung-Hsiang Cheng[3]

[1] Institute of Photonics and Nanotechnology, Vilnius University, Sauletekio al. 3, LT 10257, Vilnius, Lithuania
[2] Institute of Technical Physics, Faculty of Materials Science and Applied Chemistry, Riga Technical University, P. Valdena 3/7, Riga, LV-1048, Latvia
[3] Center for Condensed Matter Sciences and Graduate Institute of Electronic Engineering, National Taiwan University, Roosevlet Road No 1, Section 4, Taipei 10617, Taiwan
vaiva.soriute@ff.vu.lt

CANCELLED DUE TO COVID-19

Silicon materials are key semiconductors in all electronic and photonic devices and dominate the market for few decades [1]. The main drawback of Si and Ge, which are indirect band-gap semiconductors, is a lower performance in comparison to direct band-gap III-V semiconductors [2]. The development of new technology which would be able to shift photosensitivity of Si devices to the mid-infrared range, preserving the benefits of silicon, is in current effort [3]. Group IV GeSn based materials have recently shown promising optoelectronic characteristics, allowing to extend the detection range to the mid-infrared region [4]. The applications in short-wave infrared photo-sensors [5], and electrically driven lasers [6] on Si substrates show continuous improvement. Both these devices rely on the material electronic properties as carrier lifetime, carrier diffusion coefficient and diffusion length.

Therefore, in this work, we provide temperature-dependent studies of carrier lifetime, diffusion coefficient and diffusion length in $Ge_{0.95}Sn_{0.05}$ epilayer on silicon by applying contactless light-induced transient grating technique. Light-induced transient gratings is a variety of pump-probe technique, which employs an interference light field to photoexcite a sample under study. The interference field is created by two coherent laser beams (527 nm) that are made to overlap in the sample at an angle Θ. A period Λ of the resulting interference field is determined by the angle Θ and wavelength of the pump beam λ_p: $\Lambda=\lambda_p/(2\sin(\Theta/2))$. The probe (1053 nm) monitors the diffraction efficiency decay and allows to determine carrier diffusion coefficient (D) and lifetime (τ_R) from grating decay rate $1/\tau_G = 1/\tau_R + 4\pi^2 D/\Lambda^2$. The determined temperature dependences of carrier lifetime and diffusivity are provided in Fig. 1.

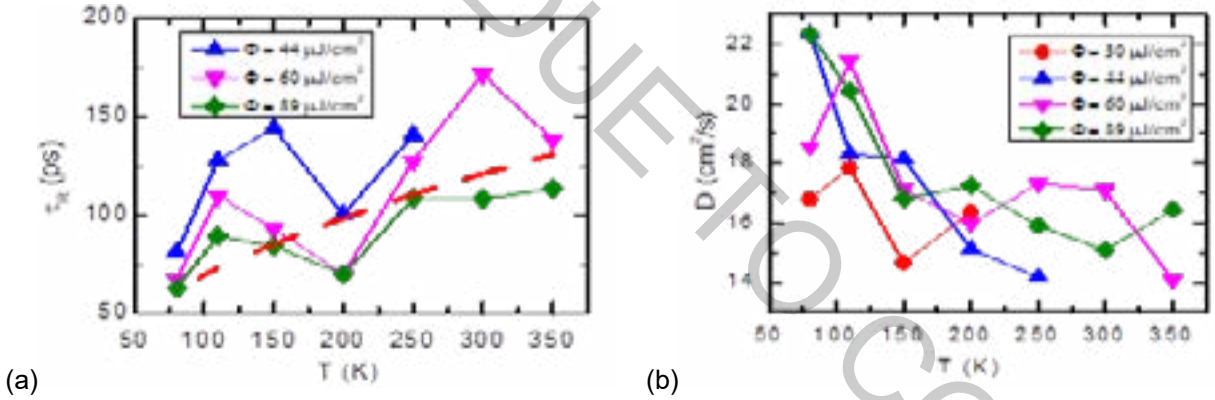

Fig. 1. Lifetime (a) and diffusion coefficient (b) temperature dependences in $Ge_{0.95}Sn_{0.05}$ epilayer.

We show rather weak temperature dependences of these parameters and explain them by defect recombination and scattering processes. Lifetime increases with temperature due to reducing carrier capture cross-section, while diffusivity decreases due to increasing scattering by acoustic phonons. Weak excitation dependences of the parameters are related to saturated trap regime.

The work was supported as part of the Program on Mutual Funds for Scientific Cooperation of Lithuania and Latvia with Taiwan project: GeSn-based photosensor – from basic research to applications.

[1] V. Narayanan, M.M. Frank, A.A. Demkov, Thin Films on Silicon, WORLD SCIENTIFIC, 2016.
[2] L. Vivien, P. Lorenzo, eds., Handbook of Silicon Photonics, 1st Editio, CRC Press, 2013. https://www.crcpress.com/Handbook-of-Silicon-Photonics/Vivien-Pavesi/p/book/9781439836101.
[3] E. Kasper, K. Lyutovich, Properties of Silicon Germanium and SiGe: Carbon, The Institution of Engineering and Technology (December 31, 1999), 1999.
[4] E. Kasper, Group IV heteroepitaxy on silicon for photonics, J. Mater. Res. 31 (2016) 3639–3648.
[5] A. Gassenq, F. Gencarelli, J. Van Campenhout, Y. Shimura, R. Loo, G. Narcy, B. Vincent, G. Roelkens, GeSn/Ge heterostructure short-wave infrared photodetectors on silicon, Opt. Express. 20 (2012) 27297.
[6] N. von den Driesch, D. Stange, D. Rainko, I. Povstugar, P. Zaumseil, G. Capellini, T. Schröder, T. Denneulin, Z. Ikonic, J.M. Hartmann, H. Sigg, S. Mantl, D. Grützmacher, D. Buca, Advanced GeSn/SiGeSn Group IV Heterostructure Lasers, Adv. Sci. 5 (2018) 1–7.

HOT CARRIER EVIDENCE IN SOLAR CELLS

Jonas Gradauskas[1,2], Steponas Ašmontas[1], Algirdas Sužiedėlis[1], Aldis Šilėnas[1], Viktoras Vaičikauskas[1], Ovidijus Žalys[1], Oleksandr Masalskyi[2]

[1] Center for Physical sciences and Technology, Lithuania
[2] Vilnius Gediminas Technical University, Lihuania
oleksandr.masalskyi@vgtu.lt

The Shockley-Queisser theory puts the limits on efficiency of a single-junction solar cell [1]. It assumes that only photons having energy close to a semiconductor forbidden energy gap are used effectively in the formation of an electrical output signal. Residual extra energy of the high energy photons not used for the electron-hole generation is scored up only through the process of carrier thermalization, i.e. through the lattice heating, and this way influencing solar cell efficiency. Low energy photons are assumed to be not absorbed at all.

We present experimental results demonstrating direct impact of the hot carriers on photoresponse of a p-n junction. As an object of investigation, GaAs p-n-junction was illuminated with 15 ns-long laser pulses of 1.06 μm wavelength. Short enough pulse and the wavelength opened possibility to observe the induced photoresponse consisting of three components. The first one, U_G, is a relatively slow component caused by a classical electron-hole pair generation. The second one, U_{HC}, is fast, follows the laser pulse shape and has opposite polarity; this is an inherent feature of the hot carrier photovoltage. The third one, U_T, has the same polarity as U_{HC} but is much slower; it is attributed to the thermoelectric electromotive force caused by the p-n junction heating. As the research reveals, each component has characteristic different dependency on laser intensity, applies bias voltage (see Fig. 1), sample temperature.

Thus, besides the usually considered thermalization of hot carriers, the magnitude of the net photoresponse depends on the result of mutual simultaneous competition between all three components. Maximum reduction of the hot carrier photovoltage contribution will boost the efficiency of a p-n junction solar cell. On the other hand, reckoning in the direct impact of the hot carriers may possibly lower the theoretical efficiency limit.

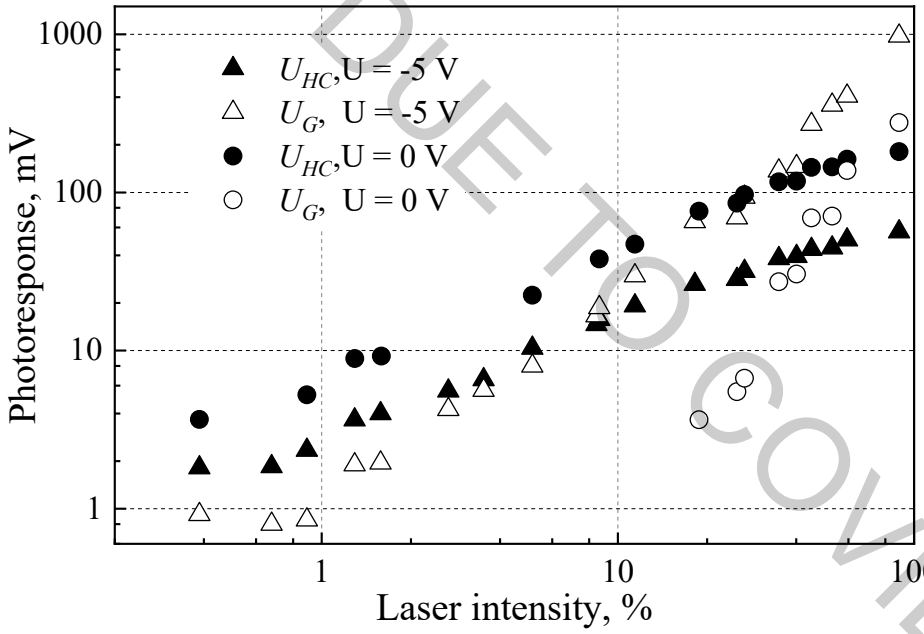

Fig. 1. Dependence of U_{HC} and U_G components on relative laser intensity at different bias voltage values.

[1] W. Shockley and H. J. Queisser, Detailed balance limit of efficiency of p–n junction solar cells, J. Appl. Phys. **32**, 510-519 (1961).

CANCELLED DUE TO COVID-19

S-METHYLTHIOURONIUM IODIDE IMPROVES PHOTOSTABILITY OF METHYLAMMONIUM LEAD IODIDE PEROVSKITES

Gabrielė Kavaliauskaitė[1], Gintarė Kuksėnaitė[1], Rokas Gegevičius[1], Vidas Pakštas[1], Viktorija Strazdienė[1], Edvinas Orentas[2], Marius Franckevičius[1], Vidmantas Gulbinas[1]

[1] Center for Physical Sciences and Technology, Saulėtekio Av. 3, LT-10257 Vilnius, Lithuania
[2] Department of Organic Chemistry, Vilnius University, Faculty of Chemistry and Geosciences, Naugarduko 24, Vilnius, LT-03225, Lithuania
gabriele.kavaliauskaite@ftmc.lt

Over the last decade, hybrid perovskites consisting of metal-halide anions and organic cations have made a breakthrough in the development of a low-cost electronic devices such as high-efficiency solar cells [1]. Although the power conversion efficiency of perovskite solar cells already surpassed 25% [2], the structural stability currently is a key challenge for their commercialization. Herein we demonstrate an application of S-methylthiouronium iodide cations $CH_3SC(NH_2)_2^+$ (SMTU) as a possible alternative for partial replacement of methylammonium cations (MA) in lead-halide perovskites towards the fabrication of more stable solar cells of the mixed $(MA)_x(SMTU)_{1-x}PbI_3$ composition. We characterized the influence of S-methylthiouronium iodide on the perovskite film quality using X-ray diffraction, absorption, fluorescence and time-correlated single-photon counting (TCSPC) spectroscopy. Comparing with a reference methylammonium iodide perovskites, S-methylthiouronium iodide perovskites show increased material stability against photooxidation in ambient air and improvement in the material quality.

[1] J. Burschka, N. Pellet, S.-J. Moon, R. Humphry-Baker et al., Sequential deposition as a route to high-performance perovskite-sensitized solar cells, Nature **499**, 316-319 (2013).
[2] NREL Best Research-Cell Efficiencies, https://www.nrel.gov/pv/assets/pdfs/best-research-cell-efficiencies.20190802.pdf (accessed: September 2019).

CANCELLED DUE TO COVID-19

RAMAN SPECTROSCOPY OF SiC LAYERS GROWN BY RAPID THERMAL CARBONIZATION OF (100) Si

Mikhail Lobanok, Stanislau Prakopyeu, Olga Korolik, Peter Gaiduk

Department of Physical electronics and nanotechnology, Belarusian State University, Minsk
mishalobanok@gmail.com

Silicon carbide is an attractive semiconductor for high power, high temperature, and high frequency electronic devices due to its superior properties [1]. An important task is the integration of SiC devices and silicon circuits within the traditional VLSI technology [1, 2]. Productive and inexpensive methods of growing the material should be developed to achieve the task. The growth of SiC/Si structures faces the problems of large lattice mismatch and very different thermal expansion constants which result in formation of dislocations, twins and stacking faults. Raman scattering is a powerful and nondestructive tool, which can be used for identifying the polytype structure of SiC as well as for stress and defect analysis. In this work, we applied Raman scattering to investigate epitaxial thin SiC layers grown during rapid thermal carbonization (RTC) of the Si wafer under high vacuum conditions.

SiC layers were grown on Si (100) by reacting Si wafer with residual carbon atmosphere at 1100 °C for 30 sec. The pressure in the chamber was about 1·10-2 Pa. Si (100) wafers were pre-cleaned in the 5% HF: H2O solution, and rinsed in deionized water. The structural properties of SiC/Si were investigated by Raman spectroscopy in backscattering configuration at room temperature with a Raman confocal microscope Nanofinder High End (Lotis TII, Belarus–Japan). Solid-state lasers at 473 or 532 nm were used for excitation. To clearly resolve the signal from SiC layer, a window in the Si substrate was etched away in HF/HNO3 solution.

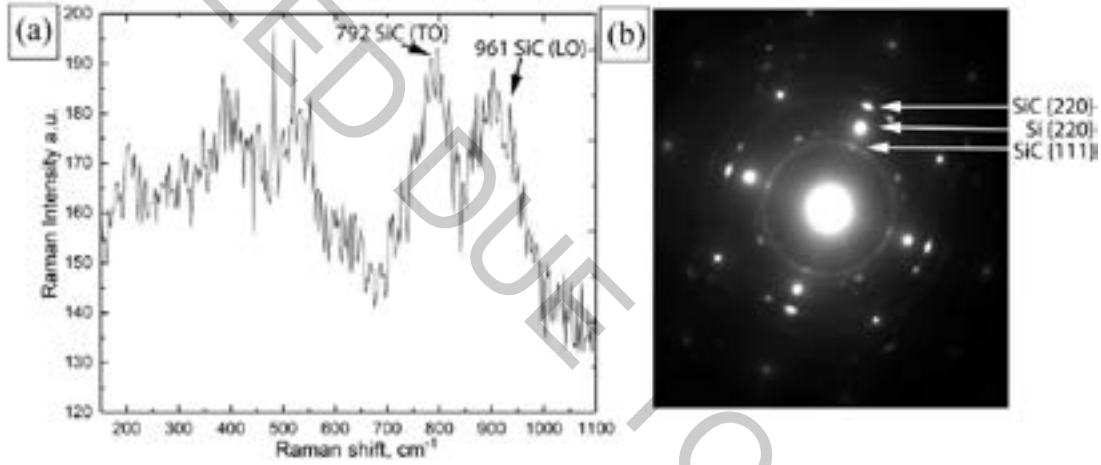

Fig. 1. Raman spectrum (a) and transmission electron diffraction pattern (b) of SiC layer grown on Si substrate at 1100 °C for 30 sec. Raman spectrum was taken at room temperature with laser excitation at 532 nm.

A typical Raman spectrum of the SiC layer RTC grown at 1100 ℃ is presented at figure 1a. The spectrum shows two peaks in the 750-800 cm-1 and 961 cm-1 range which indicate the 3C polytype of SiC. The peaks at 792 cm-1 and 961 cm-1 (arrows) correspond to transverse (TO) and longitudinal (LO) optical phonon modes, respectively. The broadening of the TO band (792) is, probably, indicative of stacking faults [3] or other defects such as anti-phase boundaries and dislocations [4]. The high structural quality of the SiC layer is confirmed by the transmission electron diffraction (Fig. 1b). In the diffraction pattern, the intensity of the polycrystalline diffraction rings is extremely low. Diffraction spots (SiC(220) and SiC(111)) correspond to the 3C SiC polytype. It could be concluded that thermal treatment of Si wafer at 1100 °C in a residual carbon atmosphere results in epitaxial growth of high quality thin silicon carbide layers.

[1] K Shenai, R. S. Scott, B. J. Baliga, Optimum semiconductors for high-power electronics, IEEE Transactions on Electron Devices, vol. 36, issue 9, pp. 1811-1823.
[2] J. Komiyama et al. // Appl. Phys. Lett.. V. 88. P. 091 901 (2006).
[3] Nakashima, S., & Harima, H. Characterization of Defects in SiC Crystals by Raman Scattering. Advanced Texts in Physics,. (2004).
[4] L.A. Falkovsky, J.M. Bluet, J. Camassel. Phys. Rev. B 57, 18, 11 283 (1998).

ACCEPTED DUE TO COVID-19

COINCIDENCE TIME RESOLUTION OF FAST INORGANIC SCINTILLATION CRYSTALS: GAGG:Ce, LYSO:Ce AND BGO

Alexei Bondarev[1], Mikhail Korjik[1], Andrei Fedorov[1], Yauheni Talochka[1], Vitali Mechinski[1]

[1] Research Institute for Nuclear Problems, Belarusian State University, Belarus
alesonep@gmail.com

With the development of fundamental and applied physics, the demand for fast inorganic scintillation crystals as a working body of ionizing radiation detectors is growing. The latter are successfully used in positron emission tomography (PET) and detectors for experimental high energy physics. At present, an important property of scintillation crystals, in addition to light yield, luminescence decay time, radiation hardness, has become the ability to resolve signals in time or coincidence time resolution (CTR). Modern experiments in high-energy physics, such as CMS detector at LHC accelerator at CERN, require CTR value of dozens ps.

Scintillator time resolution measurements requires to use a special method called the coincidence method. It allows to determine the temporal relationship between correlating values. In this work CTR was measured by using SiPMs ASD-RGB4S-P with 4x4 mm^2 active area and PDE (photon detection efficiency) exceeding 33% at 550 nm. Crystals being wrapped with Teflon® tape. The experimental setup for the CTR measurements was composed of a pair of identical detection modules equidistantly placed on the opposite sides of a ^{22}Na source simultaneously emitting two 511 keV gamma-ray photons. Each detection module included of a SiPM and a transimpedance amplifier with dual output (amplitude output and timing output with PZ-shaper). The first amplifier output was used for selection of 511 keV photopeak events by measuring the energy of the detected gamma photons. A signal for CTR measurements takes from second output. The samples under study with dimensions 3x3x5 mm^3 for LYSO:Ce and 3x3x3 mm^3 for BGO.

We approximate our scintillation pulse entering a photo-receiver in a single detector by two exponents with rise and decay components τ_r , τ_d, respectively:

$$f(t,t_0) = \frac{\exp\left(-\frac{t-t_0}{\tau_d}\right) - \exp\left(-\frac{t-t_0}{\tau_r}\right)}{\tau_d - \tau_r}\theta(t-to) \tag{1}$$

where t_0 is the moment of energy deposit in a crystal, $\theta(t-t_0)$ is a Heaviside step function. Here and after, we will exploit the first approach for time resolution.exp

Using $f(t,t_0)$, we can obtain the distribution density $p_{CTR}(\Delta t)$ of the time delay Δt for registering the same annihilation event in two identical detectors (in a coincidence scheme):

$$p_s(t) = \mathrm{C_s} Y^* f(t)\left(1 - \int_0^t f(\tau)\, d\tau\right)^{Y^*} \tag{2}$$

$$p_{CTR}(\Delta t) = \int_0^\infty p_s(t) p_s(t + |\Delta t|) dt \tag{3}$$

where Y^* – light yield, multiplied by the absorbed energy, $\mathrm{C_s}$ – normalizing constant.

The variance of the random value Δt is:

$$D[\Delta t] = \int_{-\infty}^{\infty} p_{CTR}(t)\ (t - M_{CTR}[\Delta t])^2 dt \tag{4}$$

where $M[\Delta t] = \int_{-\infty}^{\infty} p_{CTR}(t)\ t\ dt$.

ARCHIVED DUE TO COVID-19

THE INFLUENCE OF EXTERNAL LOW-FREQUENCY ACOUSTIC FIELDS ON COMBUSTION OF HEXAMINE

Ilya Zur[1], Alexander Fedotov[1]

[1] Faculty of Physics, Belarusian State University, Republic of Belarus
zur.ilya@mail.ru

Currently, much attention is being paid to the study of the influence of acoustic waves on the combustion of various fuel types [1]. Combustion of solid fuels under the influence of sound waves is less studied and needs to be further researched. The purpose of this work is to study the effect of an external low-frequency acoustic field on the combustion of hexamine $C_6H_{12}N_4$. See Fig. 1(a).

An experimental setup consisting of a functional sound generator, an acoustic speaker, a resonator chamber, and a granite platform for placing a combustible body has been designed. The range of oscillation frequencies produced by the speaker was 1 – 12.500 Hz.

It was found during the first set of experiments that hexamine combustion is being extinguished with external acoustic waves of ν = 80 Hz frequency.

The second set of experiments, conducted without a resonator chamber, showed that when a burning hexamine sample was impacted by sound waves with a frequency of ν = 80 Hz, its combustion time decreased on average by 16%. The sample weight varied from 0.5 to 2.5 gr. See Fig. 1(b).

During the third set of experiments, the dependence of the sample complete burning time on the frequency of sound waves (60 – 800 Hz) was evaluated. See Fig. 1(c).

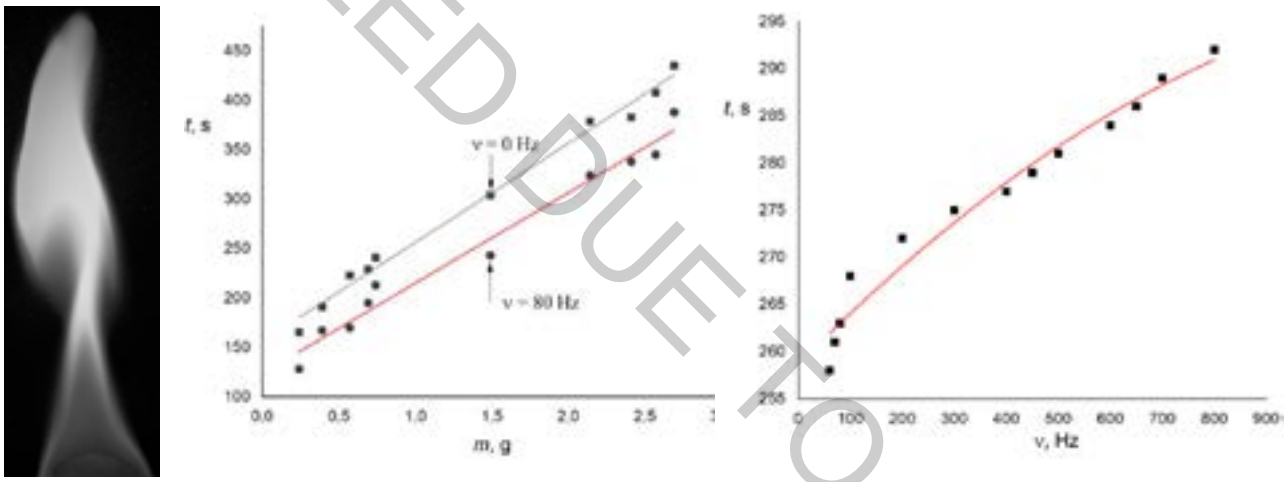

(a) (b) (c)

Fig. 1. (a) – flame of hexamine. (b) – the dependence of complete combustion time on the initial mass *m* of the sample at 80 Hz sound frequency. (c) –dependence of complete combustion time on the frequency ν for *m* = 2.0 g.

The influence of external sound waves on the combustion process is presumably explained by the fact that periodically acting acoustic waves remove the combustion products formed in the external part of the flame torch, thereby contributing to the influx of new air into the working mixture.

Obtained results will find applications in extinguishing of small localized fires that can happen in electronic sensors and controllers.

[1] Krivokorytov, M. S. Influence of acoustic vibrations on the diffusion of methane / M. S. Krivokorytov, V. V. Golub, V. V. Volodin / / Letters in ZhTF, 2012. - Vol. 38, vol. 10. - Pp. 57-63.

CANCELLED DUE TO COVID-19

CARRIER LOCALIZATION IN INGAN STRUCTURES INVESTIGATED BY LIGHT-INDUCED TRANSIENT GRATING TECHNIQUE

Mantas Vaičiulis, Kazimieras Nomeika, Ramūnas Aleksiejūnas

[1] Institute of Photonics and Nanotechnology, Faculty of Physics, Vilnius University, Saulėtekis Av. 3, LT-10257 Vilnius, Lithuania
mantas.vaiciulis@ff.stud.vu.lt

CANCELLED DUE TO COVID-19

Localization of charge carriers in shallow potential minima just below the band edges is typical for materials and structures with some level of disorder. In particular, this process is well known in III-nitrides alloys where it is believed to be the main reason for high internal quantum efficiency, in spite of high defect density [1]. The exact effect of carrier localization to carrier transport and recombination is difficult to analyze, though. Quantum wells of ternary nitride alloys is a very complex structure; thus, investigation of carrier localization demands a computational-heavy modelling [2] and sophisticated experimental methods [3].

One way to experimentally study the carrier localization is by observing the properties of carrier diffusion. In this presentation, we report the results obtained by Light-Induced Transient Grating (LITG) technique in InGaN/GaN/sapphire structures grown by MOCVD technique along the polar (*c*) crystallographic directions. We carry out LITG experiments to measure the ambipolar diffusion coefficient (*D*) of photoexcited carriers in quantum wells and thick layers. From the dependencies of *D* on carrier density and photoexcitation wavelength, we analyze the impact of carrier localization on their transport and recombination pathways.

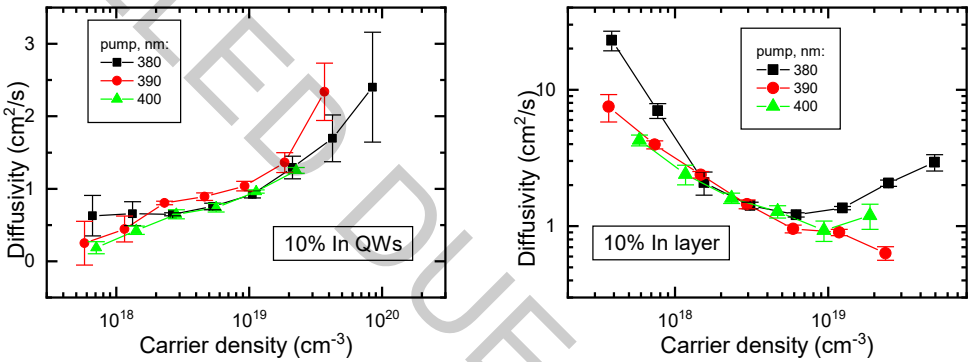

Fig. 1. Ambipolar diffusion coefficient vs. photoexcited carrier density and at different photoexcitation wavelengths in quantum wells (left) and thick layer (right) samples.

In Figure 1 we illustrate the obtained dependencies of *D* on photoexcited carrier densities in either quantum well (left) or thick layer (right) samples. In both cases, diffusivity changes in a non-trivial manner that deviates from the standard Einstein relation. We demonstrate that such a complex behavior can explained by accounting for two processes: (i) at the highest excitations, diffusivity scales with the density due to carrier degeneracy, while at low densities *D* is governed by the localization of carriers. Different dynamics of *D* in the quantum well and epilayer samples can be explained by assuming the higher localization center density with higher potential barrier in the epilayer. This somewhat unexpected result suggests that the main mechanism for hole localization is due to random indium content fluctuations rather than quantum well thickness fluctuations. The impact of carrier localization is also seen from the dependence of *D* on excitation wavelength: as the carriers are photoexcited to the localized states below the bandgap (pump wavelengths of 400 nm and 390 nm) the diffusivity value is lower than that obtained for direct band-to-band excitation (380 nm).

[1] 1.Chichibu, S., Wada, K. & Nakamura, S. Spatially resolved cathodoluminescence spectra of InGaN quantum wells. Appl. Phys. Lett. **71**, 2346–2348 (1997).
[2] Li, C.-K. et al. Localization landscape theory of disorder in semiconductors. III. Application to carrier transport and recombination in light emitting diodes. Phys. Rev. B **95**, 144206 (2017).
[3] Hahn, W. et al. Evidence of nanoscale Anderson localization induced by intrinsic compositional disorder in InGaN/GaN quantum wells by scanning tunneling luminescence spectroscopy. Phys. Rev. B **98**, 045305 (2018).

INFLUENCE OF EXCITATION RELAXATION ON LSO:CE QUANTUM YIELD

Tomas Jurgutis

Faculty of Physics, Vilnius University, Lithuania
tomas.jurgutis@ff.stud.vu

Discovery of scintillators was crucial for progress in high energy physics. Originally used scintillators to build detectors quickly became inadequate for accurate and fast measurements, thus a high demand of materials with superior qualities, such as faster luminescence rise and decay times, higher density and light yield, is the main force behind current research and development. The leading scintillator's growth technique is called Czochralski method and while it's one of the most refined methods, various parameters can be changed [1] to improve some and deteriorate other the qualities of the grown scintillator.

In this work the influence of excitation relaxation on quantum yield of commercially used LSO:Ce scintillators grown by using Czochralski method was investigated. Photoluminescence excited by various energy photons was measured and quantum yield value was evaluated using an integrating sphere method [2]. Pump-probe technique was used to evaluate charge relaxation constants. The charge was excited using 4.82 eV and 3.46 eV photon energy laser impulses, while a wide (white) spectrum probe was used to measure the relaxation. It was evident that slab (middle) part of the growing crystal had the better and more consistent parameters (fig 1.). It was also shown that higher photon energy excitations tend to have lower quantum yield due to non-radiating relaxation of charge carriers..

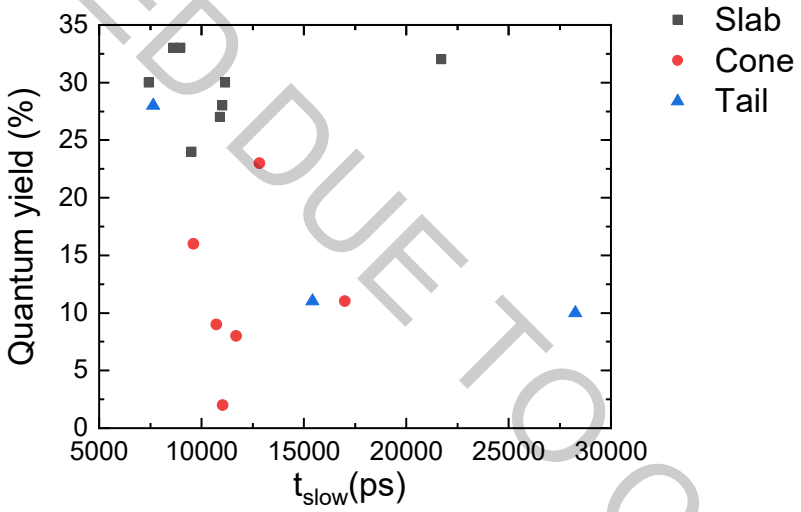

Fig 1. Quantum yield dependency on excitation relaxation constant.

[1]A. Yoshikawa, V. Chani and M. Nikl, Czochralski Growth and Properties of Scintillating Crystals. ACTA PHYSICA POLONICA A, 124,pp. 250-264 (2013)

[2] S. Leyre, E. Coutino-Gonzalez, J. J. Joos, J. Ryckaert, Y. Meuret, D. Poelman, P. F. Smet, G. Durinck, J. Hofkens, G. Deconinck, and P. Hanselaer, Absolute determination of photoluminescence quantum efficiency using an integrating sphere setup. Review of Scientific Instruments 85, 123115 (2014).

CANCELLED DUE TO COVID-19

SENSITIVE PLANAR MICROWAVE DIODES ON THE BASE OF TERNARY $AL_XGA_{1-X}AS$ SEMICONDUCTOR COMPOUND

Maksimas Anbinderis[1, 2], Algirdas SuSužiedėlis[1]

[1] Laboratory of Electronic Processes, Center for Physical Sciences and Technology, Lithuania
[2] Faculty of Electronics, Vilnius Gediminas Technical University, Lithuania
maksimas.anbinderis@ftmc.lt

Electromagnetic radiation in millimeter wavelength range attracts attention of scientists and engineers due to possible applications in modern fields of technology such as imaging of concealed objects, material homogeneity inspection, adaptive cruise control for automotive vehicles, as well as for future broadband cellular communication networks. Successive development of these technologies requires sensitive microwave detectors. For the commercial application of these technologies, microwave sensors must not only be sensitive and fast but also reliable and inexpensive. We have earlier proposed a simple design of inexpensive planar microwave (MW) diodes fabricated on the base of low resistivity gallium arsenide (GaAs) substrate [1]. The diodes were used to detect microwave continuous wave (CW) signals as well as to measure pulsed microwave power in nanoseconds time scale [2]. However, the fast diodes had low voltage responsivity, and more sensitive ones demonstrated high electrical resistance in the CW measurements. Therefore, the main issue of this report is the increase of voltage responsivity of the planar dual microwave diodes and the reduction of the spread of electrical parameters of the planar MW diodes on the base of epitaxially grown *n*-$Al_xGa_{1-x}As$ layer on semiinsulating (SI) GaAs substrate.

The *n*-$Al_xGa_{1-x}As$ layers of sub-micrometric thickness (0.4÷0.8 μm) with different aluminum arsenide (AlAs) mole fraction (x = 0; 0.15; 0.3) were grown onto semiinsulating SI GaAs substrate using liquid phase epitaxy technique. The layers were non-intentionally doped, and the charge carrier density varied from layer to layer within the range of $8 \cdot 10^{15} \div 2 \cdot 10^{17}$ cm^{-3}. First photolithography was made to define rectangular mesas of the MW diodes by means of etching the AlGaAs layer and opening the surface of the SI GaAs. The second photolithography step was used to create metallic contacts of the diodes. The thermally evaporated Ge/Ni/Au contacts were annealed in H_2 atmosphere for 2 minutes. Electrical resistance and voltage responsivity of the diodes were controlled by means of varying the area of the small contact in the vicinity of the border of the diode's mesa. Measurements of direct current and high frequency electrical parameters of separate MW diodes were carried out directly on the uncut substrate with the diode array using appropriate probe stations.

Investigation of detection properties of the dual MW diodes was performed in K_a frequency range. The voltage responsivity strongly depended on the AlAs mole fraction. The lowest value of the responsivity ranging over several volts per watt had the diodes that were fabricated on the base of GaAs epitaxial layer (x = 0). The diodes on the base of $Al_{0.15}Ga_{0.85}As$ epitaxial layer revealed higher responsivity, from tens up to one hundred V/W, depending on the value of the small contact area. The highest values of the voltage responsivity demonstrated the dual MW diodes fabricated on the base of $Al_{0.3}Ga_{0.7}As$ layer; for the diodes with small contact area of several square micrometers it exceeded 500 V/W limit.

[1] A. Sužiedėlis, S. Ašmontas, J. Gradauskas, A. Šilėnas, A. Čerškus, A. Lučun, Č. Paškevič, M. Anbinderis, O. Žalys, Planar Asymmetric Dual Diode for Millimeter Wave Detection and Power Measurement, Lithuanian Journal of Physics Vol. 57 N 4, 225–231 (2017).
[2] A. Sužiedėlis, S. Ašmontas, J. Gradauskas, A. Šilėnas, A. Lučun, A. Čerškus, Č. Paškevič, O. Žalys and M. Anbinderis, Pulsed Microwave Sensor on Heavily Doped Semiconductor Substrate, Proceedings of The 2017 Progress in Electromagnetics Research Symposium, 1037-1042 (2017).

CANCELLED DUE TO COVID-19

LINEARIZATION OF ANGULAR CHARACTERISTICS OF THE SUN SENSOR FOR THE PolyITAN-3 SATELLITE

Anatoly Ivashchuk[1], Dusheiko Mychailo[1], Mykola Koliada[1], Oleksandr Masalskyi[2]

[1]Igor Sikorsky Kyiv Polytechnic Institute, department of electronics, Ukraine
k.s.kolyada@gmail.com
[2]Vilnius Gediminas Technical University, Lihuania

CANCELLED DUE TO COVID-19

The Sun Angular Coordinate Sensor (sun sensor) of the PolyITAN-2 satellite had a number of inaccuracies in determining the Sun's coordinates, so the sensor needed modernization, that is, improved measurement accuracy [1]. Errors in determining the position of the spacecraft of this sensor are: nonlinear signals (angular characteristics), which are explained by an uneven change in the pitch of the displacement of the sunspot. The sensor support elements respond to the illumination change in two coordinate axes, which further increases the measurement inaccuracy.

In order to optimize the operation of the sensor and to resolve these inaccuracies, it is necessary to change the geometric dimensions of photosensitive elements and to investigate the effect of geometric dimensions and shape of the photocells on improving the determination of the coordinates of the sun.

The modification of the shape of the photosensitive elements was that the change in the shape of the photosensitive elements of the support and the working channels compensated the loss of power. This means that one side of each element is described by a function inversely proportional to the power loss.

Fig 1 shows the dependence of the voltage on the change in the angle of incidence of sunlight at the vertical position of the sensor. The deviation of the real characteristics from the expected are from -0.03 to 0.04 V, but they almost coincide with the real in the whole range of measurements of the angular characteristics.

When comparing the angular characteristics of the prototype sensor with the sensor mounted on the PolyITAN-2 satellite, we can conclude that the obtained characteristics of the prototype are almost linear.

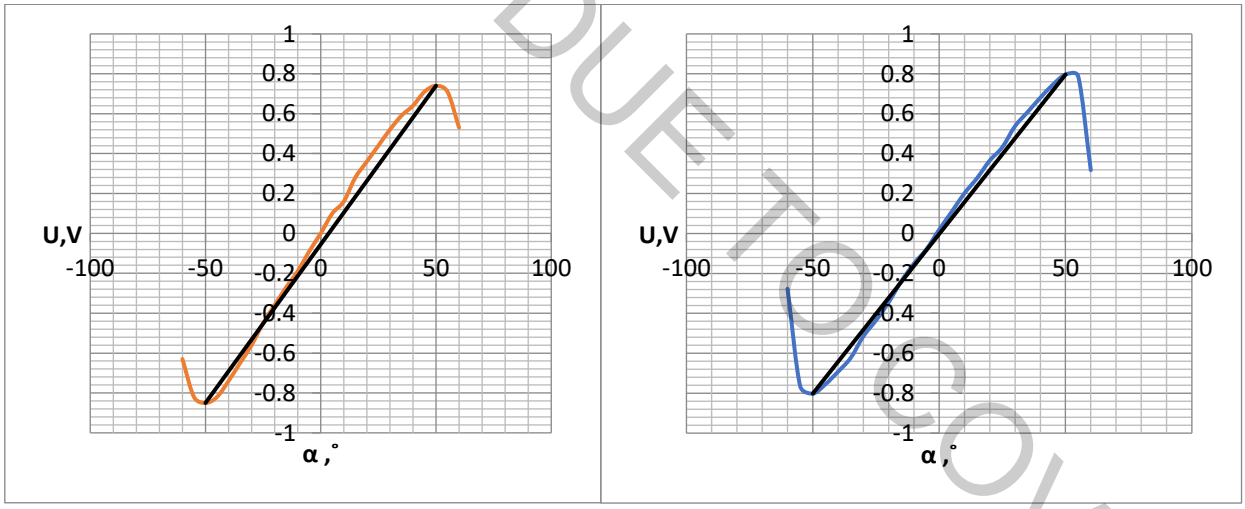

Fig 1. Dependence of differential voltage of working channels of photocells on the angle of inclination of light radiation a) - sensor mounted on the satellite "PolyItan-2", b) - for the modified sensor.

[1] Yakimenko Y.I., Ivashchuk A.V., Fadeev M.S., Koval V.M., Dusheiko M.G., Kavraska N.M. Research report «Development of 2-coordinate device for determining angular Sun coordinates on nanostructured silicon films for spacecraft », –K., 2017. – 211p.

NEAR-IR LIGHT EMITTING SOURCES: ELECTRO-OPTICAL CHARACTERISTICS

Simona Pūkienė[1], Algirdas Jasinskas[1], Virginijus Bukauskas[2], Vladimir Agafonov[2], Mindaugas Kamarauskas[2], Andrius Bičiūnas[1], Bronislovas Čechavičius[1], Arūnas Šetkus[2], Renata Butkutė[1]

[1]Department of Optoelectronics, Center for Physical Sciences and Technology, Vilnius, Lithuania
[2]Department of Fundamental Research, Center for Physical Sciences and Technology, Vilnius, Lithuania
simona.pukiene@ftmc.lt

CANCELLED DUE TO COVID-19

Recently, the infrared (IR) spectral region has attracted huge attention. Due to a number of vibrational absorption lines of organic molecules, IR becomes very important for applications in various areas, such as biomedicine, life and environmental sciences. For example, Light identification and ranging (LiDAR) called Frequency-Modulated Continuous-Wave LiDAR require narrow linewidth laser of the sub-MHz range and high power (up to 200 mW at 1550 nm). New emerging field of quantum cryptography requires single-frequency lasers at 785 nm for sending encoded information over the fiber networks and from nano-satellites down to Earth. High power, high brightness and narrow-line 785 nm lasers are on demand in Raman Spectroscopy for industrial setups and remote environmental contamination measurements. However, most of these applications are limited by the lack of efficient semiconductor IR sources and detectors. High temperature operation of semiconducting lasers is limited by losses due to non-radiative Auger recombination. Thus, the engineering and study of new materials functioning at room temperature in IR is still important and challenging. The research focuses on two objectives: first, low power, small size and weight NIR sources for applications in wireless sensing systems and, secondly, narrow linewidth and high power NIR lasers for remote applications. In this work, A3B5 compounds were used into the active area of NIR emitters operating up to 860 nm, while bismide-based A3B5 MQW structures, exhibiting strong energy bandgap reduction (70 to 90 meV/%Bi) and increased spin–orbit splitting energy ΔSO [1, 2] as well as lower temperature sensitivity [3, 4], have been employed in sources covering the 1.0 μm -1.55 μm wavelength region.

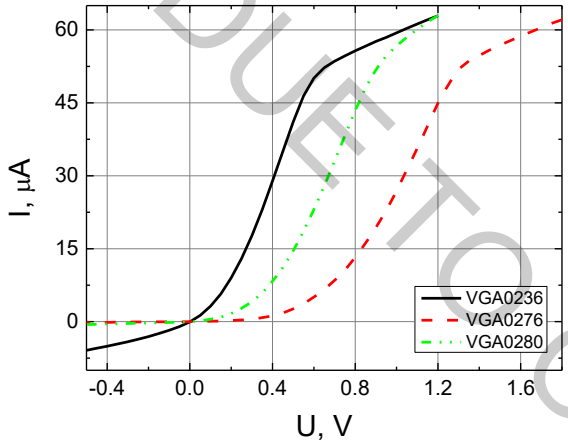

Fig. 1. I-V characteristics of several laser structures in the dark.

The diode structures were grown by molecular beam epitaxy (MBE) under optimized growth condition onto n-GaAs(100) substrate. Both the n-type and p-type AlGaAs waveguide layers were of 1.5 μm thickness and doped of 1×1018 cm-3 by silicon and beryllium, respectively. The surface morphology of the structures examined by atomic force microscopy (AFM), optical properties evaluation by measuring room-temperature photoluminescence. Grown structures were processed using UV photolithography. As-cleaved electrical properties of LDs and LEDs were investigated using Keithley 4200 semiconductor characterization system and Cascade Microtech Summit probe station. DC, pulsed current-voltage (I-V, pulsed I-V, see Fig. 1) and capacitance-voltage (C-V) dependences were measured in air at room temperature. Closed chamber was used to avoid illumination of the samples.

[1] K. Oe et al., New Semiconductor Alloy GaAs1-xBix Grown by Metal Organic Vapor Phase Epitaxy, Jpn. J. Appl. Phys., **37**, L1283(1998).
[2] S. Tixier et al., Molecular beam epitaxy growth of GaAs1−xBix, Appl. Phys. Lett., **82**, 2245 (2003).
[3] K. Oe et al., Proposal on a temperature-insensitive wavelength semiconductor lasers. IEICE Transanctions on Electrons, E79-C:1751_9(1993).
[4] W. M. Linhart et al., Temperature dependence of band gaps in dilute bismides. Semicond. Sci. Technol., **33**(7), 073001 (2018).

GaInAs/GaAs QUANTUM STRUCTURES FOR NEAR INFRARED VERTICAL-EXTERNAL-CAVITY SURFACE-EMITTING LASERS

Andrea Zelioli[1], Algirdas Jasinskas[2], Simona Pūkienė[2], Lukas Jočionis[2], Bronislovas Čechavičius[2] and Renata Butkutė[2, 3]

[1] Department of Physics, University of Modena, Italia
[2] Center for Physical Sciences and Technology, Vilnius, Lithuania
[3] Institute of Photonics and Nanotechnology, Faculty of Physics, Vilnius University, Lithuania

190558@studenti.unimore.it

CANCELLED DUE TO COVID-19

Several types of lasers, such as, solid-state, semiconductor, gas, excimer, and dye lasers, have been developed. Today lasers are used in many fields, particularly in optical fiber communication, optical digital recording, material processing, biology and medicine, spectroscopy, imaging, entertainment, and many others. Due to exceptional material properties and/or investigation conditions various application require unique set of laser parameters - emission wavelength, its tunability, beam quality, operation temperature, optical output power, as well as convenient method of laser excitation, power consumption, high-speed modulation and device size is very important.

Vertical-external-cavity surface-emitting lasers (VECSEL) also called optically pumped semiconductor lasers (OPSL) or semiconductor disk laser (SDL) belong to relatively new laser family that combines many of the desirable properties. VECSELs were developed to overcome key problems typical to conventional semiconductor lasers. In comparison to both types of electrically pumped Vertical-cavity surface-emitting lasers (VCSELs), which emit circular fundamental transverse mode beam but exhibit low power and edge emitting lasers (Fabry-Perot and DFB) that can reach high output power but an asymmetric beam with strong angular divergence, VECSELS are capable to generate high optical power with circular beam quality.

VECSEL structure is demonstrated in Fig.1. To obtain lasing it is necessary to design the Bragg mirror, gain region and surface barrier layer (window) depending on the target wavelength of the laser. The gain region is usually composed from quantum well structure calculated to match the laser optical standing wave antinodes as shown in Fig.1 (black curve).

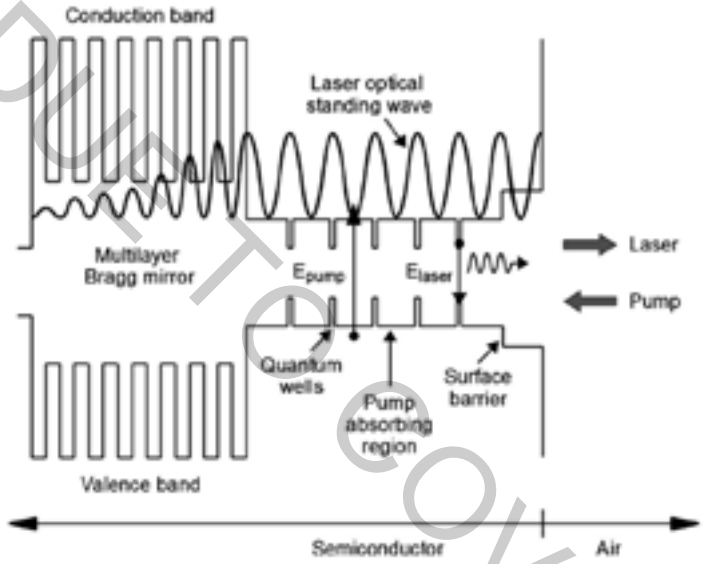

Fig. 1. Energy levels across the VECSEL structure [1].

In this work the modelling of design of VECSEL emitting at wavelength of 976nm was performed. Multiple InGaAs/GaAs quantum wells (MQWs) and AlAs/GaAs Distributed Bragg reflector (DBR) were used for VECSEL architecture. The separate layers and VECSEL structures were grown using solid-source MBE system (Veeco GENxplor R&D) equipped with standard cells for metallic Al, Ga and unique As design source generating pure arsenic dimers flux. The semi-insulating GaAs substrate oriented in (001) crystalline plane was selected for deposition of laser structures. To optimize the growth conditions In content in the well was changed from 10 to 15 %, the width of QW and barriers varied from 5 to 10 nm and from 10 to 15 nm, respectively. Quantum well number was set from 5 to 10. The reflectance of DBR was modelled for 25-30 GaAs and AlAs periods to obtain higher than 97% at central DBR wavelength of 976 nm.

All grown layers and VECSEL structures were characterized by Atomic Force Microscopy, Reflectance and Photoluminescence measurements.

1. Mark Kuznetsov, VECSEL Semiconductor Lasers: A Path to High-Power, Quality Beam and UV to IR Wavelength by Design, Semiconductor Disk Lasers. Physics and Technology. Edited by Oleg G. Okhotnikov, 2010, WILEY-VCH Verlag GmbH & Co. KGaA, Weinheim

QUANTUM MONTE-CARLO SIMULATION OF POLARON TUNNELING

Chertkova Anastasia[1,2], Vera Tiunova[2], Rubtsov Alexey[1,2]

[1]Department of Physics, Quantum Electronics Division, M.V. Lomonosov Moscow State University, 119991, Moscow, Russia

[2]Correlated Quantum Systems group, Russian Quantum Center, 121205, Moscow, Russia

chertkova.anastasia.phys@gmail.com

Theoretical investigation of polaron effects in ultracold gasses became justified due to the latest experimental results [1, 2] with tunable interaction between impurities and surrounding bosonic field via Feshbach resonance. Investigation of tunneling effects in such systems is of great interest in condensed matter physics. In the present work, for considering the dynamics of tunneling effect in the polaron task we used Frohlich Hamiltonian [3]. We study a single impurity interacting with bosonic field and its tunneling in a double-well potential. As a practical application, this system can be considered as one of the implementations of a quantum qubits [4, 5].

Since the existing theoretical techniques cannot describe the strong interacting regimes between the impurity and the surrounding condensate [6], we used numerical quantum Monte-Carlo method in terms of path integrals [7]. Nevertheless, the straightforward application of this algorithm for the simulation of polaron tunneling is limited by the exponential growth of the calculation time. This problem originates from the differences between a time scale of the polaron dynamics and the tunneling time of the particle. Therefore, we proposed the new modification of the QMC method. The main idea of the modification is to divide the calculations into two parts: at first, we integrate the action over bosons and then calculate the propagator for impurity in a double-well potential.

The modified quantum Monte-Carlo method was verified by employing the exact diagonalization in the case of the impurity interacting with two modes of BEC. For this, we used an approximation of the impuritys correlation functions at low temperatures by exponents, which lets to find the tunnel splitting. The new algorithm allows considering multimode regimes beyond the limitations on the coupling constant (i.e. on the interaction between an impurity and surrounding bosonic field) given by analytical approach.

Chertkova Anastasia acknowledges the financial support from the Foundation for the advancement of theoretical physics and mathematics BASIS.

[1] Jrgensen N. B. et al., Observation of attractive and repulsive polarons in a Bose-Einstein condensate, *Physical Review Letters* 117 (2016).

[2] Hu M. G. et al., Bose polarons in the strongly interacting regime, *Physical Review Letters* 117 (2016).

[3] Shchadilova Y. E., Grusdt F., Rubtsov A. N., Demler E., Renormalization group approach to the Frhlich polaron model: application to impurity-BEC problem, *Scientific reports* 5 (2015).

[4] Gorman J., D. G. Hasko, D. A. Williams, Charge-qubit operation of an isolated double quantum dot, *Physical review letters* 95.9 (2005).

[5] Fotue, Alain Jerve, et al., Decoherence of polaron in asymmetric quantum dot qubit under an electromagnetic field, *Am J Mod Phys* 4.3, 138-148 (2015).

[6] Chevy F. , Bose Polarons that Strongly Interact, *Physics* 9, 86 (2016).

[7] Gull, Emanuel, et al., Continuous-time Monte Carlo methods for quantum impurity models, *Reviews of Modern Physics* 83(2), 349 (2011).

CANCELLED DUE TO COVID-19

TERAHERTZ TRANSMISSION SPECTROSCOPY OF GRATING-COUPLED TWO-DIMENSIONAL ELECTRON GAS IN THE AlGaN/GaN HETEROSTRUCTURES

Daniil Pashnev*, Vadym Korotyeyev, Andrzej Urbanowicz, Irmantas Kašalynas

Department of Optoelectronics, Center for Physical Sciences and Technology, Lithuania
*Daniil.pashnev@ftmc.lt

The terahertz (THz) frequency range for many decades has attracted scientists and engineers which demonstrated various new applications of THz technology in security, telecommunication, medicine and materials science [1]. The many THz applications require compact, solid-state devices with electrical tuning of their performance which are capable to emit, detect and modulate THz waves. A promising solution in this area is associated with resonant excitation of the plasma oscillations in low-dimensional systems at the presence of metallic plasmonic elements [2-3]. Exclusive electrical robustness together with relatively high electrons mobility makes III-nitrides hetero-structures an excellent candidate for operation in the THz range. In a number of works, the excitation of a grating-gated two-dimensional (2D) plasmons and their emission at the resonant frequencies has been demonstrated [2-3].

In this work, we studied the grating-gated AlGaN/GaN heterostructures by using THz time-domain spectroscopy (TDS) system. The samples were fabricated of standard AlGaN/GaN high electron mobility (HEMT) structures grown on a 500-μm-thick semi-insulating 6H-SiC substrate by the metalorganic chemical vapour deposition method [4]. The growth began from 1-μm-thick unintentionally doped (UID) GaN and 19-nm-thick AlxGa1-xN (x = 0.25) layers with a 1-nm-thick AlN spacer in between. The metal grating was deposited on the surface of AlGaN/GaN HEMT heterostructures. The area size and filling factor of the grating was 2x2 mm and 50%; respectively. The period of the grating was varied from 600 to 1000 nm for different samples.

The transmission spectra were measured with a commercial TeraVil T-SPEC 1000 spectrometer in the frequency range from 100 GHz to 4 THz. A liquid nitrogen (LN2) cryostat with THz windows was used to study the temperature dependences of the transmission spectra in the range 80–300 K. The steel plate with two apertures with a diameter of 1.5 mm was mounted on the cold finger of the cryostat. The sample was fixed on one of the apertures. The thermocouple was fixed near the sample for accurate readings of the temperature. The radiation transmitted through the empty aperture and through the aperture with the sample was measured within a few minutes interval and used to calculate the transmission spectrum. The cryostat was fixed on a translation stage, which allowed the control of sample position in three coordinates. Sequential measurement of the signal and reference under the same conditions increased the accuracy of the experiment. The THz TDS system was purged with nitrogen to avoid water absorption lines in the transmission spectrum.

All samples demonstrated the resonant behavior which inherent for excitations of the 2DEG plasmons under the grating. The resonant features were observed in the transmission spectrum at temperature 80 K in the frequency range of 0.1-3 THz. More precisely, the sample with the grating period of 1000 nm demonstrated the well-resolved peak at the frequency of 1.4 THz. The spectral position and quality factor of the resonances were depended on the grating period and the temperature. The decrease of the grating period blue-shifted the peak position with little change of its quality factor. However, the quality factor was reduced with the increase of the temperature. And at room temperature, the resonant features were difficult to resolve in the spectrum. The resonant frequency of 2DEG plasmons was found inversely proportional to the grating period in a similar way as it has been demonstrated in [3]. The quality factor dependence on temperature was observed and it was attributed to the decrease of 2DEG mobility with the increase of the temperature which is consistent with the results obtained in [2]. In our report, detail analysis of the transmission spectra will be supported by the theoretical simulation of the Maxwell's equations using rigorous solutions [5].

[1] Yun-Shik Lee. Principles of Terahertz Science and Technology. — Springer, 2009.
[2] A.V. Muravjov et. al., Appl.Phys.Lett. **96**, 042105 (2010).
[3] V. A. Shalygin et. al. J. Appl. Phys. **126**, 183104 (2019).
[4] P. Sai et. Al. Appl. Phys. Lett. 115, 183501 (2019).
[5] Yu. M. Lyaschuk and V. V. Korotyeyev, Ukr. J. Phys. 62(10), 889 (2017).

CANCELLED DUE TO COVID-19

TERAHERTZ DETECTION WITH AlGaN/GaN BOW-TIE DIODES AT 300 K AND 80 K TEMPERATURES

Justinas Jorudas[1], Irmantas Kašalynas[1]

[1] Center for Physical Sciences and Technology (FTMC), Saulėtekio 3, LT-10257 Vilnius, Lithuania
justinas.jorudas@ftmc.lt

Imaging with terahertz (THz) radiation is appealing due to its non-ionising nature and transparency of many common industrial materials in the frequency range of 0.1 – 30 THz. However, many aspects of generation [1-2] and detection [3-4] of THz radiation are still under extensive research. A compact and sensitive THz detector with a fast response time is highly desired for the THz imaging systems.

In this work we investigate the performance of AlGaN/GaN bow-tie (BT) diodes as THz detectors in sub-THz frequency range at temperatures of 300 K and 80 K. The BT diodes were fabricated of $Al_{0.25}Ga_{0.75}N$/GaN high electron mobility transistor (HEMT) structures grown on semi-insulating SiC substrate [5]. A two-dimensional electron gas (2DEG) concentration $N_{2DEG} = 9.4 \cdot 10^{12}$ cm^{-2} and mobility $\mu = 1800$ cm^2/V·s was found at 300 K from Hall experiment. At 80 K, these parameters changed to $N_{2DEG} = 8.6 \cdot 10^{12}$ cm^{-2} and $\mu = 15830$ cm^2/V·s. Ohmic contacts were formed from Ti/Al/Ni/Au stack annealed at 830 ºC for 30 s at nitrogen ambient. The resistivity of ohmic contacts was determined using transfer length method, providing values of less than 1 Ω·mm independent on temperature in the range of 300-80 K. For electrical isolation, a 700 keV energy Al^+ ions were implanted into $Al_{0.25}Ga_{0.75}N$/GaN HEMT structures [6].

Operation of the BT diode, as a THz detector, relies on a non-uniform heating of carriers in the apex of geometrically shaped 2DEG layer under antenna-coupled electric field. Detection was studied using a quasi-optical illumination setup based on electronic multiplier chain source (VDI). Signal from detector was recorded using lock-in amplifier. Fig. 1 shows 2D profiles of 150 GHz Gaussian beam recorded with the 5 µm apex-width BT diode integrated with a hemispherical Si lens. The detected signal without applied bias was of 433 µV at the 300 K. An external bias of -0.8 V increased the signal by 20 dB resulting in the decrease of the noise equivalent power (NEP) from 249 to 4 nW/√Hz under assumption that the Johnson noise dominated in the measurements. Further signal increase is expected at 80 K due to the increase of 2DEG mobility.

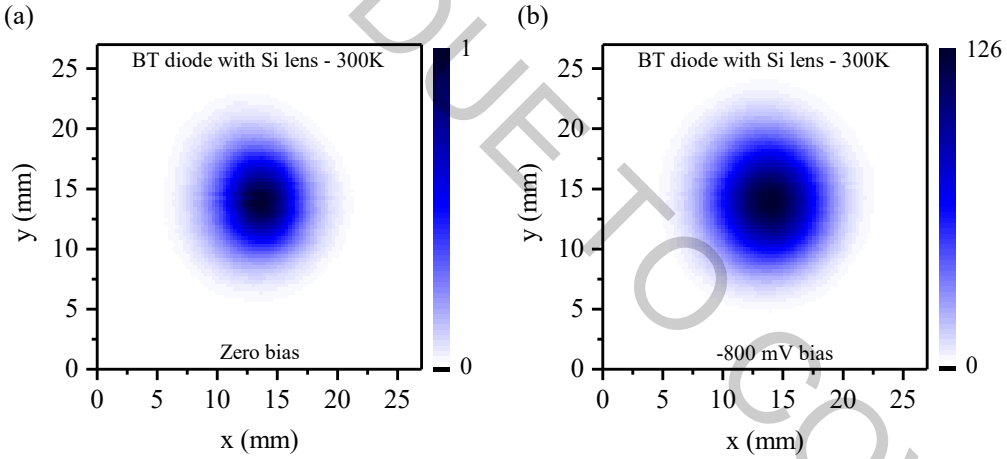

Fig. 1. Images of 150 GHz Gaussian beam recorded with BT diode of 5 µm apex width at different external bias conditions: (a) no bias (b) -0.8 V bias. Detected signal amplitudes are normalised to maximum at zero bias.

ACKNOWLEDGEMENT

This research was supported by the Research Council of Lithuania (Lietuvos mokslo taryba) under the "TERAGANWIRE" project (Grant no. S-LL-19-1). We are grateful to Vytautas Jakštas for photolithography of electric contacts and Vitalij Kovalevskij for precision processes of ions implantation.

[1] A. D. Koulouklidis *et al.*, "Observation of extremely efficient terahertz generation from mid-infrared two-color laser filaments," *Nat. Commun.*, vol. 11, no. 1, p. 292, Dec. 2020.
[2] V. A. Shalygin *et al.*, "Selective terahertz emission due to electrically excited 2D plasmons in AlGaN/GaN heterostructure," *J. Appl. Phys.*, vol. 126, no. 18, p. 183104, Nov. 2019.
[3] M. Bauer *et al.*, "A High-Sensitivity AlGaN/GaN HEMT Terahertz Detector With Integrated Broadband Bow-Tie Antenna," *IEEE Trans. Terahertz Sci. Technol.*, vol. 9, no. 4, pp. 430–444, 2019.
[4] J. Sun *et al.*, "Two-terminal terahertz detectors based on AlGaN/GaN high-electron-mobility transistors," *Appl. Phys. Lett.*, vol. 115, no. 11, p. 111101, Sep. 2019.
[5] P. Sai *et al.*, "Low frequency noise and trap density in GaN/AlGaN field effect transistors," *Appl. Phys. Lett.*, vol. 115, no. 18, p. 183501, Oct. 2019.
[6] J. Jorudas *et al.*, "Development of the planar AlGaN/GaN bow-tie diodes for terahertz detection," in *2019 44th International Conference on Infrared, Millimeter, and Terahertz Waves (IRMMW-THz)*, 2019, pp. 1–2.

CANCELLED DUE TO COVID-19

INFLUENCE OF EXCITATION WAVELENGTH ON THE EUROPIUM IONS PHOTOLUMINESCENCE IN THE GLASSY MATRIX

Paweł Dębowski, Joanna Kłosaj, Agata Jarocka, Tomasz Karol Pietrzak

Faculty of Physics, Warsaw University of Technology, Koszykowa 75, 00-662 Warsaw, Poland
pawel.debowski3.stud@pw.edu.pl

Rare earth elements (REE) based materials have wide application in many fields of technology such as screens in monitors or cell phones, telecommunication, lasers, medicine, scintillators and LED lamps. Especially lanthanides ions have remarkable optical properties due to their distinct electronic structure. They are characterized by [Xe] core, partially filled *4f* shell and outer shells that screen *4f* shell from the influence of external ions.

Recently conducted measurements of europium ions in glassy matrices have shown that the synthesis conditions (in particular time, temperature and melting atmosphere) significantly affect the luminescence spectrum of these materials by changing the ratio of Eu^{2+}/Eu^{3+} ions, and thus result in a continuous spectrum free of sharp emission lines [1]. It is worth emphasizing that the synthesis process called melt-quenching is extremely simple and cheap to implement, unlike some sophisticated methods used to achieve a similar goal [2].

Considering all above the next step in this research was to investigate influence of excitation wavelength on the samples photolumiescence. Results for four samples will be presented. Their nominal formulas and syntheses conditions are as follows: $Na_2Al_2(BO_3)_2F_3$ · 1% Eu_2O_3 (15 min, 1200°C) – A, $Na_3Al_2(BO_3)_3$ · 1% Eu_2O_3 (15 min, 1200°C) – B, $Na_3Al_2(PO_4)_2F_3$ · 1% Eu_2O_3 (15 min, 1200°C) – C, $Na_3Al_2(PO_4)_2F_3$ · 1% Eu_2O_3 (5 min, 1200°C) – D.

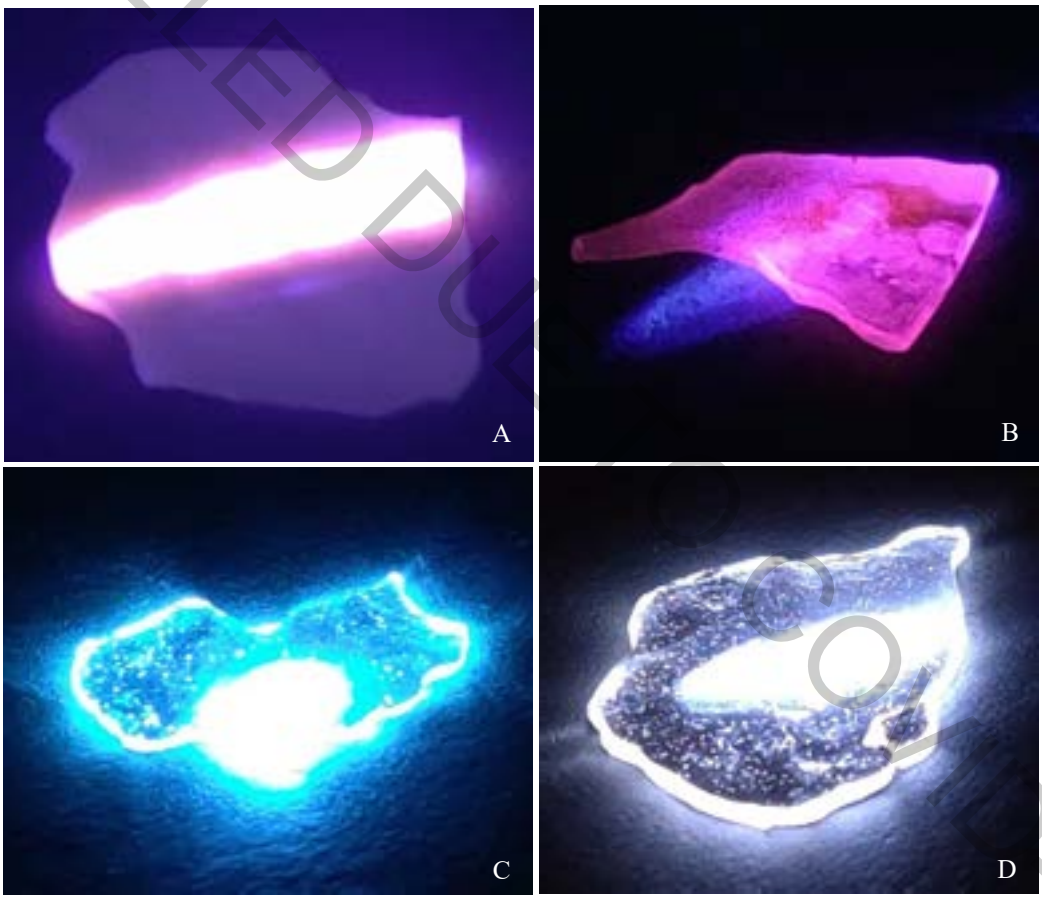

Fig. 1. Photographs of samples exctited with 405 nm laser.

[1] T.K. Pietrzak, A. Gołębiewska, J. Płachta, M. Jarczewski, J. Ryl, M. Wasiucionek, J.E. Garbarczyk: *Photoluminescence of partially reduced Eu^{2+}/Eu^{3+} active centers in a NaF–Al_2O_3–P_2O_5 glassy matrix with tunable smooth spectra*. Journal of Luminescence 208 (2019) 322–326.

[2] F. Wang, Y.-h. Chen, C.-y. Liu, D.-g. Ma: *White light-emitting devices based on carbon dots' electroluminescence.* Chem. Commun., 47 (2011) 3502–3504.

CANCELLED DUE TO COVID-19

INVESTIGATION OF OPTICAL PROPERTIES OF $CaAlBO_3F_2$ GLASSY MATRIX DOPED WITH EUROPIUM AND SAMARIUM IONS

Agata Jarocka[1], Dominika Wąs[1], Jakub Płachta[2], Tomasz K. Pietrzak[1]

[1]Faculty of Physics, Warsaw University of Technology, Koszykowa 75, 00-662 Warsaw, Poland
[2]Institute of Physics, Polish Academy of Sciences, Lotników 32/46, 02-668 Warsaw, Poland
agata.jarocka.dokt@pw.edu.pl

CANCELLED DUE TO COVID-19

Rare earth elements (REE) are widely used in today's technology – for example, in lasers based on REE-doped crystals or glasses. REE the most frequently used in lasers are lanthanides. This is due to a large variety of their *4f* configurations, which leads to a wide range of fluorescent states and wavelengths [1]. Telecommunication technologies have also benefited from the use of those elements. Oxidized and ceramic glasses doped with REE found their application in WDM technology (Wavelength Division Multiplexing), and thus a series of optical amplifiers based on REE were created. Furthermore, those elements introduced into phosphors help adjust white LED's light to the range of human vision. Therefore, they gained worldwide interest.

The atomic structure of lanthanides (group that includes considered Sm, Eu) is characterized by unfilled *4f* shell and external shells that screen *4f* shell from the influence from outside. This feature is responsible for remarkable optical properties of lanthanides. Optical spectra of those elements exhibit sharp lines characteristic for transition within the *4f* shell, known as forbidden transitions. In real terms it means that they may occur, but with low probability, according to Judd-Ofelt Theory. Aforementioned screening of *4f* shell by outer shells results in protection of optically active electrons from the influence of crystal field and as a result, REE ion's spectrum in a solid can be similar to that of a free ion spectrum [2].

The research carried out very recently in our group has shown that it is possible to prepare REE-doped glassy materials with that are characterized by strong radial transitions [3]. Therefore, it is worth to investigate different glassy matrices in order to find those of the best mechanical and chemical resistance. In our studies, $CaAlBO_3F_2$ glassy matrices doped with 1 wt% Eu_2O_3 and Sm_2O_3 were successfully prepared by a melt-quenching method. Substrates were melted for 15 min at 1300 °C.

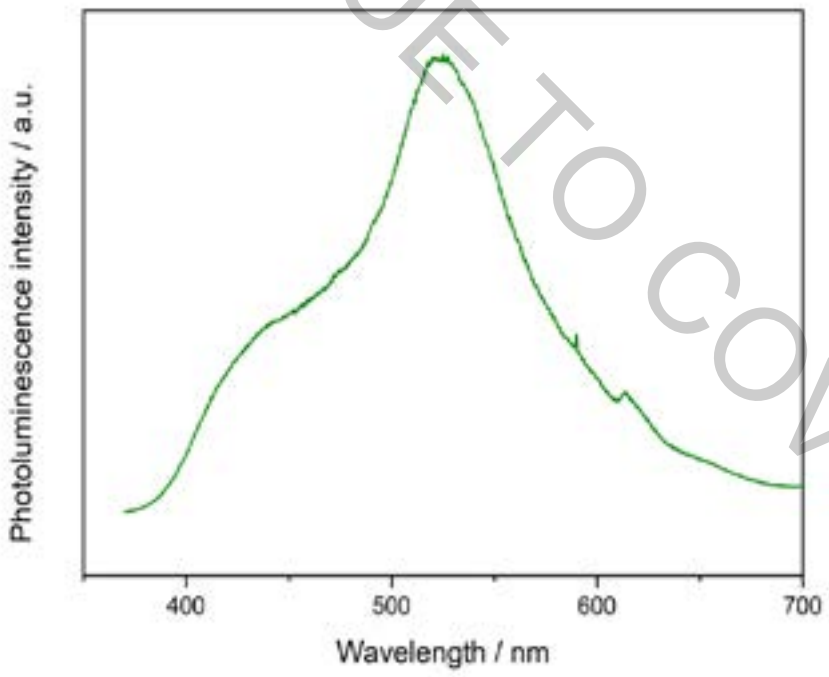

Fig. 1. Photoluminescence spectrum for sample $CaAlBO_3F_2$ doped with europium ions, excited with 325 nm laser.

[1] M. C. Gonçalves, L. F. Santos, R. M. Almeida: *Rare-earth-doped transparent glass ceramics.* Competes Rendus Chimie, 5 (2002) 845–854.
[2] B. M. Walsh: *Advances in Spectroscopy for Lasers and Sensing. Judd-ofelt theory: principles and practices*. [red.] Baldassare Di Bartolo, Ottavio Forte. Erice Italy, Springer, 2005
[3] T.K. Pietrzak, A. Gołębiewska, J. Płachta, M. Jarczewski, J. Ryl, M. Wasiucionek, J.E. Garbarczyk: *Photoluminescence of partially reduced Eu^{2+}/Eu^{3+} active centers in a NaF–Al_2O_3–P_2O_5 glassy matrix with tunable smooth spectra.* Journal of Luminescence, 208 (2019) 322–326.

INVESTIGATION OF OPTICAL PROPERTIES OF PHOSPHATE GLASSES DOPED WITH YTTERBIUM AND ERBIUM IONS

Karol Tomasz Płochocki[1], Agata Jarocka[1], Tomasz Karol Pietrzak[1]

[1] Faculty of Physics, Warsaw University of Technology, Koszykowa 75, 00-662 Warsaw, Poland
karol.plochocki.stud@pw.edu.pl

Materials based on rare earth elements (RRE) are now widely used in many fields of technology, for example: screens in monitors or cell phones, lasers, medicine and LED lamps. The reason for their use in such a broad of their applications is their amazing optical properties [1, 2].

These properties are the result of a specific electronic structure. It is characterised by [Xe] core, partially filled 4f shell and outer shells that screen 4f shell from the external field. Such an electronic structure leads, in most cases, to optical spectra of those elements consisting of sharp lines characteristic for transitions within the 4f shell, which basically are forbidden [2]. One should, however, be aware that the actual emission spectrum of a given RRE center can also depend on matrix composition. Furthermore, photoluminescence with energy upconverison is very intereting phenomenon. It is the process of emitting radiation with a lower wavelength (and therefore – higher energy), than excitation radiation. It can be possible by doping glassy matrices with Yb^{3+} and Er^{3+} ions [3].

Recently, the research carried out by group [4] has proven it is possible to synthesize RRE-doped glassy materials which photoluminescence spectrum is strong and can be controlled by changing the process conditions [4]. It has been demonstrated that the time, temperature and atmosphere of the synthesis have a significant impact on the photoluminescence spectrum. Therefore, in this work selected optical properties of ytterbium and erbium doped phosphate glasses will be presented.

Fig. 1. Shard of RRE doped glass – $Na_3Al_2(PO_4)_2F_3$ • 1% Yb_2O_3.

[1] S. Cotton: *Lanthanide and Actinide Chemistry*. John Wiley and Sons Ltd., 2006.
[2] B. M. Walsh: *Advances in Spectroscopy for Lasers and Sensing. Judd-Ofelt theory: principles and practices.* [red.] Baldassare Di Bartolo, Ottavio Forte. Erice Italy, Springer, 2005).
[3] C. Mi, Z. Tian, C. Cao, Z. Wang, C. Mao, S. Xu: *Novel Microwave-Assisted Solvothermal Synthesis of $NaYF_4$:Yb,Er Upconversion Nanoparticles and Their Application in Cancer Cell Imaging*, Langmuir (2011) 27, 14632–14637
[4] T.K. Pietrzak, A. Gołębiewska, J. Płachta, M. Jarczewski, J. Ryl, M. Wasiucionek, J.E. Garbarczyk: *Photoluminescence of partially reduced Eu^{2+}/Eu^{3+} active centers in a $Na_3Al_2(PO_4)_2F_3$ glassy matrix with tunable smooth spectra.* Journal of Luminescence 208 (2019) 322–326.

CANCELLED DUE TO COVID-19

MAGNETIC PROPERTIES OF PRUSSIAN BLUE ANALOGUE $Fe_3[Cr(CN)_6]_2 \cdot nH_2O$ NANORODS OBTAINED BY ELECTRODEPOSITION METHOD

Wojciech Sas[1*], Marcin Perzanowski[1], Magdalena Fitta[1]

[1] Institute of Nuclear Physics Polish Academy of Sciences, Radzikowskiego 152, 31-342 Kraków, Poland
wojciech.sas@ifj.edu.pl

Molecular magnets are compounds assembled out of discrete building blocks, e.g. coordination complexes or organic molecules, that exhibit magnetic properties and can be treated as multifunctional materials. The continuous increase in the interest in molecular magnets can be seen in recent years. Some of them can combine multiple attractive properties, such as low density, the high magnetic moment per unit of volume, or the sensitivity for external stimuli, including temperature and pressure. Prussian blue analogues (PBAs) are one of the best-known group of molecular magnets, especially due to their functional properties (sorption capacity, photomagnetism). The numerous methods of synthesizing samples in various forms (bulk, thin films, nanoparticles) create a possibility for the interesting research, for instance, the investigation of the influence of the size reduction on their magnetic properties.

In this work, we report the synthesis and study of magnetic properties of the nanorods of PBA belonging to the system $Fe_3[Cr(CN)_6]_2 \cdot nH_2O$. The samples were prepared by template-assisted electrochemical deposition. The porous polycarbonate (PCTE) membranes covered by a thin film of Au were used as the working electrode in a three-electrode electrochemical cell. The samples were fabricated in the polycarbonate (PCTE) membranes of two different pore size: 100 and 200 nm.

The analysis of scanning electron microscope (SEM) microphotographs confirmed that nanorods of cylindrical shape with diameters of 100 and 200 nm respectively were obtained. The measurements of magnetic properties showed that obtained materials are ferromagnets with critical temperature T_c equal to 20 K. This T_c value is comparable to that observed for bulk as well as thin films. The most important result in this study is the observation of the increase of coercive filed with the reduction of nanorods diameter.

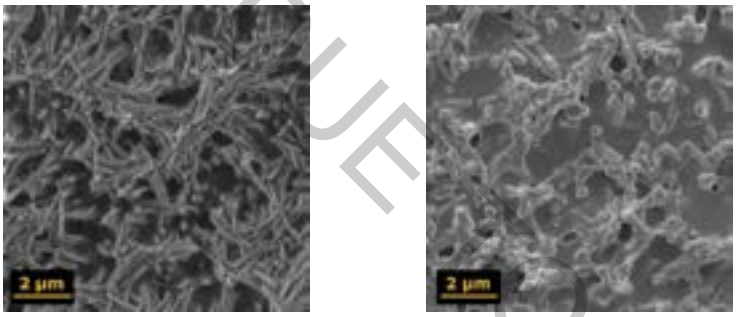

Fig. 1. Nanorods of diameter 100 nm (left) and 200 nm (right)

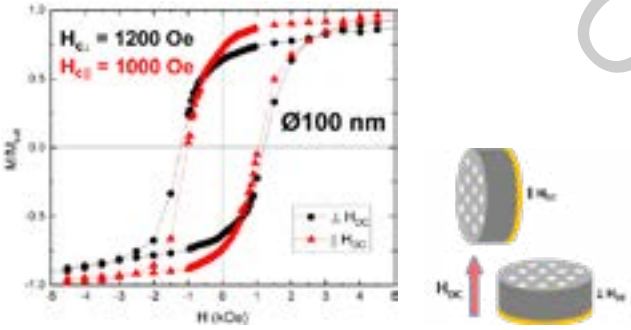

Fig. 2. Magnetic hysteresis of the sample with Ø100 nm for two different orientations with respect to the external magnetic field (explained symbolically to the right)

Acknowledgements: W.S. acknowledges the Polish National Science Centre (Grant PRELUDIUM 16: UMO-2018/31/N/ST5/03300) for financial support.

CANCELLED DUE TO COVID-19

ROBUST TECHNIQUE FOR TUNABLE PHOSPHORS PHOTOLUMNESCENCE – OPTIMIZATION OF EUROPIUM IONS REDUCTION PROCESS

Agata Jarocka[1], Tomasz K. Pietrzak[1], Jakub Płachta[2], Joanna Kłosaj[1], Michał Jarczewski[1], Jacek Ryl[3], Marek Wasiucionek[1]

[1] Faculty of Physics, Warsaw University of Technology, Koszykowa 75, 00-662 Warsaw, Poland
[2] Institute of Physics, Polish Academy of Sciences, Lotników 32/46, 02-668 Warsaw, Poland
[3] Faculty of Chemistry, Gdańsk University of Technology, Narutowicza 11/12, 80-233 Gdańsk, Poland
agata.jarocka.dokt@pw.edu.pl

CANCELLED DUE TO COVID-19

Over the past years, our group has been working on amorphous and nanocrystallised materials towards finding possible new cathode materials for Li-ion and Na-ion batteries [1], syntheses of glasses and their thermal nanocrystallisation, as well as methods to avoid oxidation of transition metals involved. Based on that experience, it was proposed to produce transparent glassy matrices doped with rare earth elements (REE), such as e.g. Eu, Pr. We studied the effects of the syntheses' conditions on REE ions reduction and adopted these correlations to control photoluminescence properties of samples.

Our recent work [2] proved that it is possible to synthesize REE-doped glassy materials whose photoluminescence spectrum can be tuned depending on synthesis conditions by using melt-quenching process. During that work we found out that one can control the relative Eu^{3+}/Eu^{2+} ions concentrations. As both Eu^{3+}/Eu^{2+} are photoluminescent in different parts of the visible range, the possibility of controlling their relative concentrations means that it is possible to "tune" photoluminescence spectrum of the material. Furthermore, emission can be "liken" to the natural light and strong UV/blue component which is present in spectra of many of today's white LEDs can be suppressed. This would make white LEDs more comfortable and healthier for the eyes than they are today [3]. It is also possible to adjust phosphors to other needed colors.

In this research, a glassy matrices based on borate and phosphate glasses were successfully synthesized by a melt-quenching process, using a double crucible method [4]. Samples obtained at different synthesis conditions were carefully investigated using X-ray diffractometry (XRD), differential thermal analysis (DTA), photoluminescence spectroscopy (PL), absorption spectroscopy and X-ray photoelectron spectroscopy (XPS).

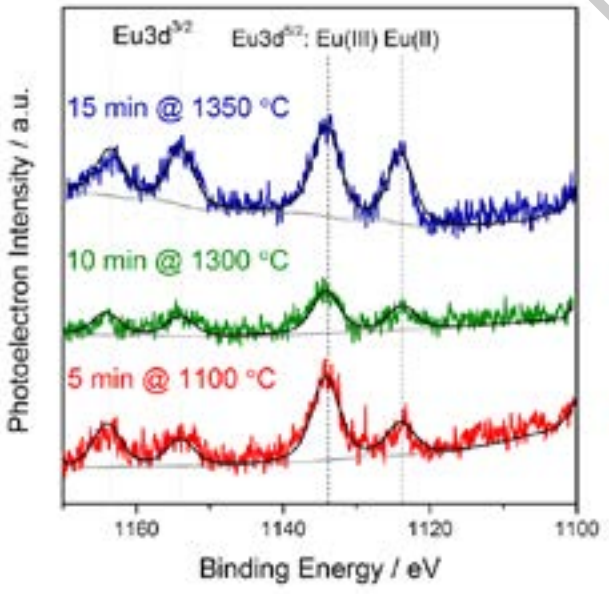

Table 1: Eu2+/Eu3+ ions ratio based on XPS analysis[2]

	Eu^{2+}	Eu^{3+}
←	42%	58%
←	36%	64%
←	33%	67%

Fig. 1. XPS studies of 3 glassy samples $Na_3Al_2(PO_4)_2F_3$ doped with Eu_2O_3. Different synthesis parameters (time and temperature) are given in the plots.

[1] T.K. Pietrzak *et al.,* Materials Science and Engineering B 213 (2016) 140-147.
[2] T.K. Pietrzak, A. Gołębiewska *et al*., Journal of Luminescence 208 (2019) 322–326.
[3] E. Chamorro *et al*., Photochemistry and Photobiology, 89 (2013) 468–473.
[4] K. Hirose *et al*., Solid State Ionics, 178 (2007) 801–807.

HOLOGRAPHIC, LOW-COST DIGITAL MICROSCOPE

Filip Łabaj[1], Witold Stępień[1], Wiktor Kulesza[1], Klaudia Gębala[1], Michał Wincel[2]

[1] Institute of Micromechanics and Photonics, Faculty of Mechatronics,
Warsaw University of Technology, Poland
[2] Institute of Metrology and Biomedical Engineering, Faculty of Mechatronics,
Warsaw University of Technology, Poland
01122428@pw.edu.pl

Digital holography is a technology providing novel solutions to the problems affecting other methods of imaging, by allowing direct numerical access to the registered complex optical field [1]. The project was focused on designing and building a low-cost Digital Holographic Microscope (DHM) system that would allow for visualization and measurement of phase objects, both biological and inorganic.

The system is based on the Mach-Zehnder interferometer architecture, with off-axis hologram recording in the image plane. Our DHM's mechanical components have been built out of LEGO parts. This provides a fast and easy way to prototype and change various modules of the microscope. Phase reconstruction from the recorded data is performed using Fourier transform method [2].

Measurements have been carried out on various biological and technical samples. Measuring standardized *poly(methyl methacrylate)* (PMMA) microspheres has shown the ability to determine their integrated phase with $\frac{\pi}{40}$ [rad] accuracy and the refractive index with accuracy to the third decimal place. We are planning on expanding our DHM's mechanical setup and software, especially to allow vertical measurements of objects, real-time monitoring of phase changes, as well as implementing automatic numerical focusing.

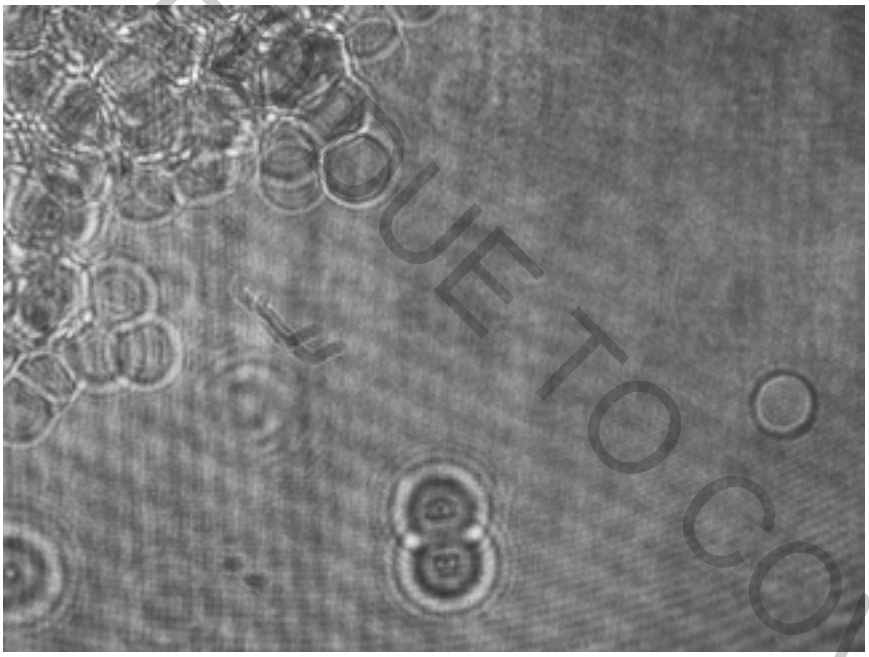

Fig. 1. Recorded hologram of microspheres in immersion fluid.

[1] M.K. Kim, *Digital Holographic Microscopy. Principles, Techniques, and Applications, chapter : Digital holographic microscopy*, pp. 149-190, Springer Series in Optical Sciences, Springer, New York (2011).

[2] V.M. Rossi, *Digital Holographic Microscopes: Design, Characterization, and Image Reconstruction*, vol. SL29 of SPIE Spotlights in Optical Design Engineering Series, RD Fiete (ed.), Bellingham, WA: SPIE Press (2017).

CANCELLED DUE TO COVID-19

ELECTRIC FIELD CONTROL OF TWO-ELECTRON STATES IN CYLINDRICALLY SYMMETRIC QUANTUM DOT

Julia Chepurnaya[1], Liliya Odanets[1], Elena Levchuk[1]

[1] Department of Applied Mathematics and Computer Science, Belarusian State University, Independence Ave. 4, 220030 Minsk, Belarus
chepurnaya.bsu@gmail.com

Semiconductor quantum dots (QDs) are increasingly being used in great number of practical applications, such as single electron transistors, photodetectors and other electronic devices [1,2]. QD structures of various geometries and configurations have been intensively studied theoretically [2,3]. However, few-electron states have been investigated mostly for QDs of a simple form. In this work, we consider two-electron states in spheroidal QDs and study the effect of external electric field on energy spectrum.

The problem is formulated as follows: the area is filled with a semiconductor with dielectric constant ε. In an external uniform electric field there is a cylindrically symmetric quantum dot in the form of a prolate or oblate spheroid. This field is directed along the axis of symmetry of the QD under study. Two types of quantum dot potential will be considered: piecewise constant and harmonic.

To calculate the system wave function Ψ and energy E, the following eigenvalue problem should be solved:

$$\left(-\frac{1}{2}\nabla_1^2-\frac{1}{2}\nabla_2^2+V(r_1)+V(r_2)+Fz_1+Fz_2+\frac{1}{|r_1-r_2|}\right)\Psi(r_1,r_2)=E\Psi(r_1,r_2), \quad (1)$$

$$\Psi(r_1,r_2)\xrightarrow[|r_1|\to\infty]{}0, \quad \Psi(r_1,r_2)\xrightarrow[|r_2|\to\infty]{}0, \quad (2)$$

where V – quantum dot potential, F – electric field strength.

The problem (1) – (2) has been solved using Hartree-Fock method. Using this method, a solution is sought in the following form:

$$\Psi(1,2)=\frac{1}{\sqrt{2}}\left(\varphi_a(1)\varphi_b(2)-\varphi_b(1)\varphi_a(2)\right), \quad (3)$$

where φ_a, φ_b are unknown functions. These functions are found from the following system:

$$-\frac{1}{2}\nabla^2\varphi_a=-\left(V+V^{bb}-V^{ab}-E_a\right)\varphi_a+E_{ab}\varphi_b, \quad (4)$$

$$-\frac{1}{2}\nabla^2\varphi_b=-\left(V+V^{aa}-V^{ba}-E_b\right)\varphi_b+E_{ba}\varphi_a, \quad (5)$$

where V^{ij} is determined from the problem for the Poisson equation:

$$\nabla^2V^{ij}=-4\pi\varphi_i^*\varphi_j. \quad (6)$$

The resulting energy can be found from the expression:

$$E=\langle\varphi_a|h|\varphi_a\rangle+\langle\varphi_b|h|\varphi_b\rangle+$$

$$+\frac{1}{2}\sum_{a,b}\langle\varphi_a|V^{bb}|\varphi_a\rangle-\frac{1}{2}\sum_{a,b}\langle\varphi_a|V^{ab}|\varphi_b\rangle, \quad (7)$$

$$h=-\frac{1}{2}\nabla^2+V.$$

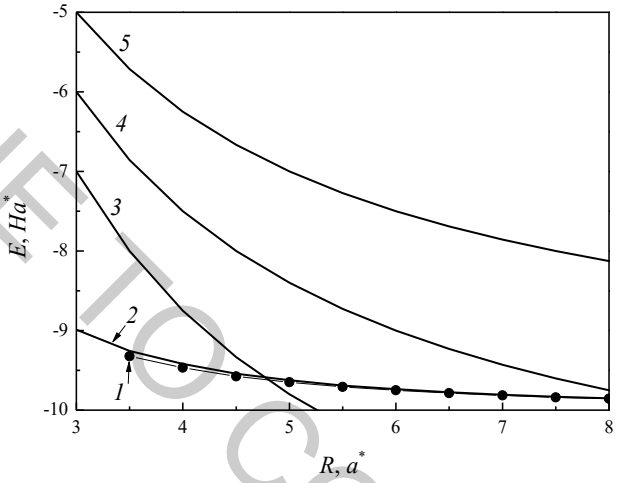

Fig. 1. The dependences of ground state energies of two electrons confined in spherical QD on characteristic QD size, calculated for different potential configurations: 1, 2 – piecewise potential with finite and infinite barrier heights, correspondingly, 3, 4, 5 – harmonic potential with the same volume.

The iterative procedure for solving the problem (4) – (7) has been implemented in the domain $[0,L]\times[0,L]$, where L is a sufficiently large number. For discretization of differential problems the finite difference method has been used.

The effect the electric field, quantum dot size (Fig. 1), the degree of elongation of a QD on the energy spectrum have been investigated. It has been found that proposed method demonstrate slower convergence rate for increasing QD size.

The developed numerical approach can be used for modeling few-electron states in cylindrically symmetric QDs of arbitrary configuration.

[1] W. Zhou, J.J. Coleman, Current Opinion in Solid State and Materials Science. Quantum dot optoelectronic devices: lasers, photodetectors and solar cells, **20**, 352–360 (2016).
[2] F.A. Zwanenburg, A.S. Dzurak et al., Silicon quantum electronics, Rev. Mod. Phys. **85**(3), 961 (2013).
[3] S.M. Reimann, M. Manninen, Electronic structure of quantum dots, Rev. Mod. Phys. **74**(4), 1283 (2002).

CANCELLED DUE TO COVID-19

YIELD AND CHEMICAL COMPOSITION OF ESSENTIAL OIL IN GERANIOL BEARING LARGE THYME (*THYMUS PULEGIOIDES*)

Vaida Vaičiulytė[1], Kristina Ložienė[1]

[1]Nature Research Centre, Institute of Botany
vaiciulyte.vaida@gmail.com

Thymus pulegioides L. is essential oil bearing medicinal and aromatic plant. Essential oil of geraniol chemotype of this species contains biologically active terpene alcohol geraniol with sweet rose aroma, therefore this essential oil is used for manufacturing of pharmaceuticals, products of perfume and cosmetic [1]. This species can be cultivated at not controlled (or semi controlled) environmental conditions, i. e. in open ground. Therefore it is very important to determine influence of meteorological conditions on *T. pulegioides* essential oil composition, in order to select the most favourable locations and conditions for cultivation. The aim of the present study was to evaluate the effects of meteorological conditions on the percentage of essential oil and geraniol in different individuals of *T. pulegioides* geraniol chemotype.

Two individual plants of *T. pulegioides* (No.1 and No.2), belonged to geraniol chemotype, were vegetative propagated and grown in the field collection of the Nature Research Centre (Mažieji Gulbinai near Vilnius, Lithuania) (N 54°46′ and E 25°17′, altitude 97 m) in 2014–2017. Plants were grown in separate square plots of 1.4 m^2, (nine sub-individuals in every plot), in the open ground under the same environmental conditions. Ground parts of *T. pulegioides* were collected separately at the full flowering stage annually and dried at room temperature. The essential oils of leaves-inflorescences were isolated by hydrodistillation in a Clevenger type apparatus during two hours. The analysis of essential oils and identification of geraniol, nerol, geranial and neral was carried out using a FOCUS GC (Thermo Scientific) gas chromatograph with a flame ionisation detector (FID) and a GC-2010 Plus instrument equipped with a GC-QP 2010 Plus (Shimadzu) series mass selective detector. Temperature (C°), precipitation (mm), photosynthetically active solar radiation (Mj/m^2) and sunshine duration (h) of April, May, June and July in 2014–2017 were obtained from the meteorological bulletins of closest station of meteorology of Lithuanian Hydrometeorological Service under the Ministry of Environment.

Results showed that same meteorological conditions can otherwise influence on accumulation of essential oil in different individuals of same chemotype of *T. pulegioides*. It could be related with genetical differences of individuals. Effect of same meteorological condition was more alike on geraniol percentage of both *T. pulegioides* samples than on essential oil: trends of effect of 6 meteorological factors (from 8) on geraniol percentage coincided in both *T. pulegioides* samples.

---

[1] B.M. Lawrence, A.O. Tucker, The genus *Thymus* as a source of commercial products, In: E. Stahl-Biskup, F. Sáez (eds) *Thyme*. The genus *Thymus*. Taylor and Francis, London and New York, England and U. S., pp 330 (2002).

CANCELLED DUE TO COVID-19

IN VITRO EVALUATION OF ANTIMICROBIAL ACTIVITY OF PROBIOTIC PRODUCED METABOLITES AGAINST PATHOGENS

Jolita Jagelaviciute, Dalia Cizeikiene

Department of Food Science and Technology, Kaunas University of Technology, Lithuania
jolita.jagelaviciute@ktu.edu

Probiotics are microorganisms which gives a beneficial health benefit on the host when is provided in suitable amounts. Probiotics in various food products such as dairy products have been used for centuries. Various studies have been shown that probiotics have a positive effect on human health, especially to normal digestive processes. Probiotics also help to maintain the animal's health. Because of that in nowadays has been increased the agricultural applications of probiotics in animal feed. The most commonly in the food and feed industry used probiotics belongs to *Lactobacillus* and *Bifidobacterium* genera [1].

In recent years a growing antibiotic-resistance has become a challenge. The number of antibiotic-resistant strains isolated from a human is increasing nowadays. Therefore, it is important to find a way to prevent the growth of pathogens which became antibiotic-resistant and is capable to colonize and adhere the mucosal surface [2].

Probiotics produce various metabolites such as lactic, acetic, citric acids and other antimicrobial substances like bacteriocins (antimicrobial peptides). Acids produced by probiotics help to acidify the medium by inhibiting the growth of pathogens [1]. Probiotics which produces bacteriocin in the gut could have an antagonistic effect on the pathogens and inhibit their growth [2].

The aim of this work was to evaluate antimicrobial activity of probiotic *Bifidobacterium* and *Lactobacillus* genera producing metabolites against pathogenic bacteria.

The ability of probiotic strains to produce antimicrobial metabolites was tested by an agar well diffusion assay. The antimicrobial activities against pathogens were determined by measuring the inhibition zones (mm) around the well. Antimicrobial activities of metabolites were evaluated in two ways: (a) the probiotics supernatants and (b) their produced bacteriocins like inhibitory substances (BLIS). Pathogens such as *Staphylococcus hyicus*, *Staphylococcus chromogenes, Staphylococcus aureus* and *Escherichia coli* were used for antimicrobial activity evaluation.

The metabolites produced by *Lactobacillus* spp. shown better inhibitory activity against pathogens comparing to strains belonging to *Bifidobacterium* genus. *Lactobacillus paracasei* subsp. *paracasei* DSM 20020, *L. paracasei* subsp. *paracasei* DSM 4905, *L. gasseri* DSM 20077 strains supernatants inhibited the growth of all 12 pathogens. *L. paracasei* subsp. *paracasei* produced BLIS also suppress the growth of several pathogens. While the metabolites of *Bifidobacterium bifidum* DSM 20082 shown antimicrobial activity against 8 from 12 pathogens. BLIS of *B. pseudolongum* DSM 20099 suppress the growth of *S. hyicus* DSM 20459. The results of this study confirm that probiotic bacteria may be used as an alternative for inhibition of pathogen growth in the host organism.

[1] D. Song, S. Ibrahim, S. Hayek, Recent application of probiotics in food and agricultural science. Probiotics, 1-34. (2012)
[2] A. Smith, C. Jones, Probiotics: Sources, Types and Health Benefits. Hauppauge.182-203 (2012)

CANCELLED DUE TO COVID-19

EXPLORING PROPERTIES OF VISCOSITY-SENSITIVE BODIPY BASED MOLECULAR ROTOR IN HUMAN MESENCHYMAL STEM CELLS

Džiugas Jurgutis[1, 2], Greta Jarockytė[1, 2], Aurimas Vyšniauskas[3],
Vitalijus Karabanovas[1, 4], Ričardas Rotomskis[1, 5]

[1] Biomedical Physics Laboratory of National Cancer Institute, Baublio 3B, Vilnius, Lithuania;
[2] Life Sciences Center, Vilnius University, Saulėtekio av. 7, Vilnius, Lithuania;
[3] Center for Physical Sciences and Technology, Saulėtekio av. 3, Vilnius, Lithuania;
[4] Department of Chemistry and Bioengineering, Vilnius Gediminas Technical University, Vilnius, Lithuania;
[5] Biophotonics group of Laser Research Centre, Vilnius University, Vilnius, Lithuania
dziugas.jurgutis@nvi.lt

CANCELLED DUE TO COVID-19

Heterogeneity is an intrinsic property of cell's structure and most biomechanical parameters. The key of such parameters – cellular viscosity, maintains cellular structure, regulates diffusion of biomolecules and significantly alters cellular behavior. Various cell mechanisms, including the differentiation of mesenchymal stem cells (MSC), apoptosis or diseases, e.g. cancer, diabetes or Alzheimer's disease results in the change of viscosity within plasma membrane and other organelles [1]. The ability to measure and visualize viscosity gradients would provide greater insight into the vital processes or even allow us to achieve earlier diagnosis of different diseases. Although there are few fluorescence-based methods for viscosity determination at the cellular level, e.g. fluorescence recovery after photobleaching (FRAP) or fluorescence correlation spectroscopy (FCS) – utilizing them would only result in single-point measurements of viscosity, which is insufficient for creating intracellular viscosity 'maps'. Therefore, a novel method is required for a spatial resolved quantitative viscosity 'mapping' in biological objects.

Viscosity-sensitive fluorophores ('molecular rotors') are the benchmark for viscosity bioimaging. One of such molecules - BODIPY-h is based on BODIPY (*4,4-difluoro-4-bora-3a,4a-diaza-s-indacene)* fluorescent dye. Phenyl ring's rotation in the BODIPY-h molecule depends on the viscosity of the surrounding micro-environment (Fig. 1): in a less viscous medium, higher intramolecular rotation gives rise to quicker deactivation from the fluorescent state via non-radiative pathway, thus resulting in a shorter fluorescence lifetime and vice versa [1], [2].

The aim of our study was to determine absorption, fluorescence spectra and fluorescence lifetime of BODIPY-h in cell growth media - Dulbecco's Modified Eagle Medium (DMEM) with fetal bovine serum (FBS) and phosphate-buffered saline (PBS), together with the uptake of the molecular rotor in human skin mesenchymal stem cells and their differentiated counterparts: adipocytes, osteocytes and chondrocytes.

Absorption, fluorescence spectra and fluorescence lifetimes of BODIPY-h were measured in PBS and cell growth media - DMEM with FBS. Fluorescence lifetimes were also measured in human skin MSC suspension with Edinburgh FLS 920 fluorimeter. For the uptake evaluation, StemPro differentiation kits (Gibco, US), were applied for specific differentiation of MSC. Cells were stained with 9 μM BODIPY-h solution diluted with DMEM (1:1000) (Gibco, US) and incubated for 60 min. The accumulation of dye was observed using Nikon Eclipse Te2000-U, confocal microscope (Nikon, Japan).

Results revealed that BODIPY-h interacts with proteins - shifting its absorption and fluorescence spectra by 5 nm and 10 nm, respectively. Fluorescence lifetime kinetics showed the same interaction: fluorescence lifetime in medium without FBS is monoexponential, while with protein it becomes biexponential and grows from 212 ps to almost 4 ns. Uptake evaluation revealed a difference in BODIPY-h localisation between undifferentiated MSC and already differentiated adipocytes. BODIPY-h accumulated in the lipid droplets, formed within the adipocytes. Meanwhile, in osteocytes, chondrocytes and undifferentiated MSC, localisation of the dye was different – molecular rotor diffuses through the membrane, stains membrane-bound organelles but is unable to pass the nuclear membrane.

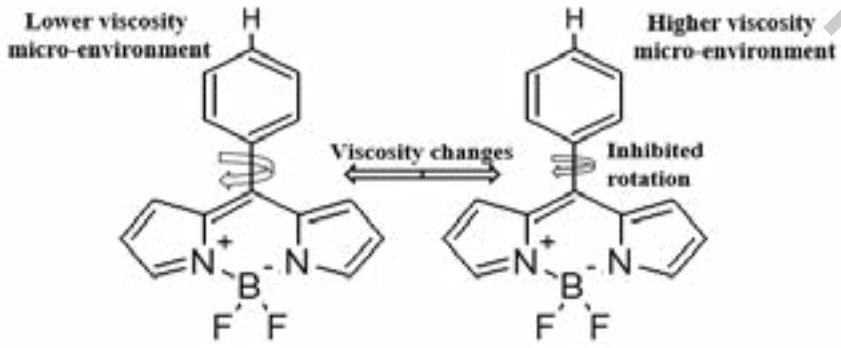

Fig. 1. Structure and rotation of molecular rotor BODIPY-h

[1] M. K. Kuimova, "Mapping viscosity in cells using molecular rotors," *Phys. Chem. Chem. Phys.*, vol. 14, no. 37, p. 12671, 2012.
[2] A. Vyšniauskas *et al.*, "Exploring viscosity, polarity and temperature sensitivity of BODIPY-based molecular rotors," *Phys. Chem. Chem. Phys.*, vol. 19, no. 37, pp. 25252–25259, 2017.

NEW LINEAR AZOL(IN)E CONTAINING ANTIMICROBIAL PEPTIDE IDENTIFICATION IN THERMOPHILIC BACTERIUM

Justas Martūnas[1], Lilija Kalėdienė[1], Arnoldas Kaunietis[1]

[1] Department of Microbiology and Biotechnology, Institute of Biosciences, Life Sciences Center, Vilnius University, Lithuania
justas.martunas@gmc.stud.vu.lt

Bacteriocins are ribosomally synthesized antimicrobial peptides produced by various bacteria. These antimicrobial peptides are usually stable at high temperatures and over a wide pH range [1]. Bacteriocins have huge potential as both food preservatives, and as next-generation antibiotics targeting the multiple-drug resistant pathogens. It has been suggested that the majority of bacterial species synthesize bacteriocins. The increasing number of reports of new bacteriocins with unique properties indicates that there is still a lot of to learn about this family of peptide antibiotics. Our goal is identification and characterization of novel bacteriocins encoded in thermophilic bacteria. In this study we have identified novel post-translationaly modiefied bacteriocin, belonging to the subclass of linear azol(in)e containing peptides (LAPs), which was encoded in Parageobacillus toebi bacterium. Here we present cloning and expression of this bacteriocin in Escherichia coli. Following the expression, we will purify and characterize its antibacterial effect on various (Para)Geobacillus spp. and other bacteria. Moreover, we will investigate its stability in various temperatures and pH values.

[1] R.H. Perez, T. Zendo, K. Sonomoto, Novel bacteriocins from lactic acid bacteria (LAB): various structures and applications, Microb. Cell Fact. 13 (2014) S3.

CANCELLED DUE TO COVID-19

THE DEVELOPMENT OF GLUCOSE BIOLOGICAL SENSORS MODIFIED BY VARIOUS GOLD DERIVATIVES

Rokas Jonaitis[1], Rugilė Chmieliauskaitė[1], Natalija German[1,2]

[1] Department of Chemistry and Bioengineering, Faculty of Fundamental Sciences, Vilnius Gediminas Technical University, Sauletekio ave.11, LT-10223, Vilnius, Lithuania
[2] Division of Immunology, State Research Institute Center for Innovative Medicine, Santariskių g. 5, LT-08406, Vilnius, Lithuania
rokas.jonaitis@stud.vgtu.lt

CANCELLED DUE TO COVID-19

In the world especially grows the interest of high-technology (nano-, bio-) application in practical analysis [1]. Biosensors are complex, high-performance laboratory instruments, which can quickly, accurately, conveniently determinate and measure the biological interactions and components [2]. Enzymatic biosensors based on the principle of the affinity were used in laboratory practice and later found a successful production progress in domestic consumption [3]. Colloidal gold and redox mediators are able to increase the electron transfer in analytical systems and improve the sensitivity of the detection [4,5]. Immobilized by enzyme and gold compounds biosensors are characterized by high selectivity, sensitivity, rapidity, reversibility, reproducibility, practical application and excellent catalytic activities [5,6].

The main aim of this research was to create glucose biosensors immobilized by glucose oxidase (GOx) and modified by different size of gold nanoparticles or electrochemically synthesized gold nanostructures in the presence of soluble (phenazine methosulfate) and insoluble (1,10-phenanthroline-5,6-dione) mediators. The enzymatic polymerization of 1,10-phenanthroline-5,6-dione was performed on modified by enzyme and gold derivatives surface of graphite rod (GR) electrode. Gold derivatives in a combination with glucose oxidase offered some advantages for the design of electrochemical glucose biosensors and are able to facilitate indirect electron transfer, via mediators and show the positive effect on the electrochemical signals [7]. During our investigations the most suitable immobilization method by gold derivatives, the kind of working electrode and of redox mediator were chosen in order to increase the sensitivity of glucose's detection. Chronoamperometry (ChA) and cyclic voltammetry (CV) were used to register analytical signals of glucose. It was evaluated, that graphite electrode is more suitable for enzymatic immobilization than glassy carbon electrode. The highest analytical signal of glucose was achieved by the use of gold nanostructures. The use of phenazine methosulfate as redox mediator in analytical system increased analytical signal of glucose about three times in the comparison of 1,10-phenanthroline-5,6-dione. However insoluble in water mediator could take more advantages (the cover of electrode, the absence of interfering compounds) in the comparison with soluble in water mediator.

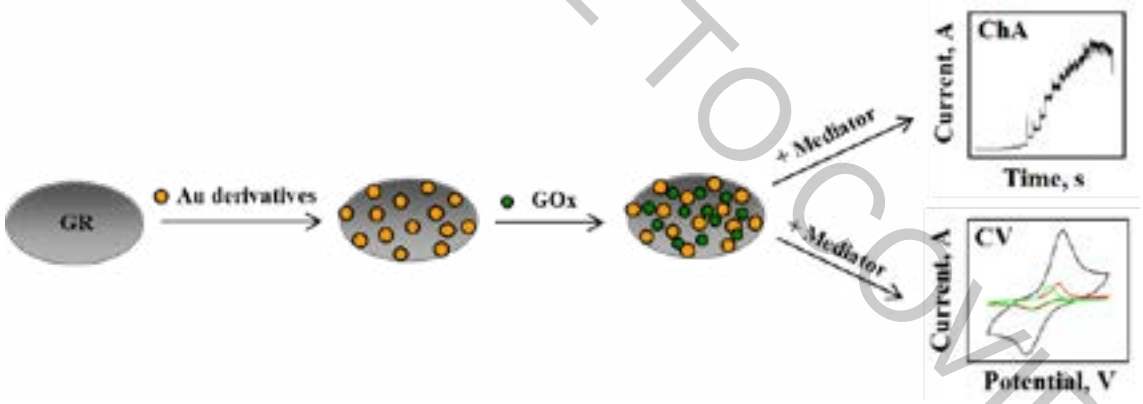

Fig.1. The presentation of GR electrode's preparation and investigation by ChA and CV.

Acknowledgment
This project has received funding from European Social Fund (project No 09.3.3-LMT-K-712-16-0006) under grant agreement with the Research Council of Lithuania (LMTLT).

[1] F. Wang, S. Hu, Electrochemical sensors based on metal and semiconductor nanoparticles, Microchim Acta **165**, 1-22 (2009).
[2] M. Pumera, S. Sánchez, I. Ichinose, J. Tang, Electrochemical nanobiosensors, Sensors and Actuators B **123**, 1195-1205(2007).
[3] A.P.F. Turner, Biosensors: sense and sensibility, Chemical Society Reviews **42**, 3184-3196 (2013).
[4] A. Ramanavicius, N. German, A. Ramanaviciene, Evaluation of electron transfer in electrochemical system based on immobilized gold nanoparticles and glucose oxidase, Journal of The Electrochemical Society **164**, G45-G49 (2017).
[5] N. German, A. Ramanavicius, A. Ramanaviciene, Electrochemical deposition of gold nanoparticles on graphite rod for glucose biosensing, Sens. Actuators B **203**, 25-34 (2014).
[6] Hs.-Ch. Liu, Ch.-Ch. Tsai, G.-J. Wang, Glucose biosensors based on a gold nanodendrite modified screen-printed electrode, Nanotechnology **24**, 215101 (8 pp) (2013).
[7] N. German, A. Ramanavicius, A. Ramanaviciene, Electrochemical deposition of gold nanoparticles on graphite rod for glucose biosensing, Sens. Actuators B: Chemical **203**, 25-34 (2014).

EVALUATION OF INTERACTION KINETICS BETWEEN FUSED CYTOKINES AND RECEPTORS USING TOTAL INTERNAL REFLECTION ELLIPSOMETRY

Aistė Lisavičiūtė[1], Ernesta Bužavaitė-Vertelienė[2], Ieva Plikusienė[3,4], Zigmas Balevičius[2], Gitana Mickienė[1], Milda Plečkaitytė[5], Gintautas Žvirblis[5]

[1]Life Sciences Center, Vilnius University, Vilnius, Lithuania
[2]Plasmonics and Nanophotonic Laboratory, Department of Laser Technology, Center for Physical Sciences and Technology, Vilnius, Lithuania
[3]Laboratory of Nanotechnology, State Research Institute Center for Physical Sciences and Technology, Vilnius, Lithuania
[4]Department of Physical Chemistry, Institute of chemistry, Faculty of Chemistry and Geosciences, Vilnius University, Naugarduko 24, Vilnius Lithuania
[5]Institute of Biotechnology, Vilnius University, Vilnius, Lithuania
aiste.lisaviciute@gmail.com

CANCELLED DUE TO COVID-19

Granulocyte-colony stimulating factor (GCSF) and stem cell factor (SCF) are cytokines that are both involved in proliferation, differentiation and survival of hematopoietic cells. It has been shown that these proteins combined can work synergistically enhancing granulopoiesis [1]. Fusion proteins are being developed to create multifunctional proteins. In addition, their therapeutic properties are improved such as increased biological activity and extended circulation half-life [2, 3]. Spectroscopic total internal reflection ellipsometry (TIRE) can be applied to measure the interaction of proteins with their receptors to evaluate their activity. By registering the analytical signal, it is possible to eventually calculate the association constant of a protein which shows how fast it binds to the immobilized receptor [4].

The aim of this study is to measure the interaction between recombinant cytokines GCSF-Lα-SCF, SCF-Lα-GCSF and their receptors using TIRE and calculate the association constants.

In this work a self-assembled monolayer (SAM) was formed by 11-mercaptoundecanoic acid (11-MUA) and activated on BK7-glass/Cr-Au slide which later was mounted inside of flow-through-cell. On top of it the layer of Protein G was created and GCSF or c-kit receptor covalently immobilized. The measurements of ligand binding to the receptor were performed in the spectral range between 300 nm and 1000 nm. The interaction kinetics of GCSF-Lα-SCF and SCF-Lα-GCSF were measured with both GCSF and c-kit receptors. Also, SCF monomer and c-kit receptor interaction was measured.

Association constants k_a were calculated for each interaction which were quite similar for SCF-Lα-GCSF and c-kit receptor, SCF-Lα-GCSF and GCSF receptor, SCF and c-kit receptor, whereas k_a for GCSF- Lα-SCF and c-kit receptor was slightly higher. Also, the association constant of GCSF- Lα-SCF and GCSF receptor could not be calculated because there was no interaction between them.

[1] Duarte, Rafael & Frank, David. (2000). SCF and G-CSF lead to the synergistic induction of proliferation and gene expression through complementary signaling pathways. Blood. 96. 3422-30.
[2] Mickiene, G., Dalgediene, I., Dapkunas, Z. *et al.* (2017) Construction, Purification, and Characterization of a Homodimeric Granulocyte Colony-Stimulating Factor. *Mol Biotechnol* 59**,** 374–384.
[3] Strohl, William. (2017). Chimeric Genes, Proteins. Reference Module in Life Sciences
[4] Z. Balevicius, J. Talbot, L. Tamosaitis et al. Modelling of immunosensor response: the evaluation of binding kinetics between an immobilized receptor and structurally-different genetically engineered ligands, Sensors and Actuators B: Chemical, Volume 297, 2019, 126770

ADDITIONAL THIOFLAVIN-T BINDING MODE IN INSULIN FIBRIL INNER CORE REGION

Mantas Žiaunys[1], Vytautas Smirnovas[1]

[1]Institute of Biotechnology, Life Sciences Center, Vilnius University, Vilnius, Lithuania
mantas.ziaunys@gmail.com

Amyloidogenic protein aggregation into fibrils is linked to several neurodegenerative disorders, such as Alzheimer's or Parkinson's disease [1]. An amyloid specific fluorescent dye thioflavin-T (ThT) is often used to track the formation of these fibrils *in vitro* [2]. Despite its wide application, it is still unknown how many types of ThT binding modes to amyloids exist, with multiple studies indicating varying numbers [3,4]. In this work we examine the binding of ThT to insulin fibrils generated at pH 2.4 and reveal a possible inner core binding mode which is not accessible to the dye molecule after aggregation occurs.

Insulin fibrils were prepared by incubating 100 or 200 µM insulin solutions (pH 2.4, 100 mM NaCl, 100 mM phosphate buffer) with or without additional ThT at 60°C without agitation for 24 hours. For each ThT concentration, excitation-emission matrices were scanned and used to determine both the maximum ThT fluorescence intensity and the position of the highest intensity peak. Absorbance measurements were used to determine the amount of free and bound ThT present in solution after sample centrifugation.

Insulin fibrils formed with ThT added before aggregation display an additional ThT binding mode, which is not accessible to ThT molecules after the fibrils are fully formed. ThT bound in this mode possesses a much higher quantum yield (Fig. 1) when compared to other bound dye molecules.

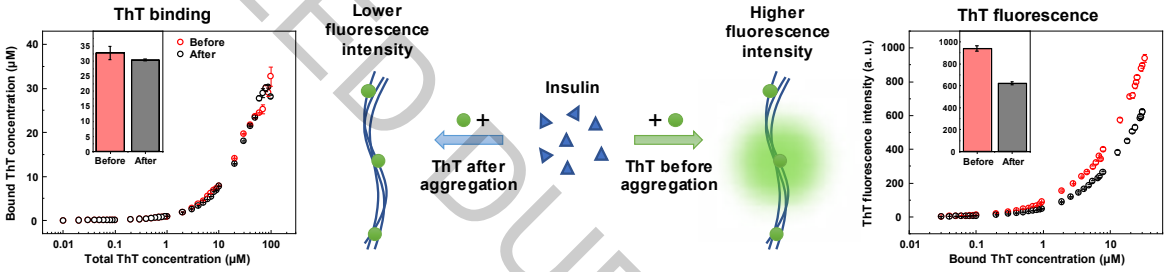

Fig. 1. Higher fluorescence quantum yield resulting from an additional ThT binding mode in insulin amyloid fibrils, which is only accessible during aggregation.

[1] Knowles, T. P. J.; Vendruscolo, M.; Dobson, C. M. The Amyloid State and Its Association with Protein Misfolding Diseases. *Nat. Rev. Mol. Cell Biol.* **2014**, *15* (6), 384–396.

[2] Xue, C.; Lin, T. Y.; Chang, D.; Guo, Z. Thioflavin T as an Amyloid Dye: Fibril Quantification, Optimal Concentration and Effect on Aggregation. *R. Soc. Open Sci.* **2017**, *4* (1), 160696.

[3] Ivancic, V. A.; Ekanayake, O.; Lazo, N. D. Binding Modes of Thioflavin T on the Surface of Amyloid Fibrils Studied by NMR. *ChemPhysChem* **2016**, *17* (16), 2461–2464.

[4] Sidhu, A.; Vaneyck, J.; Blum, C.; Segers-Nolten, I.; Subramaniam, V. Polymorph-Specific Distribution of Binding Sites Determines Thioflavin-T Fluorescence Intensity in α-Synuclein Fibrils. *Amyloid* **2018**, *25* (3), 189–196.

CANCELLED DUE TO COVID-19

ANTIMICROBIAL NUTRACEUTICALS: RASPBERRY PRESS CAKES COMBINATIONS WITH ESSENTIAL OILS AND LAB FERMENTED BOVINE COLOSTRUM

Jurga Andrėja Kazlauskaitė[1], Gražina Juodeikienė[1,2], Daiva Žadeikė[1,2], Valdas Jakštas[3], Jurga Bernatonienė[3,4], Mindaugas Marksa[3], Liudas Ivanauskas[3], Elena Bartkienė[2,3,5], Vita Lėlė[2,3,5], Pranas Viškelis[3,6]

[1] Department of Food Science and Technology, Kaunas University of Technology, Lithuania
[2] Department of Food Safety and Quality, Lithuanian University of Health Sciences, Lithuania
[3] Institute of Pharmaceutical Technologies, Lithuanian University of Health Sciences, Lithuania
[4] Department of Drug Technology and Social Pharmacy, Lithuanian University of Health Sciences, Lithuania
[5] Institute of Animal Rearing Technologies, Lithuanian University of Health Sciences, Lithuania
[6] Biochemistry and Technology Laboratory, Lithuanian Research Centre for Agriculture and Forestry, Institute of Horticulture, Lithuania
jurga.kazlauskaite@ktu.edu

CANCELLED DUE TO COVID-19

Raspberries press cake (RPC) possesses many beneficial properties for the human health related with their high content in phenolic compounds such as ellagic acid. The antimicrobial effect of RPC and essential oils mixture ("Eunutritech") against human pathogens was examined. The antimicrobial effect was determined using the agar diffusion method. Besides, in the formulations of antimicrobial nutraceuticals with *L. plantarum* fermented (LAB) and dehydrated bovine colostrum, showing antimicrobial effect, was included [1]. Phenolic compounds in lyophilized RPC and carvacrol, thymol and menthol in essential oils were evaluated for quantitative and qualitative composition by HPLC. Chromatographic separation was performed using an ACE C18 column (250 mm x 4.6 mm, 5.0 μm; Pennsylvania, USA) [2]. The total content of phenolic compounds has been evaluated using the Folin - Ciocalteu method [3].

During the experiment, two types of gels were prepared using different formulations: (a) RPC (10 %) with LAB fermented bovine colostrum (14 %); (b) RPC (10 %) with essential oils (1 %). In both cases, various combinations of jelly-forming substances (agar, pectin, gelatin) and sweeteners (erythritol, maltitol, sorbitol), were tested and selected for nutraceutical production based on texture analysis (TAXT plus texture analyzer) and optical microscope view. Gels were tested using *in vitro* digestibility assays to evaluate the release of their phenolic compounds at pH 2,0 and 7,5 [4,5].

The RPC extracts demonstrated sufficient antimicrobial effect against the inhibitory microorganisms: *Escherichia Coli*, *Salmonella Typhimurium*, *Staphylococcus Aureus*, *Bacillus Cereus*, *Pseudomonas Aeruginosa*. The study showed that susceptible structure was following RPC gel formulations: (a) sorbitol, maltitol and agar with immobilized "Eunutritech"; (b) sorbitol and agar with fermented bovine colostrum. In gels with essential oil mixture thymol was dominant antimicrobial compound (38,7 mg/50 g), while the of carvacrol and menthol concentrations were lower (0,8 mg/50 g and 18,5 mg/50 g). The highest release of phenolic compounds at different pH (2,0 and 7,5) during *in vitro* studies was obtained in nutraceuticals with RPC and LAB fermented bovine colostrum.

Acknowledgements

The authors gratefully acknowledge the COST Action CA18101 "Sourdough biotechnology network towards novel, healthier and sustainable food and bioprocesses"

The research is funded by The European Regional Development Fund by the program "Research Projects Implemented by the World-class Researcher Groups" (Grant No. 01.2.2-LMT-K-718).

[1] E. Bartkiene, M. Ruzauskas, V. Lele et al., Development of antimicrobial gummy candies with addition of bovine colostrum, essential oils and probiotics, International Journal of Food Science and Technology **53**, 1227-1235 (2017).
[2] M. Liaudanskas, P. Viškelis, V. Jakštas, Application of an Optimized HPLC Method for the Detection of Various Phenolic Compounds in Apples from Lithuanian Cultivars. Journal of Chemistry **2014**, 1-10 (2014).
[3] P. Stratil, B. Klejdus, V. Kubán, Determination of total content of phenolic compounds and their antioxidant activity in vegetables-evaluation of spectrophotometric methods. Journal of Agricultural and Food Chemistry **54**, 607-616 (2006).
[4] M. Chávarri, I. Marañón, R. Ares, Microencapsulation of a probiotic and prebiotic in alginate-chitosan capsules improves survival in simulated gastro-intestinal conditions. International Journal of Food Microbiology **142**, 185–189 (2010).
[5] N. D. Polovic, R. V. Pjanovic, L. M. Burazer, Acid-formed pectin gel delays major incomplete kiwi fruit allergen Act c 1 proteolysis in in vitro gastrointestinal digestion. Journal of the Science of Food and Agriculture **89**, 8-14 (2009).

STUDY OF INTERACTION OF S100A9 PROTEIN WITH TETHERED LIPID BILAYER MEMBRANES

Evelina Jankaitytė, Nguyen Ngoc Mai, Vytautas Smirnovas, Gintaras Valinčius, Rima Budvytytė

Life Science Center, Institute of Biochemistry, Vilnius University, Lithuania
evelina.jankaityte@gmail.com

S100A9 protein belongs to the S100 family of protein and is important factor in the regulation of most cellular processes and immune response [1]. It is associated with the development of cancer cells and neurodegeneration. S100A9 protein is involved in the amyloid-neuroinflammatory cascade in Alzheimer's disease [2]. In this work the interaction between S100A9 and membrane was studied and tethered lipid bilayer membranes (tBLM) [3] were used as simplified membrane model for these studies.

The aim of this work was to form tBLM and to optimize their electrical properties in order to use them in the study of the interaction of S100A9 protein with phospholipid bilayer and its mechanism of action. By using Electrochemical Impedance Spectroscopy and Dynamic Light Scattering methods, was shown that smaller S100A9 oligomers are more toxic to the membrane compared to larger aggregates.

[1] Markowitz J, Carson WE. Review of S100A9 biology and its role in cancer. Biochimica et Biophysica Acta (BBA) - Reviews on Cancer. 2013; 1835(1):100–9.

[2] Wang C, Klechikov AG, Gharibyan AL, Wärmländer SKTS, Jarvet J, Zhao L, Xueen J, Shankar SK, Olofsson A, Brannstrom T, Mu Y, Graslund A, Morozova-Roche LA. The role of pro-inflammatory S100A9 in Alzheimer's disease amyloid-neuroinflammatory cascade. Acta Neuropathologica. 2013; 127(4):507–22.

[3] Budvytytė R, Valinčius G, Niaura G, Voiciuk V, Mickevičius M, Chapman H, Goh HZ, Shekhar P, Heinrich F, Shenoy S, Losche M, Vanderah DJ. Structure and Properties of Tethered Bilayer Lipid Membranes with Unsaturated Anchor Molecules. Langmuir. 2013; 29(27):8645–56.

CANCELLED DUE TO COVID-19

POLYMORPHISM OF PRION PROTEIN AMYLOID FIBRILS

Ruta Snieckute, Andrius Sakalauskas, Mantas Ziaunys, Vytautas Smirnovas

Institute of Biotechnology, Life Sciences Center, Vilnius University, Vilnius, Lithuania
ruta.snieckute@gmc.stud.vu.lt

Protein aggregation into amyloid fibrils is linked to multiple neurodegenerative disorders, such as Alzheimer's, Parkinson's or Creutzfeldt-Jakob disease [1]. Usually each disease is related to aggregation of different protein or peptide, but structural polymorphism in amyloid aggregates of the same protein in vivo can lead to different pathologies [2]. It is believed that formation of structurally distinct amyloid fibrils is related either to the changes in protein amino acid sequence or to the different conditions of aggregation.

We have studied 120 samples of mouse prion protein (MoPrP 89-230) amyloid aggregates formed at six different conditions. Thioflavin T fluorescence assay revealed that polymorphism of amyloid fibrils is not only environment-dependent, but may also be observed between the samples aggregated at identical conditions. The structural differences between samples were confirmed by the assessment of the secondary structure by Fourier transform infrared spectroscopy and morphological variability observed by atomic force microscopy.

[1] H. Khanam, A. Ali, M. Asif, and Shamsuzzaman, "Neurodegenerative diseases linked to misfolded proteins and their therapeutic approaches: A review," *Eur. J. Med. Chem.*, vol. 124, pp. 1121–1141, Nov. 2016.

[2] M. Fändrich, S. Nyström, K. P. R. Nilsson, A. Böckmann, H. LeVine, and P. Hammarström, "Amyloid fibril polymorphism: a challenge for molecular imaging and therapy," *J. Intern. Med.*, vol. 283, no. 3, pp. 218–237, Mar. 2018.

CANCELLED DUE TO COVID-19

VARIATION OF BIOLOGICALLY ACTIVE COMPOUNDS OF KOMBUCHA PREPARED FROM LITHUANIAN MEDICAL HERBS

Milda Bulotaitė, Vilma Kaškonienė, Audrius Maruška

Instrumental Analysis Open Access Centre, Faculty of Natural Sciences, Vytautas Magnus University, Vileikos 8, LT-44404 Kaunas, Lithuania
mildabulotaitee@gmail.com

CANCELLED DUE TO COVID-19

Kombucha beverage considered to have originated in Northeast China (Manchuria) in 220 BC. After that, it spread around the world [1]. It is a sweet and sour taste beverage originally produced with symbiotic culture of bacteria and yeasts (SCOBY) by fermenting, sugared black or green tea (*Camellia sinensis* L.) [2]. Kombucha tea contains culture of acetic acid bacteria (e.g., *Gluconobacter* sp. and *Acetobacter* spp.), lactic acid bacteria (e.g., *Lactobacillus* sp. and *Lactococcus* sp.) and yeasts (e.g., *Schizosaccharomyces* sp., *Brettanomyces* spp. and *Zygosaccharomyces* spp.). The culture has a variable microbiological composition according to its origin, the weather, geographical location. During the fermentation process, floating cellulose biofilm is formed on the surface of medium due to the activity mainly of *Acetobacter xylinum* bacteria, for this reason kombucha culture often called as a "*tea fungus*" [3].

Kombucha consumed for its beneficial effects on health. The composition and concentration of the biologically active compounds in this beverage, are the main reasons for the health benefits. Chemical assays of kombucha beverage have indicated the presence of a variety of compounds, including organic acids, polyphenols and phenols, water-soluble vitamins, amino acids, ethanol, carbon dioxide, minerals and other metabolic products of yeasts and bacteria [4].

The aim of this research was to evaluate total amount of phenolic compounds and antioxidant activity of kombucha prepared from different Lithuanian medical herbs infusions. To our knowledge, there is no information in the literature of using specific Lithuanian herbs for kombucha fermentation, so this work gains new knowledge on the use of Lithuanian herbs, which have never been considered as a substrate for kombucha beverage.

For this research fermentation was performed using the local domestic starter culture. All experiments were done with sugared lemon balm, linden flowers, oak bark and caraway seeds infusions. Black tea was used for comparison reason. All tested herb infusions were mixed with fermentation broth containing kombucha starter culture and left for 60 days.

The total amount of phenolic compounds and antiradical activity were evaluated using spectrophotometric methods [5]. The highest amount of phenolic compounds before and after fermentation were found in lemon balm tea, 983.7±52.3 mg/L (expressed in rutin equivalents) and 417.1±22.2 mg/L, respectively. Antiradical activity varied from 222.2±6.74 to 733.3±9.7 mg/L in the herbal infusions before fermentation. The highest activity was observed in the black tea. In kombucha beverage antiradical activity varied from 102.03±3.40 mg/L to 320.97±3.16 mg/L. The highest activity was also observed in the kombucha made from black tea. The pH of tested kombucha decreased from 7.68-6.88 to 3.43-3.34 after 60 days fermentation.

According to Jayabalan et al. the concentration of the biologically active compounds in the kombucha depends on the type of tea, temperature, fermentation period, etc. [4]. Gaggìa et al. using different teas (green, black and rooibos) for kombucha preparation found that the content of polyphenolic compounds reaches a maximum value on day 7 of fermentation and then decreases statistically with the duration of fermentation [6]. A similar tendency was observed in the antioxidant activity of the kombucha drink [6].

Both total phenolic compounds content and antiradical activity reduced after fermentation of herbal infusions by kombucha culture for 60 days. The results obtained in this study do not fully coincide with those published by other scientists. The biodegradation of some specific compounds might occur due enzymes excreted by yeast or bacteria during prolonged fermentation [7]. Different types of herbs need to be evaluated and tested at more frequent intervals to evaluate the optimal fermentation time.

[1] P. Blanc, Characterization of tea fungus metabolites, Biotechnology Letters **18(2)**, 139-142 (1996).
[2] A. S. Velićanski, D. D. Cvetković, V. S. Šaponjac, J. Vulić, Antioxidant and antibacterial activity of the beverage obtained by fermentation of sweetened lemon balm (Melissa officinalis L.) tea with symbiotic consortium of bacteria and yeasts. Food Technology and Biotechnology **52(4)**, 420-429 (2014).
[3] M. I. Watawana, N. Jayawardena, C. B. Gunawardhana, V. Y. Waisundara, Enhancement of the antioxidant and starch hydrolase inhibitory activities of king coconut water (Cocos nucifera var. aurantiaca) by fermentation with Kombucha "tea fungus". International Journal of Food Science & Technology **51(2)**, 490-498 (2016).
[4] R. Jayabalan, R. V. Malbasa, E. S. Loncar, J. S Vitas, M. Sathishkumar, A review on kombucha tea microbiology, composition, fermentation, beneficial effects, toxicity, and tea fungus, Comprehensive Reviews in Food Science and Food Safety **13(4)**, 538-550 (2014).
[5] M. Stankevičius, I. Akuneca, I. Jakobsone, A. Maruška, Comparative analysis of radical scavenging and antioxidant activity of phenolic compounds present in everyday use spice plants by means of spectrophotometric and chromatographic methods, Journal of Separation Science **34(11)**, 1261-1267 (2011).
[6] F. Gaggìa, L. Baffoni, M. Galiano et al., Kombucha beverage from green, black and rooibos teas: A comparative study looking at microbiology, chemistry and antioxidant activity. Nutrients **11(1)**, (2018).
[7] R. Jayabalan, S. Marimuthu, K. Swaminathan, Changes in content of organic acids and tea polyphenols during kombucha tea fermentation. Food Chemistry **102(1)**, 392-398 (2007).

MICROBIAL CHOLESTEROL OXIDASE: PRODUCTION CHARACTERISTICS AND FEATURES OF ENZYMATIC CATALYSIS

Aleksandra A. Dobysh, Michail A. Shapira, and Aleksei V. Yantsevich

Institute of Bioorganic Chemistry, National Academy of Sciences, Belarus
alexandra.dobysh@gmail.com

Cholesterol serves as a precursor for the synthesis of various steroid hormones, bile acids, vitamin D and other biologically active substances in the human body. The determination of serum cholesterol is used in diagnostics for the assessment of atherosclerosis or coronary heart disease, estimating the risk of thrombosis and cardiovascular disease. Cholesterol oxidase is a group of enzymes that catalyzes conversion of cholesterol to cholest-4-en-3-one (Fig. 1) [1]. These enzymes are widely employed by laboratories for the determination of cholesterol concentrations in clinical samples, food and others, in enzyme-assisted derivatization for sterol analysis (EADSA) in combination with LC-ESI-MS analysis [2,3]. These enzymes are used as biocatalyst for steroid drug production.

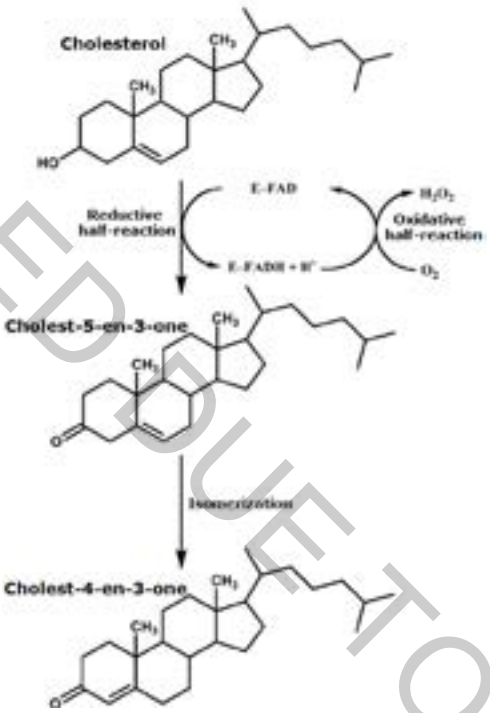

Fig. 1. Mechanism of cholesterol oxidase action [1].

Among other things, microbials cholesterol oxidases are a pathogenicity factor and can be considered as potential targets in antibiotic therapy [4]. Thereby all of the above indicates the necessity to obtain recombinant forms of cholesterol oxidases and to conduct its structure-function relation.

Thus, the biosynthesis and investigation of cholesterol oxidases from *Pseudomonas aeruginosa* and *Streptomyces lavendulae* are an important aid for development of new biosensors and for antibiotic therapy.

We obtained cholesterol oxidases from *Pseudomonas aeruginosa PAO1* and *Streptomyces lavendulae* and established the physicochemical properties of these proteins and the features of enzymatic catalysis. In addition, we characterized the catalytic activity of these enzymes, established the products of catalysis and suggested structural determinants of enzyme specificity.

[1] Vrielink, A.; Ghisla, S. Cholesterol oxidase: biochemistry and structural features, FEBS J. 276, 6826–6843 (2009).
[2] Doukyu. N. Characteristics and biotechnological applications of microbial cholesterol oxidases, Appl Microbiol Biotechnol 83, 825–837 (2009).
[3] Griffiths, W.J.; Crick, P.J.; Wang, Y.; Ogundare, M.; Tuschl, K.; Morris, A.A.; Bigger, B.W.; Clayton, P.T.; Wang, Y. Analytical strategies for characterization of oxysterol lipidomes: liver X receptor ligands in plasma, Free Radic Biol Med 59, 69–84 (2013).
[4] Reiss, R.; Faccio, G.; Thöny-Meyer, L.; Richter, M. Cloning, expression and biochemical characterization of the cholesterol oxidase CgChoA from Chryseobacterium gleum, BMC Biotechnol., 14, 46-56 (2014).

CANCELLED DUE TO COVID-19

PREPARATION OF NISIN-LOADED PECTIN-CHITOOLIGOSACCHARIDES PARTICLES

Jolita Pachaleva[1], Ruta Gruskiene[1], Alma Bockuviene[2], Jolanta Sereikaite[1*]

[1]Department of Chemistry and Bioengineering, Vilnius Gediminas Technical University, Vilnius, Lithuania
[2] Department of Polymer Chemistry, Vilnius University, Vilnius, Lithuania
jolita.buividaviciute@stud.vgtu.lt

CANCELLED DUE TO COVID-19

Nowadays, food preservation plays a tremendous role in food industry. However, the majority of food preservatives are synthetic chemicals and most of them have a harmful effect on human health. Nisin is the one of the commonly used natural additives for dairy and canned food products. This bacteriocin is generally recognized as safe (GRAS) and has a number E234. Nisin is a small 3510 Da cationic peptide composed of 34 amino acid residues. Nisin is produced by *Lactococcus lactis* subsp. *lactis* and has the broad-spectrum antimicrobial activity against Gram – positive bacteria [1]. The action is based on the formation of pore in the bacterial cell wall [2].

The antimicrobial activity of nisin depends on its interactions with food components, other food additives and conditions used for food production. The encapsulation of nisin into micro/nano particles is a promising way to achieve nisin stability and extend its antimicrobial activity in food products for a longer time [3]. Various biopolymer systems can be used for the incorporation of nisin into particles.

This study is aimed to prepare nisin-loaded particles with different surface charge, i.e. positive and negative using biopolymers pectin and chitooligosaccharides. For nisin-loading, three different types of anionic pectin biopolymer, i.e. high methoxyl pectin (HMP), low methoxyl pectin (LMP) and pectic acid (PecA) were used. The complexation process between nisin and pectin at different pH in the range of 4.0-7.0 was performed. Prepared complexes were additionally coated using different amounts of chitooligosaccharides (Fig. 1). The final concentration of nisin and pectin was 0.1 mg/ml and 0.2 mg/ml, respectively. The concentration of cationic chitooligosaccharides was in the range of 0.025-0.5 mg/ml.

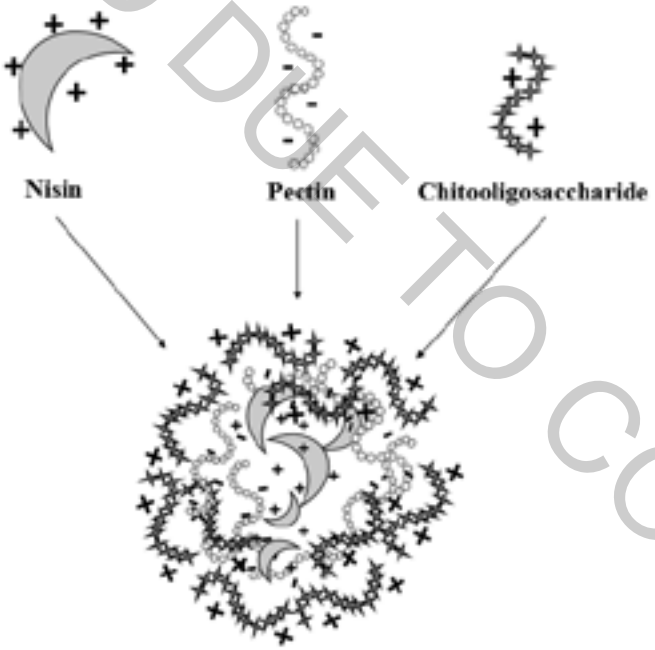

Fig. 1. Nisin-loaded pectin-chitooligosaccharides particle

Three-component particles were analyzed by measuring their zeta-potential using Zetasizer NanoZS device. The values of zeta-potentials increased with increasing chitooligosaccharides concentration and reached positive values when chitooligosaccharides concentration was in the range of 0.1-0.3 mg/ml. The isoelectric point depended on the pH of the solution and the degree of esterification of the pectin. The nisin-loaded particles with the different surface charge could be used for the investigation of particles interactions with cells applying emerging pulse electric fields technology.

[1] L. J. de Arauz, A. F. Jozala, P. G. Mazzola, T. C. V. Penna. Nisin biotechnological production and application: a review. Trends in Food Science & Technology, 20(3-4), 146-154 (2009).
[2] T. Krivorotova, R. Staneviciene, J. Luksa, E. Serviene, J. Sereikaite., Impact of pectin esterification on the antimicrobial activity of nisin-loaded pectin particles. Biotechnology progress, 33(1), 245-251 (2017).
[3] I. Khan, D. H. Oh. Integration of nisin into nanoparticles for application in foods. Innovative Food Science & Emerging Technologies, 34, 376-384 (2016).

NEW NISIN-ULVAN PARTICLES: LOADING EFFICIENCY

Edita Kodyte[1*], Ruta Gruskiene[1], Jolanta Sereikaite[1]

[1] Department of Chemistry and Bioengineering, Vilnius Gediminas Technical University, Lithuania
edita.kodyte@stud.vgtu.lt

Nisin is the most popular antimicrobial peptide which has been used in the food sector for improving food safety [1]. It exhibits a wide spectrum antimicrobial activity against Gram-positive bacteria and is produced by Lactococcus lactis subsp. lactis. Nisin is a cationic peptide composed of 34 amino acid residues.

To protect nisin from the interaction with food components and to ensure the stability of antimicrobial peptide during food processing and storage period, nisin, as the core material, is coating with the wall materials. There are a variety of food-grade wall materials including proteins, polysaccharides and lipid. In this work, for particles preparation ulvan was used. Ulvan is a water soluble anionic sulfated polysaccharide which can potentially form complexes with oppositely charged molecules [2]. Significant biological activities of ulvan has been demonstrated in both animal and plant systems in in vitro and in vivo studies [3].

In this work, the complexation process between nisin and ulvan at different pH in the range of 4.0-7.0 was performed. The final concentration of ulvan in the product was 0.4 mg/mL, and the nisin concentration was in the range of 0.1-1 mg/ml. The loading efficiency was determined by capillary zone electrophoresis method using 7100 Capillary Electrophoresis unit (Agilent Technologies). The loading efficiency was found to be 100 percent at all pH values with nisin concentration up to 0.3 mg/ml. The subsequent increase in nisin concentration especially at lowest pH values is followed by incomplete encapsulation. The lowest nisin loading efficiency was found at pH 4.0, and the highest one was found at pH 7.0.

Nisin-loaded ulvan particles obtained by the simple and inexpensive complexation method could find their application in food industry.

Acknowledgements: We thank Professor Vassilios Roussis from the University of Athens for the gift of the ulvan sample used in this study.

1] A. Bahrami, R. Delshadi, S. M. Jafari et al., Nanoencapsulated nisin: An engineered natural antimicrobial system for the food industry, Trends in Food Science and Technology **94**, 20-31 (2019).
[2] L. A. Tziveleka, E. Ioannou, V. Roussis, Ulvan, a bioactive marine sulphated polysacharide as a key constituent of hybrid biomaterials: A review, Carbohydrate Polymers **218**, 355-370 (2019).
[3] J. T. Kidgell, M. Magnusson, R. Nys et al., Ulvan: A systematic review of extraction, composition and function, Algal Research **39**, 101422 (2019).

CANCELLED DUE TO COVID-19

GEL COMPOSITES FOR CAPILLARY ELECTROCHROMATOGRAPHY

Vita Tumosaitė, Mantas Stankevičius, Tomas Drevinskas, Audrius Maruška

Instrumental Analysis Open access center, Faculty of Natural Sciences, Vyautas Magnus university, Kaunas, Lithuania
vita.tumosaite@vdu.lt

Capillary electrochromatography is considered among one of the most efficient separation techniques. This separation technique has advantages of both capillary electrophoresis and high-performance liquid chromatography [1]. Capillary electrochromatography can be applied for analyzing various complex biological and synthetic mixtures including pharmaceuticals, chiral molecules and natural compounds [1]. Not only charged but also neutral molecules can also be separated according to their molecular mass using capillary electrochromatography. To our knowledge, yet there is no report of capillary electrochromatography for size exclusion separation of the macromolecules.

In size exclusion mode, separation is possible due to electroosmotic flow, which drives uncharged molecules through the column filled with stationary phase. Stationary phase in column acts as a molecular sieve and allows to distribute molecules according to their molecular mass. Agarose is a linear polysaccharide polymer forming three-dimensional gel that can be used as a stationary phase for capillary electrochromatography [2].

The aim of this work is to create new stationary phases for separation of neutral macromolecules using capillary electrochromatography and contactless conductivity detection [3].

Agarose gel was used to make a stationary phase for capillary columns. Neutral agarose gel was mixed with another polymer that has a charge in order to create gel composites suitable for neutral molecules separation with capillary electrochromatography. Agarose was used to create optimal pore size and provide suitable mechanical properties of gel composite and charged polymer was used to create a zeta potential of the composite. Optimal pore size and zeta potential are necessary to create electroosmotic flow. Varying the ratio of charged and uncharged polymers, we optimized electroosmosis flow which is necessary for the separation. 75 μm I.D. fused silica capillaries were filled with prepared gel composite for the analysis of neutral macromolecules using electrical field.

In order to evaluate exclusion limits of created gel composites, different molecular mass dextran standard solutions were used. Dextran standards were selected due to the fact, that in the separation medium (background electrolyte pH 3) they are neutral. Elution of dextran standards provided a possibility to build up calibration curves that are used for determination of molecular mass of neutral molecules in real samples. Obtained experimental results will be presented in this presentation.

Acknowledgements: Financial support from Research Council of Lithuania project Nr. 09.3.3-LMT-K-712-16-0064 is acknowledged.

[1] A. Maruška, U. Pyell, Capillary electrochromatography: normal-phase mode using silica gel and cellulose-based packing materials. Journal of Chromatography, A **782** (2), 167-174 (1997).

[2] A. Maruška, O. Kornyšova, Homogeneous reversed-phase agarose thermogels for electrochromatography. Journal of Chromatography A **1044**, 223-227 (2004).

[3] T. Drevinskas, et al, Electrophoretic separation of pressurized hot water extracts of Hibiscus sabdariffa L. using vitamin C as background electrolyte and contactless conductivity detection. Chemija **25** (4), 206-212 (2014).

CANCELLED DUE TO COVID-19

GENETICAL IDENTIFICATION OF ANTIBACTERIAL AGENTS PRODUCING MICROORGANISMS, ANALYSIS OF THEIR BACTERIOCINS AND KILLER TOXINS AND FOOD FERMENTATION ASSAY

Domantas Armonavičius, Audrius Maruška, Tomas Drevinskas

Instumental Analysis Open Access Centre, Faculty of Natural Sciences, Vytautas Magnus University, Lithuania
domantas.armonavicius@stud.vdu.lt

In general, various preservatives are used to prevent the growth of pathogenic microorganisms in food. Recently, chemical supplements have been seeking to be replaced by more natural substances, such as bacteriocins secreted by lactic acid bacteria, which are widely researched worldwide for their antimicrobial properties and safety for human consumption [1]. In addition to lactic acid bacteria, various leavens also contain yeast, which produce killer toxins [2].

Searching for lactic acid bacteria and yeast in natural foods and investigating their application possibilities are relevant worldwide. In Lithuania, the use of yeast secreted killer toxins as natural antimicrobial agents and research on its impact on human health are new. Depending on the environmental conditions, the microorganisms adapt, resulting in different strains that can produce antimicrobial substances with different properties. Therefore, it is important to evaluate their stability against various environmental factors and to determine influence on food fermentation.

The aim of this work is genetically identify lactic acid bacteria and yeast, to produce killer toxins and bacteriocin based resistance to various enviromental factors, as well as food (milk) fermentation and capillary electroforesis analysis. Polymerase chain reaction (PCR), antibacterial activity assay and capillary electroforesis integrated with electrophoresis data segmentation method were used for this task [3-5]. *Leuconostoc mesenteroides* lactic acid bacteria and *Kluyveromyces marxianus*, *Debaromyces hansenii*, C*andida zeylanoides*, *Candida inconspicua* yeasts were identified during this work. Antibacterial activity of the isolated yeast killer toxins supernatants was investigated at 40-121°C, pH 2-12 in 5, 8, 10% NaCl medium. After capillary electrophoresis analysis and electrophoresis data segmentation method application it was found which substances, produced by *Leuconostoc mesenteroides* and *Debaryomyces hansenii* have potentially antibacterial properties. Detailed results of the work will be presented during the conference.

Acknowledgements:
This project was financed by Research Council of Lithuania, grant No. 09.3.3-LMT-K-712-16-0067.

[1] Kaškonienė V., Stankevičius M., Bimbiraitė-Survilienė K., Naujokaitytė G., Šernienė L., Mulkytė K., Malakauskas M., Maruška A., Current State of Purification, Isolation and Analysis of Bacteriocins Produced by Lactic Acid Bacteria, Applied Microbiology and Biotechnology 101, 1323-1335 (2017).
[2] Buyuksirit T., Kuleasan H., Antimicrobial Agents Produced by Yeasts, International Journal of Biological, Biomolecular, Agricultural, Food and Biotechnological Engineering 8, 1114-1117 (2014).
[3] Kormin S., Rusul G., Radu S., Ling F.H., Bacteriocin-Producing Lactic Acid Bacteria Isolated from Traditional Fermented Food, The Malaysian Journal of Medical Sciences: MJMS 8, 63-68 (2001).
[4] Drevinskas T., Stankevičius M., Bimbiraitė-Survilienė K., Naujokaitytė G., Šernienė L., Kornyšova O., Malakauskas M., Maruška A., Optimiation of capillary zone electrophoresis-contactless conductivity detection method for the determination of nisin, Electrophoresis 39, 2425-2430 (2018).
[5] Drevinskas T., Maruška A., Telksys L., Hjerten S., Stankevičius M., Lelešius R., Mickienė R., Karpovaitė A., Salomskas A., Tiso N., Ragažinskienė O., Chromatographic data segmentation method: A hybrid analytical approach for the investigation of antiviral substances in medicinal plant extracts, Analytical Chemistry, 91, 1080-1088, (2019).

CANCELLED DUE TO COVID-19

RECYCLING OF WASTE MONEY BILLS BY USING MICROBIAL HYDROLYSIS AND ETHANOL FERMENTATION

Tomas Nenartavičius[1], Neringa Kuliešienė[1], Sandra Sakalauskaitė[1], Samy Yousef[2], Rimantas Daugelavičius[1]

[1]Department of Biochemistry, Vytautas Magnus University, Kaunas, Lithuania.
[2]Department of Production Engineering, Faculty of Mechanical Engineering and Design, Kaunas University of Technology, Kaunas, Lithuania.
neringa.kuliesiene@vdu.lt

CANCELLED DUE TO COVID-19

Increasing gas prices and environmental concerns have become the driving force for developing alternative energy sources in recent years. The most popular second-generation biofuels are bioethanol, produced from non-food biomass. Waste money bills (WMBs) are potential material that can be used to produce ethanol because it contains about 95 % of cellulose [1]. According to the Cash Department of the Bank of Lithuania comment, WMBs are non-recyclable materials in Europe. Therefore, the filamentous fungus *Trichoderma reesei* is well-known as the best cellulase producer and it can be used for enzymatic hydrolysis of cellulose based material. Furthermore, *Ogataea polymorpha* is known as thermotolerant yeasts. The ability to grow at 50 °C is necessary to combine hydrolysis with ethanol fermentation [2].

The aim of this study is to optimize hydrolysis and ethanol production from the WMBs by using the filamentous fungus *Trichoderma reese* ATCC 26921 and the thermotolerant yeasts *Ogataea polymorpha* ΔCAT8.

In this study, the pretreated WMBs samples (treated by milling and alkali treatment) were used as carbon sources for cellulase production in shake flask fermentation. The total cellulase activity was determined by filter paper assay [3]. Cellulase activity was expressed as filter paper unit for 1 g substrate (FPU/g).

Cellulase production could be significantly influenced by the effect of nitrogen sources [4]. We found that the use of soybean meal or yeast extract as nitrogen sources resulted in the highest cellulases activity (5 FPU/g). The same activity was exposed in standard Mandels medium that consists of mixture of yeast extract, urea and ammonium sulfate [5]. These medium components could be replaced with other types of nitrogen sources (e.g. soybean meal) to achieve lower costs of hydrolysis process.

Physical changes of the WMBs were detected by Scanning Electron Microscope (SEM). The decomposition of cellulose fibers were detected after 7 days (Fig. 1.) of shake flask fermentation with soybeans meal. Significant break down of fiber surface and coverage of fungal biomass was observed.

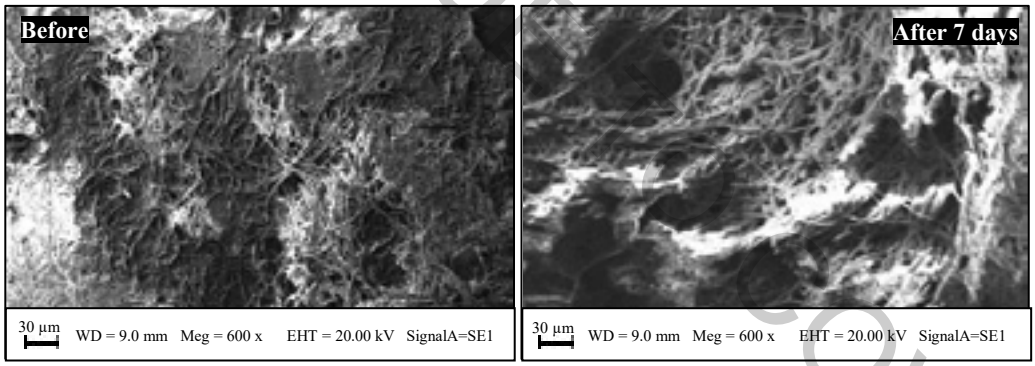

Fig. 1. SEM images of morphology of the WMB samples before and after 7 days.

Additionally, we determined the hydrolysis rate by using pretreated WMBs samples and fungal cellulases from shake flask fermentation (enzyme filtrate). For ethanol production we combined saccharification (hydrolysis of cellulose) and ethanol fermentation at the same time by adding yeasts to enzyme filtrate. We discovered the glucose recovery yield was 6.4 % during hydrolysis. Also, ethanol concentration was 10.5 mM. It demonstrates that WMBs could be used in ethanol production. However, the yield of ethanol is low. Therefore, different temperature and inoculation times of yeasts will be tested for further researches.

This study was supported by joint project of Vytautas Magnus University and Kaunas University of Technology funding grant CotEtha.

[1] Sheikh, M. M. I., Kim, C. H., Lee, J. Y., Kim, S. H., Kim, G. C., Le, J. Y., Kim, J. W. (2013). Production of bioethanol from waste money bills-A new cellulosic material for biofuels. Food and Bioproducts Processing, 91(1), 60–65.
[2] Lehnen, M., Ebert, B. E., & Blank, L. M. (2019). Elevated temperatures do not trigger a conserved metabolic network response among thermotolerant yeasts. BMC Microbiology, 19(1), 100.
[3] Adney, B., Baker, J., 1996. Measurement of cellulase activities. Lab. Anal.
[4] Wang, H., Kaur, G., Pensupa, N., Uisan, K., Du, C., Yang, X., & Lin, C. S. K. (2018). Textile waste valorization using submerged filamentous fungal fermentation. Process Safety and Environmental Protection, 118, 143–151.
[5] Mandels, M., & Reese, E. T. (1956). Induction of cellulase in *Trichoderma viride* as influenced by carbon sources and metals.

BIOSYNTHESIS AND CHARACTERIZATION OF RECOMBINANT VIRUS-LIKE PARTICLES OF *TORULASPORA DELBRUECKII* VIRUS TDV-1

Ona Bartininkaitė[1], Aleksandras Konovalovas[1], Justas Lazutka[2], Saulius Serva[1], Elena Servienė[3]

[1] Institute of Biosciences, Life Sciences Center, Vilnius University, Lithuania
[2] Institute of Biotechnology, Life Sciences Center, Vilnius University, Lithuania
[3] Laboratory of Genetics, Institute of Botany, Nature Research Center, Vilnius, Lithuania
ona.bartininkaite@gmail.com

CANCELLED DUE TO COVID-19

Yeast are widely used model microorganism for virus research. Yeast harbour double-stranded RNA viruses that are considered as non-infectious since no naturally occurring extracellular route of transmission has been identified [1]. Yeast are also an attractive platform to synthesize virus-like particles due to numerous advantages such as capability for post-translational modifications, easy cultivation procedure and high yield of recombinant protein.

In these studies, the dsRNA virus TdV-1 of the *Partitiviridae* virus family was identified in nonconventional yeast *Torulaspora delbrueckii*. *Partitiviridae* virus hosts include filamentous fungi, plants, and protozoa [2]. Therefore, TdV-1 is the first virus to be discovered in non-filamentous fungi, belonging to the *Partitiviridae* family. The aim of the study was to characterize the properties of the capsid encoded by TdV-1 virus. Viral particles of 30 nm in diameter were purified from the wild-type yeast strain of *Torulaspora delbrueckii*. Plasmids encoding recombinant capsid protein were constructed and protein biosynthesis induction in *S. cerevisiae* has been performed. Microscopic analysis of TEM revealed that the recombinant capsid protein is capable of forming virus-like particles of the same size as produced by the wild-type virus. Further studies sought to evaluate the structure of the capsid protein influence on VLPs assembly and cellular localization of the virus. To accomplish these goals, the recombinant capsid protein was fused with the fluorescent protein mCherry and biosynthesis of modified VLPs in *S. cerevisiae* yeast was performed. According to TEM microscopy results, mCherry does not interfere with virus-like particle assembly. Fluorescence microscopy analysis revealed that the capsid protein does not exhibit specific cellular localization.

Results of this study provide the first glimpse on the TdV-1 virus structure so facilitating it‘s applicability in future biotechnologic applications.

[1] R. B. Wickner et al., Viruses and Prions of Saccharomyces cerevisiae, Advances in Virus Research 86, 1–36 (2013).
[2] E. J. Vainio et al., ICTV virus taxonomy profile: Partitiviridae, Journal of General Virology 99, 17-18 (2018).

THE CHARACTERISTICS OF AN ANTIMICROBIAL PEPTIDE FROM *PEDIOCOCCUS ACIDILACTICI* JEM-1

Augustė Rastenienė[1], Kamilė Šimelytė[1], Monika Kisieliūtė[1], Rūta Gruškienė[1], Ramunė Stanevičienė[2], Elena Servienė[1,2], Jolanta Sereikaitė[1*]

[1] Vilnius Gediminas Technical University, Lithuania
[2]Nature Research Centre, Lithuania
auguste.rasteniene@stud.vgtu.lt

CANCELLED DUE TO COVID-19

Nowadays there is a growing demand of natural products without synthetic preservatives. However, such products tend to lose their quality over time and can cause food poisoning. Moreover, inappropriate and excessive use of antibiotics has induced the development of antibiotic resistance in some bacteria. Bacteriocins produced by lactic acid bacteria could solve both of the problems but their industrial use is still limited because of challenging procedures of the purification.

Among all characterized bacteriocins only nisin and pediocin PA-1/AcH are approved to be used as food additives [1]. Nevertheless, a large number of pediocins exist which are different by their biochemical features, mode of action and even antimicrobial spectrum [2].

At first, an antimicrobial peptide from *Pediococcus acidilactici* JEM-1 was purified based on its feature to adsorb onto producer cells. This process is strongly influenced by the pH [3]. After all purification steps from 500 mL of cultivation medium of *Pediococcus acidilactici* JEM-1 about 39 μg of pediocin is obtained. Its purity was determined by Tricine-SDS-PAGE and capillary zone electrophoresis. The molecular weight calculated from Tricine-SDS-PAGE gel is about 4.4 kDa. In addition, purified bacteriocin was tested for its antimicrobial activity against *Bacillus subtilis* bacteria. Our study also showed that the antimicrobial peptide from *Pediococcus acidilactici* JEM-1 can be successfully encapsulated into nano/microparticles with polysaccharides.

Acknowledgements: This research was funded by the European Social Fund under the No 09.3.3-LMT-K-712 "Development of Competences of Scientists, Other Researchers and Students through Practical Research Activities" measure. Grant No 09.3.3-LMT-K-712-16-0029.

[1] A. A. T. Barbosa, H. C. Mantovani, S. Jain, Bacteriocins from lactic acid bacteria and their potential in the preservation of fruit products, Critical Reviews in Biotechnology **37**, 852-864 (2017).
[2] B. Kumar, P. P. Balgir, B. Kaur et al., Cloning and expression of bacteriocins of *Pediococcus* spp.: a review. Archives of Clinical Microbiology **2**, 1-18 (2011).
[3] R. Yang, M. C. Johnson, B. Ray, Novel method to extract large amounts of bacteriocins from lactic acid bacteria. Applied and Environmental Microbiology **58**, 3355-3359 (1992).

SYNTHESIS AND INVESTIGATION OF OLIGOMERIZED AROMATIC AMINE FOR LACCASE ACTIVITY ASSAY

Justinas Babinskas[1], Inga Matijošytė[1]

[1] Sector of Applied Biocatalysis, Institute of Biotechnology, Life Sciences Center, Vilnius University, Lithuania
justinas.babinskas@gmail.com

Laccases are multi-copper oxidases (EC 1.10.3.2), containing T1, T2 and T3 copper sites. The catalytic mechanism consists of several stages: i) the transfer of one electron and proton from the substrate to T1 Cu (oxidation); ii) the transfer of one electron from T1 to T2/T3 Cu cluster; iii) the T2/T3 cluster reduces one oxygen molecule to two water molecules, by using four electrons and protons. The reaction byproduct is water; therefore this enzyme has high potential for industrial application [1]. Their natural substrates are aromatic compounds containing at least one hydroxyl, thiol, primary or secondary amine functional group.

Thought the years of investigating various laccases, a lot of information has already been accumulated: redox potentials, enzyme sources, reorganization energies, catalytic mechanism, etc. However, tangible application of laccases is hindered by the unresolved drawbacks such as poor stability, commercial unavailability, lack of efficient expression systems, low immobilization yields, etc.

One of the shortcomings for discovering laccases with new and/or novel features is a lack of substrates suitable for high-throughput screening and functional analysis. Currently, the most common compounds used for laccase functional analysis are 2,2'-azino-bis(3-ethylbenzothiazoline-6-sulphonic acid) under the trivial name ABTS and 4-[[2-[(3,5-dimethoxy-4-oxocyclohexa-2,5-dien-1-ylidene)methyl]hydrazinyl]methylidene]-2,6-dimethoxycyclohexa-2,5-dien-1-one known as syringaldazine [2,3]. Spectrophotometric activity assays with these substrates give acceptable results, but these compounds have poor stability, low specificity and are rather expensive.

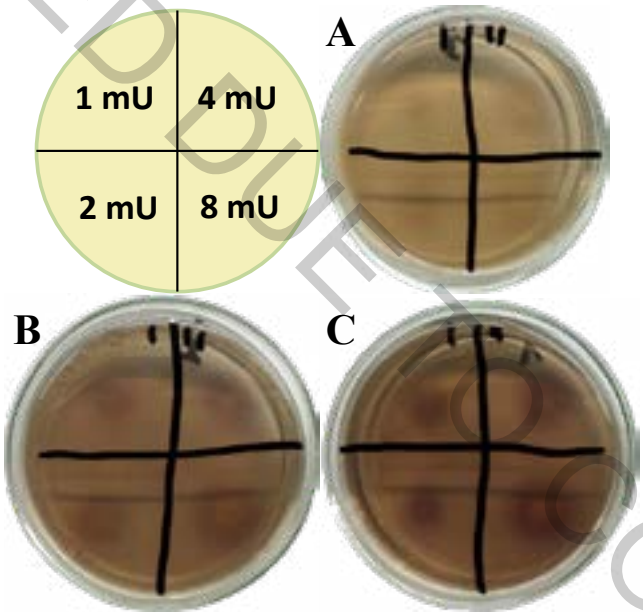

Fig. 1. The amount of laccase enzymatic activity units used for reaction on LB-agar plate with different concentrations of the substrate: **A** – 200 µM; **B** – 300 µM; **C** – 400 µM.

By our investigation, we present the synthesis of a new substrate for laccase high-throughput agar-plate screening. This compound was synthesized via a single pot reaction using relevantly low priced aromatic amine – N,N-dimethylphenylenediamine. The latter substrate was tested with commercially available laccase Novozym 51003 from *Aspergillus oryzea* on LB-agar and YEPD-agar growth medium plates (Fig. 1). The results in more detail will be presented during the poster session.

[1] Jones S. M., Solomon E. I. Electron transfer and reaction mechanism of laccases, Cellular and Molecular Life Sciences **72**, 869-883 (2014).
[2] Call H. P, Mücke I. History, overview and applications of mediated lignolytic systems, especially laccase-mediator-systems (Lignozym®-process), Journal of Biotechnology **53**, 163-202 (1997).
[3] Lucas M. F. et al. Simulating Substrate Recognition and Oxidation in Laccases: From Description to Design, Journal of Chemical Theory and Computation **13**, 1462-1467 (2017).

CANCELLED DUE TO COVID-19

FLT3 RECEPTOR AS A POTENTIAL PROGNOSTIC BIOMARKER AND THERAPEUTIC TARGET IN PANCREATIC CANCER

Julius Andriuškevičius[1], Eglė Žalytė[1], Marija Ger[1], Marius Petrulionis[2,3], Benediktas Kurlinkus[3], Audrius Šileikis[2,3], Mindaugas Valius[1]

[1] Proteomics Center, Institute of Biochemistry, Vilnius University Life Sciences Center, Vilnius, Lithuania
[2] Center of Abdominal Surgery, Vilnius University Hospital Santaros Klinikos, Vilnius, Lithuania
[3] Institute of Clinical Medicine, Clinic of Gastroenterology, Nephrourology and Surgery, Faculty of Medicine, Vilnius University, Vilnius, Lithuania
julius.andriuskevicius@chf.stud.vu.lt

CANCELLED DUE TO COVID-19

Pancreatic ductal adenocarcinoma (**PDAC**) is among the most aggressive and difficult to cure cancer types, therefore the discovery of possible diagnostic and treatment biomarkers and therapeutic targets is very important. One of the potential candidate biomarkers is receptor tyrosine kinase **FLT3**. FLT3 is mainly expressed in haematopoietic progenitor cells, but was also identified as a specific pancreatic cancer prognostic biomarker using proteomic analysis [1].

In this study we examined the level of FLT3 receptor in surgically removed PDAC tumors. Tissue samples obtained from surgery due to nonmalignant diseases of pancreas or duodenum were used as nonmalignant (healthy) control. Also primary cell cultures from PDAC tumors were obtained by outgrowth method. A correlation between better survival of PDAC patients and the FLT3 receptor expression in tumors as identified by mass spectrometry was observed. **PDAC-specific expression** of FLT3 receptor was confirmed by Western Blot analysis in tumor samples, compared to healthy pancreatic tissue, and in PDAC patient-derived primary cell lines. Next step was to evaluate the activity of FLT3 receptor. We showed the relative levels of FLT3 ligand expression in primary cell cultures utilizing the quantitative polymerase chain reaction (qPCR) method. Analysis indicated the **FLT3 ligand expression** and allowed us to confirm that FLT3 receptor can be activated in primary PDAC cultures. Finally, the effects on primary cell lines from FLT3 receptor inhibitor ASP2215 alone or in combination with other chemotherapeutic agents were measured. Analysis of cell dissemination from spheroids that mimics invasiveness showed that **ASP2215 can inhibit cancer cell invasiveness**. Several of primary cell cultures analysed were sensitive to FLT3 inhibition by ASP2215. Moreover, we demonstrated that a combination of ASP2215 with FGF (fibroblast growth factor) receptor inhibitor BGJ398 is **cytotoxic to all primary PDAC cell cultures** analysed.

These findings led us to propose FLT3 receptor as a potential prognostic biomarker and therapeutic target in pancreatic ductal adenocarcinoma.

[1] Ger et. al. (2018); *Proteomic Identification of FLT3 and PCBP3 as Potential Prognostic Biomarkers for Pancreatic Cancer*; Anticancer Research, 38(10), 5759–5765.

BIOCOMPATIBLE CARBOXYLATED $CuInS_2$/ZnS QUANTUM DOTS FOR BRAIN TUMOR DIAGNOSTICS

Viktoras Mažeika[1,2], Dominyka Dapkutė[1,2], Artiom Skripka[3], Riccardo Marin[3], Patrizia Canton[4], Fiorenzo Vetrone[3], Vitalijus Karabanovas[2,5]

[1] Life Sciences Center, Vilnius University, Saulėtekio av. 7, LT-10257, Vilnius, Lithuania
[2] Biomedical Physics Laboratory, National Cancer Institute, P. Baublio 3B, LT-08406, Vilnius, Lithuania
[3] Institut National de la Recherche Scientifique, Centre Énergie, Matériaux et Télécommunications, Université du Québec, 1650 Boulevard Lionel-Boulet, Varennes, Quebec, Canada
[4] Department of Molecular Sciences and Nanosystems, Ca' Foscari University of Venice, Via Torino 155/b, I-30170, Venezia-Mestre, Italy
[5] Department of Chemistry and Bioengineering, Vilnius Gediminas Technical University, Saulėtekio av. 11, LT-10223 Vilnius, Lithuania
vitalijus.karabanovas@nvi.lt

Despite ongoing research on its therapy and diagnostics, cancer still remains one of the leading causes of death. Currently used imaging methods, mainly computed tomography (CT) and magnetic resonance imaging (MRI), allow for effective diagnostics of cancer, but the equipment is expensive and requires extensive training to be used effectively. Therefore, other diagnostic techniques are being explored for possible application. Among them, optical methods, such as fluorescence spectroscopy, have the advantage of requiring cheaper equipment which is not as difficult to use as CT and MRI. They also allow intraoperative use as a visual aid for surgeons [1].

Even though optical techniques possess some advantages over currently used cancer diagnostic methods, they have several drawbacks which cannot be ignored. Poor stability in biological media and low quantum yield of organic dyes used for imaging limit the application of these techniques. Such issues could be solved by using quantum dots (QDs). These nanoparticles possess superior optical properties and stability compared with organic dyes [2]. In addition, QDs can be modified to allow for better targeting of tumors or to combine them with therapeutic compounds, developing a theranostic (therapy + diagnostics) platform.

In this work, we investigated the potential use of carboxylated $CuInS_2$/ZnS QDs for cancer diagnostics. These QDs are free of toxic heavy metals, such as cadmium or lead, thus being better suited for biological applications. Optical and morphological properties of $CuInS_2$/ZnS QDs, as well as their stability in different media, were investigated. We also studied their accumulation in cancer cells, their effect on cell viability and overall biocompatibility. U87 glioblastoma cell line was selected for these experiments, as diagnostics and treatment of brain tumors using optical methods still remain a challenge. The main obstacle is the difficulty of transporting dye molecules through the blood-brain barrier (BBB). QDs could be used to overcome this problem, as they can be modified to allow easier passage through the BBB [3]. Results of the experiments show the potential of $CuInS_2$/ZnS QDs as agents for cancer diagnostics.

[1] F. Vasefi, N. MacKinnon, D. L. Farkas and B. Kateb, Review of the potential of optical technologies for cancer diagnosis in neurosurgery: a step toward intraoperative neurophotonics, Neurophotonics **4**, 011010 (2016).
[2] K.J. McHugh, L. Jing, A.M. Behrens et al., Biocompatible Semiconductor Quantum Dots as Cancer Imaging Agents, Advanced Materials **30**, 1706356 (2018).
[3] Y. Liu, J. Liu, J. Zhang et al., Noninvasive Brain Tumor Imaging Using Red Emissive Carbonized Polymer Dots across the Blood–Brain Barrier, ACS Omega **3**, 7888–1896 (2018).

CANCELLED DUE TO COVID-19

ACETAMINOPHEN AS A REGULATOR OF NEUTROPHILS' ROS AND RHS PRODUCTION

Veronika Reut[1], Daria Grigorieva[1]

[1] Department of Physics, Belarusian State University, Belarus
ReutVE@bsu.by

Acetaminophen (APAP) is a frequently prescribed over-the-counter drug to reduce fever and pain in the event of inflammatory process. As neutrophils are relevant cells in inflammatory processes, the putative interaction of APAP with these cells or with reactive oxygen (ROS) and halogens (RHS) species, produced by them, is of a great importance [1]. As oxidative stress is due to primary antioxidant deficiency or to excess production of ROS, attention should aim to scavenge ROS or to inhibit their production [2]. The present study was undertaken to evaluate the effect of APAP in human neutrophils' superoxide ($\bullet O2^-$) and hypochlorous acid (HOCl) production.

In previous studies it was shown that gallocyanine (GC) and celestine blue B (CB) dyes are sensitive sensors of "turn-on" type to $\bullet O2^-$ and HOCl-derivatives production respectively [3].

Sodium citrate, phorbol 12-myristate 13-acetate (PMA), N-formyl-met-leu-phe (fMLP), GC, CB, APAP were obtained from "Sigma", USA; dextran T70 – from "Roth", Germany; histopaque – from "Nycomed", Norway; others – from "Reachem", Russia and "Belmedpreparaty", Belarus. Neutrophils were isolated from venous blood of healthy donors as described elsewhere [4]. Cells were suspended in a phosphate buffered saline (PBS) containing 10 mM Na2HPO4/KH2PO4, 137 mM NaCl, 2.7 mM KCl, 0.9 mM CaCl2, 0.5 mM MgCl2, 5 mM D-glucose (pH 7.4) and stored at 4 ºC. Changes in fluorescent characteristics of GC (5 μM in PBS, λex.=360 nm, λem.=490 nm), CB (20 μM in 20 % water glycerin solution, λex.=460 nm, λem.=590 nm) were registered on a spectrofluorimeter CM 2203 "Solar" (Minsk, Belarus). Oxidation rate (v), defined as the slope of the initial linear portion of the fluorescence intensity curve, and reaction amplitude (h), defined as changes in fluorescence intensity of the solution compared to the background level at 7 min (for GC) or 15 min (for CB), were used to describe this process.

Data obtained in the complex study of 100 μM APAP effect on chemosensors fluorescent properties changes in suspensions of 50 nM PMA or 0.5 μM fMLP-activated neutrophils (1×10^6 cells/ml) are given in the table 1.

Table 1. Effect of 100 μM APAP on chemosensors fluorescent properties (% of stimulant effect, *$p < 0.05$ compared to stimulant effect).

stimulant	parametr	GC	CB	stimulant	parametr	GC	CB
fMLP	*v*, %	153±38	-	PMA	*v*, %	125±28	226±30*
	h, %	179±39*	-		*h*, %	129±11*	201±12*

The results presented in table 1 indicate that APAP at in vivo relevant therapeutic concentration enhance both $\bullet O2^-$ and HOCl production compared to the control (stimulant only) its well-known role of H2O2 scavenger. It is notably that in cell-free system APAP directly interacts with HOCl to produce chlorinated adducts as has been shown by increase of CB fluorescence intensity (data not shown). Based on our results, it follows that using CB method to test the activity of neutrophils in the presence of pharmacological preparations, it is necessary to take into account their possibility of modification with the formation of halogenated products that will directly interact with this dye. According to results undertaken, it is necessary to limit the concentration of the drug in plasma to those where the effect of the peroxide interceptor is strong, but there is no such accumulation of halogenated products (corresponding a single oral dose less than 1 gram).

This study was supported by Russian Foundation for Basic Research (19-54-04004) and Belarusian Republican Foundation for Fundamental Research (B18R-058).

[1] M. Freitas, V. M. Costa, D. Ribeiro et al., Acetaminophen prevents oxidative burst and delays apoptosis in human neutrophils, Toxicology Letters 219 (2), 170-177 (2013).
[2] N. D. Vaziri, B. Rodríguez-Iturbe, Mechanisms of Disease: oxidative stress and inflammation in the pathogenesis of hypertension, Nature Clinical Practice Nephrology 2 (10), 582-593 (2006).
[3] V. E. Lutsenko, D. V. Grigorieva, S. N. Cherenkevich et al., Fluorescent method for estiment neutrophils functional activity, Russian journal of biological physics and chemistry 3 (3), 612-618 (2018).
[4] I. V. Gorudko, A. V. Mukhortava, B. Caraher et al., Lectin-induced activation of plasma membrane NADPH oxidase in cholesterol-depleted human neutrophils, Archives of biochemistry and biophysics, 516, 173-181 (2011)

CANCELLED DUE TO COVID-19

ANTI-INFLAMMATORY PROPERTIES OF ARTEMISIA TILESII BIOTECHNOLOGICAL RAW MATERIAL

Oleksandr Ladan[1], Volodymyr Bessarabov[1], Galyna Kuzmina[1], Ganna Kharitonenko[1], Iryna Pashchenko[1], Nadiya Matvieieva[2]

[1] Department of Pharmaceutical Industry, Kyiv National University of Technologies and Design, Ukraine
[2] Laboratory of Adaptative Biotechnology of Institute of Cell Biology and Genetic Engineering NAS of Ukraine, Ukraine
o.ladan@kyivpharma.eu

CANCELLED DUE TO COVID-19

Plants that grow in extreme climatic conditions are a potential source of biologically active substances. Artemisia tilesii is a common herb in the Arctic Circle but has been virtually unexplored, making it a potential candidate for pharmaceutical use [1].

Artemisia tilesii seeds were used to induce in vitro culture. The seeds are stored in the seed bank of the Institute of Cell Biology and Genetic Engineering of NAS of Ukraine. Plants of Artemisia tilesii are cultured in vitro by hormone-free micropropagation [2].

The effect of Artemisia tilesii extract on the activity of 15-lipoxygenase in the reaction of enzymatic oxidation of linoleic acid was experimentally determined.

The studies were performed using a spectrophotometric method, recording an increase in the degree of absorption of the reaction mixture over time at a wavelength of 235 nm. This wavelength corresponds to the maximum absorption of the conjugated diene chromophore in a linoleic acid hydroperoxide molecule (molar absorption coefficient – 23 000 $M^{-1} \cdot cm^{-1}$) [3].

The activity of the enzyme was evaluated by the value of steady-state reaction rate (V_{st}) as the arithmetic mean of the three measurements with a deviation of not more than 5%.

The effect of Artemisia tilesii on the activity of 15-lipoxygenase was determined. The data obtained are presented in Figure 1 for concentrations of 25 μM, 50 μM and 100 μM Artemisia tilesii extract, respectively.

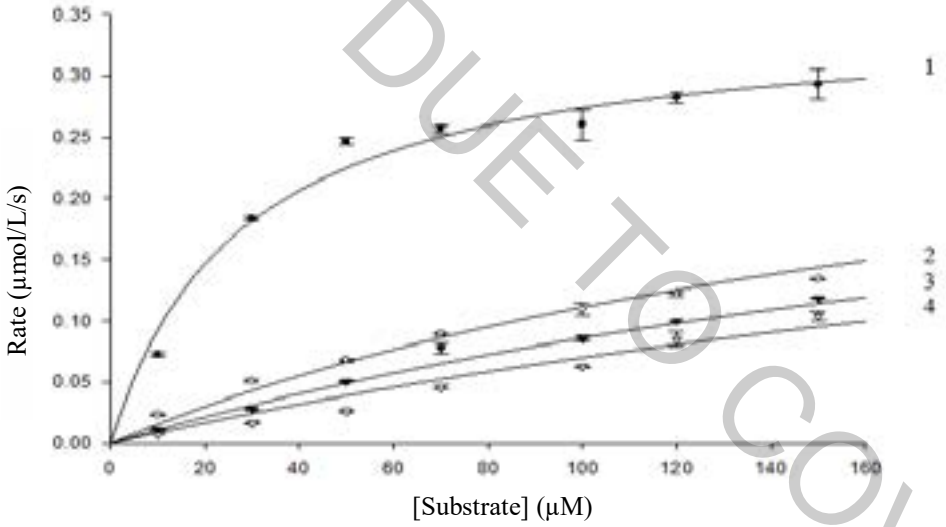

Fig. 1. Dependence of the steady-state conversion rate of the substrate by 15-lipoxygenase depending on the concentrations of the substrate without inhibitor (curve 1) and in the presence of Artemisia tilesii extract at concentrations of 25 μM (curve 2), 50 μM (curve 3), 100 μM (curve 4).

Conducted research have shown that Artemisia tilesii extract is an effective inhibitor of 15-lipoxygenase by a mixed (partial) inhibition mechanism. The results obtained suggest that Artemisia tilesii extract can be potentially used as an API for anti-inflammatory drugs because it has high efficacy as a 15-lipoxygenase inhibitor.

[1] Tunon M., Garcia-Mediavilla M., Sanchez-Campos S., Gonzalez-Gallego J. Potential of Flavonoids as Anti-inflammatory Agents: Modulation of Pro – Inflammatory Gene Expression and Signal Transduction Pathways. Current Drug Metabolism. 2009. Vol. 10, № 3. P. 256-271.
[2] Matvieieva N.A., Shakhovsky A.M., Belokurova V.B., Drobot K.O. Artemisia tilesii Ledeb hairy roots establishment using Agrobacterium rhizogenes-mediated transformation. Prep. Biochem. Biotechnol. 2016. Vol. 46, № 4. P. 342-345. doi: 10.1080/10826068.2015.1031393.
[3] Kharitonenko G.I., Skaterna T.D., Melnyk A.K. etc. Interaction of 5-lipoxygenase with an allosteric effector - sodium dodecyl sulfate. Ukrainian Biochemical Journal. 2008. № 3. P. 31–39.

SPECTROPHOTOMETRIC ANALYSIS OF PURE EXTRACTS AND THEIR FRACTIONS FROM DIFFERENT PARTS *OF ARTEMISIA DUBIA* WALL.

Dovilė Jurevičiūtė[1], Audrius Sigitas Maruška[1],Vita Tilvikienė[2], Aušra Bakšinskaitė[2]

[1]Instrumental Analysis Open Access Centre, Faculty of Natural Sciences, Vytautas Magnus University, Kaunas, Lithuania

[2] Lithuanian Research Centre for Agriculture and Forestry, Akademija, Kėdainiai distr., Lithuania

dovile.jureviciute@vdu.lt

Energy crops are crops that produce large amounts of biomass and belong to one of the fastest growing fields of alternative energy. However, some energy crops may not only be used for energy production but may exhibit antimicrobial, allelopathic, antioxidant or insecticidal properties and not all plants have been evaluated for such co-activity [1]. *Artemisia dubia* Wall. is one of the energy crops grown in Lithuania. The potential of this plant has not yet been fully disclosed, and it is very important to evaluate which plant compounds or fractions are associated with a particular activity [2]. Plants are known to adapt to the surrounding environment and have their own genotypes and chemotypes, so it is very important to evaluate the local *Artemisia dubia* Wall. biological activity in certain edaphoclimatic conditions.

The *main aim* of the study is to determine the total amount of phenolic compounds, total flavonoids and antiradical activity of different *Artemisia dubia* Wall. plant parts extracts and fractions, thus assessing the antioxidant properties of the plant.

A. dubia was collected from Akademija, Kedainiai district. (55.3896° N, 23.8624° E). Collected raw material was air-dried or frozen in Vytautas Magnus university in Kaunas. Collected raw material was ground to ca. 3-5 mm size fraction. The extracts were prepared using 0.5 g of dried raw or frozen material and 20 mL 75% methanol. Suspensions were left in a shaker for 24 h, and filtered afterwards using filtering paper. Modified spectrophotometric analysis methods were used: Folin-Ciocalteu reagent was used to determine total amount of phenolic compounds and $AlCl_3$ method was used to determine flavonoids and DPPH method was used to determine the antiradical activity of different plant parts extracts and fractions, which are obtained by solid phase extraction [3].

Spectrophotometric analysis showed that the total amount of phenolic compounds, total amount of flavonoids and antioxidant activity differed significantly between extracts of different parts of the plant. The experiment also showed that different amounts of phenolic compounds are released depending on the raw material preparation (air-dried or frozen).

The report will include an evaluation of total amount of phenolic compounds, flavonoids and antiradical activity of different plant parts and fractions by using solid phase extraction of the *Artemisia dubia* Wall. and a statistical analysis.

Acknowledgements:

This project was financed by Research Council of Lithuania project No. 09.3.3-LMT-K-712-16-0066.

[1] E Masarovičová, K Kráľová, M Peško, Energetic plants – cost and benefits, Ecological Chemistry and Engineering S , Vol. 16, No. 3 (2009).

[2] A. Kryževičienė, L. Šarūnaitė, V. Stukonis, Z. Dabkevičius, Daugiamečių kiečių (*Artemisia vulgaris* L. ir *Artemisia dubia* Wall.) potencialo biokuro gamybai įvertinimas. No. 1, p. 32–40 (2010).

[3] M. Stankevičius, I. Akuņeca, I. Jākobsone, A. Maruška, Analysis of phenolic compounds and radical scavenging activities of spice plants extracts, Maisto Chemija Ir Technologija, ISSN 1392-0227, T 44, Nr. 2 (2010).

CANCELLED DUE TO COVID-19

ROLE OF SCV-LA VIRUS IN TRANSPOSITION FREQUENCY OF YEAST *SACCHAROMYCES CEREVISIAE*

Gerda Skinderytė[1], Saulius Serva[1], Aleksandras Konovalovas[1]

[1]Department of Biochemistry and Molecular Biology, Vilnius University, Lithuania
gerda.skinderyte@gmail.com

Yeast *Saccharomyces cerevisiae* is one of the best understood eukaryotic model organisms. It is used for research of various biological processes like gene expression, cell cycle, metabolism and also for virus research. L-A-1 is a dsRNA yeast virus belonging to *Totiviridae* family, with unknown extracellular phase and not interfering with cell growth rate. Another endogenous yeast element is mobile genetic elements – transposons. Five families of transposons Ty1-Ty5 belonging to LTR-retrotransposons are known in yeast. In this work, interactions between L-A-1 virus and Ty1 retrotransposon and virus role in transposition were studied.

The transposition rates in yeast BY4741 strains carrying deletions of genes affecting L-A-1 virus replication cycle were tested using model plasmid, containing Ty1 transposon sequence and reporter gene. Range of mutant strains were analyzed along with control strain that possess the L-A-1 virus, and strain cured from the virus. The influence of transposition efficiency on L-A virus replication was tested by extracting and analyzing nucleic acids of BY4741 strains carrying deletions of genes coding for proteins known to affect the rate of transposition. It was established that the change of transposition efficiency does not influence replication of virus, whereas elimination of virus increases the rate of transposition. Also, two proteins modulating both the transposition and the replication of L-A virus were identified. The experiment design for new transposition rate test of higher efficiency suitable for wild type yeast strains was developed and a functional fluorescent reporter gene that will be used in the further development of method was constructed.

CANCELLED DUE TO COVID-19

PHYSICOCHEMICAL CHARACTERIZATION OF IMMOBILIZED LIPOLYTIC GDEST-LIP ENZYME AND ITS APPLICATION FOR TRANSESTERIFICATION REACTION

Agnė Savickaitė, Eglė Lastauskienė, Renata Gudiukaitė

Institute of Biosciences, Life Sciences Center, Vilnius University, Sauletekis ave. 7, LT-10257 Vilnius, Lithuania
agne.savickaite@gf.stud.vu.lt

Microbial lipases and esterases are highly used biocatalysts due to their particular characteristics such as the ability to utilize a wide range of substrates, high activity and stability in organic solvents, tolerance to broad pH and temperature ranges, regio- and/or enantioselectivity. These enzymes are currently being applied in a variety of biotechnological processes, including detergent preparation, cosmetics and paper production, food processing, biodiesel and biopolymer synthesis, and the biocatalytic resolution of pharmaceutical derivatives [1]. One of the reactions performed by these enzymes is transesterification, which is used in biodiesel production. Transesterification reactions involving lipolytic enzymes are suitable for biodiesel production due to the ability to more easily isolate glycerol, which is a by-product of the biofuel production process [1]. The major barrier to large-scale application of this system is the cost of producing lipolytic enzymes. The most important aspects of such biological tools are stability and reusability. Nowadays, immobilization of enzymes is commonly used to achieve these properties. One of the most effective enzyme immobilization techniques is enzyme entrapment in calcium alginate hydrogel.

In this study, immobilization conditions of GDEst-lip [2] enzyme were optimized. To achieve the most stable structure 3 % of sodium alginate and 150 mM of CaCl was used. The characteristics, including thermostability, substrate specificity and ability to catalyze reactions at different temperatures, were also evaluated. Transesterification reaction was performed using different oils and alcohols and obtained products were visualized using thin layer chromatography. Principal scheme of research is showed in Fig. 1.

This research is important for the future development of cost-effective immobilized enzyme systems that can be used in industry for transesterification or other by lipolytic biocatalysts performed reactions.

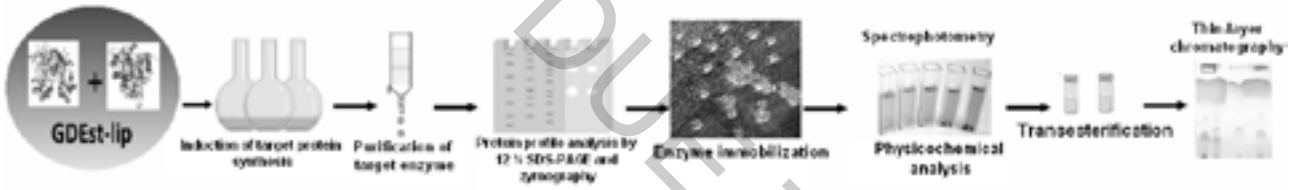

Fig. 1. Principal scheme of research.

Acknowledgment. This research was funded by the European Social Fund under the No 09.3.3-LMT-K-712 "Development of Competences of Scientists, other Researchers and Students through Practical Research Activities" measure, Grant No. 09.3.3.-LMT-K-712-16-0020.

[1] C. D. Anobom, A. S. Pinheiro, R. A. De-Andrade et al., From structure to catalysis: recent developments in the biotechnological applications of lipases, Biomed Res Int., 1-11 (2014).
[2] R. Gudiukaite, M. Sadauskas, A. Gegeckas et al., Construction of a novel lipolytic fusion biocatalyst GDEst-lip for industrial application, J Ind Microbial Biotechnol, 799-815 (2017).

CANCELLED DUE TO COVID-19

OPTICAL PROPERTIES ANALYSIS OF THE NATURAL PHOTOSENSITIZERS

Deimantė Purytė[1], Irina Buchovec[1], Pranciškus Vitta[1]

[1] Institute of Photonics and Nanotechnology, Faculty of Physics, Vilnius University, Lithuania
deimante.puryte@ff.stud.vu.lt

Usually bacteria prefer to live in the communities called biofilms. They could be found in industrial places, food facilities, water systems, hospitals and, also in spacecrafts.[1] It is known that biofilms are much more resistant to physical and chemical treatments, including antibiotics. Their resistance to antibiotics is an enormous problem in the world. Therefore, the development of alternative technologies could help to solve this problem. The one of promising approaches to treat biofilms is the use an antimicrobial photoinactivation (API). API is a modern biophotonic technology involving the employment of the photosensitizers (PS) that selectively accumulates in the target cells which are then illuminated. The interaction of PS and light, in the presence of oxygen results in a plethora of cytotoxic reactions and consequently, induces selective destruction of the target microorganism [2]. The efficacy of API is influenced by many factors but especially by physical and chemical properties of the PSs. For spacecraft applications it is necessary to use PSs which are chemically pure and water-soluble, with a stable shelf-life, not bleaching and easy to produce. This study focuses on natural PSs.

The first used PS was riboflavin (vitamin B2) (Fig. 1a) which plays an important role in the cell metabolism process and can be considered safe when administered to humans [3]. RF crystals have a yellow-orange color, whereas neutral solutions of RB have a green color. This is why they are used as the food coloring known as E101. Also, RF has been generally known to have antimicrobial properties. It is heat-stable but easily degraded by light, especially to UV irradiation. Therefore, light-induced activation of RF can selectively damage pathogen [4]. Although this PS belongs to the group of water-soluble vitamins it is, in fact, one of the least soluble in water (12 mg/100 mL at 25 °C).

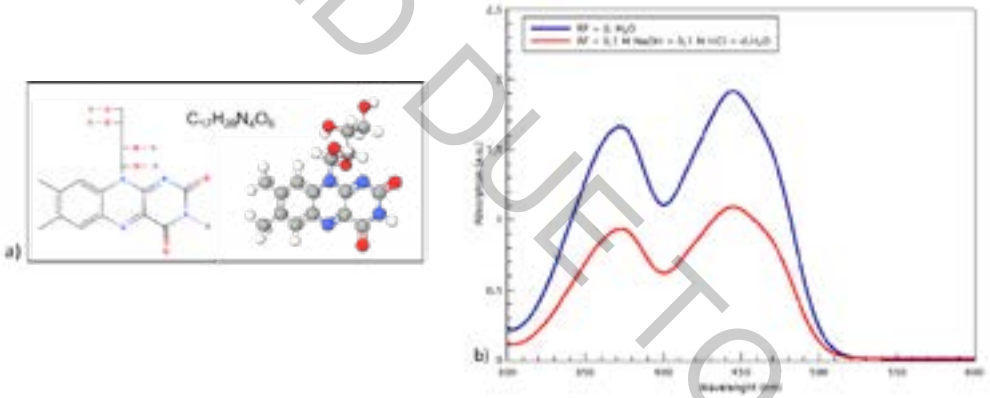

Fig. 1. a) Riboflavin chemical structure in 2D and 3D models; b) Absorption spectra of 10^{-4} M RF.

In the first stages of this work, we have prepared the aqueous solution of stock RF (concentration $10^{-4)}$. It was used two dissolution ways: 1) RF was agitated in distilled water (d. H_2O) on a magnetic stirrer at temperature 25 °C in the dark (pH~7); 2) RF was dissolved in the dark in a solution of 0,1 M NaOH, 0,1 M HCl and d H_2O (pH~7.2). The final analyzed concentrations of RF in both cases were from 10^{-6} to 10^{-4}. It is known that RF absorbance spectra have four maximums: 223, 267, 373, 444 nm [5]. We choose absorbance window from 300 nm till 600 nm because we were interested only in two peaks: 373 and 444 nm. The absorption measurements were recorded using a Perkin Elmer, Lambda 950, UV-Vis spectrometer at a spectral resolution of 0,05 nm. The concentration dependence of the absorption spectra of both RF solutions was investigated in this region. Unfortunately, 10^{-6} M concentration of RF was too low to obtain significant absorption results. However, at 10^{-4} M concentration in the first solution (dissolved in d. H_2O) RF molecules had about two times higher absorptions than in the second solution (dissolved in 0,1 M NaOH, 0,1 M HCl, d. H_2O) (Fig. 1b). Furthermore fluorescence and absorption spectra of RF in different buffers were measured, because their concentration and ionic strength have an important role in the photodegradation of RF in aqueous solution[5]. Along with the spectral-luminescence measurements, thermostability of PSs was analyzed. In conclusion we show that riboflavin is a promising candidate to be used as natural photosensitizer in spacecraft applications, but further investigation has to be performed.

[1] N. Høiby, "A short history of microbial biofilms and biofilm infections," *Apmis*, vol. 125, no. 4, pp. 272–275, 2017.
[2] T. G. S. Denis and M. R. Hamblin, "An introduction to photoantimicrobials : photodynamic therapy as a novel method of microbial pathogen eradication," in *Science against microbial pathogens: comunicating current research and technological advances*, 3rd ed., no. May, A. Mendez-Vilas, Ed. Formatex, 2011, pp. 675–683.
[3] T. Maisch *et al.*, "Fast and effective photodynamic inactivation of multiresistant bacteria by cationic riboflavin derivatives," *PLoS One*, vol. 9, no. 12, 2014.
[4] A. Ahgilan, V. Sabaratnam, and V. Periasamy, "Antimicrobial properties of vitamin B2," *Int. J. Food Prop.*, vol. 19, no. 5, pp. 1173–1181, 2016.
[5] M. A. Sheraz, S. H. Kazi, S. Ahmed, Z. Anwar, and I. A. Review, "Photo, thermal and chemical degradation of riboflavin," *Beilstein J. Org. Chem*, vol. 10, 2014.

SPIE-ED DUE TO COVID-19

PRODUCTION OF RECOMBINANT EXTRACLLULAR MATRIX MIMICKING PEPTIDES IN TOBACCO PLANT

Lukas Budginas[1], Rytis Rugienius[2], Jurgita Vinskienė[2], Danas Baniulis[2], Vidmantas Stanys[2]

[1] Vytautas Magnus University, Faculty of Natural Sciences, Kaunas
[2] Lithuanian Research Centre for Agriculture and Forestry, Institute of Horticulture, Babtai
lukas.budginas@vdu.lt

Application of the plant cultivation in the closed system (*in vitro*) technology for production of recombinant proteins provides a cost and product quality effective alternative as compared to traditional sources and it could be easily adapted for the large-scale industrial production [1]. Tobacco is one of the most popular plant-based expression systems, and it is widely used in producing antibodies, pharmaceutical and industrial proteins [2]. Composite mixtures of polymers and animal tissue specific extracellular matrix proteins – such as collagen, fibronectin, laminin – are being used for biomaterial production. However, specific functions of the extracellular matrix proteins could be readily reproduced using relatively short segments of their structure – peptides mimicking extracellular matrix. Therefore, aim of our research was to develop a closed type plant tissue cultivation system using tabaco plants (*Nicotiana tabacum*) dedicated for production for production of the recombinant peptide mimicking fibronectin typeIII domain 9-10 segments (FN9-10).

DNA construct with constant p35S promotor and t35S terminator was prepared and pDGB3_alpha1 based plasmid vector was developed using the GoldenBraid 2.0 cloning system. The construct included a green fluorescent protein (avGFP) marker for the recombinant protein expression analysis, polyhistidine (6xHis) tag for protein affinity purification and a cleavage site for the WELQut protease for the separation of target peptide (Fig. 1). Tobacco leave tissues were transformed using *Agrobacterium tumefaciens*. Selection of tabaco transformants was carried out using different concentrations of antibiotic. It was established that concentration of kanamycin and geneticin suitable for transformed callus tissue selection was 150mg/L and 40 mg/L, respectively. To eliminate agrobacteria, thimetin was used at 300 mg/L with no adverse effect on tabaco callus viability. Further, selection of transformed tabaco callus tissues was carried out based on fluorescence of the avGFP marker.

Expression of the recombinant peptide construct in different transformed callus and cell suspension lines was estimated quantitatively using a combined avGFP fluorescence and fluorescein diacetate based cell metabolic activity assay. Expression of recombinant FN9-10 fragments was further confirmed by immunoblot analysis using antibodies specific to the FN9-10 domain of fibronectin. Purification experiments were carried out and specific binding of the recombinant protein to the Ni-ion affinity matrix was demonstrated using fluorescence and immunoblot analysis.

Fig. 1. DNA construct used for tobacco plant transformation.

Acknowledgement:
This project was financed by Research Council of Lithuania project No. 09.3.3-LMT-K-712-16-0028

[1] Conley A.J., Zhu H., Le L.C., Jevnikar A.M., Lee B.H., Brandle J.E., Menassa R. Recombinant protein production in a variety of Nicotiana hosts: a comparative analysis. Plant Biotechnol. J. 9(4): 434–444 (2011).
[2] Colgan R., Atkinson C. J., Paul M., Hassan S., Pascal M. W. Drake, Sexton A. L., Santa-Cruz S., James D., Hamp K., Gutteridge C., K-C. Ma. J. Optimisation of contained *Nicotiana tabacum* cultivation for the production of recombinant protein pharmaceuticals. P. 241–256. DOI 10.1007/s11248-009-9303-y (2010).

ON REFERENCE TO COVID-19

GENERATION OF EFFECTIVE ENDOTHELIAL CELL POPULATIONS FOR MICROFLUIDIC TECHNIQUES

Karina Vitchyk, Anastasia Lapina, Andrey Demidov, Viktor Zhilkin, Gennady Fedorov, Vladimir Glotov

Department of Human Anatomy, Smolensk State Medical University, Smolensk, Russia
forssma@yandex.ru

Development of techniques for self-developing capillary endothelial networks in vitro [1, 2] has led to the nessecery for accelerated production of effective, diverse and mobile populations of free endothelial cells ex tempore for microfluidic biotechnical systems and platforms.

To solve this problem, a biotechnical platform can be proposed: an endothelial cell generator, that includes a hermetic container designed to accommodate an umbilical cord or other morphological formation with the connection of their hemocirculatory systems to the platform's circulation system.

After microsurgical implantation of the umbilical cord or other morphological formation, the hermocotainer is filled through one of the hermoports with a special nutrient mixture that provides long-term maintenance of vital processes in the biological object. Hermetic ports are also designed for controlled connection with the external environment and circulation of physiological fluids.

A peristaltic pump with a display control processor pumps special physiological fluid through the vessels of the umbilical cord or other morphological formation.

The processor-display module regulates and controls the speed and volume of the pumped liquid and displays information on the screen. The recirculating flask is intended for accumulation and buffering of the circulating liquid. The peristaltic pump selects the physiological fluid from the recirculating flask, pumps it through the vessels of the umbilical cord or other morphological formation, after which the liquid flows back into the recirculating flask. Then the process is repeated cyclically. During the working cycle of the platform, the dynamics of changes in the concentration of free endothelial cells is monitored and their identification is carried out.

The endothelial cell generator has a special interface for connecting external microfluidic biotechnical systems and platforms that implement technologies of self-developing capillary endothelial networks in vitro.

The proposed endothelial cell generator makes it possible to exclude the stage of obtaining a primary endothelial culture with classical methods from the biotechnological cycle of generating self-developing endothelial capillary networks in vitro. It greatly simplifies and reduces the cost of biotechnologies for obtaining artificial tissue-like formations with specified biological properties based on microfluidic technologies of self-developing endothelial capillary networks in vitro.

[1] Глотов В. А. Перспективы получения саморазвивающихся и функционирующих капиллярных сетей in vitro на основе клеточных культур эндотелия. //Стволовые клетки и перспективы их использования в здравоохранении. Материалы конференции (Приложение к журналу "Бюллетень экспериментальной биологии и медицины"). М.: Издательство РАМН, 2003. – С. 64-68.

[2] Sudong Kim, Hyunjae Lee, Minhwan Chunga, Noo Li Jeon. Engineering of functional, perfusable 3D microvascular networks on a chip Lab Chip, 2013,13, 1489-1500.

CRNFIELDOE TO COVID-19

MECHANISM OF EFFECTIVE QUENCHING OF CALCEIN FLUORESCENCE BY IRON. AB INITIO STUDY

Valentinas Černiauskas, Alytis Gruodis, Raminta Rodaitė-Riševičienė, Gintautas Saulis

Laboratory of Biophysics for Bionanotechnology and Medicine, Faculty of Natural Sciences, Vytautas Magnus University, Kaunas, Lithuania
valentinas.cerniauskas@vdu.lt

Cell electroporation – a temporal increase of the cell membrane permeability occurring due to the action of the pulses of strong electric field (up to 300 kV/cm) – is widely used in cell biology, biotechnology, and medicine [1]. When a high–voltage pulse is applied to the electrolyte solution, a variety of electrolysis reactions occur [2]. One of the most popular materials utilized for electrodes, which are used to electroporate the cells, is stainless–steel. In such a case, iron ions (Fe^{2+} and Fe^{3+}) are released from the anode under the action of high–voltage electric pulses. When a non-inert metal electrode is used, the release of the metal ions from the electrode into the solution occurs. These ions can, for example, react with fluorescent molecules and decrease the intensity of their fluorescence. Meanwhile, fluorescence microscopy is often used for studying cell electroporation phenomenon.

The aim of this study was to study the influence of the solution treated by high-voltage pulses and iron ions on the fluorescence of calcein as well as the mechanism of quenching.

[1] Andrei G. Pakhomov, Damijan Miklavcic, Marko S. Markov. Advanced Electroporation Techniques in Biology in Medicine. Boca Raton, FL: CRC Press. (2010) 124.
[2] Milazzo G. Electrochemistry: Theoretical Principles and Practical Applications. 1963. Elsevier, Amsterdam.

CANCELLED DUE TO COVID-19

GENERATION OF REACTIVE OXYGEN SPECIES INDUCED BY GOLD NANOCLUSTERS STABILIZED BY HUMAN BLOOD PLASMA PROTEINS

Gintarė Surplytė[1,2], Vilius Poderys[1], Vitalijus Karabanovas[1,2], Ričardas Rotomskis[1,3]

[1]Biomedical Physics Laboratory, National Cancer Institute, P. Baublio 3b, LT-08406 Vilnius
[2]Department of Chemistry and Bioengineering, Vilnius Gediminas technical university, Saulėtekio al. 11, LT-10223, Vilnius
[3]Biophotonics Group of Laser Research Centre, Vilnius University, Saulėtekio 9, LT-10222 Vilnius
gintare.surplyte@stud.vgtu.lt

CANCELLED DUE TO COVID-19

Gold nanoclusters (AuNCs) are promising luminescent nanomaterials which consist of several to tens of gold atoms. It's excitation causes the production of cytotoxic reactive oxygen species (ROS), such as hydroxyl radicals (•OH), superoxide anions ($O2^{\bullet-}$), singlet oxygen ($^1O_2$), which induce damage to cellular biomolecules in cancer cells what leads to its destruction [1]. Because of this property they are highly attractive for photodynamic therapy. Combining AuNCs and biomaterials like polymers and proteins can improve the therapeutic properties of nanoparticles, such as their biocompatibility, biodistribution, colloidal stability and lower toxicity. Capping nanostructures with human serum albumin (HSA) which is a non-toxic, stable and biodegradable protein might help to provide necessary properties.

Gold nanoclusters were synthesized according to the previously reported procedure [2] with slight modifications. Filtered and diluted human blood plasma (3,2 mL) was mixed with aqueous NaOH (320 µL, c = 1 M) and $HAuCl_4$ (c = 1,88 × 10^{-2} M, 1,8 mL) solutions and the reaction was allowed to proceed under vigorous stirring for 17 h at a temperature of 37 °C. Synthesis were carried out using human blood plasma containing rhesus negative (Rh-) or rhesus positive (Rh+) factor.

Photoluminescence spectrum of human blood plasma proteins stabilized gold nanoclusters solution (λ_{ex} = 405 nm) has two bands in the visible region: a main peak with a maximum at 641 nm and another band of lower intensity at 467 nm. Moreover, these gold nanoclusters show considerably longer lifetime (> 1 µs) than that of organic fluorophores (1-5 ns) [3]. Long lifetime of AuNCs is favorable condition for excited particle to interact with surrounding molecules like oxygen and generate reactive oxygen species.

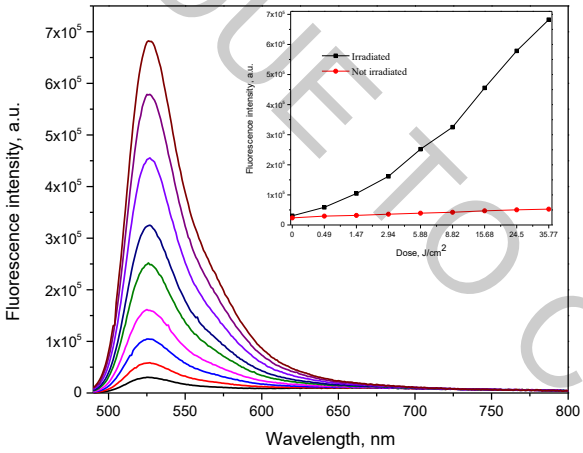

Fig.1. Fluorescence spectra of DHR123 and AuNCs stabilized by human blood plasma (Rh-) proteins mixture after irradiation with various doses (0 J/cm^2 to 35 J/cm^2) 405 nm light.

AuNCs potential to generate reactive oxygen species (ROS) was investigated using Dihydrorhodamine 123 (DHR 123). DHR 123 is a non-fluorescent dye that in the presence of reactive oxygen species is oxidized to fluorescent rhodamine. Fig. 1 presents spectra of AuNCs solution with DHR 123 after irradiation with various doses (0 J/cm^2 to 35 J/cm^2) of 405 nm light. Irradiation of solution increases intensity of rhodamine green fluorescence band while not irradiated solution doesn't show significant increase of signal. Observed DHR 123 fluorescence intensity increase was higher for AuNCs stabilized by human blood plasma (Rh-) proteins compared to AuNCs stabilized by human blood plasma (Rh+) proteins.

Our experiments show that AuNCs stabilized by human blood plasma during irradiation generates ROS and can be further investigated as potential photosensitive drugs for photodynamic cancer therapy.

[1] Misawa M., Takahashi J. 2011 Generation of reactive oxygen species induced by gold nanoparticles under x-ray and UV irradiations, *Nanomedicine* **7**(5), 604–614. DOI:10.1016/j.nano.2011.01.014;
[2] Xie J., Zheng Y., Ying J.Y. 2009. Protein-Directed Synthesis of Highly Fluorescent Gold Nanoclusters, *Journal of the American Chemical Society* 131(3): 888–889. DOI: 10.1021/ja806804u;
[3] An F., Zhang X. 2017. Strategies for Preparing Albumin-based Nanoparticles for Multifunctional Bioimaging and Drug Delivery, *Theranostics* 7(15). DOI: 10.7150/thno.19365.

INVESTIGATION OF MODIFIED SACCHAROMYCES CEREVISIAE USING AMPEROMETRIC AND IMPEDANCE SPECTROSCOPY METHODS

Vilius Aukscionis[1], Antanas Zinovicius[1], Aura Kisieliute[1], Almira Ramanaviciene[1], Arunas Ramanavicius[1,2]

[1] Vilnius University, Faculty of Chemistry and Geosciences, Vilnius, Lithuania
[2] State Research Institute Centre for Physical Sciences and Technology, Laboratory of Bio-nanotechnology, Vilnius, Lithuania
vilius.aukscionis@gmc.stud.vu.lt

Enzymes, antibodies, and whole cells can be employed in sensing and electrical current generating devices. Electrochemical systems utilizing biological components have some advantages compared to purely physical and chemical ones i.e. certain biological materials possess high binding specificity, can self-replicate, regenerate, self-assemble, etc., which are desirable characteristics when designing sensitive, long-lasting devices.

Saccharomyces cerevisiae (*S. cerevisiae*) is a species of single-celled fungi (yeast) that has great importance in science and the food industry, as it is one of the most studied eukaryotic model organisms and is instrumental in winemaking, brewing, and baking. Traits like fast replication, simple growth requirements, and high metabolic activity make *S. cerevisiae* a suitable candidate for bioelectrochemical research and applications.

However, bioelectrochemical systems have drawbacks, such as low efficiency, the need for electron transfer mediating substances, instability and sensitivity to changes in storage and operation conditions that prevent or complicate their practical use. Possible solutions to these problems are biological and/or electrical component modification and immobilization techniques e.g. conductive matrices.

In our study, we focused on yeast cell modification with an in situ polymerized polypyrrole [1], which is acknowledged for its conductivity and biocompatibility, and its effect on the system's electrochemical activity and impedance [2]. The polymer forms in proximity to the cell's membrane and in the cell's wall, which affects the cell's mechanical and electrical properties.

We used scanning electrochemical microscopy [3] to perform localized amperometric and electrochemical impedance spectrometric measurements of differently modified (varying pyrrole concentrations) *S. cerevisiae* cells using a dual electron transfer mediator system.

The variations in the mediator's reduced form in the suspension gave a measurable electronic signal from which electrochemical parameters could be calculated. This in turn demonstrated that there were changes in the electron transduction pathway due to the modification of the system/cells.

This project has received funding from European Social Fund (project No 09.3.3.-LMT-K-712-16-0286) under grant agreement with the Research Council of Lithuania (LMTLT).

[1] Andriukonis E, Stirke A, Garbaras A, Mikoliunaite L, Ramanaviciene A, Remeikis V, Thornton B, Ramanavicius A. Yeast-assisted synthesis of polypyrrole: Quantification and influence on the mechanical properties of the cell wall. Colloids and Surfaces B: Biointerfaces. 2018 Apr 1;164:224-31.

[2] He Z, Mansfeld F. Exploring the use of electrochemical impedance spectroscopy (EIS) in microbial fuel cell studies. Energy & Environmental Science. 2009;2(2):215-9.

[3] Morkvenaite-Vilkonciene I, Ramanaviciene A, Ramanavicius A. 9, 10-Phenanthrenequinone as a redox mediator for the imaging of yeast cells by scanning electrochemical microscopy. Sensors and Actuators B: Chemical. 2016 Jun 2;228:200-6.

CANCELLED DUE TO COVID-19

EVALUATION OF BIOLOGICAL ACTIVITY OF *PICEA ABIES* (L.) KARST SEEDS COLECTED IN LITHUANIA

Ieva Nekrošiūtė, Vilma Kaškonienė, Rūta Mickienė, Audrius Maruška

Instrumental Analysis Open Access center, Vytautas Magnus University, Lithuania
ieva.nekrosiute@stud.vdu.lt

*Picea abies (*L.) Karst is one of the most important forest trees in Europe, both economically and ecologically [1]. Studies show that *Picea abies* bark extracts exhibit different biological activity [2,3]. Stilbene glycosides, phenolic acids, aromatic compounds, free stilbenes and flavonoids are the main compounds detected in the bark of *Picea abies* [3]. It is possible, that other parts of the plant also have biologically active compounds. To our knowledge, the literature data about biological activity of *Picea abies* seeds are scarce.

Different biological activities have been evaluated in different plants, such as antioxidant, antibacterial, antifungal, anticancer, anti-inflammatory, allelophatic, etc. Various classes of chemical compounds are responsible for different actions. Antioxidants inactivate free radicals and protects the cells from the effects of oxidative stress [4]. Antimicrobial activity prevents microorganisms (bacteria, viruses, fungi) life-threatening effects [5]. Allelophatic, can identify the positive or harmful effect of one plant to another plant [6]. Phenolic compounds and flavonoids protect plants from different biotic and abiotic stresses and act as unique UV filters, signal molecules, allopathic compounds, phytoalexins, detoxicants and are antimicrobial defense [4, 7].

The aim of the study was to evaluate antioxidant, antibacterial and allelophatic activities of *Picea abies* (L.) Karst seeds extracts and their essential oils. Antioxidant activity in methanolic extracts and essential oils of the seeds were evaluated by spectrophotometric tests. Antibacterial activity methanolic extracts and essential oils were evaluated by agar well diffusion assay against three bacterial. Chemical composition of essential oil was determined by gas chromatography.

CANCELLED DUE TO COVID-19

[1] G. Caudullo, W. Tinner, D. de Rigo. European Atlas of Forest Tree Species. Publ. Of. EU, Luxembourg (2006).
[2] Z. Burčová, F. Kreps, P. Strižincová, A. Ház, M. Jablonský, I. Šurina, Š. Schmidt. Spruce bark as a source of antioxidant active substances. BioResources 14(3), 5980-5987. (2019).
[3] A. Bălaş, V. Popa. On characterization of some bioactive compounds extracted from *Picea abies* bark. Romanian Biotechnological Letters 12(3), 3209-3215(2018).
[4] N. F. Santos-Sánchez, R. Salas-Coronado, C. Villanueva-Cañongo, B. Hernández-Carlos. Antioxidant compounds and their antioxidant mechanism. Antioxidants, Emad Shalaby, IntechOpen, DOI: 10.5772/intechopen.85270 (2019). Available from: https://www.intechopen.com/books/antioxidants/antioxidant-compounds-and-their-antioxidant-mechanism
[5] B. Khameneh, M. Iranshahy, V. Soheili, B. S. Fazly Bazzaz. Review on plant antimicrobials: a mechanistic viewpoint. *Antimicrobial Resistance & Infection Control volume.* 8(118), 2047-2994 (2019).
[6] J. J. Ferguson, B. Rathinasabapathi, C. A. Chase. Allelopathy: How plants suppress other plants. UF/IFAS Extension, *HS944* (2016).
[7] A. N. Panche, A. D. Diwan, S. R. Chandra. Flavonoids: an overview. Journal of Nutritional Science 5, e47 (2016).

ELECTROPHYSIOLOGICAL TECHNIQUES REVEAL Cs^+ EFFECT ON ELECTRICAL SIGNALING IN MACROALGAE *NITELLOPSIS OBTUSA*

Vilmantas Pupkis, Indrė Lapeikaitė, Vilma Kisnierienė

Institute of Biosciences, Life Sciences Center, Vilnius University, Lithuania
vilmantas.pupkis@gmc.vu.lt

CANCELLED DUE TO COVID-19

Nitellopsis obtusa is a macroalgae found in fresh and brackish waterbodies. Its giant internodal cells (up to 30 cm in length) have been used in plant electrophysiology for decades, enabling thorough biophysical research of plant bioelectrical phenomena from investigations of single ion channel activity to cell-to-cell communication [1].

Nitellopsis cells, often called "green axons", are excitable [2]. Exposure to external stimuli of various modality (electrical, mechanical, termo- stimulation, salt stress) may evoke generation of action potentials, remarkably similar to those observed in animal cells. In plants, an over-threshold stimulus abruptly depolarizes cell plasmalemma by activating voltage-dependent Ca^{2+} and Ca^{2+}-dependent Cl^- ion channels, thus allowing Ca^{2+} ion influx and subsequent Cl^- ion efflux. Membrane repolarization is achieved by activation of voltage-dependent K^+ ion channels (K^+ efflux) as well as H^+-ATPase activity (H^+ efflux).

Our research aimed to investigate effect of Cs^+ ions (known to block K^+ channels [3]) on electrical signaling properties of *Nitellopsis obtusa*. Special attention was paid to repolarization phase of action potentials, since it is mainly governed by the activity of K^+ ion channels. *Nitellopsis* action potentials in single cell were registered using conventional sharp microelectrodes via current clamp technique. Voltage clamp technique enabled evaluation of dynamics of cell excitation current transients. Patch clamp technique was used to investigate activity of tonoplast (vacuolar membrane) K^+ ion channels.

It was confirmed that tonoplast K^+ ion channels are blocked by Cs^+ ions. Cs^+ ions substantially decrease velocity of repolarization of *Nitellopsis* action potentials and determine a characteristic shape. Unexpectedly, Cs^+ ions also increase amplitude of excitation current transient (Fig. 1). The results indicate that Cs^+ effect on electrical signaling patterns of *Nitellopsis obtusa* is complex and may involve altering activity of ion channels other than K^+ channels.

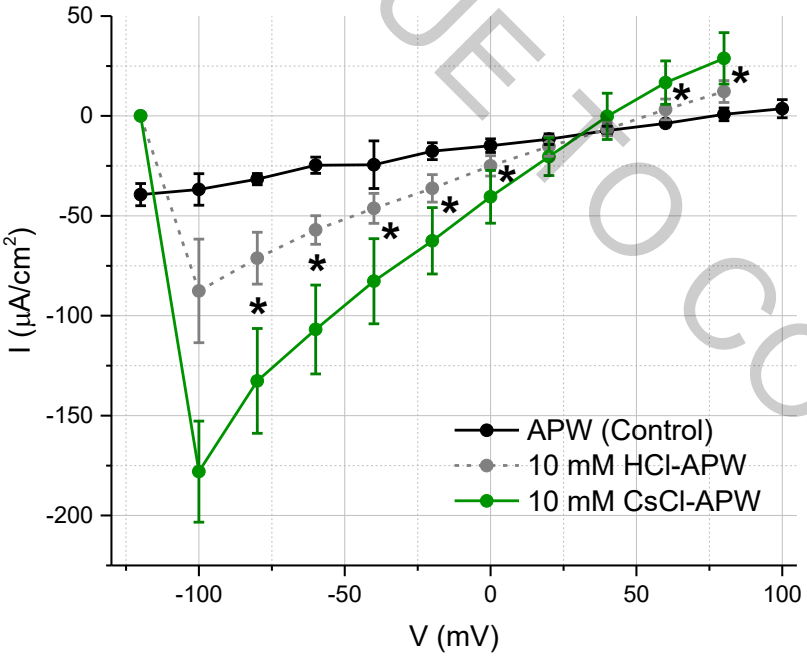

Fig. 1. I/V characteristics of excitation current transients of *Nitellopsis obtusa*. APW and 10 mM HCl-APW solutions were used as double control; 10 mM CsCl-APW solution significantly (asterisks indicate $p<0,05$) increased amplitudes of current transients during excitation.

[1] M. J. Beilby, M. T. Casanova. *The physiology of characean cells* (Springer Science & Business Media, 2014).
[2] P. R. Andjus. Harvesting the Biophysical Field of the "Green Axon." Iugosl. Physiol. Pharmacol. Acta. **34**: 1–9 (1998).
[3] G. Yellen. Ionic permeation and blockade in Ca^{2+}-activated K^+ channels of bovine chromaffin cells. The Journal of general physiology **84**(2): 157-186 (1984).

UPTAKE AND INTRACELLULAR LOCALIZATION OF $TPPS_4$ IN LIVING CELLS

Gabriele Agne Stasiukynaite[1,2], Greta Jarockyte[1,3,5], Marijus Pleckaitis[1,3,5], Saulius Bagdonas[3], Virginijus Barzda[3,4], Vitalijus Karabanovas[1,2,3], Ricardas Rotomskis[1,3]

[1]Biomedical Physics Laboratory of National Cancer Institute, P. Baublio 3B, LT-08406 Vilnius, Lithuania
[2]Department of Chemistry and Bioengineering, Vilnius Gediminas Technical University, LT-10223 Vilnius, Lithuania
[3]Biophotonics group of Laser Research Centre, Vilnius University, Sauletekio av. 9, LT-10222 Vilnius, Lithuania
[4]Department of Chemical and Physical Sciences, University of Toronto Mississauga, 3359 Mississauga Rd. N., Mississauga, ON L5L 1C6, Canada
[5]Life Sciences Center, Vilnius University, Sauletekio av. 7, LT-10257 Vilnius, Lithuania
gabriele-agne.stasiukynaite@stud.vgtu.lt

Meso-tetra(4-sulfonatophenyl) porphyrin ($TPPS_4$) is a synthetic water-soluble organic macrocycle compound, composed of a porphyrin ring (which consists of four pyrrole rings interconnected via methine bridges at their α carbon) and four sulfonatophenyl substitutes. $TPPS_4$ has been studied as a potential photosensitizer in photodynamic therapy (PDT) of cancer [1]. Due to its high triplet yield, this porphyrin is an efficient singlet oxygen generator. However, in an acidic environment, $TPPS_4$ tends to form J or H aggregates, which affect the optical and energetic properties by decreasing the quantum yields and lifetimes of excited singlet and triplet states [1]. J-aggregates have a low yield of generating reactive oxygen species. The aggregation properties of the dye also play a role in the accumulation and retention of the dye inside cells. Therefore, it is important to know the conditions at which such aggregates form. Recently, it has been predicted that $TPPS_4$ sensitizer has a potential application in non-linear microscopy (second and third harmonic generation).

This study aims to determine the localization and uptake of $TPPS_4$ in cells as well as to determine optical properties inside living cells. Some hydrophilic sensitizers are taken up by the endocytic pathway and are mainly localized in the lysosomes [2]. The initial experiment was carried out with embryonic mice fibroblast NIH/3T3 cells. After the addition of $TPPS_4$, the cells were cultivated for 24 h at 37°C, 5% CO_2. The results of confocal microscopy imaging showed that this sensitizer accumulates in vesicles around the nucleus of the cell and probably entered the cell *via* the endocytic pathway. $TPPS_4$ is distributed in a relatively uniform pattern inside the cells.

We recorded fluorescence spectra in living cells, when excited with 404 nm and 488 nm lasers, and showed that $TPPS_4$ molecules exist in a monomeric form inside NIH/3T3 cells. We compared $TPPS_4$ spectra measured inside the living cells with the spectra of the monomeric form of $TPPS_4$ in a solution (pH~7). We noticed that the peaks of the fluorescence spectra inside the cells have a shift of approximately 10 nm towards the longer wavelength of the spectrum. This is due to interactions between $TPPS_4$ and the biomolecules inside the cells.

We plan to carry out further experiments with tumor cells and perform live-cell imaging by using second and third harmonic generation microscopy, as well as PDT treatment after accumulation of $TPPS_4$ inside the cells. The study will validate a possibility of using $TPPS_4$ as a theranostic agent for targeted cancer therapy.

[1] L. P. F. Aggarwal and I. E. Borissevitch, On the dynamics of the TPPS 4 aggregation in aqueous solutions Successive formation of H and J aggregates, Spectrochim. Acta Part A **63**, 227–233 (2006)..
[2] W. S. L. Strauss, M. H. Gschwend et al, Intracellular fluorescence behaviour of meso-tetra(4-sulphonatophenyl)porphyrin during photodynamic treatment at various growth phases of cultured cells, J. Photochem. Photobiol. B Biol. **28** (2), 155–161 (1995).

CANCELLED DUE TO COVID-19

EVOLUTION OF SELF-ASSEMBLING $TPPS_4$ STRUCTURES. FROM NANO TO MACROAGGREGATES

Marijus Pleckaitis[1,2,3], Vitalijus Karabanovas[1,3,4], Saulius Bagdonas[3], Ricardas Rotomskis[1,3], Virginijus Barzda[3,5]

[1]Biomedical Physics Laboratory, National Cancer Institute, P. Baublio str. 3b, LT-08406 Vilnius, Lithuania
[2]Life Sciences Center, Vilnius University, Sauletekio av. 7, LT-10257 Vilnius, Lithuania
[3]Biophotonics group of Laser Research Center, Vilnius University, Sauletekio av. 9, LT-10222 Vilnius, Lithuania
[4]Department of Chemistry and Bioengineering, Vilnius Gediminas Technical University, Sauletekio av. 11, LT-10223 Vilnius, Lithuania
[5]Department of Chemical and Physical Sciences, University of Toronto Mississauga, 3359 Mississauga Rd. N., Mississauga, ON, Canada L5L 1C6
marijus.pleckaitis@nvi.lt

Meso-tetra (4-sulfonatophenyl) porphyrins ($TPPS_4$) are hydrophilic molecules, which under acidic conditions exist in zwitterionic forms and tend to self-assemble, forming J-aggregates. The formation occurs when positively charged porphyrin rings and negatively charged SO_3^- groups start interacting with each other [1]. Molecules of $TPPS_4$ are highly promising photosensitizers [2]. However, their tendency to aggregate in acidic environments might interfere with the photoreactivity and suppress their photosensitizing potential [3] and, thus, hindering their applicability for a photodynamic therapy. The aggregation, however, leads to enhancement of nonlinear optical response of $TPPS_4$ such as second and third harmonic generation. Recently, the nonlinear optical responses of $TPPS_4$ have been proposed for use as harmonophores, the labels for harmonic generation microscopy, in multimodal imaging applications of $TPPS_4$ J-aggregates.

In this study, we investigated the evolution of $TPPS_4$ J-aggregates and correlated their optical and structural properties. After dilution in water, $TPPS_4$ solution was prepared in 0.1 M of hydrochloric acid (to reach pH = 1). The beginning of J-aggregates formation and their continuous growth into bigger aggregates were followed by means of an atomic force microscopy and a laser scanning confocal fluorescence microscopy. Optical properties of J-aggregates were studied using absorption and fluorescence spectrometers, and applying fluorescence lifetime imaging microscopy.

The results showed that monomers of $TPPS_4$ porphyrins self-assemble into nanotubes and, given enough time, could form giant aggregates that are easily visible to the naked eye. Such giant aggregates appear as “sea urchin like” structures that can potentially be used in nanotechnology applications, for example as chiral templates for nanomaterials.

[1] Augulis R, Tamulienė J, Tamulis A, Rotomskis R. Theoretical Modeling of TPPS4 J-Aggregates. Solid State Phenomena. 2004.
[2] Wolfgang S.L. Strauss, Michael H. Gschwend, Reinhard Sailer, Herbert Schneckenburger, Rudolf Steiner, Angelika Rück, Intracellular fluorescence behaviour of meso-tetra(4-sulphonatophenyl)porphyrin during photodynamic treatment at various growth phases of cultured cells, Journal of Photochemistry and Photobiology B: Biology, Volume 28, Issue 2, 155-161, 1995.
[3] L. P. F. Aggarwal and I. E. Borissevitch, On the dynamics of the TPPS 4 aggregation in aqueous solutions Successive formation of H and J aggregates, Spectrochim. Acta Part A, 63, 227–233 (2006).

CANCELLED DUE TO COVID-19

AGGREGATION OF RECOMBINANT TAU PROTEIN ISOFORM 2N4R DEPENDENCE ON DIFFERENT ENVIRONMENTAL CONDITIONS

Lukas Krasauskas, Vytautas Smirnovas

Department of Biothermodynamics and Drug Design, Life Sciences Center, Vilnius University, Lithuania
lukas.v.krasauskas@gmail.com

Neurodegenerative diseases are one of the most widely spread disorders in the world. Sadly, despite the intensive research, the understanding of the disease mechanisms is quite moderate and all available therapies are only symptomatic. Alzheimer's disease has attracted the most of attention, because it is the most common disorder affecting around 50 million people worldwide and this number is expected to increase in the near future. It was determined that the neurofibrillary tangles formed from microtubule-associated protein Tau are the hallmark of this disease and other tauopathies. Therefore, it is imperative to understand the mechanisms affecting this process and to find the best way to tackle them. However, in order to carry out such experiments it is important to obtain Tau protein with good yield and purity. In this work, we used SUMO-fusion technology [1], to produce Tau isoform 2N4R, which allowed to reduce the time of purification and resulted in higher protein purity and yield.

For further experiments polyanion heparin has been used as amyloid-like protein aggregation inducer *in vitro*. In order to understand mechanism behind the complexity of protein Tau aggregation, different conditions were examined. Since protein Tau is classified as intrinsically disordered protein, the aggregation rate is highly dependent on different pH values changing its total net charge and solubility due to high proportion of polar and charged amino acids in protein sequence [2]. Further, high sodium chloride concentrations are expected to heavily affect aggregation rate [3]. Also, we presume that pre-formed protein Tau fibrils can induce aggregation without using polyanion heparin what would explain misfolding of monomeric protein Tau in healthy recipient neuron cells in the brains [4].

All performed aggregation kinetics were followed using Thioflavin T fluorescence assay at a range of recombinant Tau protein and heparin concentrations. Formed protein fibrils were imaged using atomic force microscopy.

[1] Peroutka III R.J., Orcutt S.J. et al., SUMO Fusion Technology for Enhanced Protein Expression and Purification in Prokaryotes and Eukaryotes, Methods in Molecular Biology (Methods and Protocols), Humana Press, vol 705 (2011).
[2] Tedeschi, G., Mangiagalli, M. et al., Aggregation properties of a disordered protein are tunable by pH and depend on its net charge per residue (2018).
[3] Goto, Y., Adachi, M. et al., Salt-induced formations of partially folded intermediates and amyloid fibrils suggests a common underlying mechanism, Biophysical reviews, 10(2), 493–502 (2018).
[4] Nizynski, B., Nieznanska, H. et al. , Amyloidogenic cross-seeding of Tau protein: Transient emergence of structural variants of fibrils, PloS one, 13(7) (2018).

CANCELLED DUE TO COVID-19

MODIFICATION OF ERYTHROCYTES UNDER THE ACTION OF CARBON NANOTUBES FUNCTIONALIZED BY POLYMERS

Alena Kavalenka, Alexei Svechko, Ekaterina Sobolevskaya

Department of Biophysics, Faculty of Physics, Belarusian State University, Belarus
ai0628k@gmail.com

Carbon nanotubes (CNTs) are promising systems for biomedical imaging, diagnostics, therapy and can be applied as a component of biosensors and implants. Thereby, it is necessary to study the effects of CNTs on various biological systems and such investigations underway in various research centres [1–5]. The different types of polymer molecules can be used to increase the dispersibility of CNT suspensions and other purposes. The aim of this work is to identify changes in the structure and properties of human erythrocytes exposed to CNTs functionalized by polymers.

Carboxylated multi-walled CNTs (MCNTs) with a length of about 1 μm and single-walled CNTs (SCNTs) with a length of about 400 nm synthesized by the CVD method were used (fig. 1, a). Polyethylene glycol (PEG, unionogenic hydrophilic polymer) and deoxyribonucleic acid (DNA, anionic polymer) were non-covalently attached to CNTs. Erythrocytes were isolated from healthy donor blood by washing in 0.15 M NaCl and suspended in Earl's balanced saline solution (pH 7.3). MCNTs-PEG or SCNTs-DNA were added into erythrocyte suspensions up to the final concentrations from 1 to 100 μg/ml and incubated at 37 °C. The geometric parameters of erythrocytes after treatment with CNTs were studied by nephelometry and light microscopy methods. The levels and type of hemoglobin in extracellular medium of erythrocytes were determined by analysis of absorption spectra at 380–700 nm. The kinetic dependencies of HCl-induced erythrocyte lysis were measured as the kinetic dependencies of light scattering intensity at an angle of 7° in order to evaluate deformability changes of the cells exposed to MCNTs-PEG or SCNTs-DNA.

Significant impact of MCNTs-PEG or SCNTs-DNA at concentration of 1 and 2.5 μg/ml on erythrocytes were not revealed. It was found that MCNTs-PEG and SCNTs-DNA at high concentrations of 5–100 μg/ml induce deformation and damage of erythrocytes and an increase of hemoglobin release into extracellular medium from cells. These changes were more significant at the highest concentration of CNTs. The partial transformation of oxy-form of hemoglobin to met-form has been detected at action of MCNTs-PEG but not at influence of SCNTs-DNA. The acceleration of acid lysis of erythrocytes was observed after preincubation of the cells with SCNTs-DNA at high concentrations (fig.1, b).

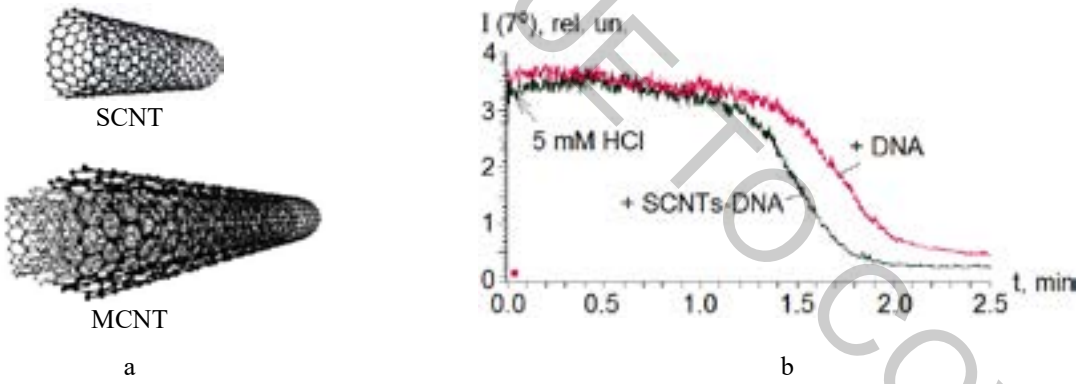

a b

Fig. 1. Illustration of single-walled and multi-walled CNTs (a) and kinetic dependences of the light scattering intensity of erythrocyte suspensions during HCl-induced cell lysis (b). SCNTs-DNA concentration was 5 μg/ml.

The obtained data indicate that SCNT-DNA and MCNT-PEG can have a cytotoxic effect on human erythrocytes. The cytotoxicity of CNTs against erythrocytes was also observed by other researchers [2–5]. Moreover, interaction of CNTs with cells is depends on their length and physical and chemical surface properties as was found in our research particularly.

[1] Z. Liu, et al., Carbon materials for drug delivery and cancer therapy, Materials today **14**, 316–323 (2011).
[2] V. Kumar, et al. Elucidation of in-vitro toxicity screening of carboxylated Multi-walled carbon nanotubes using red blood cells, Der Pharmacia Lettre. **8(4)**, 299–303 (2016).
[3] V. Yuvaraj, et al., Toxicity assessment of carbon nanotubes on erythrocyte morphology and lymphocytes in vitro, Asian J. Pharmac. Clinic. Res. **9(2)**, 278–280 (2016).
[4] Y. Heo, et al., Rheological alteration of erythrocytes exposed to carbon nanotubes, Clin. Hemorheology Microcirculation. **65(1)**, 49–56 (2017).
[5] S. Sachar, et al. Cytotoxic effect of poly-dispersed single walled carbon nanotubes on erythrocytes in vitro and in vivo, PLoS ONE. **6(7)**, e22032 (2011).

CANCELLED DUE TO COVID-19

EFFECTS OF MULTI-WALLED CARBON NANOTUBES ON NEUTROPHIL ACTIVITY IN VITRO

Alena Kavalenka, Ekaterina Sobolevskaya, Alexei Svechko, Tatsiana Kulahava

Department of Biophysics, Faculty of Physics, Belarusian State University, Belarus
ai0628k@gmail.com

Carbon nanomaterials (CNM) such as graphene oxide, carbon nanotubes, fullerenes and nanodiamonds have many promising applications in biomedical technologies [1–4]. The prospects for CNM using in biomedical applications depend on their ability to decompose in organism into products which can be easily eliminated from the body. When they enter the body, CNM interact with immune system parts including neutrophils which are the first cells involved in inflammatory reactions. It was found that the both types of phagocytes (neutrophils and macrophages) can implement slow enzymatic digestion of multi-walled and single-walled nanotubes (MCNTs and SCNMs) for a period of time exceeding several days [4–8]. The purpose of our work was to investigate the effect of carboxylated MCNTs *in vitro* on activity of human blood neutrophils in the first minutes and hours of their interaction. In order to improve the dispersibility, carbon nanotubes was modifies non-covalently by polyethylene glycol (unionogenic hydrophilic polymer) or deoxyribonucleic acid (anionic polymer).

Unactivated neutrophils have a rounded shape, but upon activation they adhere to the surface and spread out, increasing significantly in size (fig. 1, a). The shape of neutrophils upon activation changes greatly and these cells polarize and stretch (fig. 1, a). Neutrophil activation was evaluated by determining the relative content of activated cells (N_a) to the total number of cells in the sample (N) with the use of light microscopy method.

An increase in the number of polarized and spread out cells was observed as a result of MCNTs effect during the first hour (fig. 1, b). These findings indicate the activation of neutrophils under MCNTs.

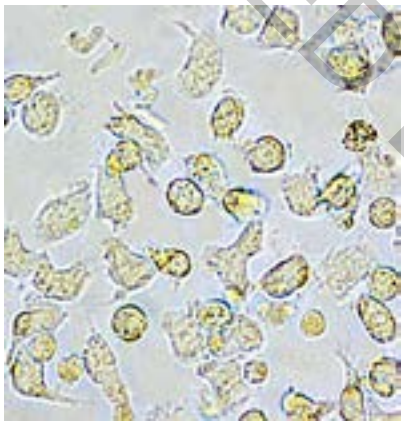

a

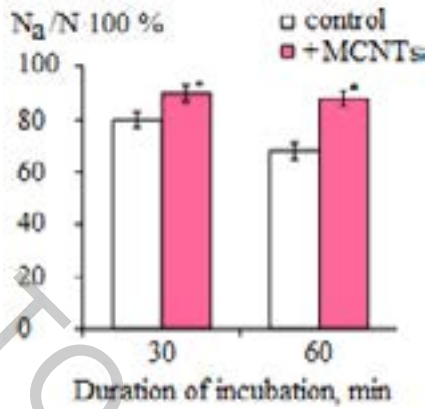

b

Fig. 1. Photograph of neutrophils activated by the chemoattractant fMLP (a) and the effect of MCNTs on the percentage of activated neutrophils in the samples according to the results of light microscopy (b)

An important indicator of neutrophil activation is the ability to generate reactive oxygen species (ROS), which was studied in the work by the method of luminol-dependent chemiluminescence. Luminol-dependent chemiluminescence of neutrophils is due to the involvement of the myeloperoxidase enzyme (MPO) in the reaction involving ROS. It should be noted that it is MPO that is considered as an enzyme capable of ensuring the destruction of CNTs [4–8].

It was found in our study that initial stimulation of neutrophil ability to generate ROS and luminol-dependent chemiluminescence occurs within 10-30 minutes under the influence of MCNTs. However, with a further increase in the duration of cell contacts with MCNTs, inhibition of neutrophil activity and a decrease in the total yield of ROS are observed.

The obtained data testify that MCNTs can have an initial stimulating effect and a later cytotoxic effect on human neutrophils.

[1] J. Simon, et al., Overview of carbon nanotubes for biomedical applications, Materials **12(4),** 624 (2019).
[2] Z. Liu, et al., Carbon materials for drug delivery and cancer therapy, Materials today, **14**, 316–323 (2011).
[3] M. Orecchioni, et al., Impact of carbon nanotubes and graphene on immune cells, J. Transl Med., **12**, 138 (2014).
[4] K. Bhattacharya, et al., Biological interactions of carbon-based nanomaterials: from coronation to degradation, Nanomedicine: Nanotechnology, Biology and Medicine, **12(2),** 333-351(2016).
[5] E. González-Lavado, et al., Biodegradable multi-walled carbon nanotubes trigger anti-tumoral effects, Nanoscale. **10(23)**, 11013-11020 (2018).
[6] I.I. Vlasova, et al., PEGylated single-walled carbon nanotubes activate neutrophils to increase production of hypochlorous acid, the oxidant capable of degrading nanotubes, Toxicol. Appl. Pharmacol., **264(1),** 131-142 (2012).
[7] C. Farrera, et al., Extracellular entrapment and degradation of single-walled carbon nanotubes, Nanoscale, **6**, 6974-6983 (2014).
[8] S. Keshavan, et al., Nano-bio interactions: a neutrophil-centric view, Cell Death. Disease, **10**, Article number: 569 (2019).

CANCELLED DUE TO COVID-19

NANOPARTICLES IN THE BIOLOGICAL ENVIRONMENT: COLLOIDAL STABILITY AND THEIR CELLULAR UPTAKE

Ksenija Godlevskaja[1,2], Evelina Voronovic[1,2], Artiom Skripka[3], Vitalijus Karabanovas[1,2], Fiorenzo Vetrone[3], Ricardas Rotomskis[1,4]

[1] Biomedical Physics Laboratory of National Cancer Institute, Baublio 3B, LT-08406, Vilnius, Lithuania
[2] Department of Chemistry and Bioengineering, Vilnius Gediminas Technical University, LT-10223 Vilnius, Lithuania
[3] National Institute of Scientific Research, University of Quebec, 1650, boulevard Lionel-Boulet, Varennes, Canada
[4] Biophotonics group of Laser Research Centre, Vilnius University, Sauletekio 9, c.3, LT-10222, Vilnius, Lithuania
ksenija.godlevskaja@stud.vgtu.lt

Upconverting nanoparticles (UCNPs) doped with trivalent lanthanide ions can convert near infrared excitation into ultraviolet, visible and shorter wavelength NIR light. For this reason, UCNPs are regarded as perspective agents for biolabeling, biosensing, theranostic, nanothermometry, solar cell, etc. [1]. UCNPs have many appealing optical and physicochemical properties that are necessary for biological applicability; such as – excitation with deep tissue penetrating light, imaging without autofluorescence, non-photobleaching and non-photoblinking, having sharp emission peaks, low toxicity, and being endowed with multifunctionality [2].

In order to use UCNPs in biomedicine it is very important to understand the effect of biological fluids on nanoparticles' (NPs) stability and biocompatibility. Immediately upon fusing with the cell growth media or corporal fluids, NPs associate with a variety of biomolecules, like proteins, following the so called "protein corona" formation. These nanoparticle-protein complexes may have generally positive effects as better accumulation in the cells, greater colloidal stability [3].

The aim of this study was to investigate the effects of human blood plasma on UCNPs, their colloidal stability, cytotoxicity and accumulation in the cancer cells.

In this work, colloidal stability of $LiYF_4$:Yb^{3+}, Tm^{3+} coated with citrate, phospholipids and silica, in biological medium was investigated using fluorescence spectroscopy. To provide a model system for the biological fluid, human plasma was added to a cell culture medium. In order to prevent plasma from clotting heparin was added to medium as well. For UCNPs biocompatibility and accumulation experiments human breast cancer MDA-MB-231 cell line was used. Cells were incubated for 24 hours with UCNPs and their viability was assessed by XTT assay. The uptake dynamics of UCNPs in cancer cells was evaluated by measuring emission of UCNPs accumulated in the cells. The qualitative evaluation of UCNPs accumulation in cells was assessed using confocal microscopy.

Research results show that silica and phospholipids coated $LiYF_4$:Yb^{3+}, Tm^{3+} NPs are more colloidally stable and possess greater accumulation rate in cancer cells than their citrate coated counterpart.

[1] M. K. Mahata et al., Photon-upconverting materials: Advances and prospects for various emerging applications, Luminescence: An Outlook on the Phenomena and their Applications, InTech (2016).
[2] H. Li et al., Recent advances of lanthanide-doped upconversion nanoparticles for biological applications, Nanotechnology **31**, 72001 (2019).
[3] V. H. Nguyen, B. J. Lee., Protein corona: a new approach for nanomedicine design, International Journal for nanomedicine **12**, 3137–3151 (2017).

CANCELLED DUE TO COVID-19

MINIATURE CRISPR-CAS SYSTEM CHARACTERIZATION

Greta Bigelyte[1], Tautvydas Karvelis[1], Joshua K. Young[2], Zhenglin Hou[2], Rimante Zedaveinyte[1], Karolina Budre[1], Sushmitha Paulraj[2], Vesna Djukanovic[2], Stephen Gasior[2], Arunas Silanskas[1], Česlovas Venclovas[1], Virginijus Siksnys[1]

[1] Institute of Biotechnology, Vilnius University, Vilnius, LT-10257, Lithuania
[2] Corteva Agriscience™ Agriculture Division of DowDuPont™, Johnston, IA 50131, USA
greta.bigelyte@bti.vu.lt

In recent years, CRISPR-associated (Cas) nucleases have revolutionized the genome editing field. Being guided by an RNA to cleave double-stranded (ds) DNA targets near a short sequence termed a protospacer adjacent motif (PAM), Cas9 and Cas12 offer unprecedented flexibility, however, more compact versions would simplify delivery and extend application. Here, we present a collection of 10 exceptionally compact (422-603 amino acids) CRISPR-Cas nucleases that recognize and cleave dsDNA in PAM dependent manner. Categorized as class 2 type V-F they come from the Cas14 family [1] and distantly related type V-U3 Cas proteins found in bacteria. Using biochemical methods, we demonstrate that a 5' T- or C-rich PAM sequence triggers double stranded (ds) DNA target cleavage [2]. Based on this discovery, we evaluated whether they can protect against invading dsDNA in *E. coli* and find that some but not all can. Altogether, our findings show that miniature Cas nucleases are functional CRISPR-Cas defense systems and have the potential to be harnessed as programmable nucleases for genome editing.

[1] Harrington LB, Burstein D, Chen JS, Paez-Espino D, Ma E, Witte IP, et al. Programmed DNA destruction by miniature CRISPR-Cas14 enzymes. Science. 2018 Nov 16;362(6416):839-842.
[2] Karvelis T, Bigelyte B, Young JK, Hou Z, Zedaveinyte R, Pociute K, Silanskas A, Venclovas Č, Siksnys V. PAM recognition by miniature CRISPR-Cas14 triggers programmable double-stranded DNA cleavage. BioRxiv 654897 [Preprint]. 2019 May 30 doi: https://doi.org/10.1101/654897.

CANCELLED DUE TO COVID-19

THE ROLE OF TARGET SEQUENCE LENGTH FOR DNA INTERFERENCE IN THE TYPE I-F CRISPR-CAS SYSTEM

Danguolė Norkūnaitė[1], Tomas Šinkūnas[1]

[1] Institute of biotechnology, Vilnius university, Lithuania
danguole.norkunaite@gmail.com

CRISPR (Clustered Regularly Interspaced Short Palindromic Repeats) – Cas (CRISPR Associated) is the immune system of bacteria or archaea that provides resistance against invasive genetic elements [1]. Proteins encoded by *cas* genes together with a mature crRNA molecule that carries a sequence (spacer) of extracellular nucleic acid origin form an effector complex, which destroys foreign nucleic acids [2]. In type I CRISPR-Cas systems, ribonucleoprotein complex, termed Cascade (CRISPR-associated complex for antiviral defence), recognises and binds intruding DNA, which has (i) a spacer-complementary sequence, named protospacer, and (ii) a protospacer adjacent motif (PAM). Cascade binding to DNA target triggers a Cas3 helicase/nuclease, which destroys the intruder [3].

In type I-E systems, Cascade-DNA target interaction is destabilised by mutations at the PAM distal end of the protospacer [4]. Otherwise, the influence of mutations at the protospacer distal end for a type I-F system, which is the phylogenetically closest for type I-E, was not yet investigated [5]. In this work, we show the importance of these nucleotides for interference in the type I-F system from *Aggregatibacter actinomycetemcomitans* D7S-1 bacteria. Mutations at the PAM distal end of the protospacer do not inhibit interactions between the Cascade complex and DNA target. Cascade complexes have a similar affinity for truncated protospacers and form R-loops the length of which depends on spacer-protospacer complementarity. However, R-loop of at least 32nt is necessary to trigger Cas2/3 protein for target DNA destruction.

[1] Barrangou, Boyaval, P. *et al.* (2007) 'CRISPR Provides Acquired Resistance Against Viruses in Prokaryotes', 315(March), pp. 1709–1713.
[2] Grissa, I., Vergnaud, G. and Pourcel, C. (2007) 'The CRISPRdb database and tools to display CRISPRs and to generate dictionaries of spacers and repeats', 10, pp. 1–10. doi: 10.1186/1471-2105-8-172.
[3] Koonin, E. V, Makarova, K. S. and Zhang, F. (2017) 'Diversity, classification and evolution of CRISPR-Cas systems.', *Current opinion in microbiology*, 37, pp. 67–78. doi: 10.1016/j.mib.2017.05.008.
[4] Rollins, M. F. *et al.* (2017) 'Cas1 and the Csy complex are opposing regulators of Cas2/3 nuclease activity', *Proceedings of the National Academy of Sciences*, 1, p. 201616395. doi: 10.1073/pnas.1616395114.
[5] Szczelkun, M. D. *et al.* (2014) 'Direct observation of R-loop formation by single RNA-guided Cas9 and Cascade effector complexes', 111(27). doi: 10.1073/pnas.1402597111.

CANCELLED DUE TO COVID-19

CRISPR-CAS EFFECTOR COMPLEX OPTIMIZATION FOR SINGLE MOLECULE STUDIES

Konstanty Keda[1], Irmantas Mogila[1], Gintautas Tamulaitis[1], Virginijus Šikšnys[1]

[1]Institute of Biotechnology, Life Science Center, Vilnius University, Lithuania
konstanty.keda.kk@gmail.com

CRISPR-Cas systems provide prokaryotes with adaptive immunity against viral and plasmid-borne infections which are destroyed by associated effector complexes [1]. Streptococcus thermophilus Type III-A CRISPR-Cas effector complex, called StCsm, is composed of several protein subunits and a crRNA molecule which acts as a guide against foreign transcripts [2]. StCsm complex is activated upon binding to nascent RNA transcript: it begins to shred transcribed DNA and produce signaling molecules for associated effectors [3, 4]. However, molecular mechanism of StCsm regulation by RNA has not been elucidated. This problem could be tackled by delicate single molecule studies allowing to monitor effector complex interaction with nucleic acids in real time. It is absolutely necessary to produce homogenous StCsm sample for these experiments, yet heterologous expression in E. coli yields different StCsm complexes carrying crRNAs of different sizes. During this work we have tried two approaches to purify homogenous StCsm: by using self-cleaving ribozymes to obtain crRNA of desired length, and by employing size-exclusion chromatrography for complex selection. Our results indicate that we were able to purify StCsm containing a crRNA of a distinct length. This complex will be used for single molecule experiments.

[1] Makarova, K. S. et al. Evolutionary classification of CRISPR-Cas systems: a burst of class 2 and derived variants. Nat. Rev. Microbiol. 18, 67–83 (2020).
[2].Tamulaitis, G., Venclovas, Č. & Siksnys, V. Type III CRISPR-Cas Immunity: Major Differences Brushed Aside. Trends in Microbiology 25, 49–61 (2017).
[3] Niewoehner, O. et al. Type III CRISPR-Cas systems produce cyclic oligoadenylate second messengers. Nature 548, 543–548 (2017).
[4] Kazlauskiene, M., Kostiuk, G., Venclovas, Č., Tamulaitis, G. & Siksnys, V. A cyclic oligonucleotide signaling pathway in type III CRISPR-Cas systems. Science 357, 605–609 (2017).

CANCELLED DUE TO COVID-19

AMYLOIDOPHILIC MOLECULE INTERACTIONS ON THE SURFACE OF AMYLOID FIBRILS : COOPERATIVE BINDING AND FLUORESCENCE QUENCHING

Kamilė Mikalauskaitė, Mantas Žiaunys, Vytautas Smirnovas

Department of Biothermodynamics and Drug Design, Institute of Biotechnology, Life Sciences Center, Vilnius University, Vilnius, Lithuania
kamile.mikalauskaite@chgf.stud.vu.lt

CANCELLED DUE TO COVID-19

Protein aggregation into amyloid fibrils is associated with several neurodegenerative disorders, such as Alzheimer's, Parkinson's, or prion diseases [1]. Amyloid aggregates are formed by conformational changes in the native protein structure and subsequent elongation [2]. Amyloidophilic dye molecules, such as thioflavin-T (ThT) and Congo red (CR), which bind to grooves formed by beta-sheets on the fibril's surface or 8-anilinonaphthalene-1-sulfonic acid (ANS) – which binds to the fibril's hydrophobic regions, can be applied to track amyloid formation and in some cases, such as methylene blue, they can act as potential aggregation inhibitors [3-5]. The changes to dye fluorescence intensity or absorbance spectra are considered to be caused by an increase or decrease in the concentration of fibrils. However, this could be the result of how such molecules interact with the fibril's surface or with one another, leading to inaccuracies in amyloid assays. In this work, the interaction of amyloidophilic molecules on the surface of amyloid fibrils was investigated using absorption and fluorescence spectroscopy.

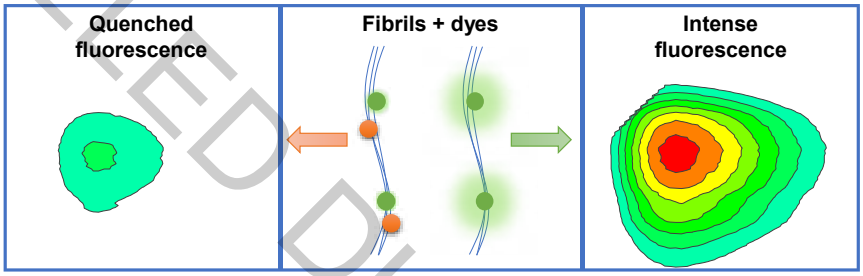

Fig. 1. Fluorescence quenching due to dye cross-interactions.

Insulin, lysozyme and mouse prion protein amyloid fibrils were prepared at 60°C. The absorbance spectra and excitation-emission matrices (EEM) of the samples were measured after mixing the fibrils, dye and PBS in the range from 200 to 800 nm. In many cases, amyloidophilic molecules, such as ThT, CR, Dapoxyl, ANS or MB assist each other in binding to amyloid fibrils, but this does not increase the fluorescence intensity of ThT, ANS, Dap. Often, there is a noticeable decrease in fluorescence (Fig. 1). Similar effect was observed using all three proteins.

[1] Chiti, F. & Dobson, C. M. Protein misfolding, amyloid formation, and human disease: a summary of progress over the last decade. Annu. Rev. Biochem. 86, 27–68 (2017).
[2] Eisenberg, D. ir Jucker, M. The Amyloid State of Proteins in Human Diseases. Cell 148, 1188–1203 (2012).
[3] Buell, A. K., Dobson, C. M., Knowles, T. P. J. ir Welland, M. E. Interactions between Amyloidophilic Dyes and Their Relevance to Studies of Amyloid Inhibitors. Biophys. J. 99, 3492–3497 (2010).
[4] Xue, C., Lin, T. Y., Chang, D. ir Guo, Z. Thioflavin T as an amyloid dye: fibril quantification, optimal concentration and effect on aggregation. R. Soc. Open Sci. 4, 160696 (2017).
[5] Yakupova, E. I., Bobyleva, L. G., Vikhlyantsev, I. M. ir Bobylev, A. G. Congo Red and amyloids: history and relationship. Biosci. Rep. 39, (2019).

SPECIFICITY OF THE ARGONAUTE PROTEIN FROM *ARCHAEOGLOBUS FULGIDUS* TO THE 5‘-END OF THE GUIDE

Mindaugas Zaremba, Elena Manakova, Edvardas Golovinas, Saulius Gražulis and Virginijus Šikšnys

Institute of biotechnology, Vilnius university, Lithuania
edvardas.golovinas@gmc.vu.lt

Argonaute proteins (Agos) are widespread in all three domains of life (bacteria, archaea and eukaryotes) [1]. In eukaryotic organisms, eAgos are the functional core of the RNA-silencing machinery, which is critical for regulation of gene expression, silencing of mobile genome elements, and defence against viruses. Prokaryotic Ago proteins (pAgo), in contrast, remain poorly understood and might hold a potential for development of novel genome editing tools, discovering new intracellular mechanisms and pathways.

In Agos, target recognition is facilitated by specific recognition of complementarity between the target and the Ago-bound strand (RNA or DNA). The 5’-end of the guide strand is anchored in the evolutionarily conserved pocked of the MID domain. eAgos and pAgos usually show a preference for a specific 5’-nucleotide of the guide strand (e.g. human Ago2 for a 5’-U, while bacterial TtAgo and CbAgo for a 5’-dC and 5‘-dA, respectively).

The Argonaute protein from an archaeaon *Archaeoglobus fulgidus* (AfAgo) has previously been well crystallographically characterized and provided initial information on the molecular mechanism of RNA interference (RNAi) in eukaryotes [2-5]. In this work we present biochemical and structural studies showing that AfAgo has specificity for a 5‘-dATT base pairs at the end of the DNA duplex, interacting with the nucleobases from both the guide and the target strands.

[1] Willkomm S, Makarova KS, Grohmann D. DNA silencing by prokaryotic Argonaute proteins adds a new layer of defense against invading nucleic acids. FEMS Microbiol Rev. 42(3):376-387 (2018).
[2] Parker JS, Roe SM, Barford D. Crystal structure of a PIWI protein suggests mechanisms for siRNA recognition and slicer activity. EMBO J. 23(24):4727-37 (2004).
[3] Ma JB, Yuan YR, Meister G, Pei Y, Tuschl T, Patel DJ. Structural basis for 5'-end-specific recognition of guide RNA by the *A. fulgidus* Piwi protein. Nature 434(7033):666-70 (2005).
[4] Parker JS, Roe SM, Barford D. Structural insights into mRNA recognition from a PIWI domain-siRNA guide complex. Nature 434(7033):663-6 (2005).
[5] Parker JS, Parizotto EA, Wang M, Roe SM, Barford D. Enhancement of the seed-target recognition step in RNA silencing by a PIWI/MID domain protein. Mol Cell. 33(2):204-14 (2009).

CANCELLED DUE TO COVID-19

ANTIFUNGAL ACTIVITY OF PYRIDINIUM COMPOUNDS IN COMBINATION WITH FLUCONAZOLE AGAINST *CANDIDA ALBICANS* PLANKTONIC CELLS AND BIOFILMS

Deimantė Galalytė, Neringa Kuliešienė, Simona Vaitkienė, Rimantas Daugelavičius

Department of Biochemistry, Vytautas Magnus University, Vileikos 8, Kaunas 44404, Lithuania
deimante.galalyte@vdu.lt

CANCELLED DUE TO COVID-19

Candida albicans (*C. albicans*) is a dimorphic pathogenic fungus which causes life-threatening candidemia and disseminated candidiasis [1]. Pathogenic fungi can form biofilms on medical catheters, implanted devices, heart valves, dentures and others, hereby protecting themselves with self-produced extracellular matrix and biofilm cells become resistant to antifungals [2]. *C. albicans* formed biofilms can develop highly resistance to a first-choice drug fluconazole, which is used to treat *C. albicans* infections [3]. Therefore, combined antifungal treatment is considered as a relevant tool.

Aim. To evaluate the synergistic antifungal effects of pyridinium compounds (IB-254, IB-358 and IB-385) in combination with fluconazole against *C. albicans* biofilms and planktonic cells.

Material and methods. The susceptibility of *C. albicans* standard strain ATCC® 10231™ and clinical strain 11017, isolated from patients' ascitic fluid was tested against combinations of fluconazole and pyridinium compounds. For planktonic cells studies the overnight culture was transferred to 96-well polystyrene plates with modified RPMI-1640 medium, supplemented with 2% glucose and L-glutamine, without sodium bicarbonate, and buffered with 0.165 M 4-morpholinepropanesulfonic acid (MOPS) to pH 7.0 in the presence of different concentrations of fluconazole (0,002 – 1 μg/ml) and constant concentration of pyridinium compounds (4 μg/ml of IB-254 and IB-358, 2 μg/ml of IB-385). The cells were incubated for 24 h without shaking at 37 ˚C. To assess the growth, ODs of planktonic yeast suspensions were measured spectrophotometrically at 612 nm using the TECAN GENios Pro™ plate reader.

For better adherence biofilms of *C. albicans* were developed in the medium without glucose in 96-well flat bottom polystyrene plates for 90 min at 37 ˚C, washed twice with PBS. Biofilms were grown for 24 h in the presence of tested compounds and their combinations. Metabolic activity of biofilm cells was determined using 2,3-bis(2-methoxy-4-nitro-5-sulfophenyl)-2H-tetrazolium-5-carboxanilide (XTT) assay.

Results. In case of fluconazole, 1 μg/ml efficiently inhibited the growth of planktonic cells of both *C. albicans* strains, while biofilms were more resistant. Fluconazole at concentration of 2048 μg/ml was not able to completely inhibit biofilm formation. Pyridinium compounds, at concentrations of 4 μg/ml for IB-254 and IB-358, 2 μg/ml for IB-385, had no significant fungicidal effect on the tested *C. albicans* cells. Whereas, in combination with a low concentration of fluconazole (4 μg/ml) pyridinium compounds demonstrated significant synergism against *C. albicans* biofilms and planktonic cells of standard and clinical strains.

Conclusions. Our study demonstrated that combination of pyridinium compounds with fluconazole is effective against *C. albicans*. Pyridinium compounds could be promising candidates in the development of new antifungal drugs.

---

[1] J. H. Lee, Y. G. Kim, V. K. Gupta, R. K. Manoharan, and J. Lee. Suppression of fluconazole resistant Candida albicans biofilm formation and filamentation by methylindole derivatives, *Front. Microbiol.* 9: 10 (2018).

[2] E. M. Scott, V. N. Tariq, and R. M. McCrory. Demonstration of synergy with fluconazole and either ibuprofen, sodium salicylate, or propylparaben against Candida albicans in vitro, *Antimicrob. Agents Chemother.*39: 2610–2614 (1995).

[3] C. Juin *et al.*, Anti-biofilm activity of a semi-synthetic molecule obtained from resveratrol against Candida albicans biofilm, *Med. Mycol. 00:* 1–13 (2019).

IDENTIFICATION OF AMINO ACIDS RESPONSIBLE FOR ACTIVITY OF THE HYDROLASE MO13 SELECTED FROM METAGENOME

Matas Tiškus[1], Nina Urbelienė[1], Audrius Laurynėnas[2], Rolandas Meškys[1]

[1]Department of Molecular Microbiology and Biotechnology, Institute of Biochemistry, Life Sciences Center, Vilnius Univesity

[2]Department of Bioanalysis, Institute of Biochemistry, Life Sciences Center, Vilnius University

matas.tiskus@gf.stud.vu.lt

CANCELLED DUE TO COVID-19

Unculturable microbiomes lead to the discovery of new genes, biocatalysts, natural compounds and bioproducts. Screening for novel enzymes that are capable of catalyzing new reactions is constantly needed because the discovery of new enzymes might provide new approaches for designing enzymatic processes.

During this study it was aimed to apply a site-directed mutagenesis for the hydrolase MO13, that was selected from metagenomics library on mineral agar plate with N^4-benzoyl-2'-deoxycytidine as the sole source of uridine. Bioinformatics analysis showed that the selected MO13 clone contained ORF sharing 56% sequence identity with the hypothetical alpha/beta hydrolase (WP_119118064.1) from *Bacillus asahii* belonging to the tannase/feruloyl esterase family. The sequence analysis together with the proteins tertiary structure prediction revealed three amino acids –aspartate 429, histidine 467 and Serine 195 as a potential catalytic triad. Further investigation using a site-directed mutagenesis confirmed that these amino acids were crucial for the enzymatic activity of MO13 hydrolase. This was proved *in vivo* using uridine auxotrophic *Escherichia coli* strain DH10B *ΔpyrFEC* and N^4-benzoyl-2'-deoxycytidine (the sole source of uridine) and *in vitro* with various substrates. The further site-directed mutagenesis targeting two amino acids (Ala146, Arg111) surrounding the proposed enzyme active center showed that the changes at these positions had effect on a substrate specificity of the hydrolase MO13. Changing of Ala146 amino acid to Trp (A146W) and Arg111 to Ala (R111A) strongly inhibited the enzymes ability to hydrolyze terephthalic acid derivatives such as *bis*(2-hydroxyethyl) terephthalate and dimethyl terephthalate. A146W mutant also lost its ability to hydrolyze capecitabine whereas R111A mutant still retained a weak activity towards this substrate.

ENZYME/PRODRUG SYSTEMS FOR CANCER TREATMENT

Greta Koženevska[1,2], Augustina Naciūtė[1,2], Karolina Kavaliauskaitė[1], Kamilė Butkutė[1], Daiva Tauraitė[1,2]

[1] Department of Molecular Biology and Biotechnology, Institute of Biochemistry, Life Sciences Center, Vilnius University, Lithuania
[2] Department of Chemistry and Bioengineering, Faculty of Fundamental Sciences, Vilnius Gediminas Technical University, Lithuania
greta.kozenevska@stud.vgtu.lt

Fluorouracil is a chemotherapy drug used to treat different cancers including breast, skin, stomach, pancreatic, bowel. However, at its therapeutic dose it causes significant side effects such as mucositis, myelosuppression, dermatitis, and cardial toxicity [1]. Due to these side effects, its application as prodrug in the form of fluorocytosine in combination with cytosine deaminase has gained attention in the past decades. The cytosine deaminase/5-fluorocytosine system is among the best explored enzyme/prodrug systems for cancer therapy [2]. In this system, 5-fluorocytosine, non-toxic prodrug, is converted to its active form 5-fluorouracil by cytosine deaminase activity. The use of this system has some drawbacks, such as the non-specific targeting of normal cells that are located in the vicinity of the tumor [3] and also the deleterious effects of 5-fluorocytosine to the organism ranging from minor side effects such as nausea, vomiting and diarrhea to serious ill-effects such as hepatotoxicity and bone-marrow depression have been reported in a number of clinical studies [4]. Recently, a new 5-fluoroisocytosine/isocytosine deaminase system has been proposed. This novel enzyme/prodrug pair alleviates the toxic side effects, and could be used as an improved the cancer therapy [5,6].

In this study, new promising enzyme/prodrug systems were investigated. We synthesized novel 5-fluorocytosine/isocytosine and uridine acylated derivatives as possible prodrugs and tested the ability of hydrolases to convert these compounds into the drug 5-fluorouracil (Fig. 1).

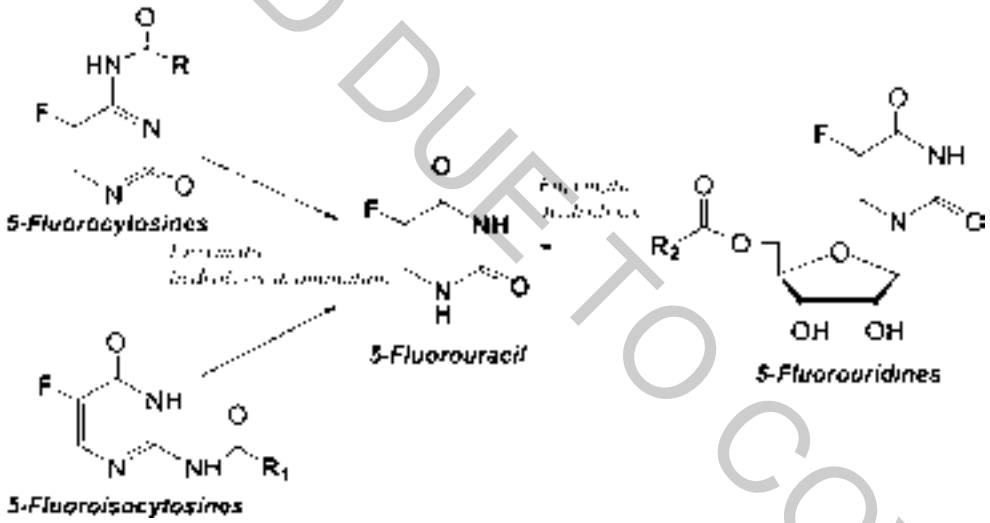

Fig. 1. Enzymatic conversion of inactive prodrugs into toxic drug 5-fluorouracil.

[1] O. M. Malekshah, X. Chen, A. Nomani et al., Enzyme/prodrug systems for cancer gene therapy, Curr. Pharmacol. Rep. **2**, 299–308 (2016).
[2] A. Raza, V. Kohila, S. S. Ghosh, Redesigned *Escherichia coli* cytosine deaminase: a new facet of suicide gene therapy, J. Gene Med. **17**, 132–139 (2015).
[3] V. K Yata, P. Gopinath, S. S. Ghosh, Emerging implications of nonmammalian cytosine deaminases on cancer therapeutics, Appl. Biochem. Biotechnol., **167**, 2103–2116 (2012).
[4] A. Vermes, H. J. Guchelaar, J. Dankert, Flucytosine: a review of its pharmacology, clinical indications, pharmacokinetics, toxicity and drug interactions, J. Antimicrob. Chemother., **46**, 171–179 (2000).
[5] A. Aučynaitė, R. Rutkienė, D. Tauraitė et al., Discovery of bacterial deaminases that convert 5-fluoroisocytosine into 5-fluorouracil. Frontiers in Microbiology **9**, 2375 (2018).
[6] A. Kazlauskas, A. Darinskas, R. Meškys et al., Isocytosine deaminase Vcz as a novel tool for the prodrug cancer therapy, BMC Cancer **19**, 197 (2019).

CANCELLED DUE TO COVID-19

RESPONSE OF OXIDATIVE STRESS AND NEUROTOXICITY BIOMARKER IN RAINBOW TROUT (*Oncorhynchus mykiss*) AFTER EXPOSURE TO SIX-METALS MIXTURES

Reda Nalivaikienė[1], Virginija Kalcienė[2], Laura Butrimavičienė[1]

[1] Nature Research Centre, Institute of Ecology, Akademijos Str. 2, LT-08412 Vilnius, Lithuania
[2] Vilnius University, Life Sciences Center, Institute of Biosciences, Saulėtekio av. 7, LT-10257 Vilnius, Lithuania
reda.eglinskaite@gamtc.lt

Heavy metals toxicity to aquatic organisms includes their ability to induce oxidative stress due to an imbalance between the production of reactive oxygen species and the activity of antioxidant defence system. Catalase (CAT) is one of the most important enzymes in the antioxidant defence system, which protects organisms from oxidative stress. Acetylcholinesterase (AChE) is a key enzyme in the nervous system and its activity is a widely used as biomarker of neurotoxicity in various organisms after different metals exposure [1, 2, 3]. Adverse effects of metals on the structure or function of the organism 's central or peripheral nervous system is described [4, 5], but it is still lacking information on the toxicity effects of metals mixtures.

The aim of this study was to assess two different biochemical parameters – liver CAT and brain AChE activity of rainbow trout (*Oncorhynchus mykiss*) after exposure for 7 and 14-days with: 1) six metals (Zn – 0.1, Cu – 0.01, Ni – 0.034, Cr – 0.01, Pb – 0.014 and Cd – 0.0015 mg/L) mixture (metals in a mixture were at maximum permissible concentrations (MPC) (2013/39/EB; 2008/105/EB)) and 2) the same six metals mixtures, with reduced concentration of Cu and Cr ions for 10 times, respectively.

The experimental treatment was conducted on one-year-old O. *mykiss*, acclimated fish were exposed for 7 and 14-days with six metals mixtures. After exposure rainbow trouts were dissected, brain and liver tissues for biochemical analysis were collected. Later in the laboratory the brain and liver tissues were homogenized and centrifuged for 20 min. at 15 000× g (4 °C). The supernatants were used immediately and were frozen at −80 ◦C for CAT and AChE assays, respectively. Total protein concentrations were determined according to the Bradford method [6] using bovine albumin as the standard. CAT activity was determined according to the method of Aebi [7] with minor modifications. CAT activity was calculated as μmol H_2O_2 decomposed/min/mg protein. AChE was determined using a modified Ellman method [8]. AChE activity was expressed in nmol of hydrolysed acetylthiocholine iodide/min/mg protein.

Statistically significant increase of catalase and acetylcholine esterase activity (26 % and 29 % respectively) was observed in rainbow trout (*Oncorhynchus mykiss*) after 7-days exposure to six-metals mixture at MPC. However, after 14-days treatment, neither CAT nor AChE did not show significant response to this mixture exposure. Six metals mixtures, where concentrations of Cu or Cr were reduced 10 times, inhibited liver catalase activity in the rainbow trout after 7 days exposure (20% for Cu and 22% for Cr, respectively). After 14-days treatment CAT did not showed significant response. The levels of AChE activity after 7 and 14 days of exposure, with reduced Cu or Cr ions concentrations in a mixture, did not vary significantly in comparison to control groups.

The results of present work suggest, that exposure for 7 and 14-days with six metals (Zn, Cu, Ni, Cr, Pb and Cd, metals are at MPC) mixture and with mixtures where Cu or Cr ions were reduced for 10 times, induce oxidative stress and neurotoxicity as metal's toxicity response in *O. mykiss* tissues. It's known that fish utilize enzymatic defence and cells are protected by an interacting antioxidant enzyme against oxidative stress [2, 3, 5]. In addition, the results provide evidence that enzymic biomarkers of oxidative stress and neurotoxicity can be sensitive indicators of aquatic pollution.

[1] M. Sevcikova, H. Modra, A. Slaninova, Z. Svobodova, Metals as a cause of oxidative stress in fish: a review, Veterinaria Medicina, 56 (11), 537-546 (2011).
[2] G. Souid, N. Souayed, F. Yaktiti, K. Maaroufi, effect of acute cadmium exposure on metal accumulation and oxidative stress biomarkers of *sparus aurata*, ecotoxicology and environmental safety, 89, 1-7 (2013).
[3] A. C. Elia, G. Magara, M. Righetti, A. J. M. Dörr, T. Scanzio, N. Pacini, M. C. Abete, M. Prearo,. Oxidative stress and related biomarkers in cupric and cuprous chloride-treated rainbow trout. Environmental Science and Pollution Research International, 24: 10205-10219, (2017).
[4] N. A. Ossana, B. L. Eissa, F. G. Baudou, P. M. Castañé, L. Ferrari, S. Soloneski, Multibiomarker response in ten spotted live-bearer fish Cnesterodon decemmaculatus (Jenyns, 1842) exposed to Reconquista river water, Ecotoxicology and environmental safety, 133, 73-81 (2016).
[5] K. C. C. Silva, C. R. D. Assis, V. M. Oliveira, L. B. Carvalho, R. S. Bezerra, Kinetic and physicochemical properties of brain acetylcholinesterase from the peacock bass (*Cichla ocellaris*) and *in vitro* effect of pesticides and metal ions, Aquatic Toxicology, 126, 191-197, (2013)
[6] M. M. Bradford A rapid and sensitive method for the quantitation of microgram quantities of protein utilizing the principle of protein-dye binding. Analytical Biochemistry, 72, 248-254, (1976).
[7] H Aebi, Catalase *in vitro*, Methods in Enzymology, 105, 121-126, (1984).
[8] G. L. Ellman, K. D. Courtney, V. J. Andres, R. M. Featherstone, A new and rapid colorimetric determination of acetylcholinesterase activity, Biochemical Pharmacology, 7, 88-95 (1961).

Acknowledgment: This study was funded by the Research Council of Lithuania through the project ACTIS S-MIP-17-10.

CORRECTED PROOF COVID-19

AB INITIO CONFDORMATIONAL AND ELECTRINIC STRUCTURE ANALYSIS OF INOSITOL PHOSPHATES

Wojciech Marciniak[1] , Joanna Marciniak[1], Karolina Olszewska[2]

[1] Institute of Physics, Faculty of Materials Engineering and Technical Physics, Poznan University of Technology, Piotrowo 3, 61-138 Poznań, Poland

[2]Institute of Materials Research and Quantum Engineering, Faculty of Materials Engineering and Technical Physics, Poznan University of Technology, Piotrowo 3, 61-138 Poznań, Poland

wojciech.robe.marciniak@doctorate.put.poznan.pl

Inositol phosphates fulfil plenty of roles in living cells, including regulatory purposes, as well as lower inositol phosphates, constituting a part of the metabolic cycle of legumes, beans, grain and other plants [1]. Myo-inositol hexakisphosphate and myo-inositol trispyrophosphate are considered good candidates for allosteric effector of haemoglobin, promising in threating hypoxia which can be a result of carcinogenesis or cardiovascular system malfunction [2].

Despite the fact of the undeniable importance of inositol phosphates, only a few recent results are discussing physical and chemical properties related to the evolution of molecules electronic structure and conformation in changing environment. The goal of the presented research is a determination of possible augmentation for red blood cell oxygen transport and lifecycle regulatory purposes [3], with particular attention to erythrocyte cell membrane permeability, as the band 3 protein, identified as the inositol phosphates transport channel, were proven to be highly selective [4].

In the presented study, a wide range of inositol phosphates are studied with the use of density functional theory. Theoretical calculations of conformational space of varying protonation states in standard generalised gradient approximation methods (PBE if applicable) from different computational codes are compared with Raman spectra of the molecules. Results are further validated by the comparison of thermodynamical and chemical parameters from molecular dynamics based on the derived model with known experimental values.

The work has been funded by Polish Ministry of Science and Higher Education under the grant DI2017/007947 in the Diamont Grant programme 2018 edition. We want to thank Marian W. Radny for valuable insights and suggestions.

[1] Frank, A. (2013). *Chemistry of plant phosphorus compounds*. Elsevier.

[2] Kieda C., Greferath R., Silva C.C.D., Fylaktakidou K.C., Lehn J.M. and Nicolau C. *Suppression of hypoxia-induced HIF-1α and of angiogenesis in endothelial cells by myo-inositol trispyrophosphate-treated erythrocytes*, PNAS, **103 (42)** 15576 (2006). doi:10.1073/pnas.0607109103.

[3] Kieda C., Hafny-Rahbi B.E., Collet G., Lamerant-Fayel N., Grillon C., Guichard A., Dulak J., Jozkowicz, A., Kotlinowski J., Fylaktakidou K.C., Vidal A., Auzeloux P., Miot-Noirault E., Beloeil J.C., Lehn J.M. and Nicolau C. *Stable tumor vessel normalization with pO2 increase and endothelial PTEN activation by inositol trispyrophosphate brings novel tumor treatment*. Journal of Molecular Medicine, **91 (7)** 883 (2013). doi:10.1007/s00109-013-0992-6.

[4] Fylaktakidou K.C., Lehn J.M., Greferath R. and Nicolau C. *Inositol tripyrophosphate: a new membrane permeant allosteric effector of haemoglobin*. Bioorganic & Medicinal Chemistry Letters, **15 (6)** 1605 (2005). doi:10.1016/j.bmcl.2005.01.064.

CANCELLED DUE TO COVID-19

HARNESSING THE DIVERSITY OF CAS9 ORTHOLOGS FOR GENOME EDITING

Tomas Urbaitis[1,3], Giedrius Gasiunas[1], Joshua K. Young[2], Monika Jasnauskaite[1], Mantvyda Grusyte[1], Sushmitha Paulraj[2], Jennifer L. Curcuru[4], Megumu Mabuchi[4], Ryan T. Fuchs[4], Ezra Schildkraut[4], G. Brett Robb[4] and Virginijus Siksnys[1,3]

[1] CasZyme, Vilnius, LT-10257, Lithuania
[2] Department of Molecular Engineering, Corteva Agriscience™ Agriculture Division of DowDuPont™, Johnston, IA 50131, USA
[3] Institute of Biotechnology, Vilnius University, Vilnius, LT-10257, Lithuania
[4] New England Biolabs, Ipswich, MA 01938, USA
tomas.urbaitis@gmc.vu.lt

The Cas9 protein from CRISPR (Clustered Regularly Interspaced Palindromic Repeats)-Cas (CRISPR Associated) bacterial defense systems has been adopted as a robust and multifaceted genome editing tool. The Cas9 RNA guided DNA endonuclease can be directed to cleave, nick or bind a specific site in the chromosomal DNA just by changing the guide RNA sequence. Cas9-based tools have been used to edit genomic DNA, modulate gene expression, visualize genomic loci in cells and deaminate nucleotide bases. However, for Cas9 to bind a given target, a short nucleotide sequence motif, termed PAM, is required. This PAM constraint as well as insufficient specificity are major obstacles for Cas9 genome editing. Thus, analysis of natural Cas9 orthologs could offer an increased diversity of PAM sequences and biochemical properties which may be beneficial to genome editing applications.

Cas9 nucleases are abundant in microbes. To explore this large uncharacterized diversity of Cas9 orthologs, we established a phylogeny-guided bioinformatic selection approach and developed biochemical screens based on cell-free recombinant protein expression and interrogation of plasmid libraries containing randomized PAM sequences for the rapid characterization of novel Cas9 proteins and identification of PAM requirements. Guide RNAs for each Cas9 ortholog were designed *in silico* by identifying putative tracrRNA (trans-activating CRISPR RNA) coding regions in respective native loci. The examined set revealed nucleases that exhibit a wide range of distinctive T-, A-, C- and G-rich PAM preferences, ranging from two to more than four nucleotides, as well as generate staggered-end breaks or require longer spacers to function robustly. Our results indicate that the natural diversity of Cas9 orthologs provides a source of various PAM recognition sequences and other potentially desirable properties that may be used to expand the genome editing toolbox.

CANCELLED DUE TO COVID-19

PROTEIN KINASE C SIGNALING IN STIMULATED MYOMETRIUM

Oleksii Fedorenko, Valentina Tararina , Olesya Moroz

ESC "Institute of Biology and Medicine", Taras Shevchenko National University of Kyiv, Ukraine
alefeoreno@gmail.com

Protein kinase C (PKC) is a family of Ca2+-activated phospholipid-dependent serine/threonine protein kinases which regulates a lot of crucial processes in various types of cells and in particular – calcium sensitization and contractility of smooth muscles [1]. PKC is supposed to participate in oxytocin (Ox) effect in myometrium [2] but rather few studies elucidate its role in pathophysiologal uterine contractions. Investigation of PKC effects was conducted to find out its role in Ox-induced contractions and hypotonic stress response with usage of its specific antagonist chelerythrine (Che).

Experiments were done on pregnant rat myometrium (18 -22 days of gestation) and human myometrium at term. Tissue samples were obtained from pregnant women near term during elective caesarian section. All volunteers gave written informed consent. All experiments on animals were also conducted in accordance to bioethics principals and the study was approved by the Institutional Ethics Committee for Research. Contractility was studied with isolated tissue bath method [3]. Myometrium strips were perfused in modified physiolological salt solution of normal and reduced (220 mOsmol/L) tonicity. Ox (10 nM, Sigma, USA) and Che (1 μM, Sigma, USA) were administered to the bath solution. Calculations and statistical analysis were made in Clampfit and OriginPro.

Effect of the PKC antagonist was studied by analyzing changes in several parameters of contractions – Peak Amplitude, Area under the curve, Half-width ($T_{1/2}$), Rise Tau and Decay Tau. When Che was used in combination with Ox all parameters were lower than those after oxytocin application only. Also in these experiments Peak Amplitude and Area under the curve that demonstrates the load developed by muscular strip were increased in comparison to control contractions. Similar changes have been observed for Rise and Decay Tau, indicating that the phase of contraction and relaxation were depressed under these experimental conditions, as can be seen in Figure 1.

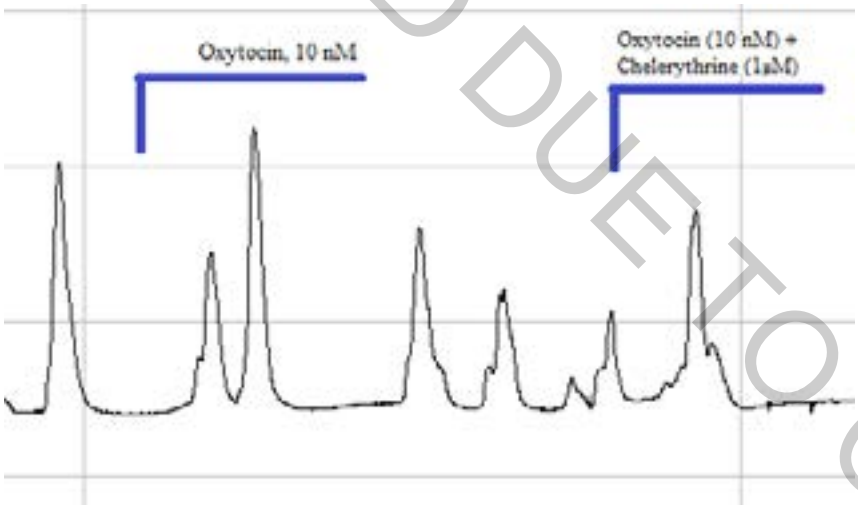

Figure 1. Contraction of human pregnant myometrium at term in response to Ox and under Ox together with Che.

Che under hypotonic solution showed light the elevation in Half-width, Rise Tau and Decay Tau and fall in Peak Amplitude and Area under the curve . Because these changes were not significant we can conclude that PKC pathway could hardly be considered to participate in contractile response to mechanical stretch.

Results demonstrate that PKC play the minor role in the process of hormonal regulation of myometrium contractility. The contractile response of myometrium to hypotonic stress is PKC-independent. .

[1] Chen, J., Zheng, D., Cui, H., Liu, S., Zhang, L., & Liu, C. (2017). Roles and mechanisms of TRPC3 and the PLCγ/PKC/CPI-17 signaling pathway in regulating parturition. Molecular Medicine Reports

[2] Arrowsmith, S., & Wray, S. (2014). Oxytocin: Its Mechanism of Action and Receptor Signalling in the Myometrium. Journal of Neuroendocrinology, 26(6), 356–369.

[3] Arrowsmith, S., Keov, P., Muttenthaler, M., & Gruber, C. W. (2018). Contractility Measurements of Human Uterine Smooth Muscle to Aid Drug Development. Journal of Visualized Experiments, (131).

CANCELLED DUE TO COVID-19

CAPACITY OF *IRPEX LACTEUS* TO DECOLORIZE VARIOUS TEXTILE DYES

Marius Žagunis[1], Nicola Tiso[1], Jurgita Mikašauskaitė[2], Audrius Maruška[1]

[1] Instrumental Analysis Open Access Center, Faculty of Natural Sciences, Vyautas Magnus university, Kaunas, Lithuania
[2]Department of Food Science and Technology, Faculty of Chemical Technology, Kaunas University of Technology Kaunas, Lithuania
marius.zagunis@vdu.lt

Synthetic dyes are often used because of their simplicity and color variety, although the increased usage of synthetic dyes creates worldwide environmental ecological problems. It has been estimated that during the manufacturing process of synthetic dyes a high amount of dye is lost and gets released into the environment as effluent [1]. Effluent containing textile dyes is particularly harmful, since a very small amount of dye is enough to cause a visible difference and that synthetic dyes often contain cancerogenic compounds [2]. Traces of dye should be processed and removed from the effluent before releasing it into the environment in order to minimize the damage caused. Traditional methods are quite ineffective or expensive which is why an alternative method for the removal of textile dyes is sought for. One of these methods is the use of microorganisms, in particular white rot fungi [3].

This study describes the ability of a Basidyomycetes fungi isolate - *Irpex lacteus* to decolorize various textile dyes of three different types: acid, reactive and direct. The ability of the isolate *Irpex lacteus* to biodegrade textile dyes in Petri dishes containing malt extract agar supplemented by textile dyes was evaluated during a 7-day incubation period [4]. It was determined that *Irpex lacteus* proved to be an efficient degrader of all the investigated types and colors of textile dyes within the 7-day period. Furthermore, the degradation ability of *Irpex lacteus* was quantitatively evaluated in liquid medium supplemented with textile dyes. The absorbance of the samples and the control were compared daily at a determined wavelength for each textile dye by means of UV-vis spectrophotometer [5]. It was determined that *Irpex lacteus* can degrade up to 99% of the textile dye contained in the liquid medium within 7 days after inoculation.

Acknowledgements: Financial support from Research Council of Lithuania project Nr. 09.3.3-LMT-K-712-16-0053 is acknowledged.

[1] M. Kaykhaii, M. Sasani, S. Marghzari. Removal of Dyes from the Environment by Adsorption Process. Chemical and Materials Engineering **6,** 31–35 (2018).
[2] P. Sathiya Moorthi, S. Periyar Selvam, A. Sasikalaveni et al., Decolorization of textile dyes and their effluents using white rot fungi. African Journal of Biotechnology **6** (4), 424–429 (2007).
[3] I. M. Banat, P. Nigam, D. Singh et al. Microbial Decolorization of Textile-Dye Containing Effluents: a Review. Bioresource Technology **58**, 217–227 (1996).
[4] F. Munari, T. A. Gaio, R. Calloni et al. Decolorization of textile dyes by enzymatic extract and submerged cultures of *Pleurotus sajor-caju*. World Juornal of Microbiology and Biotechnology **24** (8), 1383–1392 (2018).
[5] N. Šekuljica, N. Ž. Prlainovic, A.B. Stefanovic et al., Decolorization of Anthraquinonic Dyes from Textile Effluent Using Horseradish Peroxidase: Optimization and Kinetic Study. The Scientific World, 1–13 (2015).

CANCELLED DUE TO COVID-19

EVALUATION OF MICROORGANISMS, ISOLATED FROM BEES PRODUCTS

Aušrinė Venckaitytė, Vilma Kaškonienė, Rūta Mickienė, Audrius Maruška

Instrumental Analysis Open Access center, Vytautas Magnus University, Lithuania
ausrine.venckaityte@stud.vdu.lt

Beekeeping is one of the most important subjects of agriculture and economic well–being of human [1]. The products of bees are recognised worldwide for their positive effects on human health. The most important characteristic of propolis is that it has extremely strong bactericidal and disinfectant characteristics. It is used to cure colds, treat ulcer, wounds, frostbites and joints diseases [2]. Bee pollen on the other hand provides organism with nutrients such as B group vitamins, minerals and unsaturated fatty acids. It also helps to overcome metabolic problems, reduces the activity of harmful bacteria. Therefore, bee pollen is often referred to as "fully balanced food" or "life–giving dust" [3]. Bee bread strengthens immune and nervous systems, improves blood circulation, it is considered a potential source of polyunsaturated fatty acids in the human diet [4].

From the products of bees there has been isolated lactic acid bacteria (LAB). Bacterial genus, such as *Bacillus*, are found as the major bacterial genus that can be isolated from varieties of stingless bee species. Moreover, other bacterial genera including *Streptomyces*, *Clostridium*, *Staphylococcus*, *Enterobacter*, *Ralstonia*, *Pantoea*, *Neisseria*, *Pseudomonas*, *Lysinibacillus* and *Fructobacillus* also have be found associated with stingless bees [5]. It is very important because LAB produces natural antibiotics, so called bacteriocins, that gained a huge attention of the scientists in the last century, in order to reduce the usage of synthetic food additives [6]. Moreover, bacteriocins can increase phenolic compounds, antioxidant activity or produce volatile compounds during fermentation of medicinal plants [7]. Hence, the broad spectrum of antibacterial activity of bacteriocins makes it possible to use them as biological preservatives in many foods. The composition of bacteria depends on the objects, geographic location, and according to our data there are no such studies in Lithuania, so it is important to evaluate.

Research purpose is to isolate microorganisms from bee products (bee bread, bee pollen and propolis) and after obtaining results to check if metabolites of these microorganisms inhibit the growth of other bacteria.

CANCELLED DUE TO COVID-19

[1] Molan, P. C. Why honey is effective as a medicine. Its use in modern medicine. *Bee World*, **80**, 80-92 (1999).
[2] Paulino N., Coutinho L. A., Coutinho J. R., Vilela G. C., da Silva Leandro V. P., Paulino A. S. Antiulcerogenic effect of Brazilian propolis formulation in mice. *Pharmacology & Pharmacy*. 6(12):p. 580 (2015).
[3] Feás X., Vázquez-Tato M. P., Estevinho L., Seijas J. A., Iglesias A. Organic bee pollen: botanical origin, nutritional value, bioactive compounds, antioxidant activity and microbiological quality. 17(7):8359–8377 (2012).
[4] Kaplan M., Karaoglu O., Eroglu N., Silici S. Fatty Acid and Proximate Composition of Bee Bread. *Food Technol Biotechnol*. 54(4): 497–504 (2016).
[5] Ngalimat MS, Raja Abd Rahman RNZ, Yusof MT, Syahir A, Sabri S. Characterisation of bacteria isolated from the stingless bee, *Heterotrigona itama*, honey, bee bread and propolis. *PeerJ*. 7:e7478. (2019).
[6] Kaškonienė, V., Stankevičius, M., Bimbiraitė-Survilienė, K. *et al.* Current state of purification, isolation and analysis of bacteriocins produced by lactic acid bacteria. *Appl Microbiol Biotechnol* 101, 1323–1335 (2017).
[7] Bartkiene E, Mozuriene E, Juodeikiene G, Zadeike D, Maruska A, Stankevicius M, Ragazinskiene O, Cizeikiene D. Pork meat products functional value and safety parameters improving by using lactic acid fermentation of savory plants. *J Food Sci Technol* 52:7143-7152 (2015).

COMPARISON OF BEE POLLEN ANTIOXIDANT PROFILE AFTER ENZYMATIC HYDROLYSIS AND LACTIC ACID FERMENTATION

Vaida Adaškevičiūtė, Vilma Kaškonienė, Audrius Maruška

Instrumental Analysis Open Access Centre, Vytautas Magnus University, Lithuania
vaida.adaskeviciute@stud.vdu.lt

Bee pollen is one of the most popular product of natural origin, which is known and is used for thousand years for its nutritional and medicinal properties. Recently, this natural product gain a huge attention of the due to its chemical composition, therapeutic properties and possibilities of uses. However, pollen wall structure is resistant to the human digestion system and limited bioavailability is determined. New tendencies in food biotechnology induce to use fermentation or enzymatic treatments due to make products more usable. Also, these processes help to increase amount of nutrients, peptides, amino acids, probiotics and vitamins [1].

The aim of this study was to compare the effect of fermentation with lactic acid bacteria and enzymatic hydrolysis on bee pollen antioxidant activity. Nine samples of bee pollen from Sweden, Spain, Italy, The Netherlands, Poland, Lithuania, Denmark, Malta and Slovakia were fermented and hydrolyzed using lactic acid fermentation and enzymes, respectively. Three types of bee pollen treatment were performed: spontaneous fermentation, bacterial fermentation with *L. rhamnosus* and enzymatic hydrolysis (using Viscozyme L, Clara-diastase, lipase, protease, amyloglucosidase and cellulase enzymes). Total phenolic compound content, total flavonoid content and antioxidant activity were determined in the bee pollen extracts by spectrophotometric methods in order to evaluate amount of bioactive compounds [2, 3, 4]. The total content of phenolic compounds was measured using Folin–Ciocalteu reagent. The total flavonoid content analysis was carried out performing colorimetric reaction with aluminum chloride. Antiradical activity, characterized by the total radical scavenging activity, was measured using 2,2-diphenyl-1-picrylhydrazyl (DPPH) free radical. Also, the oxidation-reduction potential (ORP) was measured with platinum electrode using a standard multimeter [5].

Additionally, the fermentation process or enzymatic treatment helps to break the bee pollen wall and increase total phenolic, total flavonoid compounds content or antioxidant activity. The following conclusion of which type of treatment has the greatest potential in obtaining high available biologically active compounds will be presented during the conference.

CANCELLED DUE TO COVID-19

Acknowledgements:
This project was financed by Research Council of Lithuania project No. 09.3.3-LMT-K-712-16-0030.

[1] S. Yan, Q. Li, X. Xue, K. Wang, L. Zhao, L. Wu. Analysis of improved nutritional composition of bee pollen (*Brassica campestris* L.) after different fermentation treatments, International Journal of Food Science & Technology **54**(6), 2169-2181 (2019).

[2] V. Kaškonienė, A. Katilevičiūtė, P. Kaškonas, A. Maruška The impact of solid state fermentation on bee pollen phenolic compounds and radical scavenging capacity, Chemical Papers, 1-6 (2018).

[3] V. Kaškonienė, G. Ruočkuvienė, P. Kaškonas, I. Akuneca, A. Maruška, Chemometric analysis of bee pollen based on volatile and phenolic compound compositions and antioxidant properties, Food Analytical Methods **8**(5), 1150-1163 (2015).

[4] M. Stankevičius, I. Akuneca, I. Jakobsone, A. Maruška, Comparative analysis of radical scavenging and antioxidant activity of phenolic compounds present in everyday use spice plants by means of spectrophotometric and chromatographic methods, Journal of Separation Science **34**(11), 1261-1267 (2011).

[5] L. D. Mello, G. P. Quadros. Correlation between antioxidant activity and total phenolic content with physicochemical parameters of blended extracts of *Camellia sinensis*, Acta Scientiarum **36**, 97–103 (2014).

ENHANCEMENT OF BLEOMYCIN CYTOTOXIC EFFECT AND REGULATION OF GENE EXPRESSION USING SIMULTANEOUS PLASMID DNA AND BLEOMYCIN ELECTOTRANSFER

Aistė Rimgailaitė, Paulius Ruzgys, Sonam Chopra, Saulius Šatkauskas

Biophysical Research Group, Faculty of natural sciences, Vytautas Magnus university, Kaunas, Lithuania, aiste.rimgailaite@stud.vdu.lt

CANCELLED DUE TO COVID-19

Electrochemotherapy (ETC) is an effective physical technique that enables cytotoxic drugs to have direct access to the cytosol. This budding mode of therapy uses electroporation and anticancer drugs (mainly bleomycin) to trigger cell death in cancerous cells. At this moment, various methods are being explored to increase the impact of ETC, such as gene transfer.

Our preliminary studies have shown that plasmid DNA and bleomycin in the medium allows simultaneous transport of these molecules. In addition, we have shown that the presence of DNA in the medium can increase bleomycin transport and thereby cytotoxicity, whereas the presence of bleomycin may alter the strength and timing of gene expression. These effects can be used to increase the efficiency of ECT (due to more efficient BLM electrotransfer) and to regulate the immune response, by delivering genes, encoding specific cytokines.

In this work, the cytotoxicity effect of the electrotransfer of different concentrations of bleomycin and different size of plasmid DNA by using the same parameters of the electric pulses on Chinese Hamster Ovary cells was determined. Electroporation was performed by using combination of 1 electric pulse of 1400 V/cm pulse strength and 100 µs pulse duration. pMAX GFP (3.5 kb), pEGFP (4.7 kb) and piggyBac (7.1 kb) coding plasmids in concentrations of 200 µg/ml were used.

The obtained results showed that a combination of plasmid DNA, bleomycin, and electroporation increases the cytotoxic effect of the anticancer drug but achieves lower transfection efficiency. Further studies have shown that the cytotoxic effects of anticancer drug (BLM) and transfection efficiency are dependent on plasmid DNA size.

Acknowledgements: This project was financed by Research Council of Lithuania project No. 09.3.3-LMT-K-712-16-0146.

ESTABLISHMENT AND CHARACTERIZATION OF A NEW HUMAN PANCREATIC CANCER CELL LINE CAPAN-26

Eglė Žalytė[1], Kęstutis Strupas[2], Mindaugas Valius[1]

[1] Institute of Biochemistry, Proteomics Center, Vilnius University Life Sciences Center, Vilnius, Lithuania;
[2] Institute of Clinical Medicine, Clinic of Gastroenterology, Nephrourology and Surgery, Faculty of Medicine, Vilnius University, Vilnius, Lithuania
egle.zalyte@gmail.com

CANCELLED DUE TO COVID-19

Pancreatic ductal adenocarcinoma (PDAC) is one of the deadliest forms of human cancer. It is basically resistant to all mainstream cancer treatment modalities, such as chemotherapy and radiotherapy, and a surgical resection is effective for only 15-25% of patients [1]. A key to a successful therapy could be individualized treatment, which employs new pancreatic cancer cell lines, derived from patient tissue. Such lines represent a clinically relevant *in vitro* model of a tumor and can be used for drug testing.

In this study we present a new pancreatic cancer cell line Capan-26, which was derived from PDAC tissue of a 65-year old female Lithuanian patient. We determined cell doubling time and showed expression of E-cadherin and two PDAC markers CEACAM6 and CA19-9 in 2D and 3D Capan-26 culture. *Ras* sequencing detected a point mutation E76→K76, which is claimed to be oncogenic in both *in vitro* and *in vivo* PDAC models [2]. We believe that Capan-26 will be a valuable tool for human PDAC studies in the future.

[1] Goodman MD, Saif MW. Adjuvant therapy for pancreatic cancer. JOP : Journal of the pancreas. 2014; 15: 87-90

[2] Guo Z, Lu Y, Oakes S, Britton A, King T, Huang K, Tzenova V, Ferraro J, Apelian D, Franzusoff A. Trans-national patterns of pancreas cancer ras mutations and discovery of a new ras mutation with oncogenic synergy when found with ras codon 12 mutations. American Assotiation for Cancer Research. 2008; 14.

TRYPANOSOMA CRUZI CHAPERONE HSP90 AS A TARGET FOR CHAGAS DISEASE TREATMENT

Dovilė Daunoraitė, Marius Gedgaudas, Aurelija Mickevičiūtė, Egidijus Kazlauskas, Daumantas Matulis

Department of Biothermodynamics and Drug Design, Institute of Biotechnology, Vilnius University, Vilnius, Lithuania
dovile.daunoraite@gf.stud.vu.lt

Parasitic protozoan organisms contribute to the high burden of infectious diseases that are prevalent in both developing and developed countries and cause over a million deaths each year. *Trypanosoma cruzi*, which is the subject of our research, is the causing agent of Chagas disease, also known as American trypanosomiasis. The disease is characterized by cardiac, neurologic and digestive tract pathologies that can lead to sudden death. Although mostly widespread in Latin America, due to international immigration the disease threatens people living in other areas as well. Unwanted side effects of current drugs and the ability of parasites to quickly develop resistance mechanisms require new treatment options [1, 2].

Heat shock protein 90 (Hsp90) is a dimeric molecular chaperone, which is involved in many eukaryotic cell pathways ensuring proteostasis. The chaperone has a role in folding, maturation and degradation of select client proteins. As well as other protozoan parasites, *T. cruzi* relies on its functionality for survival, stage differentiation and adaptation to stressful conditions during infection. The fact that healthy human cells are significantly less sensitive to partial Hsp90 inhibition than parasitic protozoa makes it an attractive drug target for treatment of the Chagas disease [3, 4].

We aim to develop antiparasitic drugs based on Hsp90 inhibition. To achieve that, we first had to acquire a viable protein model for ligand binding assays. Since full length proteins are often difficult to obtain, we chose to work with isolated N-terminal domain of Hsp90, which binds ATP molecules and Hsp90-selective inhibitors of interest [5]. Fluorescence thermal shift assay was used to assess protein stability and determine binding affinities for the Hsp90 inhibitors.

[1] Fletcher, S. M.et al., Enteric Protozoa in the Developed World: A Public Health Perspective. *Clin. Microbiol. Rev.* 2012, *25* (3), 420–449.
[2] Sales Junior, P. A.et al., Experimental and Clinical Treatment of Chagas Disease: A Review. *Am. J. Trop. Med. Hyg.* 2017, *97* (5), 1289–1303.
[3] Shonhai, A.; et al., Intracellular Protozoan Parasites of Humans: The Role of Molecular Chaperones in Development and Pathogenesis. *Protein Pept. Lett.* 2011, *18* (2), 143–157.
[4] Schopf, F. H. et al.,The HSP90 Chaperone Machinery. *Nat. Rev. Mol. Cell Biol.* 2017, *18*, 345.
[5] Gewirth, D. T., Paralog Specific Hsp90 Inhibitors – a Brief History and a Bright Future. *Curr. Top. Med. Chem.* 2016, *16* (25), 2779–2791.

CANCELLED DUE TO COVID-19

CHARACTERIZATION OF TOXIN-ANTITOXIN SYSTEM IN THE VICINITY OF CRISPR-CAS OPERON

Inga Songailienė[1], Jonas Juozapaitis[1], Giedrė Tamulaitienė[1], Giedrius Sasnauskas[1], Audronė Rukšėnaitė[2], Virginijus Šikšnys[1]

[1]Department of Protein - DNA Interactions, Institute of Biotechnology, Life Sciences Center, Vilnius University, Lithuania
[2]Department of Biological DNA Modification, Institute of Biotechnology, Life Sciences Center, Vilnius University, Lithuania
jonas.juozapaitis@bti.stud.vu.lt

Bacteriophages (viruses of bacteria) represent a lethal threat to bacteria. In the course of evolution, microbes developed many tools to fight viral infections. CRISPR-Cas system in prokaryotes functions as an adaptive immune system that provides acquired resistance against invasive genetic elements like viruses or plasmids. CRISPR-Cas systems are very diverse and differ by gene arrangement and composition of the effector complex [1]. During recent years molecular mechanisms of CRISPR-Cas were established [2–6].

Auxiliary genes are found quite often in the vicinity of CRISPR-Cas systems; however, their role in the CRISPR-provided bacterial immunity remains unclear [1, 7].

The study aims to characterize a toxin-antitoxin (TA) module, located in the same operon with a Type I CRISPR-Cas system in cyanobacteria. The link between CRISPR-Cas and particular TA system is unknown, while biochemical and structural data on the TA system is also lacking.

Genes of interest were cloned in heterologous host *E. coli. In vivo* assays showed that the two-gene module forms an active toxin-antitoxin system. Protein expression conditions were optimized and proteins were purified from *E. coli*. Amino acids, critical for the function of the TA system, were determined both *in vivo* and *in vitro*. Finally, protein crystals, suitable for X-ray crystallography, were obtained. Collected data was sufficient to determine the ternary structures of the toxin and toxin-antitoxin complex.

[1] K. S. Makarova et al., Evolutionary classification of CRISPR–Cas systems: a burst of class 2 and derived variants, Nat. Rev. Microbiol. **18**, (2020).
[2] G. Gasiunas, R. Barrangou, P. Horvath, and V. Siksnys, Cas9-crRNA ribonucleoprotein complex mediates specific DNA cleavage for adaptive immunity in bacteria, Proc. Natl. Acad. Sci. **109**, E2579–E2586 (2012).
[3] T. Sinkunas et al., In vitro reconstitution of Cascade-mediated CRISPR immunity in Streptococcus thermophilus, EMBO J. **32**, 385–394 (2013).
[4] O. O. Abudayyeh et al., C2c2 is a single-component programmable RNA-guided RNA-targeting CRISPR effector, Science **353**, aaf5573 (2016).
[5] M. Kazlauskiene, G. Tamulaitis, G. Kostiuk, Č. Venclovas, and V. Siksnys, Spatiotemporal Control of Type III-A CRISPR-Cas Immunity: Coupling DNA Degradation with the Target RNA Recognition, Mol. Cell **62**, 295–306 (2016).
[6] W. X. Yan et al., Functionally diverse type V CRISPR-Cas systems, Science **363**, 88–91 (2019).
[7] S. A. Shmakov, K. S. Makarova, Y. I. Wolf, K. V. Severinov, and E. V. Koonin, Systematic prediction of genes functionally linked to CRISPR-Cas systems by gene neighborhood analysis, Proc. Natl. Acad. Sci. **115**, E5307–E5316 (2018).

CANCELLED DUE TO COVID-19

OPTIMIZATION OF CULTURE CONDITIONS FOR THE EXPRESSION OF MEMBRANE SCAFFOLD PROTEIN 1 FOR THE DESIGN OF DISCOIDAL PHOSPHOLIPID BILAYER NANOPARTICLES

Maryia Kisel[1*], Irina Haidukevich[1], Tatsiana Sushko[2], Andrei Gilep[1]

[1] Institute of Bioorganic Chemistry of the National Academy of Sciences of Belarus, Minsk, Belarus
[2]The Graduate School of Engineering, The University of Tokyo, 4-6-1 Shirokanedai, Tokyo 108-8639
marusenka95@iboch.by

CANCELLED DUE TO COVID-19

Membrane proteins account for 70 % of all known pharmacological targets and 50 % of potential new drug targets due to their direct involvement in a wide range of diseases, including diabetes, cancer and neurological disorders. As promising as the studies of membrane proteins are, it remains difficult to investigate them due to the complexity of preparation and stabilization of membrane proteins in aqueous solutions [1].

One of the most effective systems for studying the structure of membrane proteins, as well as refolding, protein-protein and protein-lipid and protein-ligand interactions, are nanodiscs – particles in the form of a flat lipid bilayer with a diameter of 8 – 16 nm, surrounded by a "belt" of amphipathic helices 2 polypeptide chains of the MSP protein (Membrane Scaffold Protein) [2]. Their main advantages over other methods of stabilization of membrane proteins (bicelles, flat lipid bilayer, proteoliposomes) are a clearly defined relatively small size, the possibility of embedding the monomeric form of the protein, stability in aqueous solutions, the availability of both sides of the membrane and the possibility to accurately control the lipid composition.

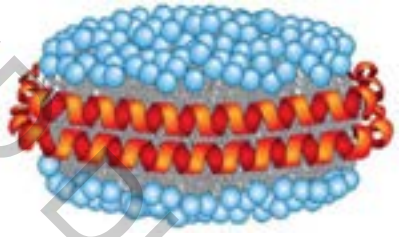

Fig. 1. Nanodiscs are discoidal lipid bilayer stabilized by encircling amphipathic helical scaffoldproteins termed MSPs [1].

The following parameters of heterologous expression of MSP1 were optimized: type of producer strain, type of culture medium, time of post-induction growth. MSP1 was obtained in the standard expression system pET28(b). Since MSPs are sensitive to proteolysis, and long-term post-induction growth leads to a significant decrease in the yield of MSP, expression time was limited and the incubation temperature decreased from 37 to 28 °C after 1 hour of expression [3].

When using *E. coli* BL21(DE3)C41 cells as a producer strain, the cell mass yield was minimal (3.2 g of wet cells per 1 liter of culture), and when using *E. coli* BL21(DE3) strain, the yield of wet cell pellet was 5 – 6 g with 1 liter of culture medium. The cultivation of *E. coli* BL21(DE3) cells in 2xYT growth medium also led to a relatively low yield (2.8 g per 1 liter of culture) compared to using TB medium (5 – 6 g per 1 liter of culture medium). An increase in the duration of post-induction growth using 0.5 L of TB medium did not significantly affect the number of cells obtained (2.4 g, 2.5 g, 2.2 g of cells 4, 7, and 13 hours after induction, respectively). Two-step purification of MSP1 by metalloaffinity chromatography and dialysis methods yielded 1.8 mmol of protein with 1 L of culture medium. Correspondence of the molecular weight of the obtained protein preparation MSP1 was confirmed using MALDI mass spectrometry and electrophoresis under denaturing conditions.

Thus, a technique was developed to obtain the preparation MSP1, which is necessary for the reconstruction of membrane proteins. The following parameters were chosen as the parameters of MSP1 expression: type of producer strain – *E. coli* BL21(DE3), type of growth medium – TB medium, growth duration after induction – 4 hours. It is planned to use this technique to obtain nanodiscs with incorporated membrane proteins, in particular, CYP2 family enzymes. Reconstitution of P450 cytochromes in nanodisks will allow us to study the interactions of various CYP2C isoforms, as well as the effect of the protein environment and lipid bilayer composition on the catalytic and ligand-binding properties of enzymes of this group.

[1] W. LiGuo, T. LiGe, Membrane protein reconstitution for functional and structural studies, Science China Life Sciences, **58(1)**, 66 – 74 (2015).
[2] I. G. Denisov, S. G. Sligar, Nanodiscs for structural and functional studies of membrane proteins, Nature Structural & Molecular Biology, **23(6)**,481 – 486 (2016).
[3] T. K. Ritchie et al., Reconstitution of Membrane Proteins in Phospholipid Bilayer Nanodiscs, Methods in Enzymology, **464**, 211 – 231 (2009).

CHARACTERIZATION OF MULTILAMELLAR LIPID VESICLES

Akvilė Milašiutė, Rima Budvytytė, Tadas Ragaliauskas, Gintaras Valinčius

Institute of Biochemistry, Vilnius University Life Sciences Center
akvile.milasiute@gmc.stud.vu.lt

Biological membrane is responsible for multiple physiological functions, so its research is very important. However, due to membrane complexity, these studies are a serious challenge. Model membrane system is used to make it easier. The most common model is tethered bilayer lipid membrane. Tethered bilayer lipid membrane can be formed using multillamelar lipid vesicles. This technique is new and there is not much information about the effect of multillamelar lipid vesicles on tBLM formation [1].

The aim of this work was to find sizes of various multillamelar lipid vesicles and check their ability to form tethered bilayer lipid membrane using electrochemical impedance spectroscopy.

The results have shown that when the concentration of cholesterol and the total concentration of both lipids (DPPC and cholesterol) is increasing multilamellar lipid vesicle size is getting bigger. The size of multilamellar lipid vesicle is decreasing when the concentration of DOPC is rising. Number of defects in tethered membrane depends on cholesterol concentration [2]. Also, tethered bilayer membrane can be formed when DOPC concentration is 0,25 mM and bigger. The size of liposomes is independent from time and they are suitable to use for 2 weeks.

[1] G. Valincius, T. Meskauskas, F. Ivanauskas, Electrochemical Impedance Spectroscopy of Tethered Bilayer Membranes, Langmuir **28**, 977-990 (2011).
[2] R. Budvytyte, M. Mickevicius, D.J. Vanderah, F. Heinrich, G. Valincius, Modification of Tethered bilayers by Phospholipid Exchange with Vesicles, Langmuir **29**, 4320-4327 (2013).

CANCELLED DUE TO COVID-19

INVESTIGATION OF THE INFLUENCE OF DIFFERENT MICROORGANISMS ON PLANT BIOMASS

Kornelija Beresnevičiutė[1], Rūta Mickienė[1], Vilma Kaškonienė[1], Audrius Maruška[1]

[1]Instrumental Analysis Open Access Centre, Vytautas Magnus University, Vileikos str. 8, LT–44404 Kaunas, Lithuania
kornelija.beresneviciute@stud.vdu.lt

Microorganisms are an integral part of the soil that helps it thrive and establishes beneficial relationships with the plants that grow on it. They break down various organic matter and pollutants and restore the natural structure of the soil. The processes of synthesis of humid substances and the decomposition of residues depend on the biological activity of the soil – group and species composition of microbes and abundance of microorganisms, especially bacteria. The purpose of this study is to investigate and evaluate the influence of different soil bacteria and fungi on the growth of plant biomass by purifying these microorganisms and transferring them to a selected plant. Studies have shown that plants can increase the dispersion of organic pollutants in the immediate root background (rhizosphere). Several plant species capable of decomposing pollutants in soil were selected and their biomass change was monitored. The plants were grown with bacteria and fungi isolated from clean and contaminated polycyclic aromatic hydrocarbon soils. The plant biomass obtained from above and below-ground parts of the plant and estimated per unit area of land per unit of time is calculated. Microorganisms that promote plant biomass growth have been discovered and can be applied in crop production in the future and used for further research on plant biomass.

Keywords: soil, microorganisms, plant

Acknowledgements: The study was financed by Research Council of Lithuania project No. 01.2.2-LMT-K-718-01-0074 (REMTECH)

CANCELLED DUE TO COVID-19

NON-CLASSICAL BINDING MODE BETWEEN ORTHO-, PARA-DISUBSTITUTED FLUORINATED PRIMARY BENZENESULFONAMIDES AND NATIVE OR MUTATED HUMAN CARBONIC ANHYDRASES

Kristina Gluščiukaitė, Vaida Paketurytė, Alexey Smirnov, Vaida Juozapaitienė, Daumantas Matulis

Department of Biothermodynamics and Drug Design, Institute of Biotechnology, Vilnius University, Vilnius, Lithuania

kristina.glusciukaite@gf.stud.vu.lt

The mode of sulfonamide binding to human carbonic anhydrases has been demonstrated in more than 500 crystallographic structures deposited in PDB database [1]. This binding mode is characterized by the formation of coordination bond between sulfonamide nitrogen atom and Zn(II) cation located in the ~15 Å-deep cone-shaped cavity formed of a hydrophobic and hydrophilic regions [2]. However, we were able to obtain several unusual crystal structures of CA XIII in complex with ortho-, para- disubstituted fluorinated primary sulfonamide compounds (VD12-15, VD12-09) where the fully reversed orientation of the inhibitor was observed. There was no coordination bond and the sulfonamide group was exposed towards the solvent.

Several CA mutants were generated utilizing PCR-mediated site-specific mutagenesis in order to determide structural reasons for such unusual ligand positioning. Two recombinant active site mutant proteins (CA II Thr199Val, Ca XIII Val201Thr) were constructed in this study. For expression of the active site mutant proteins, plasmids carrying mutations were transformed into E.coli. proteins were purified by IMAC, ion exchange and affinity chromatography. Fluorescent thermal shift assay (FTSA) was used for evaluation of dissociation constants. Three X-ray crystallographic structures of mutated protein and ligands were solved and analyzed.

Despite the hypothesis, we were unable to detect reverse-orientation ligand positioning in the active site of mutated proteins. Consequently, we decided that unexpected ligand position was an artifact due to acidic pH (4.0) buffer used for crystallization. However, mutation in CA II active site did not influence ligand upside down positioning towards solvent. Still, one amino acid substitution in protein active site could influence the binding affinities in mutant proteins in some cases.

Fig. 1. Interactions between sulfonamide inhibitor and the CA XIII, CA II isoforms.

[1]. RCSB PDB - Search Results. https://www.rcsb.org/pdb/results/results.do?tabtoshow=Current&qrid=939A8999.

[2]. Baranauskienė, L. & Matulis, D. Overview of Human Carbonic Anhydrases. in *Carbonic Anhydrase as Drug Target* (ed. Matulis, D.) 3–14 (Springer International Publishing, 2019).

CANCELLED DUE TO COVID-19

The effect of newly synthesized derivative of dehydroepiandrosterone on glioma cell proliferation and reactive oxygen species generation

Valeryia Klopava[1], Jan Panada[2,3], Tatsiana Kulahava[1,4], Yaroslav Faletrov[2,3], Vladimir Shkumatov[2,3]

[1] Department of Biophysics, Physics faculty, Belarusian State University, Minsk, Belarus
[2] Chemistry faculty, Belarusian State University, Minsk, Belarus
[3]Research Institute for Physical Chemical Problems, Belarusian State University, Minsk, Belarus
[4]Research Institute for Nuclear Problems of Belarusian State University
fiz.klopova@bsu.by

Gliomas are one of the most common types of malignant tumors worldwide, however, an effective therapeutic strategy have not yet been fully determined [1]. In gliomas and glioblastomas, an increased basal level of reactive oxygen species (ROS) play an important role as chemical mediators in the regulation of signal transduction [2]. H_2O_2, which can oxidize signaling proteins, inducing the formation of a disulfide bond in phosphatase and kinase domains, regulates glioma cell apoptosis, proliferation, and survival. Novel therapeutic alternatives are now focused on immune recognition and immune response enhancing, blocking of survival metabolism pathways, and modulating cellular redox status. Drug resistance in cancer cells is closely related to their redox status [3]. To modify the net physiologic balance between interconvertible oxidized and reduced equivalents within subcellular compartments that remain in dynamic equilibrium, the change of concentration of either ROS or antioxidants can be induced.

Steroid hormones may influence the glioma progression through interaction with their receptors and metabolism and transcription of target genes regulation [4]. We synthesized a new derivative of dehydroepiandrosterone (DHEA) namely N-(3-indolylethyl)-3β-hydroxyandrost-5-en-17β-amine (IS-1). The aim of this work was to investigate the effects of DHEA, IS-1 and abiraterone acetate (known anticancer agent) on proliferative activity and ROS generation of C6 glioma cells. It is worth saying, that no oxidation of IS-1 into 3-ketosteroid, a requisite for hormonal activity in biogenic steroids, were detected in C6 glioma cells exposed to IS-1 for 24 h using mass spectrometry. Therefore, it can be implied that the mode of action of indole steroids does not involve signaling via steroid receptors or interference with CYP17A1 activity.

DHEA-derived decrease in cell proliferation was revealed. At 10·μM, abiraterone acetate decrease cell proliferation by 36±12 %, whereas IS-1 do so by 52±13 %. And at 1 μM, abiraterone acetate leads to the decrease in cell proliferation by 28±13 %, whereas IS-1 do so by 22±11 %. Treatment of cells with IS-1, abiraterone acetate for 30-60 min did not cause cell viability.

As shown in [5], the intracellular ROS levels gradually increased with the rising of concentration of DHEA in cancer cells. At the addition of IS-1 and abiraterone acetate at 1-10 μM concentration, the ROS level was the same as in control samples. These results indicate, that steroid derivatives could not induce ROS generation in glioma cells, as DHEA. Such data may be due to the high level of antioxidants in the cells. So, the antioxidant status of C6 glioma cells needs further investigation.

[1] Xiao X. et al., Pregnenolone, a cholesterol metabolite, induces glioma cell apoptosis via activating extrinsic and intrinsic apoptotic pathways, Oncology letters 8, 645-650 (2014).
[2] Aleli Salazar-Ramiro, et al., Role of Redox Status in Development of Glioblastoma, Front Immunol 7: 156 (2016).
[3] Dalavaikodihalli Nanjaiah N, et al., Survival of glioblastoma cells in response to endogenous and exogenous oxidative challenges: possible implication of NMDA receptor-mediated regulation of redox homeostasis, Cell Biol Int. (2019).
[4] Gatson W. et al., *Endocrinology*, 2008, 149:2028-2034.
[5] Zishui F. et al., Effects of G6PD activity inhibition on the viability, ROS generation and mechanical properties of cervical cancer cells, Biochimica et Biophysica Acta, 2245-2254 (2016).

CANCELLED DUE TO COVID-19

PLEIOTROPIC EFFECTS OF STATINS

Shamish Ganpule[1], Giulio Preta[2]

[1] Department of Biochemistry, Vilnius University, Lithuania
[2] Department of Biochemistry, Vilnius University, Lithuania
shamish.ganpule@gmc.vu.lt

Statins are known to be potent 3-hydroxy-3-methylglutaryl CoA reductase inhibitors and are widely used to treat cardiovascular diseases. However, the recent clinical trials have demonstrated that overall benefits observed with statins are greater than changes in lipid level alone, indicating the benefits beyond cholesterol inhibition termed as "pleiotropic effects." Accumulating evidences suggest that some of the pleiotropic effects involve interaction and modification of membrane bilayers. Using the combined approach of biophysical and biological methods, we demonstrate that lipophilic, but not hydrophilic statins are capable enough to lower the damage caused by cholesterol dependent cytolysins. This protective ability of statins correlates with lipophilicity and its capability to interact with lipid bilayer. Our experimental results suggest that lipophilic statins portray the ability to associate with the membrane and hinder the ability of cholesterol dependent cytolysin to bind to membrane cholesterol. Further evaluation of capability of statins to modify cell membrane properties can be of great interest to develop better therapeutic approach for cardiovascular diseases, atherosclerotic plaque stabilization, neurodegenerative diseases etc. Better understanding of the potential of statins can also be useful as adjuvants for drug delivery.

CANCELLED DUE TO COVID-19

TRPV4 in rat myometrium contractility

Lavryk Roman, Sukha Iryna, Moroz Olesya

[1]Department of Biophysics and Medical Informatics, Taras Shevchenko National University of Kyiv, Ukraine
Roman.Lavryk@outlook.com

In recent years the importance at the study of the participation of ion channels in regulatory and signaling pathways both as effectors and as mediators, a lot consideration is given to transient receptor channels of potential (TRP), the expression of which is described for epithelial, smooth muscle and nerve cells [1]. Also the urgent problem such as preterm labor, that included premature birth of babies (globally near 10% average) and its increasing in most countries with reliable time trend data requires new avenues in understanding its mechanisms and potent therapy including investigation of the role TRPV4 in this problem.

The strips of rat uterine smooth muscle (myometrium) on 19-22 days of pregnancy were affected by Oxytocin, 10 nM (Gedeon Richter,Hungary), selective TRPPV4 agonist GSK1016790A? 0.3 μM (Sigma, USA), selective TRPV4 antagonist HC067047, 1 μM (Sigma, USA). Modified Krebs solution and hypotonic Krebs solution were used to perfuse muscle strips. Experiments were conducted on the research-tissue bath with force transducers, which was assembled at the department of Biophysics in KNU, the force contraction was recorded by force sensors, ADC and its related software. Studies of the contractile function of myometrium were performed by the method tensometry on several groups of smooth muscle preparations. This method register the muscle's contraction in isometric mode [2]. This study was approved by Institutional Bioethics committee.

Application of the selective TRPV4 channels agonist reduced force of phasic contractions by 26% ($p<0.05$). Duration of contractions was calculated at 50% of peak force and showed the increase up to 30%, without statistically significant difference. Area under the curve was reduced by up to 22% ($p<0.05$). These results indicate that there is a possible mechanism for reducing the excitability of uterus with the progress of labor, which could serve for protection of both the fetus and the organ. Probable mechanism of this phenomenon may include the activation of BK_{Ca} cannels, which, in turn, cause hyperpolarization of the myocytes plasma membrane [3]. Further electrophysiological studies are needed to address this hypothesis.

In experiments with hypotonic environment that was chosen as model of such pathologic conditions as hypertonic disease, diabetes and preeclampsia and activate mechanosensitive channels, myometrium strips responded with enforced contractibility, with the increase of fore amplitude up to 60% ($p<0.05$). TRPV4 by being sensitive to the cell stretch could also be involved in this phenomenon.

[1] J. P. M. White, M. Cibelli, L. Urban, B. Nilius, J. G. McGeown, і I. Nagy, «TRPV4: Molecular Conductor of a Diverse Orchestra», *https://doi.org/10.1152/physrev.00016.2015*, 2016.

[2] S. Arrowsmith, P. Keov, M. Muttenthaler, і C. W. Gruber, «Contractility Measurements of Human Uterine Smooth Muscle to Aid Drug Development», *J. Vis. Exp.*, no 131, 2018.

[3] M. S. Grace, S. J. Bonvini, M. G. Belvisi, і P. McIntyre, «Modulation of the TRPV4 ion channel as a therapeutic target for disease», *Pharmacology and Therapeutics*, vol 177. pp 9–22, Bep-2017.

CANCELLED DUE TO COVID-19

STRUCTURAL PROPERTIES AND IRON-BINDING CAPACITY OF LACTOFERRIN DURING OXIDATIVE/HALOGENATIVE STRESS

Maria Terekhova[1], Anatoli Kokhan[1], Daria Grigorieva[1]

[1]Department of Physics, Belarussian State University, Belarus
rrchypp@gmail.com

Lactoferrin (Lf) is an iron-binding glycoprotein, contained in most external secretions: milk, saliva, tears, etc., and in polymorphonuclear leucocytes [1]. Main property of Lf is antimicrobial activity, which depends on protein iron-binding capacity. Apart from that, Lf possesses a number of important properties, among them antiviral, antifungal, immunomodulatory and even anticancer activity [2, 3]. One of the promising application of this protein is development of the drugs, especially using recombinant human lactoferrin (rhLf), produced from the milk of transgenic animals [2]. Lf is released from the secondary granules of neutrophils during degranulation. This process is accompanied by production of reactive oxygen and halogen species (ROS and RHS), which leads to the development of oxidative and halogenative stress [4]. Thus, a large number of ROS and RHS surround Lf and other proteins. We showed previously that this oxidants can affect structure and properties of myeloperoxidase, protein which is closely associated with the production of RHS [5], and that modification of rhLf by HOCl changes it's structure, as well as ability to activate neutrophils.

Little is known about the effect of other ROS and RHS, such as HOBr, Tau-Cl, Tau-Br, H_2O_2 and HOSCN, on the structure and other important biological and biophysical properties of Lf molecule. Thus, this work aims to study the structural properties of Lf and it iron-binding capacity during modification by different ROS and RHS.

It was showed that modification of rhLf by HOCl, HOBr and Tau-Br led to the destruction of tryptophan residues, that was measured by intrinsic fluorescence of tryptophan ($\lambda_{ex.}$=285 nm, $\lambda_{em.}$=340 nm). Modification of rhLf by RHS in molar ratios from 1:10 to 1:50 showed that HOBr and Tau-Br had more potent effect then HOCl, but at the molar ratio of 1:100 HOCl, HOBr, Tau-Br all destroyed tryptophan residues. H_2O_2, HOSCN and Tau-Cl had no significant effect on tryptophan fluorescence.

Modification of primary amines (Lys and Arg) by ROS and RHS was studied with the help of fluorescent probe fluorescamin ($\lambda_{ex.}$=390 nm, $\lambda_{em.}$=490 nm). Only modification by HOCl at the molar ratios 1:50 and 1:100 showed significant effect on the change of the structure of primary amines of rhLf.

Structural properties of the whole protein globe were studied by the fluorescent probe ANS ($\lambda_{ex.}$=350 nm, $\lambda_{em.}$=510 nm). Modification of rhLf by HOCl have showed sights of protein unfolding, whereas modification by Tau-Br likely led to the formation of aggregates of rhLf molecules.

Changes of iron-binding capacity of rhLf, which is the key factor for many biological activities of this protein, were studied by monitoring the absorption at λ=465 nm while adding the Fe^{3+} ($NH_4Fe(SO_4)_2$) salt to the suspension. Modification of rhLf by HOBr, HOCl and Tau-Br led to the loss of the iron-binding capacity of this protein.

In this work we showed that modification of rhLf molecule by different forms of RHS (HOCl, HOBr, Tau-Br) led to the loss of antimicrobial activity of rhLf, but at the same time mechanisms of this effect are vastly different, as shown by analysis of change of protein structure by different fluorescent probes and techniques.

[1] J Zhang, L Li, Y Cai [et al.] Expression of active recombinant human lactoferrin in the milk of transgenic goats, Protein Expression and Purification **57**, 127-135 (2008).
[2] D Legrand, E Elass, M Carpentier, J Mazurier Lactoferrin: a modulator of immune and inflammatory responses, Cell. Mol. Life Sci. **62 (22)**, 2549-2559 (2005).
[3] L Adlerova, A Batroskova, M Faldyna Lactoferrin: a review, Veterinarni Medicina **53**, 457-468 (2008).
[4] P Lacy Mechanisms of degranulation in neutrophils, Allergy Asthma Clin. Immunol. **2(3)**, 98-108 (2006).
[5] T V Vakhrusheva [et al.] Enzymatic and bactericidal activity of myeloperoxidase in conditions of halogenative stress, Biochem. Cell Biol. **96**, 580-591 (2018).

ACCEPTED PRIOR TO COVID-19

SPECTRAL-KINETIC PROPERTIES OF LOWER EXCITED ELECTRONIC STATES IN OXYHEMOGLOBIN

Arthur F. Chaikovskii

Center for Photonics and photochemistry of molecules, Institute of Physics of the NAS of Belarus, Minsk, Belarus
arthur.chaykovski@gmail.com

The presence of an extensive system of low-energy levels located below the triplet $\pi\pi^*$-state is intrinsic to oxyhemoglobin (HbO_2), as well as to many hemoproteins. These levels correspond to the excited states of the charge-transfer (*CT*) nature. Four such levels are reliably known from oxyhemoglobin literature. Earlier, we studied the third excited *CT*-state by means with nanosecond laser spectroscopy [1]. Accompanied by the fourth one, it forms the low-intensity band located in the near infrared region (λ_{max} = 925 nm) and corresponding to electron transfers from porphyrin π-orbitals to a mixed orbital formed from iron *d*-orbital and free π-orbital of molecular oxygen. Photodissociation was found to not observe upon excitation into this band (λ_{ex}=1064 nm). In this case the primary quantum yield of photodissociation can be estimated as $\gamma_0 \leq 0.7$ %.

The purpose of the present work was to determine the spectral-kinetic characteristics of the energetically most high-lying excited state of the *CT* nature ($^{1,3}CT_{\pi d}$). Accomplishing this purpose is of a significant step towards elucidation of intraheme processes and photodissociation, which in turn will enable to develop methods of photodissociation control and to create artificial blood substitute.

Flash-photolysis measurements of transient absorption spectra were carrying out on femtosecond time-resolved laser kinetic absorption spectrometer. The device is made on the basis of femtosecond pulse Ti:Sp generator synchronously pumped by a pulsed Nd:YAG laser. The wavelengths of 780 and 390 nm were used in the work. The pulse duration at half-height was about 150 fs. Generated after beam passing through an adjustable delay line, femtosecond supercontinuum was used as a source of probing light.

In the present study solutions of human oxyhemoglobin were investigated at two different concentrations: 2.0 mM (λ_{ex}=780 nm) and 30 μM (λ_{ex}=390 nm). All measurements were performed at room temperature 21 ± 1°C using 50 mM Tris-HCl pH 8.3 buffer. For each laser pulse, the spectra of probing radiation transmitted through a sample were recorded by CCD matrix coupled to a computer.

HbO_2 photodissociation upon excitation at a wavelength of 390 nm is studied well, and transient spectrum similar to that obtained in the work [2] was observed in the spectral region 417–456 nm. This spectrum evolved over time of ~300 fs and was replaced by another one corresponding to the spectrum of heated hemoglobin. Despite of the position of the triplet $^3\pi\pi^*$-state cannot be identified for oxyhemoglobin, by analogy with other metalloporphyrins, it is placed in the region of ~14000 cm^{-1}. Thus, photodissociation can be believed to occur in exactly that state. A detailed scheme of HbO_2 photoinduced dissociation and a justification of the heme energy exchange processes accompanying was presented in the work [1]. Hence, a state with a lifetime of ~300 fs is the photodissociating triplet $^3\pi\pi^*$-state into which HbO_2 transfers from the singlet $^1\pi\pi^*$-state as result of the intersystem crossing.

An energy of 12800 cm^{-1} was transferred to HbO_2 molecule at λ_{ex}=780 nm. This value is lower than the energy of the triplet level, but is sufficient to populate the $^{1,3}CT_{\pi d}$ state. After that, a transient absorption spectrum was observed in the region of 620–666 nm. Using the singular decomposition, it was possible to identify the presence of two components in this difference spectrum. However, taking into account the duration of the excitation pulse, it was possible to reliably determine only the duration of the short component that is 380 fs. The spectrum of this short component was first measured. This difference spectrum is believed to correspond to absorption in the $^{1,3}CT_{\pi d}$ state. Though, it is worth to note there were difficulties in determining the percentage contribution of the two-photon absorption effect (390 nm), therefore it is impossible to unequivocally state there is no contribution of the oxyhemoglobin spectrum in the triplet state or the deoxyhemoglobin spectrum. Nevertheless, taking into account the high optical density in the two-photon absorption region one can consider the photodissociation does not occur upon excitation at a wavelength of 780 nm.

This study was supported by The State Research Program “Photonics and Opto- and Microelectronics 1.4.01” (2016–2020) of The Republic of Belarus.

[1] B. M. Dzhagarov, S. V. Lepeshkevich, A. Yu. Panarin et al., Photoinduced breaking of the Fe–O_2 bond in hemoglobin: dissociation quantum yield, excited electronic states, and nonradiative relaxation processes, Optics and Spectroscopy **125** (1), 123-129 (2018).

[2] J. W. Petrich, C. Poyart and J. L. Martin, Photophysics and reactivity of heme proteins: a femtosecond absorption study of hemoglobin, myoglobin, and protoheme, Biochemistry **27**, 4049-4060 (1988).

CORRECTED PROOF COVID-19

ANALYSIS OF RELEASE PROCESSES OF TEMOPORFIN (mTHPC) FROM DEXTRAN70-POLY (N-ISOPROPYLACRYLAMIDE) COPOLYMER IN BLOOD SERUM

Ivan Kablov[1], Yulia Kuziv[2]

[1] Department of Biophysics, Faculty of Physics, Belarussian State University, Minsk, Belarus
[2] Faculty of Chemistry, Taras Shevchenko National University of Kyiv, Kyiv, Ukraine
iv.kablov@gmail.com

CANCELLED DUE TO COVID-19

One of the ways to solve the problem of low drug watersolubility is to use special delivery systems based on nanostructured materials. An important factor in the development of such technologies is the monitoring of drug release from the nanocarriers.

In this work we carried out the monitoring of 5,10,15,20-tetra(m-hydroxyphenyl)chlorin (mTHPC) release from dextran70-poly(N-isopropylacrylamide) copolymers (D70-PNIPAM) using the spectral approach. mTHPC is one of the most promising clinically approved second generation photosensitizers [1]. The main limitation of its application in photodynamic therapy is a low watersolubility. To prevent mTHPC aggregation and facilitate its administration several special formulations, such as liposomes,bioconjugates, copolymers have been proposed [2].

D70-PNIPAM copolymers are in the condensed state at temperatures above the critical point. At temperatures between 34-35 °C, there is a phase transition, which leads to significant changes in the structure of the polymer molecule. mTHPC could be simply encapsulated into the D70-PNIPAM copolymers at the temperature above critical one. It was demonstrated, that the addition copolymers to the aqueous mTHPC solution is accompanied with complete monomerization of photosensitizer. Indeed, photosensitizer molecules penetrate into a rigid polymer matrix resulting in the increase of mTHPC fluorescence polarization degree up to 0,33. When cooling to below critical temperatures, mTHPC molecules release from the complexes forming molecules aggregates in the aqueous surrounding. Meanwhile in the serum solutions, the release process is accompanied with the binding of mTHPC to the plasma proteins (mainly to high density lipoproteins and low density lipoproteins).

Spectral data analysis has shown that the shape of mTHPC excitation spectrum in serum and complexes with D70-PNIPAM significantly differs (Fig.1) allowing us monitor temperature-induced redistribution of mTHPC from copolymers to serum proteins (Fig.2).

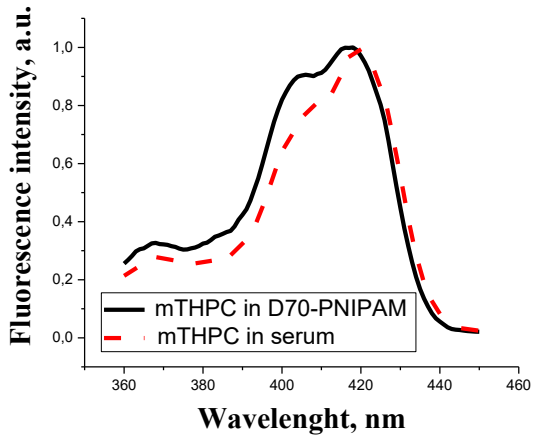

Fig. 1. Normalized fluorescence excitation spectra of mTHPC in D70-PNIPAM and serum.

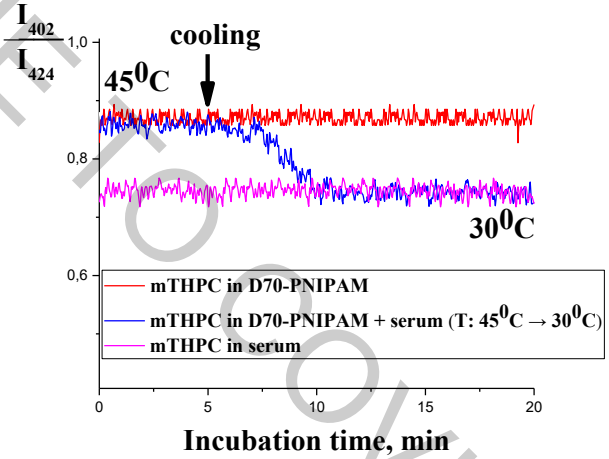

Fig. 2. Temperature-induced redistribution of mTHPC from D70-PNIPAM to serum. λem = 652 nm.

Based on the measurements of the ratio of intensities of fluorescence excited at 402 nm and 424 nm, the redistribution rate of mTHPC between D70-PNIPAM and serum can be estimated.

Acknowledgements: The work was carried out with the financial support of the Belarusian Republican Foundation for Fundamental Research (BRFFR) [grant number M19UKRG-002]; the Ministry of the Education and Science of Ukraine: joint Ukrainian-Belarusian research and development projects № M110-2019.

[1] M. Senge, mTHPC – A drug on its way from second to third generation photosensitizer?, Photodiagnosis and Photodynamic Therapy 9, 170-179 (2012)
[2] I. Yakavets, M. Millard, V. Zorin, H-P. Lassalle, L. Bezdetnaya, Current state of the nanoscale delivery systems for temoporfin-based photodynamic therapy: Advanced delivery strategies, Journal of Controlled Release 304, 268-287 (2019)

THE ANTIMICROBIAL ACTIVITY OF GEOBACILIN 26: ARTIFICIAL VS BACTERIAL CELL MEMBRANE

Mantė Rakauskaitė[1,*], Marija Jankunec[2], Arnoldas Kaunietis[1]

[1]Institute of Biosciences, Life Sciences Center, Vilnius University, Vilnius, Lithuania
[2]Institute of Biochemistry, Life Sciences Center, Vilnius University, Vilnius, Lithuania
*mante.rakauskaite@gmc.stud.vu.lt

Geobacillin 26 is a heat-labile, high molecular weight antibacterial protein from a thermophilic Gram-positive bacteria *Geobacillus stearothermophilus* 15 and it has a narrow antibacterial spectrum against other thermophilic bacteria. Its mode of action differs from similar bacteriolysins. In recent studies, it was proven, that geobacillin 26 is not a cell wall degrading enzyme, but its specific mode of action is unknown [1]. Bacteriocins, including geobacillin 26, have a great potential in the food industry where contamination with thermophilic bacteria is unwanted.

The study aimed to determine the mode of action of geobacillin 26 using Atomic Force Microscopy (AFM). AFM is a surface-sensitive technique that allows to visualize three-dimensional topographic views of a specimen under physiological conditions. Thus we established protocols to immobilize and visualize directly the activity of protein on bacterial and artificial cell membranes (tBLM – tethered bilayer lipid membrane).

Bacterial cells of sensitive strain *Parageobacillus genomospecies* 1 NUB36187 (9A11) were spread on NB-agar plate and incubated overnight at 55 °C. After the incubation biomass from the plate was transferred to NB medium and incubated overnight at 55 °C. The next morning the cell suspension was inoculated to the NB medium (55 °C) in the ratio 1:50. The cell suspension adjusted to OD (600 nm) of 0,6 and then affected with geobacillin 26. The cell suspension was washed with PBS (pH 7,4) buffer two times. The suspension was spread out on poly-L-lysine modified mica. Surface topography and force curves (elasticity and adhesion properties) of bacteria were analyzed.

The artificial cell membranes were prepared as described elsewhere [2]. To imitate bacterial cell membrane, tBLMs were formed from 1,2-dioleoylphosphatidylglycerol/1,2-dioleoyl-*sn*-glycero-3-phosphoethanolamine7/3 multilamellar vesicle solutions .The effect of geobacilin 26 on the artificial bacterial membrane was detected via time-lapse capturing (Figure 1).

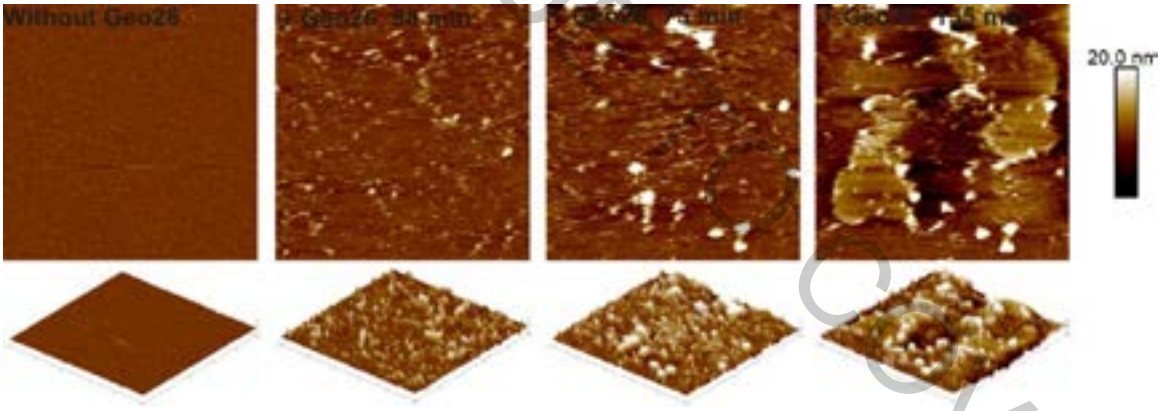

Figure 1. Time-lapse capturing of the effect of geobacilin 26 on the artificial bacterial cell membrane.

[1] Vaičikauskaitė M., Ger M., Valius M., Maneikis A., Lastauskienė E., Kalėdienė L., Kaunietis A. Geobacilin 26 – high molecular weight bacteriocin from a thermophilic bacterium. International Journal of Biological Macromolecules 2019 (141): 333-344.
[2] Ragaliauskas T., Mickevicius M., Rakovska B., Penkauskas T., Vanderah D.J., Heinrich F., Valincius G. Biochimica et BiophysicaActa (BBA)-Biomembranes 2017 (1859): 669-678.

CANCELLED DUE TO COVID-19

MINIATURIZED GLUCOSE BIOSENSOR BASED ON LOCALIZED ELECTROCHEMICAL IMPEDANCE SPECTROSCOPY

Antanas Zinovicius[1], Juste Rozene[2], Inga Morkvenaite-Vilkonciene [2,3], Almira Ramanaviciene[1], Arunas Ramanavicius[1,3]

[1]Vilnius University, Faculty of Chemistry and Geosciences, Naugarduko 24, Vilnius, Lithuania
[2] Vilnius Gediminas Technical University, Faculty of Mechanics, J. Basanavičiaus g. 28, 03224 Vilnius, Lithuania
[3]Center for Physical Sciences and Technology, Saulėtekio 3, 10257 Vilnius, Lithuania
antanas.zinovicius@chgf.vu.lt

Electrochemical impedance spectroscopy is successfully applied in biosensors, where the recognition element (enzymes or cells) is immobilized directly on the electrode [1]. The reaction products diffuse into the solution and have to be registered by the electrode, but it is blocked by the recognition element itself. Using localized impedance spectroscopy, the recognition element and the recording electrode are at a certain distance from each other, which allows the reaction products to be recorded. Localized impedance spectroscopy is performed in tandem with scanning electrochemical microscopy (SECM), using ultramicroelectrode.

To evaluate immobilization efficiency and activity of glucose oxidase, SECM and localized impedance were employed. This method was chosen as non-destructive, an operator can choose the precise location and measurements can be performed in the optimal medium [2]. Also, changes in electrochemical activity can be recorded in real time. SECM can be combined with electrochemical impedance spectroscopy (SEIM), which showed great results for the characterization of a glucose oxidase based detection of glucose [3]. SEIM can be used to obtain more advanced mapping of the electrochemical system and the results can be visualized by plotting one of the calculated parameters, e.g. charge transfer resistance or double-layer capacitance as a function of 3D coordinates [4].

During research different glucose oxidase surface concentration were immobilized on the dielectric surface. Using SEIM method the lowest detectable amount of enzyme was found. Obtained results show suitability of localized electrochemical impedance spectroscopy for the development of miniaturized glucose biosensor.

Acknowledgements

This research was funded by the European Social Fund according to the activity "Development of Competencies of Scientists, other Researchers and Students through Practical Research Activities" measure No Project Nr.09.3.3.-LMT-K-712-16-0211

[1] N. Bhalla, P. Jolly, N. Formisano, and P. Estrela, "Introduction to biosensors," *Essays Biochem.*, vol. 60, no. 1, pp. 1–8, 2016.
[2] M. M. N. Zhang, Y. T. Long, and Z. Ding, "Filming a live cell by scanning electrochemical microscopy: Label-free imaging of the dynamic morphology in real time," *Chem. Cent. J.*, vol. 6, no. 1, pp. 1–6, 2012.
[3] I. Morkvenaite-Vilkonciene, P. Genys, A. Ramanaviciene, and A. Ramanavicius, "Scanning electrochemical impedance microscopy for investigation of glucose oxidase catalyzed reaction," *Colloids Surfaces B Biointerfaces*, vol. 126, pp. 598–602, 2015.
[4] I. Morkvenaite-Vilkonciene, A. Valiūnienė, J. Petroniene, and A. Ramanavicius, "Hybrid system based on fast Fourier transform electrochemical impedance spectroscopy combined with scanning electrochemical microscopy," *Electrochem. commun.*, vol. 83, pp. 110–112, 2017.

CANCELLED DUE TO COVID-19

INVESTIGATION OF ELECTROPORATION EFFECTS BY MEDIATED AMPEROMETRY AT YEAST MODIFIED ELECTRODES

Povilas Šimonis[1], Rasa Garjonytė[2], Arūnas Stirkė[1]

[1] Laboratory of Bioelectrics, [2] Laboratory of Spektroelectrochemistry,
State Research Institute, Center for Physical Sciences and Technology,
Saulėtekio al. 3, Vilnius, Lithuania
povilas.simonis@ftmc.lt

CANCELLED DUE TO COVID-19

Budding yeast (*Saccharomyces cerevisiae*) is one of the most well-studied and understood eukaryotic organisms. Yeast cells could be used for whole-cell bioprocesses such as biocatalysis and recombinant protein fermentation, but natural barrier functions of the cell wall and cell membrane often retards entry of substrates and release of products [1]. One of the possible techniques which could be used to improve permeability for target molecules is pulsed electric field (PEF), yet there is still a lack of sufficient data related to the effects of PEF on yeast cells especially in combination with whole-cell bioprocesses.

In this study we modified electrodes with whole yeast cells to detect electroporation effects. For the analysis, PEF-treated cells were immobilized on carbon paste electrodes which were then immersed into solution with potassium ferricyanide or menadione acting as mediators and producing measurable currents through oxidizing at electrode surface. Menadione-mediated amperometry was used for measurement of redox activity inside the yeast cells [2], while ferricyanide currents from amperometric sensor for lactic acid reflected membrane permeability (Fig 1.) [3]. Viability of cells was evaluated by counting colony-forming units. Leakage of intracellular compounds was evaluated by measuring fluorescence of supernatant or staining it with Ellman's reagent. Cells were exposed to single square shaped electric field pulses with pulse duration τ = 300 µs and electric field strengths (E) up to 16 kV/cm.

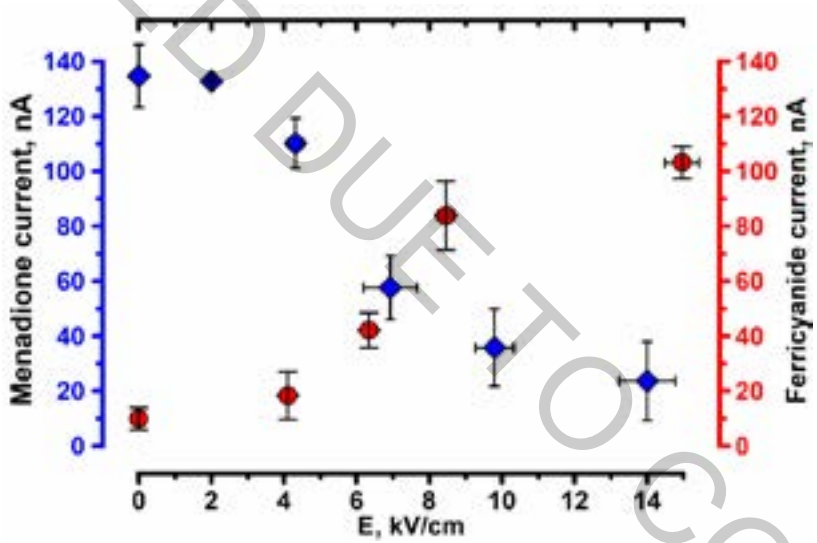

Fig. 1. Effect of electric field strength on current responses of yeast-modified electrode. Squares: 67 µM menadione at an operating potential 0.3 V in phosphate buffer at pH 6.5. Circles: 0.2 mM lactic acid at yeast-modified electrodes at an operating potential 0.3 V in phosphate buffer at pH 7.3 containing 0.5 mM mediator $K_3[Fe(CN)_6]$.

We showed that after exposure to PEF, permeability of cell membrane/wall increased while viability decreased. Yeast-modified electrode responses to lactic acid and menadione were dependent on PEF exposure. Currents obtained from amperometric biosensor with treated cells increased from 9.9 ± 4 nA (E = 0 kV/cm) up to 103.2 ± 5.8 nA (E = 15 ± 0.5 kV/cm). PEF treated yeast cells also showed lower redox activity which decreased (from 135 ± 11 nA to 24 ± 14 nA) with raise in electric field strength (0 kV/cm up to 14 ± 0.8 kV/cm). Decrease of menadione-mediated current showed similar pattern with viability. Viability of yeast cells decreased (from 100 % up to 1.5 ± 0.5 %) with raise in electric field strength (E = 9.6 kV/cm). We conclude that amperometric measurements can be effectively used for investigation of various cellular responses after PEF treatment.

[1] Chen, R., "Permeability issues in whole-cell bioprocesses and cellular membrane engineering" Applied Microbiology and Biotechnology 74, 730-738 (2007).
[2] R. Garjonyte, V. Melvydas, and A. Malinauskas, "Mediated amperometry reveals different modes of yeast responses to sugars", Bioelectrochemistry 107, 45–49 (2016).
[3] R. Garjonyte, V. Melvydas, and A. Malinauskas, "Effect of yeast pretreatment on the characteristics of yeast-modi fi ed electrodes as mediated amperometric biosensors for lactic acid", Bioelectrochemistry 74, 188–194 (2008).

SYNTHESIS AND ANTIBACTERIAL ACTIVITY EVALUATION OF CARBAZOLE-BASED COMPOUNDS

Kestutis Dabravolskas[1], Ilona Jonuskiene[2], Simona Sutkuviene[3,4], Dalius Gudeika[1]

[1]Kaunas University of Technology, Department of Polymer Chemistry and Technology Radvilėnų 19, Kaunas, Lithuania

[2]Kaunas University of Technology, Department of Organic Chemistry Radvilėnų 19, Kaunas, Lithuania

[3]Department of Biochemistry, Faculty of Medicine, Lithuanian University of Health Sciences, Tilzes Str. 18, LT47181, Kaunas, Lithuania

[4]Department of Biochemistry, Faculty of Natural Sciences, Vytautas Magnus University, Vileikos Str. 8, LT44404, Kaunas, Lithuania

kestutis.dabrovolskas@ktu.edu

CANCELLED DUE TO COVID-19

Even though there are many antibacterial agents multidrug resistant bacteria poses a huge threat to public health and has become one of the biggest health problems in the last decade. Therefore, there is an urgent need to develop and provide novel and more potent antibacterial agents to overcome drug resistance [1].

Carbazole is a nitrogen containing aromatic heterocyclic compound, which can be found in nature as carbazole alkaloid that is isolated from various part of the plan [2]. Such carbazole ring containing alkaloids are carbomycins that were first isolated from *Streptoverticillium ehimense* and showed good activity against various organisms, which made carbazoles a desirable target for further biological research [3].

It has been observed that carbazole compounds exhibit multiple mechanisms of antibacterial activity action. One is that carbazole compounds increase membrane permeability by inhibiting specific enzymatic processes. Increased penetration of free radicals in violates integrity of bacterial cell [4]. Second, mechanism of action is that carbazole compounds can interact with bacterial DNA by forming non-covalent interactions with DNA gyrase [5]. Therefore, various N and C substituted carbazoles are attractive target to develop and produce new antibacterial agents with two possible antibacterial mechanism of action, that could help resolve drug resistance problem.

In this work, various mono-, di- and tri-substituted carbazole derivatives, containing appropriate halogens, cyano and alkyl groups were synthesized and evaluated for their antibacterial activities against two bacteria (*Bacillus subtilis* and *Escherichia coli*) using disk diffusion method. Screening of their antibacterial activity has displayed that against *Bacillus subtilis* the most active antibacterial agents 3-cyano-9*H*-carbazole, 3-iodo-9*H*-carbazole and 3,6-diiodo-9*H*-carbazole, they suppressed the growth of bacteria at concentration 31.25 μg ml^{-1}. *Escherichia coli* bacteria was the most sensitive to 1,3,6-tribromo-9*H*-carbazole, which inhibited their growth at concentration of 31.25 μg ml^{-1}.

Antioxidative activities were evaluated using free 1,1-diphenyl-2-picryl-hydrazyl radical scavenging assay and ferric reducing antioxidant power methods. Antioxidant activity assay revealed that tested compounds displayed from none to very weak antioxidant activity according to tested methods.

Table 1. The antibacterial activity results against *Bacillus subtilis* and *Escherichia coli* strains of selected compounds 1a-5 at different concentrations**.**

Strain		*Bacillus subtilis*				*Escherichia coli*			
Concentration (μg ml^{-1})		1000	125	62.5	31.25	1000	125	62.5	31.25
Zone of inhibition (mm)	**1a**	10.5	8.0	7.9	5.3	10.45	6.30	NA	NA
	1b	9.50	NA	NA	NA	9.67	NA	NA	NA
	2a	8.00	7.95	8.20	5.47	10.20	8.60	6.17	NA
	2b	9.00	7.18	7.20	6.33	10.20	9.65	6.00	NA
	3	10.30	7.68	7.40	NA	9.67	8.70	7.67	5.95
	4	8.50	7.15	NA	NA	7.75	NA	NA	NA
	5	NA	NA	NA	NA	NA	NA	NA	NA

Acknowledgement.

This research was supported by the Research, Development and Innovation Fund of Kaunas University of Technology and the Research Fund of Lithuanian University of Health Sciences / the Research, Development and Innovation Fund of Vytautas Magnus University (SLOPSINT). We are grateful to dr. Eigirdas Skuodis and dr. Gintare Krucaite for provided compounds.

[1] S.T. Cole, Philosophical Transactions of The Royal Society B, 369, 1 (2014).

[2] T. Indumathi, T. Brant, M. Zeller, K. J. R. Prassad, Indian Journal of Chemistry, 52B, 405 (2013).

[3] S. Chakraborty, B. Chakraborty, A. Saha et al., Indian Journal of Chemistry, 56B, 701 (2017).

[4] Y. J. Eun, M. H. Foss, D. Kiekebusch et al., Journal of the American Chemical Society, 134(28), 11322 (2012).

[5] Y. Zhang, V. K. R. Tangadanchu, Y. Cheng et al., ACS Medicinal Chemistry Letters, 9(3), 244 (2018).

EARLY AND PROLONGED MESENCHYMAL INDUCTION FOR CHONDROGENIC DIFFERENTIATION OF HUMAN DERMAL FIBROBLAST-DERIVED INDUCED PLURIPOTENT STEM CELLS

Jolanta Bukauskaite[1], Edvardas Bagdonas[1], Ausra Unguryte[1], Paulius Lukas Tamosiunas[2], Vaidas Dirse[3], Dainius Daunoravicius[4], Ali Mobasheri[1,5], Eiva Bernotiene[1].

[1] State Research Institute Centre for Innovative Medicine, Lithuania
[2] Vilnius University Life Science Center, Institute of Biotechnology, Lithuania
[3] Hematology, Oncology and Transfusion Medicine Center, Vilnius University Hospital, Santaros Klinikos, Lithuania
[4] Vilnius City Clinical Hospital, Lithuania
[5] Faculty of Medicine, Research Unit of Medical Imaging, Physics and Technology, University of Oulu, Findland
jolantaco@gmail.com

CANCELLED DUE TO COVID-19

Induced pluripotent stem cells (iPSCs) hold a great promise in regenerative medicine due to large self-renewal capacity, no ethical controversies and possibility to rise every cell type of the body. Defined three germ layers formation of mesoderm, ectoderm and endoderm during iPSCs differentiation is a crucial step for the further wanted cell differentiation. So far, several early lineage commitment protocols have been developed for mesodermal induction of iPSCs in monolayer or embryoid body formation with defined growth factors Activin A, Wnt3, bFGF (and others) alone or in combinations. Second step is the prolonged mesodermal differentiation of early induced mesenchymal cells. However, current methods of mesenchymal induction are not finally understood and developed, for this reason effective and eligible differentiation may not be reached.

For this study, we derived hiPSCs from several human dermal fibroblasts, which showed normal karyotype and endogenous expression of pluripotent markers like OCT4, SOX2, NANOG (by RT-PCR), TRA-1-60, SSEA4 (by Flow cytometry) and TRA-1-60, ALP (by ICF) were detected. Chondrogenic differentiation was induced through early and prolonged mesenchymal differentiation in monolayer or pellets cultures with diverse combination of growth factors. Morphological and cell growth changes were typical for the stage of differentiation. Expression of pluripotency or differentiation related genes, including OCT4, SOX2, ATF3, TGIF1, CAV1.2, COL1, COL2, ACAN, SOX9 were evaluated in iPSCs differentiation. Dynamical changes in expression of those genes demonstrated the mesenchymal induction and efficient chondrogenic differentiation as determined on days 3, 14 and 21. Histochemical staining with Safranin-O and immunohistochemical Collagen type II detection confirmed chondrogenic differentiation.

ACKNOWLEDGEMENT: This research is/was funded by the European Social Fund under the No 09.3.3 LMT K 712 “Development of Competences of Scientists, other Researchers and Students through Practical Research Activities” and according to the activity ‘Improvement of researchers qualification by implementing world class R&D projects’ of Measure No. 09.3.3 LMT K71200.

PULSED CURRENT AS AN INDICATOR OF SUCCESSFUL TUMOR ELECTROCHEMOTHERAPY

Veronika Malyško[1], Vitalij Novickij[1], Augustinas Želvys[2], Austėja Balevičiūtė[2], Auksė Zinkevičienė[2], Jurij Novickij[1], Gediminas Staigvila[1] and Irutė Girkontaitė[2]

[1]Department of Electrical Engineering, Vilnius Gediminas Technical University, Lithuania
[2]Department of Immunology, State Research Institute Centre for Innovative Medicine, Vilnius, Lithuania
vitalij.novickij@vgtu.lt

Pulsed electric field (PEF) is used for ablation of tumors [1] or intratumoral drug delivery [2], however, the possibilities for real-time evaluation of the treatment efficacy are limited. In this work, we have used microsecond and nanosecond non-thermal PEF (<10 J) for electrochemotherapy of Sp2/0 tumors with doxorubicin and evaluated the feasibility of current measurement as an indicator of successful tumor electrochemotherapy. The changes in pulsed current amplitude during the *in vivo* experiments were compared to the changes of the permeabilization rate of the cells *in vitro*. It was shown that the current varies in a similar tendency as the permeabilization rate. It was also shown that changes in tumor conductivity can be used as an indicator of permeabilization efficiency, however, limited to non-thermal PEF treatments. The results can be used for development and optimization of electrochemotherapy protocols and techniques for real time prediction of treatment outcome.

Acknowledgement: The research was funded by Research Council of Lithuania, Grant Nr. S-MIP-19-22.

[1] Stam, Anita GM, and Tanja D. de Gruijl. "From local to systemic treatment: leveraging antitumor immunity following irreversible electroporation." Irreversible Electroporation in Clinical Practice. Springer, Cham, 249-270, (2018).
[2] Falk, H., et al. "Calcium electroporation for treatment of cutaneous metastases; a randomized double-blinded phase II study, comparing the effect of calcium electroporation with electrochemotherapy." Acta Oncologica 57.3, 311-319 (2018).

CANCELLED DUE TO COVID-19

APPLICATOR PROTOTYPE FOR DIELECTROPHORESIS-ENHANCED ELECTROTRANSFER OF MOLECULES INTO BIOLOGICAL CELLS

Arūnas Murauskas[1], Gediminas Staigvila[1,2], Vitalij Novickij[1,2]

[1] Department of Electrical Engineering, Vilnius Gediminas Technical University, Lithuania
[2] Institute of High Magnetic Fields, Vilnius Gediminas Technical University, Lithuania
vitalij.novickij@vgtu.lt

CANCELLED DUE TO COVID-19

Various carriers are used to locally increase the membrane permeability for drugs and/or other molecules [1]. However, pulsed electric field induced electroporation phenomenon is an alternative physical method to increase membrane permeability [2]. At the same time, alternating pulsed electric fields can be also used to manipulate the motion of the biological cells using dielectrophoresis [3], which is based on polarization of cells in non-homogeneous fields. In this work, we present a cuvette prototype and a concept for dielectrophoresis-enhanced electroporation. The finite element method model of the pulse applicator and the generated pulsed electric field is presented. It is shown that the gradient of electric field is sufficient to trigger controllable dielectrophoresis accompanied by cell permeabilization, which indicates opportunity to significantly improve/manipulate the electrotransfer rate. The influence of needle type electrode density and shape is also investigated and further recommendations are provided.

Acknowledgement: The research was funded by Research Council of Lithuania, Grant Nr. S-MIP-19-13.

[1] Jahangirian, Hossein, et al. "A review of drug delivery systems based on nanotechnology and green chemistry: green nanomedicine." International journal of nanomedicine **12**, 2957 (2017).
[2] Weaver, James C., and Yuri Chizmadzhev. "Electroporation." Biological and Medical Aspects of Electromagnetic Fields, Fourth Edition. CRC Press, 243-284, (2018)
[3] Pethig, Ronald R. Dielectrophoresis: Theory, methodology and biological applications. John Wiley & Sons, (2017).

EFFECTS OF ESSENTIAL OILS AND THEIR COMPOUNDS ON MEALWORMS (*TENEBRIO MOLITOR* L.) LARVAE

Gabrielė Bumbulytė[1,2], Vincas Būda[2]

[1]Vilnius University Faculty of Natural Sciences, Vilnius
[2]The Nature Research Centre, Laboratory of Chemical and Behavioural Ecology, Vilnius
gabriele.bumbulyte@gmail.com

CANCELLED DUE TO COVID-19

Entomophagy is not a new phenomenon in our society. Insects have been eaten by humans from prehistoric times. Nowadays people eat insects not only as an exotic snack, but in some soceties insects are the main food source. According to the Food and Agriculture Organization of the United Nations [1], population growth, urbanization and the increase of human population of average income has increased global demand for food products, in particular those with great source of protein. One of the main aspects why insect eating is an alternative to the animal meat is because insects are very nutritious, they multiply fast and do not contaminate the environment. Currently the ecological insect farms are very popular and attempt to include insects in the daily diet of humans.

Mealworms (*Tenebrio molitor* L.) are easily cultivated, have a relatively large increase in biomass, are nutritious and a great source of protein. Because of these characteristics mealworms are the best example of insect food for humans. It is very important to increase the effectiveness of the collection of insect larvae biomass for the insect breeders. One of the possibilities could be the manipulation of insect larvae behavior using natural repellents. Natural repellents could ivert larvae from their food source to the collection points since this is related to the food industry, most of materials should be non-toxic to humans. Essential oils as natural repellents could be perfectly used for controlling insect behavior. The current thesis describes the impact of natural essential oils on the behavior of mealworm larvae. The results showedhat the best repellents for the mealworm larvae were the essential oils of thyme (*Thymus vulgaris* L.) and mint (*Mentha spicata* L.). The effect of active compounds of essential oils was also tested. The best repellency was recorded for 100 mM concentration of citronelool and 100 mM of linalool. It has been observed that in control plates without stimulus, the larvae spend most of their time on the periphery, not in the central zone. The effect of 3-methylbutanol, a product of mold metabolism, has been studied on the largest larvae of mealworms. However, this substance has not shown affect to larvae locomotorics.

[1] FAO. Edible Insects. Future Prospects for Food and Feed Security; 2013

OPTIMIZATION OF CONDITIONS FOR GENETIC TRANSFORMATION OF THERMOPHILIC BACTERIA

Aušra Kondrataitė[1], Arnoldas Kaunietis[1]

[1] Department of Microbiology and Biotechnology, Vilnius University, Lithuania
ausra.kondrataite@gf.stud.vu.lt

Thermophilic bacteria are considered to be useful biotechnological objects, since this type of bacteria has a lot of possible uses in various industrial fields, where these microorganisms serve as a source of many thermostable enzymes as well as biotechnologically produced metabolites. However, due to the lack of reliable genetic transformation systems for thermophiles, industrial application remains a challenging approach. Thus, optimization of genetic transformation of thermophilic bacteria is highly required.

The aim of this research was to broaden current knowledge of genetic manipulation of thermophilic bacteria in order to find the method of transforming the three bacterial strains - *Geobacillus stearothermophilus* 15, *Aeribacillus pallidus* 8 and *Parageobacillus toebii* DSM 14590^T. Shuttle vectors used in this study were methylated and non-methylated, containing replication initiation proteins from different species of thermophilic bacteria. Unfortunately, we did not obtain any transformants, which confirms that transformation efficiency is not strongly dependent on these factors.

Further studies concentrate on the vector methylation using recombinant restriction-modification (R-M) systems encoded by the thermophilic bacteria strains. Using the Restriction Enzyme Database (REBASE), we identified the R-M systems in the thermophiles and transferred these genes to the *Escherichia coli* strains. The extracted shuttle-vectors are later used for genetic transformation of thermophiles. We hope that using the heterologous expression of R-M system genes from thermophilic bacteria will allow exogenous DNA to avoid restriction by the host R-M system.

Overall, we believe that this work has a great potential and could be useful in future researches associated with genetic engineering of thermophilic microorganisms.

CANCELLED DUE TO COVID-19

EVALUATION OF ESSENTIAL OILS COMPOSITION OF *ARTEMISIA ABSINTHIUM* L. USING GC-MS

Sandra Saunoriūtė[1], Ona Ragažinskienė[2], Liudas Ivanauskas[3], Mindaugas Marksa[3]

[1]Faculty of Natural Science, Vytautas Magnus University, Vileikos 8, Kaunas, LT-44404, Lithuania
[2]Scientific Sector of Medicinal and Aromatic Plants, Vytautas Magnus University, Botanical Garden, Ž. E. Žilibero 6, LT- 46324 Kaunas, Lithuania
[3]Department of Analytical and Toxicological Chemistry, Lithuanian University of Health Science, Sukilėlių 13, LT-50162, Kaunas, Lithuania
sandra.saunoriute@vdu.lt

Chemical analysis of spice, aromatic plants at different vegetation stages can serve for the optimal collection of plant raw material revealing the period when the plant possesses the highest biological activity and accumulates the highest content of biologically active compounds, which could be used in pharmacy, medicine, food or cosmetic industry [1].

The aim of this study was to investigate the qualitative and quantitative composition of essential oils obtained from *A. absinthium* during different vegetation stages.

The object of investigation was *Artemisia absinthium* L. a perennial medicinal, aromatic plant of *Asteraceae* (Bercht. & J. Presl) family. *A. absinthium* is widely used in the Lithuanian folk medicine mainly for stomachic and anthelmintic activity, also for healing gall-bladder and kidneys diseases, against insomnia, diarrhea [3, 5, 6, 7]. Raw material of *A. absinthium* was collected during different vegetation stages of vegetation cycle in Spice – Melliferous plants collection *ex situ* of Botanical Garden at Vytautas Magnus University in 2018. Five stages have been separated: growth and leaf production, flower bud development, beginning of the flowering, massive flowering, end of the flowering [4]. The essential oils have been extracted by hydrodistillation method and analysed by the chromatographic techniques in the gas phase and chromatography in gas phase coupled with mass spectrometry (GC/MS) so as to determine their chemical composition. The percentage composition of the essential oils was computed from GC peak areas without correction factors. Qualitative analysis was based on a comparison of retention times, indexes and mass spectra with the corresponding data in the literature [2] and computer mass spectra libraries.

There were studied 5 samples of *A. absinthium* considering different vegetation stages. A total of 81 different compounds were found in the essential oils. The data showed that amounts of compounds with the content of major constituents varried significantly from (0.02 to 66.38%). The highest content and diversity of compounds was determined during the the massive flowering stage. To the major constituents belonged *trans*-sabinyl acetate, *cis*-chrysanthenol, *trans*-pinocarvyl acetate, *cis*-myroxide, β-myrcene, linalool.

[1] Abad M. J., Bedoya L. M., Apaza L., Bermejo P. The *Artemisia* L. Genus: A Review of Bioactive Essential Oils. Molecules, 17, 2542-2566 (2012).
[2] Adams R. P. Identification of Essential Oil Components by Gas Chromatography/Mass Spectrometry. Allured Publishing Corporation, Carol Stream, IL (1995).
[3] Altunkaya A., Yildirim B., Ekici K., Terzioglu O. Determining essential oil composition, antibacterial and antioxidant activity of water wormwood extracts GIDA 39, 17-24 (2014).
[4] European pharmacopoeia. 9 Edition. Strasbourg: Council of Europe. 2, 5145 (2017).
[5] Judzentiene A., Budiene J., Gircyte R., Masotti V., Laffont-Schwob I. Toxic Activity and Chemical Composition of Lithuanian Wormwood (*Artemisia absinthium* L.) Essential Oils. Rec. Nat. Prod. 6 (2), 180-183 (2012).
[6] Lachenmeier D.W. Wormwood (*Artemisia absinthium* L.): A curious plant with both neurotoxic and neuroprotective properties? Journal *of* Ethnopharmacol, 131(1), 224-227 (2010).
[7] Lopes-Lutz D., Alviano D. S., Alviano C. S., Kolodziejczyk P. P. Screening of chemical composition, antimicrobial and antioxidant activities of *Artemisia essential* oils. Phytochemistry, 69 (8), 1732-1738 (2008).

CANCELLED DUE TO COVID-19

EFFECT OF *ESCHERICHIA COLI* ENDOTOXIN ON VITAL FUNCTIONS OF RATS AFTER INTRANASAL INJECTION

Zhanna Hladkova

Institute of Physiology of the National Academy of Sciences of Belarus, Minsk, Republic of Belarus
gladkova_z@mail.ru

It has been experimentally proven that endotoxins are involved in the pathogenesis of neurodegenerative diseases such as Alzheimer's disease, Parkinson's disease, multiple sclerosis, amyotrophic lateral sclerosis. It happens due to the fact that endotoxin during intranasal administration is the closest to the natural way of penetration of a foreign agent into the body. In this regard, study of the effect of lipopolysaccharide from *Escherichia coli* (LPS) on somatic and visceral functions of the body is very important [1,2].

The aim of the study is to analyze changes in blood pressure, deep body temperature and the latent period of nociceptive reaction with prolonged intranasal administration of LPS.

The experiments were carried out with male Wistar rats weighing 280-320 g (n = 28), which were instilled intranasally with LPS daily (1; 10; 100 μg / ml) in a volume of 25 μl daily for 21 days. An apyrogenic saline solution (ASS) was used as a solvent for LPS, and it was used as a control. The parameters were recorded before the start, then - weekly on the 7th, 14th, 21st day of the experiment. All animals were divided into 4 groups depending on the dose of the injected substances: group 1 - ASS, group 2 - LPS 1 μg / ml, group 3 - 10 μg / ml, group 4 - 100 μg / ml. All experiments were carried out taking into account the recommendations of the European Convention on Humane Treatment of Laboratory Animals [3].

It has been established that the intranasal administration of ASS does not affect the latent period of nociceptive reaction, blood pressure, and deep body temperature.

On the 7th, 14th and 21st days of the experiment, a dose-dependent increase in blood pressure was recorded in all the studied groups of experimental animals. An increase in deep body temperature was observed in the third group of animals on the 21st day of the experiment (39.3 ± 0.2 ° C) relative to the control group of animals (38.5 ± 0.2 ° C). In the fourth group, an increase in deep body temperature was recorded already on the 7th (39.1 ± 0.5 ºC), the 14th (39.0 ± 0.5 ºC) and the 21st day (39.0 ± 0, 4 ºC) experiment. A decrease in latent period nociceptive reaction was observed only in the fourth group of rats on the 14th and 21st days (5.9 ± 0.6 s and 7 ± 1.6, respectively, $p < 0.05$). The values of blood pressure, deep body temperature and the nociceptive reaction period returned to the initial values 7 days after the end of the experiment.

It was shown in experiments that intranasal infusion of *E. coli* lipopolysaccharide is accompanied by a decrease in the threshold level (hyperalgesia), a dose-dependent increase in blood pressure and an increase in deep body temperature. The data obtained indicate that with chronic penetration of endotoxin into the body through the mucous membrane of the nasal cavity, the thermoregulatory and cardiovascular system reacts primarily and nociceptive sensitivity threshold decreases only two weeks later.

[1] Hunter, R. L., Cheng, B., Choi, D.-Y. et al., Intrastriatal lipopolysaccharide injection induces parkinsonism, Journal of Neuroscience Research **8** (2009). doi:10.1002/jnr.22012
[2] Chae C. U., Lee R. T., et al. Blood pressure and inflammation in apparently healthy men, Hypertension **38**, 399–403 (2001).
[3] European Convention for the protection of vertebrate animals used for experimental and other scientific purposes, Europ. Treaty Series **123**, (1986).

ARTICLE DUE TO COVID-19

RESPONSE PATTERNS OF BIOMARKERS IN DIFFERENT FISH SPECIES EXPOSED TO MULTICOMPONENT METAL (Cd, Cr, Cu, Ni, Pb and Zn) MIXTURE

Gintarė Sauliutė[1]*, Arvydas Markuckas[2], Brigita Čapukoitienė[1], Milda Stankevičiūtė[1]

[1]Nature Research Centre, Akademijos St. 2, LT-08412 Vilnius, Lithuania
[2]Vilnius University, Life Sciences Center, Department of Biochemistry and Molecular Biology, Saulėtekio av. 7, 10223 Vilnius, Lithuania
gintare.sauliute@gamtc.lt

Toxicity to fish of multicomponent metal mixtures at maximum-permissible-concentrations (MPC: Cd – 0.005, Cr – 0.01, Cu – 0.01, Ni – 0.01, Pb – 0.005 and Zn – 0.1 mg/L) set for EU inland waters was evaluated using the whole-mixture approach. The study on the biological effects of multicomponent metal mixtures on three ecologically different fish species, i.e. *Perca fluviatilis, Rutilus rutilus,* and *Salmo salar*, which are valuable bioindicators for monitoring water pollution, is reported. The aim of this study was to assess response patterns of biomarkers (erythrocytic nuclear abnormalities (ENAs), metal accumulation and metallothioneins) in tissues of ecologically different fish species following 14-day treatment with multicomponent metal mixtures at MPC and multicomponent metal mixtures with one of its components (single-metal) at reduced MPC (↓). Tissues of all tested fish species demonstrated different patterns of metal accumulation. After treatments with Cu↓ and Cr↓, the lowest amount of Ni was found in all tissues (except the liver) of all the three fish species tested. After Zn↓ and Pb↓ treatments, the amount of Ni in muscle of all the tested fish species significantly decreased. The highest amounts of Cr in gills and Pb in muscle were detected in all the tested fish species after treatments with Ni↓ and Cd↓ mixtures, respectively. *R. rutilus* accumulated significantly larger amounts of metals than *P. fluviatilis* and *S. salar.* The data obtained show that tissues of the omnivorous *R. rutilus* exposed to metal mixtures accumulated higher amounts of Cr, Cu, Ni and Zn, while tissues of the exposed carnivorous fish *S. salar* and *P. fluviatilis* higher amounts of Cd and Pb. The analysis of ENAs revealed concentration-dependent responses, indicating Cu↓ and Cr↓ treatments as causes of higher geno- and cytotoxicity levels. Our study highlights the impact that even changes in low metal concentration (MPC) exposure have on increased geno-, cytotoxicity risk in erythrocytes of *S. salar* and *P. fluviatilis* as well as on changes in accumulated metal amounts in all fish species.

CANCELLED DUE TO COVID-19

HAEMATOLOGICAL RESPONSES UNDER MULTIPLE STRESS EXPOSURE IN PERCH (*Perca fluviatilis*)

Brigita Čapukoitienė[1*], Gintarė Sauliutė[1], Tomas Makaras[1], Svetlana Markovskaja[1], Milda Stankevičiūtė[1]

[1]Nature Research Centre, Akademijos St. 2, LT-08412 Vilnius, Lithuania
brigita.capukoitiene@gamtc.lt

The aim of the present study was to evaluate haematological responses induced by multiple stress (parasitic infestation and metal mixture exposure) in European perch (*Perca fluviatilis*). In order to represent multiple stress, fish were exposed to two parasites: ectocommensal protozoan parasite (*Trichodina* sp. (naturally infected) and pathogenic oomycete *Saprolegnia parasitica* (experimentally infected)), and metal mixture (MIX: Zn, Cu, Ni, Cr, Pb and Cd). Uninfected and infected fish were exposed for 14 days period to MIX at a concentration corresponding to Maximum-Permissible-Concentrations (MPC) accepted for the inland waters in EU. Haematological parameters such as hemoglobin concentration (Hb, g/l), hematocrit level (Ht, %), erythrocytes (RBC × 10^6/μL), leukocytes (WBC × 10^3/μL) and thrombocytes (TC/500 leucocytes) count were determined [1]. Additionally, differential leucocyte count, mean cell volume (MCV), mean cell hemoglobin (MCH), and mean cell hemoglobin concentration (MCHC) were calculated [2, 3]. Multiple stressors (parasitic infestation + MIX) elicited significant decrease in WBC, RBC, TC and Ht, except Hb, in comparison to single stressor (uninfected MIX). No significant differences of differential leucocytes count, MCV, MCH and MCHC between multiple stressors exposed and control *P. fluviatilis* were observed.

[1] Z. Svobodova, D. Pravda, J. Palackova (1991) Unified methods of haematological examination offFish. Research Institute of Fish culture and Hydrobiology, Vodnany,Czecho Slivakia, 31 pp.
[2] M. Witeska, E. Kondera, M. Szymańska, M. Ostrysz (2010) Hematological changes in common carp (*Cyprinus carpio* L.) after short-term Lead (Pb) exposure. Pol. J. Environ. Stud, 19(4): 825–831.
[3] M. P. Natt, C. A. Herrick (1952) A new blood diluent for counting the erythrocytes and leucocytes of the chicken. Poultry Science, 31: 735–738.

CANCELLED DUE TO COVID-19

TROPHIC ECOLOGY OF SMALL MAMMALS IN COMMERCIAL ORCHARDS: INSIGHTS FROM STABLE ISOTOPE STUDIES

Vitalijus Stirkė[1*], Linas Balčiauskas[1], Laima Balčiauskienė[1], Raminta Skipitytė[2], Andrius Garbaras[2]

[1]Nature Research Centre, Lithuania
[2]Center for Physical Sciences and Technology, Lithuania
vitalijus.stirke@gamtc.lt

CANCELLED DUE TO COVID-19

Foraging strategies in various animal species in recent years are mainly determined by their isotopic niche which is defined by means of stable isotope analysis. According the trophic peculiarities small mammals of the middle latitudes are grouped into herbivores, granivores, omnivores and insectivores. Herbivores (*Microtus* spp.) mainly feed on the green plant material, granivores (*Apodemus* and *Micromys* spp.) on seeds, fruits and/or foods of animal origin, omnivores (*Myodes glareolus*) on both low and high energetic plant resources and animal food, and insectivores (*Sorex* spp.) on foods of animal origin.

In 2018–2019 we trapped small mammals in 15 commercial orchards, berry plantations and neighboring control habitats, mainly meadows [1]. In total, 1087 individuals (11 species) were trapped. In the orchards dominant species was common vole (*Microtus arvalis*), 37.9% of all trapped individuals, while in the control habitats dominant was striped field mouse (*Apodemus agrarius*) with the share of 29.0%.

Knowing the trophic ecology of the species that occur in a given location is crucial for understanding the factors that allow their co-existence. Values of the stable isotopes provide trophic-level information that is a time-integrated approximation of assimilated diet. We used hair of the trapped small mammals to investigate $\delta^{13}C$ and $\delta^{15}N$ stable isotope signatures. Carbon and nitrogen stable isotope ratios were measured using an elemental analyzer (EA) (Flash EA1112) coupled to an isotope ratio mass spectrometer (IRMS) (Thermo Delta V Advantage) via a ConFlo III interface (EA-IRMS). The accuracy of measurements were better than 0.15 ‰ for carbon and 0.2 ‰ for nitrogen isotope ratio.

Species position according $\delta^{15}N$ values formed one group of all herbivores and the yellow-necked mouse (*Apodemus flavicollis*) and the second of omnivore bank vole *M. glareolus* with the rest of granivore species. $\delta^{15}N$ values in *Sorex* species exceed all mentioned groups 2–3-fold [2]. Compared to natural habitat of the floode meadows [2], distribution of $\delta^{13}C$ values in commercial orchards was very wide (Fig. 1), especially in harvest mouse (*Micromys minutus*). Most distinct trophic position was characteristic to the commensal house mouse (*Mus musculus*).

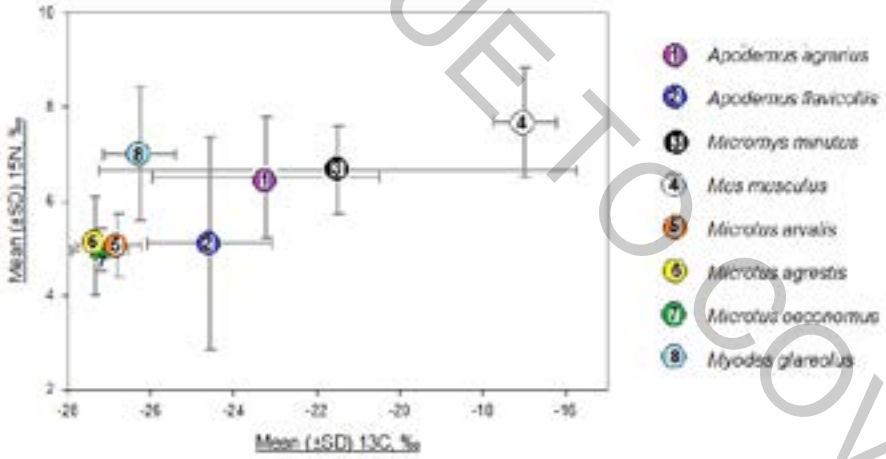

Fig. 1. Differences in the trophic space of granivores (1–4), herbivores (5–7) and omnivores (8) in commercial orchards.

Concluding, we found that (1) small mammal diet in the orchards did not differ significantly from the surrounding meadows – this implies also migration of the animals between orchards and meadows; (2) according distribution of $\delta^{15}N$ and $\delta^{13}C$ values, dietary niche in the orchards is segregated between small mammal species and groups; and (3) according small mammal community composition and diet, commercial gardens are in between natural and the other agricultural habitats. We presume possible effects of season, intensity of agricultural practices and crop type on the amplitude of the trophic niche of dominant species. Preliminary, the influence of habitat on the isotopic trophic niche is species-dependent and not unidirectional, thus being difficult to make general predictions of species response.

VS, LB and LB were financed by grant MoA Lithuania, No MT-18-3.

[1] Balčiauskas, L., Balčiauskienė, L., Stirkė, V., Mow the grass at the mouse's peril: diversity of small mammals in commercial fruit farms, Animals, **9(6)**, art. no. 334 (2019).
[2] Balčiauskas, L., Skipitytė, R., Balčiauskienė, L., Jasiulionis, M., Resource partitioning confirmed by isotopic signatures allows small mammals to share seasonally flooded meadows, Ecology and Evolution, **9(9)**, 5479-5489 (2019).

ISOLATION OF A HIGH MOLECULAR MASS PLASMID FROM OPPORTUNISTIC PATHOGEN *Acinetobacter baumannii*

Vaidas Mačiulskis[1*], Jūratė Skerniškytė[1], Edita Sužiedėlienė[1]

[1] Institute of Biosciences, Life Sciences Center, Vilnius University, Vilnius, Lithuania
*vaidas.maciulskis@gmc.stud.vu.lt

Acinetobacter baumannii is a gram-negative aerobic bacterium regarded as opportunistic pathogen due to ability to cause severe illness in persons with deficient immune system, particularly in hospital patients, although community-acquired cases are known as well [1]. Strains belonging to international clonal lineages I (IC I) and II (IC II) are associated with hospital outbreaks and high virulence. Clinical isolates frequently express multi-drug resistance (MDR) including resistance to colistin, a drug of last resort for gram-negative MDR species which highly contributes to worldwide concern about *A. baumannii* as an emerging threat to human health [2]. *A. baumannii* isolates exhibit diversity in variously sized plasmids they harbor [3]. Small to medium sized plasmids containing antibiotic resistance genes are studied extensively unlike large conjugative plasmids which remain mainly uncharacterized and their influence on *A. baumannii* virulence characteristics yet to be elucidated.

During previous laboratory investigations, characteristics of multiple clinical IC I and IC II isolates were described [4]. We speculate that phenotype differences related to pathogenicity among IC II isolates could be attributed to p2AB52 plasmid. *A. baumannii* isolate, harboring this 67 kb conjugative plasmid, was demonstrated to possess more hydrophobic cell surface and reduced lethality in animal infection model compared to another *A. baumannii* isolate, which lacks p2AB52. To confirm this hypothesis pulsed-field gel electrophoresis (PFGE) was performed as described by Barton *et al*. in order to isolate p2AB52 [5]. Single plasmid was isolated by cutting out a piece of agarose in the place of approximately 70 kb size band from the gel, digesting the piece with agarase and precipitating p2AB52 from the solution using isopropanol.

Further assays include transformation of isolated p2AB52 into *A. baumannii* isolate and determination of the phenotype of transformants such as cell surface hydrophobicity and lethality in animal infection model.

[1] Harding CM, Hennon SW, Feldman MF. Uncovering the mechanisms of *Acinetobacter baumannii* virulence. *Nat Rev Microbiol.* 2018;16(2):91–102.

[2] Qureshi ZA, Hittle LE, O'Hara JA *et al*. Colistin-Resistant *Acinetobacter baumannii*: Beyond Carbapenem Resistance. *Clinical Infectious Diseases.* 2015;60(9):1295-303.

[3] Salto PI, Torres GT, Wibberg D *et al.* Comparative genomic analysis of *Acinetobacter* spp. plasmids originating from clinical settings and environmental habitats. *Sci Rep.* 2018;8(1):7783.

[4] Skerniškytė J, Krasauskas R, Péchoux C *et al*. Surface-Related Features and Virulence Among *Acinetobacter baumannii* Clinical Isolates Belonging to International Clones I and II. *Front. Microbiol.* 2019;9(1):3116.

[5] Barton BM, Harding GP, Zuccarelli AJ. A general method for detecting and sizing large plasmids. *Analytical biochemistry.* 1995;226(2):235–240.

CANCELLED DUE TO COVID-19

THE EFFECTS OF CLASS-3 SEMAPHORIN PROTEINS ON ANGIOGENESIS *IN VITRO* SYSTEM

Giedrė Miniotaitė[1], Indrė Valiulytė[1], Arūnas Kazlauskas[1]

[1]Lithuanian University of Health Sciences, Neuroscience Institute, Laboratory of Molecular Neurooncology;
Eivenių st. 2, Kaunas LT-50161, Lithuania
miniotaitegiedre@gmail.com

Semaphorins are a large family of secreted, transmembrane, or GPI-anchored proteins that are found in variety of tissues and organ systems: nervous, cardiovascular, endocrine, gastrointestinal, immune, reproductive, respiratory, and other systems [1,2]. Semaphorins are best known for their roles in nervous system development, but they also are involved in tumorigenesis by regulating angiogenesis process which in abnormal conditions is a key mediator in cancer development [3,4]. Recent research works suggest that class-3 semaphorins (Sema3) fulfill important regulatory roles in multiple forms of cancer [5]. Depending on the specificity of the tissue, malignancy of the tumor, receptors on the surface of the cytoplasmic membrane, growth factors and ability of proteases to cleave semaphorins, Sema3 can promote or inhibit tumor angiogenesis processes [6]. For example, Sema3C can inhibit angiogenesis in pathologic retinopathy but also can function as angiogenesis promoting protein in gastric cancer [7,8].

The aim of this study was to investigate the effects of Sema3 (B, D, E, and G) on angiogenesis process *in vitro* system. First, expression vectors encoding Sema3 (B, D, E, and G) and a green fluorescent protein Venus or EGFP were constructed. Their construction was verified by performing restriction analysis. Then, human embryonal kidney cells 293FT were transfected with these vectors. The transfection efficiency was checked with fluorescent microscope and the expression of Sema3 (B, D, E and G) proteins in cells and cell media was confirmed by reverse transcription polymerase chain reaction (RT-PCR) and western-blot analysis. The medium of transfected cells, as a source of Sema3 proteins, was collected and used in angiogenesis *in vitro* assay with human umbilical vein endothelial cells (HUVEC). After 16 hours of incubation photos of microcapillary structures formed by endothelial HUVEC cells were taken (Fig. 1). Then, the parameters of microcapillary structures such as number of meshes, mean mesh size, number of junctions, number of master junctions, number of master segments and total length of master segments were analysed with „ImageJ Angiogenesis analyser“ program. Due to the inhibitory function of Sema3A on angiogenesis process [9], in our study it was used as negative control. Finally, statistical analysis (Student's t test) of the resulting quantitative data was performed using GraphPad Software Inc.'s Prism 8 software. The results revealed that among Sema3 (B, D, E, and G) proteins, Sema3B significantly promoted the formation of microcapillary structures. Other proteins (Sema3D, Sema3E and Sema3G) did not show any significant effects on the angiogenesis process *in vitro* compared to control.

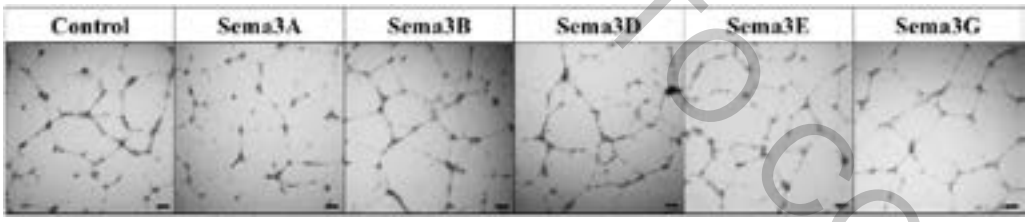

Fig. 1 Analysis of Sema3 effects on formation of the microcapillary HUVEC structures
Photos were taken after 16 hours of incubation. The black line in the lower right corner of the photo represents the 100 μm scale

[1] Hu S, Zhu L. Semaphorins and their receptors: From axonal guidance to atherosclerosis. Front Physiol. 2018;9:1–11.
[2] Alto LT, Terman JR. Semaphorins and their signaling mechanisms. Methods Mol Biol. 2017;1493(2):1–25.
[3] Verlinden L, Vanderschueren D, Verstuyf A. Semaphorin signaling in bone. Mol Cell Endocrinol. 2016;432:66–74.
[4] Li T, Kang G, Wang T, Huang H. Tumor angiogenesis and anti-angiogenic gene therapy for cancer. Oncol Lett. 2018;16(1):687–702.
[5] Toledano S, Nir-Zvi I, Engelman R, Kessler O, Neufeld G. Class-3 semaphorins and their receptors: Potent multifunctional modulators of tumor progression. Int J Mol Sci. 2019;20(3):556–76.
[6] Gaur P, Bielenberg DR, Samuel S, Bose D, Zhou Y, Gray MJ, et al. Role of class 3 semaphorins and their receptors in tumor growth and angiogenesis. Clin Cancer Res. 2009;15(22):6763–70.
[7] Yang W, Hu J, Uemura A, Tetzlaff F, Augustin HG, Fischer A. Semaphorin - 3C signals through Neuropilin - 1 and PlexinD1 receptors to inhibit pathological angiogenesis. EMBO Mol Med. 2015;7(10):1267–1284.
[8] Miyato H, Tsuno NH, Kitayama J. Semaphorin 3C is involved in the progression of gastric cancer. Cancer Sci. 2012;103(11):1961–1966.
[9] F. Maione, F. Molla, C. Meda, R. Latini, L. Zentilin, M. Giacca, et. al. Semaphorin 3A is an endogenous angiogenesis inhibitor that blocks tumor growth and normalizes tumor vasculature in transgenic mouse models. J. Clin. Invest. 2009; 119:3356–3372.

CORRECTED PUBLICATION COVID-19

IDENTIFICATION OF NEW ANTIMICROBIAL PEPTIDES FROM THERMOPHILIC BACTERIA

Ana Koniuchovaitė, Lilija Kalėdienė, Arnoldas Kaunietis

Department of Microbiology and Biotechnology, Institute of Biosciences, Life Sciences Center, Vilnius University, Lithuania
arnoldas.kaunietis@gmc.vu.lt

CANCELLED DUE TO COVID-19

Bacteriocins comprise a huge family of ribosomally synthesized peptides. They are heat-stable, produced by various bacteria and have antibacterial activity towards closely related strains, although there are an increasing number of bacteriocins reported to have broad range antimicrobial activity. Interest in bacteriocin research has gained great momentum due to its potential as both a natural food preservative and as next-generation antibiotics targeting the multiple-drug resistant pathogens. They are especially attractive for various applications.

Thermophilic bacilli are a potential contaminant in various industries that maintain higher temperatures (40-65°C) in the manufacturing process as food industry. Bacteriocins acting against thermophilic bacteria could be a solution to this problem. Thermophilic bacteria proteins are usually thermostable, therefore bacteriocins derived from these bacteria could be also thermostable, even with a higher thermostability than those encoded in mesophilic bacteria.

This study aimed to synthesize and characterize new antibacterial peptides. We analyzed genomes of thermophilic bacteria species and identified gene clusters encoding potential bacteriocins. One novel bacteriocin (circularin-like) was encoded in *Geobacillus thermoleovorans* strain. It is post-translationally modified head-to-tail cyclized peptide, whose N- and C-termini are linked by a peptide bond. Another one (lacticin-like) was found in genome of *Parageobacillus thermoglucosidasius*. It is leaderless bacteriocin and do not contain unusual post-translational modifications. We have cloned the bacteriocin biosynthesis genes into expression vectors and performed their heterologous biosynthesis in *Escherichia coli* to obtain active antibacterial peptides. The synthesized bacteriocins will be purified, characterized and evaluated for their antibacterial activity against various bacteria strains including pathogens.

UTILISING CRISPR-Cas9 TO TAG ENDOGENOUS GENE LOCI WITH C-TERMINAL FLUORESCENT PROTEIN FUSIONS IN PREIMPLANTATION MOUSE EMBRYOS

Miriama Pekľanská[1], Federica Serati[1] & Alexander William Bruce[1*]

[1] Laboratory of Early Mammalian Developmental Biology, Department of Molecular Biology and Genetics, University of South Bohemia, Czech Republic
miriama.peklanska@gmail.com

A complete understanding of preimplantation stages of mouse embryo development is still lacking. A technical mainstay of research into the specific function of individual genes/proteins during these stages has been the use of antibodies to detect expression and sub-cellular localisation using microscopic immuno-fluorescent staining approaches [1]. However, this method is not 100% reliable, as antibodies are not always as specific as claimed and not all proteins have available and reliable anti-sera.

Hence, one option to study specific proteins is to create transgenic embryos that incorporate genetically encoded fluorescence reporter proteins as fusions with endogenous candidate genes [2]. Thus, permitting the expression level and subcellular localisation of specific genes to be assayed, across preimplantation developmental time, in both live and fixed embryos. We are currently adopting one such method to achieve this aim that exploits the CRISPR-Cas9 system to fluorescently tag candidate cell-fate related genes in mouse embryos.

The main goal of my study is to create the necessary *in vitro* derived RNAs (i.*e.* biotinylated candidate gene specific guide RNAs/sgRNA and Cas9-Strepavidin mRNA) needed (Figure 1). Such RNAs will be co-microinjected into one cell stage zygotes or 2-cell stage mouse embryos, together with generated (by myself) and engineered recombinant DNA repair templates that target the candidate gene loci to ensure C-terminal tagging with the fluorescent protein mCherry. We will then microscopically assay the expression and sub-cellular localisation of these candidate genes, via the fused mCherry fluorescent tag, up to the peri-implantation blastocyst stages.

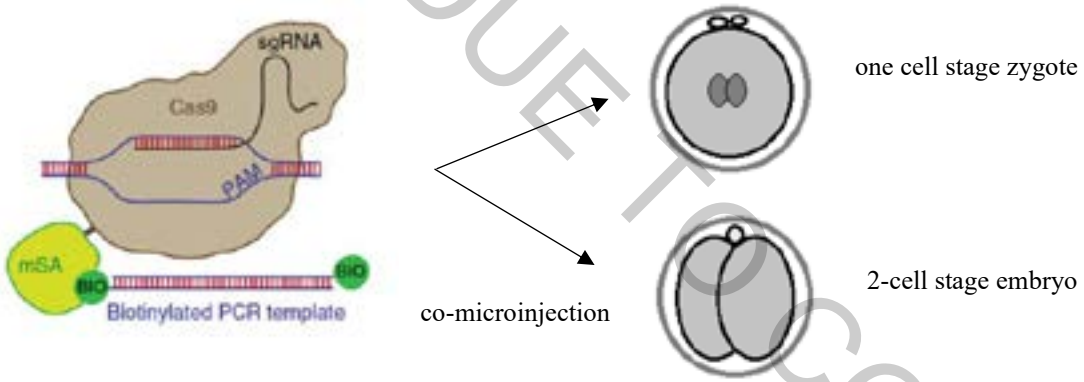

Fig. 1. Schematic showing the Cas9 complex [2] and the process of co-microinjection.

[1] Crivat, G., & Taraska, J. W. (2012). Imaging proteins inside cells with fluorescent tags. *Trends in Biotechnology*, *30*(1), 8–16.
[2] Gu, B., Posfai, E., & Rossant, J. (2018). Efficient generation of targeted large insertions by microinjection into two-cell-stage mouse embryos. *Nature Biotechnology*, *36*(7), 632–637.

CANCELLED DUE TO COVID-19

GEOBACILLIN 19, NOVEL BACTERIOCIN FROM A THERMOPHILIC BACTERIUM

Saulė Ulinauskaitė [1], Algirdas Kaupinis [2], Mindaugas Valius [2], Lilija Kalėdienė [1], Arnoldas Kaunietis [1]

[1]Vilnius University, Life Sciences Center, Institute of Biosciences, Department of Microbiology and Biotechnology, Lithuania

[2]Vilnius University, Life Sciences Center, Institute of Biochemistry, Proteomics Centre, Lithuania

saule.ulinauskaite@gf.stud.vu.lt

The genus *Geobacillus* is represented by obligately thermophilic bacteria able to grow in the temperature range of 35–75°C. Growth at high temperatures makes *Geobacillus* species promising agents in biotechnological processes. They can be sources of various thermostable enzymes. Also, *Geobacillus* spp. can produce bacteriocins, it is ribosomally synthesized antimicrobial peptides or proteins, which has narrow antagonistic activity spectrum against bacterial strains closely related to the strain-producer. The activity of bacteriocins against foodborne and pathogenic bacteria opens wide opportunities for their application in medicine and food industry [1].

Little is known about bacteriocins of thermophilic bacteria. *Geobacillus stearothermophilus* 15 produces two bacteriocins geobacillin 26 (Geo26) and geobacillin 19 (Geo19). Whereas Geo26 have been well characterized and its amino acid sequence determined [2], native Geo19 still needed characterization. In this study we tested several different growth mediums for bacteriocin production and purification. After medium optimization different protein chromatographic strategies have been used to purify Geo19. Using mass spectrometry analysis, we determined the amino acid sequence of Geo19. Bioinformatics tool BLASTp at NCBI database revealed gene sequence coding Geo19 protein in the genome of *Geobacillus stearothermophilus* 15. Our focus now is in cloning and heterologous expression of recombinant Geo19 in *Escherichia coli* for further characterization.[i]

[1] G. Novik, V. Savich, and O. Meerovskaya, "Geobacillus Bacteria: Potential Commercial Applications in Industry, Bioremediation, and Bioenergy Production," 2018.

[2] M. Vaičikauskaitė *et al.*, "Geobacillin 26 - high molecular weight bacteriocin from a thermophilic bacterium," *Int. J. Biol. Macromol.*, vol. 141, pp. 333–344, Dec. 2019.

CANCELLED DUE TO COVID-19

TAGGING *A. BAUMANNII* TYPE VI SECRETION SYSTEM COMPONENTS WITH A GREEN FLUORESCENT PROTEIN

Julius Martinkus, Renatas Krasauskas, Jūratė Skerniškytė, Julija Armalytė, Edita Sužiedėlienė

Institute of Biosciences, Life Sciences Center, Vilnius University, Vilnius, Lithuania
julius.martinkus@gmc.stud.vu.lt

Acinetobacter baumannii is a Gram-negative opportunistic pathogen responsible for hospital-acquired nosocomial infections [1], [2]. It is a successful pathogen due to its ability to resist desiccation, disinfectants and major antimicrobials [3]. Previously identified *A. baumannii* two-component signal transduction system BfmRS was shown to be responsible for regulating virulence-related traits such as biofilm production, resistance to antibiotics, type VI secretion system (T6SS) regulation, survival in human ascites fluid and serum [4]. T6SS is also related to *A. baumannii* virulence and responsible for inter-bacterial competition and bacterial interactions with eukaryotic cells [5]. Secretion systems are usually regulated by two-component signal transduction systems. However, T6SS regulation and BfmRS role in it are not fully understood. Therefore, in this work, we aimed to fluorescently label T6SS components in *A. baumannii*.

Markerless gene deletion technique was used to generate Δ*bfmRS*, Δ*hcp*, and Δ*bfmRS*Δ*hcp* mutants. The total protein content of mutants was visualized using SDS-PAGE. The inter-bacterial competition assay was performed by incubating mixed bacterial strains at the aggressor (*A. baumannii*) and prey (*E. coli*) ratio 10:1, respectively. Components of T6SS (Hcp and TssB) were fused with a green fluorescent protein by the PCR-based overlap extension method. Labeled proteins were tracked by a fluorescent microscope with a 600x-1000x magnification range.

Protein secretion profiles of *A. baumannii* clinical strain and its Δ*bfmRS* mutant revealed that the mutant displayed a reduction of Hcp protein, which is essential for the assembly of the T6SS apparatus. However, competition assays showed that loss of bfmRS did not impair the killing phenotype. To evaluate the assembly state of T6SS in the mutant, Hcp protein was fluorescently labeled with a green fluorescent protein in N- and C- termini. However, fluorescent labels *per se* impaired killing phenotype and Hcp tracking did not reveal any information about the state of T6SS. Therefore, we then fluorescently labeled sheath protein TssB and evaluated T6SS activity.

Fluorescently labeled T6SS with Hcp protein was non-functional. However, T6SS component TssB looks like a promising candidate to track T6SS in *A. baumannii*.

[1] C.-R. Lee et al., 'Biology of Acinetobacter baumannii: Pathogenesis, Antibiotic Resistance Mechanisms, and Prospective Treatment Options', Front. Cell. Infect. Microbiol., vol. 7, Mar. 2017, doi: 10.3389/fcimb.2017.00055.
[2] F. C. Morris, C. Dexter, X. Kostoulias, M. I. Uddin, and A. Y. Peleg, 'The Mechanisms of Disease Caused by Acinetobacter baumannii', Front. Microbiol., vol. 10, 2019, doi: 10.3389/fmicb.2019.01601.
[3] M. S. Ramirez et al., 'Identification of Potential Virulence Factors in the Model Strain Acinetobacter baumannii A118', Front. Microbiol., vol. 10, 2019, doi: 10.3389/fmicb.2019.01599.
[4] E. Geisinger, N. J. Mortman, G. Vargas-Cuebas, A. K. Tai, and R. R. Isberg, 'A global regulatory system links virulence and antibiotic resistance to envelope homeostasis in Acinetobacter baumannii', PLoS Pathog., vol. 14, no. 5, May 2018, doi: 10.1371/journal.ppat.1007030.
[5] S. Coulthurst, 'The Type VI secretion system: a versatile bacterial weapon', Microbiol. Read. Engl., vol. 165, no. 5, pp. 503–515, 2019, doi: 10.1099/mic.0.000789.

CANCELLED DUE TO COVID-19

USING OF HESPERIDINE FOR PREVENTION POISONING OF PHOSPHORORGANIC SUBSTANCES

Volodymyr Vasylenko[1], Volodymyr Bessarabov[1], Galyna Kuzmina[1], Victoria Chumak[1], Marina Sidorenko[2], Saulius Mickevičius[2]

[1] Department of Pharmaceutical Industry, Kyiv National University of Technologies and Design, Ukraine
[2] Faculty of Natural Sciences, Vytautas Magnus University, Lithuania
v.vasylenko@kyivpharma.eu

CANCELLED DUE TO COVID-19

According to the World Health Organization, about 3 million pesticide poisonings occur worldwide each year. The use of organophosphorus substances is poorly regulated and their easy accessibility is a consequence of a large number of self-poisonings [1]. The main pathogenetic mechanism of action of organophosphorus compounds is based on the inhibition of the activity of cholinesterases - enzymes that hydrolyze acetylcholine and butyrylcholine and play an important role in the process of synaptic transmission of nerve impulse in cholinergic entities [2]. Therefore, the development of new ways of preventing poisoning with organophosphorus toxic substances is relevant.

As a model substance used paraoxone. The aim of the study was to determine the activity of human serum butyrylcholinesterase in the presence of paraoxon and with the preliminary inhibition of the enzyme by the model flavonoid hesperidin.

The study is based on the determination of *ex vivo* human serum butyrylcholinesterase activity using a modified Ellman method. This method is based on the ability of the thiocholine, the reaction product, to restore potassium hexacyanoferrate (III), which is colored yellow, to potassium hexacyanoferrate (II), which is practically unpainted. This allows direct photometric registration of the rate of enzymatic reaction.

According to the results of the study, diagrams of changes in the activity of human serum butyrylcholinesterase in the presence of paraoxon (0.01 mkM) and with the preliminary addition of hesperidin (50; 100; 200 mkM) were constructed (Fig. 1).

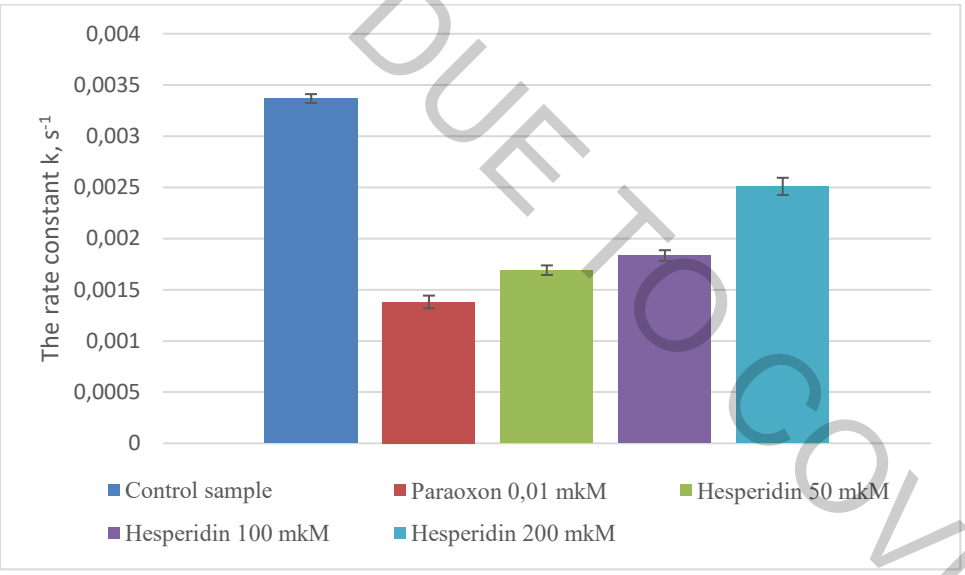

Fig. 1. Changes in the activity of human serum butyrylcholinesterase in the presence of paraoxone (0.01 mkM) and with the preliminary addition of hesperidin (50; 100; 200 mkM).

With the addition of paraoxone, the activity of butyrylcholinesterase decreased dramatically. But in the next experiment, when previously added to the system of hesperidin, the degree of inhibition of butyrylcholinesterase by paraoxone is reduced by almost 45%. It is shown that the higher the concentration of hesperidin, – the higher the activity of butyrylcholinesterase. Hesperidin is a reversible inhibitor. Prior to the addition of hesperidin to the serum, it binds to the active center of butyrylcholinesterase, leaving no room for paraoxon. Over time, hesperidine exits the active center and the enzyme activity is restored.

The established effect can be used in the development of new drugs for the prevention of poisoning by organophosphorus toxic substances.

[1] Y.H. Hou et al., An analysis of the clinical and epidemiological characteristics of acute poisoning patients in general hospital, Zhonghua lao dong wei sheng zhi ye bing za zhi. **7**(34), 506-509 (2016).
[2] Y. Li. et al., Clinical toxicology in China: current situation and future development, Clinic toxicol. 47, 263-269 (2009).

NEURAL GENE EXPRESSION PATTERNS OF DIFFERENTIATED HUMAN AMNIOTIC FLUID STEM CELLS

Elizabet Beržanskytė[1], Aistė Zentelytė[1], Giedrė Valiulienė[1], Rūta Navakauskienė[1]

[1] Department of Molecular Cell Biology, Institute of Biochemistry, Life Sciences Center, Vilnius University
LT-10257 Vilnius, Lithuania
elizabet.berzanskyte@gmc.stud.vu.lt

CANCELLED DUE TO COVID-19

Amniotic fluid is a promising source of stem cells in regenerative medicine, since these cells are easy to isolate from amniocentesis samples, they display high proliferation potential as well as the ability to differentiate towards lineages from all three germ layers [1]. As neural tissue has restricted regeneration potential, amniotic fluid stem cells (AFSC) could be an attractive option for therapeutic purposes. Therefore the aim of this study was to evaluate the potential of AFSC to differentiate towards neural cell lineage under different induction conditions.

Stem cells were obtained using a two-stage isolation protocol and expanded in monolayer culture where they displayed typical spindle shaped morphology. Cells were characterized and were positive for pluripotent stem cell markers (Nanog, Sox2, Oct4, Rex1) and mesenchymal stem cell markers (CD44, CD73, CD90, CD105, CD146, CD166). In order to initiate neural differentiation of AFSC we used several induction protocols (Fig. 1) which comprised commercial supplement NeuroCult™ and biomolecules such as NGF, BDNF, cAMP, IBMX, retinoic acid and KCl. Later the expression of neural genes (*NES*, *NSE*, *TUBB3*, *GFAP*, etc.) was examined. Results of this study revealed some differences in expression of specific genes when using distinct combinations for neurogenic induction. In addition, the dependence of differentiation efficiency on chosen differentiation inducing agents was highlighted. Differentiated cells were also characterized by specific proteins (Tubulin B3, Vimentin and NCAM) using fluorescence microscopy. As a positive control for neuronal cell culture model human neuroblastoma SH-SY5Y cell line [2] was used.

The results of this work bring new insights about the ability of AFSC to differentiate into neural-like cells and the importance of differentiation induction conditions, however, a more in-depth research is required to acquire functional AFSC-derived neural cells.

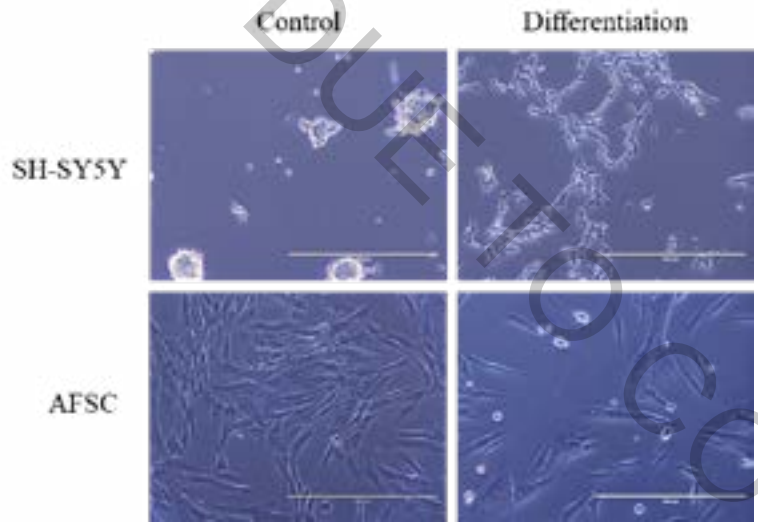

Fig. 1. Representative images of AFSCs and SH-SY5Ys after 3 days of differentiation induction. Scale bar = 400 µm. Differentiation was performed using the following protocols: BrainPhys with NeuroCult, antibiotics, 10 µM RA, BDNF and NGF supplements for SH-SY5Y cells; DMEM/F12 with antibiotics and 1mM 8-bromo-cyclic AMP for AFSC cells.

[1] Bonaventura et al., Different Tissue-Derived Stem Cells: A Comparison of Neural Differentiation Capability, PLOS ONE (2015).
[2] McLaughlin et al., Stable expression of a neuronal dopaminergic progenitor phenotype in cell lines derived from human amniotic fluid cells, Journal of Neuroscience Research (2006).

NITROGEN AS A KEY NUTRIENT AMONG POPULATIONS OF *PHALARIS ARUNDINACEA*

Edvina Krokaitė[1*], Tomas Rekašius[1,2], Lina Jocienė[1], Donatas Žvingila[3], Eugenija Kupčinskienė[1]

[1] Department of Biology, Vytautas Magnus University, Vileikos str. 8, LT-44404, Kaunas, Lithuania
[2] Vilnius Gediminas Technical University, Saulėtekio al. 11, LT-10223, Vilnius, Lithuania
[3]Nature Research Centre, Akademijos str. 2, LT-08412, Vilnius, Lithuania
[3]Vilnius University, Saulėtekio al. 7, LT-10257, Vilnius, Lithuania
*edvina.krokaite@gmail.com

Currently bigger attention started to be paid to the quality of inland waters, which receive substantial nutrient inputs such as nitrogen (N). Although data regarding riparian species response to pollution by nutrients are very poor in Lithuania. Among water macrophytes of our country, reed canary grass (*Phalaris arundinacea* L.) is a common and frequently occurring species. Due to huge biomass much attention is paid to this plant for its use as biofuel, for bioremediation, for forage or ornamental purposes.

We investigated leaf N concentration differences and compared it among populations of *P. arundinacea* growing in different sites of Lithuanian rivers. Our study involved over 60 populations, sampled on Nemunas, Venta, Lielupė and coastal river catchments of Lithuania. Nitrogen concentrations were determined using Kjeldahl method and expressed as percentage of dry mass (d. m.) of the leaf tissue.

Mean leaf N concentration for all populations of *P. arundinacea* was 3.50 % d. m. The lowest N concentration (3.03 % d. m.) was documented in population sampled on the bank of the river Merkys, while the highest (3.69 % d. m.) was observed in population near the Neris river, the most contrasting ones differed by 1.32 times ($p < 0.05$). Leaf N concentrations of *P. arundinacea* were compared to the same parameter of some other riparian plant species: in respect to N concentrations, *P. arundinacea* was of intermediate position: higher than *Lythrum salicaria* or *Stuckenia pectinata, although lower compared to Bidens frondosa*. *Phragmites australis, Nuphar lutea or Echinocystis lobata*.

To determine the potential impact of the rivers and their environment on the N concentration in the plant, populations of *P. arundinacea* were classified into five groups according to: the land cover and use type of the areas neighboring riverbank (based on classification system of COoRdinate Information on the Environment; CORINE) [1].

Agricultural areas near the *P. arundinacea* sites were the most common type of the land use, accounting for 72 % (44 of all populations) cases. Mean leaf N concentration in populations near the riverbanks of the agricultural areas was 2.83 % d. m. Forestry areas near the *P. arundinacea* sites were the less common and constituted 11 % (7) of all populations, where mean leaf N concentration was 2.72 % d. m. Mean leaf N concentration in populations near the artificial areas was 3.17 % d. m.

According to the occurrence of populations in the river fragments of different state, defined by Water Framework Directive, *P. arundinacea* was described as very resistant species to pollution [2]. The biggest number (57 %) of populations, were collected in the South-East part of Lithuania representing the least polluted rivers (0.6–2.1 mg N L^{-1} in 1992–1996) [3]. In our case reed canary grass growing near the river segments of poor (14 % of populations) or bad (3 % of populations) condition, did not contain significantly higher leaf N concentrations.

The largest number (49 %) of populations were located along medium size (100-1000 km^2) rivers, the smallest number (13 %) – along extra-large size (>10000 km^2) rivers. Banks of the small size rivers were missing among sites of *P. arundinacea.* There was no significant leaf N concentration between the populations along the rivers of the different size.

The highest number (79 %) of populations for *P. arundinacea*, were located along the natural river segments, where mean value of leaf N concentration of populations was 2.91 % d. m., while N concentration of populations from regulated river parts was 2.73 % d. m. No significant differences of leaf N concentrations were found between populations in regulated and natural river segments. Overall, our results revealed that leaf N concentration of *P. arundinacea* populations of Lithuania were not stronger influenced by the river segments exposed to different anthropogenic effect.

[1] CORINE Land Cover Nomenclature Conversion to Land Cover Classification System (2006). http://www.igeo.pt/gdr/pdf/CLC2006_nomenclature_addendum.pdf
[2] Directive 2000/60/EC of the European Parliament and of the Council of 23 October 2000 establishing a framework for Community action in the field of water policy. The Official Journal of the European Communities, L 327/1–327/72 (2000).
[3] R. Tumas. Regularities of river water quality under the interactions of physical geography factors and farming intensity. Proceedings of Nordic Hydrological Conference. Helsinki, Finland, 100–108 (1998).

CANCELLED DUE TO COVID-19

SOME PECULIARITIES OF *LYTHRUM SALICARIA* NUTRITION

Edvina Krokaitė[1*], Dinara Shakeneva[1], Tomas Rekašius[1,2], Lina Jocienė[1], Donatas Žvingila[3], Eugenija Kupčinskienė[1]

[1] Vytautas Magnus University, Vileikos str. 8, LT-44404, Kaunas, Lithuania
[2] Vilnius Gediminas Technical University, Saulėtekio al. 11, LT-10223, Vilnius, Lithuania
[3]Vilnius University, Saulėtekio al. 7, LT-10257, Vilnius, Lithuania
*edvina.krokaite@gmail.com

CANCELLED DUE TO COVID-19

Nowadays much attention is paid to the quality of wetlands and waters. Environmental data on pollutants are not sufficient to understand the direct effects of negative compounds on aquatic flora. There is also the question of human impact on the environment. Land use is facing a major pollution load, in particular due to the use of fertilizers in agriculture, which falls in inland waters. Nitrogen (N) is the main mineral nutrient needed for plants and it plays an essential role in the plant life cycle. The nutrient evaluation could help to understand the affection level for environment.

Lythrum salicaria is riparian plant species, naturally occurring the riverbanks in Europe but is invasive in the United States of Amerika and Canada. This plant used for medical purposes, has many secondary metabolites and is important as indicator of soil salinity. There are genetical evaluations of this plant, but there is a lack of information about ecophysiological parameters, especially in the Baltic countries.

Our task was to evaluate leaf N concentration differences and compared it among populations of *L. salicaria* growing in different sites of Lithuanian rivers. Our study involved 29 populations of selected plant species, sampled on the Nemunas river and seafront catchments. Three independent batches of healthy leaves were dried, turned to the powder and analyzed by Kjeldahl method. Nitrogen concentrations were expressed as percentage of dry mass (d.m.).

Mean leaf N concentration for *L. salicaria* populations was 2.98 % d.m. The lowest N concentration (2.35 % d.m.) was documented in population sampled on the bank of the river Nemunas, while the highest (3.94% d.m.) was observed in population near the river Neris. Difference between the most contrasting populations was 1.68 times ($p < 0.05$). The mean values of leaf N concentration of Lithuanian populations of *L. salicaria* were lower than other neighbouring plant species like *Phalaris arundinacea Stuckenia pectinata, Bidens frondosa, Phragmites australis, Nuphar lutea or Echinocystis lobata*. Compared to the other species, among populations of *Lythrum. salicaria* differences in leaf N concentrations were the highest.

In order to determine the potential effect of rivers and their environment on nitrogen concentration in plants, *L. salicaria* populations were divided into five groups according to: the land cover type (based on classification system of COoRdinate Information on the Environment; CORINE) [1], river state, geographical location, river size and riverbed origin. Significantly higher ($p < 0.05$) leaf N concentrations were found for *L. salicaria* populations growing near agricultural areas (3.2 % d.m.) compared to populations found near artificial areas (2.8 % d.m.) or forest (2.7% d.m.). Significantly higher ($p < 0.05$) concentrations of leaf N concentrations were found for *L. salicaria* populations growing near the small rivers (3.4% DM) compared to the large ones (2.8 % d.m.). The higher N concentration than the median value was determined for *L. salicaria* growing in the centre of Kaunas city, it might be related to point sources of pollution [2]. The highest number (77 %) of *L. salicaria* populations, were located in the natural river parts, where mean value of leaf N concentration of populations was lower (2.9 % d.m.) compared to N concentration of populations from regulated river parts (3.2 % d.m.) [3].

It can be assumed that *L. salicaria* populations are affected by neighboring agricultural areas, in addition, N nutrition conditions are different comparing the rivers of the different size.

[1] CORINE Land Cover Nomenclature Conversion to Land Cover Classification System (2006). http://www.igeo.pt/gdr/pdf/CLC2006_nomenclature_addendum.pdf

[2] A. S. Šileika, M. Wallin, K. Gaigalis. Assessment of nitrogen pollution reduction options in the river Nemunas (Lithuania) using FyrisNP model. Journal of Environmental Engineering and Landscape Management, 21 (2): 141–152 (2013).

[3] E. Krokaitė, D. Shakeneva, E. Juškaitytė, T. Rekašius, J. Nemaniūtė-Gužienė, J. Butkuvienė, J. Patamsytė, V. Rančelienė, R. Vyšniauskienė, L. Duchovskienė, L. Jocienė, Z. Sinkevičienė, D. Naugžemys, V. Kleizaitė, D. Chmura, N. O. Anderson, D. Žvingila, E. Kupčinskienė. Nitrogen concentration of the aquatic plant species in relation to land cover type and other variables of the environment. Zemdirbyste-Agriculture, 106 (3): 203–212 (2019).

COMPARISON OF INTELLECTUAL DISABILITY ASSOCIATED GENES IN X CHROMOSOME AND AUTOSOMES

Austėja Dapkutė[1], Egle Preikšaitienė[2]

[1] Faculty of Medicine, Vilnius University, Lithuania
[2] Department of Human and Medical Genetics, Institute of Biomedicine sciences, Faculty of Medicine, Vilnius University, Lithuania
austeja.dapkute@mf.stud.vu.lt

CANCELLED DUE TO COVID-19

Despite of many extensive studies held on an intellectual disability, it still remains one of the most mysterious neuropsychiatric disorders. The prevalence of an intellectual disability (2-3% of the population) [1] and its variability induce active research of the etiology of this disorder. Frequently, such research directs to genetic causes of an intellectual disability. The epidemiology of this disorder is quite astonishing – there can be around 20 % more males, affected by intellectual disability, than there are females. [2] Such prevalence can explain extensive studies held on the research of X chromosome linked mutations potentially causing intellectual disorders.

After reviewing the most significant articles, published during the last 20 years and currently ongoing international studies which investigate the linkage of X chromosome and intellectual disability, it was observed that there was a constant increase of genes, associated with X-linked intellectual disability. However, it is very difficult to interpret this result because with a notable improvement of laboratory equipment many genes were identified on other chromosomes, as well. It is often a topic for debates whether all chromosomes should be acknowledged as having the same significance for the cause of intellectual disability or X chromosome is still yielding more potential to cause this disorder. [3] To address this question, we aimed to calculate the ratio of genes, associated with intellectual disability in each chromosome and to compare this ratio between the data of X chromosome and autosomes.

We listed genes associated with intellectual disability, found in OMIM and DECIPHER databases. To access the data of all protein coding genes in each chromosome, Ensembl database was used.

It was calculated that the average ratio between intellectual disability associated genes and all protein coding sequences in the chromosome was 5,43% (SD=2,72) for autosomes and 17,12% for X chromosome (Fig. 1). This difference was statistically significant ($p<0,05$).

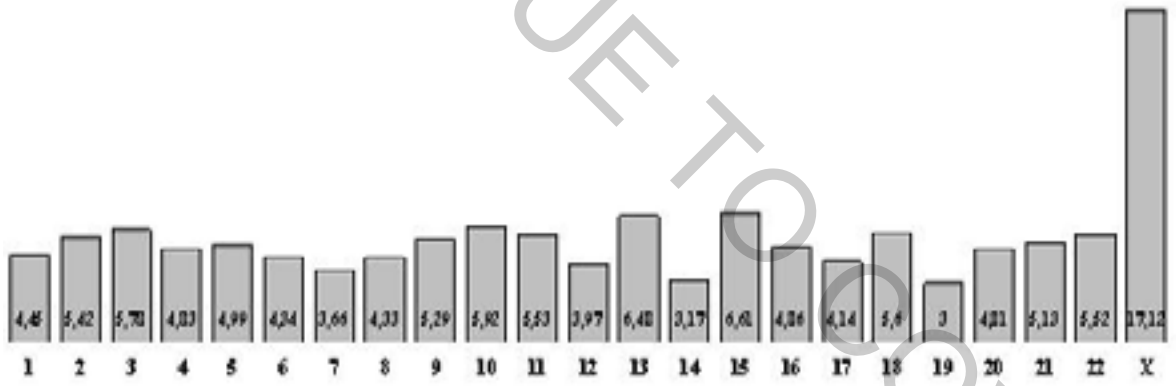

Fig. 1. Percentage of intellectual disability associated genes in every chromosome

According to our results, it can be concluded that with the current knowledge, the diagnosis of X-linked intellectual disability is much more likely to occur in comparison with autosomal mutation caused intellectual disability. It is speculated that the reason for X chromosome genes to be involved in the intelligence at such a high level might be the chromosome's sequence conservation and lower recombination frequency [4] or a skewed X-inactivation when a heterozygous mutation occurs. [5]

[1] Raugalė A, Bubnaitienė V, Ėmužytė R, Grinkevičiūtė D, Gurskis V, Kėvalas R, et al. Vaikų ligos: 4 tomas: Infekcinės ligos. Alerginės ligos. Imunodeficito būklės. Reanimacija ir intensyvioji terapija. Vaikų elgesio ir psichikos sutrikimai. Vilniaus universiteto leidykla; 2005.
[2] Stevenson RE, Schwartz CE. X-linked intellectual disability: unique vulnerability of the male genome. Dev Disabil Res Rev 2009; 15: 361–8.
[3] Chiurazzi P, Pirozzi F. Advances in understanding – genetic basis of intellectual disability. F1000Research 2016; 5.
[4] Knight SJL. Genetics of mental retardation: an overview encompassing learning disability and intellectual disability. Karger Medical and Scientific Publishers; 2010.
[5] Plenge RM, Stevenson RA, Lubs HA, Schwartz CE, Willard HF. Skewed X-chromosome inactivation is a common feature of X-linked mental retardation disorders.Am J Hum Genet 2002; 71: 168–73.

MIRNAS AS THE POTENTIAL BIOMARKERS FOR CHRONIC PERIODONTITIS

Benita Buragaite-Staponkiene[1], Kristina Stuopelyte[1], Adomas Rovas[2], Egle Punceviciene[3], Irena Butrimiene[3], Alina Puriene[1,2], Sonata Jarmalaite[1]

[1] Human Genome Research Group, Life Sciences Center, Vilnius University, Vilnius, Lithuania
[2] Vilnius University Hospital Zalgiris Clinic, Vilnius, Lithuania
[3] Vilnius University Hospital Santaros Clinics, Vilnius, Lithuania
benita.buragaite@gmc.stud.vu.lt

CERTIFIED PUF COVID-19

Chronic periodontitis (CP) is a highly prevalent oral disease affecting 20-50% of human population worldwide. Besides its negative impact on quality of life, CP is also strongly associated with higher risk of life-threatening conditions such as cardiovascular diseases, type 2 diabetes etc. Various mechanisms of pathogenesis of CP are epigenetically regulated and microRNAs (miRNAs) are considered as one of the key modulators that influences periodontal homeostasis. The aim of this study is to analyze miRNA expression profile in gingival tissues by applying high-throughput technologies, searching for potential biomarkers of CP that may facilitate early diagnostics of the disease.

miRNA expression analysis was performed in 8 inflamed and 8 healthy gingival tissue samples by using microarray platform (Human miRNA Microarrays, 8x60K format). Fifteen significantly differently expressed miRNAs were selected for validation in 80 gingival tissue specimens from 48 CP patients and 32 controls by using quantitative reverse transcription PCR and the associations with clinical-pathological characteristics were assessed.

The microarray analysis indicated a large number of differently expressed miRNAs in patients with CP compared to healthy controls (Fig. 1). The comparison of 15 selected miRNAs in CP-affected *vs.* healthy gingiva demonstrated overexpression of ten miRNAs, out of which miR-A ($P<0.001$), miR-B ($P=0.006$), miR-C ($P=0.041$) were upregulated significantly ($FC\geq1.5$). Furthermore, the expression of miR-A and miR-C were also increased in a group of patients with periapical lesions compared to control group. Therefore, abovementioned miRNAs were chosen for further miRNA analysis in human bodily fluids.

The application of high-throughput technologies enables effective identification of periodontitis-specific miRNA expression profile. The results of present study suggest miRNAs as potential biomarkers of periodontal disease that could be applied for early diagnostics and treatment purposes.

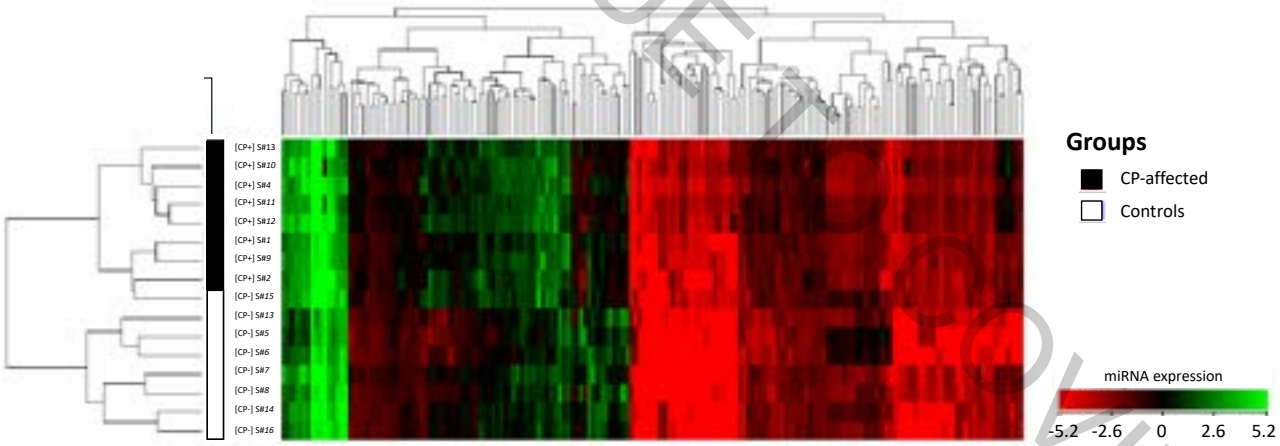

Fig. 1. miRNA expression profile of chronic periodontitis (CP)-affected and control samples. 177 miRNAs were differentially expressed at least 1.5-fold ($P\leq0.05$) between CP-affected group and healthy control group.

* – censored due to patent application

MODELING NATURAL HABITATS WITH LIQUID CRYSTALS: MOTILE BACTERIA IN ANISOTROPIC ENVIRONMENT

Illia Kostiuk[1], Daria Hamova[1], Mariia Harkusha-Omelchenko[1], Yuliia Faidiuk[1,2], Pavlina Zelena[1], Larysa Skivka[1], Oleksandr Tereshchenko[3], Oleksandr Bului[3], Vasyl Nazarenko[3]

[1]Taras Shevchenko National University of Kyiv, ESC "Institute of Biology and Medicine"
[2]D.K. Zabolotny Institute of Microbiology and Virology of the NAS of Ukraine
[3]Institute of Physics of the NAS of Ukraine
kilyapo@gmail.com

CANCELLED DUE TO COVID-19

Liquid crystals (LC) are compounds that retain the properties of a liquid, such as fluidity, and those of a crystal: highly ordered orientation of constituents underlies the ability of a LC to exhibit variations in physical properties along different molecular axes (anisotropy). The orientation of anisotropic medium imposes constraints on moving objects placed inside it. Among examples of such are motile bacteria that naturally occur in habitats with physical characteristics similar to LC. Soil, solid tissues of plant and animal organisms represent the environments with local anisotropy. Colonization of such environments, a process that largely depends on bacterial motility, until recently has been studied without taking into account the physical characteristics and the structural organization of the medium. Yet the anisotropy of natural biotopes can affect both the dynamics of bacteria movement and intercellular signaling, exerting an effect on the differentiation of cells and their response to exogenous stressors, including antibiotic substances.

In our study we have used disodium cromoglycate (DSCG), a biocompatible lyotropic chromonic LC that exhibits phase transitions from isotropic to anisotropic state as a function of both temperature and concentration. As a motile object, a bacterial strain *Proteus vulgaris* Hauser 1885 UKM B-905 was chosen. It is a pleomorphic peritrichous bacteria with multiple flagella located on its surface, responsible for its motility. The bacterium inhabits the intestinal tract of humans and animals, but as an opportunistic pathogen can cause urinary tract infections. In case of *P. vulgaris*, the colonization of the surfaces is performed by specialized differentiated cells 'swarmers'– elongated multinucleoid hyper flagellated structures, with a type of motility called 'swarming'. The latter are reported to be virulent forms with enhanced production of hemolysins and proteases.

We have developed and adjusted a system that allows for combining a LC and active motile bacteria: a set of nutrient media for bacteria cultivation and LC preparation was tested, the growth parameters in batch culture calculated, morphology of cells studied using transmission electron microscopy. Observation (using polarization microscopy) of bacterial behavior was performed in microchambers with oriented LC of various concentrations and temperature, in different solvent media, and within various time intervals. After being transferred to a different medium, majority of bacterial cells differentiated into large swarmer cells reaching 10μm. In an isotropic phase (under 10wt% of LC) their movement was chaotic, while in anisotropic phase bacterial behavior was drastically different: they moved parallel to the orientation of LC director. The movement was nonpolar, that is, approximately the same number of bacteria moving to the right and to the left.

The orientation order of LC reveals new facets of the dynamics of the bacterial movement up to providing a tool to control individual trajectories of bacteria. Studying behavioral patterns of bacteria in an anisotropic environment as an approximation of biological *in vitro* experiment to such *in vivo* opens the prospect of extending existing ideas about the interaction of macro- and microorganisms, as well as improvement in the technology of antimicrobial agent development.

ACETYLTRANSFERASE CHEA IN *ACINETOBACTER BAUMANNII* STRESS RESPONSE

Gabija Šakalytė[1], Julija Armalytė[1], Edita Sužiedėlienė[1]

[1] Institute of Biosciences, Life Sciences Center, Vilnius University, Vilnius, Lithuania
gabija.sakalyte@gf.stud.vu.lt

Acinetobacter baumannii is a gram-negative opportunistic pathogen, causing pneumonia, bacteremia and urinary tract infections in immunocompromised patients [1]. Due to its ability to quickly acquire antibiotic resistance, form biofilms on plastic surfaces and persist desiccation, *A. baumannii* was able to spread in the hospitals worldwide as well as in Lithuania. Rapidly increasing *A. baumannii* resistance to most antibiotics is a serious threat, thus more research is needed to understand the virulence and survival mechanisms of this bacterium and find new potential targets for antimicrobial treatment.

GNAT N-acetyltransferases are enzymes widely distributed among eukaryotic and prokaryotic organisms. These proteins usually transfer an acetyl group from acetyl-CoA to a large array of substrates, ranging from proteins and peptides to small molecules such as aminoglycosides [2]. In bacteria, GNAT acetyltransferases are associated with response to reactive oxygen species, toxins, iron acquisition and other cellular stress inducing factors. Moreover, it has been proved that some GNAT acetyltransferases transfer acetyl group to the aminocyclitol ring of a wide variety of aminoglycoside antibiotics and contribute to antibiotic resistance in bacteria [2].

In this work, we analysed the role of conservative *A. baumannii* N-acetyltransferase CheA in bacterial physiology, concentrating on the virulence and survival related traits. We have constructed an *A. baumannii ΔcheA* mutant and compared its properties with the wild type *A. baumannii* isolate.

[1]. Gonzalez-Villoria, A. M. & Valverde-Garduno, V. Antibiotic-Resistant Acinetobacter baumannii Increasing Success Remains a Challenge as a Nosocomial Pathogen. J Pathog 2016, (2016).
[2]. Favrot, L., Blanchard, J. S. & Vergnolle, O. Bacterial GCN5-Related N-Acetyltransferases: From Resistance to Regulation. Biochemistry 55, 989–1002 (2016).

CANCELLED DUE TO COVID-19

THE STUDY OF M6A EPIMODIFICATION REGULATING GENES EXPRESSION AND M6A EPIMARK LEVEL IN HUMAN ASTROCYTOMAS

Katažyna Samaitė[1], Arimantas Tamašauskas[1], Giedrius Steponaitis[1]

[1] Laboratory of Molecular Neurooncology, Neuroscience Institute, Lithuanian University of Health Sciences
Eivenių st. 2, Kaunas LT-50161, Lithuania
katazynasamaite@gmail.com

Astrocytomas are astrocytes derived, diffusely infiltrating and the most frequent primary tumors in human brain. Astrocytomas according to tumor malignancy are classified into 4 grades of which the most common and aggressive are 4th grade tumors called glioblastomas (GBM) [1]. Glioblastoma is a life-threatening brain tumor showing a median overall patient survival between 10 and 20 months after the resection. The incidence of glioblastoma is approximately 3-4/100,000, increases with age, and peaks in patients aged 50-60 years [2]. Epitranscriptome, in general can be understood as a chemical modifications of RNA bases, is recently discovered as an additional regulation level of biological information. More than 170 chemical modifications types of RNA are known up to date. Abundant levels of RNA modification are found in tRNA and rRNA, and slightly lower levels in mRNA and ncRNA [3, 4]. Methylation of adenosine at N6 position- m6A is identified as the most frequent modification in mRNA, microRNA and lncRNA and is also associated with cancer, obesity and infertility [5, 6]. m6A modification is controlled by three genes types: methyltransferases- „writers“ (METTL3, METTL14, WTAP), demethylases- „erasers“ (ALKBH5, FTO) and „readers“ (YTHDC1/2, YTHDF1/2/3) [7].

The aim of this research was to evaluate the significance of m6A epi-modification level and m6A regulating genes expression for astrocytoma malignancy, patient age and survival. The study enrolled n= 58 specimens of II and IV grade human astrocytomas (14 and 44, respectively). RNA from tumors specimens was purified applying TRIzol method following tissues cryo-homogenization. m6A modification detection was made applying fluorometric ELISA method using “EpiQuik™ m6A RNA Methylation Quantification Kit” according to the manufacturer’s recommendations. Gene expression of two m6A writers and two erasers (METTL3, WTAP and ALKBH5, FTO) were analyzed applying RT-qPCR. Results were evaluated by ΔCt method, GraphPad Prism software used for statistical calculations. Results showed that the expression of METTL3 ($p<0.0001$), ALKBH5 ($p=0.0005$) and FTO ($p<0.0001$) genes was associated with astrocytoma malignancy, patients survival (METTL3, FTO ($p<0.01$)) and IDH status (METTL3 ($p<0.0001$), ALKBH5 ($p=0.0005$), FTO ($p<0,0001$)). m6A modification level of total tumor specimens RNA did not showed any significant differences between tumor grade and patient clinical data as survival, patient age as well as IDH status. Such a data might be a result of ribosomal RNA (rRNA) which represents more than 95% of the total RNA, thus further investigation is essential to clarify the significance of N6-methyladenosine modification level in mRNA and ncRNA for astrocytomas.

To conclude, mRNA expression analysis of m6A writers and erasers revealed that METTL3, ALKBH5, FTO could serve as potential targets for astrocytoma diagnostics and prognostics.

[1] Louis DN, Perry A, Reifenberger G, et al. The 2016 World Health Organization classification of tumors of the central nervous system: a summary. Acta Neuropathol. 2016;131:803–820.
[2] Hong K. Emerging function of N6-methyladenosine in cancer (Review). ONCOLOGY LETTERS 2018;16:5519-5524.
[3] Hussain S, Aleksic J, Blanco S, Dietmann S, Frye M. Characterizing 5-methylcytosine in the mammalian epitranscriptome. Genome Biol. 2013;14:215.
[4] Machnicka MA, Milanowska K, Osman Oglou O, et al. MODOMICS: a database of RNA modification pathways-2013 update. Nucleic Acids Res. 2013;41:D262–D267.
[5] Zhang C, Fu J, Zhou Y. A Review in Research Progress Concerning m6A Methylation and Immunoregulation. Front Immunol. 2019;10:922.
[6] Wenqiang W, Xinying J, Xiangqian G, Shaoping J. Regulatory Role of N6 -methyladenosine (m6 A) Methylation in RNA Processing and Human Diseases. J Cell Biochem. 2017;118(9):2534–2543.
[7] Chen XY, Zhang J, Zhu JS. The role of m6A RNA methylation in human cancer. Mol Cancer. 2019;18(1):103.

CANCELLED DUE TO COVID-19

TECHNOLOGICAL ASPECTS OF DEPROTEINIZED CALF BLOOD HEMODERIVATIVE PREPARATION

Mariia Popova[1], Olena Saliy[1,2], Aleksey Godovskiy[2]

[1]Department of Chemical and Biopharmaceutical Technologies, Kyiv National University of Technologies and Design, Kyiv, Ukraine
[2]Ltd "BIOTESTLAB", Kyiv, Ukraine
e-mail: riia@ukr.net

Clinicians are particularly interested in drugs that improve the repair and regeneration of damaged tissues and / or tissues that are deficient in sufficient nutrients, such as Actovegin (Takeda Austria GmbH (Austria) and Solcoseryl (MEDA Pharma GmbH & Co. KG) The active substance, deproteinized calf blood hemoderivative (DCBH), is a mixture of natural substances such as inorganic electrolytes – chlorides, sodium, potassium, calcium, magnesium ions, nitrogen compounds and organic substances – glucose, acetates, lactates, amino acids, peptides, nucleosides, glycosphingolipids, and other metabolic products [1]. The studies of the neuroprotective effect of the drug based on deproteinized hemoderivative *in vitro* in cultured primary rat hippocampus neurons have confirmed the ability of the drug to exhibit neuroprotective and regenerative effects [2].

The raw material for obtaining the active substance of the drugs is cattle blood, which is subjected to deproteinization after preliminary treatment. The stages of the technological process for obtaining these drugs are not described in detail and differ depending on the manufacturers. Despite a sufficient number of cattle, Ukraine does not have its own technology for the production of DCBH. According to the results of the literature analysis, the technology for producing DCBH consists of the following stages: 1) blood defibrinization; 2) precipitation of high molecular weight proteins with various solvents (ethyl alcohol, acetone) or the breakdown of high molecular weight proteins by acid, alkaline or enzymatic hydrolysis; 3) prefiltration (0.45 μm); 4) sterilizing filtration (0.22 μm); 5) ultrafiltration (cut-off of the 5kDa fraction) [3-5].

The technological aspects of obtaining DCBH for the purpose of further industrial production have been studied. At the first stage of our research, blood was taken from the jugular vein of 2-month-old calves; the blood was defibrated for 6 hours in a thermal room at the temperature of 37°C. Defibrinated blood was subjected to hemolysis by means of a temperature difference: the blood was frozen at the temperature of -40°C for 12 hours and then the blood was incubated in water bath at the temperature of 37°C for 15 minutes, and then the temperature was raised up to 50°C and kept for 50 minutes. Hemolized blood was centrifuged at 5000 rpm for 1 hour. To determine the composition, the obtained intermediate was fractionated by gel filtration on a Sephadex column. The samples containing low molecular weight fractions were studied spectrophotometrically in the wavelength range from 100 to 750 nm in quartz cuvettes of 10 mm thickness (Fig. 1).

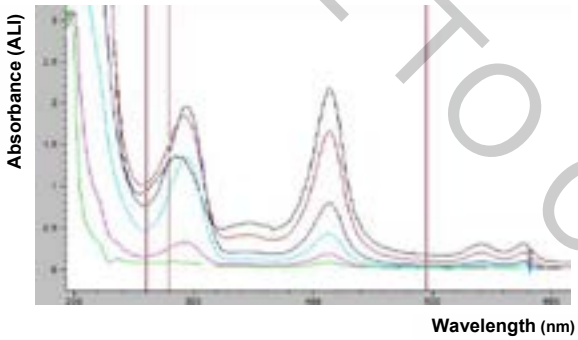

Fig. 1. Absorption spectra samples of hemolized blood

Analysis of the spectrum showed that the absorption maxima at the wavelength of 280 nm are based on the presence of tyrosine and tryptophan aromatic amino acid residues in the protein composition. Optical absorption at the wavelength of 405 nm indicates the presence of α-Amylase, alkaline phosphatase, and cholinesterase. Optical absorption at the wavelengths of 540 and 570 nm is due to the presence of hemoglobin.

Thus, a deproteinized calf blood derivative has been obtained for the subsequent studies of its low molecular weight fractions.

[1] F. Buchmayer, J. Pleiner, M.W. Elmlinger et al., Actovegin(R): a biological drug for more than 5 decades. Wien. Med. Wochenschr.; 161: 80–88 (2011).
[2] M.W Elmlinger., M. Kriebel and D. Ziegler, Neuroprotective and anti-oxidative effects of the hemodialysate actovegin on primary rat neurons *in vitro*. Neuromolecular. Med.; 13: 266–274 (2011).
[3] Dong Jisheng, Wang Jinfu, Feng Wenshan, Li Yong, Zhao Bo, Method for preparing calf-blood deproteinized extract, Worldwide applications, 2013. Patent No. CN103191151A.
[4] Gulevsky, N. Moiseyeva, O. Abakumova, I. Shchenyavsky, A. Nikolchenko, O.Gorina, Method of obtaining low molecular fraction from bovine cord blood, Ukrpatent, 2012, Patent No. UA 69652.
[5] Karl-Heinz Jaeger, Hellmut mittenzwei, Tissue cell stimulating blood extracts, United States patents, 1975, Patent No. US3973001A.

CREATED PRIOR TO COVID-19

MUTATION ANALYSIS IN LIQUID BIOPSY FROM NON-SMALL CELL LUNG CANCER PATIENTS

Agnė Šeštokaitė[1,2], Rasa Sabaliauskaitė[1], Vaida Gedvilaitė[1], Saulius Cicėnas[1], Sonata Jarmalaitė[1,2]

[1] National Cancer Institute, Vilnius, Lithuania
[2] Human Genome Research Group, Life Sciences Center, Vilnius University, Vilnius, Lithuania
agne.sestokaite@gmc.stud.vu.lt

Non-small cell lung cancer (NSCLC) is a common and rapidly progressing cancer with poor survival rates. Plasma cell-free DNA (cfDNA) has been proven to have prognostic potential as well as being useful for molecular profiling and monitoring disease burden [1]. Next-generation sequencing (NGS) is the most efficient and sensitive method to detect mutations from cfDNA.

The aim of this study was to screen Lithuanian NSCLC liquid biopsy samples for common lung cancer-related mutations by targeted NGS and to determine their associations with disease progression.

Analysis was conducted in NSCLC patient plasma samples before treatment and after clinical progression. Sequencing libraries were prepared from DNA using Oncomine Lung panel targeting 11 gene 180 hotspot mutation regions.

Out of all 39 analysed plasma samples, in 24 taken before treatment largely from patients with advanced NSCLC, we identified 32 protein-coding pathogenic single nucleotide variants (SNV) and 2 small insertions/deletions. Most common pathogenic SNVs in Lithuanian population were in *KRAS* (10/24; 42%) and *PIK3CA* (14/24; 58%). Moreover, higher mutation load was detected in patient samples after clinical progression *vs* before treatment. Specifically, in a group of patients (n=4) overall mutation count was 4-fold higher in samples after immediate progression diagnosed during routine check-up at end of the treatment as compared to patient samples before treatment (p=0.203) (Fig. 1).

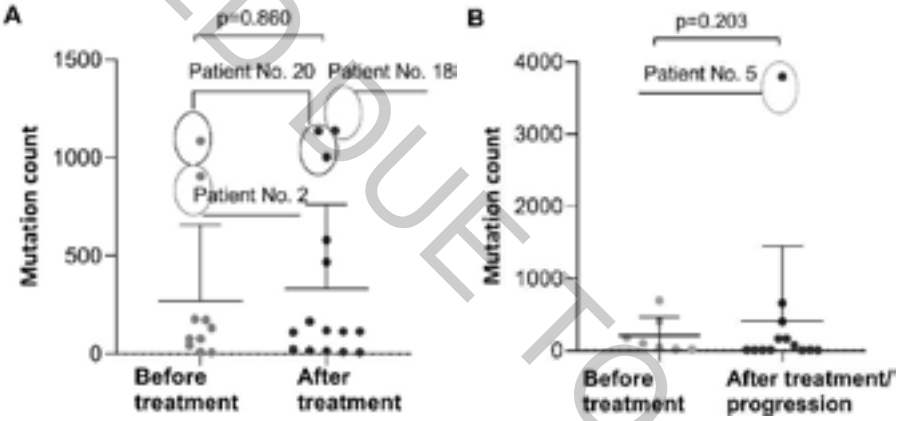

Fig. 1. Overall mutation count difference in plasma samples from NSCLC patient groups after treatment (A) and after treatment/progression (B) as compared to before treatment.

In conclusion, plasma cfDNA is useful for molecular profiling of NSCLC patients to capture clinically relevant somatic alterations in advanced stage patients and could be used as prognostic biomarker.

[1] N. Yang, Y. Li et al., The characteristics of ctDNA reveal the high complexity in matching the corresponding tumor tissues. BMC cancer, 18(1), 319 (2018).

CANCELLED DUE TO COVID-19

ANALYSIS OF METALLO-B-LACTAMASES FROM *CHRYSEOBACTERIUM* SPP. OF SOIL ORIGIN

Ignas Ragaišis[1], Laurita Klimkaitė[1], Renatas Krasauskas[1], Julija Armalytė[1], Edita Sužiedėlienė[1]

[1] Life Sciences Centre, Vilnius University, Lithuania
ignasraga@gmail.com `

World Health Organisation has announced antibiotic resistance as one of the biggest global health problems [1]. Antibiotics are substances naturally produced by microorganisms to combat bacteria, and have been used in clinical settings since 1941 to treat bacterial infections. Due to reckless use of antibiotics, many pathogenic bacteria are becoming more resistant to them, causing hardly treatable diseases. Most widely used antibiotic class is β-lactams, the compounds targeting bacterial cell wall synthesis by inhibiting transpeptidation of peptidoglycan, resulting in death of the cell. Resistant bacteria often have enzymes called β-lactamases that degrade these antibiotics. Genes of various β-lactamases can be easily transferred from one bacteria to the other, accelerating the spread of resistance [2].

Many soil microbes are naturally exposed to antibiotics and thus, have developed resistance to the compounds over millions of years. Some soil dwellers can also cause infections to patients with a suppressed immune system, thus becoming opportunistic pathogens. For example, *Chryseobacterium* genus consists of common soil bacteria, which can also cause urinary tract infections, sepsis or bacteraemia. *Chryseobacterium indologenes*, the most virulent species in the genus, have started to be associated with urinary tract infections in 1996 but nowadays more species are discovered to cause a variety of diseases, spreading from Taiwan, the primary source of *Chryseobacterium* infections [3]. *Chryseobacterium* are known to have a genus specific IND β-lactamase, responsible for their resistance to β-lactams [4].

In our previous study we have discovered two β-lactamases from *Chryseobacterium* spp.: IND-like and an unknown metallo-β-lactamase (MBL). Both of them gave significant resistance to β-lactam antibiotics when transferred to *Escherichia coli*. MBL gene homologues are found in almost half sequenced *Chryseobacterium* genomes and the proteins share ~40% similarity to IND β-lactamases, which are more common and found encoded in almost 60% of sequenced *Chryseobacterium* genomes. The aim of this study is to characterise these novel β-lactamases, as none of the MBL homologues have been characterised yet and less than a half of IND β-lactamases have their biochemical activities determined [5].

[1] https://www.who.int/news-room/detail/17-01-2020-lack-of-new-antibiotics-threatens-global-efforts-to-contain-drug-resistant-infections
[2] Munita, Jose M., and Cesar A. Arias, Mechanisms of Antibiotic Resistance, Microbiology Spectrum 4 (2) (2016).
[3] Mukerji, Ridhwi, Radhika Kakarala, Susan Jane Smith, and Halina G. Kusz., Chryseobacterium Indologenes: An Emerging Infection in the USA. BMJ Case Reports 2016 (April).
[4] Zeba B, De Luca F, Dubus A, et al. IND-6, a highly divergent IND-type metallo-beta-lactamase from Chryseobacterium indologenes strain 597 isolated in Burkina Faso. Antimicrob Agents Chemother. 2009;53(10):4320–4326.
[5] Naas, T.; Oueslati, S.; Bonnin, R. A.; Dabos, M. L.; Zavala, A.; Dortet, L.; Retailleau, P.; Iorga, B. I., Beta-Lactamase DataBase (BLDB) – Structure and Function. J. Enzyme Inhib. Med. Chem. 2017, 32, 917-919.

CANCELLED DUE TO COVID-19

DOXORUBICIN CELLULAR RETENTION PATTERNS CORRELATES WITH THERAPEUTIC RESPONSE IN ASCITIC LYMPHOMA BEARING MICE

Sima Garberytė[1,2], Margarita Žvirblė[1], Karolina Žilionytė[1], Jan Aleksander Kraśko[1], Nijolė Matusevičienė[1], Božena Pavliukevičienė[3], Gintaras Zaleskis[1]

[1]National Cancer Institute, Vilnius
[2]State Research Institute Centre for Innovative Medicine, Vilnius
[3]Vilnius University Life Sciences Center, Vilnius
E-mail for correspondence: Sima.garberyte@gmail.com

CANCER PREPRINTS 2019

Chemotherapy resistance (CR) greatly affects the risk of death in cancer patients. However, mechanisms of CR are not yet entirely elucidated. The mainstream of cancer research on this phenomenon call attention to genetically mediated mechanisms that lead to modified susceptibility to anticancer drugs. However non-genomic factors were also shown to trigger CR, for instance vascular permeability, stromal interstitial pressure, regions of hypoxia and some others. It has been also shown that the cellular uptake and cytotoxicity of anticancer agents might decrease with increasing cell density, an event observed *in vitro* and termed 'the inoculum effect'.

The aim of this study was to investigate Doxorubicin (Dox) plasma pharmacokinetics and cellular drug retention in C57BL/6NCr mice bearing ascitic EL4 lymphoma. Mice were inoculated intraperitoneally with $5*10^4$ EL4 lymphoma cells. Intravenous administration of Dox at a dose of 15mg/kg was given on day 3, day 5 or day 9 after tumor transplantation. These specific time points were chosen due to different tumor response characteristics attributable to tumor bearing mice (TBM) in our study. Cellular Dox content was determined by HPLC and FCM methods. Pharmacokinetic parameters were determined in plasma by HPLC and peripheral blood cell counts were done on automatic CBC analyzer.

Ascitic El4 lymphoma exhibited typical rapid proliferation in peritoneal cavity. Median survival time of untreated TBM was 14.5 days. Tumor cell numbers increased exponentially from $0.05x10^6$ (Day 0) to $202x10^6$ (Day 14). Therapeutic efficacy of Dox treatment was highly dependent on the relatively modest differences in tumor size. The median survival time of mice injected on Day 3 was 60 days with no signs of residual tumor. These mice were arbitrary designated as "cure" group. These mice also revealed the highest Dox cellular uptake in tumor cells during first 30 min after injection and tumor cells in peritoneal cavity were not detectable 72 h post-injection. TBM treated on day 5 exhibited signs of remission with median survival time of 26 days. Tumor cell counts were dramatically decreased in peritoneal cavity 72 hours after Dox administration. This group was designated as "relapse" group. Dox uptake 30 min after injection in "relapse" TBM was significantly lower as compared to "cure" group. During observable period of 12 days after drug administration cellular dox content was gradually decreasing in "relapse" TBM group. TBM treated with dox on day 9 exhibited a median survival duration of 14 days which was not different from group of untreated animals ("resistance" group). The cellular dox uptake in tumors was essentially undetectable in this group. Maximal plasma concentration of Dox was 1.33 µg/ml and it was detectable as early as 5 min post-injection. Plasma clearance half-time was 28.2 h, volume of distribution 128.4 l/kg. Plasma drug presence was below detection limit at 72 h post-injection. However, drug was retained in cellular samples of ascitic fluid, spleen and thymus up to 18 days following IV administration ("cure" group) or 10 days ("relapse" group). There were no significant differences in systemic hematopoietic toxicity observed between all three groups of TBM. Leukopenia (mostly due to decrease in lymphocyte and granulocyte counts) as well thrombocytopenia was observed on day 4 after Dox administration in all three TBM groups. Absence of differences in systemic effects between all three groups suggested that local tumor characteristics might be controlling susceptibility to dox treatment. In fact, the density of tumor cells in peritoneal cavity was rising by two orders of magnitude faster as compared to animal weight and ascites volume (ascitic fluid increase was 50-fold as compared to >5000-fold increase of cell number on day 14 after tumor transplantation). We hypothesized that the rapid increase of cell density at early avascular stage of tumor growth can govern the differences of cellular drug uptake, retention and eventually to drug susceptibility. This phenomenon is similar to "inoculum effect" reported to tumor cells exposed to cytotoxic drugs *in vitro*.

The intracellular tracking of dox in the cells of TBM might be a convenient means to further investigate this phenomenon. One additional clinical application out of these observations could be a possibility to develop a dox uptake test in blood. Importantly, dox lymphocyte uptake values exploring flow cytometric means could be performed on patient's blood. This method can be developed to show the individualized drug uptake and retention patterns in patient's blood.

[1.] Kobayashi H, Takemura Y, Ohnuma T. Relationship between tumor cell density and drug concentration and the cytotoxic effects of doxorubicin or vincristine: mechanism of inoculum effects. Cancer Chemother Pharmacol. 1992;31:6–10.
[2.] Ohnuma T, Arkin H, Holland JF. Effects of cell density on drug-induced cell kill kinetics in vitro (inoculum effect) Br J Cancer. 1986;54:415–421.

INVESTIGATION OF CYTOTOXIC RESPONSE OF HEALTHY AND PATHOLOGICAL HUMAN MYOCARDIUM-MESENCHYMAL STEM CELLS

Andre Aleksandraviciute[1], Rokas Miksiunas[1], Ieva Kulvinskiene[1], Ruta Aldonyte[1], Kestutis Rucinskas[2], Vilius Janusauskas[2], Siegfried Labeit[3], Daiva Bironaite[1]

[1] Department of Regenerative Medicine, State Research Institute Centre for Innovative Medicine, Vilnius, Lithuania.
[2] Vilnius University, Faculty of Medicine, Centre of Cardiac Surgery, Clinic of Cardiac and Vascular Diseases, Vilnius, Lithuania.
[3] Department of Integrative Pathophysiology, Universitätsmedizin Mannheim, Mannheim, Germany.
andryte.aleksandraviciute@gmail.com

Cardiomyopathies are a heterogeneous group of myocardial diseases associated with mechanical or electrical disorders of cells causing inappropriate functioning of the left ventricle [1]. Dilated cardiomyopathy (DCM) is agreed to be most common form of cardiomyopathy responsible for 40-50% of cases of heart failure leading to requirement of heart transplantation [2]. Many toxic causes, including drugs, environmental agents, substances of abuse or natural toxins and other are involved in pathophysiological mechanisms of DCM [3]. Therefore, in this study the molecular mechanisms of human healthy and dilated myocardium-derived mesenchymal stem cells (hmMSC) response to chemical and mechanical toxic exposures have been investigated. hmMSC have been isolated from human healthy and dilated myocardium biopsies, after cultivated in IMDM growth media with 10 percent FBS and were subjected to different concentrations of toxic environment mimicking naphoquinone and to an extra mechanical overload using Flexcell equipment. Healthy and pathological hmMSC response to toxic exposures have been investigated by cell viability kit CCK-8, apoptosis detection, pro and anti-oxidant mechanisms have been investigated as well. The cell viability protecting compounds and mechanisms have been also investigated.

Data of this study showed that healthy and pathological hmMSC differently responded to the toxic exposures with more prominent effect on healthy compared to the pathological cells. The obtained data also showed that possible to influence cell death-surviving mechanisms in order to improve cell regenerative potential. Investigation and targeted regulation of diseased human heart cell protection mechanisms will allow to broaden their application for therapeutic purposes searching new DCM preventing means.

[1] B. Maisch, M. Noutsias, V. Ruppert, A. Richter, S. Pankuweit, Heart Fail. Clin. 2012, 8,53.
[2] Elliott P, Andersson B, Arbustini E. Eur Heart J. 2007;29:270–276.
[3]Ghadri J-R, Wittstein IS, Prasad A, et al. Eur Heart J. 2018; 39:2032–2046.

CANCELLED DUE TO COVID-19

IDENTIFICATION AND QUALITATIVE EXPRESSION ANALYSIS OF UNUSUAL ESTERASE FROM *STAPHYLOCOCCUS SAPROPHYTICUS* AG1

Justas Šidiškis, Gintarė Povilaitytė, Lilija Kalėdienė, Alisa Gricajeva

Department of Microbiology and Biotechnology, Institute of Biosciences, Life Sciences Center, Vilnius University
justas.sidiskis@gf.stud.vu.lt; sidiskis.justas@gmail.com

It is well-known that bacterial lipolytic enzymes are extremely attractive for the sustainable industry applications due to their unique biocatalytic properties. These enzymes are valued not only for their natural ability to catalyze hydrolysis of carboxylic esters, but also for the *in vitro* promiscuity and ability to catalyze carboxylic ester bond synthesis and other non-specific activities. Easy extraction of bacterial lipolytic enzymes, their stability in various reaction conditions (extreme temperatures, pH, and chemical agents), wide range of substrates enable their applications in the fields of oleochemistry, polymer, textile, detergent, food, cosmetic industries, biodiesel production and bioremediation. With one of the most exceptional properties of enantioselectivity, bacterial lipolytic enzymes are distinguished as one of the most important biocatalysts used to produce optically pure chemical compounds [1, 2]. Their biotechnological significance is also reflected by the fact that certain microbial lipases and esterases are commercialized by the global biotechnology companies such as Fluka, Novozymes, Biocatalysts Ltd and other [3, 4]. Nevertheless, the demand for these biotechnologically relevant enzymes is not diminishing. Also, despite the current high number of identified lipolytic enzymes (~ 5000), only a small percentage (<10 %) of them are characterized [5]. Moreover, physiological relevance of these enzymes in bacteria are also underestimated and not fully understood and studied.

With the significant improvement of genome sequencing over the past decades, large amounts of data have become available in the public databases, analysis of which allows identification of new enzymes and helps to fill in the gap of knowledge regarding certain enzymes and other biological molecules. Moreover, genome-mining approach allows easy discovery of new biocatalysts more purposefully and without some expenses needed by utilizing classical microbiological enrichment culture approach or metagenomic analysis and protein engineering [6].

In this work, unusual EstAG1 esterase with unconventional conservative amino acid motives was identified to be coded in the genome of *Staphylococcus saprophyticus* AG1. Because of the unusual sequence traits of the EstAG1 enzyme, in order to preliminary evaluate its possible function and nature of the expression of the gene in the native bacterial cells, qualitative expression analysis was performed. For that purpose, bacterial cells of *S. saprophyticus* AG1 were grown in different nutrient composition media. For the amplification of EstAG1, total RNA was extracted from different growth phases of the bacteria and one-step RT-PCR method was employed.

---

[1] L. Casas-Godoy, F. Gasteazoro, F. Bordes et al., *Lipases: an overview* (Springer Nature Switzerland AG: Springer International Publishing, 2018).
[2] P.Y. Stergiou, A. Foukis, M. Filippou et al., Advances in lipase-catalyzed esterification reactions, *Biotechnology Advances* 31, 1846–1859 (2013).
[3] A. Kademi, D. Leblanc, A. Houde, *Lipases* (Enzyme Tech. Springer ASIATECH PUBLICHERS, Inc., New Deli, 2008).
[4] R. Singh, M. Kumar, A. Mittal, Microbial enzymes: industrial progress in 21st century, *3 Biotech* 6: 174 (2016).
[5] F. Kovacic, N. Babic, U. Krauss, *Classification of lipolytic enzymes from bacteria* (Springer Nature Switzerland AG: Springer International Publishing, Switzerland, 2019).
[6] A. Gricajeva, I. Bikutė, L. Kalėdienė, Atypical organic solvent tolerant bacterial hormone sensitive lipase-like homologue EstAG1 from *Staphylococcus saprophyticus* AG1: synthesis and characterization, *International Journal of Biological Macromolecules* 130, 253-265 (2019).

CRICKET DUE TO COVID-19

THE EFFECTS OF ELECTROSTIMULATION ON HUMAN MESENCHYMAL STEM CELL CHONDROGENIC DIFFERENTIATION

Raminta Vaičiulevičiūtė[1], Ilona Uzielienė[1], Vitalij Novickij[2], Ali Mobasheri[1,3], Edvardas Bagdonas[1], Narūnas Porvaneckas[4], Giedrius Kvederas[4], Eiva Bernotienė[1]

[1]Department of Regenerative Medicine, State Research Institute Centre for Innovative Medicine, Vilnius, Lithuania
[2]Faculty of Electronics, Vilnius Gediminas Technical University
[3] Research Unit of Medical Imaging, Physics and Technology, Faculty of Medicine, University of Oulu, Oulu, Finland
[4]Vilnius University, Faculty of Medicine, Vilnius, Lithuania
raminta.vaiciuleviciute@imcentras.lt

Electrostimulation (ES) is widely used in joint diseases like osteoarthritis or rheumatoid arthritis. Many studies showed safety and efficacy of transcutaneous electrostimulation for joint pain relief and improvement in their physical function [1]. But there is still a lack of knowledge on ES effects for cartilage repair *in vivo*. Cartilage tissue has limited ability to regenerate after trauma or degeneration, so mesenchymal stem cells (MSC) is a promising tool for treatment of studies of chondrogenesis induction, as they have a strong capacity to differentiate into chondrogenic lineage [2]. Increased expression of chondrogenic differentiation markers were observed after application of ES [3]. We hypothesise that efficacy of differentiation is mediated through voltage-gated Ca^{2+} channels.

The aim of this study was to evaluate effects of different intensity ES, as well as pulsed-ES (PES), as potential stimulating factors for improvement of MSC chondrogenic differentiation capacity through alteration of intracellular Ca^{2+} levels.

MSCs were isolated from bone marrows of three different patients. Additionally, human chondrocytes were isolated from articular cartilage of three different patients and compared to MSCs in all of the experiments. ES was performed for 3 days in 12 well plates under 5 V/cm electric field, pulse duration 8 ms and the frequency of pulse was 5.0 Hz. After ES, cell proliferation capacity was analyzed using cell proliferation kit 8 (CCK-8) (Spectrophotometry), intracellular Ca^{2+} concentration was measured using fluorescent dye Cal-520 (Spectrophotometry, fluorescent microscopy). Also, different nanosecond PES was applied to cells in order to analyze the differences in intracellular Ca^{2+} concentration. Chondrogenic differentiation was performed in micromasses of 200 000 cells. Chondrogenesis was evaluated by Safranin-O, Collagen type II antibody staining and by SOX9, Collagen II and Aggrecan gene expression (RT-PCR).

Results. ES has affected MSCs and chondrocyte proliferation, intracellular Ca^{2+} levels and chondrogenic differentiation capacity. Cell proliferation was significantly increased even after 1st day of stimulation (according to CCK-8 staining). Moreover, the amount of intracellular Ca^{2+} was significantly lower in cells after ES stimulation, as compared to non-stimulated cells. On the other hand, PES increased the levels of intracellular Ca^{2+} in both cell types.

In conclusion, ES and PES differently regulate intracellular Ca^{2+} levels of human MSCs and chondrocytes, which might reveal the differences in stimulation of chondrogenic differentiation response in those cells.

This work was funded by the European Social Fund according to the activity "Improvement of researchers" qualification by implementing world-class R&D projects' of Measure No. 09.3.3-LMT-K-712 (grant application code: 09.3.3-LMT-K-712-01-0157, agreement No. DOTSUT-215).

[1] T. M. Zizic, K. C. Hoffman, P. A. Holt et al., The treatment of osteoarthritis of the knee with pulsed electrical stimulation. The Journal of Rheumatology **22,** 1757–1761 (1995)
[2] R. S. Tuan, A. F. Chen, B. A. Klatt, Cartilage regeneration, The Journal of the American Academy of Orthopaedic Surgeons **21,** 303–311 (2013)
[3] H. Kwon, G. S. Lee, H. Chun, Electrical stimulation drives chondrogenesis of mesenchymal stem cells in the absence of exogenous growth factors, Scientific Reports **6,** 39302 (2016).

CANCELLED DUE TO COVID-19

THE FLOCALIN ACTION ON HEART-SPECIFIC COMBINATION OF K-ATP CHANNELS AND ITS DOSE-RESPONSE

Nataliia Shtefan[1,2], Oleksiy Boldyriev[1], Taras Vereshak[1], Yaroslav Shuba[1].

[1] Bogomoletz Institute of Physiology of the National Academy of Sciences of Ukraine, Kyiv, Ukraine
[2] National University of "Kyiv-Mohyla Academy", Kyiv, Ukraine
nataliia.shtefan@gmail.com

Activators of K-ATP (potassium ATP sensitive) channels are used as cardioprotectors in case of ischemia. The opening of K-ATP channels leads to hyperpolarization, reduction in contractility and decline in cellular metabolism. Thus it protects cardiomyocytes from damage. Flocalin is the new opener of the K-ATP channels. The presence of the fluorine group made the flocalin less toxic and more stable compared to its predecessor – pinacidil. It is known that flocalin has strong cardioprotective action against ischemia-reperfusion damage in the whole heart [1]. But there are some tissues also having K-ATP channels and the flocalin tissue specificity remains unclear. To investigate this question we developed the expression system which will artificially reproduce the K-ATP channels subunits composition of appropriate tissue. For sufficient comparing of flocalin action on different tissue-specific combinations of the K-ATP channels the estimation of its dose-response and its effective concentration is needed.

The expression system of the K-ATP channels is made as transfected HEK-293 cells with plasmid vectors containing complementary DNA sequences of K-ATP subunits appropriate to a certain tissue. The Kir6.2 and SUR2A combination of subunits is typical for heart tissue. We have found it using RT-PCR (reverse transcription-polymerase chain reaction) approach. Thus to obtain heart-specific expression we have transfected HEK-293 cell line with Kir6.2 and SUR2A subunits coding sequences. On such HEK-293 cells we have measured currents through expressed ion channels and flocalin application effect on it using the electrophysiological approach – patch-clamp.

In our previous investigations we have found that 20 uM flocalin solution activated current of lower amplitude compared to 20 uM of pinacidil. Both types of currents evoked by pinacidil and flocalin were blocked by K-ATP channel blocker – glibenclamide (10 uM) and had appropriate electrophysiological characteristics for K-ATP channels. The flocalin effect on potassium current differs depending on its concentration and is not as same as the pinacidil effect with the same concentration. According to this, it is necessary to define flocalin dose-response. It will help to compare the flocalin action on different tissues.

We measured potassium currents activated by application of 0.5, 0.75, 1,5, 10, and 20 uM flocalin. The effective concentration EC_{50} was about 5.4 uM. The obtained dose-response curve has a more sharp form than the pinacidil one comparing to the literature [2]. The current amplitude increases at low concentration. Therefore we suggest that flocalin is a more potent substance since it induces the same effect with a lower concentration than pinacidil. The less amount of substance is needed to activate the certain number of K-ATP channels.

In conclusion, we suggest that flocalin has no same effectiveness as pinacidil. Due to its stability, less toxicity, and potency the flocalin can be better than pinacidil in pharmacology issues. The data of dose-response will be used for further experiments on expressed compositions of other tissues: pancreas and bladder smooth muscle. Further experiments with flocalin on tissue-specific compositions of K-ATP channels are necessary.

[1] O.I. Voitychuk, R.B. Strutynskyi et al., Sarcolemmal cardiac K(ATP) channels as a target for the cardioprotective effects of the fluorine-containing pinacidil analogue, flocalin, British journal of pharmacology, **162(3)**, 701–11 (2011).
[2] T. Shindo, M. Yamada et al., SUR2 subtype (A and B)-dependent differential activation of the cloned ATP-sensitive K+ channels by pinacidil and nicorandil, British journal of pharmacology, **124(5)**, 985–991 (1998).

CANCELLED DUE TO COVID-19

THE INTERFACE BETWEEN CHRONOLOGICAL AGING AND KILLER MAINTENANCE IN *SACCHAROMYCES* YEASTS

Martynas Rojus Bartkus, Bazilė Ravoitytė, Ramunė Stanevičienė, Elena Servienė

Laboratory of Genetics, Institute of Botany, Nature Research Centre, Akademijos g. 2, 08412, Vilnius, Lithuania
martynas-rojus.bartkus@stud.vgtu.lt

Aging is a process affecting every cell of any living organism. Chronological life span (CLS) is the length of time that a non-dividing yeast cell survives. CLS studies is a model of aging of non-dividing cells of higher eukaryotes. Domesticated yeast *Saccharomyces cerevisiae* has been widely investigated in various fields of research, including aging [1]. *Saccharomyces paradoxus* is a closest relative of *S. cerevisiae* widespread in nature, which has been investigated in a less extent.

S. cerevisiae and *S. paradoxus* are known to possess *Totiviridae* double-stranded RNA (dsRNA) viruses, namely, L-A and satellite M [2]. M type dsRNA encodes a toxin and thus provides a killer phenotype and self-immunity to the host cell. Host cell and dsRNA virus are highly interconnected. Virus propagation and killer toxin synthesis require functions of various cellular proteins and components. To our knowledge, there is no published data on connection between cell aging and the dsRNA conferred killer phenotype in *Saccharomyces* yeast.

In this work, CLSs of *S. paradoxus* AML-15-66 and *S. cerevisiae* M437 killer strains, harbouring different dsRNA viruses [3,4], were compared. Colony forming units (CFUs) assay was used to evaluate yeast survival. Killing assays were performed to depict killer and non-killer cells in an aging population. Double-stranded RNA content of non-killer cells was investigated. Aging experiments in buffered and unbuffered growth medium were performed. Insights into the interface between aging and the killer yeast population is important for understanding adaptability of dsRNA viruses and their possible roles in cell survival upon different aging conditions.

[1] V. D. Longo, G. S. Shadel, M. Kaeberlein, B. Kennedy, Replicative and chronological aging in *Saccharomyces cerevisiae*. Cell Metab. 16(1):18–31 (2012).

[2] N. Rodríguez-Cousiño, P. Gómez, R. Esteban, Variation and distribution of L-A helper Totiviruses in *Saccharomyces sensu stricto* yeasts producing different killer toxins. Toxins (Basel), 9(10), pii: E313 (2017).

[3] I. Vepštaitė-Monstavičė, J. Lukša, A. Konovalovas, D. Ežerskytė, R. Stanevičienė, Ž. Strazdaitė-Žielienė, S. Serva, E. Servienė *Saccharomyces paradoxus* K66 killer system evidences expanded assortment of helper and satellite viruses. Viruses, 10(10): 564 (218).

[4] J. Lukša, B. Ravoitytė, A. Konovalovas, L. Aitmanaitė, A. Butenko, V. Yurchenko, S. Serva, E. Servienė, Different metabolic pathways are involved in response of *Saccharomyces cerevisiae* to L-A and M viruses, Toxins (Basel). 9(8): 233 (2017).

CANCELLED DUE TO COVID-19

THE INTRACELLULAR CALCIUM CONCENTRATION IN HUMAN MESENCHYMAL STEM CELLS AS A POTENTIAL TARGET FOR IMPROVEMENT OF CHONDROGENIC DIFFERENTIATION

Greta Rakauskienė[1], Emilija Sadauskaitė[1], Eiva Bernotienė[1], Edvardas Bagdonas[1], Ali Mobasheri[1,2,3,4], Narūnas Porvaneckas[5], Giedrius Kvederas[5], Ilona Uzielienė[1]

[1] Department of Regenerative Medicine, State Research Institute Centre for Innovative Medicine, Lithuania
[2] Research Unit of Medical Imaging, Physics and Technology, Faculty of Medicine, University of Oulu, Finland
[3] Centre for Sport, Exercise and Osteoarthritis Research Versus Arthritis, Queen's Medical Centre, United Kingdom
[4] Sheik Salem Bin Mahfouz Scientific Chair for Treatment of Osteoarthritis with Stem Cells, King Abdulaziz University, Kingdom of Saudi Arabia
[5] Vilnius University, Faculty of Medicine, Lithuania
greta.rakauskiene@gmail.com

CANCELLED DUE TO COVID-19

Human articular cartilage has a low ability to regenerate in case of damage, which is essential for development of such illnesses as osteoarthritis (OA). OA is a very common progressive disease, annually found in almost 10% of human population of which 60% are women [1]. Human mesenchymal stem cells (hMSCs) have attracted attention due to their potential application for the treatment of OA. These cells could be isolated from different types of tissues, where the classical source remain bone marrow (BM). However, due to low amounts of cells and difficulties in receiving healthy bone marrow samples, other sources, such as menstrual blood-derived hMSCs (MenMSCs), seems an attractive alternative. Intracellular calcium (iCa^{2+}) is known to have influence in regulating hMSCs differentiation, however, the basic iCa^{2+} levels in different types of hMSCs and chondrocytes and their role in stem cell chondrogenic differentiation are not elucidated [2].

The aim of this study was to evaluate association of intracellular calcium levels in human BMMSCs, MenMSCs and chondrocytes with chondrogenic differentiation capacity.

All experiments were performed on three different human cell types – MenMSCs (n=5), BMMSCs (n=5) and chondrocytes (n=5). MSCs were characterized by the expression of typical MSC surface markers (flow cytometry) as well as adipogenic and osteogenic differentiation capacity (Oil-Red O and Alizarin S staining). The cells were incubated with different types of calcium channel antagonists/agonists, including L-type voltage-operated calcium channel (VOCC) regulators and endoplasmic reticulum iCa^{2+} inhibitor for 1 and 24 hours to determine iCa^{2+} levels using Cal-520 dye (flow cytometry, fluorescent microscopy). Additionally, VOCC subunit CaV1.2 was analyzed immunocytochemically after treatment of the cells with VOCC regulators. The effects of the same calcium channel regulators on 21 day of chondrogenic differentiation of all three cell types were evaluated by Safranin-O, Collagen II antibody staining and by SOX9, Collagen II and Aggrecan gene expression (RT-PCR).

Similar stem cell properties were observed in both types of MSCs, as determined by surface marker expression and adipogenic and osteogenic differentiation. In MenMSCs and chondrocytes iCa^{2+} levels are significantly higher, which was associated with lower levels of chondrogenic differentiation capacity in those cells, as compared to BMMSCs. Stimulation with L-type calcium channel regulators resulted in improved chondrogenic differentiation potential in all cell types. In addition, iCa^{2+} channel regulators used in this study showed different effects on iCa^{2+} levels in both cell types, suggesting cell-specific regulation.

Taken together, our results demonstrate that MenMSCs exhibit similar stem cell properties to BMMSCs, however their iCa^{2+} levels are significantly higher, which may play a role in regulation of chondrogenic differentiation.

This project was supported by European Social Funds, titled: „Regulation of Intracellular Calcium Concentration in Human Menstrual Blood Mesenchymal Stem Cells During Chondrogenic Differentiation", Nr. 09.3.3-LMT-K-712.

[1] I. Uzieliene, G. Urbonaite, Z. Tachtamisevaite, A. Mobasheri, E. Bernotiene. The Potential of Menstrual Blood-Derived Mesenchymal Stem Cells for Cartilage Repair and Regeneration: Novel Aspects, Stem Cells International vol. 5748126 (2018).

[2] I. Uzieliene, E. Bernotiene, G. Rakauskiene, J. Denkovskij, E. Bagdonas, Z. Mackiewicz, N. Porvaneckas, G. Kvederas, A. Mobasheri. The Antihypertensive Drug Nifedipine Modulates the Metabolism of Chondrocytes and Human Bone Marrow-Derived Mesenchymal Stem Cells, Frontiers in Edocrinology vol. 10 756 (2019).

THE EXPRESSION OF L-TYPE VOLTAGE-OPERATED CALCIUM CHANNEL SUBUNIT CAV1.2 IN HUMAN MESENCHYMAL STEM CELL CHONDROGENIC DIFFERENTIATION

Emilija Sadauskaitė[1], Ilona Uzielienė[1], Greta Rakauskienė[1], Rokas Mikšiūnas[1], Edvardas Bagdonas[1], Daiva Bironaitė[1], Ali Mobasheri[1,2,3,4], Narūnas Porvaneckas[5], Giedrius Kvederas[5], Eiva Bernotienė[1]

[1] Department of Regenerative Medicine, State Research Institute Centre for Innovative Medicine, Vilnius, Lithuania
[2] Research Unit of Medical Imaging, Physics and Technology, Faculty of Medicine, University of Oulu, Oulu, Finland
[3] Centre for Sport, Exercise and Osteoarthritis Research Versus Arthritis, Queen's Medical Centre, Nottingham, United Kingdom
[4] Sheik Salem Bin Mahfouz Scientific Chair for Treatment of Osteoarthritis with Stem Cells, King Abdulaziz University, Jeddah, Kingdom of Saudi Arabia
[5] Vilnius University, Faculty of Medicine, Vilnius, Lithuania
esadausk@gmail.com

CANCELLED BUT TO BE PUBLISHED

Human mesenchymal stem cells (hMSC) have an ability to differentiate into diverse types of cells – osteoblasts, myocytes, adipocytes and chondrocytes. These cells are found in different tissues, such as bone marrow and less studied source – menstrual blood. The field of tissue engineering have used these cells to repair and regenerate nearly all kinds of human tissues. One of the most common applications is repair of cartilage, especially in patients with osteoarthritis.

Osteoarthritis is a degenerative disease which results in the loss of joint structure and deterioration of cartilage, it is also associated with obesity and aging. Moreover, there is evidence that osteoarthritis is often co-diagnosed with hypertension [1]. Such patients are usually prescribed cardiovascular drugs containing nifedipine (chemical name: 3,5-dimethyl-2,6-dimethyl-4-(2-nitrophenyl)-1,4-dihydropyridine3,5-dicarboxylate) which is a well-known L-type voltage-operated calcium channel (VOCC) inhibitor.

VOCC are important for intracellular intake of ions, regulating such processes as contraction, secretion, neurotransmission and gene expression in many different human tissues. CaV1.2 is one of the VOCCs subunits representing major channel's pore parts, which enable Ca^{2+} flow [2]. Alterations of calcium intake using antihypertensive drugs may influence pathogenesis of osteoarthritis, as intracellular levels of Ca^{2+} are important for chondrogenic differentiation.

The aim of this study was to evaluate the effects of VOCCs antagonist nifedipine on hMSC chondrogenic differentiation potential and expression of CaV1.2, and comparison to chondrocytes. hMSC were isolated from bone marrow (BM) or menstrual blood (Men). Human chondrocytes were isolated from articular cartilage samples. Cells were treated with nifedipine (10 μM) or VOCC agonist BayK8644 (10 μM) for 1 or 3 days and cell migration capacity was analyzed using scratch method. CaV1.2 was evaluated by staining the cells with CaV1.2 fluorescent antibodies (immunocytochemistry) and by its gene expression levels (RT-PCR). Cell metabolism (mitochondrial respiration) was measured after the treatment of the cells with nifedipine (10 μM) for 24 hours, using Agilent Seahorse. Chondrogenic differentiation was stimulated for 21 day, and the effects of nifedipine (10 μM) and BayK8644 (10 μM) were evaluated by Safranin and Collagen II antibody staining (histology) and expression profile of CaV1.2, SOX9, Collagen II genes (RT-PCR).

The levels of CaV1.2 subunit varied in different cell types. The highest expression of CaV1.2 gene (CACNAC1) was observed in chondrocytes, whereas BMMSCs and MenMSCs had similar, lower amounts of CACNAC1. Nifedipine downregulated mitochondrial respiration in all cell types, as well as their migration capacity. Different expression levels were observed during chondrogenesis in three cell types, where nifedipine reduced CaV1.2 gene expression in all cell types, however increased extracellular matrix formation, according to histological analysis.

Taken together, the results of this study might help in understanding the regulation of Ca^{2+} flow through VOCCs CaV1.2 pore during chondrogenic differentiation of hMSCs of different origins, which may help to further comprehend mechanisms of cartilage repair and lead to the development of therapies for patients with osteoarthritis.

[1] M. M. Rahman, J. A. Kopec, A. H. Anis, J. Cibere, C. H. Goldsmith, Risk of cardiovascular disease in patients with osteoarthritis: a prospective longitudinal study, Arthritis Care Res **65**, 1951-1958 (2013).
[2] W. Catterall, E. Perez-Reyes, T. P. Snutch, J. Striessnig, International Union of Pharmacology. XLVIII. Nomenclature and structure-function relationships of voltage-gated calcium channels, Rev **57**, 411-425 (2005).

MORPHOLOGY AND ELEMENTAL ANALYSIS OF LEECHES COCOONS USING SEM-EDS

Jurgita Rutkauskaitė-Sucilienė[1], Ingrida Šatkauskienė[1], Simona Tučkutė[2]

[1] Department of Biology, Faculty of Natural Sciences, Vytautas Magnus University, Lithuania
[2]Lithuanian Energy Institute, Breslaujos str. 3, Kaunas
jurgitasuciliene@gmail.com

CANCELLED DUE TO COVID-19

Some leeches during reproduction produce cocoons, which are similar to sacks. This capsule protects from drying out, also provides a microenvironment necessary for embryonic development. Leeches secrete various cocoon types depending on constraints imposed by environmental pressures and developmental strategies. For example, mechanically strong, hard-shelled cocoons are abandoned by the parent worm, leaving embryos to develop independently on nutritive cocoon fluid, meanwhile gelatinous cocoons are worn on the ventral side of the body until juveniles are born [1].

The purpose of this research is to analys morphological and chemical composition differences in different species leeches cocoons.

We examined cocoons from three leech species (i.e., *Erpobdella octoculata*, *Piscicola geometra*, and *Haemopis sanguisuga*). The unique structure was studied using several techniques – Electron Dispersive Spectroscopy (EDS) and Scanning Electron Microscopy (SEM). The last method allowed to see ultrastructural patterns on the surface of cocoons. Electron Dispersive Spectroscopy results were obtained from the cocoons wall. This analysis disclosed the chemical composition and percentage distribution of the elements. These elements were identified by the energy at which peak counts were detected. Based on primary data, carbon, oxygen and calcium prevailed in all samples, whereas magnesium, nitrogen, phosphorus, sulfur, and silicon were found in smaller quantities. There is a slight difference in the elemental composition and percentage of incidence between the surface and the inside of the cocoons wall.

Therefore, different species of leeches produce cocoons of varying shapes, sizes, and structures, which can help in species identification.

[1] A. M. Rossi, W. M. Saidel, C. J. Gravante et al., Mechanics of cocoon secretion in a segmented worm (Annelida: Hirudinidae). Micron 86, 30–35 (2016).

USE OF DIGESTATE FOR PLANT FERTILIZATION - INFLUENCE ON SOIL AND PLANT QUALITY AND GHG EMISSIONS

Aušra Bakšinskaitė, Vita Tilvikienė, Modupe Doyeni, Urtė Stulpinaitė

Lithuanian Research Centre for Agriculture and forestry, Instituto al. 1, Akademija, Kėdainiai distr.
ausra.baksinskaite@lammc.*lt*

CANCELLED DUE TO COVID-19

Climate change is one of the most important issues of our time. Recently, we are facing the consequences of human activity as we select various anomalous phenomena such as hurricanes, rain, drought, etc. Addressing these challenges requires an assessment of all areas contributing to climate change and measures to mitigate it. Lithuania is one of the countries with the highest greenhouse gas (GHG) emissions from the transport and agricultural sectors. However, direct GHG emissions are only one of the problems. Soil quality, organic matter accumulation and soil degradation are also very important when assessing the impact of agriculture on climate change. The addition of organic agricultural waste to soil plays an important role in combating environmental pollution from agricultural waste, also addressing the energy crisis and responding to global climate change. However, information on the impact of different agricultural organic wastes on soil, plant quality and GHG emissions is limited.

The aim is to compare the influence of fertilization of different digestate manures and mineral nitrogen fertilizers on soil and plant quality and GHG emissions from the soil. The digestate used in the experiment is under the anaerobic conditions in biogas plant and contains organic and mineral nutrients that are necessary and important for plant growth. The experiment was carried out at a laboratory scale. Wheat were cultivated in pots pots filled with two different soil types and fertilized with eight treatments of mineral and organic (digestate) fertilizer in three replicates. Plants were grown in climatic chambers (Climacell CLC-707-TV) at a temperature of 8 hours 10°C and 16 hours – 18°C, a humidity of 65%. GHG emissions will be determined using hoods and the gas collected will be analyzed by gas chromatography.

The results of the study will determine which organic matter in the soil releases the least GHG emissions and has lower contribution to environmental pollution.

DETERMINATION OF MINERAL COMPOSITION OF HEMP MORPHOLOGICAL PARTS (*CANNABIS SATIVA L.*) DURING VEGETATION BY MEANS ICP-MS

Solveiga Braknytė,[1] Aušra Bakšinskaitė[2], Vita Tilvikienė[2], Karolina Barčauskaitė[2]

[1] Vytautas Magnus University, Faculty of Natural Sciences, Department of Biology, Kaunas, Lithuania
[2] Lithuanian Research Centre for Agriculture and Forestry, Kaunas, Lithuania
braknyte.solveiga@vdu.lt

The current climatic and economic scenario encourages humanity to use sustainable resources to reduce our dependence on petrochemicals and reduce the negative environmental impact. Plants are valuable and natural resources because they can provide us with the chemicals that humans need. *Cannabis sativa L.,* also known as fibre hemp, is one of the oldest cultivated and herbaceous plants in the world, with many valuable natural components that have been used by folk since ancient times. For many years mankind has cultivated this plant for a variety of purposes, some as a source of food, others as a fuel or building material, and others as for medicinal purposes. Hemp plants are rich in nutrients and health-enhancing ingredients, including vitamins, mineral salts and macronutrients, and at least one hundred different cannabinoids[1]. Deficiency of mineral nutrients such as Fe, I, Zn, Ca, K, Mg is a growing nutritional problem in human populations. The versatility of hemp leaves and stems and the composition of their components can lead to the sustainable development of many products for use in the food, cosmetic and medical industries [2].

The aim of this study was to find out the amount of mineral composition of hemp morphological parts (*Cannabis Sativa L.*) during vegetation by means ICP-MS. Mineral composition of variety Felina 32 was determined during this study.

In the present study, 3 hemp raw materials (stems, leaves and blossoms) were analyzed. Samples were collected from Institute of Agriculture (LAMMC) field experiments. Investigated samples differ in their growing conditions. Different fertilization rate and density were applied. All samples were filled with concentrated nitric acid and placed in a device called MARS6 for mineralization. Mineral composition of digested hemp samples was investigated by means ICP-MS method.

Obtained results, as well as sample preparation methodology step by step, will be presented at the conference.

---

[1] F. Palazzoli, C. Citti, M. Licata, A. Vilella, L. Manca, M. Zoli, M.A. Vandelli, F. Forni, G. Cannazza, Development of a simple and sensitive liquid chromatography triple quadrupole mass spectrometry (LC–MS/MS) method for the determination of cannabidiol (CBD), Δ9-tetrahydrocannabinol (THC) and its metabolites in rat whole blood after oral administration of, J. Pharm. Biomed. Anal. **150**, 25–32 (2018).

[2] M.N. Qureshi, F. Kanwal, M. Siddique, Inayat-ur-Rahman, M. Akram, Estimation of biologically active cannabinoids in Cannabis indica by Gas Chromatography-mass Spectrometry (GC-MS), World Appl. Sci. J. **19**, 918–923 (2012).

CANCELLED DUE TO COVID-19

IDENTIFICATION OF 6 POTENTIAL SERUM MARKERS OF ASTROCYTOMA

Rūta Zabitaitė[1]; Daina Skiriutė[1], Rūta Urbanavičiūtė[1]

[1]Laboratory of Molecular Neurooncology, Neuroscience Institute, Medical Academy, Lithuanian University of Health Sciences, Eiveniu str. 4, Kaunas, LT 50009, Lithuania.

rutazabitaite@gmail.com

Astrocytoma is the most common glial tumor of the central nervous system. The most malignant form of it is grade IV Astrocytoma, also called Glioblastoma (GBM) – less than 5% of GBM patient survive more than 5 years after diagnosis. Due to its aggressiveness and lethal nature scientist are trying to find less invasive method of early prediction of this tumor, and patients' survival time. Over the past decade, YKL-40, TIMP1, TGFβ1, IP-10, ANG-1 and OPN proteins have emerged as a potential mediators of astrocytoma progression. Therefore, the aim of our study was to investigate expression of these six candidate biomarkers in the serum of astrocytoma patients.

Study group consisted of 72 astrocytoma patients (12 grade II, 60 grade IV), 60 healthy controls and 30 meningioma patients. In order to evaluate targeted proteins suitability as astrocytoma's blood markers ELISA method was used. Results of our investigation have demonstrated that TIMP-1, OPN, YKL-40 and TGF-β1 proteins serum levels were able to distinguish astrocytoma patient's group from healthy controls ($p<0.05$). There was also a statistically significant difference between TIMP-1, YKL-40, OPN proteins expression in GBM patients compared to healthy subjects ($p<0.05$), like between TIMP-1 level in grade II astrocytoma patients serum and control group ($p<0.05$). Further evaluation of our data revealed a statistically significant association between TIMP-1, OPN, TGF-β1, ANG-1 and YKL-40 proteins expression in patient serum and patient's survival time ($p <0.05$).

Results of this research confirmed that TIMP-1, OPN, YKL-40 and TGF-β1 could be a potential astrocytoma diagnostic biomarkers.

CANCELLED DUE TO COVID-19

EVALUATION OF FECUNDITY OF PERENNIAL RYEGRASS OF DIFFERENT GENETIC ORIGIN

Gintarė Šidlauskaitė[1], Žydrė Kadžiulienė[1]

[1] Department of Plant Nutrition and Agroecology, Lithuanian Research Centre for Agriculture and Forestry, Lithuania
gintare.sidlauskaite@lammc.lt

Due to climate change there is a growing interest in sustainable agriculture, which contributes to the conservation of natural resources. Grasslands of different composition do not only lead to an increase in biodiversity, but also enhance the environmental function of grasslands [2]. Perennial ryegrass has been cultivated in Europe for many years because of its good yield and good forage quality. It has started to be grown in Lithuania with the development of new varieties that are more resistant to adverse meteorological conditions. Cultivating the mixtures of different crops can also be one of the sustainable means of increasing agricultural productivity, but it is essential to optimize functional diversity by combining the distinct characteristics of not only species but also of varieties, that are best suited to local growing conditions [1].

So far studies have focused on the overall productivity of grassland and its forage value, as well as how individual species can help each other. However, only few varieties of different species have been analyzed in the mixtures. The intensity of growth of individual varieties may vary in case of different intensities and types of stress, which may affect the condition of grasslands.

Perennial ryegrass (*Lolium perenne L.*) is one of the most valuable *Poaceae* grasses and is a major component for perennial grasslands and pastures. In our study three new tetraploid perennial ryegrass 'Elena DS', 'Raminta', 'Verseka' (Lithuanian varieties) were used. The use of nutritional resources is a very important factor in the competition and compatibility of species and their quality existence, productive growth in the same place at the same time. To meet the nutrient requirements of the agroecosystem, biological nitrogen fixing legumes were used in the mixtures, which are compared to the effects of mineral fertilizers in homogeneous grasslands.

The obtained results showed differences between the cultivated perennial ryegrass varieties, however no significant differences were found between them. Perennial ryegrass 'Elena DS' had the best growth properties. The annual dry matter yield of this plant was the highest 7011 t ha $^{-1}$, the annual yield of 'Raminta' was 5.4% lower. 'Verseka' variety also showed good growth properties. The mixture of three varieties growing together showed the same growth trends as the 'Raminta' variety. Evaluation of the nutrient requirements of perennial ryegrass 'Elena DS' found out that the yield of perennial ryegrass was 15% higher with use of mineral stimulating nitrogen fertilizer rations compared to the yield of perennial ryegrass grown together with red and white clovers.

CANCELLED DUE TO COVID-19

[1].Ergon, Å., Seddaiu, G., Korhonen, P., Virkajärvi, P., Bellocchi, G., Jørgensen, M., Østrem, L., Reheul, D., Volaire, F. 2018. How can forage production in Nordic and Mediterranean Europe adapt to the challenges and opportunities arising from climate change*? European Journal of Agronomy*, vol. 92, p. 97-106.

[2].Brophy C., Finn J. A., Lüscher A. et al. (2017) Major shifts in species' relative abundance in grassland mixtures alongside positive effects of species diversity in yield: a continental-scale experiment. *Journal of Ecology* vol. 105, p. 1210–1222.

SUPPRESSING FUNGAL SOFT FRUIT PATHOGENS GROWTH USING PLANT EXTRACT

Jovita Kybartaitė[1], Lina Šernaitė[2], Neringa Rasiukevičiūtė[2], Alma Valiuškaitė[2]

[1]Vytautas Magnus University, Faculty of Nature Sciences, Vileikos Str. 8, LT-44404, Kaunas
[2]Institute of Horticulture, Lithuanian Research Centre for Agriculture and Forestry, Kauno Str. 30, LT-54333, Babtai, Kaunas dist.
jovita.kybartaite@vdu.lt

CANCELLED DUE TO COVID-19

Chemical management of pests includes herbicides, insecticides and fungicides. Side effect of fungicides are the accumulation of active substances and/or related metabolites in harvest and environment [1], however the usage of these pesticides still grows due to increased activity of pathogens [2]. Fungal pathogens cause most of diseases in horticulture and are becoming more aggressive and resistant to fungicides because of environmental changes [3]. Necrotrophic fungal pathogen *Botrytis cinerea* causes grey mold disease for more than couple hundred plants species [4], including strawberry and raspberry. In order to decrease the usage of fungicides, biological control methods like application of substances excluded from plants for food security are under investigation [3].

The laurel is well known for its aromatic leaves and there is a possibility that extract from laurel has an antifungal effect to *B. cinerea* because of the aromatic active substances. The aim of the research was to investigate the ability of laurel extract to suppress the growth of *B. cinerea* isolates from strawberry and raspberry *in vitro*. The research was carried out at LAMMC Institute of Horticulture, Lithuania. The research started from mixing different concentrations of the investigated extract with PDA and inoculating each plate with 7 mm diameter *B. cinerea* pathogen disc. The concentrations used for the test were 2600 µL/L, 2800 µL/L, 3000 µL/L. Petri plates were incubated at 20±2 ºC in the dark and measured after 2, 4 and 7 days (Fig. 1). The results showed that all used laurel concentrations have an ability to suppress the growth of *B. cinerea*. The highest concentration extract (3000 µL/L) showed more effectiveness with both *B. cinerea* isolates, especially with isolates from strawberry (Fig. 2). In conclusion, laurel extract can be used as an inhibitor for the growth of *B. cinerea*.

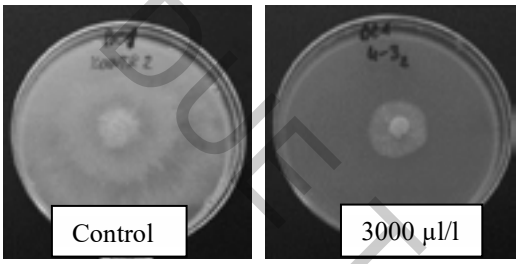

Fig. 1. *B. cinerea* isolate from strawberry after 4 days of inoculation without extract (A) and with laurel extract (B)

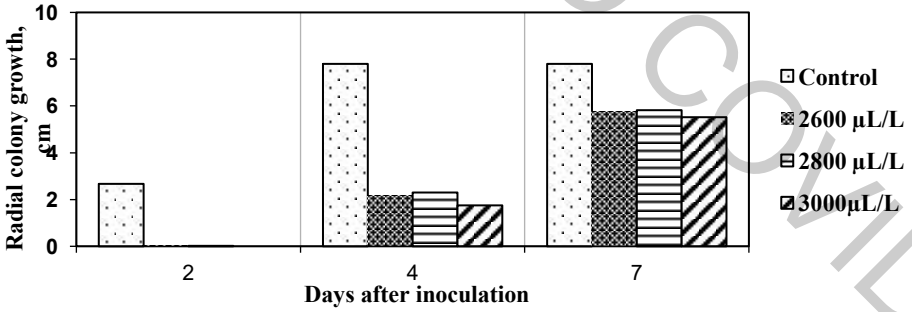

Fig. 2. Radial colony growth of *B. cinerea* isolates from strawberry affected with laurel extract

[1] European Food Safety Authority, EFSA, The 2017 European Union report on pesticide residues in food, EFSA Journal, **17(6)** (2019).
[2] A. B. Boxall, A. Hardy, S. Beulke et al., Impacts of climate change on indirect human exposure to pathogens and chemicals from agriculture, Environmental health perspectives **117(4)**, 508-514 (2008).
[3] D. S. S. Shuping, J. N., Eloff, The use of plants to protect plants and food against fungal pathogens: a review, African Journal of Traditional, Complementary and Alternative Medicines **14(4)**, 120-127 (2017).
[4] Y. Elad, I. Pertot, *Botrytis – the fungus, the pathogen and its management in agricultural systems* (Springer International Publishing, 2016).

THE PREVENTION OF POSTOPERATIVE PERITONEAL ADHESIONS IN A RAT MODEL BY THE NOVEL ANTI-ADHESION POLYSACCHARIDE-BASED FILMS

Anastasiya Kanunnikava[1,2], Vladimir Gureev[3], Arkadiy Nesterov[3], Evgenij Patrakhanov[3], Vladimir Pokrovsky[3], Vitaly Tilikin[1]

[1]Chemistry Department, Belarusian State University, Minsk, 220030, Belarus
[2]The Republican Scientific and Practical Center for Pediatric Surgery, Minsk, 220013, Belarus
[3]Belgorod State National Research University, Belgorod, 308015, Russia
a.r.kanunnikova@gmail.com

Postoperative adhesions are a serious complication often occurring after a variety of surgeries. It is characterized by a pronounced abnormal tissue growth caused by the proliferation of fibrous tissues that stick to the nearby normal organs, thus impairing their function and potentially leading to severe clinical complications, such as chronic pain, female infertility, bowel obstruction, etc. It also brings huge financial burden to the hospitals and the patient's families. Nowadays, many multiple strategies to prevent and eliminate adhesions have been proposed, but this problem still remains largely unsolved, which stimulates further research of suitable methods and/or materials [1,2].

One of the most promising therapies that prevent the formation of adhesions employs various mechanical barriers. Despite considerable efforts, limited positive results were obtained, which requires further research in this area [3].

In this work, three kinds of films based on the natural polysaccharides blends with different molar ratio of the components were prepared for studying their anti-adhesive properties.

Prior to the study, adult female Wistar rats of the same age weighing 230-270 g were housed at a constant room temperature with a 12 h light and dark cycle. Standard rodent food and water were available ad libitum. Before the inclusion in the study, the animals were kept under observation for 48 hours.

Prior the surgery, fourteen rats were randomly divided into five groups (n=8 in each): the sham group, the control group without any anti-adhesion treatment, and three experimental groups treated with polysaccharide-based film I, II, and III, respectively. Then all the rats were anesthetized by intraperitoneal injection of 300 mg/kg of Chloral hydrate and 1 mg/kg of Xylazine. In all animals, after shaving and sanitizing, a 3-cm long median laparotomy was performed. In the sham group animals underwent only laparotomy without any injury and/or suturing. In the other experimental groups, the cecum was delivered and the cecum wall was injured by 1 minute application of a cotton pad soaked in an alkaline (1 N sodium hydroxide) solution. Then the cecum was thoroughly washed with saline water. In the experimental groups, the investigated anti-adhesion films were trimmed into pieces 2×2 cm and then applied in-between the abdominal wall and the injured cecum. The cecum was put back into the abdominal cavity and fixed to the abdominal wall by a non-absorbable suture. The abdomen was closed using two-layer closure technique by a consecutive suture. To prevent infections prophylactic antibiotic (50 mg/kg Tylosin) was injected intraperitoneally after the surgery. Also, the same antibiotic was administered intraperitoneally once daily for 4 days. Until the rats were euthanized, they were observed every day and the postoperative wound was cleaned with ethanol, if necessary.

At day 14 after surgery, the animals were euthanized with lethal doses of Chloral hydrate. The abdominal cavity was opened via a U-shaped incision. The severity and the area of adhesions between the cecum and abdominal wall were examined macroscopically by a surgeon, who was blinded with respect to the animal groups. Adhesion formation was evaluated by a macroscopic inspection according to the adhesion rating scale from 0 to 5 proposed by Oncel et al. [4]. Grade 0: no adhesions; grade 1: loose filmy adhesions that can be separated by blunt dissection; grade 2: adhesions requiring <50% of sharp dissection for separation; grade 3: adhesions requiring >50% of sharp dissection for separation; grade 4: serosal injury, grade 5: full-thickness injury.

In the sham group (without prior adhesion-induced operation), six animals had no adhesions, while the other two had grade 2 adhesions. Severe grade of adhesion for the control group was 4.4. The animals treated with implanted film I had severe grade 1.6 adhesions. In the group treated by film II, the severe adhesion grade was 1.21, while in the third treated group the adhesion grade was 1.20. The overall significantly lower severity grade in the groups, where studied polysaccharide-based films were applied, points to the effectiveness of the chosen approach and materials for reducing the formation of tissue adhesion.

Obtained results demonstrated that the novel polysaccharide-based films were effective in reducing the formation of tissue adhesion.

All experiments were carried in compliance with the recommendations of the European Convention on Humane Treatment of Laboratory Animals [5].

[1] Cannata, A. et al. Postsurgical Intrapericardial Adhesions: Mechanisms of Formation and Prevention. Ann. Thorac. Surg. 95, 1818–1826 (2013).
[2] Capella-Monsonís, H.et al. Battling adhesions: from understanding to prevention. BMC Biomed. Eng. 1, 5 (2019).
[3] Li, J. et al. Polymer materials for prevention of postoperative adhesion. Acta Biomater. 61, 21–40 (2017).
[4] Oncel, M. et al. Comparison of a novel liquid (Adcon-P®) and a sodium hyaluronate and carboxymethylcellulose membrane (Seprafilm™) in postsurgical adhesion formation in a murine model. Dis. Colon Rectum 46, 187–191 (2003).
[5] European Convention for the protection of vertebrate animals used for experimental and other scientific purposes. Strasbourg: Europ. Treaty Series, 1986. № 123. P. 48.

CAMOTHEOPETHOSKP.19

SPATIAL PATTERNS OF PARTICLES&PLANKTON IN THE WARMING ARCTIC FJORD (ISFJORDEN,WEST SPITSBERGEN) IN 7 CONSECUTIVE MID-SUMMERS (2013-2019)

Marlena Szeligowska, Emilia Trudnowska, Anna Maria Dąbrowska, Rafał Boehnke, Sławomir Sagan, Józef Wiktor, Katarzyna Błachowiak-Samołyk

Department of Marine Ecology, Institute of Oceanology of the Polish Academy of Sciences, Poland
lena@iopan.pl

CANCELLED DUE TO COVID-19

The Arctic is warming at the fastest rate and thus it is facing the most rapid and substantial climate-related changes in marine ecosystems. The fjords on the western coast of Spitsbergen, Svalbard, are a unique area to study the aftermaths of warming in this polar region since they are exposed to various and dynamic forces driving local ecosystems. These fjords balance Atlantic, Arctic, brine- and freshwaters and thus different habitats exist there over relatively small spatial scales. They have only recently been recognized as important hotspots for many fish, seabirds and marine mammals. Since plankton is a key component of the Arctic pelagial and pivotal element of pelagic food web, pathways and efficiency of energy transfer to the higher trophic levels depend on the structure and dynamics of planktonic communities. However, despite a few group-specific studies on the fluctuations of either protists or zooplankton [1, 2], the nature of the progressing changes in its functioning as a whole remains poorly characterized.

Addressing the evident knowledge gap concerning the whole plankton community and suspended matter, we performed a comprehensive study on a wide range of plankton size fractions (nano-, micro-, small and large mesoplankton) and corresponding size fractions of the particles. We used two laser-based devices – Laser In Situ Scattering and Transmissometry instrument (LISST-100X) and Laser Optical Plankton Counter (LOPC) simultaneously with standard sampling methods of protists and zooplankton (Niskin bottles and plankton nets, respectively) and microscopic analyses. Our research constitutes a first such comprehensive approach to present a holistic view on spatio-temporal coupling between particles, aggregates, auto- and heterotrophic protists and zooplankton along a transect in Isfjorden - the largest Svalbard fjord system.

[1] A. M. Kubiszyn et al., The annual planktonic protist community structure in an ice-free high Arctic fjord (Adventfjorden, West Spitsbergen), Journal of Marine Systems **169**, 61-72 (2017).
[2] M. Głuchowska et al., Zooplankton in Svalbard fjords on the Atlantic–Arctic boundary, Polar Biology **39**, 1785–1802(2016).

NATURAL BIOACTIVE PRODUCTS FOR VEGETABLE DISEASE CONTROL

Simona Lukšiūtė[1], Alma Valiuškaitė[1], Neringa Rasiukevičiūtė[1]

[1]Lithuanian Research Centre for Agriculture and Forestry, Kauno st. 30, LT-54333 Babtai, Kauno district
simona.lukosiute@lammc.lt

Rising food contamination with pathogens demands precise diseases and pests control. Alternaria leaf blight and black spot are diseases caused by *Alternaria* spp. has become one of the most common carrot diseases. The use of chemical pesticides for control of various plant diseases is still a common practice, especially in developing countries. Although with the application of chemical fungicides, these diseases can be controlled, the hazardous impacts of pesticides in human health and environment are well known [1, 2, 3]. Moreover, with their excess applications, pest resistance already exists. Naturally occurring biologically active compounds, such as essential oils, are generally assumed to be more acceptable and less hazardous than synthetic compounds and represent a rich source of potential disease control agents. Crucial oils of medicinal and aromatic plants are believed to have antifungal properties [4, 5, 6]. Therefore, this study aimed to determine the in vitro effect of *Lavandula angustifolia*, *Citrus sinensis*, and *Thymus vulgaris* essential oils on *Alternaria* spp. Experiments carried out at the LAMMC Institute of Horticulture, Lithuania, 2018 - 2019. Lavender and thyme essential oils (EO) were obtained from dried material by hydrodistillation using the *Clevenger*-type apparatus, and orange blossom oil was commercial. EO separately mixed with potato dextrose agar in concentrations from 200 to 1000 µl/l, poured into Petri dishes. Small purified isolate fragment of 5 mm diameter placed in the centre of the Petri plate and incubated at 25 ± 2 °C in the dark for 7 days. The antifungal activity of EO was compared with chemical fungicide Switch® 62,5 WG (a.i. cyprodinil 375 g/kg + fludioxonil 270 g/kg). The diameter of the pathogen colony was measured 2, 5, and 7 days after inoculation (DAI). Concentrations of the essential oils, which demonstrated reduced growth of the pathogen, were considered to have an antifungal effect. The results showed that lavender EO had a weak antifungal activity at 200 and 400 µl/l concentrations. However, the most effective concentration was 800 µl/l. The orange blossom EO at 800 and 1000 µl/l concentrations had 100 % suppression of *Alternaria* spp. development 2 DAI. Chemical fungicide Switch® 62,5 WG was more effective compared with lavender and orange blossom EO at tested concentrations. However, thyme EO completely inhibited the growth of *Alternaria* spp. at concentrations above 200 µl/l. Besides, the fungicidal activity of concentrations from 200 to 1000 µl/l was even better than chemical fungicide 2 and 5 DAI and in all concentrations from 400 µl/l 7 DAI. To conclude, natural bioactive products produced from plants, especially thyme, have the potential to be control agents for diseases caused by *Alternaria* spp.

[1] N. Rasiukevičiūtė, E. Survilienė, A. Valiuškaitė. *Alternaria dauci* infekcijos prognozavimas skirtinguose agroekologiniuose regionuose su iMETOS®sm ligų prognozavimo sistema. Sodininkystė ir daržininkystė, 31 (3-4): 77-85 (2012).
[2] V. Singh, A. Shrivastava, S. Jadon, N. Wahi, A. Singh, N. Sharma. *Alternaria* diseases of vegetable crops and its management control to reduce the low production. International Journal of Agriculture Sciences, 7(13): 834–840 (2015).
[3] F. Fung, H. S. Wang, S. Menon. Food safety in the 21st century. Biomed. J. 41, 88–95. (2018)
[4] M. A. Gatto, A. Ippolito, L. Sergio, D. Di Venere. Extracts from wild edible herbs for controlling postharvest rots of fruit and vegetables. In: A. Ippolito, S. M. Sanzani, M. Wisniewski, S. Droby (eds.), Using Science to Increase Food Availability. III International Symposium on Postharvest Pathology, Bari, Italy, 1144: 349–354. (2016).
[5] A. Morkeliūnė, N. Rasiukevičiūtė, D. Burokienė, A. Valiuškaitė. Application of *Salvia officinalis* and *Pinus sylvestris* essential oils for controlling *Colletotrichum* spp. Rural Development 2019: Research and Innovation for Bioeconomy (2019).
[6] L. Šernaitė, A. Valiuškaitė, N. Rasiukevičiūtė, E. Dambrauskienė, P. Viškelis. The effect of spice extracts on strawberry pathogen *Botrytis cinerea.* Rural Development 2019: Research and Innovation for Bioeconomy. (2019).

CANCELLED DUE TO COVID-19

THE USE OF A CONDENSER MICROPHONE FOR THE STUDY OF STRIDULATION OF AQUATIC AND SEMI-AQUATIC BEETLES

Rodionova Elena Yurievna[1,2], Sazhnev Alexey Sergeevich[3]

[1] Laboratory of Chemical Commenication and Mass Rearing Insects, All-Russian Reseach institute of Biological Plant Protection, Krasnodar, Russia
[2] Department of Biology, Kubain State University, Krasnodar, Russia
[3] Laboratory of Water Invertebrate Ecology, Papanin Institute for Biology of Inland Waters Russian Academy of Sciences, Borok, Russia
rigaey@gmail.com, sazh@list.ru

The use of condenser microphone for the study of insects is a really important part of understanding behavior inside species. Insects have three main acoustic signals, which are stress, mating and predation trials. Other signals depend on the group of insects which we study. The main tools to investigate these signals are condenser microphone with different specifications and structures. Each microphone has special characteristics, such as frequency range, approximate sensitivity and approximate input-referred self-noise level. If the sensitivity level is 70 dB or less we need to use a preamplifier. Aquatic and semi-aquatic insects have a hidden way of life. Most of species can't use chemical communication because all pheromone liquid dissolve by water. In this case they use their organs (stridulatory organs) which produce different sounds. The frequency of these insects is between 0,2 to 10 kHz [1]. Many species from this group are produced when they are in the water and we use a waterproof condenser microphone. For example, many male species from the family Dytiscidae attract female only in water and the condenser microphone can't record interesting sounds for us.

Aquatic and semi-aquatic beetles were collected from the Kuban river near the All-Russian Research Institute of Biological Plant Protection (45°02'56.5"N 38°52'22.1"E) between June and September 2019. Adult beetles were collected using the superbright LED's trap. Males and females were stored in plastic containers with wet soil and kept at 20–26°C in constant climate chamber (model KBF720; Binder; Germany). Sounds were recorded from insects under stress using a measurement condenser microphone (model ECM8000; Behringer, Germany), audiophile vacuum tube preamplifier with limiter (model MIC100; Behringer, Germany) and stored as .wav files on a notebook (model HP Pavilion g series; USA). For sound processing used to the software Sony Sound Forge Pro 10.0 was used. All trials were conducted in the Laboratory of Chemical Communication and Mass Rearing Insects, at temperatures of 22–24°C.

Stress signals for *Berosus frontifoveatus* Kuwert, 1888 (Hydrophilidae) were simulated in accordance with a procedure used to create stress signals in another *B. frontifoveatus* [2]. Each adult was restrained by the appendage and sounds were recorded of 1 cm from the Behringer condenser microphone. For the recording of stress signals for *Heterocerus fenestratus* Thunberg, 1784 (Heteroceridae), each adult was held by the head and recorded 0,5 cm from the Behringer condenser microphone. Stress signals were recorded for 25 adults in each family. *B. frontifoveatus* is an aquatic species and *H. fenestratus* is a semi-aquatic species. Both are a bioindicator of water quality.

Each species has a different frequency range. For *B. frontifoveatus* the frequency range was from 935,56 to 974,85 Hz. For *H. fenestratus* the frequency range was from 1594,95 to 1698,74 Hz. Furthermore, every sound consists of pulses which has pre-pulse, main-pulse and major-pause. Sound *B. frontifoveatus* consist of seven alternating pulses (five main-pulses and two pre-pulses which separated six major-pauses). The duration of one pulse is 0.2852 s (main-pulses are 0.1692 s and pre-pulses are 0.116 s). The sound of *H. fenestratus* consist of short pre-pulse chirp trains. The duration of one pulse is 0.156 s. Both species have different locations of the stidulatory organ. *B. frontifoveatus* has abdomino-elytral stridulatory organs; *H. fenestratus* has abdomino-femoral stridulatory organs.

The use of a proper condenser microphone for bioacoustics study is a natural way to understand conversation between insects. For successful experiments, the researcher should know which condenser microphone with specific characteristics needs to the chosen. It depends on the frequency range of sounds for each species. These characteristics depend on the location of special organs which produce sound. Researchers can select which condenser microphone with special characteristics they need to use for experiments if they know about the location of these organs.

[1] S. Drosopoulos, M.F. Claridge, *Insect sound and communication: physiology, behavior, ecology and evolution* (Taylor and Francis Group, UK 2006).
[2] E. R. Van Tassell, An audiospectrographic study of stridulation as an isolating mechanism in the genus Berosus (Coleoptera: Hydrophylidae), Annals of The Entomological Society of America **58**, 407-413 (1965).

CANCELLED DUE TO COVID-19

THE NOVEL EXPERIMENTAL RAT MODEL OF POSTOPERATIVE PERITONEAL ADHESIONS

Vladimir Pokrovsky[1], Anastasiya Kanunnikava[2,3], Arkadiy Nesterov[1], Yury Linnik[3], Alexandr Filchakov[1], Ivan Arkhipov[1], Petr Lebedev[1]

[1]Belgorod State National Research University, Belgorod, 308015, Russia
[2]Chemistry Department, Belarusian State University, Minsk, 220030, Belarus
[3]The Republican Scientific and Practical Center for Pediatric Surgery, Minsk, 220013, Belarus
vmpokrovsky@yandex.ru

СТАТЬЯ ПОДГОТОВЛЕНА COVID-19

The formation of postoperative adhesions is a significant clinical problem for the present-day surgery. It involves a proliferation of fibrous tissue between two anatomically different structures, causing adherence and restricted visceral mobility. Adhesion-related complications after abdominal surgery increase mortality and morbidity, can lead to chronic pain, bowel obstruction, chronic constipation, and infertility [1] and thus significantly raise the cost of medical treatment. Due to this, there is a high demand of protocols for the treatment and prevention of these postoperative complications, which in turn can be based on the information on the underlying causes and the mechanism of adhesion growth. These studies are, however, significantly complicated by the fact that the process is affected by the variety of factors such as operation conditions, which hinders the analysis of data and prevents making unambiguous conclusions. This obstacle can be overcome by designing reliable clinical models, which involves procedures to reproducibly induce adhesions in a controllable manner. Aside from the investigation, such models can be used for developing management, treatment and prophylactic measures to be applied to this condition. At the moment most existing experimental models of peritoneal adhesions include abdominal sidewall defect and/or cecal abrasion, but the results of the different works are inconsistent [2]. Thus the objective of this study was the development of reproducible and representative experimental rat model of postoperative adhesions to further assess the efficacy of various preventative strategies for this process.

For developing the model in this work we used twenty rats of the same age and mean weight (250-300 g), which were split into four groups of five rats. Prior to the operation all rats were quarantined for 3 days in the vivarium and kept in a 12:12-h light-dark cycle with food and water available ad libitum. Them the rats were anesthetized by intraperitoneal injection of 300 mg/kg of Chloral hydrate and 1 mg/kg of Xylazine, their chest hair were removed by shaving and the skin was scrubbed with ethanol. To access the abdominal cavity a 3-cm-long lower abdominal midline incision was made. In the first group (C-group), the cecum was delivered and its wall was injured by 1 minute application of a cotton pad soaked in the alkaline (1 N sodium hydroxide) solution. In the second group (CP-group), the cecum wall and its opposite parietal peritoneum both were injured by the application of the same alkaline solution. In the third group (P-group), only the parietal peritoneum was injured. After the procedure the alkaline solution was washed out completely with saline water. In all the experimental groups, after replacing the cecum intra-abdominally, the cecum wall was fixed to the abdominal wall by a non-absorbable suture to localize adhesion sites. In the control group, necrosis was not induced and the cecum was not fixated on the parietal peritoneum. The peritoneum, the abdominal muscles, and the skin were closed by two layers of continuous sutures. To prevent infections prophylactic antibiotic (50 mg/kg Tylosin) was injected intraperitoneally immediately and once daily for 4 days after the surgery. Until the rats were euthanized, they were observed every day and the postoperative wound was cleaned with ethanol, if necessary. The rats were euthanized 14 days after the surgery.

A surgeon, who was blinded with respect to the animal groups, examined the adhesion sites between the cecal and the peritoneum macroscopically. Adhesions were evaluated by a macroscopic inspection according to the rating scale from 0 to 5 proposed by Oncel et al.[3]. Grade 0 of this scale corresponds to no adhesions, while grade 1 corresponds to loose filmy adhesions that can be separated by blunt dissection. Adhesions requiring <50% of sharp dissection for separation are assigned grade 2, while adhesions requiring >50% of sharp dissection for separation as grade 3. Grade 4 and 5 corresponds to serosal injury and full-thickness injury.

After the implementation of the protocol described above, all the animals in the sham group had severe grade 0.8 adhesions. In the CP-group, all the rats had grade 5 of adhesions, but 3 animal had to be sacrificed during the postoperative course. In the P-group, two rats had grade 2 of adhesions, one rat had grade 4 adhesions, and the remaining one had grade 1 adhesions. In the C-group, severity grade of adhesions was 4.8, which demonstrated the successful establishment of the adhesions model. Obtained results demonstrate the applicability of our novel experimental model created by alkali-induced injury of the cecal wall with its subsequent fixation to using for the comparative assessment of different potential antiadhesive agents.

All experiments comply to the European Convention on Humane Treatment of Laboratory Animals [4].

[1] Capella-Monsonís, H., Kearns, S., Kelly, J. & Zeugolis, D. I. Battling adhesions: from understanding to prevention. BMC Biomed. Eng. 1, 5 (2019).
[2] Li, J. et al. Polymer materials for prevention of postoperative adhesion. Acta Biomater. 61, 21–40 (2017).
[3] Oncel, M., Remzi, F. H., Senagore, A. J., Connor, J. T. & Fazio, V. W. Comparison of a novel liquid (Adcon-P®) and a sodium hyaluronate and carboxymethylcellulose membrane (Seprafilm™) in postsurgical adhesion formation in a murine model. Dis. Colon Rectum 46, 187–191 (2003).
[4] European Convention for the protection of vertebrate animals used for experimental and other scientific purposes. Strasbourg: Europ. Treaty Series, 1986. № 123. P. 48.

FIRE-BLIGHT PATHOGEN *ERWINIA AMYLOVORA*, PERSISTING IN UKRAINE: MULTI-APPROACH ANALYSIS

Shapoval Sofiia[1], Minchuk Yevheniia[1], Faidiuk Yuliia[1,2], Kharkhota Maksym[2], Moroz Svitlana[2], Gorb Tetiana[2], Tovkach Fedir[2]

[1]Taras Shevchenko National University of Kyiv, ESC "Institute of Biology and Medicine"
[2]D.K. Zabolotny Institute of Microbiology and Virology of the NAS of Ukraine
sonyaschapoval@gmail.com

CONTRIBUTED PAPER TO COVID-19

The enterobacterium *Erwinia amylovora (Eam)* is a devastating plant pathogen causing necrotrophic fire blight disease of rosaceous plants that has global economic importance for apple and pear production and trade. The urgency of finding an efficient method of accurate identification is due to importance to control its prevalence. Understanding of pathogen`s biology, as well as studying its closely-related species, can promote the development of antibacterial products and preventive measures, including those based on bacteriophages.

With a 5-year time interval several strains of *Eam* were isolated in Western part of Ukraine from affected quince, pear, apple trees, rowan-tree and pyracantha. Their biochemical, serological, pathogenicity properties and phage susceptibility were studied. Here we add the analysis with such features as the ability of mobile genetic elements maintaining, as well as fatty acid (FA) content, being compared to those of *Erwinia "horticola" (Eho)* – a closely-related pathogen causing similar symptoms in beech and apple trees, isolated earlier in Ukraine. Reference collection strains *Eam* 9057 and K8 were also included in the analyses.

Both the newly isolated and collection *Eam* strains carry a plasmid replicon of the same size. We presume it to be a pEA29, the most common extrachromosomal DNA in the abovementioned species. Notably, in most strains (except for typical strain *Eam* K8) it can be extracted using only harsh conditions. On the contrary, in *Eho* the variability of replicons is much bigger: from absence of any extrachromosomal DNA up to 2 and 3 large replicons. In *Eho*, as well as in strain *Eam* K8 plasmids can be easily extracted under standard conditions.

According to their FA content, the isolated *Eam* strains appeared to be a homogeneous group. Both major FA (represented by C12:0, C14:0, C16:0; C16:1, C18:1, and C17:0cyc) and minor FA percentage fully coincided with that of collection strain *Eam* 9057. Comparing to *Eho* strains, in *Eam* saturated even FA content was higher: 48.43±0.92% vs 39.30±1.36% in *Eam* and *Eho* respectively, while saturated odd FA portion was rather underrepresented:1.86±0.52% vs 5.25±1.67%. The content of unsaturated FA and hydroxy-FA was more or less similar. The major difference was revealed in in cyclic FA, being as low 2,22±0,38% in *Eam* strains, while 9,19±2,40% in *Eho.*

Again, this was not relevant for *Eam* K8: on a tree, constructed on a basis of FA content distances between strains of *Eam* and *Eho,* this strain did not cluster within *Eam* group, while appeared in a cluster of *Eho* species. Also, *Eho* as a species was revealed to represent rather heterogeneous group, varying in FA content more severely than *Eam.*

Notably, newly isolated *Eam* strains and collection strain *Eam* 9057 remain absolutely resistant to phages isolated from the same material as the bacteria, and any phage form our collection. Meanwhile, collection strain *Eam* K8, being different in FA content and plasmid replicon isolation, and suspected for being an R-variant or mutant, is the only one susceptible to phage infection.

Thus, isolated strains of *Erwinia amylovora* can be referred to as a highly conserved and homogeneous group that retains its features persisting in nature within a prolonged time. *Erwinia "horticola"* despite being closely-related are rather heterogeneous and significantly differ from *Eam.* Further investigation of underlying mechanisms that allow phages to infect *Eam* K8 and cause efficient lytic infection in it may shed the light on utility of phage-based anti-fire blight tools.

THE EFFECT OF PRISTINE C_{60} FULLERENE ON COGNITIVE DYSFUNCTIONS IN 6-OHDA–INDUCED MODEL OF PARKINSON'S DISEASE IN RATS

Anastasiia Tsymbaliuk[1], Viktoriia Stetska[1], Taisa Dovbynchuk[1], Yelyzaveta Makedon[1], Nataliia Dziubenko[1], Yuriy Prylutskyy[1], Ganna Tolstanova[1,2]

[1]ESC "Institute of Biology and Medicine" Taras Shevchenko National University of Kyiv,
[2]Institute of High Technologies Taras Shevchenko National University of Kyiv, 64/13, Volodymyrska Street, Kyiv, 01601, Ukraine
inastuska48@gmail.com

CANCELLED DUE TO COVID-19

Oxidative stress is one of the key pathological triggers of Parkinson's disease **(**PD) [1]. One of the main physicochemical properties of C_{60} fullerene (C_{60}FAS) is the ability to scavenge a large number of free radicals [2]. We assumed that C_{60}FAS due to this capacity, can efficiently reduce neuronal degeneration and changes in autonomic and cognitive functions of CNS in rats with PD.

Studies were done on male Wistar rats (220-250 g, n=15). The PD was induced by either single unilateral stereotaxic injection of 12 μg 6-OHDA. The control group was injected 2 μl 0,9 % NaCl. The C_{60}FAS was given daily for 2-11 days i.p. at doze 75 mg/kg. The percentage of destroyed dopaminergic neurons was evaluated in apomorphine test (0.5 mg/kg, i.p.) 1 and 2 weeks after surgery and by IHC staining of tyrosine hydroxylase (TH)-positive neurons in SN. The rats body weight, the water intake and behavioral test – open field were evaluated too.

C_{60}FAS treatment increased the number of TH-positive cells vs. the placebo group. The body weight in the 6-OHDA-PD rats treated with C_{60}FAS increased by 7% *vs.* placebo. The water intake in C_{60}FAS-treated rats had tendency to increase *vs.* 6-OHDA. In open field test, we found that C_{60}FAS treatment decreased 3-fold ($P < 0.01$) the latent period of the leaving of the field center and 2-fold the number of visits to the field center from the periphery vs. rats with 6-OHDA-PD.

This work confirmed that treatment with C_{60}FAS improved emotional state of the rats while did not affect locomotor and explorative activity.

[1] F. Sun, Y. Deng, X. Han et al., "A secret that underlies Parkinson's disease: The damaging cycle," Neurochemystry International, vol. 129, pp. 104484, 2019.

[2] H. Amani, R. Habibey, S. J. Hajmiresmail et al., "Antioxidant nanomaterials in advanced diagnoses and treatments of ischemia reperfusion injuries," Journal of Materials Chemystry B**,** vol. 5, no. 48, 2017.

SCREENING OF PROBIOTIC STRAINS OF BACTERIA WITH HIGH OXALATE-DEGRADING ACTIVITY

Marharyta Skovorodka[1], Iryna Akulenko[1], Hennadii Suslov[1], Tetiana Serhiychuk[1], Ganna Tolstanova[2]

[1] ESC "Institute of Biology and Medicine", Taras Shevchenko National University of Kyiv, Ukraine
[2]Institute of High Technologies, Taras Shevchenko National University of Kyiv, Ukraine
tuchishe@gmail.com

CANCELLED DUE TO COVID-19

Motivation. Excessive amounts of oxalate in the human body can be the cause of various pathological conditions, including hyperoxaluria [1]. In humans, there are no enzymes that provide the metabolism of oxalate. Human organism lack enzymes that provide the metabolism of oxalate [2]. Oxalate level can be decreased through the microorganisms that present in the gastrointestinal tract [3]. Recently, *in vivo* studies have been conducted to determine the oxalate degradation properties of microorganisms, which is a prospect to prevent kidney stone disease.

Purpose. Determine the oxalate degrading properties of existing probiotic drugs and newly isolated bacterial strains.

Materials and methods. The object of the study was newly identified strains of microorganisms from various sour-milk products (leaven, sour milk, sour cream) and probiotic drugs ("Enterogermina", "SANOFI-AVENTIS.S.p.A.", Italy; "Subalin", "BIOFARMA" LLC, Ukraine). Identification of strains was carried out using the ANAEROtest test system 23 (Erba Lachema, Czech Republic). Oxalate-degrading activity (ODA) was determined on the medium Oxalate Medium (contains sodium oxalate as the sole source of energy and carbon), MRS Broth+sodium oxalate for lactic acid bacteria and MPB+sodium oxalate for probiotic drugs "Enterogermina" and "Subalin". The ODA was determined using redoximetric titration (with KMnO4), in dynamics of 24, 48 and 72 hours. ODA expressed in %.

Results. From the sour-milk products, 12 strains of bacteria were isolated, among which 5 strains showed ODA. These strains were identified as *Lactobacillus nagelii 32* (Ln-32), *Lactobacillus rhamnosus K7* (Lr-K7), *Lactobacillus rhamnosus K8* (Lr-K8), *Lactobacillus frumenti K9* (Lf-K9), *Lactobacillus nagelii C12* (Ln-C12). Strains Lr-K7, Lr-K8, Ln-C12 have not shown grows on the Oxalate Medium (OM) medium. On the MRS Broth+sodium oxalate their ODA ranged from 1-5%. The highest level of ODA showed strain Lf-K9, the percentage of ODA in the OM amounted on 24 h - 23%, 48 h - 48% and 72 h - 52%. The Ln-32 strain on the OM medium metabolized on 24 h - 17%, 48 h - 34%, 72 h - 35%. Probiotics "Enterogermina" and "Subalin" showed a moderate ODA that was higher in the OM environment and ranged from 7-24%, and on the medium MPB+sodium oxalate from 5-18%.

Conclusions. 1) Thus, for further study with the prospect of the creation of probiotic drugs with high ODA, two strains of *Lactobacillus nagelii 32* and *Lactobacillus frumenti K9* were selected. 2) Probiotic drugs "Enterogermina" and "Subalin" have a moderate ODA.

[1] Hatch, M. and Freel, R. The Roles and Mechanisms of Intestinal Oxalate Transport in Oxalate Homeostasis. Seminars in Nephrology, **28(2)**, pp. 143-151 (2009).
[2] Abratt, V. and Reid, S. Oxalate-Degrading Bacteria of the Human Gut as Probiotics in the Management of Kidney Stone Disease. Adv Appl Microbiol., **72**, pp. 63-87 (2010).
[3] Gnanandarajah, J. and Abrahante, J. Presence of Oxalobacter formigenes in the intestinal tract is associated with the absence of calcium oxalate urolith formation in dogs. UrolRes, **40(5)**, 467-473 (2012).

CHARACTERIZATION OF L-TRYPTOPHAN IMPRINTED POLYPYRROLE DEPOSITED ON THE GRAPHITE ELECTRODE

Ernestas Brazys[1], Vilma Ratautaitė[2], Gintautas Bagdžiūnas[2], Arūnas Ramanavičius[1,2]

[1] NanoTechnas – Center of Nanotechnology and Materials Science at Vilnius University, Faculty of Chemistry and Geosciences, Institute of Chemistry, Naugarduko 24, Vilnius LT-03225, Lithuania
[2] Center for Physical Sciences and Technology, Department of Functional Materials and Electronics, Laboratory of Nanotechnology, Sauletekio av. 3, Vilnius LT-10257, Lithuania
ernestasbrazys@gmail.com

Tryptophan is an essential constituent of the diet. It plays an important role in protein synthesis, and is also the precursor of a variety of biologically active compounds including serotonin, melatonin, tryptamine, quinolinic acid and kynurenic acid. In addition, tryptophan is a precursor to the coenzymes NAD and NADP, and can replace niacin as an essential nutrient. Both excessive intake and deficiency of tryptophan are detrimental to health. Tryptophan and its metabolite niacin deficiency can cause lethargy, loss of hair, skin lesions and pellagra. Small doses of tryptophan are often used in the treatment of mild insomnia. However, large amounts of tryptophan can exhibit tremor, rigidity, hyperreactivity, myoclonus and even generalized seizures [1]. Therefore it is useful to monitor tryptophan levels in the body.

Quantitative tryptophan amino acid analysis can be carried out by high-performance liquid chromatography (HPLC) [2]. However, this method is impractical in sensor application, thus more practical and easy to produce electrochemical sensors are gaining popularity.

In this research electrochemical sensor based on molecularly imprinted polymers was used to determine L-tryptophan. Molecular imprinting allows the preparation of synthetic polymers featuring receptor or catalytically active sites. The most common form of imprinting comprises the synthesis of polymers in the presence of templates. Removal of the template from the formed polymer liberates binding sites complementary in shape and binding groups to the template structure. The resulting polymers are then used in various recognition-based applications [3].

Cyclic voltammetry was applied for electrochemical polymerization of molecularly imprinted polypyrrole (MIP) with L-tryptophan template molecules. The electrochemical synthesis was performed by potential cycling (10 potential cycles) based method, the potential was cycled in the range of 0 V – 1.0 V *vs* Ag/AgCl (3 M KCl), scan rate 50 mV/s and step potential 2.44 mV.

After the synthesis MIP's template molecules were removed by washing MIP in stirred water. The sensing ability of L-tryptophan was evaluated in a solution of Britton-Robinson buffer (BRB) with pH value of 2.50. Differential pulse voltammetry (DPV) method was chosen to determine L-tryptophan concentration in a BRB solution. Measurement parameters were as follows: step potential 5 mV, modulation amplitude 25 mV, modulation time 50 ms and interval time 500 ms, in the potential range of 0.4 V - 1.2 V *vs* Ag/AgCl (3M KCl). The results show that L-tryptophan eletrochemical oxidation peaks were observed at potential around 0.9 V *vs* Ag/AgCl (3 M KCl).

[1] E. L. Sainio, K. Pulkki, S. N. Young. L-Tryptophan: Biochemical, nutritional and pharmacological aspects. *Amino Acids*, **10**(1), 21–47 (1996).
[2] F. Wu, E. Tanoue. Sensitive Determination of Dissolved Tryptophan in Freshwater by Alkaline Hydrolysis and HPLC. *Analytical Sciences,* **17**(9), 1063–1066 (2001).
[3] B. Sellergren, A. J. Hall. Molecularly Imprinted Polymers. *Supramolecular Chemistry* (2012).

CANCELLED DUE TO COVID-19

INCREASING OF THE BIOAVAILABILITY OF MODEL FLAVONOID IN SOLID DISPERSION SYSTEM WITH UREA

Vadym Lisovyi, Iryna Povshedna, Dmytro Danylenko,
Volodymyr Bessarabov, Galyna Kuzmina

Department of Pharmaceutical Industry, Kyiv National University of Technologies and Design, Ukraine
v.lisovyi@kyivpharma.eu

CANCELLED DUE TO COVID-19

Biologically active substances (BAS) of plant origin have a positive effect on the physiological processes of the human body, increasing its resistance. One of the representatives of the flavonoid nature BAS is hesperidin. The problem of its use in the composition of drugs is its low solubility, which significantly affects the bioavailability index [1]. Therefore, it is relevant to study the direction of increasing solubility of hesperidin.

The inclusion of flavonoid in the solid dispersive system (SDS) was chosen as a research method in this work. Main objective of this study is to investigate the effect of SDS composition on the solubility of hesperidine. Solid dispersion systems are multicomponent systems containing lipophilic substances and water-soluble carriers, where the substance is in the form of a highly dispersed solid phase with the formation of intermolecular complexes of variable composition with the carrier material [2]. The formation of SDS allows to significantly increase the dissolution of flavonoids and provides a uniform release of the active substance from the system, without changing the chemical structure of the molecule of the active pharmaceutical ingredient [3]. As carriers for the manufacture of SDS used urea, polyethylene glycol (PEG) of different molecular weight, polyvinyl alcohol (PVA), propylene glycol, mannitol. The results obtained are presented in the form of a diagram (Fig.1).

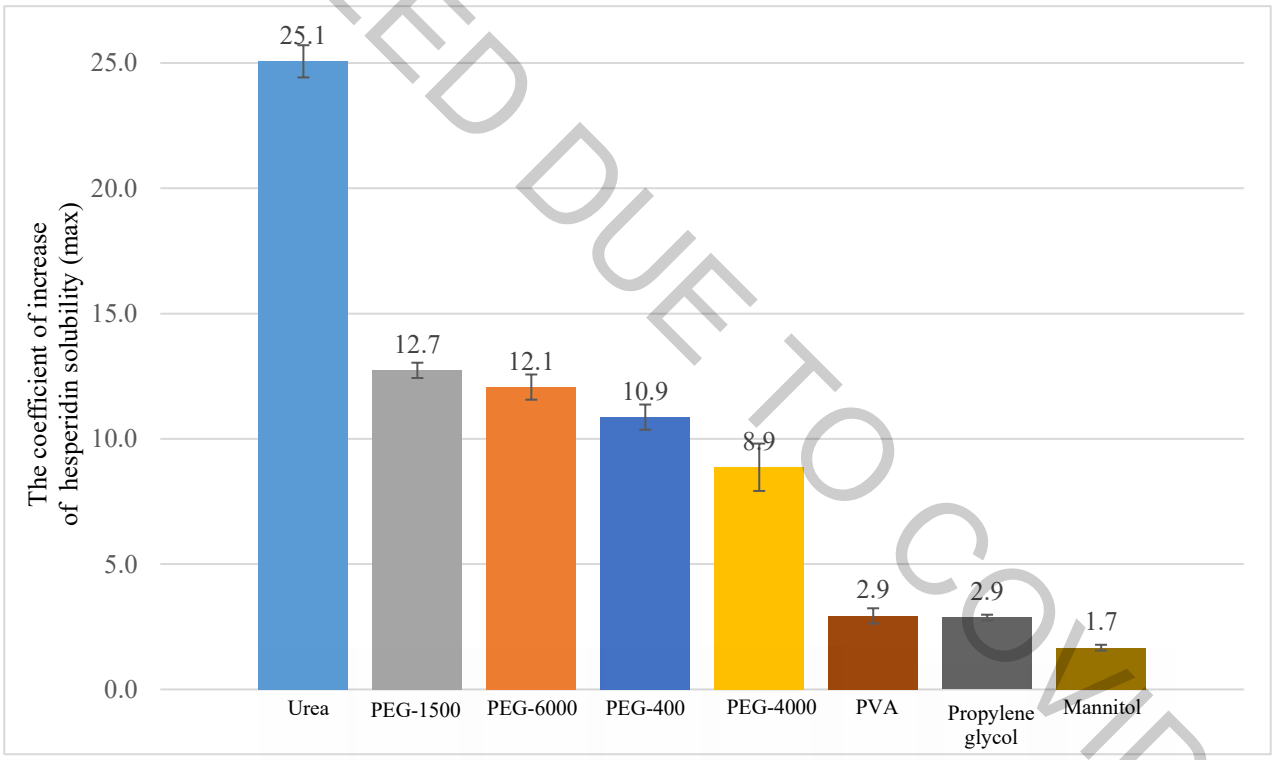

Fig. 1. Dependence of increasing solubility of hesperidin on the composition of the SDS

In conclusion, it was found that the increase in the solubility of hesperidin depends on the composition. The maximum value of solubility increase is observed in the system with urea – 25.1 times.

The authors is grateful to K. Yashchenko for her assistance with the research.

[1] Majumdar S. Solubility, Stability, Physicochemical Characteristics and In Vitro Ocular Tissue Permeability of Hesperidin: a Natural Bioflavonoid/ S. Majumdar, R. Srirangam. // Pharmaceutical Research. – 2010. – №26. – C.1217–1225.
[2] Higuchi T. Phase-solubility techniques / T. Higuchi, K. Connors. // Adv. Anal. Chem. Instrum.. – 1965. – №4. – p. 117–122
[3] Connors K. Thermodynamics of Pharmaceutical Systems: An Introduction for Students of Pharmacy / K.A Connors. – Hoboken, New Jersey: John Wiley & Sons Inc, 2002. – 360 p.

LASER INDUCED OPTICAL BREAKDOWN WITH FRACTIONAL PICOSECOND Nd:YAG 1064 NM LASER IN VIVO ON PORCINE MODEL

Justinas Baleišis[1], dr. Romualdas Rudys[1].

[1] Department of Biomodels, State Research Institute Centre for Innovative Medicine, Lithuania
Justinas.baleisis@imcentras.lt

Picosecond lasers ranging in the infrared region use the theory of selective photothermolysis by creating zones of photomechanical (photoacoustic) trauma. As a result, the picosecond laser has a high specificity for its target but with less heat generation in the epidermal and dermal layers. Acoustic waves are produced due to rapid thermal expansion and result in mechanical destruction of surrounding structures creating vacuoles like structures by optical tissue breakdown (LIOB) [1]. LIOB uses spatially precise microscopic thermal wounds in the target tissue creating microthermal treatment zones or MTZ. Fractionated lasers create coagulative, fractional, located and epidermal necrosis on MTZs. They are non-contiguous, meaning, they are separated by zones of intact tissue cells, that migrate into the damaged areas accelerating the healing processes [2].

The initiation mechanism of picosecond LIOB, begins from the production of free seed electrons by a laser pulse via multiphoton absorption. The plasma formed at the focal point then expands vaporizing materials and creating cavitation bubbles that further expand outward to the co-located tissue to generate microscopic vacuolar tissue reactions [3]. Histologically, this translates as a column-like denaturation of the epidermis and dermis. Tissue surrounding the affected area remains intact and together with the surrounding healthy tissue provides migrating cells to the damaged area within the first 24 hours [4].

Depending on the extent of the laser treatment in the skin, selecting the correct operatic wavelength can greatly determine, which specific chromophores (melanin, hemoglobin and water) are targeted and defines the penetration depth. Fractionated laser modalities target water as their chromophore, which allows to target various water-containing structures, such as collagen, blood-vessels and epidermal keratinocytes [5].

In this study, we investigated the laser-tissue interactions brought by the picosecond domain Nd:YAG laser. The modality operates at two switchable wavelengths (1064/532nm), generating 250±20 mJ and 150 ps pulses. The effects of the ultrashort pulses are not currently described, and the area is absent of *in vivo* animal studies, that could correlate with human skin. *In vivo* studies with longer pulse duration than 150 ps, used in our study, conducted with patients demonstrated pronounced effect on new collagen formation with no pain, little to no side-effect, no social downtime[6].

For this purpose, we designed an experiment by using a *in vivo* porcine model, as it offers great similarity to human skin, as described in literature [7]. We analyzed the formation of the MTZ, microscopic epidermal necrotic debris, collagen, epidermal integrity staining and conducted macroscopic examination of the treated skin after 1 hour, 2 and 10 days.

No pigmentary changes, blistering, scarring or other side effects were observed in the treated area during the post-treatment follow-ups. The appearance of erythema and edema implied that the treatment was effective, and a skin healing response was expected to occur. The histopathological examination of the tissue samples was prepared using histochemistry and immunohistochemistry methods. They confirmed the formation of MTZs in the dermal-epidermal junction. Based on our finding, the Nd:YAG laser operating on 1064 nm wavelength and 150 ps, depending on the energy in use, is safe on *in vivo* porcine skin models and can be applicable generating reproducible dermal or epidermal lesions, where target depth is only defined by the focusing optics. LIOB could be applied for direct extracellular matrix remodelling, removal of senescent fibroblasts, addressing mast cells and resident cells related disorders, tattoo removal and sebaceous gland treatment.

[1] T. Ohshiro, T. Ohshiro, K Sasaki et al., Picosecond pulse duration laser treatment for dermal melanocytosis in Asians: A retrospective review. Laser Ther. ;25(2):99–104 (2016).
[2] C. Tziotzios, C. Profyris, J. Sterling, Cutaneous scarring: Pathophysiology, molecular mechanisms, and scar reduction therapeutics: Part II. Strategies to reduce scar formation after dermatologic procedures. J Am Acad Dermatol [Internet]. 66(1):13–24 (2012). Available from: http://dx.doi.org/10.1016/j.jaad.2011.08.035
[3] B. Varghese , M. Jurna, J. Palero et al., Influence of absorption induced thermal initiation pathway on irradiance threshold for laser induced breakdown. Biomed Opt Express. 6(4):1234 (2015).
[4] R.L. Torbeck, L. Schilling, H. Khorasani et al., Evolution of the Picosecond Laser: A Review of Literature. Dermatologic Surg. 45(2):183–94 (2019).
[5] I. Bogdan Allemann, J. Kaufman, Fractional photothermolysis-an update. Lasers Med Sci. 25(1):137–44 (2010).
[6] M.H. Gold, Dual wavelength treatment protocol with a picosecond laser for the reduction of facial wrinkles. J Cosmet Laser Ther [Internet]. 21(3):147–51 (2019). Available from: https://doi.org/10.1080/14764172.2018.1481514.
[7] A. Summerfield, F. Meurens, M.E. Ricklin, The immunology of the porcine skin and its value as a model for human skin. Mol Immunol. 66(1):14–21 (2015).

ORIGINAL ARTICLE COVID-19

OPEN READINGS 2020 ORGANIZERS

Faculty of Physics

SPIE. STUDENT CHAPTER VILNIUS UNIVERSITY

OSA Vilnius University Student Chapter

CENTER FOR PHYSICAL SCIENCES AND TECHNOLOGY

EPS Young Minds

SPONSORS

LIGHT CONVERSION

EKSPLA

BROLIS SEMICONDUCTORS

OPTOGAMA

EKSMA OPTICS

MONO SPEKTRA

Standa

Altechna

femtika

PULSAR

HOLTIDA

LIDARIS LIDT Service

TERAVIL

OPTOMAN IBS HERO

Optoteka

Quantum Light Instruments

3photon

integrated optics

QS LASERS

EKSMA

AgriFood DIH Lithuania

Go Vilnius

THORLABS

Gudobelė

akvilė

BARLEY BROS SOFT BREW